SEMI-ANALYTICAL ESTIMATES OF PERMEABILITY

OBTAINED FROM CAPILLARY PRESSURE

A Thesis

by

CAROLINE CECILE HUET

Submitted to the Office of Graduate Studies of
Texas A&M University
in partial fulfillment of the requirements for the degree of

MASTER OF SCIENCE

December 2005

Major Subject: Petroleum Engineering

APPENDIX A
DERIVATION OF PERMEABILTY
AND RELATIVE PERMEABILITY FROM CAPILLARY PRESSURE

Introduction

By definition, relative permeability is a measure of the ability of a rock to conduct one fluid when two or more fluids are present. The relative permeability is controlled by pore geometry of rock, wettability characteristics, fluid saturation and saturation history. In the past, many papers about analytical expressions for relative permeability have been published. These relationships are good approximations for "clean" rocks with limited cementation. But these methods are not valid for rocks with high amount of clay or very heterogeneous. In this appendix, we derive the equation estimating permeability and relative permeability from capillary pressure.

Derivation of permeability from capillary pressure

Derivation of permeability equation follows Willie and Gardner [A-1] approach. This approach describes a porous medium as a capillary model with a random connection of pore spaces. Some assumptions are made to simplify the model:

1. Two-phase immiscible displacement,
2. One dimensional linear flow,
3. Darcy's law.

Willie and Gardner introduce the capillary model. This model consists to a buddle of capillary tubes running parallel to the direction of the flow (**Fig. A-1**). There are different sizes of capillary tubes. They use a distribution function $\alpha(r)$ — i.e., $\alpha(r)dr$ capillary radii between r and $r+dr$. This bundle is cut into a large number of thin slices. The short pieces of a tube in each slice are arranged randomly and then are reassembled. So, capillary tubes from one slice to the next are not completely aligned.

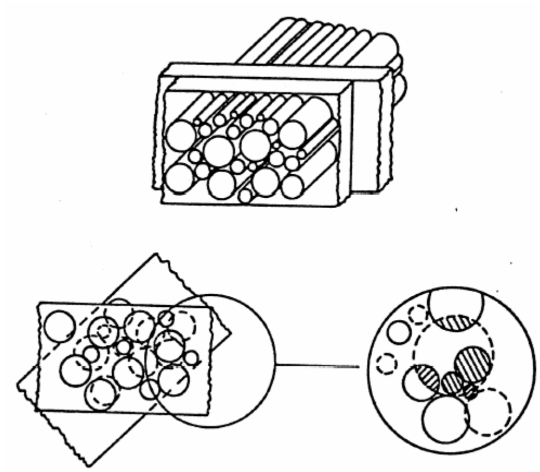

Figure A.1 – Idealized capillary model of a porous medium showing probability of inter-connection of pore spaces [A-1].

In this model, they assume that when wetting and non-wetting phases flow in the same time in a porous media, each phase flow in different pathways. Since the medium is water-wet, some water stays immobile, that constitutes the irreducible water saturation S_{wi}. In the capillary model, displacement of liquid is complete, so there is no immobile water on the walls of capillary tubes. So the porosity of the model is:

$$\phi^* = \phi(1 - S_{wi}) \quad \text{(A-1)}$$

Water saturation for the model is:

$$S_w^* = \frac{S_w - S_{wi}}{1 - S_{wi}} \quad \text{(A-2)}$$

The two primary assumptions in this derivation are that permeabilities and capillary pressures in the model and the porous media are the same. For a single-tube, capillary pressure is defined by:

$$p_c = \frac{2\gamma}{r} \quad \text{(A-3)}$$

where

$$\gamma = \sigma \cos(\theta) \quad \text{(A-4)}$$

They assume that at water saturation S_w^* and capillary pressure p_c, water occupies all small pores with radii from r_1 to R and oil occupies larger pores with radii from R to r_2. The wetting phase saturation S_w^* is related to the radius R and the pore size distribution by the equation:

$$S_w^* = \frac{\int_{r_2}^{R} \pi r^2 \alpha(r) dr}{\int_{r_1}^{r_2} \pi r^2 \alpha(r) dr} \quad \text{(A-5)}$$

The area effectively occupied by water in any slice of the model is $(\phi^* S_w^* A)$, where A is the total area of the slice. An equal area is occupied by water in the neighboring slice. Owing to the random distribution of the pores in each slice, these areas have a common part whose area is smaller. Indeed, the probability that it lies in the first area is $(\phi^* S_w^*)$ and the probability that it lies in the second area is $(\phi^* S_w^*)$, then the probability that lies both area is $(\phi^* S_w^*)^2$.

Consider a single pore filled with water. This pore abuts against pores in the next slice of which some are filled with water also. Assuming that the water-filled pores are randomly distributed, it follows by a similar argument that the area common to the single pore in the first slice and all water-filled pores may be taken as $(\pi r^2 \phi^* S_w^*)$.

Thus the water passes through a pore whose area is πr^2 but whose ends are constricted to a fraction $(\phi^* S_w^*)$ of this area. It is also influenced by the way in which the exit area is distributed over the ends of the pore. A constant n reflects the manner in which the available interconnecting pore is divided (**Fig. A-2**). If $n = 1$, it indicate that all the exit area are connected in one pore. It can be expected that $n \geq 1$.

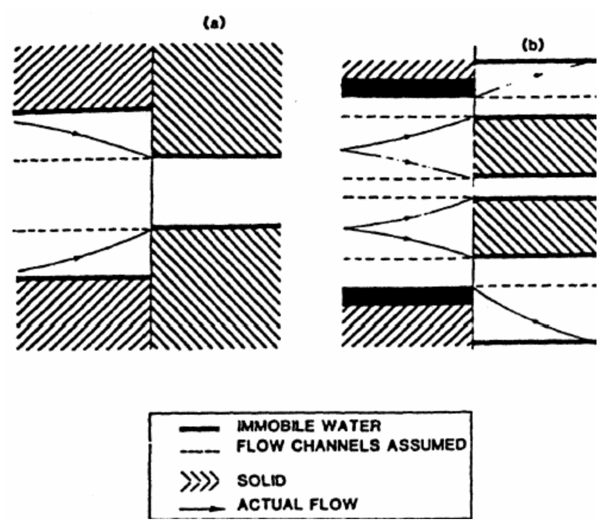

Figure A.2 – Schematic representation of value of geometric factor β and n: (a) n=1; (b) n>1.

Since the flow of water through a constricted pore depends on the distribution of the exit area — it can be expected only on the basis of an average distribution. An equivalent pore radius $\bar{r}$ is defined as:

$$\bar{r} = \frac{(\phi^* S_w^*)^{\frac{1}{2}} r}{n^{1/2}} \qquad \text{(A-6)}$$

This radius is proportional to the exit area for all pores. Poiseuille's law is used to calculate the flow through each pore on the assumption that the effective radius is given by Eq. A-6.

$$q = \frac{\pi \bar{r}^4}{8\mu}\left[\frac{\Delta p}{L}\right] \qquad \text{(A-7)}$$

Since there are n exit areas per pore, Eq. A-7 becomes:

$$q = \frac{\pi \bar{r}^4}{8\mu}\left[\frac{\Delta p}{L}\right]\left[\frac{\beta}{n}\right] \qquad \text{(A-8)}$$

The parameter β is inserted to recognize the fact that flow through a pore radius r overemphasizes the impedance because it ignores the larger areas available for exit flow at either side of the constrictions formed where pores abut. Thus it may be expected that $\beta \geq 1$ and that β is a function of the average shape of pores in the medium that the model represents. By substituting Eq. A-6 into Eq. A-8, we obtain:

$$q = \left[\frac{\Delta p}{L}\right]\frac{\pi}{8\mu}(\phi^* S_w^*)^2 r^4 \left[\frac{\beta}{n}\right] \qquad \text{(A-9)}$$

From Eq. A-9, the total flow may be computed by integrated for flowrate through pores with radii between r_1 and R.

$$Q = \left[\frac{\Delta p}{L}\right]\frac{\pi}{8\mu}(\phi^* S_w^*)^2 \left[\frac{\beta}{n}\right]\int_{r_1}^{R} r^4 \alpha(r)dr \qquad \text{(A-10)}$$

The total pore area of the cross-section may be written as:

$$\phi^* A = \int_{r_1}^{r_2} \pi r^2 \alpha(r)dr \qquad \text{(A-11)}$$

Dividing Eq. A-10 by Eq. A-11, we obtain:

$$\frac{Q}{A}=\left[\frac{\Delta p}{L}\right]\frac{\pi}{8\mu}\phi^{*3}S_w^{*2}\left[\frac{\beta}{n}\right]\frac{\int_{r_1}^{R} r^4\alpha(r)dr}{\int_{r_1}^{r_2} r^4\alpha(r)dr} \qquad \text{(A-12)}$$

Taking the derivative of Eq. A-12, and replacing R by r, we obtain:

$$dS_w^* = \frac{r^2\alpha(r)dr}{\int_{r_1}^{r_2} r^4\alpha(r)dr} \qquad \text{(A-13)}$$

We can eliminate r from Eq. A-12 by using Eqs. A-3 and A-13 and the fact that $R=r_1$, $S_w^*=0$, *at* $R=R$, $S_w^*=S_w^*$ and at $R=r_2$, $S_w^*=1$. Therefore Eq. A-12 becomes:

$$\frac{Q}{A}=\left[\frac{\Delta p}{L}\right]\phi^{*3}S_w^{*2}\frac{\gamma^2}{2\mu}\left[\frac{\beta}{n}\right]\int_0^{S_w^*}\frac{dS_w^*}{p_c^2} \qquad \text{(A-14)}$$

With Darcy's law for flow of water

$$\frac{Q}{A}=\frac{k_{rw}k}{\mu}\left[\frac{\Delta p}{L}\right] \qquad \text{(A-15)}$$

Substitute Eq. A-15 into Eq. A-14, we obtain:

$$k_{rw}k=\phi^{*3}S_w^{*2}\frac{\gamma^2}{2\mu}\left[\frac{\beta}{n}\right]\int_0^{S_w^*}\frac{dS_w^*}{p_c^2} \qquad \text{(A-16)}$$

But $k_{rw}=1$ when $S_w^*=1$; so,

$$k=\phi^{*3}\frac{\gamma^2}{2}\frac{\beta}{n}\int_0^1\frac{dS_w^*}{p_c^2} \qquad \text{(A-17)}$$

Converting Eq. A-17 in field units gives:

$$k(md)\left[9.869\times10^{-12}\ \frac{cm^2}{md}\right]=\phi^{*3}\frac{\beta}{n}\frac{\gamma^2}{2}\left[\frac{dyne}{cm}\right]^2\int_0^1\frac{1}{p_c^2(psia^2)\left[6.8947\times10^4\ \frac{dyne/cm^2}{psia}\right]^2}dS_w^*$$

$$k(md)=\left[\frac{1md}{9.869\times10^{-12}\ \frac{cm^2}{md}}\right]\left[\frac{psi}{6.8947\times10^4\ \frac{dyne}{cm^2}}\right]^2\phi^{*3}\frac{\beta}{n}\frac{\gamma^2}{2}\left[\frac{dyne}{cm}\right]^2\int_0^1\frac{1}{p_c^2(psia^2)}dS_w^*$$

$$k(md) = 10.66\left[\frac{md\ psia^2}{\frac{dyne}{cm^2}}\right]\phi^{*3}\,\frac{\beta}{n}\gamma^2\left[\frac{dyne}{cm}\right]^2\int_0^1 \frac{1}{p_c^2\,(psia^2)}\,dS_w^*$$

$$k = 10.66\phi^{*3}\,\frac{\beta}{n}\gamma^2\int_0^1 \frac{1}{p_c^2}\,dS_w^* \qquad \text{(A-18)}$$

At this point, k is in md and p_c in psia. Isolating the integral in Eq. A-18 we have:

$$I = \int_0^1 \frac{1}{p_c^2}\,dS_w^* \qquad \text{(A-19)}$$

Brook and Corey[A-2] define the following capillary pressure model:

$$p_c = p_d S_w^{*-1/\lambda} \qquad \text{(A-20)}$$

Substituting Eq. A-20 into Eq. A-19 gives

$$I = \frac{1}{p_d^2}\int_0^1 S_w^{*2/\lambda}\,dS_w^*$$

$$I = \frac{1}{p_d^2}\,\frac{1}{1+2/\lambda}\,S_w^{*(1+2/\lambda)}\Big|_0^1$$

then,

$$I = \frac{1}{p_d^2}\left[\frac{\lambda}{\lambda+2}\right] \qquad \text{(A-21)}$$

Substituting Eq. (A-21) into Eq. (A-18)

$$k = 10.66\phi^{*3}\,\frac{\beta}{n}\gamma^2\,\frac{1}{p_d^2}\left[\frac{\lambda}{\lambda+2}\right] \qquad \text{(A-22)}$$

<u>Relative Permeability Correlation</u>

From Nakornthap and Evans,[A-3] the wetting and non-wetting phase relative permeability functions are given as:

$$k_{rw} = k_{rw}^o S_w^{*(3+2/\lambda)} \qquad \text{(A-23)}$$

and

$$k_{rn} = k_{rn}^o (1-S_w^*)^2\left[1 - S_w^{*(1+2/\lambda)}\right] \qquad \text{(A-24)}$$

Rearranging Eq. B-23 and B-24 we have:

$$\frac{k_{rw}}{k_{rw}^{o}}\frac{1}{S_w^{*(3+2/\lambda)}}\equiv 1 \qquad \text{(A-25)}$$

and

$$\frac{k_{rn}}{k_{rn}^{o}}\frac{1}{(1-S_w^*)^2\left[1-S_w^{*(1+2/\lambda)}\right]}\equiv 1 \qquad \text{(A-26)}$$

Setting the equality in the Eq. A-25 for two separate conditions, we have:

$$\frac{k_{rw_1}}{k_{rw_1}^{o}}\frac{1}{S_{w_1}^{*\ (3+2/\lambda_1)}}=\frac{k_{rw_2}}{k_{rw_2}^{o}}\frac{1}{S_{w_2}^{*\ (3+2/\lambda_2)}} \qquad \text{(A-27)}$$

Solving for k_{rw_2} we obtain:

$$k_{rw2}=\frac{k_{rw2}^{o}}{k_{rw1}^{o}}\frac{S_{w2}^{*\ (3+2/\lambda_2)}}{S_{w1}^{*\ (3+2/\lambda_1)}}k_{rw1} \qquad \text{(A-28)}$$

Setting the equality in Eq. A-26 for two separate conditions gives

$$\frac{k_{rn_1}}{k_{rn1}^{o}}\frac{1}{(1-S_w^*)^2\left[1-S_w^{*(1+2/\lambda_1)}\right]}=\frac{k_{rn_2}}{k_{rn2}^{o}}\frac{1}{(1-S_w^*)^2\left[1-S_w^{*(1+2/\lambda_2)}\right]} \qquad \text{(A-29)}$$

Solving for k_{rn_2}

$$k_{rn_2}=\frac{k_{rn2}^{o}}{k_{rn1}^{o}}\frac{(1-S_w^*)^2\left[1-S_w^{*(1+2/\lambda_2)}\right]}{(1-S_w^*)^2\left[1-S_w^{*(1+2/\lambda_1)}\right]}k_{rn_1} \qquad \text{(A-30)}$$

For completeness, we should substitute Eq. A-2 into A-28 and A-30 — this gives:

$$k_{rw2}=\frac{k_{rw2}^{o}}{k_{rw1}^{o}}\frac{\left[\dfrac{S_{w2}-S_{wi2}}{1-S_{wi2}}\right]^{(3+2/\lambda_2)}}{\left[\dfrac{S_{w1}-S_{wi1}}{1-S_{wi1}}\right]^{(3+2/\lambda_1)}}k_{rw1} \qquad \text{(A-31)}$$

$$k_{rn_2} = \frac{k^o_{rn2}}{k^o_{rn1}} \frac{\left[1-\left[\frac{S_{w_2}-S_{wi_2}}{1-S_{wi_2}}\right]\right]^2 \left[1-\left[\frac{S_{w_2}-S_{wi_2}}{1-S_{wi_2}}\right]^{(1+2/\lambda_2)}\right]}{\left[1-\left[\frac{S_{w_1}-S_{wi_1}}{1-S_{wi_1}}\right]\right]^2 \left[1-\left[\frac{S_{w_1}-S_{wi_1}}{1-S_{wi_1}}\right]^{(1+2/\lambda_1)}\right]} k_{rn_1} \quad \text{(A-32)}$$

References

A.1. Wyllie, M.R.J., and Gardner, G.H.F.: "The Generalized Kozeny–Carman Equation: Part II," *World Oil*, (1958), 146(5): 210–228.

A.2. Brooks, R.H., and Corey A.T.: "Hydraulic Properties of Porous Media," Hydrol. Paper 3, Colo. State Univ., Fort Collins, CO, 1964.

A.3. Nakornthap, K. and Evans, R.D.: "Temperature-Dependent Relative Permeability and Its Effect on Oil Permeability and Its Effect on Oil Displacement by Thermal Methods," SPE 11217 *SPERE* (1986)

Nomenclature

k	=	permeability, md
k_{rw}	=	relative permeability to wetting phase, fraction
k_{rnw}	=	relative permeability to non-wetting phase, fraction
n	=	geometrical constant in the model porous medium
p_d	=	displacement pressure, psia
p_c	=	capillary pressure, psia
q	=	volume flowrate in single capillary, B/D
Q	=	flowrate, B/D
r	=	pore radius, in
$\bar{r}$	=	radius of an equivalent pore in the modifier porous medium, in
R	=	arbitrary radius, in
S_{wi}	=	irreducible saturation, fraction
S_w	=	water saturation in the actual porous medium, fraction
S_w^*	=	water saturation in the model porous medium, fraction
$\alpha(r)$	=	distribution function governing capillary radii
β	=	geometrical factor in the model porous medium
γ	=	interfacial tension, dynes/cm
θ	=	contact angle, degrees
λ	=	pore geometric factor (or index of pore-size distribution)

APPENDIX B
DERIVATION OF A FUNCTION FOR THE NORMALIZATION OF CAPILLARY PRESSURE CURVES

Introduction

Capillary pressure curves are usually determined in the laboratory by three methods — mercury injection, restored state cell (porous plate) and centrifuge. Reservoir calculations require a normalized curve for the capillary pressure measurements which are obtained from several plug samples. Because of reservoir heterogeneity, no single capillary pressure curve can be used for the entire reservoir. Several attempts have been made to correlate to correlate capillary pressure curves with the petrophysical properties of the reservoir rock. Leverett[B-1] was the first to introduce a dimensionless capillary pressure correlation function. This function accounts for change of permeability, porosity and wettability of the reservoir as long as the general pore geometry remains constant. However, this function correlated to a formation fails to correlate capillary pressure data of another formation.

An improvement of a J-Function is derived in this Appendix.

Derivation of a Normalized capillary pressure function

The Burdine[B-2] relation is derived from a bundle of capillary tubes model and is given by:

$$k = 10.66\phi^3 (1 - S_{wi})^3 \frac{\beta}{n} \gamma^2 \int_0^1 \frac{1}{p_c^2} dS_w^* \quad \text{(B-1)}$$

The Brooks and Corey[B-3] model for capillary pressure is

$$p_c = p_d S_w^{*-1/\lambda} \quad \text{(B-2)}$$

Substituting Eq. B-2 into Eq. B-1 gives:

$$k = 10.66\phi^3 (1 - S_{wi})^3 \frac{\beta}{n} \gamma^2 \frac{1}{p_d^2} \left[\frac{\lambda}{\lambda + 2}\right] \quad \text{(B-3)}$$

A correlation function for the *β/n* term has recently been proposed (ref. B-3). This relation is given by:

$$\frac{\beta}{n} = \alpha \frac{(1 - S_{wi})}{\phi} \quad \text{(B-4)}$$

where α is an empirical adjustment constant. Substituting Eq. B-4 in B-3 gives:

$$k = 10.66\alpha(\gamma_{ab})^2 (1 - S_{wi})^4 \phi^2 \frac{1}{(p_d)^2} \left[\frac{\lambda}{\lambda + 2}\right] \quad \text{(B-5)}$$

Solving Eq. B-5 for the displacement pressure, p_d, gives:

$$p_d = \sqrt{10.66}\sqrt{\alpha}(1-S_{wi})^2 \frac{\phi\gamma}{\sqrt{k}}\sqrt{\frac{\lambda}{\lambda+2}} \quad \text{(B-6)}$$

Eq. B-6 is a "semi-analytical" expression for relating the displacement pressure to formation properties. By equating Eq. B-6 for two separate flow conditions yields:

$$\frac{p_{d_1}}{p_{d_2}} = \frac{\sqrt{\alpha_1}}{\sqrt{\alpha_2}} \frac{(1-S_{wi,1})^2}{(1-S_{wi,2})^2} \frac{\dfrac{\phi_1\gamma}{\sqrt{k_1}}}{\dfrac{\phi_2\gamma}{\sqrt{k_2}}} \frac{\sqrt{\dfrac{\lambda_1}{\lambda_1+2}}}{\sqrt{\dfrac{\lambda_2}{\lambda_2+2}}} \quad \text{(B-7)}$$

or

$$p_{d_1} = \frac{\sqrt{\alpha_1}}{\sqrt{\alpha_2}} \frac{(1-S_{wi,1})^2}{(1-S_{wi,2})^2} \frac{\phi_1\gamma_1\sqrt{k_2}}{\phi_2\gamma_2\sqrt{k_1}} \frac{\sqrt{\lambda_1(\lambda_2+2)}}{\sqrt{\lambda_2(\lambda_1+2)}} p_{d_2} \quad \text{(B-8)}$$

From Eq. B-7, we can intuitively suggest that:

$$\frac{p_{d_1}}{p_{d_2}} \approx \frac{p_{c_1}}{p_{c_2}} \quad \text{or} \quad p_{c_2} = \frac{p_{d_2}}{p_{d_1}} p_{c_1} \quad \text{(B-9)}$$

So by analogy with Eq. B-8, we have

$$p_{c_2} = \sqrt{\frac{\alpha_2}{\alpha_1}} \frac{(1-S_{wi,2})^2}{(1-S_{wi,1})^2} \frac{\phi_2\gamma_2}{\phi_1\gamma_1} \sqrt{\frac{k_1}{k_2}} \frac{\sqrt{\lambda_2(\lambda_1+2)}}{\sqrt{\lambda_1(\lambda_2+2)}} p_{c_1} \quad \text{(B-10)}$$

Eq. B-10 could be used to "convert" laboratory-derived data into data at reservoir conditions. This concept is similar to the Leverett "J-Function" which is given by:

$$J_L(S_w) = \frac{1}{\gamma}\sqrt{\frac{k}{\phi}} p_c \quad \text{(B-11)}$$

Assuming that $J_{L,1}(S_w) = J_{L,2}(S_w)$ we have:

$$p_{c_2} = \frac{\gamma_2}{\gamma_1}\sqrt{\frac{k_1}{k_2}\frac{\phi_2}{\phi_1}} p_{c_1} \quad \text{(B-12)}$$

We note that Eq. B-12 is the "standard" application of the Leverett *J*-Function. Both Eqs. B-10 and B-12 "rescale" capillary pressure data in the sense that if we assume that the data have the same character (*i.e.*, shape) then these concepts should suffice. However, we immediately recognize from Eq. B-2 that capillary pressure data will not, as a general behavior, exhibit the same shape.

This forces us to pursue the concept of a "universal" capillary pressure curve — as Leverett[B-1] believed he had established using his *J*-Function. Unfortunately, we cannot establish a "universal" trend, but we can develop an equality condition using the Brooks and Corey capillary pressure relation. Recalling Eq. B-2, we have:

$$p_c = p_d S_w^{*-1/\lambda} \qquad \text{(B-2)}$$

Setting Eq. B-2 as an equality (*i.e.*, $p_c \,/\, p_d S_w^{*1/\lambda} \equiv 1$)

$$\frac{p_{c_1}}{p_{d_1}} S_w^{*1/\lambda_1} = \frac{p_{c_2}}{p_{d_2}} S_w^{*1/\lambda_2} \qquad \text{(B-13)}$$

or, solving for p_{c_2}, we have:

$$p_{c_2} = \frac{p_{d_2}}{p_{d_1}} \frac{S_w^{*1/\lambda_1}}{S_w^{*1/\lambda_2}} p_{c_1} \qquad \text{(B-14)}$$

Recalling the definition of the "effective" saturation function, S_w^*, we have

$$S_w^* = \frac{S_w - S_{wi}}{1 - S_{wi}} \qquad \text{(B-15)}$$

Substituting Eq. B-15 into Eq. B-14 we have:

$$p_{c_2} = \frac{p_{d_2}}{p_{d_1}} \frac{\left[\dfrac{S_w - S_{wi,1}}{1 - S_{wi,1}}\right]^{1/\lambda_1}}{\left[\dfrac{S_w - S_{wi,2}}{1 - S_{wi,2}}\right]^{1/\lambda_2}} p_{c_1} \qquad \text{(B-16)}$$

Substituting Eq. B-7 into Eq. B-16 we have:

$$p_{c_2} = \sqrt{\frac{\alpha_2}{\alpha_1}} \frac{(1 - S_{wi,2})^2}{(1 - S_{wi,1})^2} \frac{\phi_2 \gamma_2}{\phi_1 \gamma_1} \sqrt{\frac{k_1}{k_2}} \frac{\sqrt{\lambda_2 (\lambda_1 + 2)}}{\sqrt{\lambda_1 (\lambda_2 + 2)}} \frac{\left[\dfrac{S_w - S_{wi,1}}{1 - S_{wi,1}}\right]^{1/\lambda_1}}{\left[\dfrac{S_w - S_{wi,2}}{1 - S_{wi,2}}\right]^{1/\lambda_2}} p_{c_1} \qquad \text{(B-17)}$$

Recall that α_1 and $\alpha_2 \approx 1$; so without any additional information we can assume that $\sqrt{\alpha_1/\alpha_2} \approx 1$. This assumptions leads to our final form:

$$p_{c_2} = \frac{(1-S_{wi,2})^2}{(1-S_{wi,1})^2}\frac{\phi_2\gamma_2}{\phi_1\gamma_1}\sqrt{\frac{k_1}{k_2}}\frac{\sqrt{\lambda_2(\lambda_1+2)}}{\sqrt{\lambda_1(\lambda_2+2)}}\frac{\left[\dfrac{S_w-S_{wi,1}}{1-S_{wi,1}}\right]^{1/\lambda_1}}{\left[\dfrac{S_w-S_{wi,2}}{1-S_{wi,2}}\right]^{1/\lambda_2}}p_{c_1} \quad \text{(B-18)}$$

References

B.1. Leverett, M.C.: "Capillary Behavior in Porous Solids," *Trans*, AIME **142**, (1941) 152.

B.2. Burdine, N. T.: "Relative Permeability Calculations from Pore Size Distribution Data", *Trans*. AIME **198**, (1953) 71.

B.3. Ali, L., personal communication with T. Blasingame (1995).

B.4. Brooks, R.H., and Corey A.T.: "Hydraulic Properties of Porous Media," Hydrol. Paper 3, Colo. State Univ., Fort Collins, CO, 1964.

Nomenclature

k	=	permeability, md
n	=	geometrical constant in the model porous medium
$J_L(S_w)$	=	Leverett J-Function, dimensionless
p_d	=	displacement pressure, psi
p_c	=	capillary pressure, psi
S_{wi}	=	irreducible saturation, fraction
S_w	=	water saturation in the actual porous medium, fraction
S_w^*	=	water saturation in the model porous medium, fraction
α	=	empirical adjustment constant
β	=	geometrical factor in the model porous medium
γ	=	interfacial tension, dynes/cm
θ	=	contact angle, degrees
λ	=	index of pore-size distribution
ϕ	=	porosity

APPENDIX C

COMPARISON WITH TIMUR'S PERMEABILITY MODEL

Timur[C.1] proposed a generalized equation for permeability as follows:

$$k_{Timur} = A\frac{\phi^B}{S_{wi}^C} \quad \text{(C.1)}$$

where: (*A, B, C* are generalized constants)

k_{Timur} = Timur correlation for permeability, md
ϕ = porosity, fraction of pore volume
S_{wi} = irreducible wetting phase saturation, fraction of pore volume

Eq. C.1 can be evaluated in terms of the statistically determined parameters *A*, *B*, and *C*. Timur applied a reduced major axis method of regression analysis to data obtained by laboratory measurements conducted on 155 sandstone samples from three different oil fields from North America. Based both on the highest correlation coefficient and on the lowest standard deviation, Timur chose the following result for permeability.

$$k_{Timur} = 0.136\frac{\phi^{4.4}}{S_{wi}^2} \quad \text{(C.2)}$$

Our approach to the derivation of Timur's base relation (Eq. C.1) is to note that, in a general form, Timur's base relation can be written as:

$$k_{Timur} = \alpha\phi^{\beta}S_{wi}^{\chi} \quad \text{(C.3)}$$

where α, β, χ are generalized constants. Our goal in this particular proof is to provide a specific combination of relations that, upon combination, yield the form given by Eq. C.3 (or at least a result that is an essentially identical form).

The model based model for permeability for this work is given in the form of a generalized correlation as:

$$k = a_1\frac{1}{(p_d)^{a_2}}\left[\frac{\lambda}{\lambda+2}\right]^{a_3}(1-S_{wi})^{a_4}\,\phi^{a_5} \quad \text{(C.4)}$$

Clearly, Eq. C.4 is almost in the "Timur" form in terms of the porosity (ϕ) and irreducible wetting phase saturation (S_{wi}) — however, we note that because we use (1-S_{wi}), then our final model written in the "Timur" form should be:

$$k_{Timur} = \alpha \phi^{\beta} (1-S_{wi})^{\delta} \quad \text{(C.5)}$$

For simplicity, we will use a form of Eq. C.4 that is written in terms of λ, rather than $\lambda/(\lambda+2)$. This modification will not seriously affect the character of the correlation given by Eq. C.4, and will provide the algebraic form that should mimic our rendering of the Timur correlation (*i.e.*, Eq. C5).

The "modified" formulation of Eq. C.4 (*i.e.*, the permeability correlation) is given as:

$$k = a_1 (p_d)^{a2} \lambda^{a3} (1-S_{wi})^{a4} \phi^{a5} \quad \text{(C.6)}$$

As discussed in the body of this work, the generalized correlation proposed for the capillary displacement pressure (p_d) is given by:

$$p_d = b_1 \phi^{b_2} k^{b_3} (1-S_{wi})^{b_4} \quad \text{(C.7)}$$

Lastly, the index of pore-size distribution (λ) is represented by the following generalized correlation as:

$$\lambda = c_1 \phi^{c_2} k^{c_3} (1-S_{wi})^{c_4} p_d^{c_5} \quad \text{(C.8)}$$

We first need to substitute Eq. C.7 into Eq. C.82 and reduce Eq. C.8 into a form that only contains ϕ, k, and S_{wi}. Making this substitution yields:

$$\begin{aligned}
\lambda &= c_1 \phi^{c_2} k^{c_3} (1-S_{wi})^{c_4} p_d^{c_5} \\
&= c_1 \phi^{c_2} k^{c_3} (1-S_{wi})^{c_4} \left[b_1 \phi^{b_2} k^{b_3} (1-S_{wi})^{b_4} \right]^{c_5} \\
&= c_1 \phi^{c_2} k^{c_3} (1-S_{wi})^{c_4} \left[b_1{}^{c_5} \phi^{b_2 c_5} k^{b_3 c_5} (1-S_{wi})^{b_4 c_5} \right] \\
&= (c_1 b_1{}^{c_5})\, k^{(c_3+b_3 c_5)}\, \phi^{(c_2+b_2 c_5)}\, (1-S_{wi})^{(c_4+b_4 c_5)}
\end{aligned} \quad \text{(C.9)}$$

We now substitute Eq. C.7 into Eq. C.6 to reduce Eq. C.6 into a form that only contains ϕ, k, S_{wi}, and λ. This substitution gives us:

$$\begin{aligned}
k &= a_1 (p_d)^{a_2} \lambda^{a_3} (1-S_{wi})^{a_4} \phi^{a_5} \\
&= a_1 \left[b_1 \phi^{b_2} k^{b_3} (1-S_{wi})^{b_4} \right]^{a_2} \lambda^{a_3} (1-S_{wi})^{a_4} \phi^{a_5} \\
&= a_1 \left[b_1{}^{a_2} \phi^{a_2 b_2} k^{a_2 b_3} (1-S_{wi})^{a_2 b_4} \right] \lambda^{a_3} (1-S_{wi})^{a_4} \phi^{a_5} \\
&= (a_1 b_1{}^{a_2})\, k^{a_2 b_3}\, \phi^{(a_5+a_2 b_2)}\, (1-S_{wi})^{(a_4+a_2 b_4)}\, \lambda^{a_3}
\end{aligned} \quad \text{(C.10)}$$

As an intermediate result, we raise Eq. (C.9) (λ) to the power of a_3, which yields:

$$\lambda^{a_3} = \left[(c_1 b_1{}^{c_5})\, k^{(c_3+b_3c_5)}\, \phi^{(c_2+b_2c_5)}\, (1-S_{wi})^{(c_4+b_4c_5)} \right]^{a_3}$$
$$= (c_1{}^{a_3} b_1{}^{c_5 a_3})\, k^{(c_3+b_3c_5)a_3}$$
$$\times\ \phi^{(c_2+b_2c_5)a_3}\, (1-S_{wi})^{(c_4+b_4c_5)a_3}$$
$$= (c_1{}^{a_3} b_1{}^{c_5 a_3})\, k^{(a_3c_3+a_3b_3c_5)}$$
$$\times\ \phi^{(a_3c_2+a_3b_2c_5)}\, (1-S_{wi})^{(a_3c_4+a_3b_4c_5)}$$

$$\lambda^{a_3} = (c_1{}^{a_3} b_1{}^{c_5 a_3})\, k^{(a_3c_3+a_3b_3c_5)}$$
$$\times\ \phi^{(a_3c_2+a_3b_2c_5)}\, (1-S_{wi})^{(a_3c_4+a_3b_4c_5)}$$

We now substitute the previous result into Eq. (C.10) which gives us the "composite equation", which is defined as:

$$k = (a_1 b_1{}^{a_2})\, k^{a_2b_3}\, \phi^{(a_5+a_2b_2)}\, (1-S_{wi})^{(a_4+a_2b_4)}\, \lambda^{a_3}$$
$$= (a_1 b_1{}^{a_2})\, k^{a_2b_3}\, \phi^{(a_5+a_2b_2)}\, (1-S_{wi})^{(a_4+a_2b_4)}$$
$$\times\ (c_1{}^{a_3} b_1{}^{a_3c_5})\, k^{(a_3c_3+a_3b_3c_5)}$$
$$\times\ \phi^{(a_3c_2+a_3b_2c_5)}\, (1-S_{wi})^{(a_3c_4+a_3b_4c_5)}$$
$$= \left[k^{a_2b_3}\, k^{(a_3c_3+a_3b_3c_5)} \right]$$
$$\times\ \left[(a_1 b_1{}^{a_2})(c_1{}^{a_3} b_1{}^{a_3c_5}) \right]$$
$$\times\ \left[\phi^{(a_5+a_2b_2)}\, \phi^{(a_3c_2+a_3b_2c_5)} \right]$$
$$\times\ \left[(1-S_{wi})^{(a_4+a_2b_4)}\, (1-S_{wi})^{(a_3c_4+a_3b_4c_5)} \right]$$
$$= \left[k^{(a_2b_3+a_3c_3+a_3b_3c_5)} \right]$$
$$\times\ \left[a_1 b_1{}^{a_2+a_3c_5}\, c_1{}^{a_3} \right]$$
$$\times\ \left[\phi^{(a_2b_2+a_3b_2c_5+a_3c_2+a_5)} \right]$$
$$\times\ \left[(1-S_{wi})^{(a_2b_4+a_3c_4+a_3b_4c_5+a_4)} \right]$$

where this form reduces to:

$$k^{1\text{-}(a_2b_3+a_3c_3+a_3b_3c_5)} = \left[a_1 b_1{}^{a_2+a_3c_5}\, c_1{}^{a_3} \right]$$
$$\times\ \left[\phi^{(a_2b_2+a_3b_2c_5+a_3c_2+a_5)} \right]$$
$$\times\ \left[(1-S_{wi})^{(a_2b_4+a_3c_4+a_3b_4c_5+a_4)} \right]$$

Or, solving for *k*, we have

$$k = \left[a_1 b_1{}^{a_2+a_3c_5} c_1{}^{a_3}\right]^{\frac{1}{1-(a_2b_3+a_3c_3+a_3b_3c_5)}}$$

$$\times\ \phi^{\frac{(a_2b_4+a_3c_4+a_3b_4c_5+a_4)}{1-(a_2b_3+a_3c_3+a_3b_3c_5)}}$$

$$\times\ (1-S_{wi})^{\frac{(a_2b_4+a_3c_4+a_3b_4c_5+a_4)}{1-(a_2b_3+a_3c_3+a_3b_3c_5)}}$$

Upon final reduction, we obtain:

$$k = \alpha\phi^{\beta}(1-S_{wi})^{\delta} \quad \text{(C.11)}$$

where:

$$\alpha = \left[a_1 b_1{}^{a_2+a_3c_5} c_1{}^{a_3}\right]^{\frac{1}{1-(a_2b_3+a_3c_3+a_3b_3c_5)}} \quad \text{(C.12)}$$

$$\beta = \frac{(a_2b_4+a_3c_4+a_3b_4c_5+a_4)}{1-(a_2b_3+a_3c_3+a_3b_3c_5)} \quad \text{(C.13)}$$

$$\delta = \frac{(a_2b_4+a_3c_4+a_3b_4c_5+a_4)}{1-(a_2b_3+a_3c_3+a_3b_3c_5)} \quad \text{(C.14)}$$

In this work we have tuned Eqs. C.6, C.7, C.8, and C.11 to our database, and the results of this tuning exercise yields:

$$k = 385008.942\frac{1}{(p_d)^{1.8284}}\lambda^{1.0262}(1-S_{wi})^{2.3490}\phi^{1.8727} \quad \text{(C.15)}$$

$$p_d = 751.3360\phi^{0.8469}\,k^{-0.5166}\,(1-S_{wi})^{0.0489} \quad \text{(C.16)}$$

$$\lambda = 0.00084\phi^{-1.0485}\,k^{0.5498}\,(1-S_{wi})^{-2.2790}\,p_d^{0.9939} \quad \text{(C.17)}$$

$$k = 566169.5767\,\phi^{1.5869}(1-S_{wi})^{-6.1696} \quad \text{(C.18)}$$

Eqs. C.15-C.17 are combined as prescribed by Eqs. C.12 through C.14, and the results are plotted with the tuned Timur relation (Eq. C.18) in **Fig. C.1**. We note good agreement — the points are identical, indicating that our algebraic exercise is correct.

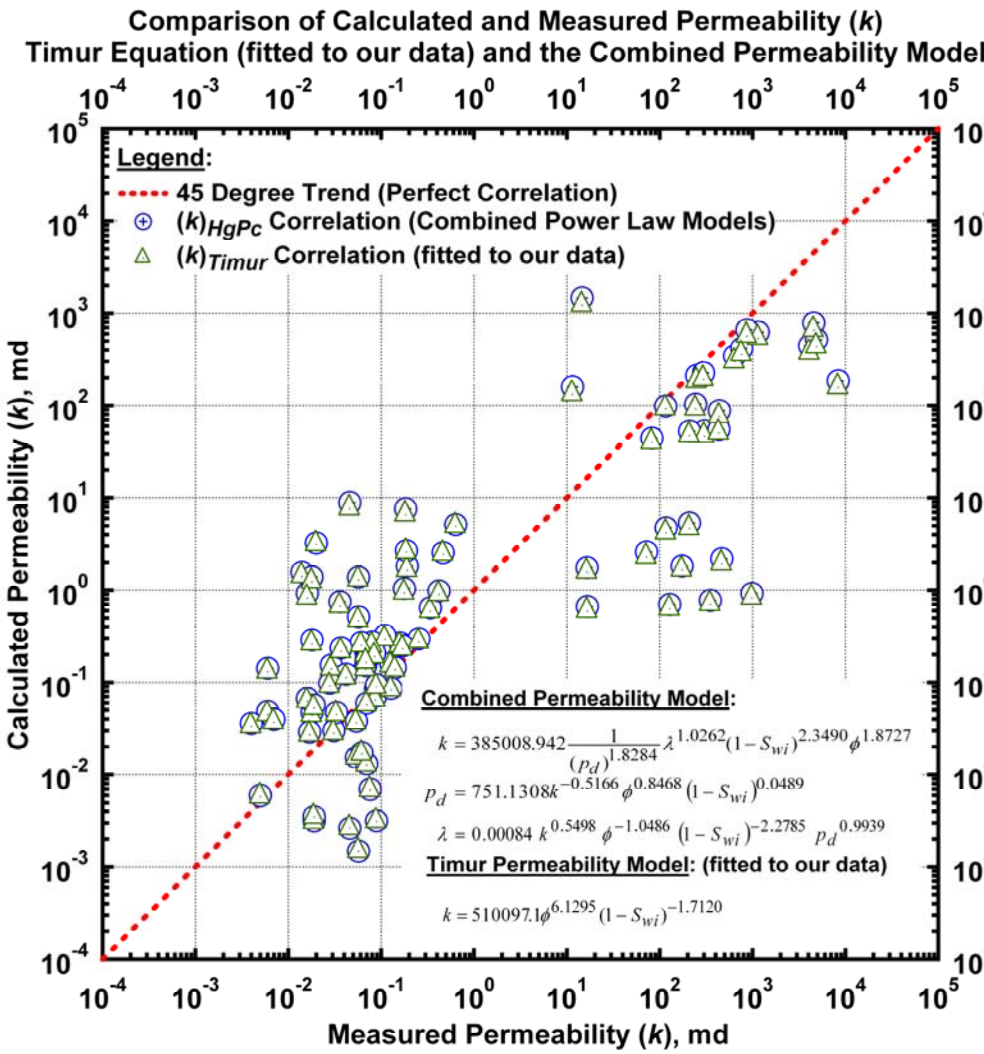

Figure C.1 – Comparison of tuned Timur relation (Eq. C.1) to the combination solution (Eqs. C.7 to C.10) for the data set used in this work.

This exercise proves that the Timur formulation can be derived from a fundamental formulation, albeit the relation must be tuned to a particular dataset.

References

C.1. Timur, A.: "An Investigation of Permeability, Porosity, and Residual Water Saturation Relationships for Sandstone Reservoirs," *The Log Analyst* , Vol. 9, No. 4, 8-17..

Nomenclature

k	=	permeability, md
p_d	=	displacement pressure, psi
p_c	=	capillary pressure, psi
S_{wi}	=	irreducible saturation, fraction
S_w	=	water saturation in the actual porous medium, fraction
λ	=	index of pore-size distribution
ϕ	=	porosity

APPENDIX D

SUMMARY OF DATA USED IN THIS STUDY

Table D.1 – Summary of data used in this study

No.	Reservoir Name	Input Data ϕ (fraction)	k (md)	p_d, S_{wi} and λ Calibration Results S_{wi} (fraction)	p_d (psia))	λ (dim-less)
1	2-40 HS1	0.076	0.087	0.130	400.00	2.100
2	2-41 HS1	0.084	0.127	0.107	380.00	2.250
3	2-42 HS1	0.077	0.090	0.100	390.00	2.100
4	3-01 HS1	0.092	0.159	0.095	290.00	1.500
5	3-03 HS1	0.090	0.068	0.035	460.00	1.300
6	3-19 HS1	0.094	0.255	0.090	260.00	1.800
7	3-24 HS1	0.091	0.171	0.090	300.00	1.750
8	4-02 HS1	0.083	0.142	0.110	320.00	1.800
9	4-11 HS1	0.166	0.166	0.065	300.00	1.600
10	4-15 HS1	0.072	0.031	0.110	320.00	2.000
11	6-02 HS1	0.083	0.041	0.050	400.00	0.750
12	6-06 HS1	0.075	0.016	0.030	400.00	0.800
13	6-21 HS1	0.096	0.110	0.030	340.00	1.120
14	6-25 HS1	0.095	0.080	0.010	440.00	1.250
15	6-32 HS1	0.071	0.018	0.010	640.00	0.950
16	6-34 HS1	0.086	0.029	0.010	600.00	1.050
17	6-36 HS1	0.066	0.031	0.020	430.00	1.000
18	6-42 HS1	0.086	0.068	0.010	425.00	1.250
19	7-03 HS1	0.069	0.007	0.010	1250.00	1.220
20	7-08 HS1	0.066	0.017	0.010	640.00	1.064
21	7-16 HS2	0.071	0.006	0.010	1500.00	1.250
22	Archie1B	0.220	116.0	0.350	18.00	2.000
23	Archie1J	0.371	14.6	0.100	53.00	0.778
24	Archie1K	0.265	11.5	0.012	70.00	1.121
25	FAC1_17152	0.287	640.0	0.170	10.00	3.000
26	FAC1_17160	0.316	1150.0	0.170	10.00	3.000
27	FAC2_17066	0.320	868.0	0.160	10.00	2.150
28	FAC2_17077	0.309	4110.0	0.060	5.50	2.000
29	FAC2_17136	0.266	250.0	0.160	17.00	1.100
30	FAC2_17142	0.272	296.0	0.120	14.00	1.014
31	FAC2_17171	0.297	764.0	0.160	10.00	1.800
32	FAC2_17174	0.335	4570.0	0.100	6.00	2.100
33	FAC6_17147	0.313	4890.0	0.100	5.00	1.700
34	No21-6 2-01	0.046	0.019	0.030	450.00	1.150
35	No21-6 2-02	0.046	0.019	0.100	500.00	1.300
36	No21-6 2-06	0.106	0.339	0.095	205.00	1.350
37	No21-6 2-07	0.114	0.420	0.092	190.00	1.320
38	No21-6 2-09	0.092	0.061	0.110	435.00	1.200
39	No21-6 2-10	0.067	0.054	0.120	490.00	2.300
40	No30-4 3-01	0.051	0.076	0.100	190.00	1.000
41	No30-4 3-02	0.056	0.054	0.180	320.00	1.600
42	No30-4 3-03	0.071	0.070	0.150	330.00	1.450
43	No30-4 3-04	0.075	0.128	0.170	220.00	1.200
44	No30-4 3-06	0.077	0.089	0.110	380.00	1.800
45	No30-4 3-07	0.089	0.085	0.060	390.00	1.300
46	No30-4 3-08	0.088	0.069	0.040	330.00	0.850
47	No30-4 3-1	0.116	0.178	0.037	250.00	0.850
48	No30-4 3-11	0.127	0.191	0.065	290.00	1.000
49	No31-2 4-1					1.500
		0.056	0.070	0.110	290.00	

Table D.1 – Summary of data used in this study

		Input Data		p_d, S_{wi} and λ Calibration Results		
No.	Reservoir Name	ϕ (fraction)	k (md)	S_{wi} (fraction)	p_d (psia))	λ (dim-less)
50	No31-2 4-3	0.103	0.057	0.070	375.00	0.750
51	No31-2 4-4	0.091	0.037	0.048	450.00	0.770
52	No31-2 4-6	0.069	0.033	0.100	530.00	1.350
53	No31-2 4-7	0.083	0.042	0.020	470.00	1.000
54	No4-2 1-1	0.039	0.057	0.110	275.00	2.000
55	No4-2 1-2	0.044	0.089	0.120	230.00	1.800
56	No4-2 1-4	0.043	0.046	0.130	360.00	1.900
57	No4-2 1-5	0.059	0.062	0.120	320.00	1.600
58	Off1 1-16 AH	0.235	438.0	0.100	12.00	1.500
59	Off1 2-11 AH	0.204	82.3	0.200	17.00	1.000
60	Off1 2-18 AH	0.234	244.0	0.200	15.00	2.200
61	Off1 3-05 AH	0.207	434.0	0.260	8.00	1.200
62	Off1 3-34 AH	0.214	303.0	0.140	11.00	1.600
63	Off1 3-62 AH	0.209	210.0	0.210	14.00	2.000
64	Off1 3-71 AH	0.265	8340.0	0.100	3.80	3.000
65	Qars3-13159	0.115	985.0	0.010	3.00	0.350
66	Qars3-13164	0.110	128.0	0.010	4.50	0.550
67	Qars3-13275	0.125	174.0	0.110	7.30	2.100
68	Qars3-13193.0	0.132	467.0	0.020	3.00	0.750
69	Qars3-13208	0.110	351.0	0.070	2.80	0.750
70	Qars5-13388.6	0.148	117.0	0.060	15.00	1.082
71	Qars5-13419.8	0.126	16.5	0.060	24.00	1.000
72	Qars5-13423.6	0.109	16.6	0.010	14.50	0.700
73	Qars5-13433.2	0.136	72.2	0.010	9.00	0.800
74	Qars5-13448	0.153	209.0	0.010	9.00	0.840
75	Stevens A1-R 13203	0.166	0.046	0.010	652.50	0.750
76	Stevens A1-R 13207.15	0.162	0.184	0.008	348.00	0.700
77	Stevens A1-R 13217.1	0.068	0.004	0.007	1450.00	0.590
78	Stevens A1-R 13221	0.095	0.018	0.020	942.50	0.600
79	Stevens A1-R 13226.05	0.085	0.006	0.008	1305.00	0.480
80	Stevens A1-R 13227.15	0.123	0.018	0.008	797.50	0.450
81	Stevens A1-R 13239	0.139	0.636	0.300	108.75	1.460
82	Stevens A1-R 13240.2	0.125	0.187	0.300	152.25	1.200
83	Stevens A1-R 13246	0.111	0.036	0.015	406.00	0.560
84	Stevens A1-R 13250	0.129	0.020	0.300	725.00	1.200
85	Stevens A1-R 13253	0.073	0.019	0.020	638.00	0.806
86	Stevens A1-R 13254	0.079	0.028	0.054	522.00	0.925
87	Stevens A1-R 13262	0.117	0.057	0.180	406.00	1.000
88	Stevens A1-R 13265.15	0.050	0.005	0.070	964.25	1.060
89	Stevens A1-R 13288	0.124	0.465	0.300	159.50	1.250

APPENDIX E
CORRELATIONS FOR PERMEABILITY (*k*) DERIVED FROM THE DATA IN THIS WORK

In this Appendix we present the correlations derived in this work which are based on given permeability and porosity data, as well as the results of the regression of the semi-analytical Brooks-Corey[E-1] capillary pressure model (recall that the regression of this model to data yields displacement (or threshold) pressure (p_d), irreducible wetting phase saturation (S_{wi}), and the "pore geometric factor" (or the "index of pore size distribution") (λ), where λ was introduced by Brooks and Corey [E-1]).

Model 1

The "base" permeability model is taken from our modification of the Nakornthap and Evans[E-2] extension of the Burdine-Purcell-Wyllie-Spangler permeability model derived for the model of a porous media based on a "bundle of capillary tubes." This model serves as a "proof-of-concept" for the bundle of capillary tubes types of models.

$$k = a_1 \frac{1}{(p_d)^{a_2}} \left[\frac{\lambda}{\lambda+2}\right]^{a_3} (1-S_{wi})^{a_4} \phi^{a_5} \quad \text{(E.1)}$$

Table E.1 – Regression Summary for Permeability — Model 1.

Optimized coefficients for k (*Eq.* E.1):

Coefficient	Optimized Value
a_1	1233562.51 md
a_2	-1.8139352
a_3	1.4385928
a_4	2.2764176
a_5	1.7296397

Statistical summary for k (*Eq.* E.1):

Statistical Variable	Value
Sum of Squared Residuals	2.3865 ln(md)^2
Variance	369278.5839 md^2
Standard Deviation	607.6830 md
Average Absolute Error	26.4580 percent

Substituting the coefficients from **Table E.1** into Eq. E.1, we have:

$$k = 123356.512 \frac{1}{(p_d)^{1.8139}} \left[\frac{\lambda}{\lambda+2}\right]^{1.4385} (1-S_{wi})^{2.2761} \phi^{1.7296} \quad \text{(E.2)}$$

The permeability correlation given by Eq. E-2 is illustrated in **Fig. E.1** — we note a very reasonable correlation of the calculated and measured data, which validates our concept of using a power law basis for representing permeability in terms of other the other intrinsic variables (*i.e.*, ϕ, p_d, S_{wi}, and λ).

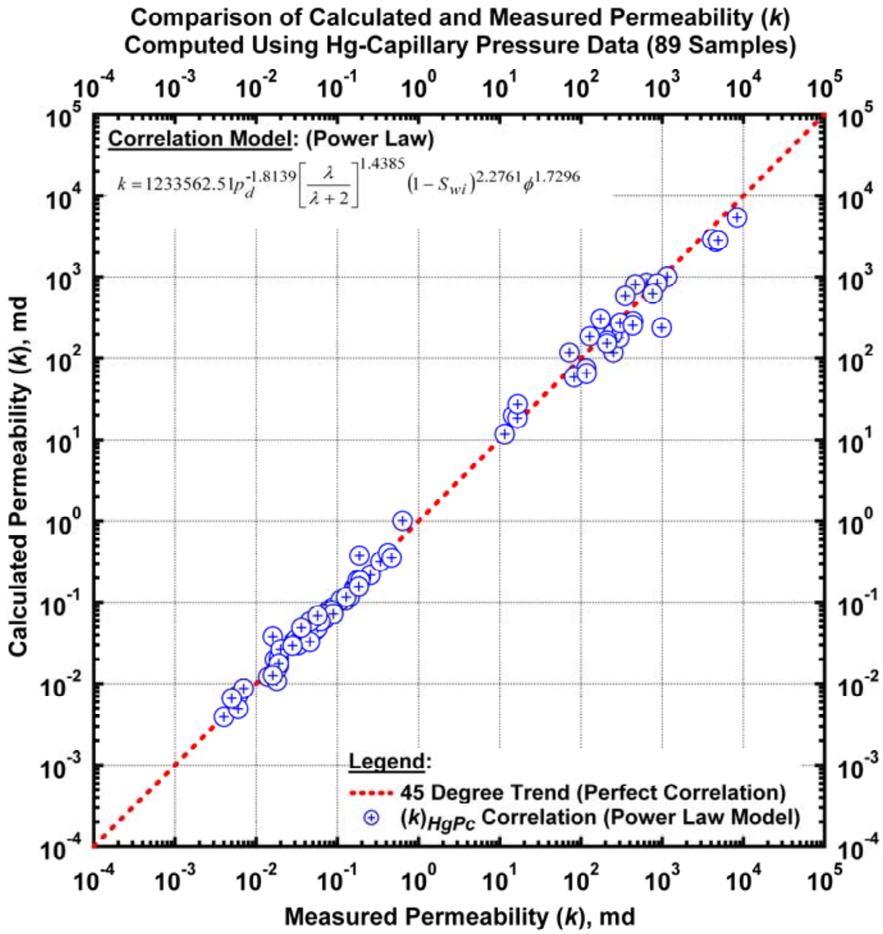

Figure E.1 – Permeability correlation based on mercury capillary pressure data (Eq. E.1 used for regression), *AAE* (average absolute error) = 26.46 percent).

Model 2

Model 2 is an extension of the base "power-law" model (Model 1) — this particular form is a "non-linear" power-law model (used by analogy with PVT correlations).

$$k = a_6\left[a_1 p_d{}^{a_2}\left[\frac{\lambda}{\lambda+2}\right]^{a_3}(1-S_{wi})^{a_4}\phi^{a_5}+a_7\right]^{a_8} \quad \text{(E.3)}$$

Table E.2 – Regression Summary for Permeability — Model 2.

Optimized coefficients for k (*Eq.* E.3):

Coefficient	Optimized Value
a_1	2590.43 md
a_2	-0.8567
a_3	0.7367
a_4	0.9960
a_5	0.8173
a_6	0.0610
a_7	0.1015
a_8	2.2135

Statistical summary for k (*Eq.* E.3):

Statistical Variable	Value
Sum of Squared Residuals	1.6592 $\ln(\text{md})^2$
Variance	593310.5224 md^2
Standard Deviation	770.2650 md
Average Absolute Error	22.8300 percent

Substituting the coefficients from **Table E.2** into Eq. E.3, we have:

$$k = 0.0610\left[2590.43\,p_d^{-0.8567}\left[\frac{\lambda}{\lambda+2}\right]^{0.7367}(1-S_{wi})^{0.9960}\,\phi^{0.8173} + 0.1015\right]^{2.2135} \quad \text{......................(E.4)}$$

The permeability correlation given by Eq. E-4 is illustrated in **Fig. E.2** — we note a very reasonable correlation of the calculated and measured data. We note that Model 2 provides more statistical accuracy than Model 1, but this form requires 3 more model parameters.

<u>Model 3</u>

This model is the exponential form of the power-law model. This is a mathematical equivalent of Model 1. This is an intermediate model which allows us to compare the more complex models of this same type which follow.

$$k = \exp\left[a_1 + a_2\ln(p_d) + a_3\ln\left[\frac{\lambda}{\lambda+2}\right] + a_4\ln(1-S_{wi}) + a_5\ln(\phi)\right] \quad \text{..(E.5)}$$

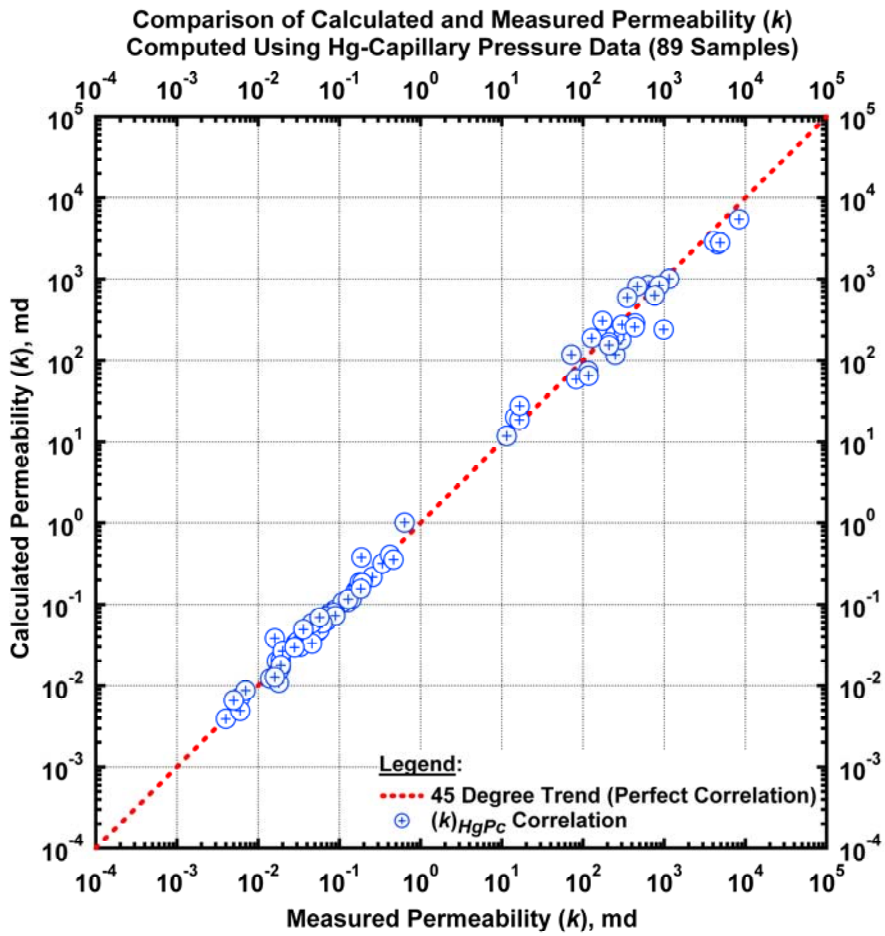

Figure E.2 – Permeability correlation based on mercury capillary pressure data (Eq. E.3 used for regression), *AAE* (average absolute error) = 26.46 percent).

Table E.3 – Regression Summary for Permeability — Model 3.

Optimized coefficients for k (*Eq.* E.5):

Coefficient	Optimized Value
a_1	14.0253 md
a_2	-1.8139
a_3	1.4385
a_4	2.2764
a_5	1.7296

Table E.3 – Regression Summary for Permeability — Model 3. (Continued)

Statistical summary for k (*Eq.* E.5):

Statistical Variable	Value
Sum of Squared Residuals	2.0106 $\ln(\text{md})^2$
Variance	369278.5839 md^2
Standard Deviation	607.6824 md
Average Absolute Error	26.4680 percent

Substituting the coefficients from **Table E.3** into Eq. E.5, we have:

$$k = \exp\left[14.0253 - 1.8139\ln(p_d) + 1.4385\ln\left[\frac{\lambda}{\lambda+2}\right] + 2.2764\ln(1-S_{wi}) + 1.7296\ln(\phi)\right] \text{..................(E.6)}$$

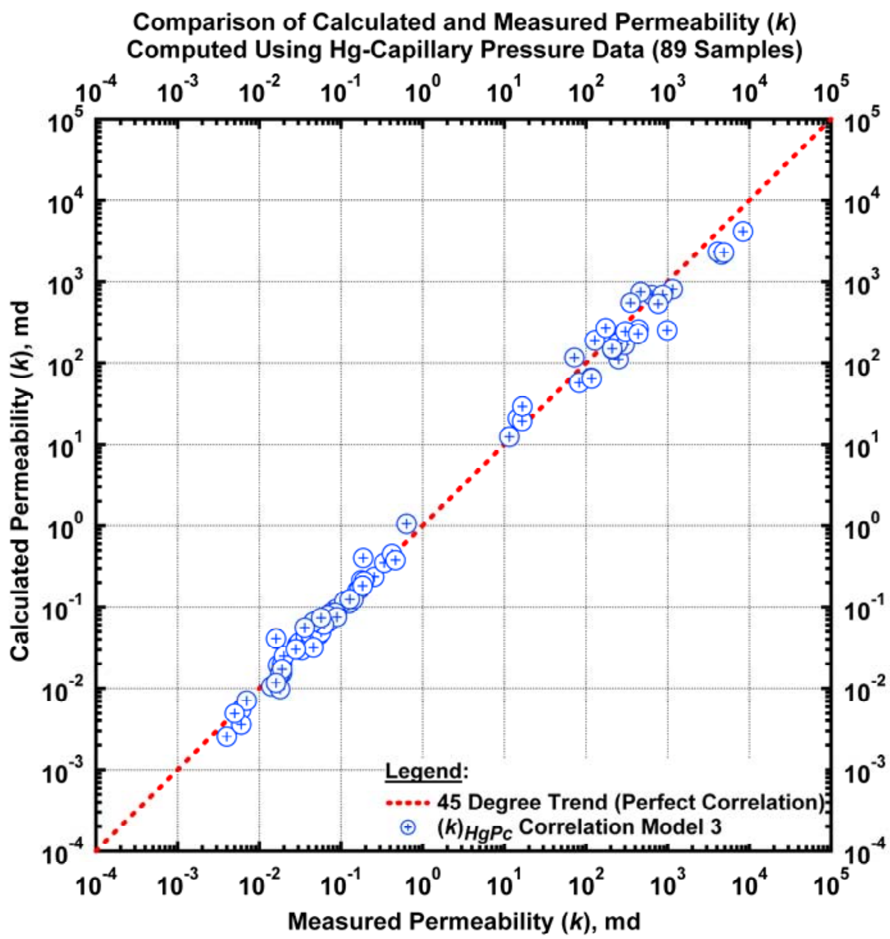

Figure E.3 – Permeability correlation based on mercury capillary pressure data (Eq. E.5 used for regression).

The permeability correlation given by Eq. E-6 is illustrated in **Fig. E.3** — we note a very reasonable correlation of the calculated and measured data. Results are identical to Model 1.

Model 4

Model 4 is a generalized exponential model, and is based on a linear extension of Eq. E.5.

$$k = \exp\left[\begin{array}{l} a_1 + a_2 \ln p_d + a_3 \ln \dfrac{\lambda}{\lambda+2} + a_4 \ln(1-S_{wi}) + a_5 \ln\phi + a_6 \ln p_d \ln \dfrac{\lambda}{\lambda+2} \\ + a_7 \ln p_d \ln(1-S_{wi}) + a_8 \ln p_d \ln\phi + a_9 \ln \dfrac{\lambda}{\lambda+2} \ln\phi + a_{10} \ln \dfrac{\lambda}{\lambda+2} \ln(1-S_{wi}) \\ + a_{11} \ln\phi \ln(1-S_{wi}) + a_{12} \ln\phi \ln(1-S_{wi}) \ln \dfrac{\lambda}{\lambda+2} + a_{13} \ln\phi \ln(1-S_{wi}) \ln p_d \\ + a_{14} \ln\phi \ln \dfrac{\lambda}{\lambda+2} \ln p_d + a_{15} \ln(1-S_{wi}) \ln \dfrac{\lambda}{\lambda+2} \ln p_d \\ - a_{16} \ln(1-S_{wi}) \ln \dfrac{\lambda}{\lambda+2} \ln p_d \ln\phi \end{array}\right] \quad \text{.............(E.7)}$$

Table E.4 – Regression Summary for Permeability — Model 4.

Optimized coefficients for k (*Eq.* E.7):

Coefficient	Optimized Value
a_1	18.3238
a_2	-1.8915
a_3	2.4842
a_4	21.6208
a_5	5.2947
a_6	0.3809
a_7	2.2876
a_8	-0.2808
a_9	18.8029
a_{10}	17.7095
a_{11}	1.5474
a_{12}	0.5485
a_{13}	0.8697
a_{14}	0.0123
a_{15}	14.6168
a_{16}	-0.1252

Statistical summary for k (*Eq.* E.7):

Statistical Variable	Value
Sum of Squared Residuals	1.1438 $\ln(\text{md})^2$
Variance	1073182.5224 md^2
Standard Deviation	1038.9453 md
Average Absolute Error	19.8664 percent

Substituting the coefficients from **Table E.4** into Eq. E.7, we have:

$$k = \exp\begin{bmatrix} 18.3238 - 1.8915 \ln p_d + 2.4842 \ln \dfrac{\lambda}{\lambda+2} + 21.6208 \ln(1-S_{wi}) + 5.2947 \ln\phi \\ + 0.3809 \ln p_d \ln \dfrac{\lambda}{\lambda+2} + 2.2876 \ln p_d \ln(1-S_{wi}) - 0.2808 \ln p_d \ln\phi \\ + 18.8029 \ln \dfrac{\lambda}{\lambda+2} \ln\phi + 17.7095 \ln \dfrac{\lambda}{\lambda+2} \ln(1-S_{wi}) + 1.5474 \ln\phi \ln(1-S_{wi}) \\ + 0.5485 \ln\phi \ln(1-S_{wi}) \ln \dfrac{\lambda}{\lambda+2} + 0.8697 \ln\phi \ln(1-S_{wi}) \ln p_d \\ + 0.0123 \ln\phi \ln \dfrac{\lambda}{\lambda+2} \ln p_d + 14.6168 \ln(1-S_{wi}) \ln \dfrac{\lambda}{\lambda+2} \ln p_d \\ - 0.1252 \ln(1-S_{wi}) \ln \dfrac{\lambda}{\lambda+2} \ln p_d \ln\phi \end{bmatrix} \quad \text{.....................(E.8)}$$

The permeability correlation given by Eq. E-8 is illustrated in **Fig. E.4**. As with Model 3, we note a very good correlation of the calculated and measured data.

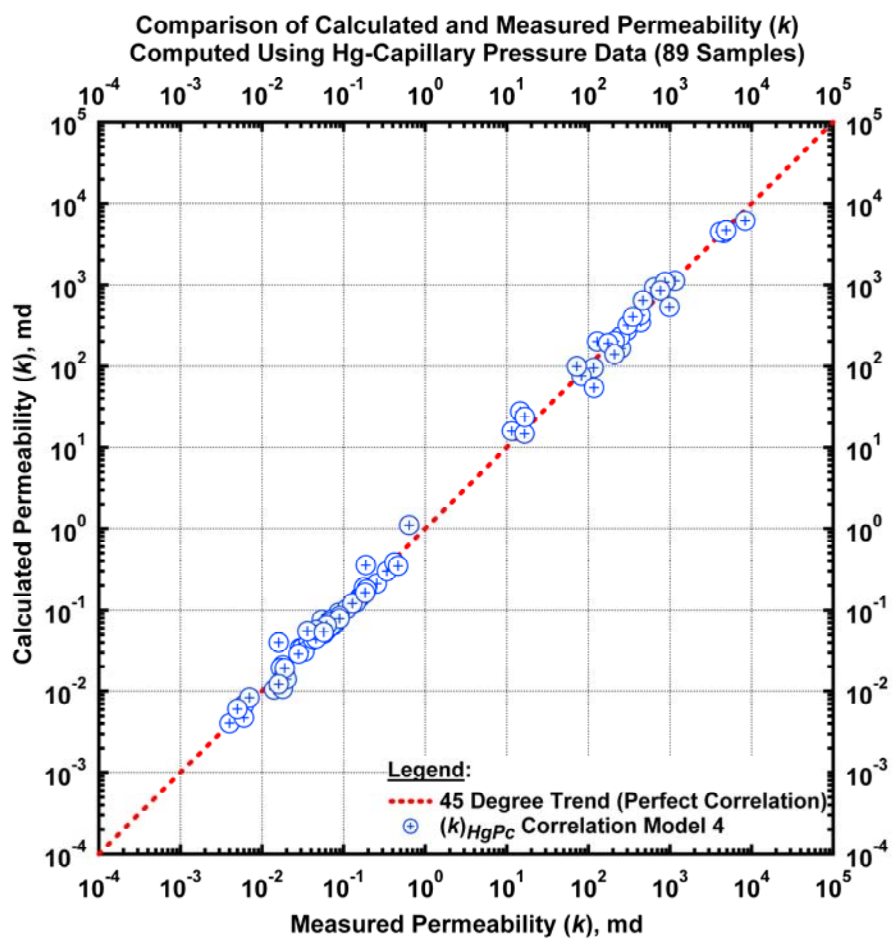

Figure E.4 – Permeability correlation based on mercury capillary pressure data (Eq. E.7 used for regression).

Using the correlation given by Eq. E.8, we note that it is possible that we are over-fitting the data in this case (*i.e.*, fitting the errors in the data, as well as the underlying correlation of the variables)).

Model 5

Model 5 is a generalized exponential model formulated as a rational function (*i.e.*, one function divided by another). This correlation model is based on using Eq. E.7 as the numerator and denominator in a rational formulation.

$$k = \exp\left[\frac{\begin{array}{l} a_1 + a_2 \ln p_d + a_3 \ln \frac{\lambda}{\lambda+2} + a_4 \ln(1-S_{wi}) + a_5 \ln\phi + a_6 \ln p_d \ln \frac{\lambda}{\lambda+2} \\ + a_7 \ln p_d \ln(1-S_{wi}) + a_8 \ln p_d \ln\phi + a_9 \ln\frac{\lambda}{\lambda+2}\ln\phi \\ + a_{10} \ln\frac{\lambda}{\lambda+2}\ln(1-S_{wi}) + a_{11}\ln\phi\ln(1-S_{wi}) + a_{12}\ln\phi\ln(1-S_{wi})\ln\frac{\lambda}{\lambda+2} \\ + a_{13}\ln\phi\ln(1-S_{wi})\ln p_d + a_{14}\ln\phi\ln\frac{\lambda}{\lambda+2}\ln p_d + a_{15}\ln(1-S_{wi})\ln\frac{\lambda}{\lambda+2}\ln p_d \\ + a_{16}\ln(1-S_{wi})\ln\frac{\lambda}{\lambda+2}\ln p_d \ln\phi \end{array}}{\begin{array}{l} 1 + a_{17}\ln p_d + a_{18}\ln\frac{\lambda}{\lambda+2} + a_{19}\ln(1-S_{wi}) + a_{20}\ln\phi + a_{21}\ln p_d\ln\frac{\lambda}{\lambda+2} \\ + a_{22}\ln p_d\ln(1-S_{wi}) + a_{23}\ln p_d\ln\phi + a_{24}\ln\frac{\lambda}{\lambda+2}\ln\phi + a_{25}\ln\frac{\lambda}{\lambda+2}\ln(1-S_{wi}) \\ + a_{26}\ln\phi\ln(1-S_{wi}) + a_{27}\ln\phi\ln(1-S_{wi})\ln\frac{\lambda}{\lambda+2} + a_{28}\ln\phi\ln(1-S_{wi})\ln p_d \\ + a_{29}\ln\phi\ln\frac{\lambda}{\lambda+2}\ln p_d + a_{30}\ln(1-S_{wi})\ln\frac{\lambda}{\lambda+2}\ln p_d - \\ a_{31}\ln(1-S_{wi})\ln\frac{\lambda}{\lambda+2}\ln p_d\ln\phi \end{array}}\right] \quad \text{.......(E.9)}$$

Table E.5 – Regression Summary for Permeability — Model 5.

Optimized coefficients for k (*Eq.* E.9):

Coefficient	Optimized Value	Coefficient	Optimized Value
a_1	-1.1662 md	a_{11}	-0.6519
a_2	-17.4834	a_{12}	0.0246
a_3	3250.9090	a_{13}	-141.3981
a_4	-237.7238	a_{14}	1.2541
a_5	214.99223	a_{15}	-0.2865
a_6	-559.9114	a_{16}	140.9318
a_7	-42.6880	a_{17}	5.2919
a_8	-25.7582	a_{18}	162.7202
a_9	1189.6335	a_{19}	6.8905
a_{10}	1084.4966	a_{20}	39.7913

Optimized coefficients for k (*Eq.* E.9): (Continued)

Coefficient	Optimized Value	Coefficient	Optimized Value
a_{21}	6.5984	a_{27}	624315
a_{22}	9.5643	a_{28}	-19.9661
a_{23}	-13.7159	a_{29}	-0.5488
a_{24}	-7.4197	a_{30}	-5.649
a_{25}	68.3802	a_{31}	-0.0019
a_{26}	35.0810		

Statistical summary for k (*Eq.* E.9):

Statistical Variable	Value
Sum of Squared Residuals	0.9779 ln(md)^2
Variance	1145308.5541 md^2
Standard Deviation	1070.1908 md
Average Absolute Error	17.2631 percent

Substituting the coefficients from **Table E.5** into Eq. E.9, we have:

$$k = \exp\left[\frac{\begin{array}{l} -1.1662 - 17.4834 \ln p_d + 3250.9090 \ln \frac{\lambda}{\lambda+2} - 237.7238 \ln(1-S_{wi}) \\ + 214.9225 \ln \phi - 559.9114 \ln p_d \ln \frac{\lambda}{\lambda+2} - 42.6880 \ln p_d \ln(1-S_{wi}) \\ - 25.7582 \ln p_d \ln \phi + 1189.6335 \ln \frac{\lambda}{\lambda+2} \ln \phi + 1084.4966 \ln \frac{\lambda}{\lambda+2} \ln(1-S_{wi}) \\ - 0.6519 \ln \phi \ln(1-S_{wi}) + 0.0246 \ln \phi \ln(1-S_{wi}) \ln \frac{\lambda}{\lambda+2} \\ - 141.3981 \ln \phi \ln(1-S_{wi}) \ln p_d + 1.2541 \ln \phi \ln \frac{\lambda}{\lambda+2} \ln p_d \\ - 0.2865 \ln(1-S_{wi}) \ln \frac{\lambda}{\lambda+2} \ln p_d + 140.9318 \ln(1-S_{wi}) \ln \frac{\lambda}{\lambda+2} \ln p_d \ln \phi \end{array}}{\begin{array}{l} 1 - 5.2919 \ln p_d + 162.7202 \ln \frac{\lambda}{\lambda+2} + 6.8905 \ln(1-S_{wi}) + 39.7913 \ln \phi \\ + 6.5984_{21} \ln p_d \ln \frac{\lambda}{\lambda+2} + 9.5643 \ln p_d \ln(1-S_{wi}) - 13.7159 \ln p_d \ln \phi \\ - 7.4197 \ln \frac{\lambda}{\lambda+2} \ln \phi + 68.3802 \ln \frac{\lambda}{\lambda+2} \ln(1-S_{wi}) + 35.0810 \ln \phi \ln(1-S_{wi}) \\ + 62.4315 \ln \phi \ln(1-S_{wi}) \ln \frac{\lambda}{\lambda+2} - 19.9661 \ln \phi \ln(1-S_{wi}) \ln p_d \\ - 0.5488 \ln \phi \ln \frac{\lambda}{\lambda+2} \ln p_d - 5.6490 \ln(1-S_{wi}) \ln \frac{\lambda}{\lambda+2} \ln p_d \\ - 0.0019 \ln(1-S_{wi}) \ln \frac{\lambda}{\lambda+2} \ln p_d \ln \phi \end{array}}\right] \quad \text{................(E.10)}$$

The permeability correlation given by Eq. E-10 is illustrated in **Fig. E.5** — we note an excellent correlation, but we also note that this correlation contains 31 parameters — and has almost certainly "over-fit" the data. This is the very best correlation that we have obtained.

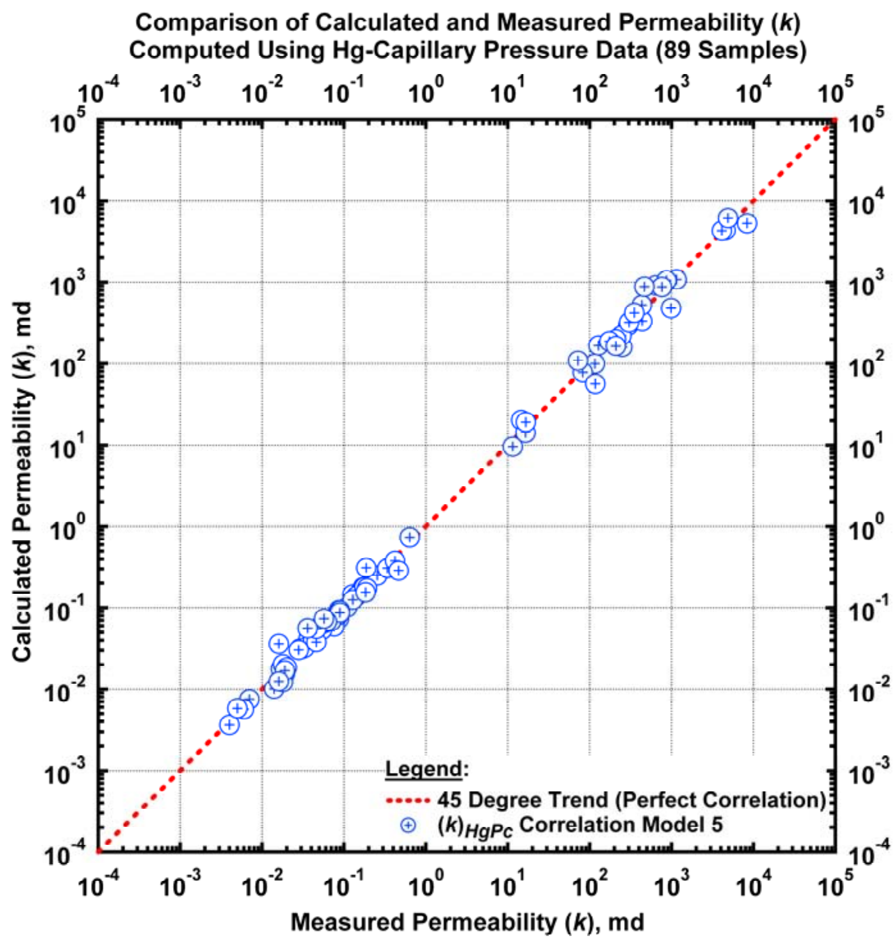

Figure E.5 – Permeability correlation based on mercury capillary pressure data (Eq. E.9 used for regression).

Model 6

The pore geometric factor (λ), is a variable with a relatively small range of values (0.5–2.25). The following model has been proposed to test the influence of the pore geometric factor.

$$k = \left[a_1\, p_d^{a_2} (1-S_{wi})^{a_3} \phi^{a_4} \left[\frac{\lambda}{\lambda+2} \right]^{\left[a_5 + a_6 p_d + a_7 (1\text{-}S_{wi}) + a_8 \phi + a_9 \left[\frac{\lambda}{\lambda+2} \right] \right]} \right] \quad \text{......................................(E.11)}$$

Table E.6 – Regression Summary for Permeability — Model 6.

Optimized coefficients for k (*Eq.* E.11):

Coefficient	Optimized Value
a_1	13217682.3 md
a_2	-1.9184
a_3	1.4516
a_4	0.1528
a_5	3.6014
a_6	-2.6093
a_7	2.07150
a_8	-0.0004
a_9	6.0762

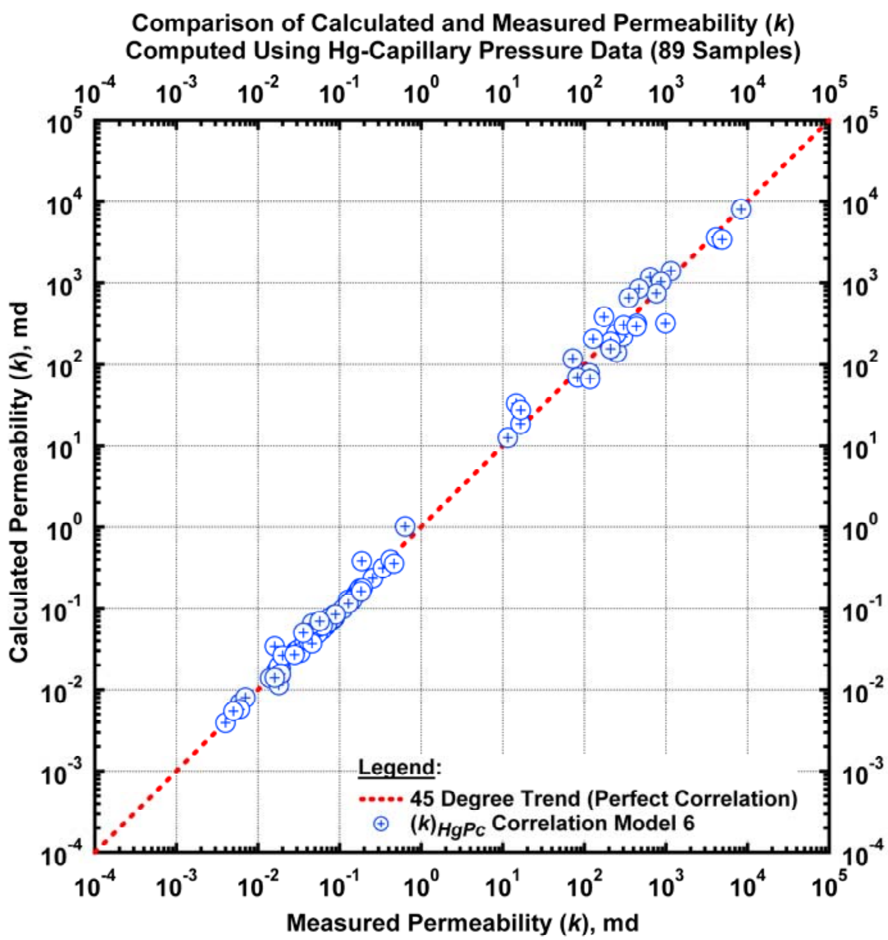

Figure E.6 – Permeability correlation based on mercury capillary pressure data (Eq. E.11 used for regression).

Table E.6 – Regression Summary for Permeability — Model 6. (continued)

Statistical summary for k (*Eq.* E.11):

Statistical Variable	Value
Sum of Squared Residuals	1.6097 $\ln(\text{md})^2$
Variance	1130725.5521 md^2
Standard Deviation	1063.6830 md
Average Absolute Error	22.9942 percent

Substituting the coefficients from **Table E.6** into Eq. E.11, we have:

$$k = \begin{bmatrix} 13217682.36\, p_d^{-1.9184} (1 - S_{wi})^{1.4516} \phi^{0.1528} \\ \mathbf{x} \left[\dfrac{\lambda}{\lambda + 2} \right]^{\left[3.6014 - 2.6093 p_d + 2.0715(1 - S_{wi}) - 0.0004\phi + 6.0762 \left[\frac{\lambda}{\lambda+2} \right] \right]} \end{bmatrix} \quad \text{(E.12)}$$

The permeability correlation given by Eq. E-12 is illustrated in **Fig. E.6** — we note a better correlation of the calculated and measured data than the model 1.

Model 7

We propose the following model as the final case which serves as a mechanism to again test the influence of the pore geometric factor:

$$k = a_{10} \left[a_1\, p_d^{a_2} (1 - S_{wi})^{a_3} \phi^{a_4} \left[\frac{\lambda}{\lambda + 2} \right]^{\left[a_5 + a_6 p_d + a_7 (1 - S_{wi}) + a_8 \phi + a_9 \left[\frac{\lambda}{\lambda+2} \right] \right]} + a_{11} \right]^{a_{12}} \quad \text{(E.13)}$$

Table E.7 – Regression Summary for Permeability — Model 7.

Optimized coefficients for k (*Eq.* E.13):

Coefficient	Optimized Value
a_1	13217682.3 md
a_2	-1.9184
a_3	1.4516
a_4	0.1528
a_5	3.6014
a_6	-2.6093
a_7	2.07150
a_8	-0.0004
a_9	6.0762
a_{10}	1084.4966
a_{11}	-0.6519
a_{12}	0.0246

Table E.7 – Regression Summary for Permeability — Model 7. (continued)

Statistical summary for k (Eq. E.13):

Statistical Variable	Value
Sum of Squared Residuals	1.7513 $\ln(\text{md})^2$
Variance	618398.8353 md^2
Standard Deviation	786.3834 md
Average Absolute Error	22.3800 percent

Substituting the coefficients from **Table E.7** into Eq. E.13, we have:

$$k = 1435.17\left[\begin{array}{l} 0.1125 + 6.1155\, p_d^{-0.3822}(1-S_{wi})^{0.3417}\phi^{0.6337} \\ \mathbf{x}\left[\dfrac{\lambda}{\lambda+2}\right]^{\left[-0.2281+0.0007\,p_d+0.2813(1-S_{wi})+0.73\phi+0.4066\left[\frac{\lambda}{\lambda+2}\right]\right]} \end{array}\right]^{5.9156} \quad \text{....................(E.14)}$$

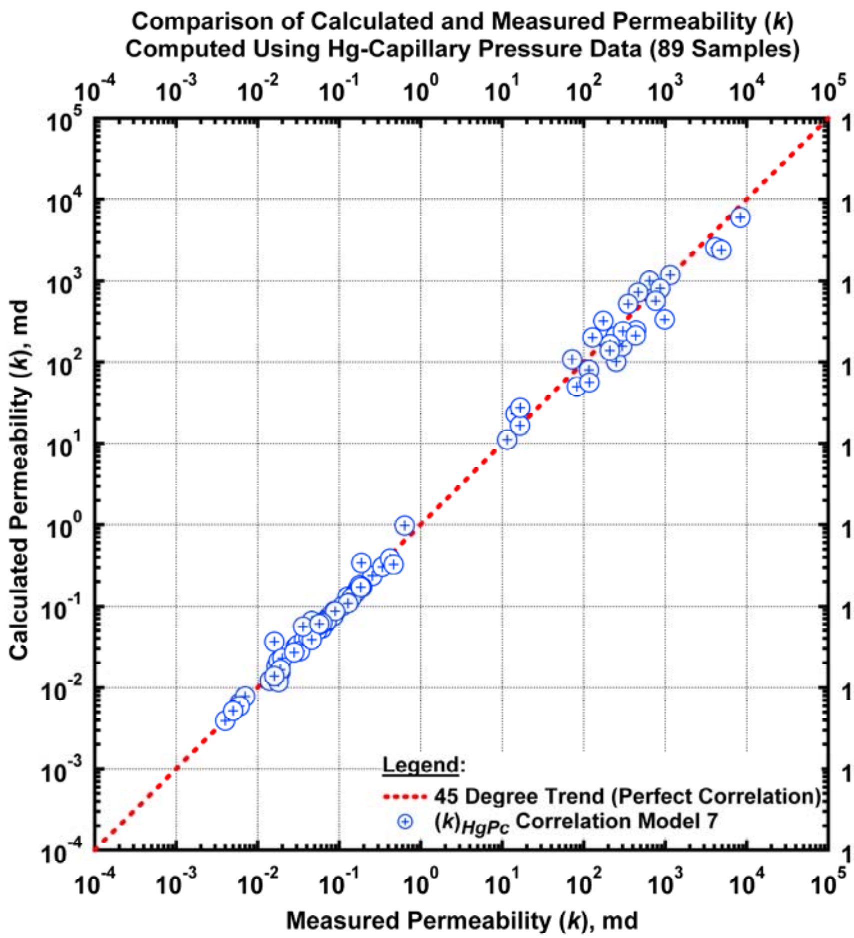

Figure E.7 – Permeability correlation based on mercury capillary pressure data (Eq. E.13 used for regression).

The permeability correlation given by Eq. E-14 is illustrated in **Fig. E.7** — we note a good reasonable correlation of the calculated and measured data.

References

E.1. Brooks, R.H., and Corey A.T.: "Hydraulic Properties of Porous Media," Hydrol. Paper 3, Colo. State Univ., Fort Collins, CO, 1964.

E.2. Nakornthap, K. and Evans, R.D.: "Temperature-Dependent Relative Permeability and Its Effect on Oil Permeability and Its Effect on Oil Displacement by Thermal Methods," SPE 11217 *SPERE* (1986)

Nomenclature

k	=	permeability, md
p_d	=	displacement pressure, psi
p_c	=	capillary pressure, psi
S_{wi}	=	irreducible saturation, fraction
S_w	=	water saturation in the actual porous medium, fraction
λ	=	index of pore-size distribution
ϕ	=	porosity

APPENDIX F
CORRELATIONS FOR DISPLACEMENT PRESSURE (p_d) DERIVED FROM THE DATA IN THIS WORK

In this Appendix we present the correlations of displacement pressure derived in this work — which are based on the permeability and porosity data used in this work, as well as the results of the regression of the semi-analytical Brooks-Corey[F-1] capillary pressure model.

Model 1

The power-law model form is used as a mechanism to correlate the displacement pressure (p_d). In this case, we correlate the displacement pressure (p_d) in terms of permeability, porosity and irreducible wetting phase saturation.

$$p_d = b_1 \phi^{b_2} k^{b_3} (1 - S_{wi})^{b_4} \quad \text{(F.1)}$$

Table F.1 – Regression Summary for Displacement Pressure — Model 1.

Optimized coefficients for p_d (Eq. F.1):

Coefficient	Optimized Value
b_1	751.3360 (psia)
b_2	0.8469
b_3	-0.5166
b_4	0.0489

Statistical summary for p_d (Eq. F.1):

Statistical Variable	Value
Sum of Squared Residuals	1.2239 $\ln(\text{psia})^2$
Variance	113392.3297 psia^2
Standard Deviation	336.7378 psia
Average Absolute Error	22.2482 percent

Substituting the coefficients in **Table F.1** into Eq. F.1, we have:

$$p_d = 751.3360 \phi^{0.8469} k^{-0.5166} (1 - S_{wi})^{0.0489} \quad \text{(F.2)}$$

The displacement pressure correlation given by Eq. F-2 is illustrated in **Fig. F.1** — we note a reasonable correlation of the calculated and measured data, which validates our concept of using a power law basis for representing displacement pressure in terms of other the other intrinsic variables (*i.e.*, ϕ, p_d and S_{wi}).

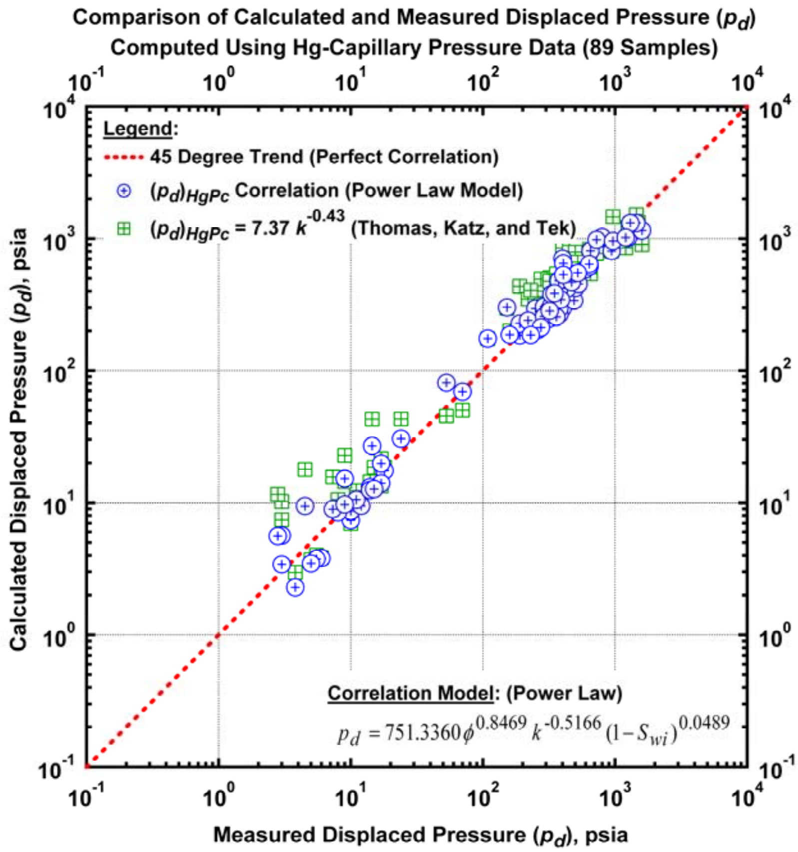

Figure F.1 – Displacement pressure (p_d) correlation based on mercury capillary pressure data (Eq. F.1 used for regression).

Model 2

Model 2 is an extension of the base "power-law" model (Model 1) — this particular form is a "non-linear" power-law model (used by analogy with PVT correlations).

$$p_d = b_5\left[b_1 k^{b_2}\ \phi^{b_3}(1-S_{wi})^{b_4} + b_6\right]^{b_7} \quad \text{(F.3)}$$

Table F.2 – Regression Summary for Displacement Pressure — Model 2.

Optimized coefficients for p_d (*Eq.* F.3):

Coefficient	Optimized Value
b_1	31539.5170 (psia)
b_2	-2.4108
b_3	3.7970
b_4	-0.4579
b_5	72.5043
b_6	$1.6568\text{x}10^{-6}$
b_7	0.2178

Statistical summary for p_d (Eq. F.3):

Statistical Variable	Value
Sum of Squared Residuals	1.1213 $\ln(\text{psia})^2$
Variance	116427.1317 psia^2
Standard Deviation	341.2142 psia
Average Absolute Error	21.7110 percent

Substituting the coefficients in **Table F.2** into Eq. F.3, we have:

$$p_d = 72.5043\left[31539.5170k^{-2.4108}\,\phi^{3.7970}(1-S_{wi})^{-0.4579} + 1.6568\times10^{-6}\right]^{0.2178} \quad \text{(F.4)}$$

The displacement pressure correlation given by Eq. F.4 is illustrated in **Fig. F.2** — we note a very reasonable correlation of the calculated and measured data. We note that Model 2 provides more statistical accuracy than Model 1, but this form requires 3 more model parameters.

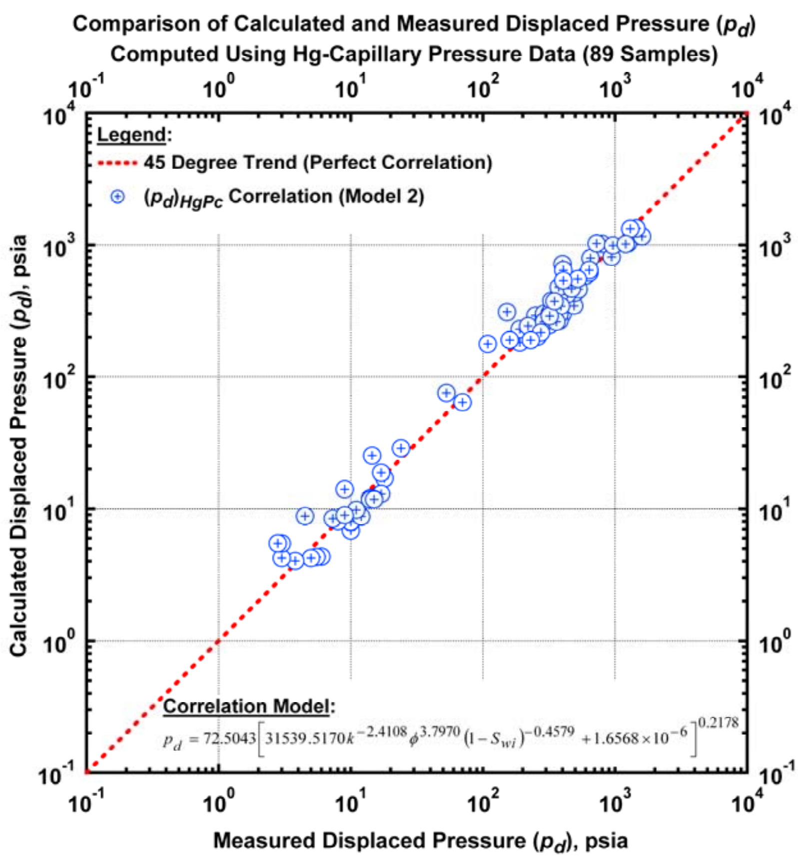

Figure F.2 – Displacement pressure (p_d) correlation based on mercury capillary pressure data (Eq. F.3 used for regression).

Model 3

This model is the exponential form of the power-law model. This is a mathematical equivalent of Model 1. This is an intermediate model which allows us to compare the more complex models of this same type which follow for the displacement pressure:

$$p_d = \exp\left[b_1 + b_2 \ln k + b_3 \ln \phi + b_4 \ln(1 - S_{wi})\right] \quad \text{(F.5)}$$

Table F.3 – Regression Summary for Displacement Pressure — Model 3.

Optimized coefficients for p_d (*Eq.* F.5):

Coefficient	Optimized Value
b_1	6.1810 (psia)
b_2	6.6129
b_3	-0.5166
b_4	0.8450

Statistical summary for p_d (*Eq.* F.5):

Statistical Variable	Value
Sum of Squared Residuals	1.2239 ln(psia)^2
Variance	113392.3297 psia^2
Standard Deviation	336.7378 psia
Average Absolute Error	22.2481 percent

Substituting the coefficients in **Table F.3** into Eq. F.5, we have:

$$p_d = \exp\left[6.1810 + 6.6129 \ln k - 0.5166 \ln \phi + 0.8450 \ln(1 - S_{wi})\right] \quad \text{(F.6)}$$

The displacement pressure correlation given by Eq. F-6 is illustrated in **Fig. F.3** — we note a reasonable correlation of the calculated and measured data. The results are identical to Model 1.

Model 4

Model 4 is a generalized exponential model, and is based on a linear extension of Eq. F.5.

$$p_d = \exp\begin{bmatrix} b_1 + b_2 \ln\phi + b_3 \ln k + b_4 \ln(1 - S_{wi}) + b_5 \ln\phi \ln k \\ + b_6 \ln\phi \ln(1 - S_{wi}) + b_7 \ln k \ln(1 - S_{wi}) + b_8 \ln k \ln\phi \ln(1 - S_{wi}) \end{bmatrix} \quad \text{(F.7)}$$

Table F.4 – Regression Summary for Displacement Pressure — Model 4.

Optimized coefficients for p_d (*Eq.* F.7):

Coefficient	Optimized Value
b_1	6.4343
b_2	0.8264
b_3	-0.4127
b_4	0.4688
b_5	0.0598
b_6	-0.6248
b_7	0.0028
b_8	-0.3103

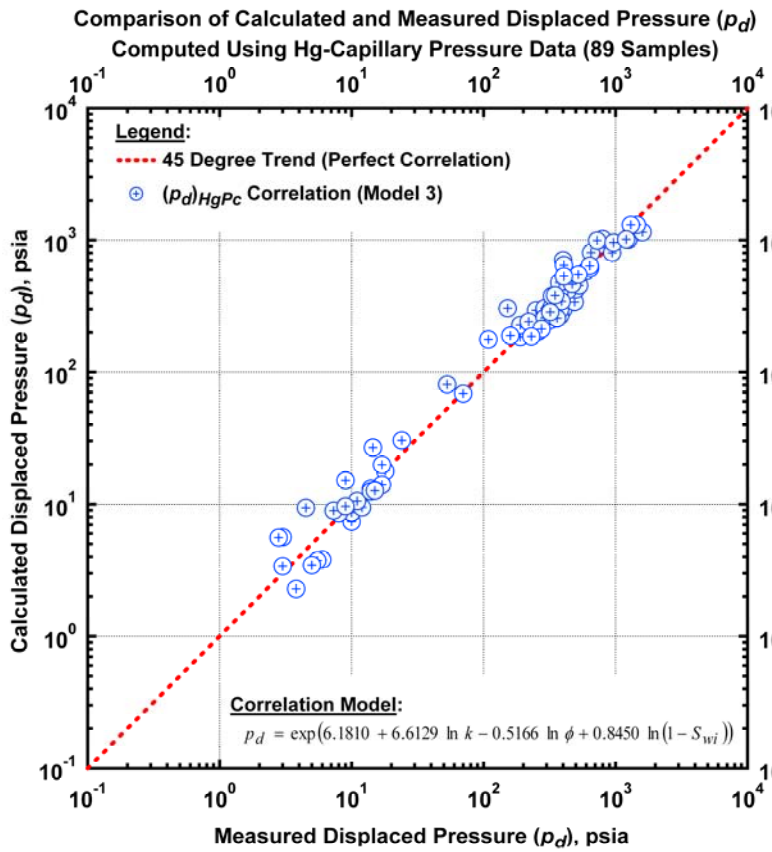

Figure F.3 – Displacement pressure (p_d) correlation based on mercury capillary pressure data (Eq. F.5 used for regression).

Table F.4 – Regression Summary for Displacement Pressure — Model 4. (continued)

Statistical summary for p_d (*Eq.* F.7):

Statistical Variable	Value
Sum of Squared Residuals	0.7506 ln(psia)^2
Variance	134532.3199 psia^2
Standard Deviation	336.7865 psia
Average Absolute Error	17.2332 percent

Substituting the coefficients in **Table F.4** into Eq. F.7, we have:

$$p_d = \exp\begin{bmatrix} 6.4343 + 0.8264 \ln \phi - 0.4124 \ln k + 0.4688 \ln(1 - S_{wi}) \\ + 0.0598 \ln \phi \ln k - 0.6248 \ln \phi \ln(1 - S_{wi}) \\ + 0.0028 \ln k \ln(1 - S_{wi}) - 0.3103 \ln k \ln \phi \ln(1 - S_{wi}) \end{bmatrix} \quad \text{(F.8)}$$

The displacement pressure correlation given by Eq. F-8 is illustrated in **Fig. F.4.** As with Model 3, we note a very good correlation of the calculated and measured data..

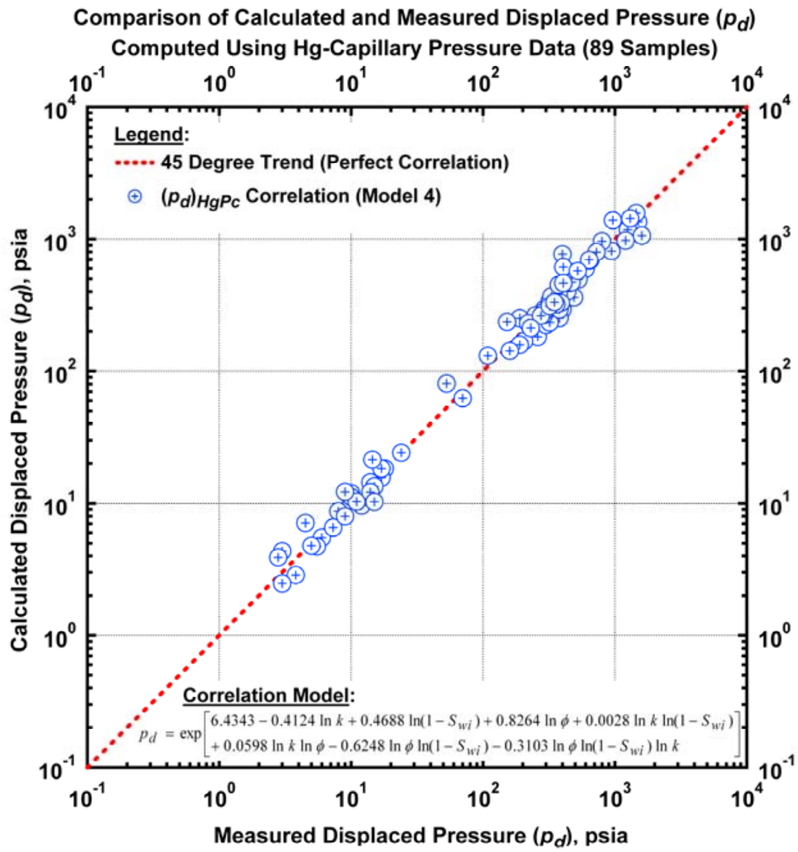

Figure F.4 – Displacement pressure (p_d) correlation based on mercury capillary pressure data (Eq. F.7 used for regression).

Model 5

Model 5 is a generalized exponential model formulated as a rational function (*i.e.*, one function divided by another). This correlation model is based on using the form of Eq. F.7 as the numerator and denominator in a rational formulation.

$$p_d = \exp\left[\frac{\begin{array}{l} b_1 + b_2 \ln\phi + b_3 \ln k + b_4 \ln(1-S_{wi}) + b_5 \ln\phi \ln k \\ + b_6 \ln\phi \ln(1-S_{wi}) + b_7 \ln k \ln(1-S_{wi}) + b_8 \ln k \ln\phi \ln(1-S_{wi}) \end{array}}{\begin{array}{l} 1 + b_9 \ln\phi + b_{10} \ln k + b_{11} \ln(1-S_{wi}) + b_{12} \ln\phi \ln k \\ + b_{13} \ln\phi \ln(1-S_{wi}) + b_{14} \ln k \ln(1-S_{wi}) + b_{15} \ln k \ln\phi \ln(1-S_{wi}) \end{array}}\right] \quad \text{(F.9)}$$

Table F.5 – Regression Summary for Displacement Pressure — Model 5.

Optimized coefficients for p_d (*Eq*. F.9):

Coefficient	Optimized Value
b_1	6.5325
b_2	0.8603
b_3	-0.2141
b_4	1.1769
b_5	0.1737
b_6	0.0029
b_7	-0.0305
b_8	0.1971
b_9	-0.0002
b_{10}	0.0519
b_{11}	-0.8402
b_{12}	0.0264
b_{13}	-0.4981
b_{14}	0.0027
b_{15}	0.0084

Statistical summary for p_d (*Eq*. F.9):

Statistical Variable	Value
Sum of Squared Residuals	0.5978 ln(psia)^2
Variance	115533.5473 psia^2
Standard Deviation	339.9023 psia
Average Absolute Error	14.9016 percent

Substituting the coefficients in **Table F.5** into Eq. F.9, we have:

$$p_d = \exp\left[\frac{\begin{array}{l} 6.5325 + 0.8603\ln\phi - 0.2141\ln k + 1.1769\ln(1-S_{wi}) + 0.1737\ln\phi\ln k \\ + 0.0029\ln\phi\ln(1-S_{wi}) - 0.0305\ln k\ln(1-S_{wi}) + 0.1971\ln k\ln\phi\ln(1-S_{wi}) \end{array}}{\begin{array}{l} 1 - 0.0002\ln\phi + 0.0519\ln k - 0.8402\ln(1-S_{wi}) + 0.02647\ln\phi\ln(1-S_{wi}) \\ - 0.4981\ln\phi\ln(1-S_{wi}) + 0.0027\ln k\ln(1-S_{wi}) + 0.0084\ln k\ln\phi\ln(1-S_{wi}) \end{array}}\right] \quad \text{..............} \ (\text{F.10})$$

The displacement pressure correlation given by Eq. F-10 is illustrated in **Fig. F.5** but we also note that this correlation contains 15 parameters — and has probably "over-fit" the data. This is the very best correlation that we have obtained.

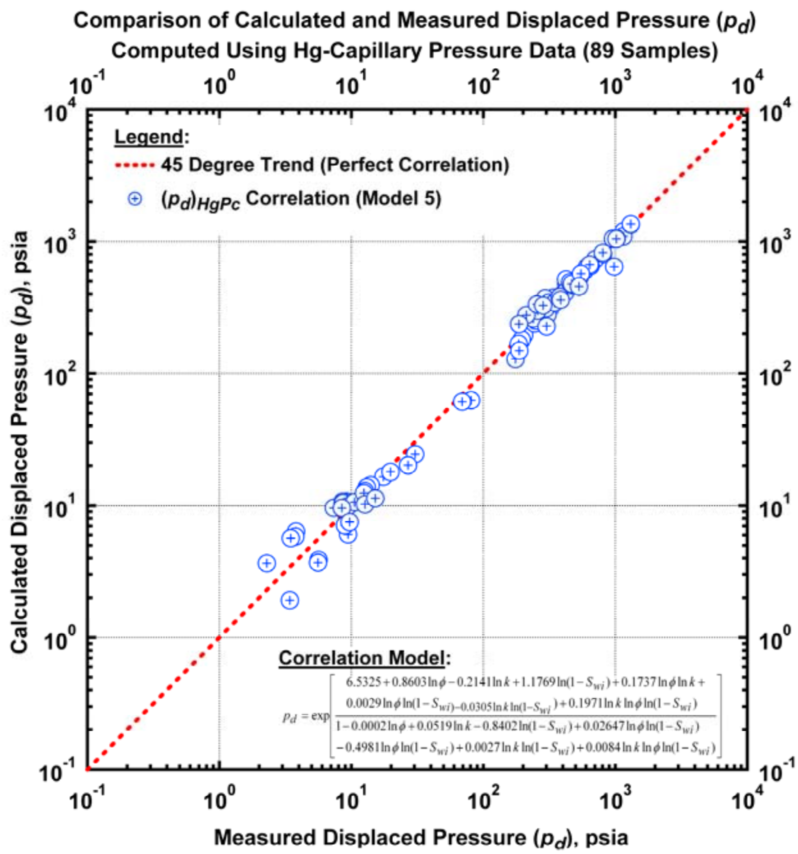

Figure F.5 – Displacement pressure (p_d) correlation based on mercury capillary pressure data (Eq. F.9 used for regression).

References

F.1. Brooks, R.H., and Corey A.T.: "Hydraulic Properties of Porous Media," Hydrol. Paper 3, Colo. State Univ., Fort Collins, CO, 1964.

Nomenclature

k	=	permeability, md
p_d	=	displacement pressure, psi
p_c	=	capillary pressure, psi
S_{wi}	=	irreducible saturation, fraction
S_w	=	water saturation in the actual porous medium, fraction
λ	=	index of pore-size distribution
ϕ	=	porosity

APPENDIX G

CORRELATIONS FOR PORE GEOMETRIC FACTOR (λ) DERIVED FROM THE DATA IN THIS WORK

In this Appendix we present the correlations of pore geometric factor (or the "index of pore-size distribution") (λ) derived in this work which are based on given permeability and porosity data, as well as the results of the regression of the semi-analytical Brooks-Corey[G-1] capillary pressure model.

Model 1

We correlate the pore geometric factor (λ) with permeability, porosity, irreducible wetting phase saturation and capillary displacement pressure, again using a power-law model.

$$\lambda = c_1 \phi^{c_2} k^{c_3} (1-S_{wi})^{c_4} p_d^{c_5} \quad \text{(G.1)}$$

Table G.1 – Regression Summary for Pore Geometric Factor (λ) — Model 1.

Optimized coefficients for λ (*Eq.* G.1):

Coefficient	Optimized Value
c_1	0.00084
c_2	-1.0485
c_3	0.5498
c_4	-2.2790
c_5	0.9939

Statistical summary for λ (*Eq.* G.1):

Statistical Variable	Value
Sum of Squared Residuals	1.0262
Variance	0.1943
Standard Deviation	0.4408
Average Absolute Error	18.9111 percent

Substituting the coefficients in **Table G.1** into Eq. G.1, we have:

$$\lambda = 0.00084 \phi^{-1.0485} k^{0.5498} (1-S_{wi})^{-2.2790} p_d^{0.9939} \quad \text{(G.2)}$$

The index of pore geometric factor correlation given by Eq. G-2 is illustrated in **Fig. G.1** — we note a very reasonable correlation of the calculated and measured data, which validates our concept of using a power law basis for representing index of pore-size distribution in terms of other the other intrinsic variables (*i.e.*, ϕ, p_d, S_{wi}, and k).

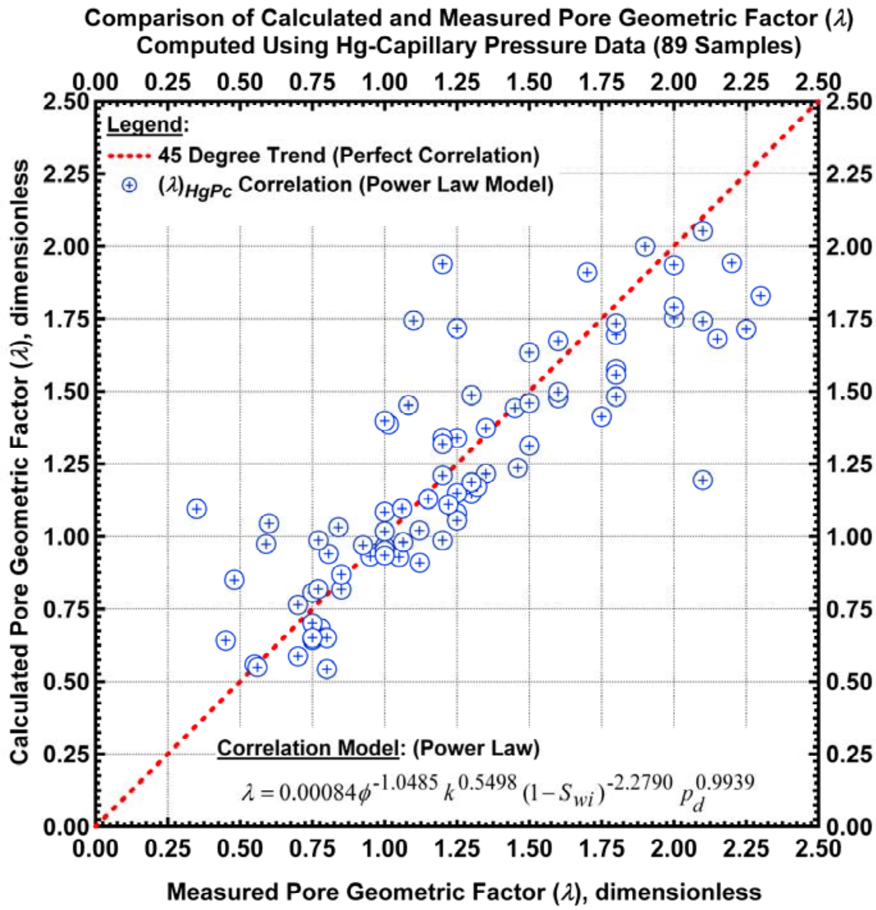

Figure G.1 – Pore geometric factor (λ) correlation based on mercury capillary pressure data (Eq. G.1 used for regression).

Model 2

Model 2 is an extension of the base "power-law" model (Model 1) — this particular form is a "non-linear" power-law model (used by analogy with PVT correlations).

$$\lambda = a_6 \left[a_1 k^{a_2} \phi^{a_3} (1 - S_{wi})^{a_4} \, p_d^{a_5} + a_7 \right]^{a_8} \text{ .... (G.3)}$$

Table G.2 – Regression Summary for Pore Geometric Factor (λ) — Model 2.

Optimized coefficients for λ (*Eq.* G.3):

Coefficient	Optimized Value
c_1	0.0003
c_2	1.084
c_3	-2.0070
c_4	-3.9226
c_5	1.9978
c_6	0.0220
c_7	27.3709
c_8	0.9208

Statistical summary for λ (*Eq.* G.3):

Statistical Variable	Value
Sum of Squared Residuals	0.9904
Variance	0.2257
Standard Deviation	0.4751
Average Absolute Error	18.2095 percent

Substituting the coefficients in **Table G.2** into Eq. G.3, we have:

$$\lambda = 0.0220\left[0.0003k^{1.084}\phi^{-2.0070}(1-S_{wi})^{-3.9226}\,p_d^{\,1.9978} + 27.3709\right]^{0.9208} \quad \text{................................ (G.4)}$$

The index of pore geometric factor correlation given by Eq. G-4 is illustrated in **Fig. G.2** — we note a very reasonable correlation of the calculated and measured data. We note that Model 2 provides more statistical accuracy than Model 1, but this form requires 3 more model parameters.

Model 3

This model is the exponential form of the power-law model. This is a mathematical equivalent of Model 1. This is an intermediate model which allows us to compare the more complex models of this same type which follow.

$$\lambda = \exp\left[c_1 + c_2\ \ln(k) + c_3\ \ln(\phi) + c_4\ \ln(1-S_{wi}) + c_5\ \ln(p_d)\right] \quad \text{.. (G.5)}$$

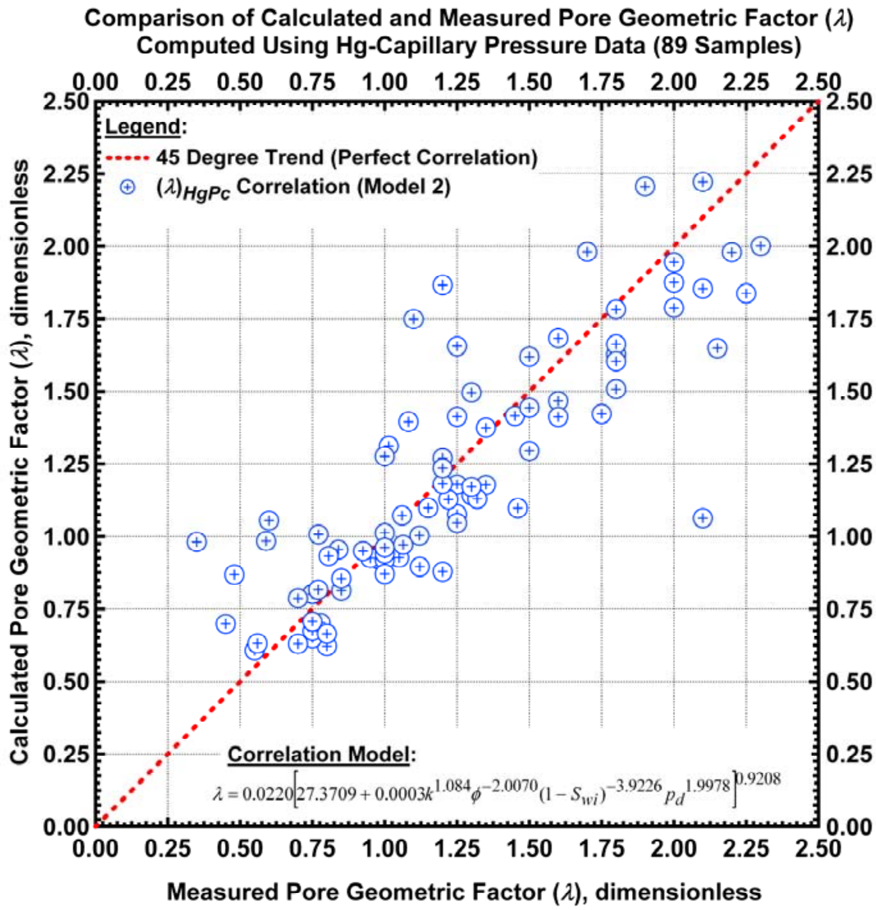

Figure G.2 – Pore geometric factor (λ) correlation based on mercury capillary pressure data (Eq. G.3 used for regression).

Table G.3 – Regression Summary for Pore Geometric Factor (λ) — Model 3.

Optimized coefficients for λ (*Eq.* G.5):

Coefficient	Optimized Value
c_1	-7.0829
c_2	-1.0488
c_3	0.5499
c_4	-2.2787
c_5	0.9942

Statistical summary for λ (*Eq.* G.5):

Statistical Variable	Value
Sum of Squared Residuals	1.0262
Variance	0.1943
Standard Deviation	0.4408
Average Absolute Error	18.9103 percent

Substituting the coefficients in **Table G.3** into Eq. G.5, we have:

$$\lambda = \exp\left[-7.08296 - 1.0488\ln(k) + 0.5499\ln(\phi) - 2.2787\ln(1-S_{wi}) + 0.9942\ln(p_d)\right] \text{ .... (G.6)}$$

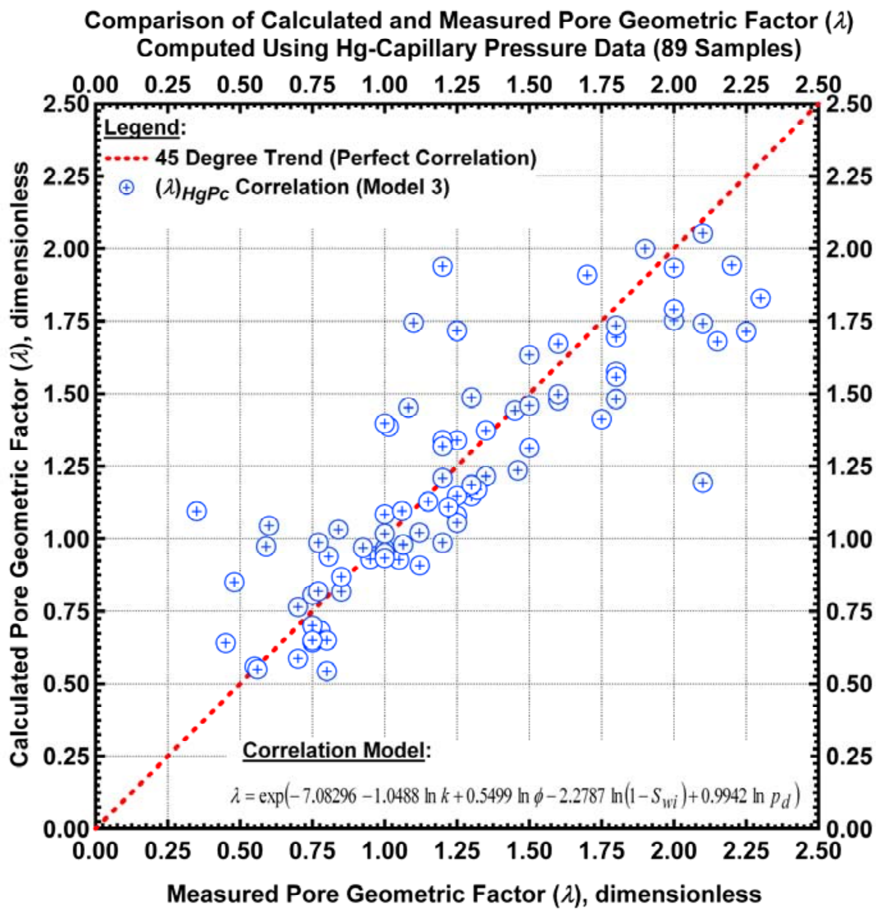

Figure G.3 – Pore geometric factor (λ) correlation based on mercury capillary pressure data (Eq. G.5 used for regression).

Model 4

Model 4 is a generalized exponential model, and is based on a linear extension of Eq. G.5.

$$\lambda = \exp\begin{bmatrix} c_1 + c_2 \ln p_d + c_3 \ln k + c_4 \ln(1-S_{wi}) + c_5 \ln\phi \\ + c_6 \ln p_d \ln k + c_7 \ln p_d \ln(1-S_{wi}) + c_8 \ln p_d \ln\phi \\ + c_9 \ln k \ln\phi + c_{10} \ln k \ln(1-S_{wi}) + c_{11} \ln\phi \ln(1-S_{wi}) \\ + c_{12} \ln\phi \ln(1-S_{wi}) \ln k + c_{13} \ln\phi \ln(1-S_{wi}) \ln p_d \\ + c_{14} \ln\phi \ln k \ln p_d + c_1 5 \ln(1-S_{wi}) \ln k \ln p_d \\ + c_{16} \ln(1-S_{wi}) \ln k \ln p_d \ln\phi \end{bmatrix} \text{ .... (G.7)}$$

Table G.4 – Regression Summary for Pore Geometric Factor (λ) — Model 4.

Optimized coefficients for λ (*Eq.* G.5):

Coefficient	Optimized Value
c_1	-2.7818
c_2	0.2799
c_3	0.2730
c_4	0.1813
c_5	0.2233
c_6	0.0101
c_7	0.6473
c_8	-0.1938
c_9	-1.3494
c_{10}	0.0041
c_{11}	0.1554
c_{12}	1.9845
c_{13}	0.3963
c_{14}	-0.0085
c_{15}	-0.4542
c_{16}	0.1181

Statistical summary for λ (*Eq.* G.7):

Statistical Variable	Value
Sum of Squared Residuals	0.7762
Variance	0.2076
Standard Deviation	0.4457
Average Absolute Error	16.6527 percent

Substituting the coefficients in **Table G.4** into Eq. G.7, we have:

$$\lambda = \exp\begin{bmatrix} -2.7818 + 0.2799 \ln p_d + 0.2730 \ln k + 0.1813 \ln(1-S_{wi}) + 0.2233 \ln\phi \\ +0.0101 \ln p_d \ln k + 0.6473 \ln p_d \ln(1-S_{wi}) - 0.1938 \ln p_d \ln\phi \\ -1.3494 \ln k \ln\phi + 0.0041 \ln k \ln(1-S_{wi}) + 0.1554 \ln\phi \ln(1-S_{wi}) \\ +1.9845 \ln\phi \ln(1-S_{wi}) \ln k + 0.3963 \ln\phi \ln(1-S_{wi}) \ln p_d \\ -0.0085 \ln\phi \ln k \ln p_d - 0.4542 \ln(1-S_{wi}) \ln k \ln p_d \\ +0.1181 \ln(1-S_{wi}) \ln k \ln p_d \ln\phi \end{bmatrix} \quad \text{............................. (G.8)}$$

The index of pore geometric factor correlation given by Eq. G-8 is illustrated in **Fig. G.4**. As with Model 3, we note a very good correlation of the calculated and measured data.

Using the correlation given by Eq. G.8, we note that it is possible that we are over-fitting the data in this case (*i.e.*, fitting the errors in the data, as well as the underlying correlation of the variables).

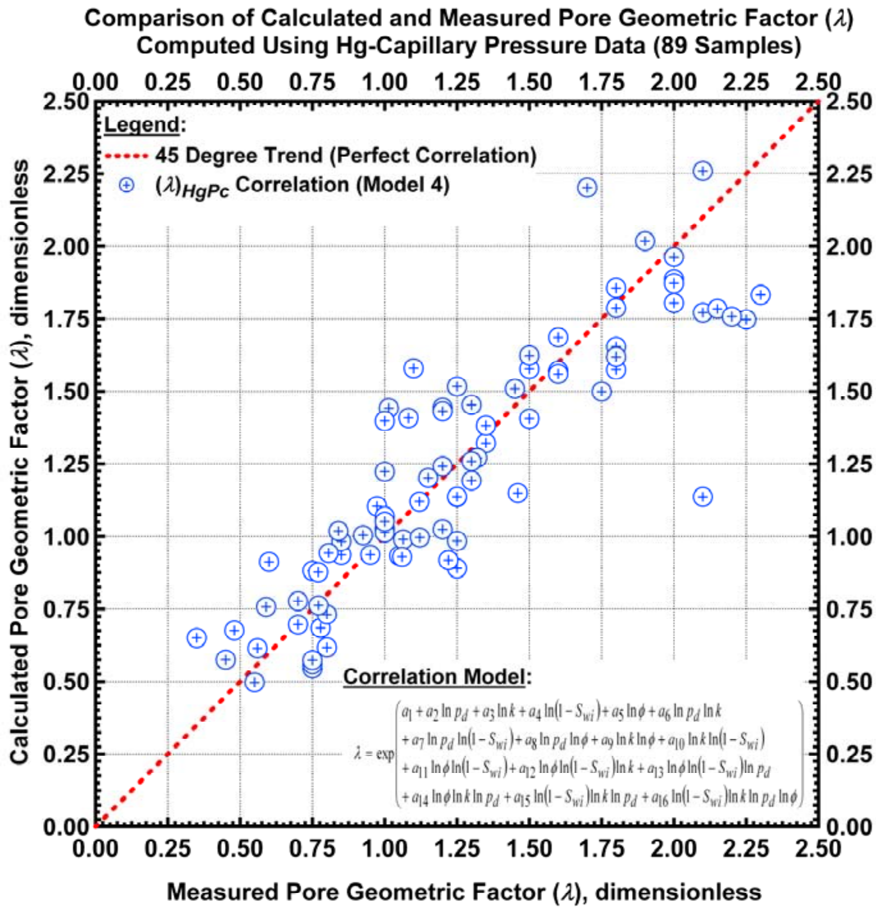

Figure G.4 – Pore geometric factor (λ) correlation based on mercury capillary pressure data (Eq. G.7 used for regression).

Model 5

Model 5 is a generalized exponential model formulated as a rational function (*i.e.*, one function divided by another). This correlation model is based on using Eq. G.7 as the numerator and denominator in a rational formulation.

The index of pore geometric factor correlation given by Eq. G-10 is illustrated in **Fig. G.5** — we note an excellent correlation, but we also note that this correlation contains 31 parameters — and has almost certainly "over-fit" the data. This is the very best correlation that we have obtained for the pore geometric factor.

$$\lambda = \exp\left[\frac{\begin{array}{l} c_1 + c_2 \ln p_d + c_3 \ln k + c_4 \ln(1-S_{wi}) \\ + c_5 \ln\phi + c_6 \ln p_d \ln k + c_7 \ln p_d \ln(1-S_{wi}) \\ + c_8 \ln p_d \ln\phi + c_9 \ln k \ln\phi + c_{10} \ln k \ln(1-S_{wi}) \\ + c_{11} \ln\phi \ln(1-S_{wi}) + c_{12} \ln\phi \ln(1-S_{wi}) \ln k \\ + c_{13} \ln\phi \ln(1-S_{wi}) \ln p_d + c_{14} \ln\phi \ln k \ln p_d \\ + c_{15} \ln(1-S_{wi}) \ln k \ln p_d + c_{16} \ln(1-S_{wi}) \ln k \ln p_d \ln\phi \end{array}}{\begin{array}{l} 1 + c_{17} \ln p_d + c_{18} \ln k + c_{19} \ln(1-S_{wi}) \\ + c_{20} \ln\phi + c_{21} \ln p_d \ln k + c_{22} \ln p_d \ln(1-S_{wi}) \\ + c_{23} \ln p_d \ln\phi + c_{24} \ln k \ln\phi + c_{25} \ln k \ln(1-S_{wi}) \\ + c_{26} \ln\phi \ln(1-S_{wi}) + c_{27} \ln\phi \ln(1-S_{wi}) \ln k \\ + c_{28} \ln\phi \ln(1-S_{wi}) \ln p_d + c_{29} \ln\phi \ln k \ln p_d \\ + c_{30} \ln(1-S_{wi}) \ln k \ln p_d + c_{31} \ln(1-S_{wi}) \ln k \ln p_d \ln\phi \end{array}}\right] \quad \text{...} \quad (G.9)$$

Table G.5 – Regression Summary for Pore Geometric Factor (λ) — Model 5.

Optimized coefficients for λ (*Eq.* G.9):

Coefficient	Optimized Value	Coefficient	Optimized Value
c_1	0.1510	c_{17}	-0.1925
c_2	-0.0184	c_{18}	-0.0656
c_3	-0.0009	c_{19}	-0.0934
c_4	0.0285	c_{20}	0.4324
c_5	0.0301	c_{21}	-0.0012
c_6	-0.0011	c_{22}	0.1501
c_7	0.0573	c_{23}	-0.0834
c_8	0.0003	c_{24}	0.2989
c_9	0.0312	c_{25}	-0.0274
c_{10}	0.0074	c_{26}	0.2394
c_{11}	0.1425	c_{27}	-0.0551
c_{12}	0.0162	c_{28}	-0.0585
c_{13}	-0.0007	c_{29}	-0.0013
c_{14}	0.0005	c_{30}	0.2336
c_{15}	0.0848	c_{31}	-0.0467
c_{16}	-0.0038		

Statistical summary for λ (*Eq.* G.9):

Statistical Variable	Value
Sum of Squared Residuals	0.7762
Variance	0.2076
Standard Deviation	0.4457
Average Absolute Error	16.6527 percent

Substituting the coefficients in **Table G.5** into Eq. G.9, we have:

$$\lambda = \exp\left[\frac{\begin{array}{l} 0.1510 - 0.0184\ln p_d - 0.0009\ln k + 0.0285\ln(1-S_{wi}) \\ +0.0301\ln\phi - 0.0011\ln p_d\ \ln k + 0.0573\ln p_d\ \ln(1-S_{wi}) \\ +0.0003\ln p_d\ \ln\phi + 0.0312\ln k\ln\phi + 0.0074\ln k\ln(1-S_{wi}) \\ +0.1425\ln\phi\ln(1-S_{wi}) + 0.01620\ln\phi\ln(1-S_{wi})\ln k \\ -0.0007\ln\phi\ln(1-S_{wi})\ln p_d + 0.0005\ln\phi\ln k\ln p_d \\ +0.0848\ln(1-S_{wi})\ln k\ln p_d - 0.0038\ln(1-S_{wi})\ln k\ln p_d\ \ln\phi \end{array}}{\begin{array}{l} 1 - 0.1925\ln p_d - 0.0656\ln k - 0.0934\ln(1-S_{wi}) \\ +0.4324\ln\phi - 0.0012\ln p_d\ \ln k + 0.1501\ln p_d\ \ln(1-S_{wi}) \\ -0.0834\ln p_d\ \ln\phi + 0.2989\ln k\ln\phi - 0.0274\ln k\ln(1-S_{wi}) \\ +0.2394\ln\phi\ln(1-S_{wi}) - 0.0551\ln\phi\ln(1-S_{wi})\ln k \\ -0.0585\ln\phi\ln(1-S_{wi})\ln p_d - 0.0013\ln\phi\ln k\ln p_d \\ +0.2336\ln(1-S_{wi})\ln k\ln p_d - 0.0467\ln(1-S_{wi})\ln k\ln p_d\ \ln\phi \end{array}}\right] \quad \text{.................................. (G.10)}$$

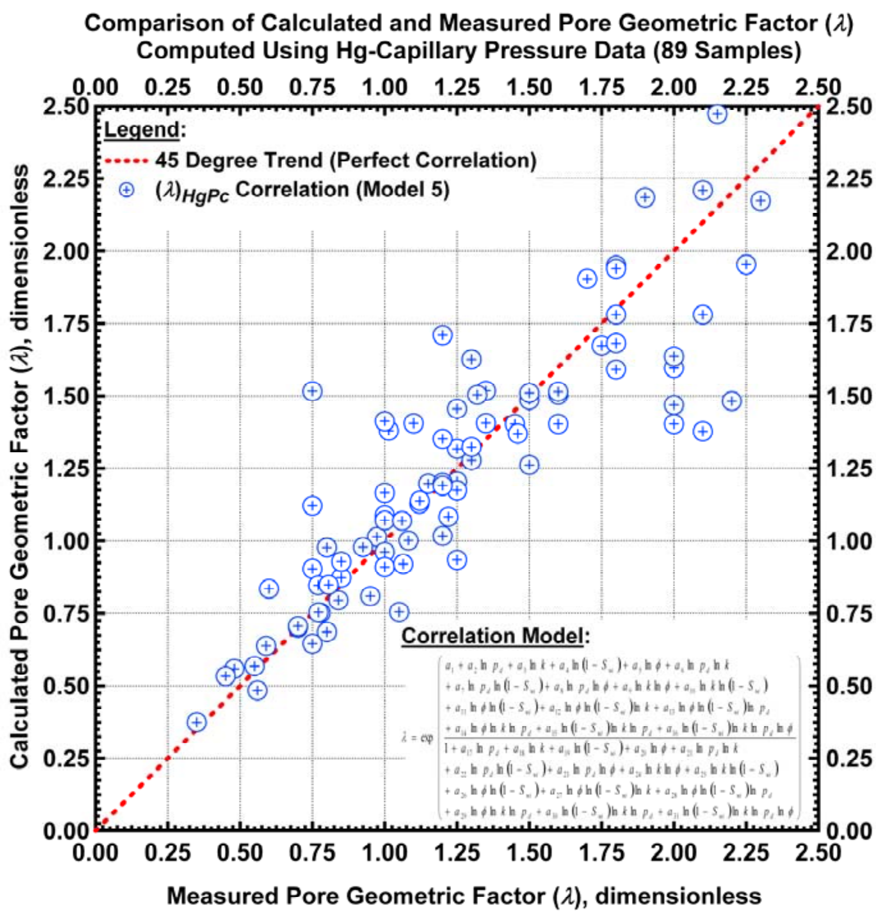

Figure G.5 – Pore geometric factor (λ) correlation based on mercury capillary pressure data (Eq. G.9 used for regression).

References

G.1. Brooks, R.H., and Corey A.T.: "Hydraulic Properties of Porous Media," Hydrol. Paper 3, Colo. State Univ., Fort Collins, CO, 1964.

Nomenclature

k	=	permeability, md
p_d	=	displacement pressure, psi
p_c	=	capillary pressure, psi
S_{wi}	=	irreducible saturation, fraction
S_w	=	water saturation in the actual porous medium, fraction
λ	=	index of pore-size distribution
ϕ	=	porosity

APPENDIX H
NON-PARAMETRIC REGRESSIONS
DERIVED FROM THE DATA IN THIS WORK

The non-parametric correlation is the optimal fit of the data — this is not a "model-based" regression, but a point-by-point correlation of the data[H1-H8]. And we note that any (model-based) regression that achieves a better fit than the non-parametric regression algorithm has fitted the errors in the data.

Non-Parametric Regression for Permeability

Table H.1 – Statistical summary for k

Statistical Variable	Value
Sum of Squared Residuals	1.1395 $\ln(\text{md})^2$
Variance	1188906.8074 md^2
Standard Deviation	1090.3700 md
Average Absolute Error	18.9947 percent

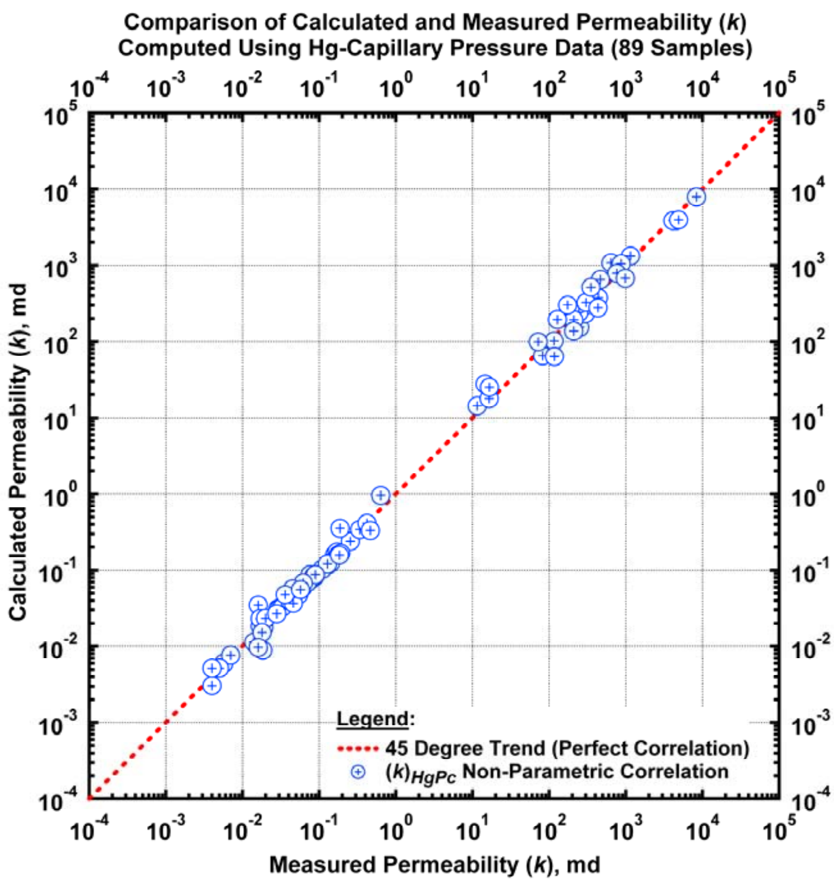

Figure H.1 – Non-parametric correlation for permeability based on mercury p_c data.

Non-Parametric Regression for the Displacement Pressure (mercury capillary pressure data)

Table H.2 – Statistical summary for p_d

Statistical Variable	Value
Sum of Squared Residuals	0.5401 ln(psia)^2
Variance	124402.6310 psia^2
Standard Deviation	352.7076 psia
Average Absolute Error	13.9832 percent

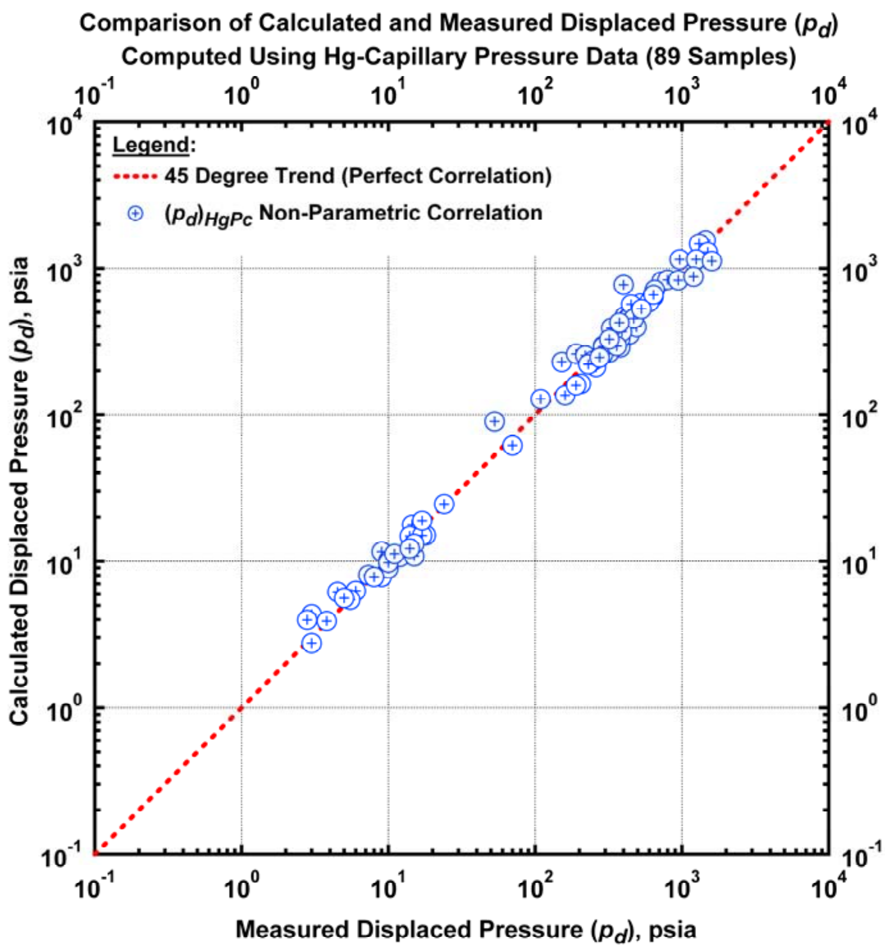

Figure H.2 – Non-parametric correlation for displacement pressure (p_d) based on mercury p_c data.

Non-Parametric Regression for the Pore Geometric Factor (mercury capillary pressure data)

Table H.3 – Statistical summary for λ

Statistical Variable	Value
Sum of Squared Residuals	0.7305
Variance	0.1766
Standard Deviation	0.4202
Average Absolute Error	15.2642 percent

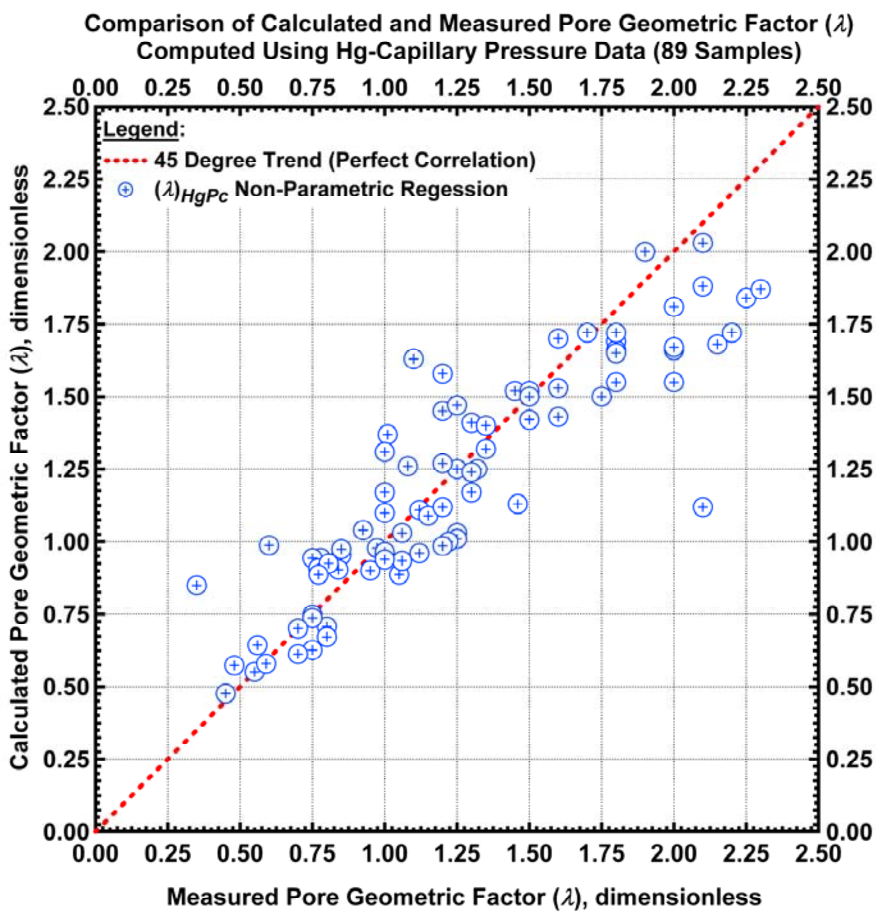

Figure H.3 – Non-parametric correlation for pore geometric factor (λ) based on mercury p_c data.

References

H.1.Breinan, L. and Friedman, J.: "Estimation Optimal Transformations for Multiple Regression and Correlation," *Journal of the American Statistical Association*, Vol. 80, No.391 (Sept. 1985).

H.2. Breinan, L. and Meisel, W.S.: "General Estimates of the Intrinsic Variability of Data in Nonlinear Regression Models," *Journal of the American Statistical Association*, Vol. 71, No.354 (Jun. 1976).

H.3.Breinan, L. and Freedman, D.: "How Many Variables Should be Entered in a Regression Equation?," *Journal of the American Statistical Association*, Vol. 78, No.381 (Mar. 1983).

H.4. Emerson, J.D. and Stoto, M.A.: "Choosing a Symmetrizing Power Transformation: Rejoinder," *Journal of the American Statistical Association*, Vol. 79, No.385 (Mar. 1984).

H.5. Emerson, J.D. and Stoto, M.A.: "Exploratory Methods for Choosing Power Transformations," *Journal of the American Statistical Association*, Vol. 77, No.377 (Mar. 1982).

H.6. Stoto, M.A.: "The Accuracy of Population Projections," *Journal of the American Statistical Association*, Vol. 78, No.381 (Mar. 1983).

H.7. Wang, D. and Murphy, M.: "Estimating Optimal Transformations for Multiple Regression Using the ACE Algorithm," *Journal of Data Science*, Vol. 2, (Mar. 2004), 329-346.

H.8. Xue, G. et *al.*: "Optimal Transformations for Multiple Regression: Application to Permeability Estimation from Well Logs," SPE 35412 presented at the Improved Oil Recovery Symposium held in Tulsa, Oklahoma, 21 April 1996.

Nomenclature

k	=	permeability, md
p_d	=	displacement pressure, psi
p_c	=	capillary pressure, psi
λ	=	index of pore-size distribution

APPENDIX I

LIBRARY OF CAPILLARY PRESSURE VERSUS WETTING PHASE SATURATION PLOTS — CARTESIAN CAPILLARY PRESSURE FORMAT

To calibrate the proposed power models, we have used mercury-injection capillary-pressure data .
This Appendix presents the calibration of the capillary displacement pressure (p_d), irreducible wetting-phase saturation (S_{wi}), and the index of pore-size distribution (λ) on a sample-by-sample basis using the Brooks-Corey $p_c(S_w)$ model .
In this Appendix, we provide for each data a plot of capillary pressure (p_c) vs. wetting phase saturation (S_w).

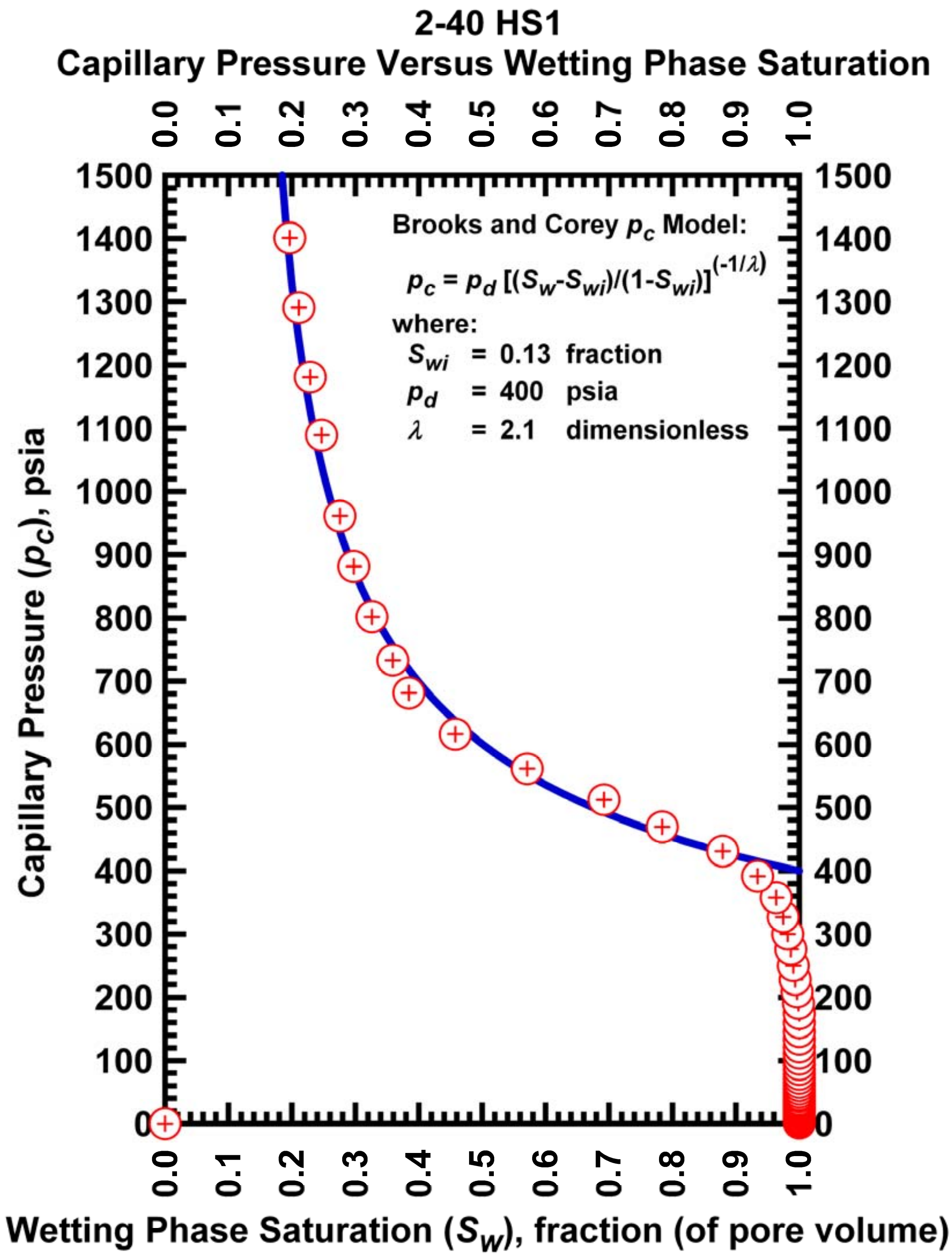

Figure I.1 — Plot of capillary pressure (p_c) vs. wetting phase saturation (S_w) — Case 2-40 HS1.

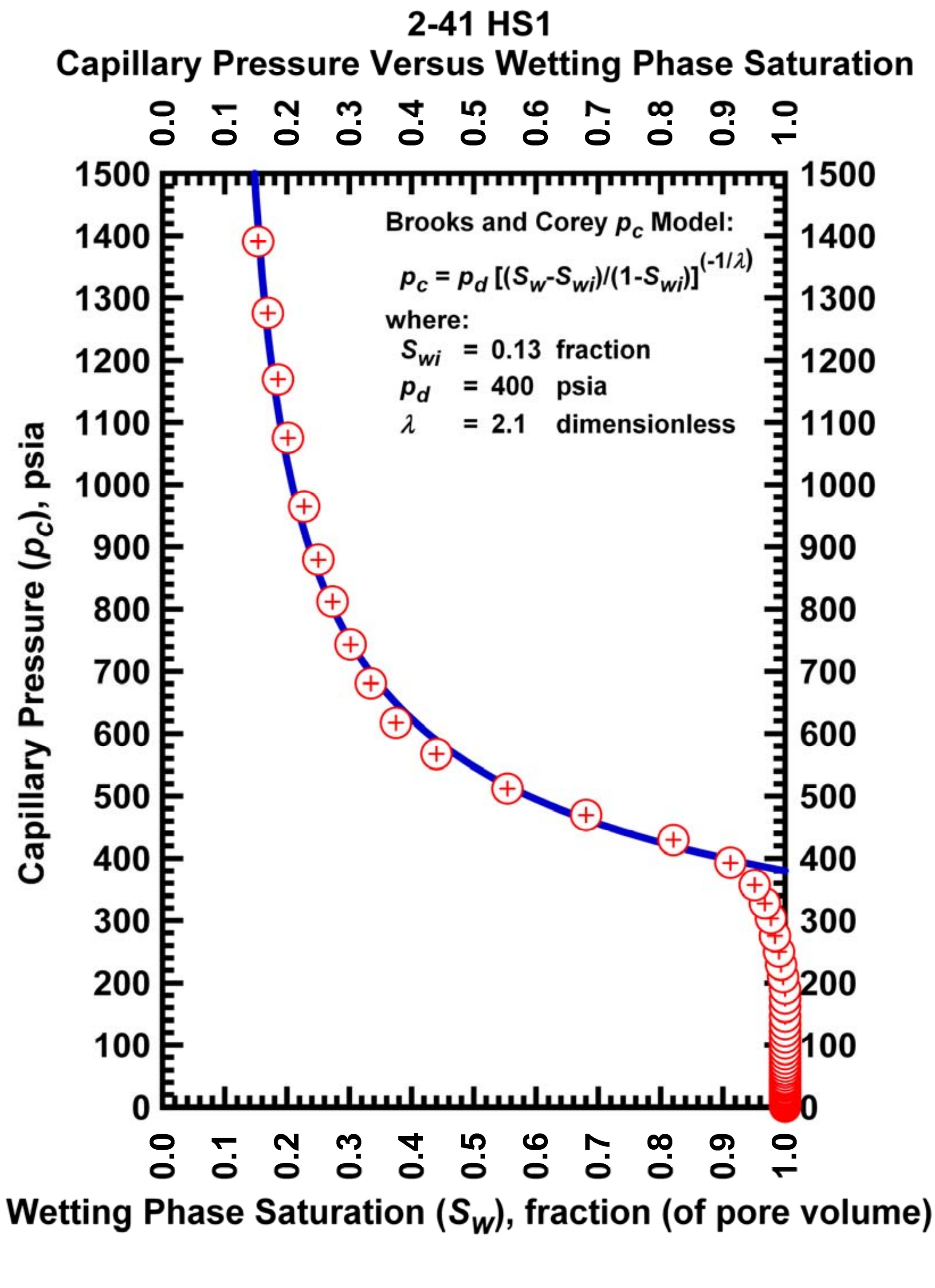

Figure I.2— Plot of capillary pressure (p_c) vs. wetting phase saturation (S_w) — Case 2-41 HS1.

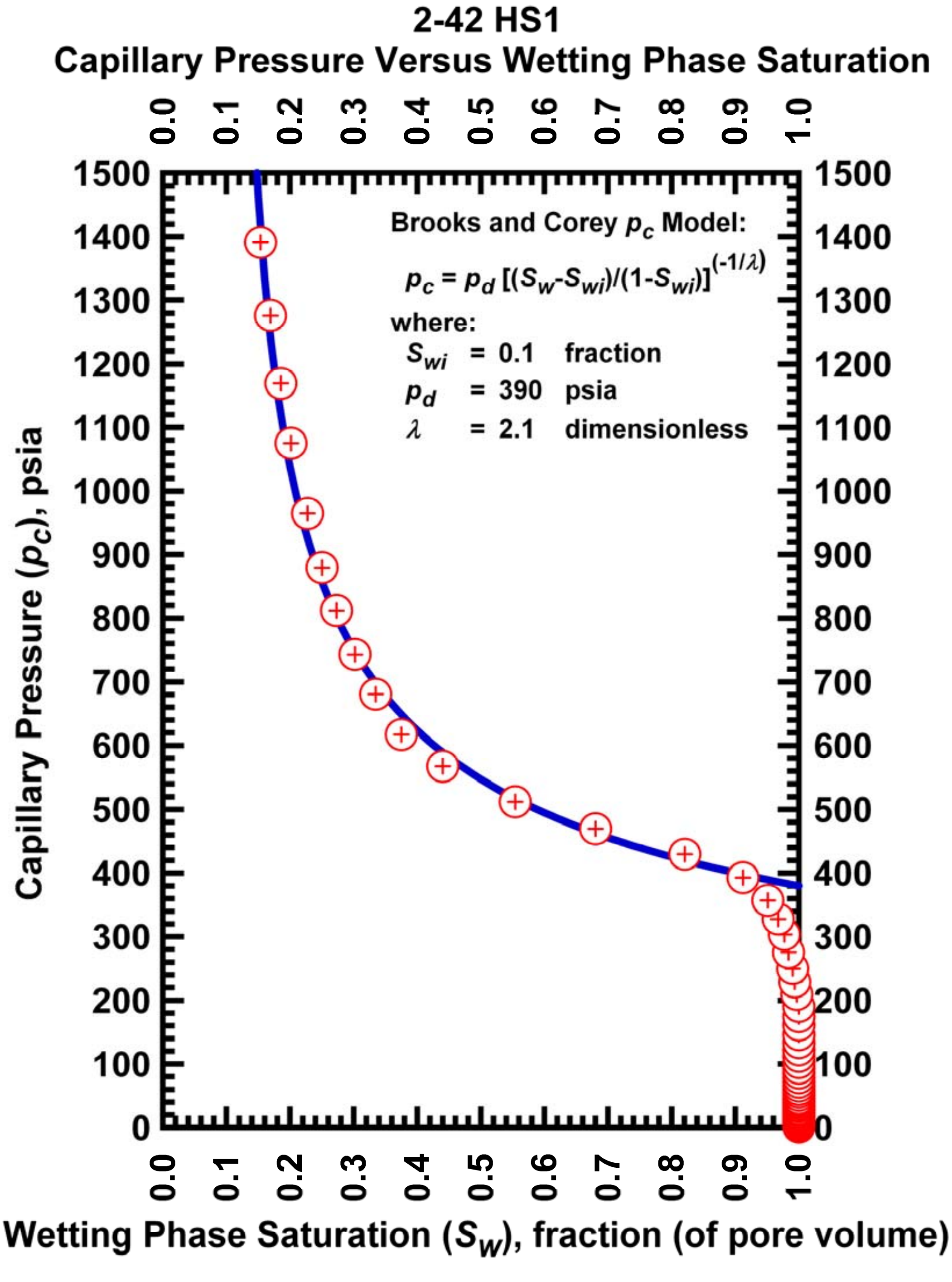

Figure I.3 — Plot of capillary pressure (p_c) vs. wetting phase saturation (S_w) — Case 2-42 HS1.

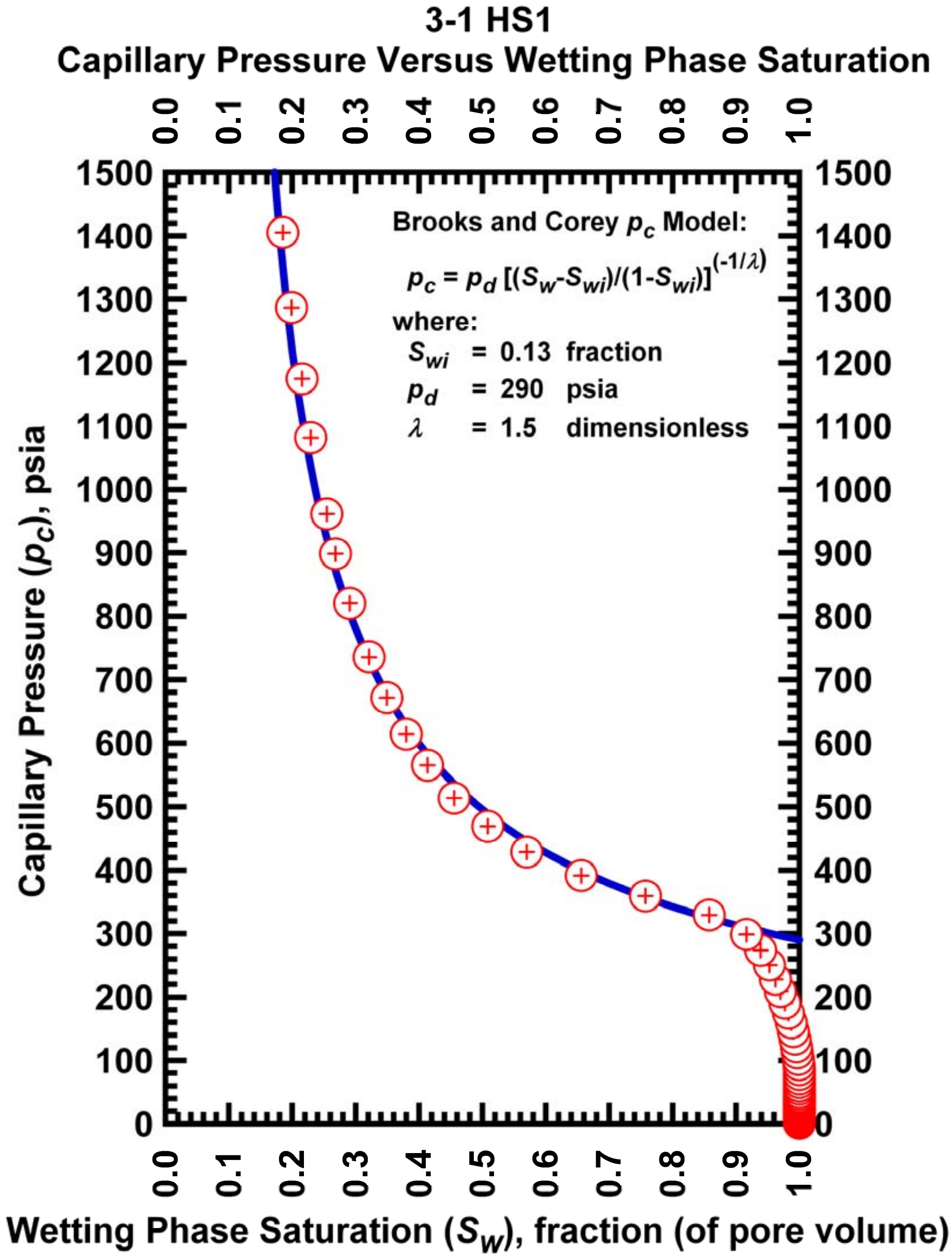

Figure I.4 — Plot of capillary pressure (p_c) vs. wetting phase saturation (S_w) — Case 3-1 HS1.

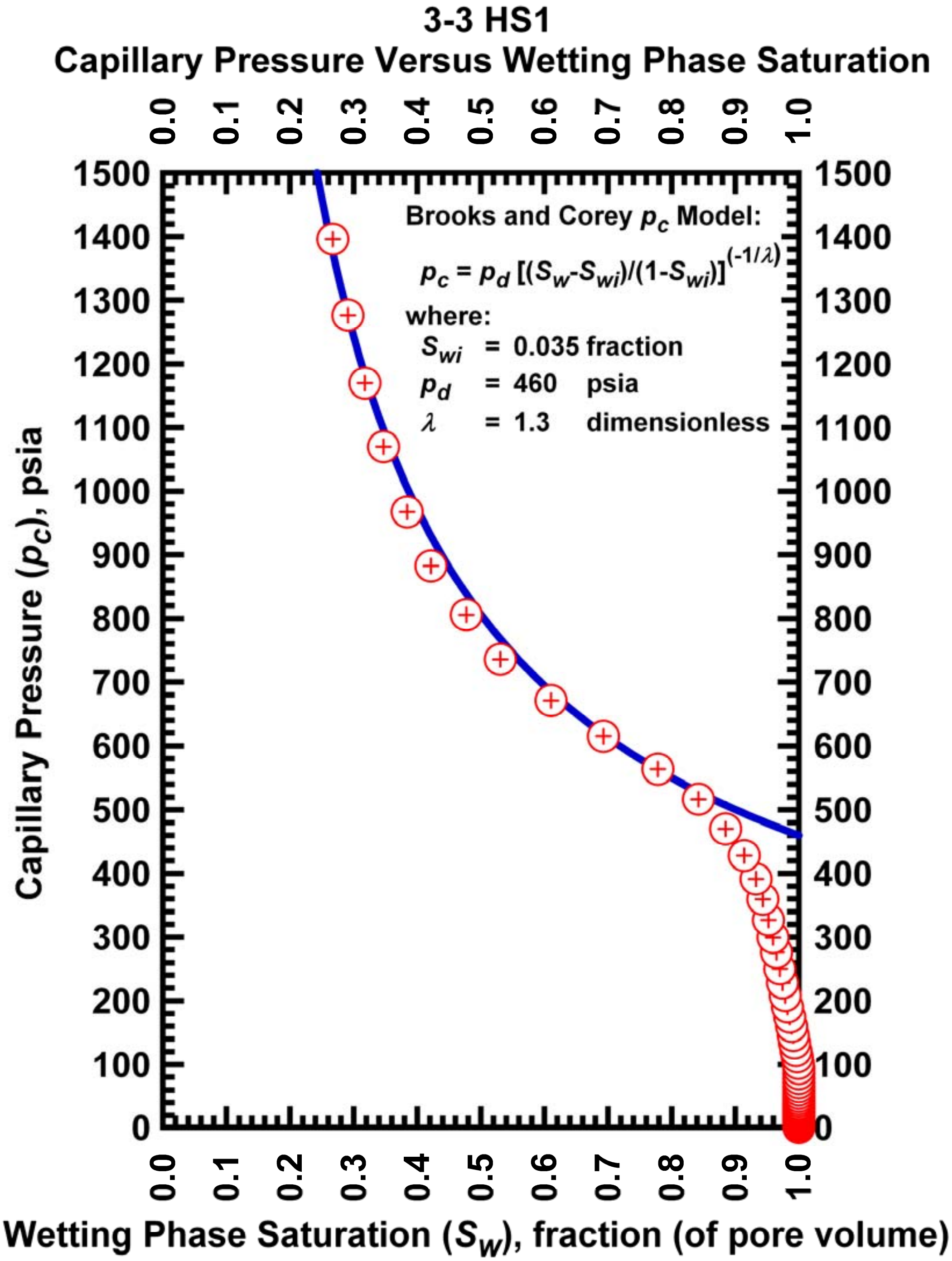

Figure I.5 — Plot of capillary pressure (p_c) vs. wetting phase saturation (S_w) — Case 3-3 HS1.

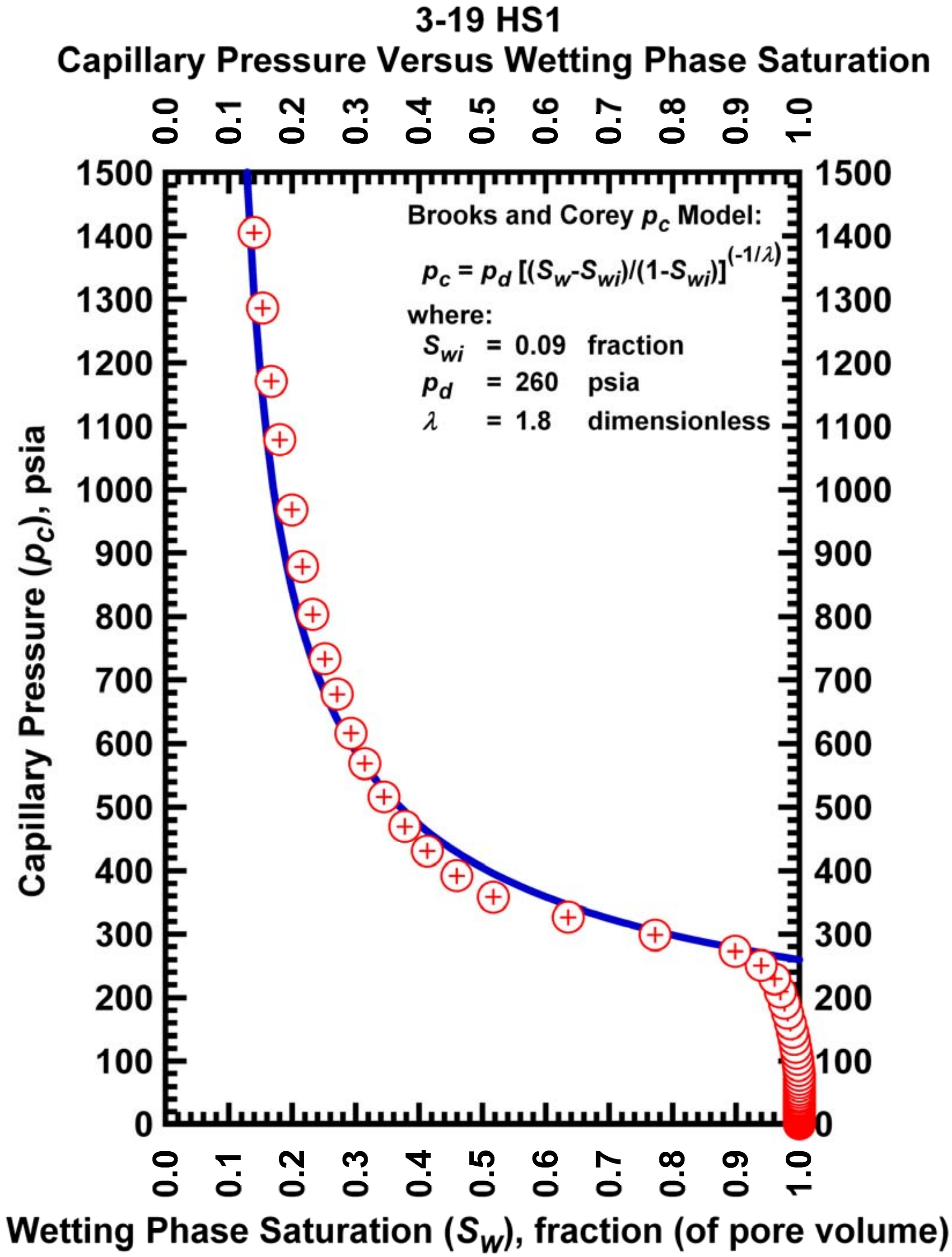

Figure I.6 — Plot of capillary pressure (p_c) vs. wetting phase saturation (S_w) — Case 3-19 HS1.

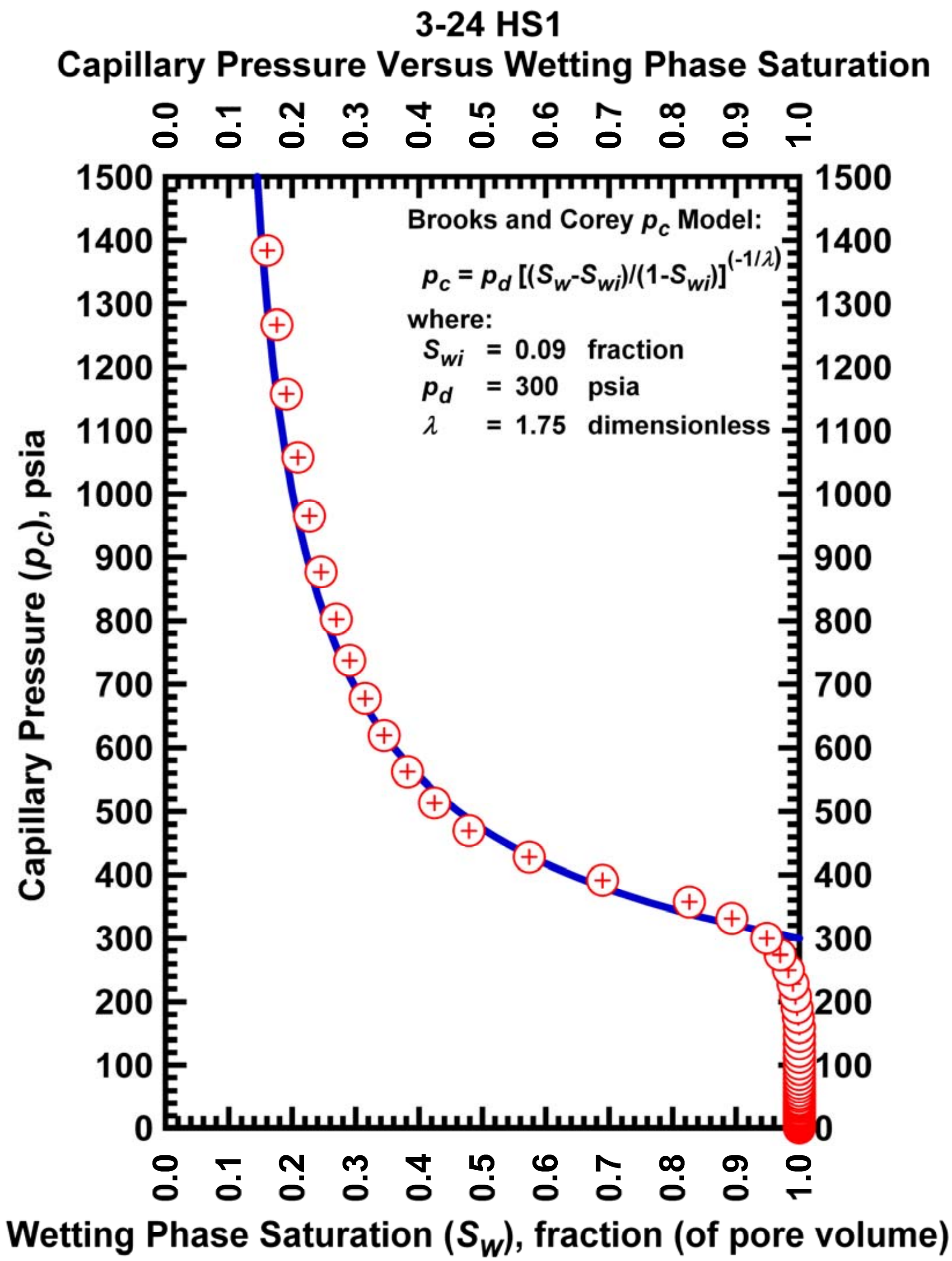

Figure I.7 — Plot of capillary pressure (p_c) vs. wetting phase saturation (S_w) — Case 3-24 HS1.

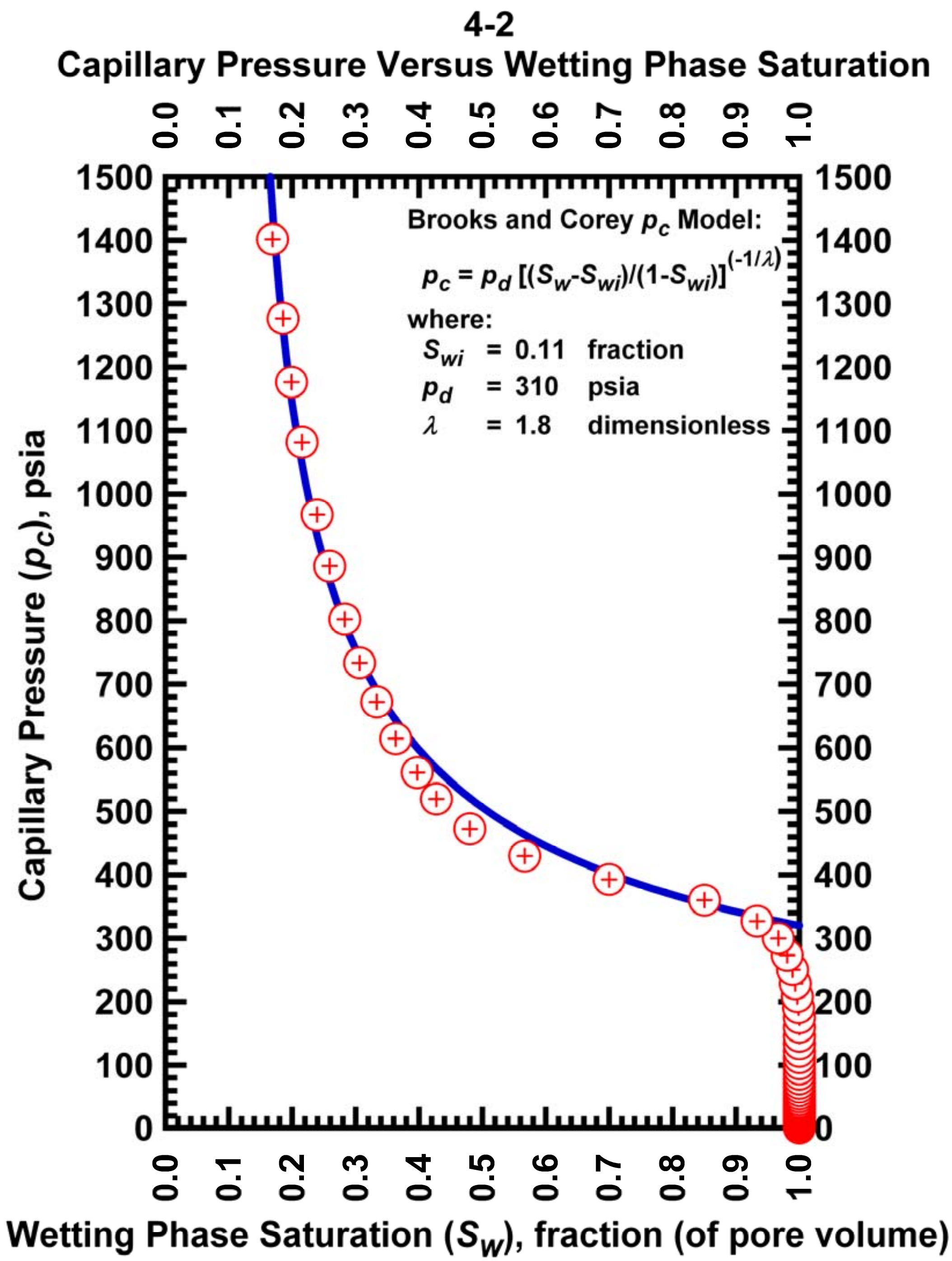

Figure I.8 — Plot of capillary pressure (p_c) vs. wetting phase saturation (S_w) — Case 4-2 HS1.

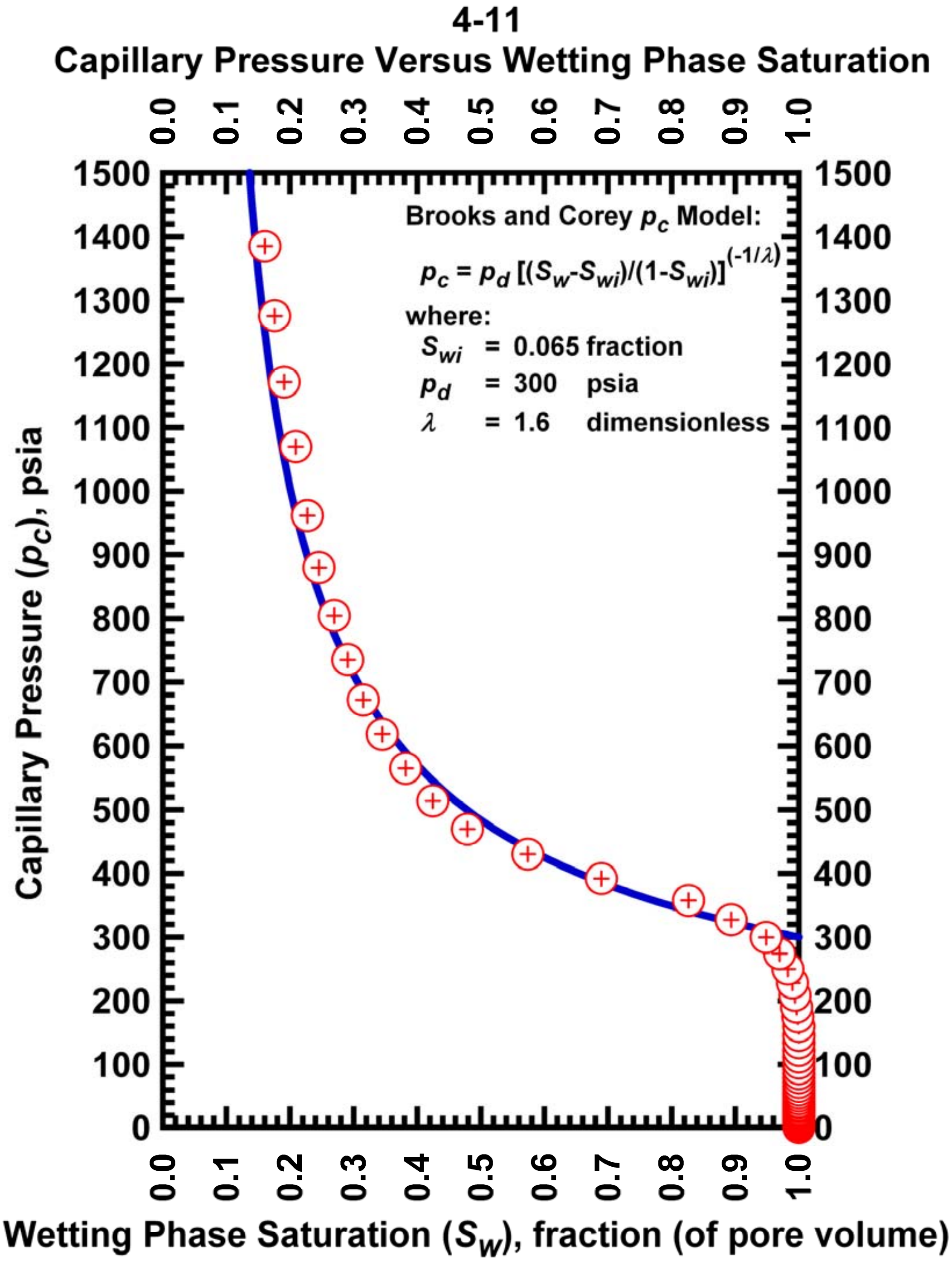

Figure I.9 — Plot of capillary pressure (p_c) vs. wetting phase saturation (S_w) — Case 4-11 HS1.

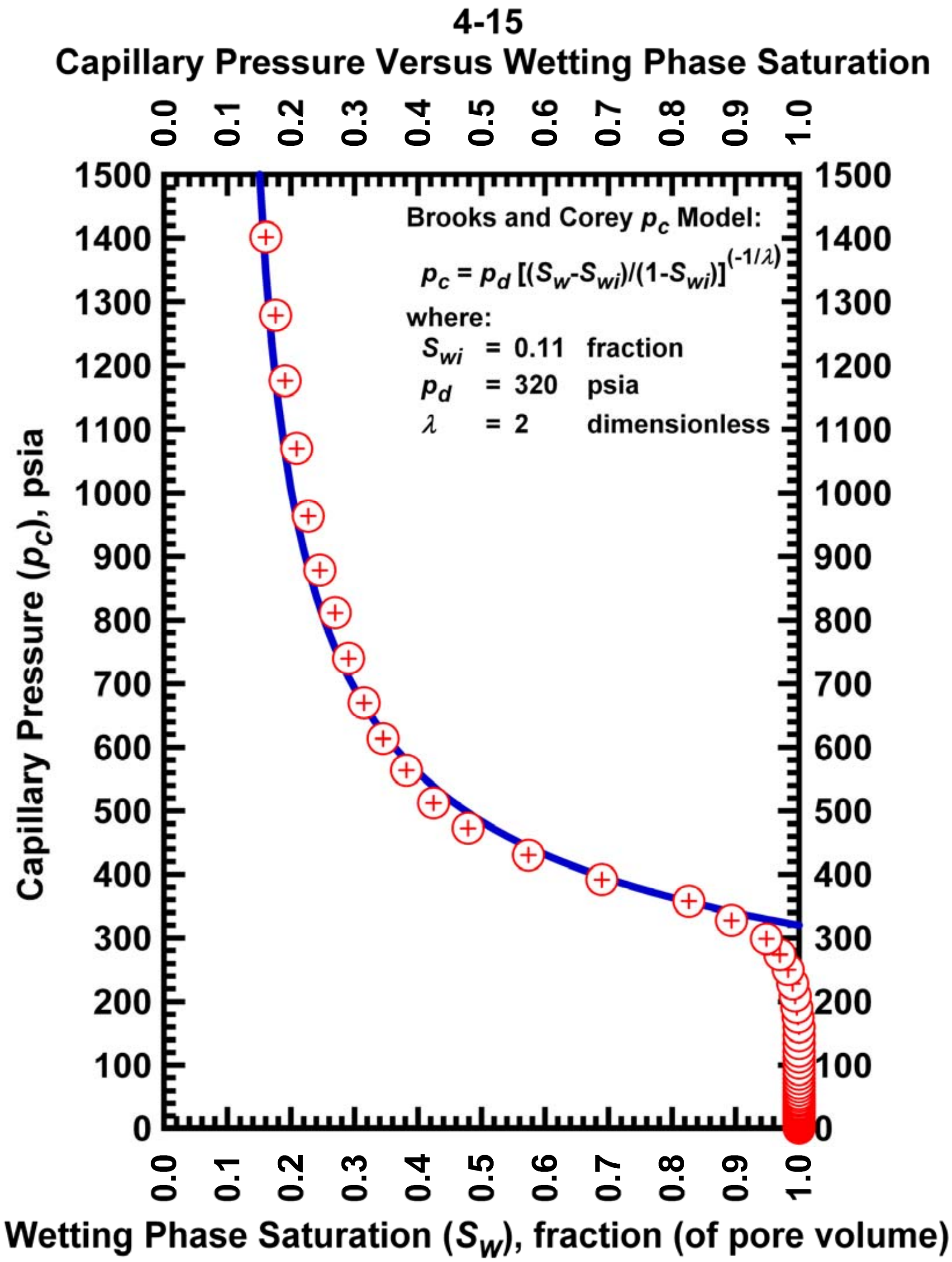

Figure I.10 — Plot of capillary pressure (p_c) vs. wetting phase saturation (S_w) — Case 4-15 HS1.

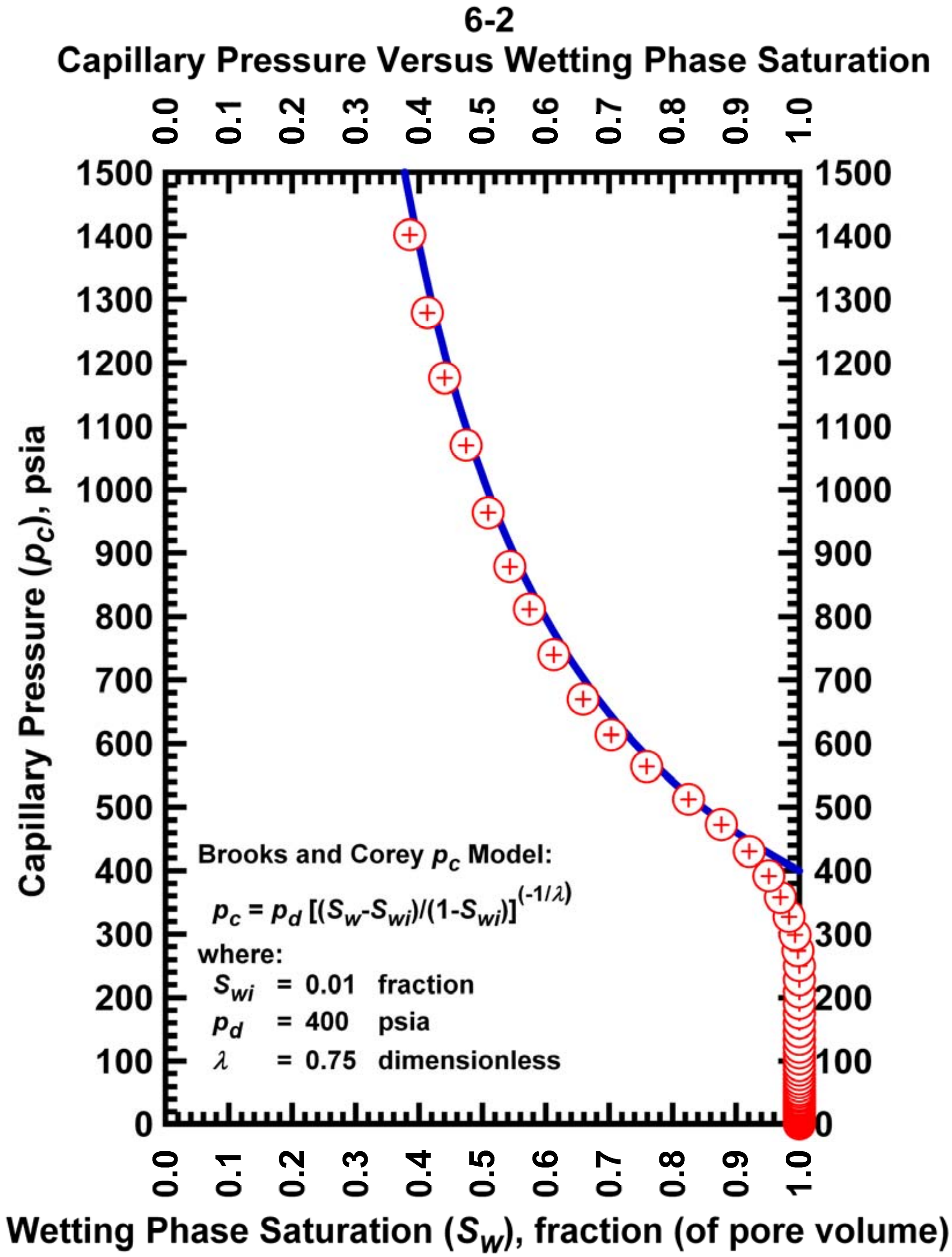

Figure I.11 — Plot of capillary pressure (p_c) vs. wetting phase saturation (S_w) — Case 6-2 HS1.

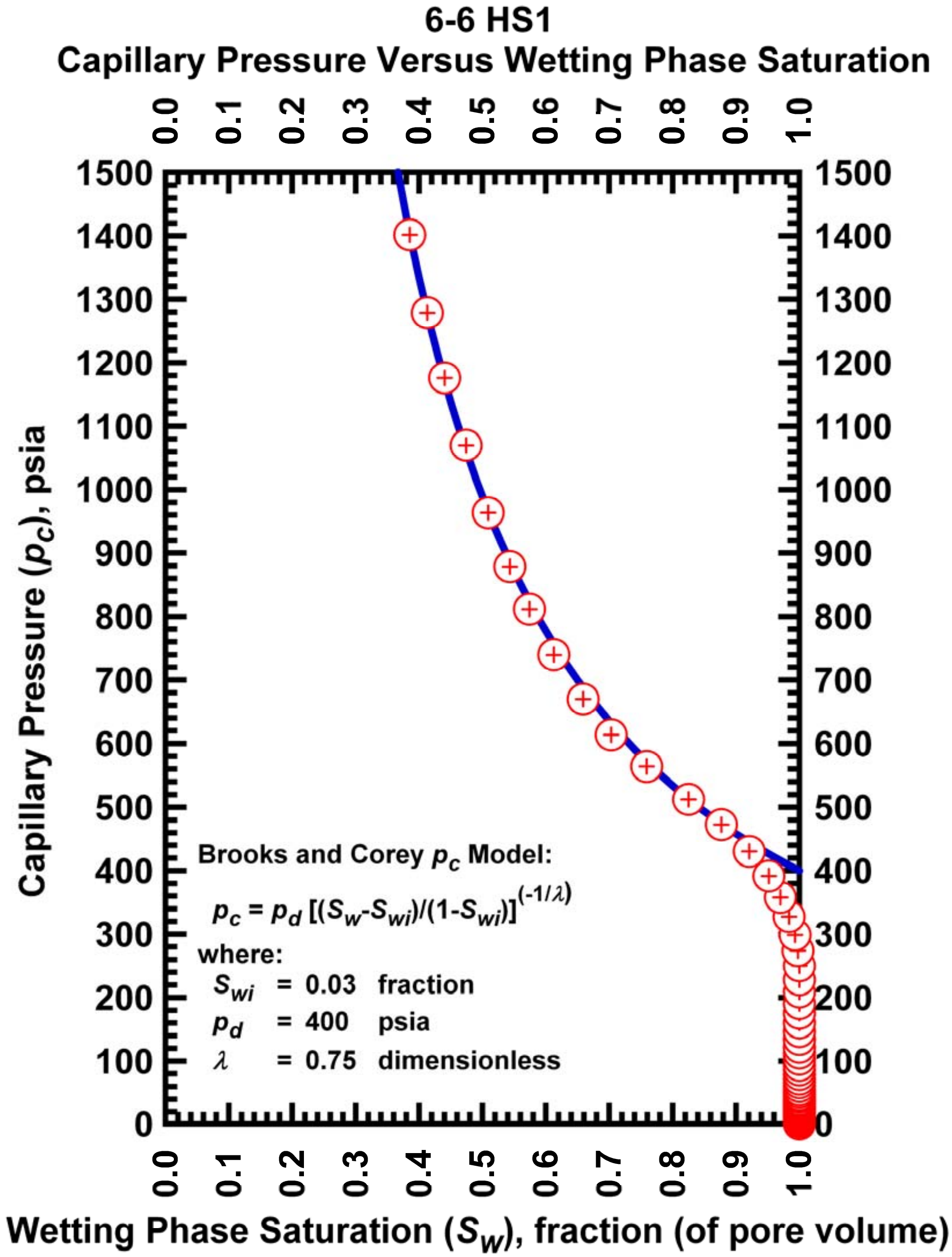

Figure I.12 — Plot of capillary pressure (p_c) vs. wetting phase saturation (S_w) — Case 6-6 HS1.

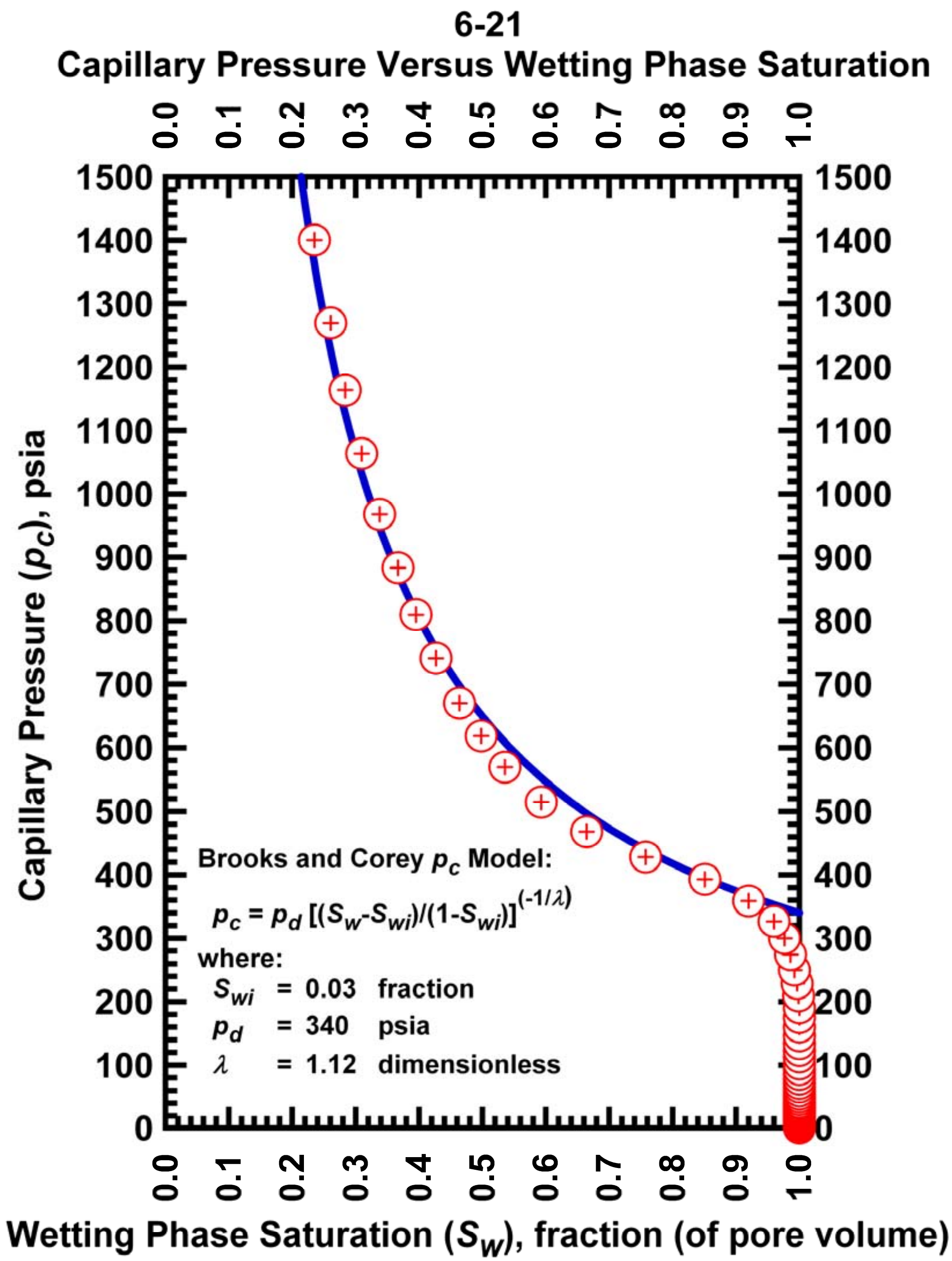

Figure I.13 — Plot of capillary pressure (p_c) vs. wetting phase saturation (S_w) — Case 6-21 HS1.

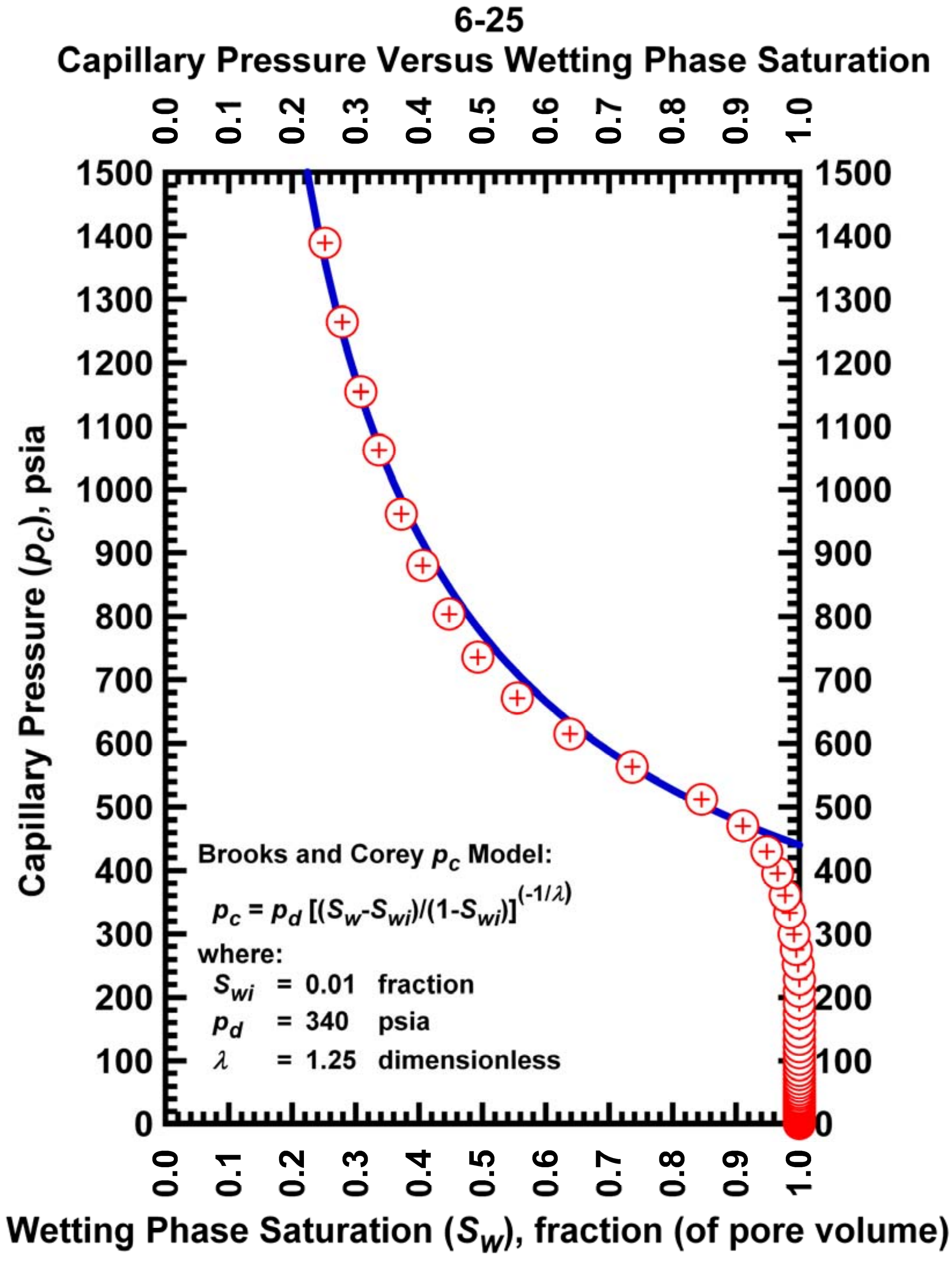

Figure I.14 — Plot of capillary pressure (p_c) vs. wetting phase saturation (S_w) — Case 6-25 HS1.

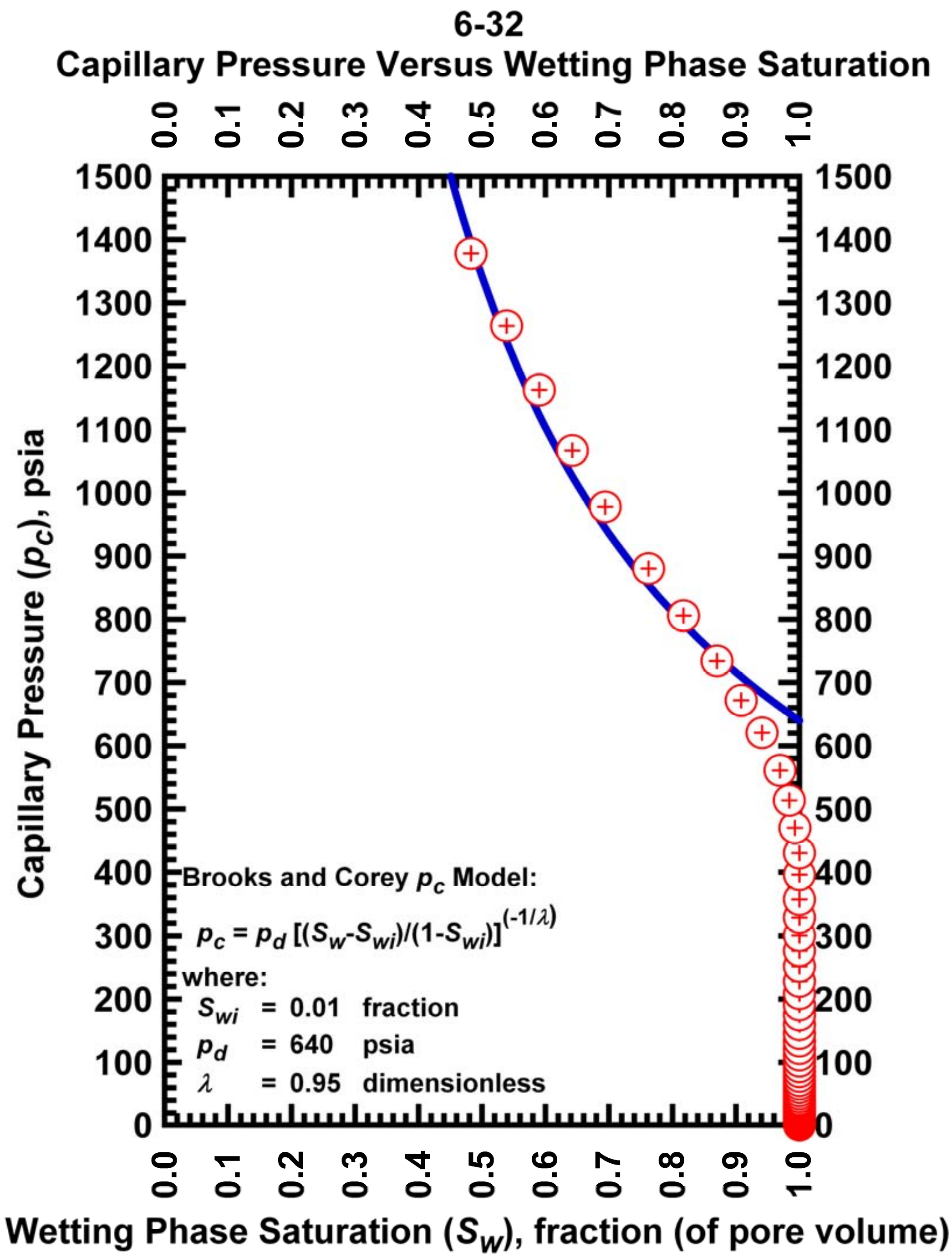

Figure I.15 — Plot of capillary pressure (p_c) vs. wetting phase saturation (S_w) — Case 6-32 HS1.

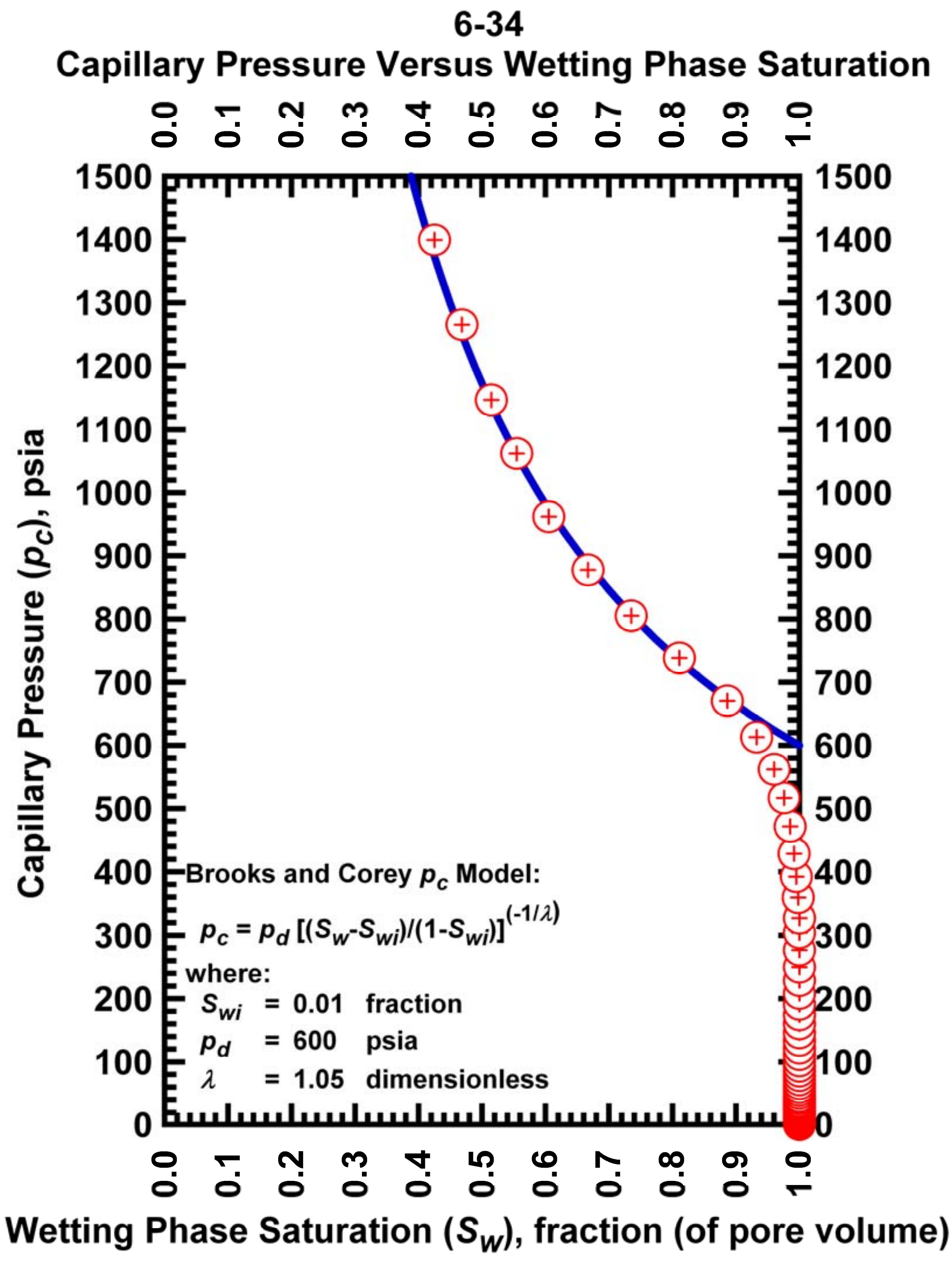

Figure I.16 — Plot of capillary pressure (p_c) vs. wetting phase saturation (S_w) — Case 6-34 HS1.

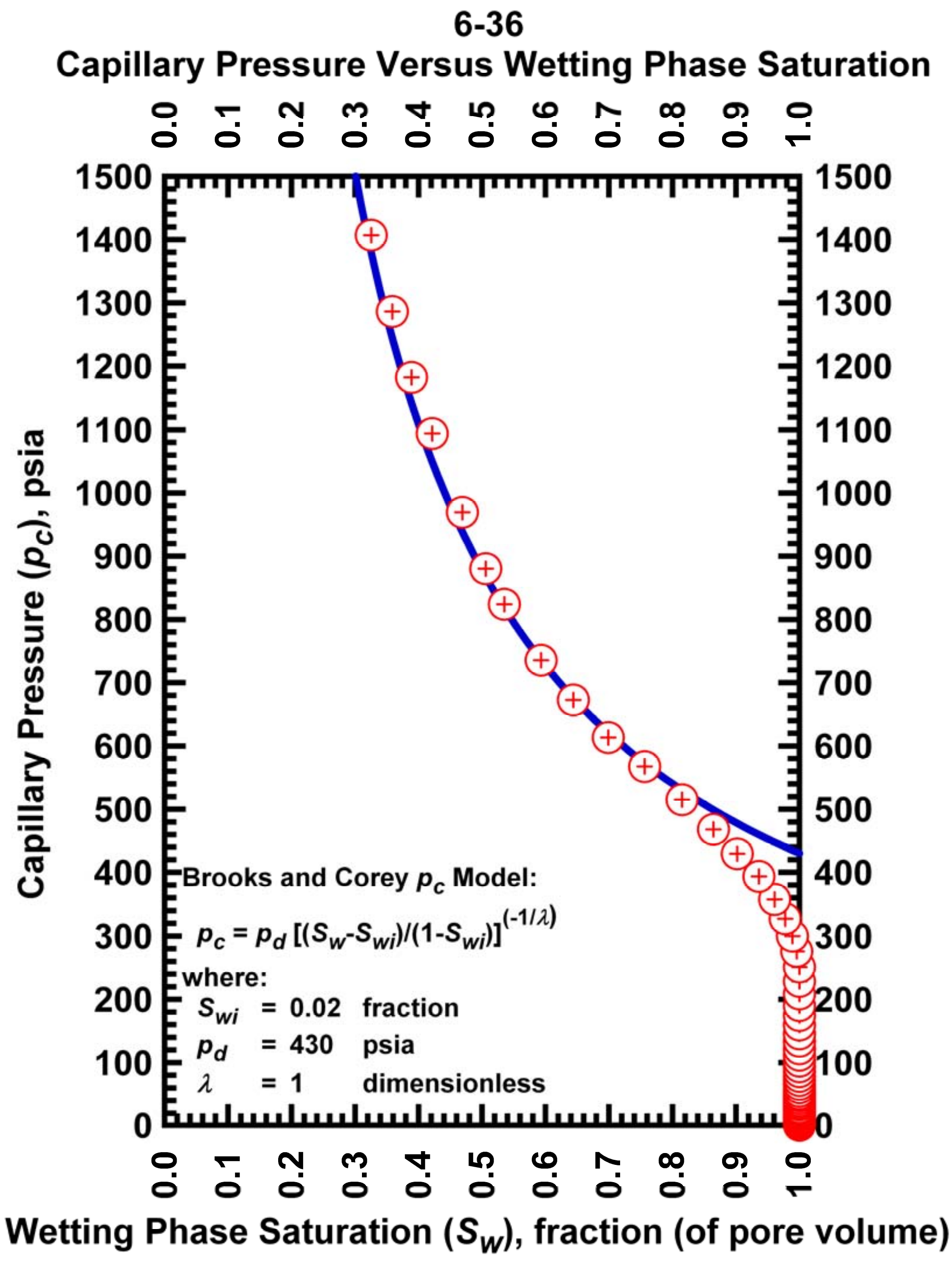

Figure I.17 — Plot of capillary pressure (p_c) vs. wetting phase saturation (S_w) — Case 6-36 HS1.

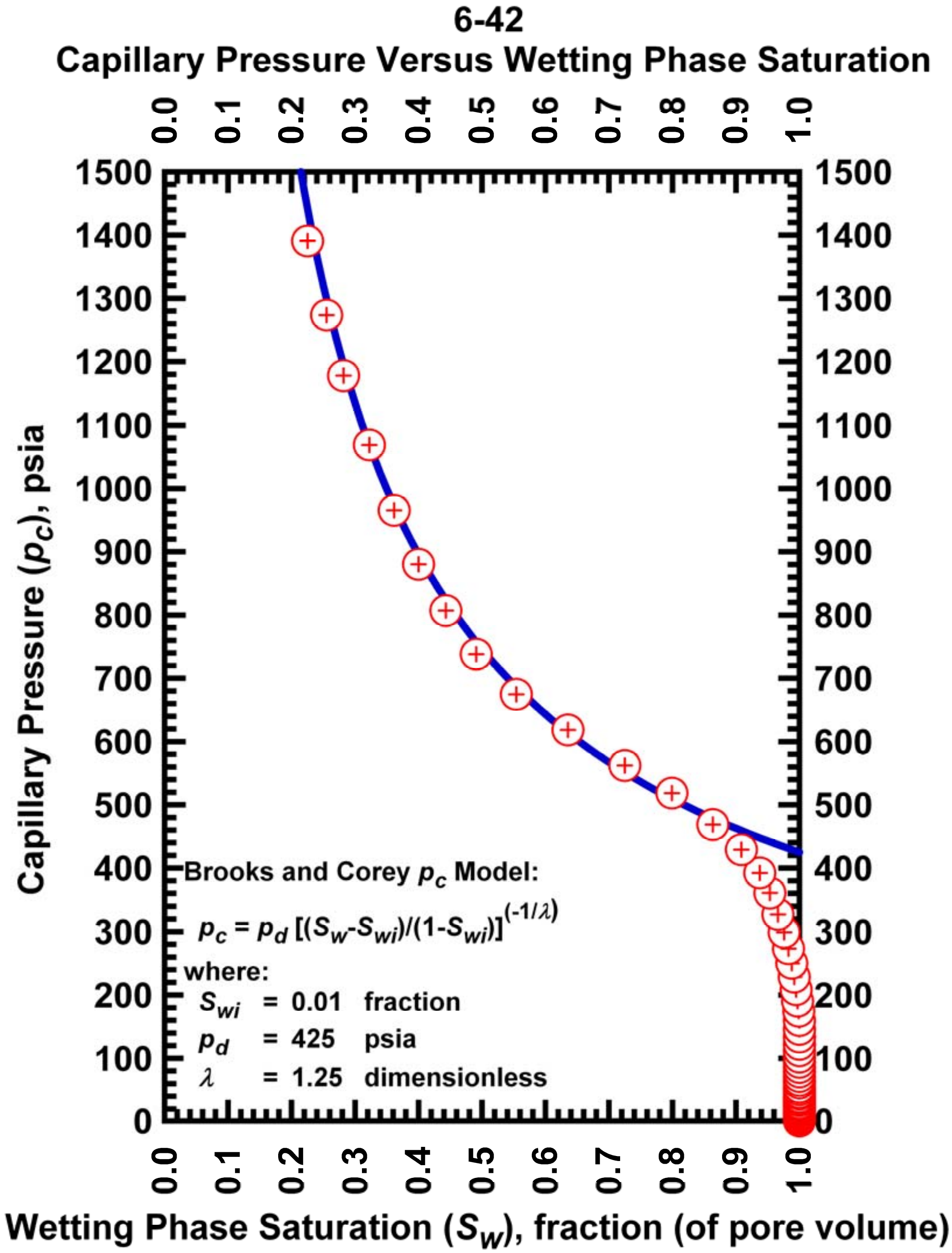

Figure I.18 — Plot of capillary pressure (p_c) vs. wetting phase saturation (S_w) — Case 6-42 HS1.

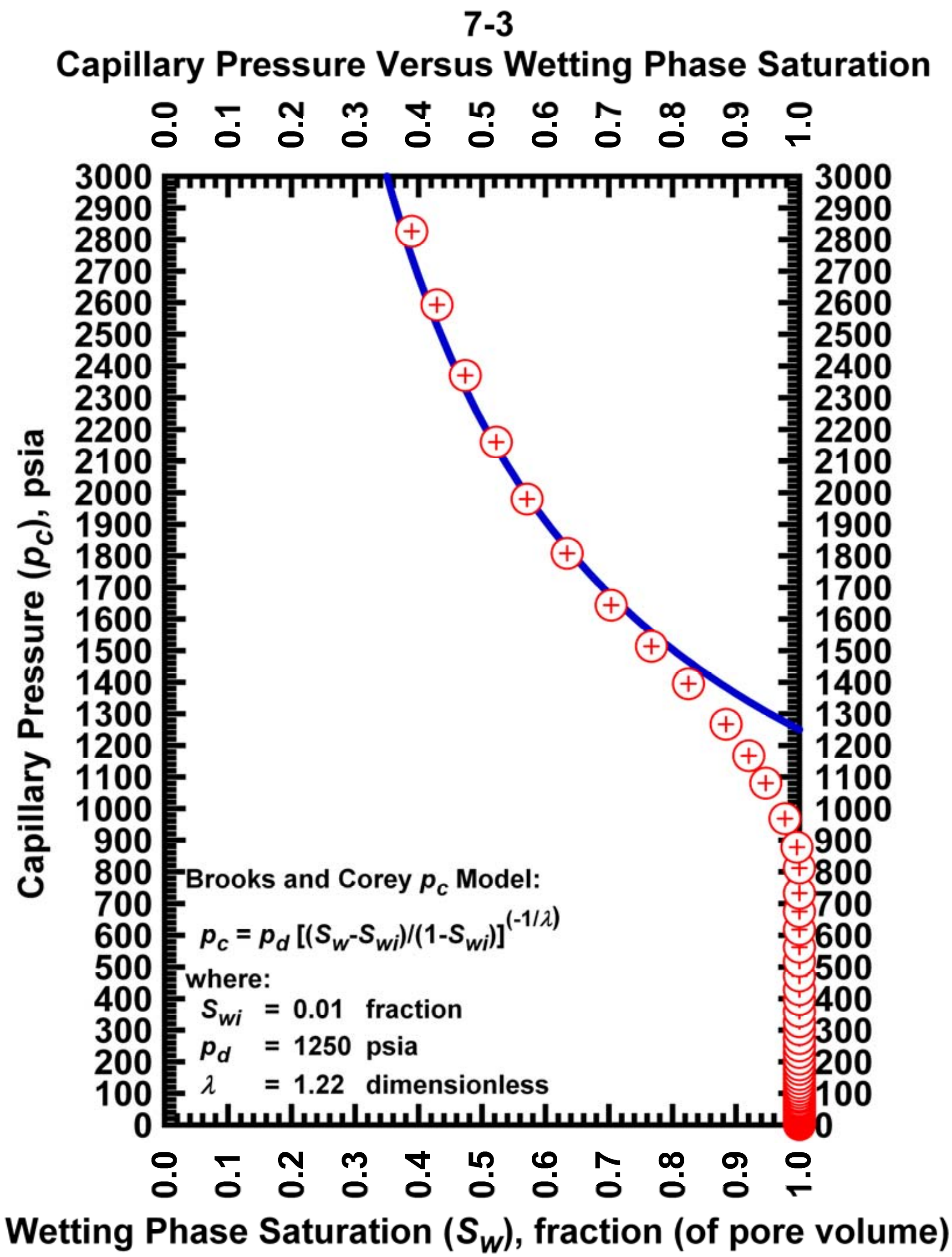

Figure I.19 — Plot of capillary pressure (p_c) vs. wetting phase saturation (S_w) — Case 7-3 HS1.

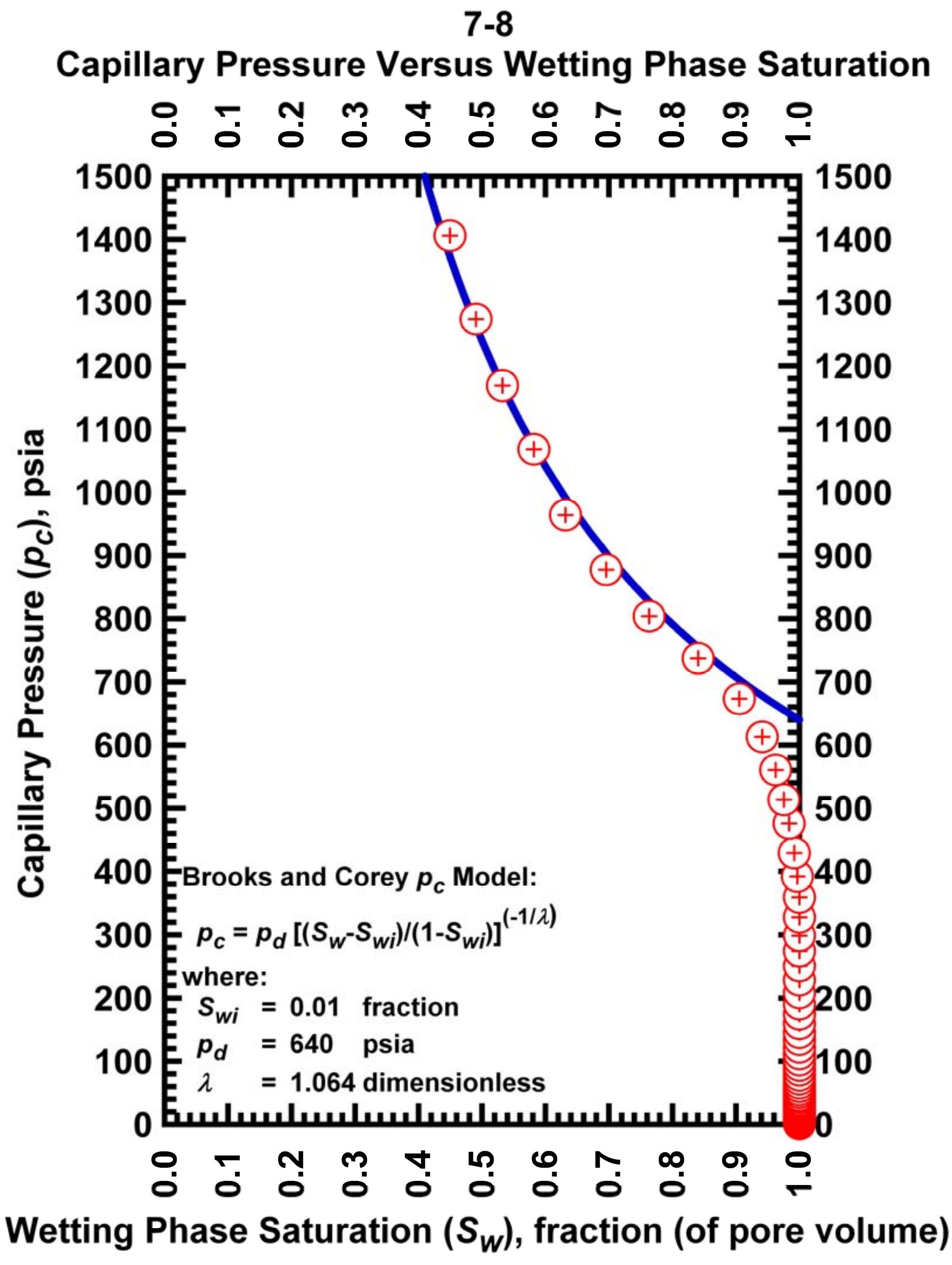

Figure I.20 — Plot of capillary pressure (p_c) vs. wetting phase saturation (S_w) — Case 7-8 HS1.

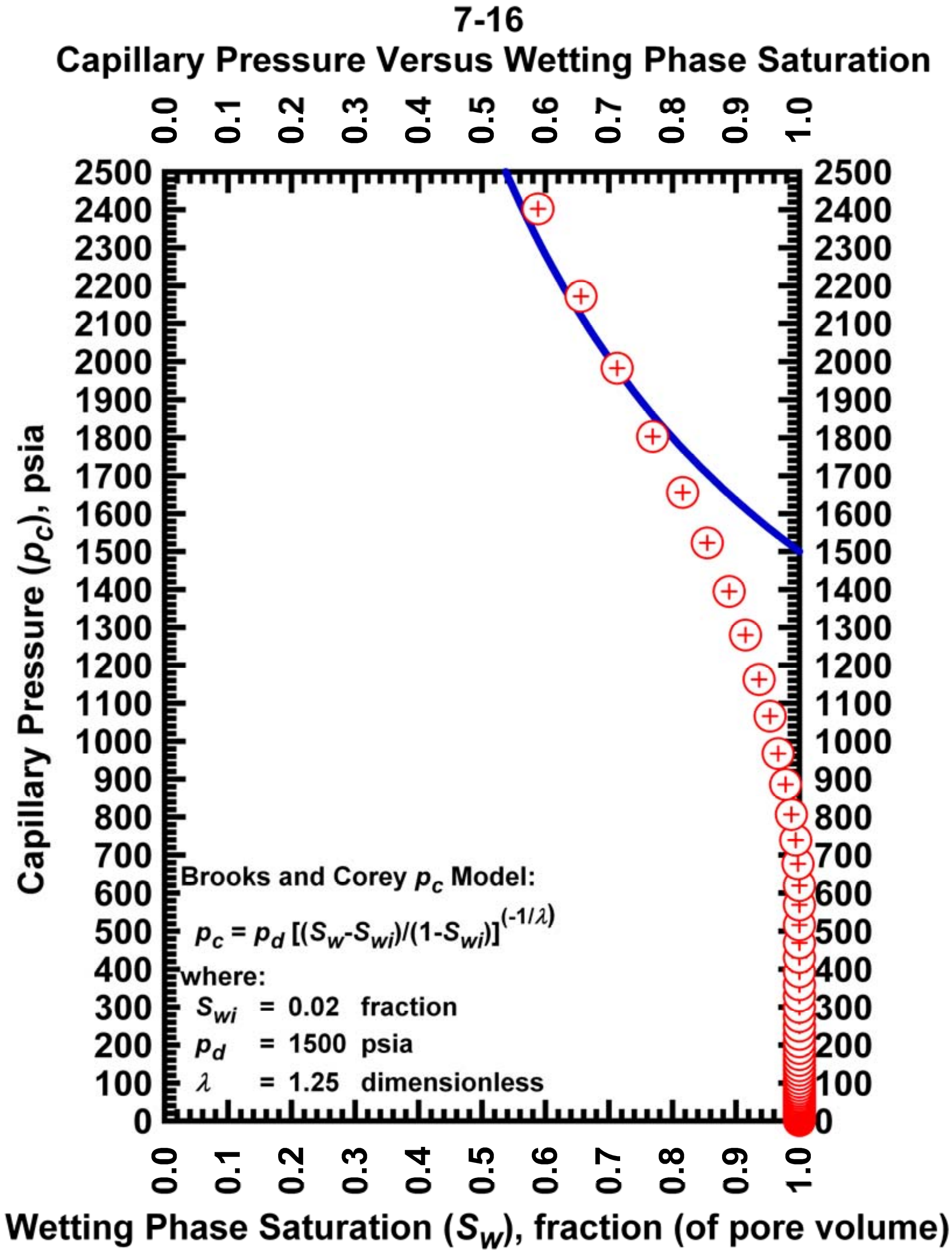

Figure I.21 — Plot of capillary pressure (p_c) vs. wetting phase saturation (S_w) — Case 7-16 HS1.

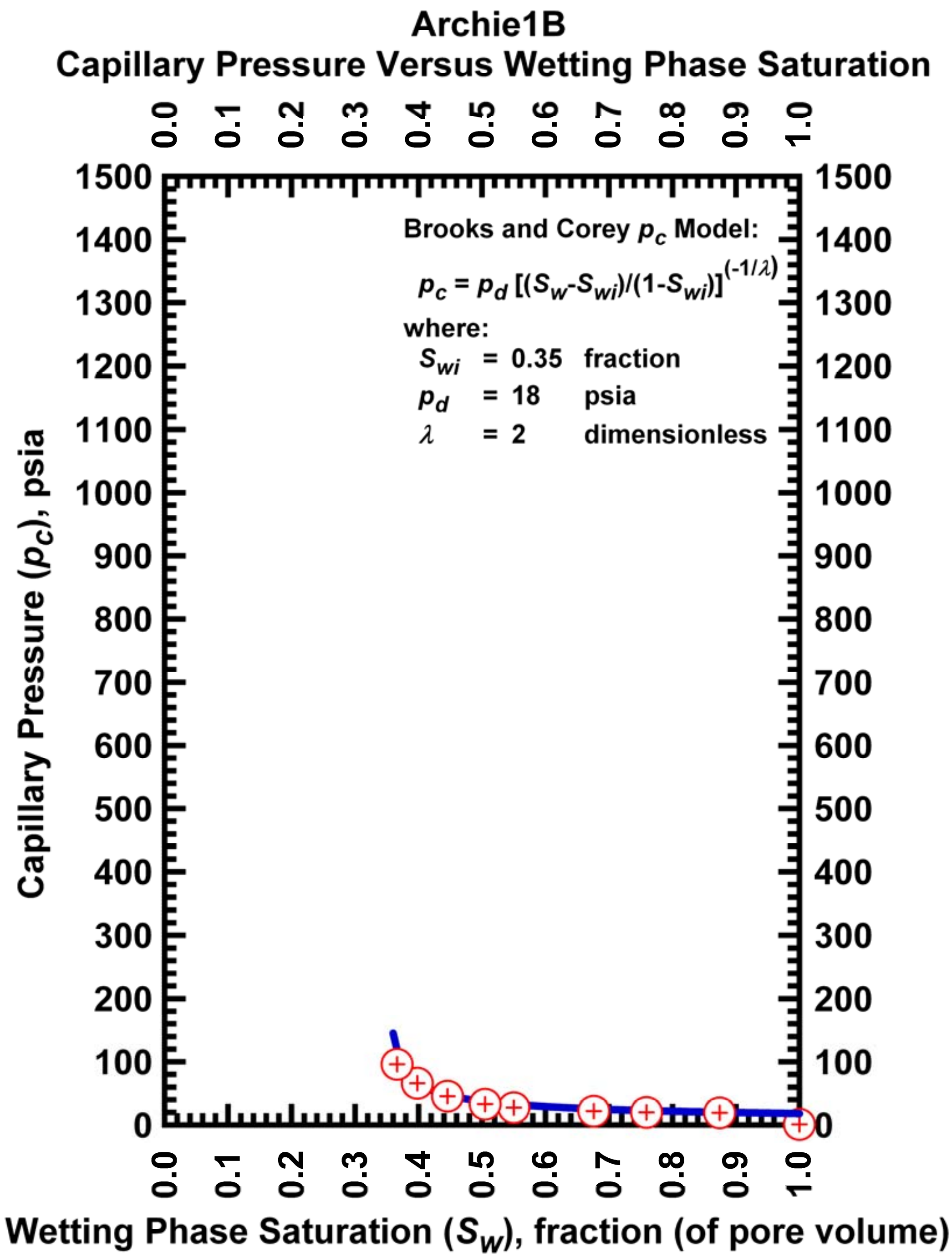

Figure I.22 — Plot of capillary pressure (p_c) vs. wetting phase saturation (S_w) — Case Archie1B.

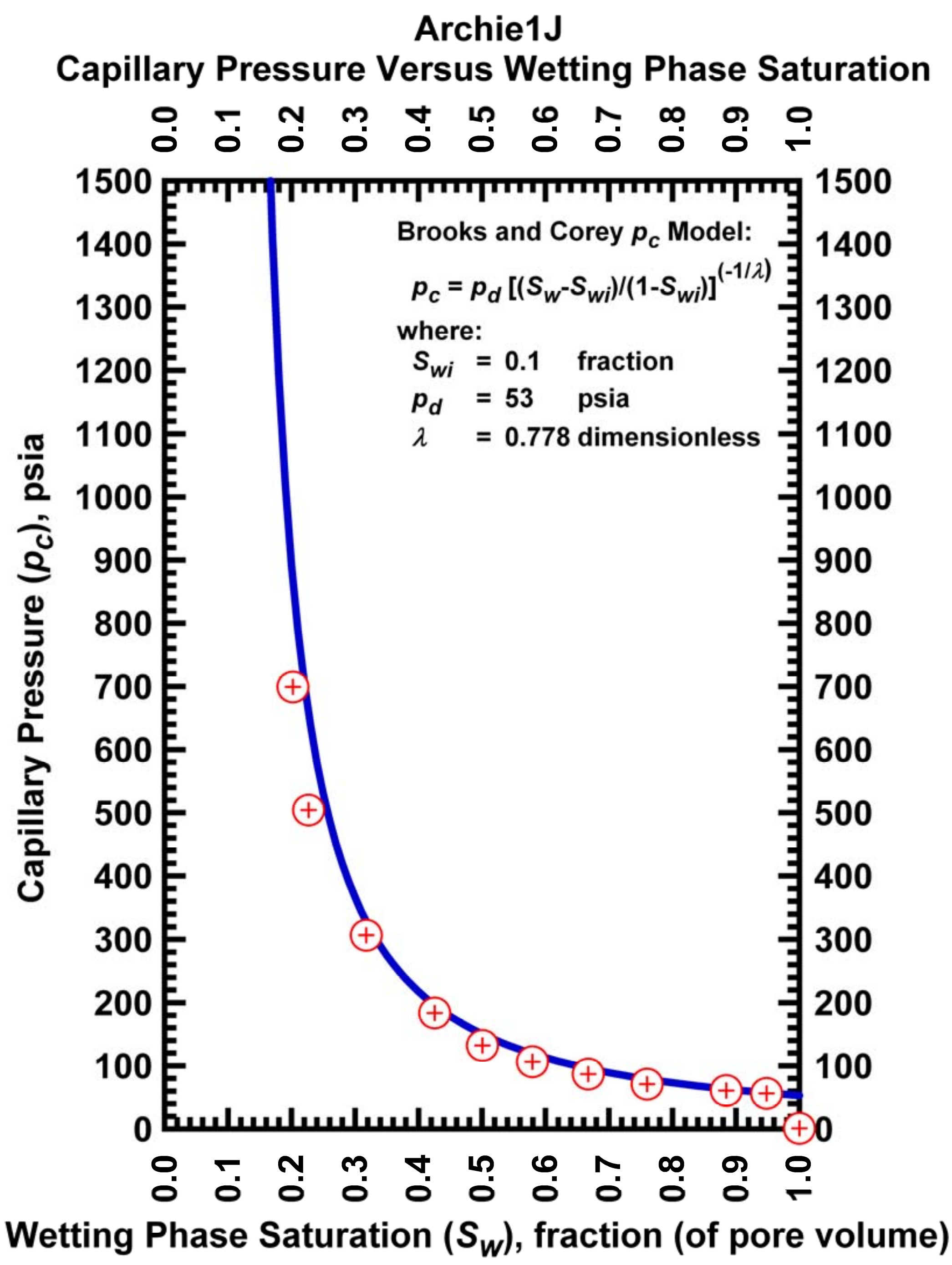

Figure I.23 — Plot of capillary pressure (p_c) vs. wetting phase saturation (S_w) — Case Archie1J.

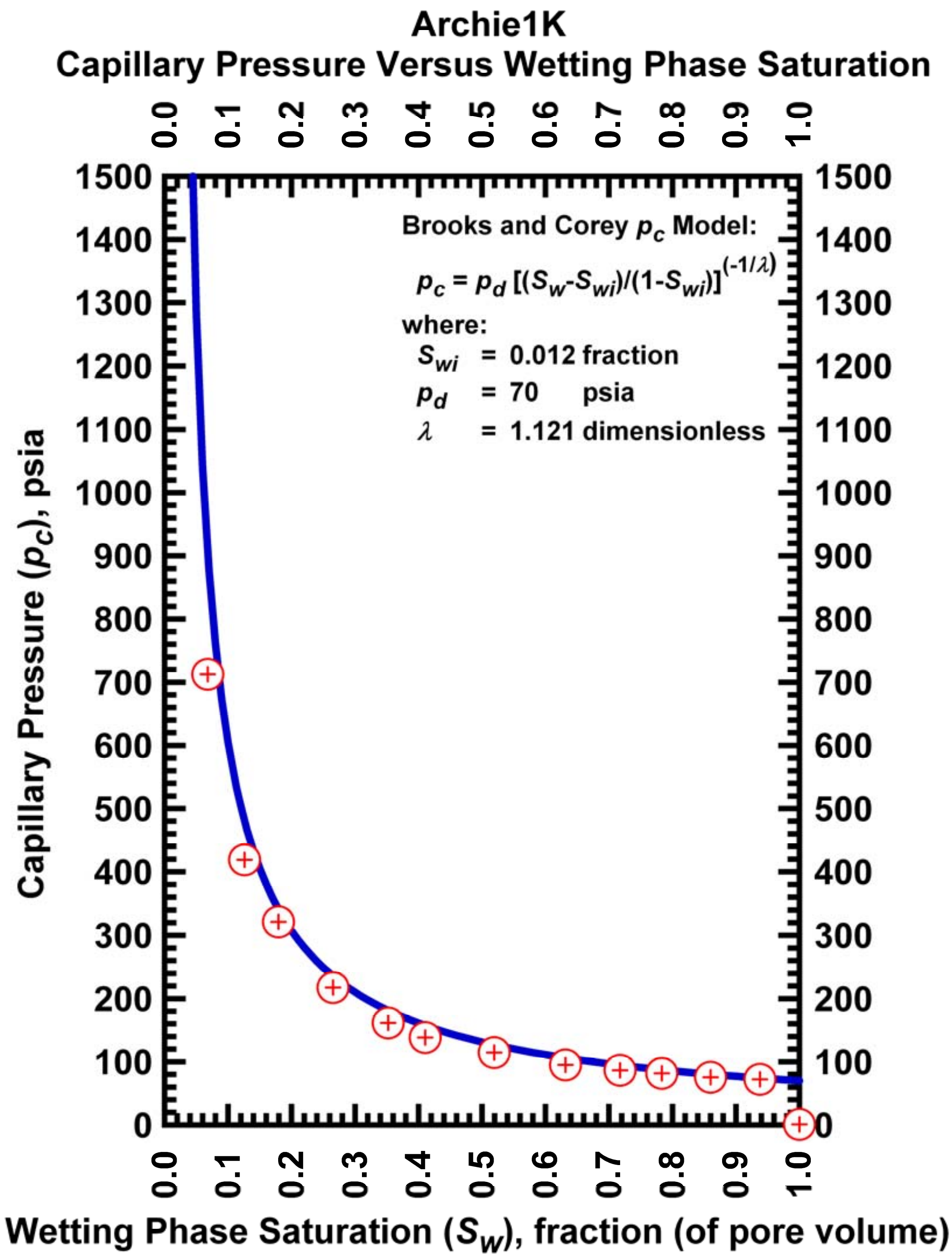

Figure I.24 — Plot of capillary pressure (p_c) vs. wetting phase saturation (S_w) — Case Archie1J.

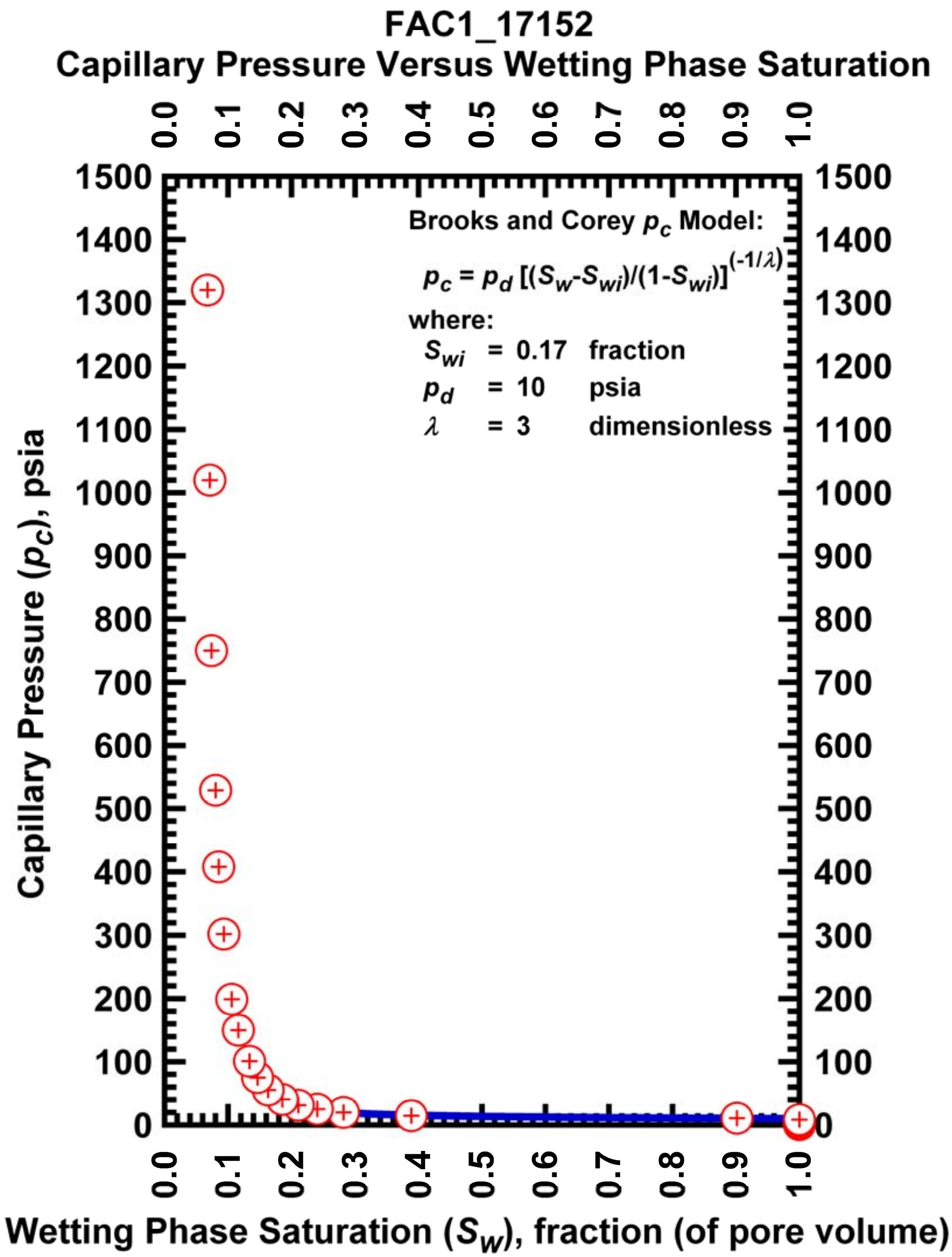

Figure I.25 — Plot of capillary pressure (p_c) vs. wetting phase saturation (S_w) — Case FAC1_17152.

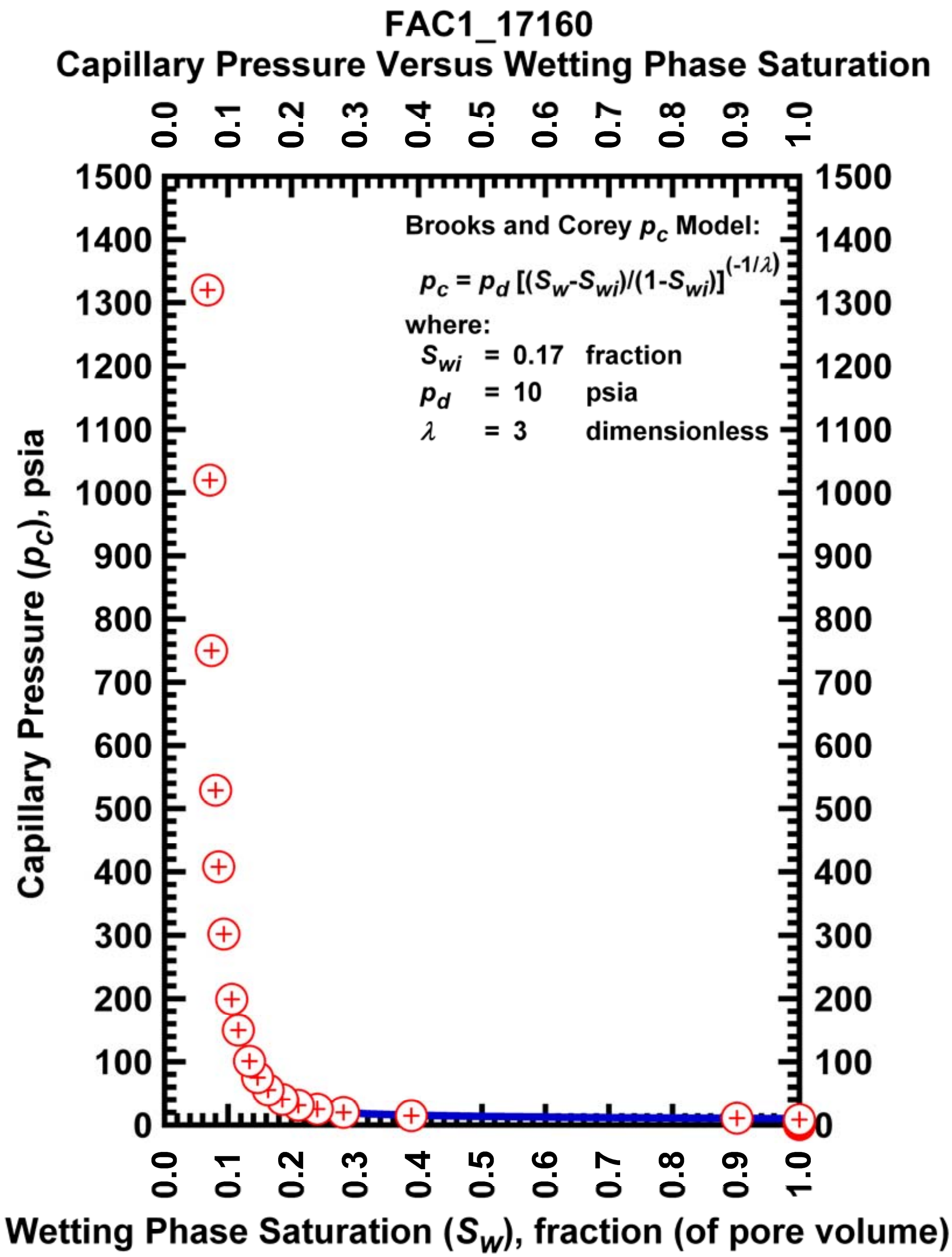

Figure I.26 — Plot of capillary pressure (p_c) vs. wetting phase saturation (S_w) — Case FAC1_17160.

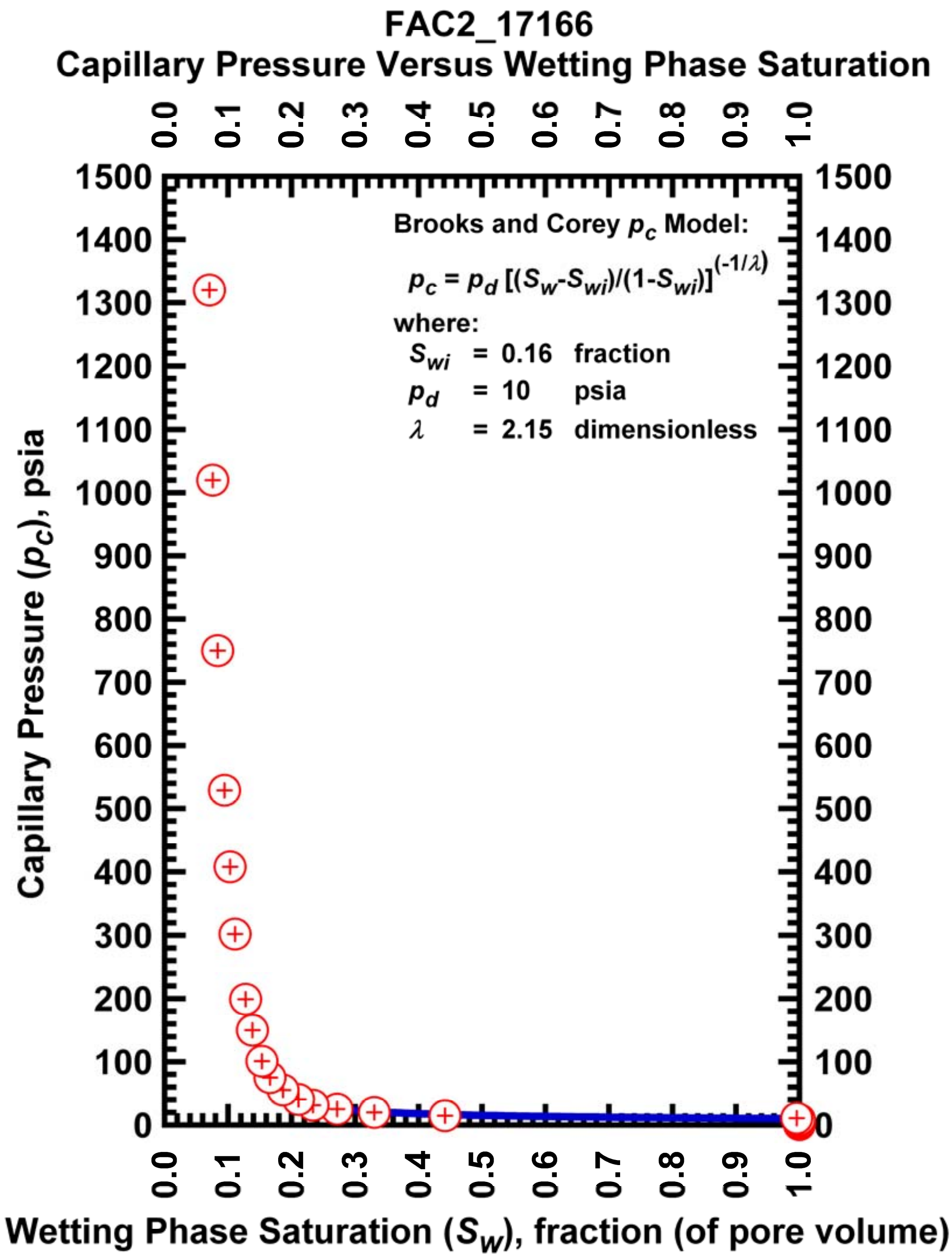

Figure I.27 — Plot of capillary pressure (p_c) vs. wetting phase saturation (S_w) — Case FAC1_17166.

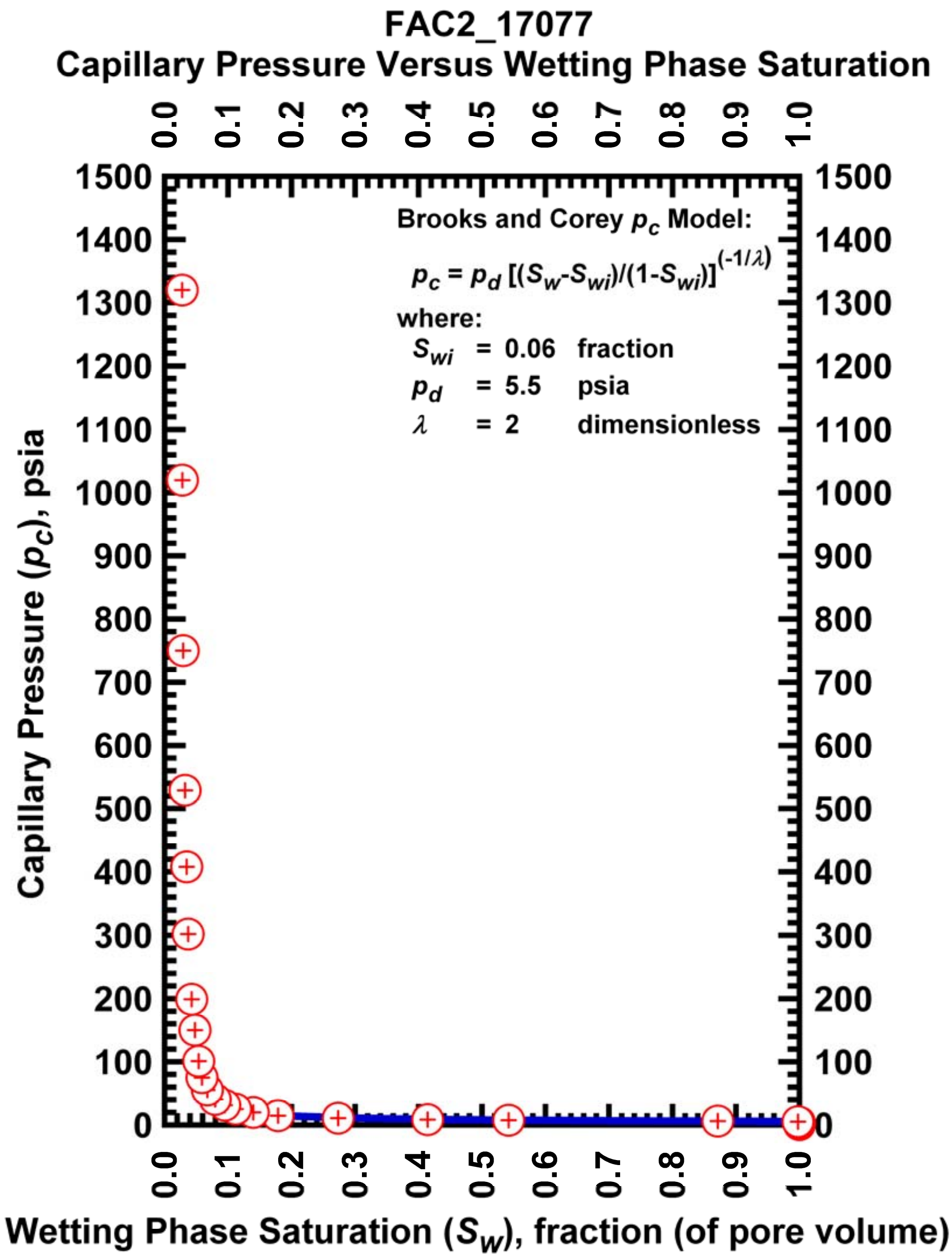

Figure I.28 — Plot of capillary pressure (p_c) vs. wetting phase saturation (S_w) — Case FAC2_17077.

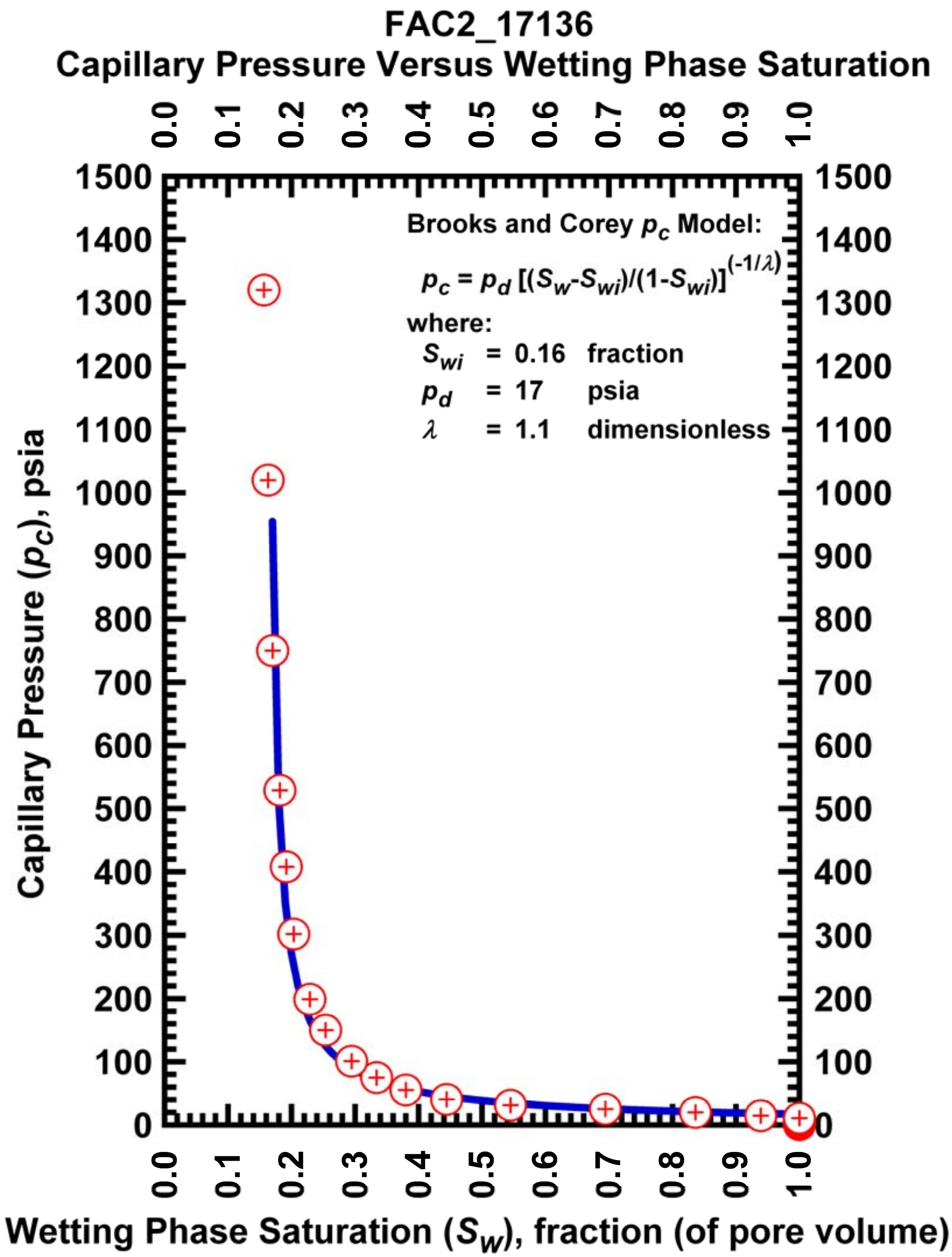

Figure I.29 — Plot of capillary pressure (p_c) vs. wetting phase saturation (S_w) — Case FAC2_17136.

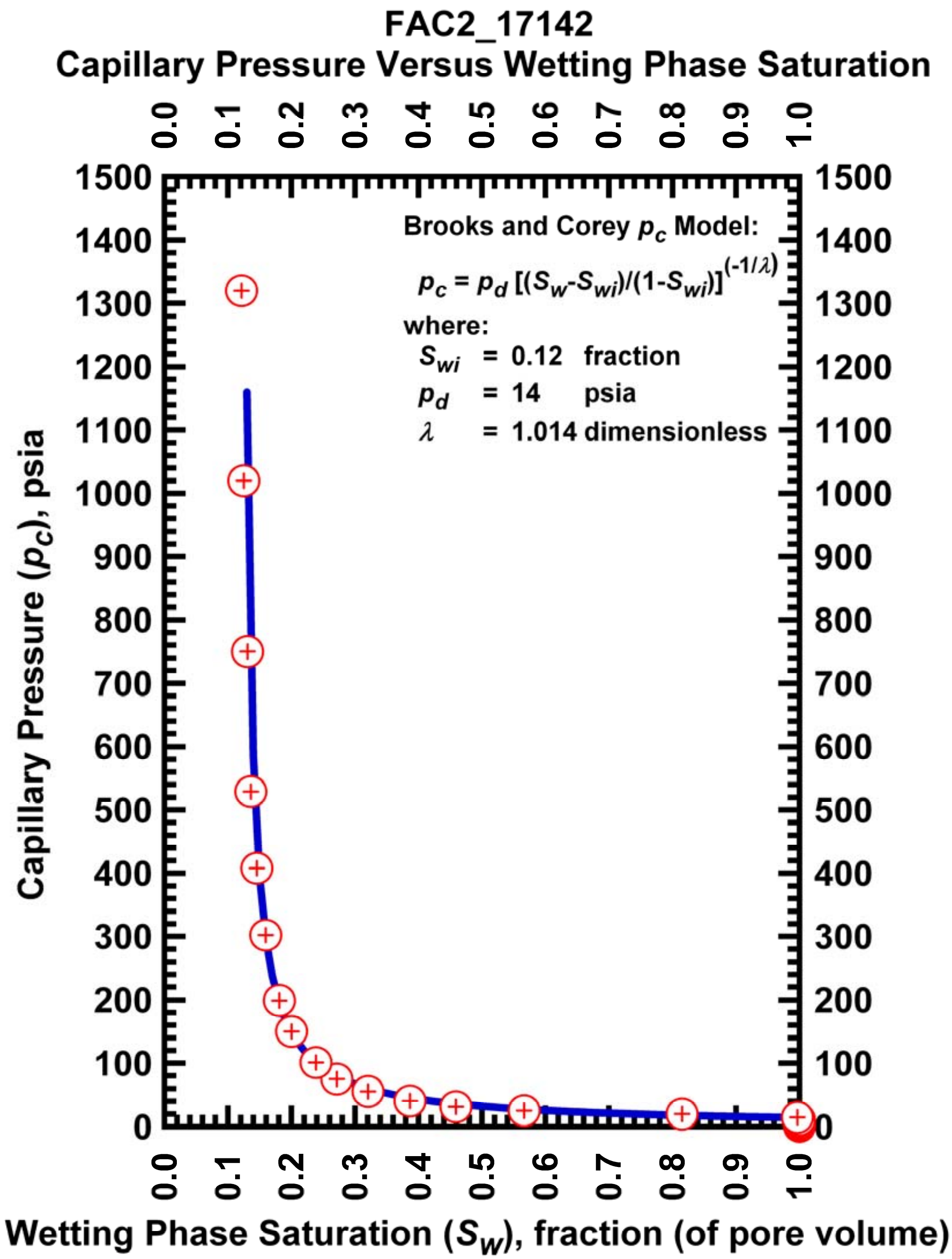

Figure I.30 — Plot of capillary pressure (p_c) vs. wetting phase saturation (S_w) — Case FAC2_17142.

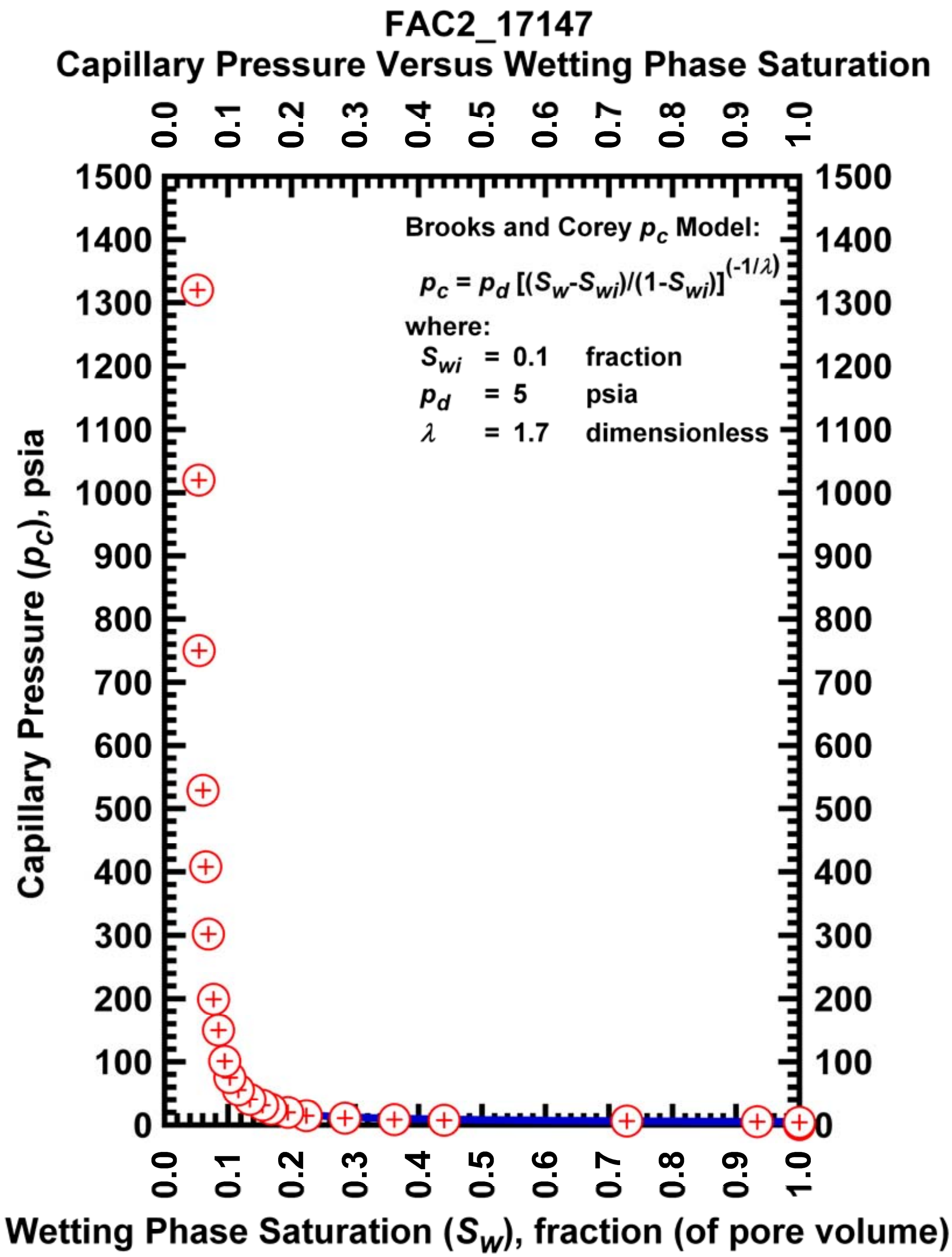

Figure I.31 — Plot of capillary pressure (p_c) vs. wetting phase saturation (S_w) — Case FAC2_17147.

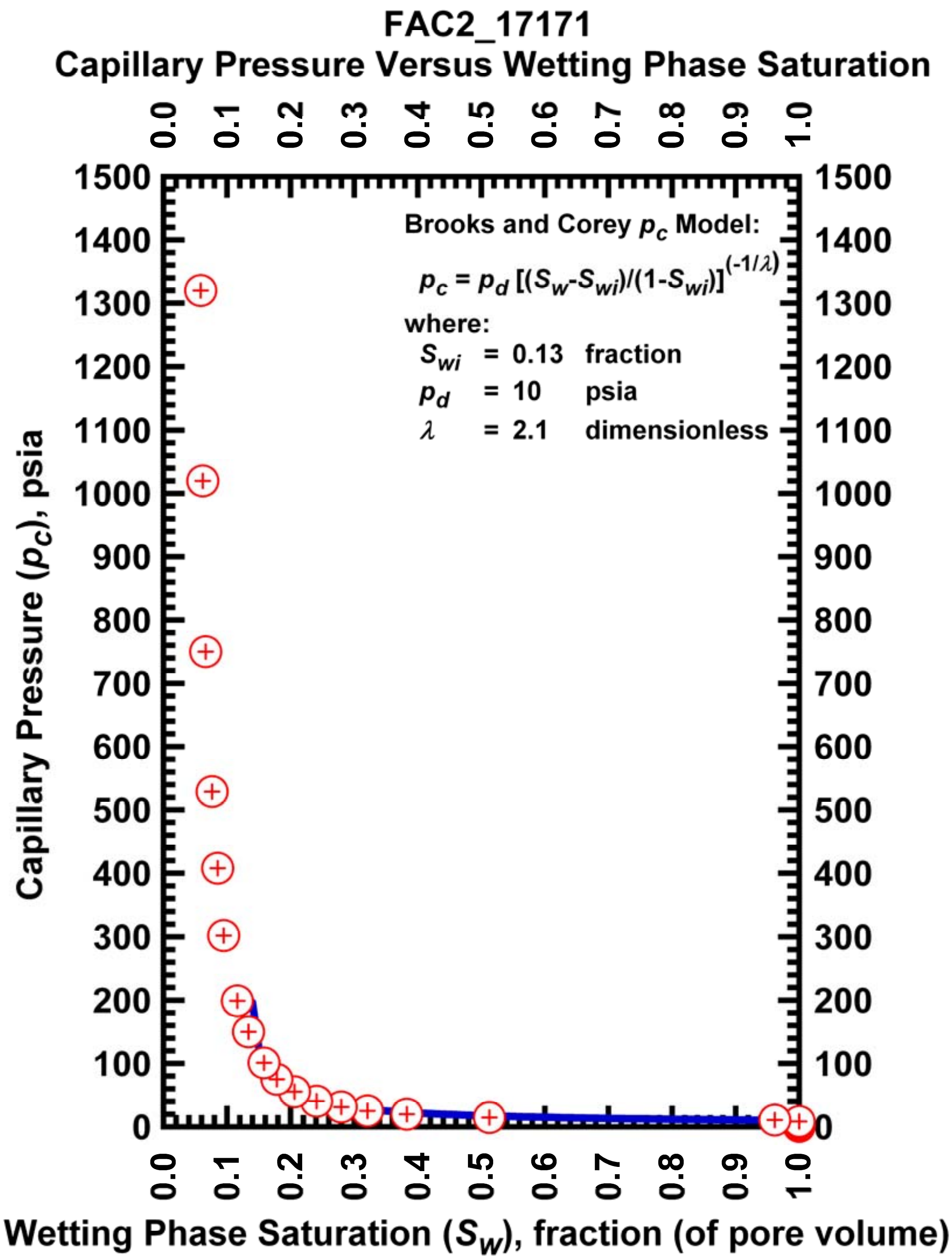

Figure I.32 — Plot of capillary pressure (p_c) vs. wetting phase saturation (S_w) — Case FAC2_17171.

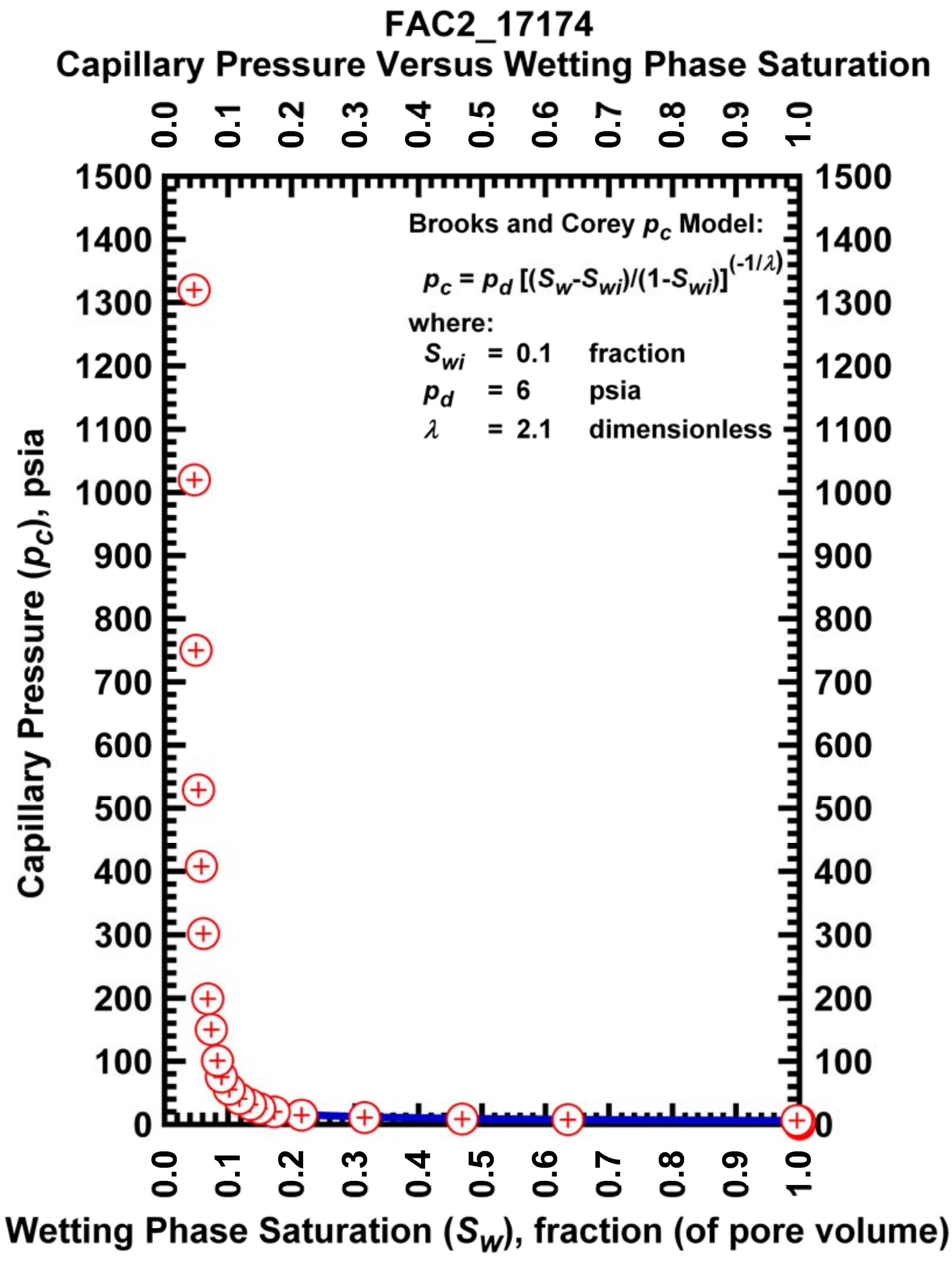

Figure I.33 — Plot of capillary pressure (p_c) vs. wetting phase saturation (S_w) — Case FAC6_17174.

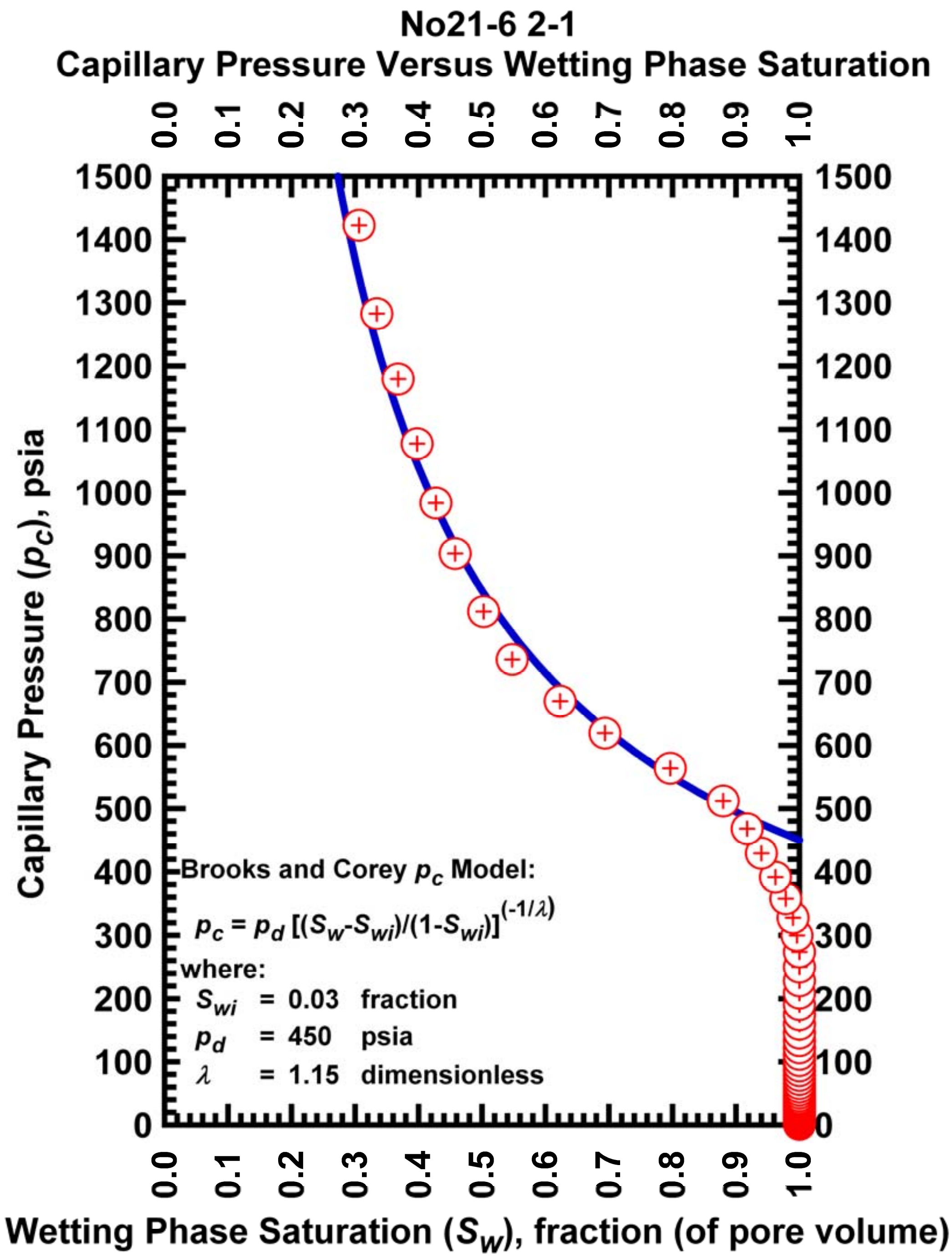

Figure I.34 — Plot of capillary pressure (p_c) vs. wetting phase saturation (S_w) — Case No21-6 2-1.

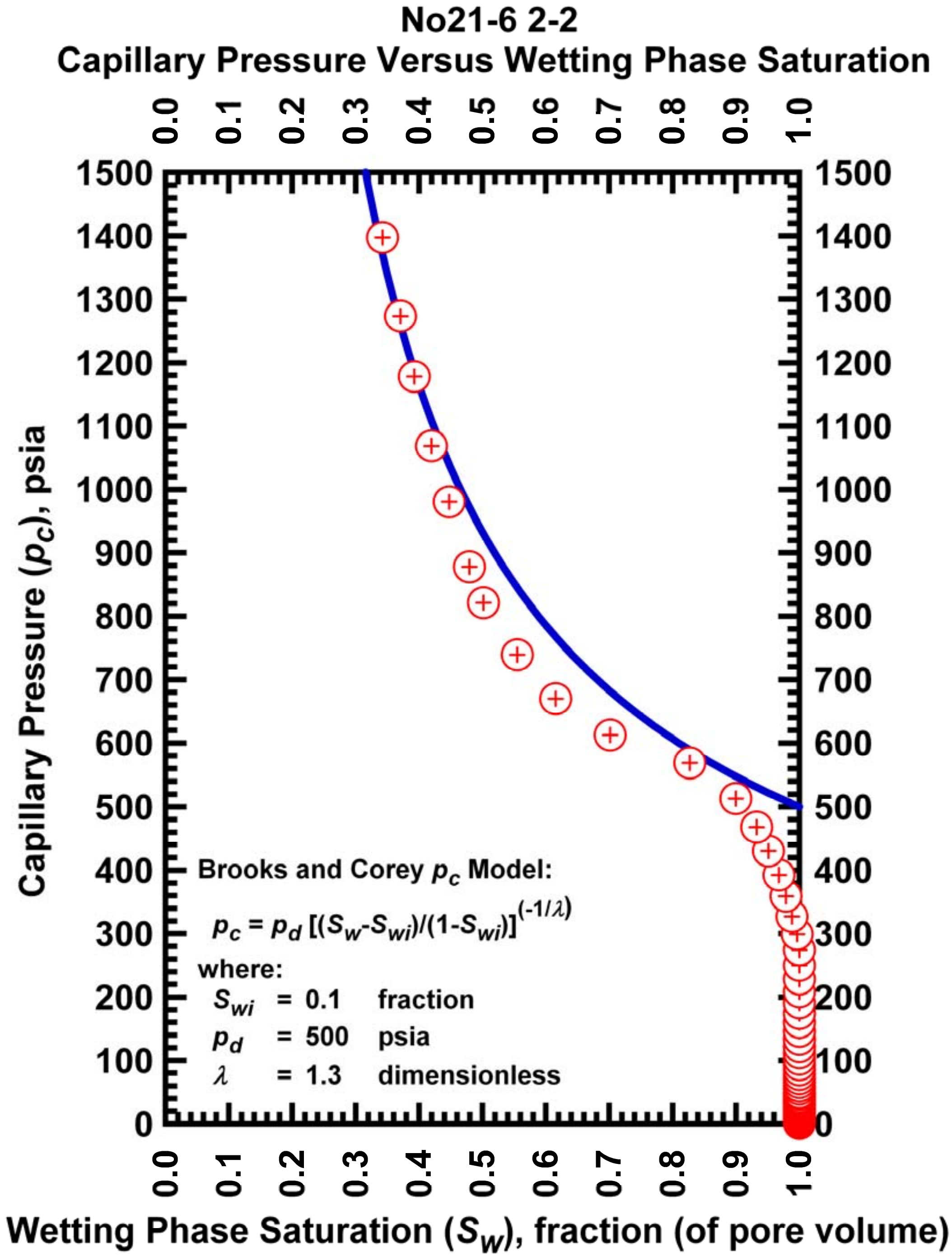

Figure I.35 — Plot of capillary pressure (p_c) vs. wetting phase saturation (S_w) — Case No21-6 2-2.

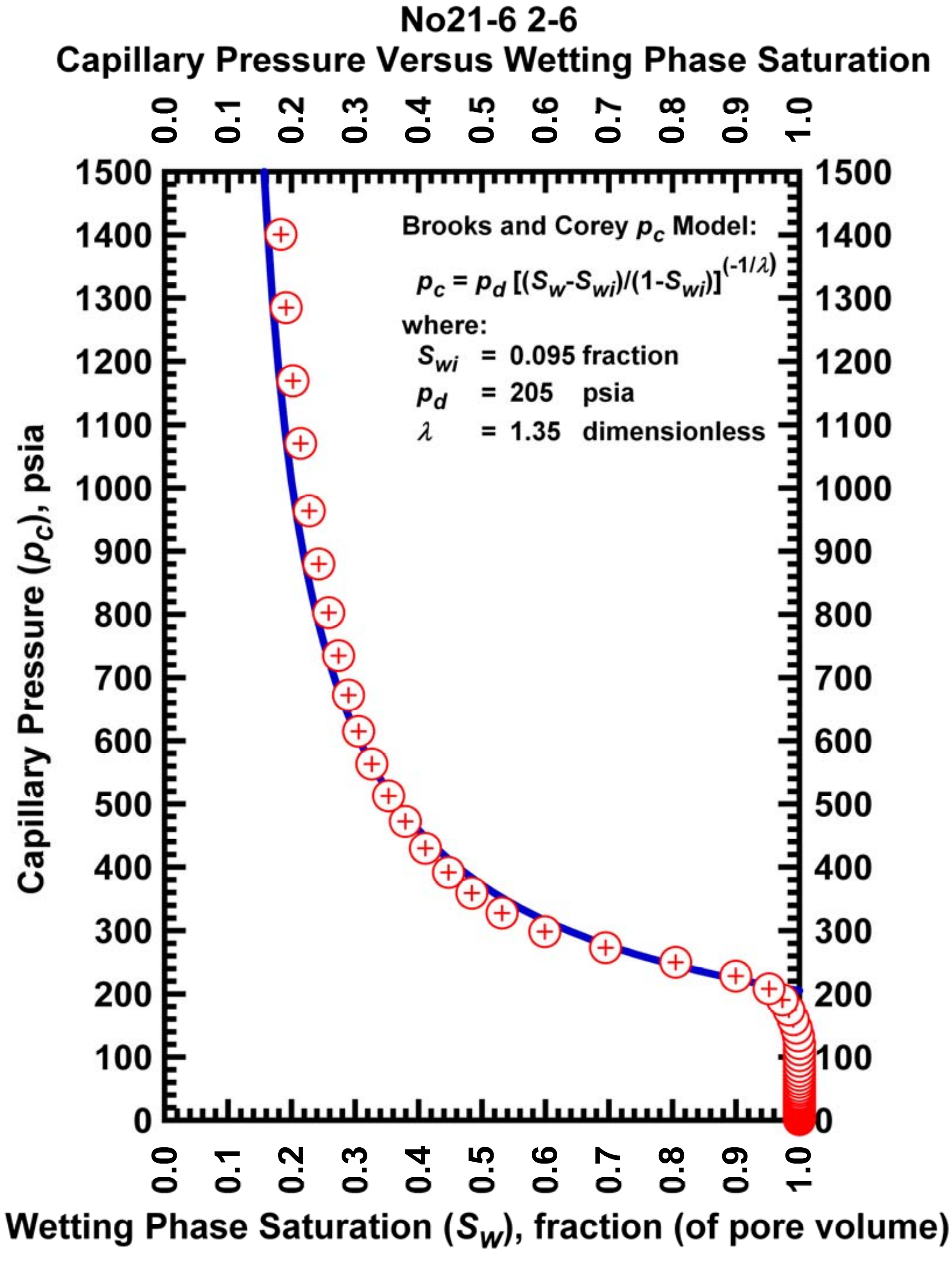

Figure I.36 — Plot of capillary pressure (p_c) vs. wetting phase saturation (S_w) — Case No21-6 2-6.

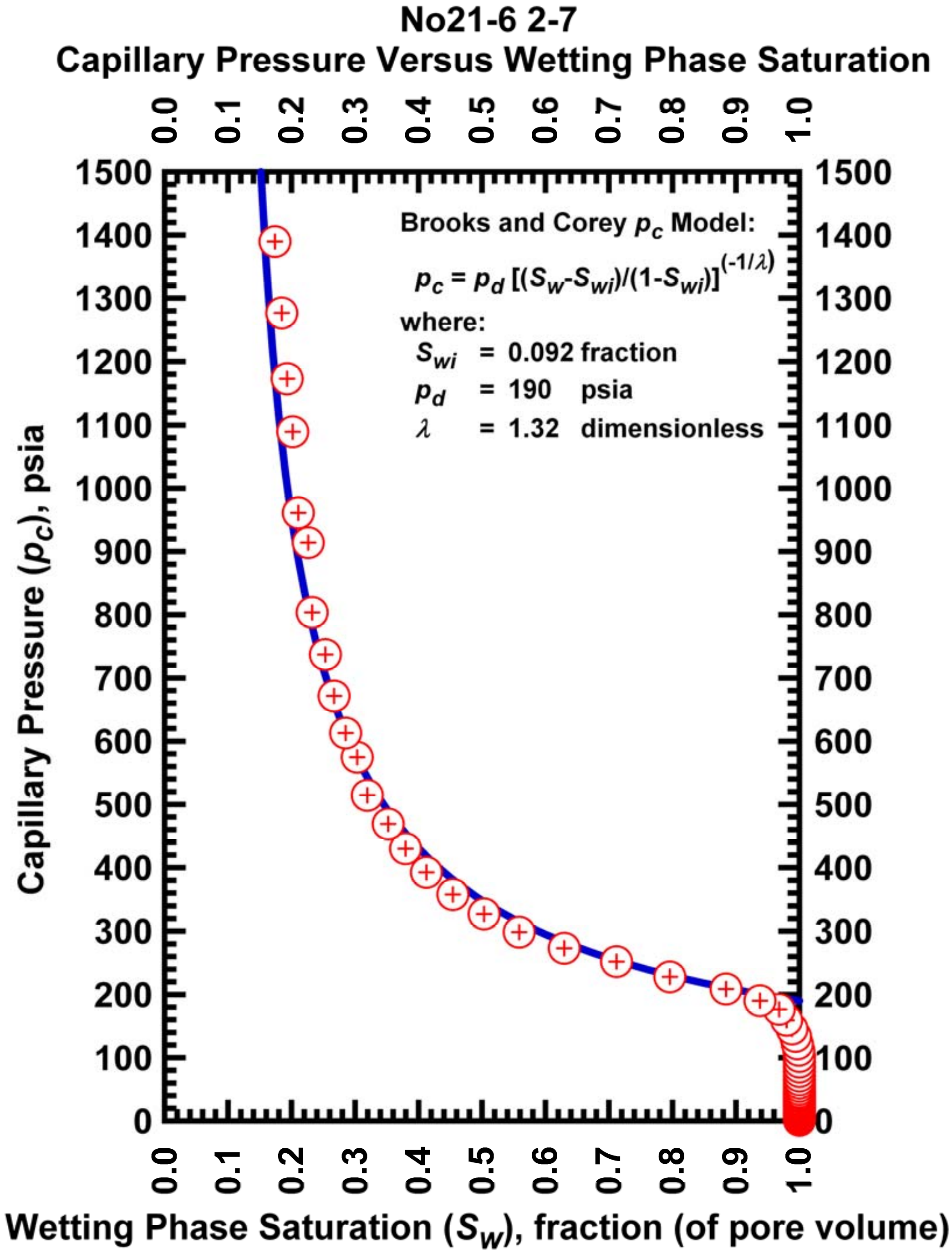

Figure I.37 — Plot of capillary pressure (p_c) vs. wetting phase saturation (S_w) — Case No21-6 2-7.

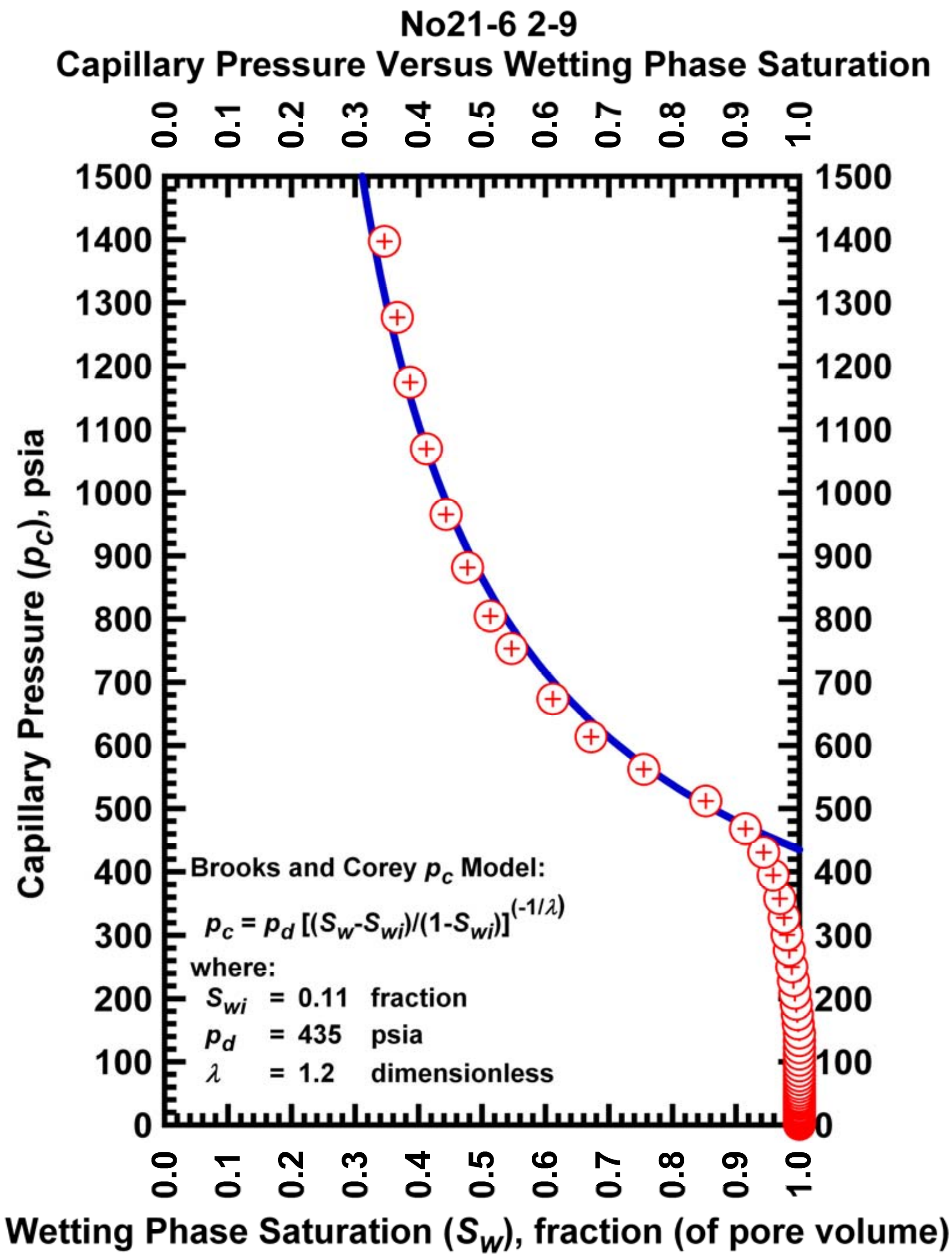

Figure I.38 — Plot of capillary pressure (p_c) vs. wetting phase saturation (S_w) — Case No21-6 2-9.

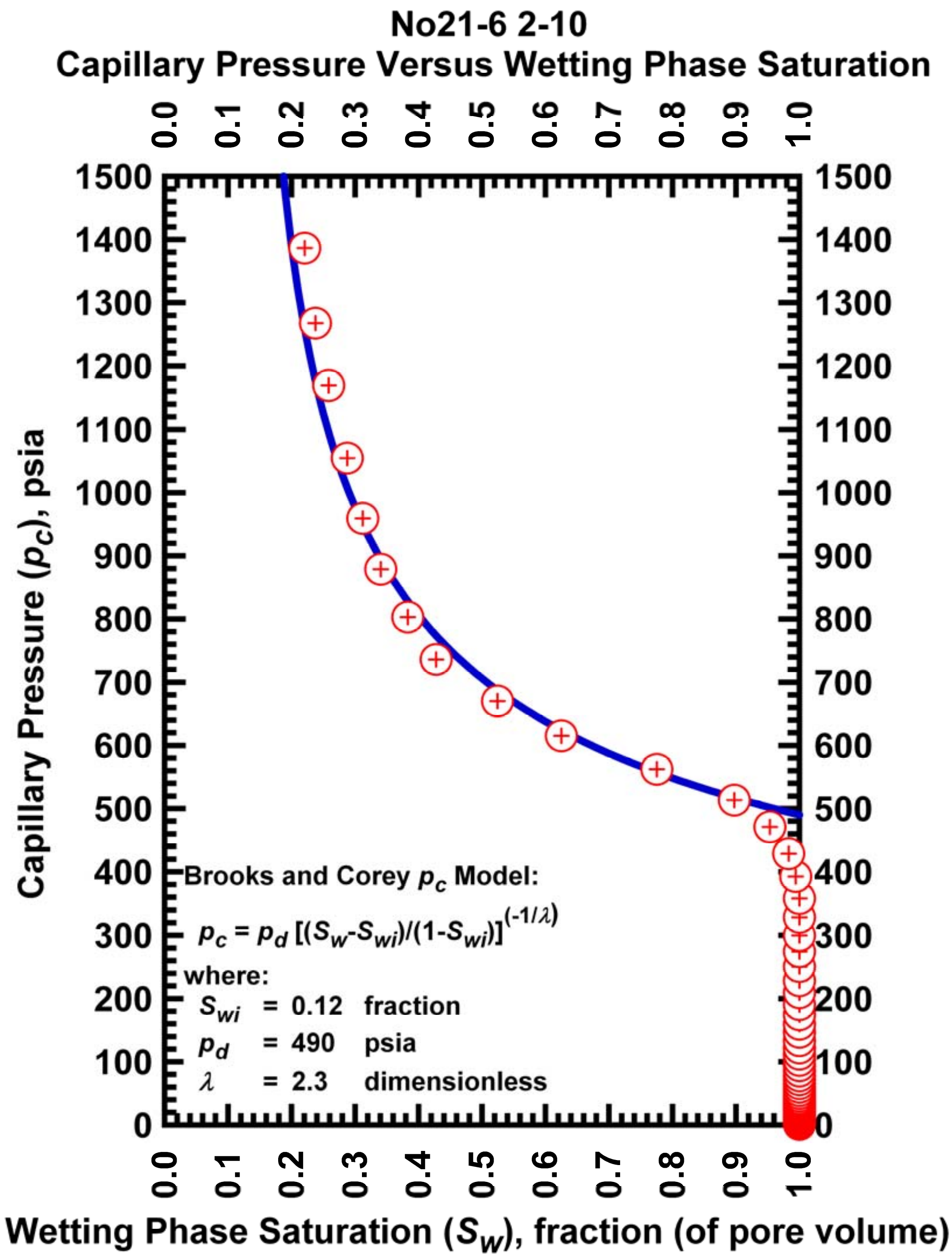

Figure I.39 — Plot of capillary pressure (p_c) vs. wetting phase saturation (S_w) — Case No21-6 2-10.

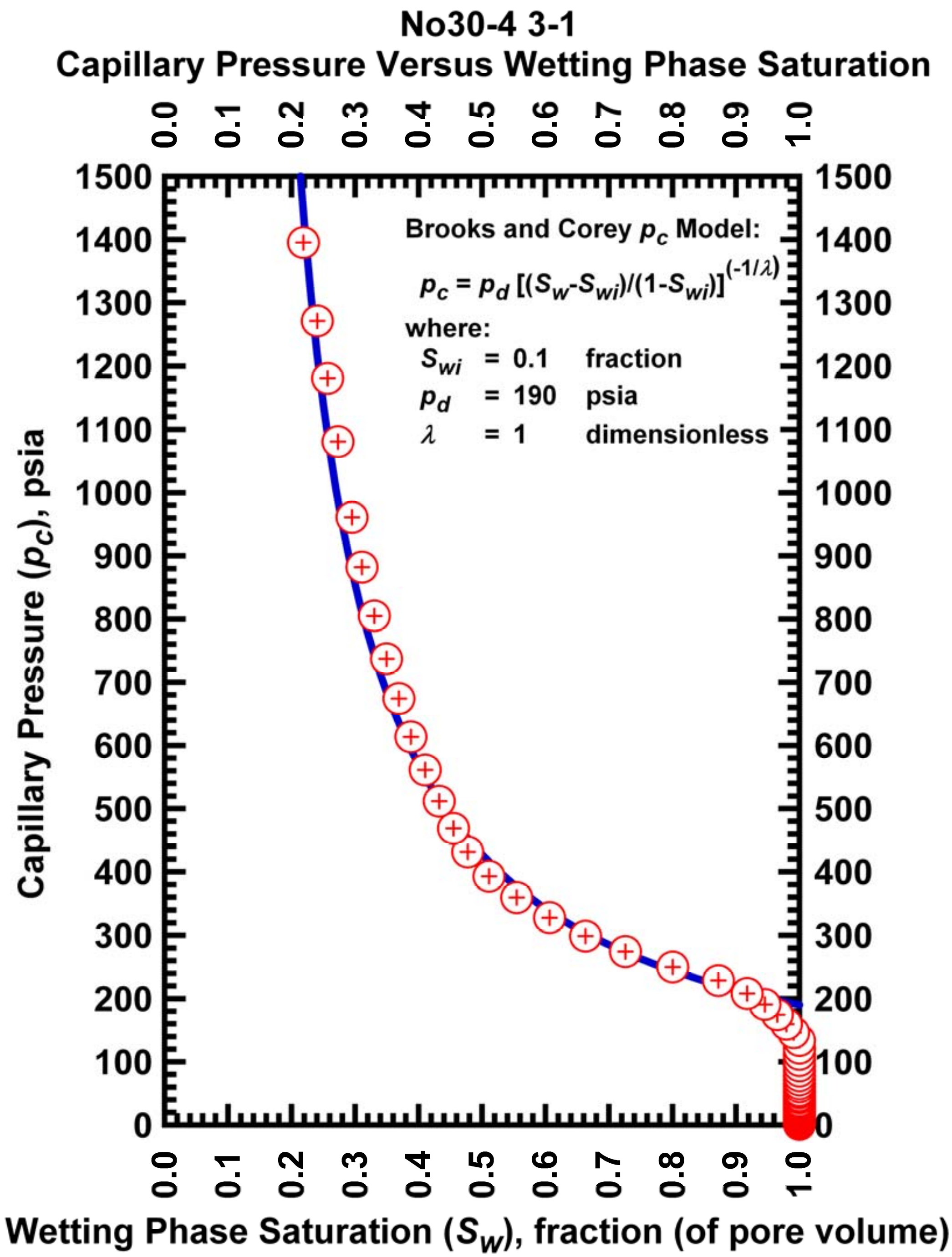

Figure I.40 — Plot of capillary pressure (p_c) vs. wetting phase saturation (S_w) — Case No30-4 3-1.

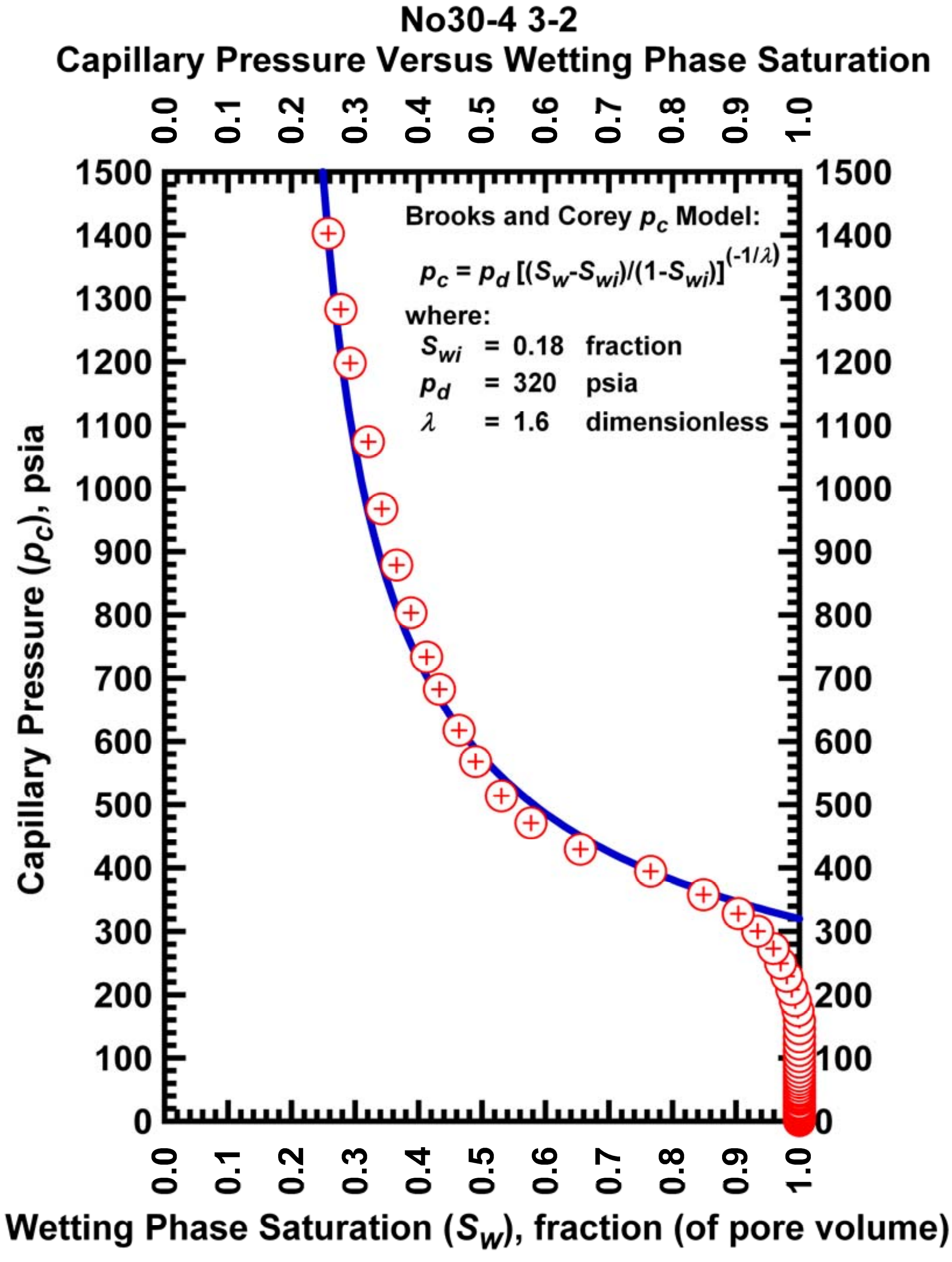

Figure I.41 — Plot of capillary pressure (p_c) vs. wetting phase saturation (S_w) — Case No30-4 3-2.

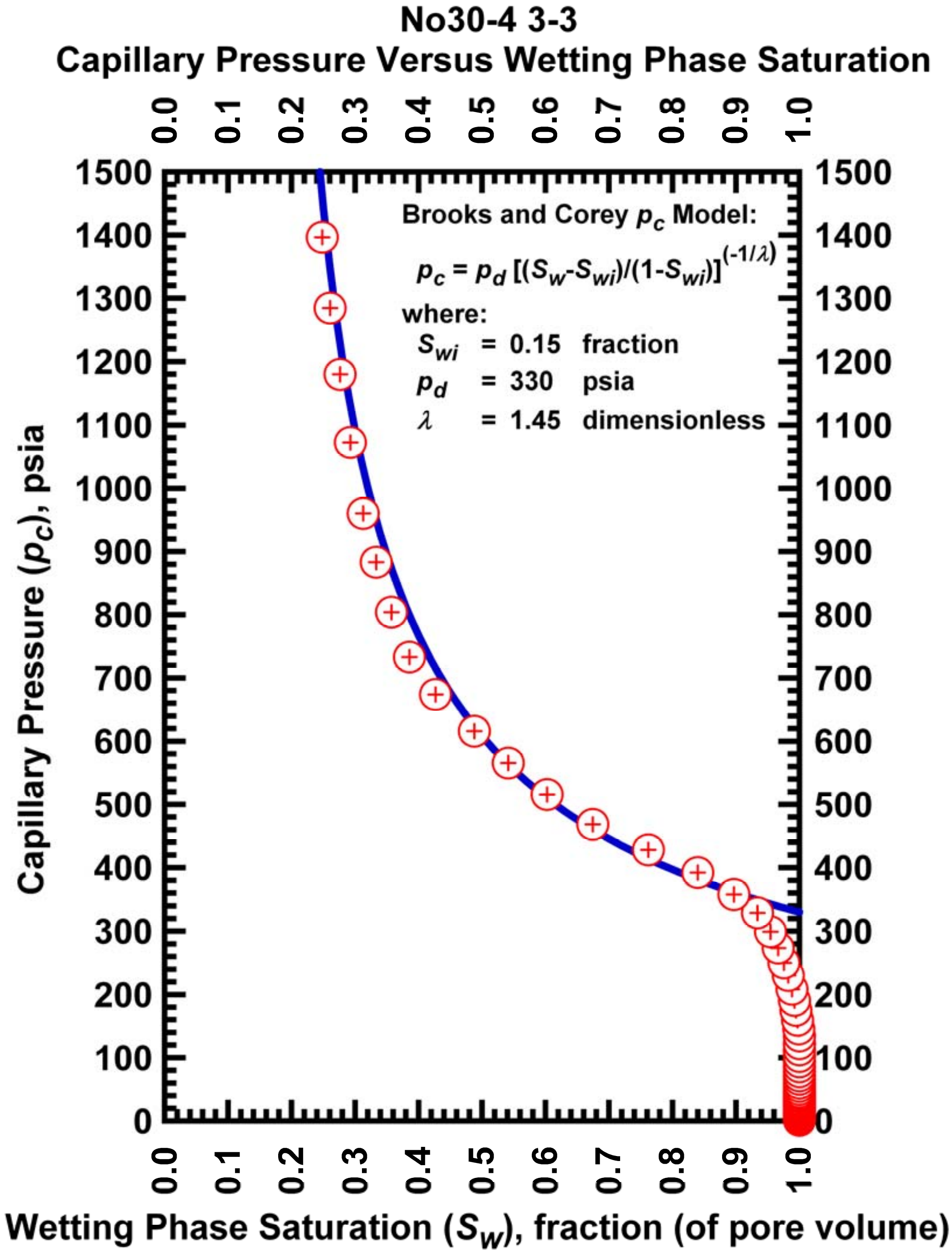

Figure I.42 — Plot of capillary pressure (p_c) vs. wetting phase saturation (S_w) — Case No30-4 3-3.

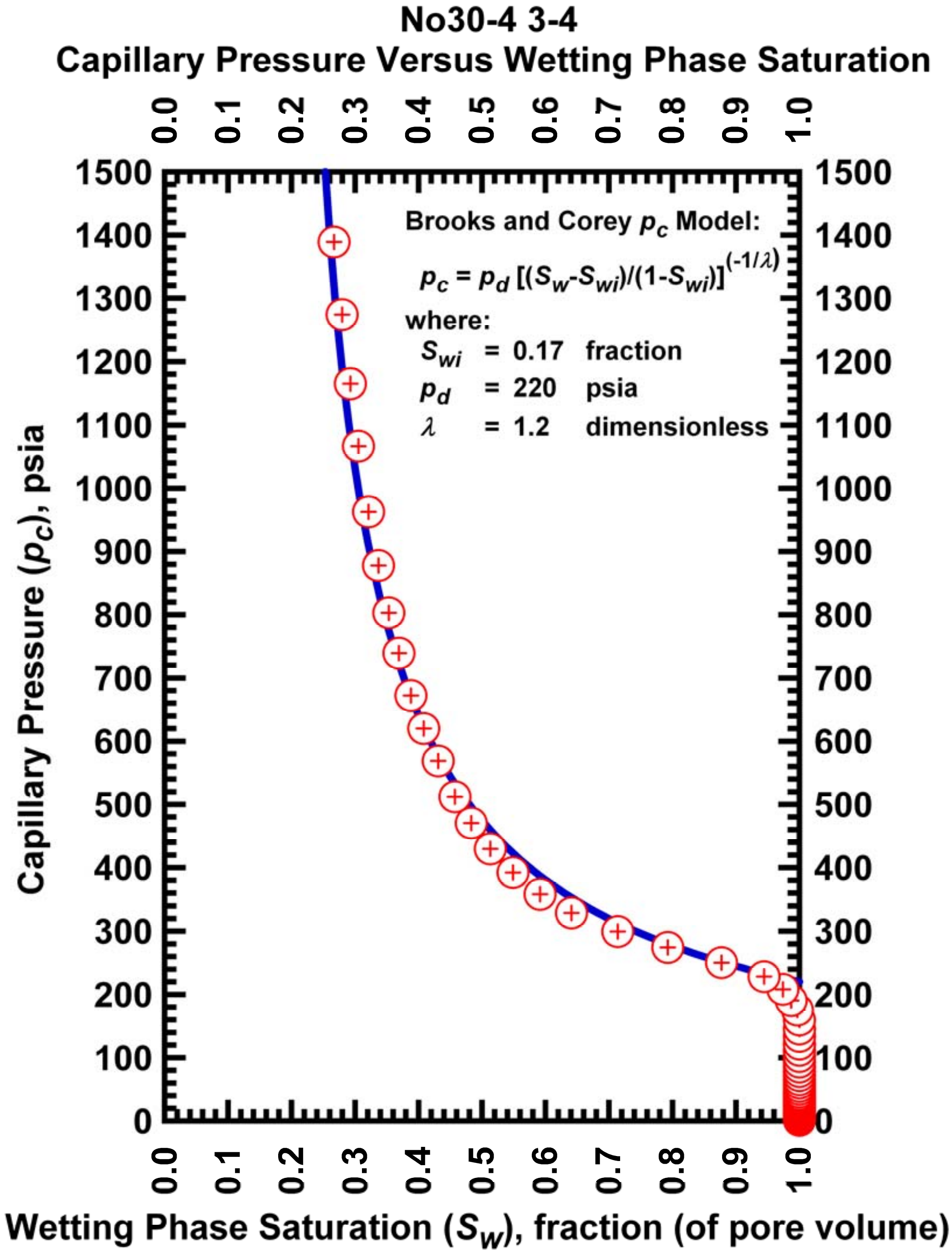

Figure I.43 — Plot of capillary pressure (p_c) vs. wetting phase saturation (S_w) — Case No30-4 3-4.

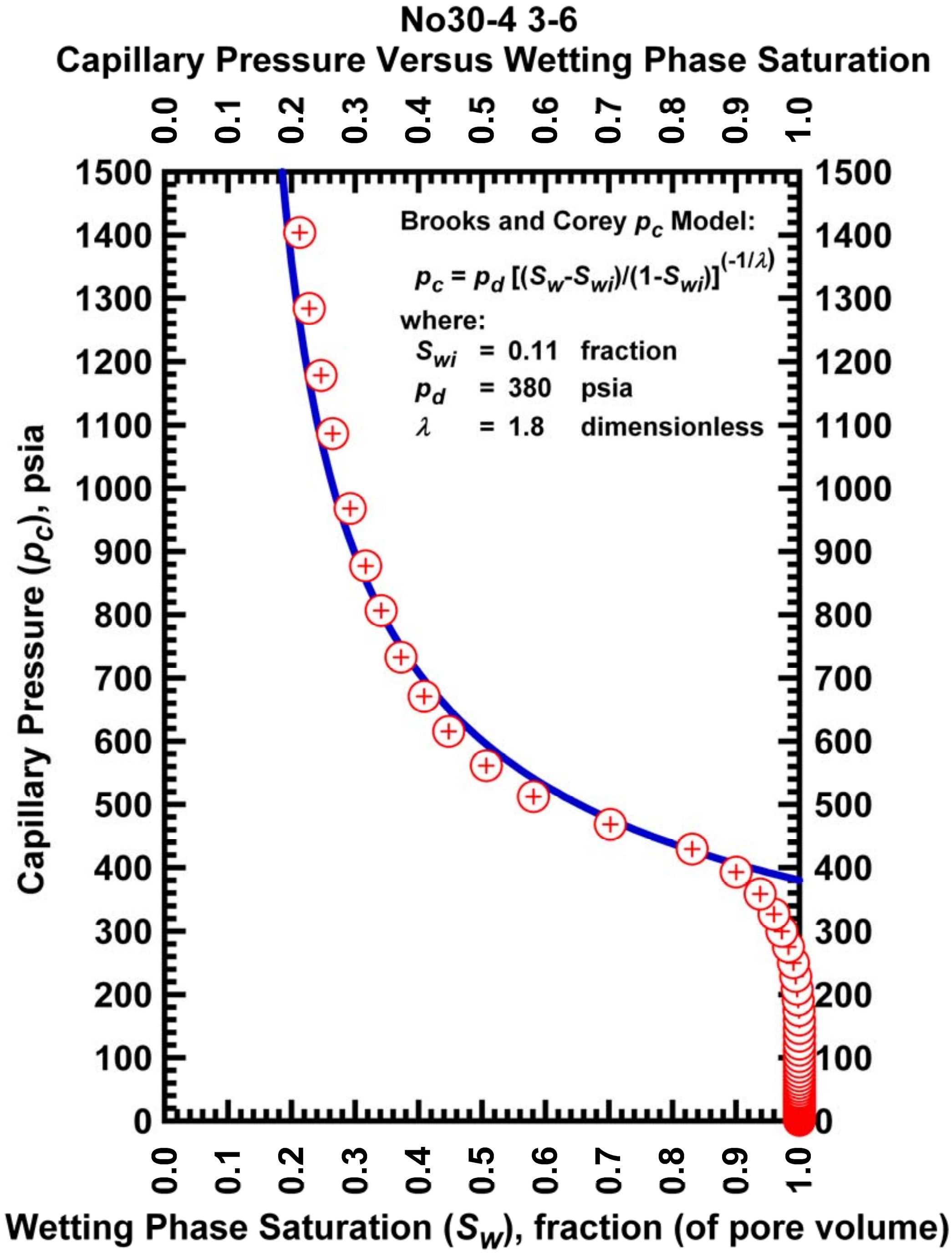

Figure I.44 — Plot of capillary pressure (p_c) vs. wetting phase saturation (S_w) — Case No30-4 3-6.

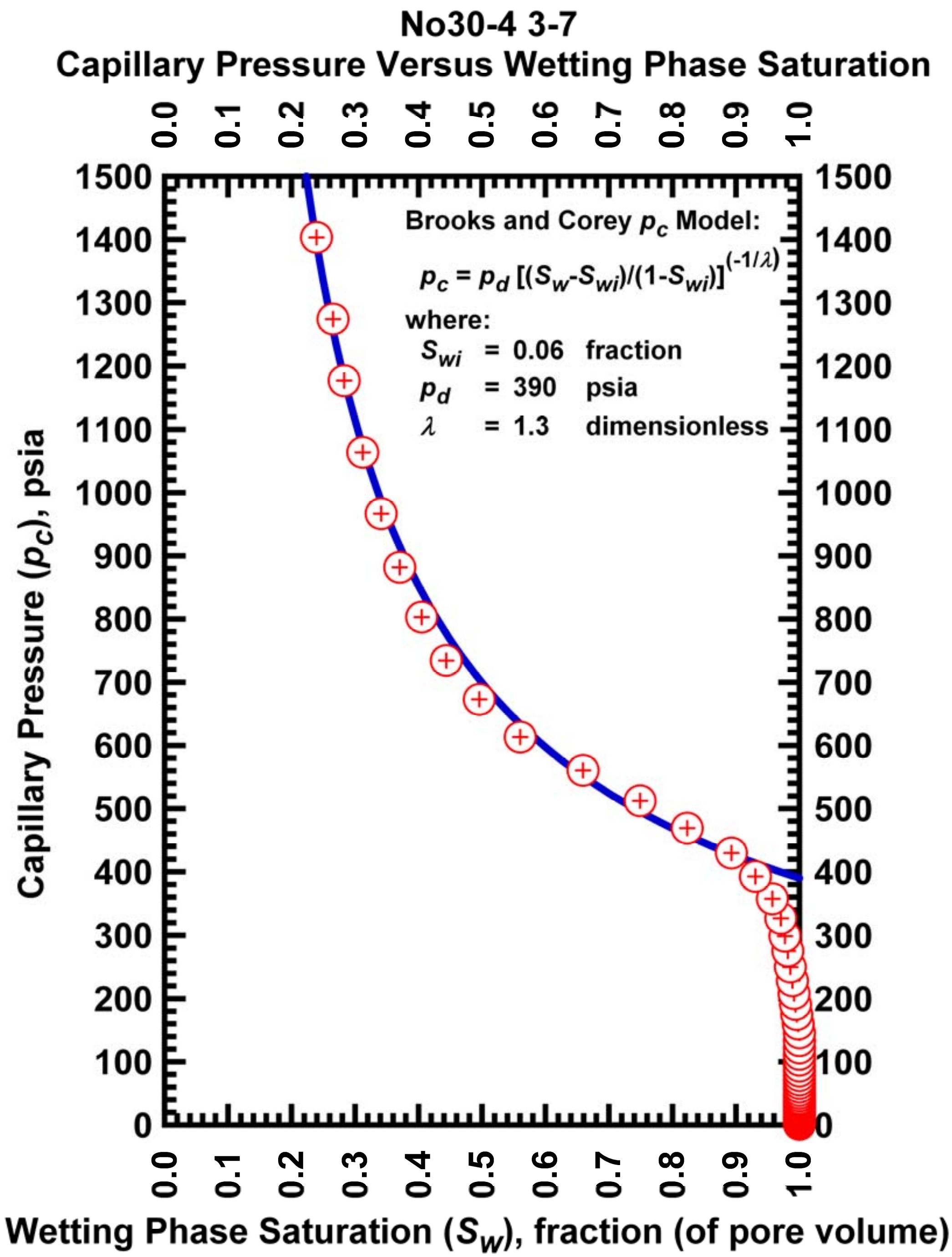

Figure I.45 — Plot of capillary pressure (p_c) vs. wetting phase saturation (S_w) — Case No30-4 3-7.

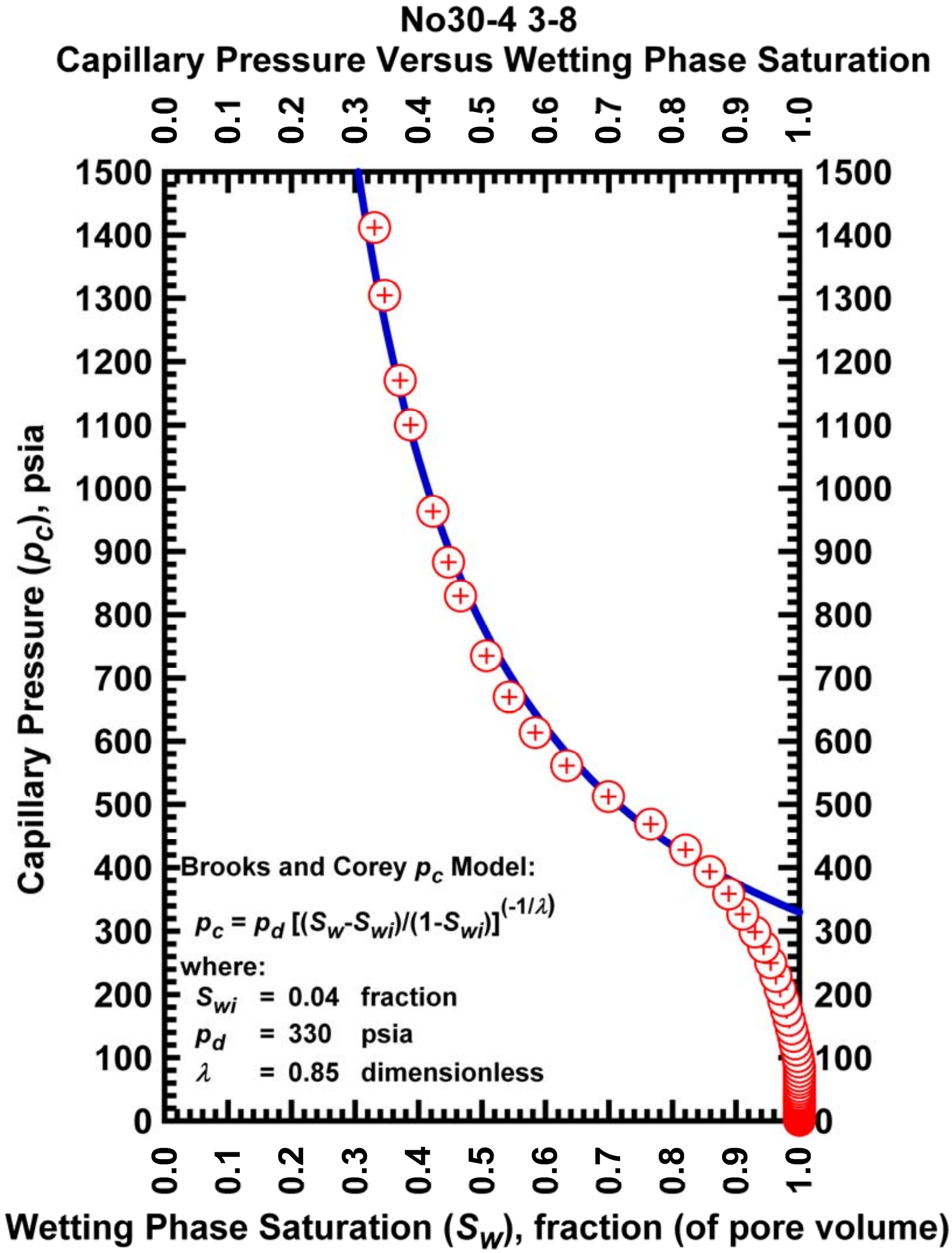

Figure I.46 — Plot of capillary pressure (p_c) vs. wetting phase saturation (S_w) — Case No30-4 3-8.

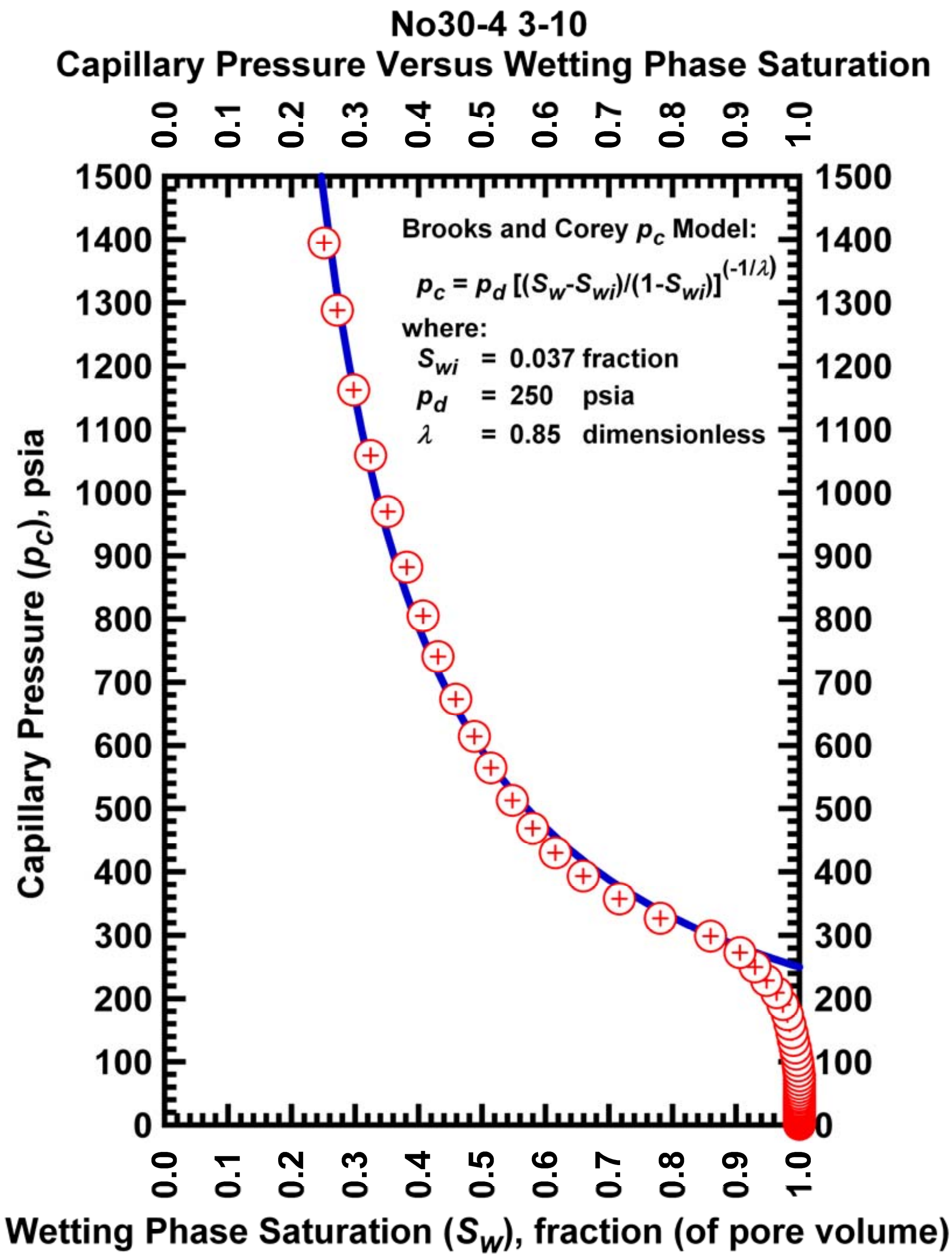

Figure I.47 — Plot of capillary pressure (p_c) vs. wetting phase saturation (S_w) — Case No30-4 3-10.

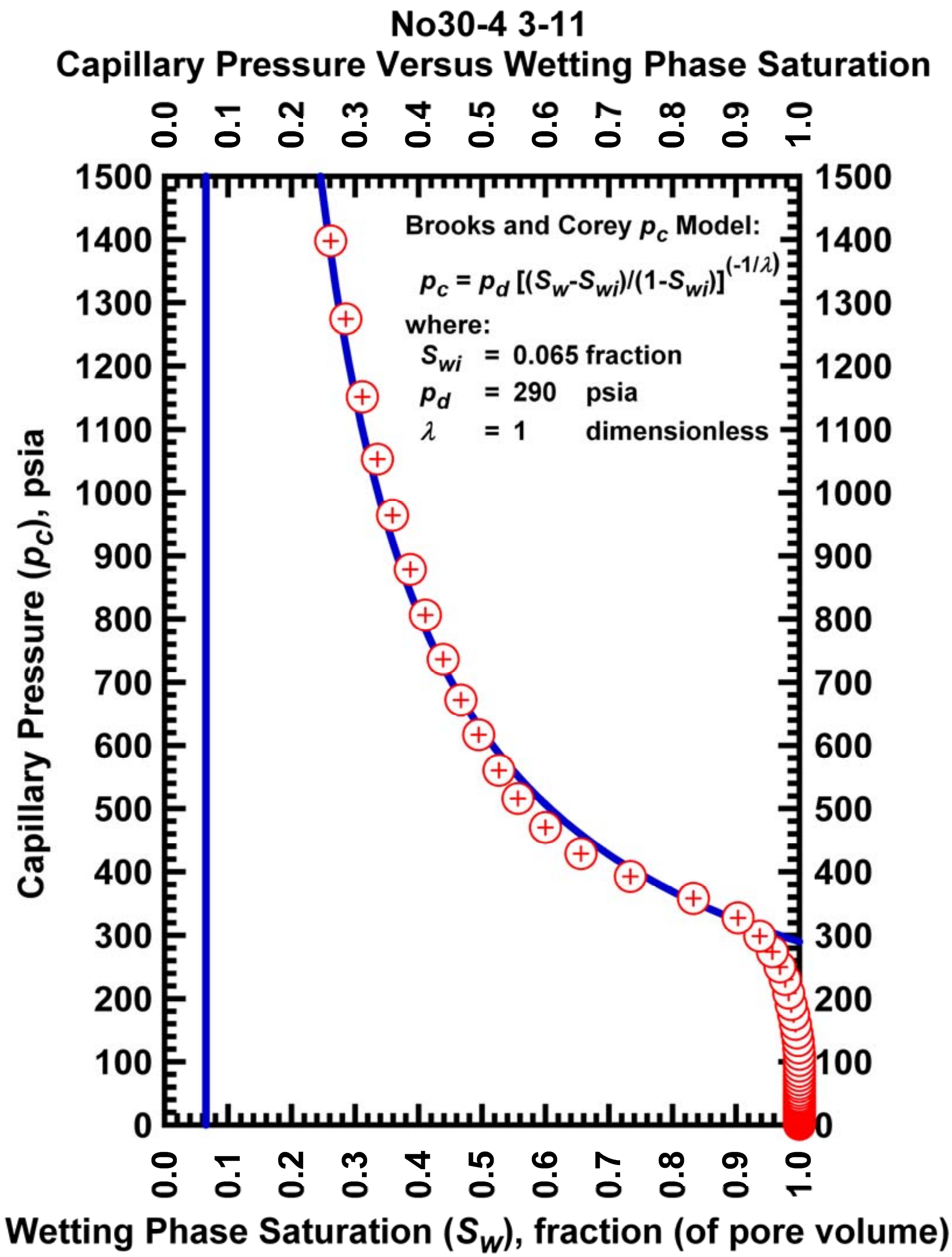

Figure I.48 — Plot of capillary pressure (p_c) vs. wetting phase saturation (S_w) — Case No30-4 3-11.

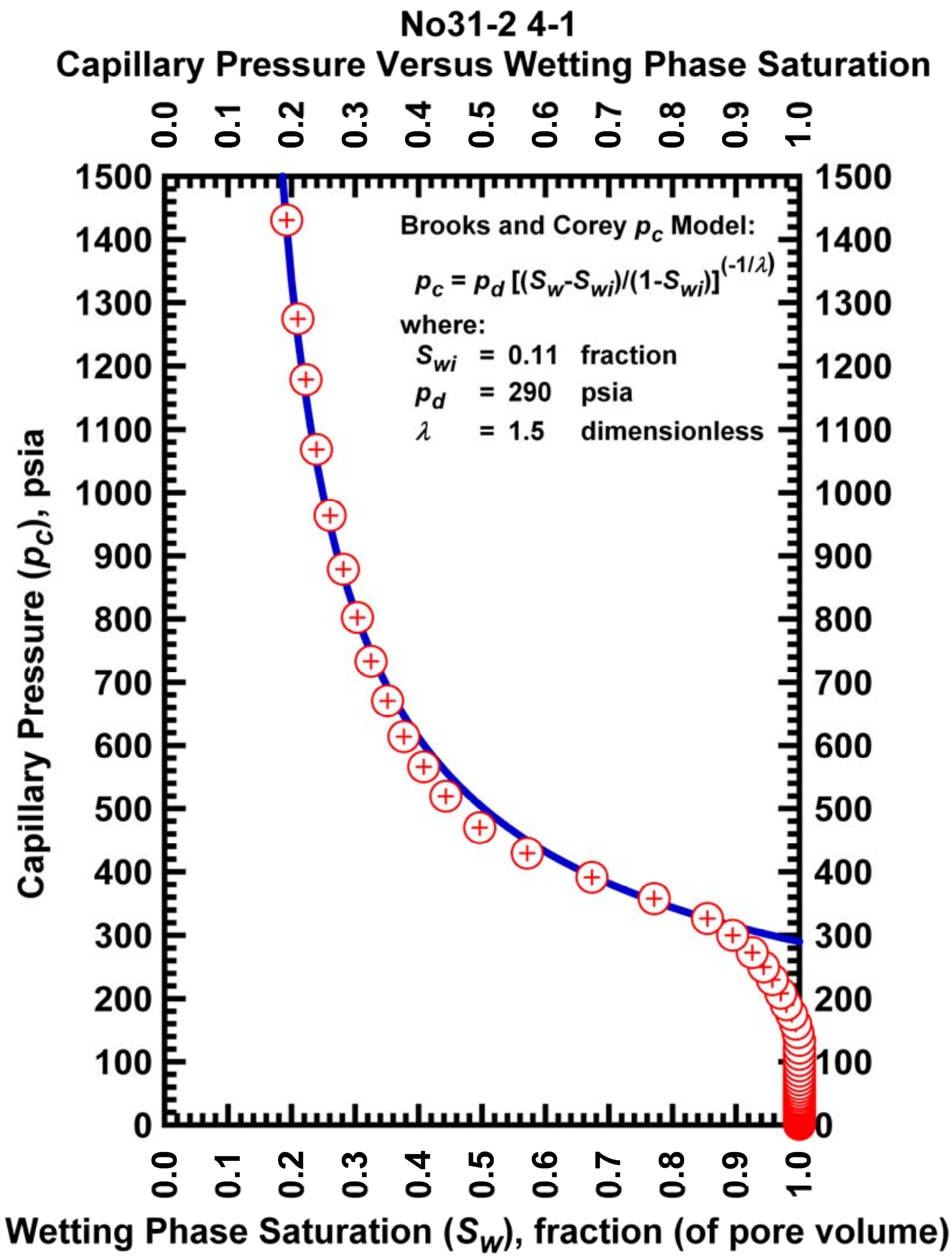

Figure I.49 — Plot of capillary pressure (p_c) vs. wetting phase saturation (S_w) — Case No31-2 4-1.

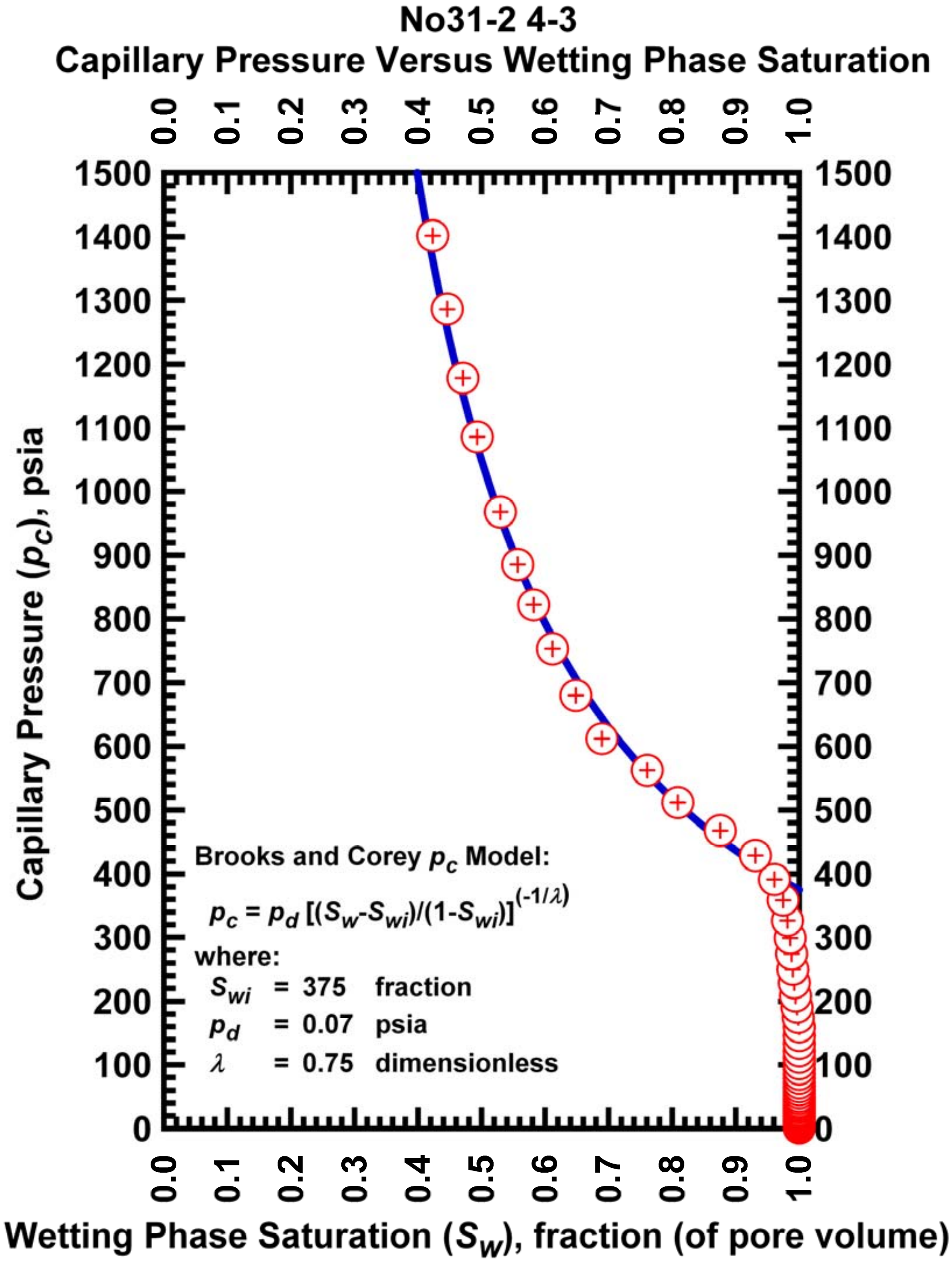

Figure I.50 — Plot of capillary pressure (p_c) vs. wetting phase saturation (S_w) — Case No31-2 4-3.

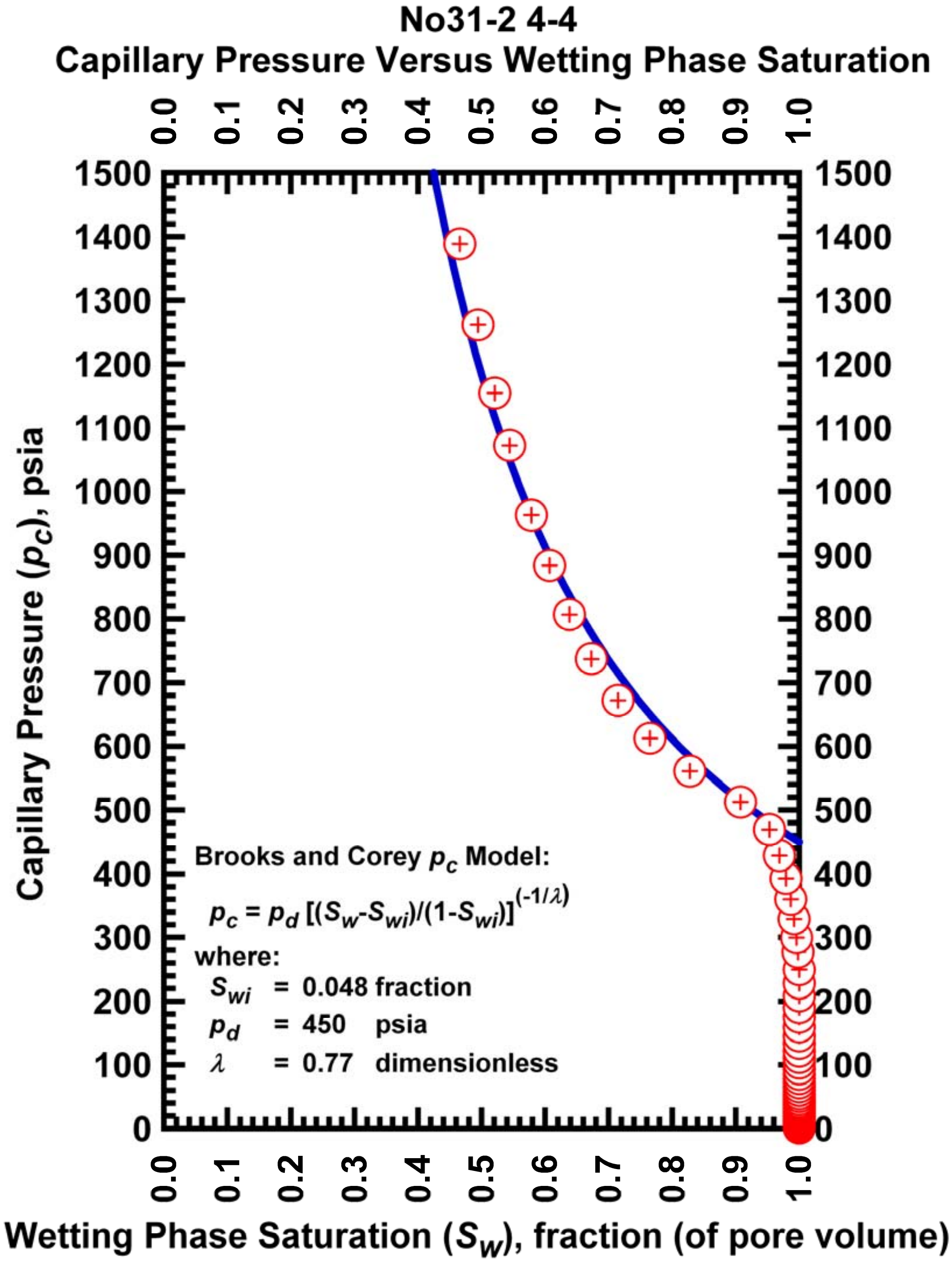

Figure I.51 — Plot of capillary pressure (p_c) vs. wetting phase saturation (S_w) — Case No31-2 4-4.

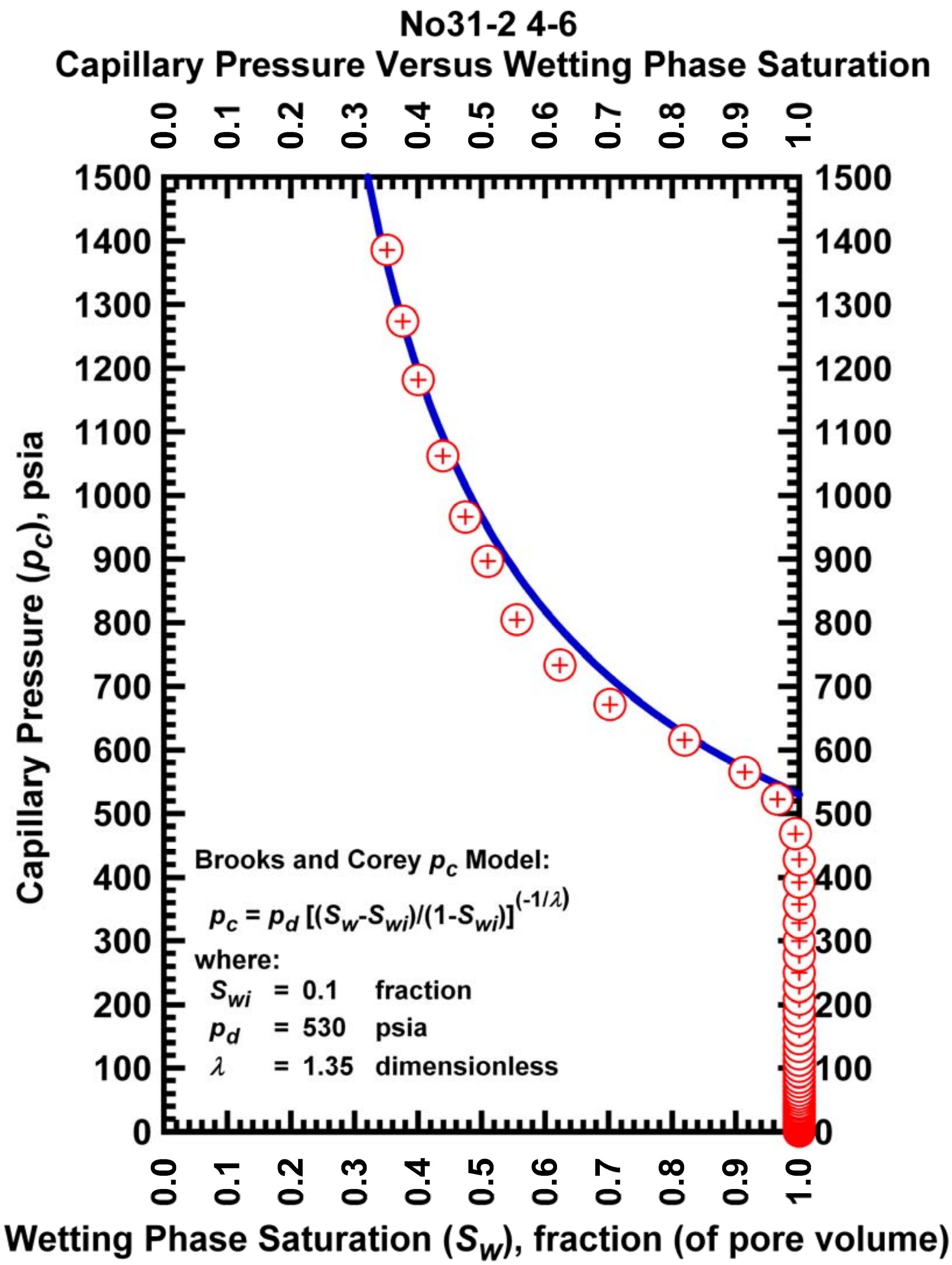

Figure I.52 — Plot of capillary pressure (p_c) vs. wetting phase saturation (S_w) — Case No31-2 4-6.

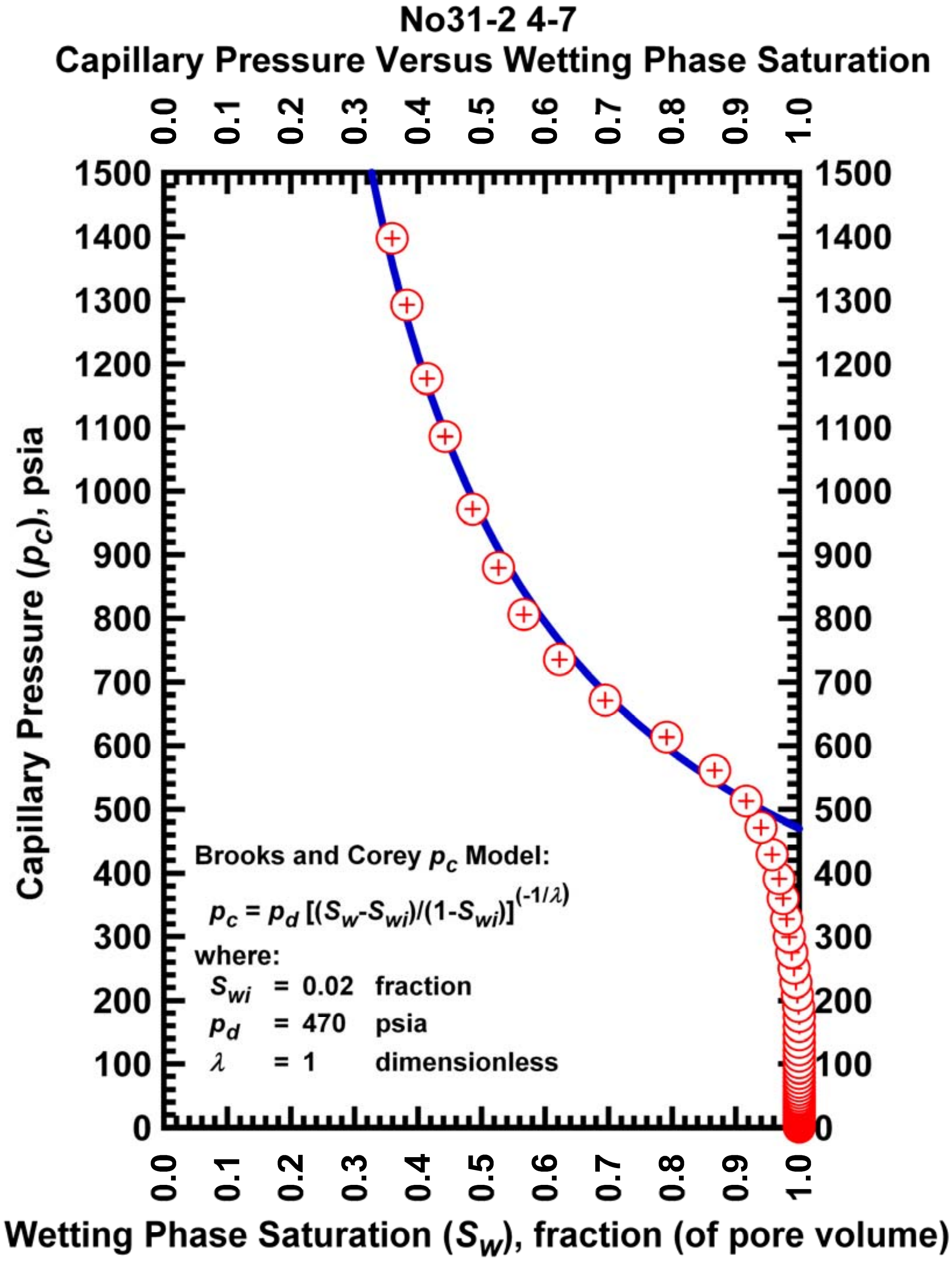

Figure I.53 — Plot of capillary pressure (p_c) vs. wetting phase saturation (S_w) — Case No31-2 4-7.

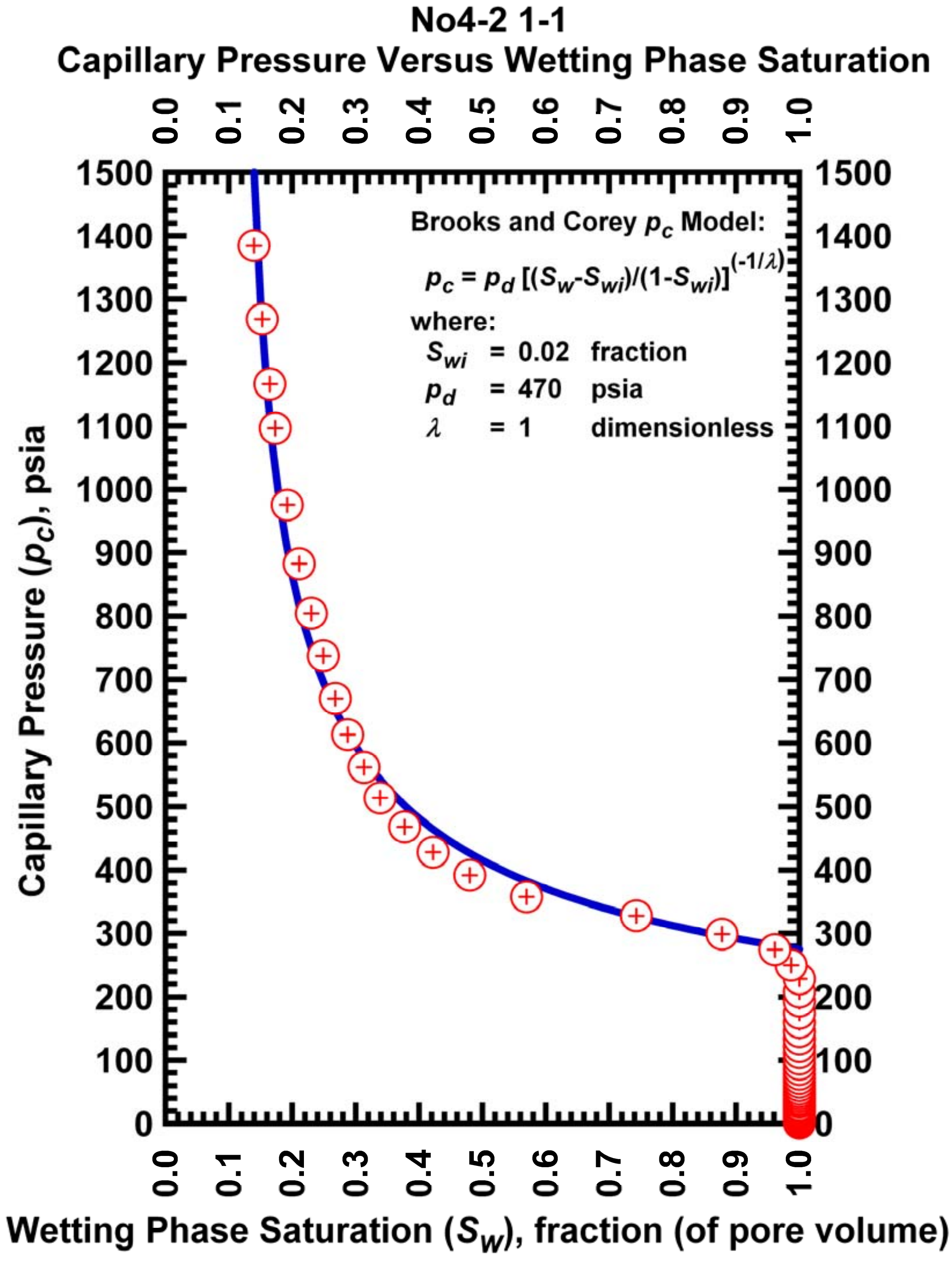

Figure I.54 — Plot of capillary pressure (p_c) vs. wetting phase saturation (S_w) — Case No4-2 1-1.

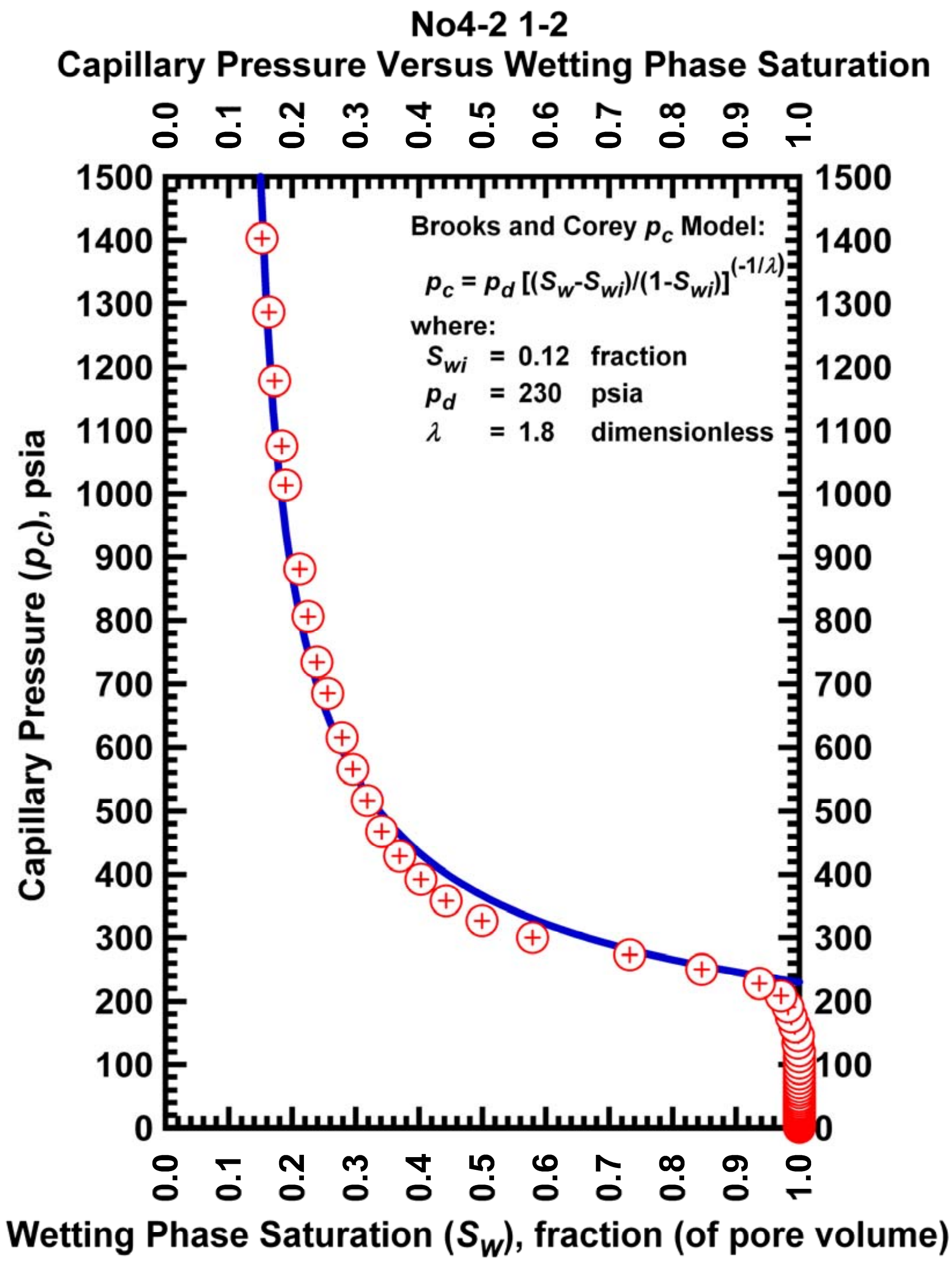

Figure I.55 — Plot of capillary pressure (p_c) vs. wetting phase saturation (S_w) — Case No4-2 1-2.

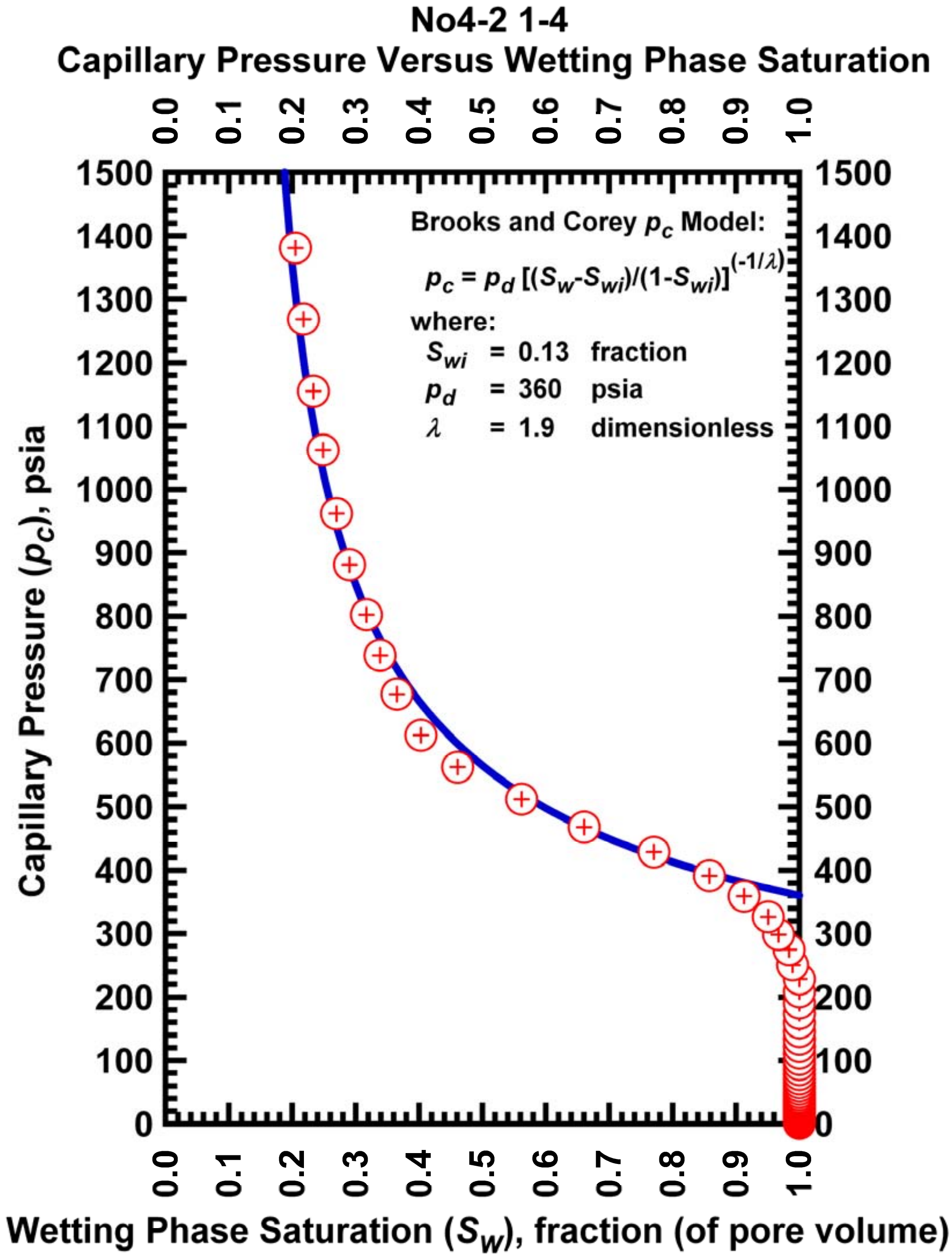

Figure I.57 — Plot of capillary pressure (p_c) vs. wetting phase saturation (S_w) — Case No4-2 1-4.

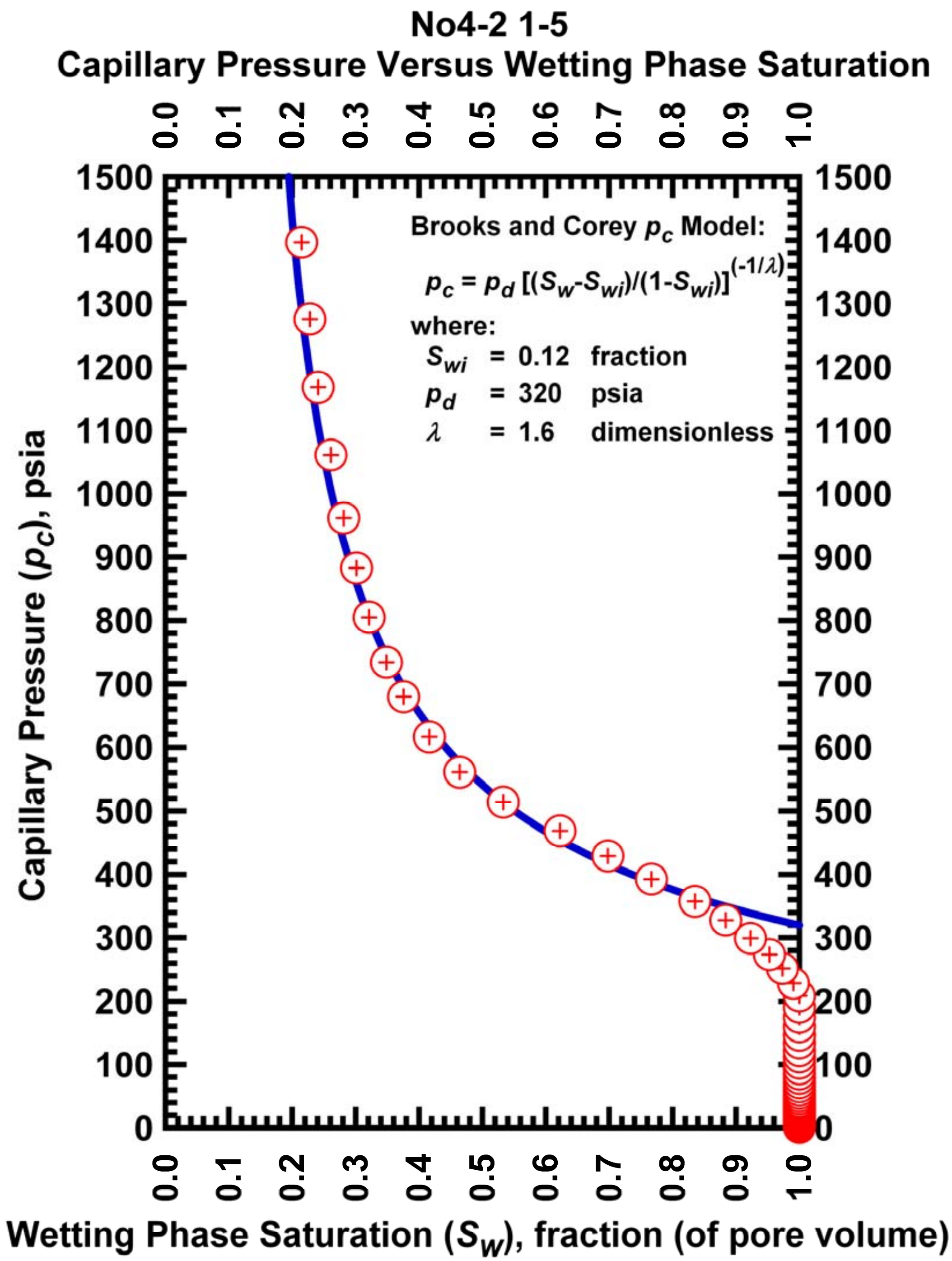

Figure I.58 — Plot of capillary pressure (p_c) vs. wetting phase saturation (S_w) — Case No4-2 1-5.

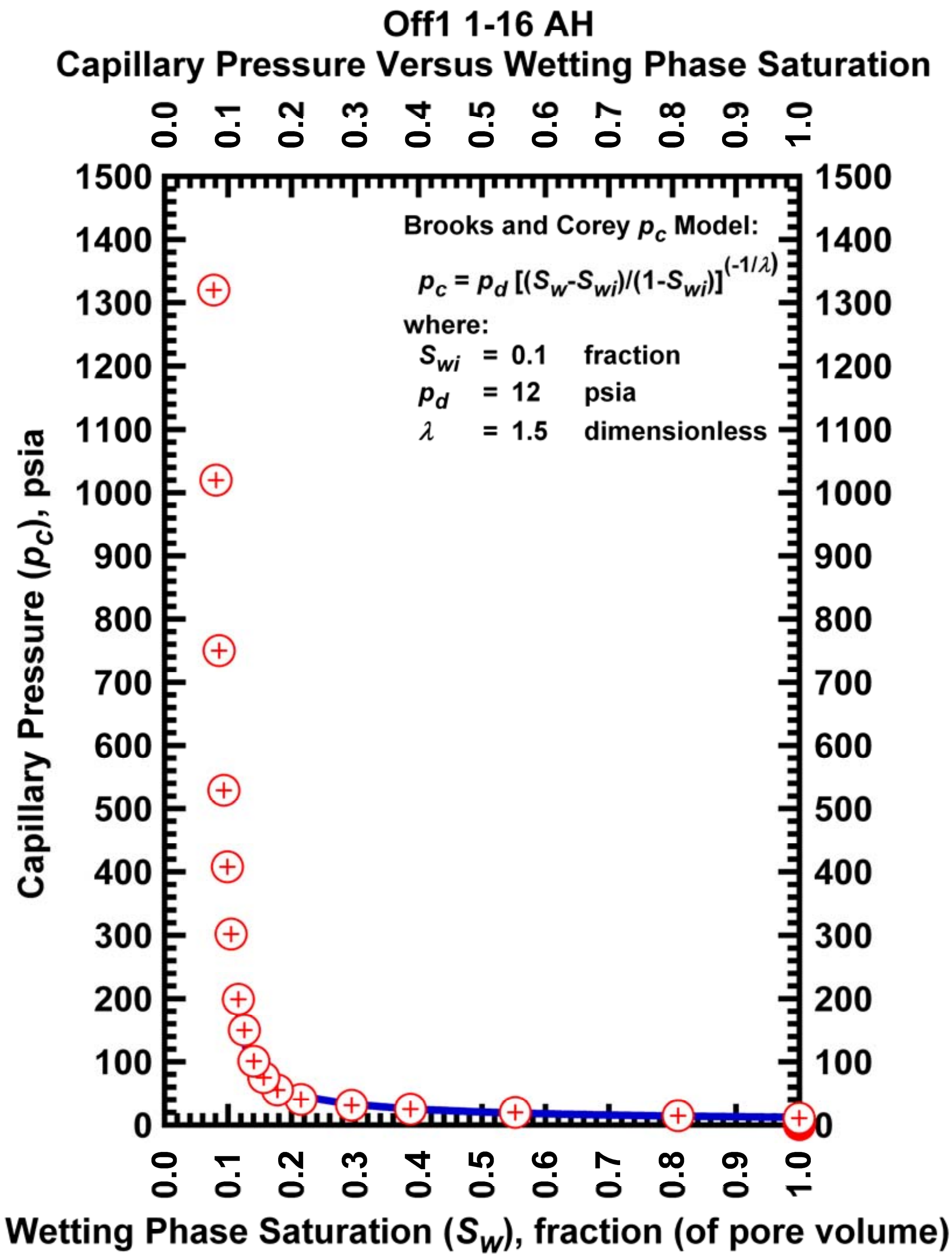

Figure I.59 — Plot of capillary pressure (p_c) vs. wetting phase saturation (S_w) — Case Off1 1-16AH.

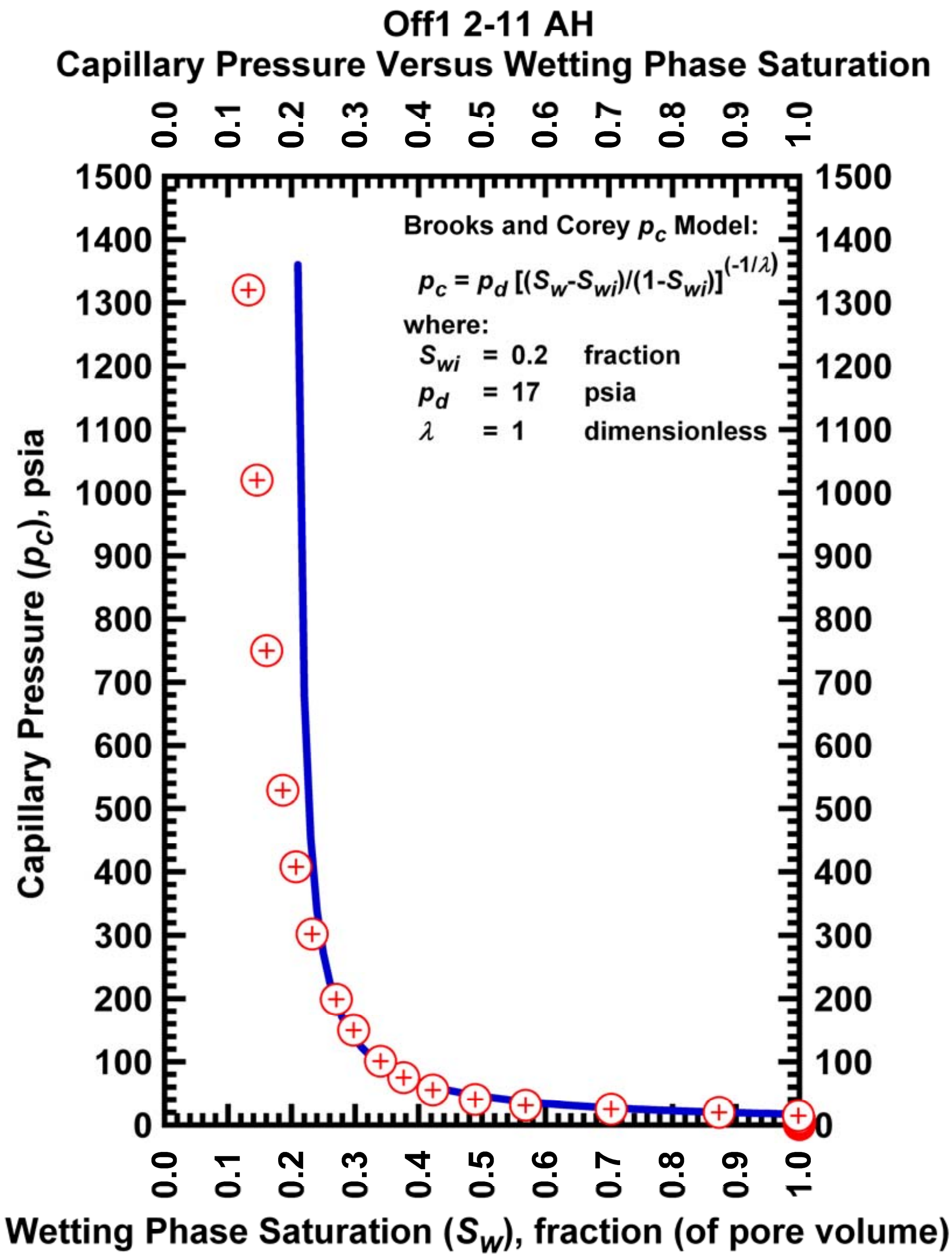

Figure I.60 — Plot of capillary pressure (p_c) vs. wetting phase saturation (S_w) — Case Off1 2-11AH.

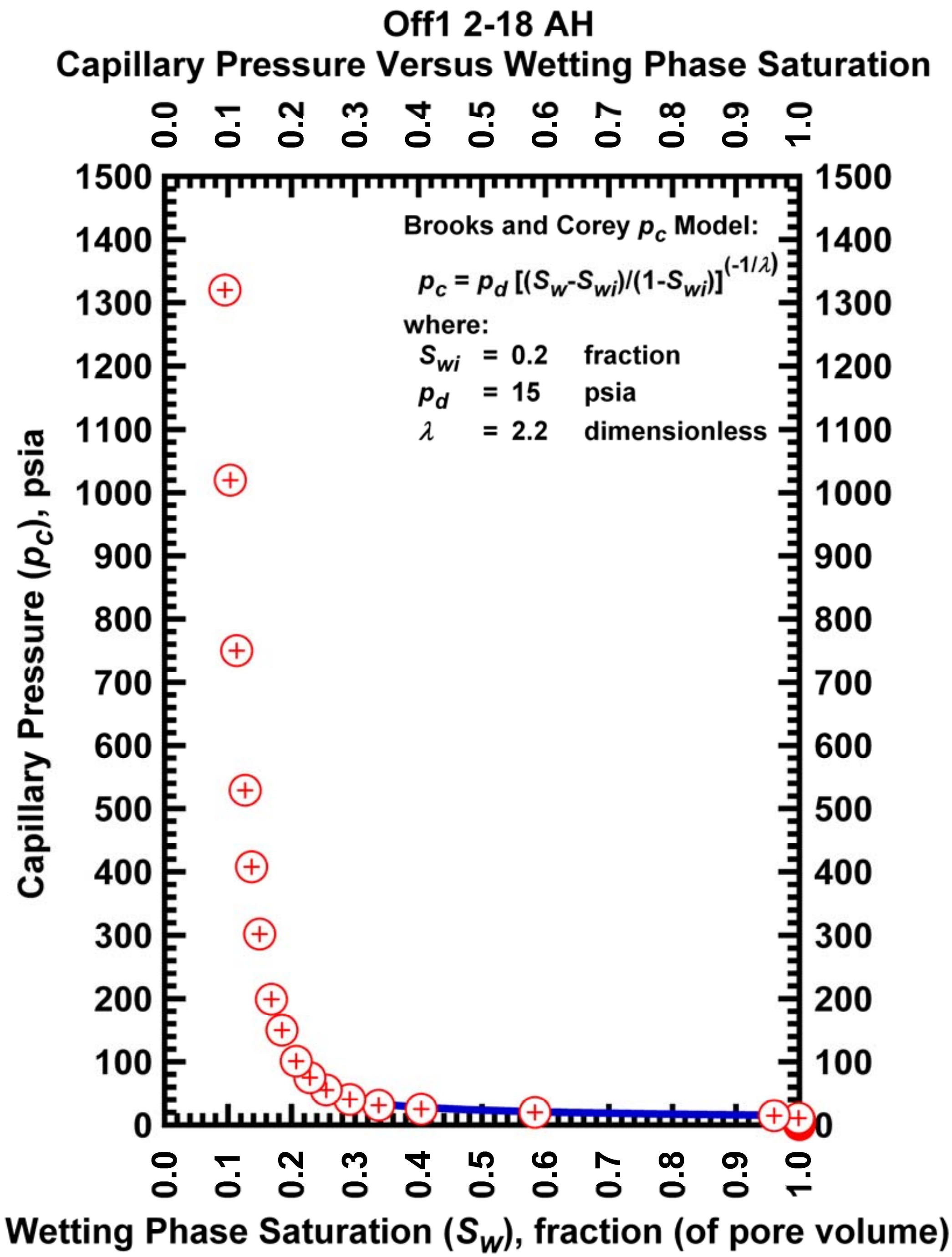

Figure I.60 — Plot of capillary pressure (p_c) vs. wetting phase saturation (S_w) — Case Off1 2-18AH.

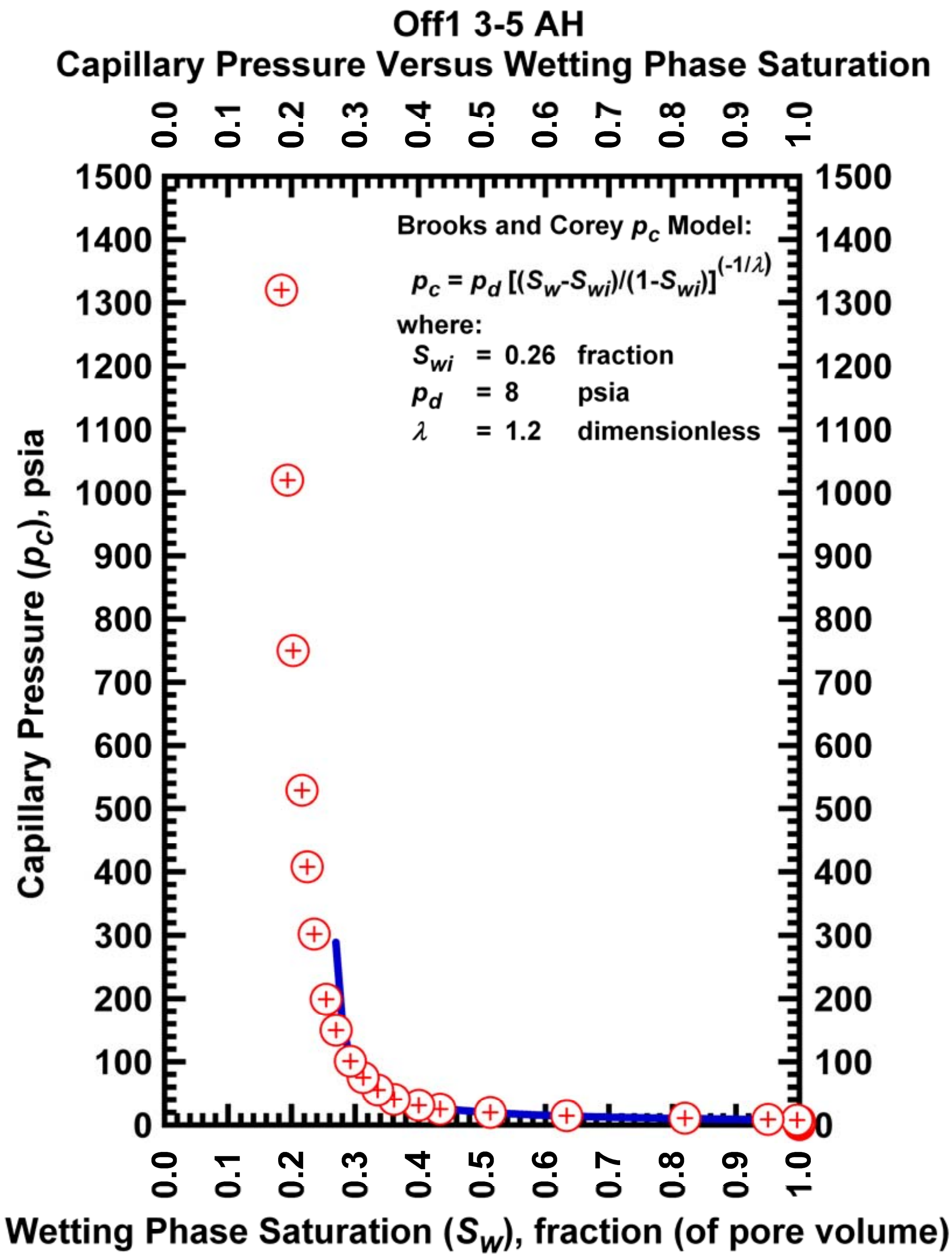

Figure I.61 — Plot of capillary pressure (p_c) vs. wetting phase saturation (S_w) — Case Off1 3-5AH.

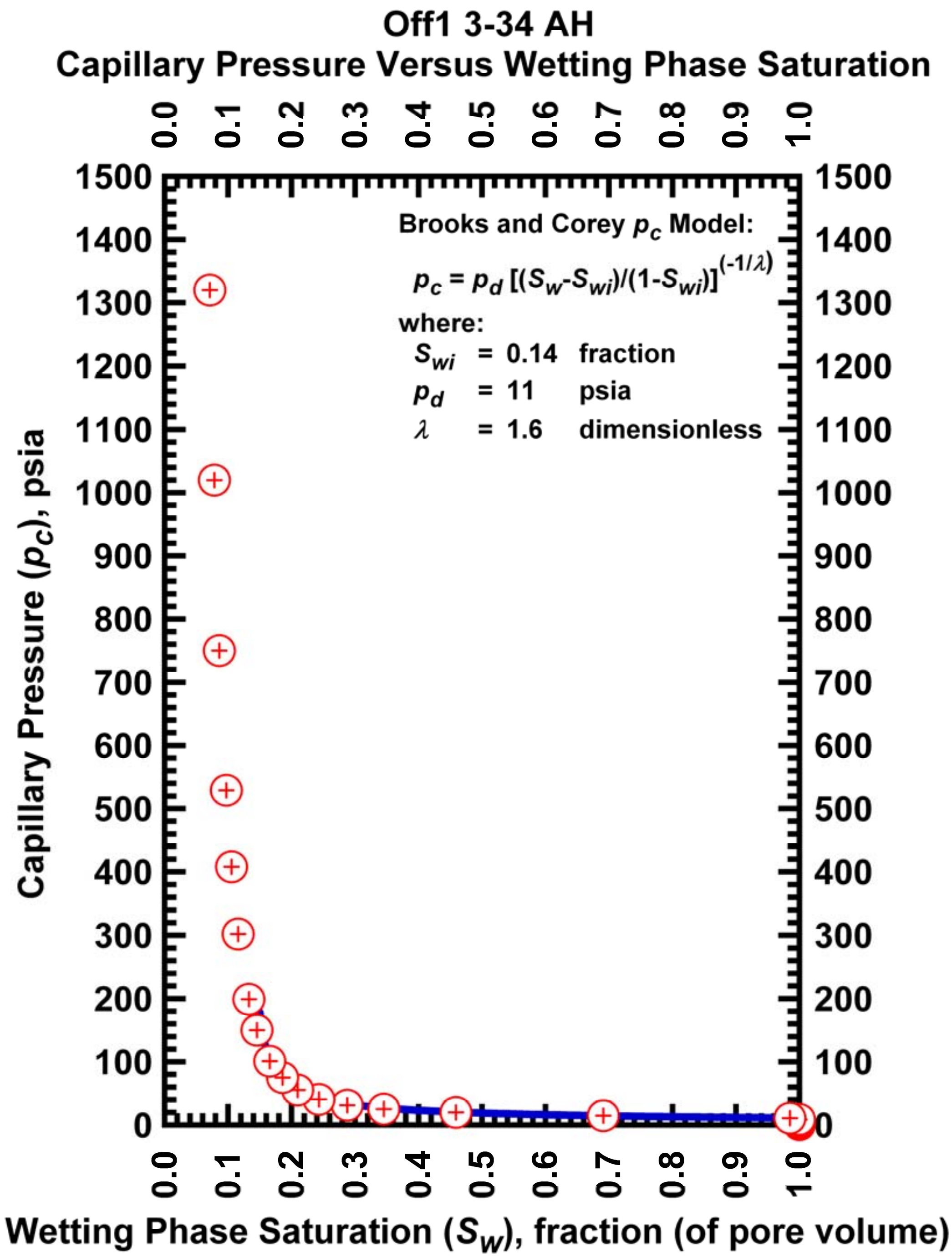

Figure I.62 — Plot of capillary pressure (p_c) vs. wetting phase saturation (S_w) — Case Off1 3-34AH.

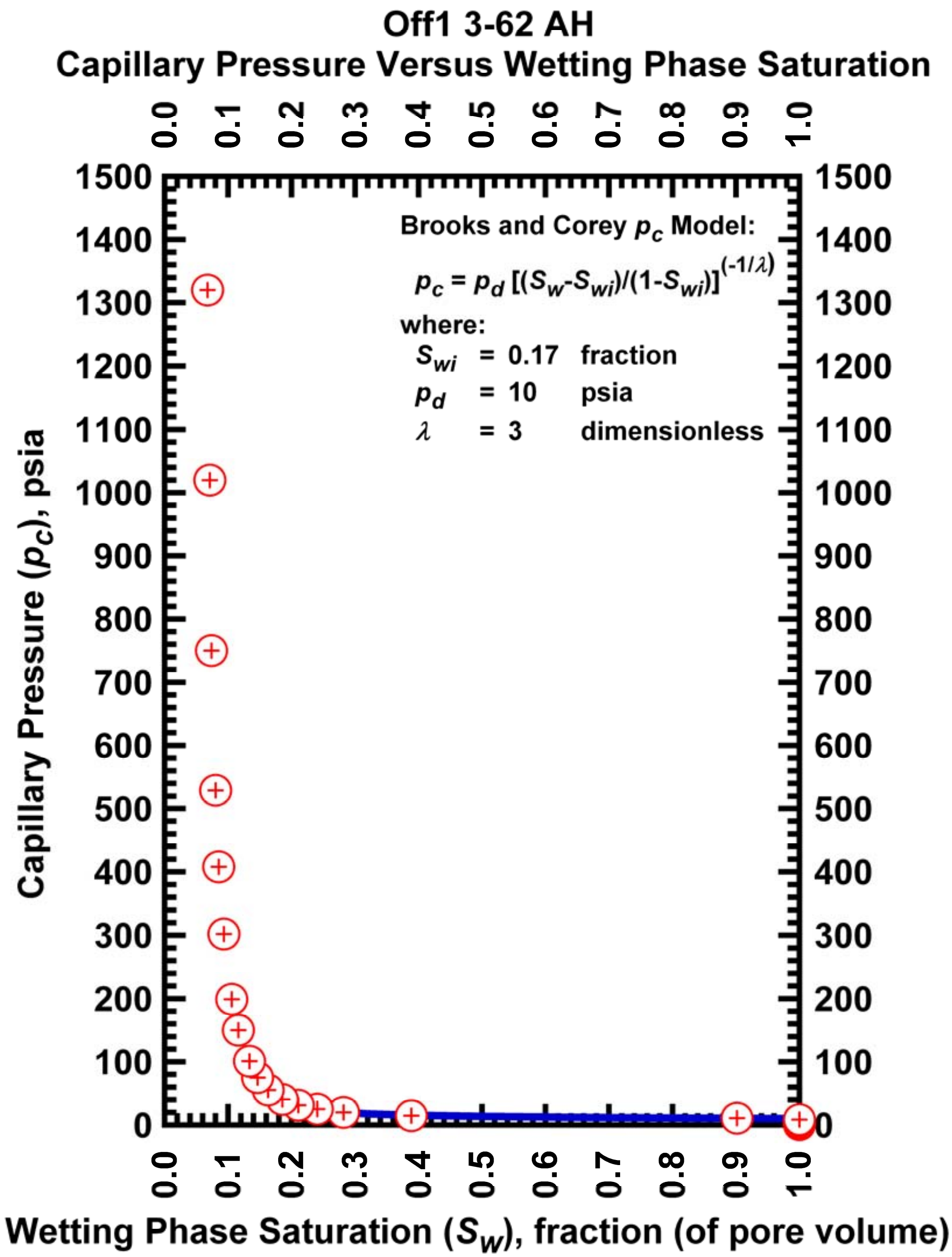

Figure I.63 — Plot of capillary pressure (p_c) vs. wetting phase saturation (S_w) — Case Off1 3-62AH.

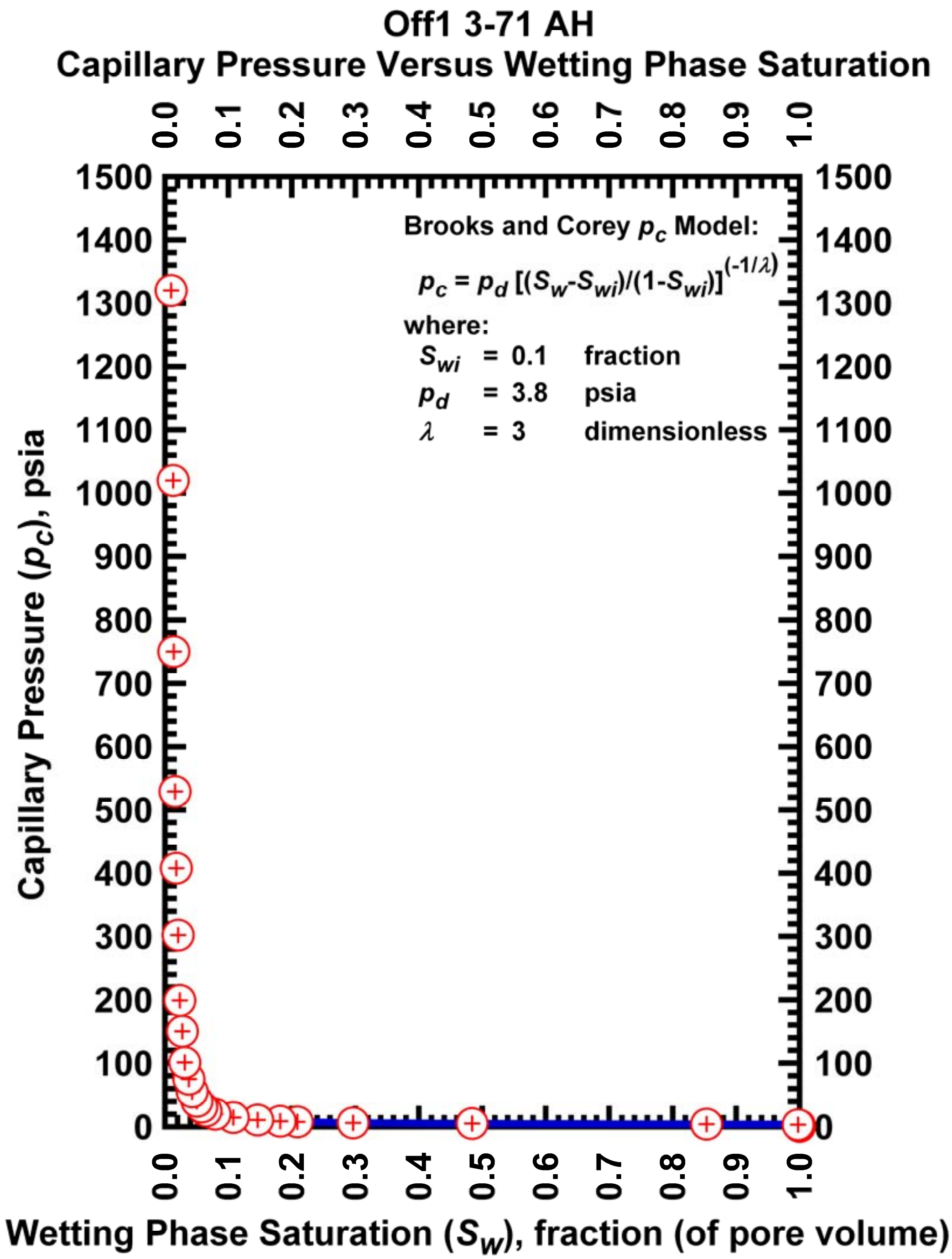

Figure I.64 — Plot of capillary pressure (p_c) vs. wetting phase saturation (S_w) — Case Off1 3-71AH.

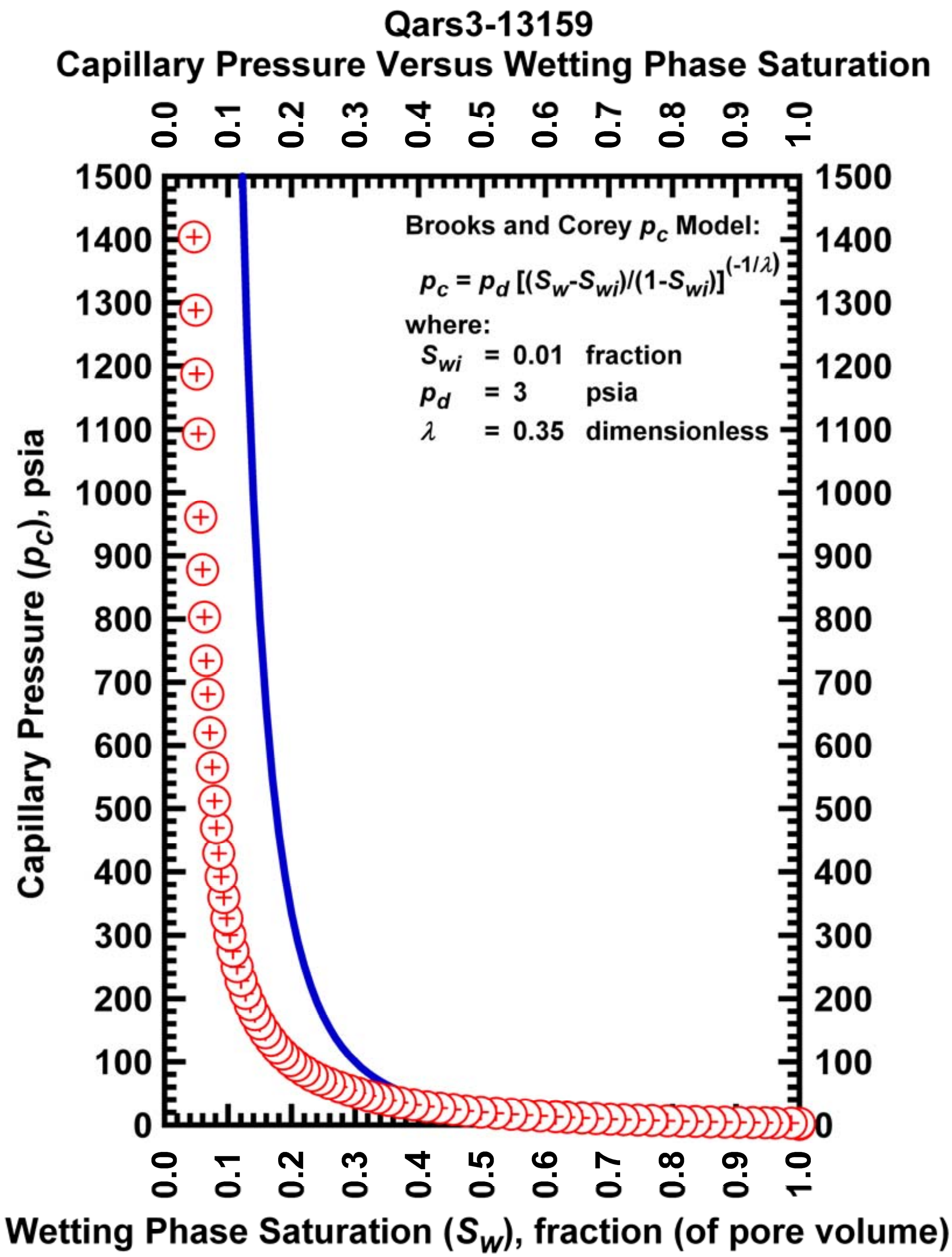

Figure I.65 — Plot of capillary pressure (p_c) vs. wetting phase saturation (S_w) — Case Qars3-13159.

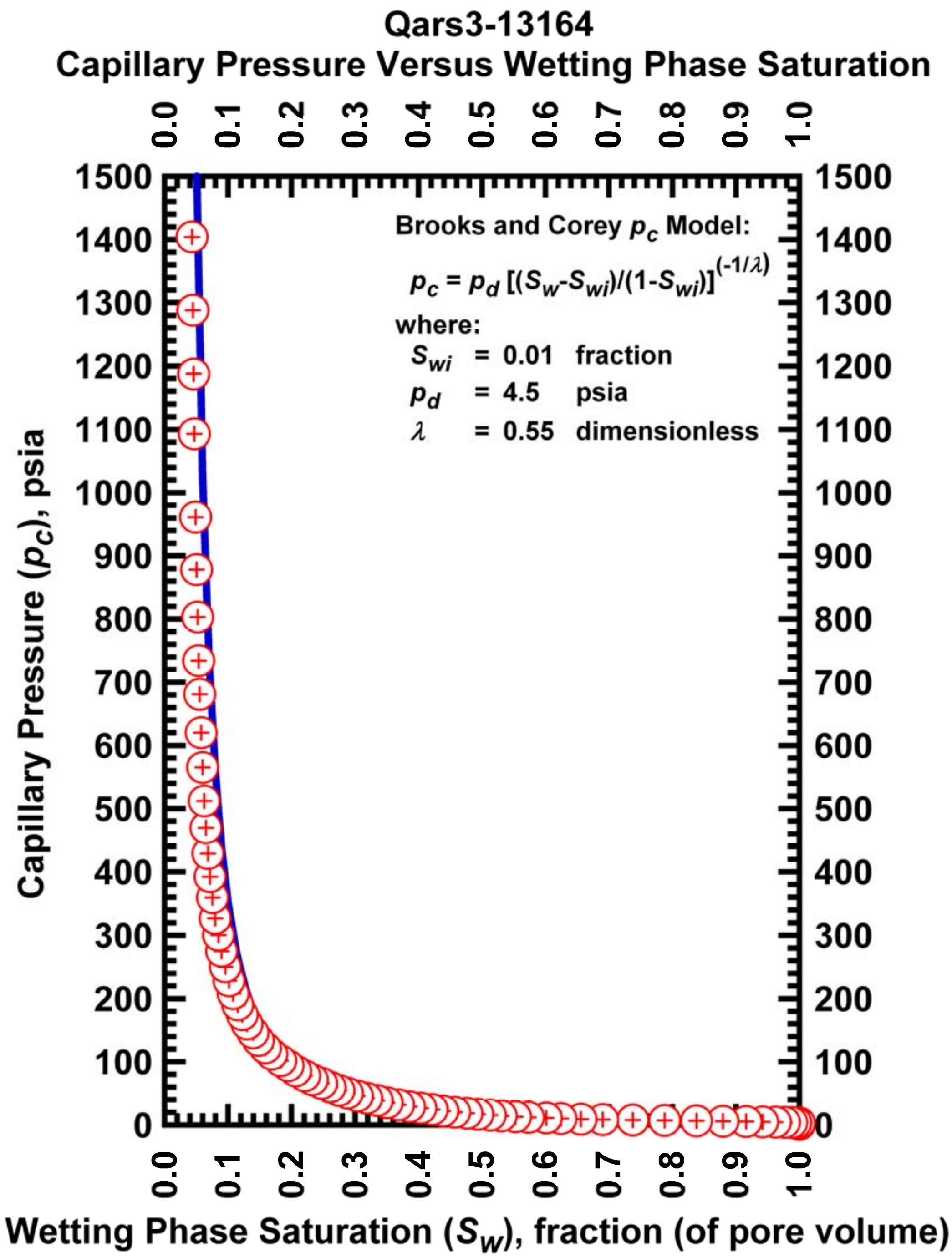

Figure I.66 — Plot of capillary pressure (p_c) vs. wetting phase saturation (S_w) — Case Qars3-13164.

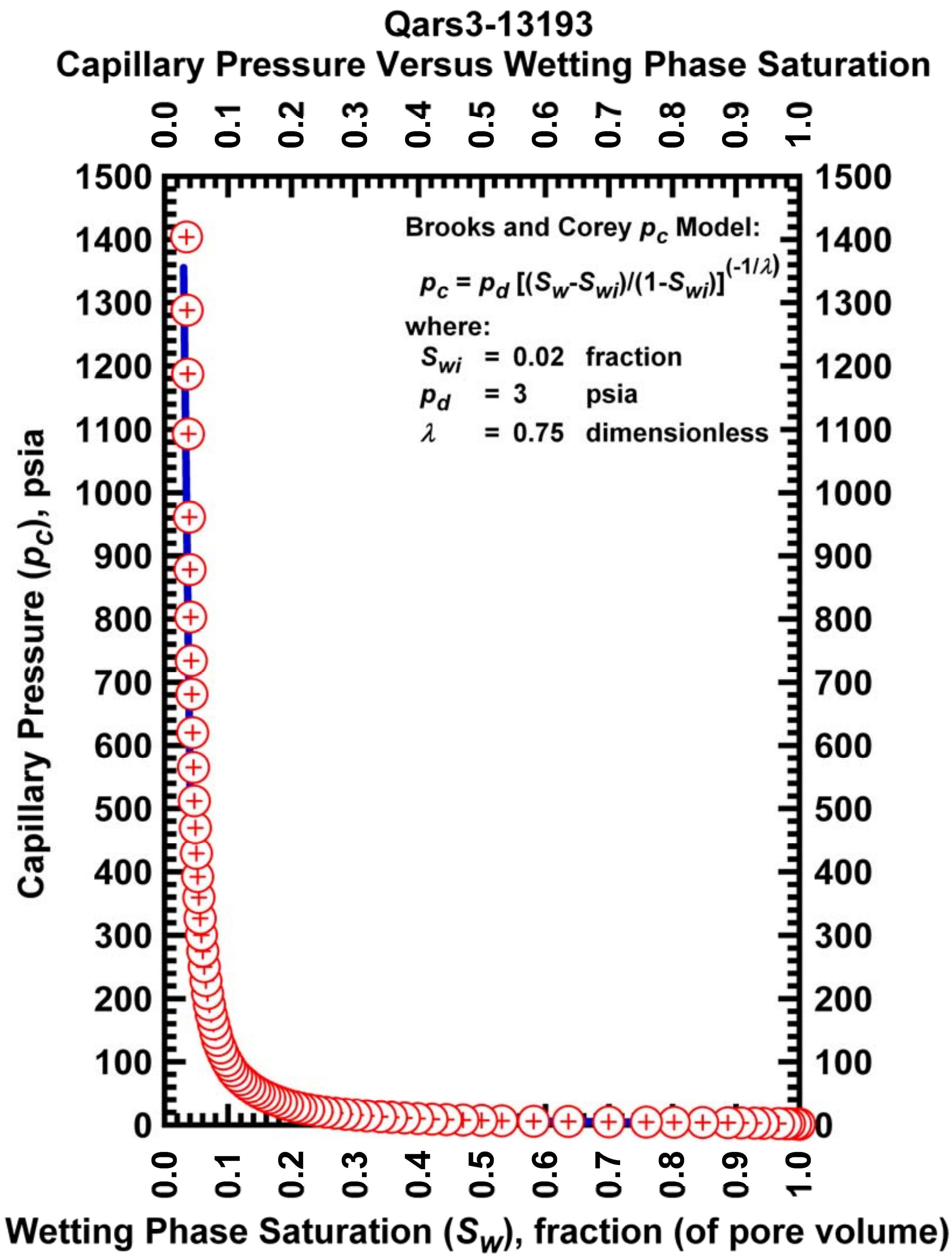

Figure I.67 — Plot of capillary pressure (p_c) vs. wetting phase saturation (S_w) — Case Qars3-13193.

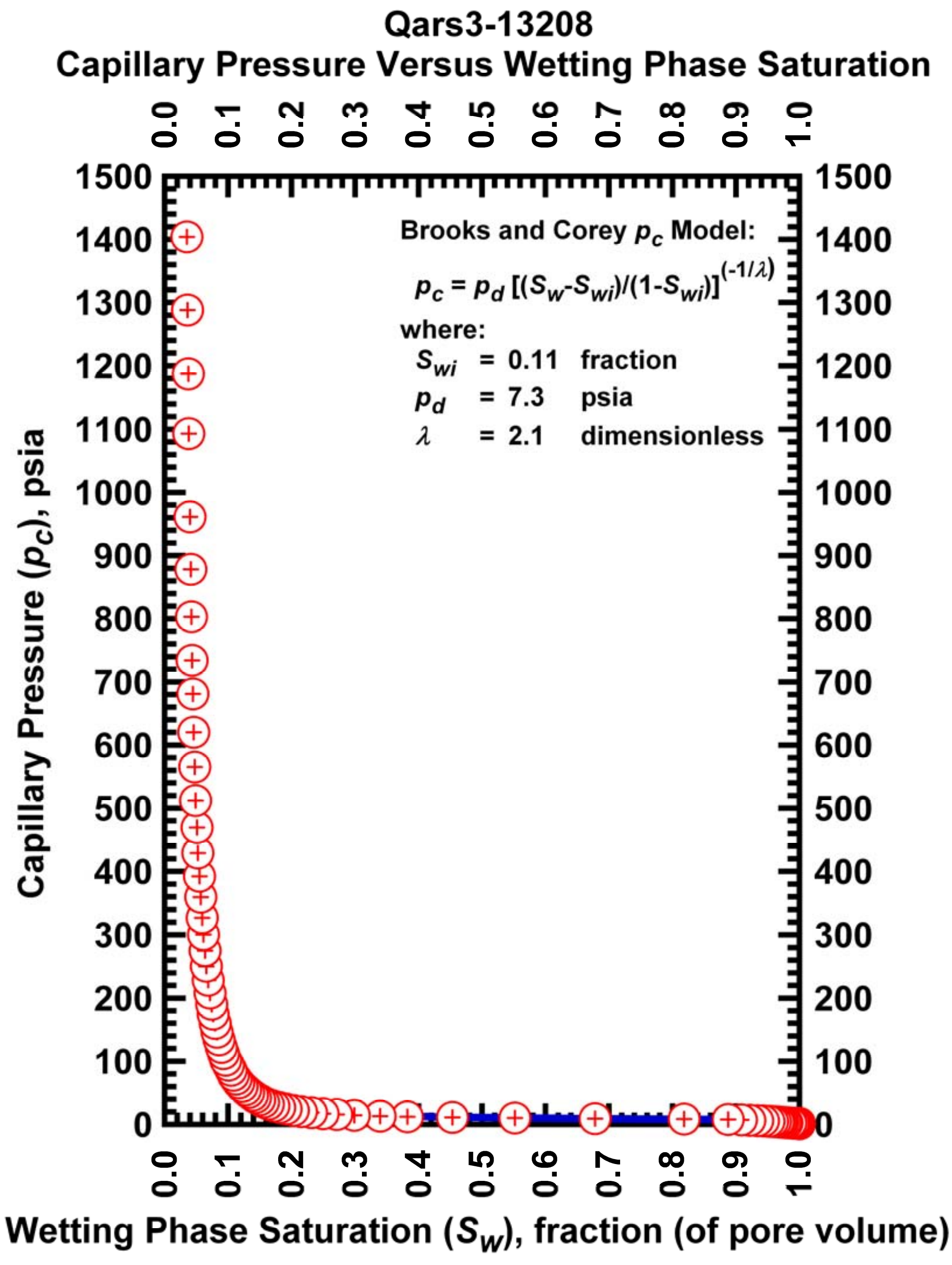

Figure I.68 — Plot of capillary pressure (p_c) vs. wetting phase saturation (S_w) — Case Qars3-13208.

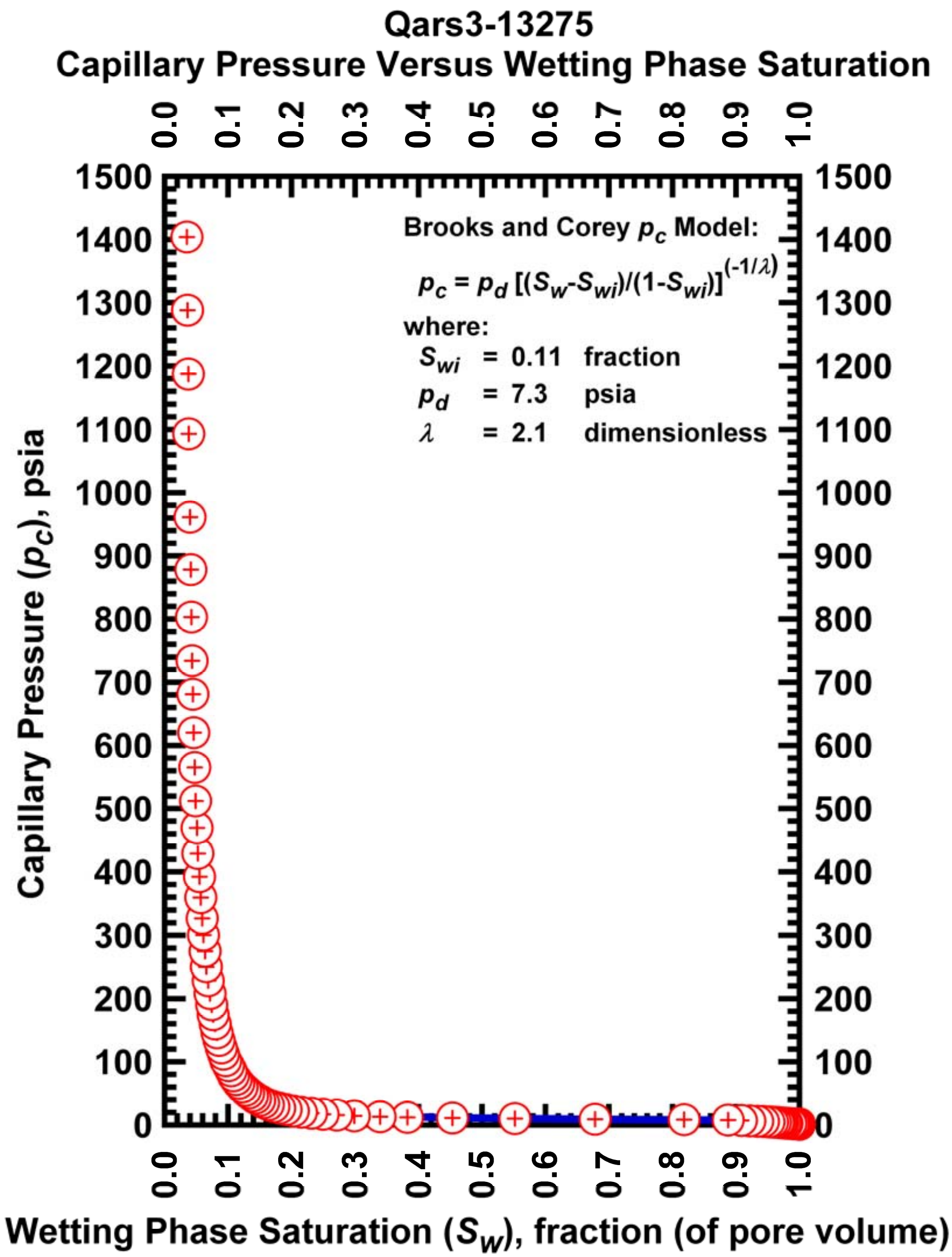

Figure I.69 — Plot of capillary pressure (p_c) vs. wetting phase saturation (S_w) — Case Qars3-13275.

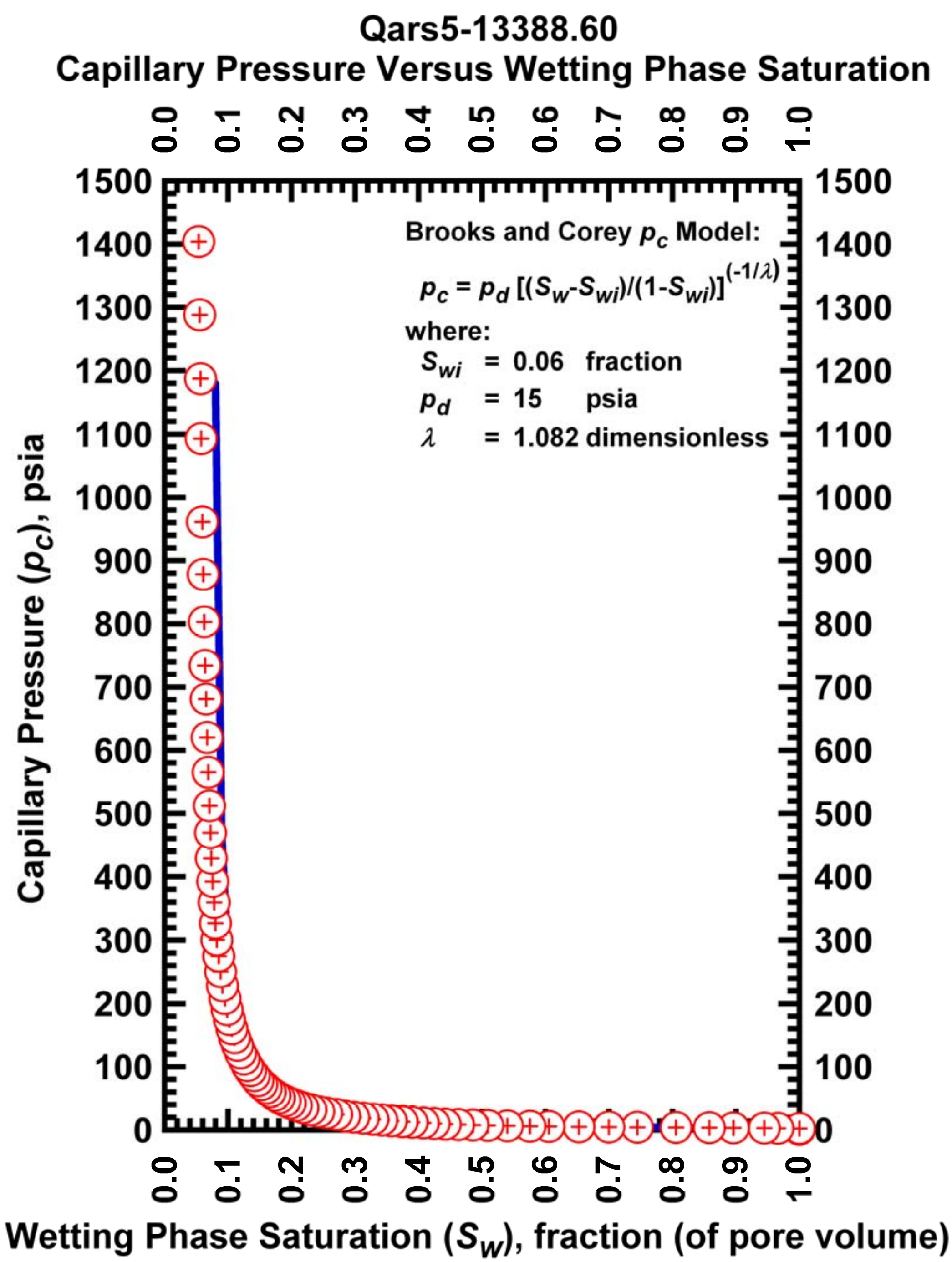

Figure I.70 — Plot of capillary pressure (p_c) vs. wetting phase saturation (S_w) — Case Qars5-13388.

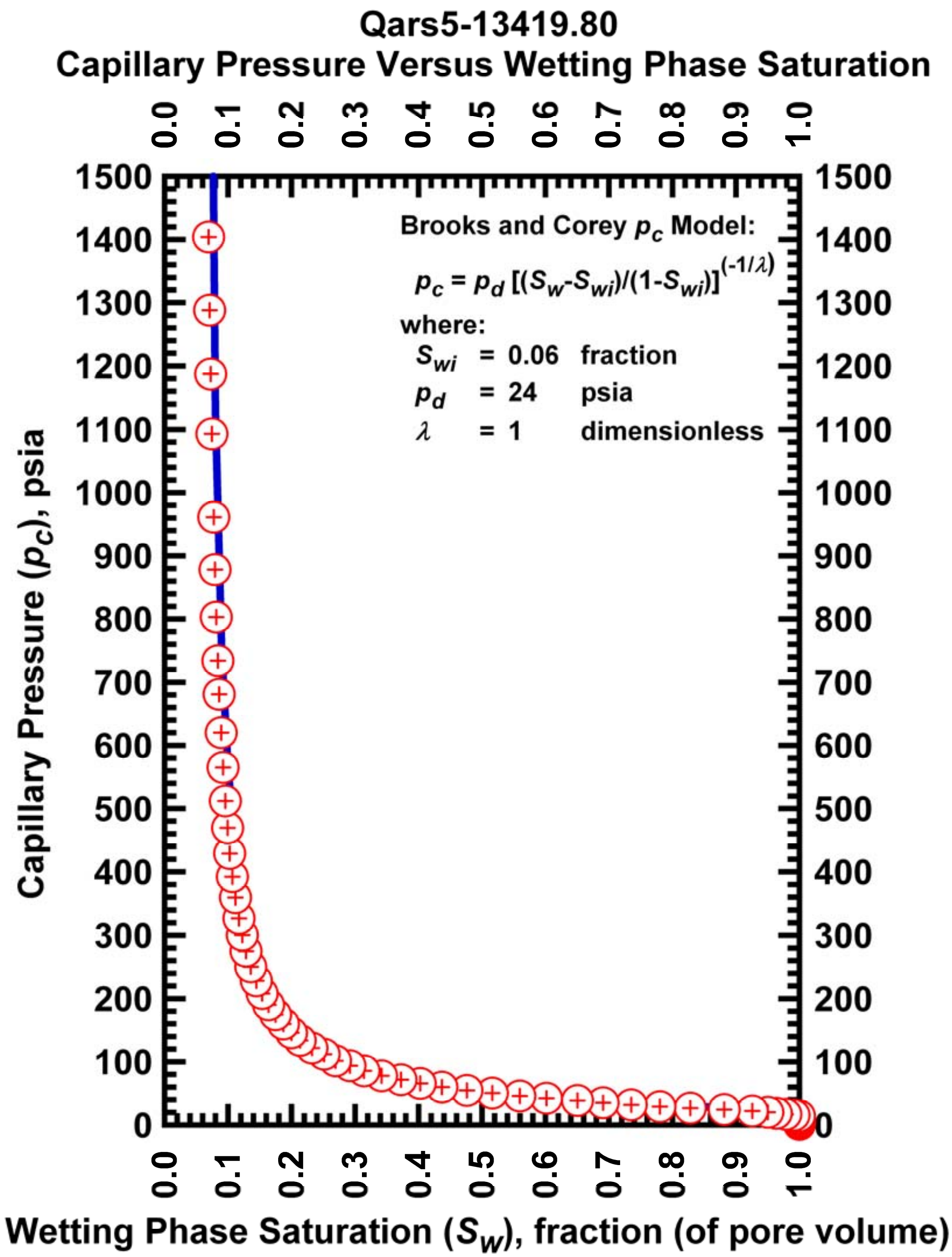

Figure I.71 — Plot of capillary pressure (p_c) vs. wetting phase saturation (S_w) — Case Qars5-13419.

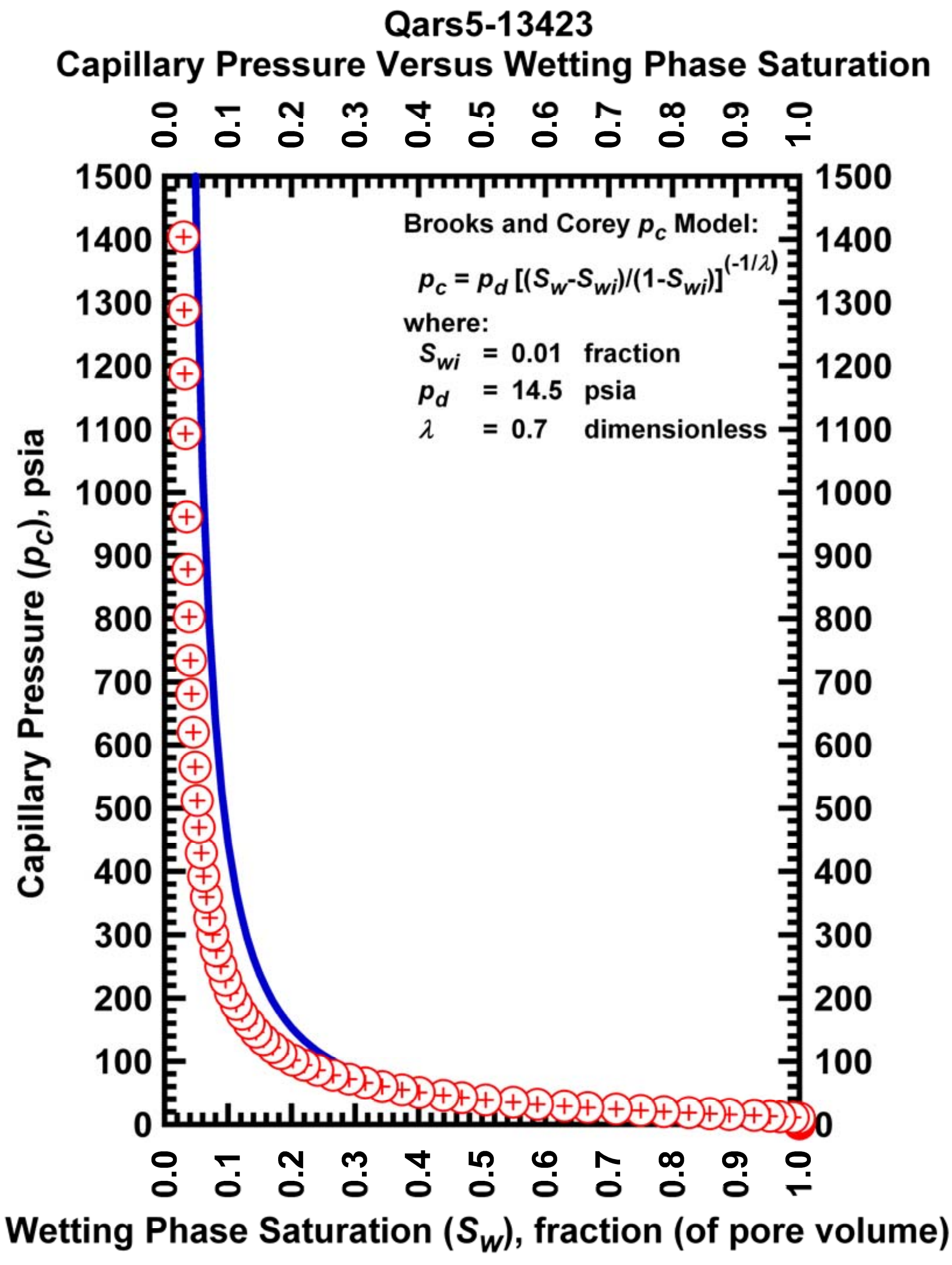

Figure I.72 — Plot of capillary pressure (p_c) vs. wetting phase saturation (S_w) — Case Qars5-13423.

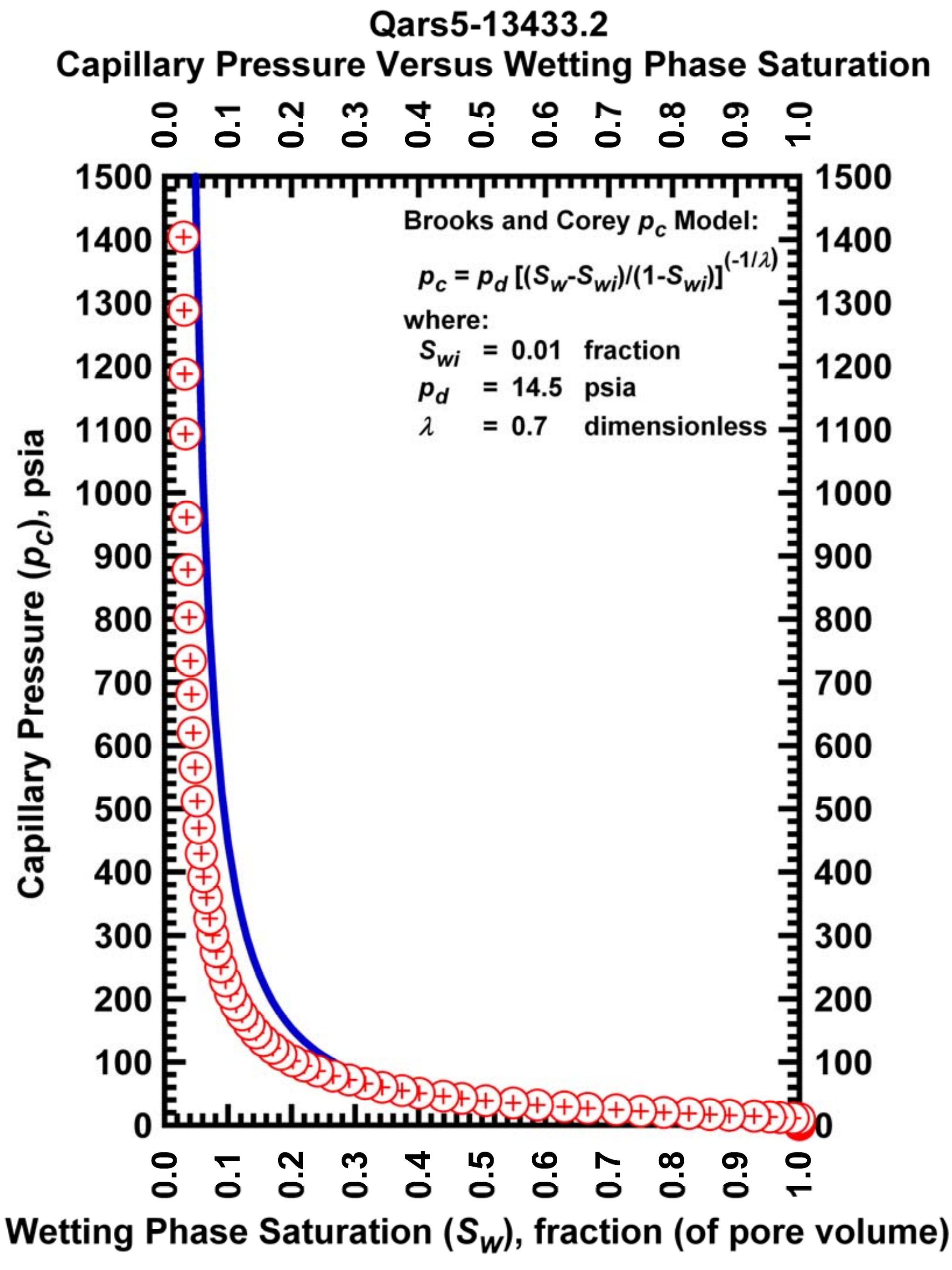

Figure I.73 — Plot of capillary pressure (p_c) vs. wetting phase saturation (S_w) — Case Qars5-13433.

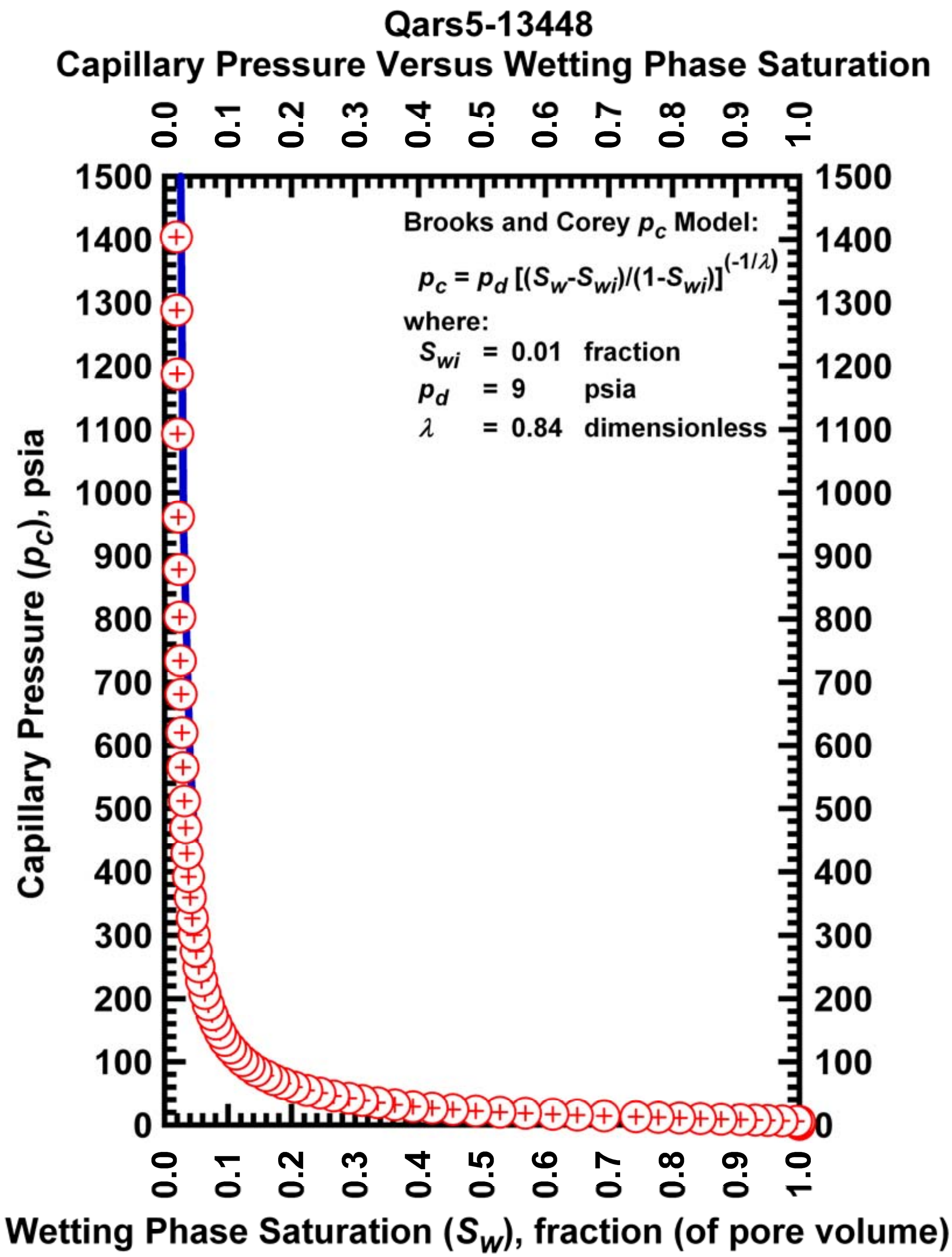

Figure I.74 — Plot of capillary pressure (p_c) vs. wetting phase saturation (S_w) — Case Qars5-13448.

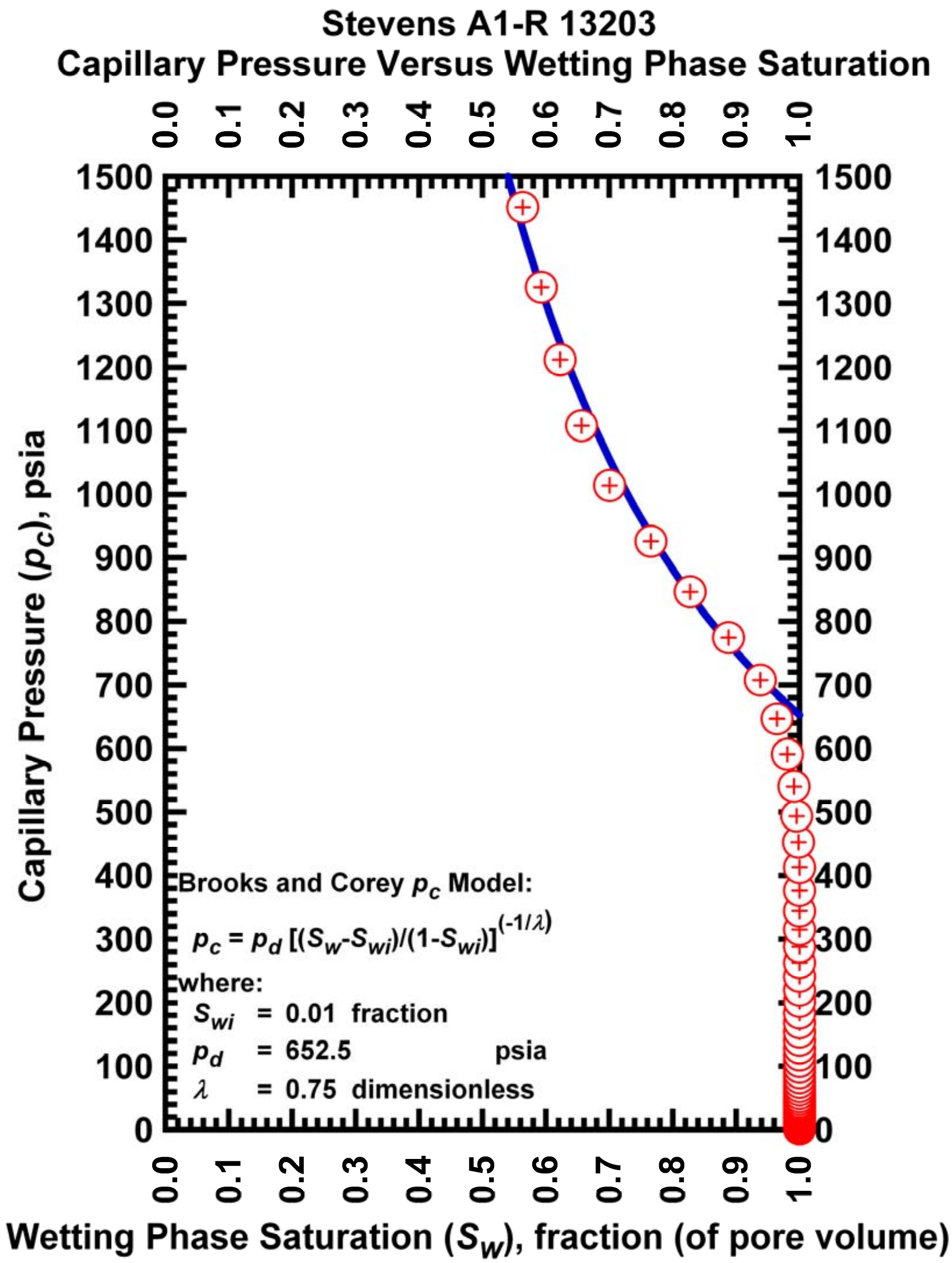

Figure I.75 — Plot of capillary pressure (p_c) vs. wetting phase saturation (S_w) — Case Stevens A1-R 13203

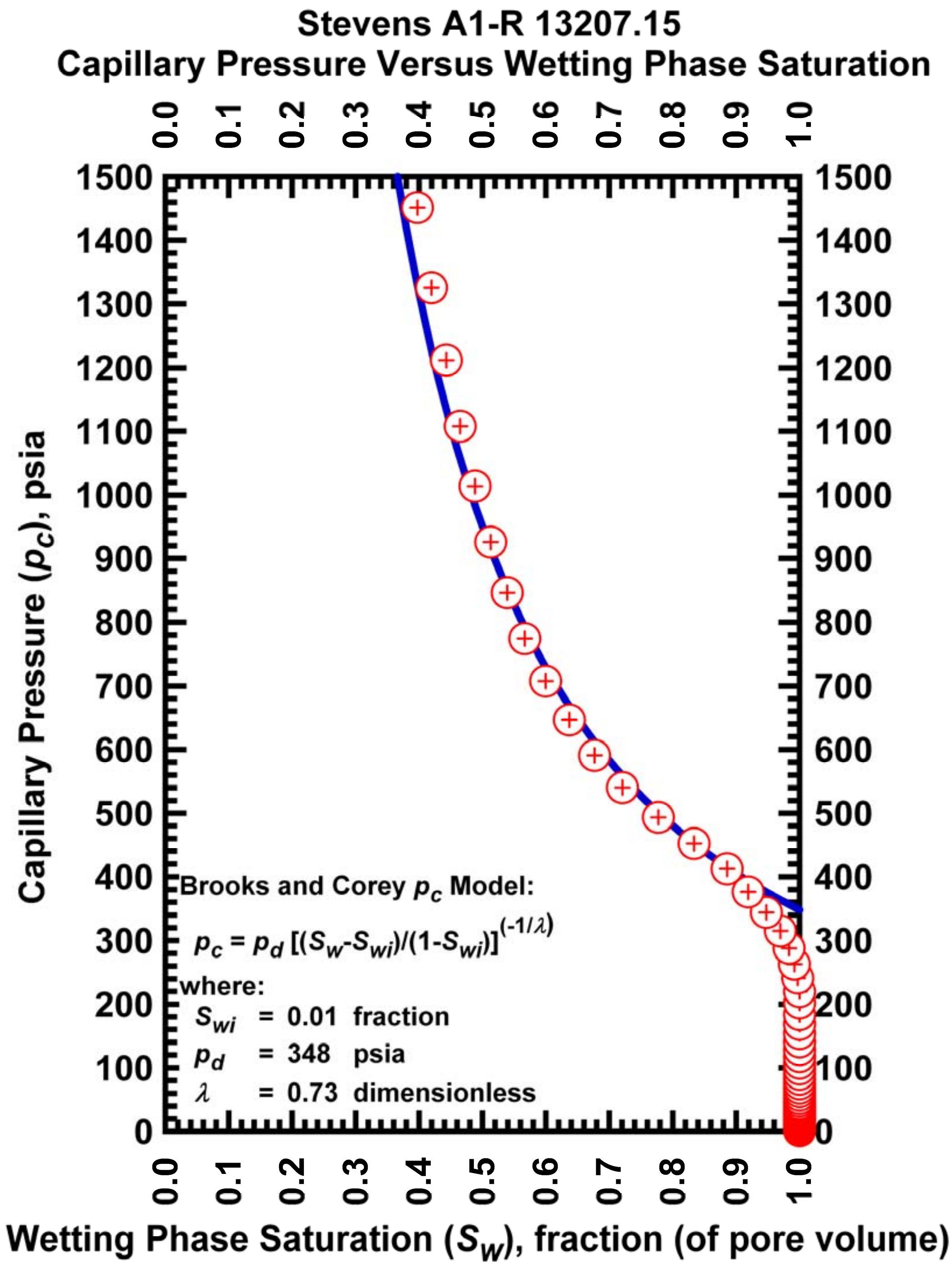

Figure I.76 — Plot of capillary pressure (p_c) vs. wetting phase saturation (S_w) — Case Stevens A1-R 13207.15

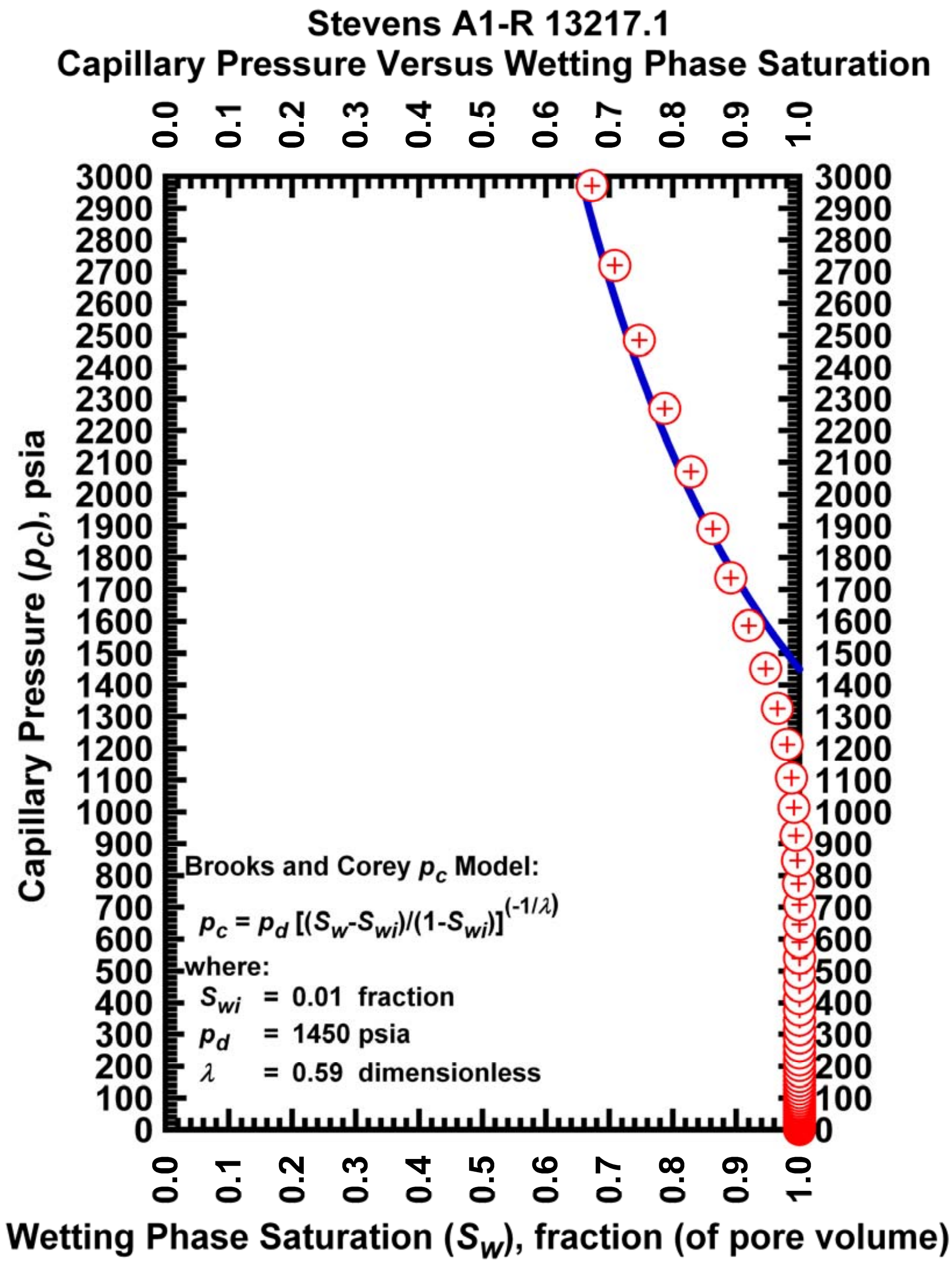

Figure I.77 — Plot of capillary pressure (p_c) vs. wetting phase saturation (S_w) — Case Stevens A1-R 13217.1

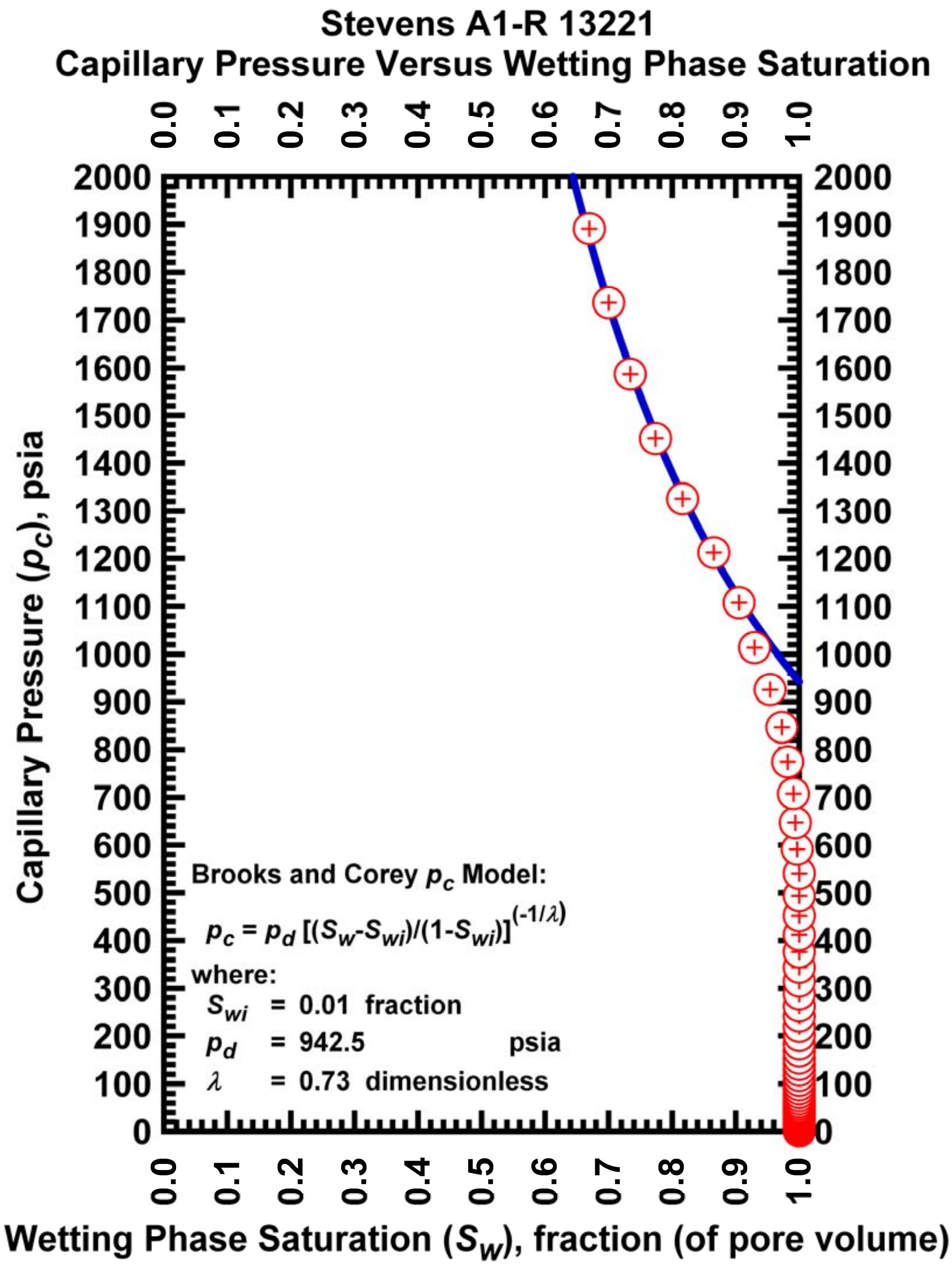

Figure I.78 — Plot of capillary pressure (p_c) vs. wetting phase saturation (S_w) — Case Stevens A1-R 13221

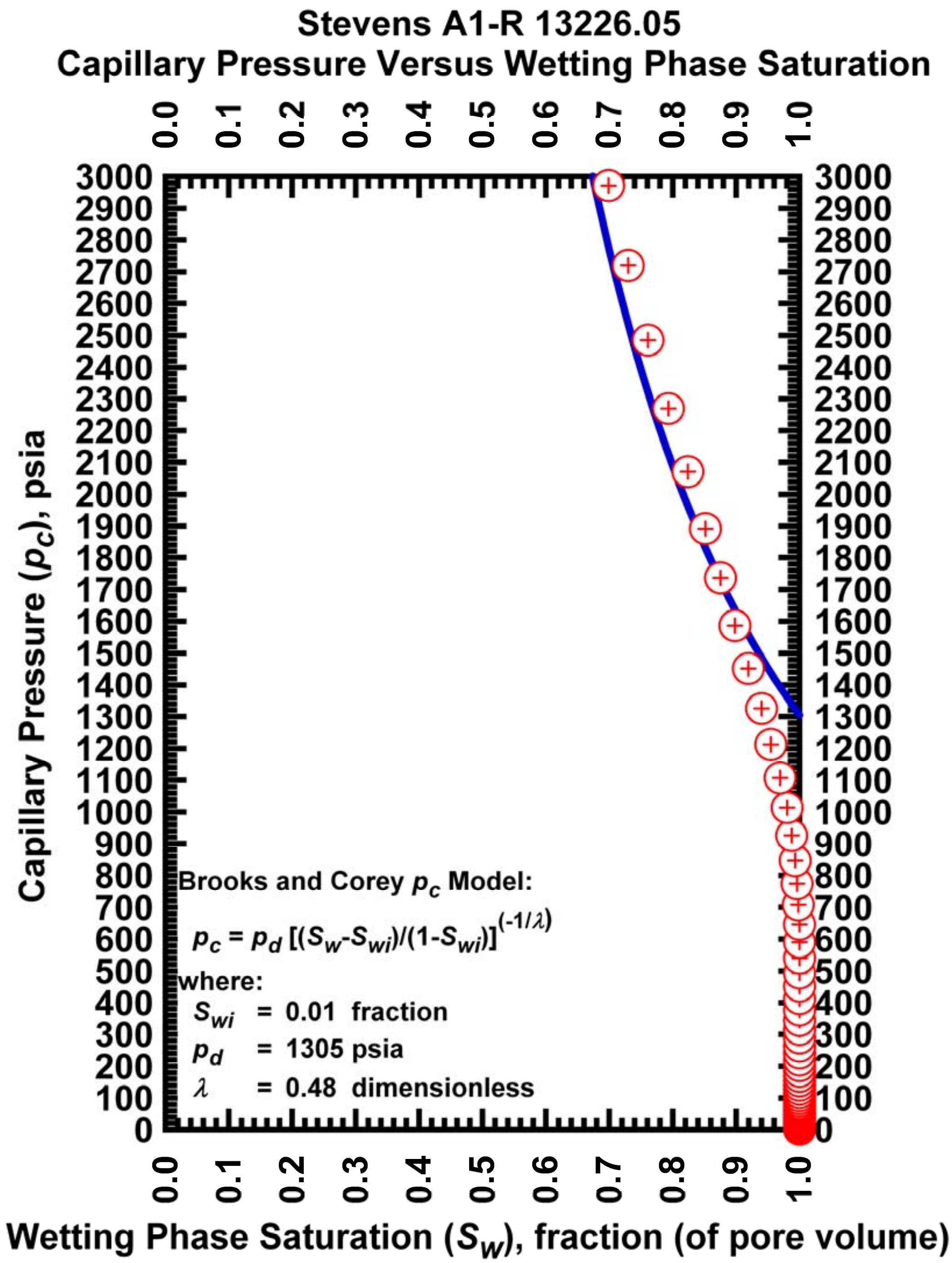

Figure I.79 — Plot of capillary pressure (p_c) vs. wetting phase saturation (S_w) — Case Stevens A1-R 13226.05

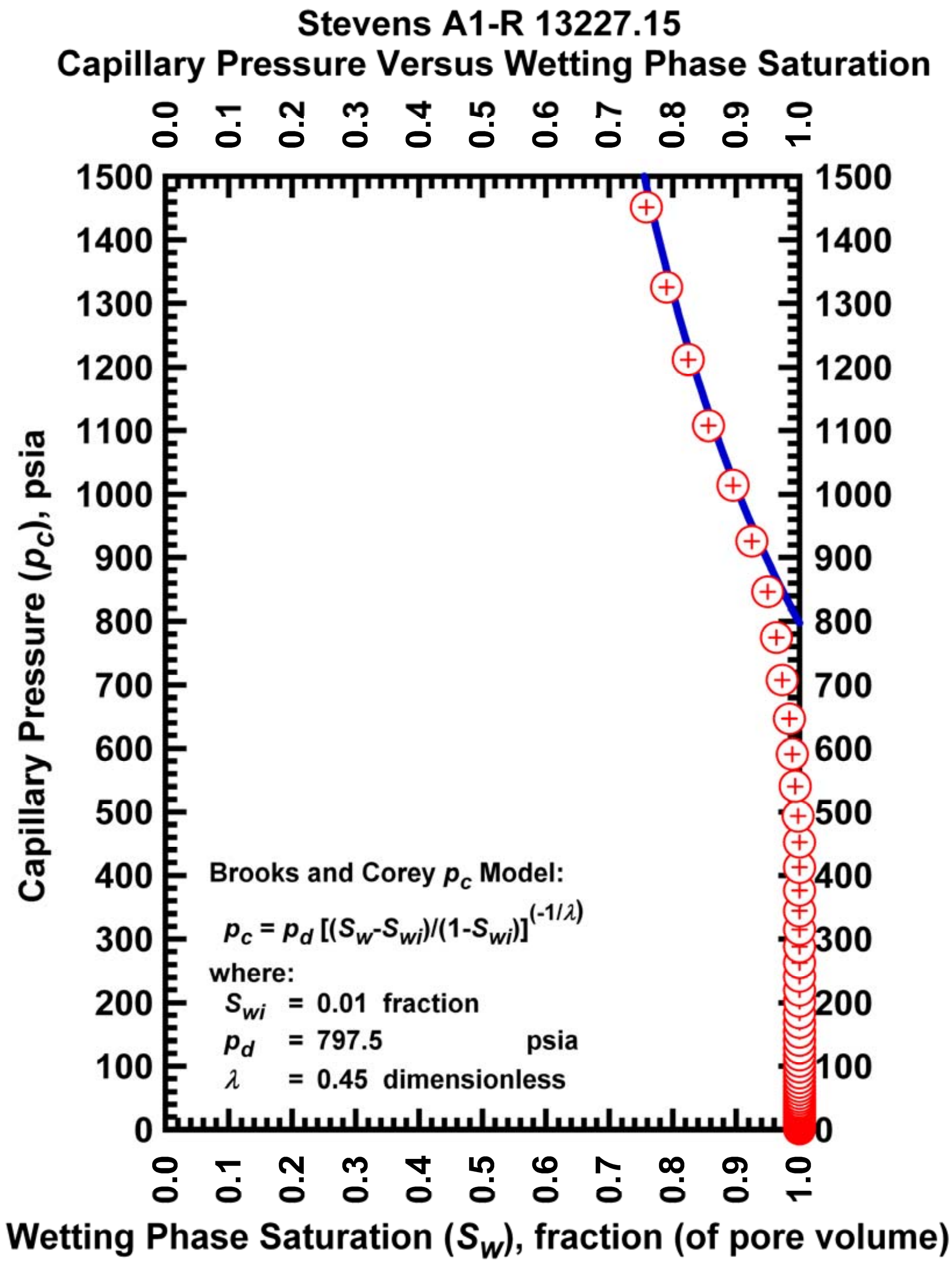

Figure I.80 — Plot of capillary pressure (p_c) vs. wetting phase saturation (S_w) — Case Stevens A1-R 13227.15

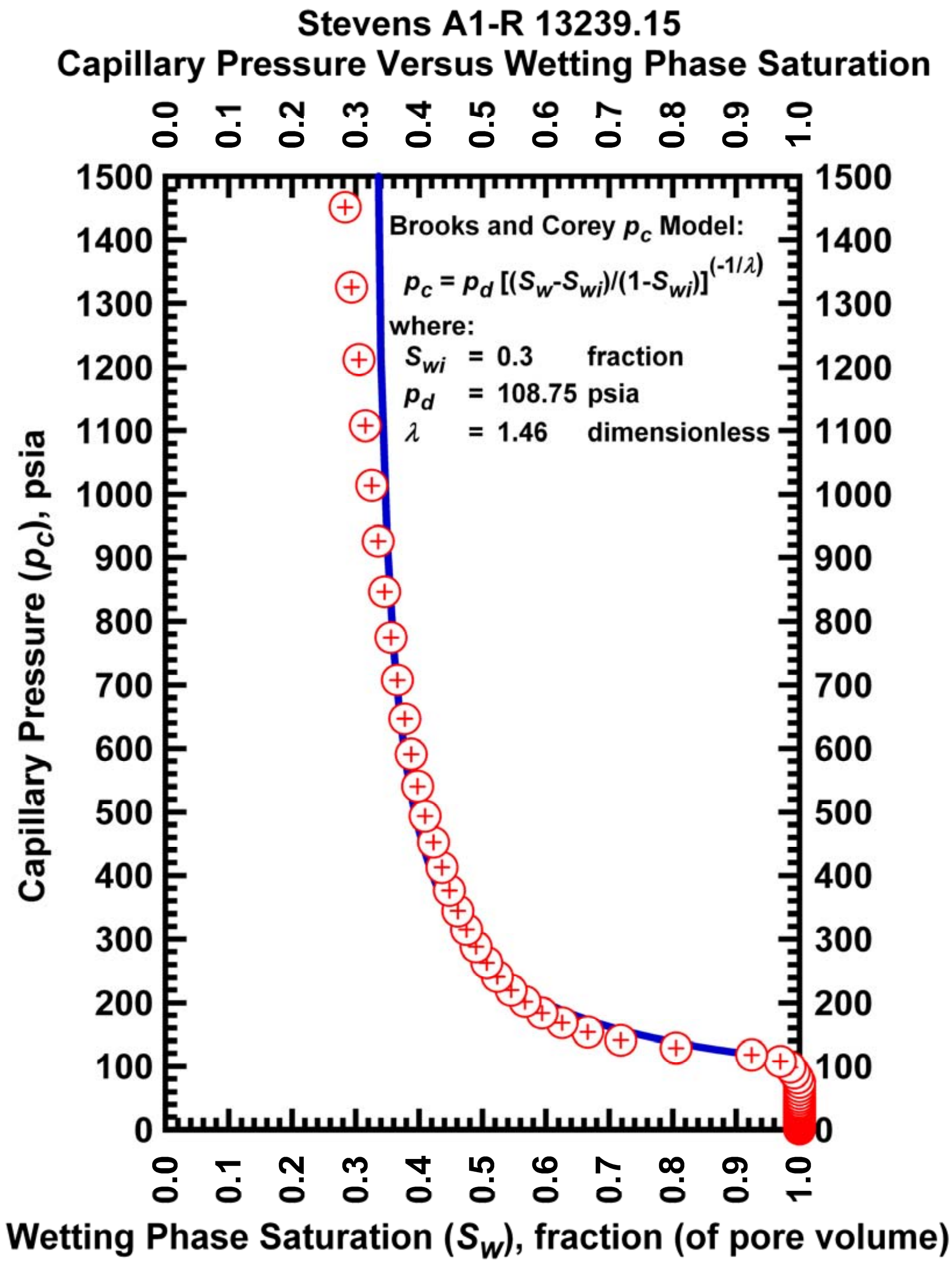

Figure I.80 — Plot of capillary pressure (p_c) vs. wetting phase saturation (S_w) — Case Stevens A1-R 13227.15

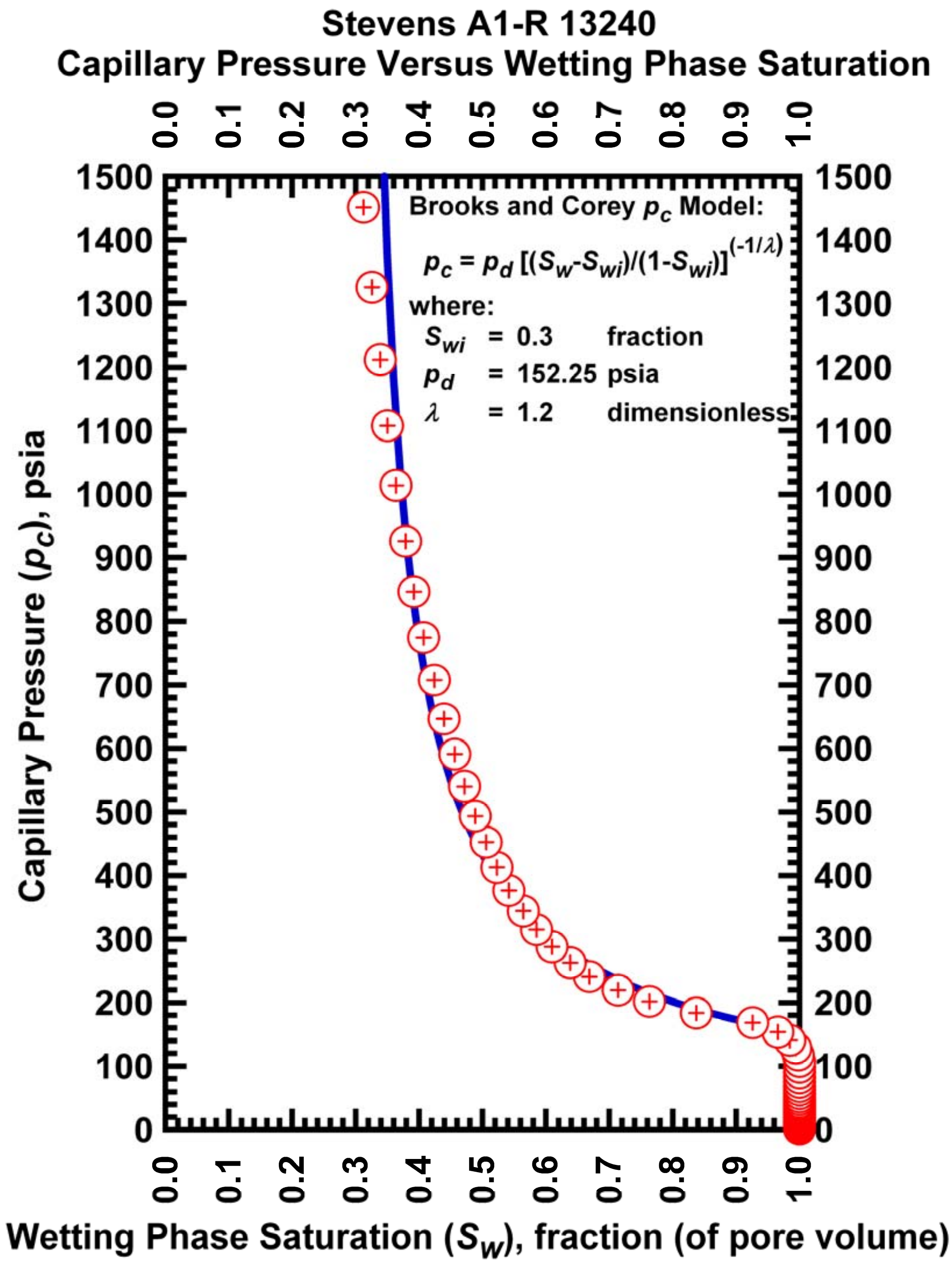

Figure I.82 — Plot of capillary pressure (p_c) vs. wetting phase saturation (S_w) — Case Stevens A1-R 13240

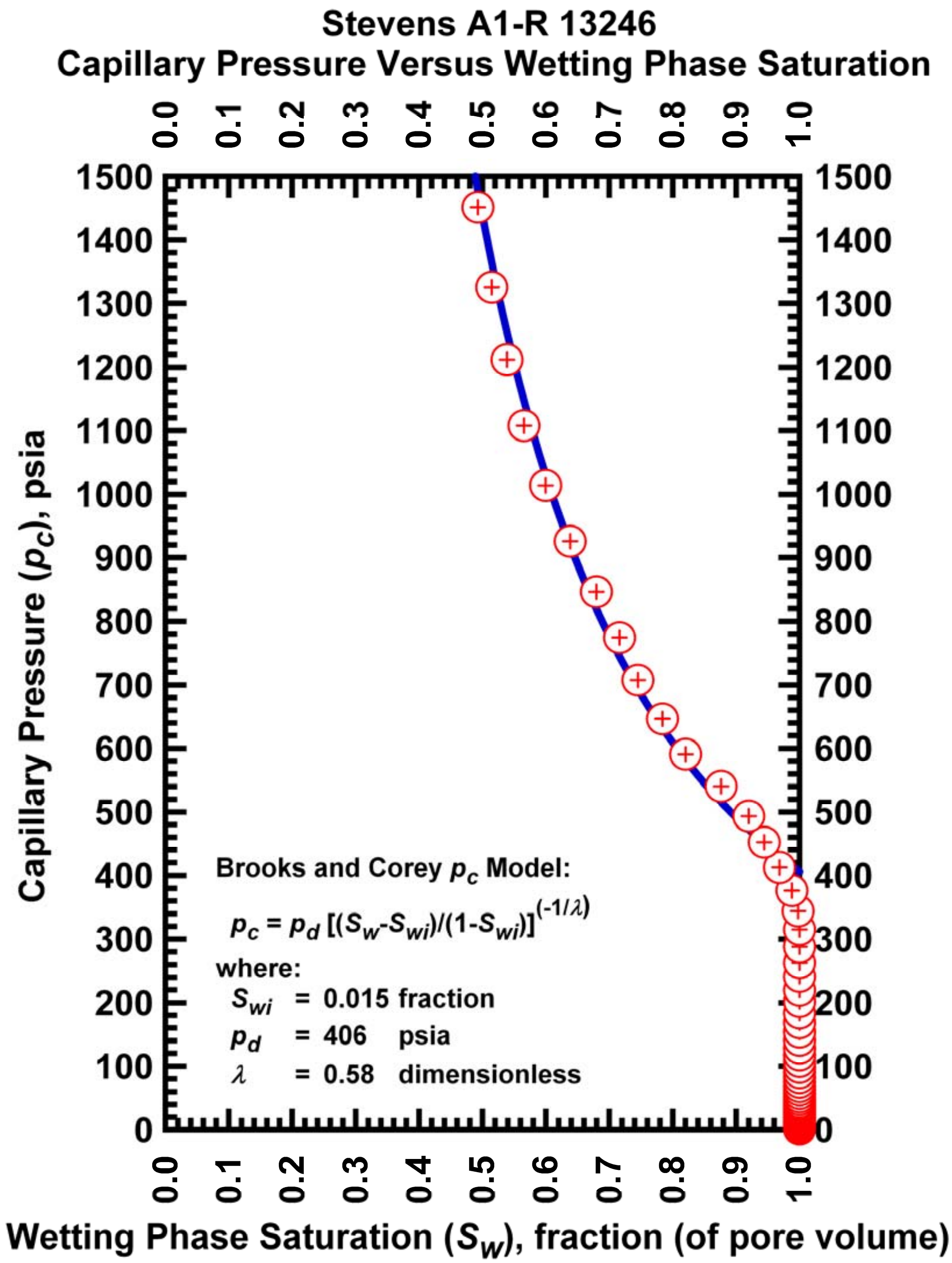

Figure I.83 — Plot of capillary pressure (p_c) vs. wetting phase saturation (S_w) — Case Stevens A1-R 13246

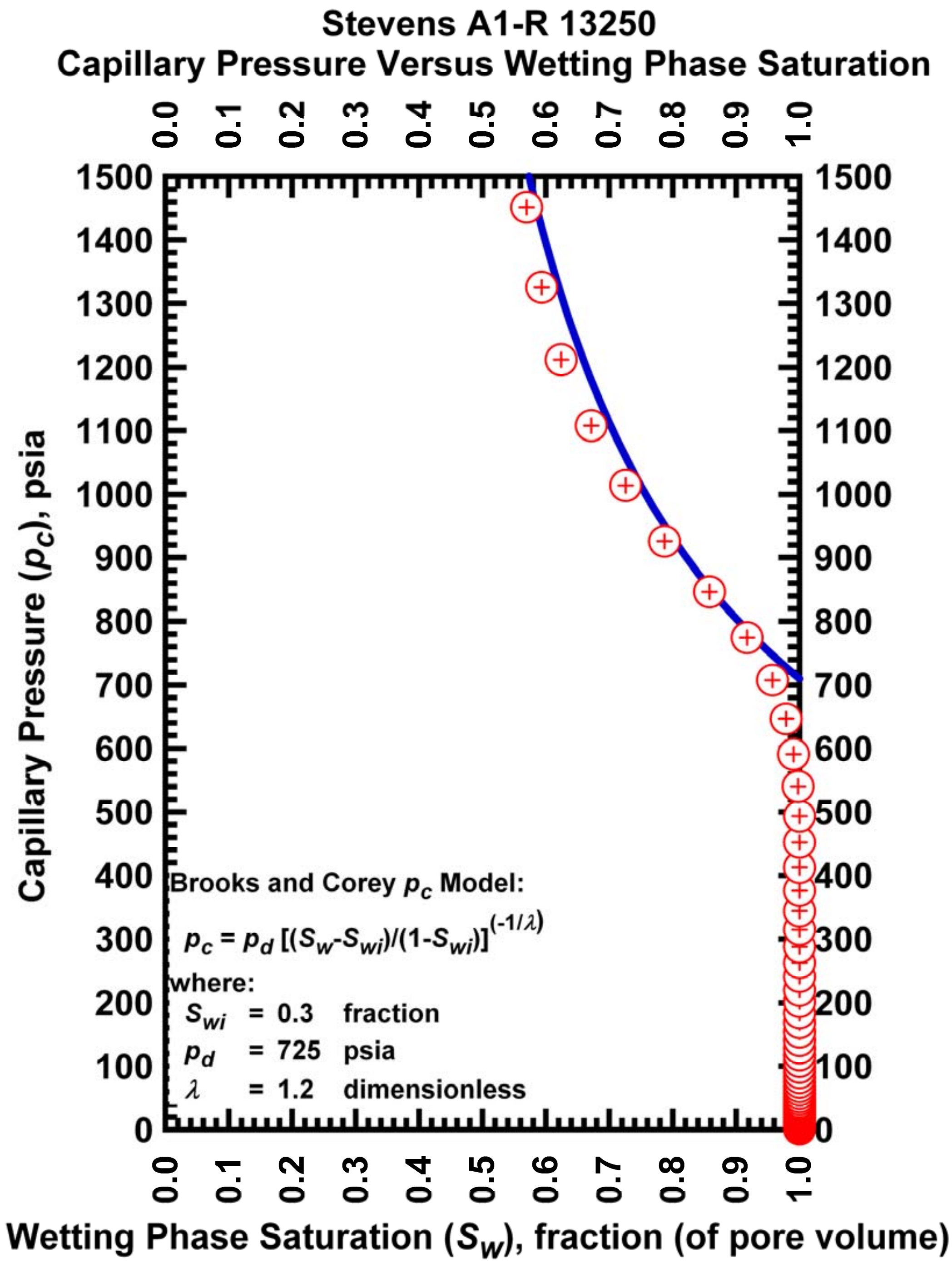

Figure I.84 — Plot of capillary pressure (p_c) vs. wetting phase saturation (S_w) — Case Stevens A1-R 13250

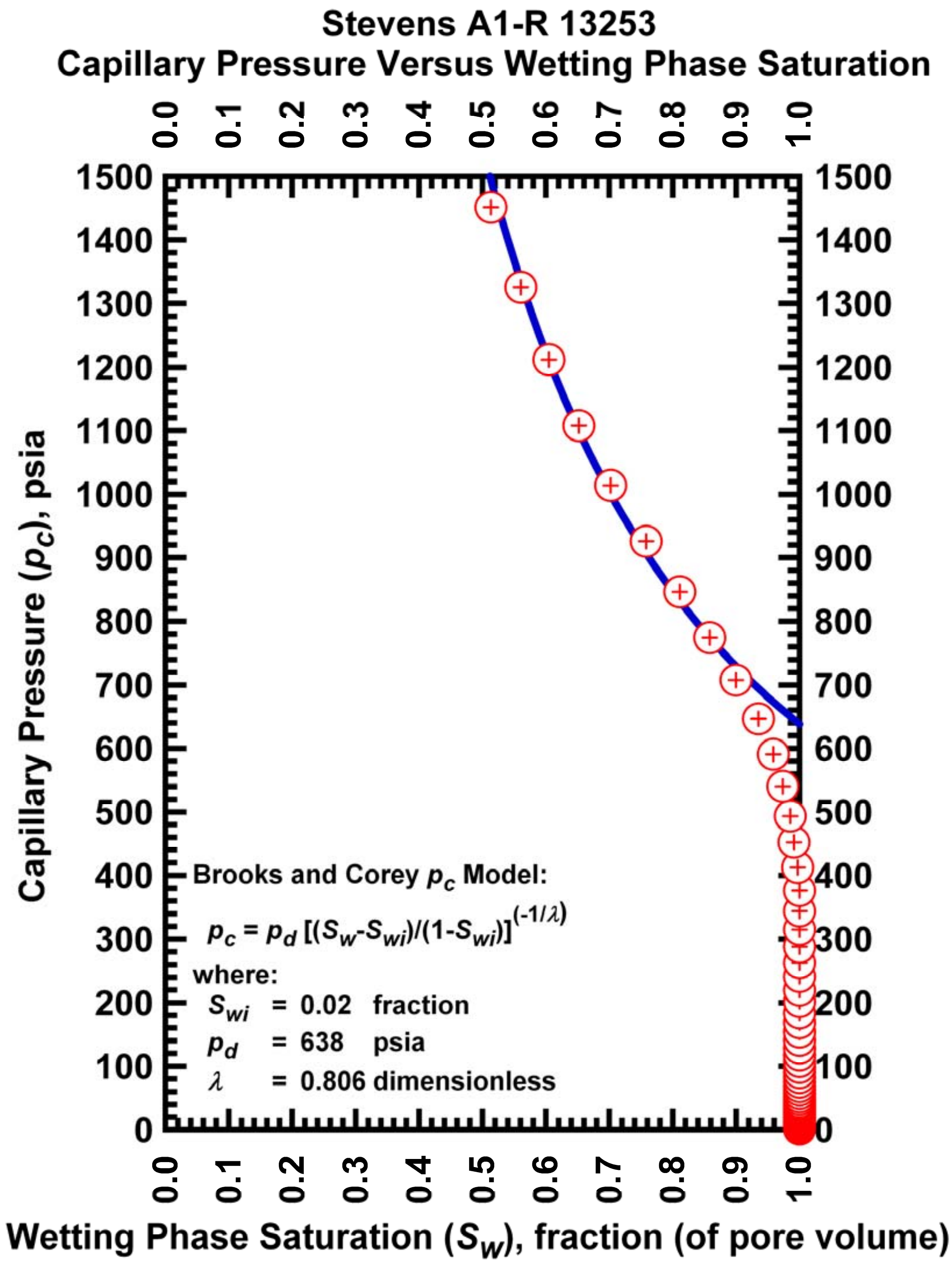

Figure I.85 — Plot of capillary pressure (p_c) vs. wetting phase saturation (S_w) — Case Stevens A1-R 13253

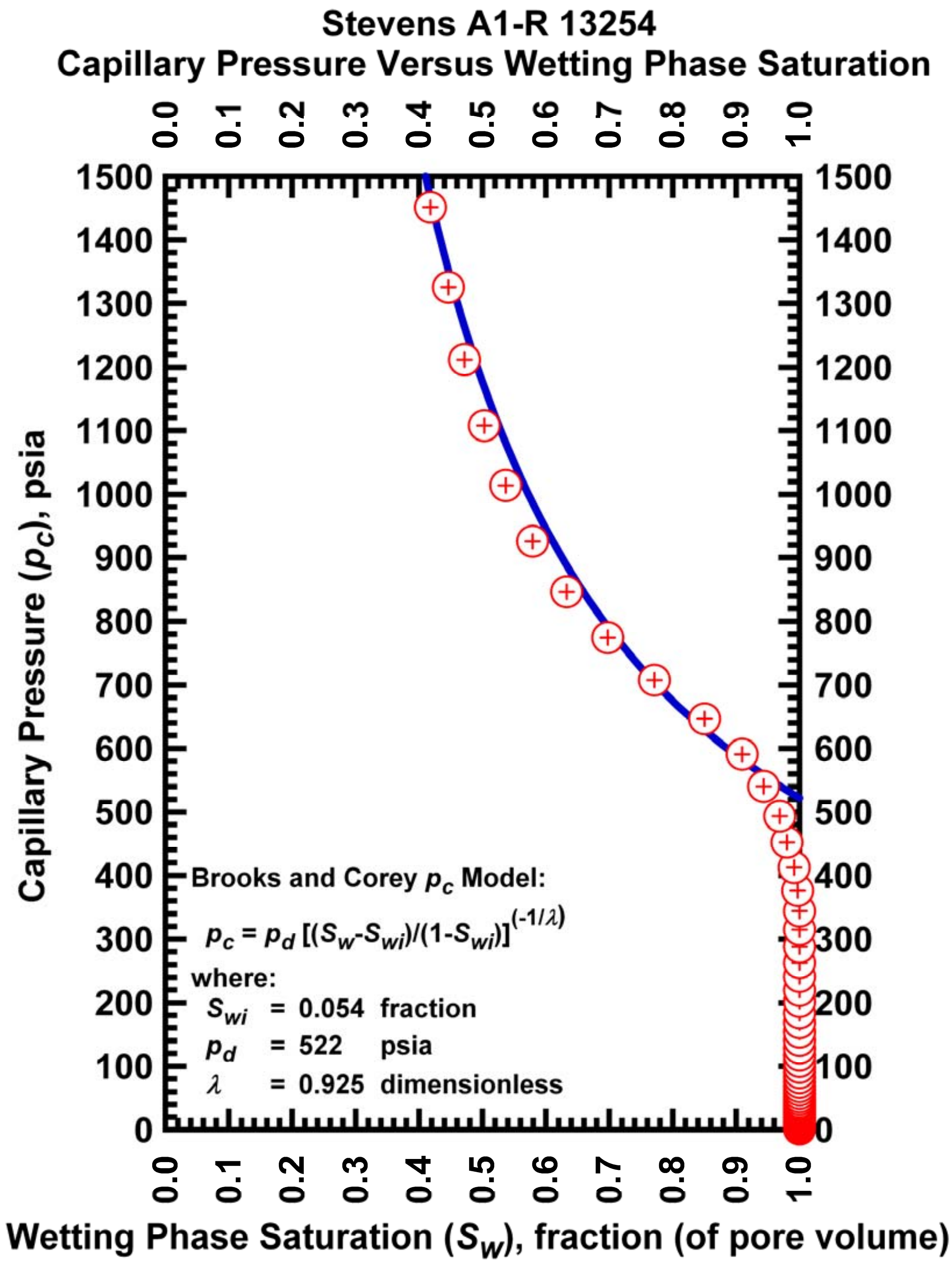

Figure I.86 — Plot of capillary pressure (p_c) vs. wetting phase saturation (S_w) — Case Stevens A1-R 13254

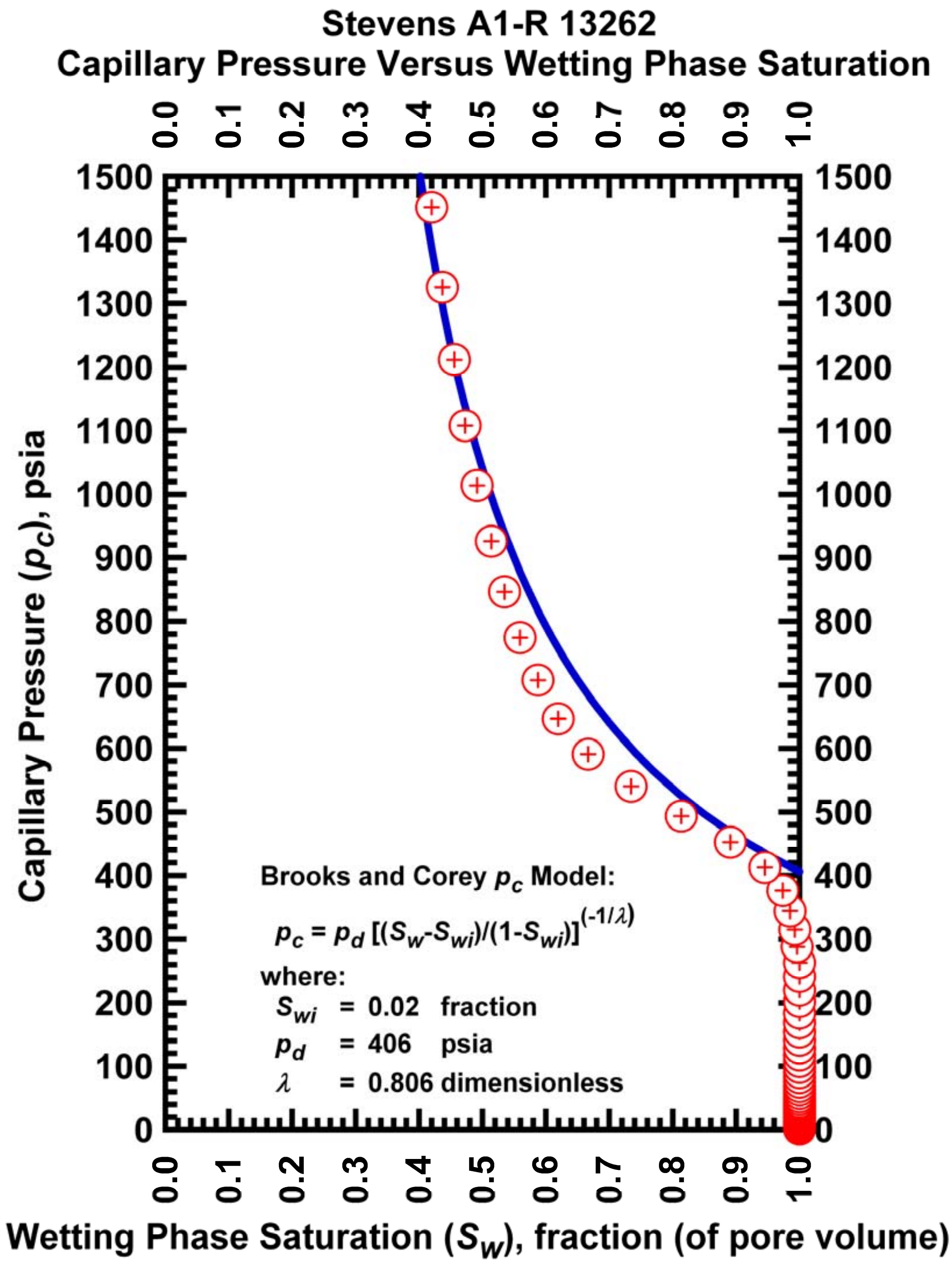

Figure I.87 — Plot of capillary pressure (p_c) vs. wetting phase saturation (S_w) — Case Stevens A1-R 13262

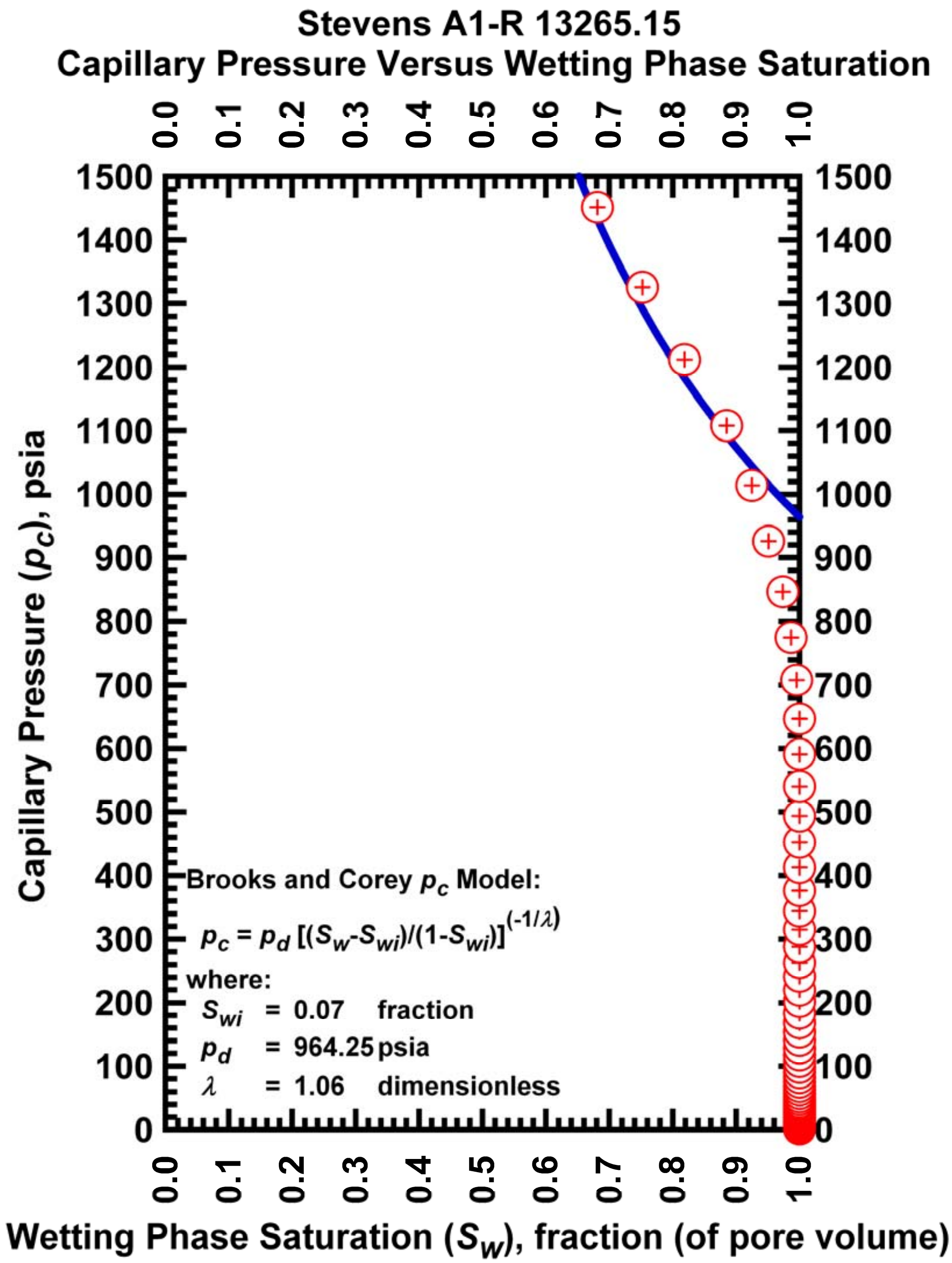

Figure I.88 — Plot of capillary pressure (p_c) vs. wetting phase saturation (S_w) — Case Stevens A1-R 13265.15

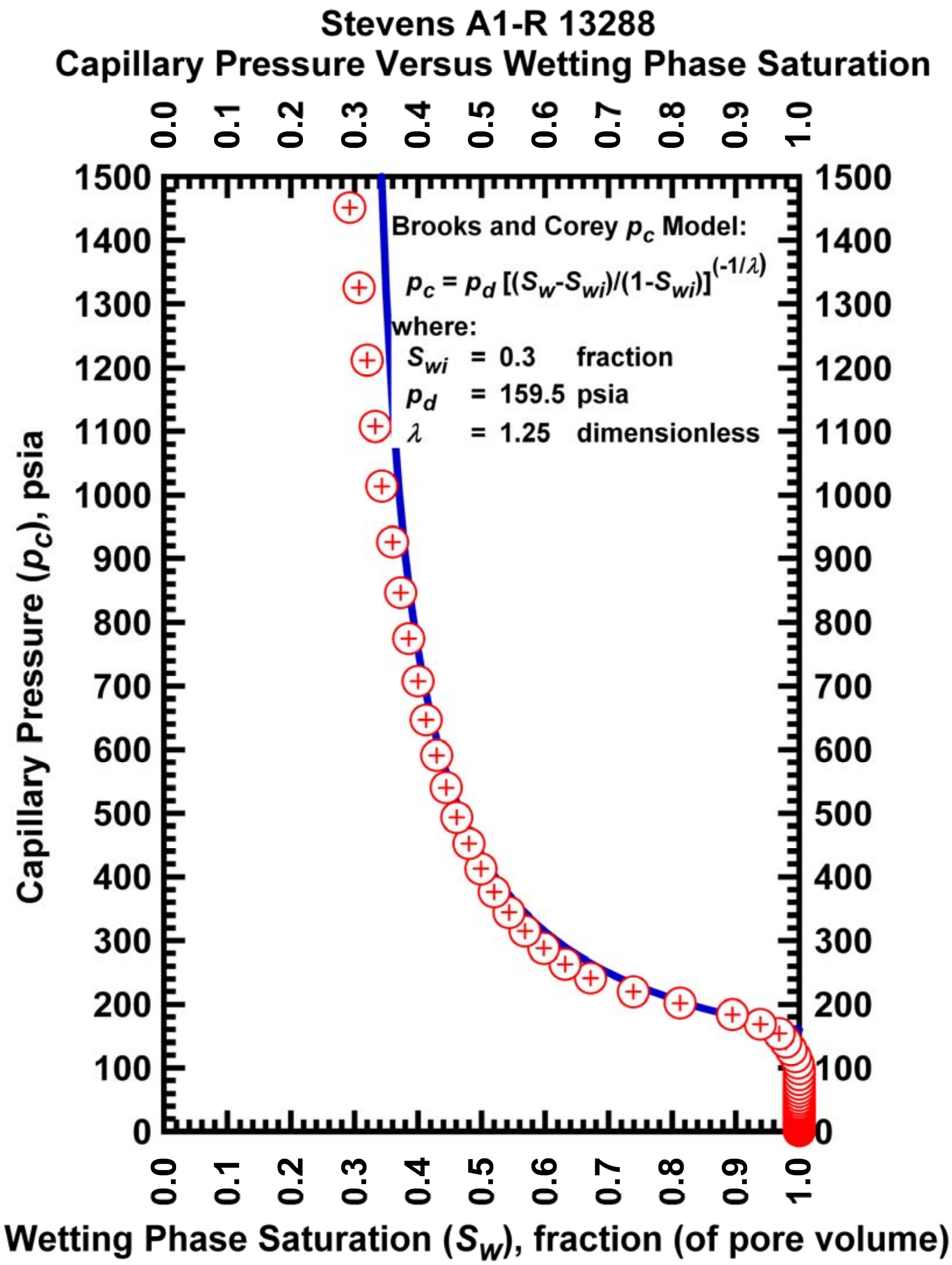

Figure I.89 — Plot of capillary pressure (p_c) vs. wetting phase saturation (S_w) — Case Stevens A1-R 13288

APPENDIX J

LIBRARY OF CAPILLARY PRESSURE VERSUS WETTING PHASE SATURATION PLOTS — LOGARITHMIC CAPILLARY PRESSURE FORMAT

This Appendix presents the calibration of the capillary displacement pressure (p_d), irreducible wetting-phase saturation (S_{wi}), and the index of pore-size distribution (λ) on a sample-by-sample basis using the Brooks-Corey $p_c(S_w)$ model .

In this Appendix, we provide for each data a plot of capillary pressure (p_c) vs. wetting phase saturation (S_w) – logarithmic capillary pressure format.

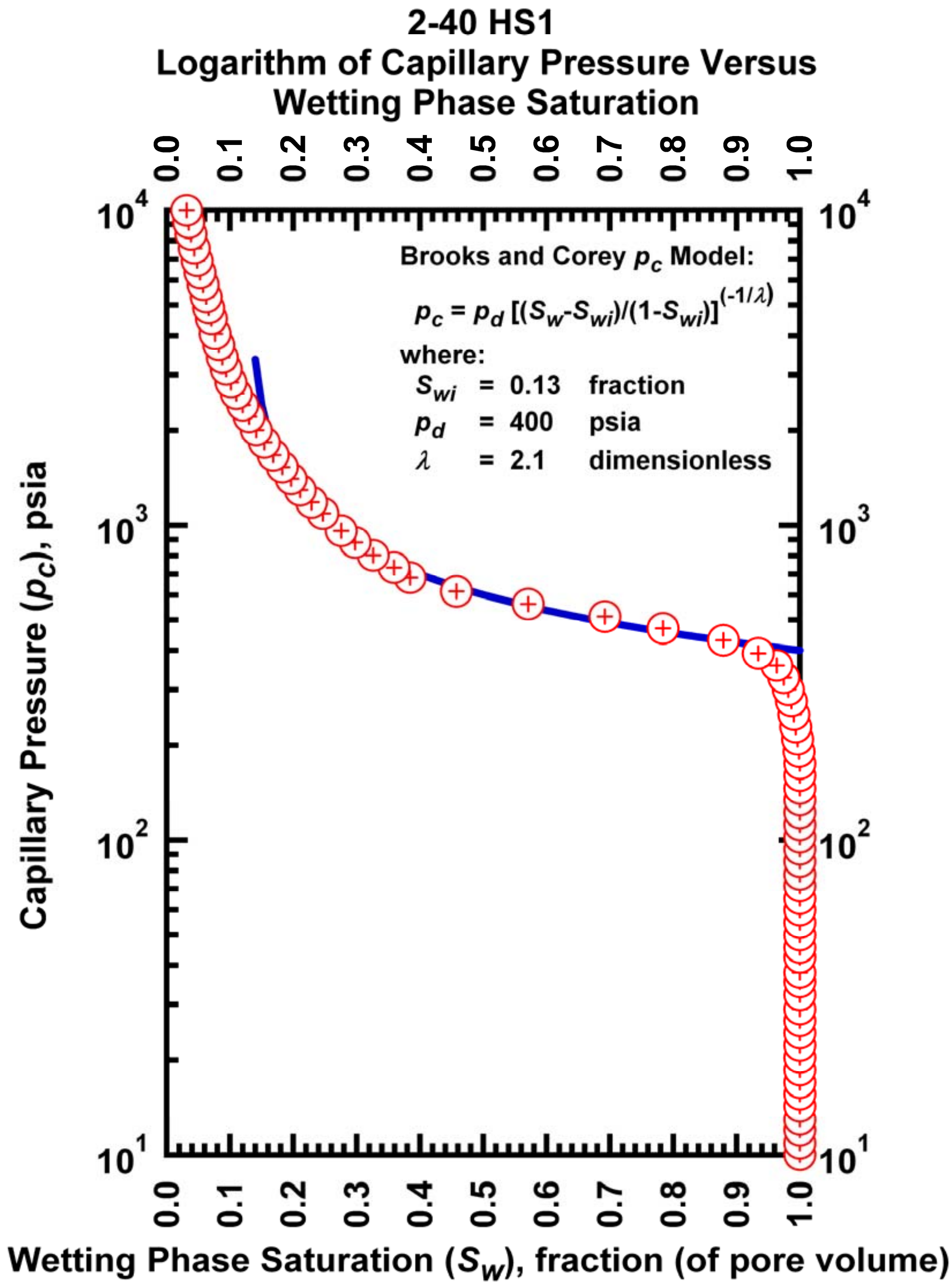

Figure J.1 – Plot of logarithm of capillary pressure vs. wetting phase saturation — Case 2-40 HS1.

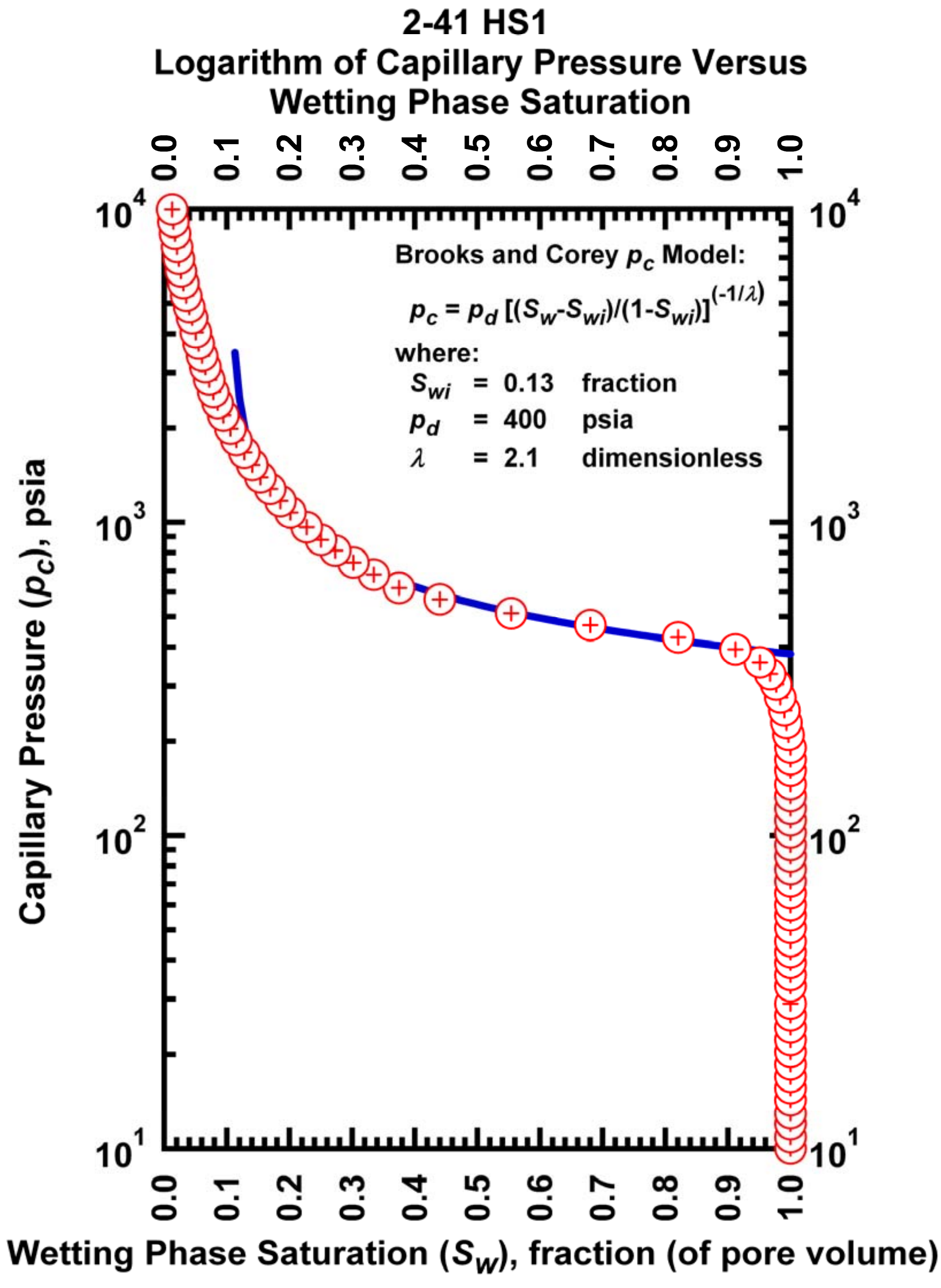

Figure J.2 – Plot of logarithm of capillary pressure vs. wetting phase saturation — Case 2-41 HS1.

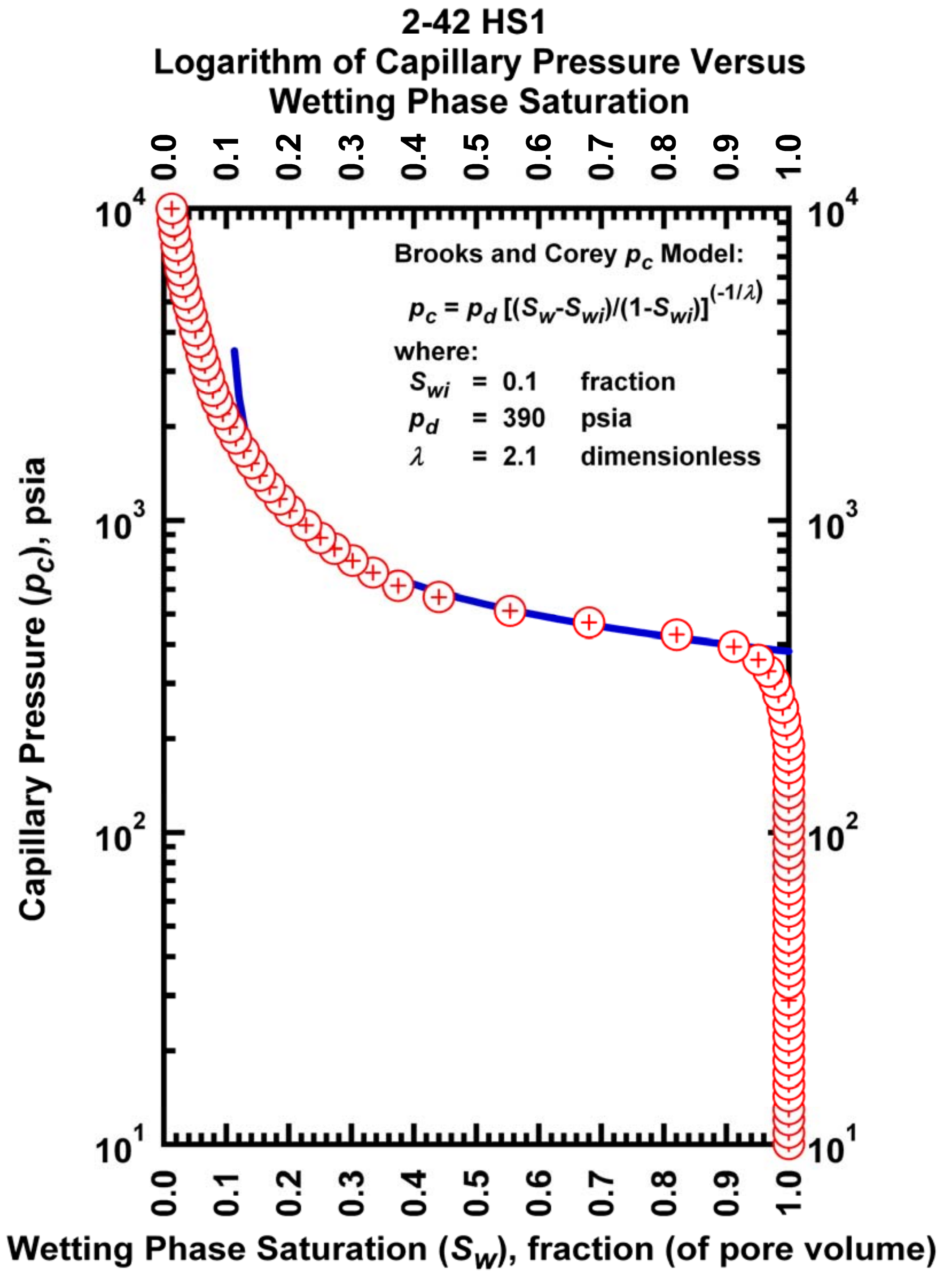

Figure J.3 – Plot of logarithm of capillary pressure vs. wetting phase saturation — Case 2-42 HS1.

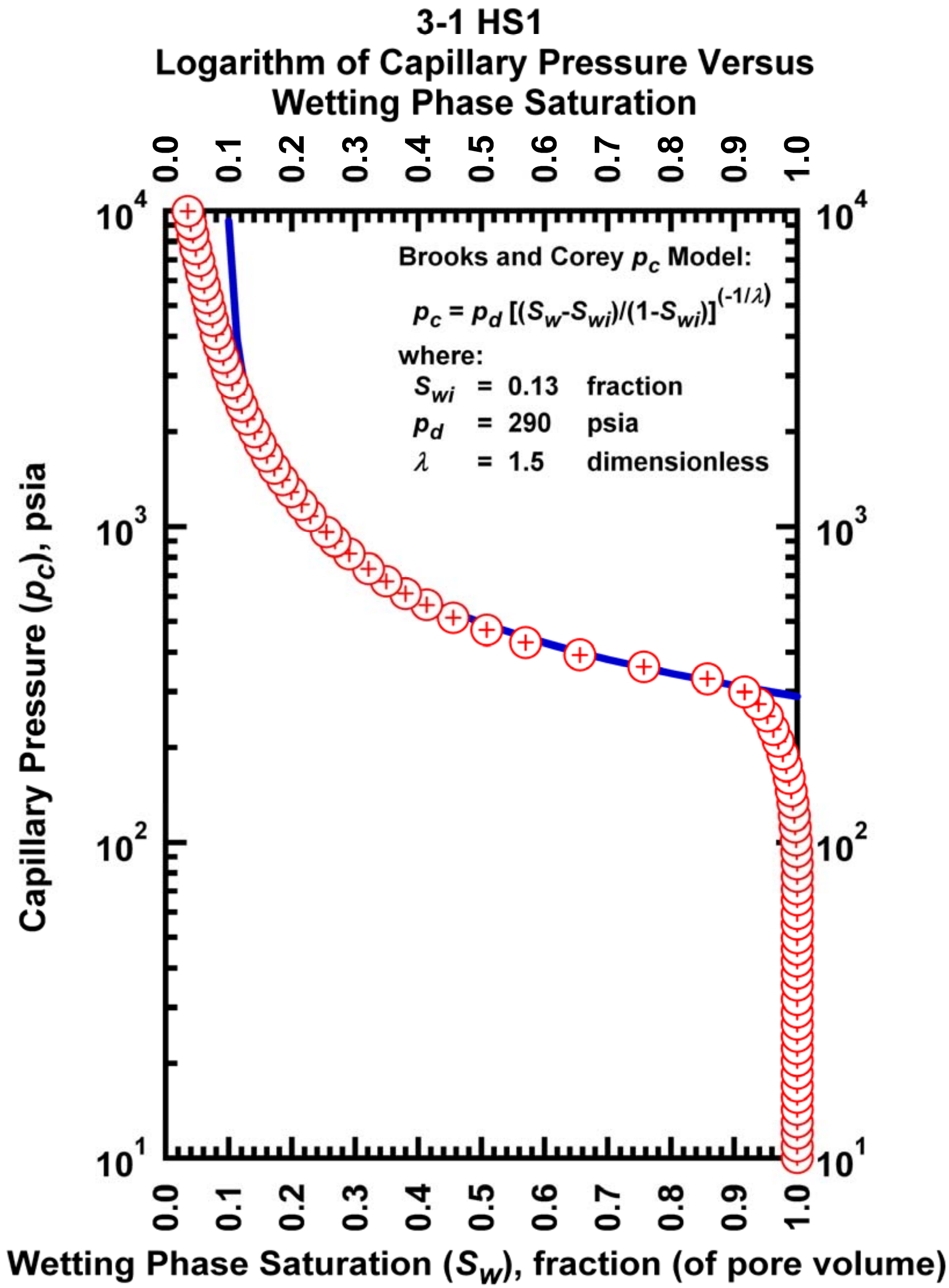

Figure J.4 – Plot of logarithm of capillary pressure vs. wetting phase saturation — Case 3-1 HS1.

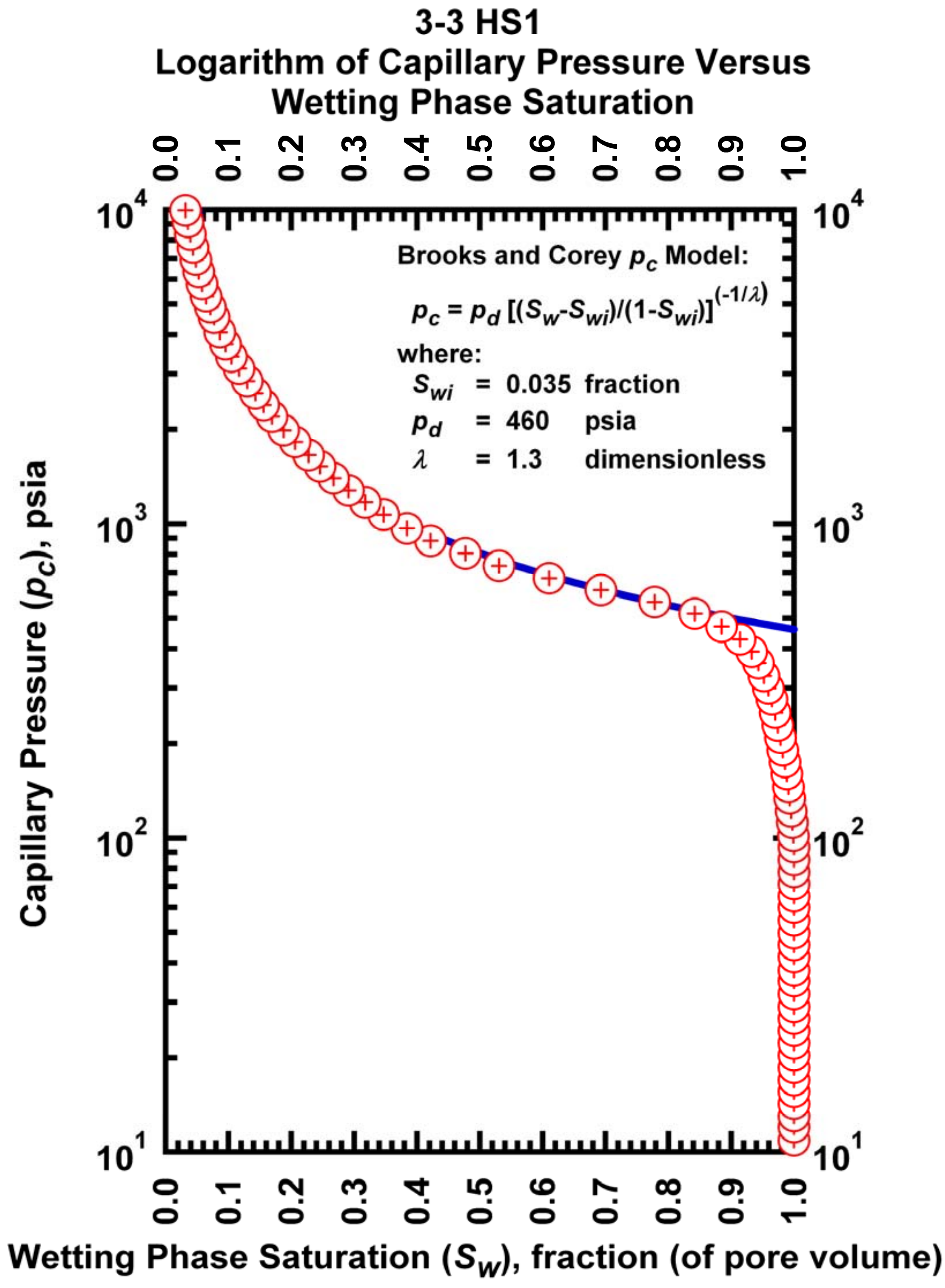

Figure J.5 – Plot of logarithm of capillary pressure vs. wetting phase saturation — Case 3-3 HS1.

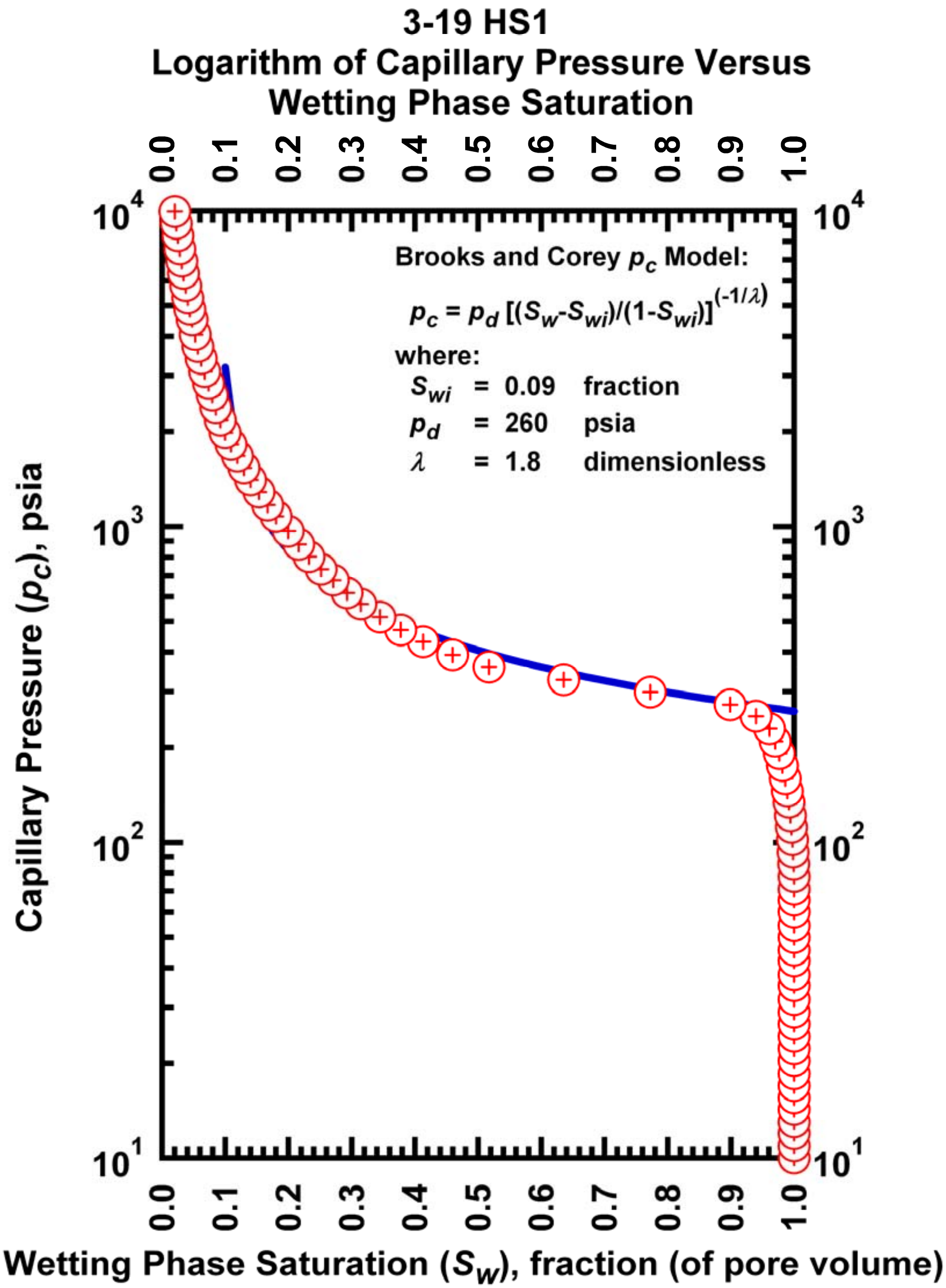

Figure J.6 – Plot of logarithm of capillary pressure vs. wetting phase saturation — Case 3-19 HS1.

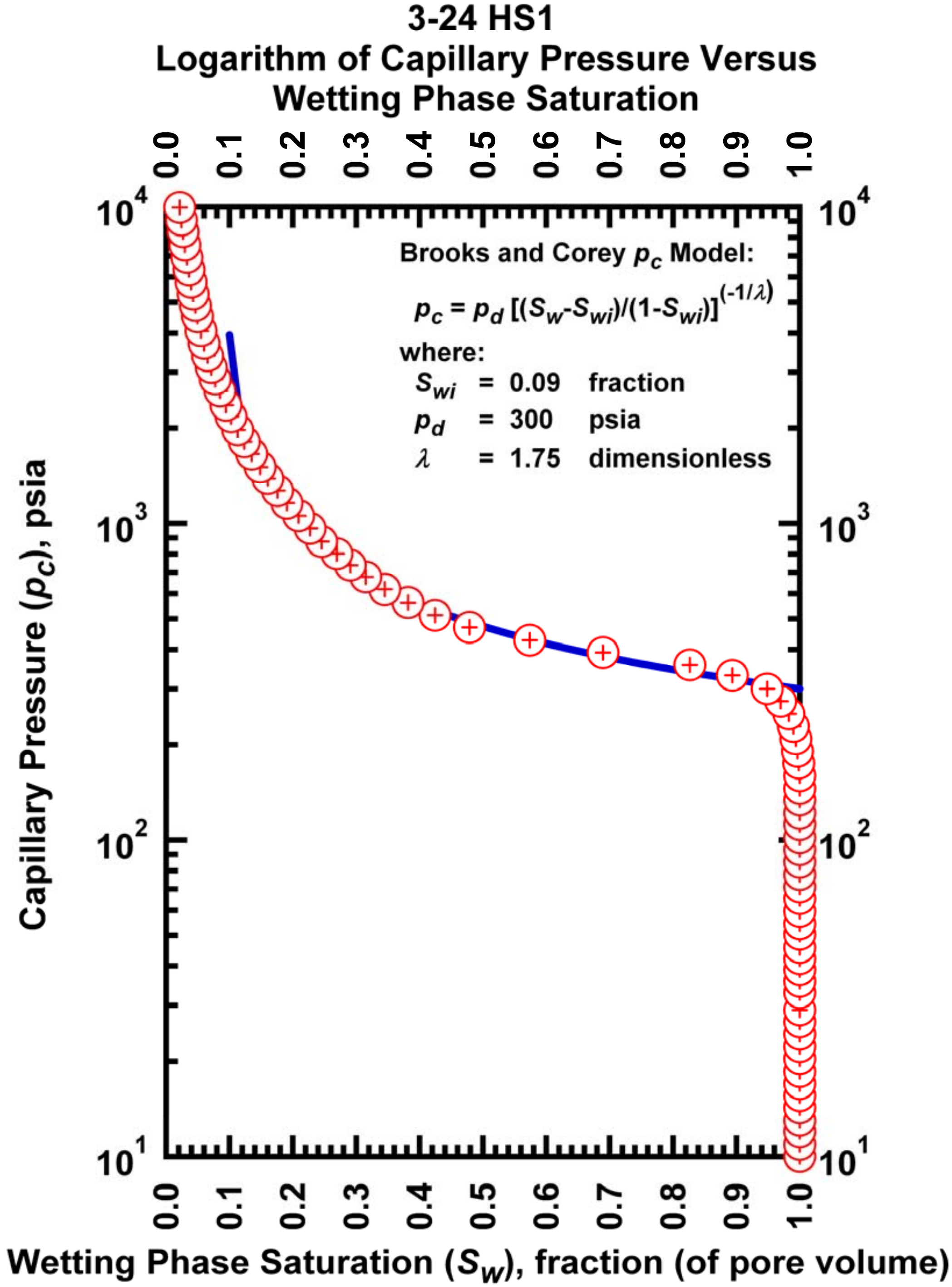

Figure J.7 – Plot of logarithm of capillary pressure vs. wetting phase saturation — Case 3-24 HS1.

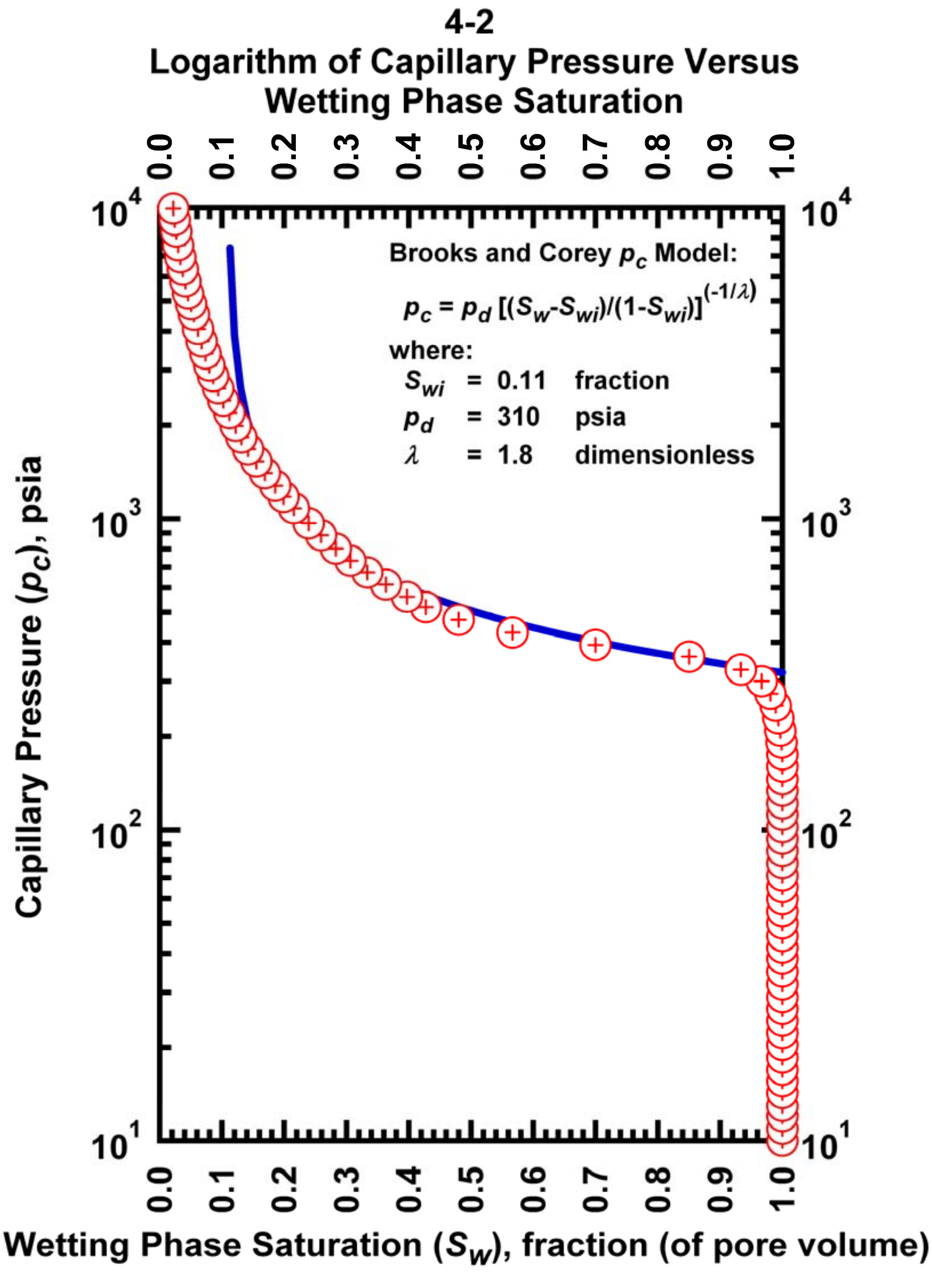

Figure J.8 – Plot of logarithm of capillary pressure vs. wetting phase saturation — Case 4-2 HS1.

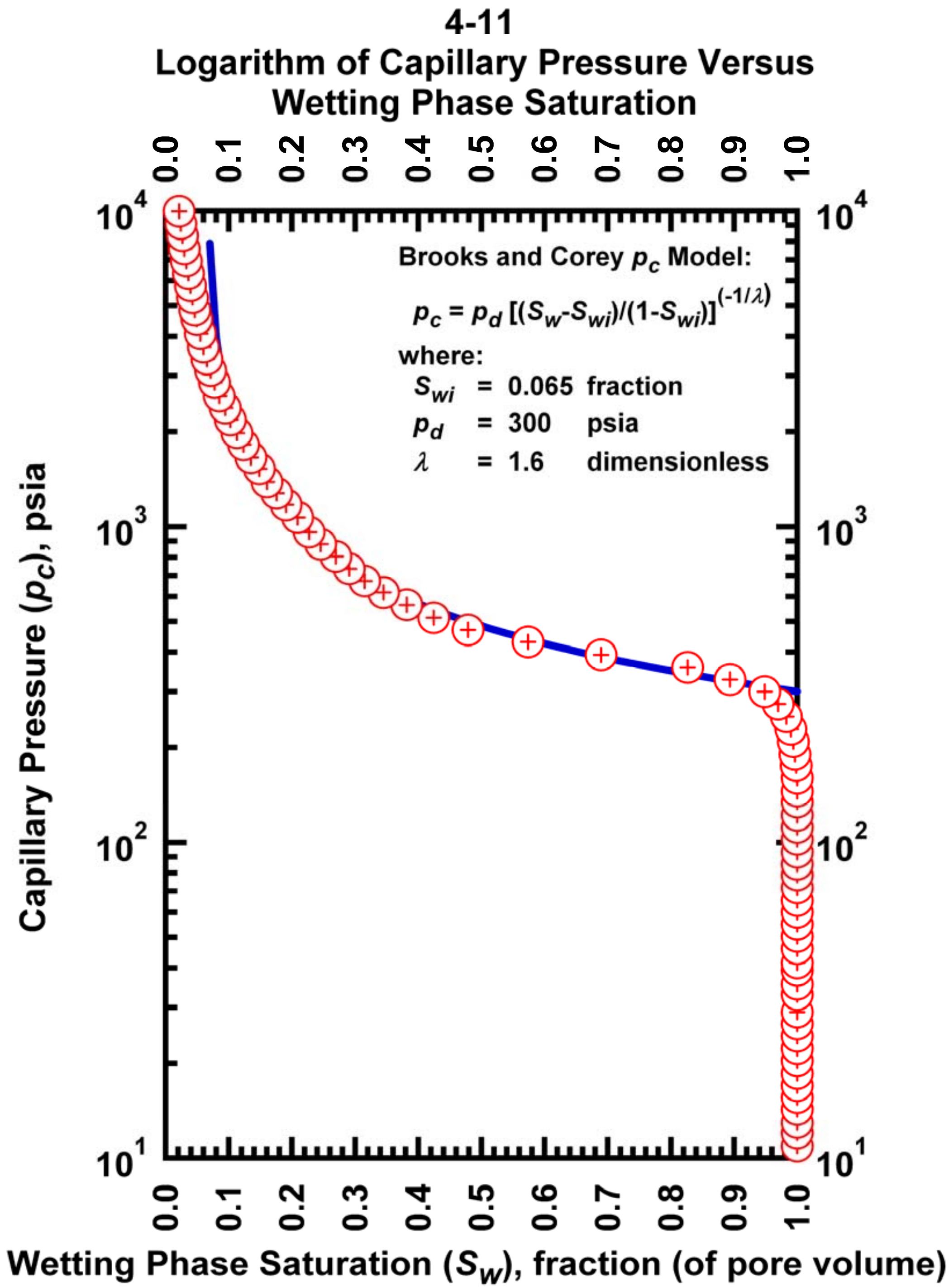

Figure J.9 – Plot of logarithm of capillary pressure vs. wetting phase saturation — Case 4-11 HS1.

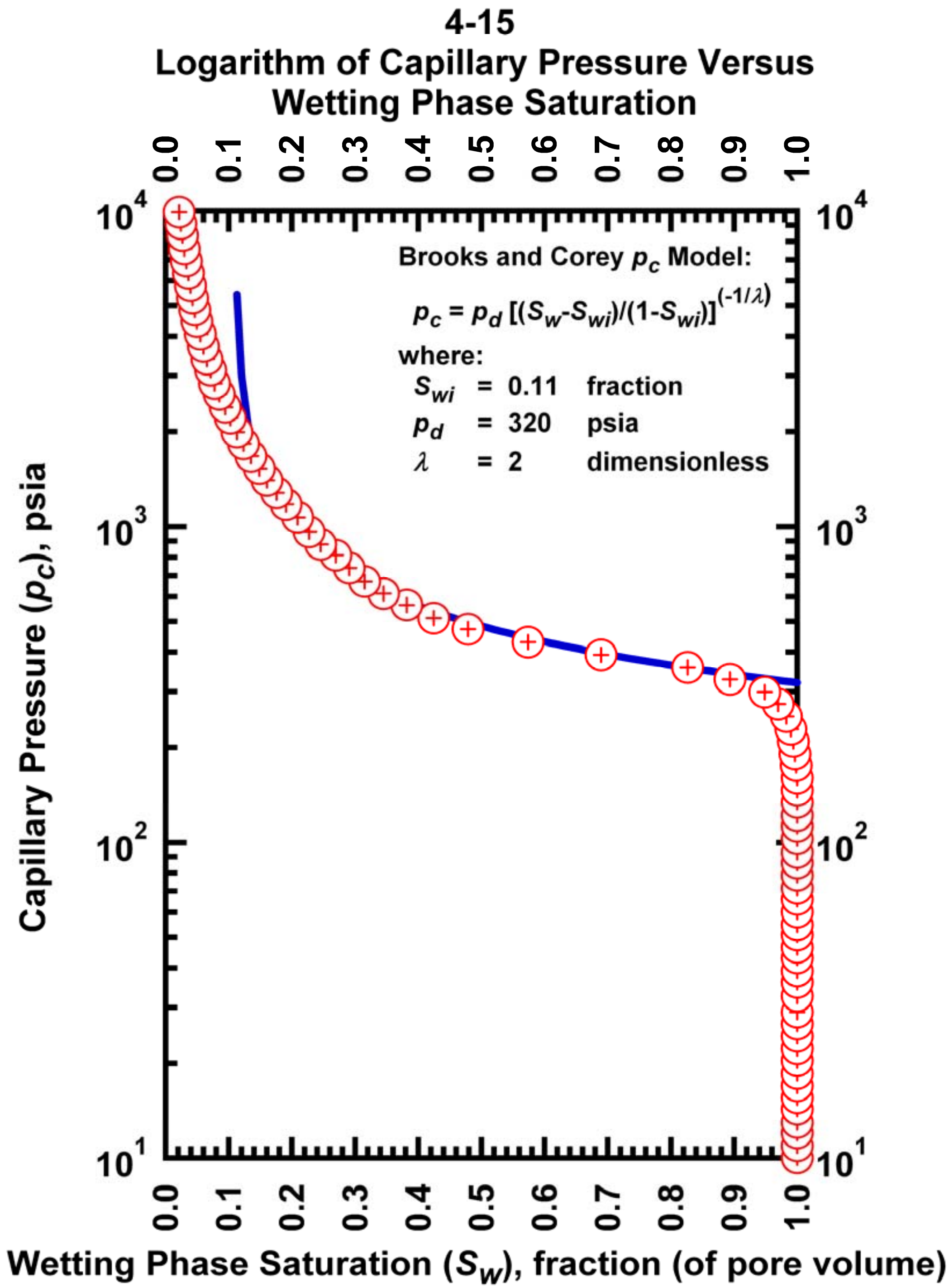

Figure J.10 – Plot of logarithm of capillary pressure vs. wetting phase saturation — Case 4-15 HS1.

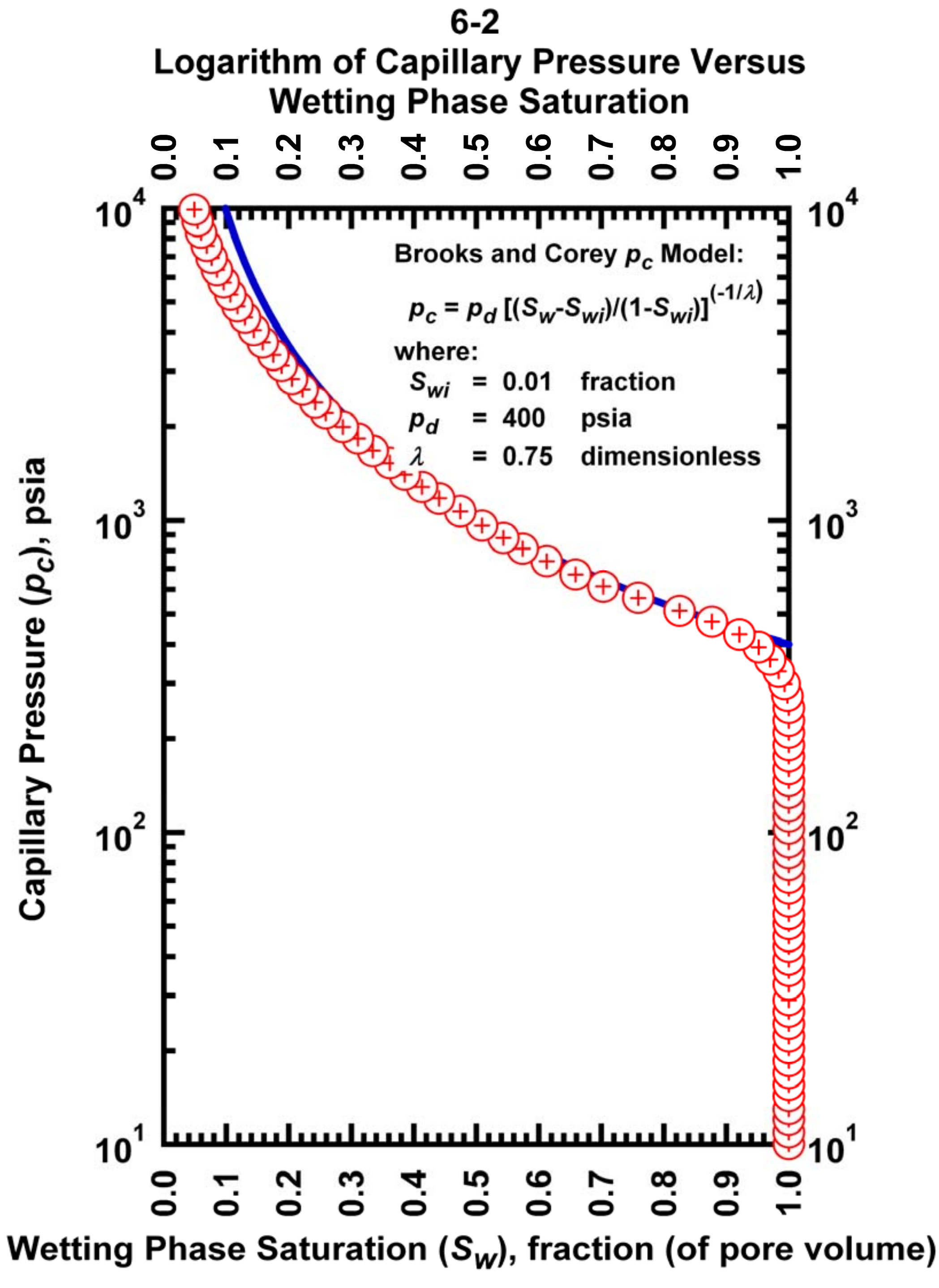

Figure J.11 – Plot of logarithm of capillary pressure vs. wetting phase saturation — Case 6-2 HS1.

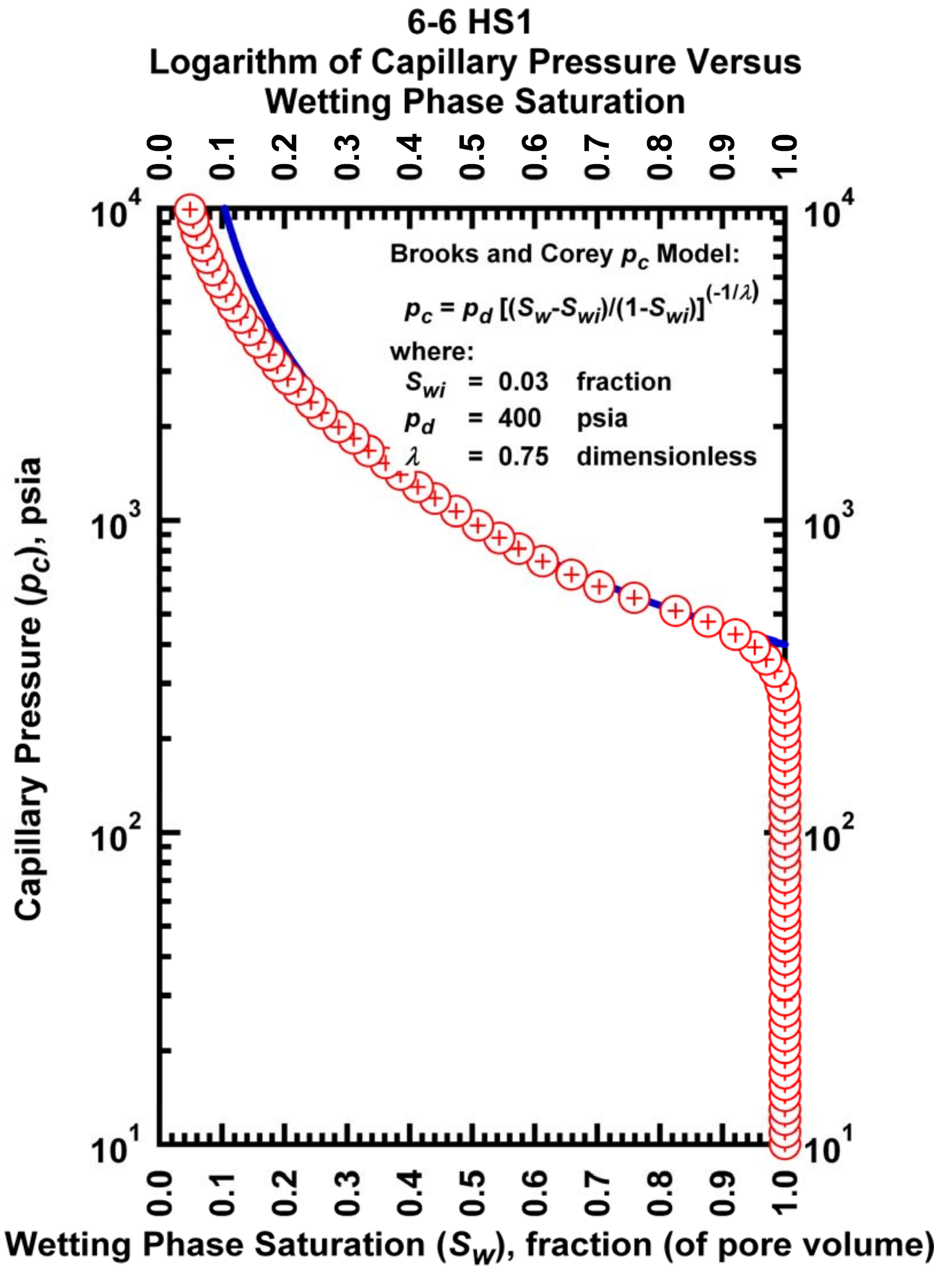

Figure J.12 – Plot of logarithm of capillary pressure vs. wetting phase saturation — Case 6-6 HS1.

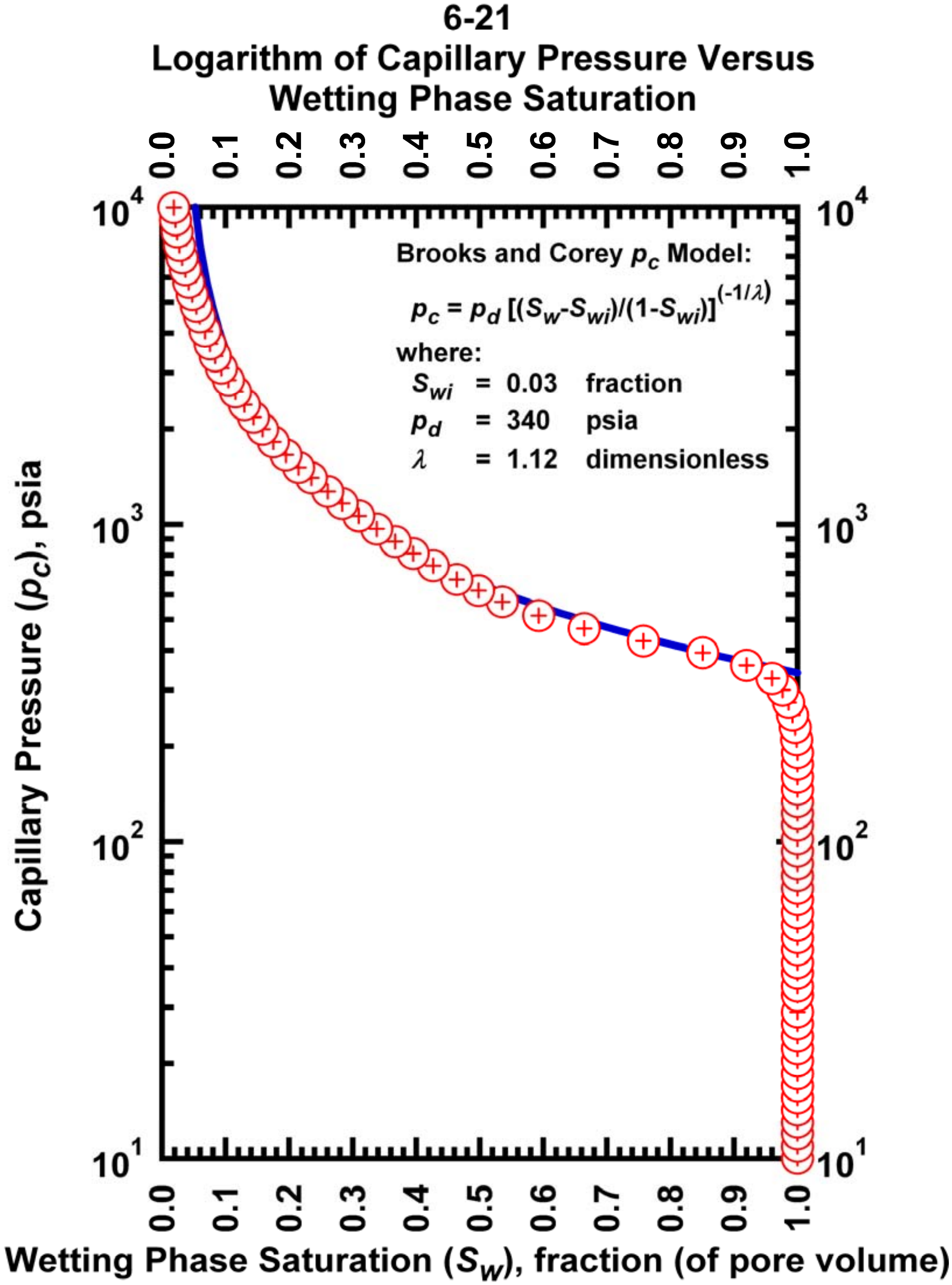

Figure J.13 – Plot of logarithm of capillary pressure vs. wetting phase saturation — Case 6-21 HS1.

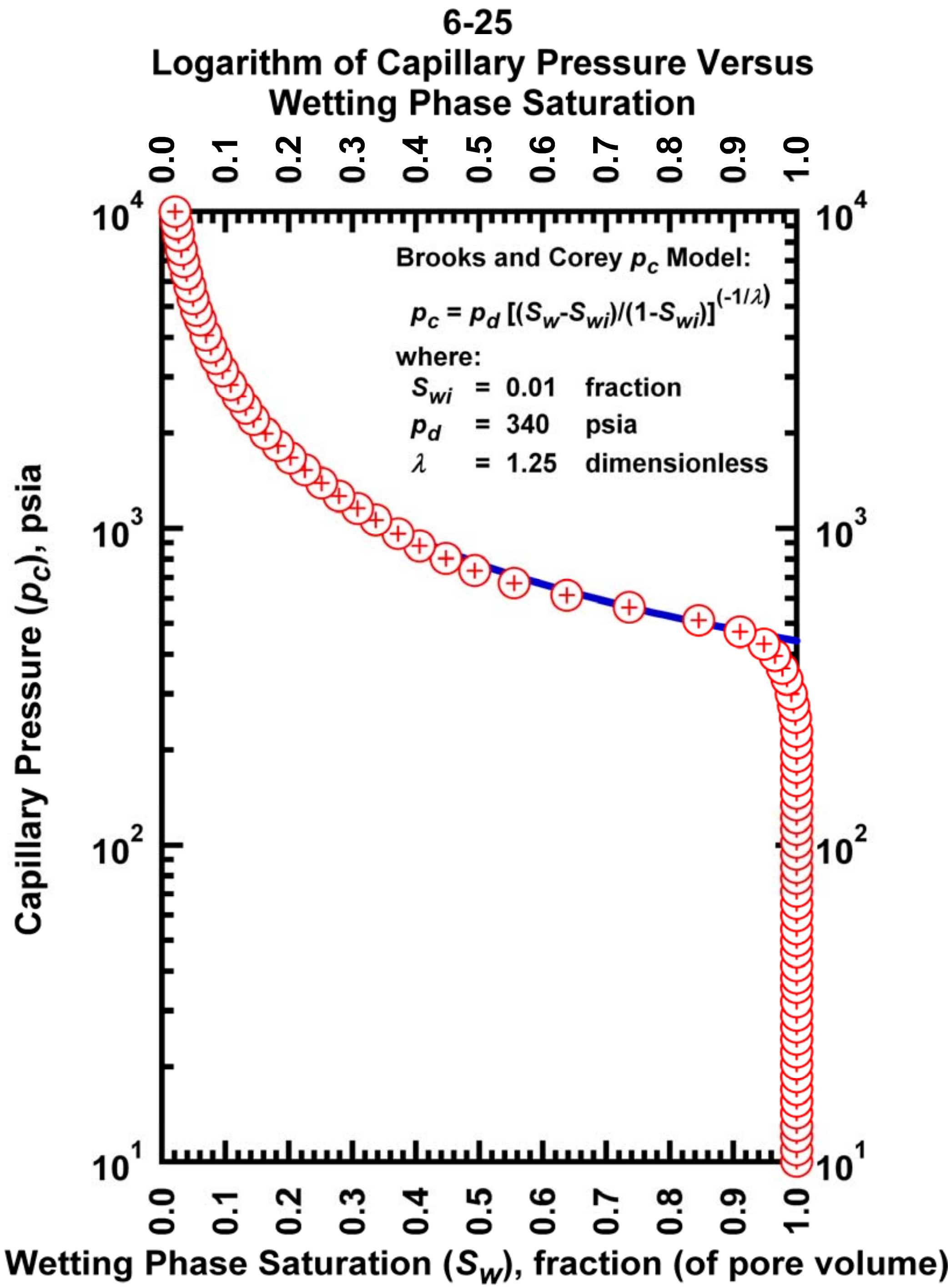

Figure J.14 – Plot of logarithm of capillary pressure vs. wetting phase saturation — Case 6-25 HS1.

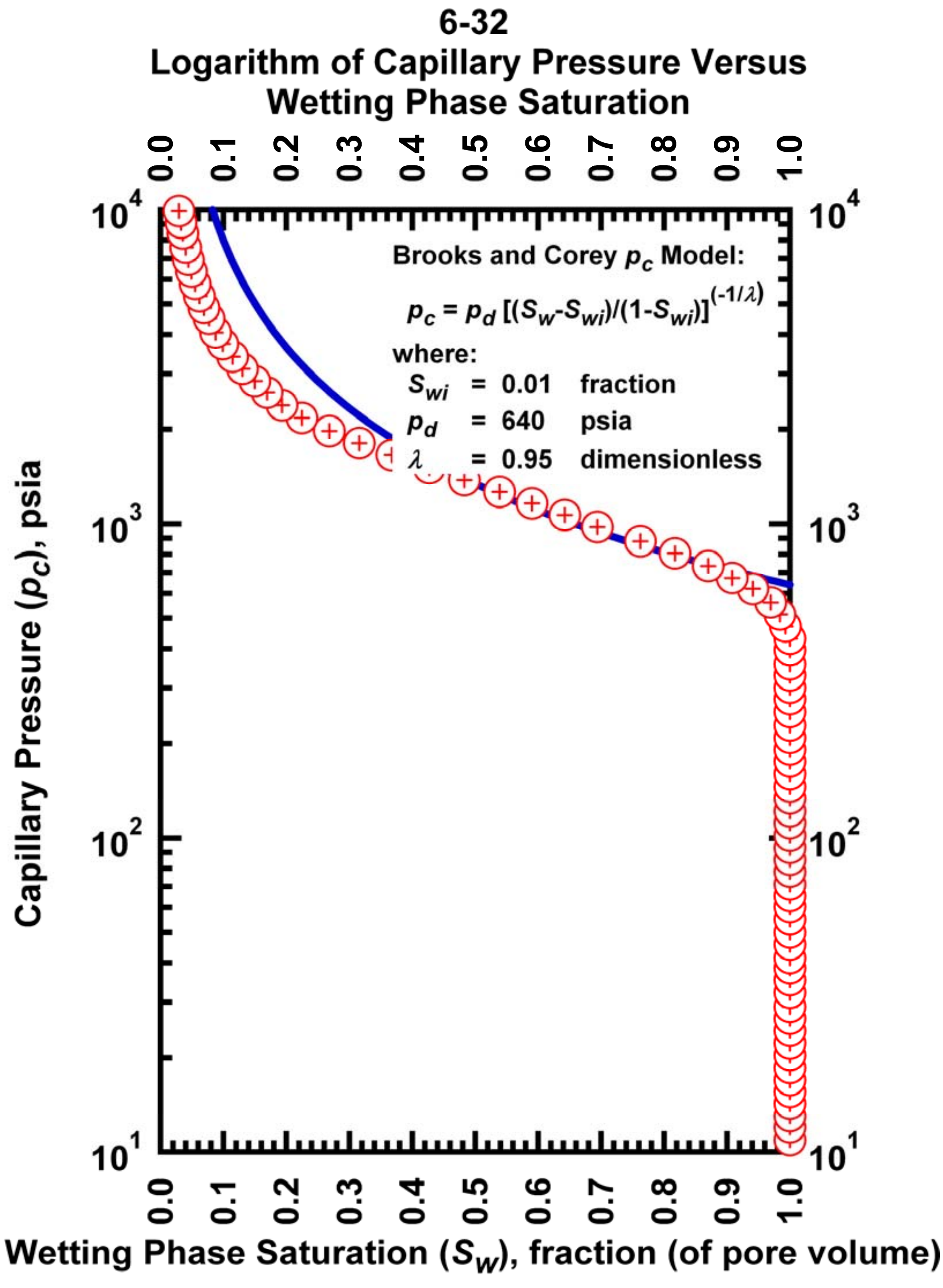

Figure J.15 – Plot of logarithm of capillary pressure vs. wetting phase saturation — Case 6-32 HS1.

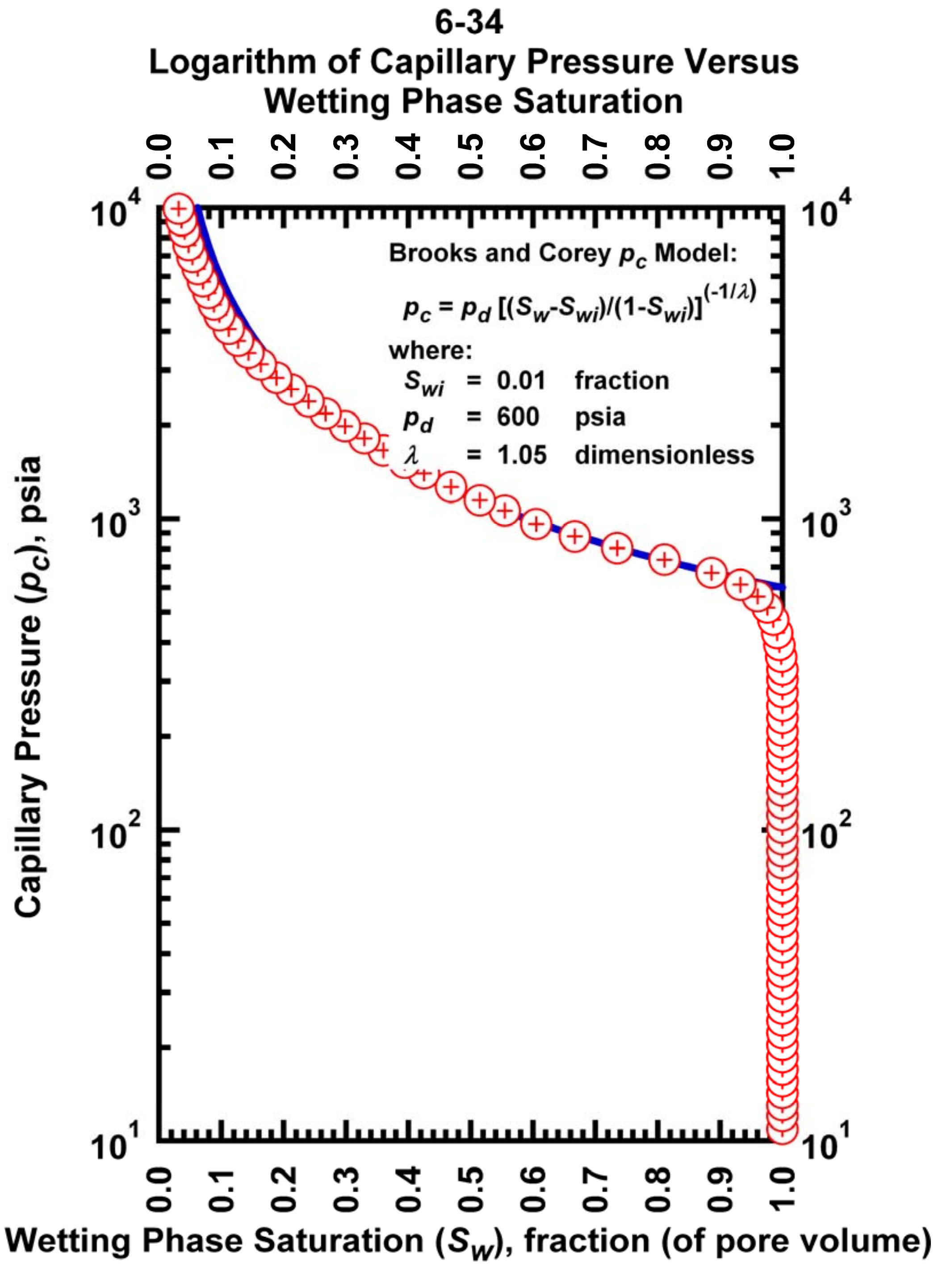

Figure J.16 – Plot of logarithm of capillary pressure vs. wetting phase saturation — Case 6-34 HS1.

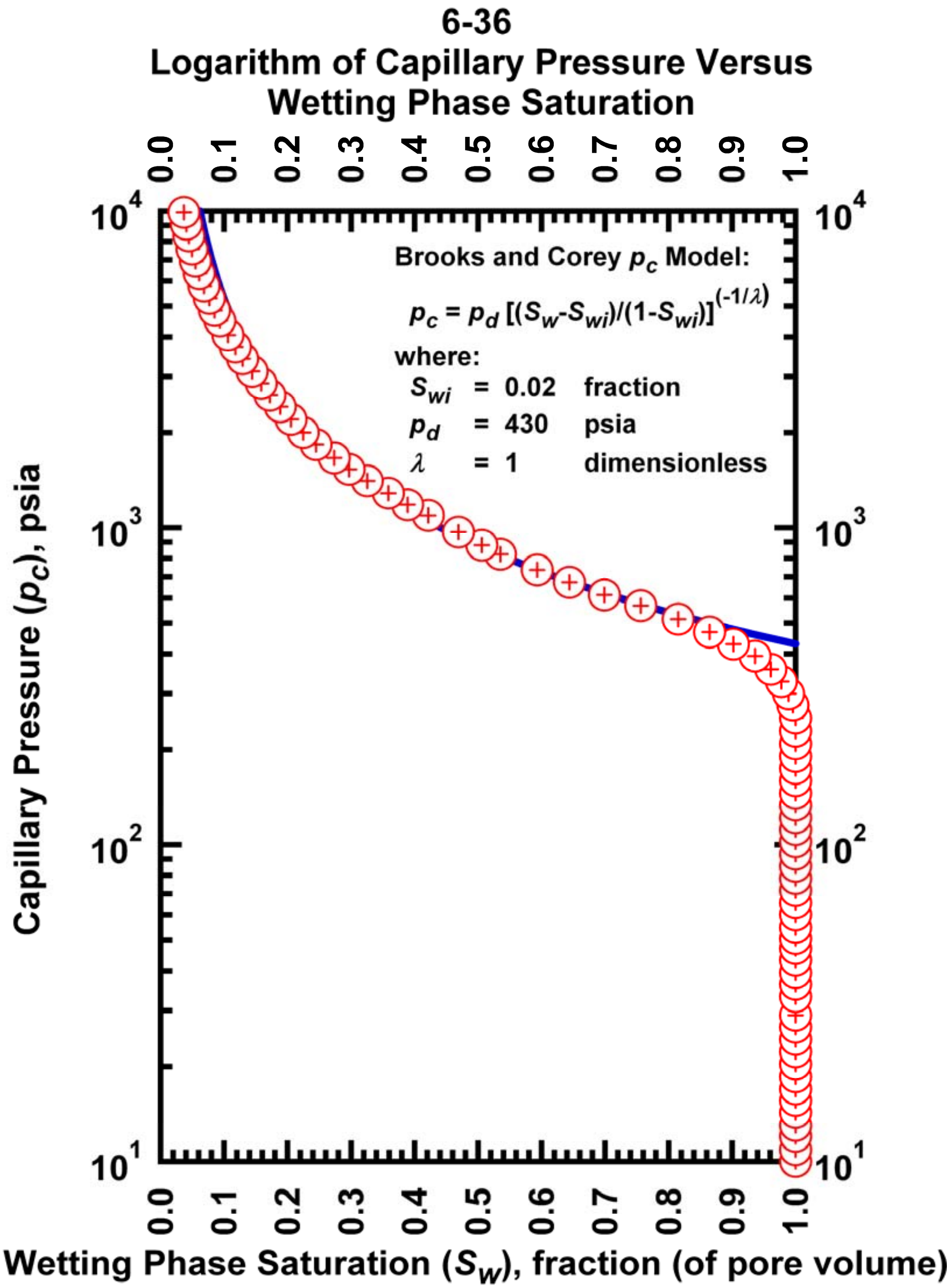

Figure J.17– Plot of logarithm of capillary pressure vs. wetting phase saturation — Case 6-36 HS1.

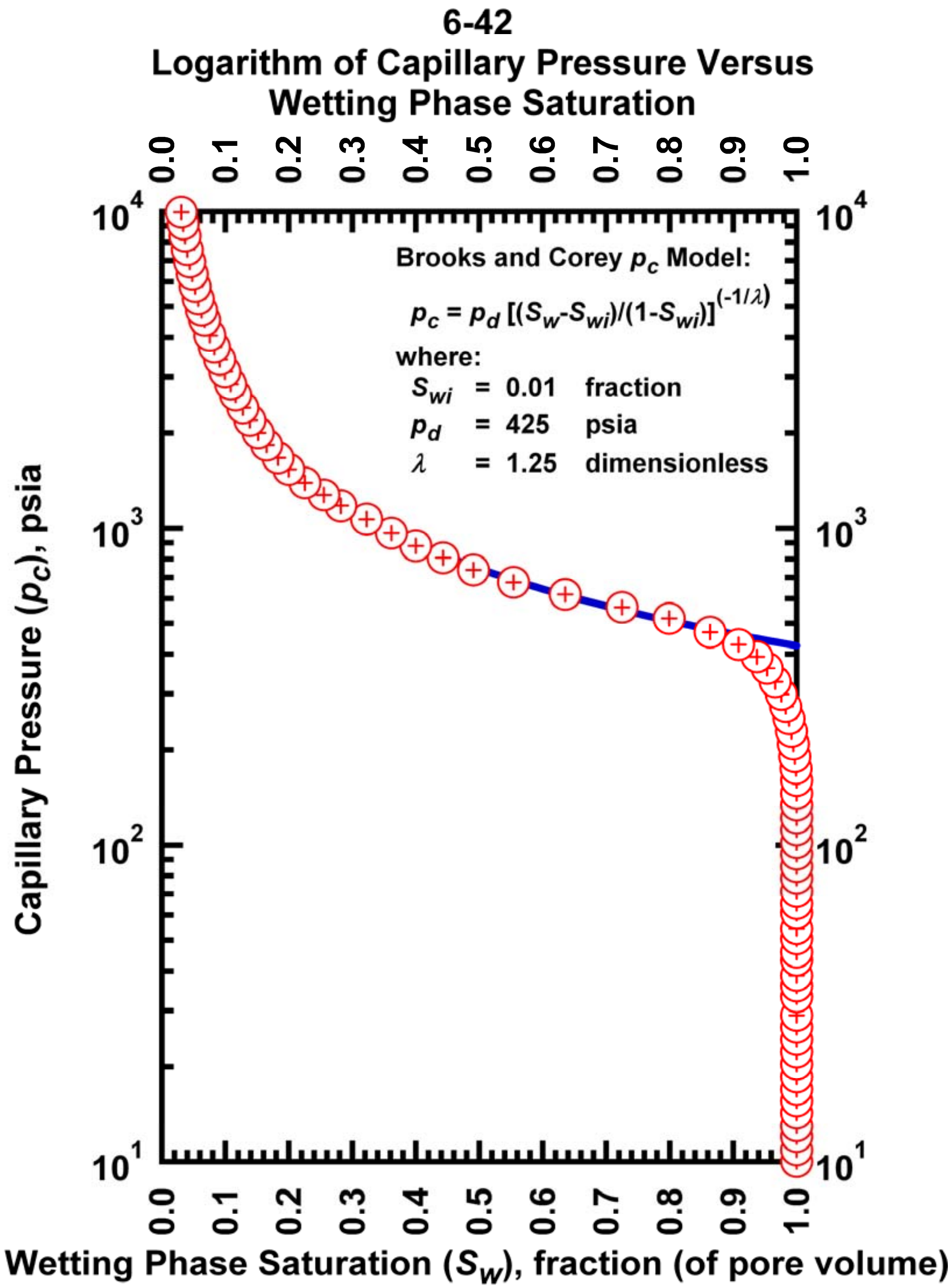

Figure J.18 – Plot of logarithm of capillary pressure vs. wetting phase saturation — Case 6-42 HS1.

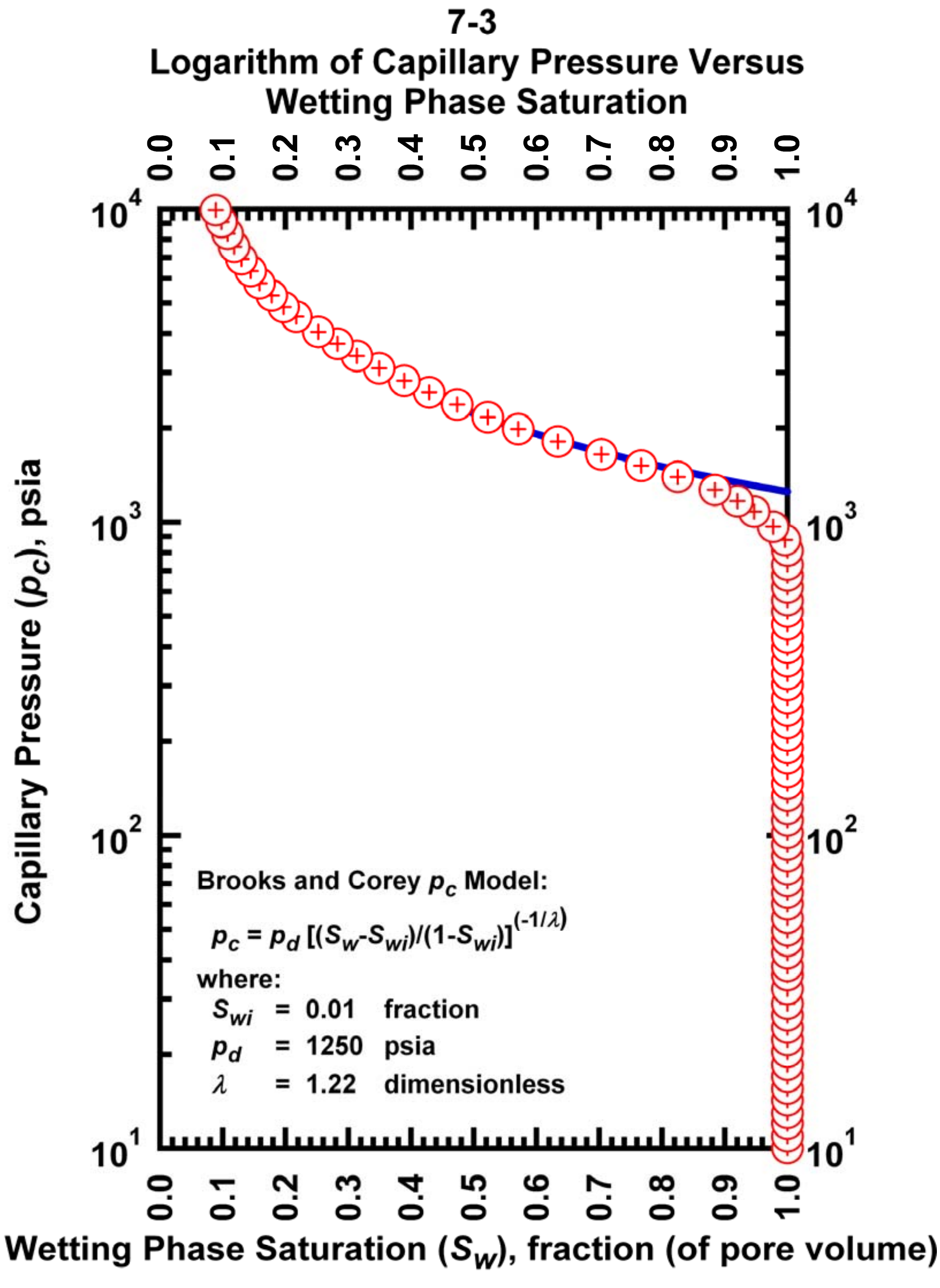

Figure J.19 – Plot of logarithm of capillary pressure vs. wetting phase saturation — Case 7-3 HS1.

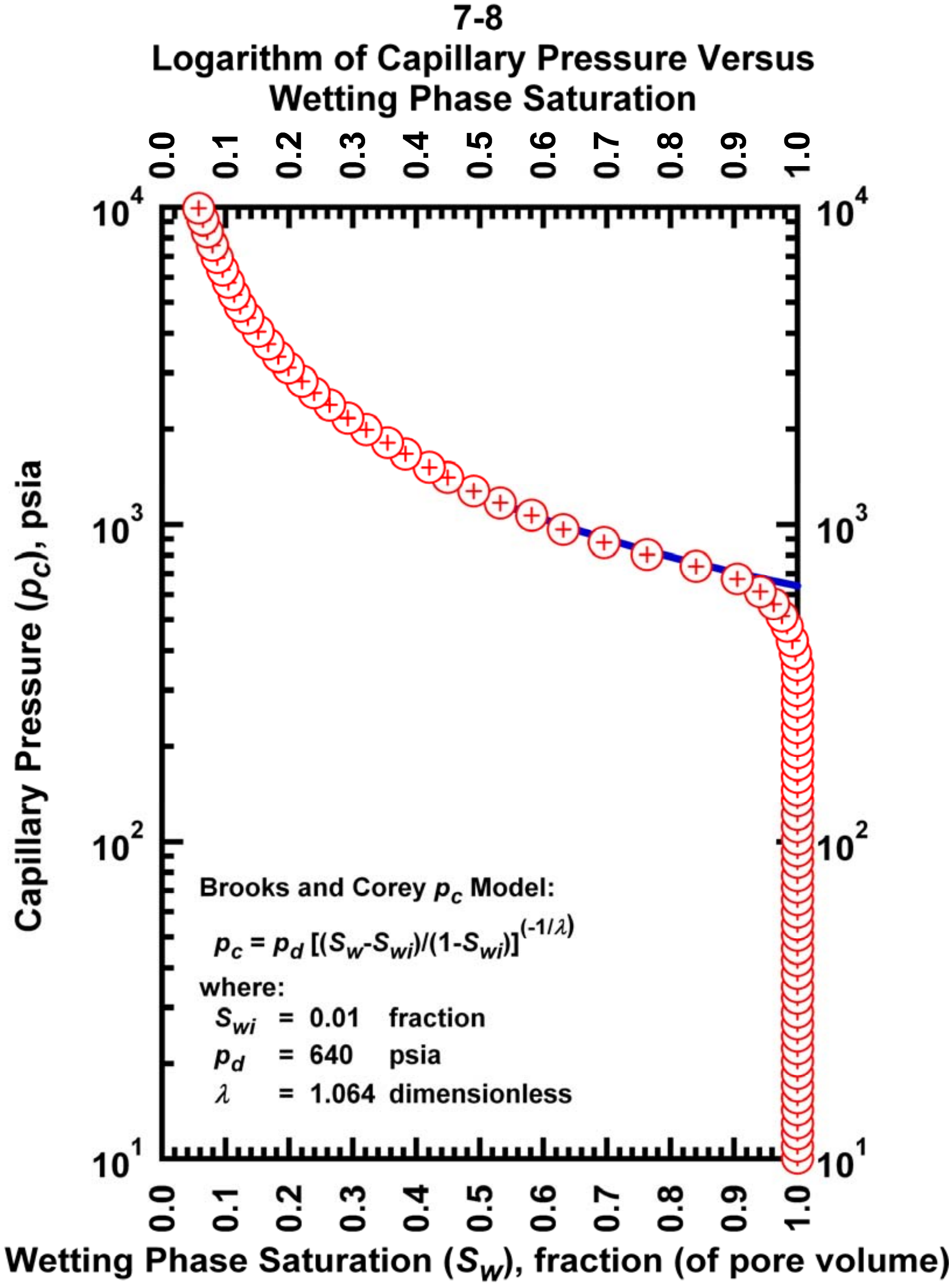

Figure J.20 – Plot of logarithm of capillary pressure vs. wetting phase saturation — Case 7-8 HS1.

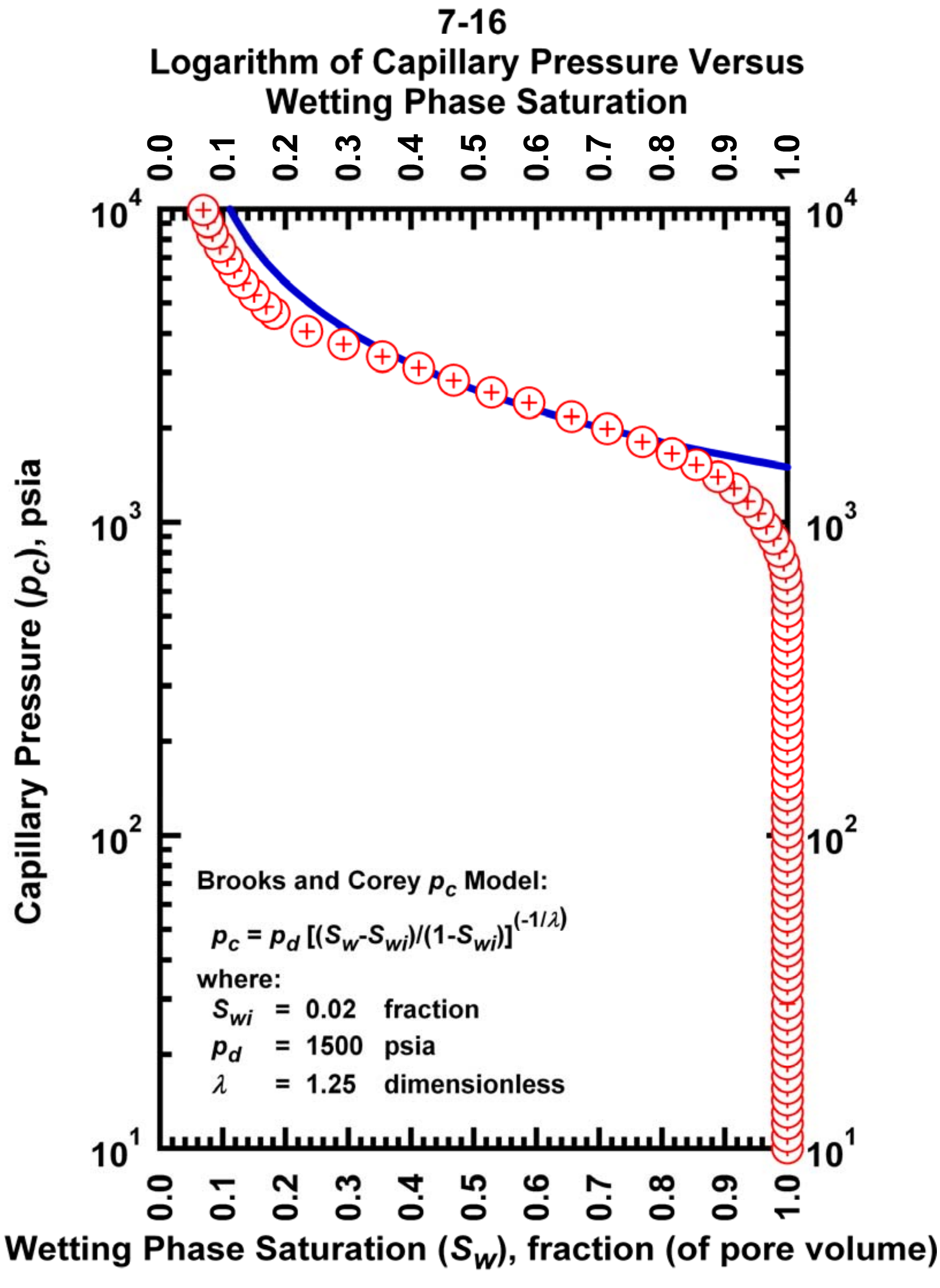

Figure J.21 – Plot of logarithm of capillary pressure vs. wetting phase saturation — Case 7-16 HS1.

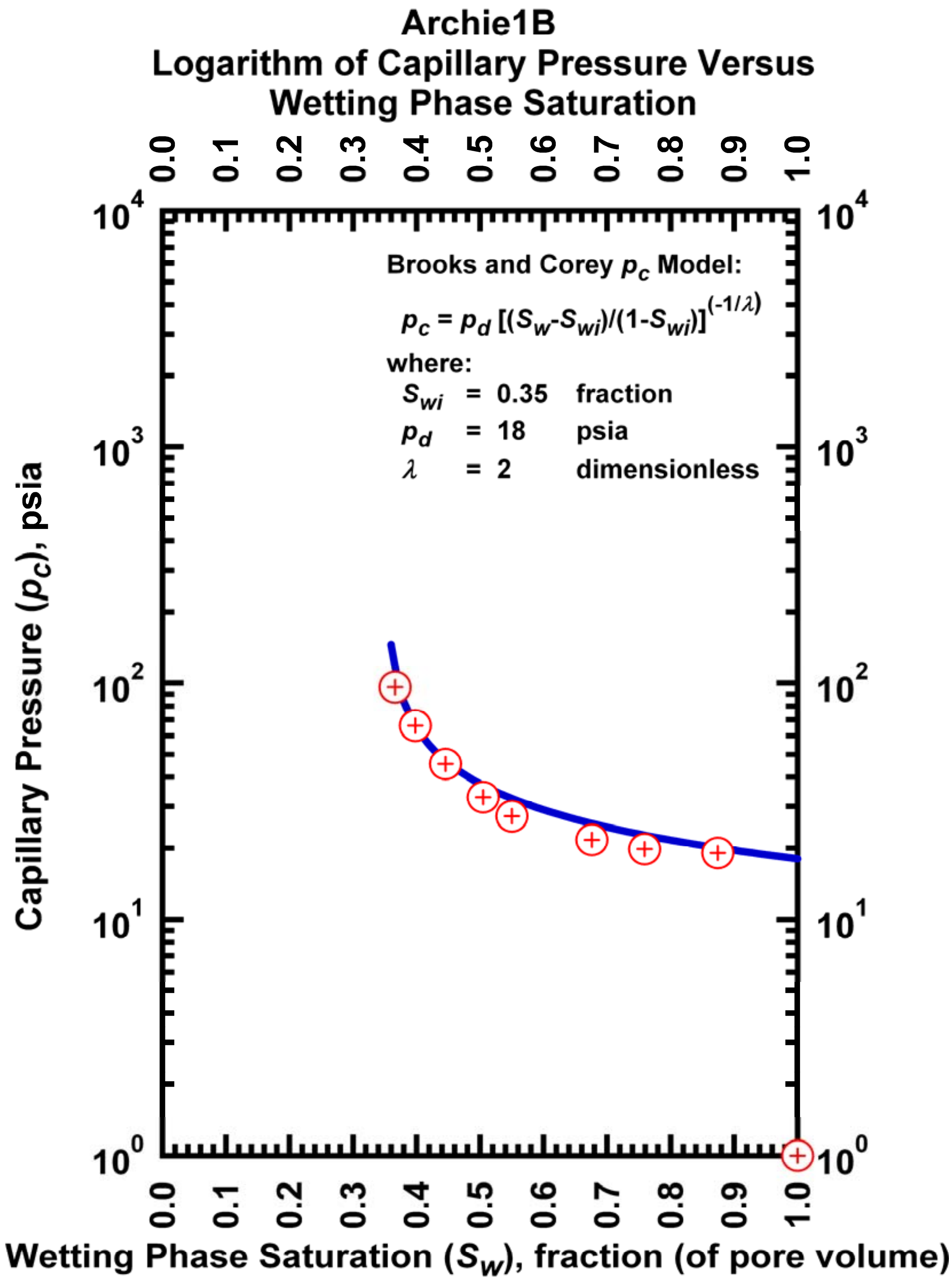

Figure J.22 – Plot of logarithm of capillary pressure vs. wetting phase saturation — Case Archie1B.

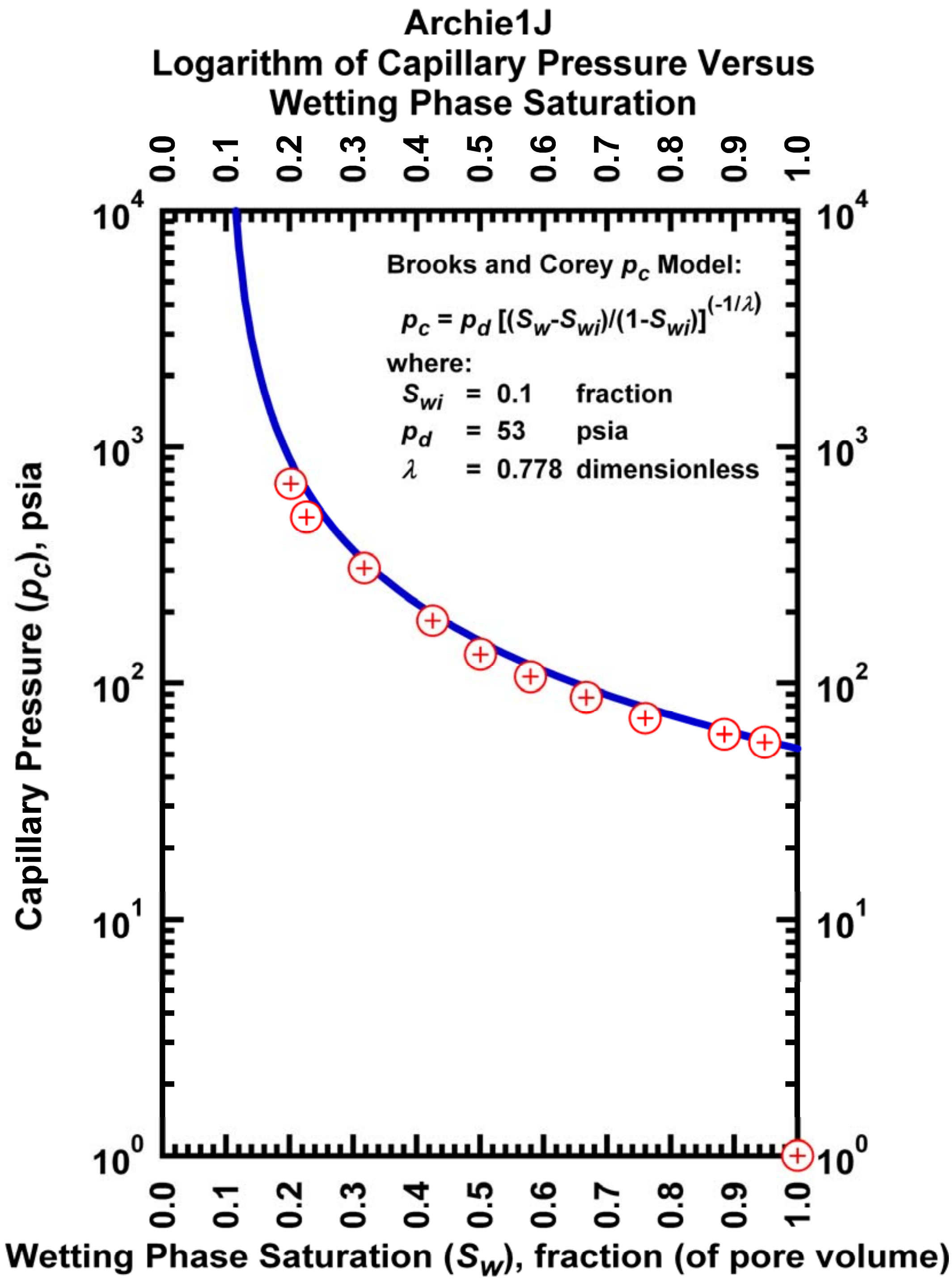

Figure J.23 – Plot of logarithm of capillary pressure vs. wetting phase saturation — Case Archie1J.

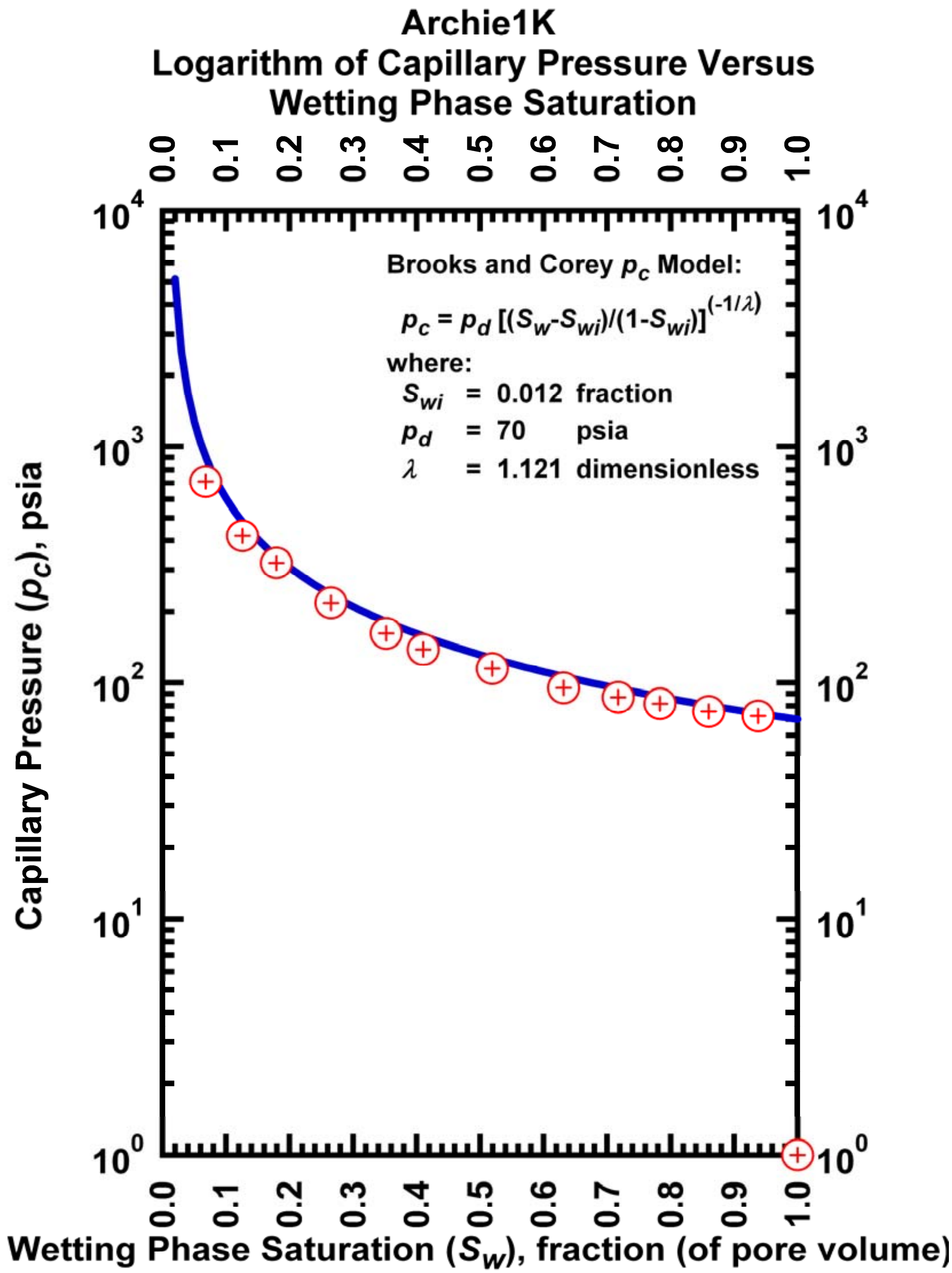

Figure J.24– Plot of logarithm of capillary pressure vs. wetting phase saturation — Case Archie1K.

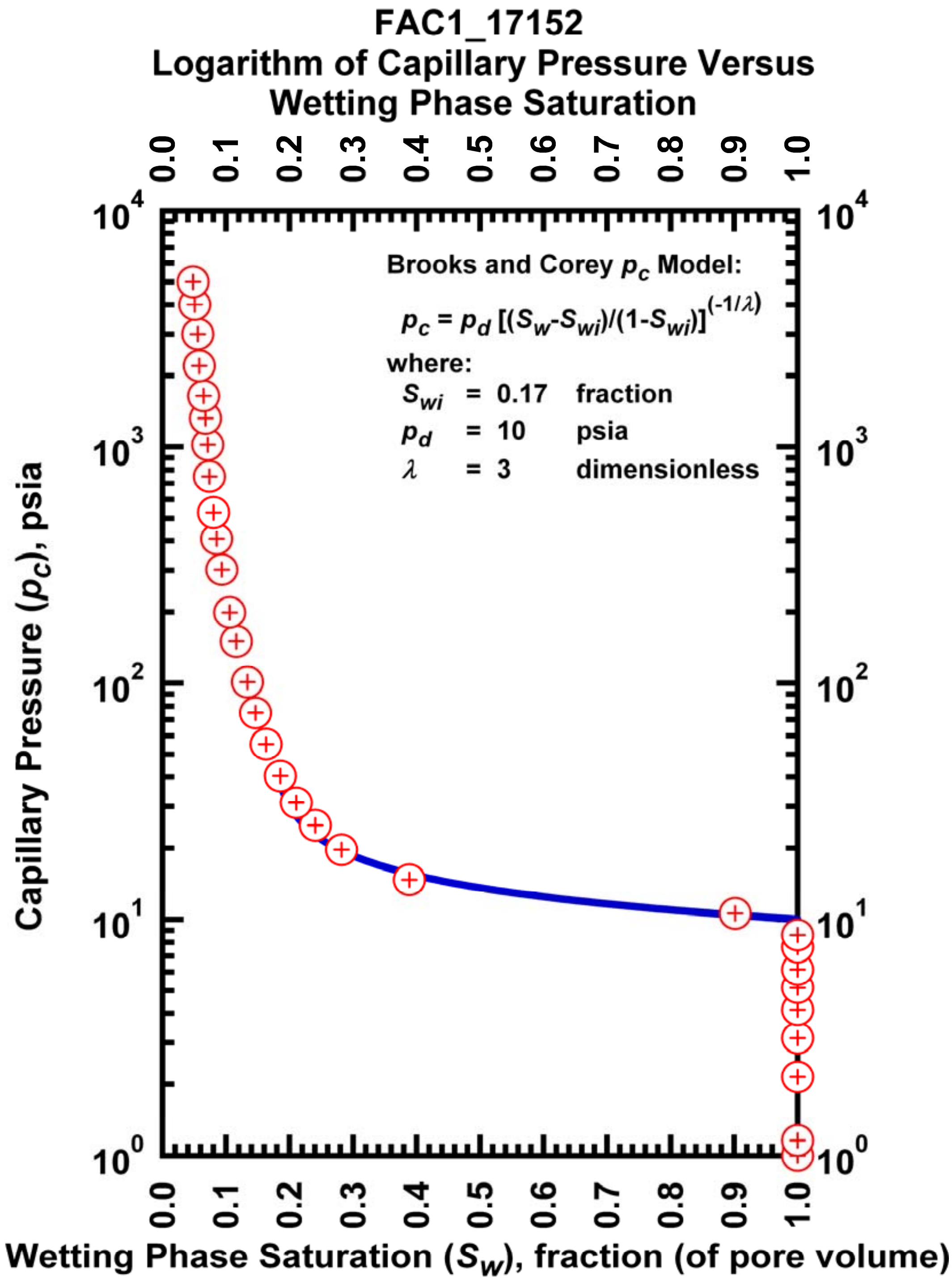

Figure J.25 – Plot of logarithm of capillary pressure vs. wetting phase saturation — Case FAC1_17152.

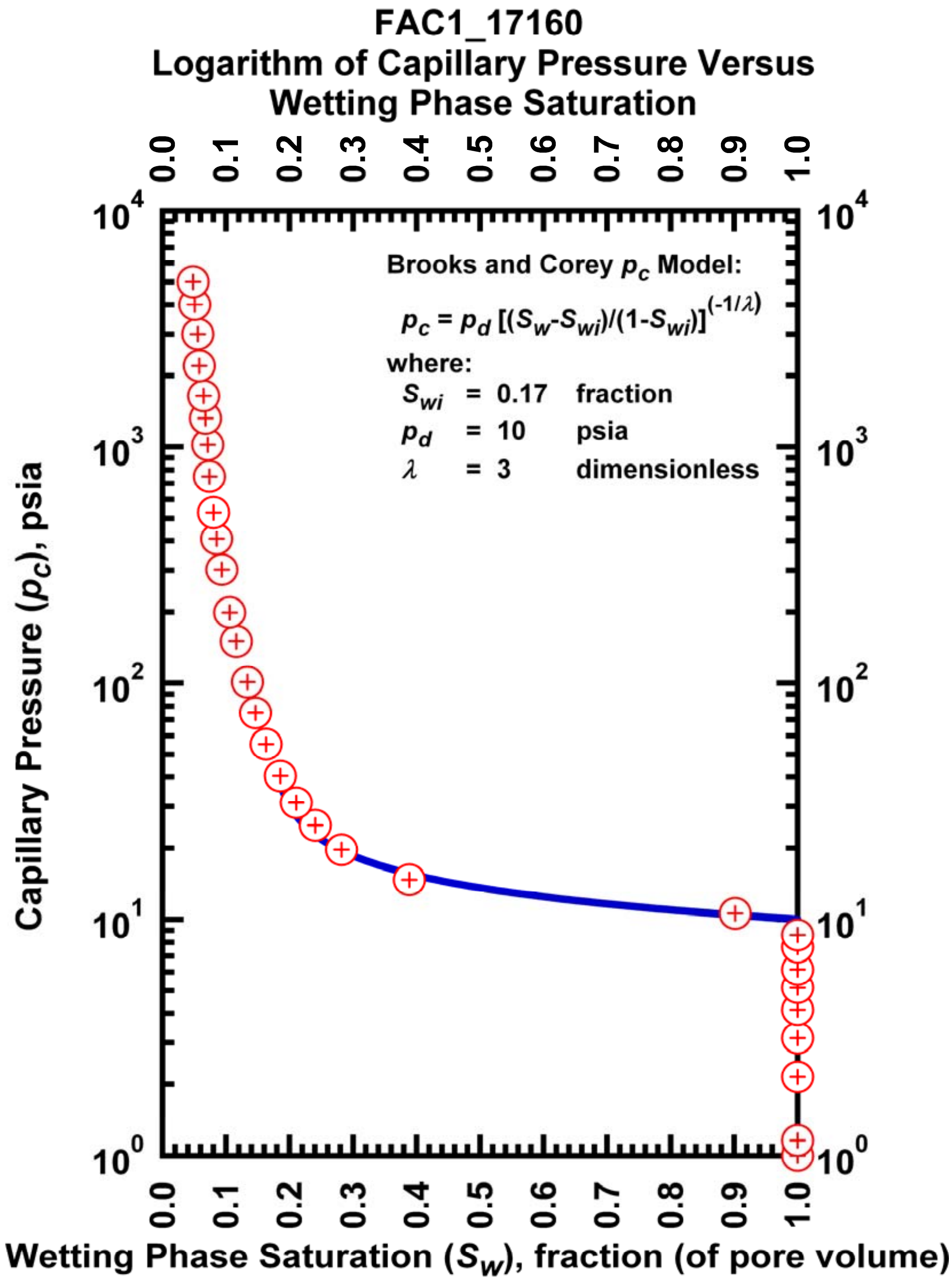

Figure J.26 – Plot of logarithm of capillary pressure vs. wetting phase saturation — Case FAC1_17160.

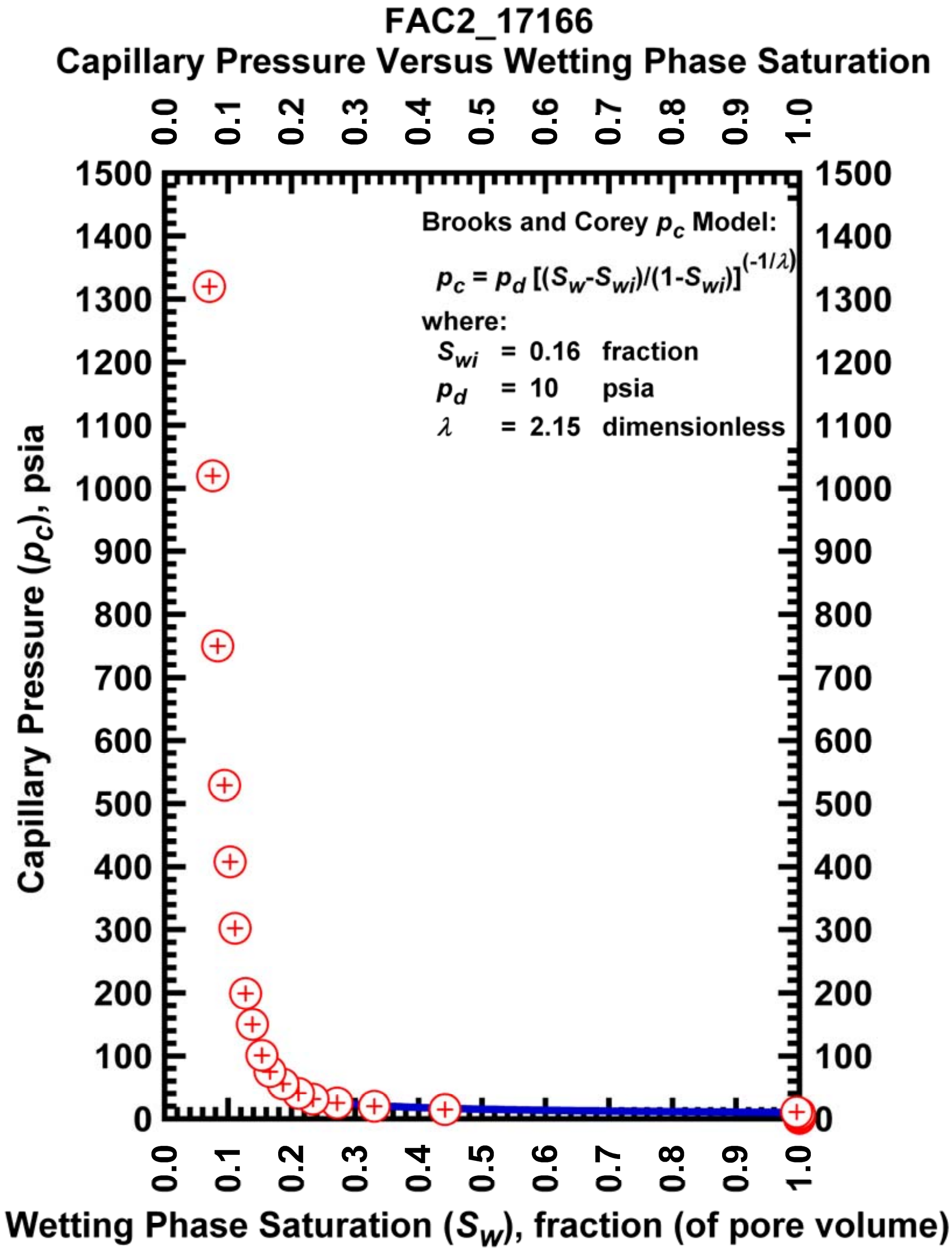

Figure J.27 – Plot of logarithm of capillary pressure vs. wetting phase saturation — Case FAC2_17066.

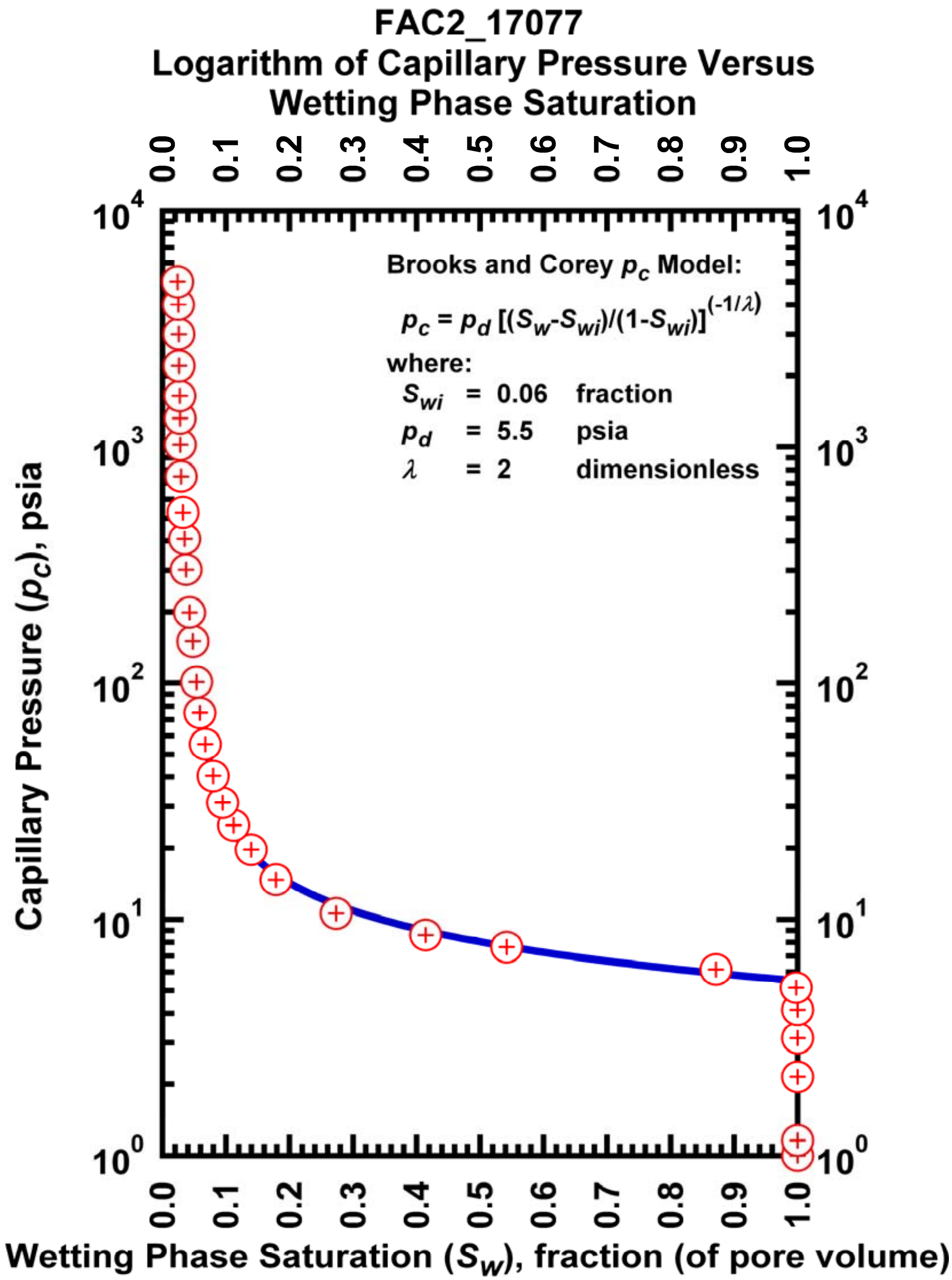

Figure J.28 – Plot of logarithm of capillary pressure vs. wetting phase saturation — Case FAC2_17077.

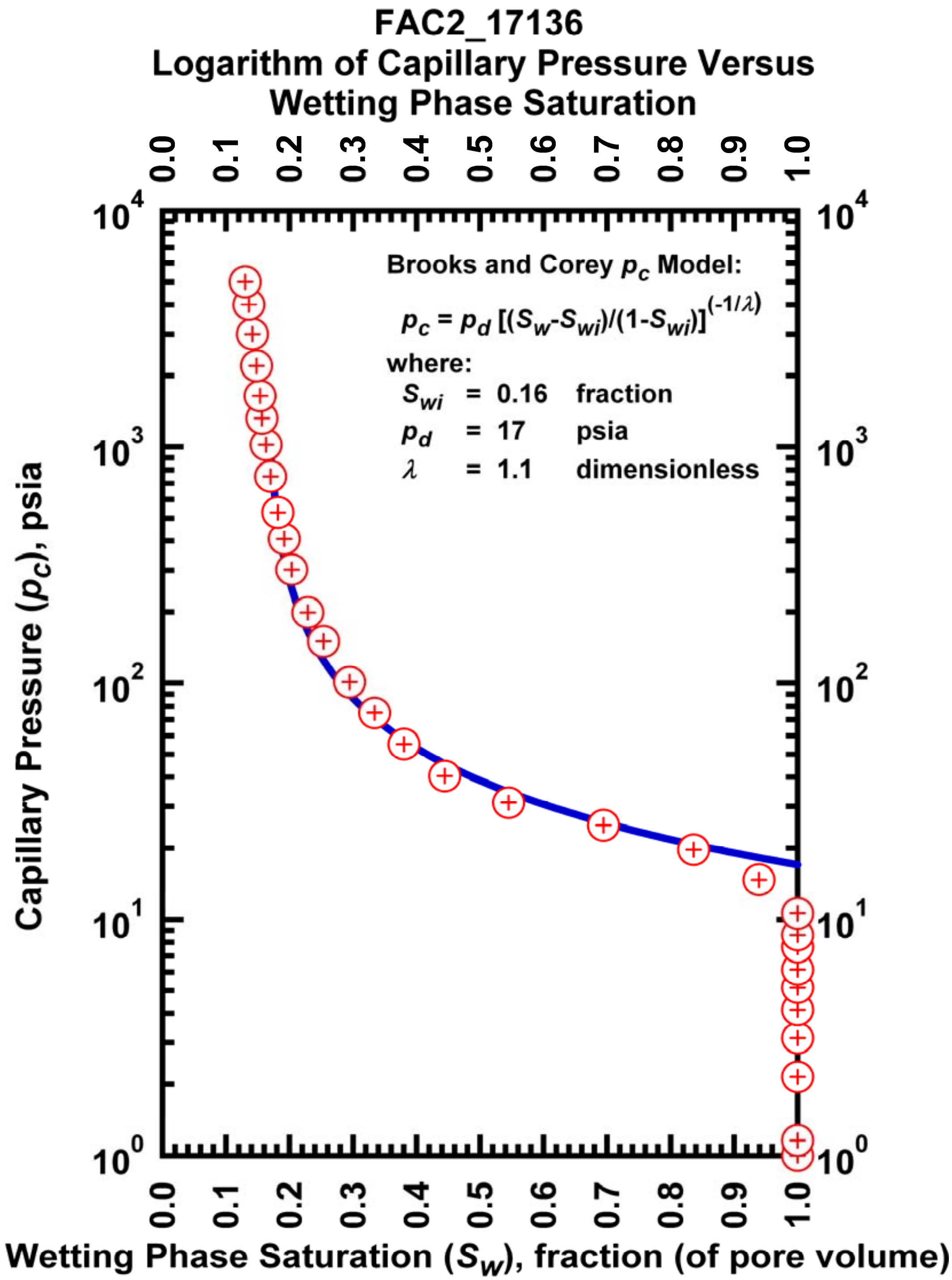

Figure J.29 – Plot of logarithm of capillary pressure vs. wetting phase saturation — Case FAC2_17136.

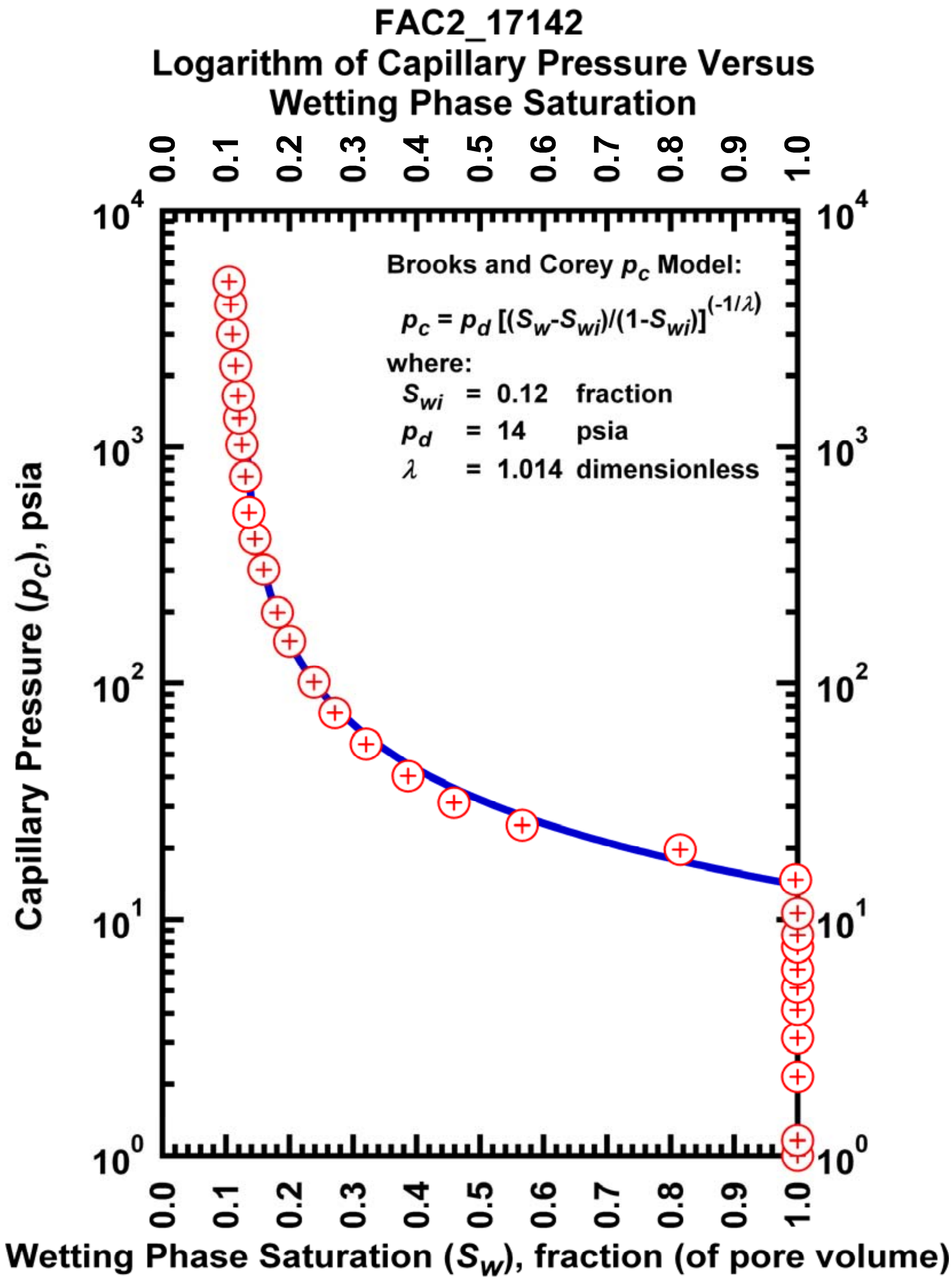

Figure J.30 – Plot of logarithm of capillary pressure vs. wetting phase saturation — Case FAC2_17142.

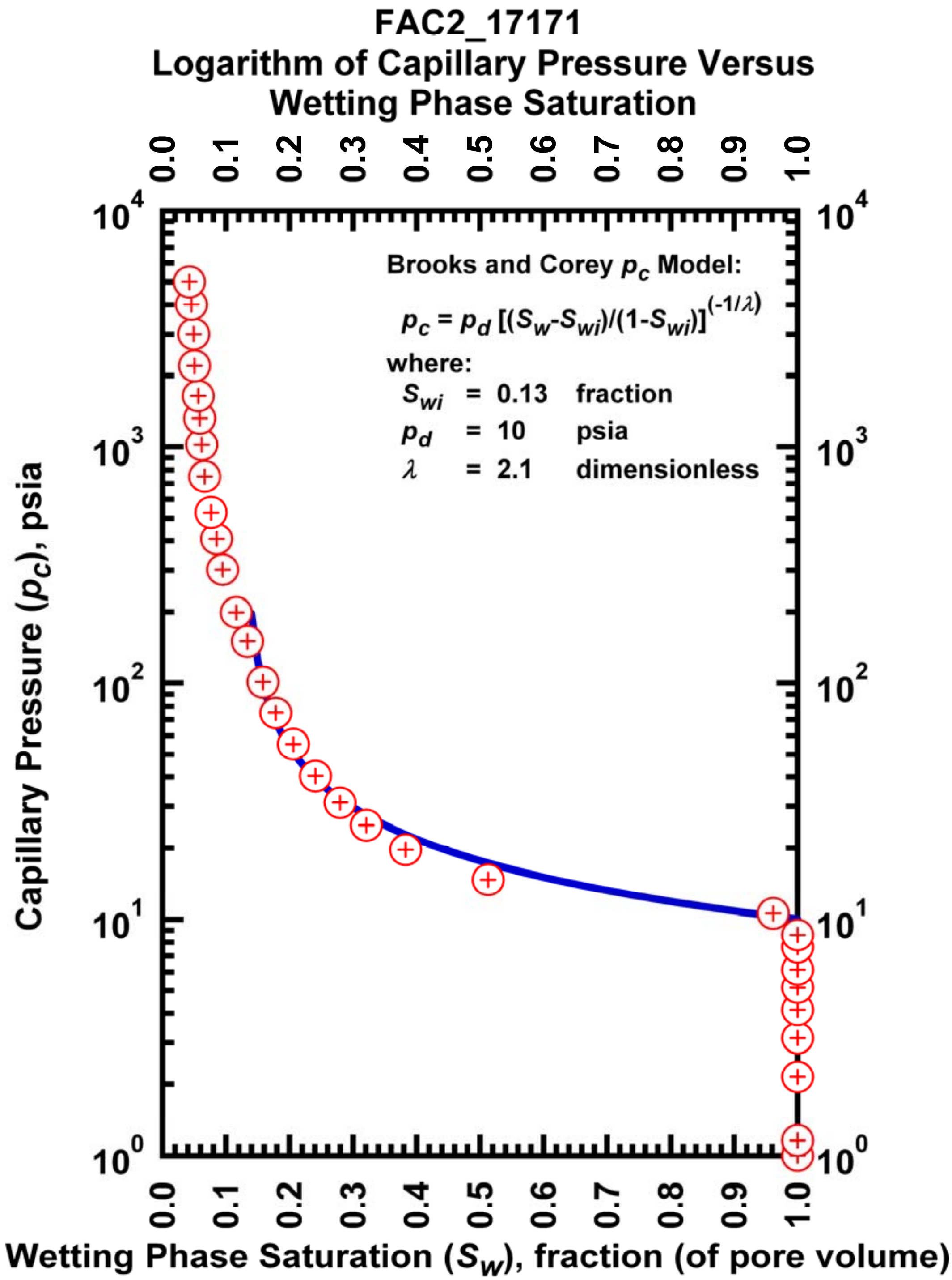

Figure J.31 – Plot of logarithm of capillary pressure vs. wetting phase saturation — Case FAC2_17171.

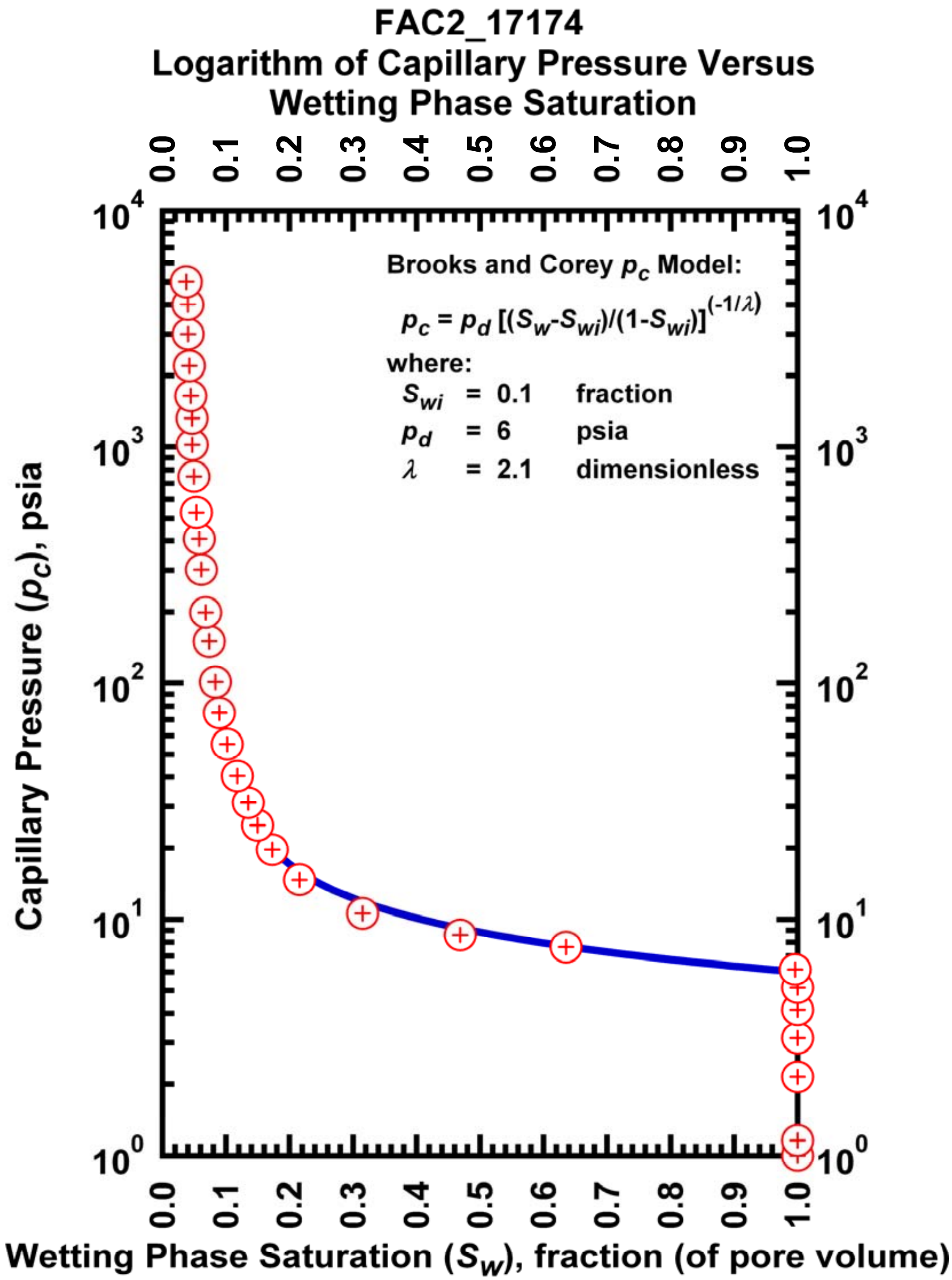

Figure J.32 – Plot of logarithm of capillary pressure vs. wetting phase saturation — Case FAC2_17174.

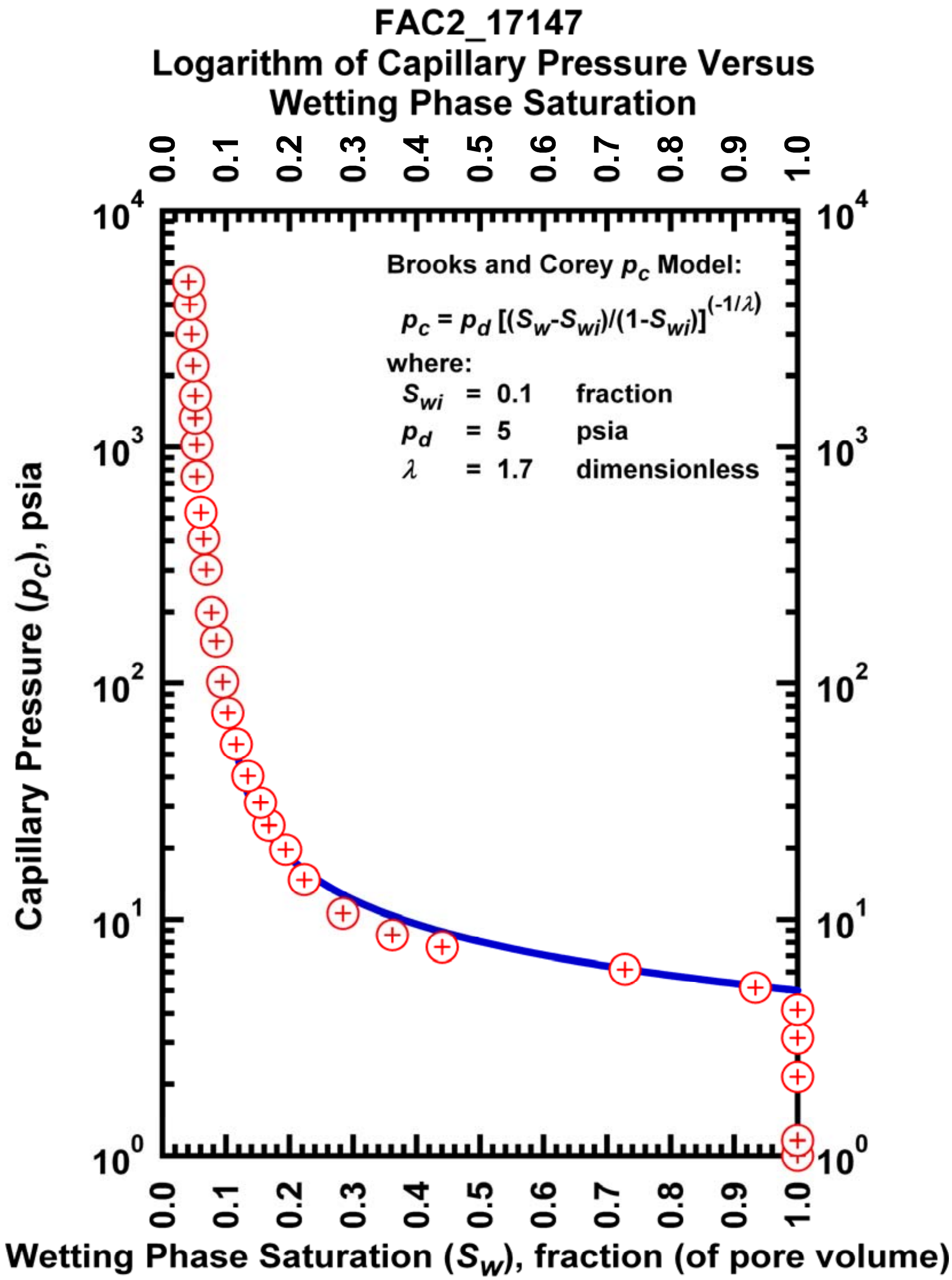

Figure J.33– Plot of logarithm of capillary pressure vs. wetting phase saturation — Case FAC6_17147.

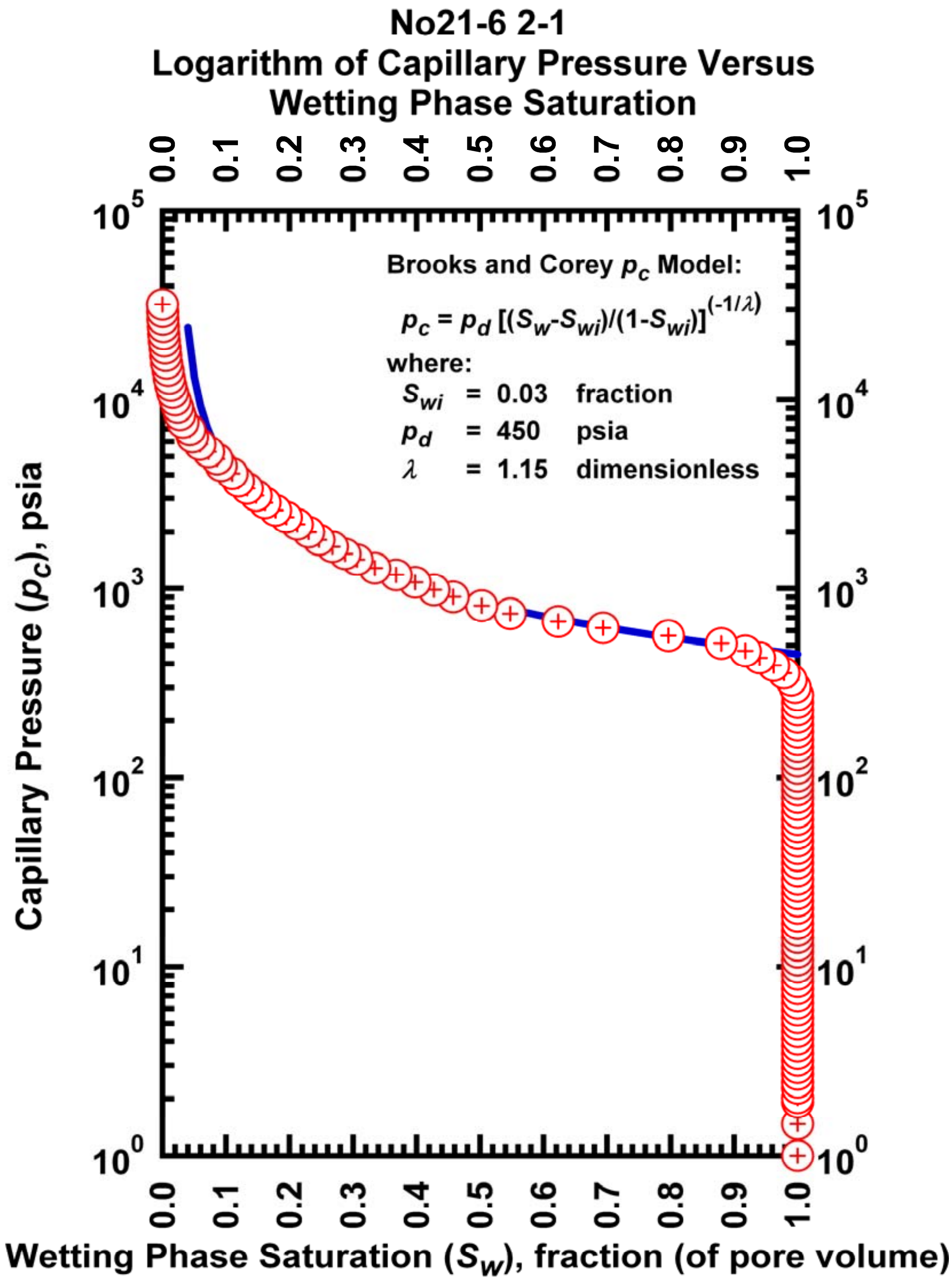

Figure J.34– Plot of logarithm of capillary pressure vs. wetting phase saturation — Case No21-6 2-1.

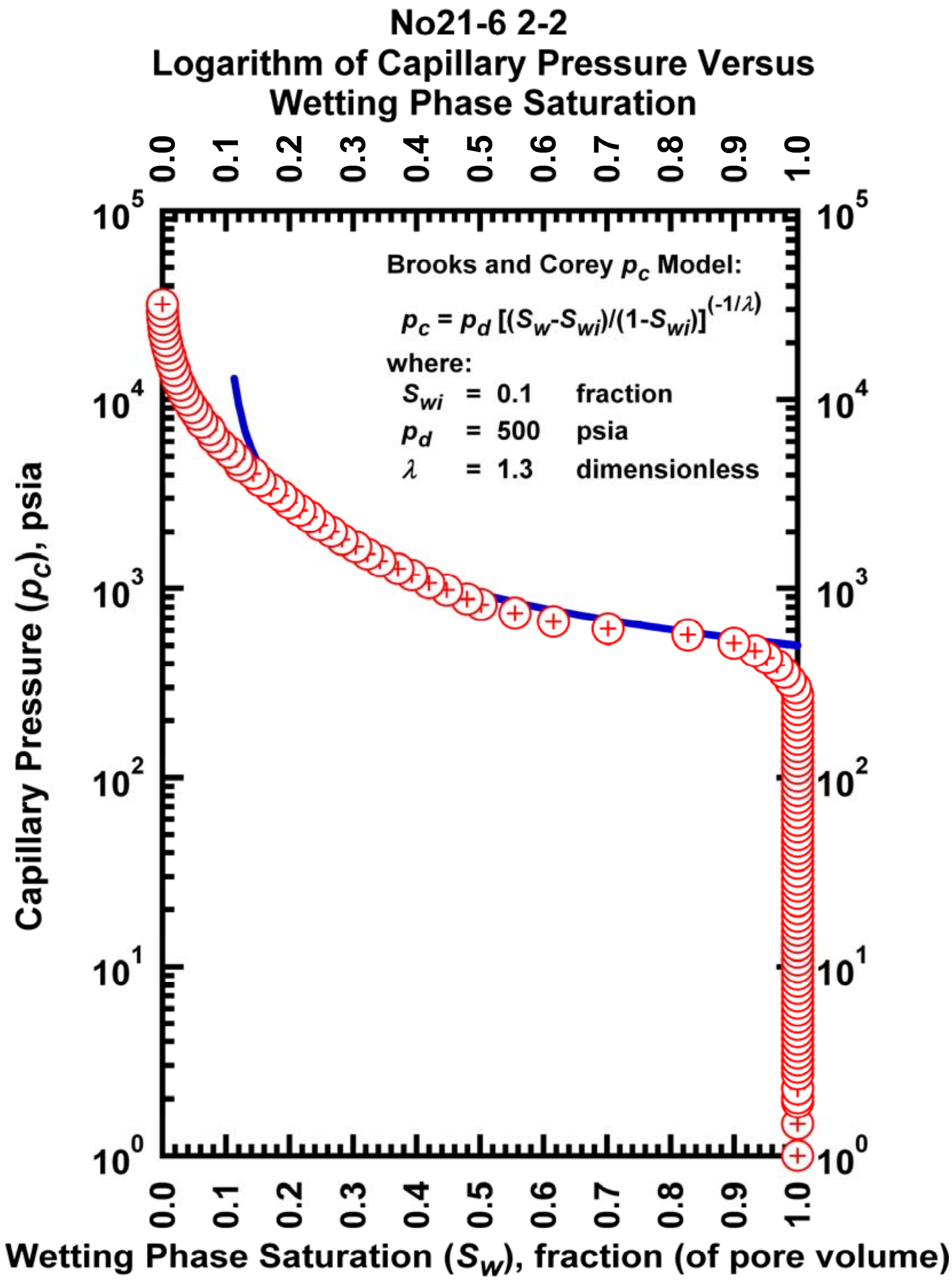

Figure J.35 – Plot of logarithm of capillary pressure vs. wetting phase saturation — Case No21-6 2-2.

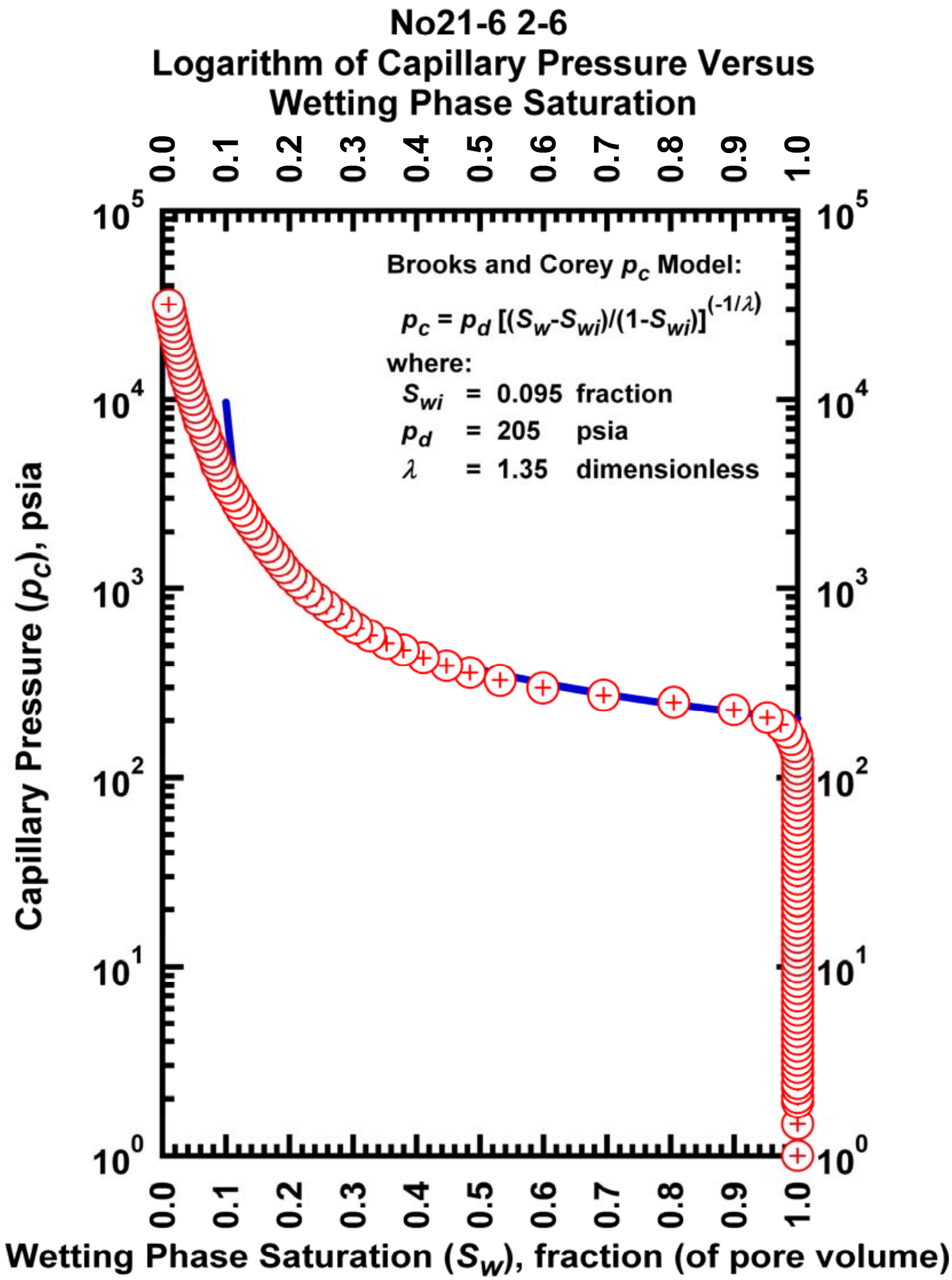

Figure J.36 – Plot of logarithm of capillary pressure vs. wetting phase saturation — Case No21-6 2-6.

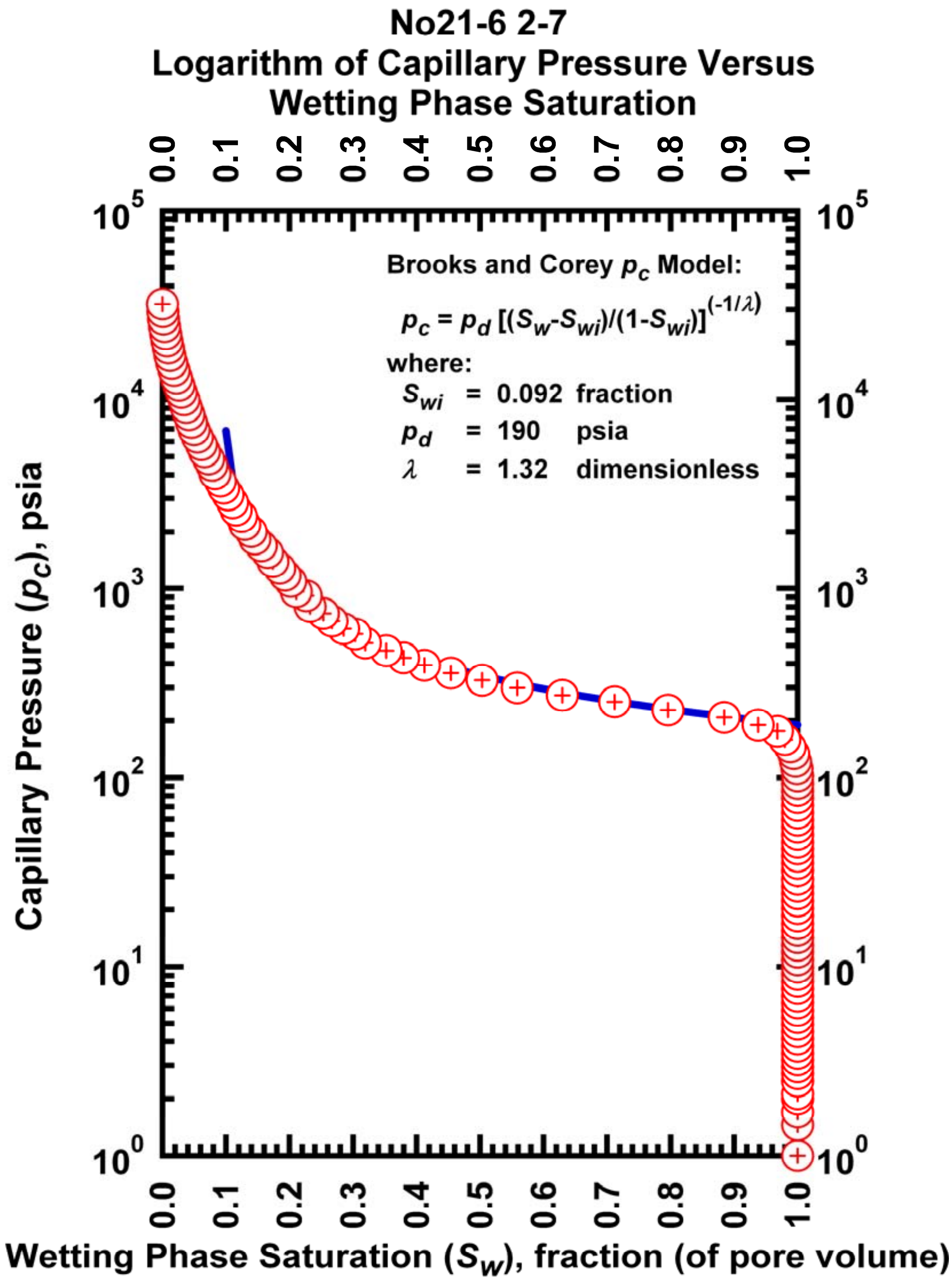

Figure J.37– Plot of logarithm of capillary pressure vs. wetting phase saturation — Case No21-6 2-7.

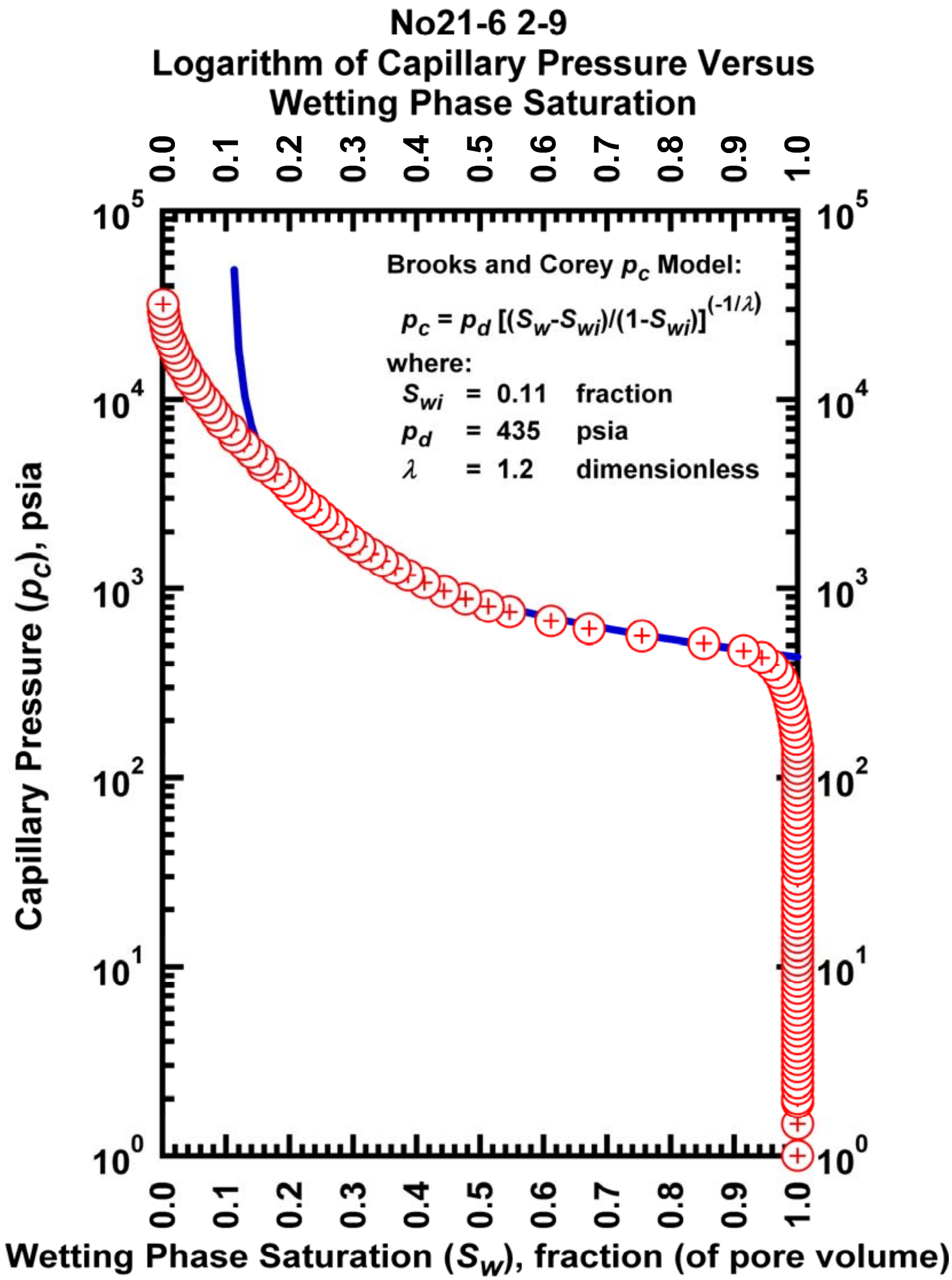

Figure J.38 – Plot of logarithm of capillary pressure vs. wetting phase saturation — Case No21-6 2-9.

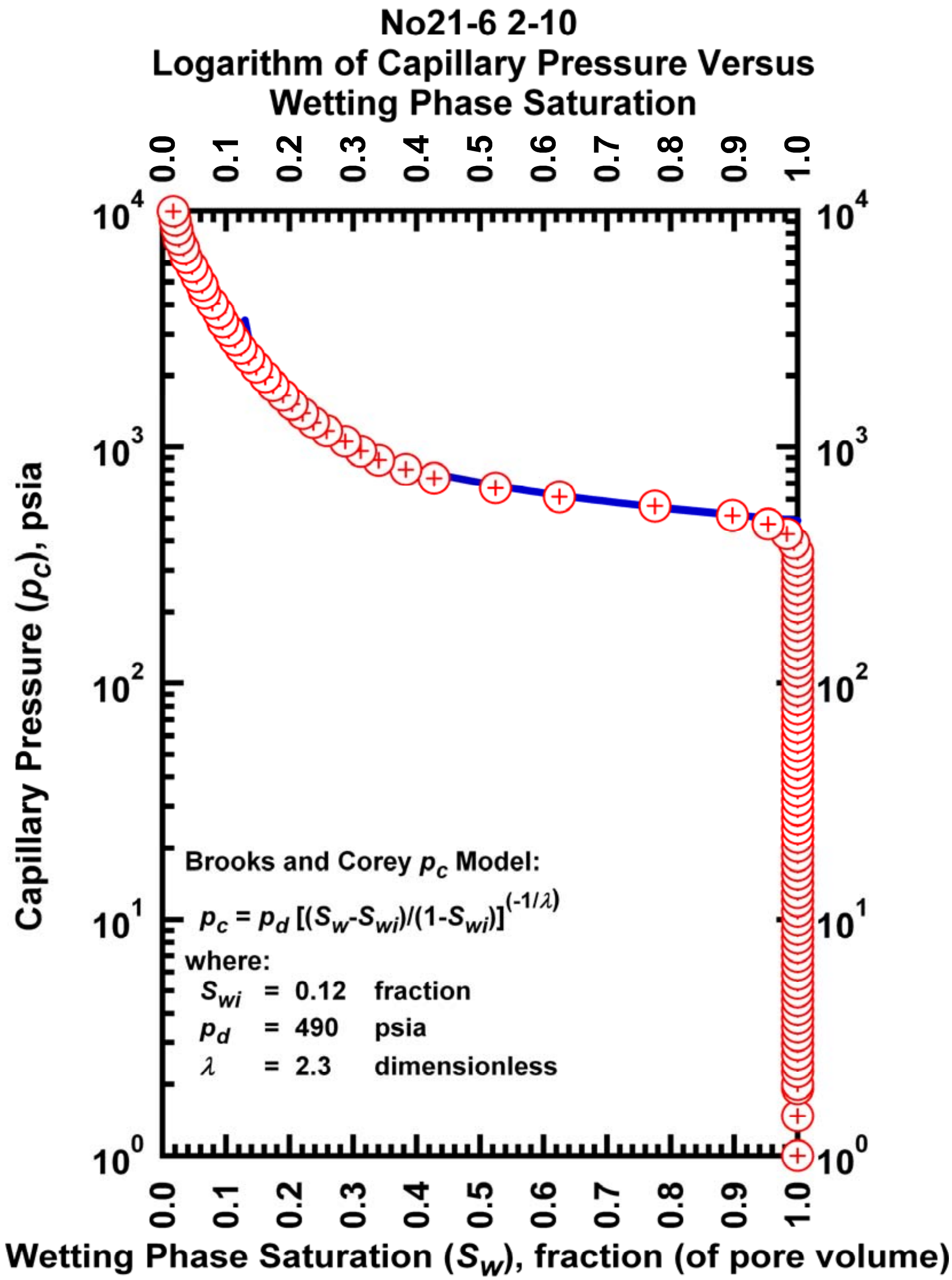

Figure J.39 – Plot of logarithm of capillary pressure vs. wetting phase saturation — Case No21-6 2-10.

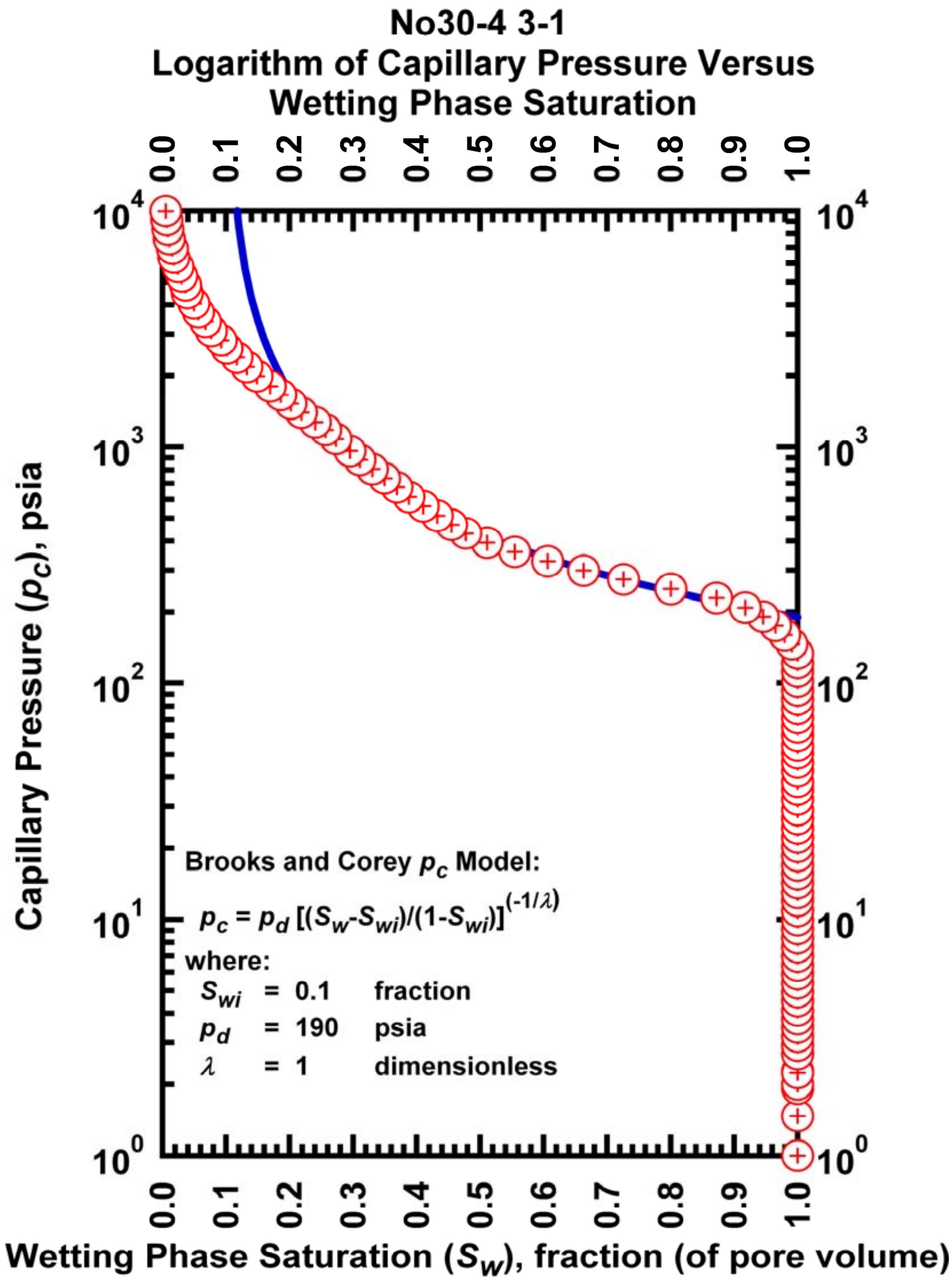

Figure J.40 – Plot of logarithm of capillary pressure vs. wetting phase saturation — Case No30-4 3-1.

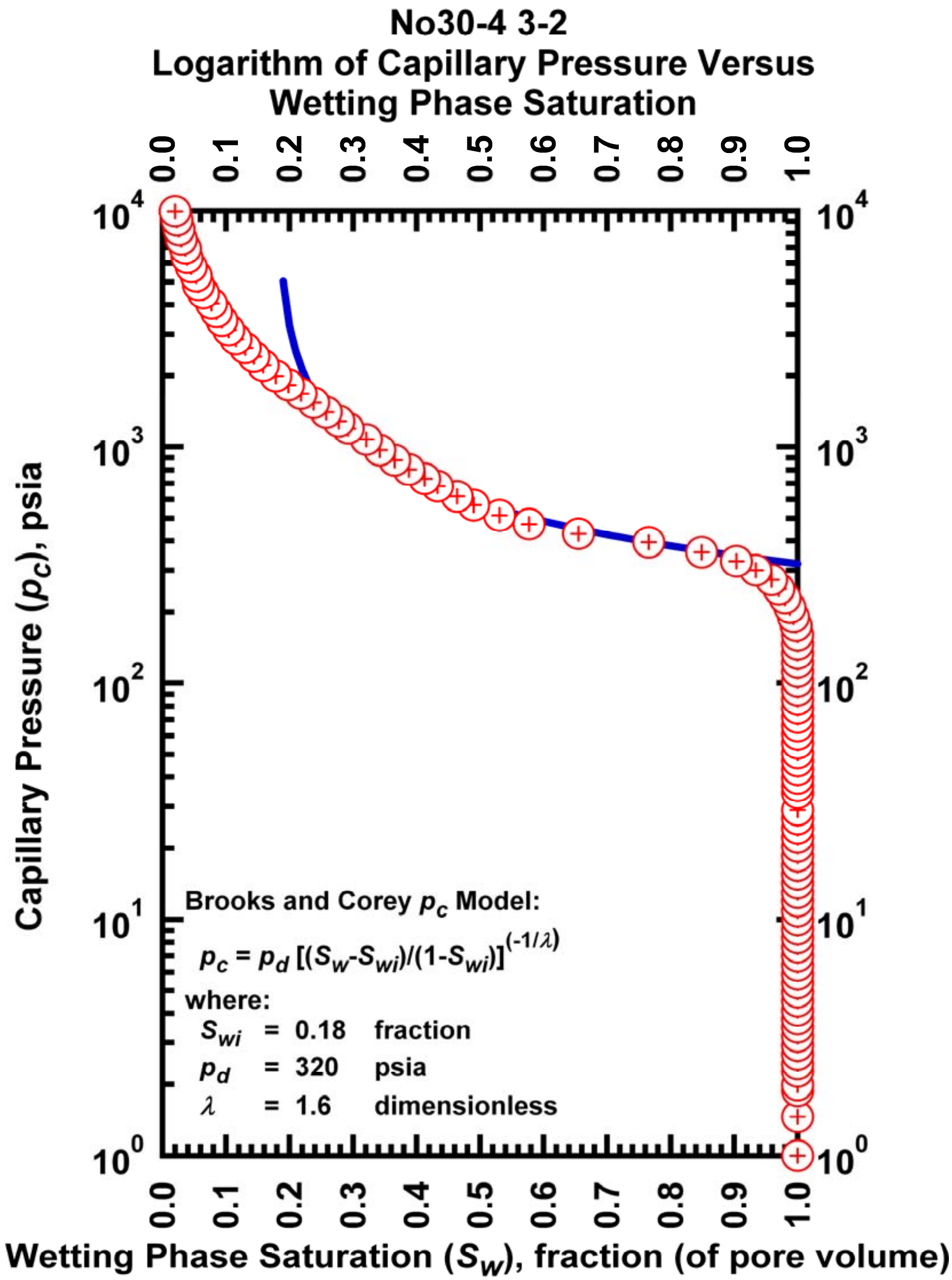

Figure J.41 – Plot of logarithm of capillary pressure vs. wetting phase saturation — Case No30-4 3-2.

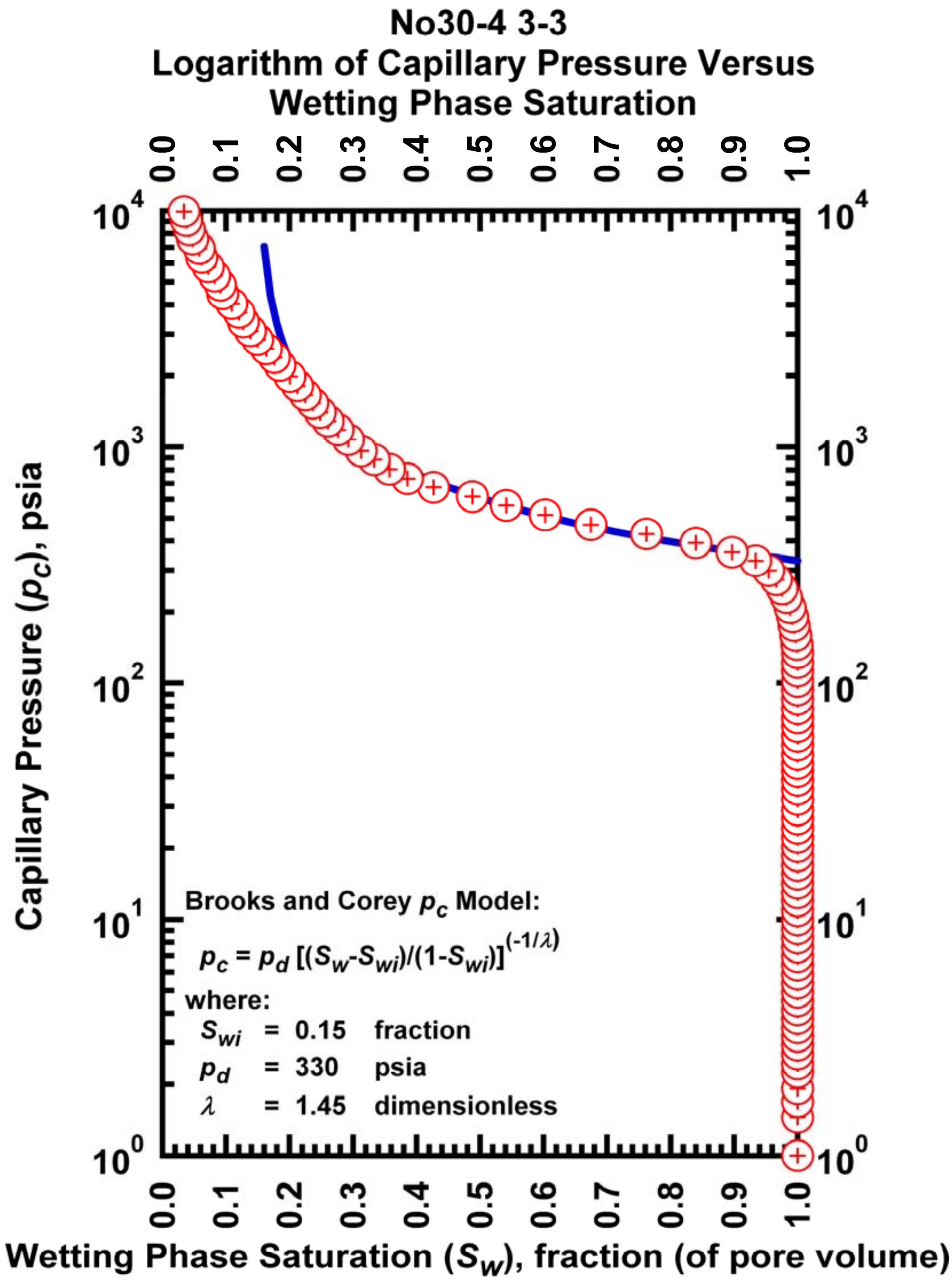

Figure J.42 – Plot of logarithm of capillary pressure vs. wetting phase saturation — Case No30-4 3-3.

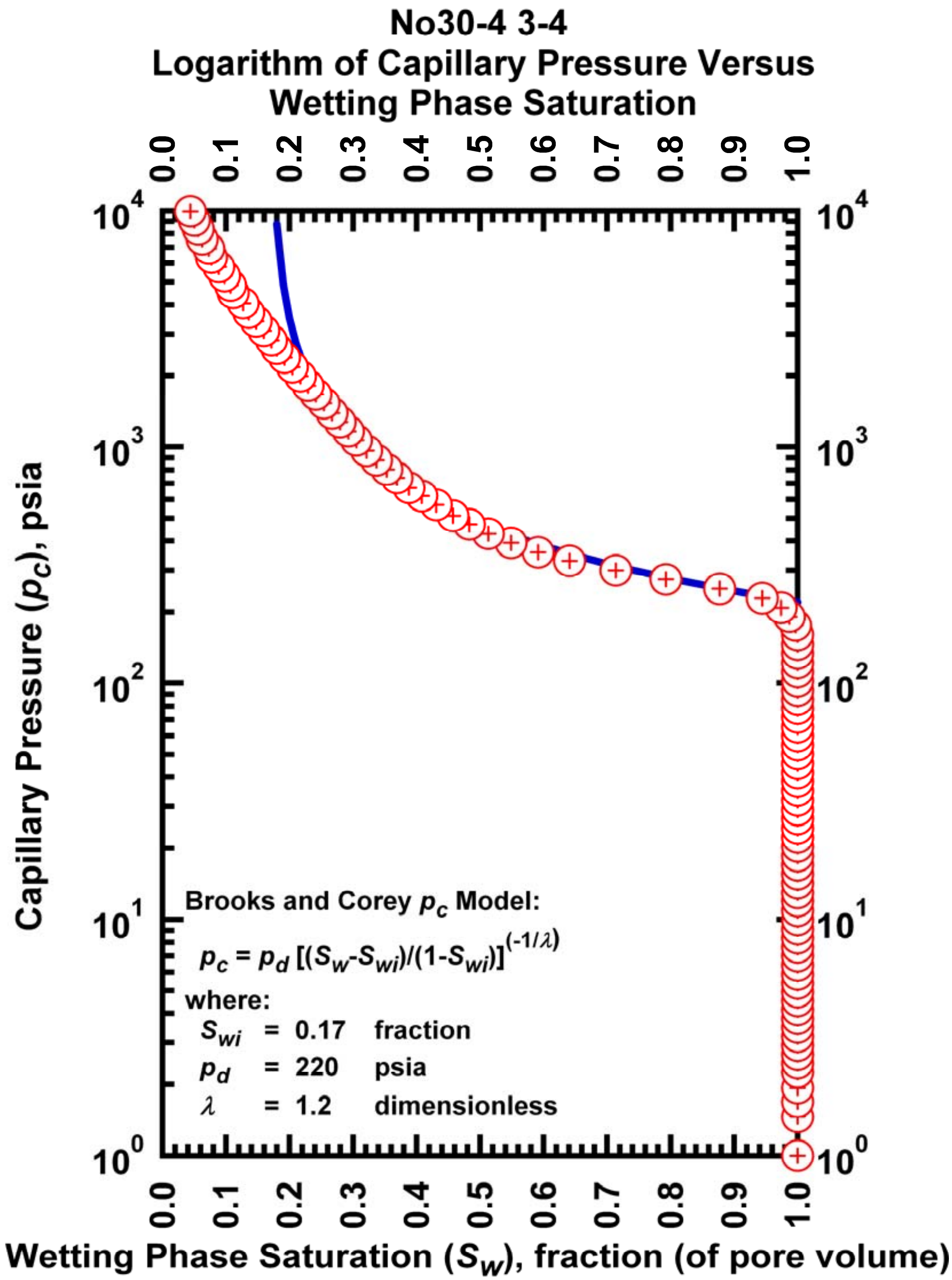

Figure J.43 – Plot of logarithm of capillary pressure vs. wetting phase saturation — Case No30-4 3-4.

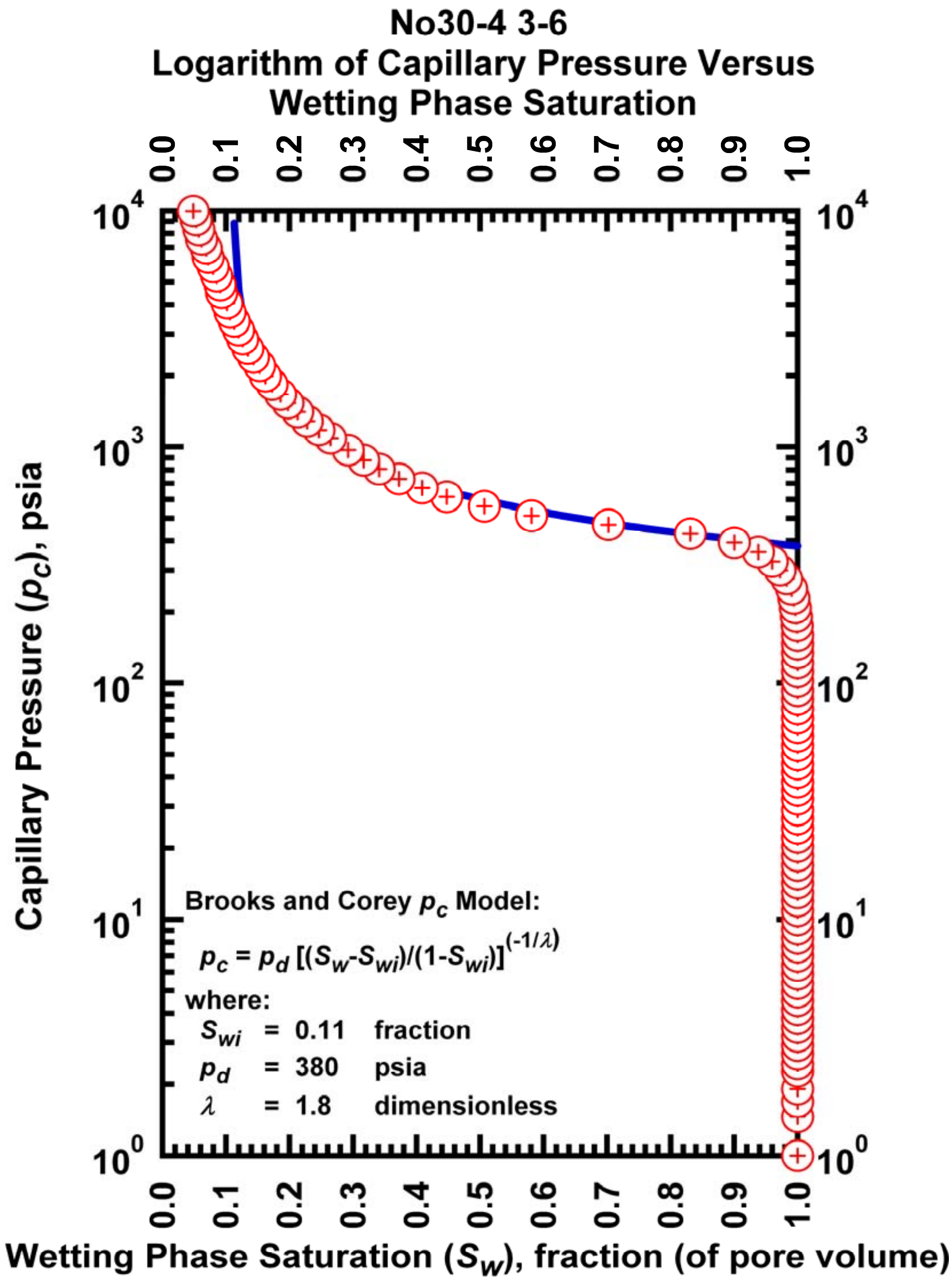

Figure J.44– Plot of logarithm of capillary pressure vs. wetting phase saturation — Case No30-4 3-6.

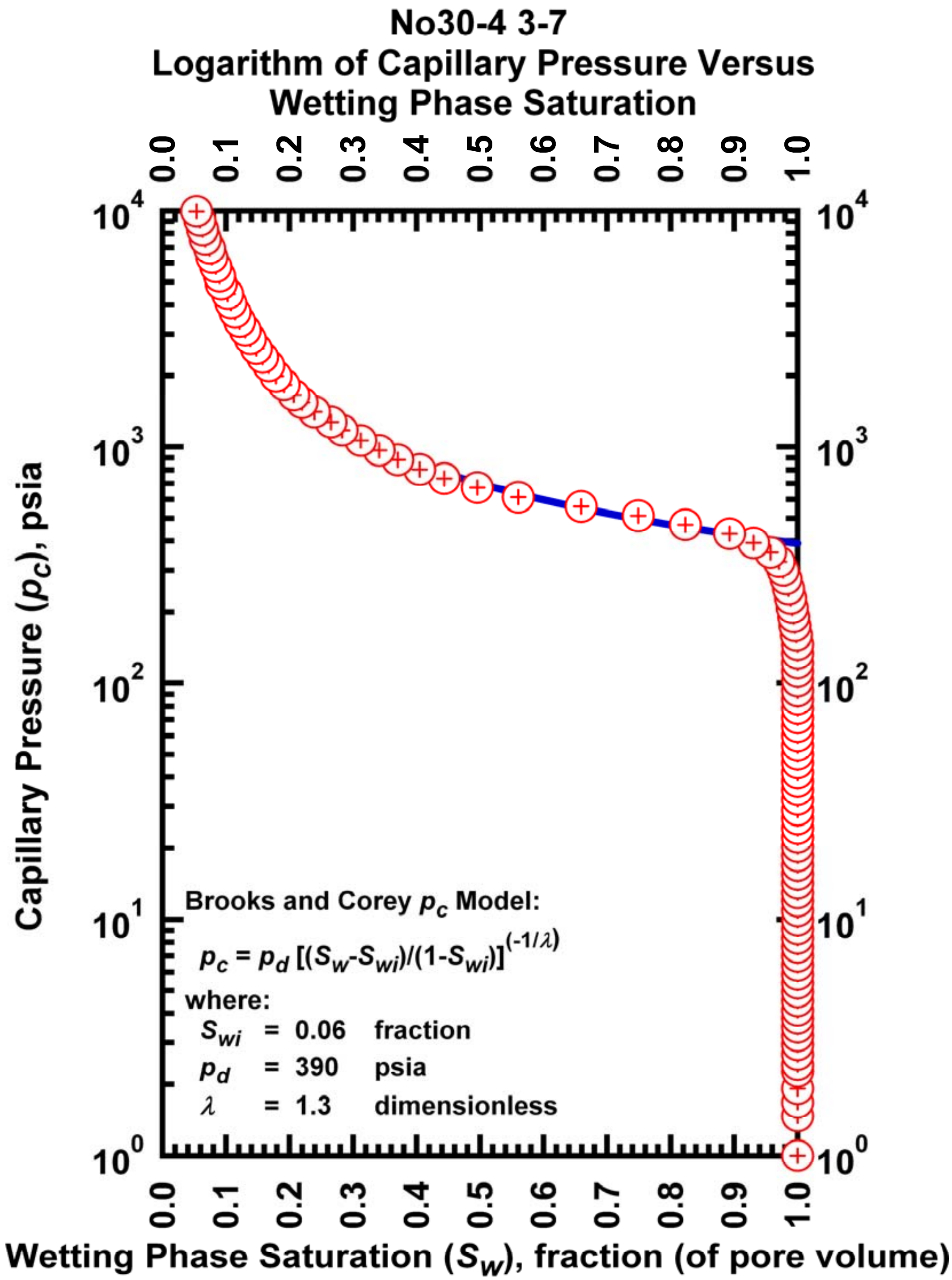

Figure J.45 – Plot of logarithm of capillary pressure vs. wetting phase saturation — Case No30-4 3-7.

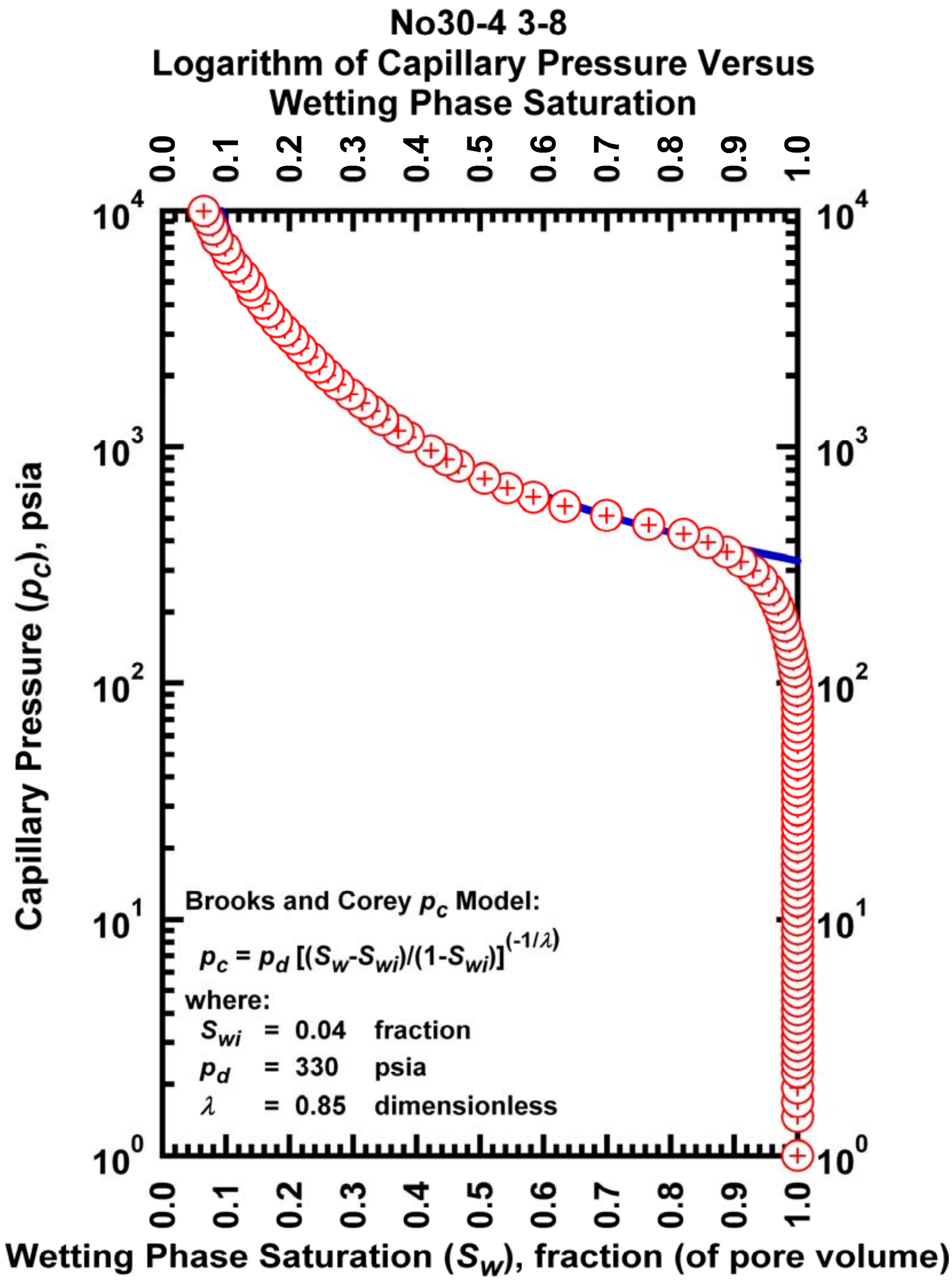

Figure J.46 – Plot of logarithm of capillary pressure vs. wetting phase saturation — Case No30-4 3-8.

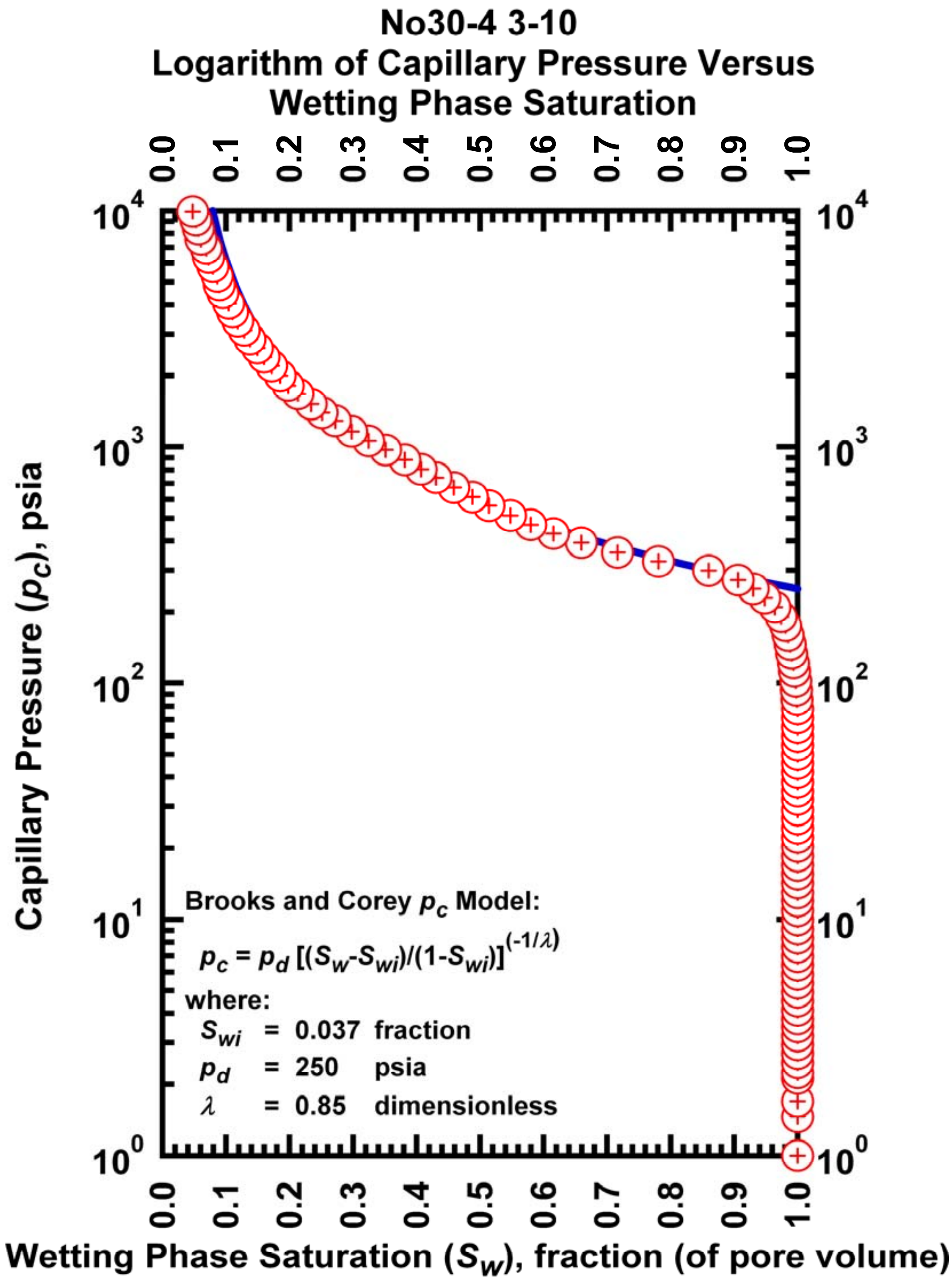

Figure J.47 – Plot of logarithm of capillary pressure vs. wetting phase saturation — Case No30-4 3-10.

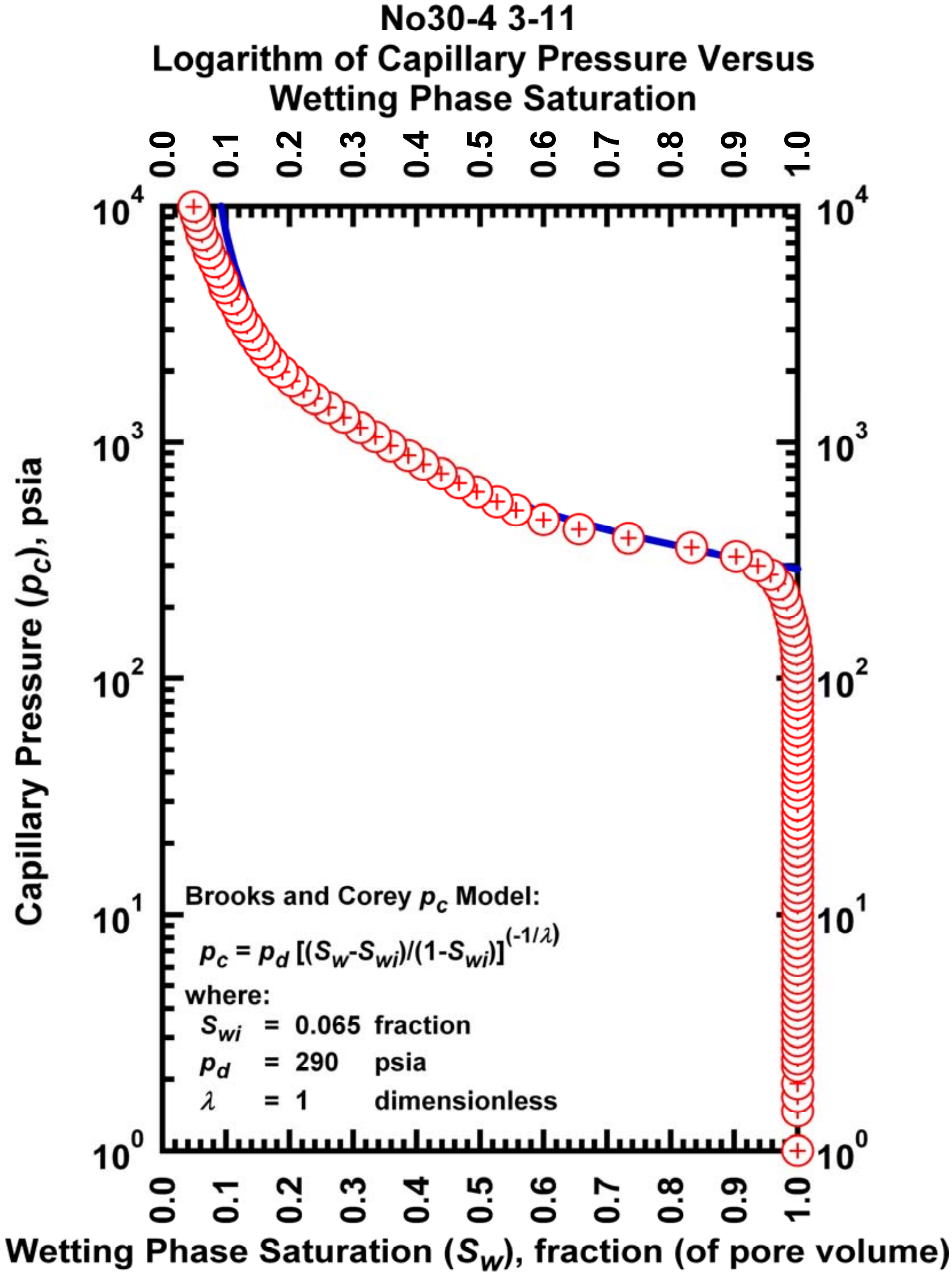

Figure J.48 – Plot of logarithm of capillary pressure vs. wetting phase saturation — Case No30-4 3-11.

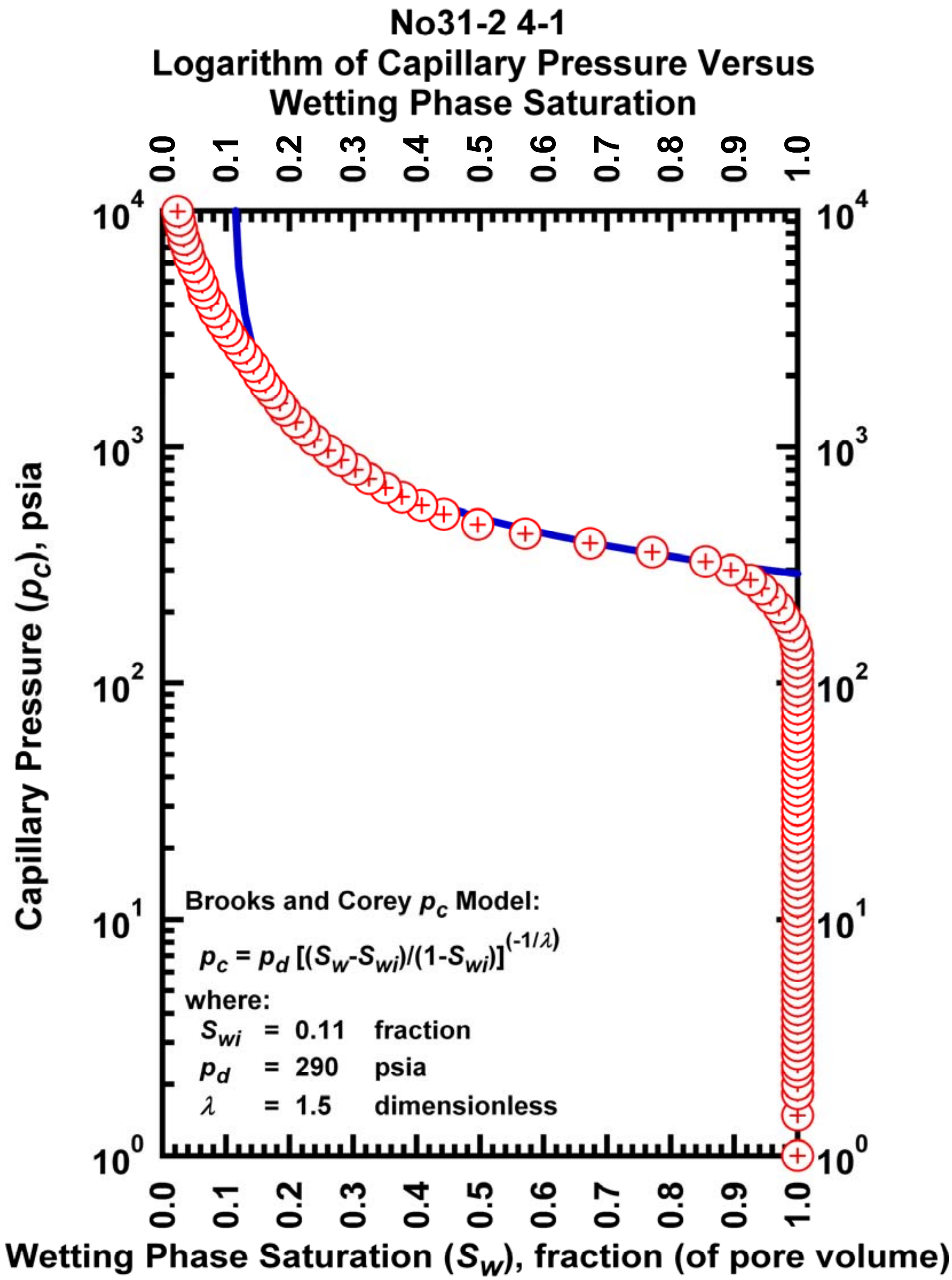

Figure J.49 – Plot of logarithm of capillary pressure vs. wetting phase saturation — Case No31-2 4-1.

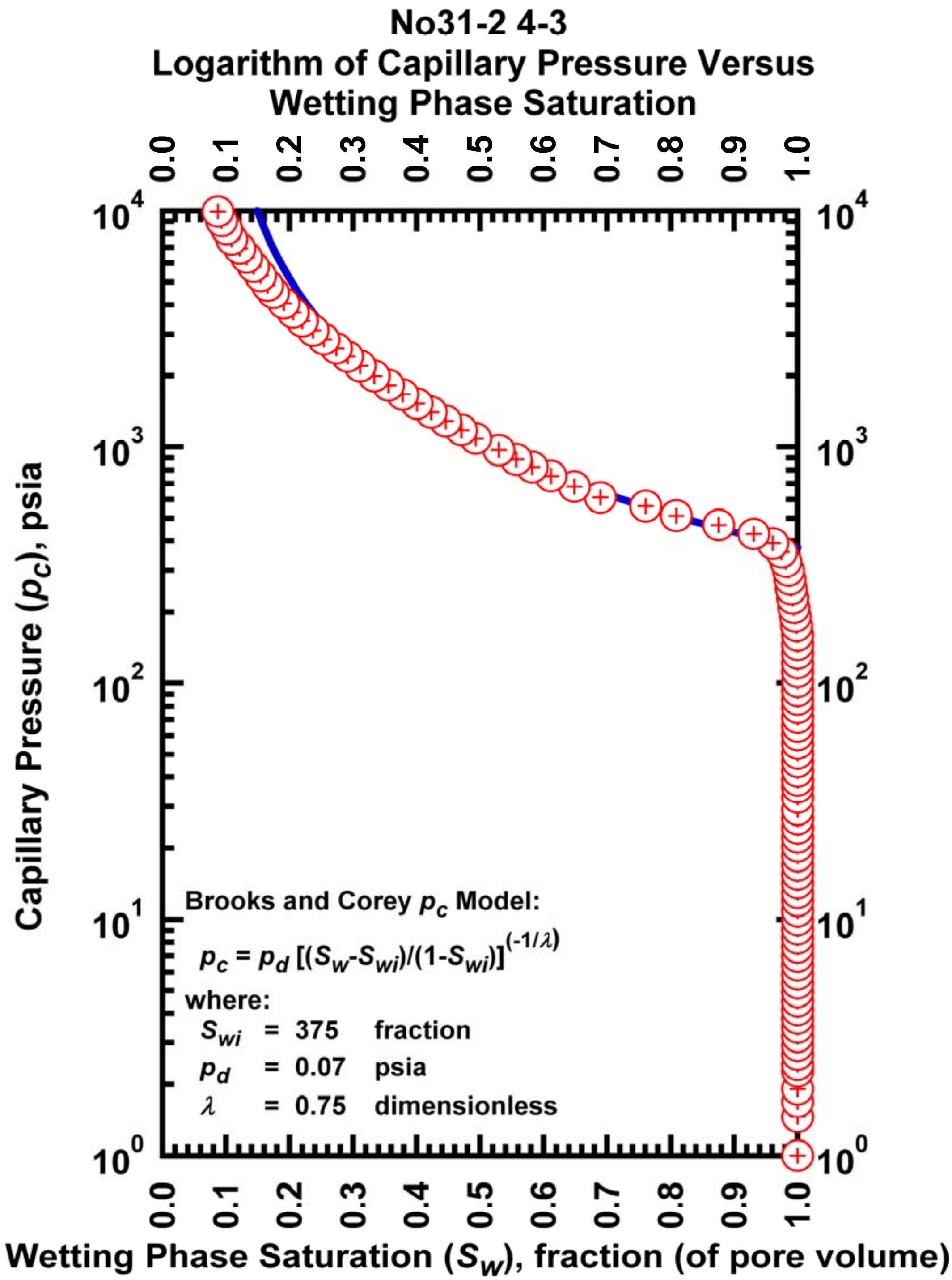

Figure J.50 – Plot of logarithm of capillary pressure vs. wetting phase saturation — Case No31-2 4-3.

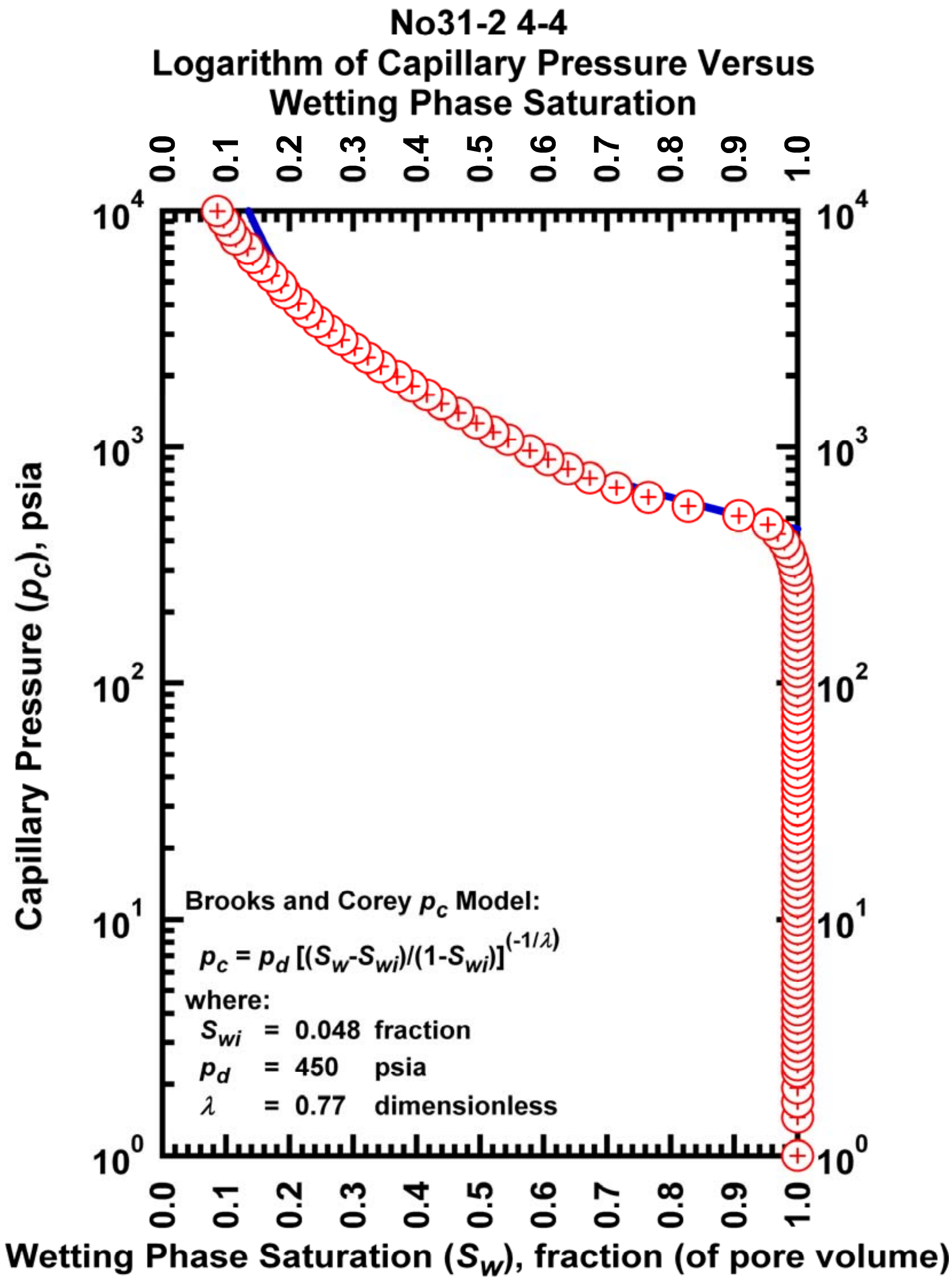

Figure J.51 – Plot of logarithm of capillary pressure vs. wetting phase saturation — Case No31-2 4-4.

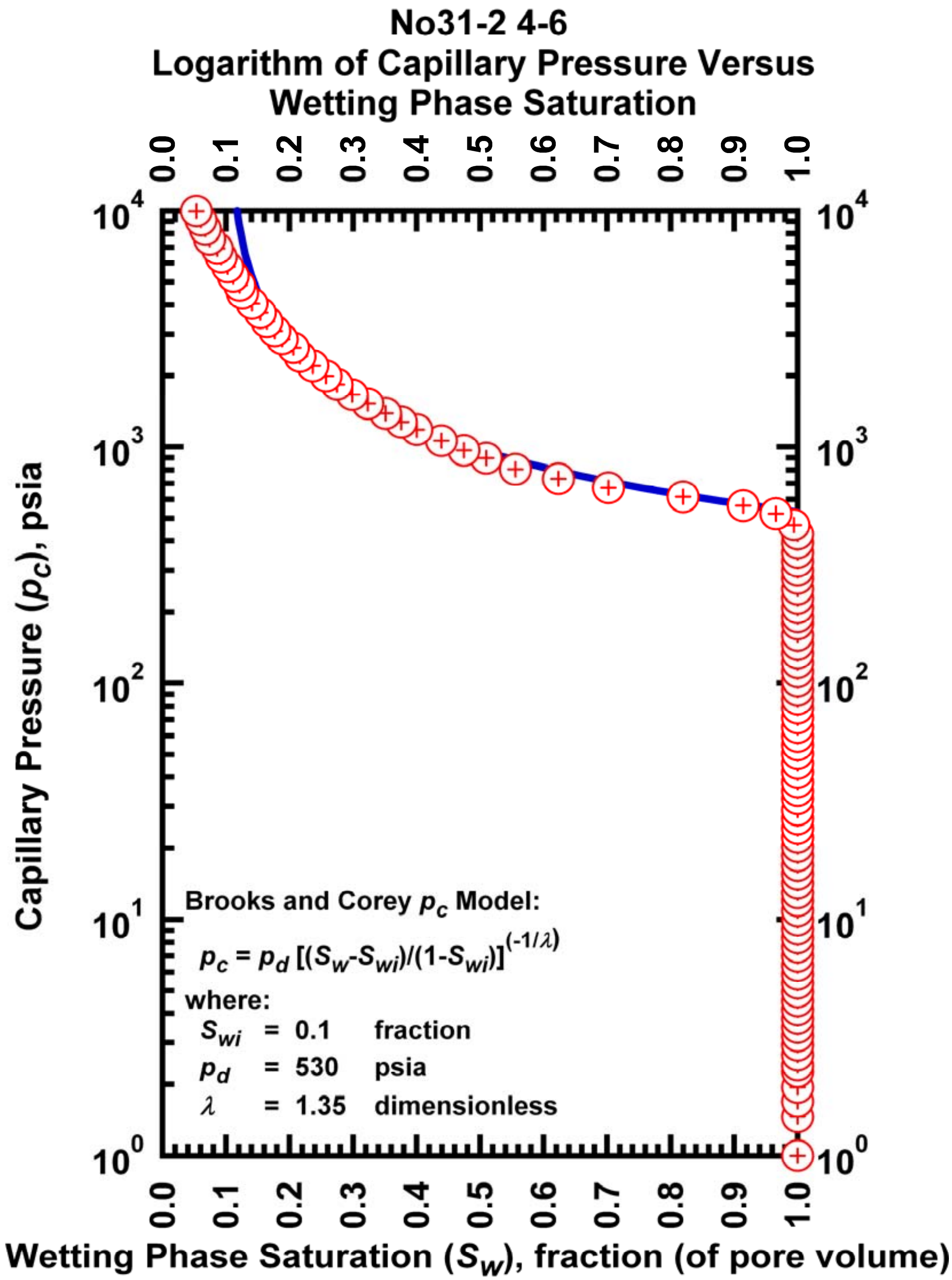

Figure J.52 – Plot of logarithm of capillary pressure vs. wetting phase saturation — Case No31-2 4-6.

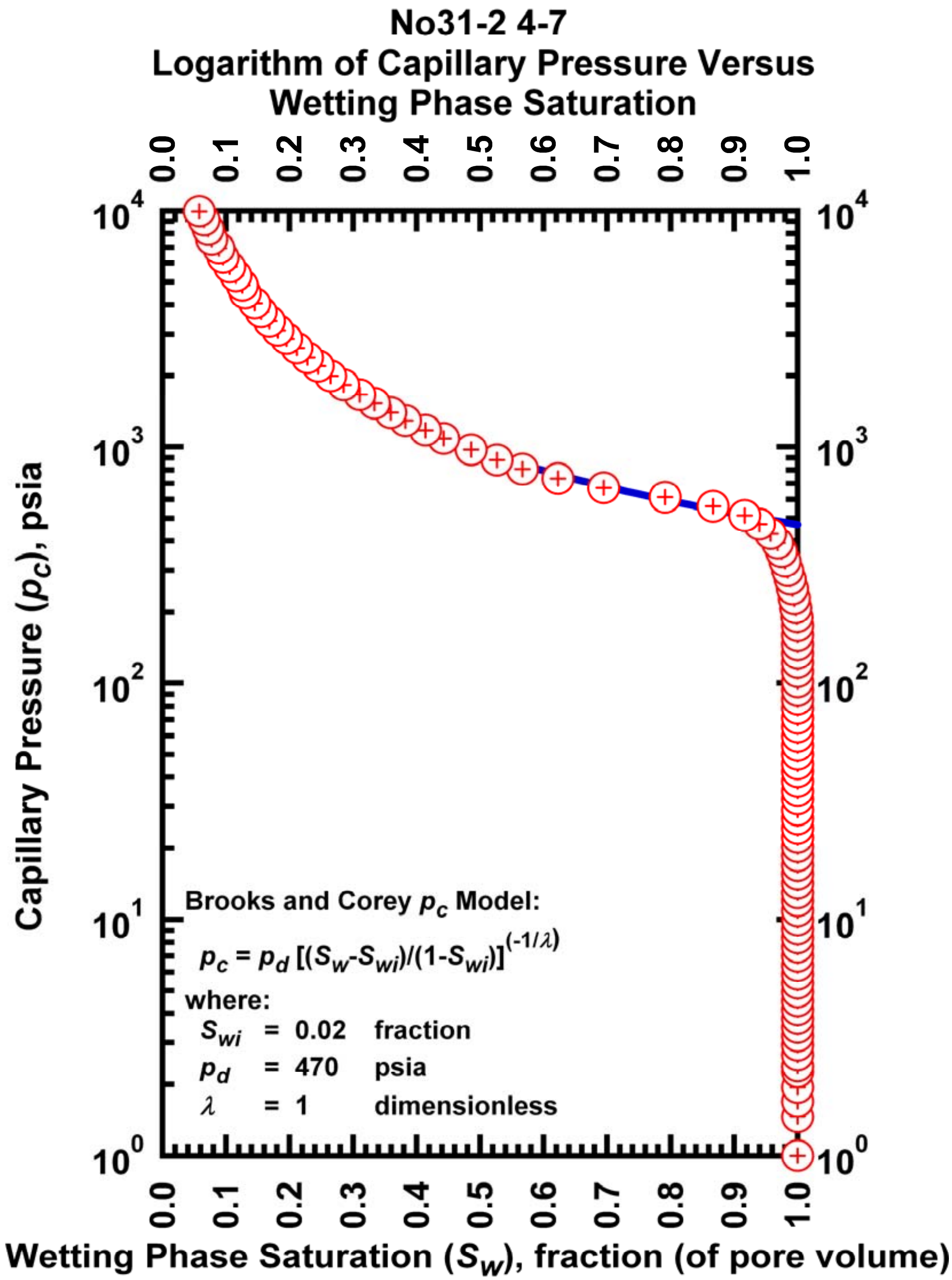

Figure J.53– Plot of logarithm of capillary pressure vs. wetting phase saturation — Case No31-2 4-7.

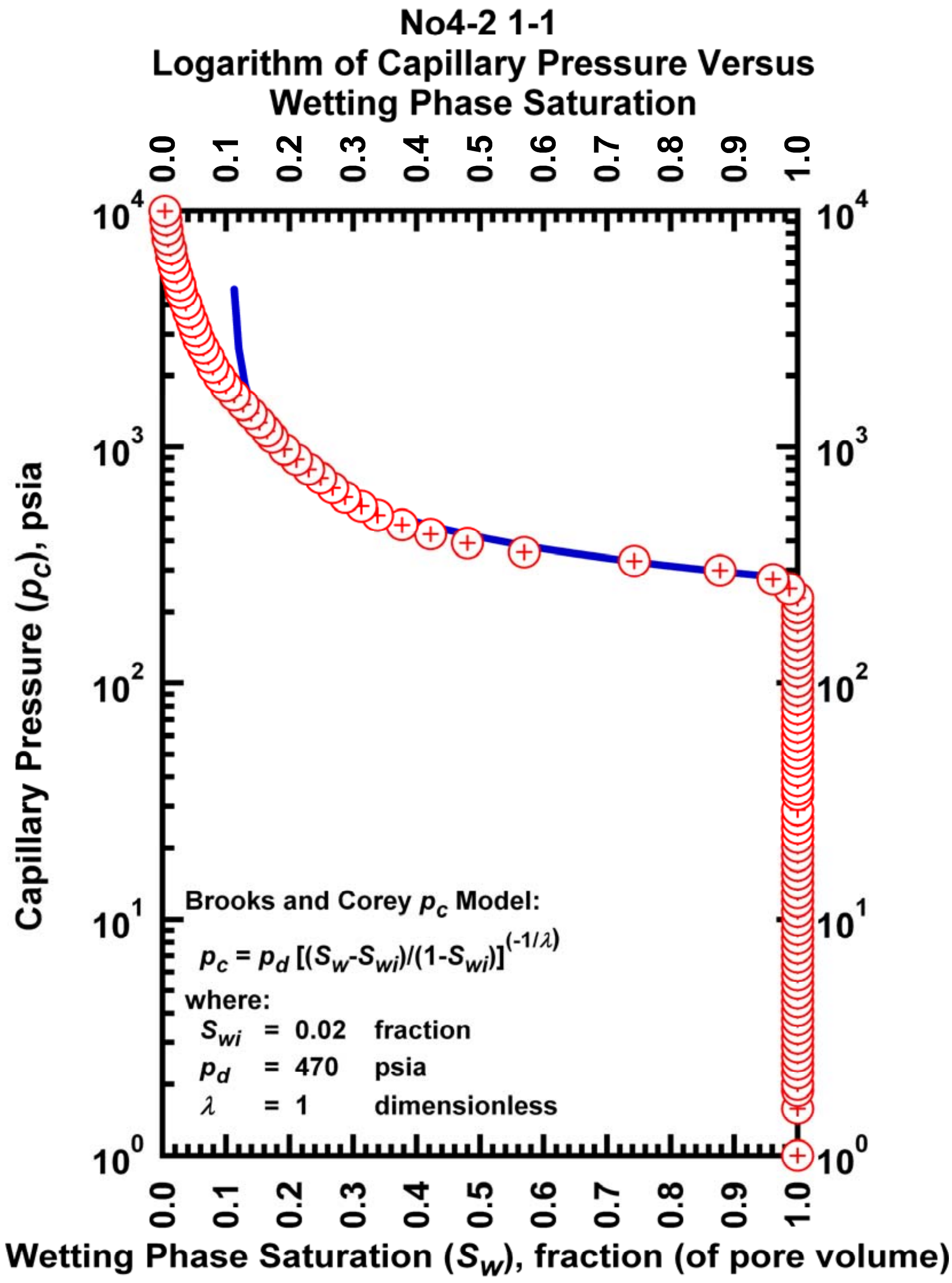

Figure J.54– Plot of logarithm of capillary pressure vs. wetting phase saturation — Case No4-2 1-1.

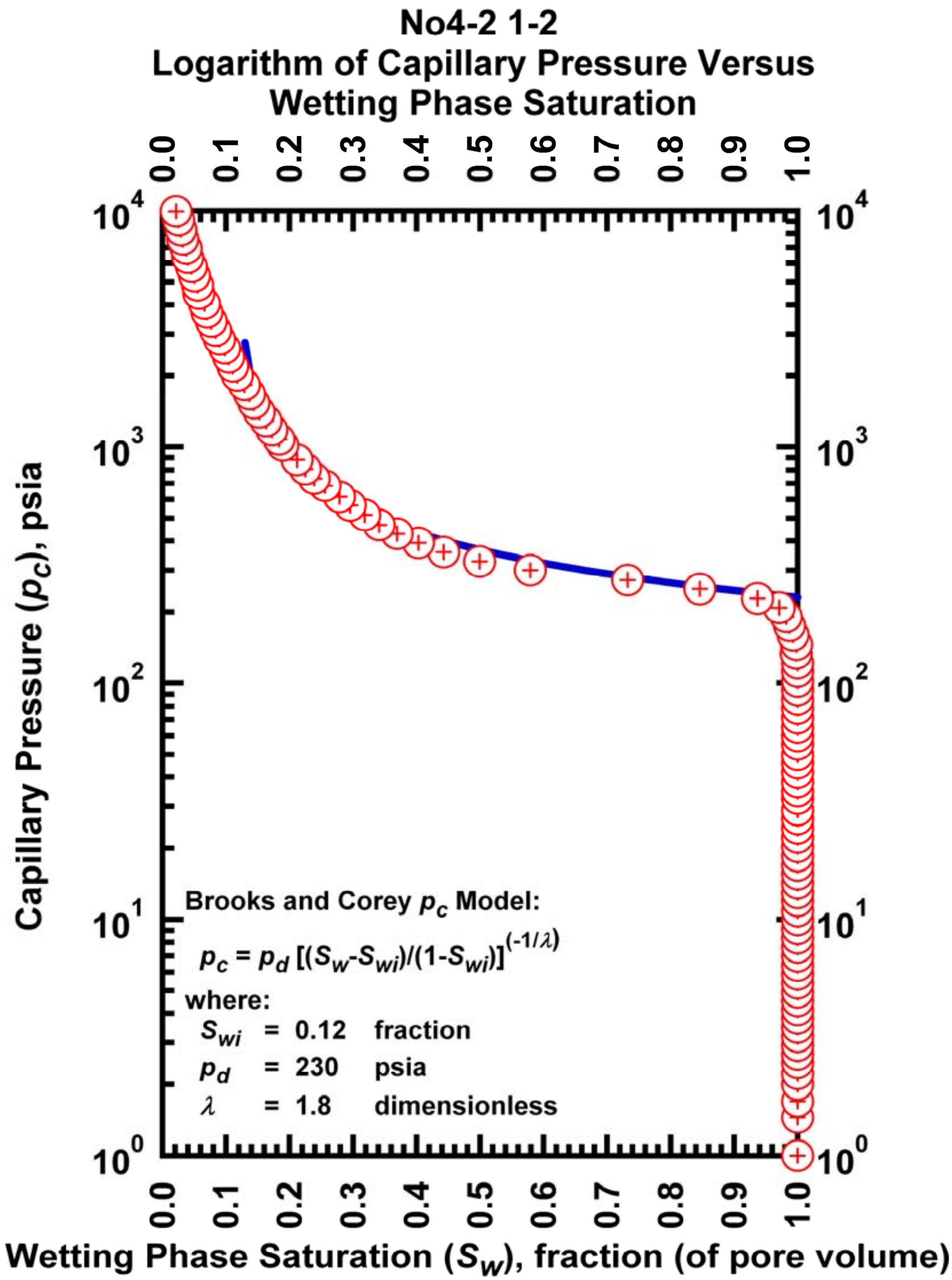

Figure J.55 – Plot of logarithm of capillary pressure vs. wetting phase saturation — Case No4-2 1-2.

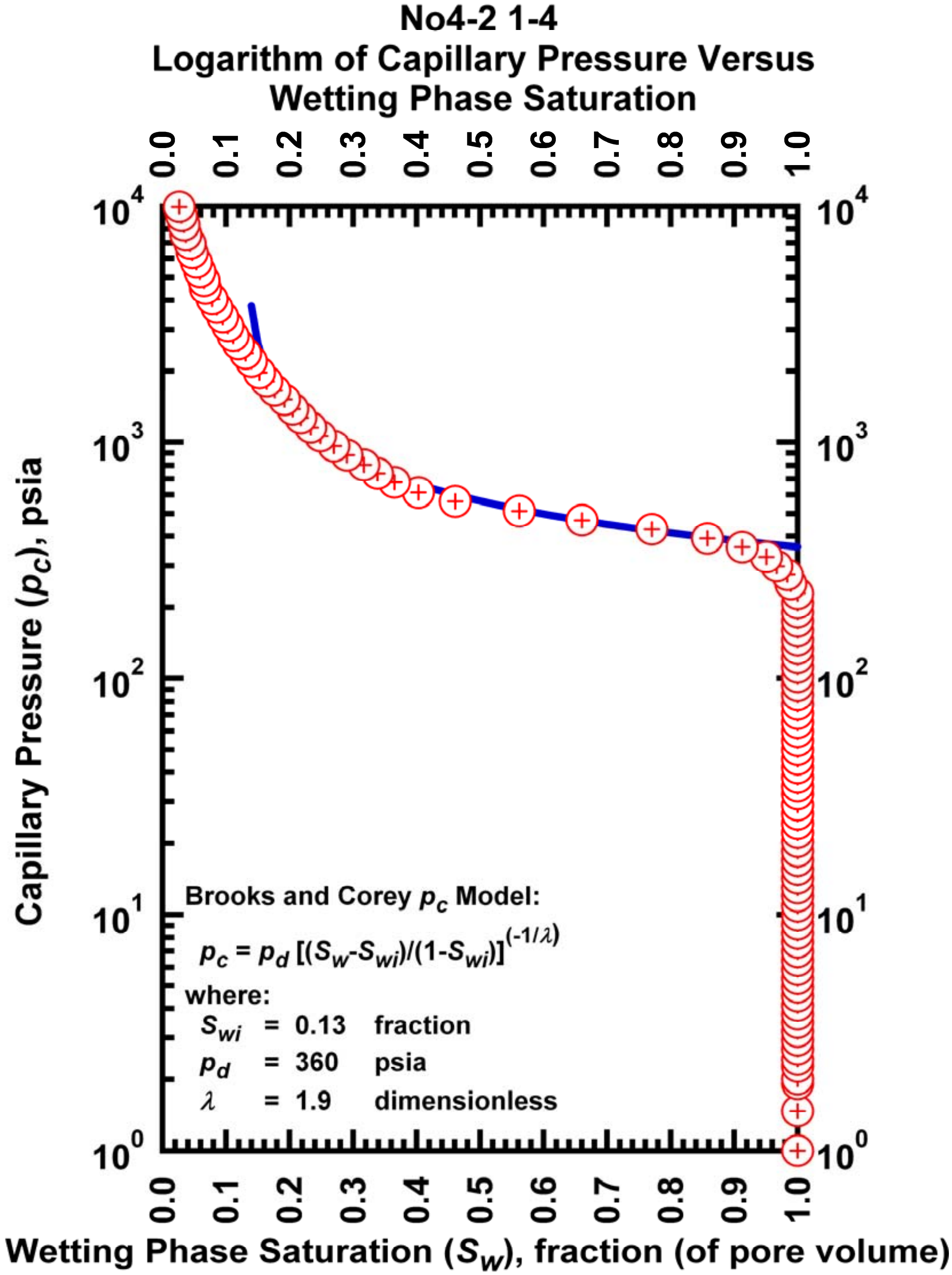

Figure J.56 – Plot of logarithm of capillary pressure vs. wetting phase saturation — Case No4-2 1-4.

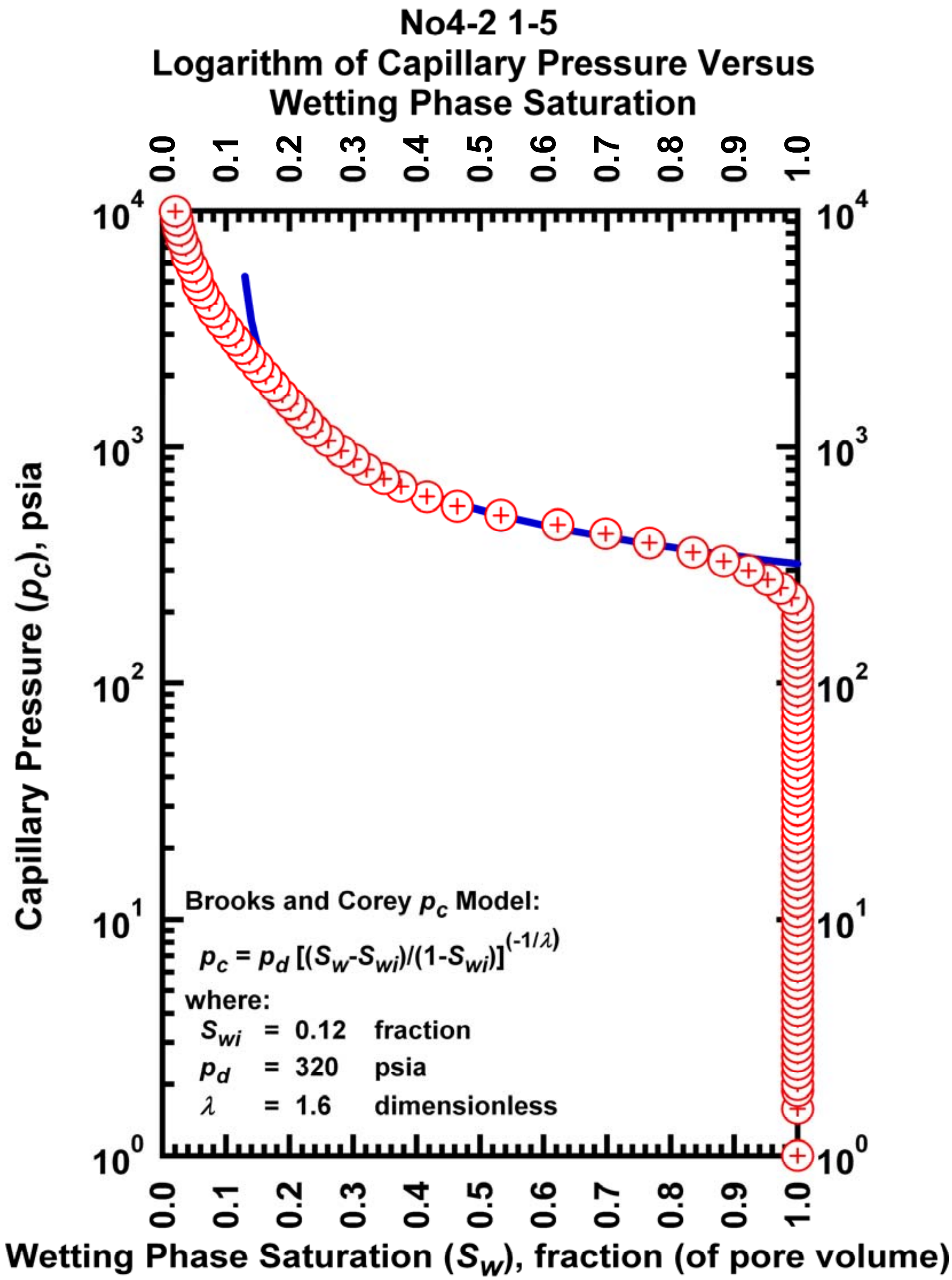

Figure J.57 – Plot of logarithm of capillary pressure vs. wetting phase saturation — Case No31-2 4-5.

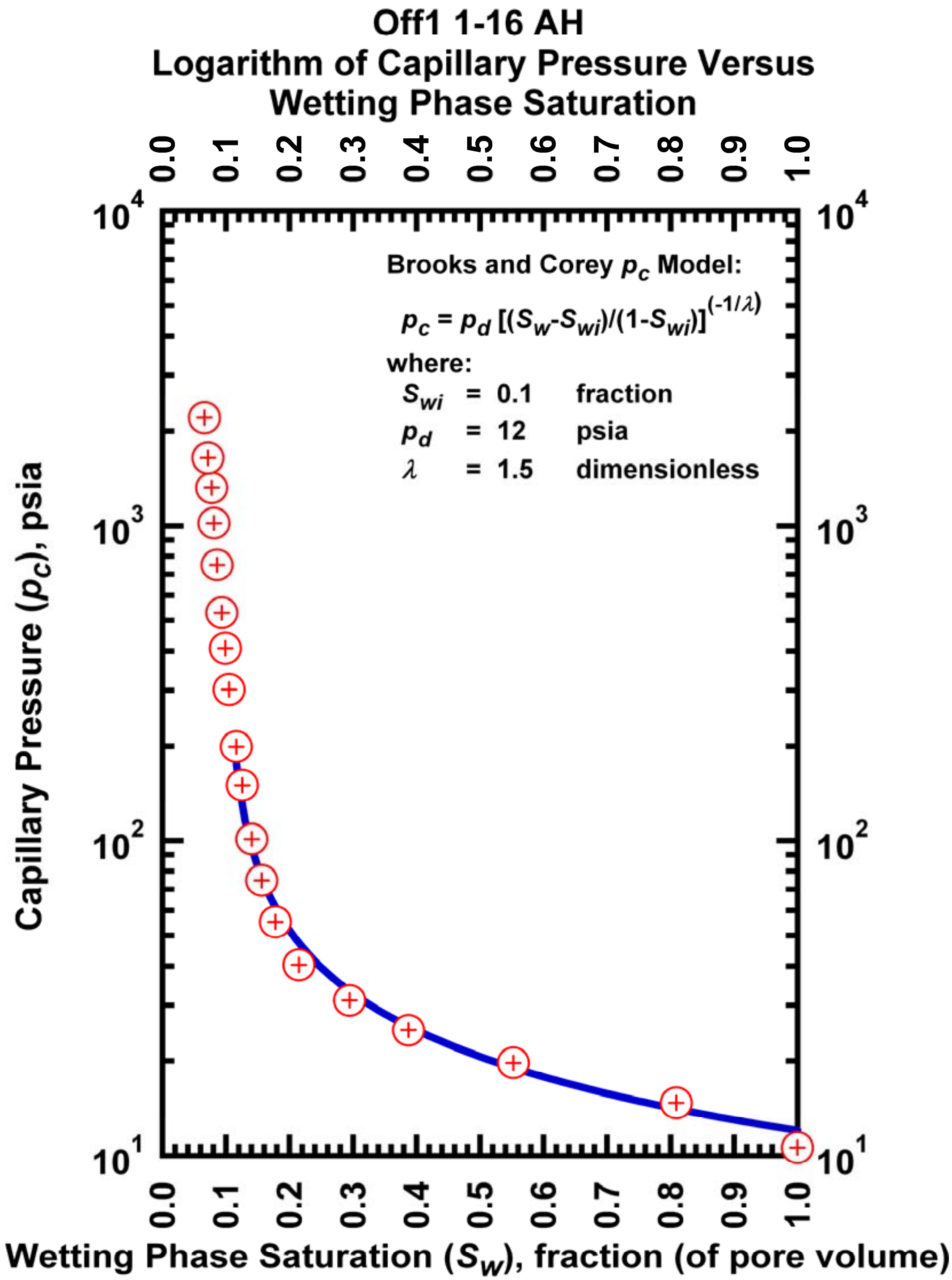

Figure J.58 – Plot of logarithm of capillary pressure vs. wetting phase saturation — Case Off1 1-16 AH.

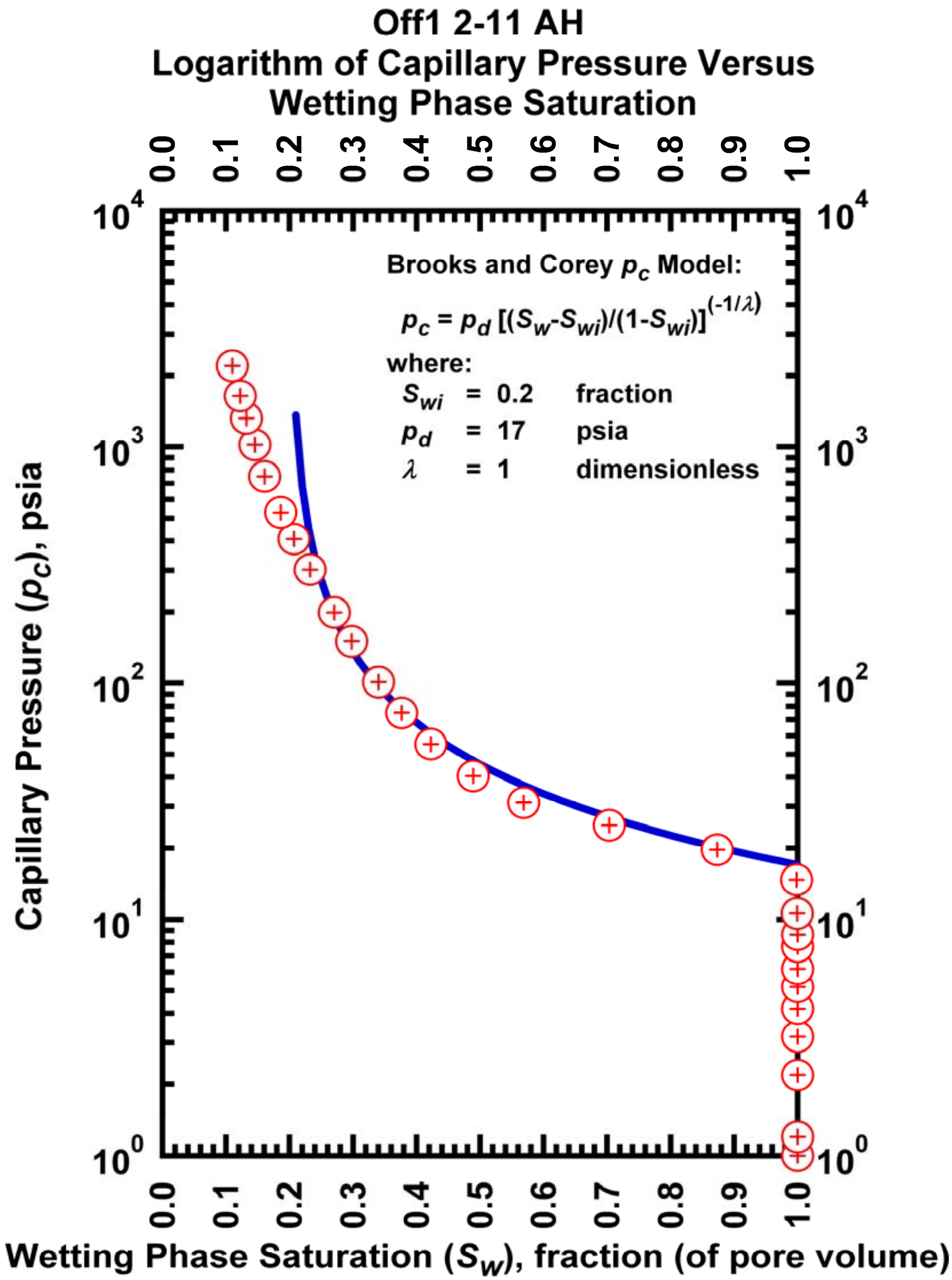

Figure J.59 – Plot of logarithm of capillary pressure vs. wetting phase saturation — Case Off1 2-11 AH.

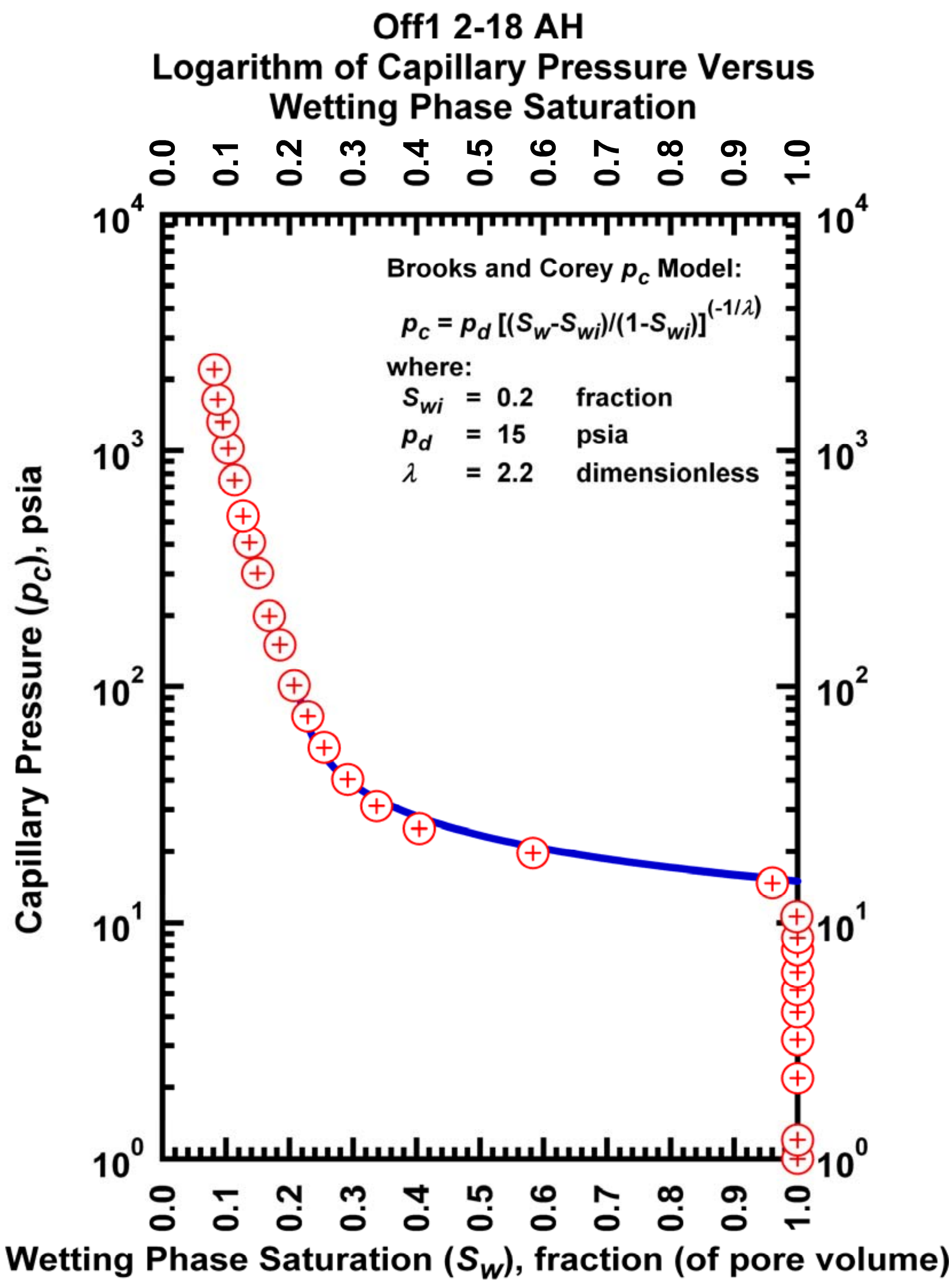

Figure J.60 – Plot of logarithm of capillary pressure vs. wetting phase saturation — Case Off1 2-18 AH.

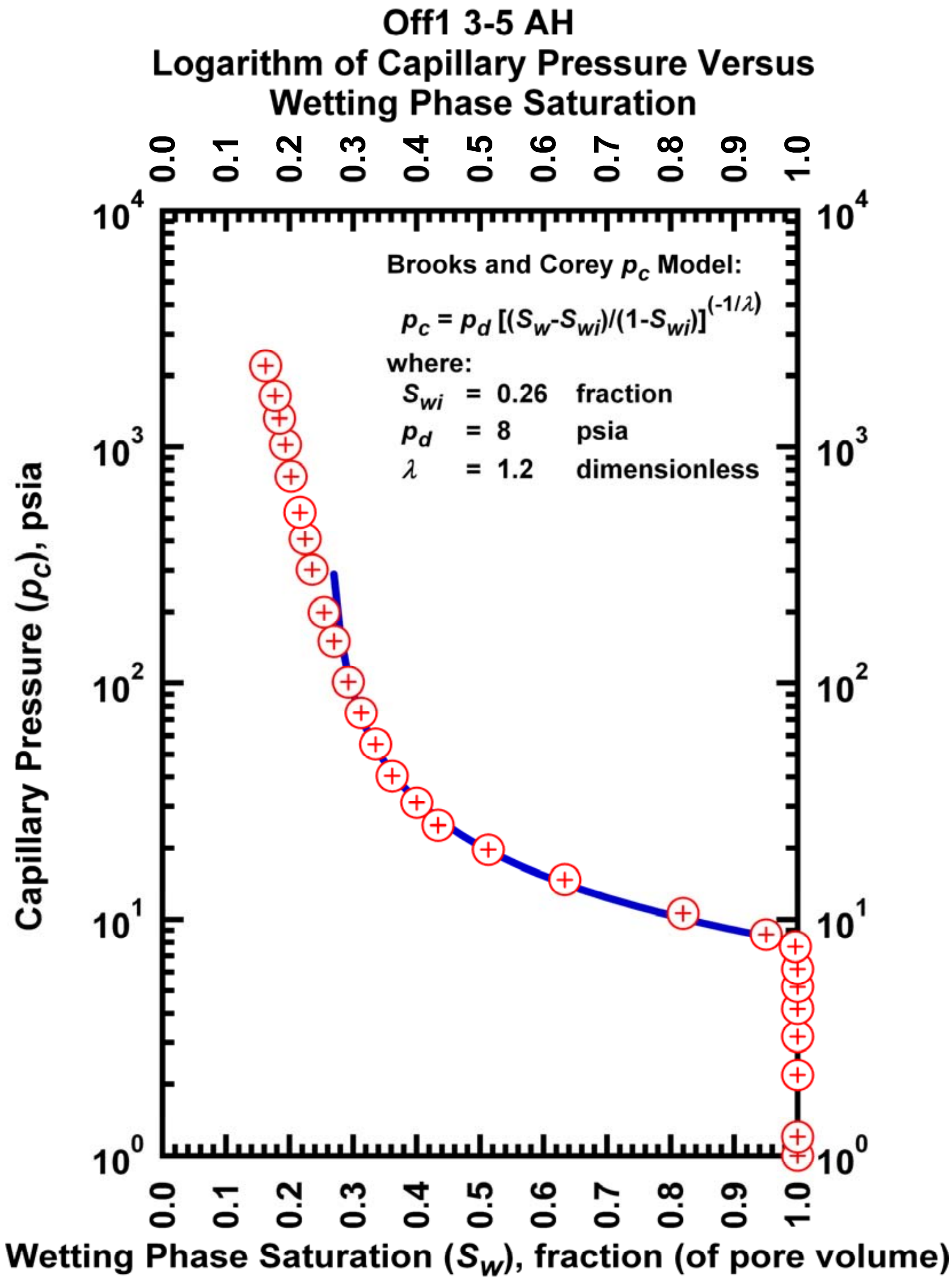

Figure J.61 – Plot of logarithm of capillary pressure vs. wetting phase saturation — Case Off1 3-5 AH.

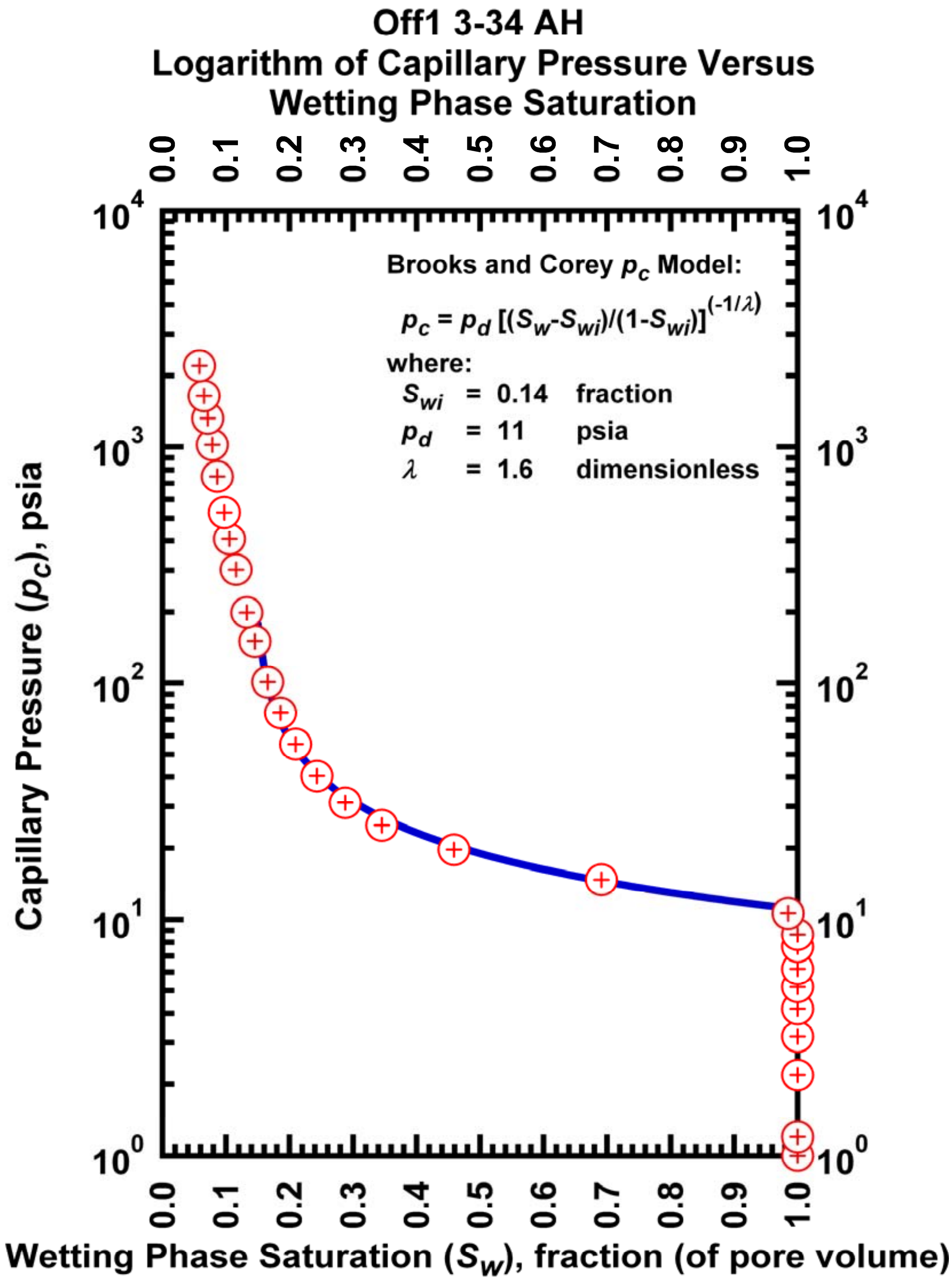

Figure J.62 – Plot of logarithm of capillary pressure vs. wetting phase saturation — Case Off1 3-34 AH.

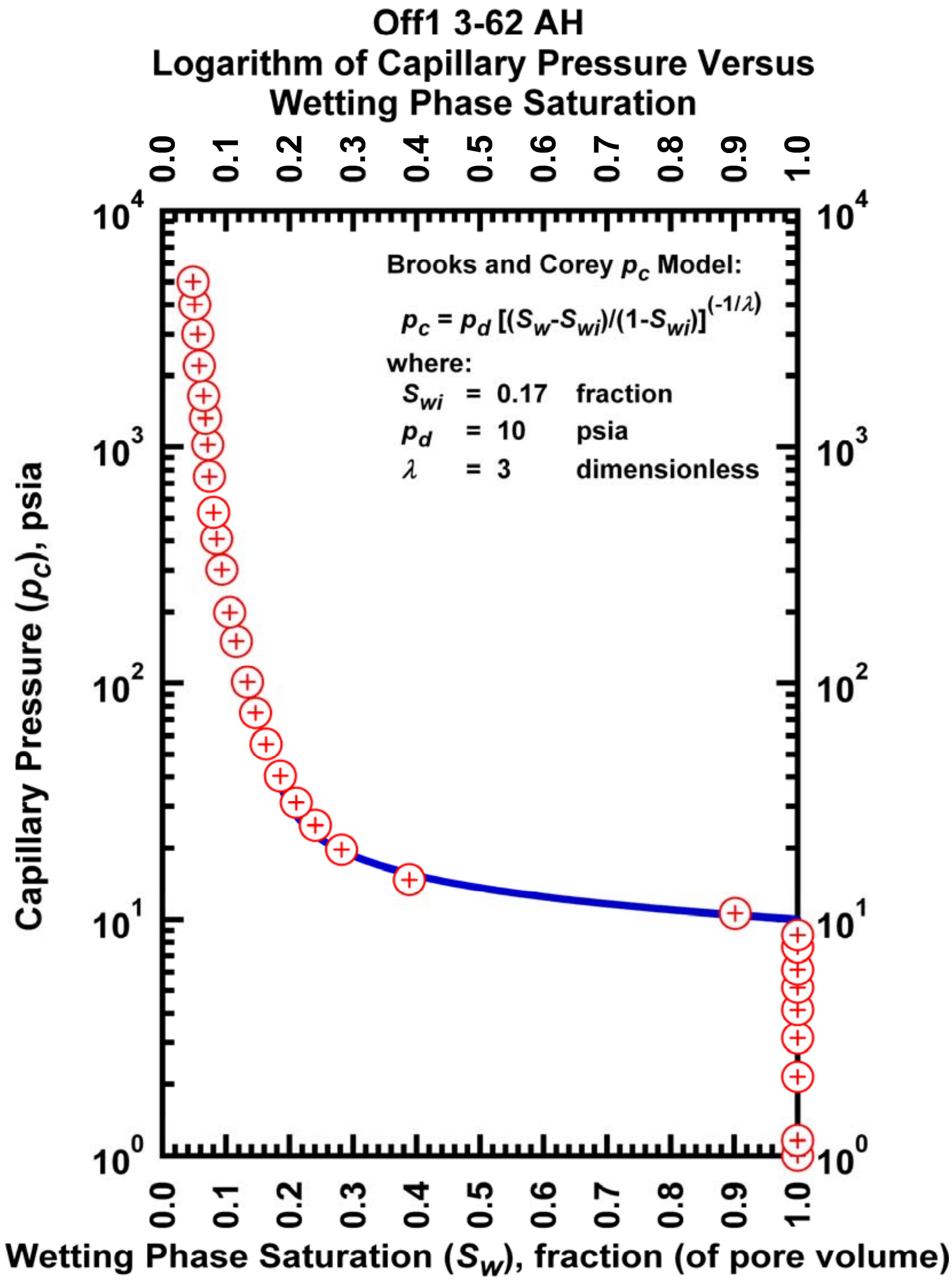

Figure J.63 – Plot of logarithm of capillary pressure vs. wetting phase saturation — Case Off1 3-62 AH.

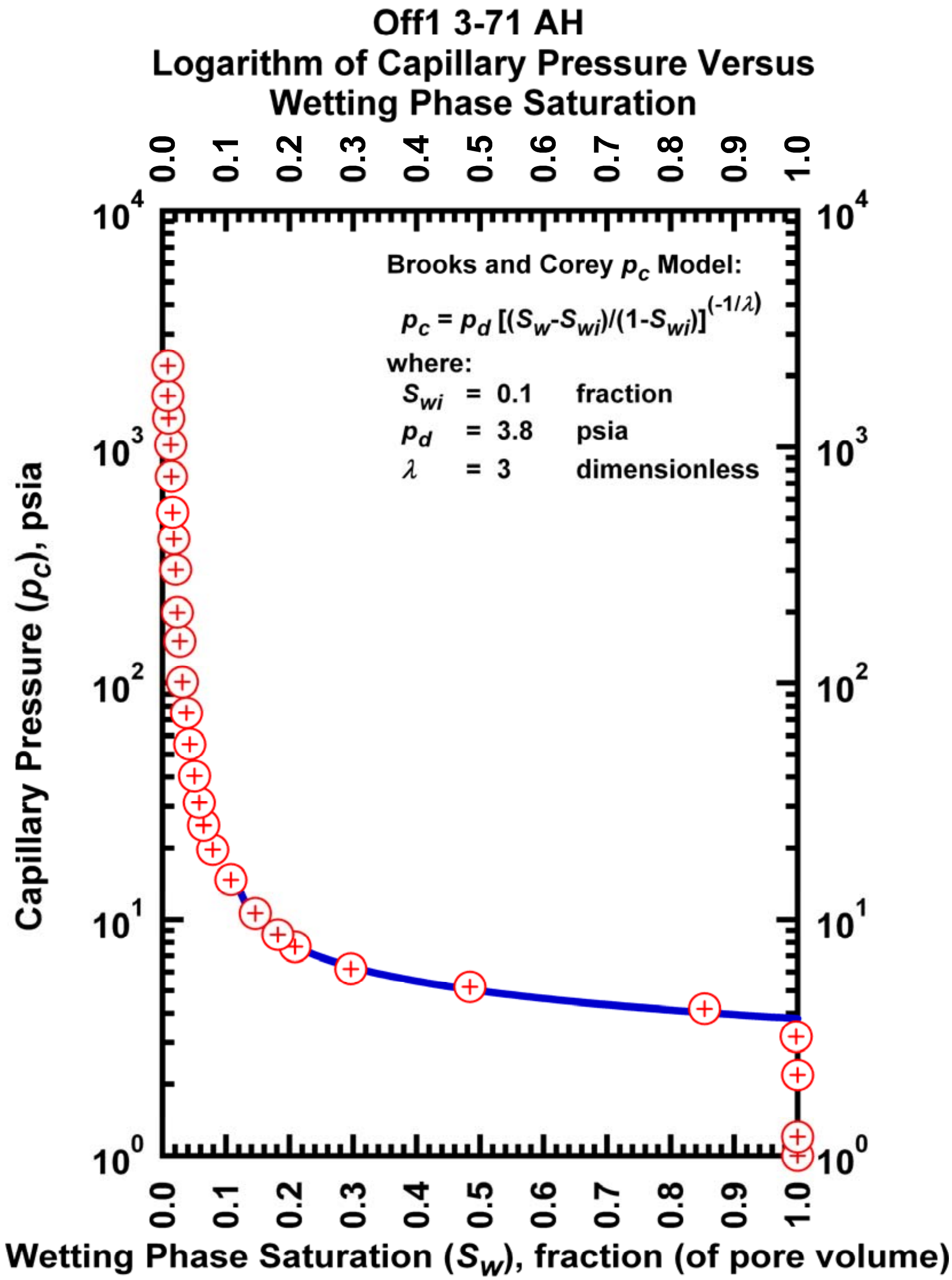

Figure J.64– Plot of logarithm of capillary pressure vs. wetting phase saturation — Case Off1 3-71 AH.

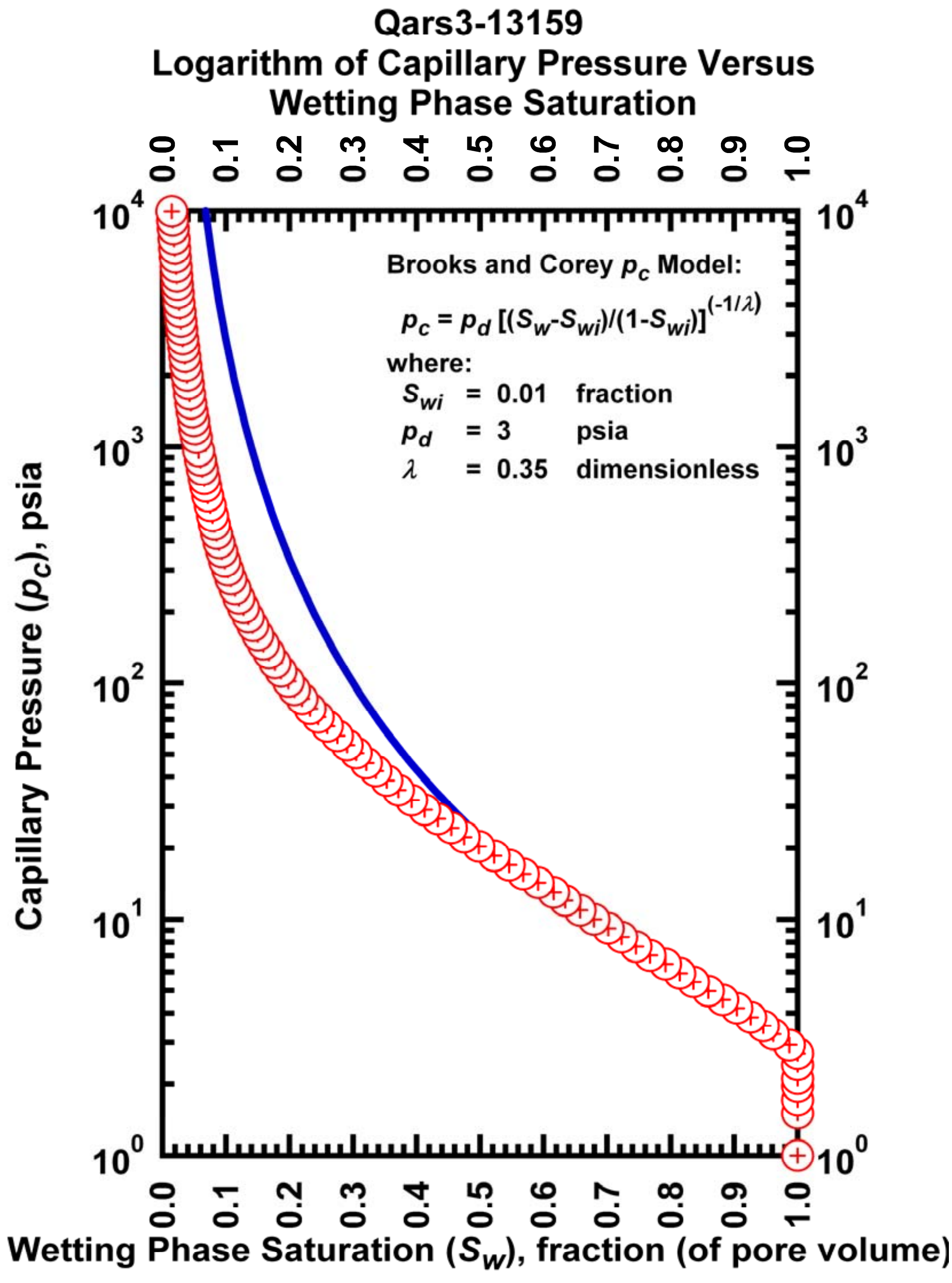

Figure J.65 – Plot of logarithm of capillary pressure vs. wetting phase saturation — Case Qars3-13159.

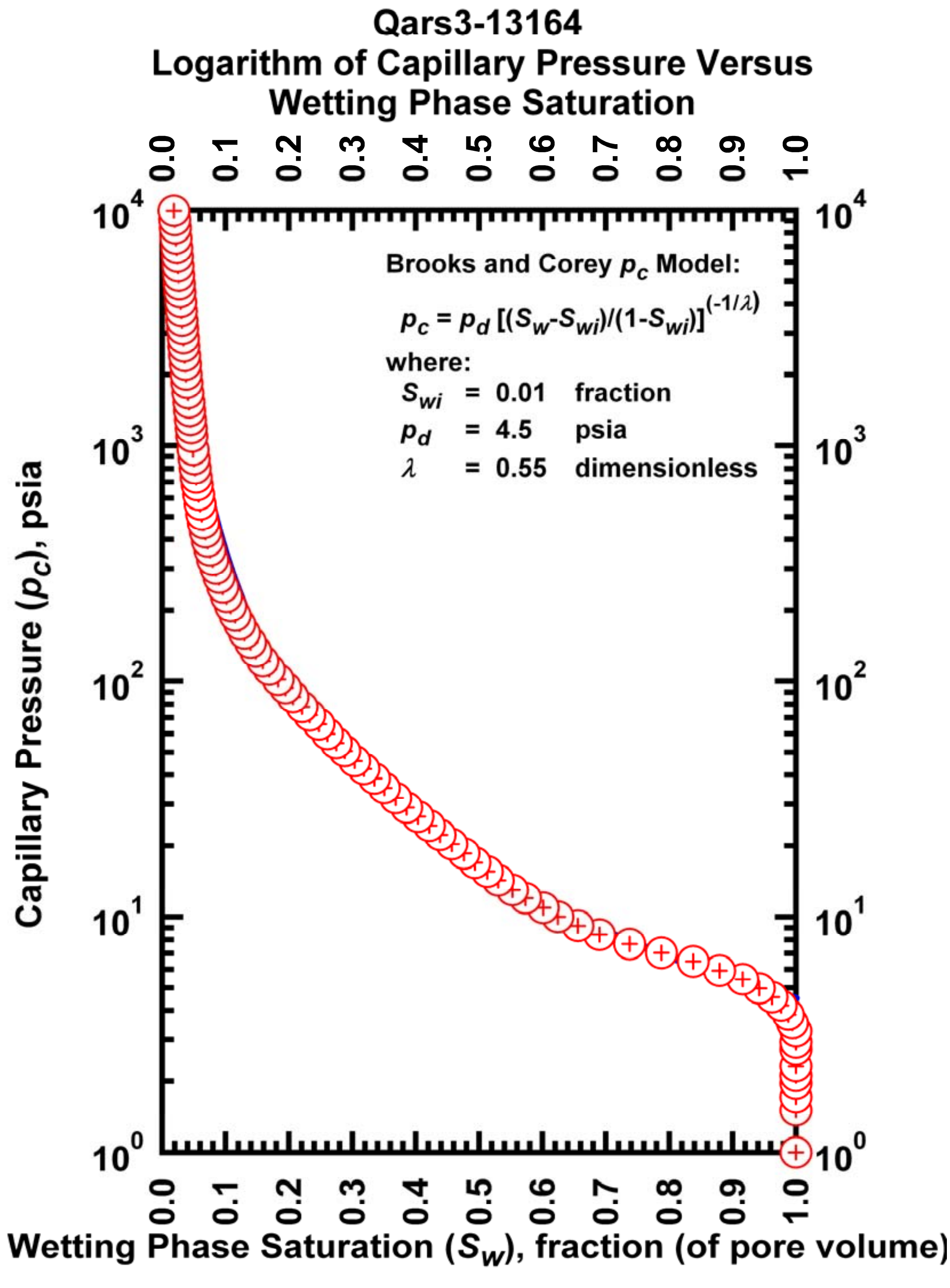

Figure J.66 – Plot of logarithm of capillary pressure vs. wetting phase saturation — Case Qars3-13164.

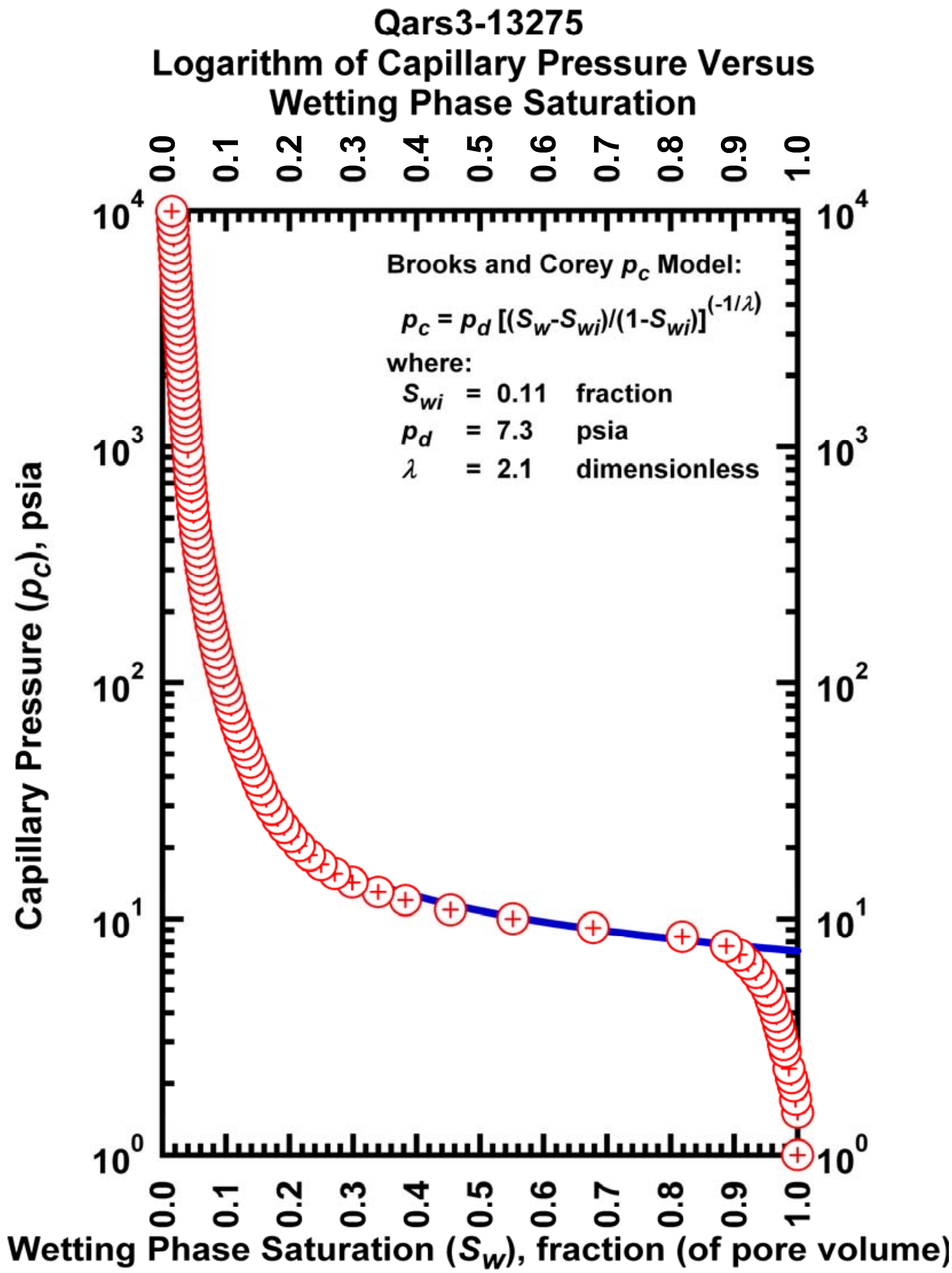

Figure J.67 – Plot of logarithm of capillary pressure vs. wetting phase saturation — Case Qars3-13175.

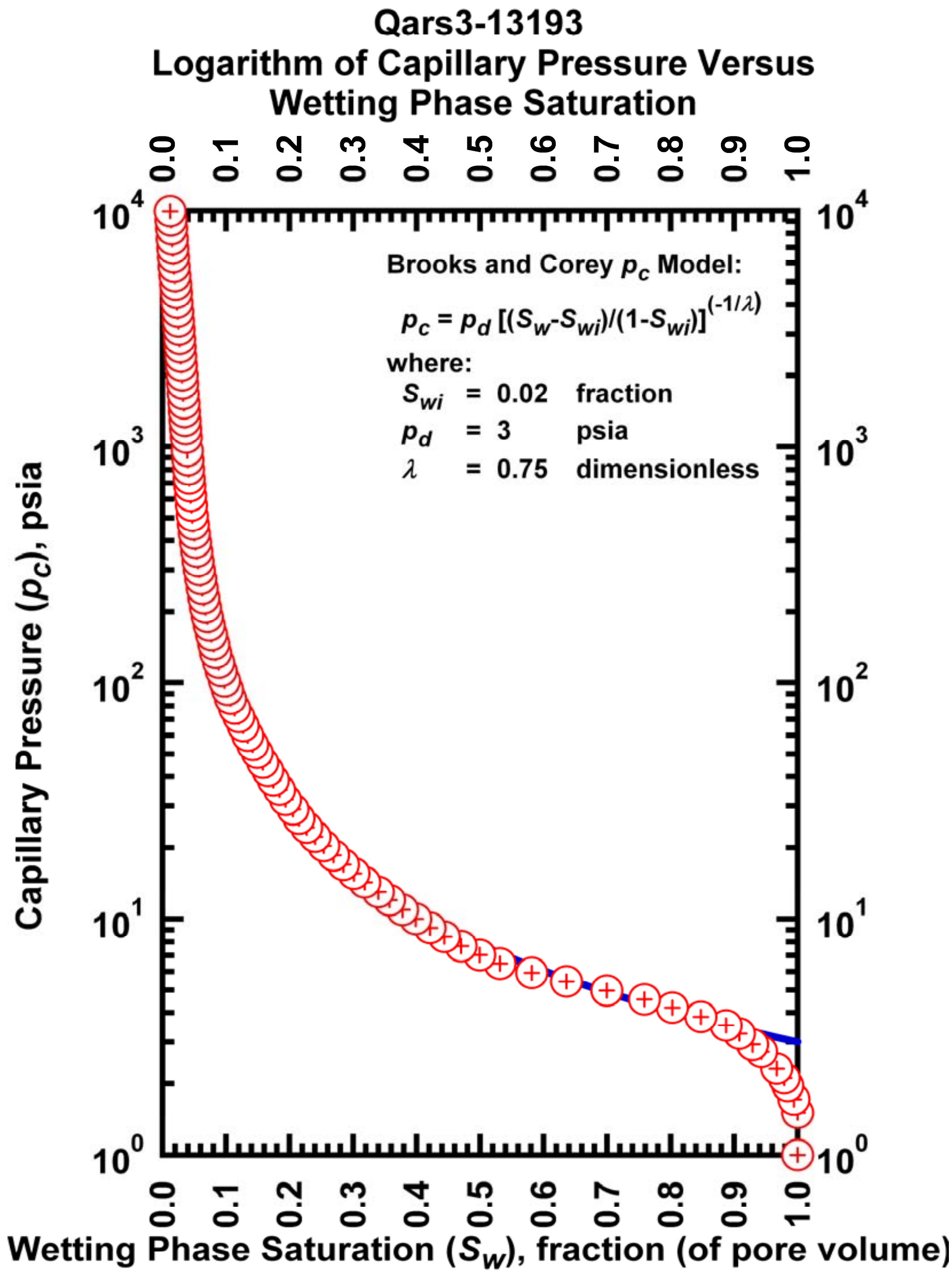

Figure J.68 – Plot of logarithm of capillary pressure vs. wetting phase saturation — Case Qars3-13193.

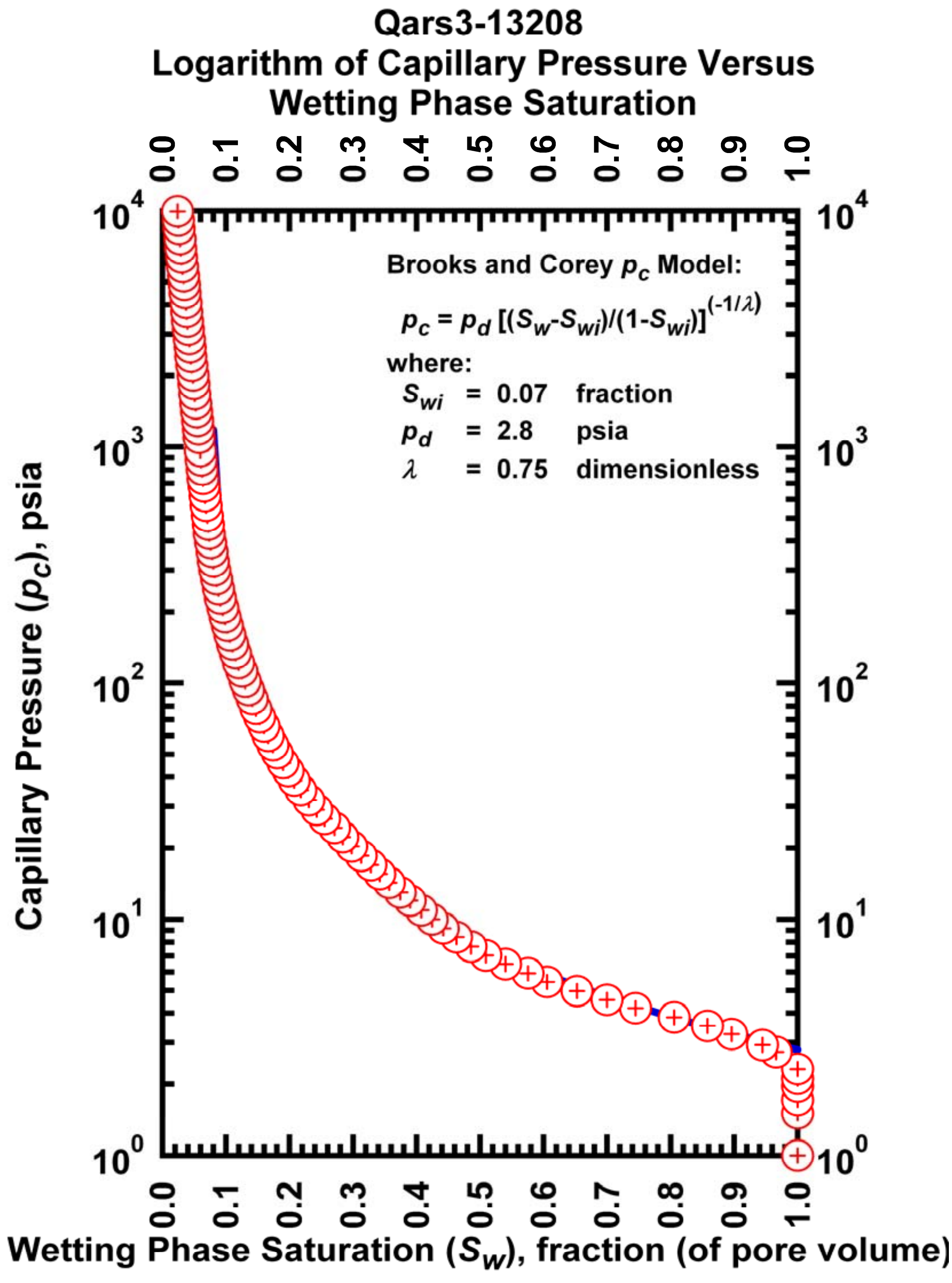

Figure J.69 – Plot of logarithm of capillary pressure vs. wetting phase saturation — Case Qars3-13208.

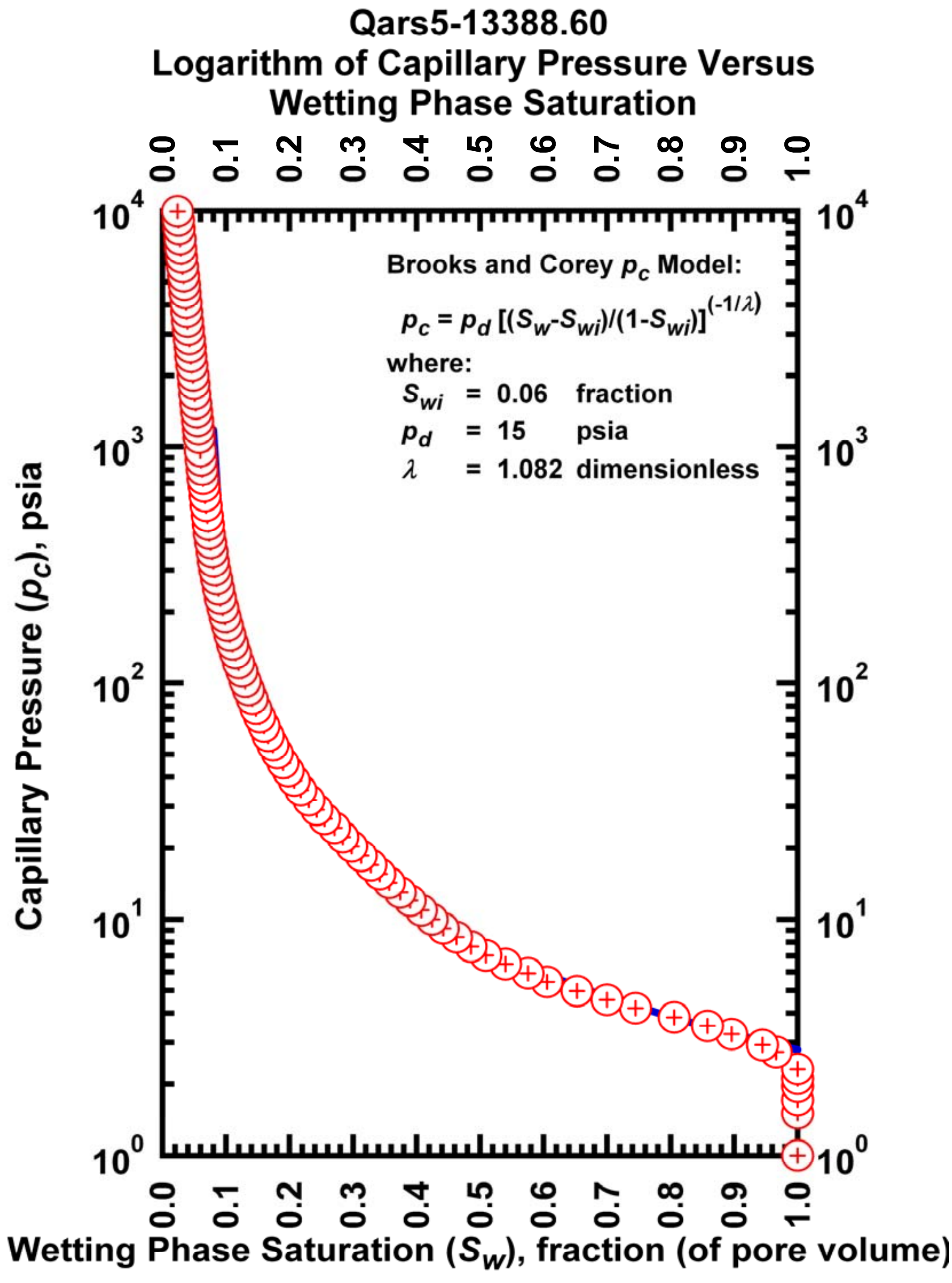

Figure J.70 – Plot of logarithm of capillary pressure vs. wetting phase saturation — Case Qars5-13288.

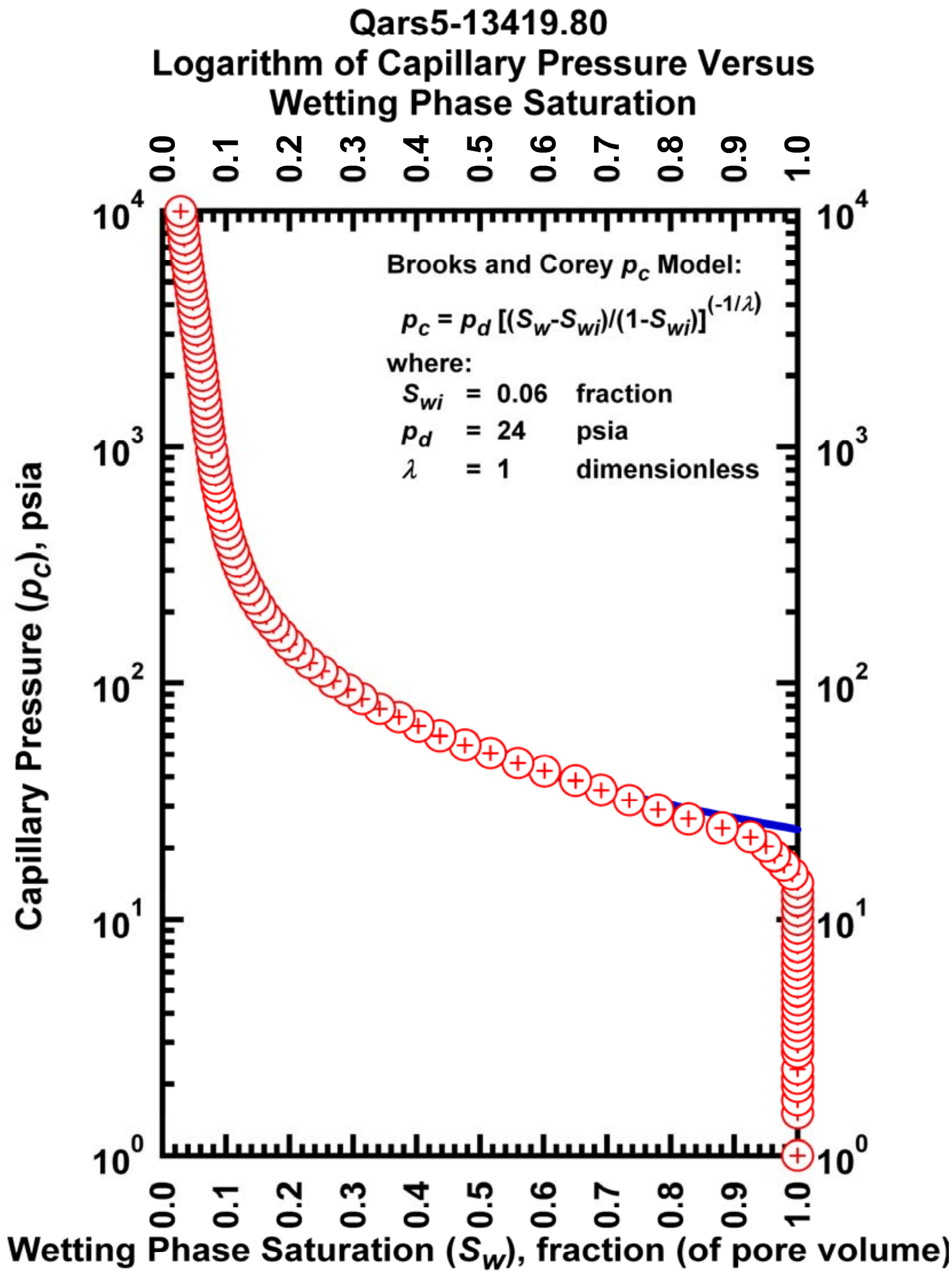

Figure J.71 – Plot of logarithm of capillary pressure vs. wetting phase saturation — Case Qars5-13419.8.

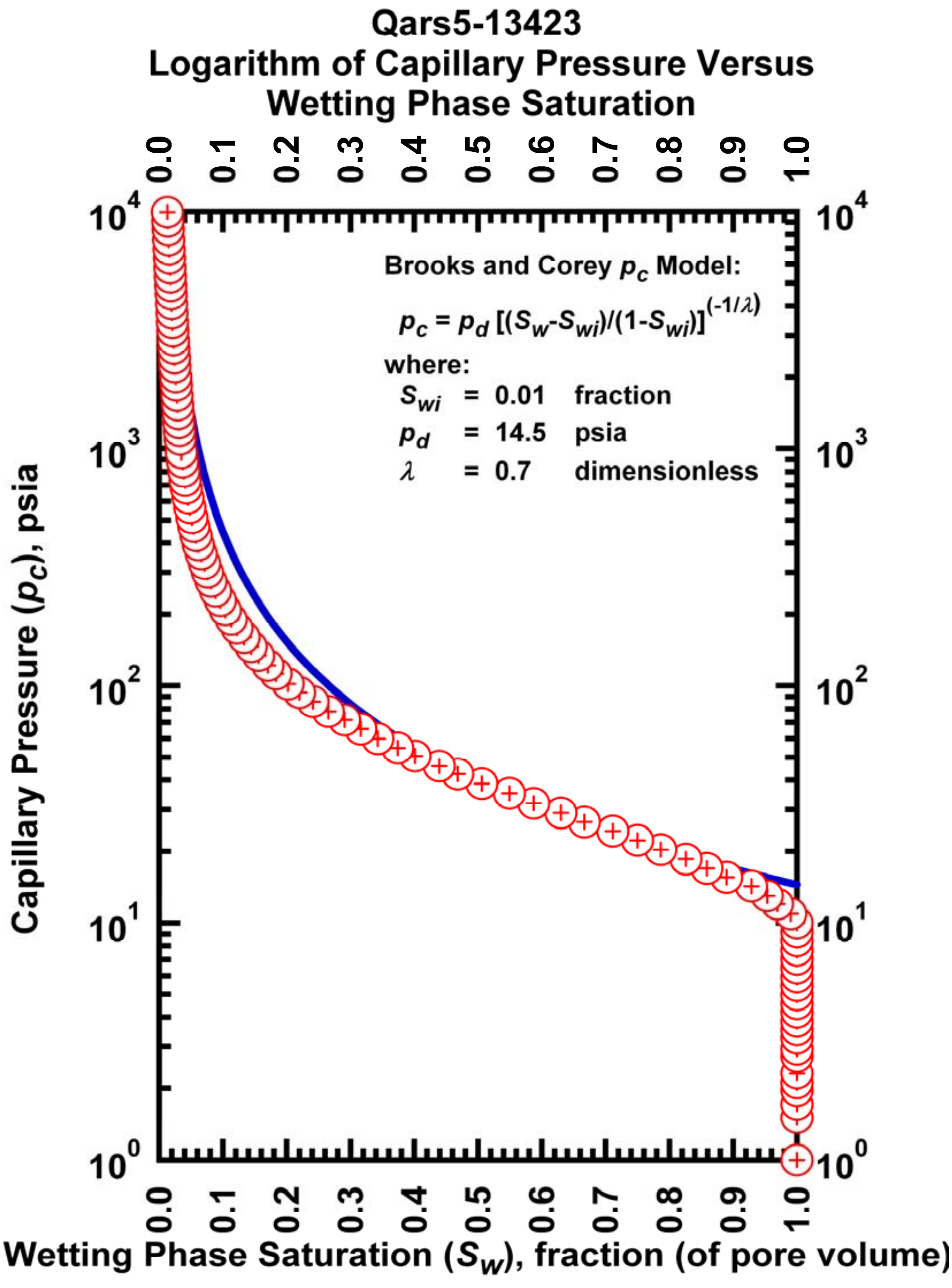

Figure J.72 – Plot of logarithm of capillary pressure vs. wetting phase saturation — Case Qars5-13423.

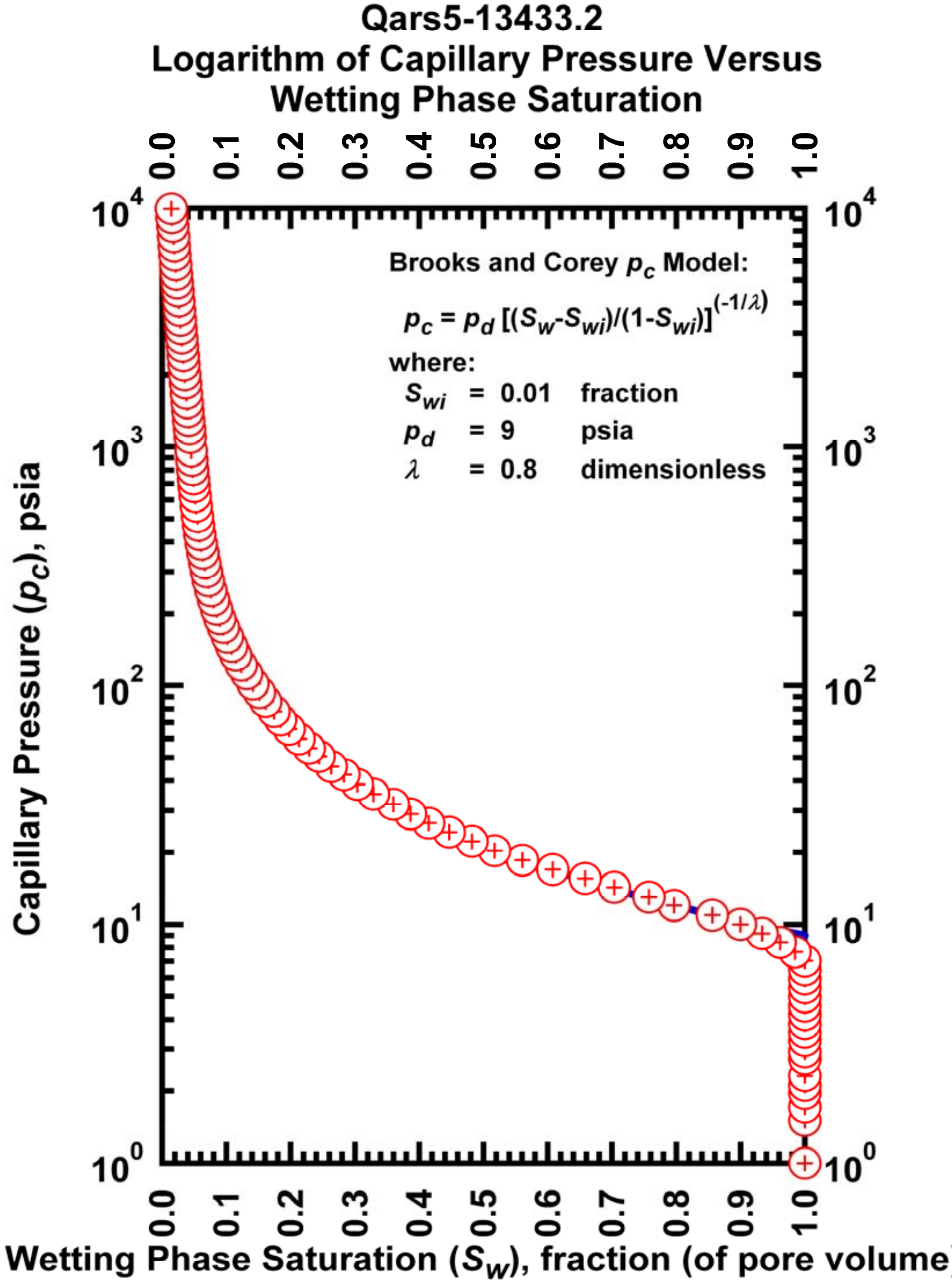

Figure J.73 – Plot of logarithm of capillary pressure vs. wetting phase saturation — Case Qars5-13433.

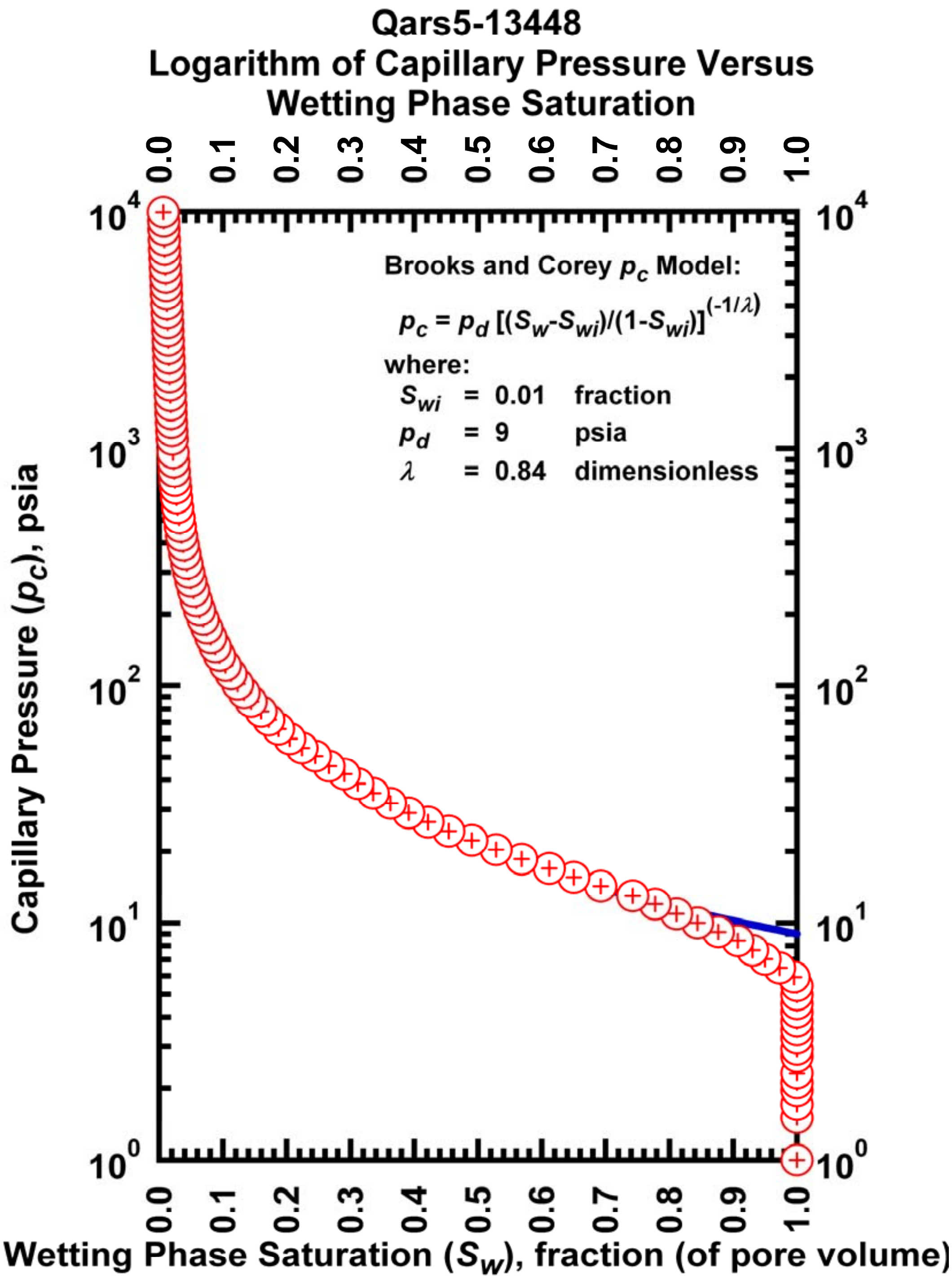

Figure J.74– Plot of logarithm of capillary pressure vs. wetting phase saturation — Case Qars5-13448.

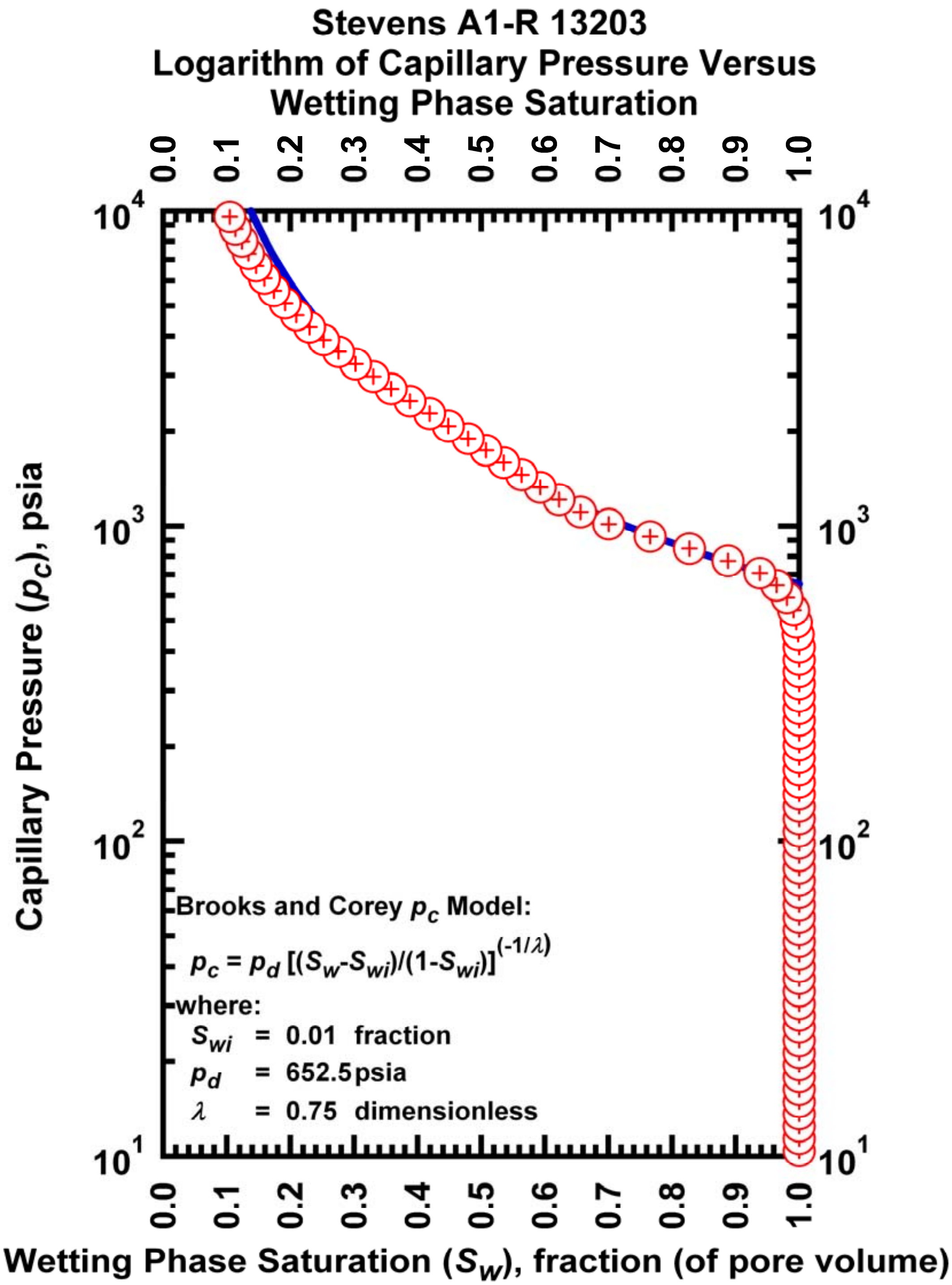

Figure J.75 – Plot of logarithm of capillary pressure vs. wetting phase saturation — Case Stevens A1-R 13203.

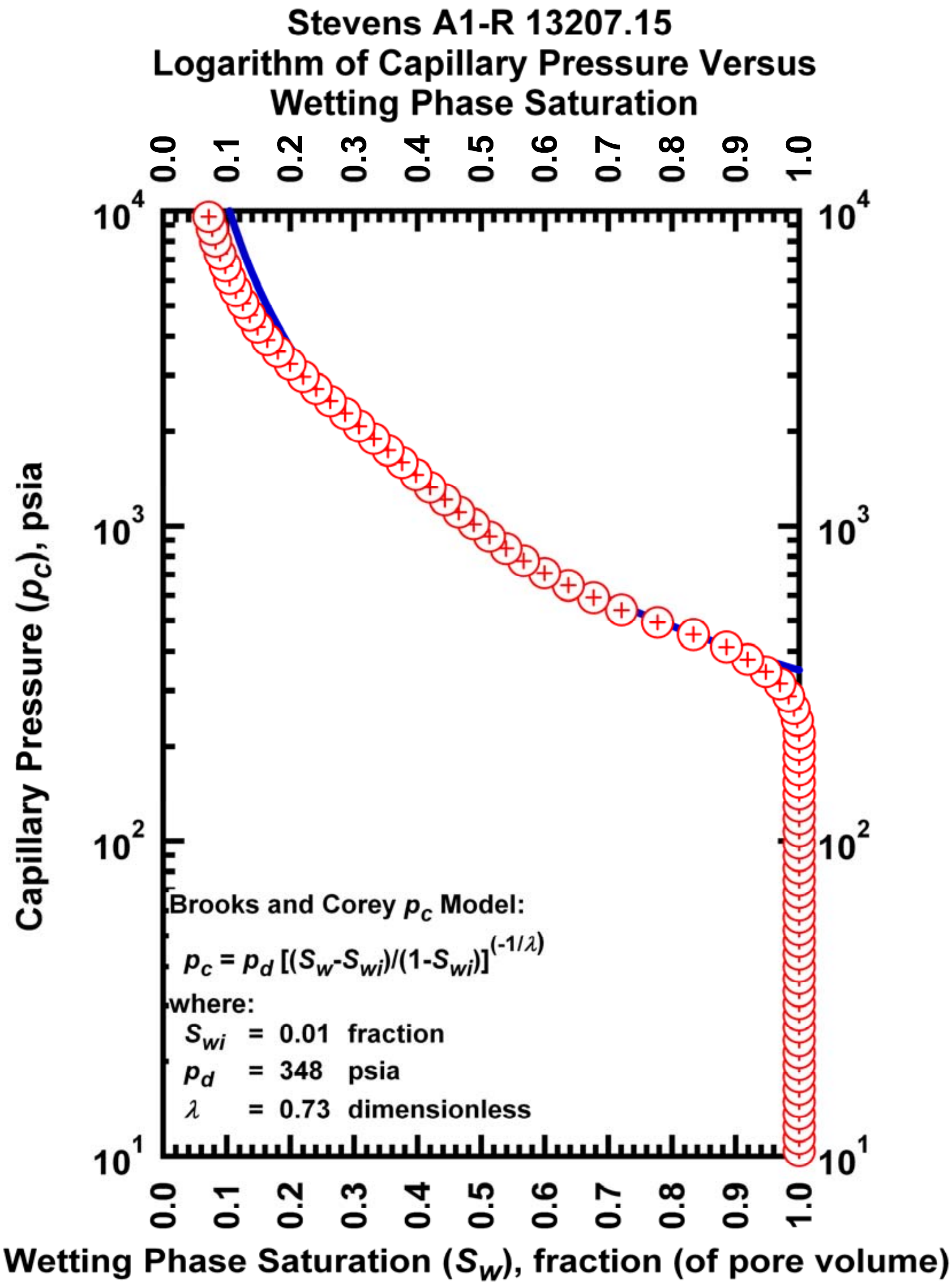

Figure J.76 – Plot of logarithm of capillary pressure vs. wetting phase saturation — Case Stevens A1-R 13207.15.

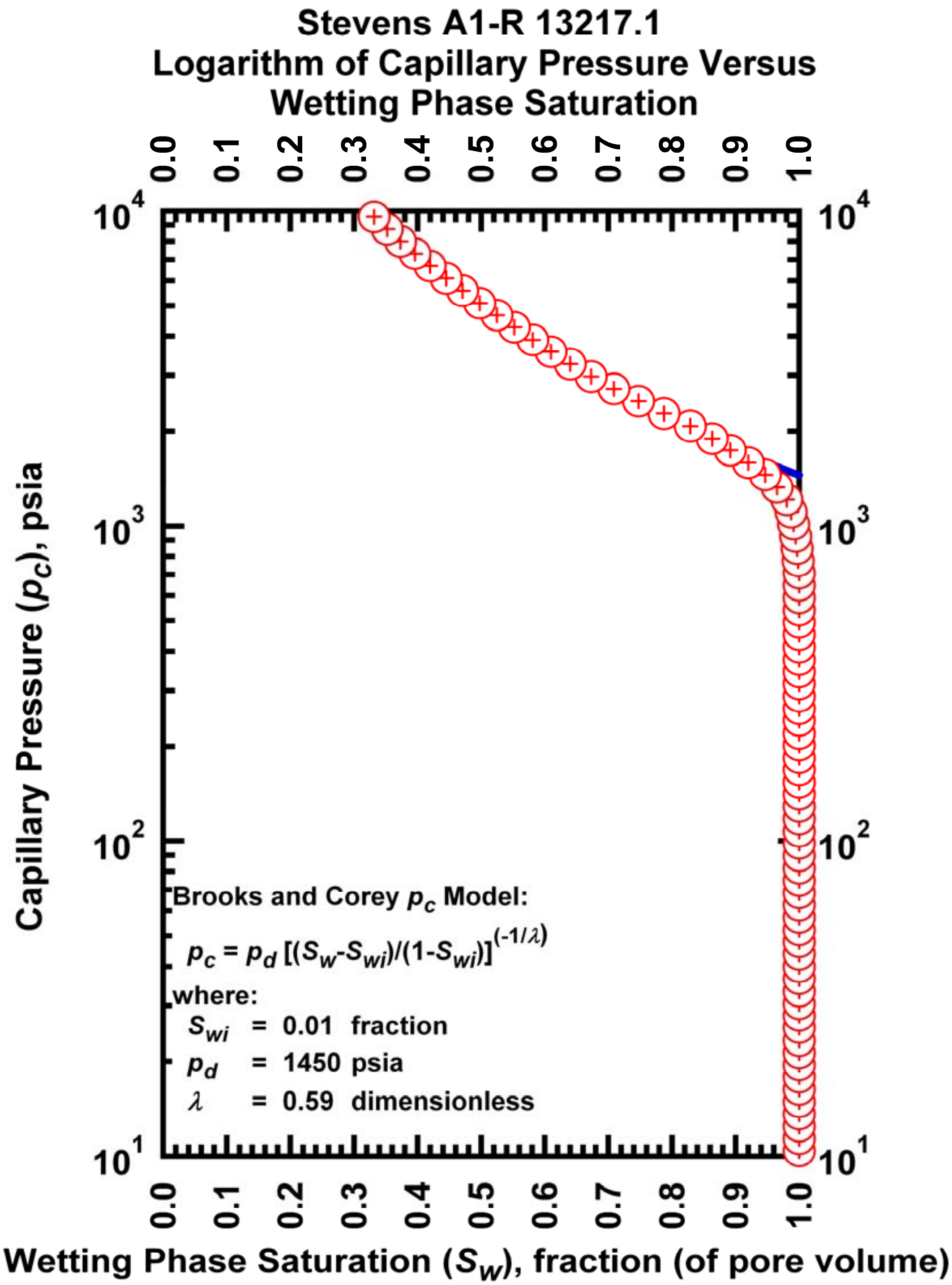

Figure J.77– Plot of logarithm of capillary pressure vs. wetting phase saturation — Case Stevens A1-R 13217.1.

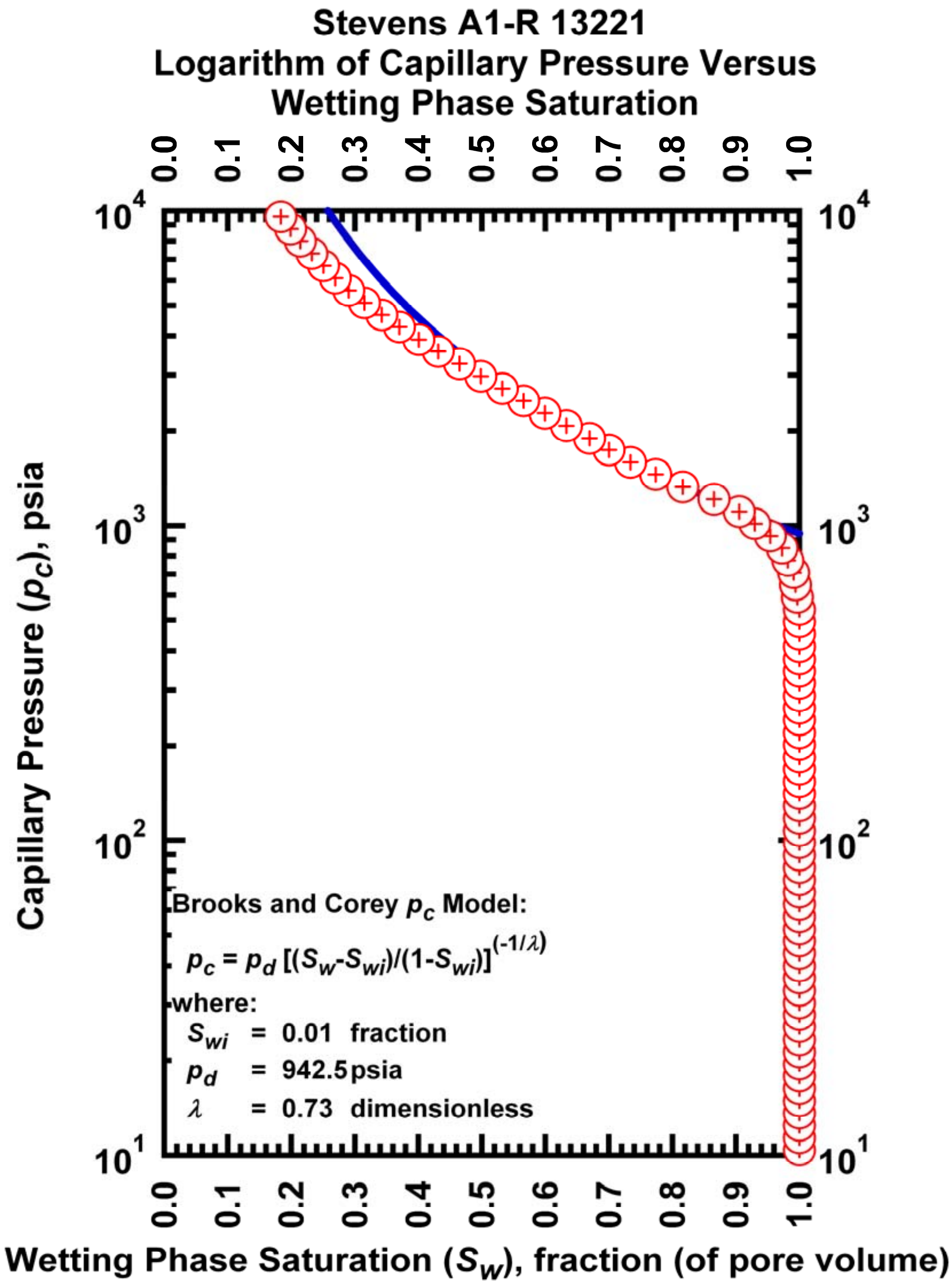

Figure J.78– Plot of logarithm of capillary pressure vs. wetting phase saturation — Case Stevens A1-R 13221.

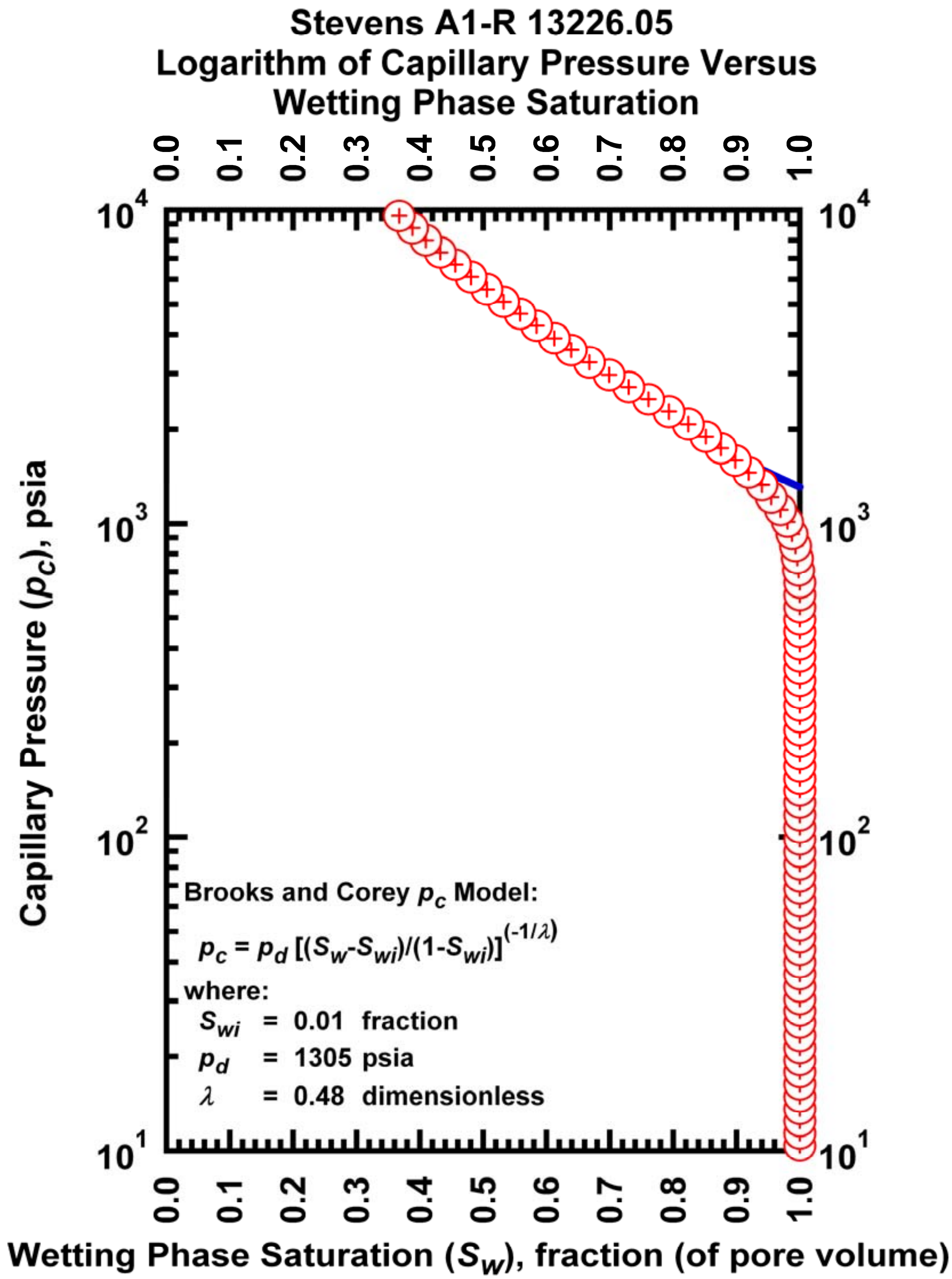

Figure J.79 – Plot of logarithm of capillary pressure vs. wetting phase saturation — Case Stevens A1-R 13226.05.

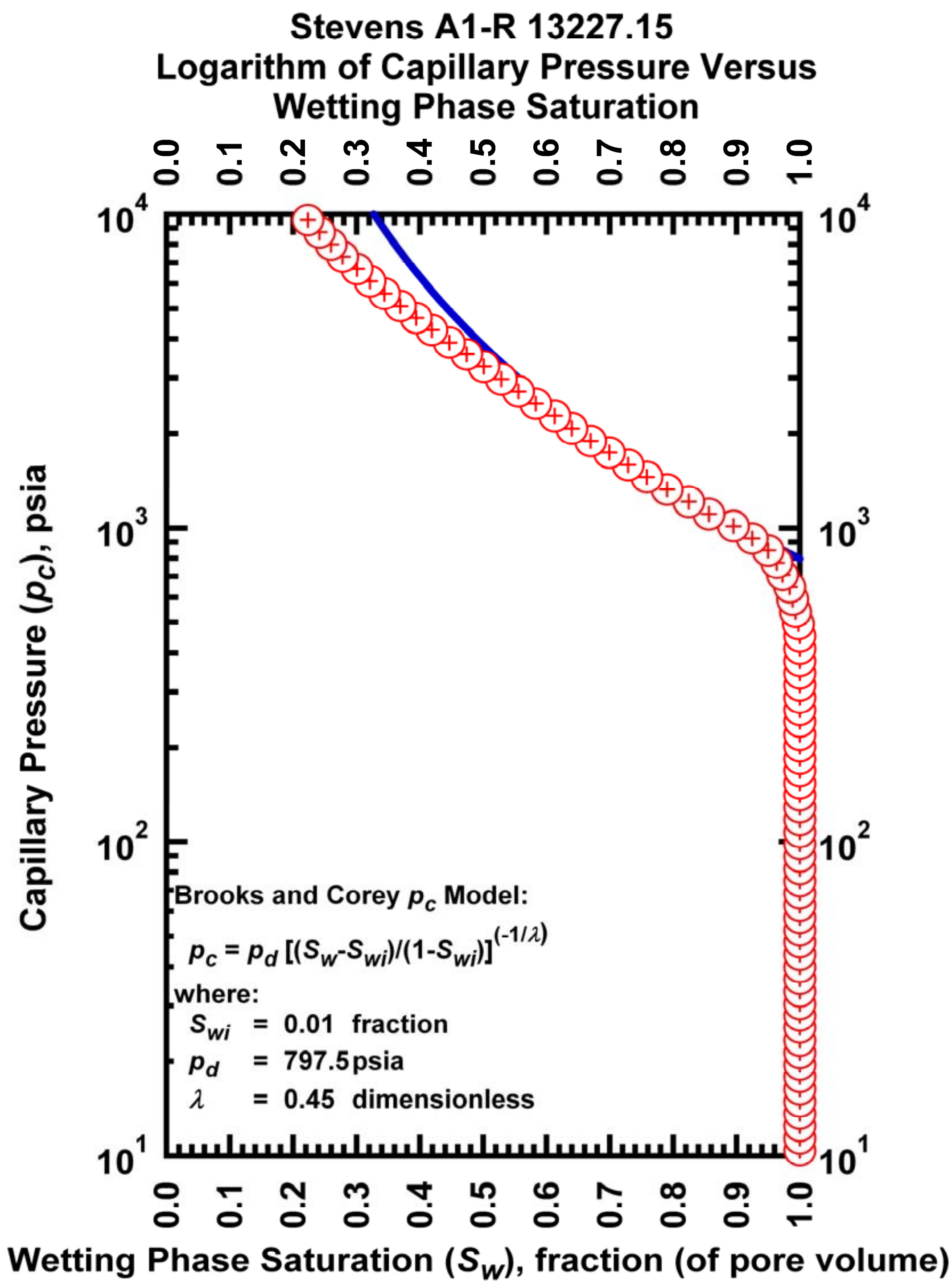

Figure J.80 – Plot of logarithm of capillary pressure vs. wetting phase saturation — Case Stevens A1-R 13227.15.

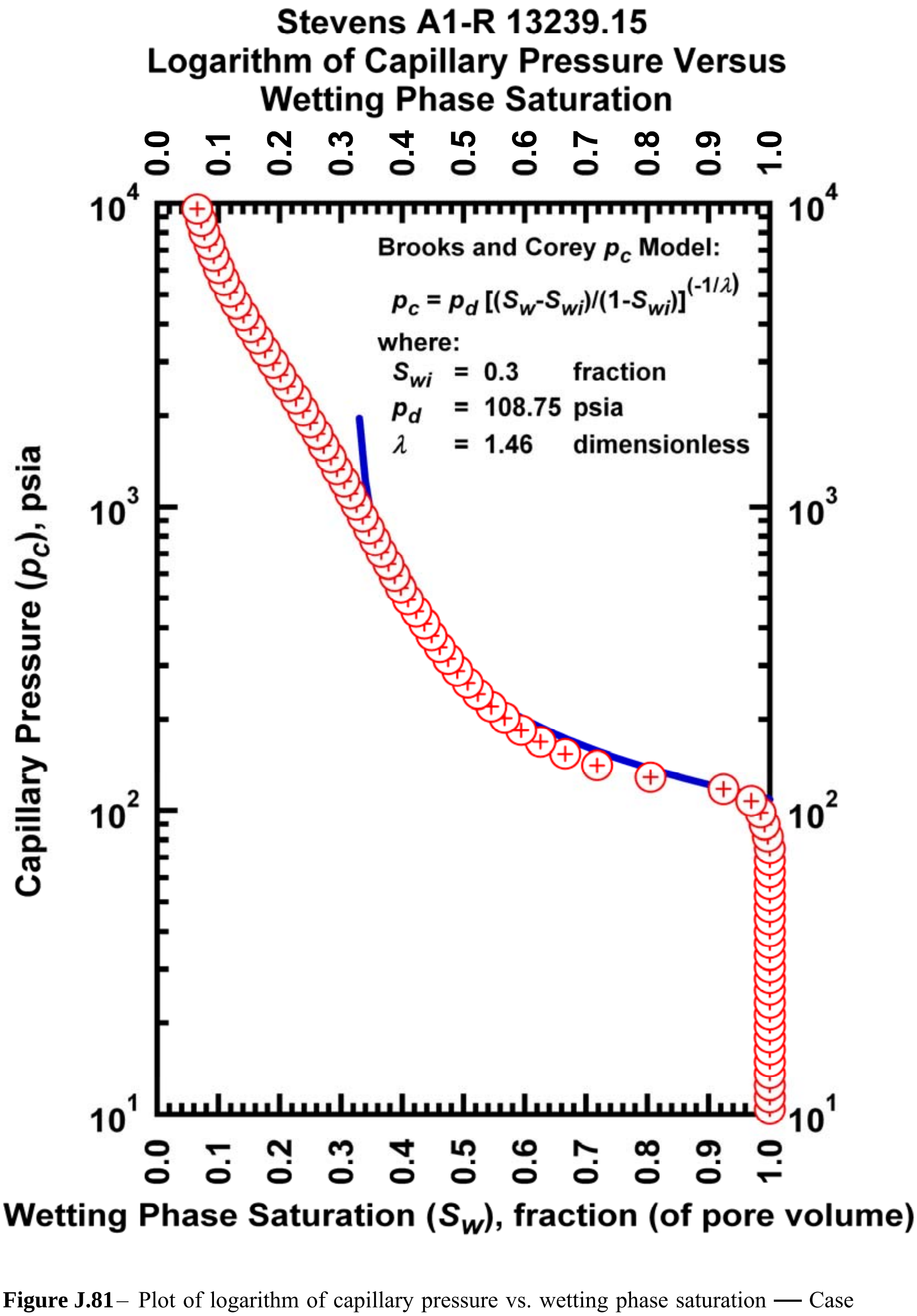

Figure J.81 – Plot of logarithm of capillary pressure vs. wetting phase saturation — Case Stevens A1-R 13239.15.

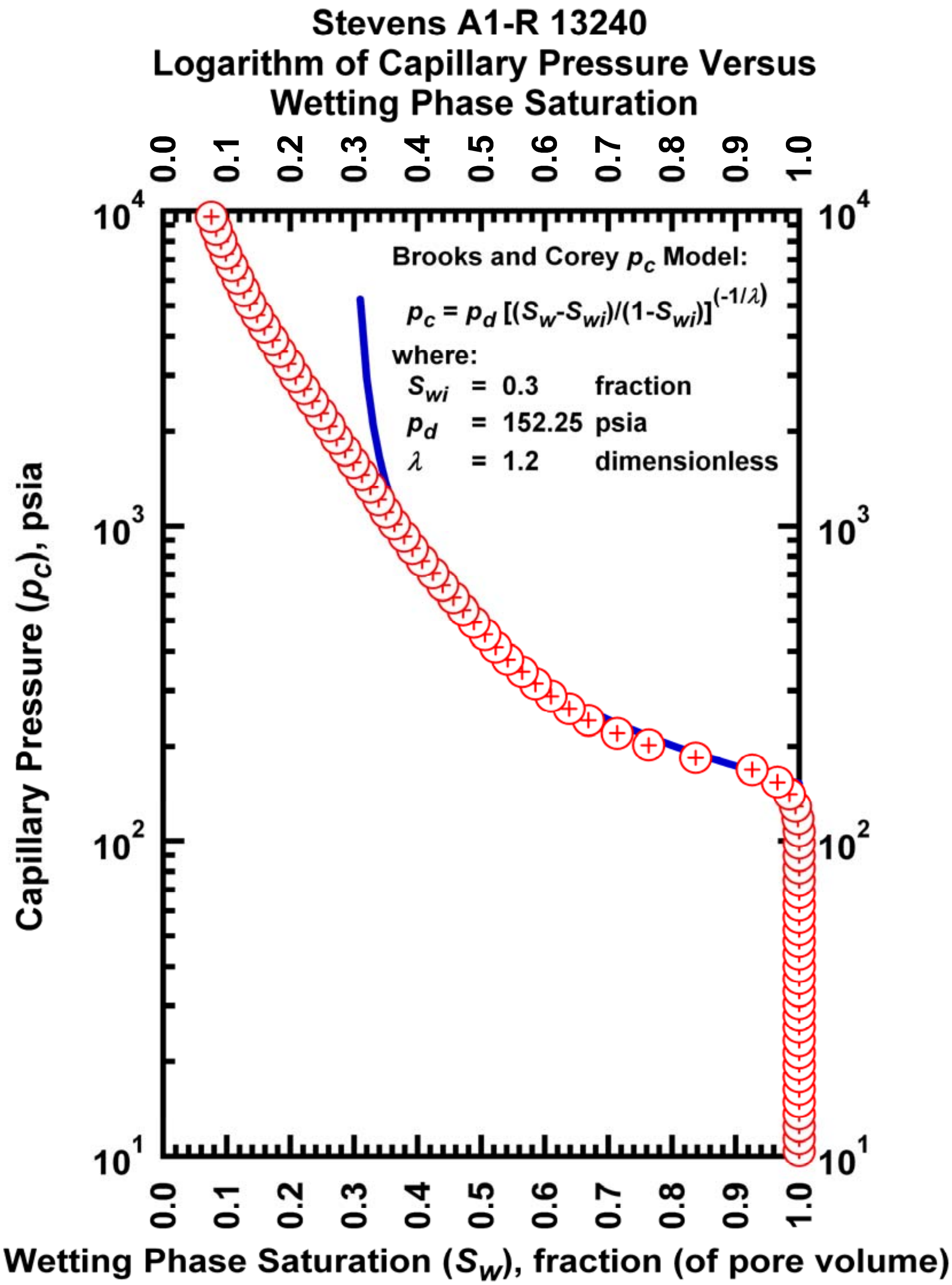

Figure J.82 – Plot of logarithm of capillary pressure vs. wetting phase saturation — Case Stevens A1-R 13240.

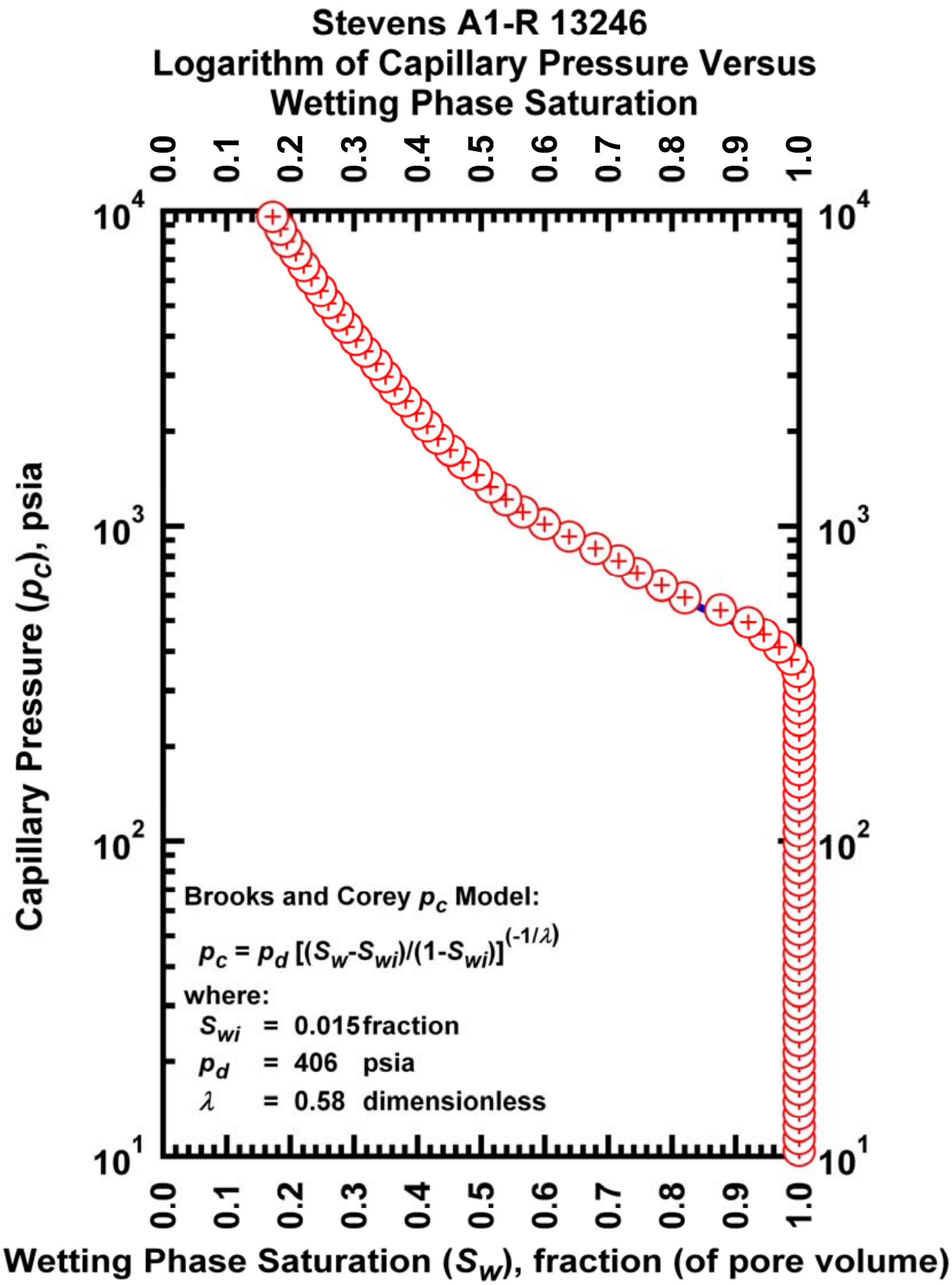

Figure J.83 – Plot of logarithm of capillary pressure vs. wetting phase saturation — Case Stevens A1-R 13246.

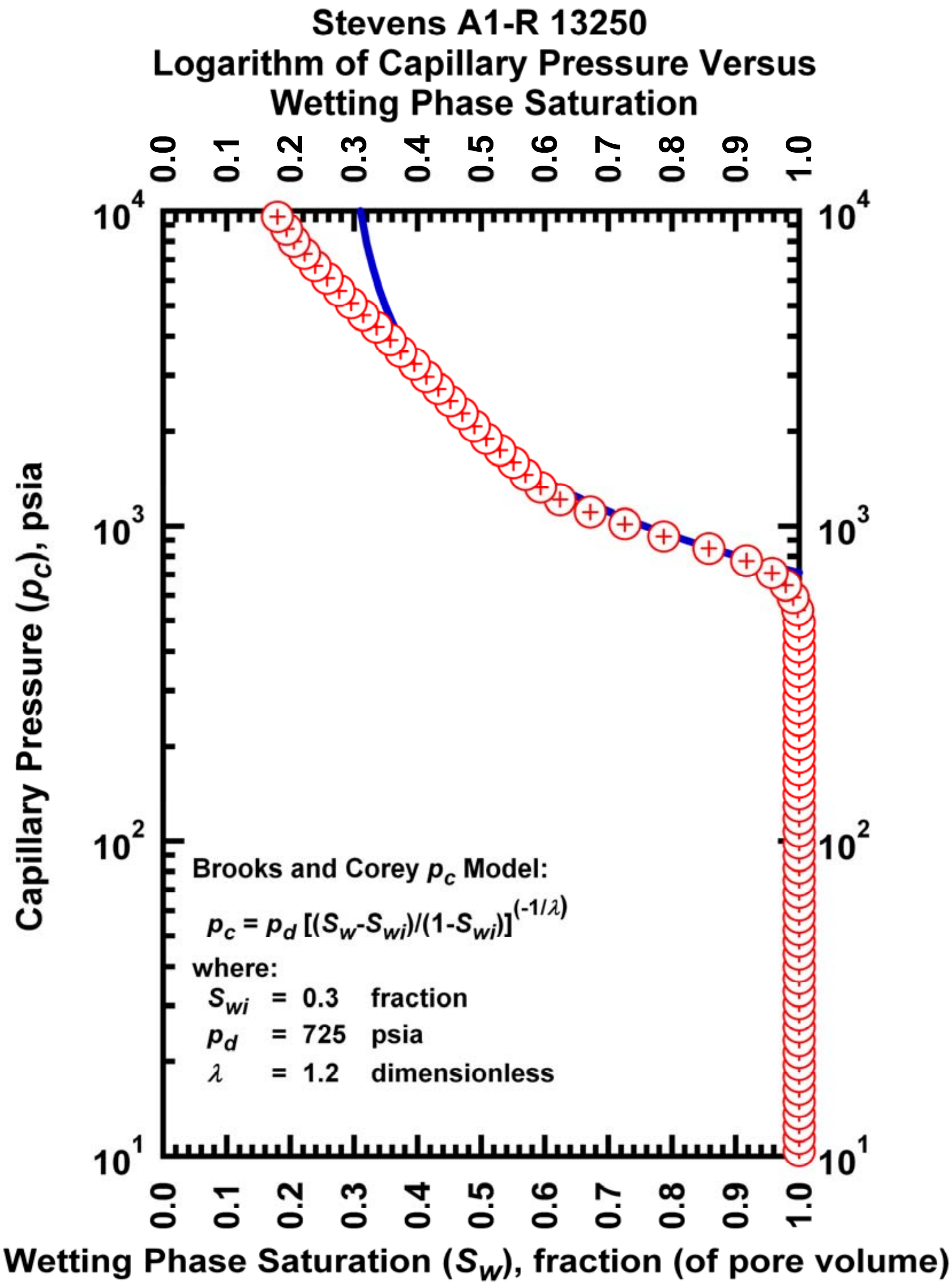

Figure J.84– Plot of logarithm of capillary pressure vs. wetting phase saturation — Case Stevens A1-R 13250.

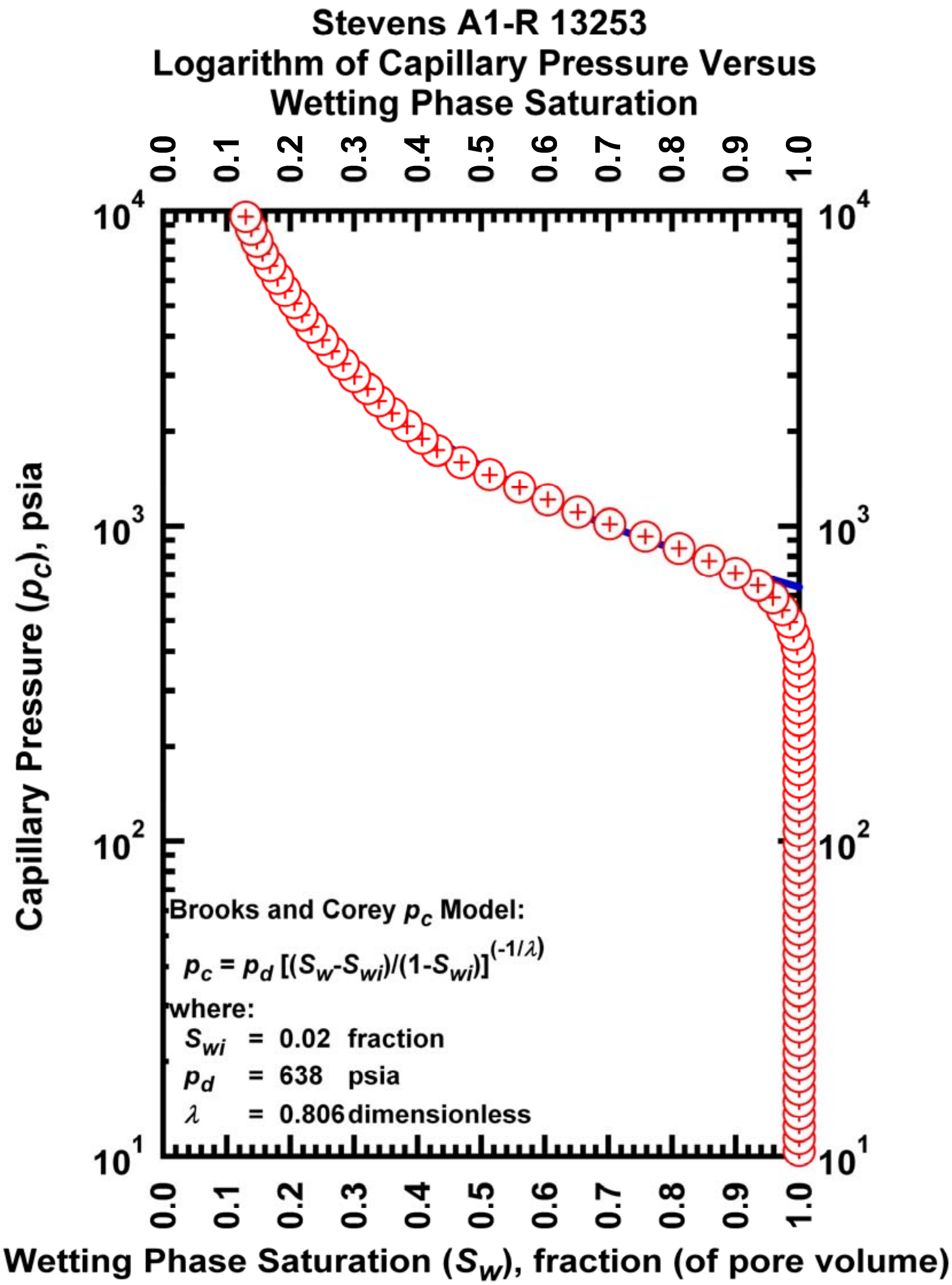

Figure J.85– Plot of logarithm of capillary pressure vs. wetting phase saturation — Case Stevens A1-R 13253.

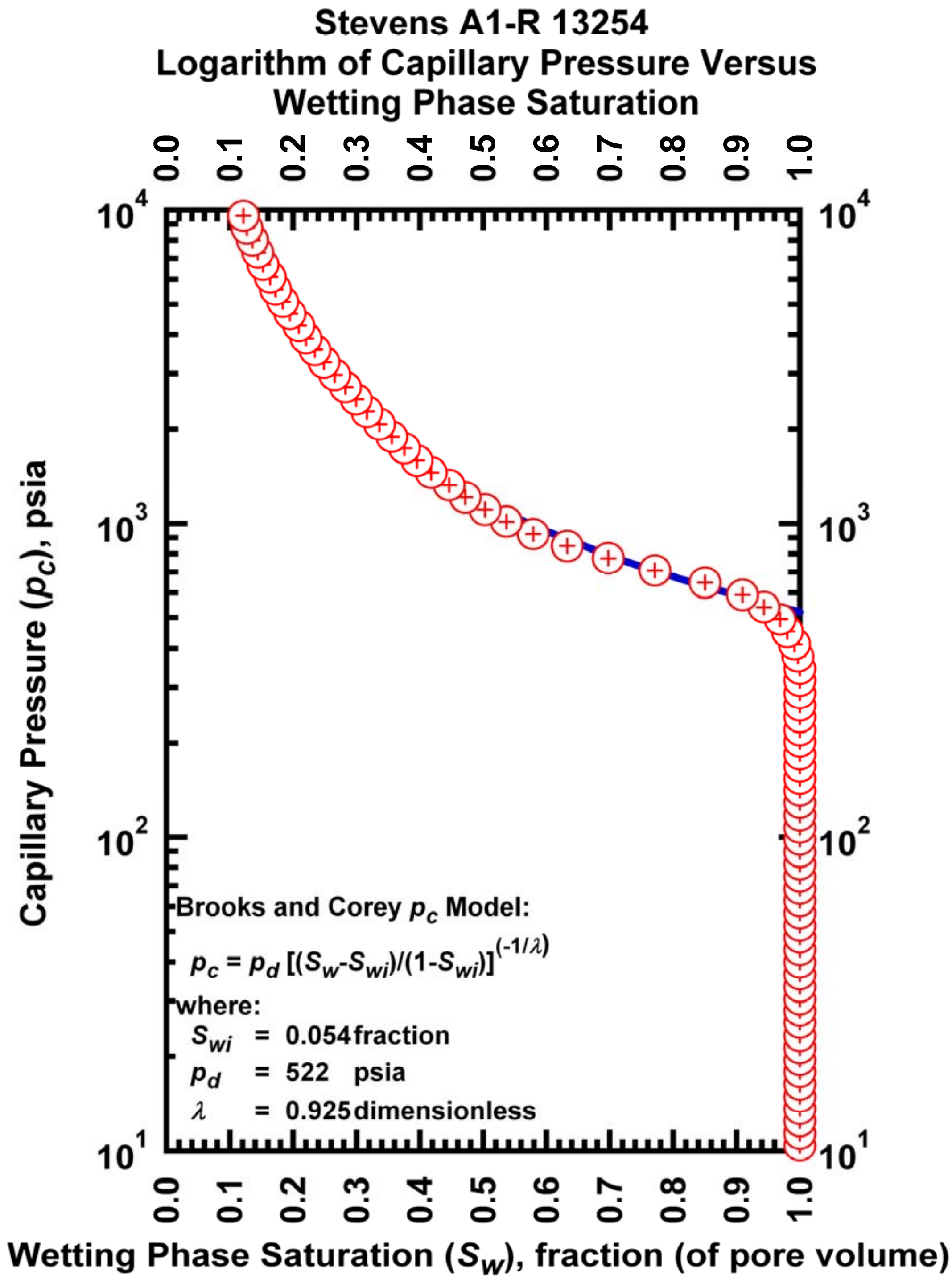

Figure J.86 – Plot of logarithm of capillary pressure vs. wetting phase saturation — Case Stevens A1-R 13254.

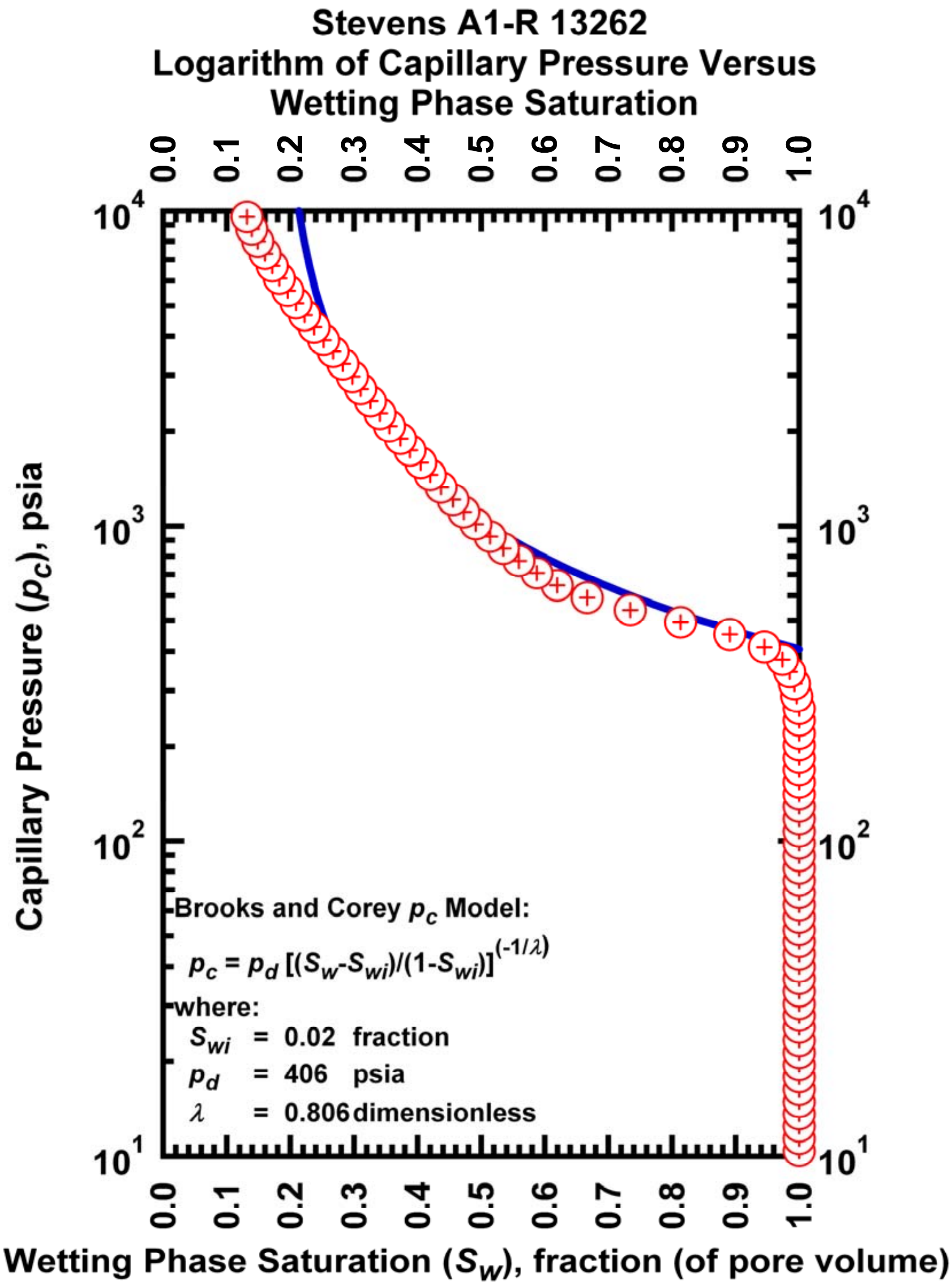

Figure J.87 – Plot of logarithm of capillary pressure vs. wetting phase saturation — Case Stevens A1-R 13262.

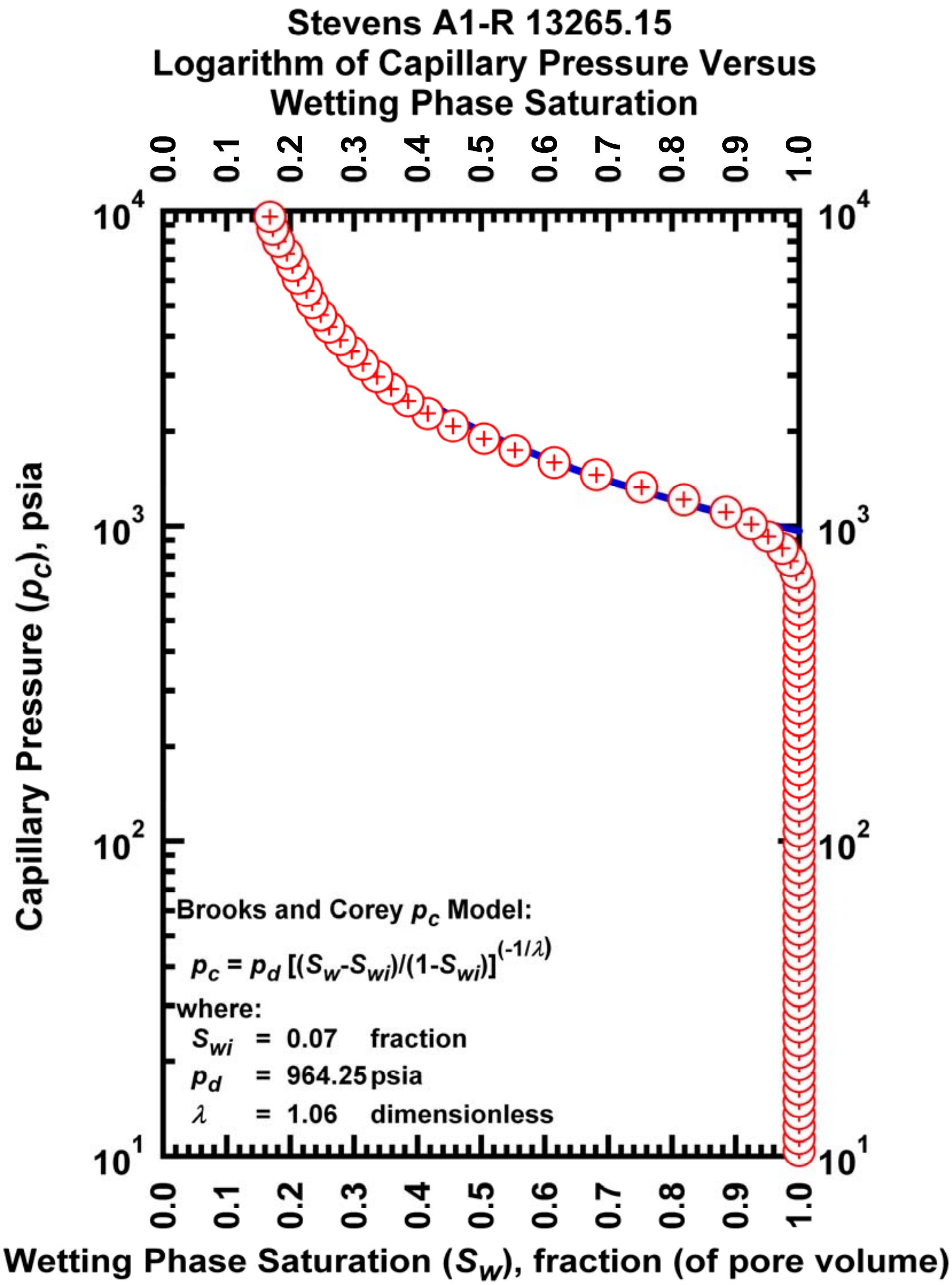

Figure J.88 – Plot of logarithm of capillary pressure vs. wetting phase saturation — Case Stevens A1-R 13265.15.

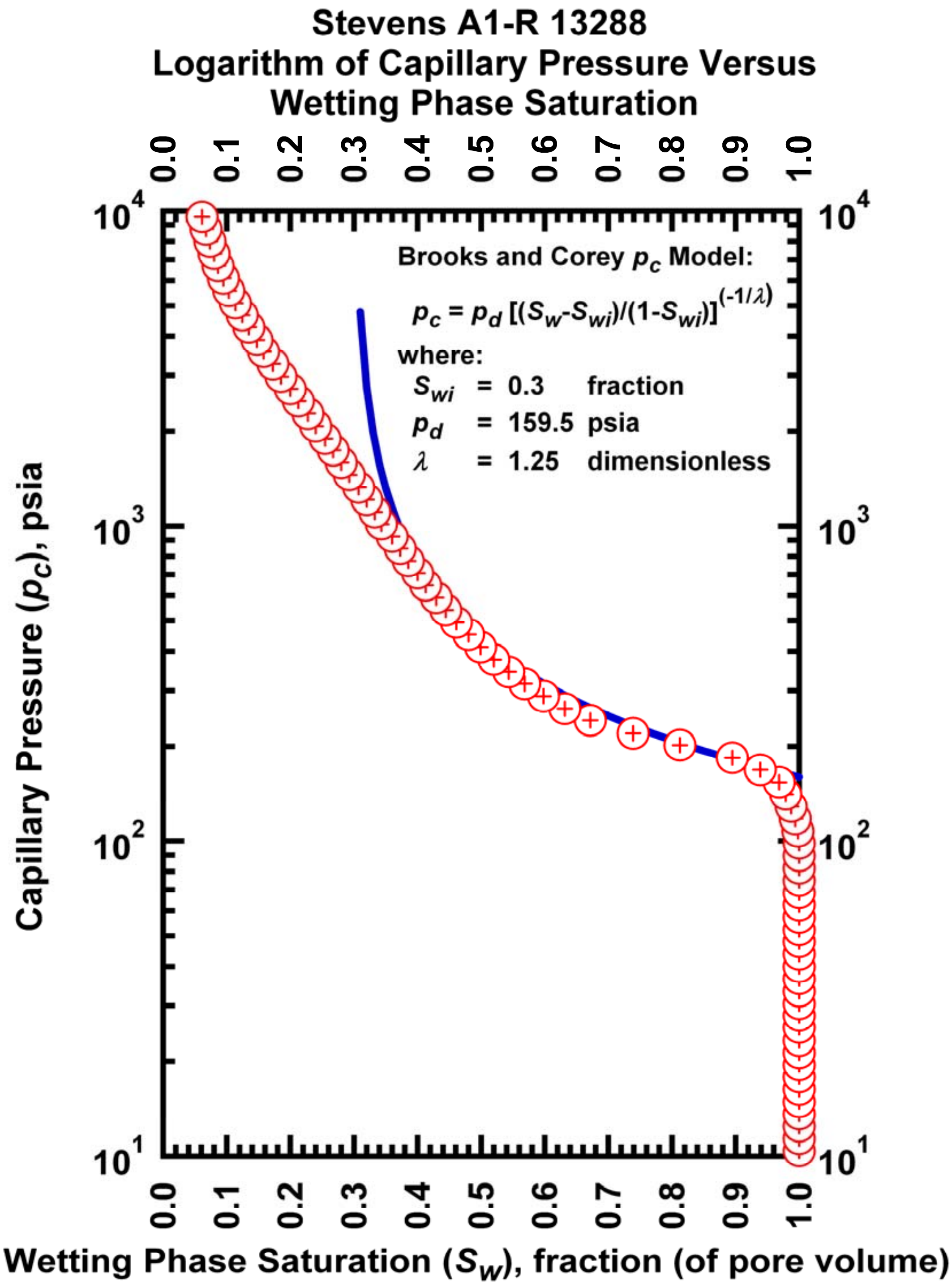

Figure J.89– Plot of logarithm of capillary pressure vs. wetting phase saturation — Case Stevens A1-R 13288.

APPENDIX K

LIBRARY OF CAPILLARY PRESSURE VERSUS NORMALIZED WETTING PHASE SATURATION PLOTS — LOGARITHMIC CAPILLARY PRESSURE FORMAT

This Appendix presents the calibration of the capillary displacement pressure (p_d), irreducible wetting-phase saturation (S_{wi}), and the index of pore-size distribution (λ) on a sample-by-sample basis using the Brooks-Corey $p_c(S_w)$ model .

In this Appendix, we provide for each data a plot of capillary pressure (p_c) vs. normalized wetting phase saturation (S_w) – logarithmic capillary pressure format.

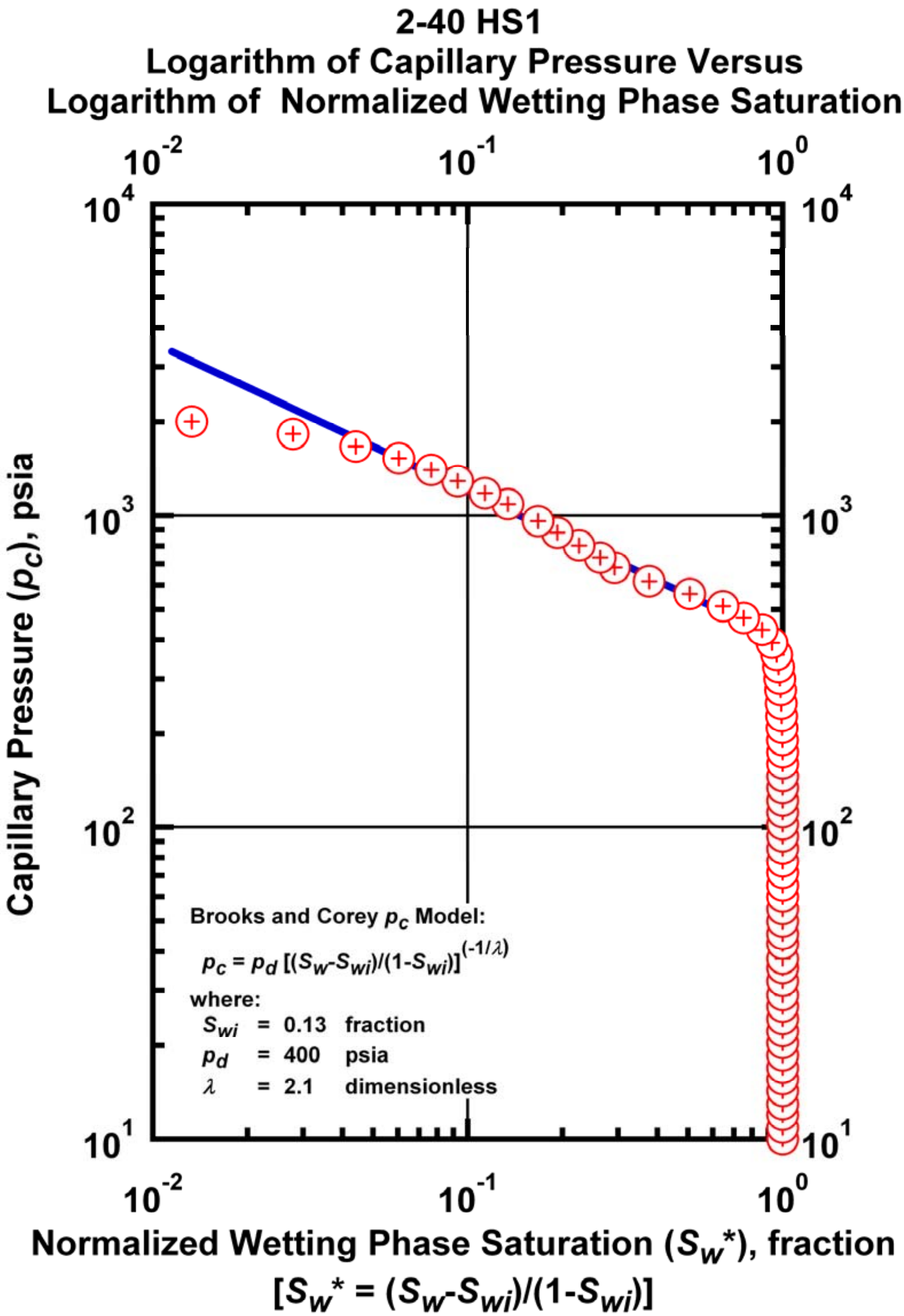

Figure K.1 – Plot of logarithm of capillary pressure vs. logarithm of normalized wetting phase saturation — Case 2-40 HS1.

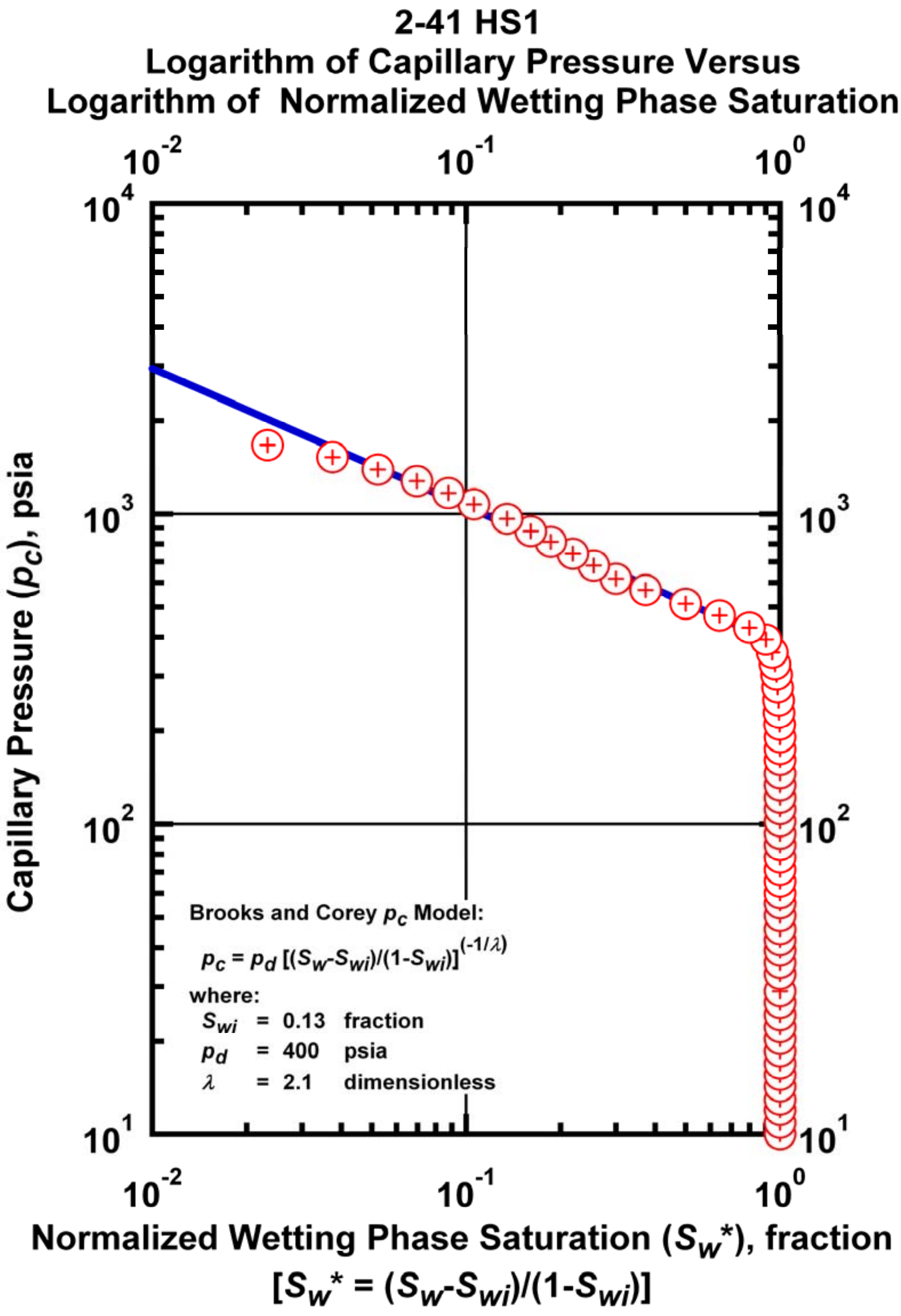

Figure K.2 – Plot of logarithm of capillary pressure vs. logarithm of normalized wetting phase saturation — Case 2-41 HS1.

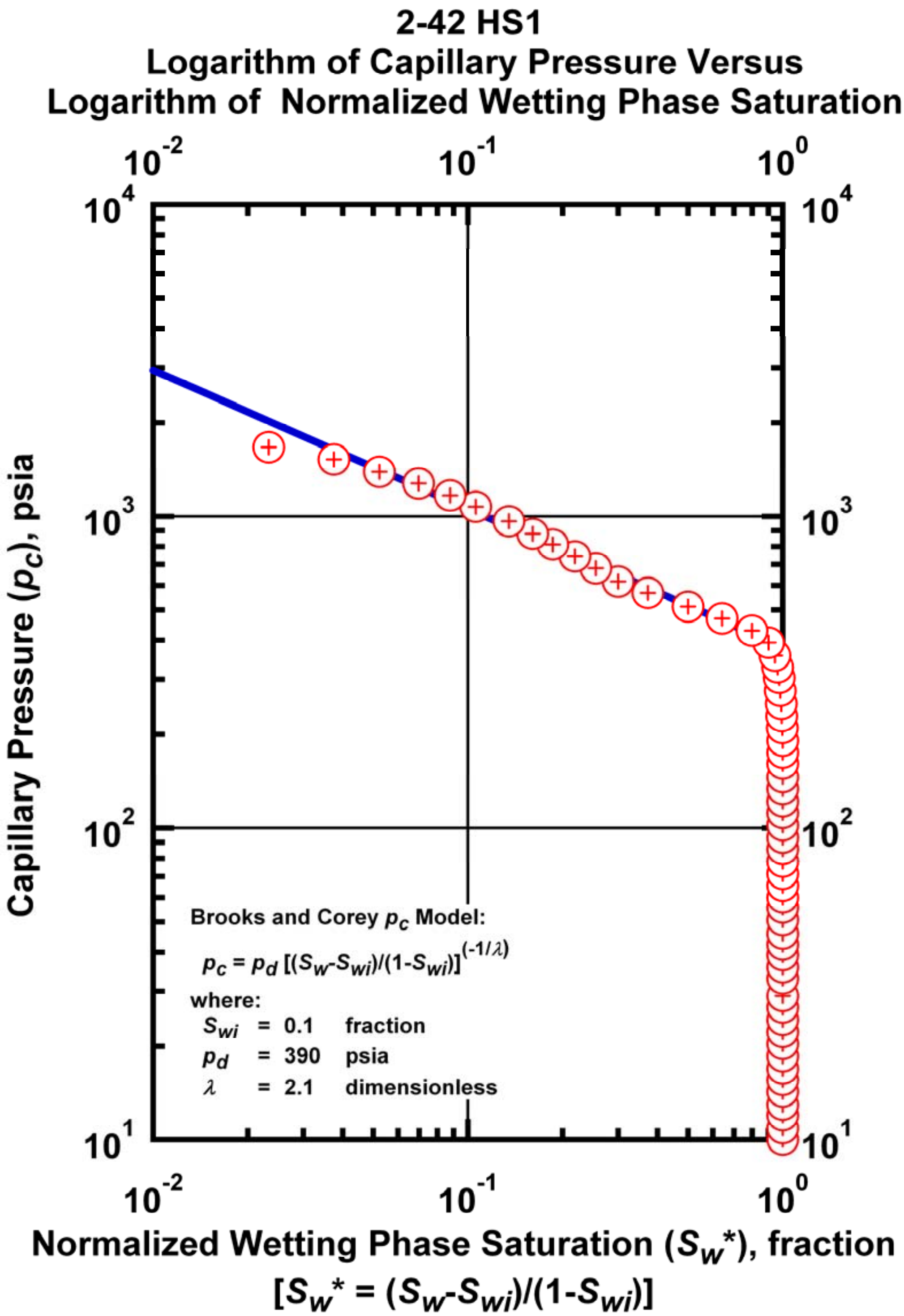

Figure K.3 – Plot of logarithm of capillary pressure vs. logarithm of normalized wetting phase saturation — Case 2-42 HS1.

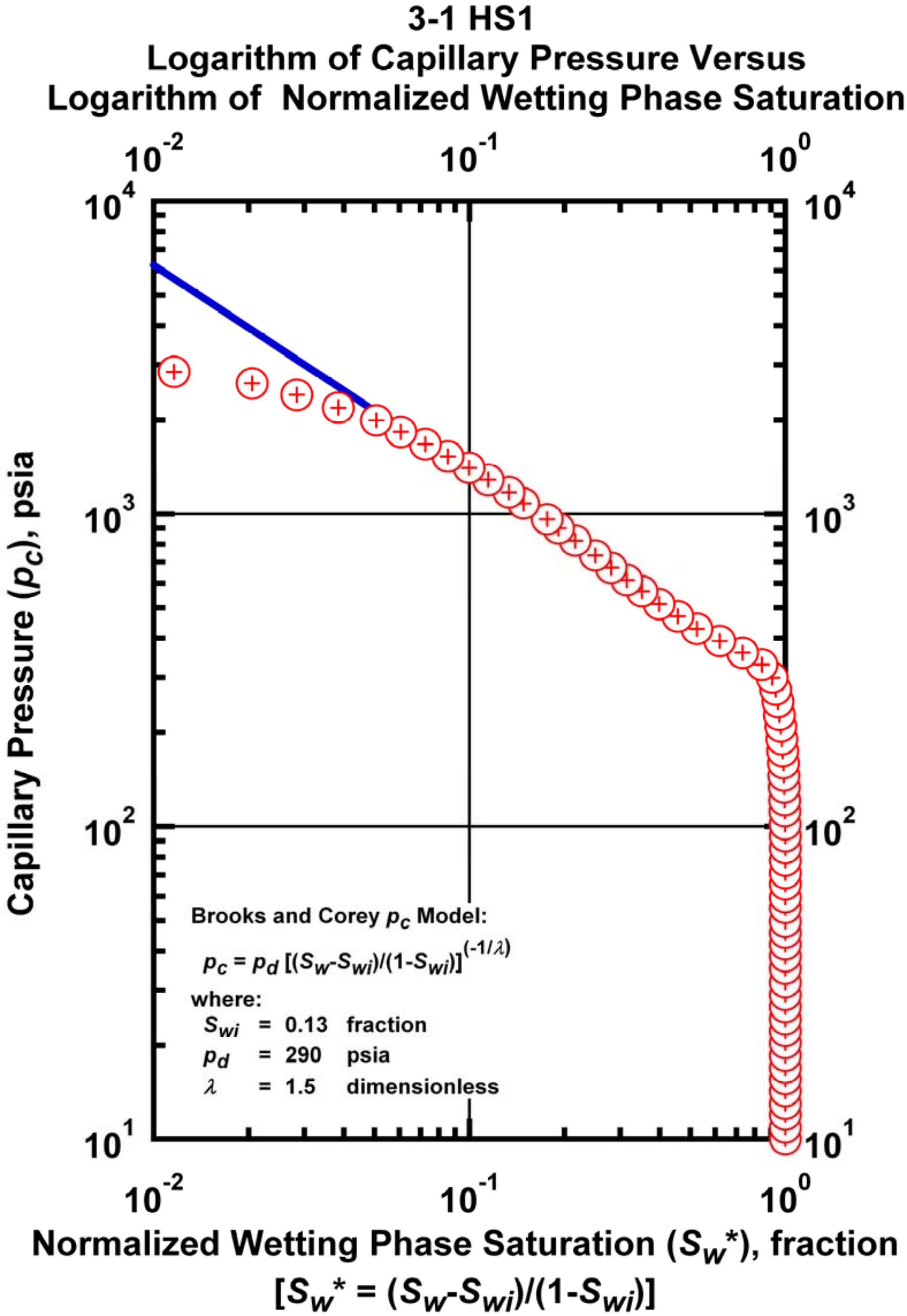

Figure K.4 – Plot of logarithm of capillary pressure vs. logarithm of normalized wetting phase saturation ── Case 3-1 HS1.

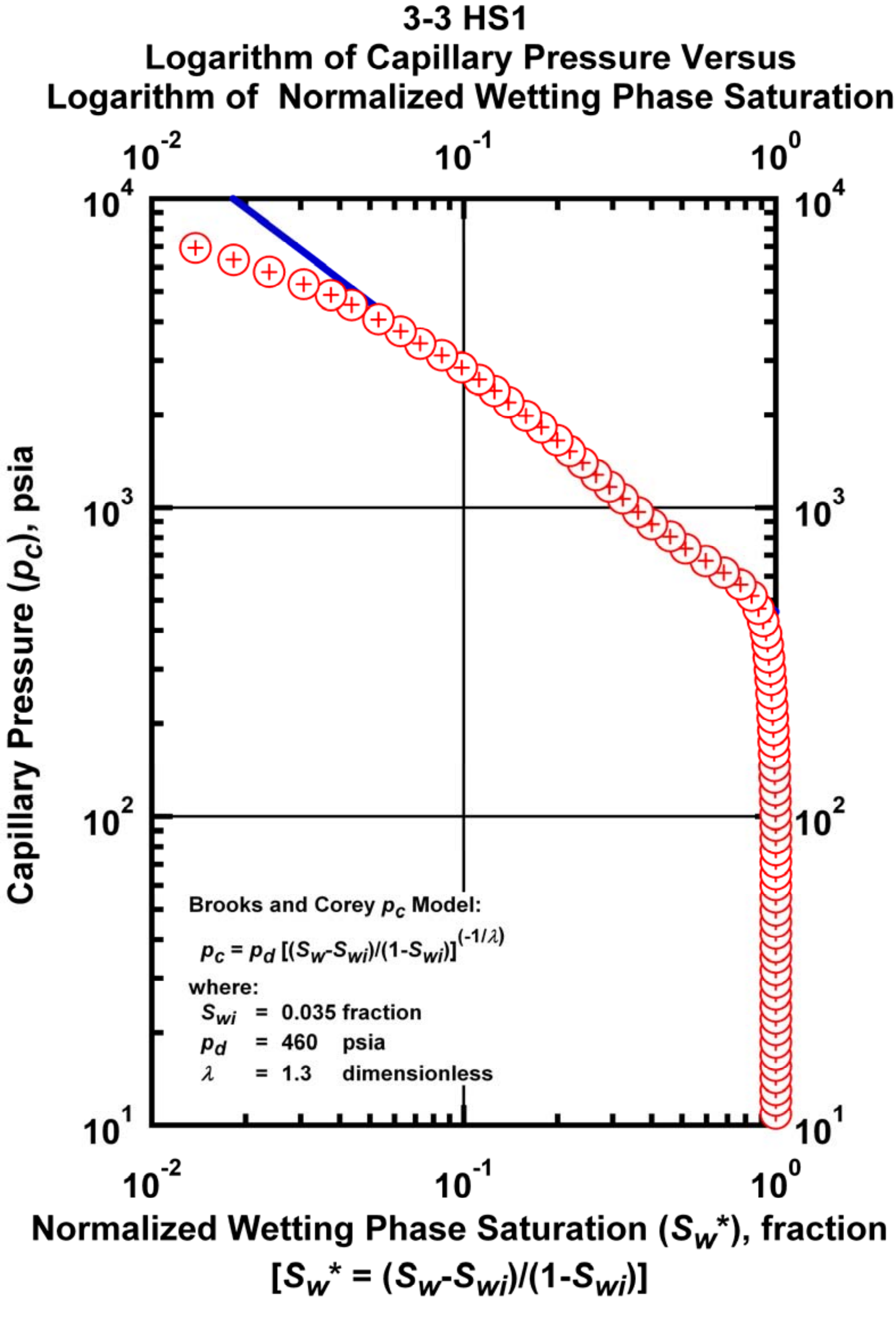

Figure K.5 – Plot of logarithm of capillary pressure vs. logarithm of normalized wetting phase saturation — Case 3-3 HS1.

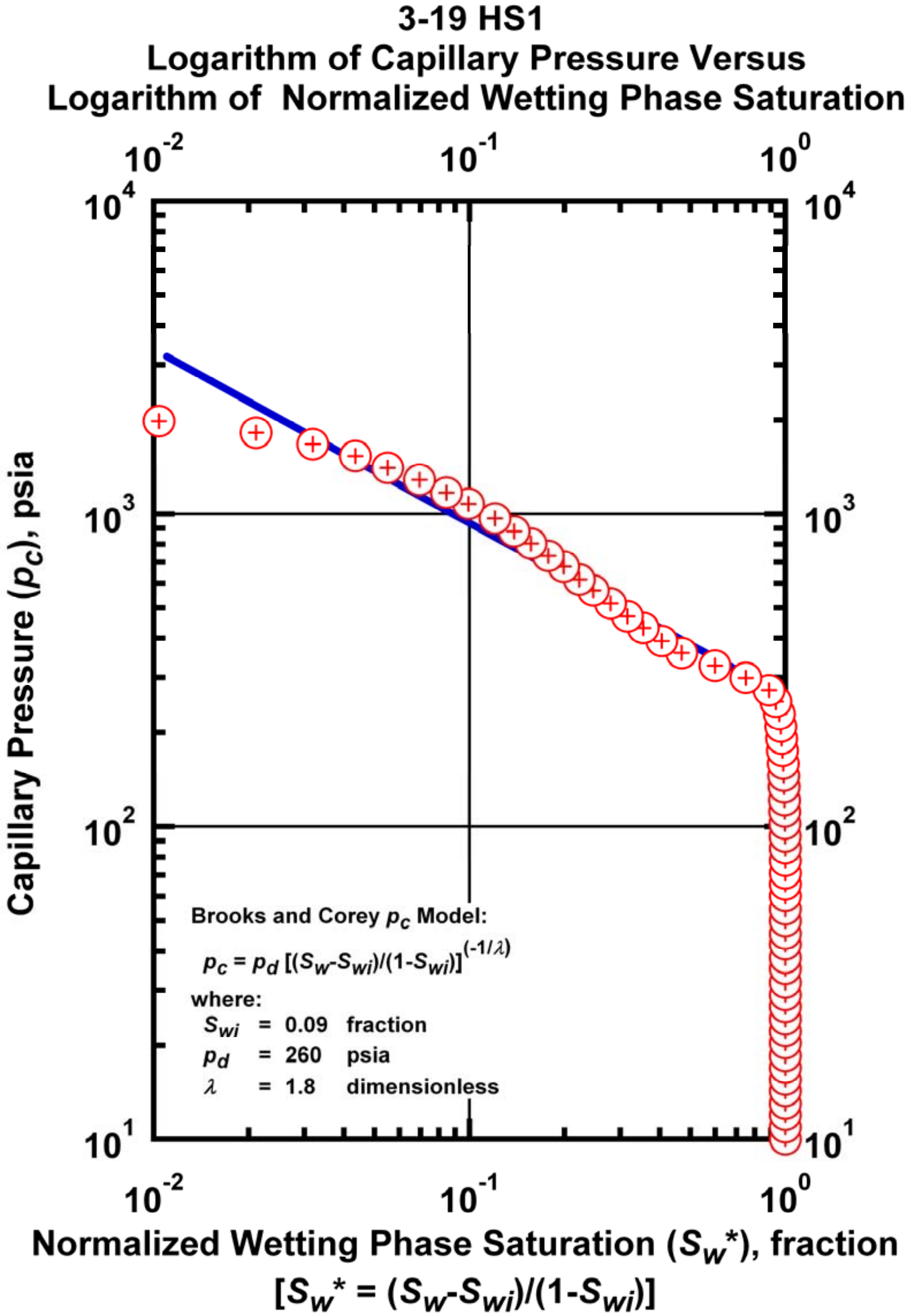

Figure K.6 – Plot of logarithm of capillary pressure vs. logarithm of normalized wetting phase saturation — Case 3-19 HS1.

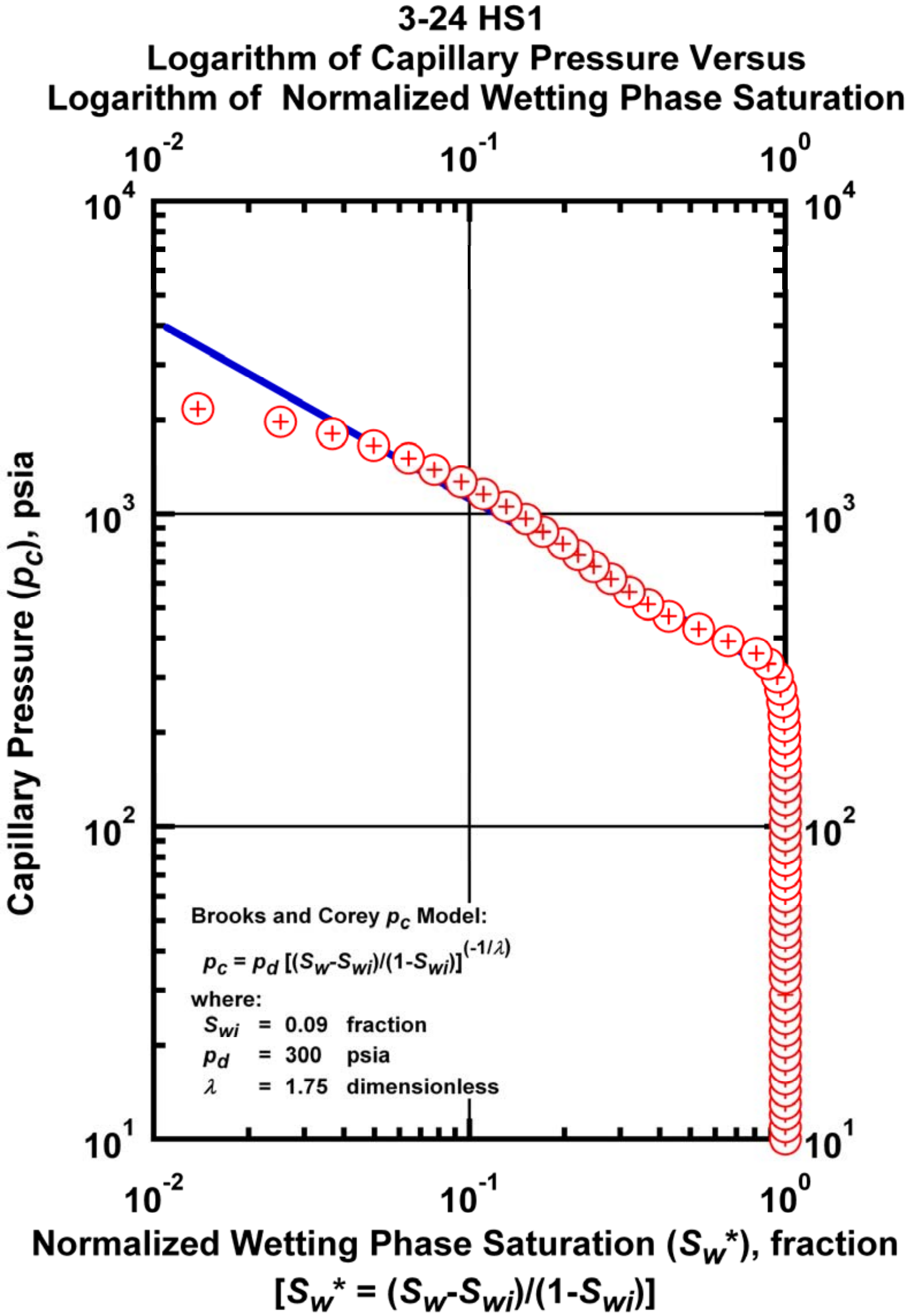

Figure K.7 – Plot of logarithm of capillary pressure vs. logarithm of normalized wetting phase saturation — Case 3-24 HS1.

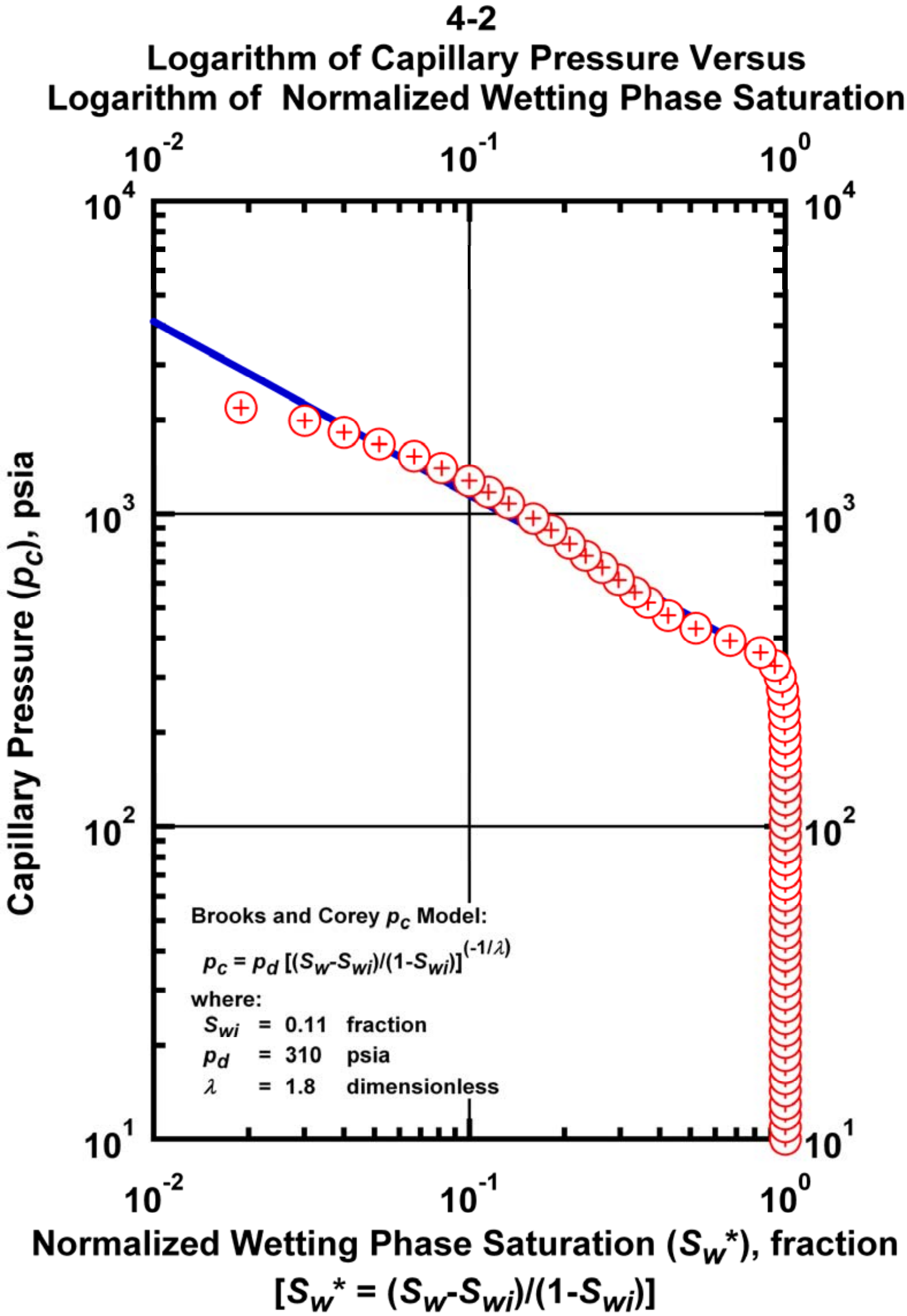

Figure K.8 – Plot of logarithm of capillary pressure vs. logarithm of normalized wetting phase saturation — Case 4-2 HS1.

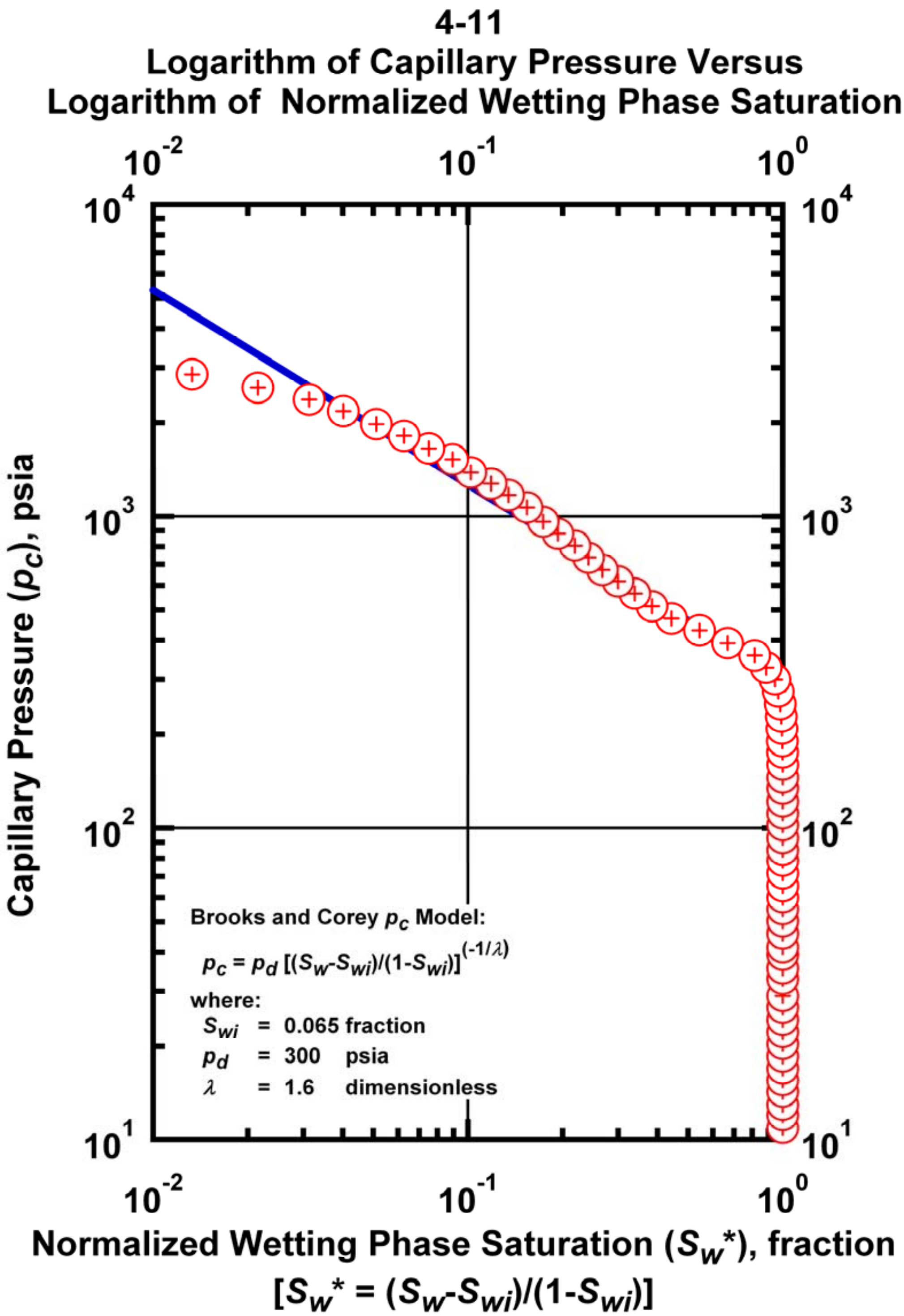

Figure K.9 – Plot of logarithm of capillary pressure vs. logarithm of normalized wetting phase saturation — Case 4-11 HS1.

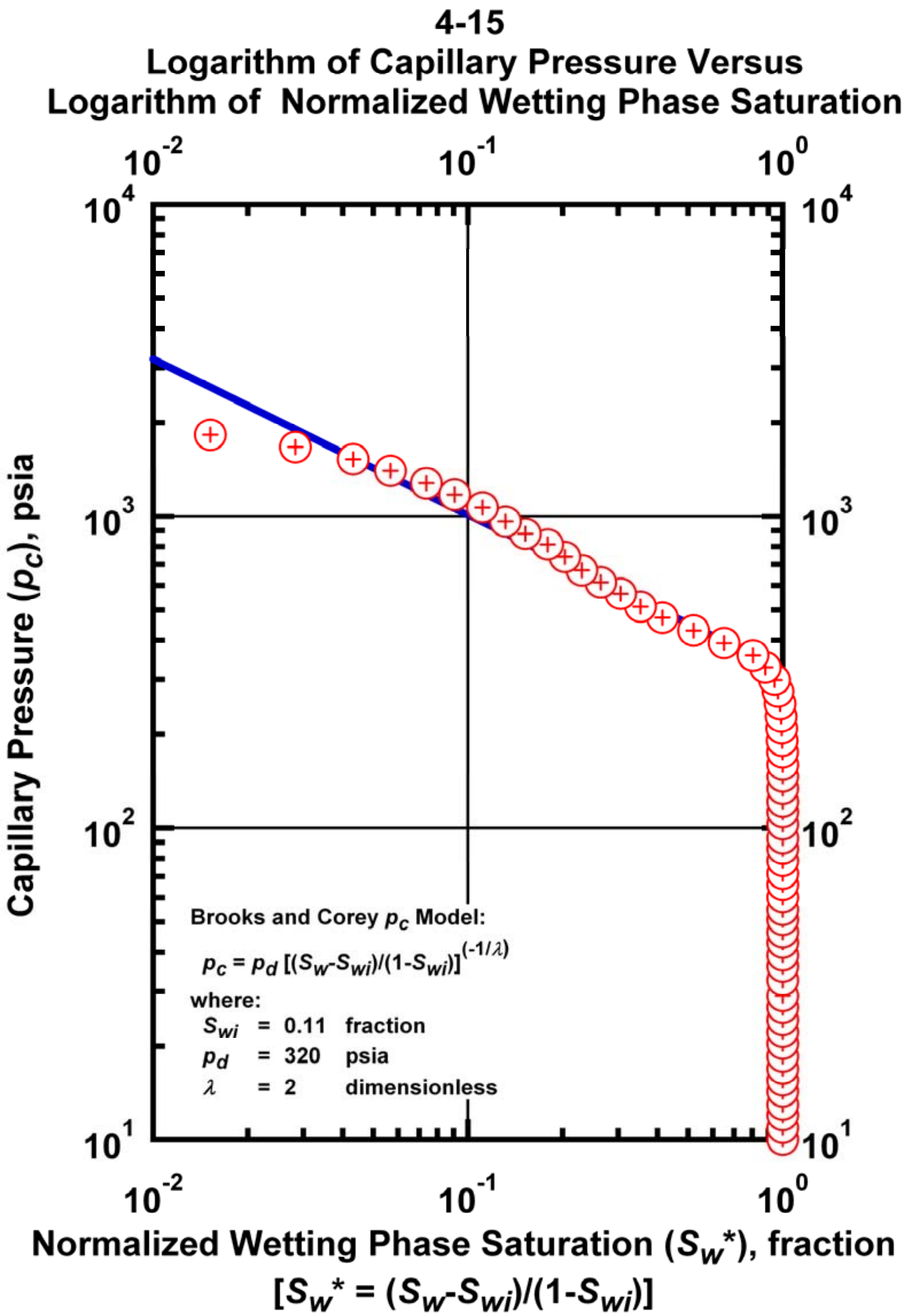

Figure K.10 – Plot of logarithm of capillary pressure vs. logarithm of normalized wetting phase saturation — Case 4-15 HS1.

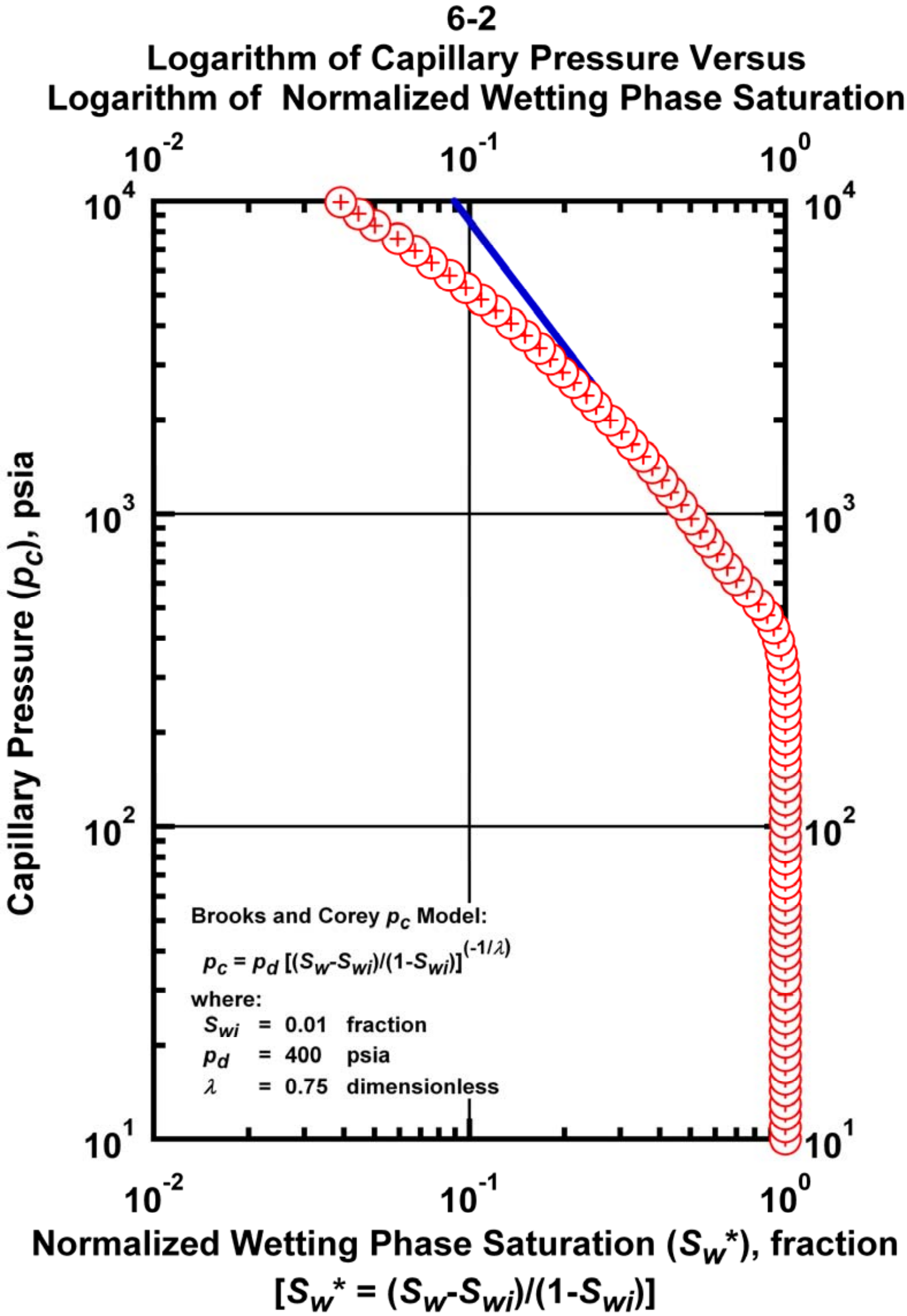

Figure K.11 – Plot of logarithm of capillary pressure vs. logarithm of normalized wetting phase saturation — Case 6-2 HS1.

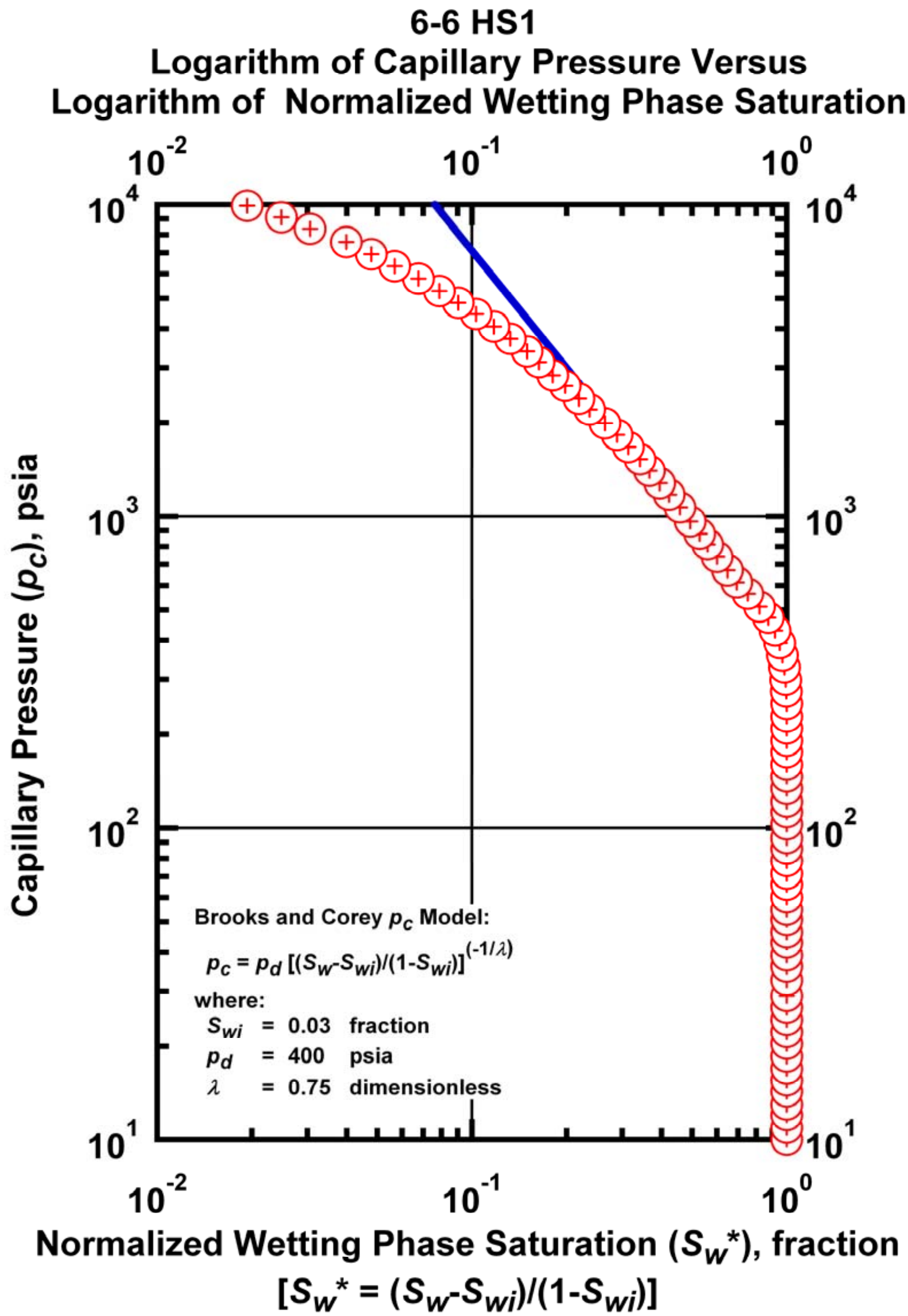

Figure K.12 – Plot of logarithm of capillary pressure vs. logarithm of normalized wetting phase saturation — Case 6-6 HS1.

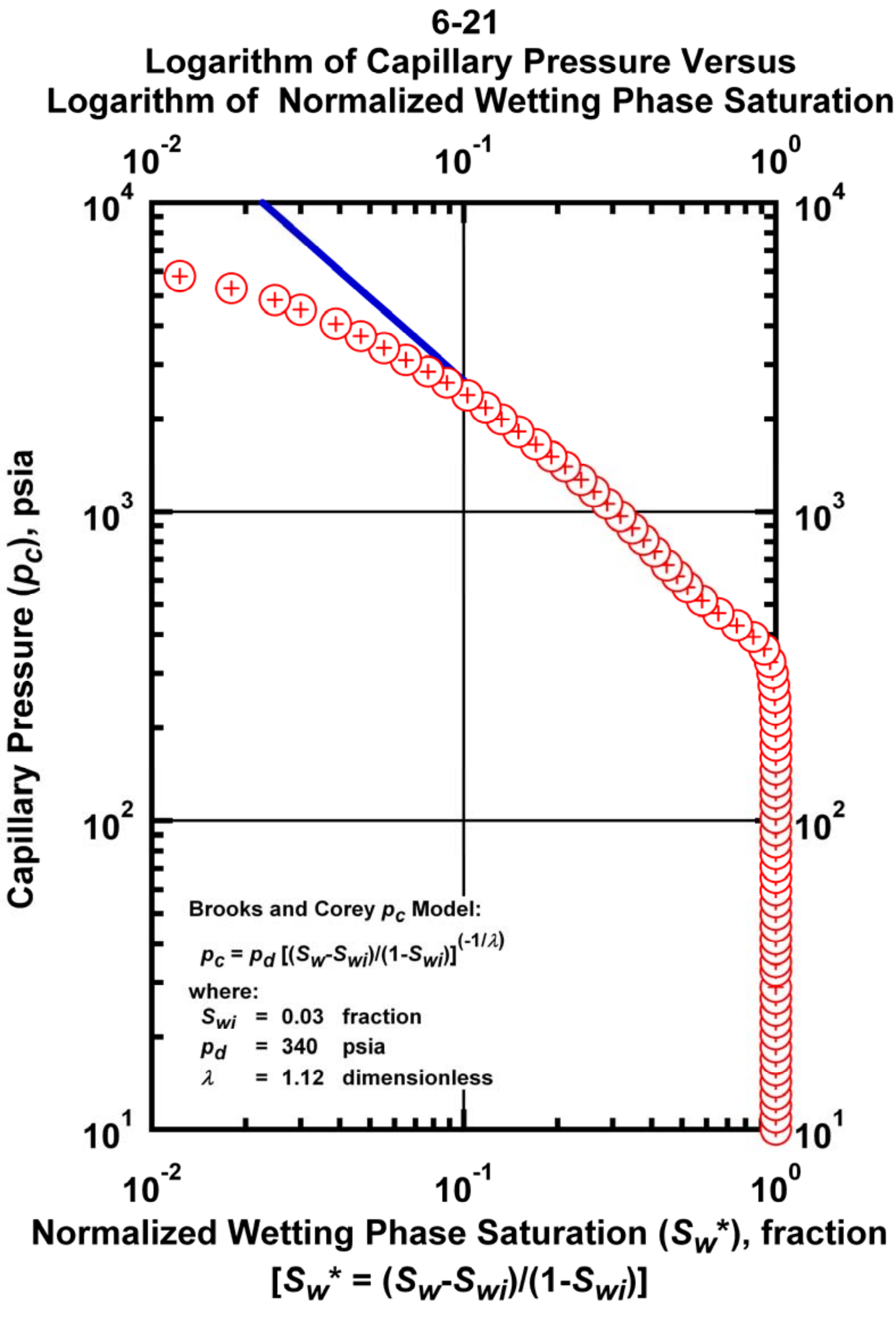

Figure K.13 – Plot of logarithm of capillary pressure vs. logarithm of normalized wetting phase saturation — Case 6-21 HS1.

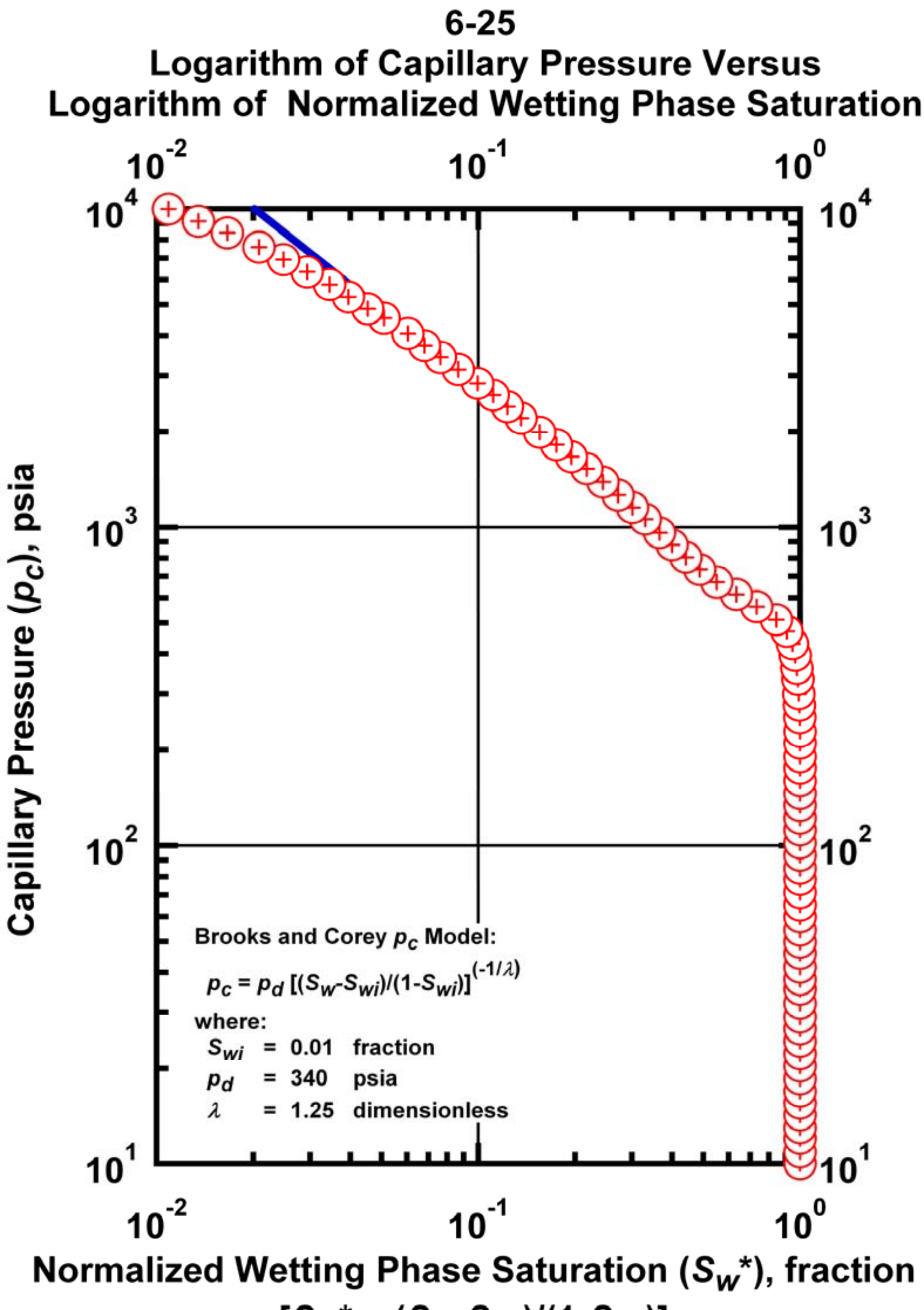

Figure K.14 – Plot of logarithm of capillary pressure vs. logarithm of normalized wetting phase saturation — Case 6-25 HS1.

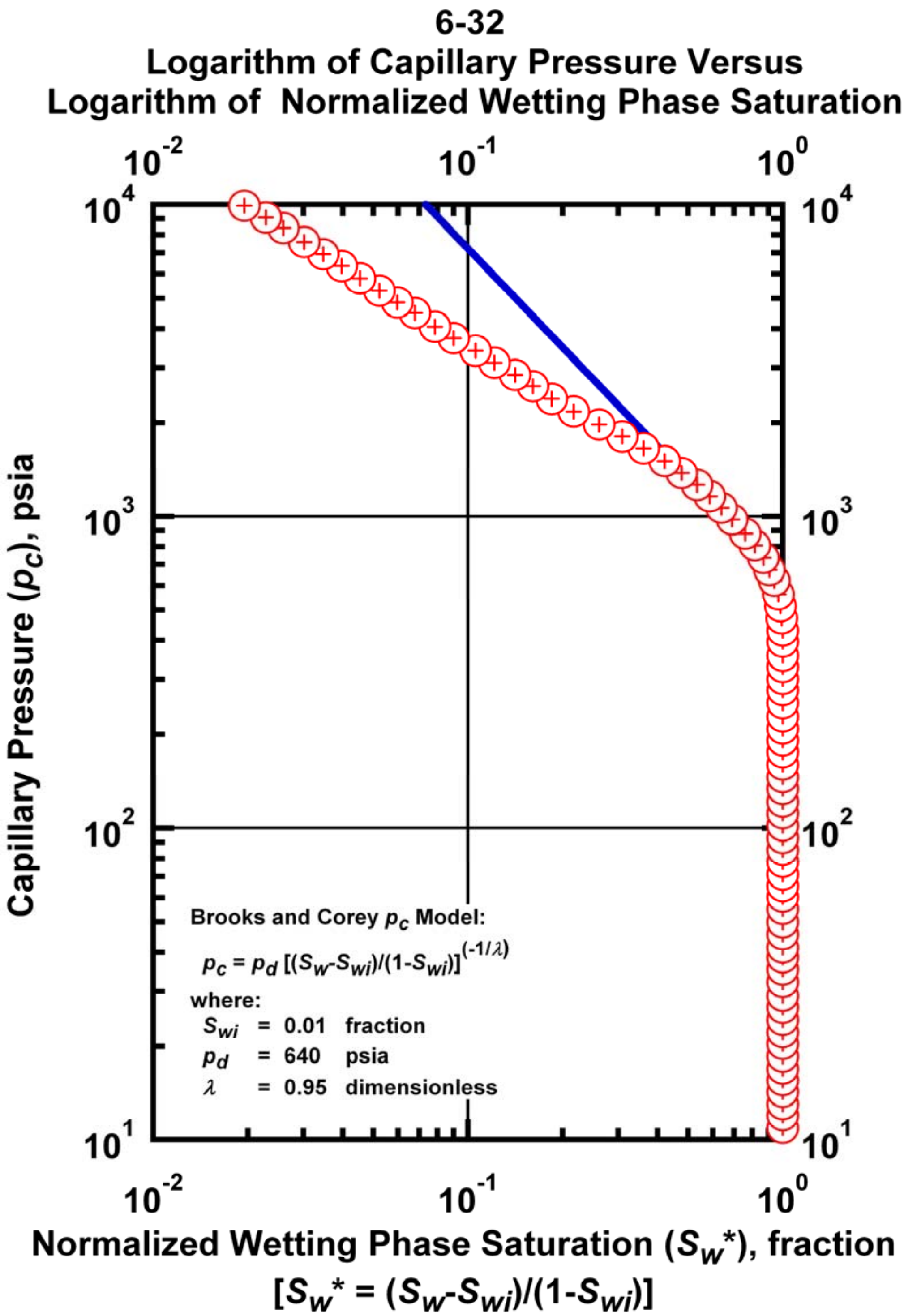

Figure K.15 – Plot of logarithm of capillary pressure vs. logarithm of normalized wetting phase saturation — Case 6-32 HS1.

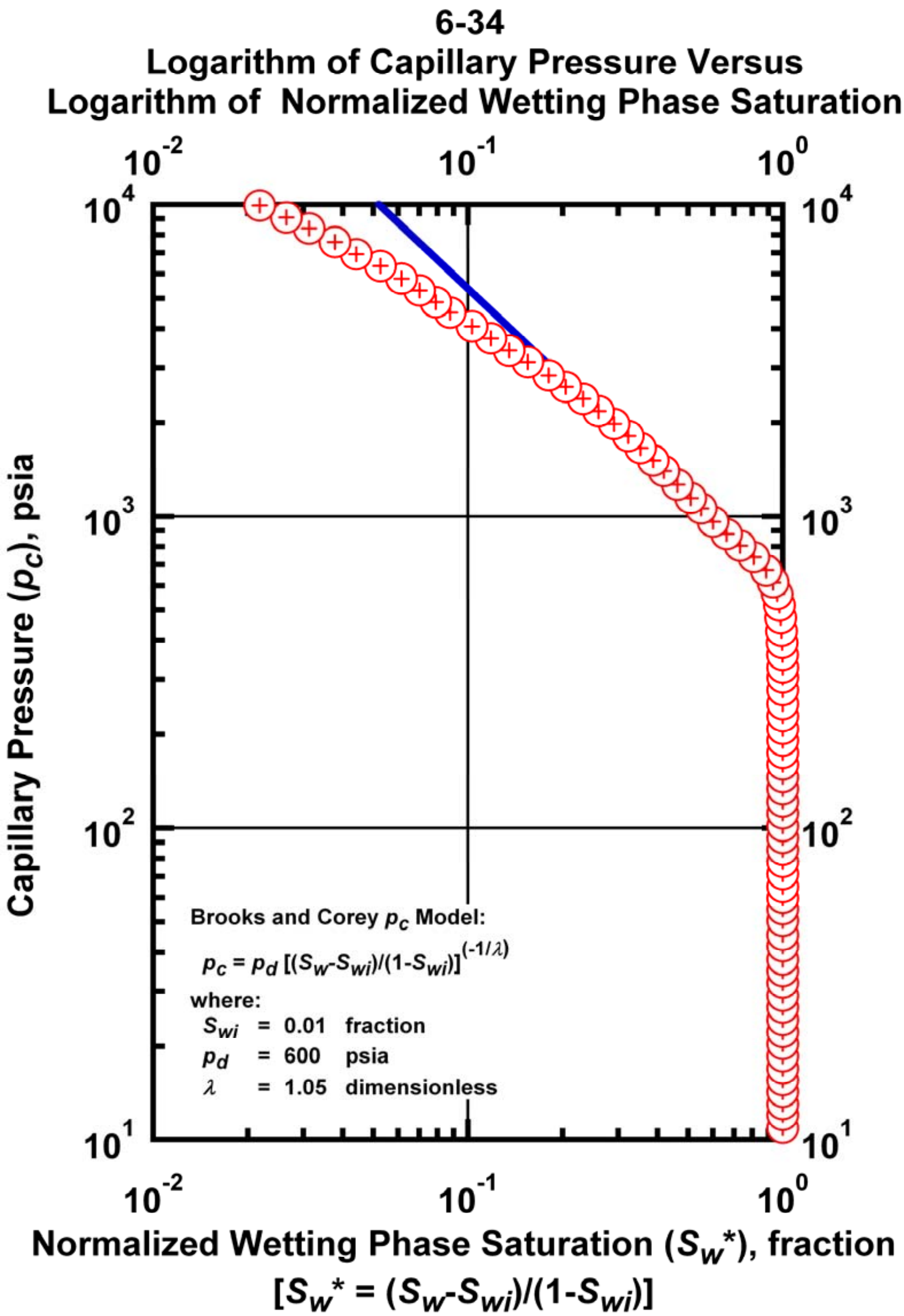

Figure K.16 – Plot of logarithm of capillary pressure vs. logarithm of normalized wetting phase saturation — Case 6-34 HS1.

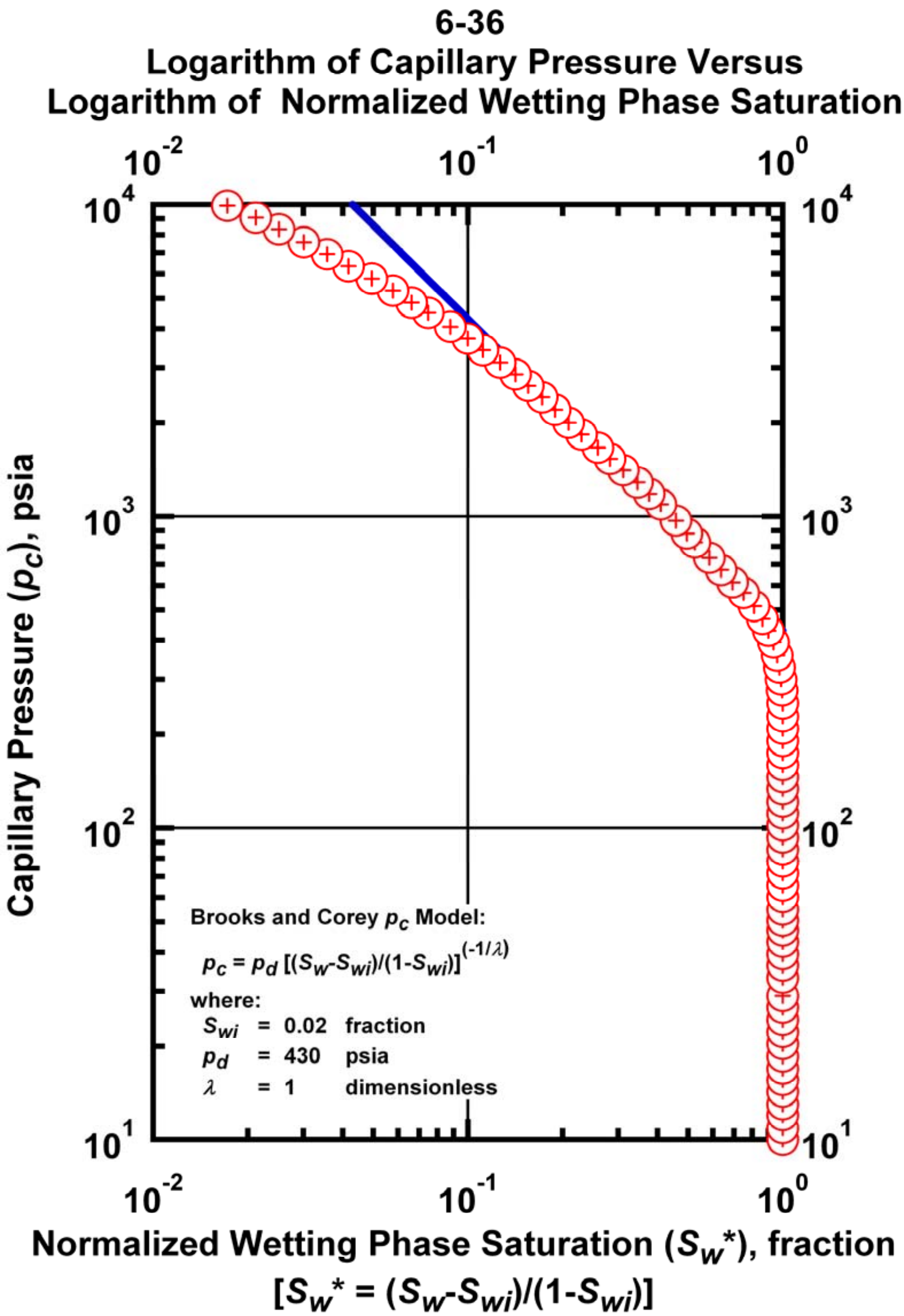

Figure K.17 – Plot of logarithm of capillary pressure vs. logarithm of normalized wetting phase saturation — Case 6-36 HS1.

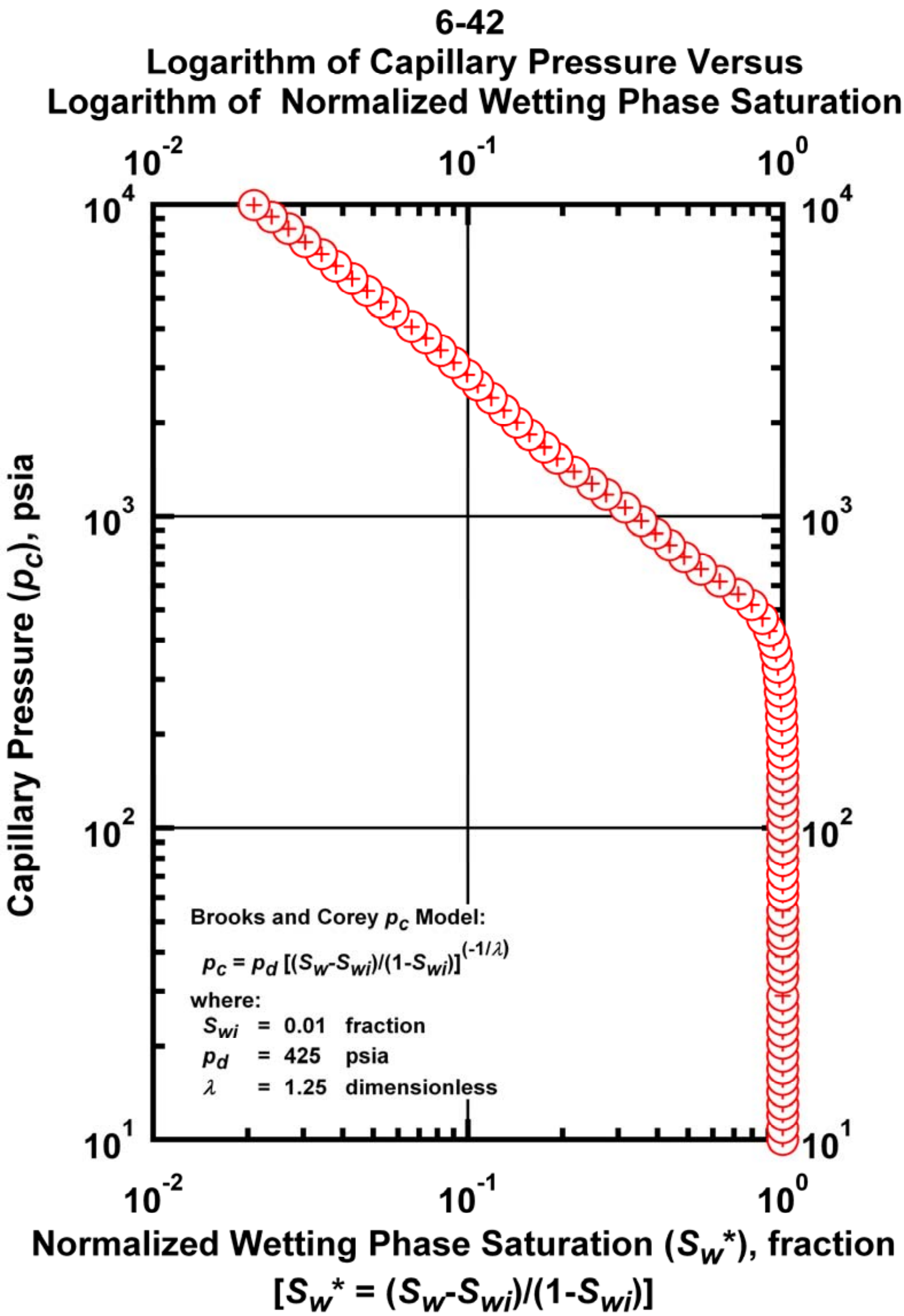

Figure K.18 – Plot of logarithm of capillary pressure vs. logarithm of normalized wetting phase saturation — Case 6-42 HS1.

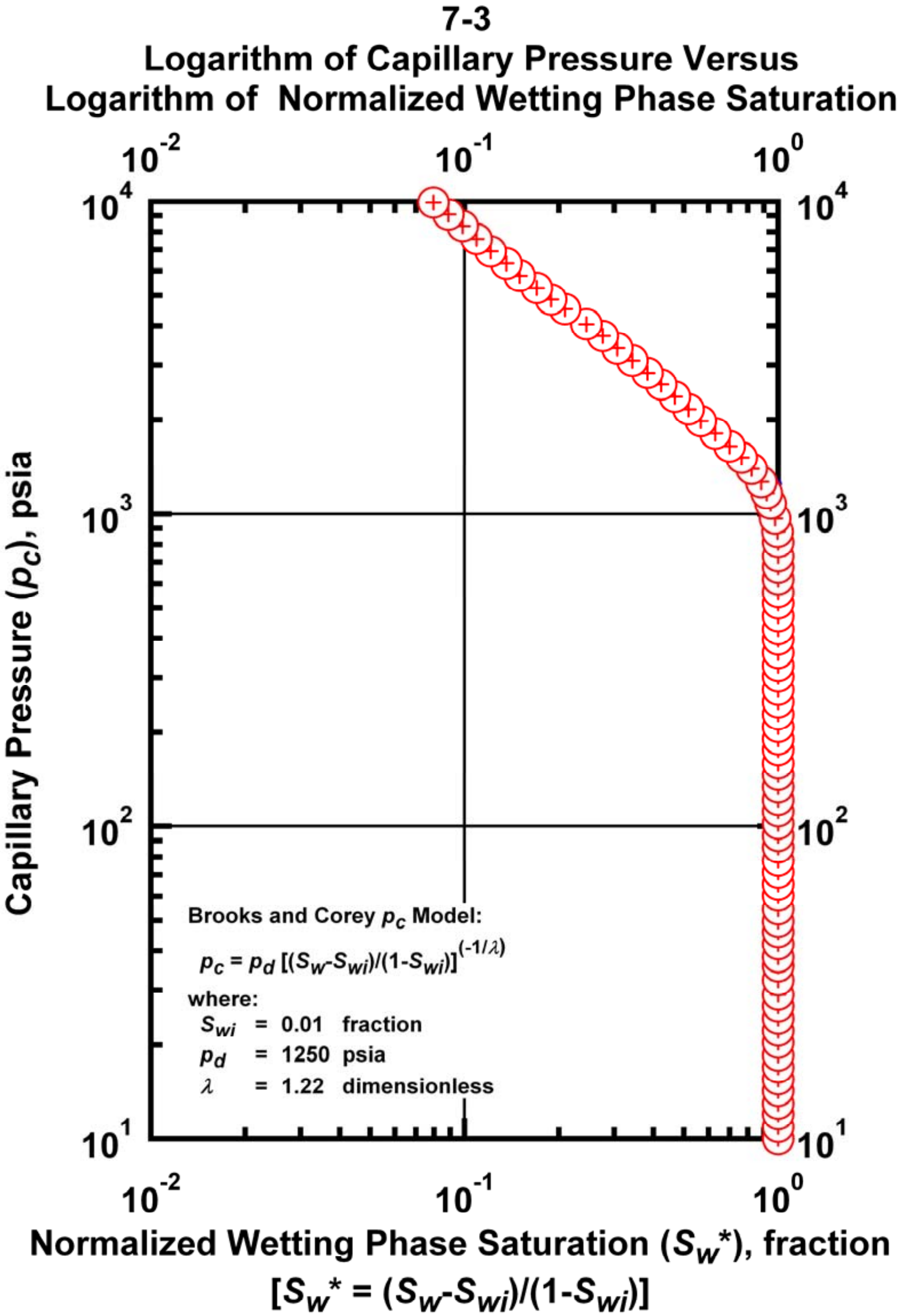

Figure K.19 – Plot of logarithm of capillary pressure vs. logarithm of normalized wetting phase saturation — Case 7-3 HS1.

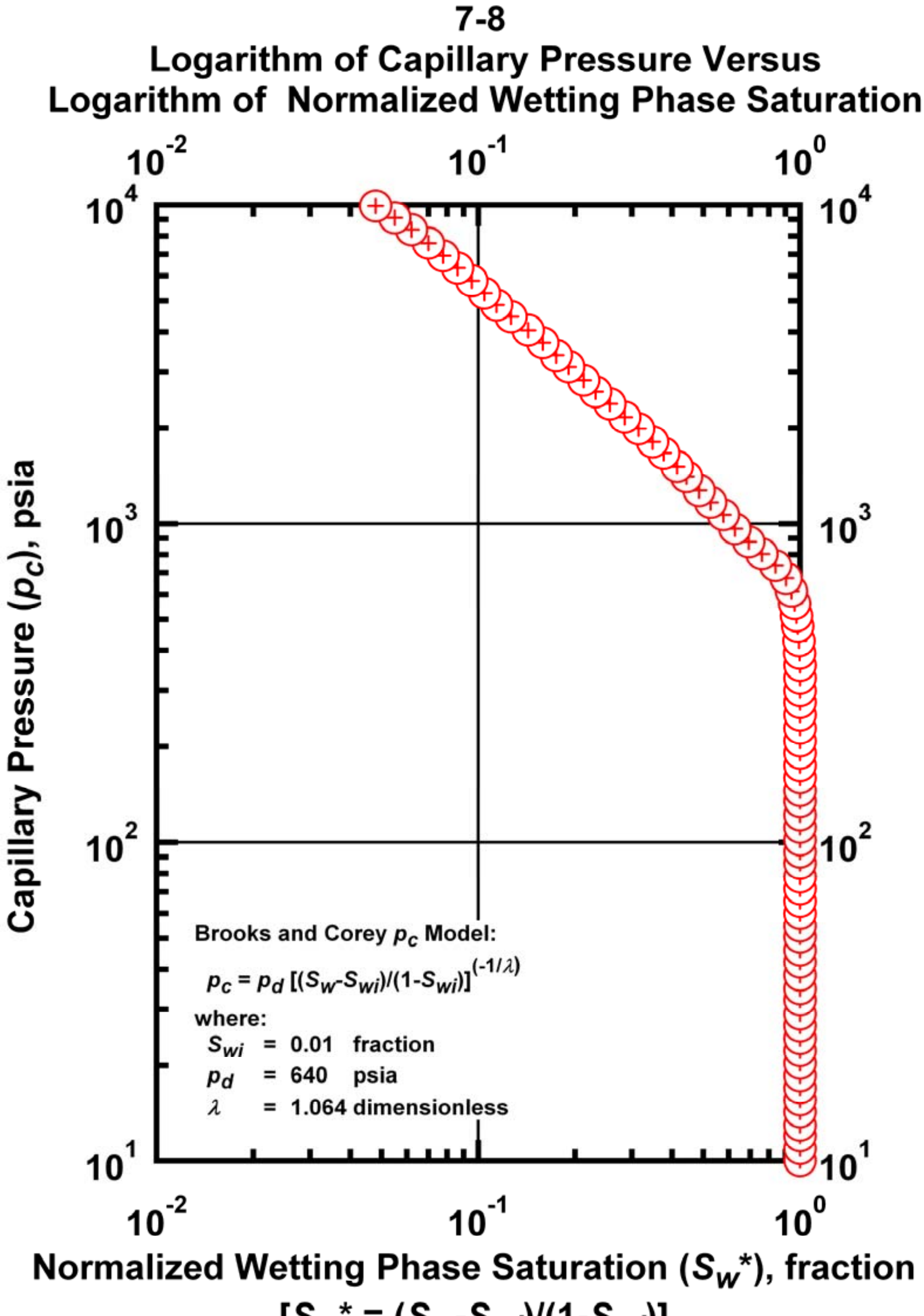

Figure K.20 – Plot of logarithm of capillary pressure vs. logarithm of normalized wetting phase saturation — Case 7-8 HS1.

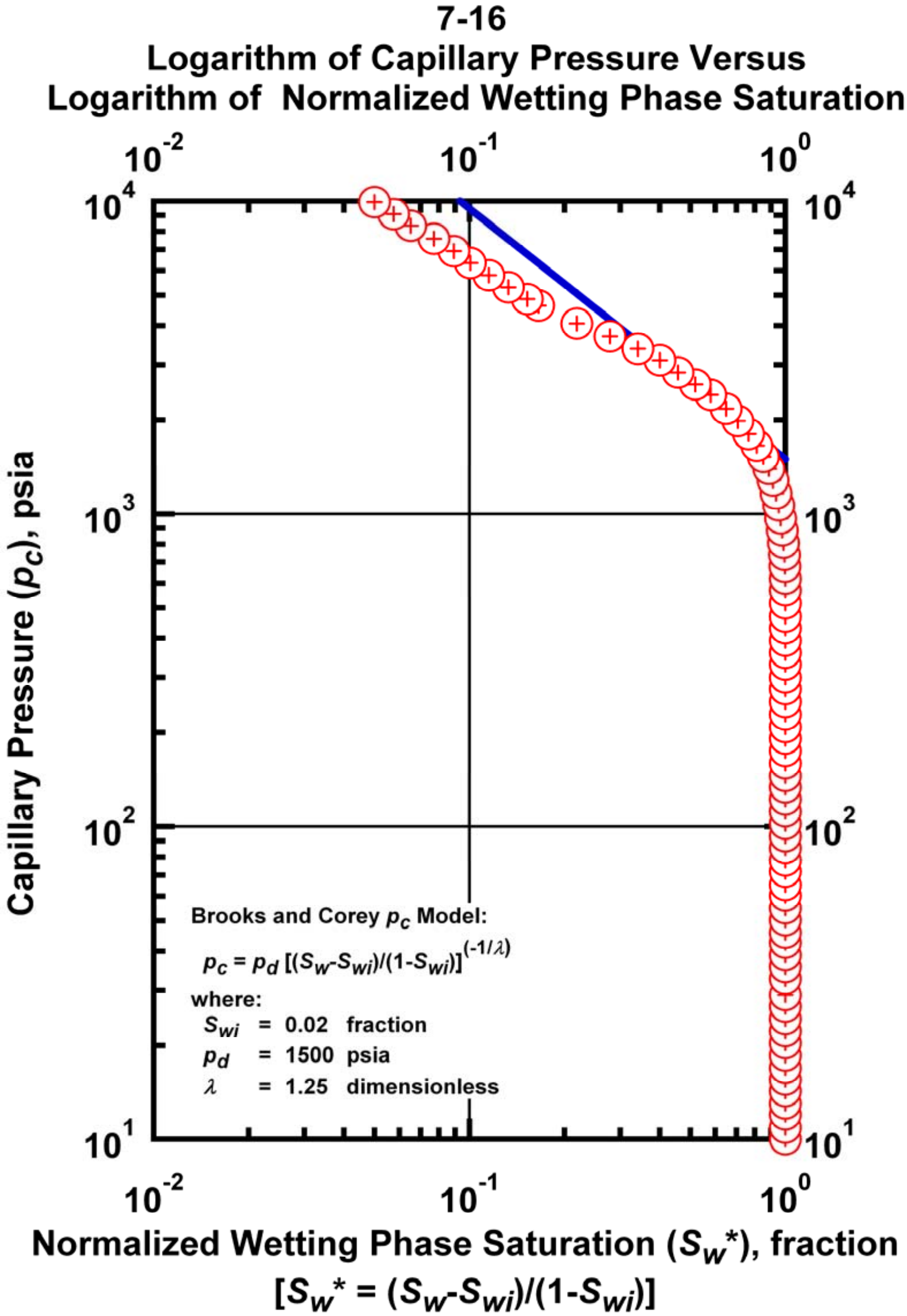

Figure K.21 – Plot of logarithm of capillary pressure vs. logarithm of normalized wetting phase saturation — Case 7-16 HS1.

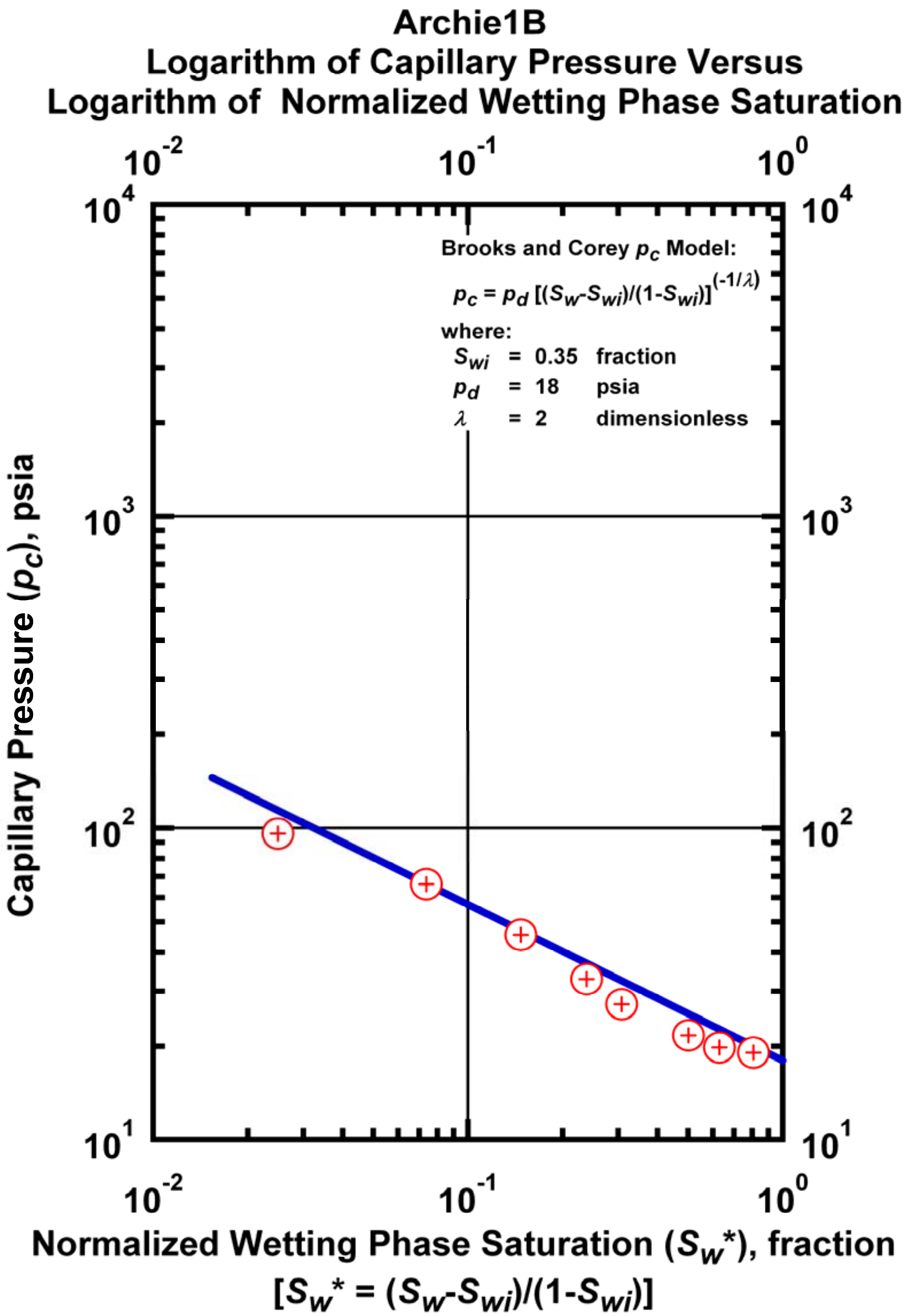

Figure K.22 – Plot of logarithm of capillary pressure vs. logarithm of normalized wetting phase saturation — Case Archie1B.

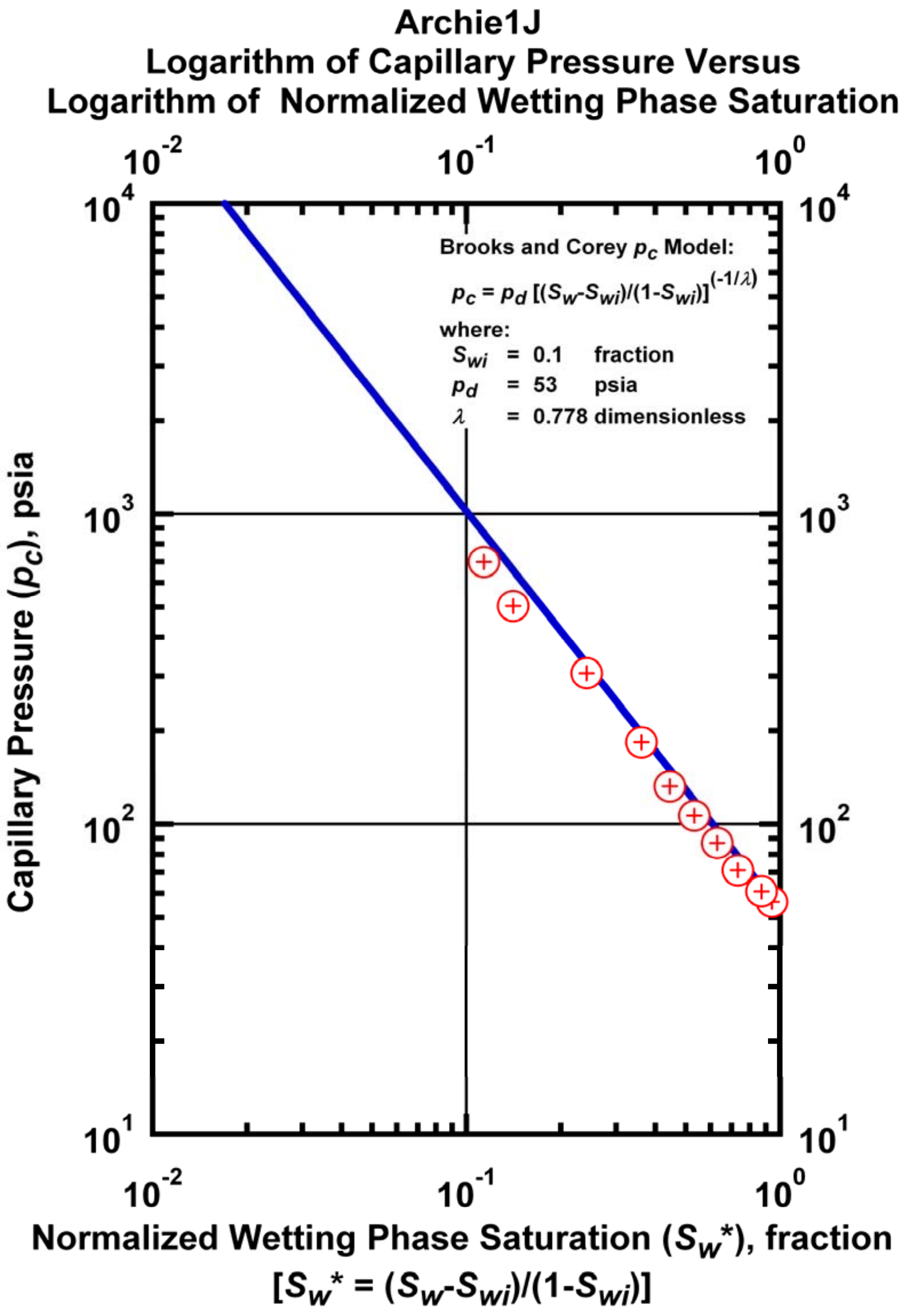

Figure K.23 – Plot of logarithm of capillary pressure vs. logarithm of normalized wetting phase saturation — Case Archie1J.

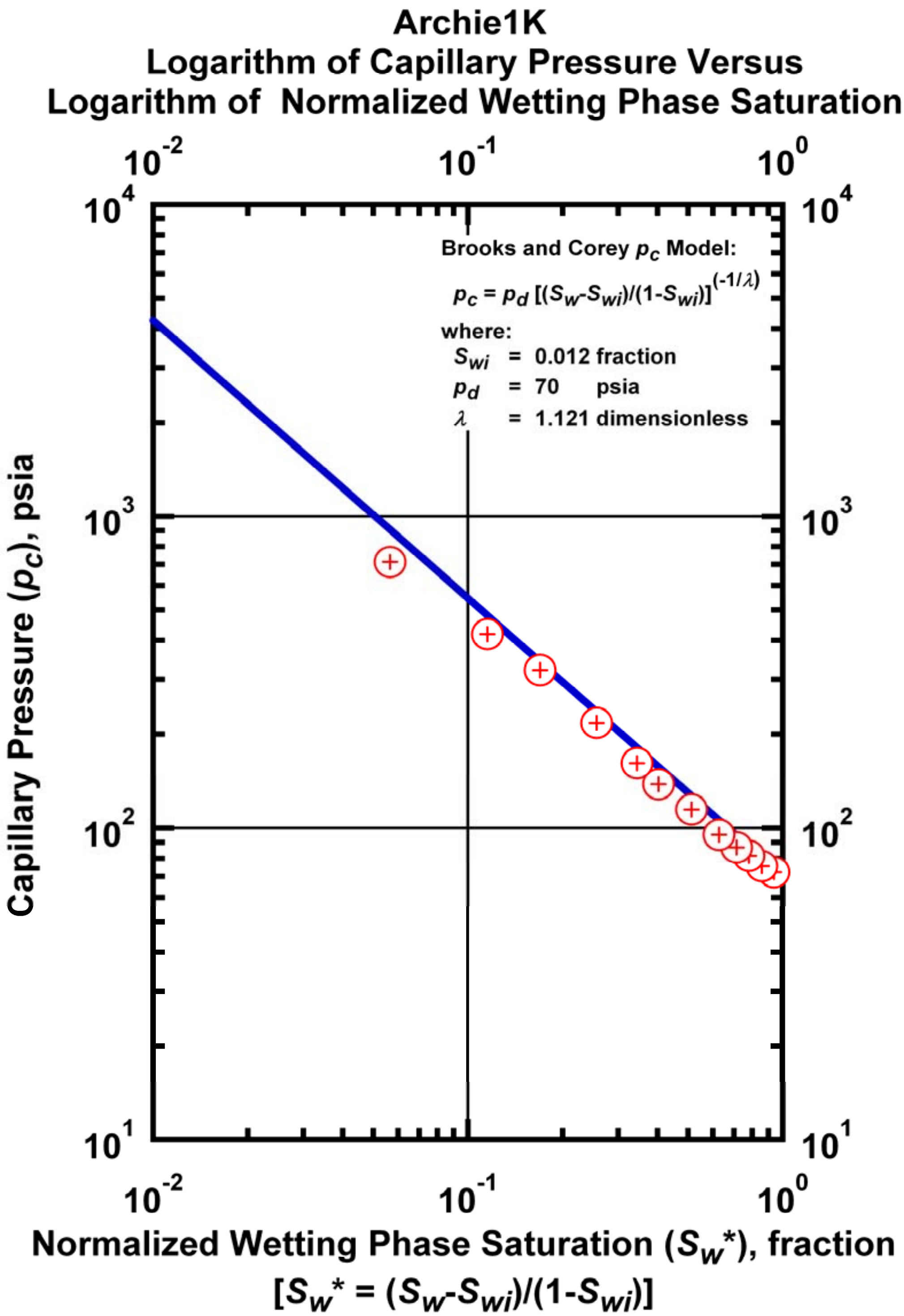

Figure K.24 – Plot of logarithm of capillary pressure vs. logarithm of normalized wetting phase saturation — Case Archie1K.

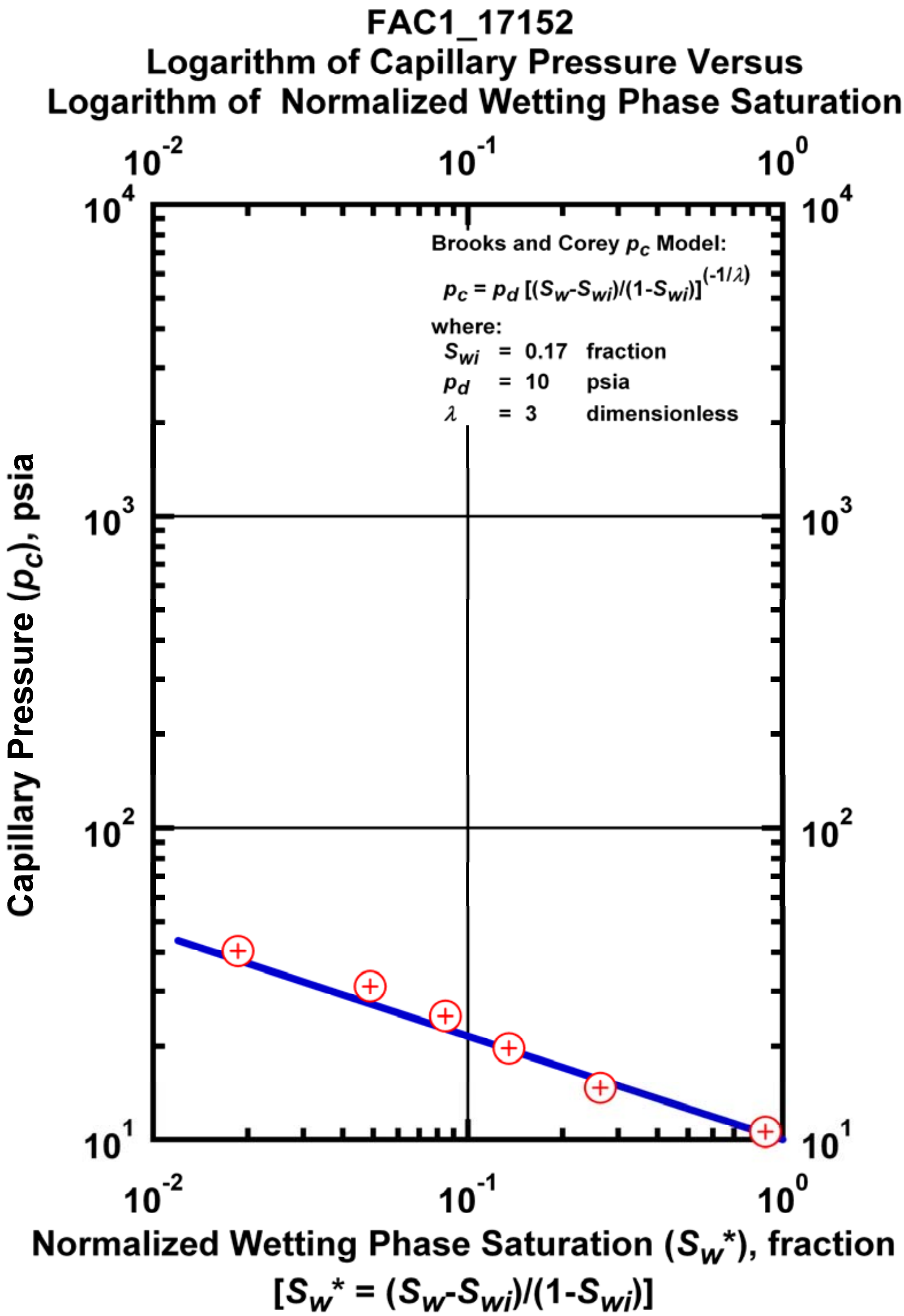

Figure K.25 – Plot of logarithm of capillary pressure vs. logarithm of normalized wetting phase saturation — Case FAC1_17152.

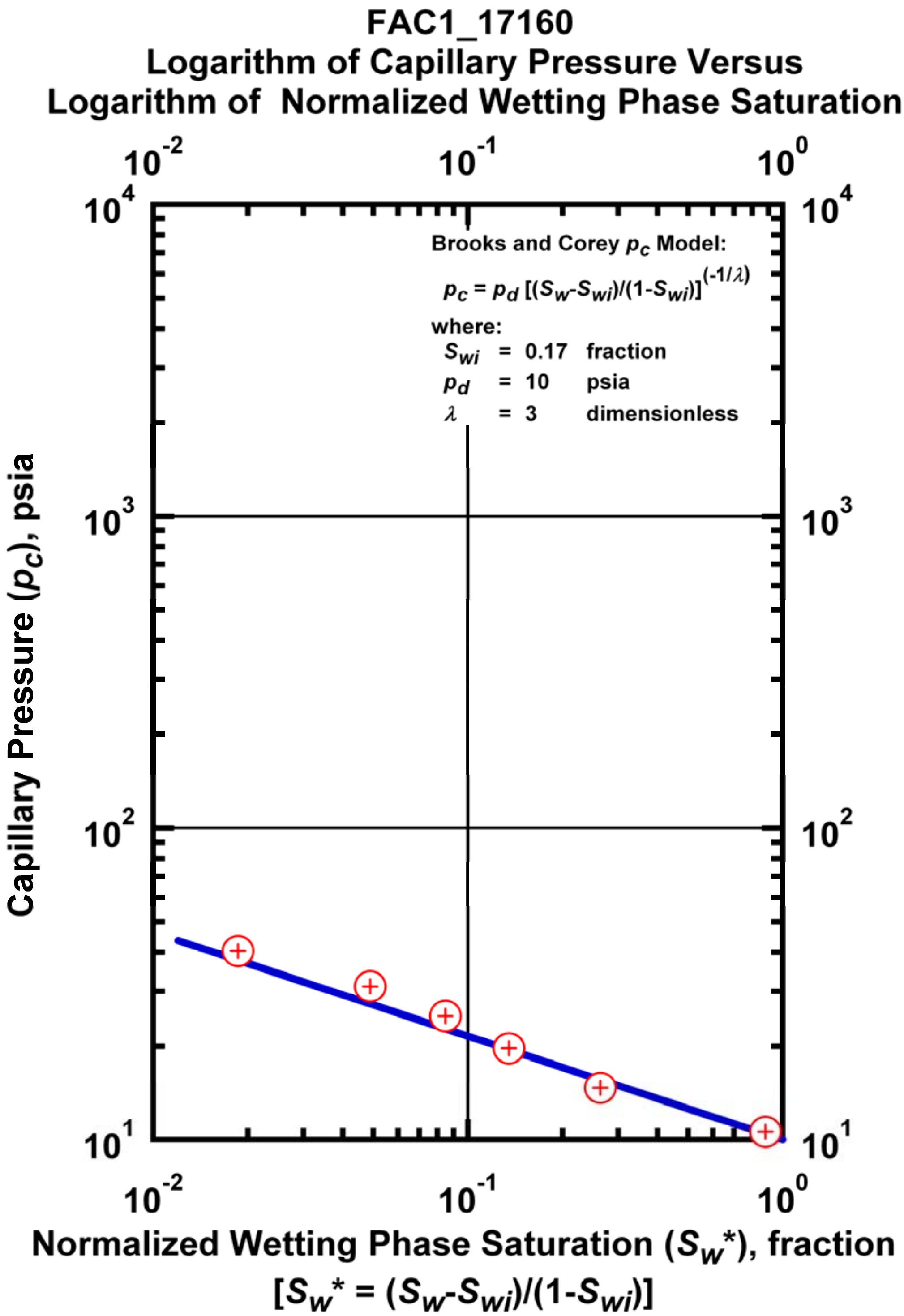

Figure K.26 – Plot of logarithm of capillary pressure vs. logarithm of normalized wetting phase saturation — Case FAC1_17160.

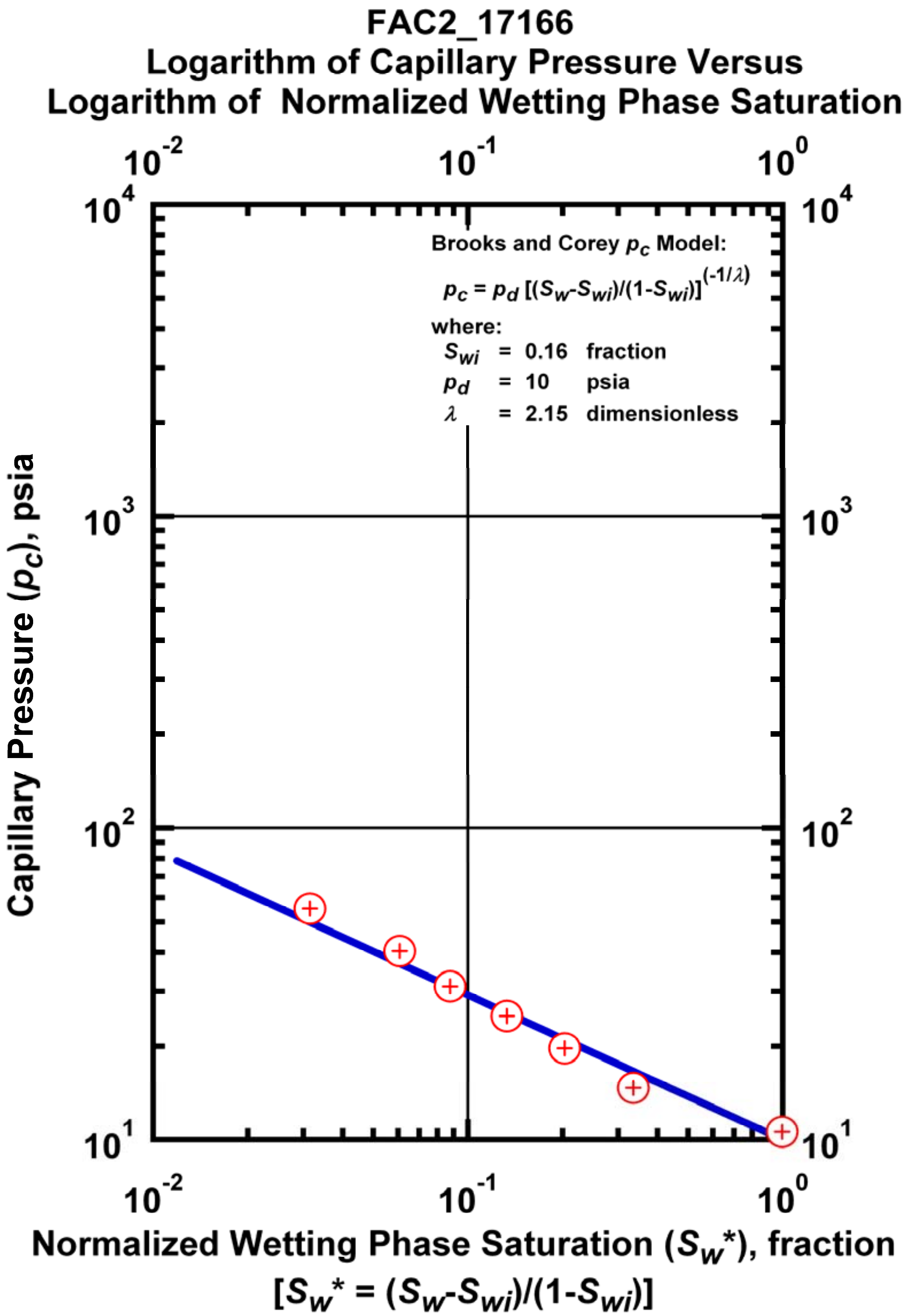

Figure K.27 – Plot of logarithm of capillary pressure vs. logarithm of normalized wetting phase saturation — Case FAC2_17166.

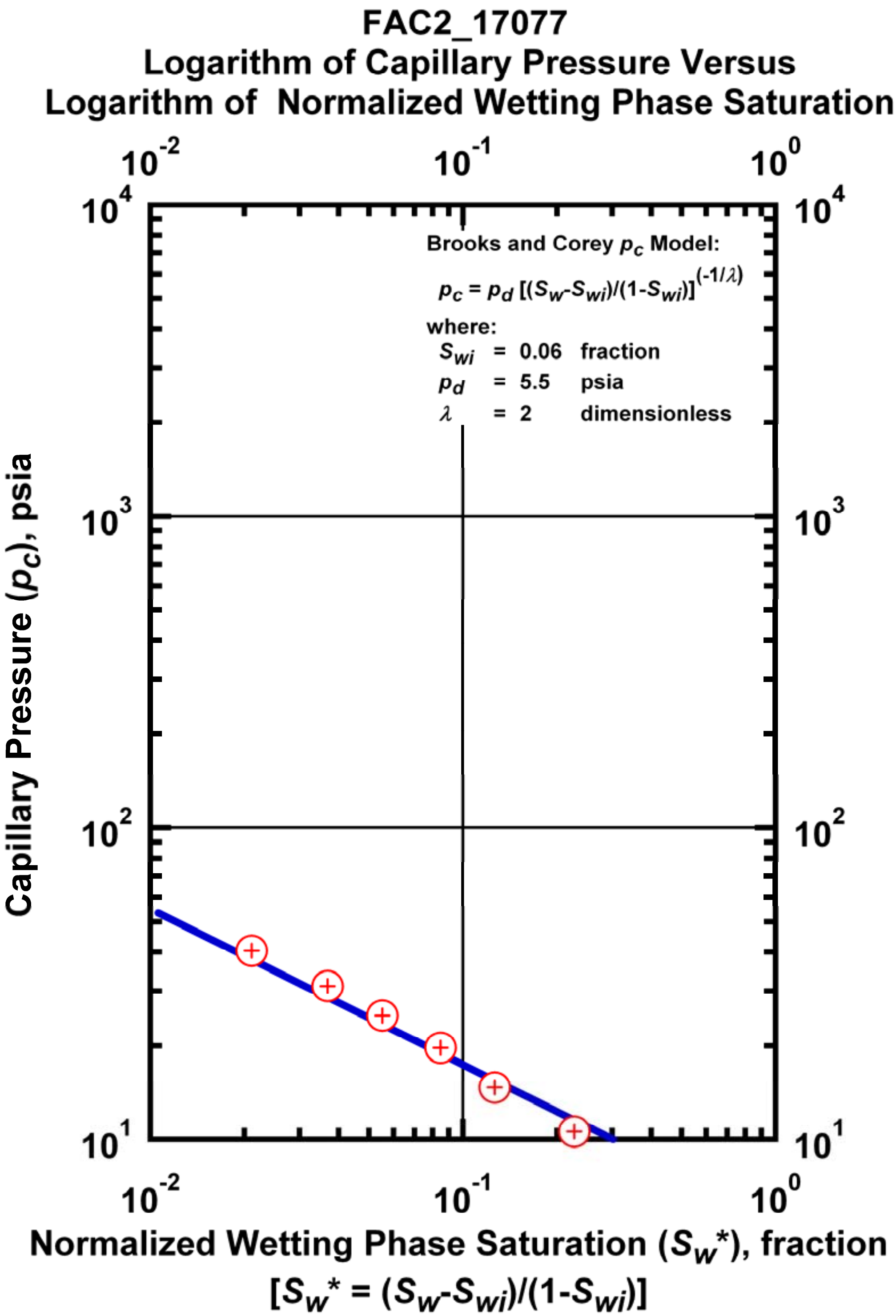

Figure K.28 – Plot of logarithm of capillary pressure vs. logarithm of normalized wetting phase saturation — Case FAC2_17077.

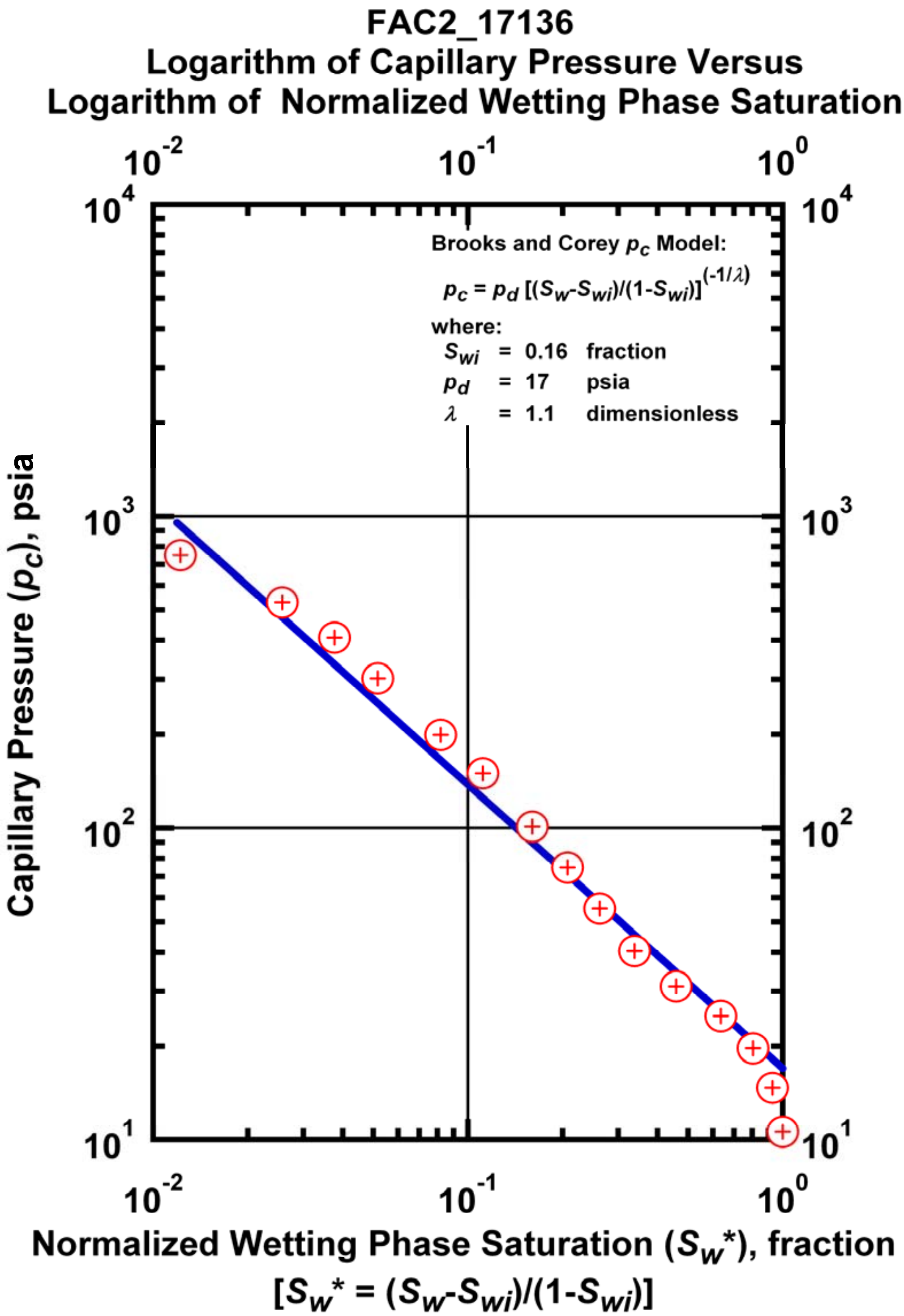

Figure K.29 – Plot of logarithm of capillary pressure vs. logarithm of normalized wetting phase saturation — Case FAC2_17136.

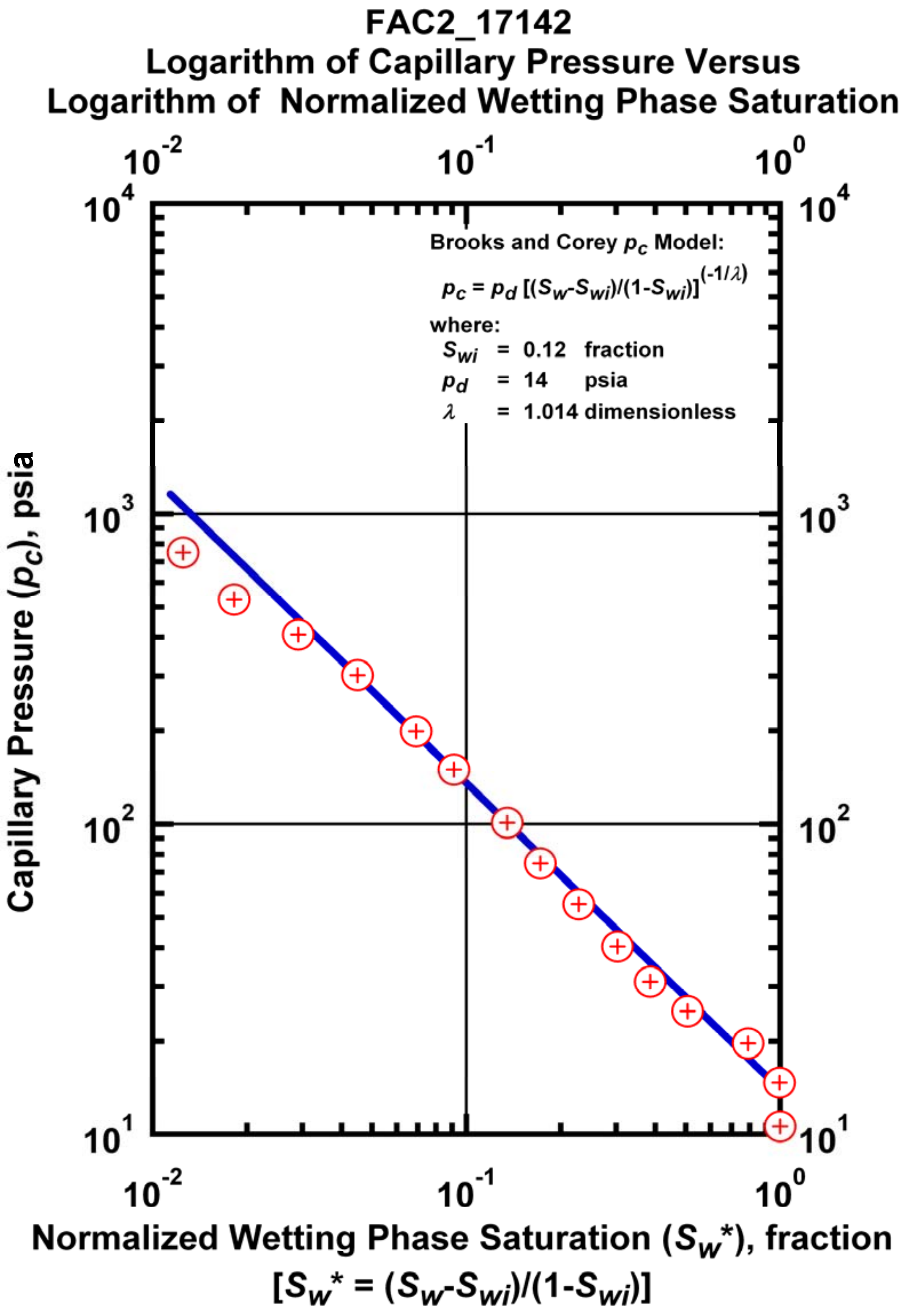

Figure K.30 – Plot of logarithm of capillary pressure vs. logarithm of normalized wetting phase saturation — Case FAC2_17142.

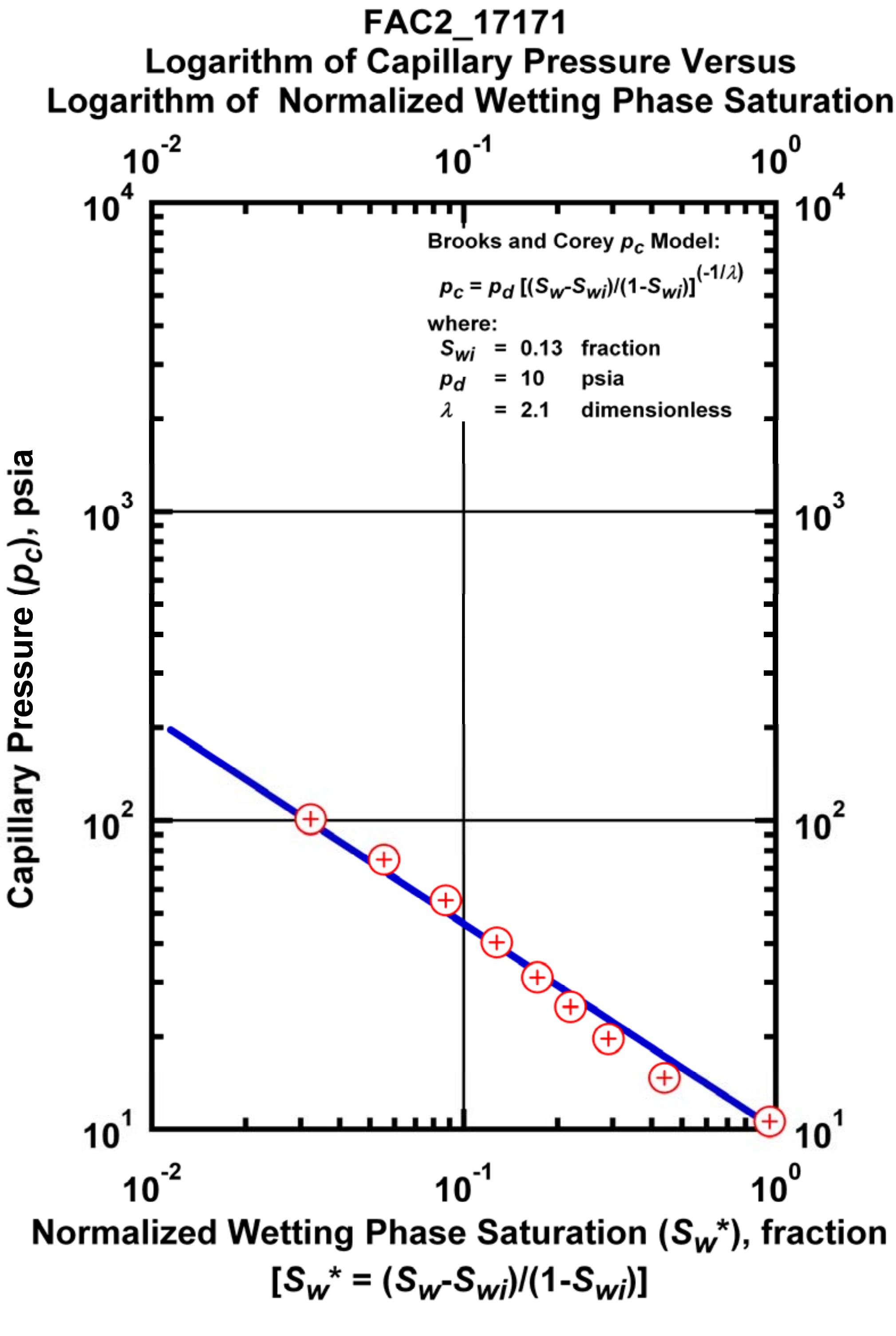

Figure K.31 – Plot of logarithm of capillary pressure vs. logarithm of normalized wetting phase saturation — Case FAC2_17171.

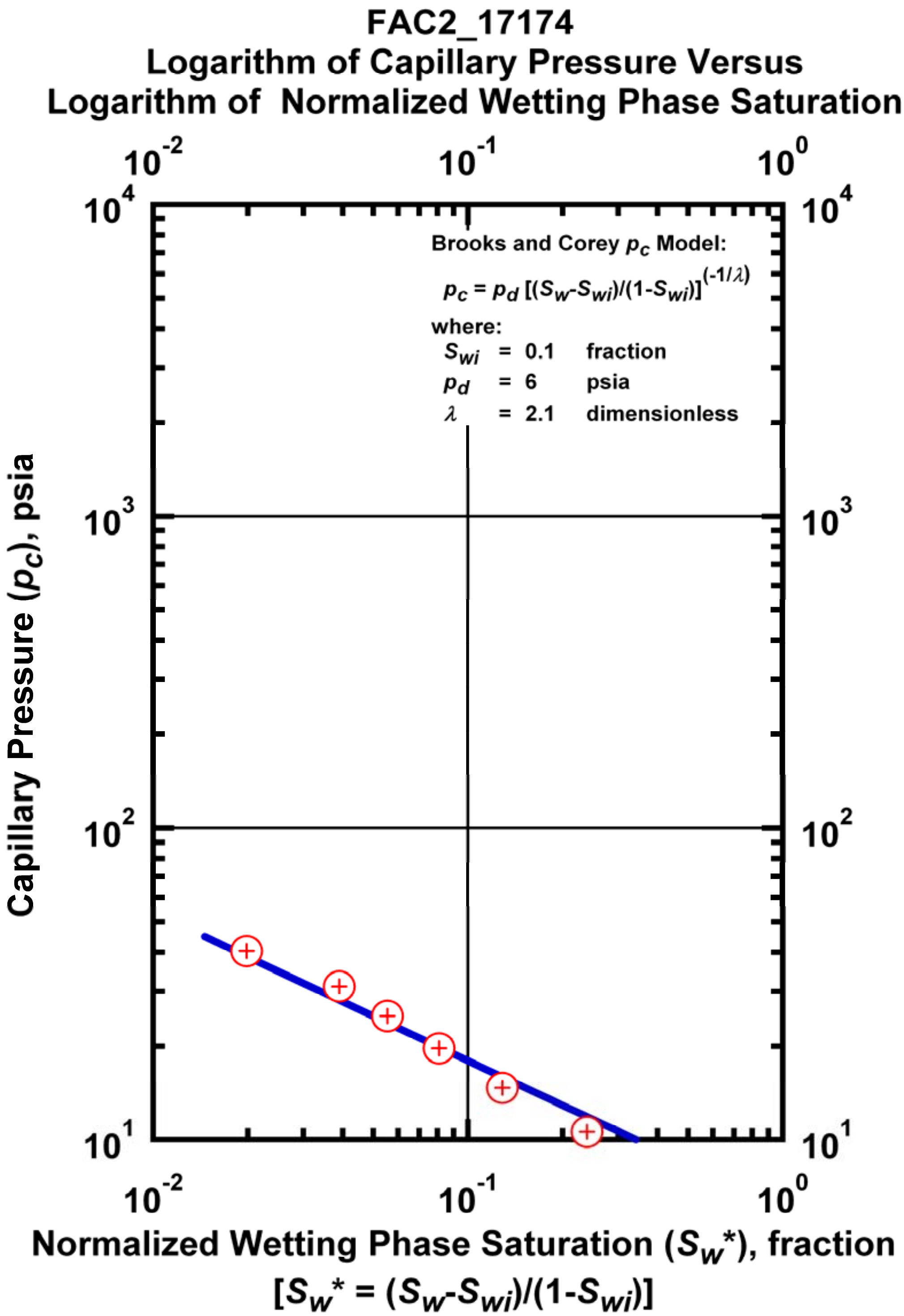

Figure K.32 – Plot of logarithm of capillary pressure vs. logarithm of normalized wetting phase saturation — Case FAC2_17174.

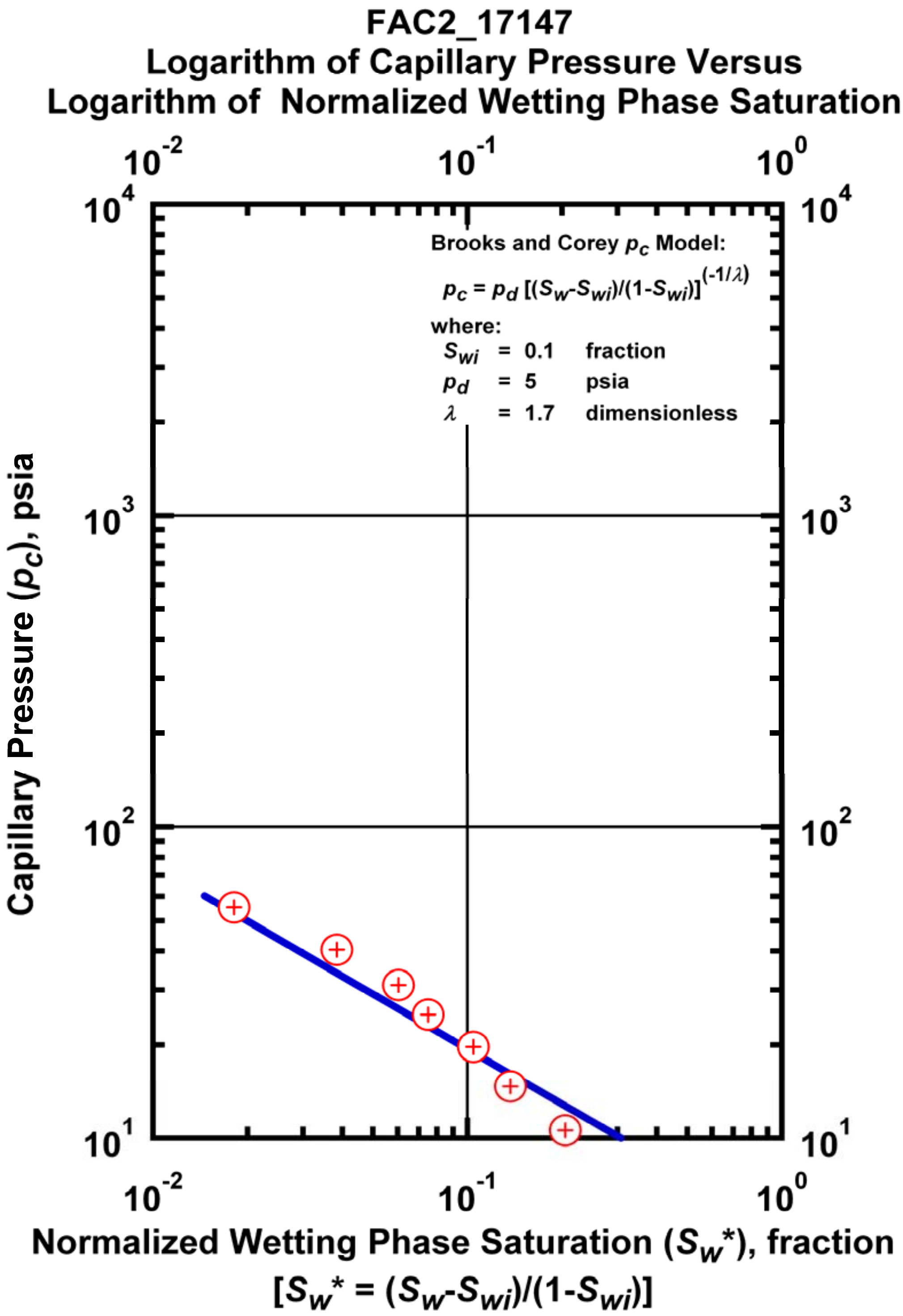

Figure K.33 – Plot of logarithm of capillary pressure vs. logarithm of normalized wetting phase saturation — Case FAC2_17147.

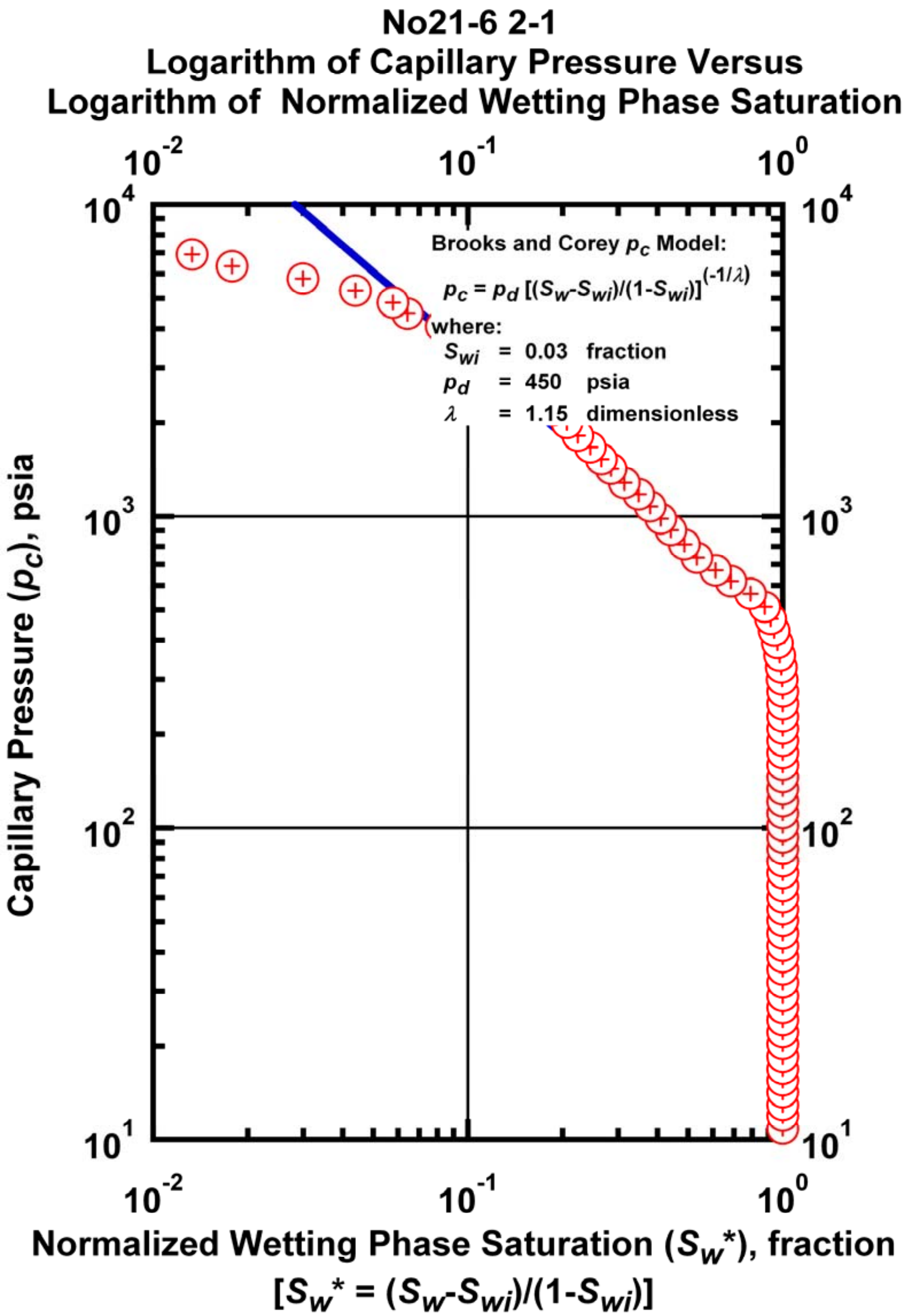

Figure K.34 – Plot of logarithm of capillary pressure vs. logarithm of normalized wetting phase saturation — Case No21-6 2-1.

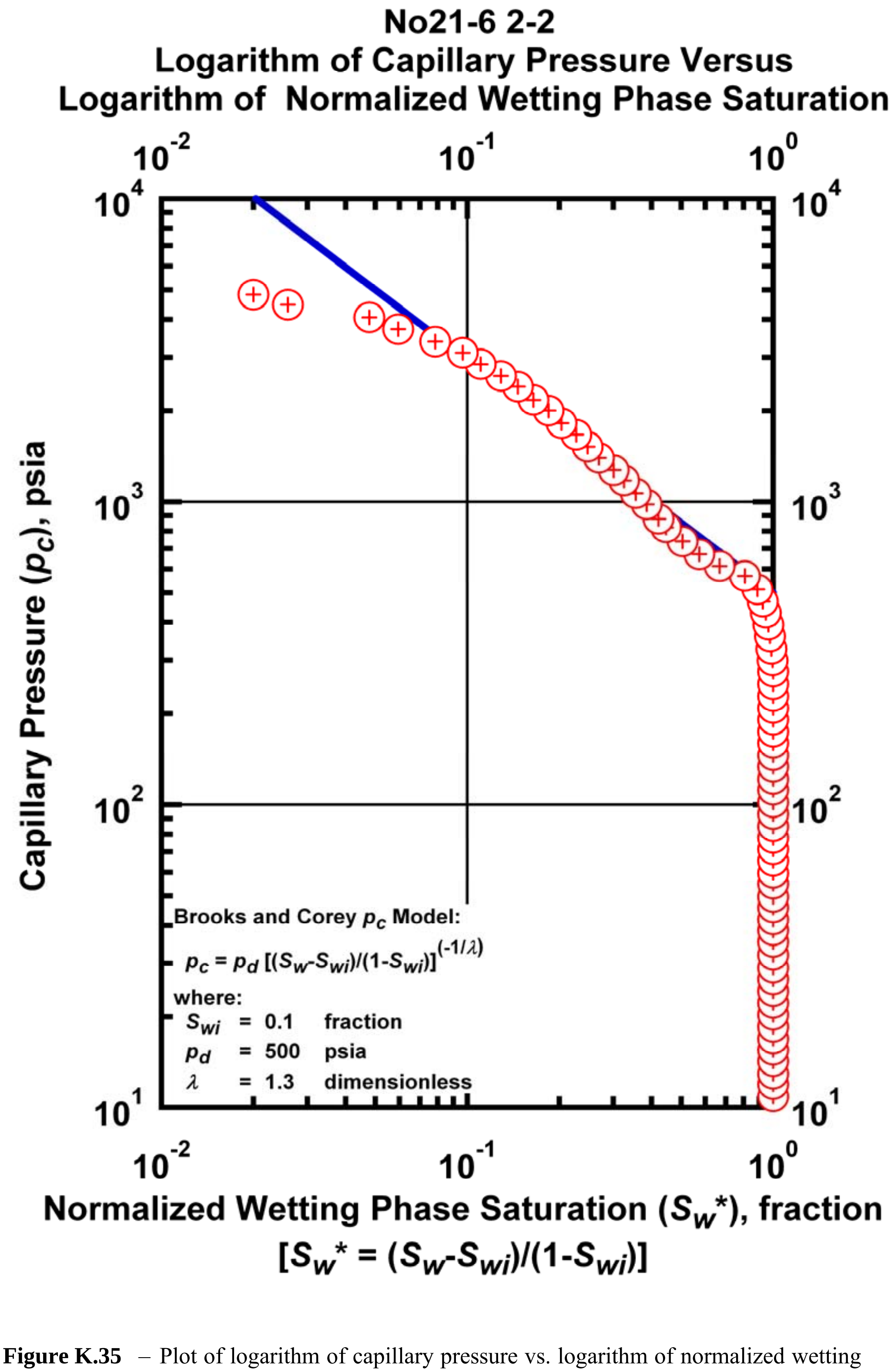

Figure K.35 – Plot of logarithm of capillary pressure vs. logarithm of normalized wetting phase saturation — Case No21-6 2-2.

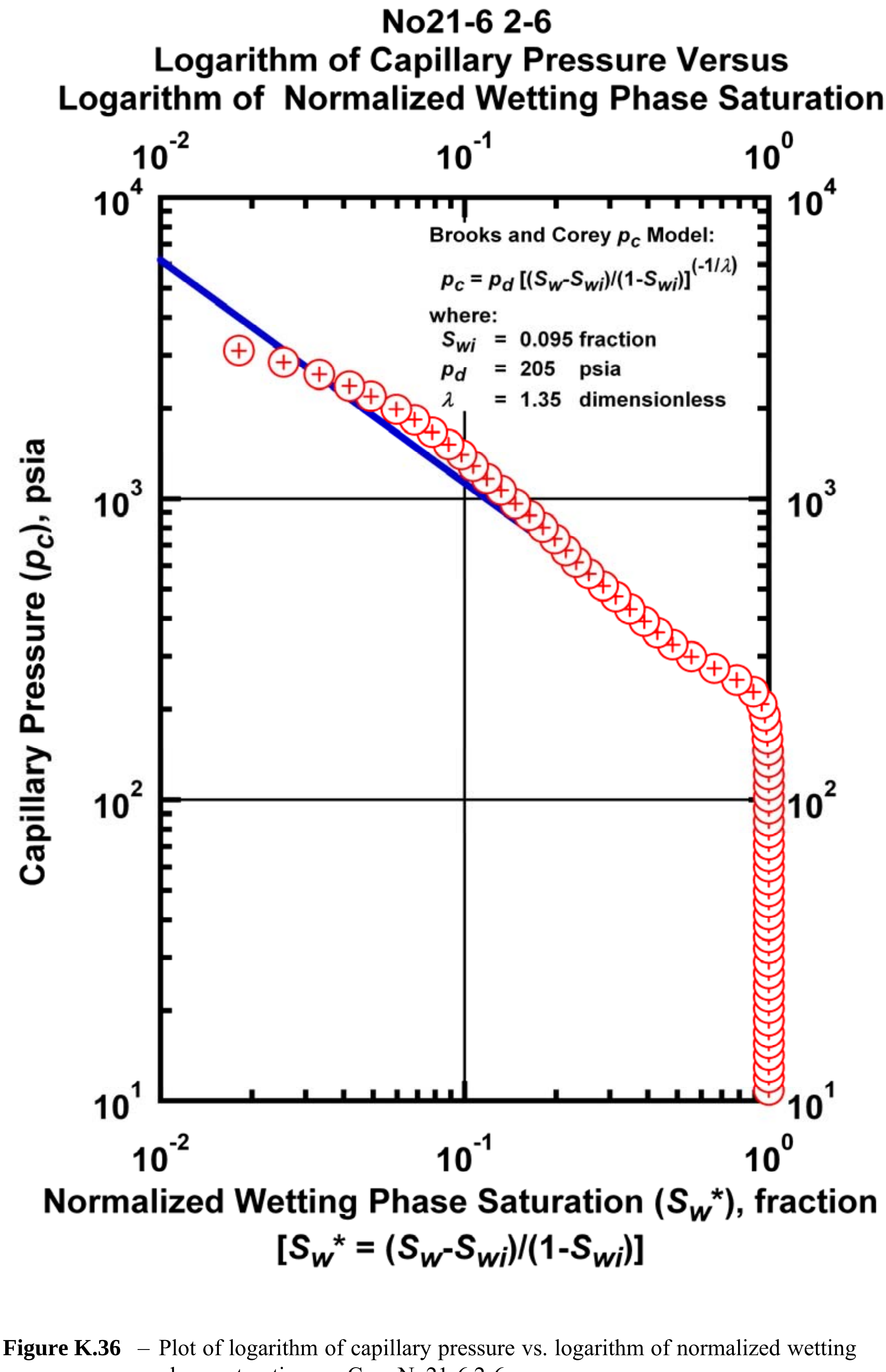

Figure K.36 – Plot of logarithm of capillary pressure vs. logarithm of normalized wetting phase saturation — Case No21-6 2-6.

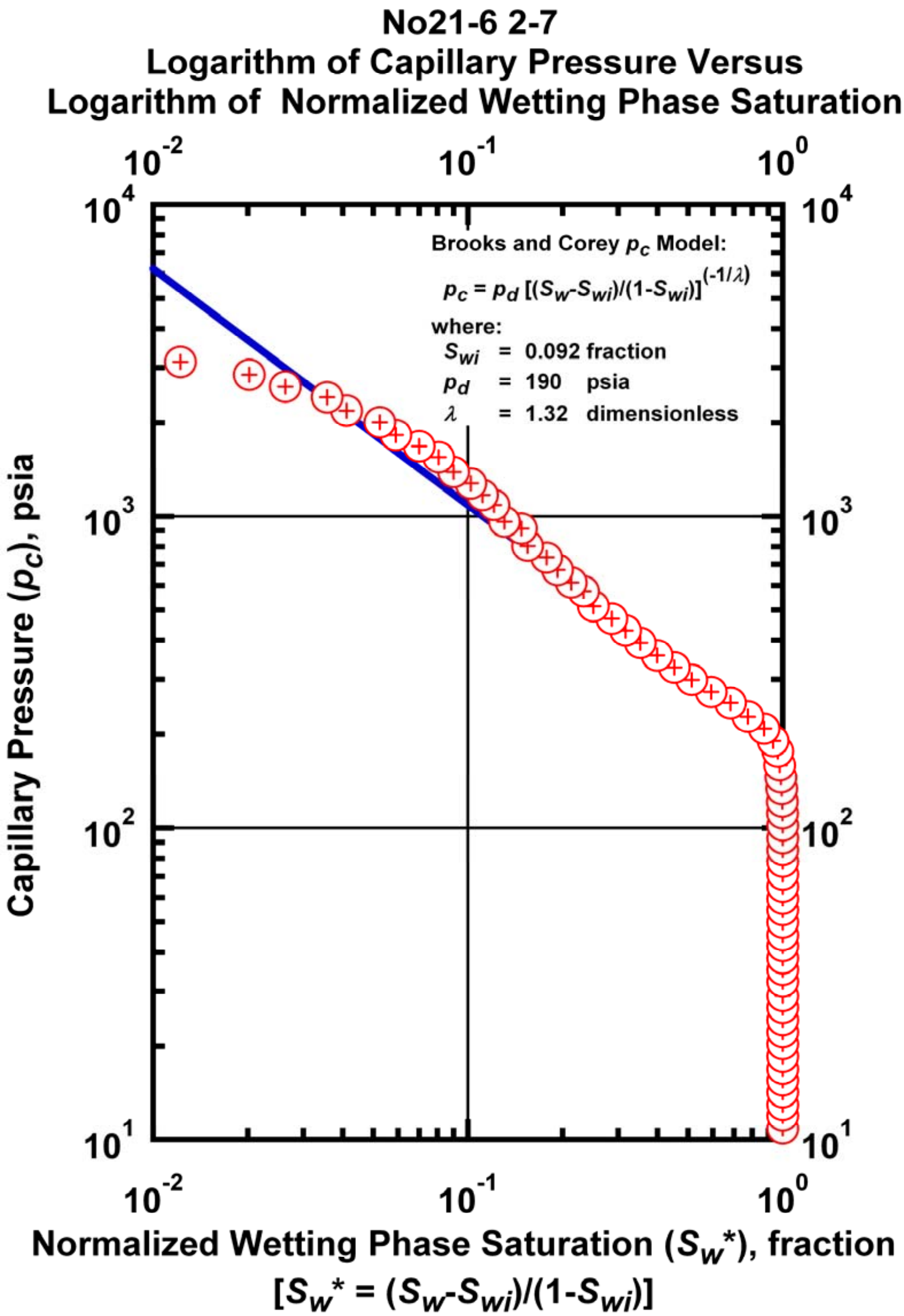

Figure K.37 – Plot of logarithm of capillary pressure vs. logarithm of normalized wetting phase saturation — Case No21-6 2-7.

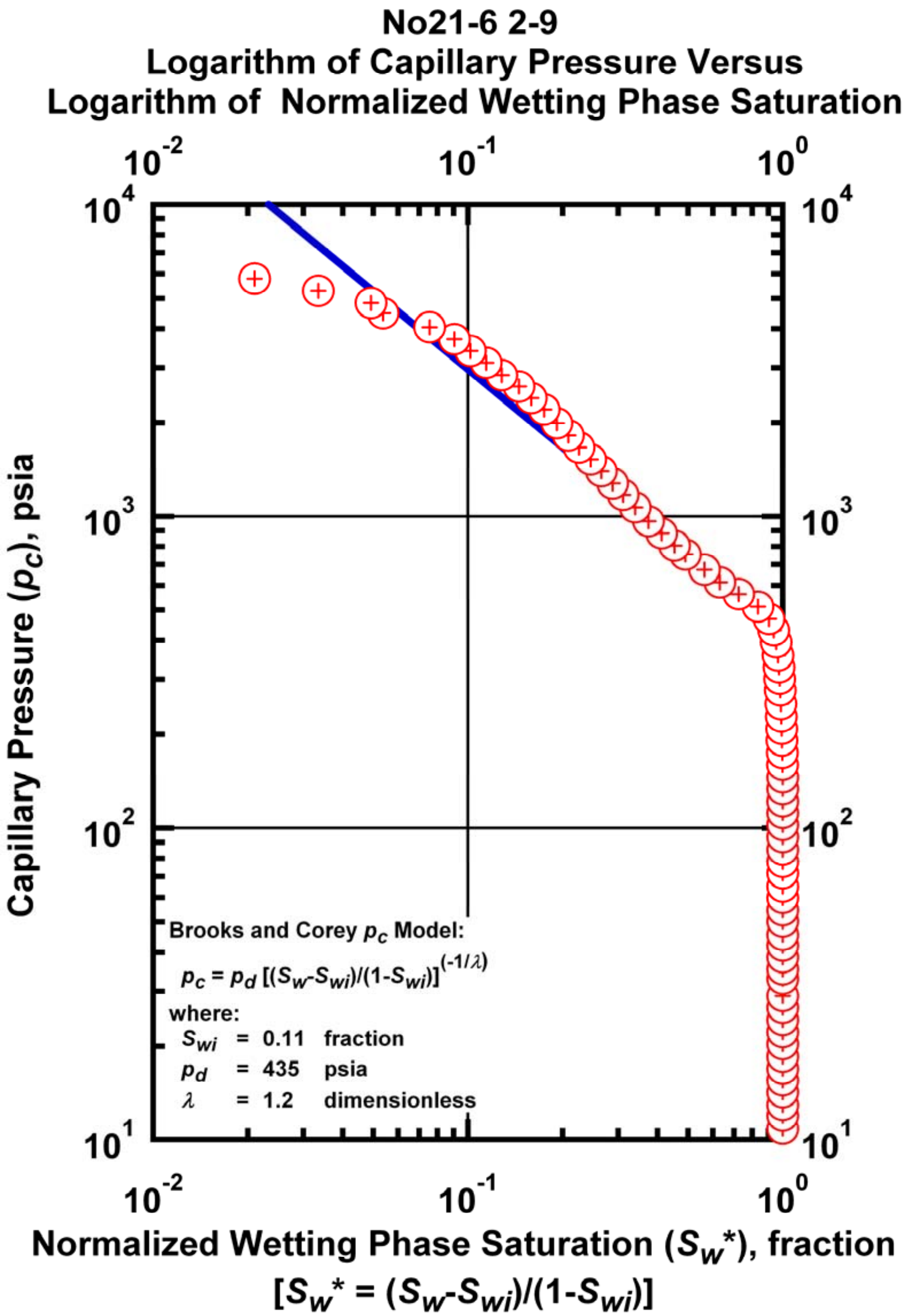

Figure K.38 – Plot of logarithm of capillary pressure vs. logarithm of normalized wetting phase saturation — Case No21-6 2-9.

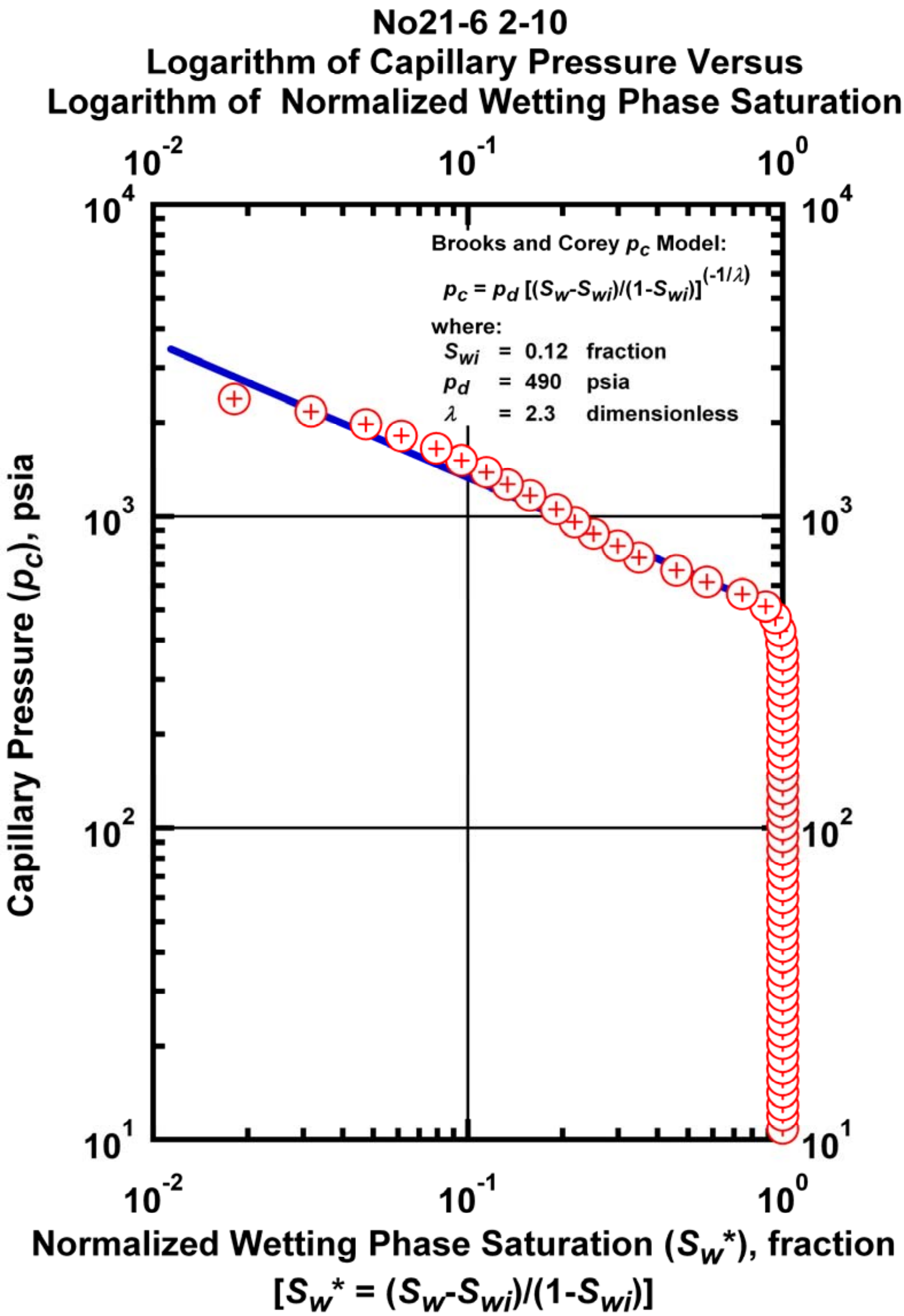

Figure K.39 – Plot of logarithm of capillary pressure vs. logarithm of normalized wetting phase saturation — Case No21-6 2-10.

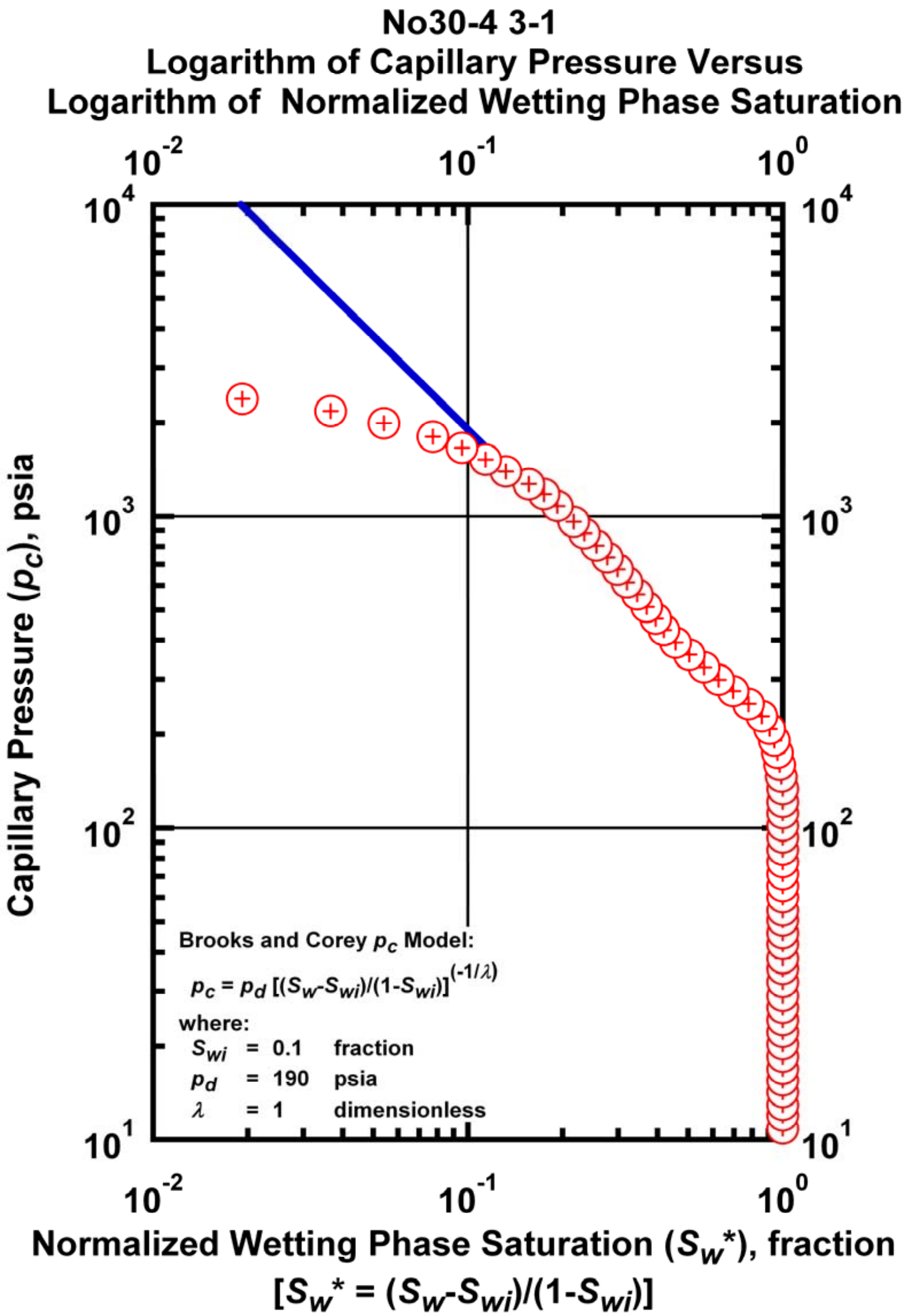

Figure K.40 – Plot of logarithm of capillary pressure vs. logarithm of normalized wetting phase saturation — Case No30-4 3-1.

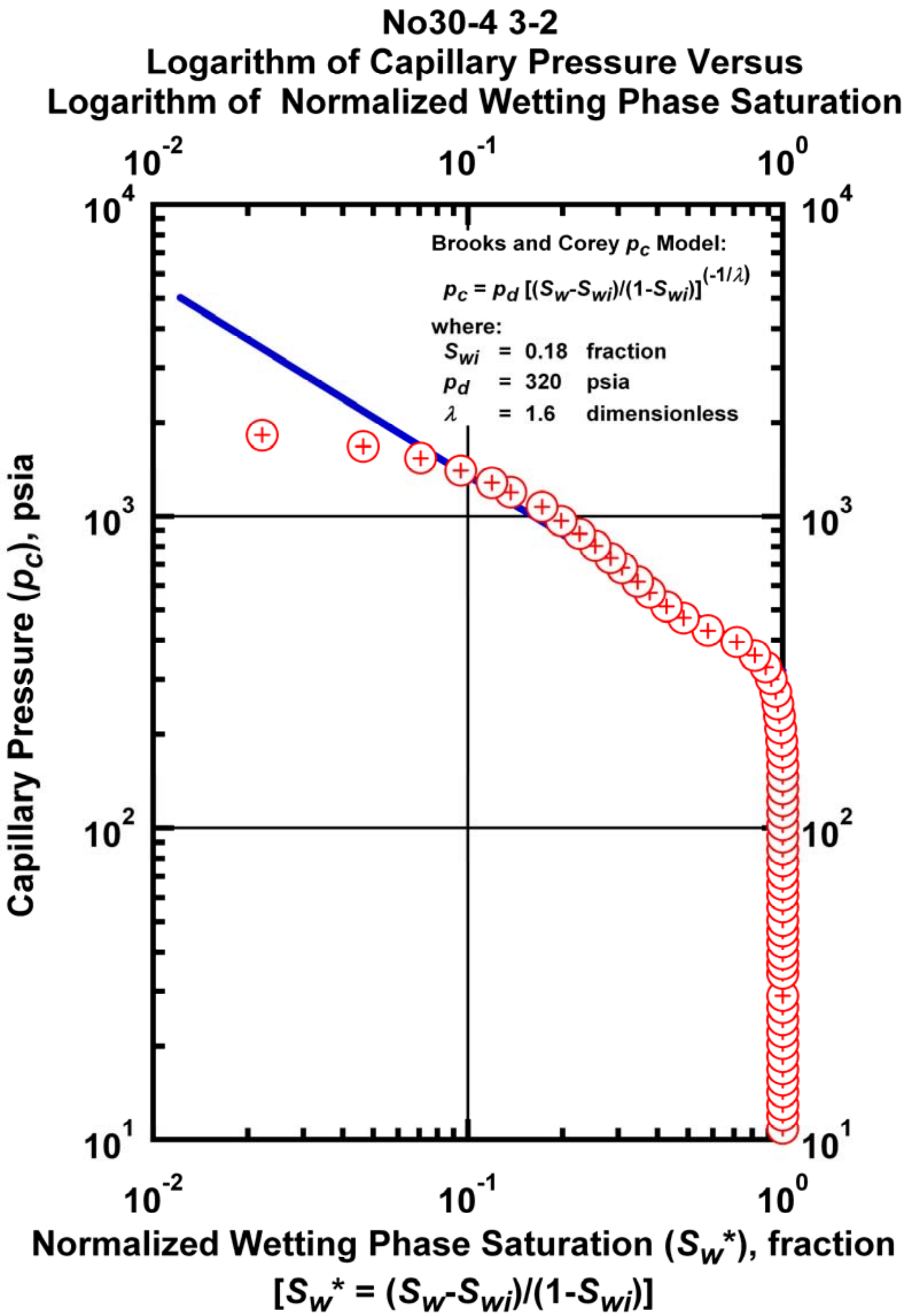

Figure K.41 – Plot of logarithm of capillary pressure vs. logarithm of normalized wetting phase saturation — Case No30-4 3-2.

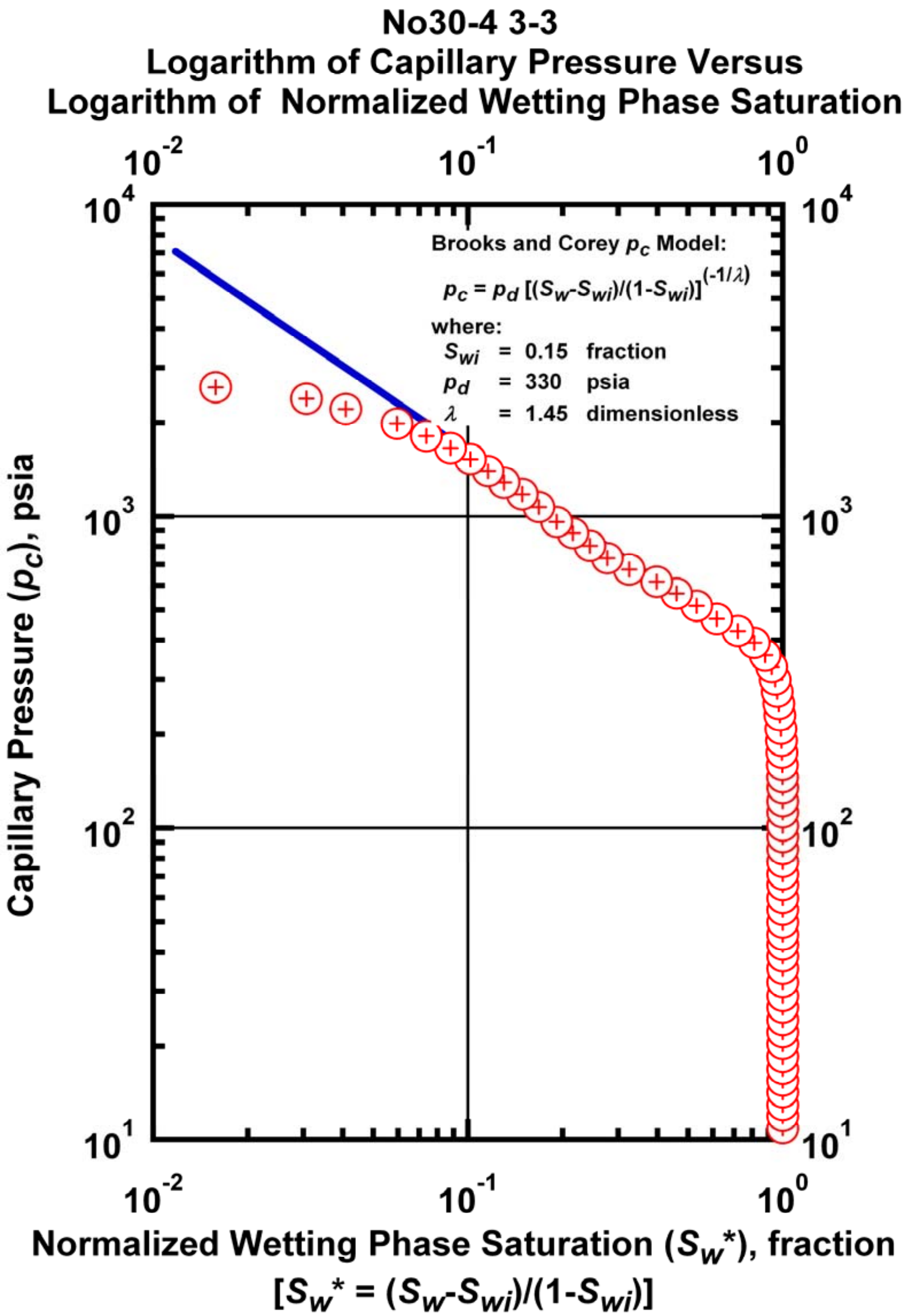

Figure K.42 – Plot of logarithm of capillary pressure vs. logarithm of normalized wetting phase saturation — Case No30-4 3-3.

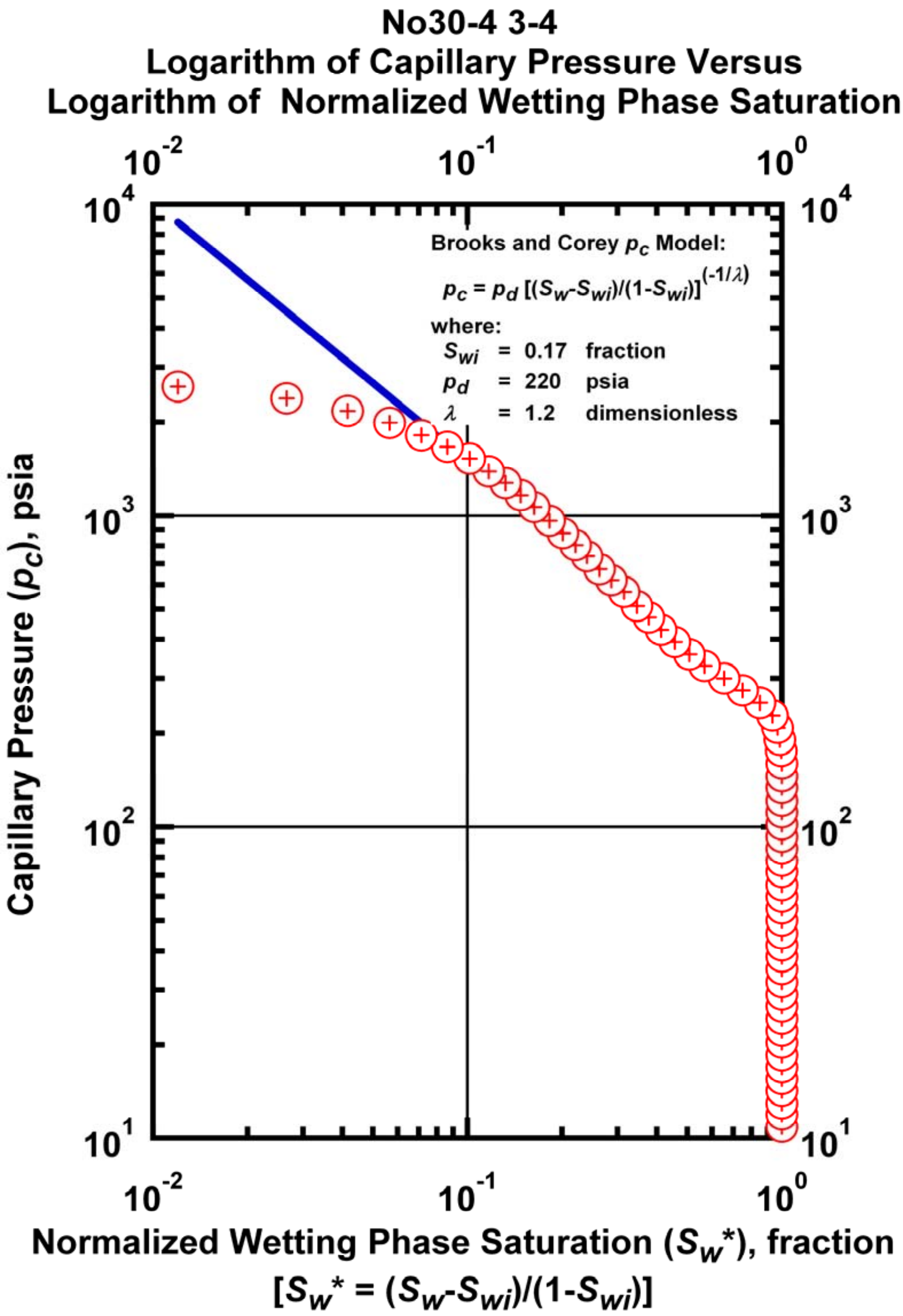

Figure K.43 – Plot of logarithm of capillary pressure vs. logarithm of normalized wetting phase saturation — Case No30-4 3-4.

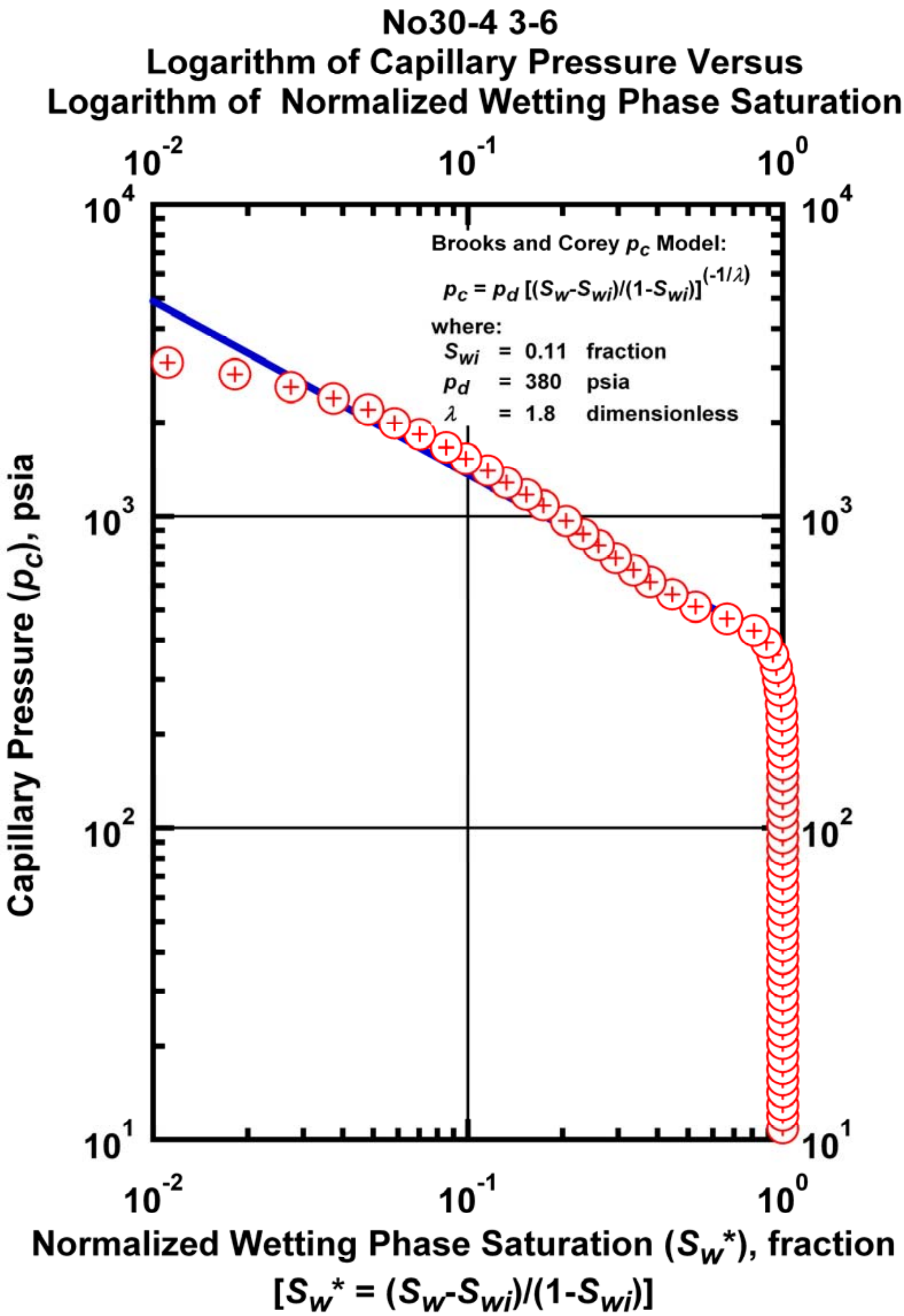

Figure K.44 – Plot of logarithm of capillary pressure vs. logarithm of normalized wetting phase saturation — Case No30-4 3-6.

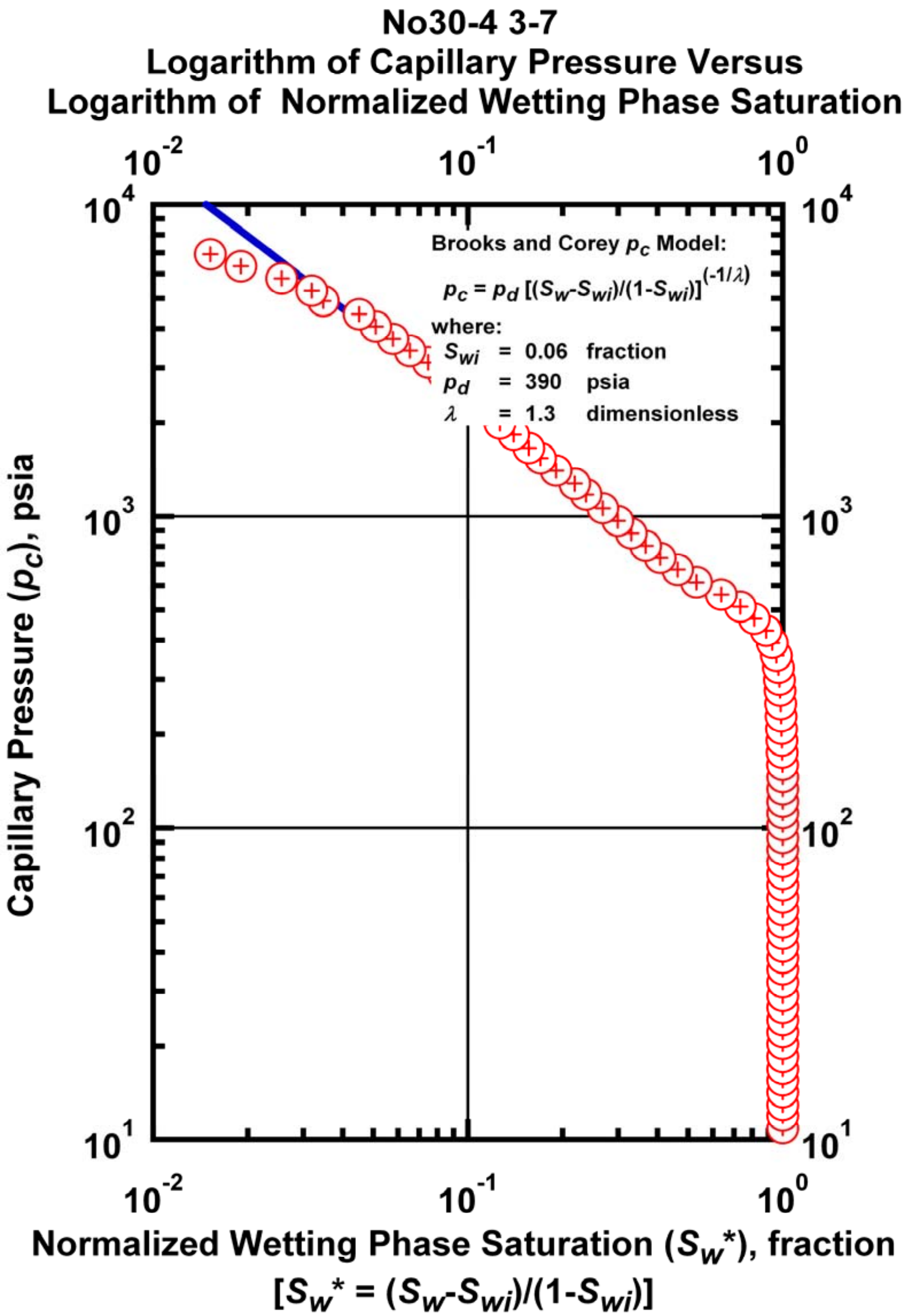

Figure K.45 – Plot of logarithm of capillary pressure vs. logarithm of normalized wetting phase saturation — Case No30-4 3-7.

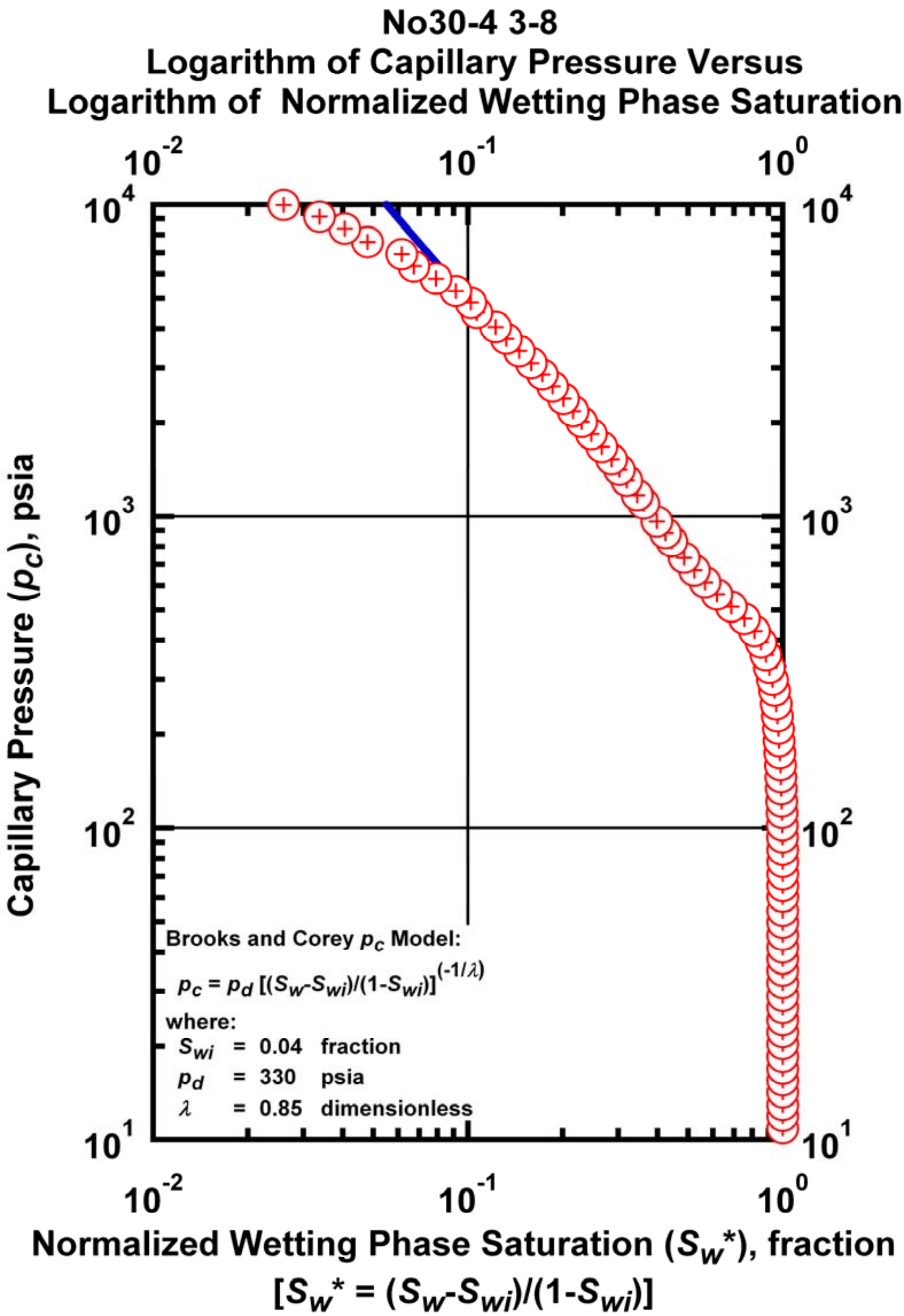

Figure K.46 – Plot of logarithm of capillary pressure vs. logarithm of normalized wetting phase saturation — Case No30-4 3-8.

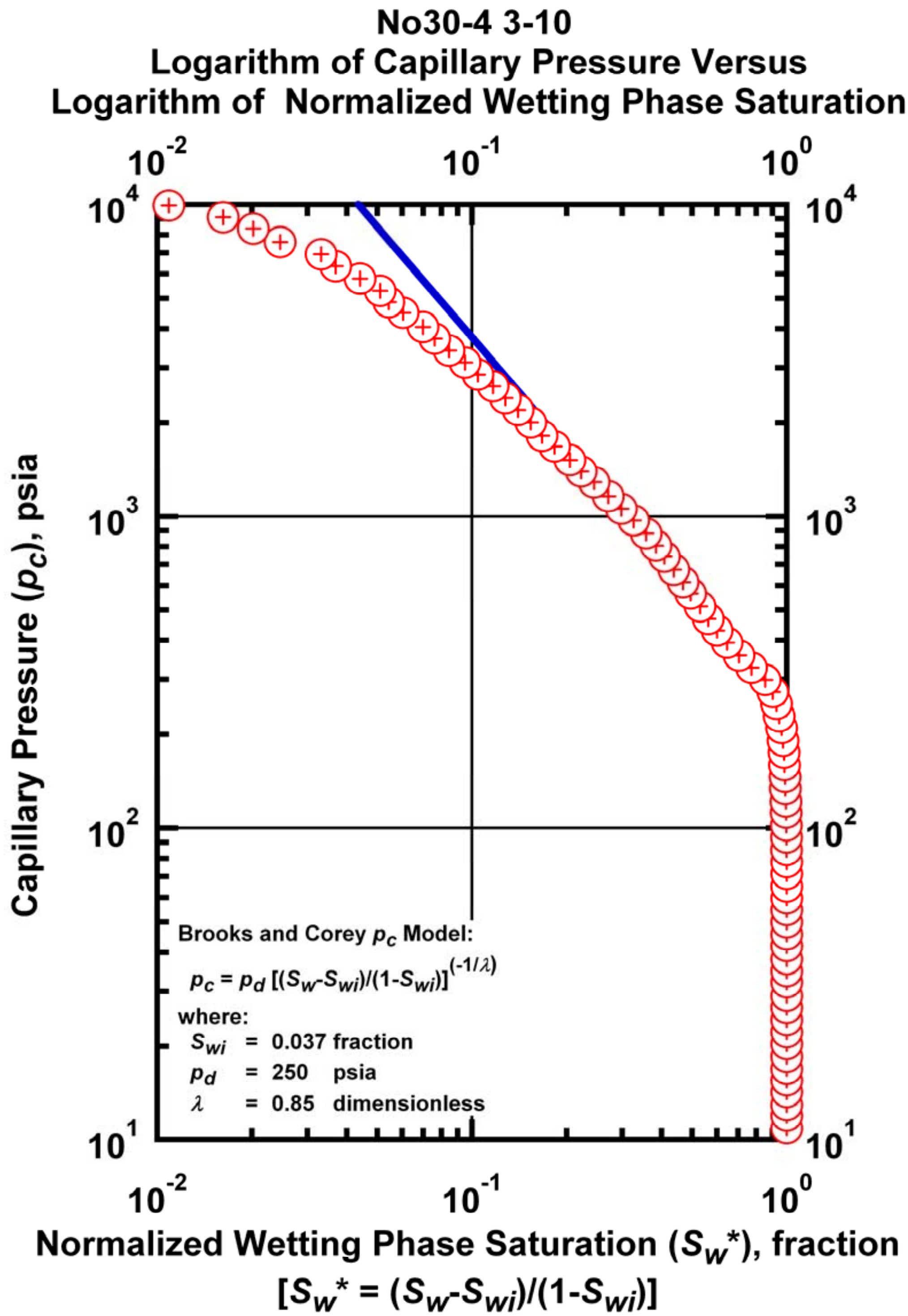

Figure K.47 – Plot of logarithm of capillary pressure vs. logarithm of normalized wetting phase saturation — Case No30-4 3-10.

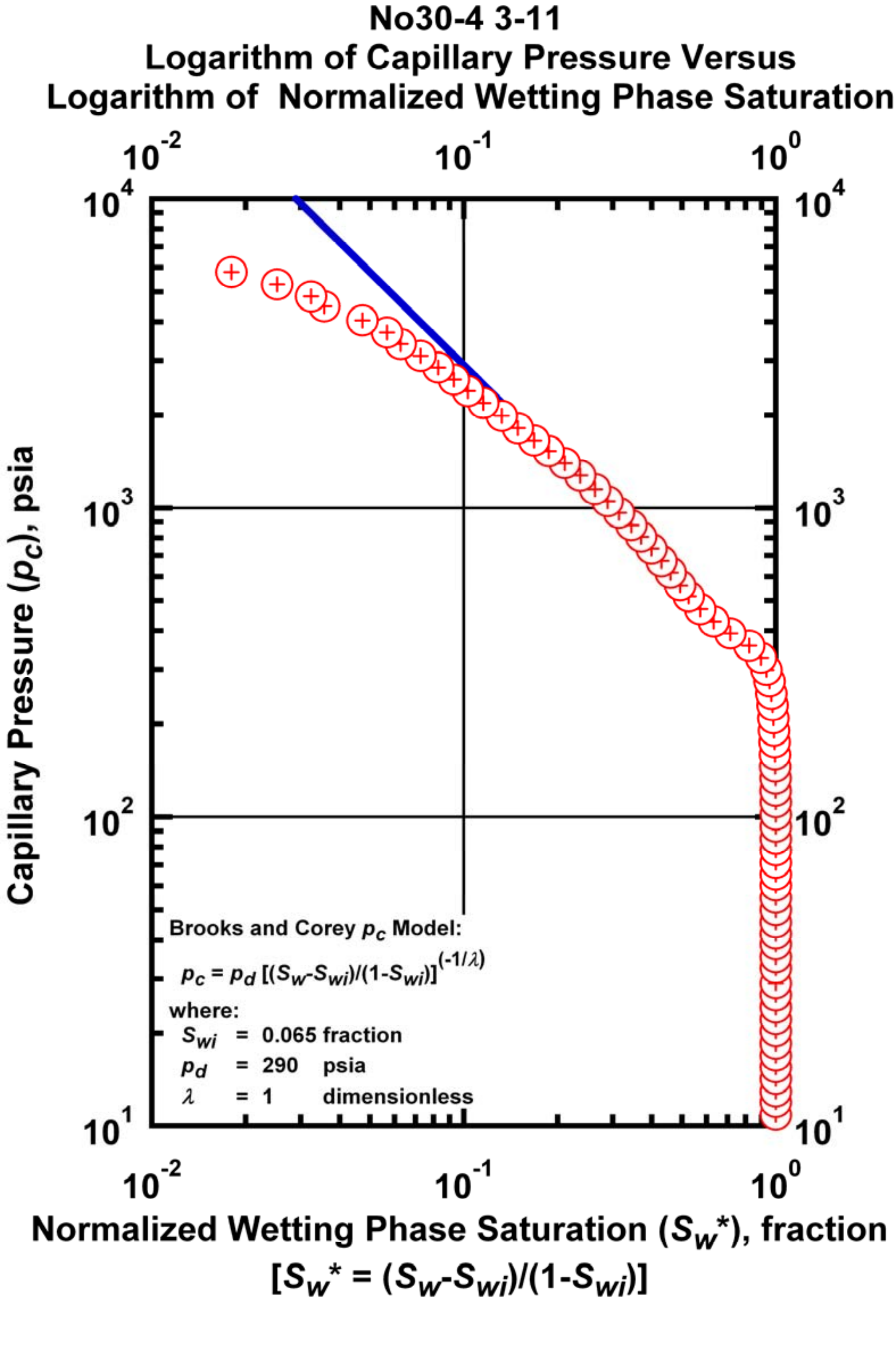

Figure K.48 – Plot of logarithm of capillary pressure vs. logarithm of normalized wetting phase saturation — Case No30-4 3-11.

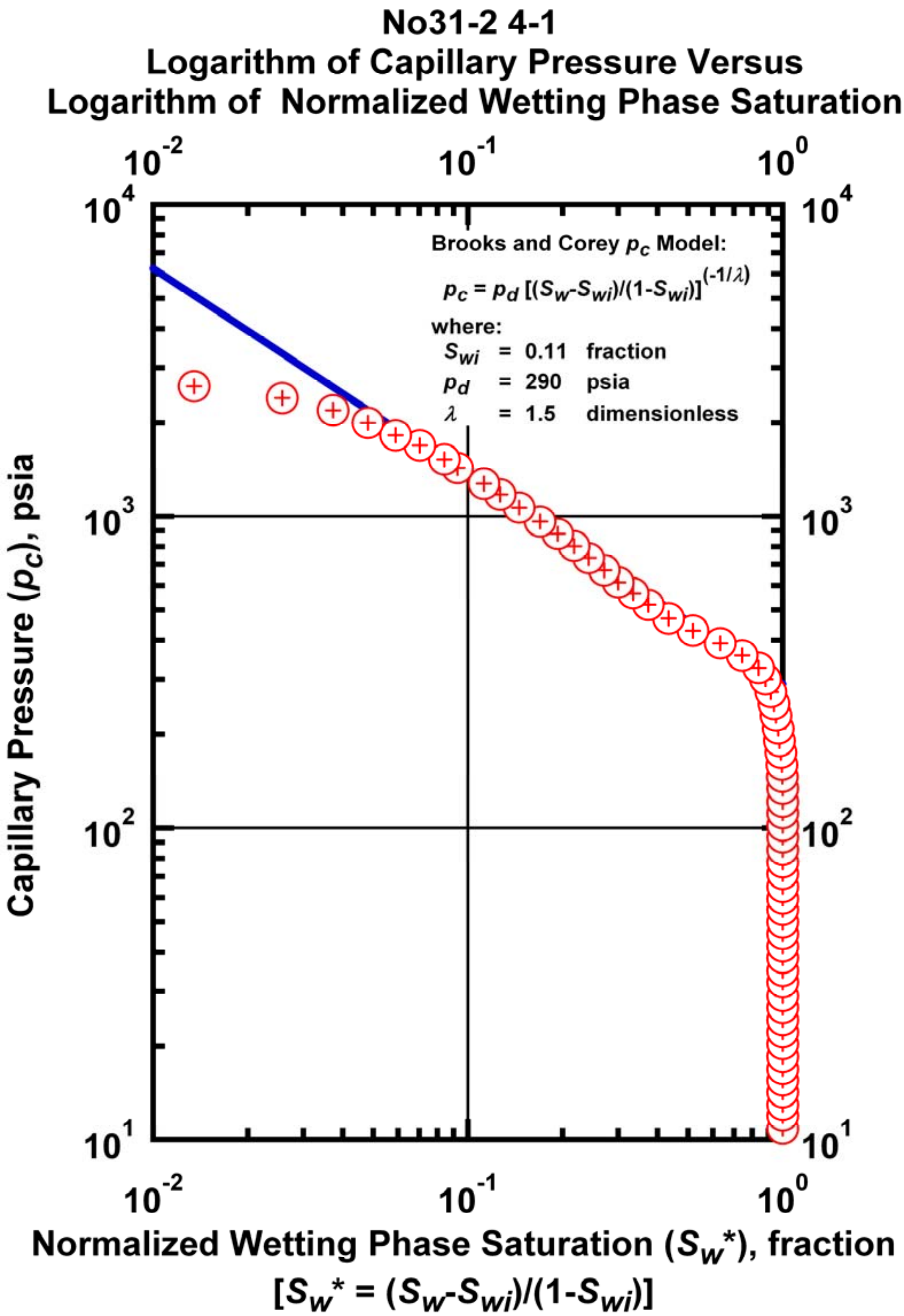

Figure K.49 – Plot of logarithm of capillary pressure vs. logarithm of normalized wetting phase saturation — Case No31-2 4-1.

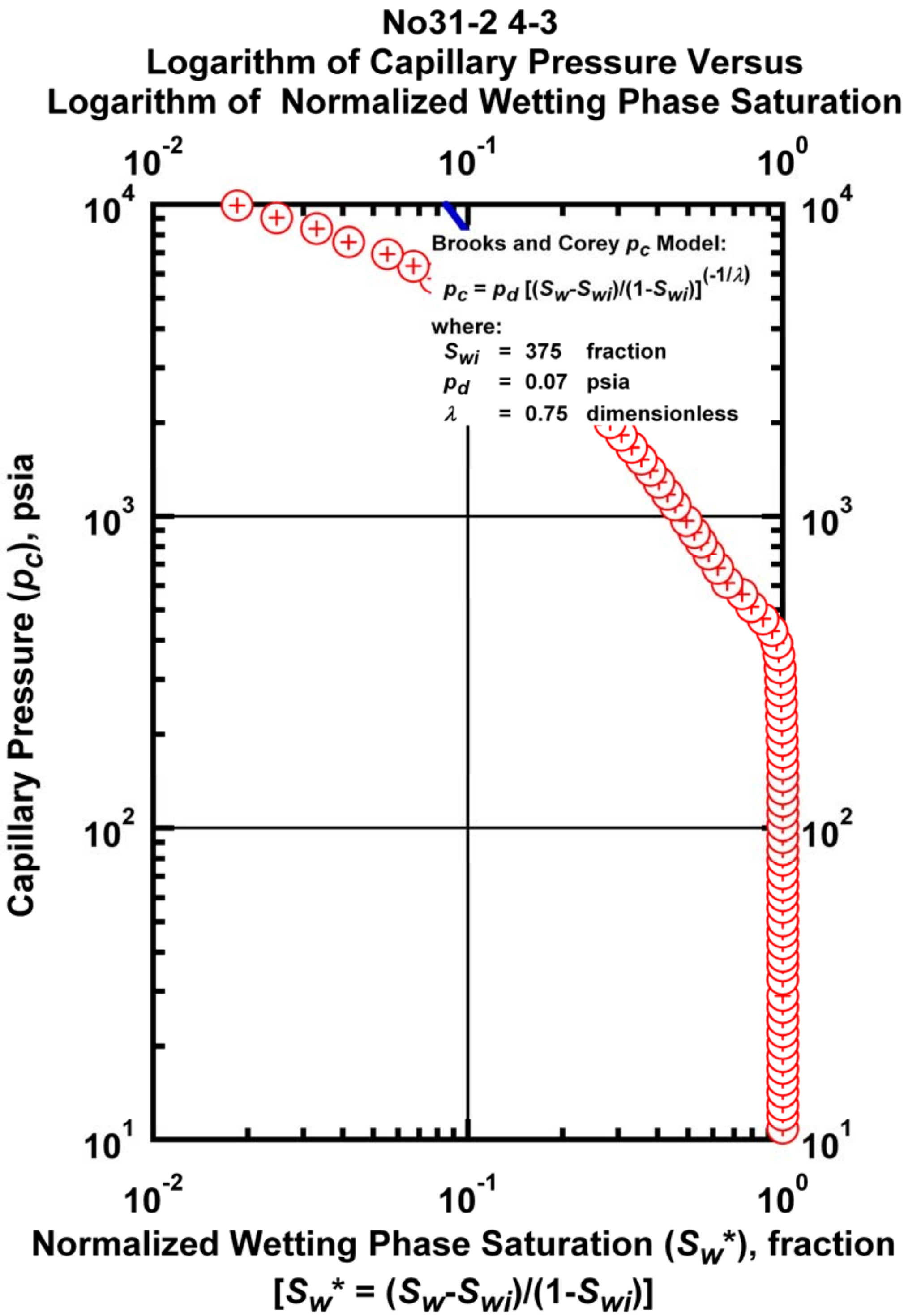

Figure K.50 – Plot of logarithm of capillary pressure vs. logarithm of normalized wetting phase saturation — Case No31-2 4-3.

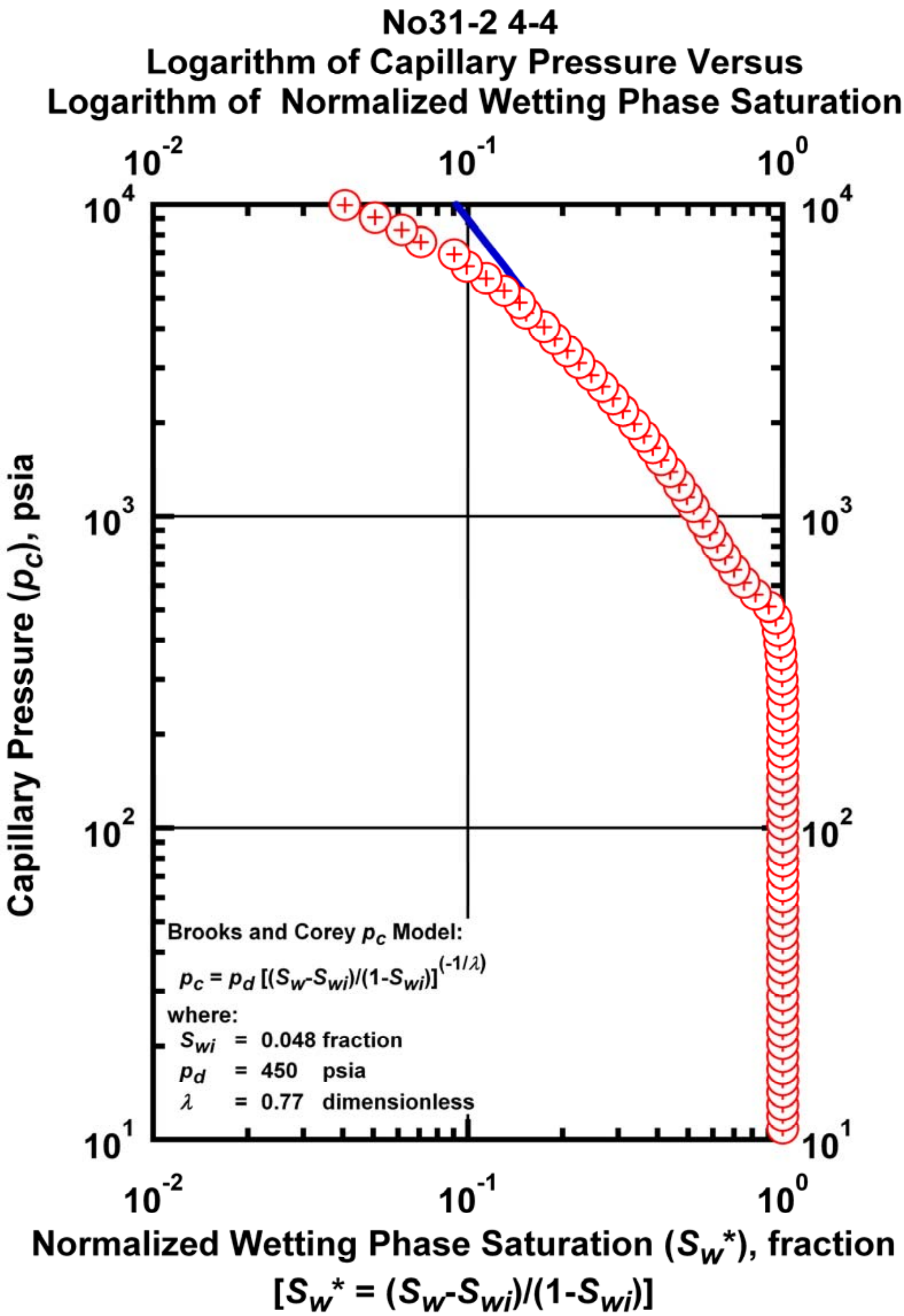

Figure K.51 – Plot of logarithm of capillary pressure vs. logarithm of normalized wetting phase saturation ― Case No31-2 4-4.

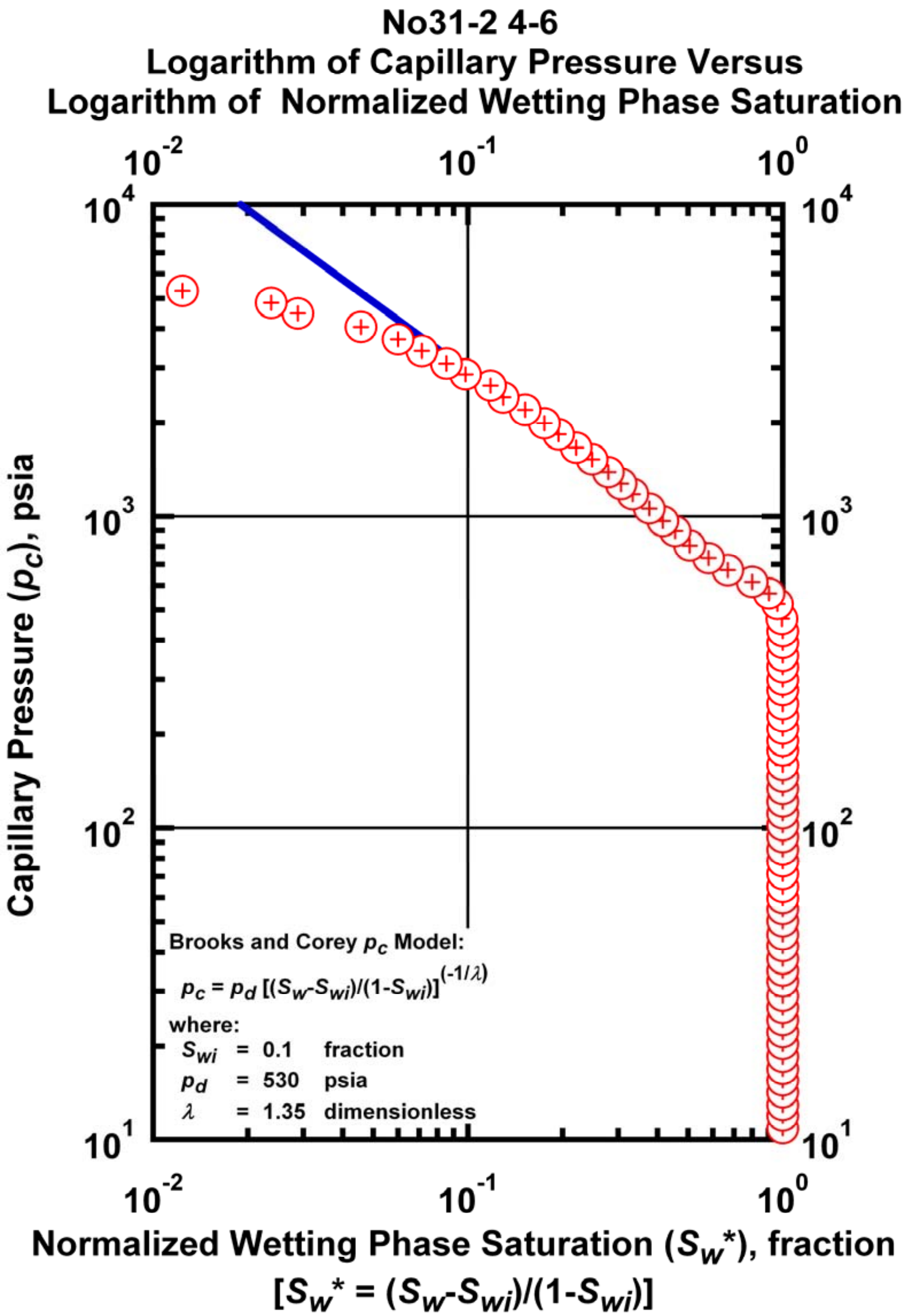

Figure K.52 – Plot of logarithm of capillary pressure vs. logarithm of normalized wetting phase saturation — Case No31-2 4-6.

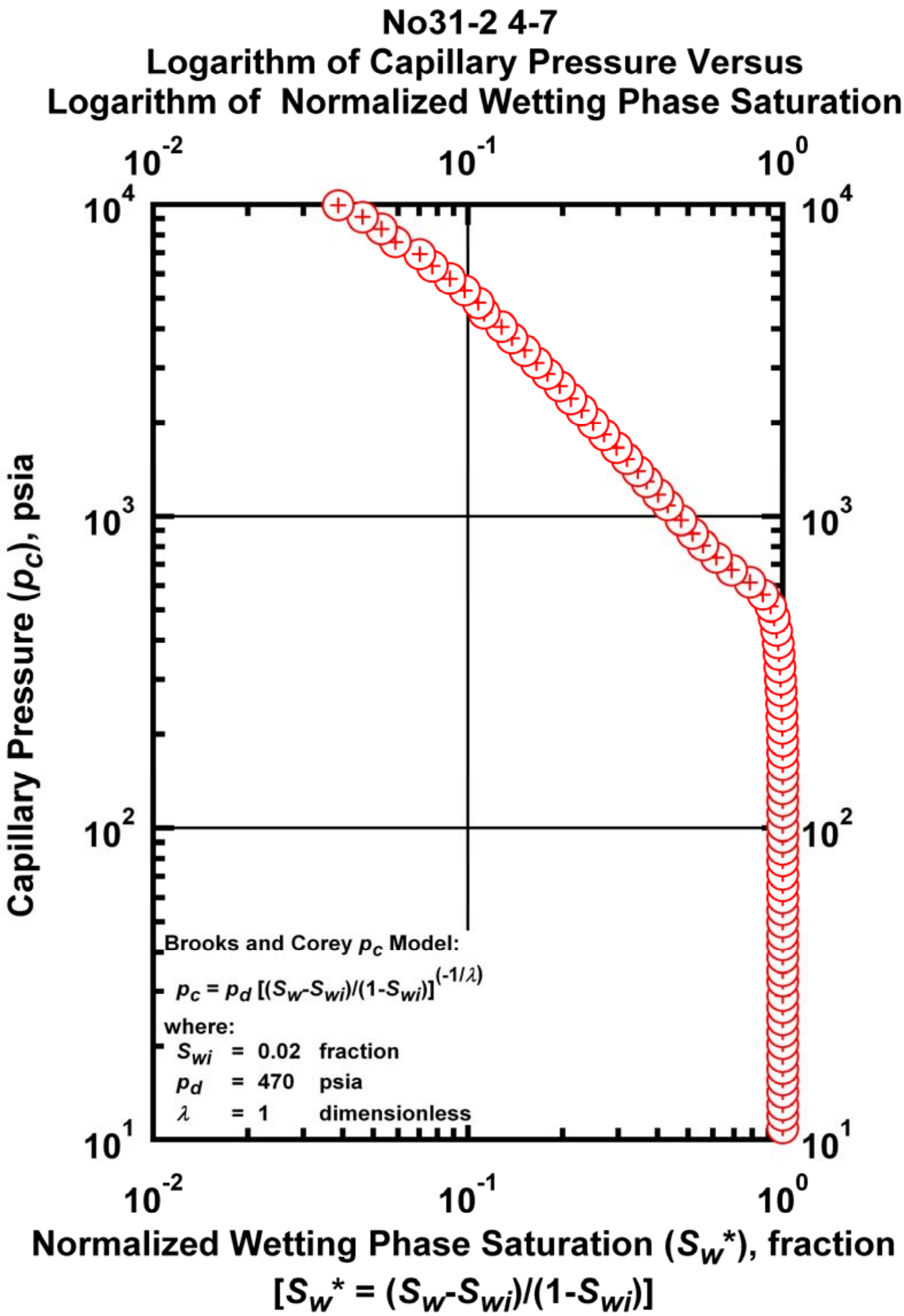

Figure K.53 – Plot of logarithm of capillary pressure vs. logarithm of normalized wetting phase saturation — Case No31-2 4-7.

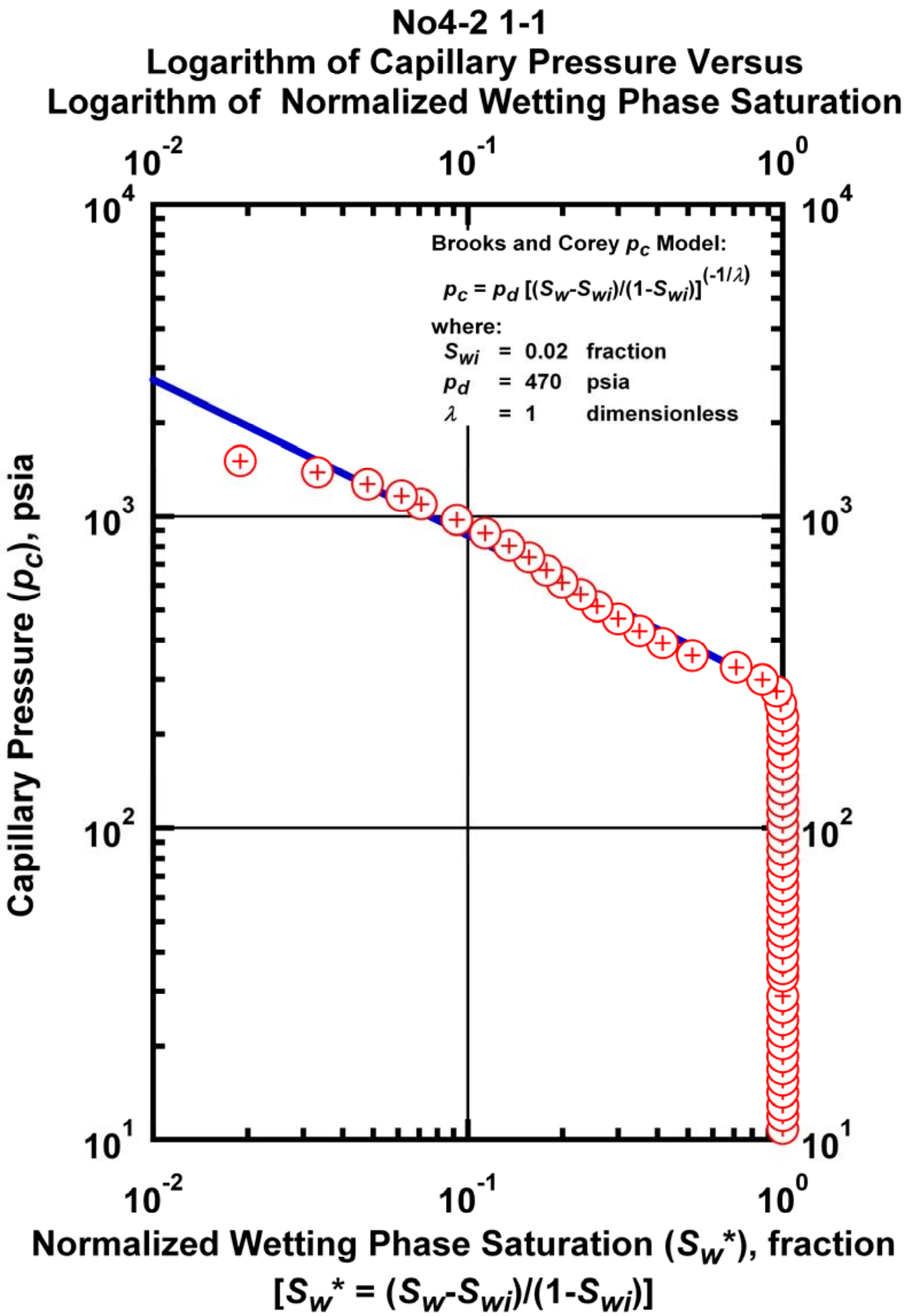

Figure K.54 – Plot of logarithm of capillary pressure vs. logarithm of normalized wetting phase saturation — Case No4-2 1-1.

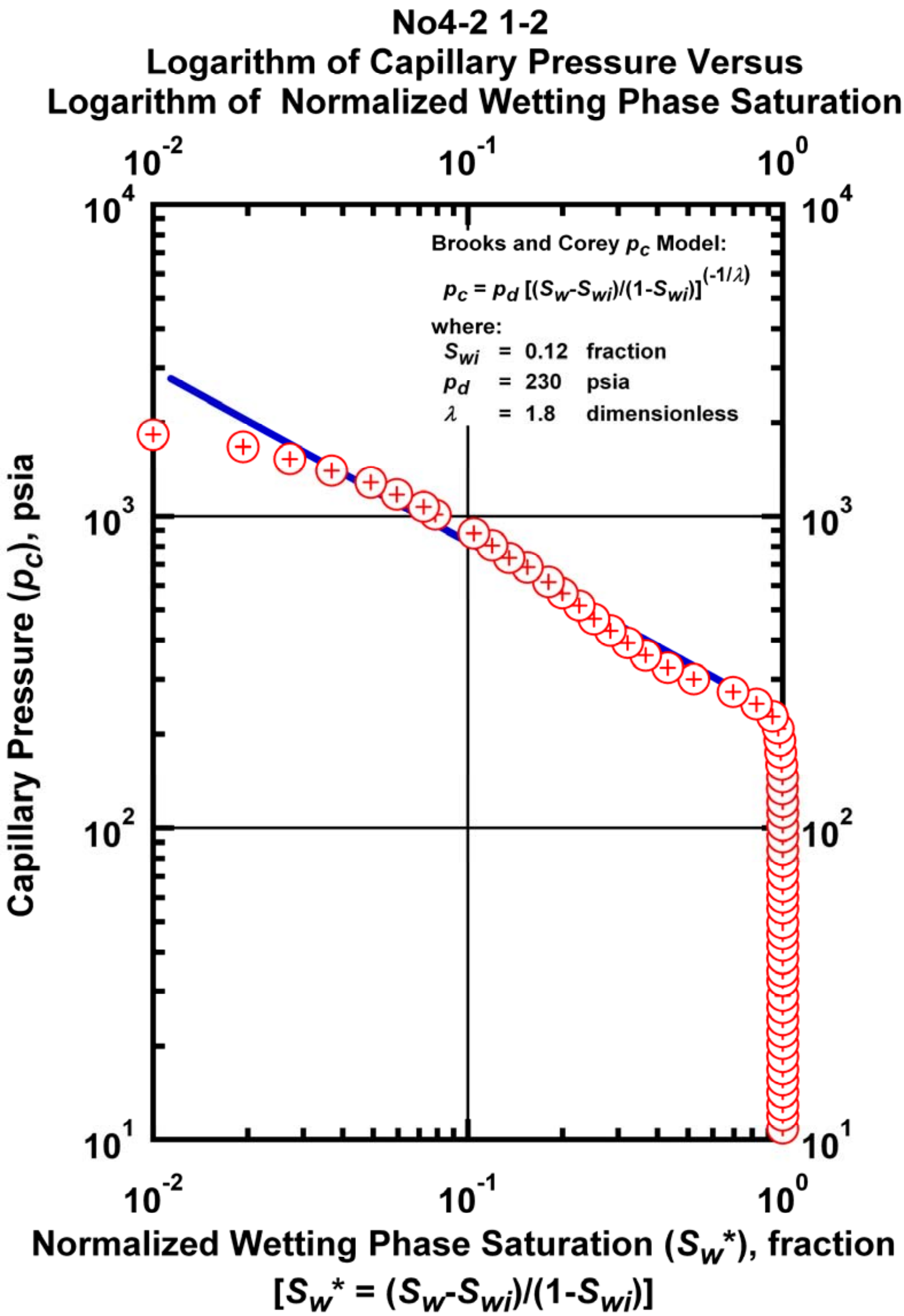

Figure K.55 – Plot of logarithm of capillary pressure vs. logarithm of normalized wetting phase saturation — Case No4-2 1-2.

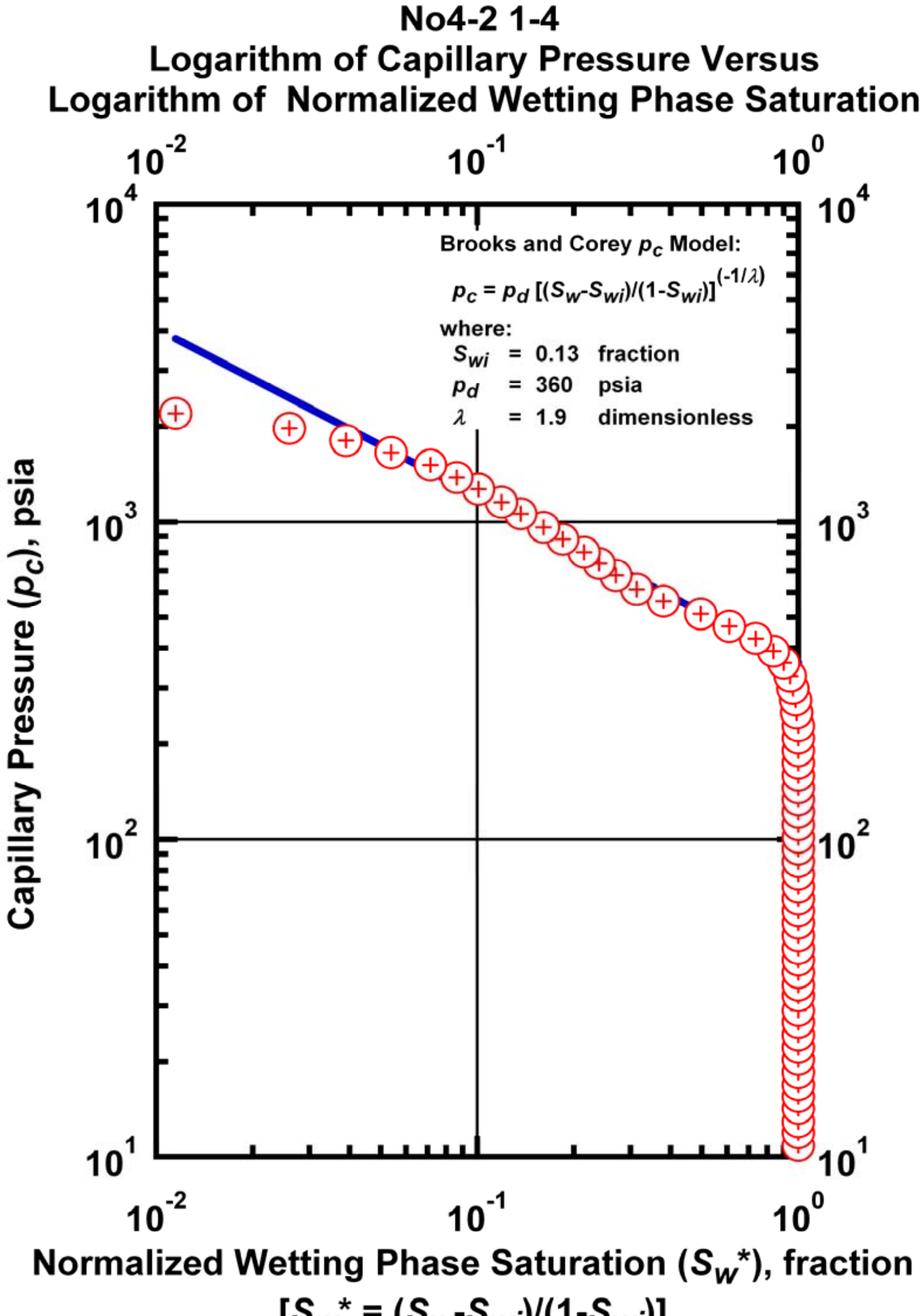

Figure K.56 – Plot of logarithm of capillary pressure vs. logarithm of normalized wetting phase saturation — Case No4-2 1-4.

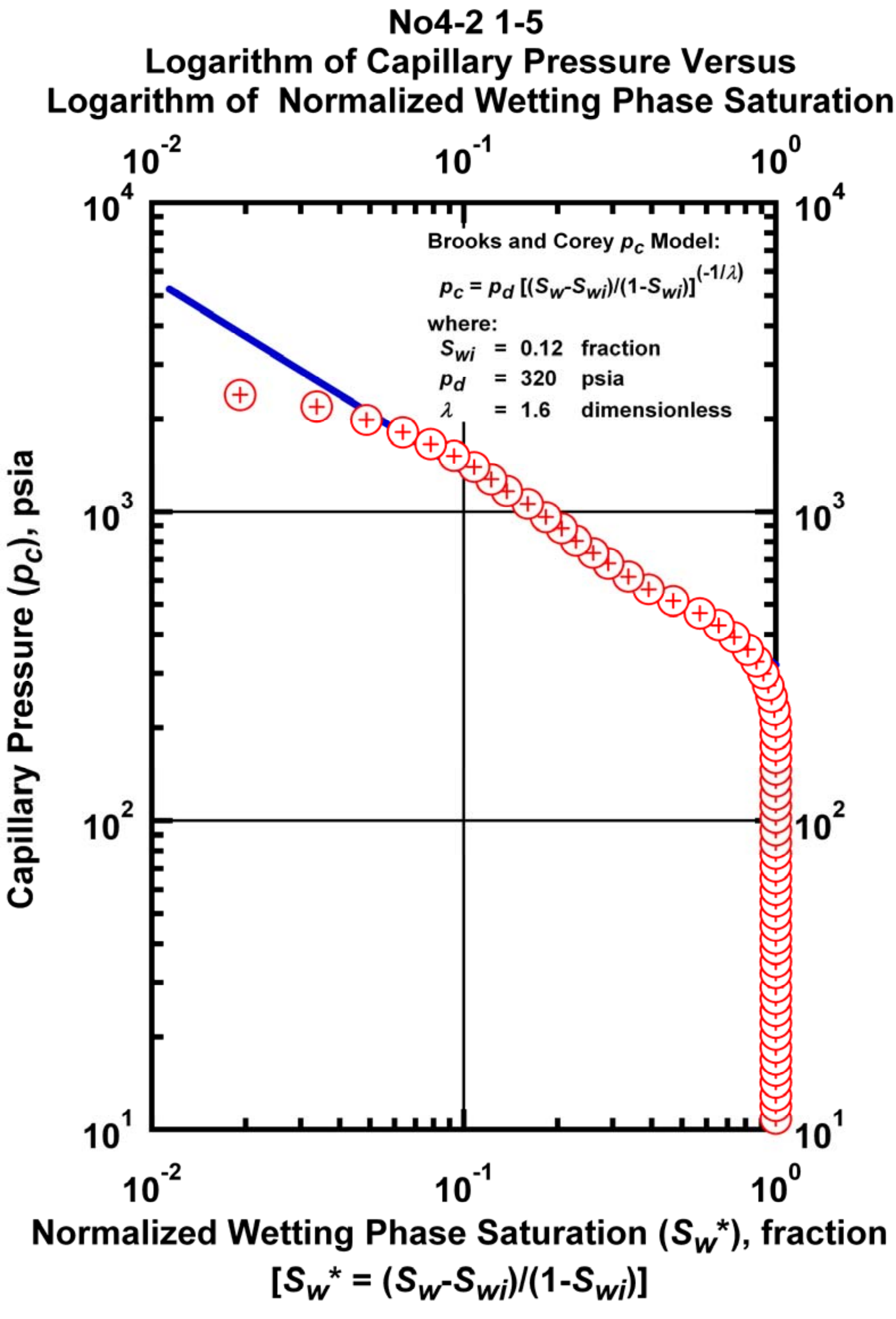

Figure K.57 – Plot of logarithm of capillary pressure vs. logarithm of normalized wetting phase saturation — Case No4-2 1-5.

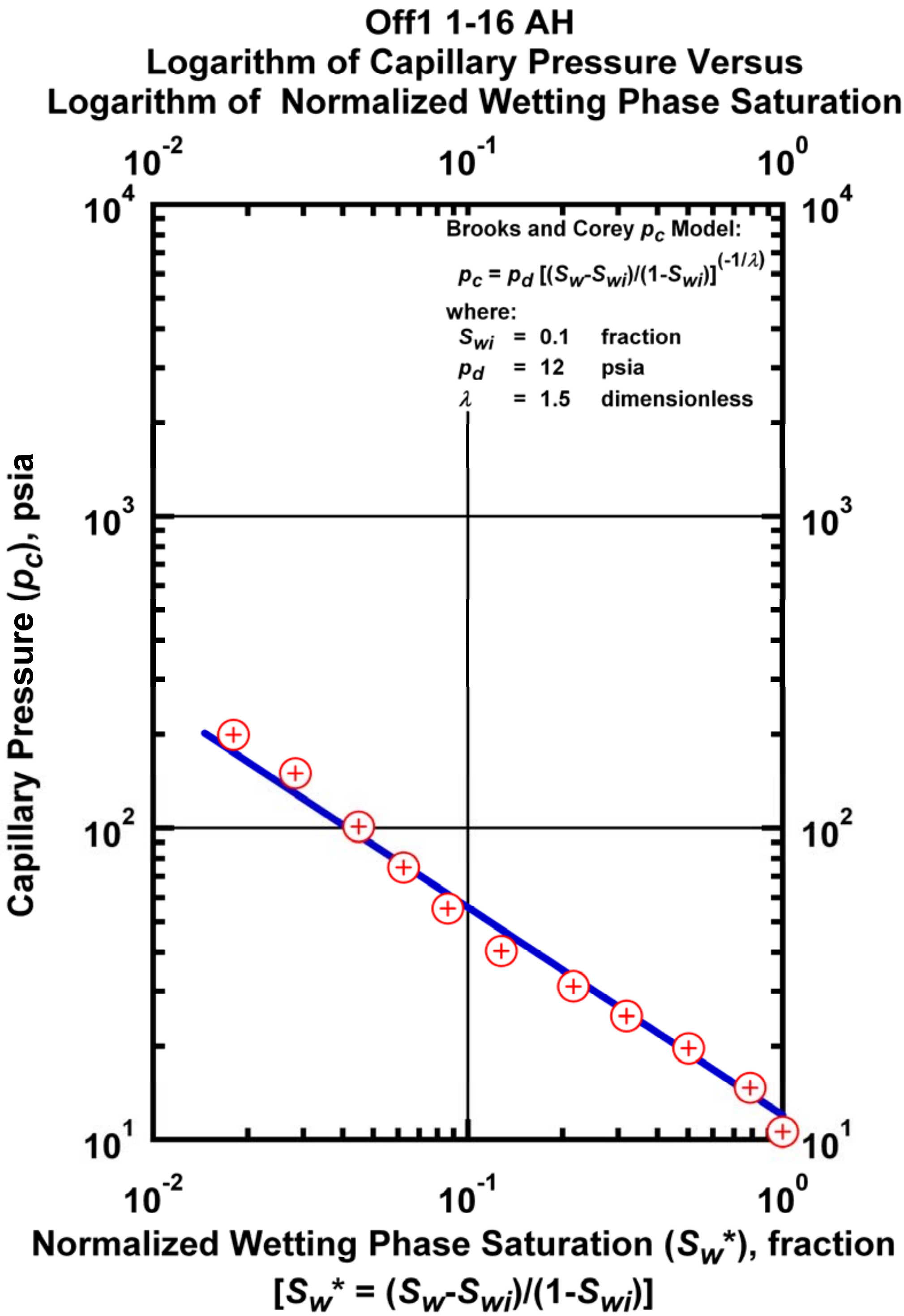

Figure K.58 – Plot of logarithm of capillary pressure vs. logarithm of normalized wetting phase saturation — Case Off1 1-16 AH.

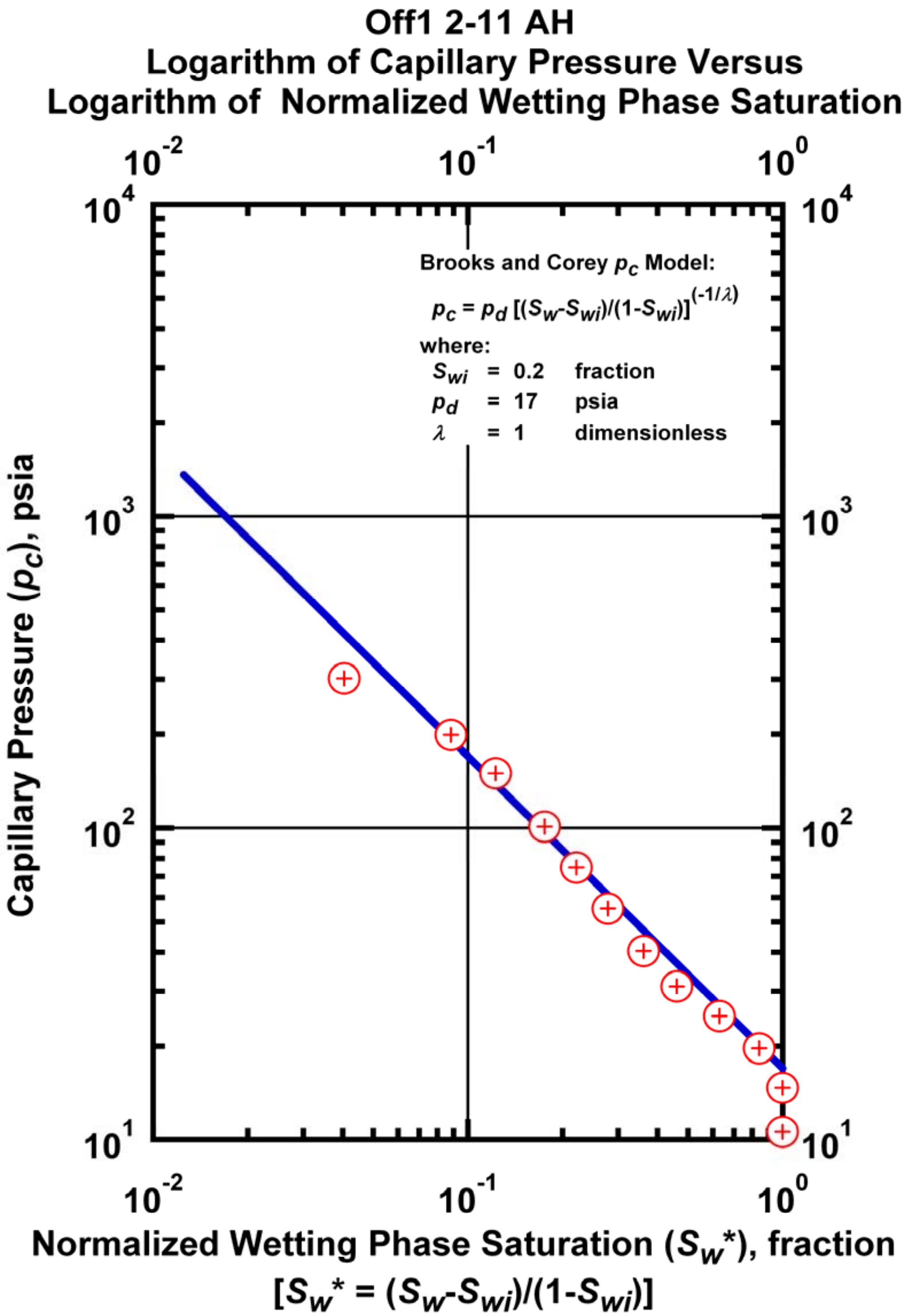

Figure K.59 – Plot of logarithm of capillary pressure vs. logarithm of normalized wetting phase saturation — Case Off1 2-11 AH.

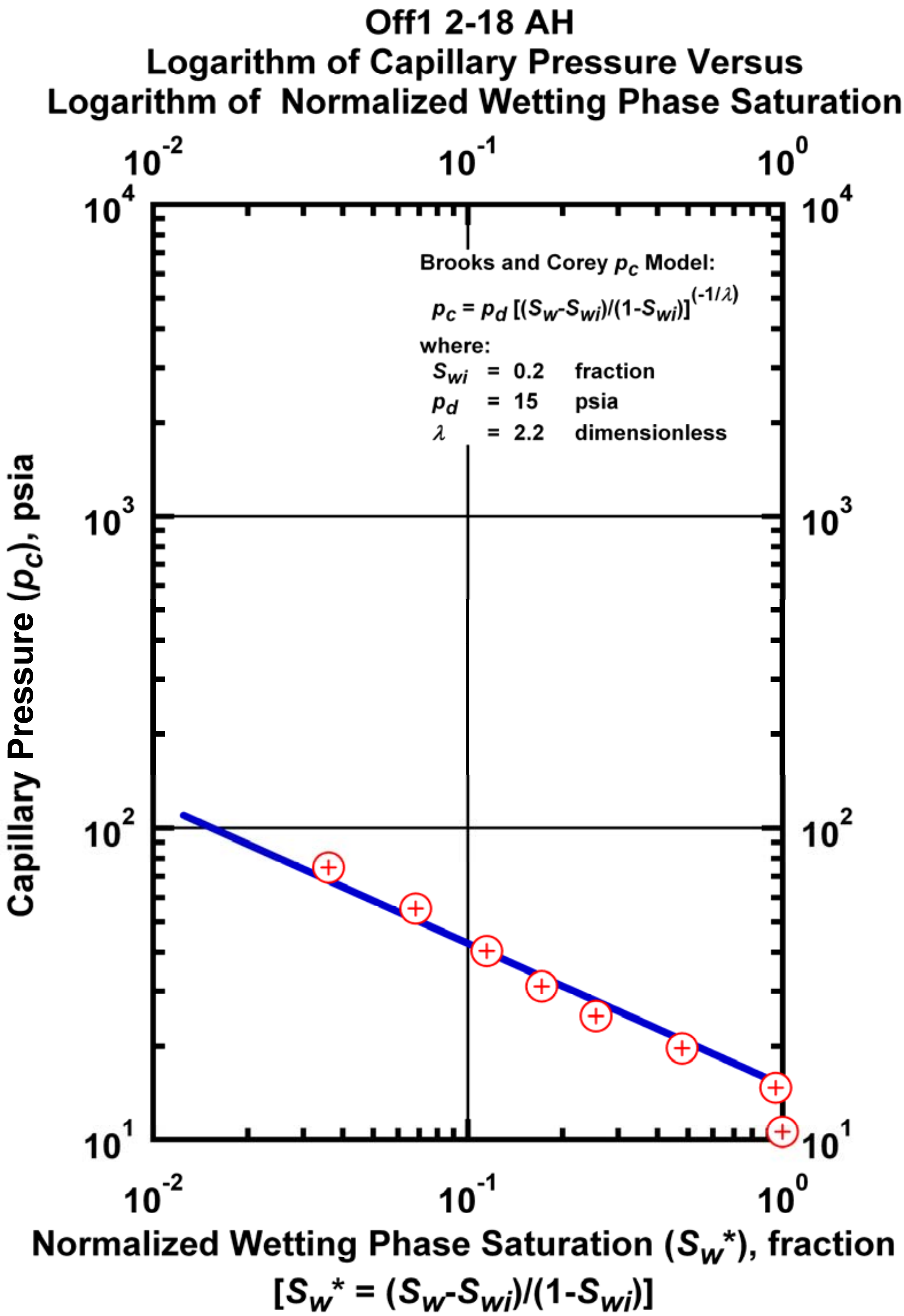

Figure K.60 – Plot of logarithm of capillary pressure vs. logarithm of normalized wetting phase saturation — Case Off1 2-18 AH.

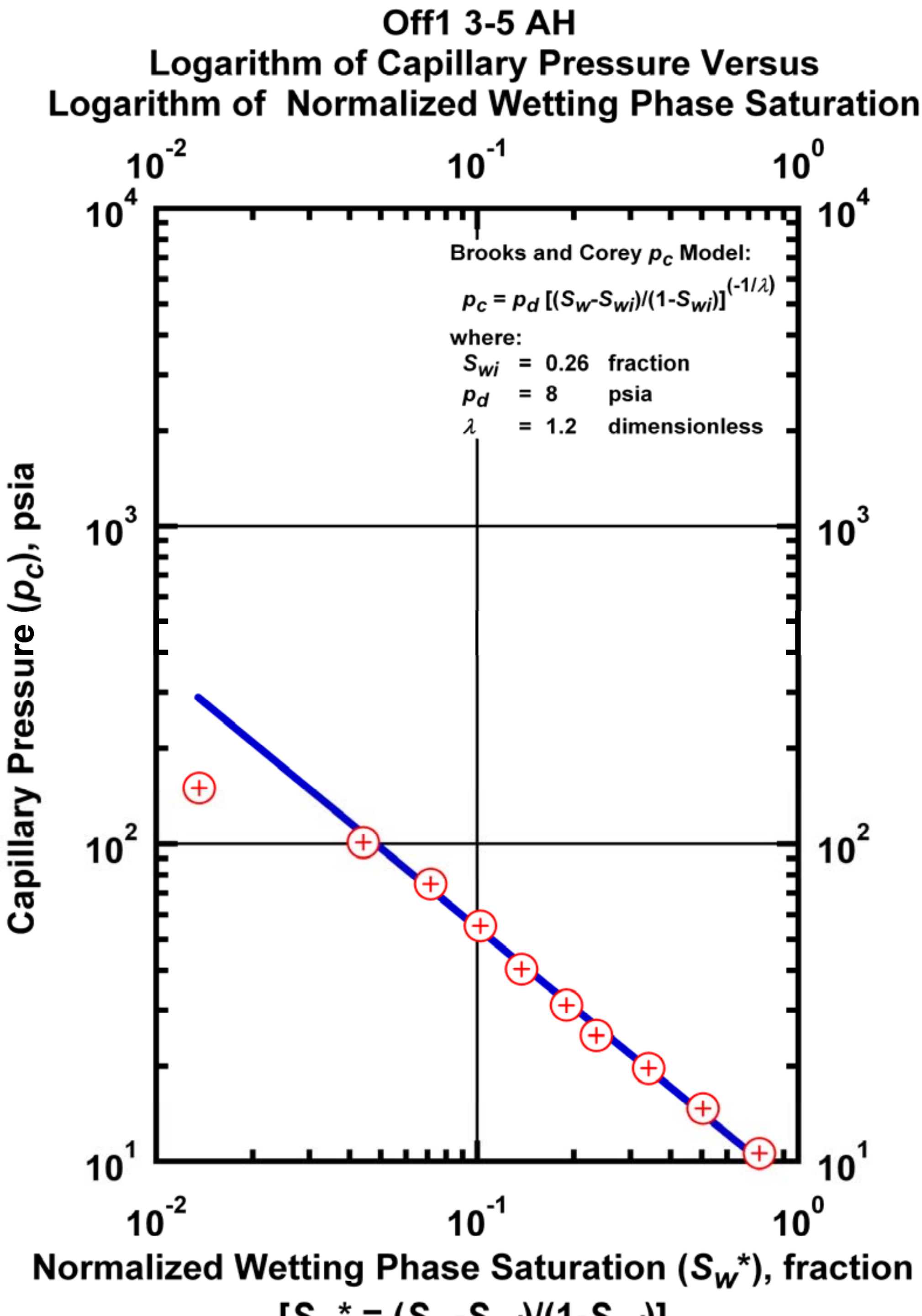

Figure K.61 – Plot of logarithm of capillary pressure vs. logarithm of normalized wetting phase saturation — Case Off1 3-5 AH.

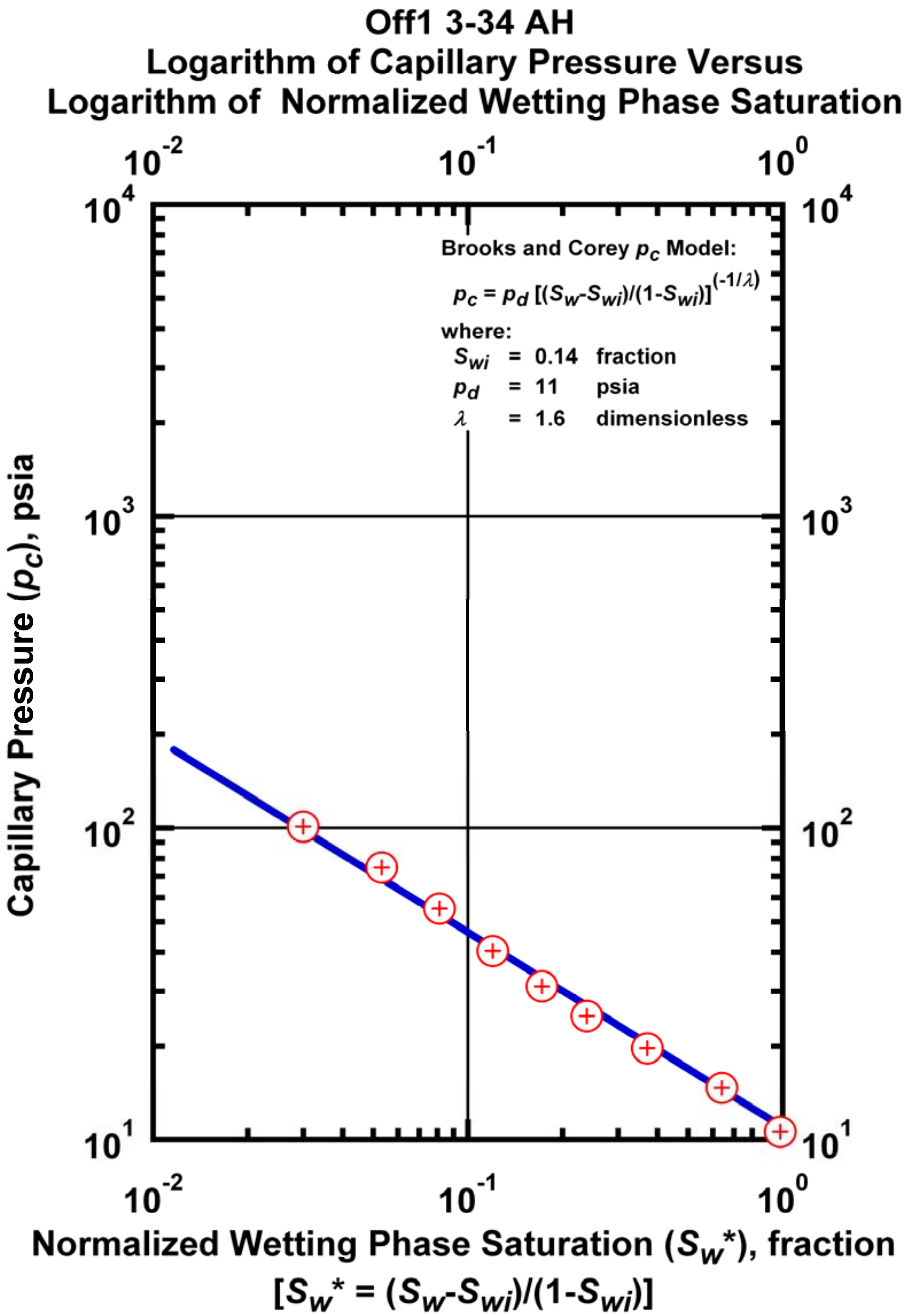

Figure K.62 – Plot of logarithm of capillary pressure vs. logarithm of normalized wetting phase saturation — Case Off1 3-34 AH.

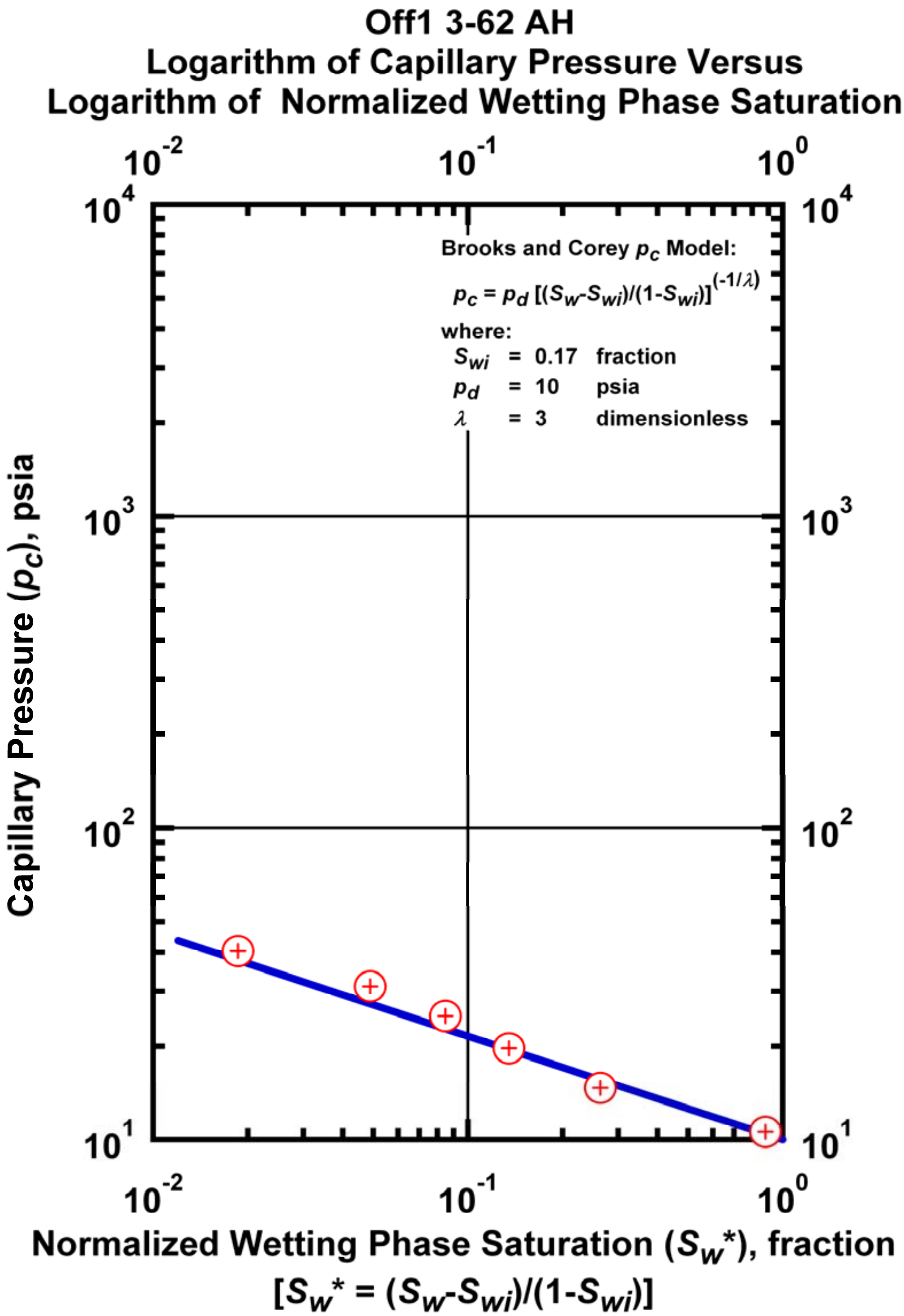

Figure K.63 – Plot of logarithm of capillary pressure vs. logarithm of normalized wetting phase saturation — Case Off1 3-62 AH.

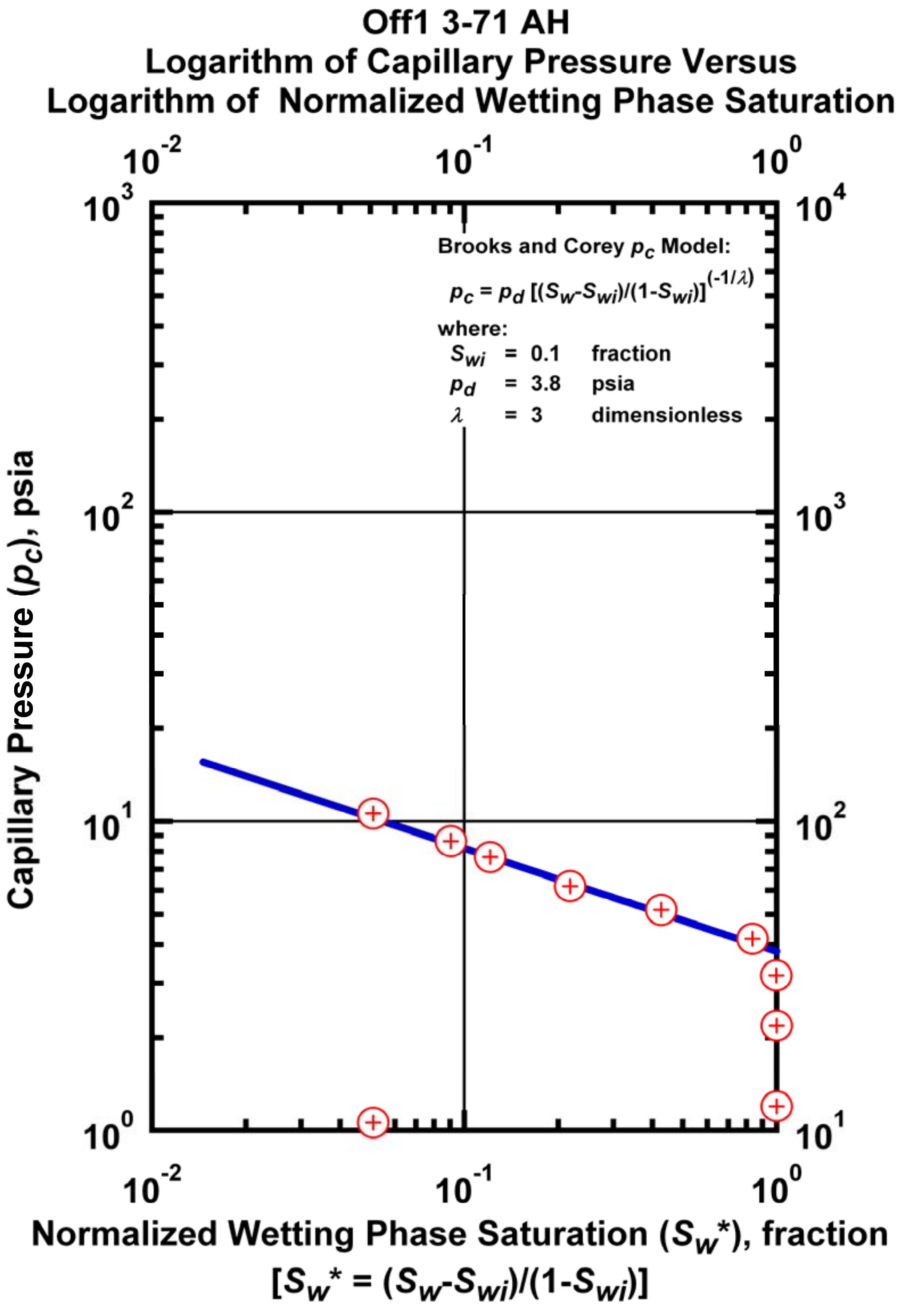

Figure K.64 – Plot of logarithm of capillary pressure vs. logarithm of normalized wetting phase saturation — Case Off1 3-71 AH.

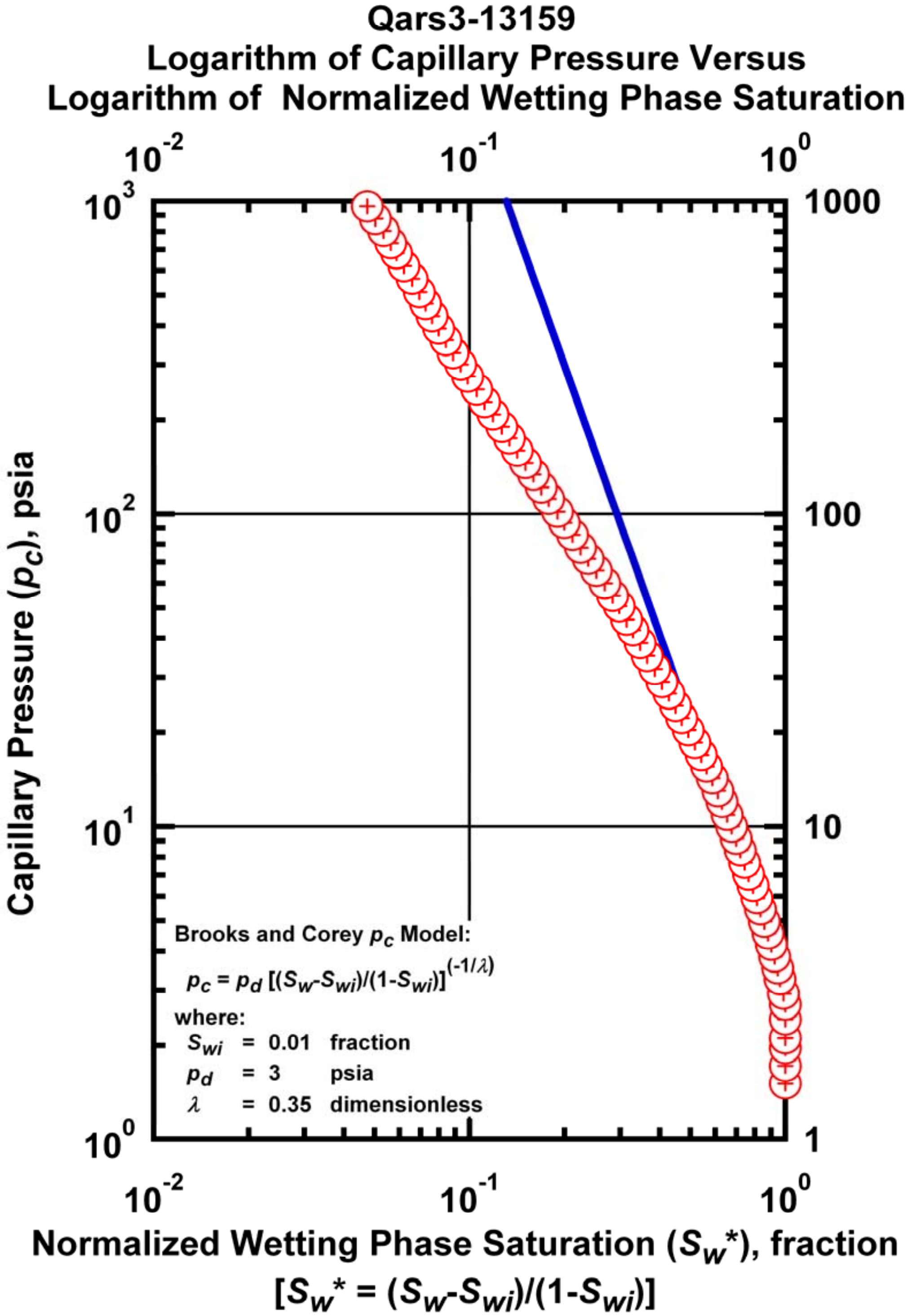

Figure K.65 – Plot of logarithm of capillary pressure vs. logarithm of normalized wetting phase saturation — Case Qars3-13159.

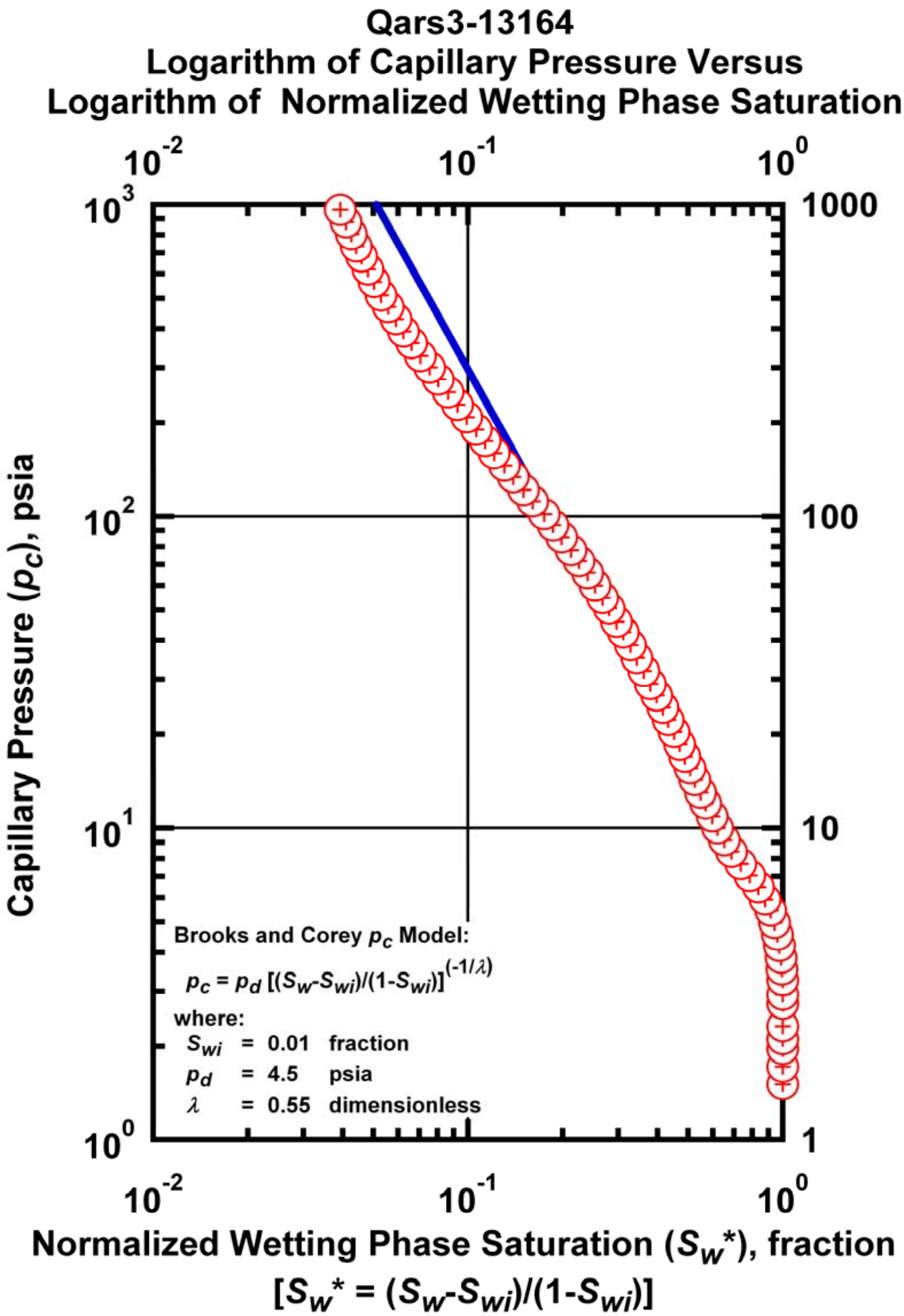

Figure K.66 – Plot of logarithm of capillary pressure vs. logarithm of normalized wetting phase saturation — Case Qars3-13164.

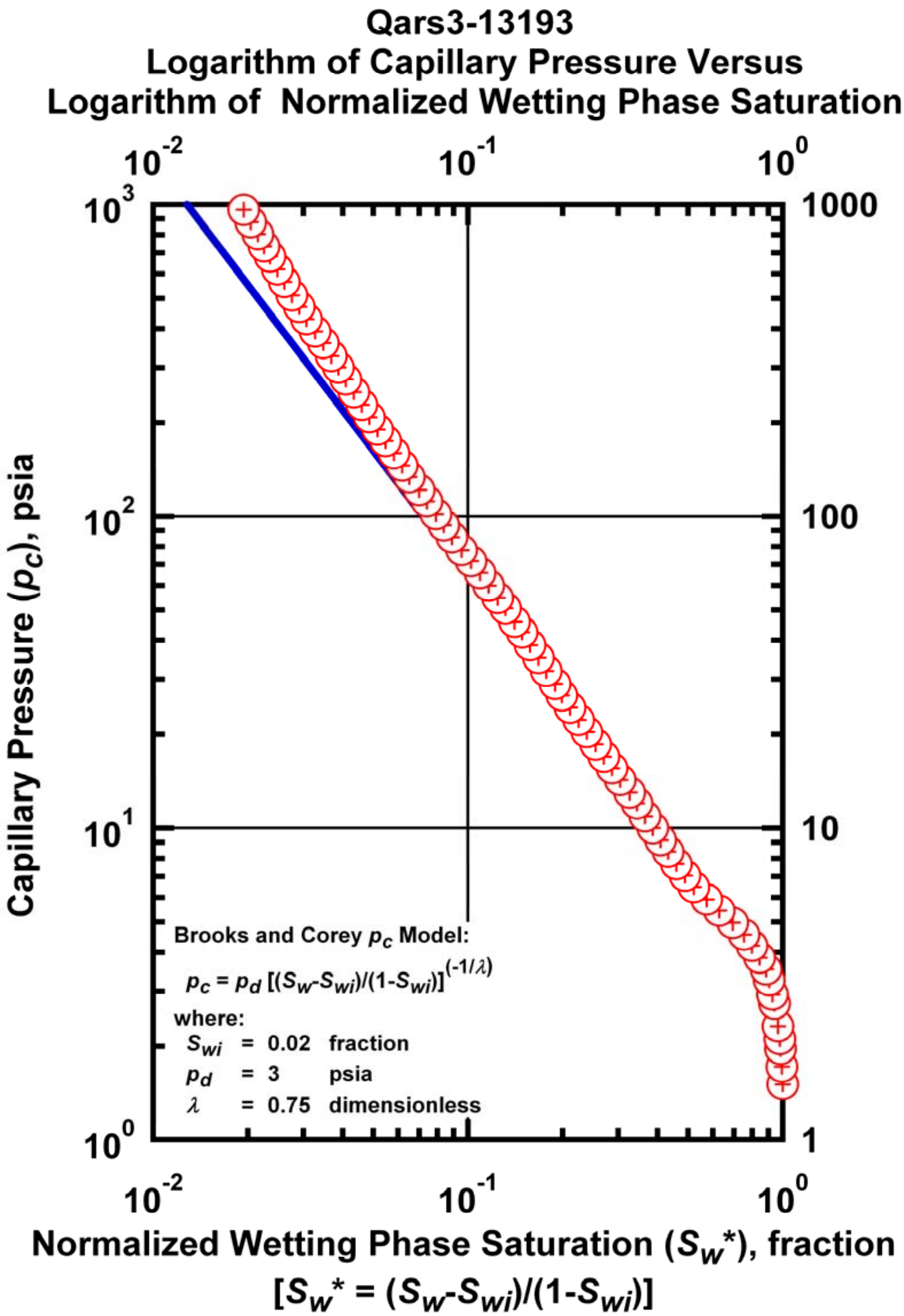

Figure K.67 – Plot of logarithm of capillary pressure vs. logarithm of normalized wetting phase saturation — Case Qars3-13193.

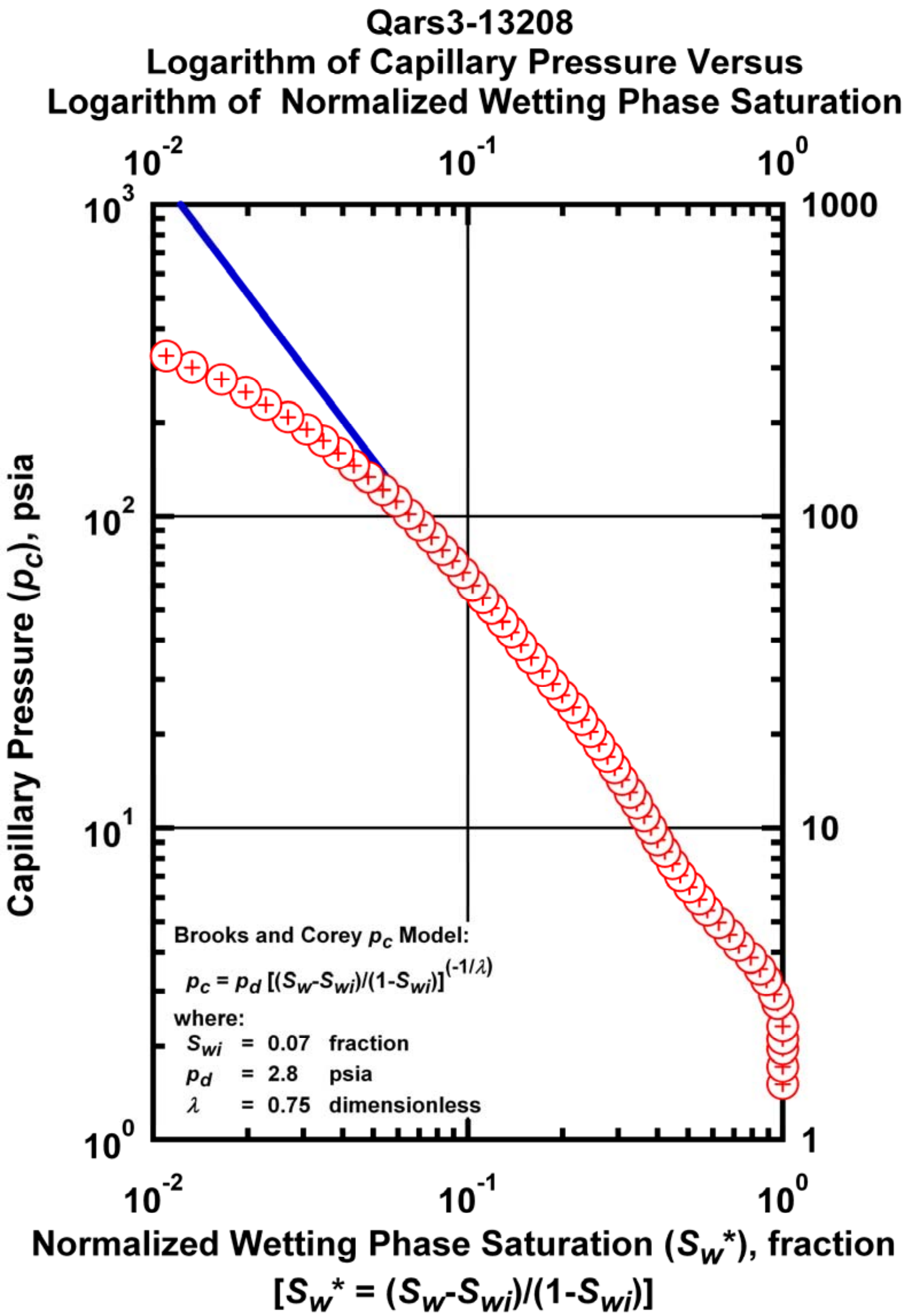

Figure K.68 – Plot of logarithm of capillary pressure vs. logarithm of normalized wetting phase saturation — Case Qars3-13208.

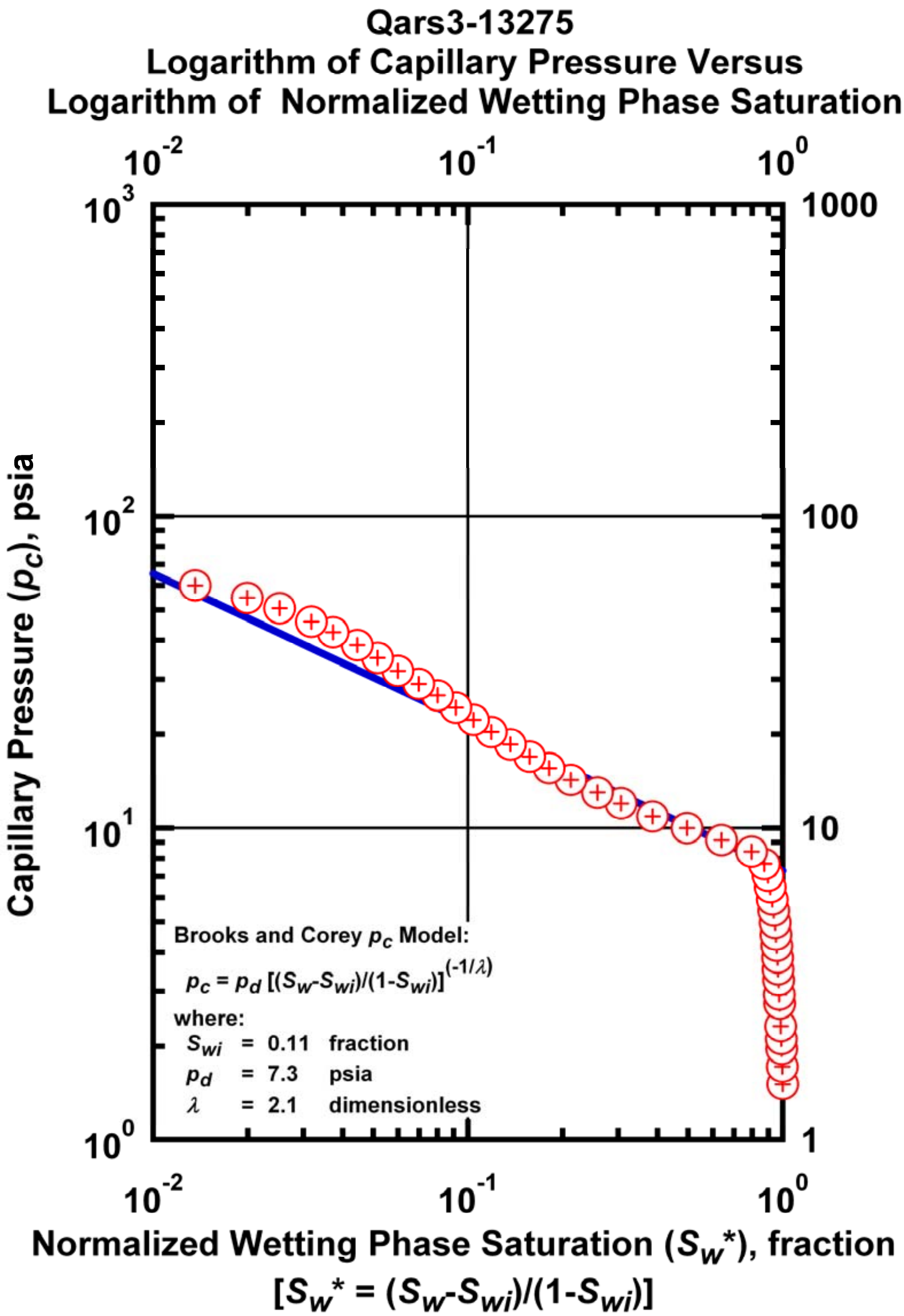

Figure K.69 – Plot of logarithm of capillary pressure vs. logarithm of normalized wetting phase saturation — Case Qars3-13275.

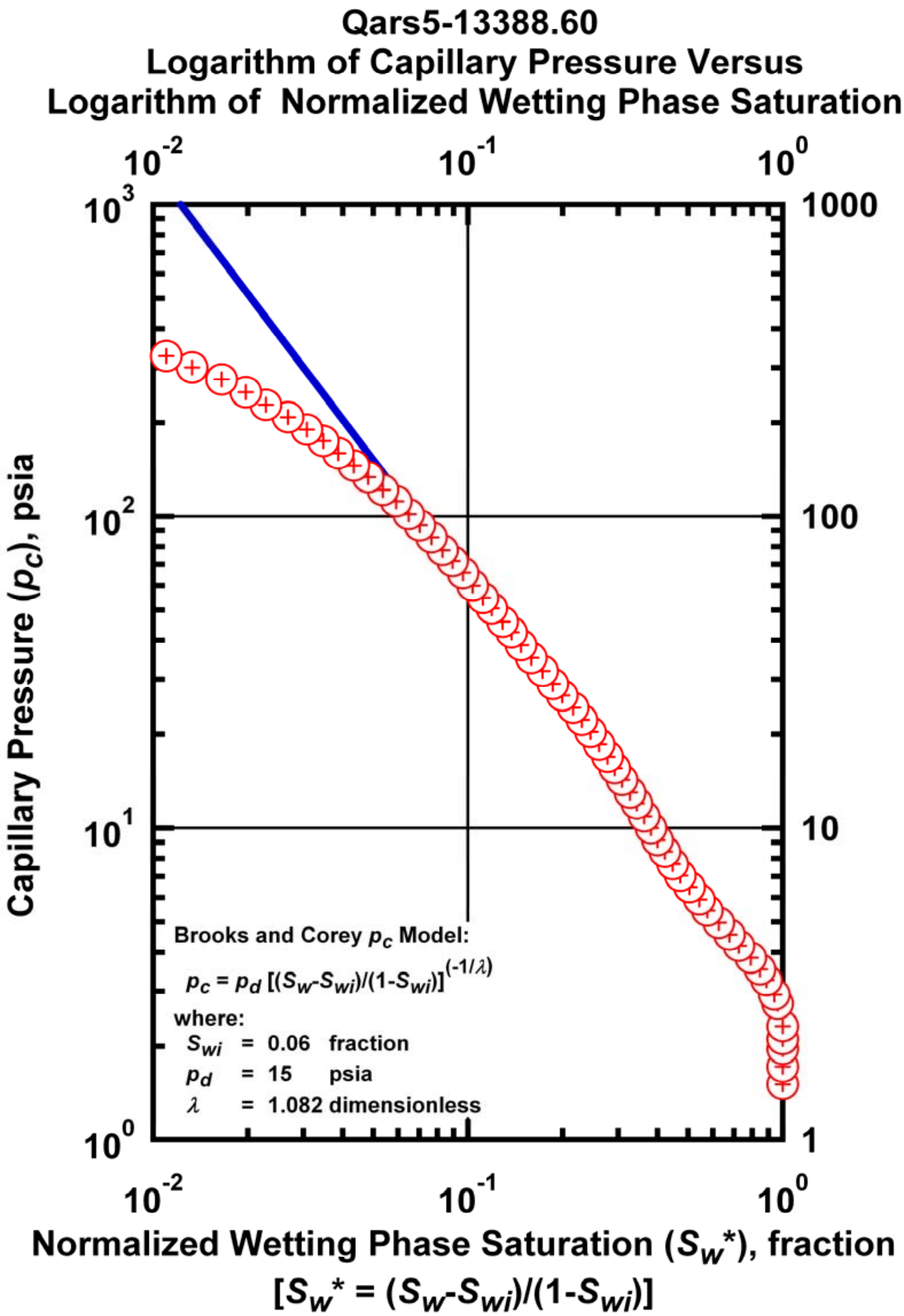

Figure K.70 – Plot of logarithm of capillary pressure vs. logarithm of normalized wetting phase saturation — Case Qars5-13388.6.

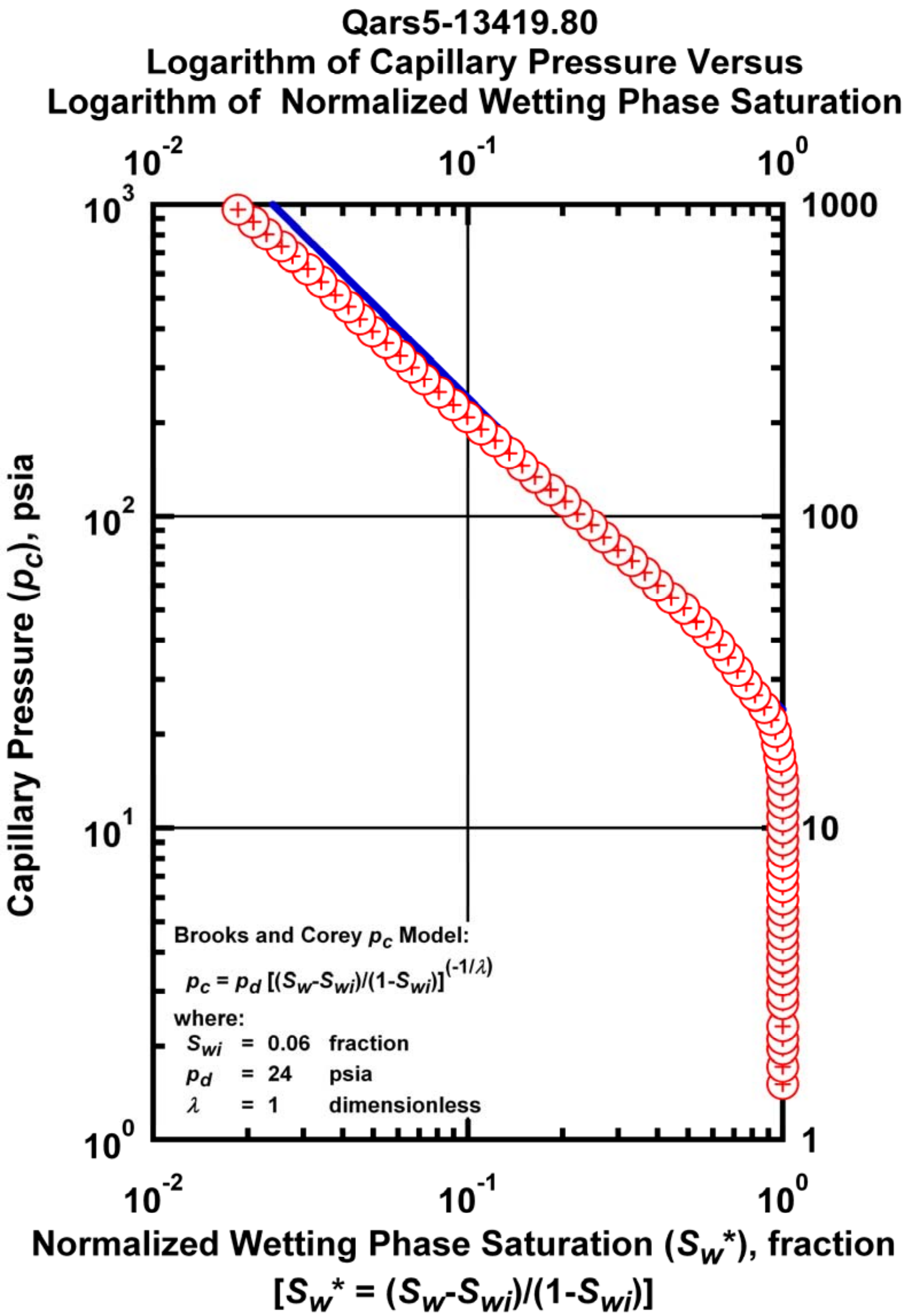

Figure K.71 – Plot of logarithm of capillary pressure vs. logarithm of normalized wetting phase saturation –– Case Qars5-13419.8.

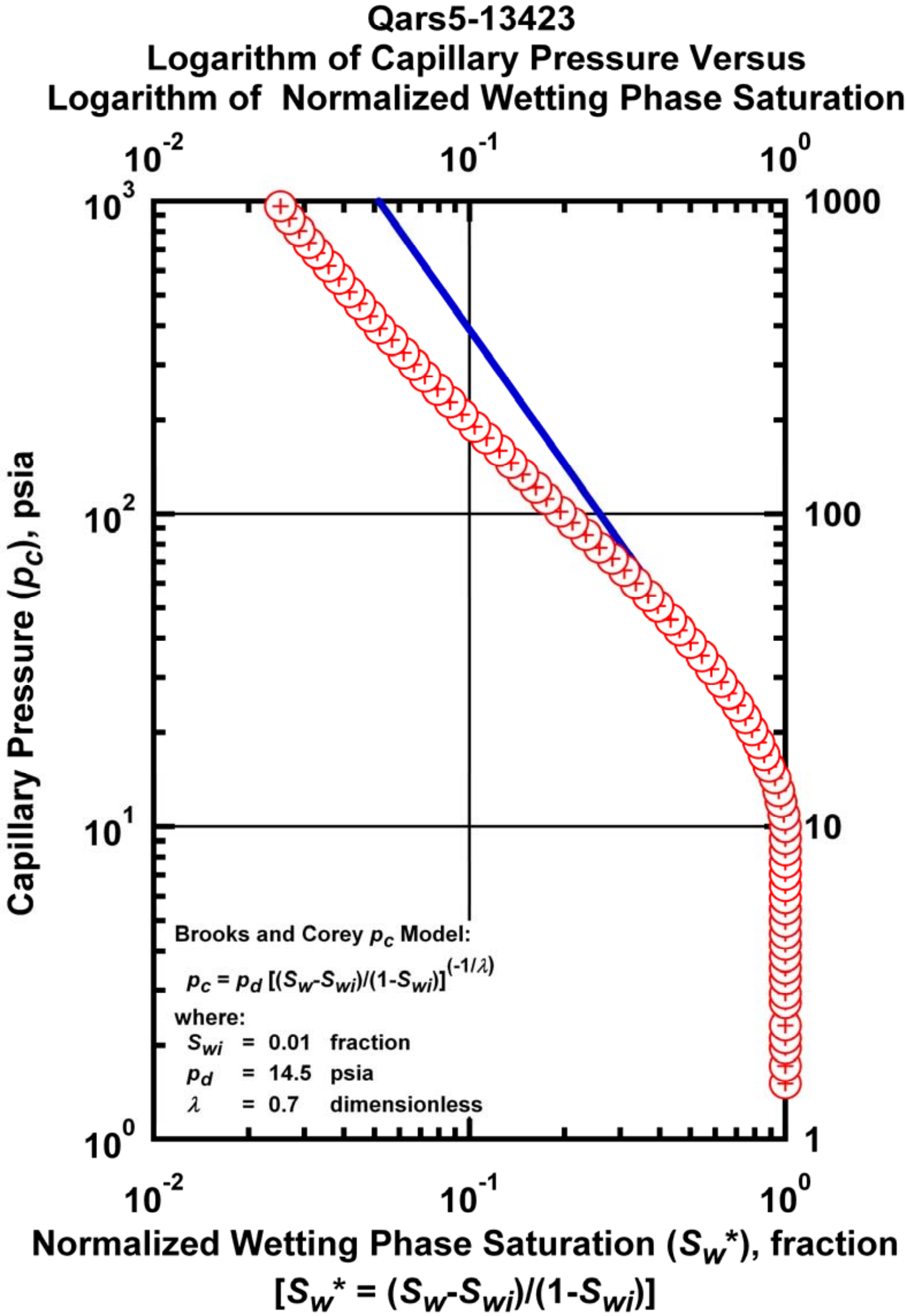

Figure K.72 – Plot of logarithm of capillary pressure vs. logarithm of normalized wetting phase saturation — Case Qars5-13423.

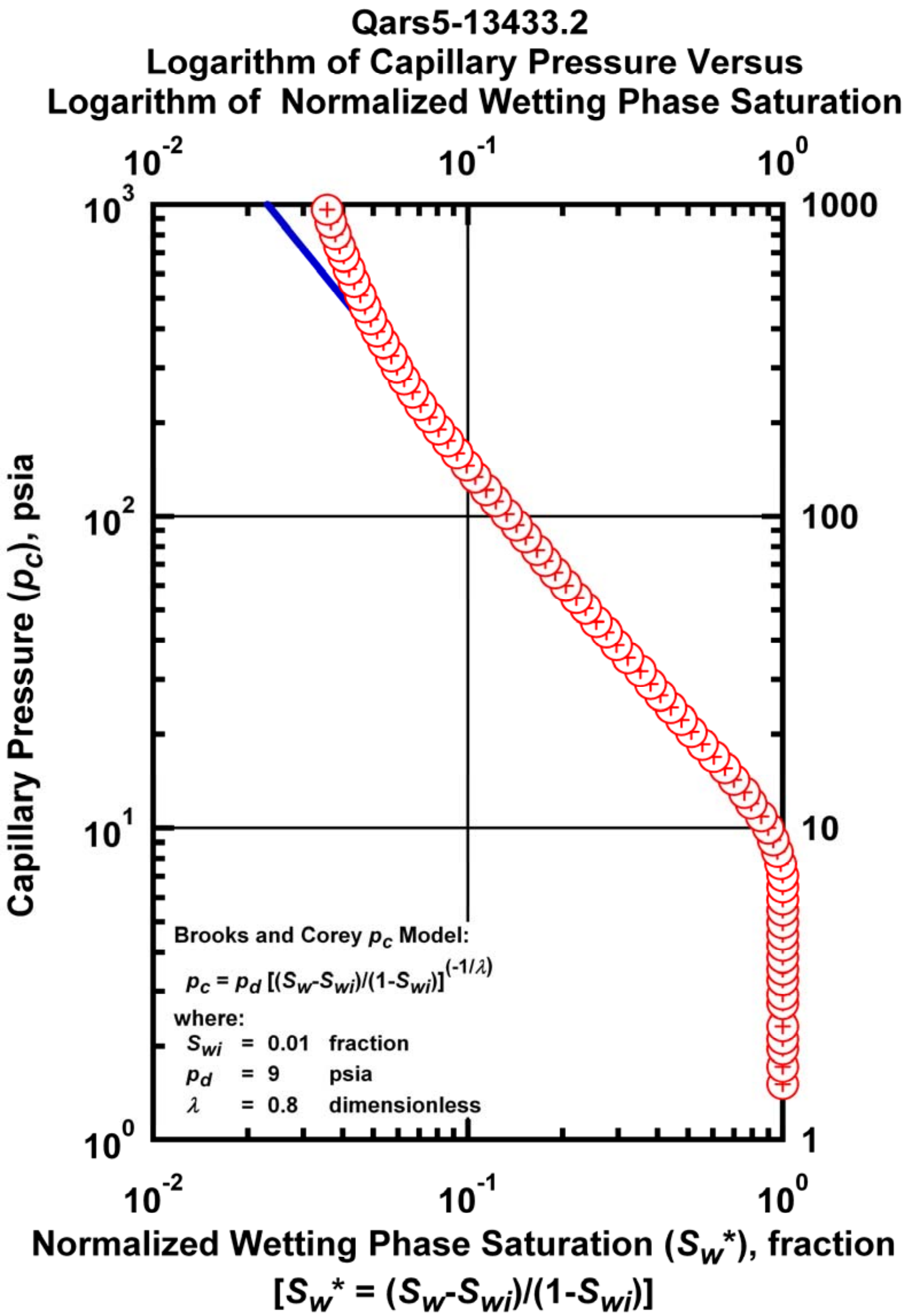

Figure K.73 – Plot of logarithm of capillary pressure vs. logarithm of normalized wetting phase saturation — Case Qars5-13433.2.

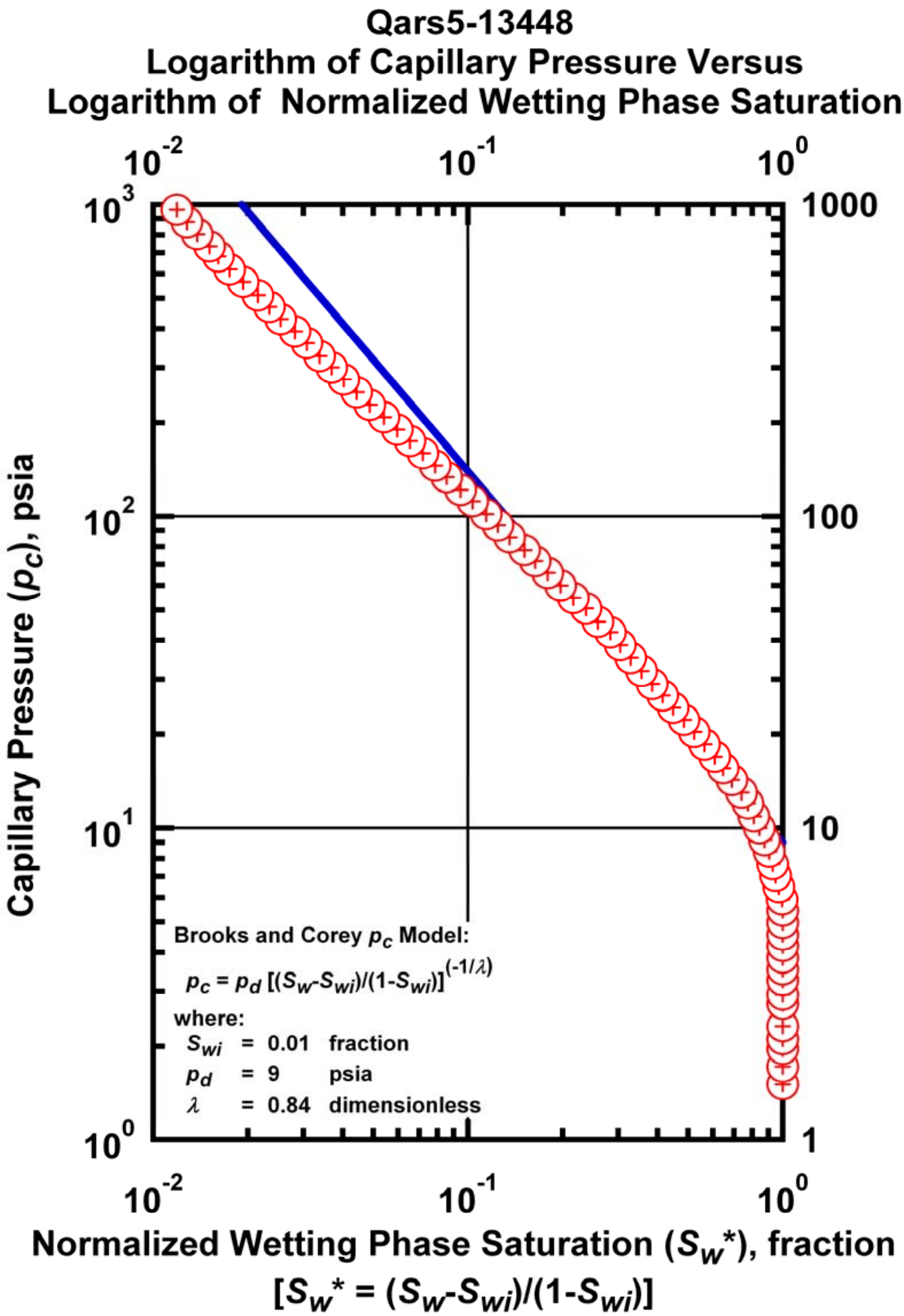

Figure K.74 – Plot of logarithm of capillary pressure vs. logarithm of normalized wetting phase saturation — Case Qars5-13448.

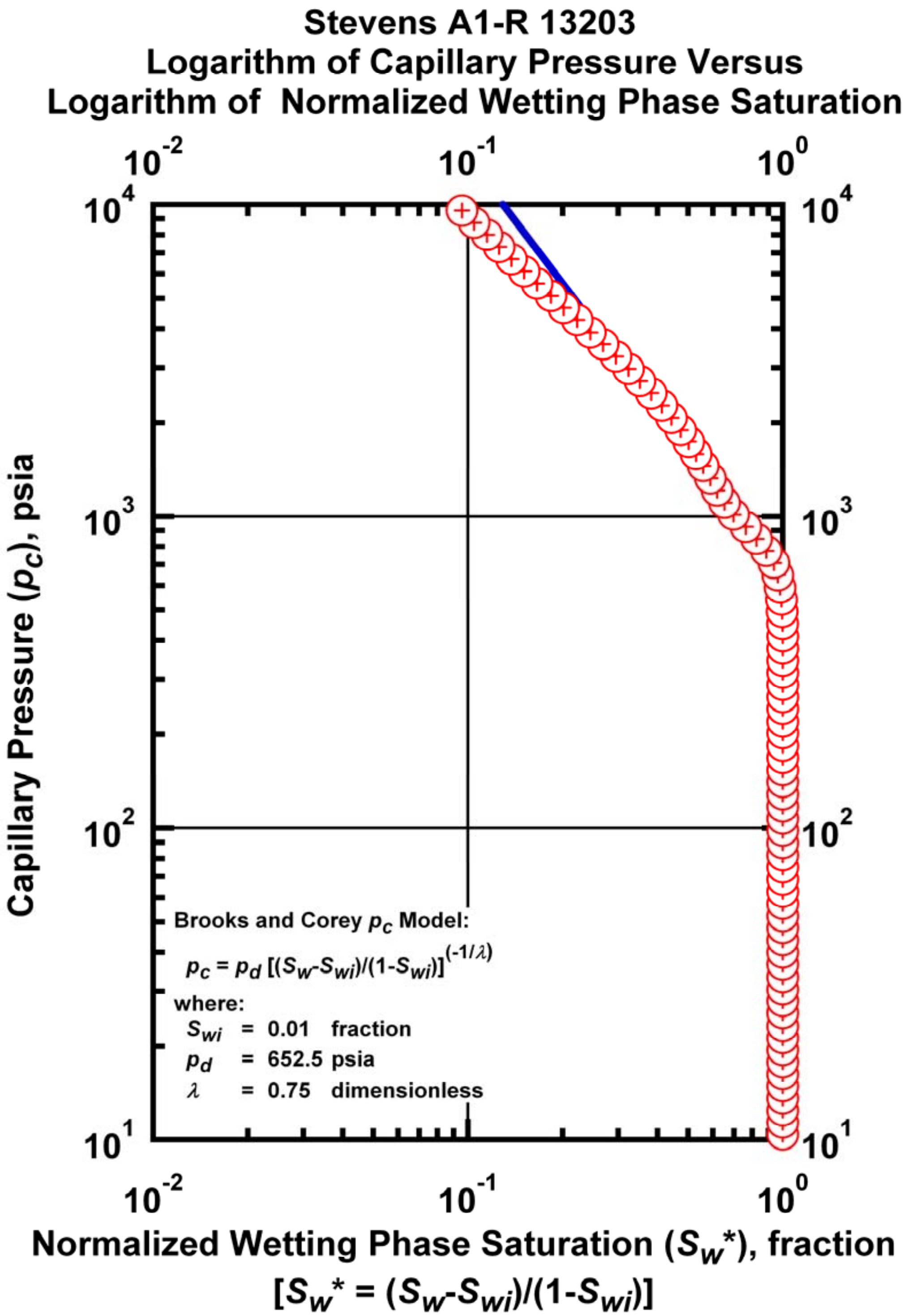

Figure K.75 – Plot of logarithm of capillary pressure vs. logarithm of normalized wetting phase saturation — Case Stevens A1-R 13203.

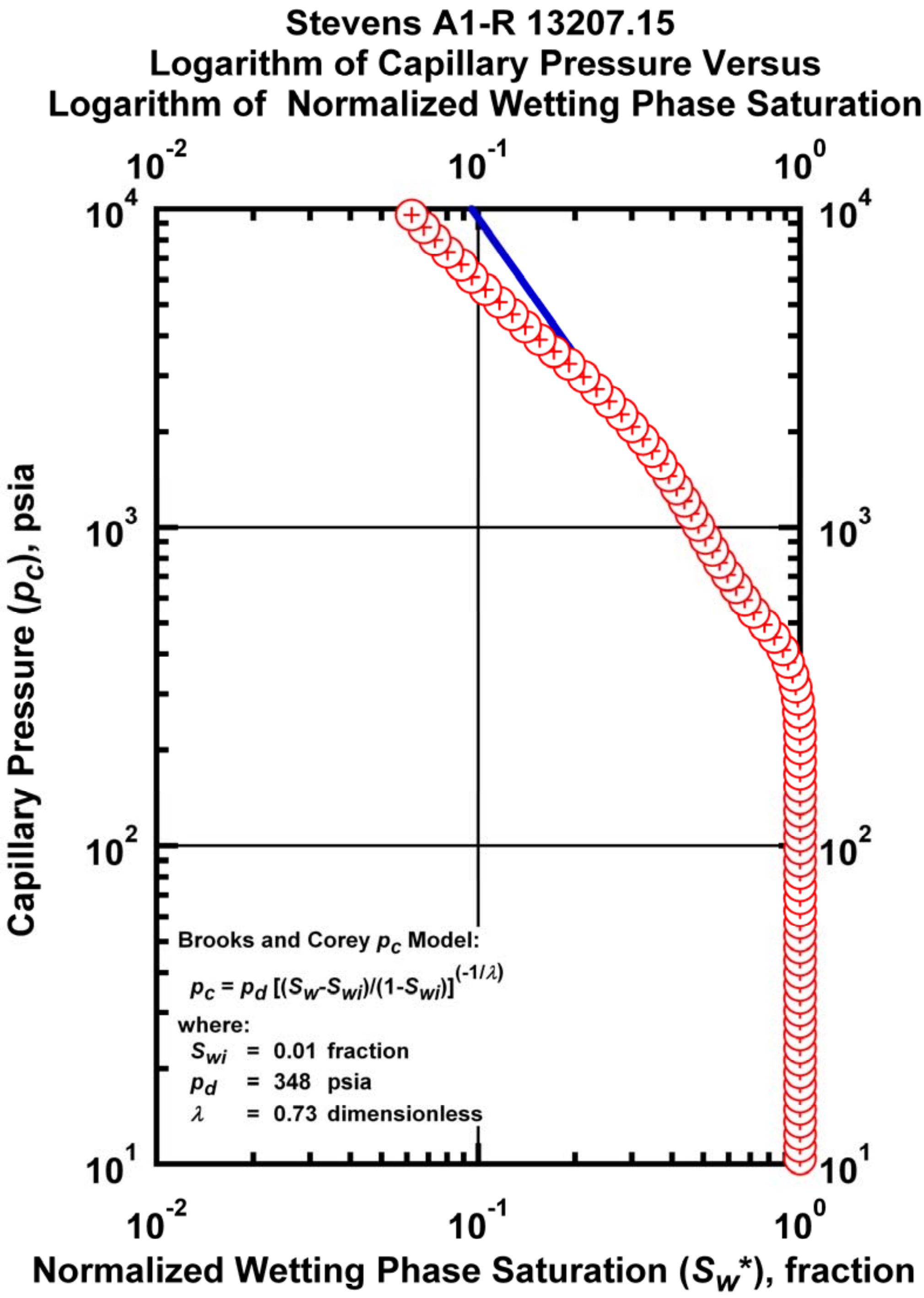

Figure K.76 – Plot of logarithm of capillary pressure vs. logarithm of normalized wetting phase saturation — Case Stevens A1-R 13207.15.

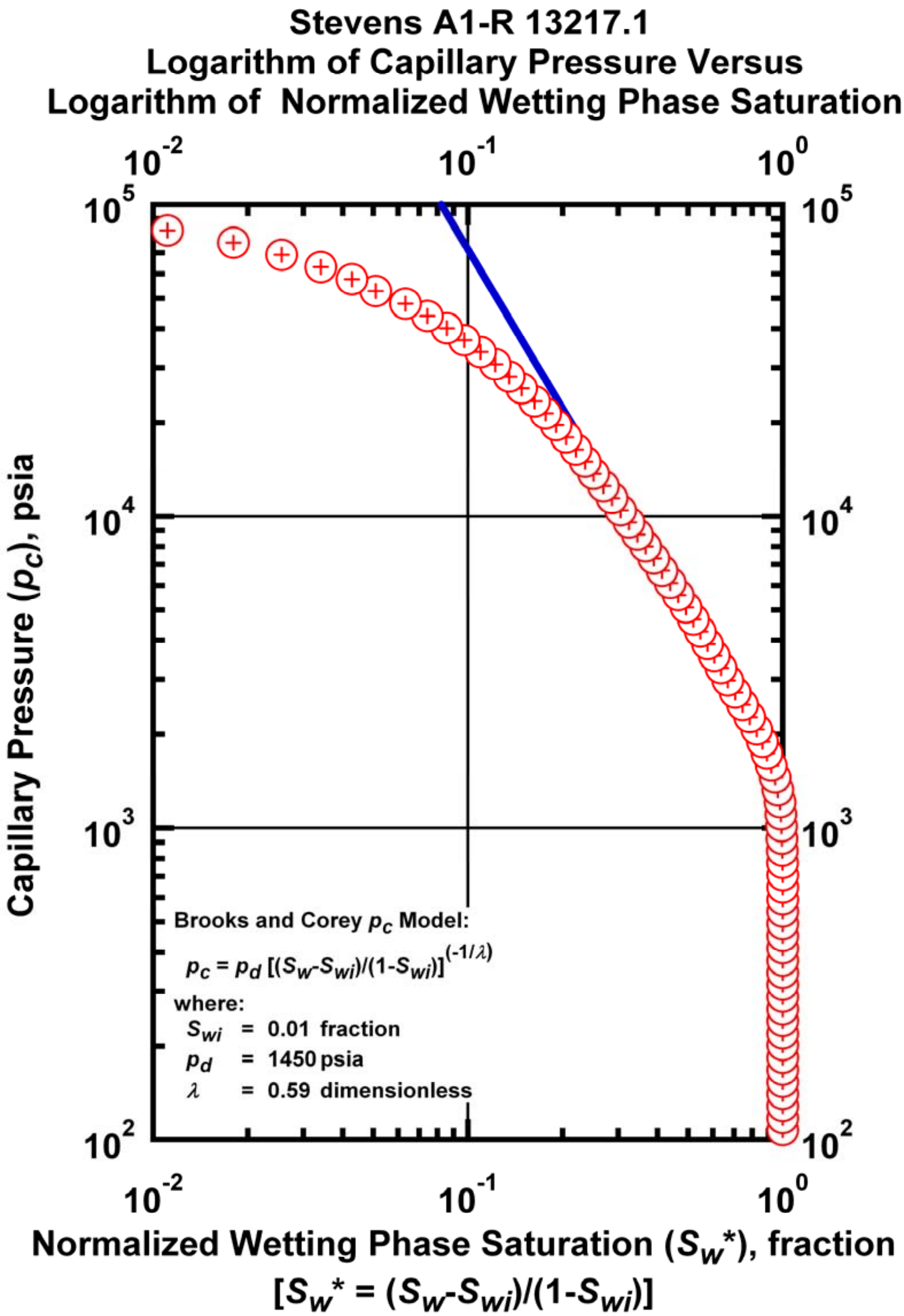

Figure K.77 – Plot of logarithm of capillary pressure vs. logarithm of normalized wetting phase saturation — Case Stevens A1-R 13217.1.

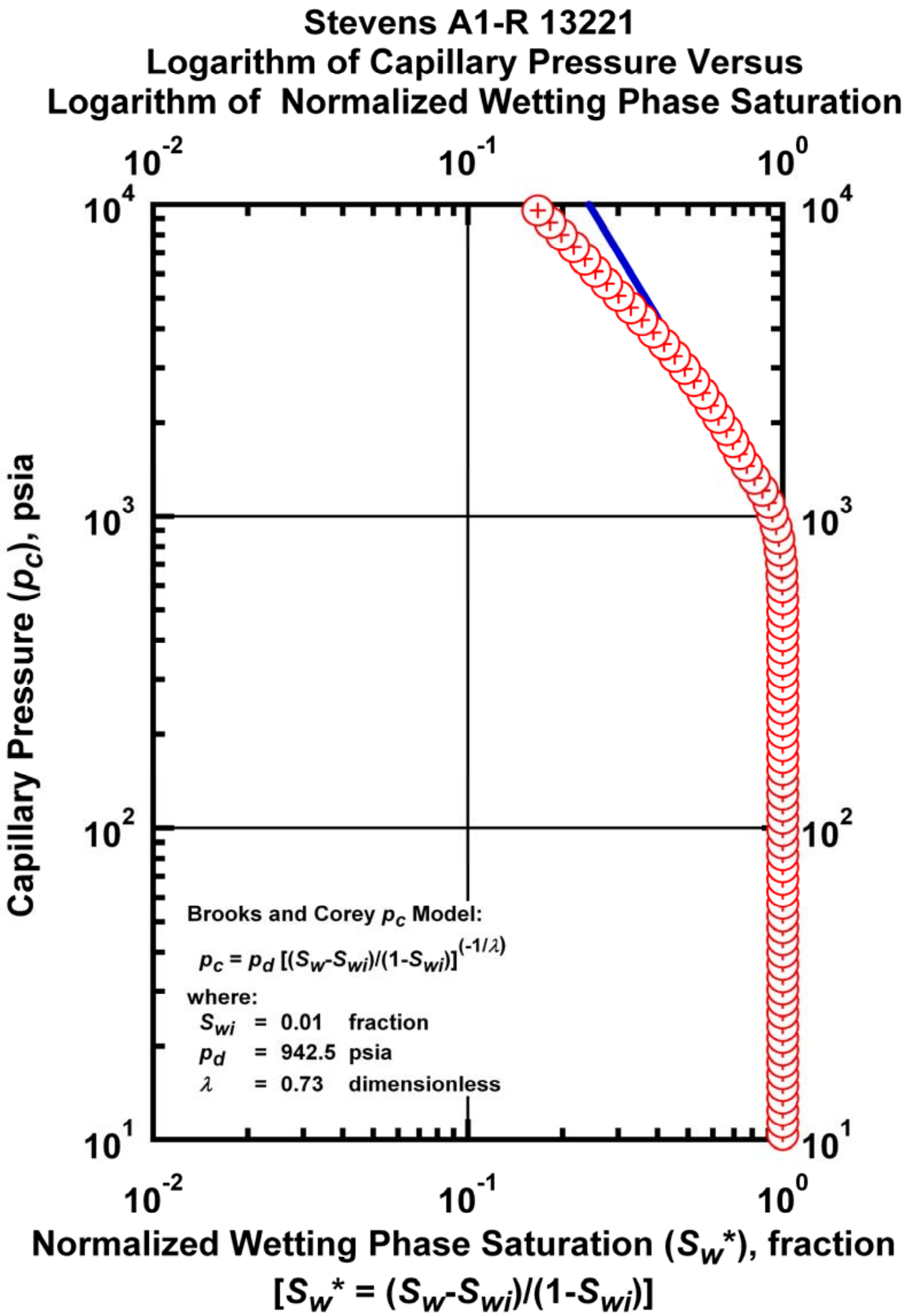

Figure K.78 – Plot of logarithm of capillary pressure vs. logarithm of normalized wetting phase saturation — Case Stevens A1-R 13221.

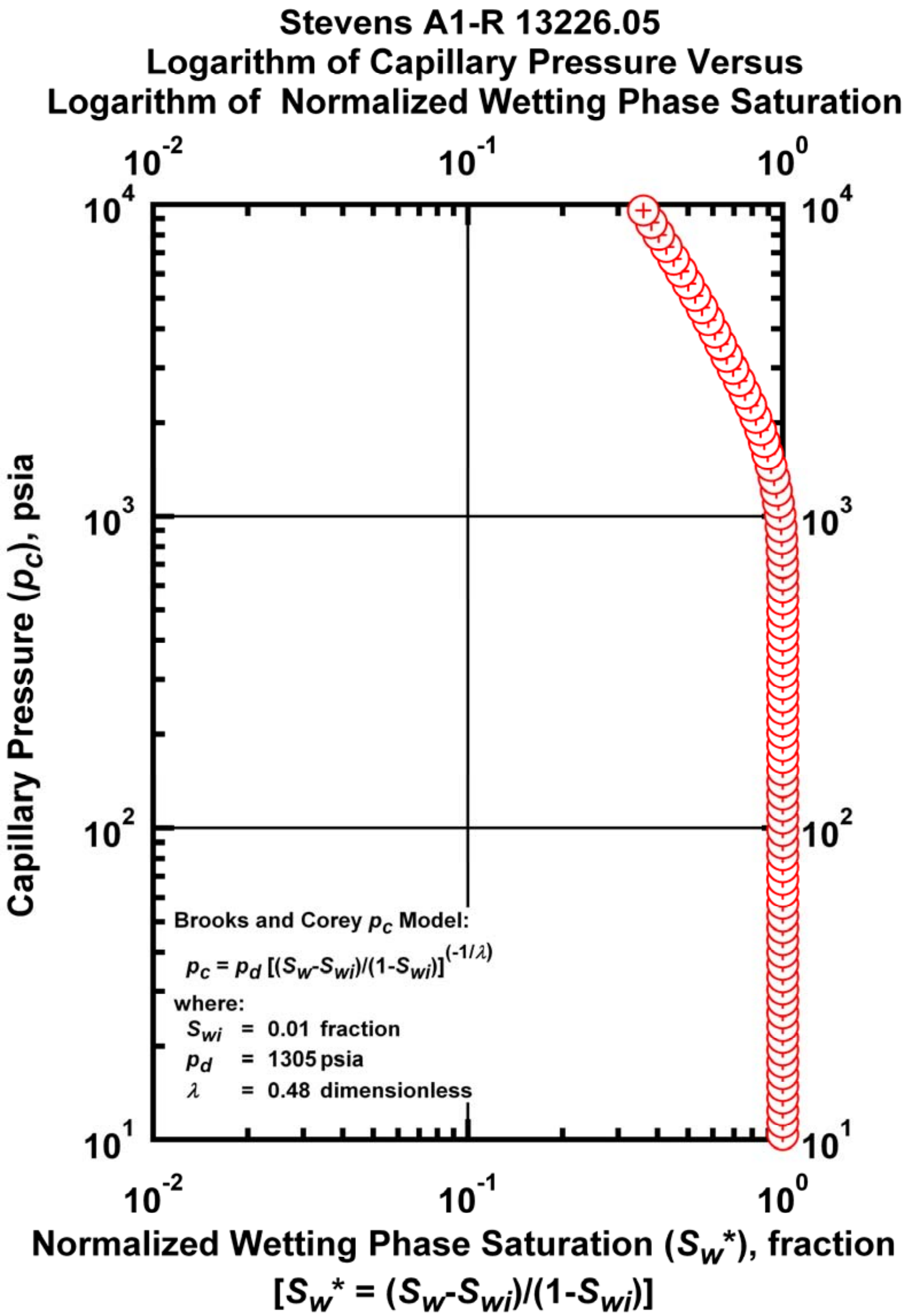

Figure K.79 – Plot of logarithm of capillary pressure vs. logarithm of normalized wetting phase saturation — Case Stevens A1-R 13226.05.

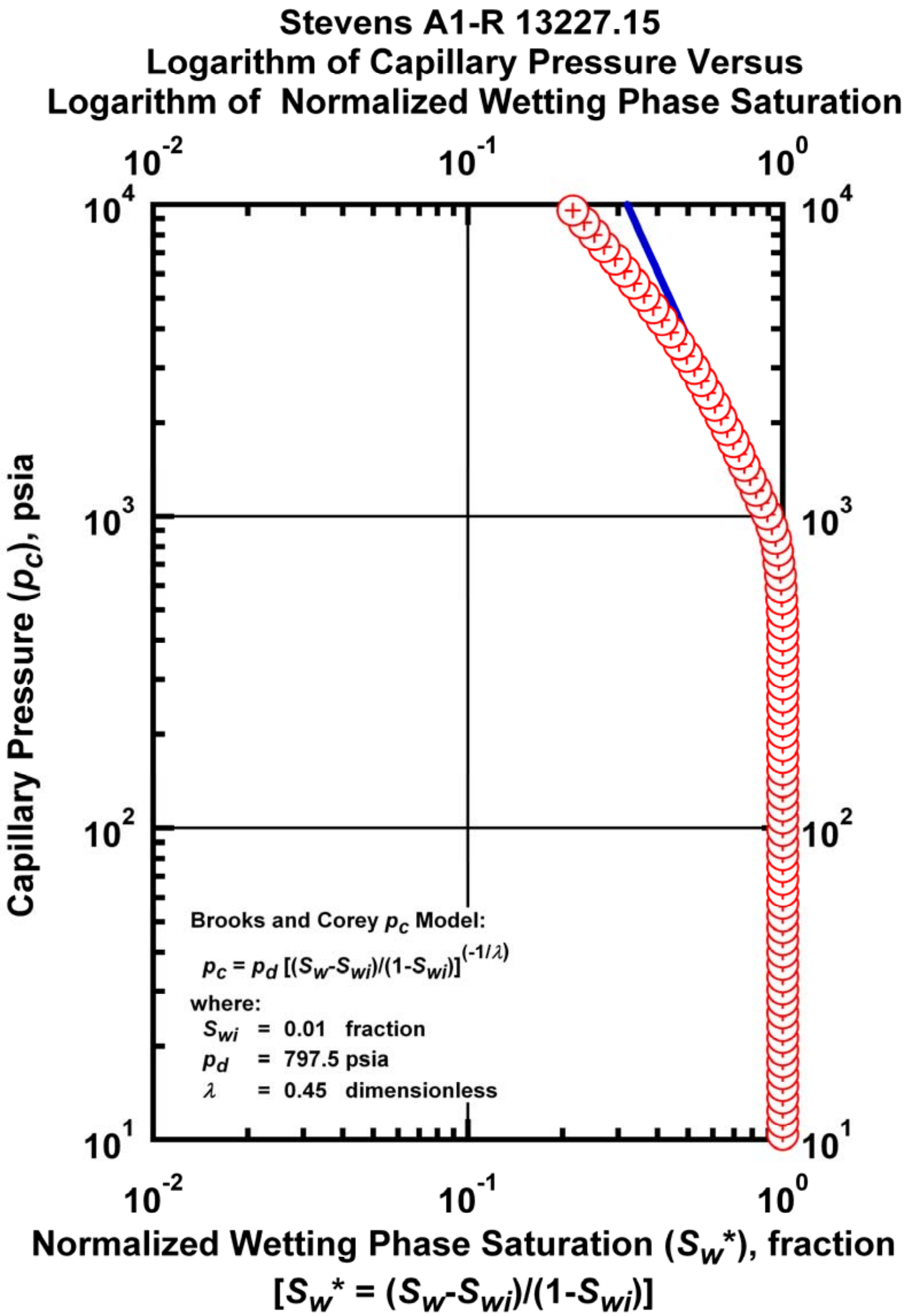

Figure K.80 – Plot of logarithm of capillary pressure vs. logarithm of normalized wetting phase saturation — Case Stevens A1-R 13227.15.

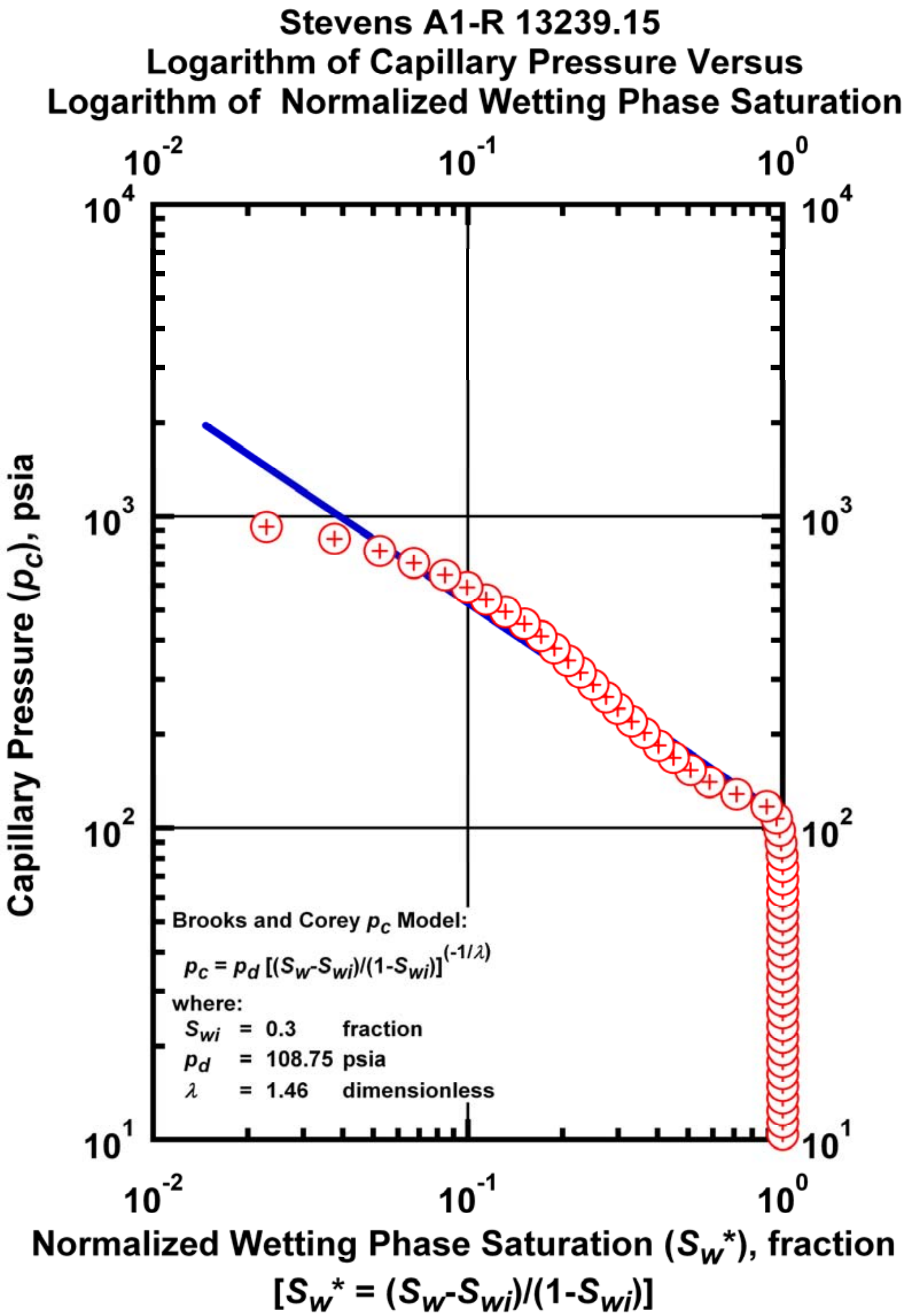

Figure K.81 – Plot of logarithm of capillary pressure vs. logarithm of normalized wetting phase saturation — Case Stevens A1-R 13239.15.

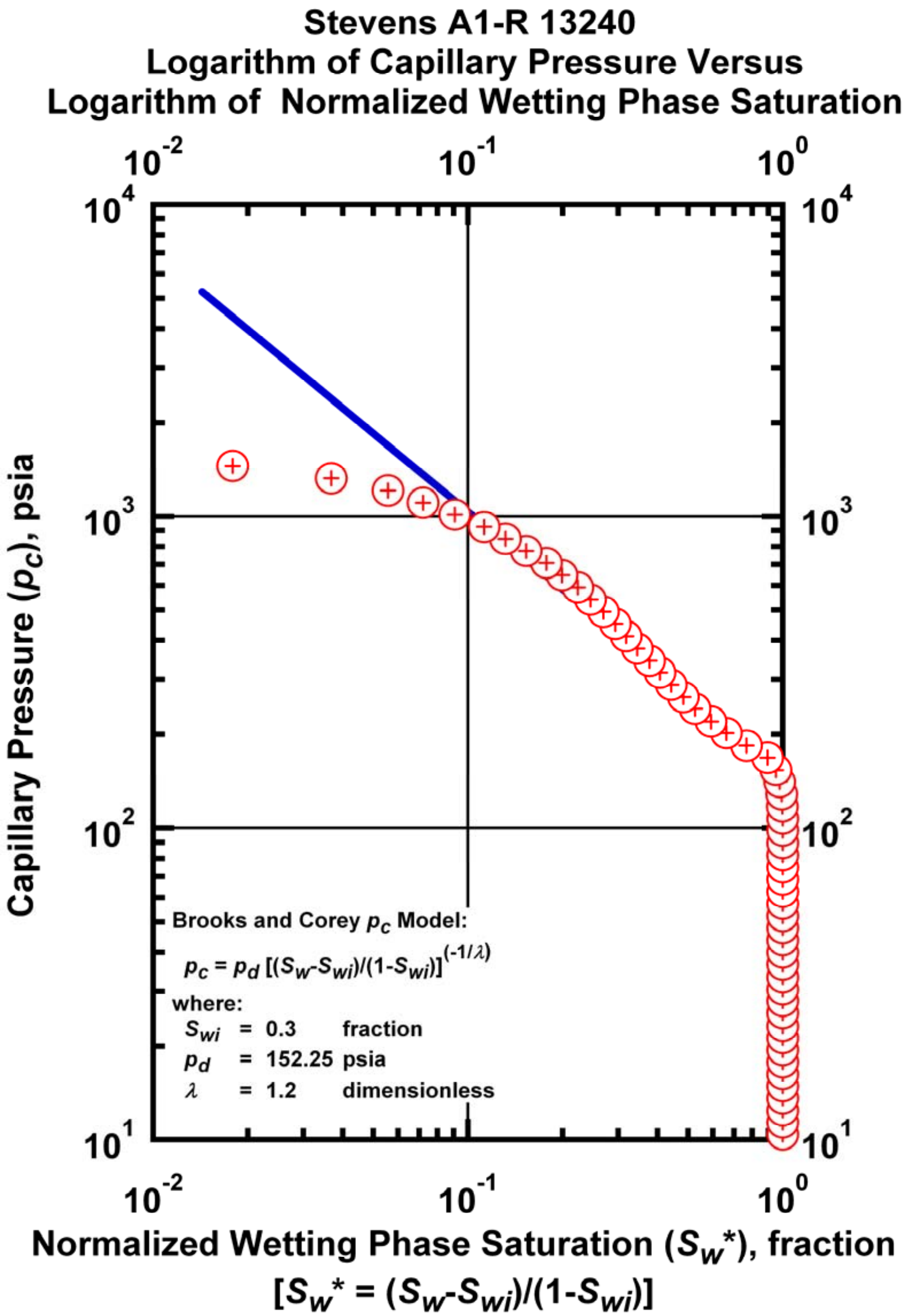

Figure K.82 – Plot of logarithm of capillary pressure vs. logarithm of normalized wetting phase saturation — Case Stevens A1-R 13240.

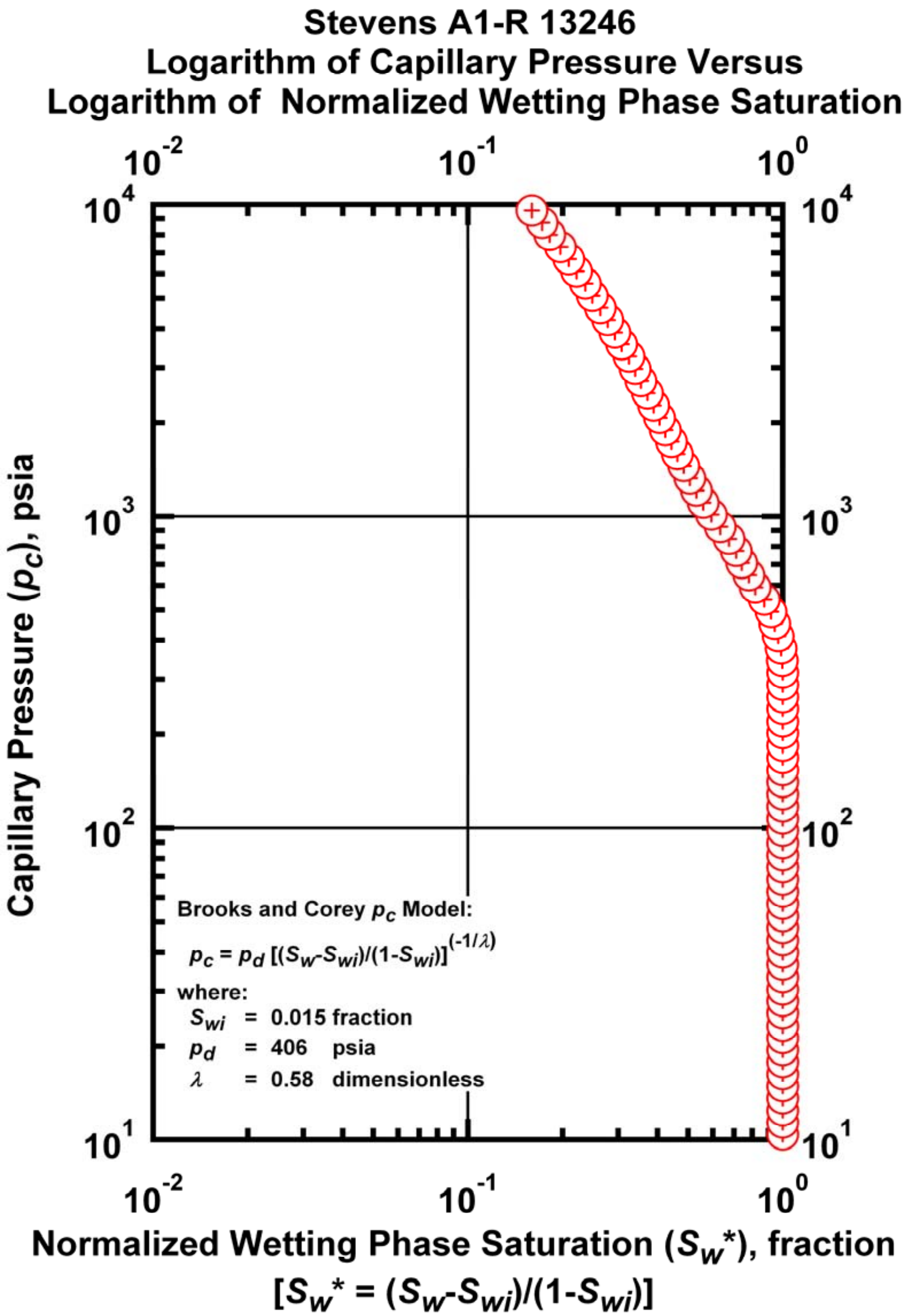

Figure K.83 – Plot of logarithm of capillary pressure vs. logarithm of normalized wetting phase saturation — Case Stevens A1-R 13246.

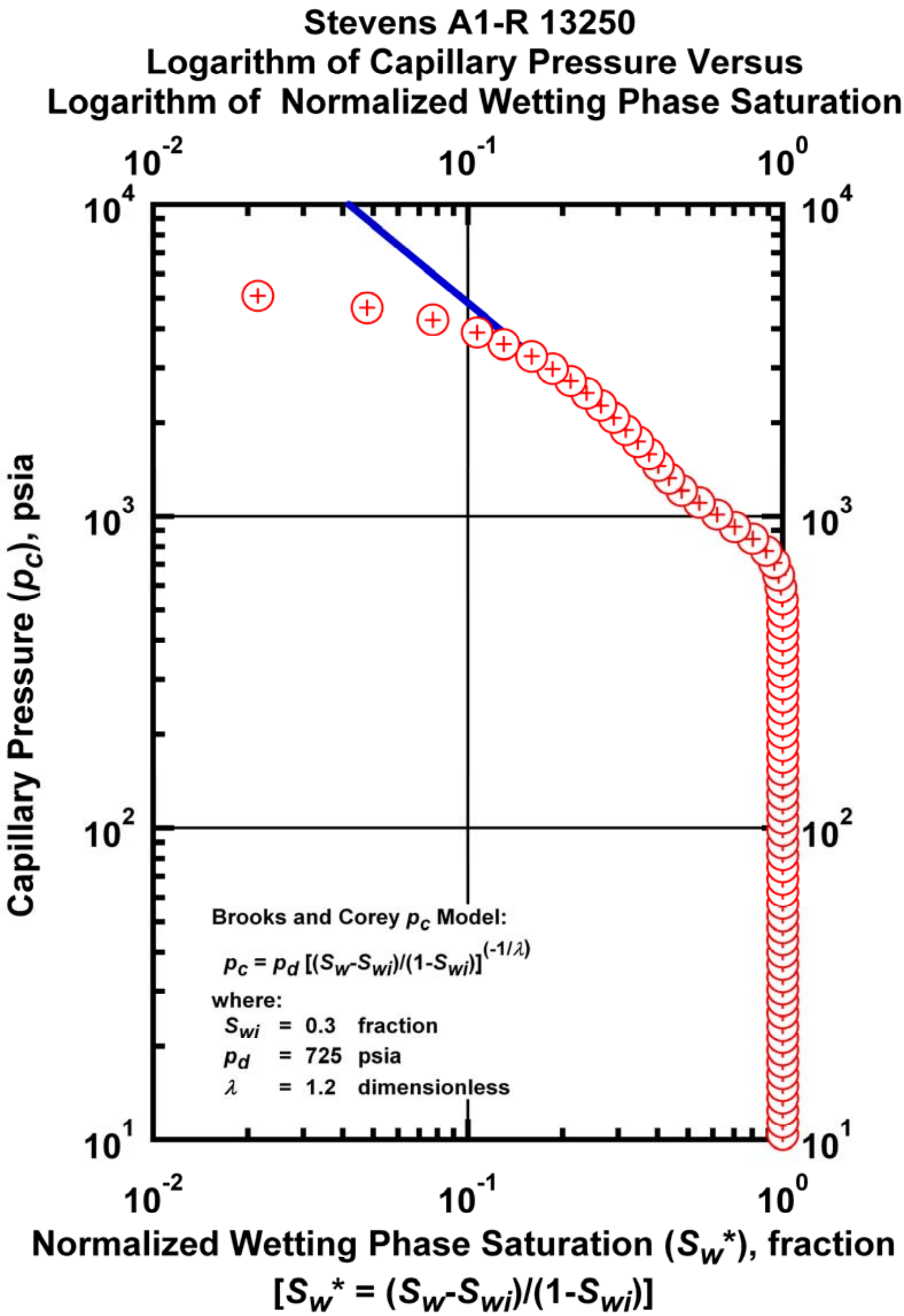

Figure K.84 – Plot of logarithm of capillary pressure vs. logarithm of normalized wetting phase saturation — Case Stevens A1-R 13250.

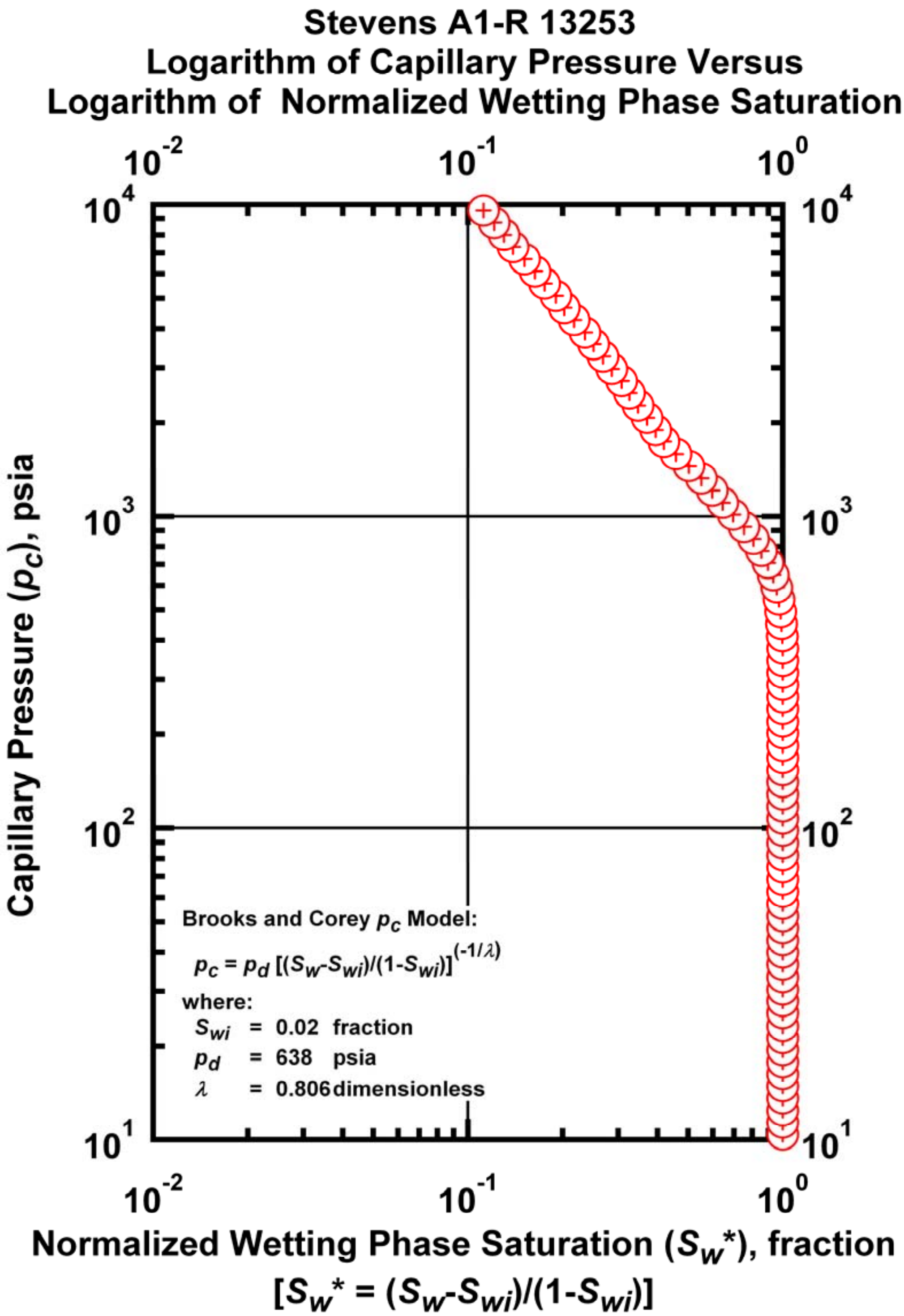

Figure K.85 – Plot of logarithm of capillary pressure vs. logarithm of normalized wetting phase saturation — Case Stevens A1-R 13253.

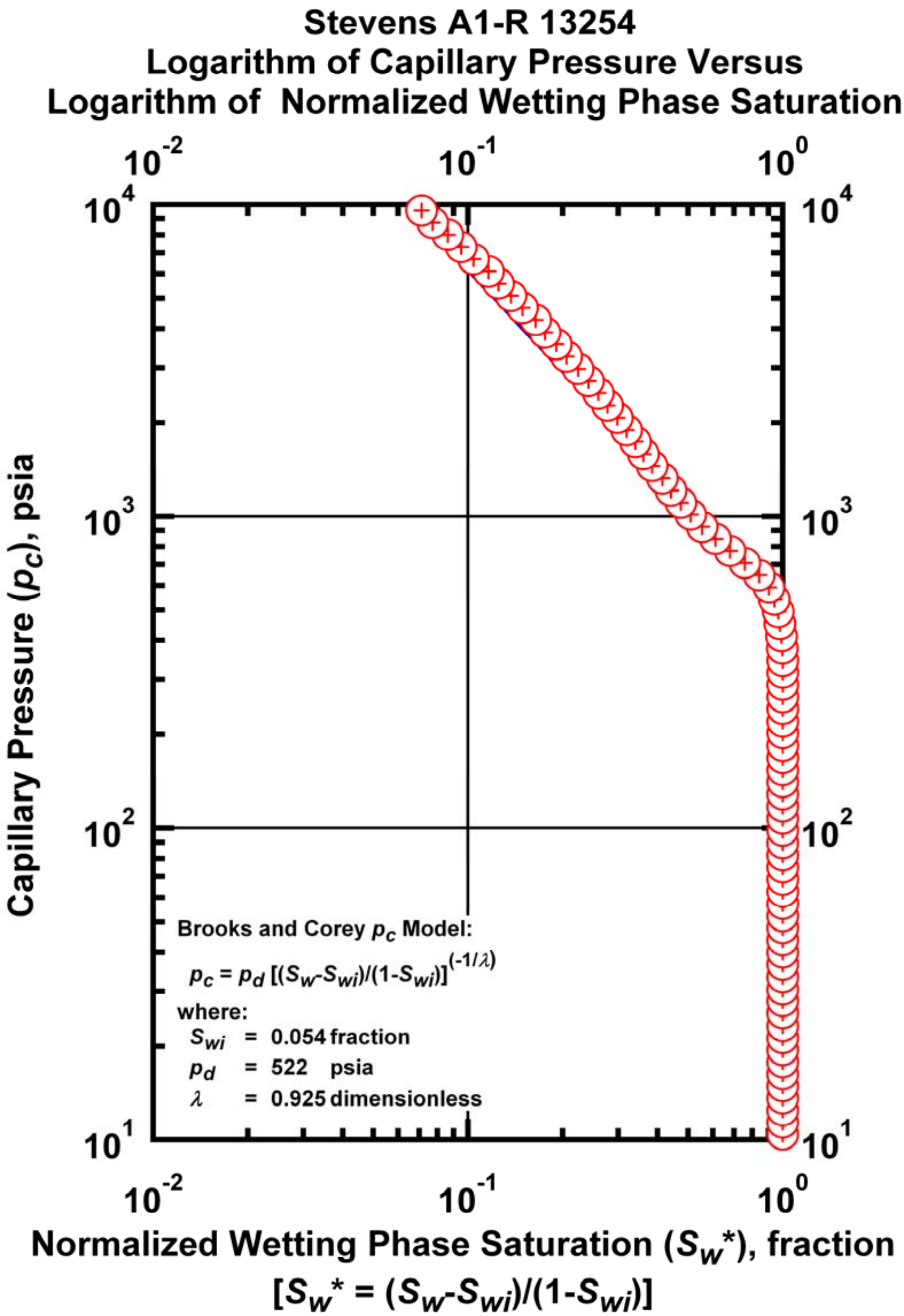

Figure K.86 – Plot of logarithm of capillary pressure vs. logarithm of normalized wetting phase saturation — Case Stevens A1-R 13254.

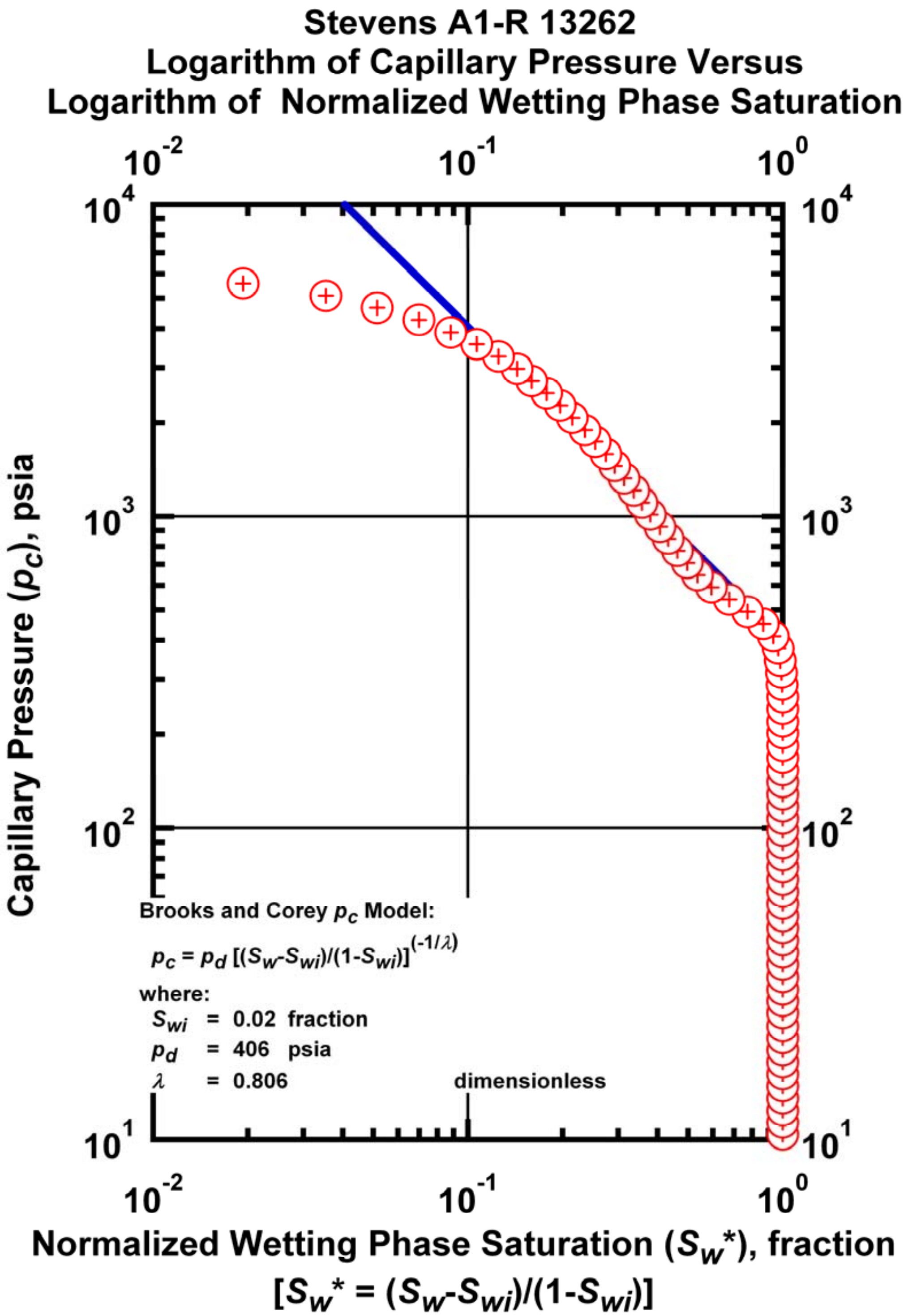

Figure K.87 – Plot of logarithm of capillary pressure vs. logarithm of normalized wetting phase saturation — Case Stevens A1-R 13262.

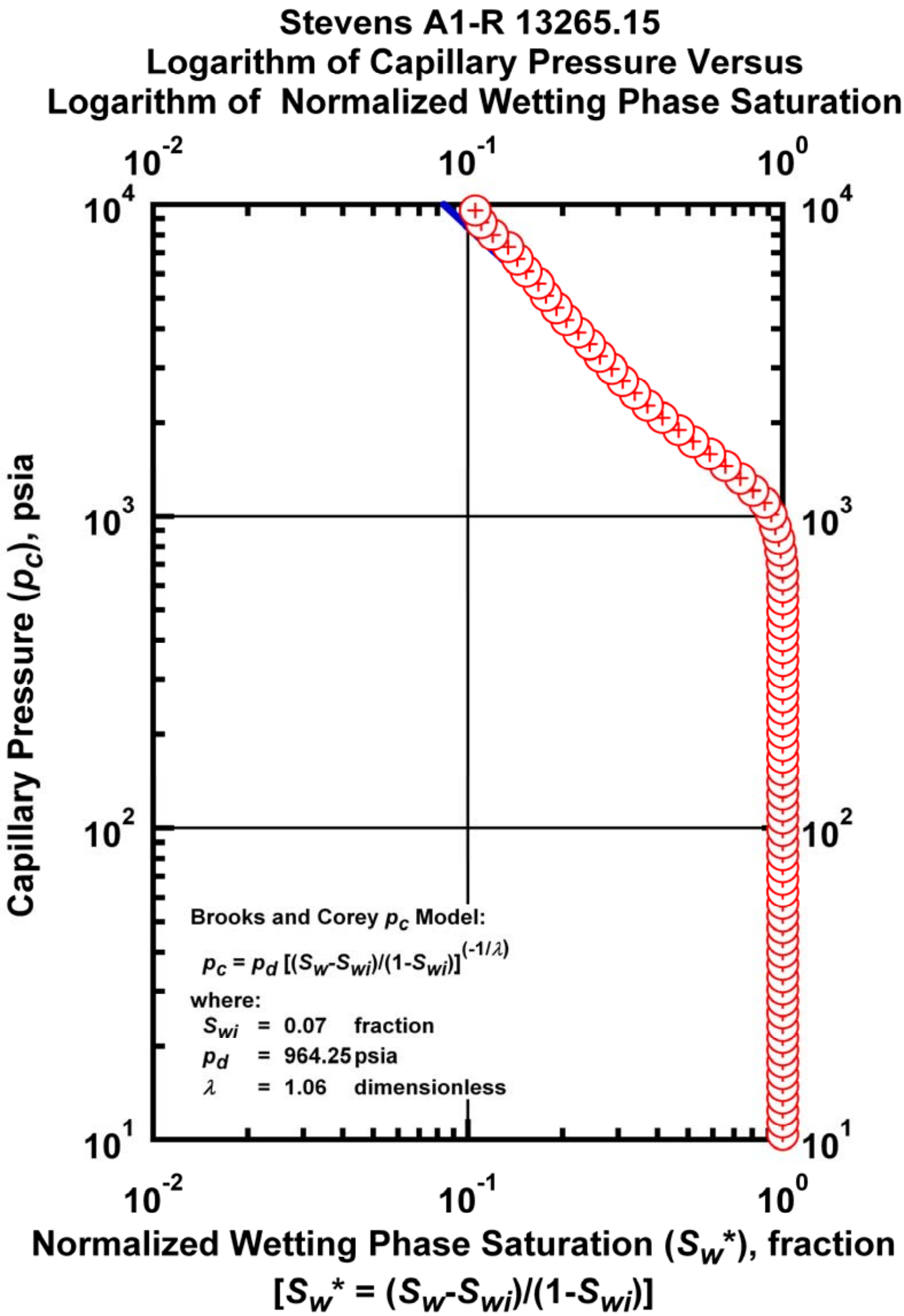

Figure K.88 – Plot of logarithm of capillary pressure vs. logarithm of normalized wetting phase saturation — Case Stevens A1-R 13265.15.

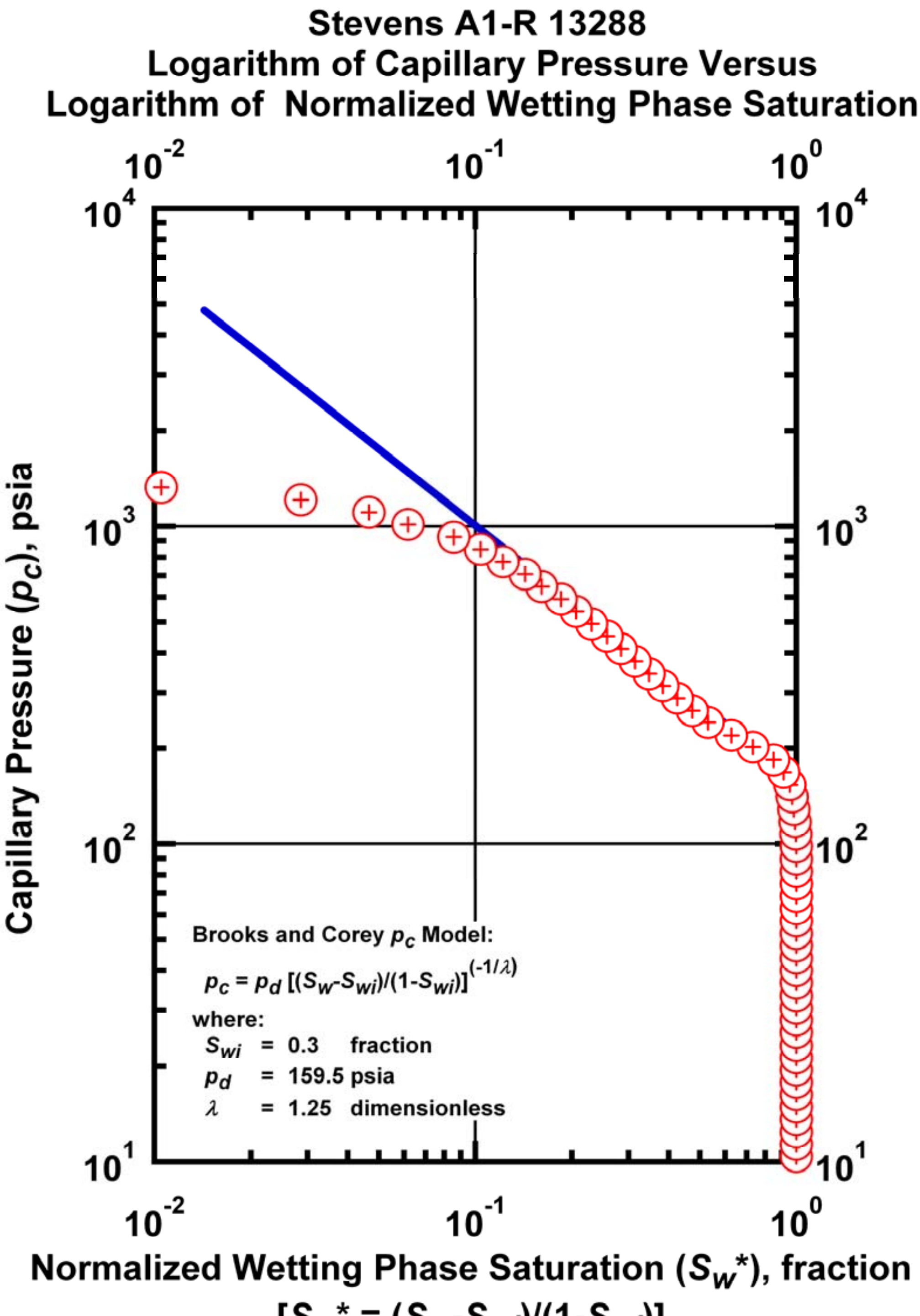

Figure K.89 – Plot of logarithm of capillary pressure vs. logarithm of normalized wetting phase saturation — Case Stevens A1-R 13288.

APPENDIX L

LIBRARY OF DIMENSIONLESS CAPILLARY PRESSURE VERSUS NORMALIZED WETTING PHASE SATURATION PLOTS — LOG-LOG FORMAT "TYPE CURVE" FOR CAPILLARY PRESSURE (BROOKS AND COREY CAPILLARY PRESSURE MODEL)

This Appendix presents the calibration of the capillary displacement pressure (p_d), irreducible wetting-phase saturation (S_{wi}), and the index of pore-size distribution (λ) on a sample-by-sample basis using the Brooks-Corey $p_c(S_w)$ model .

In this Appendix, we provide for each data a plot of dimensionless capillary pressure (p_c) vs. normalized wetting phase saturation (S_w) – log-log format "type curve" for capillary pressure.

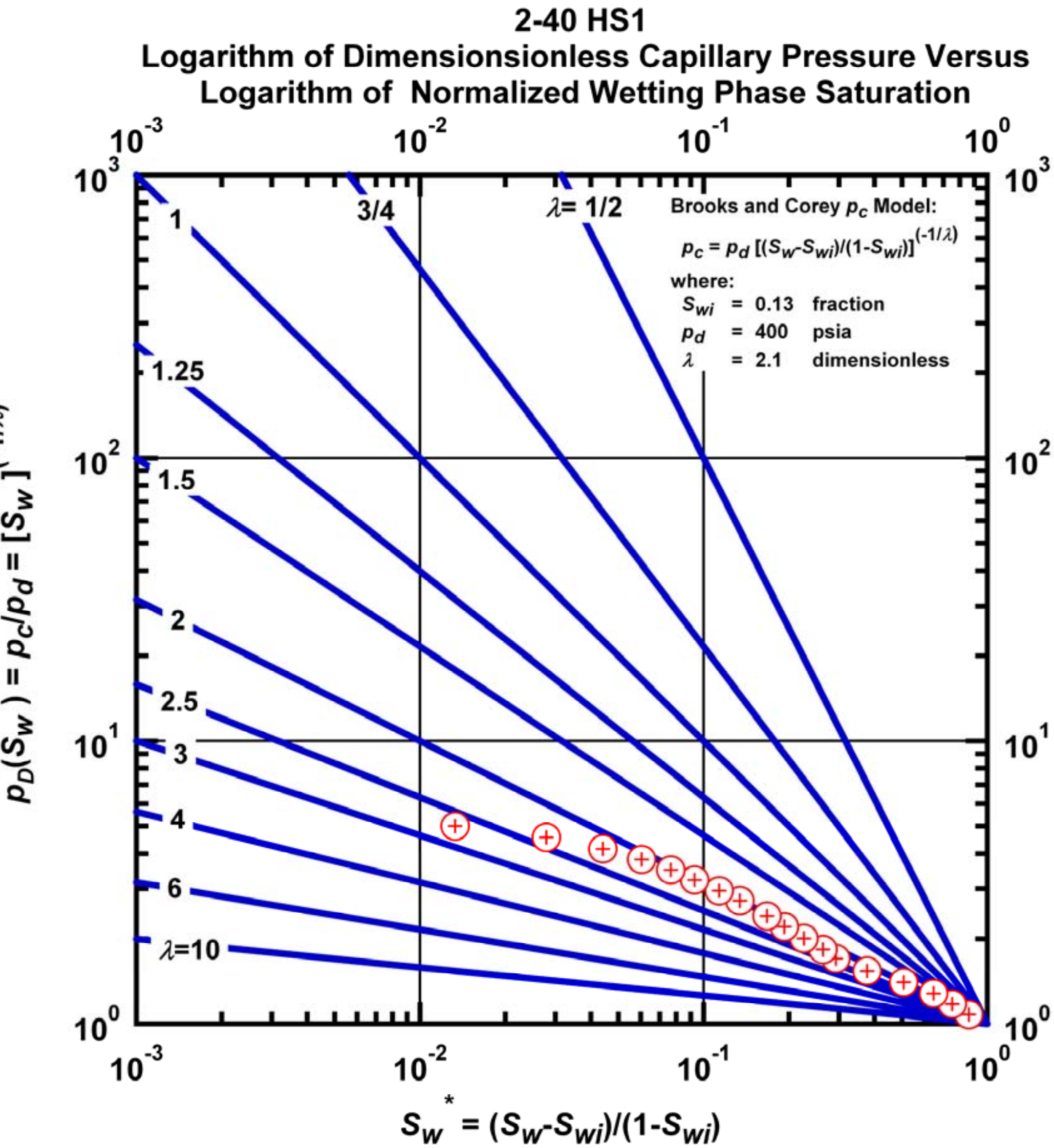

Figure L.1 – Plot of logarithm of dimensionless capillary pressure vs. logarithm of normalized wetting phase saturation — Case 2-40 HS1.

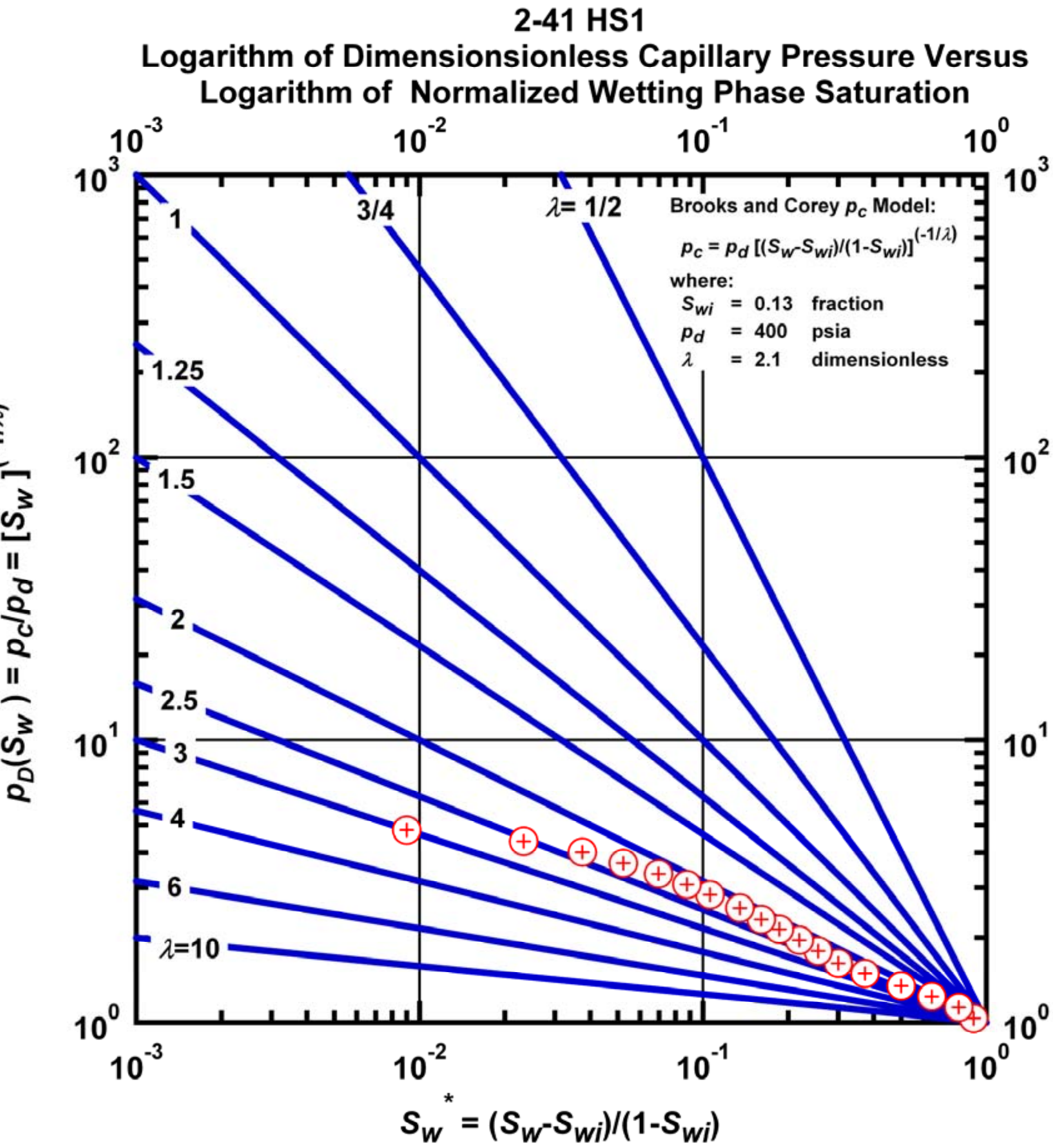

Figure L.2 – Plot of logarithm of dimensionless capillary pressure vs. logarithm of normalized wetting phase saturation — Case 2-40 HS1.

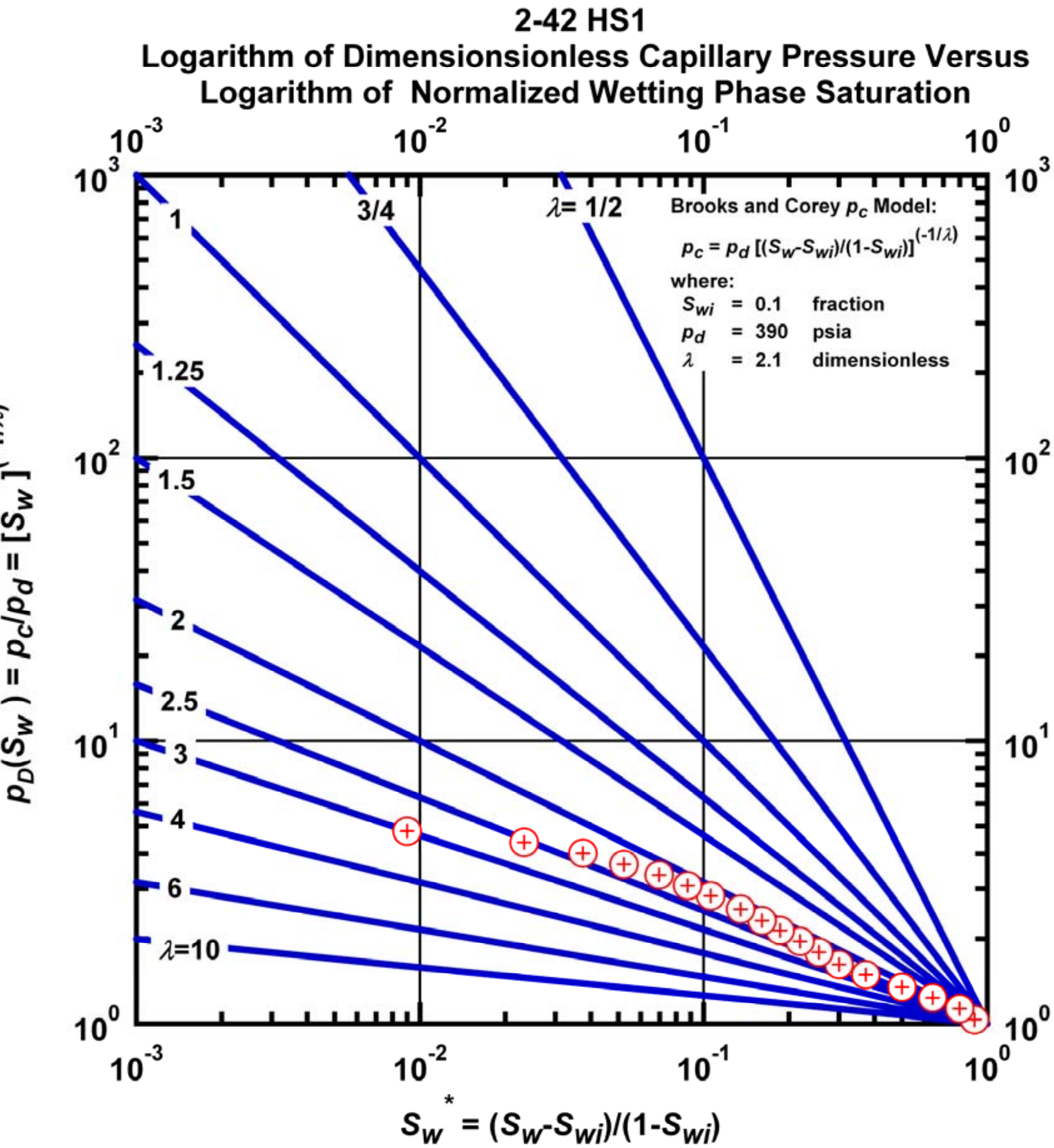

Figure L.3 – Plot of logarithm of dimensionless capillary pressure vs. logarithm of normalized wetting phase saturation — Case 2-42 HS1.

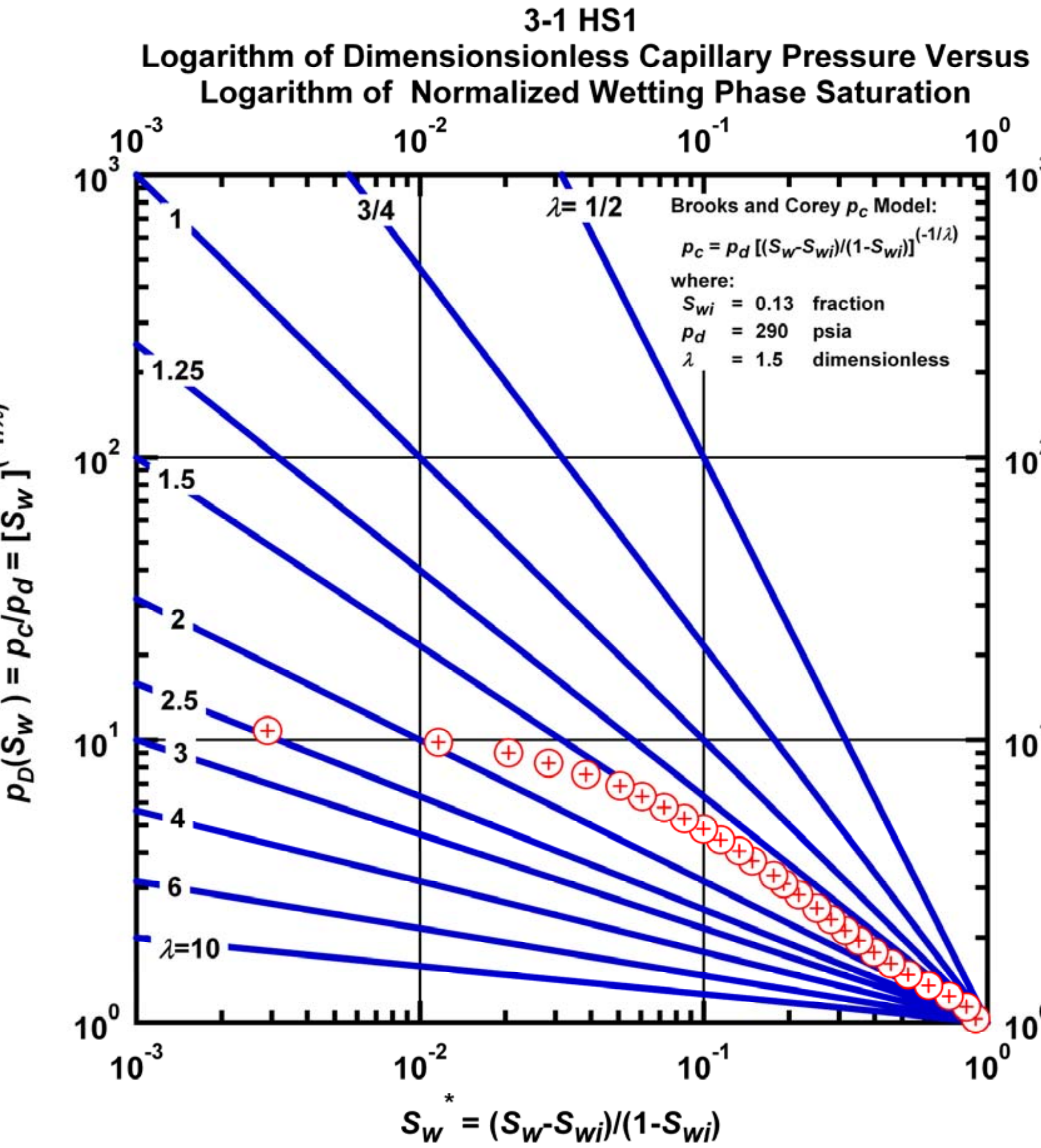

Figure L.4 – Plot of logarithm of dimensionless capillary pressure vs. logarithm of normalized wetting phase saturation — Case 3-1 HS1.

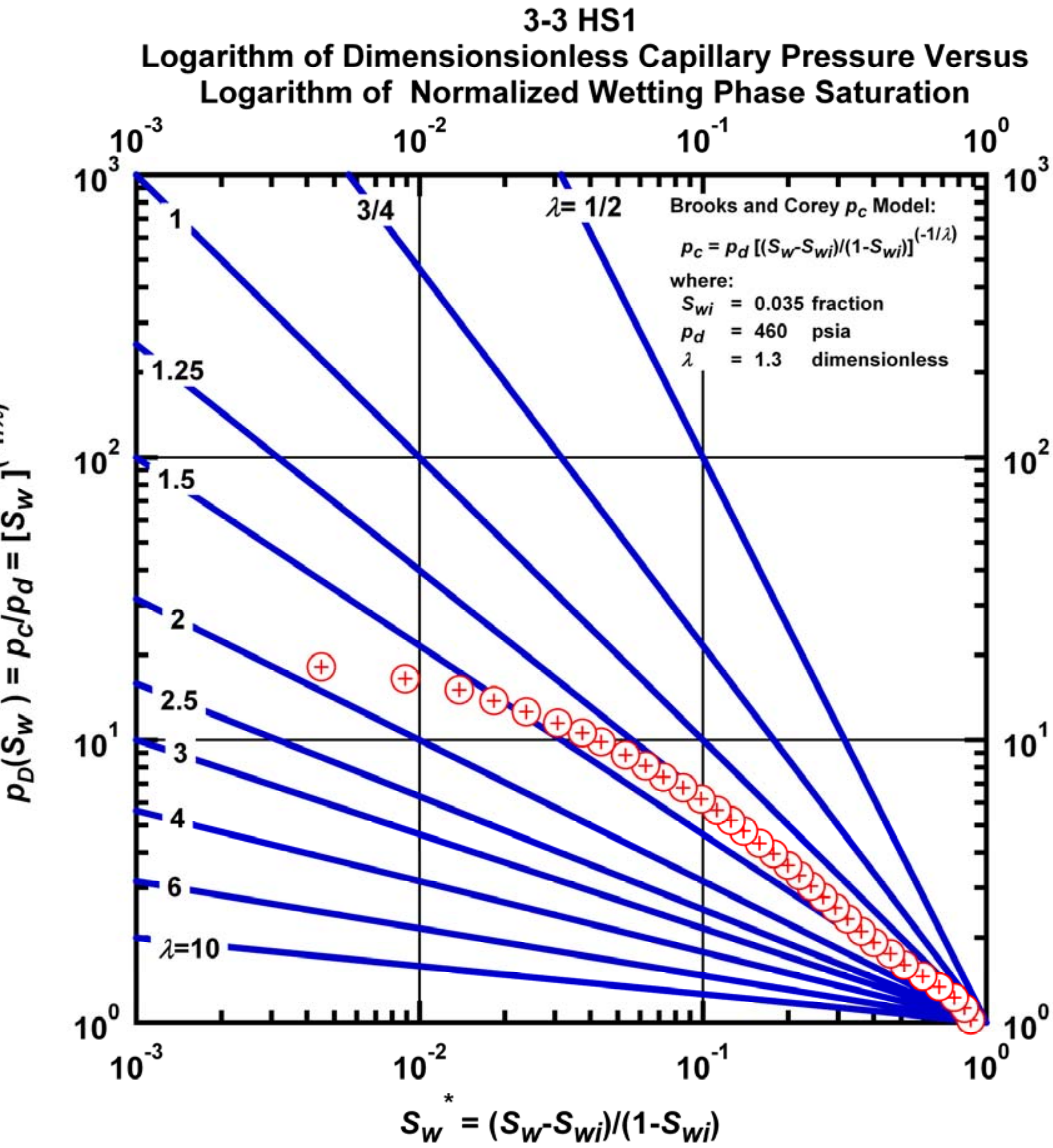

Figure L.5 – Plot of logarithm of dimensionless capillary pressure vs. logarithm of normalized wetting phase saturation — Case 3-3 HS1.

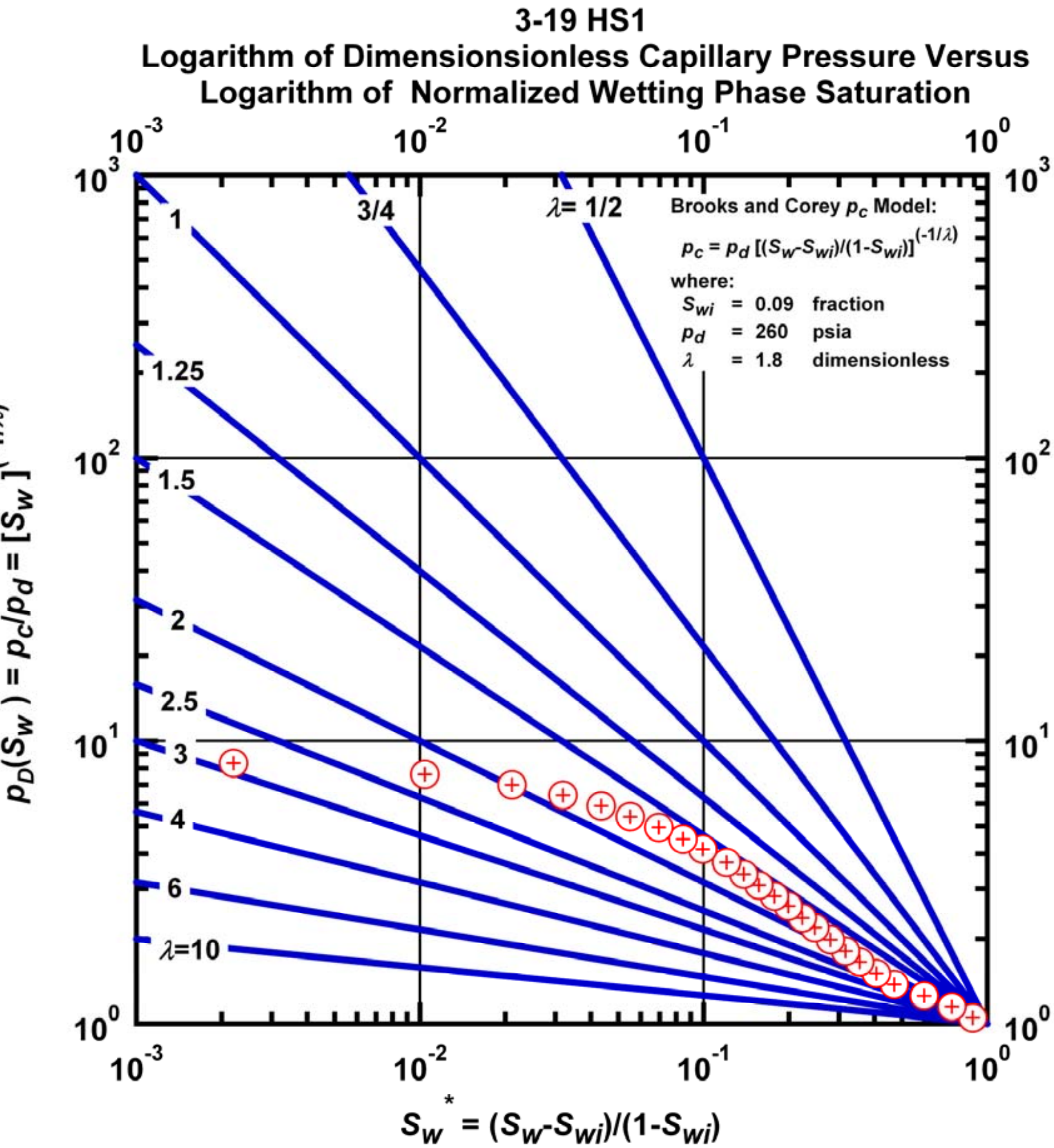

Figure L.6 – Plot of logarithm of dimensionless capillary pressure vs. logarithm of normalized wetting phase saturation — Case 3-19 HS1.

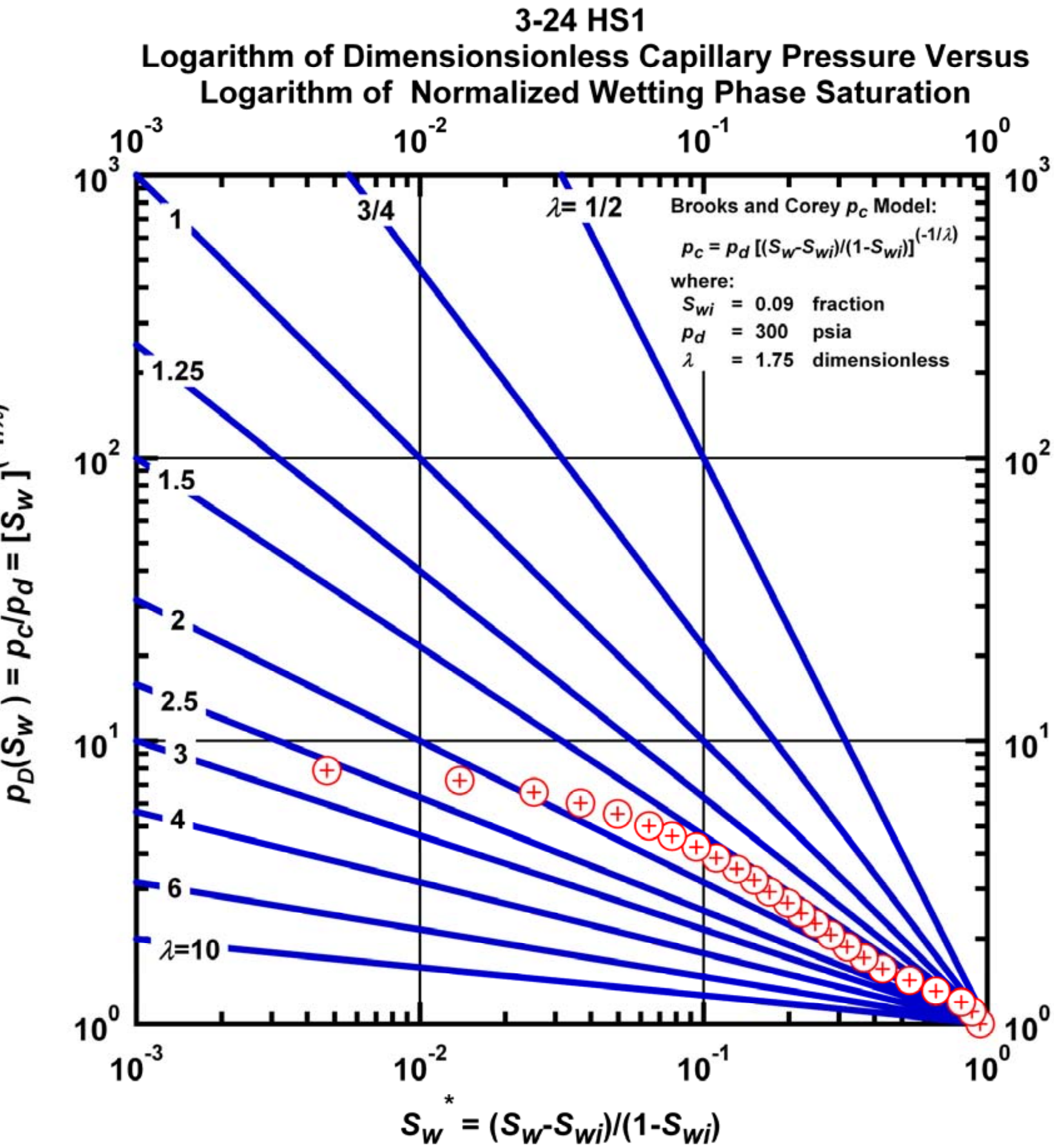

Figure L.7 – Plot of logarithm of dimensionless capillary pressure vs. logarithm of normalized wetting phase saturation — Case 3-24 HS1.

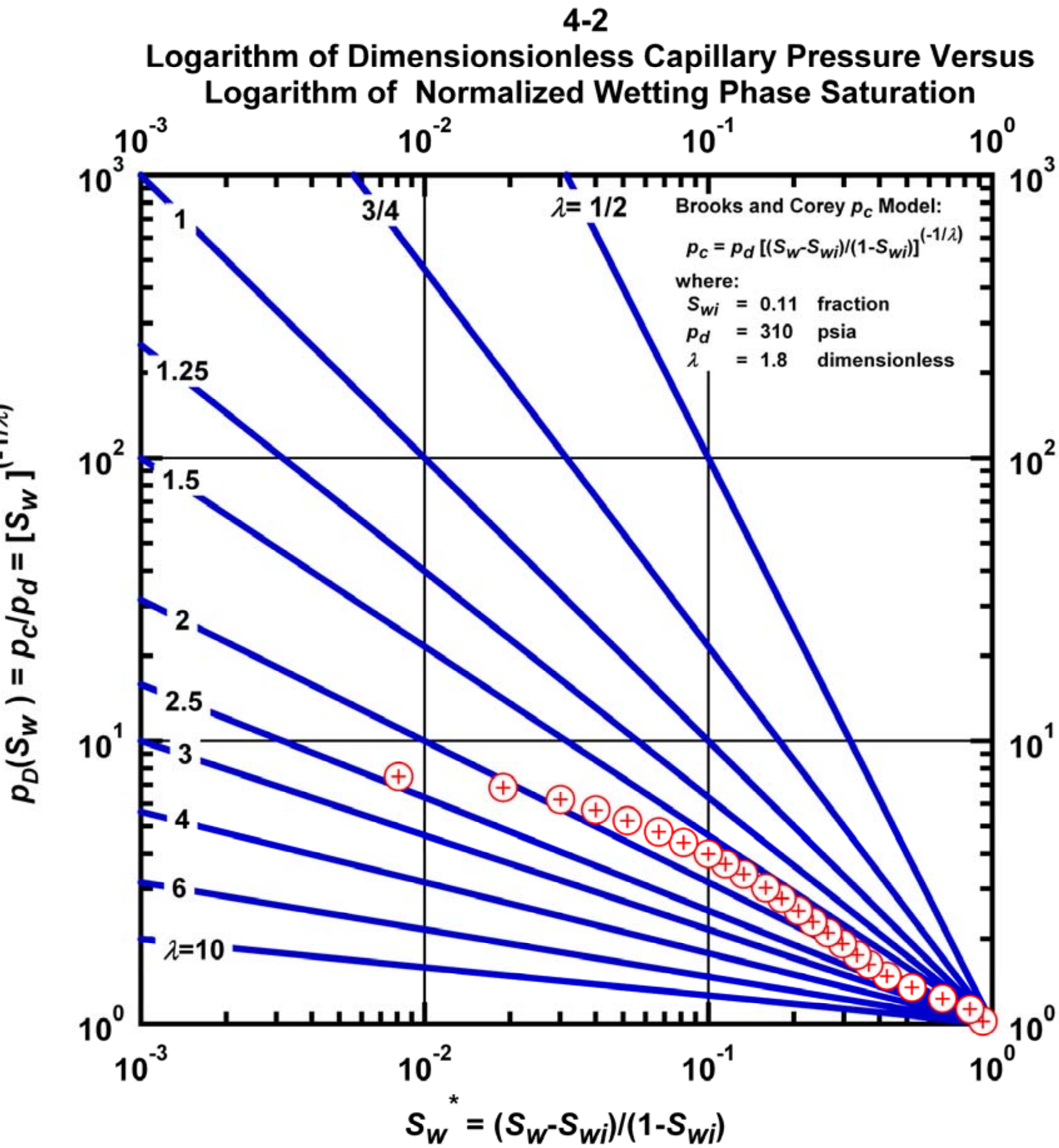

Figure L.8 – Plot of logarithm of dimensionless capillary pressure vs. logarithm of normalized wetting phase saturation — Case 4-2 HS1.

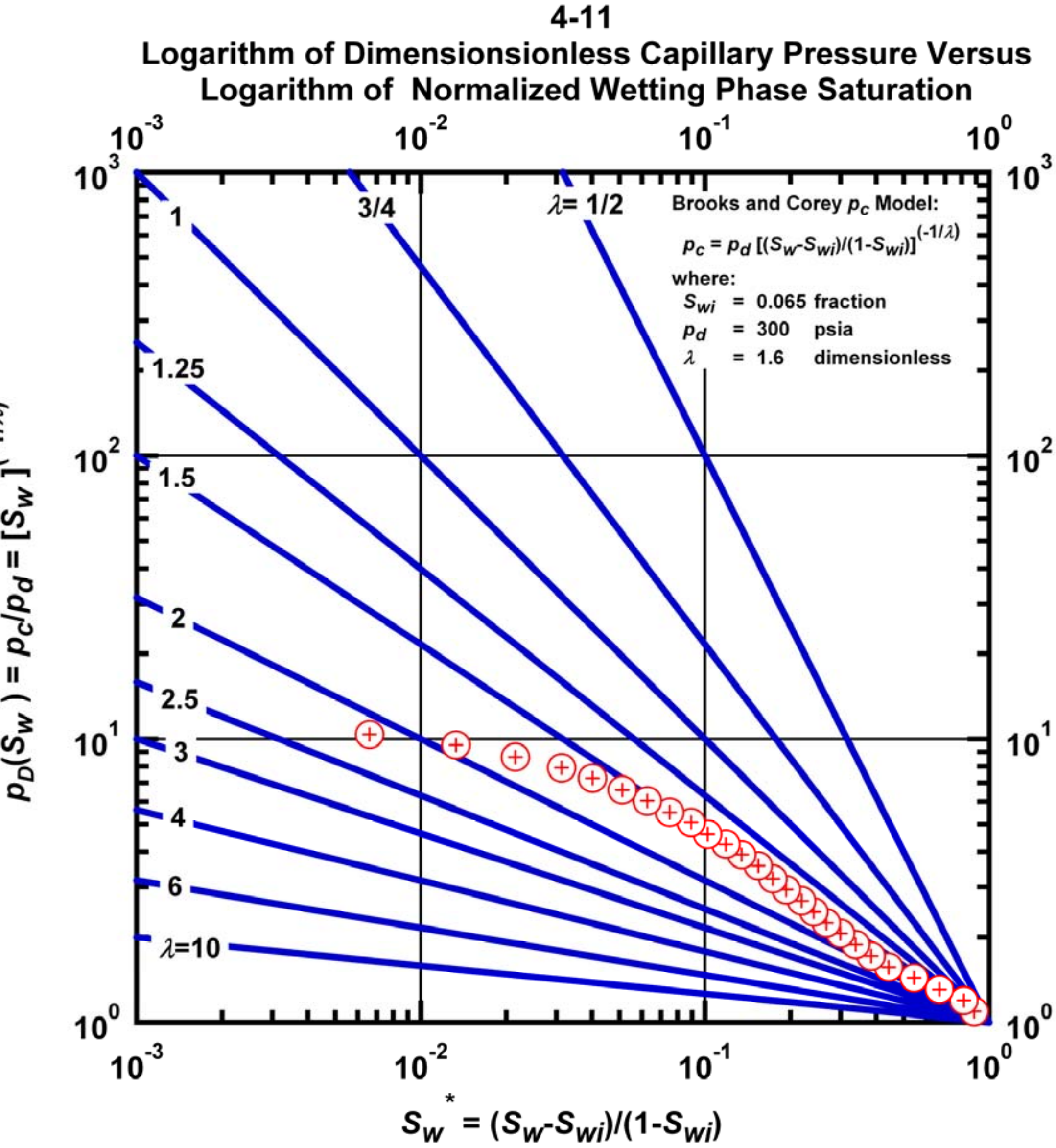

Figure L.9 – Plot of logarithm of dimensionless capillary pressure vs. logarithm of normalized wetting phase saturation — Case 4-11 HS1.

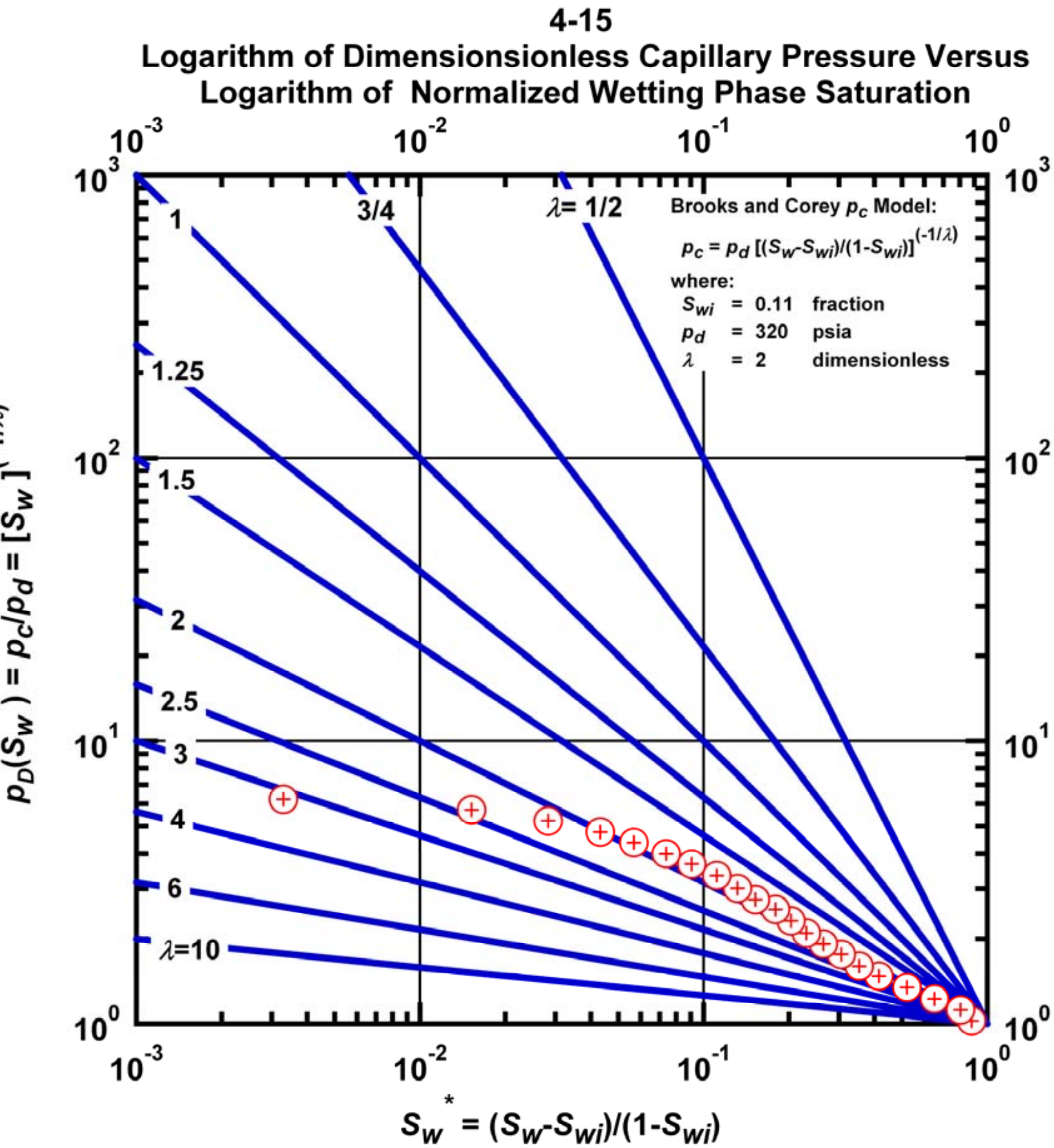

Figure L.10 – Plot of logarithm of dimensionless capillary pressure vs. logarithm of normalized wetting phase saturation — Case 4-15 HS1.

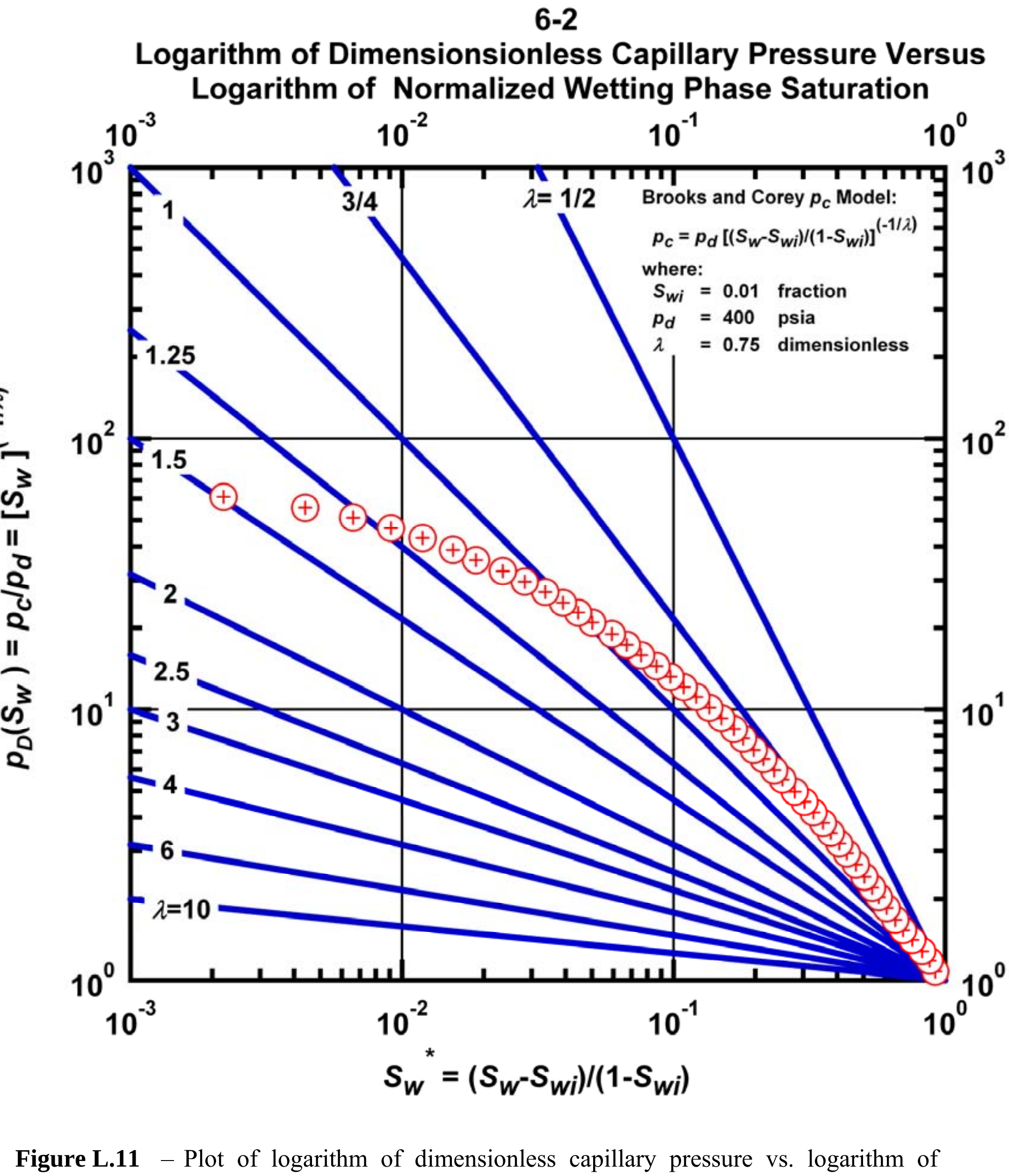

Figure L.11 – Plot of logarithm of dimensionless capillary pressure vs. logarithm of normalized wetting phase saturation — Case 6-2 HS1.

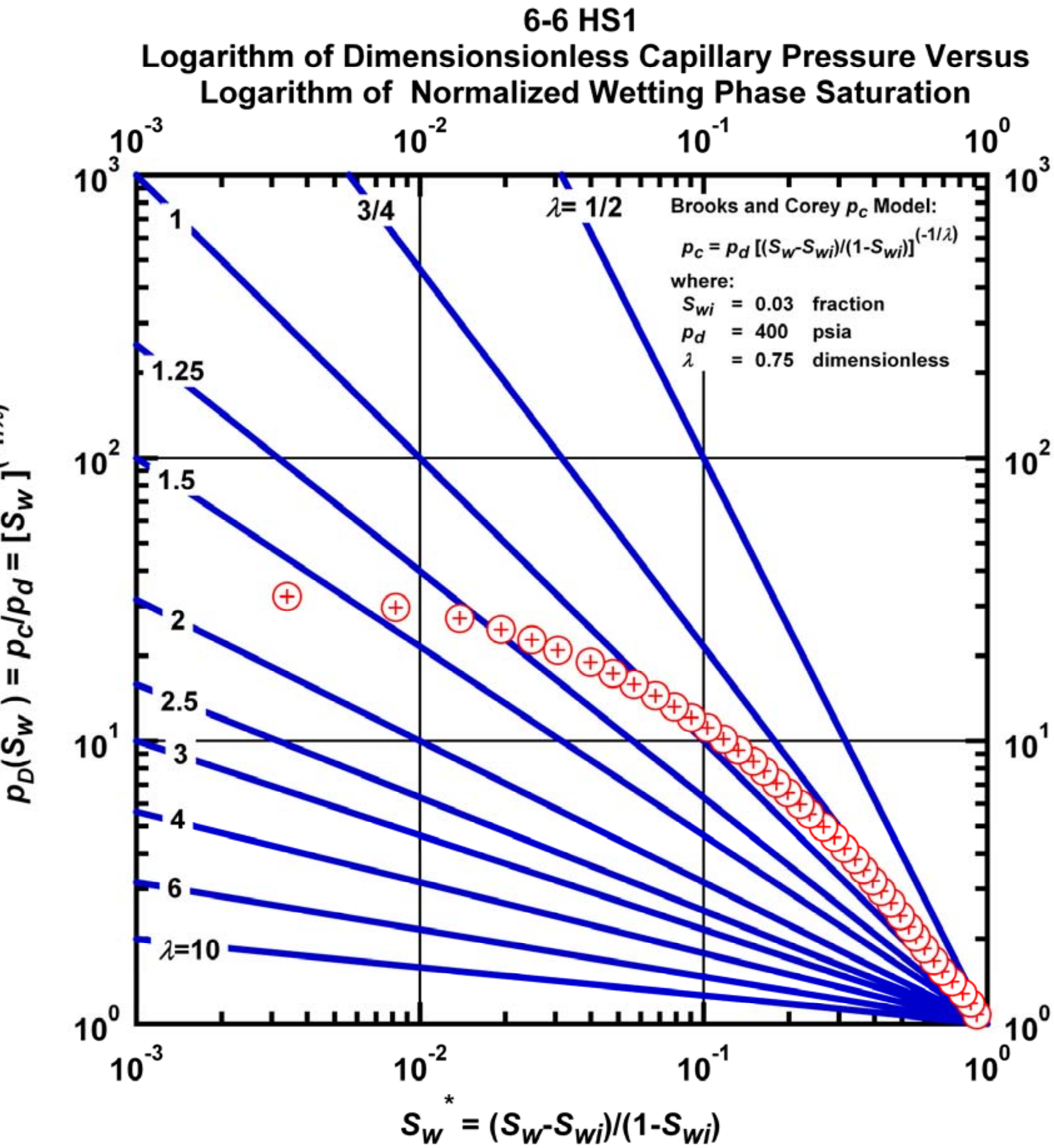

Figure L.12 – Plot of logarithm of dimensionless capillary pressure vs. logarithm of normalized wetting phase saturation — Case 6-6 HS1.

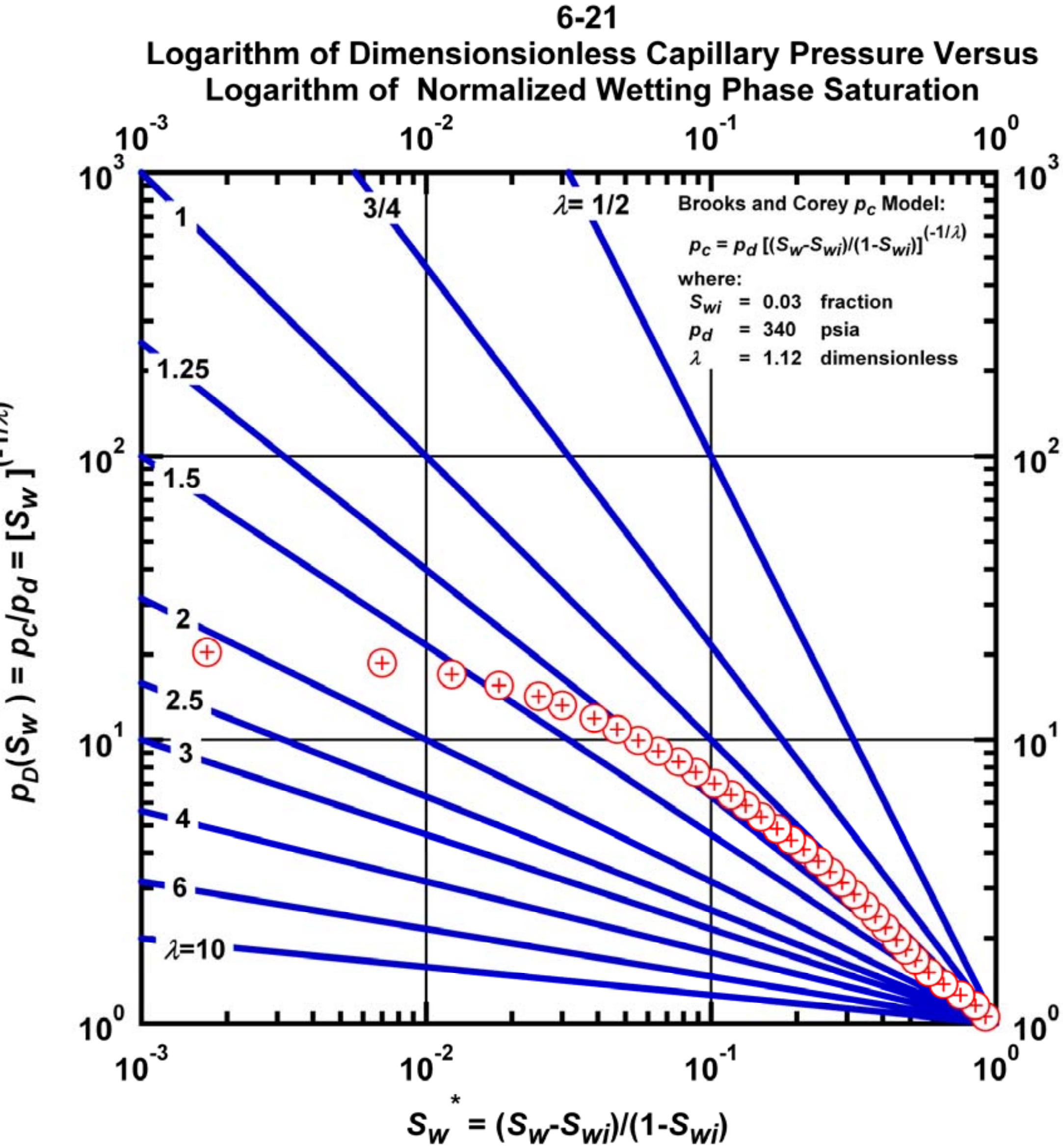

Figure L.13 – Plot of logarithm of dimensionless capillary pressure vs. logarithm of normalized wetting phase saturation — Case 6-21 HS1.

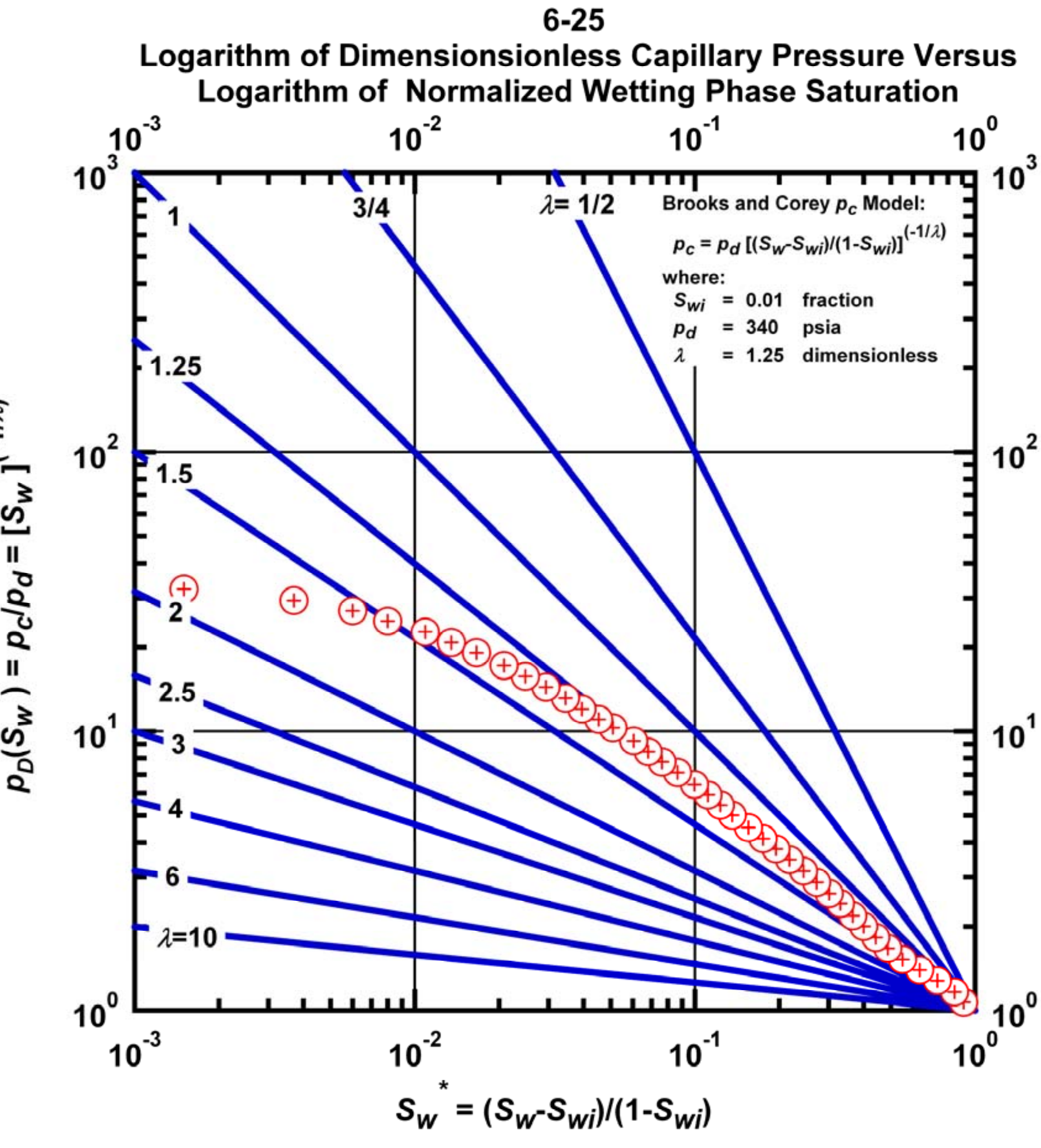

Figure L.14 – Plot of logarithm of dimensionless capillary pressure vs. logarithm of normalized wetting phase saturation ── Case 6-25 HS1.

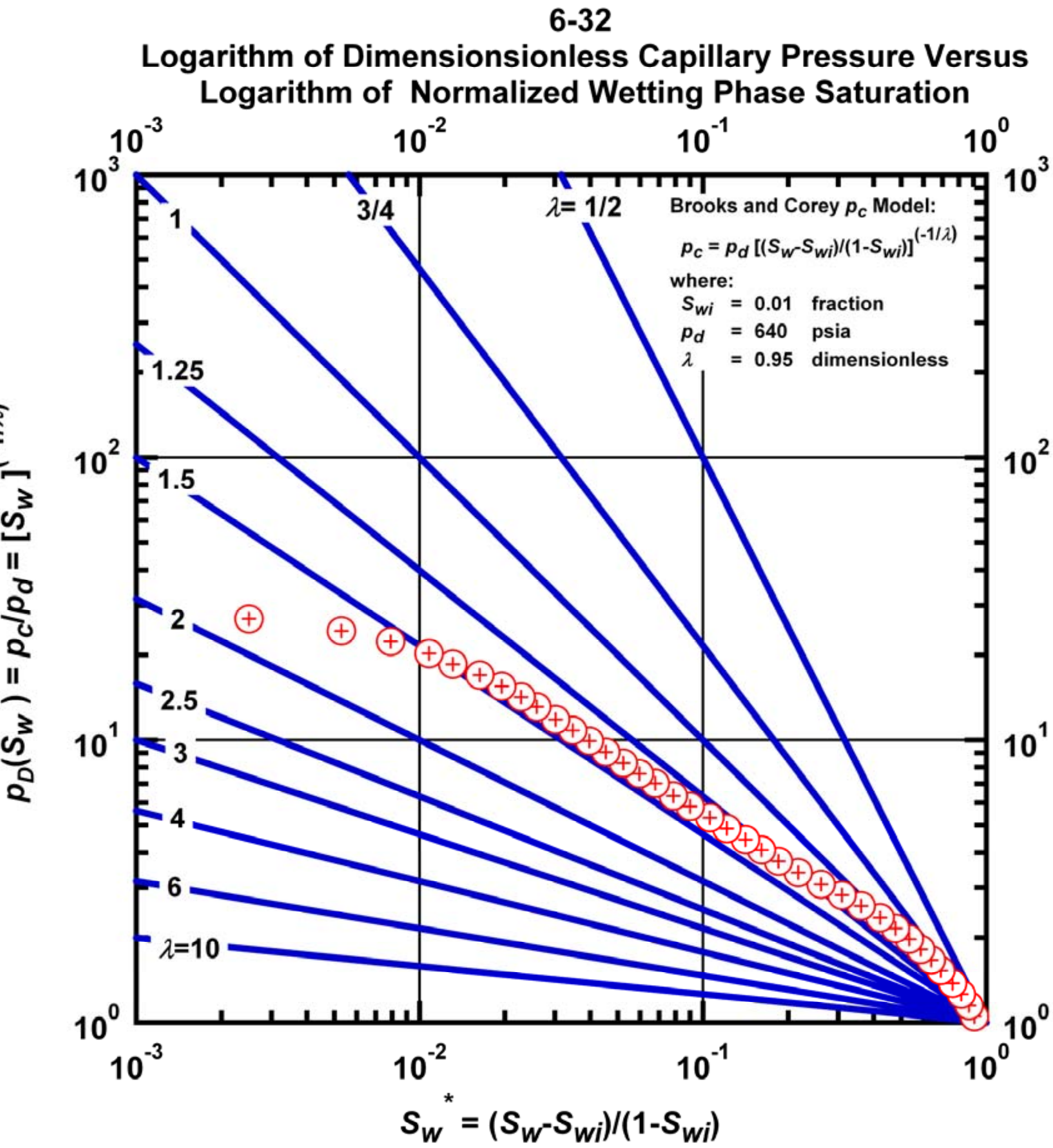

Figure L.15 – Plot of logarithm of dimensionless capillary pressure vs. logarithm of normalized wetting phase saturation — Case 6-32 HS1.

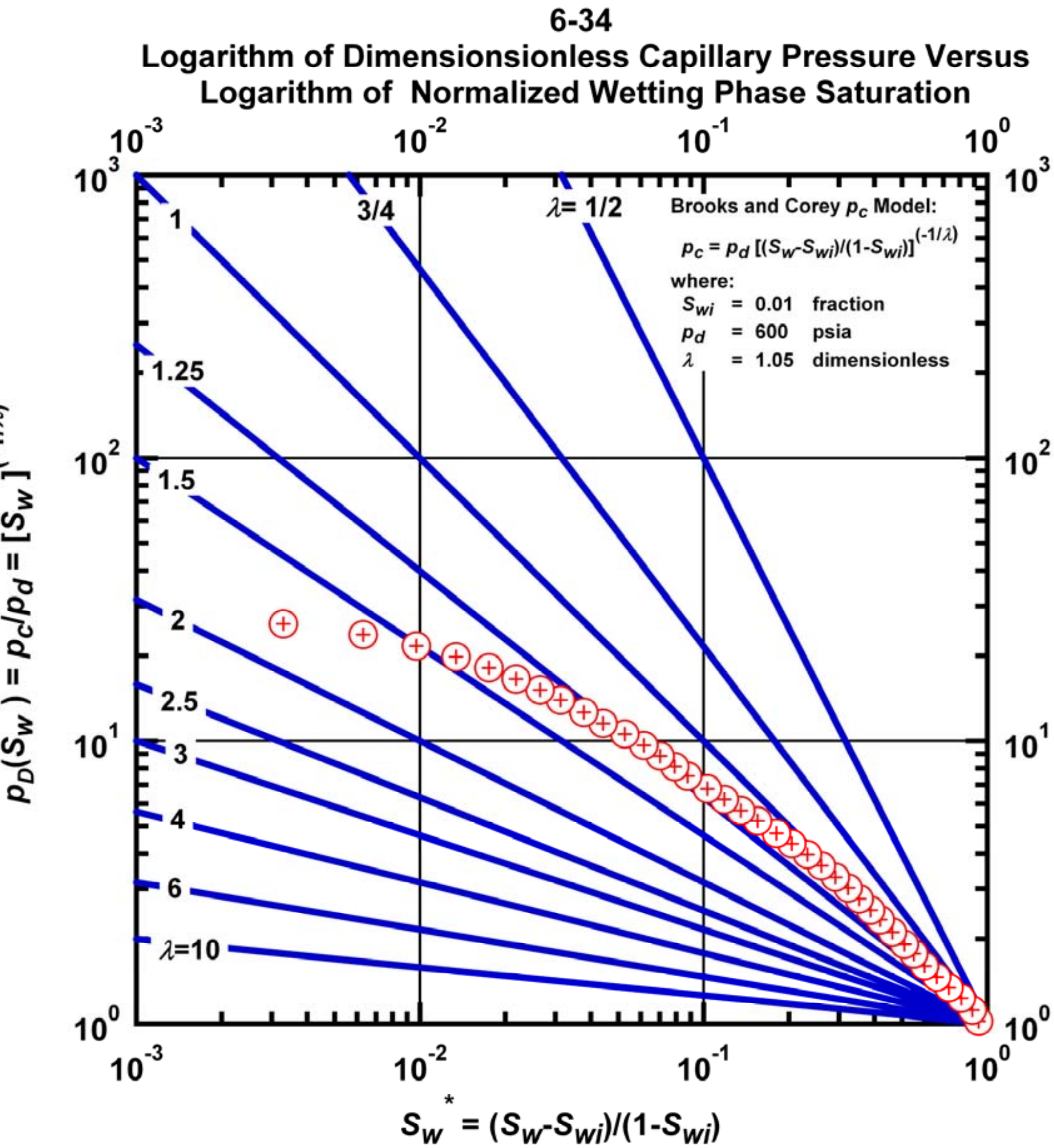

Figure L.16 – Plot of logarithm of dimensionless capillary pressure vs. logarithm of normalized wetting phase saturation — Case 6-34 HS1.

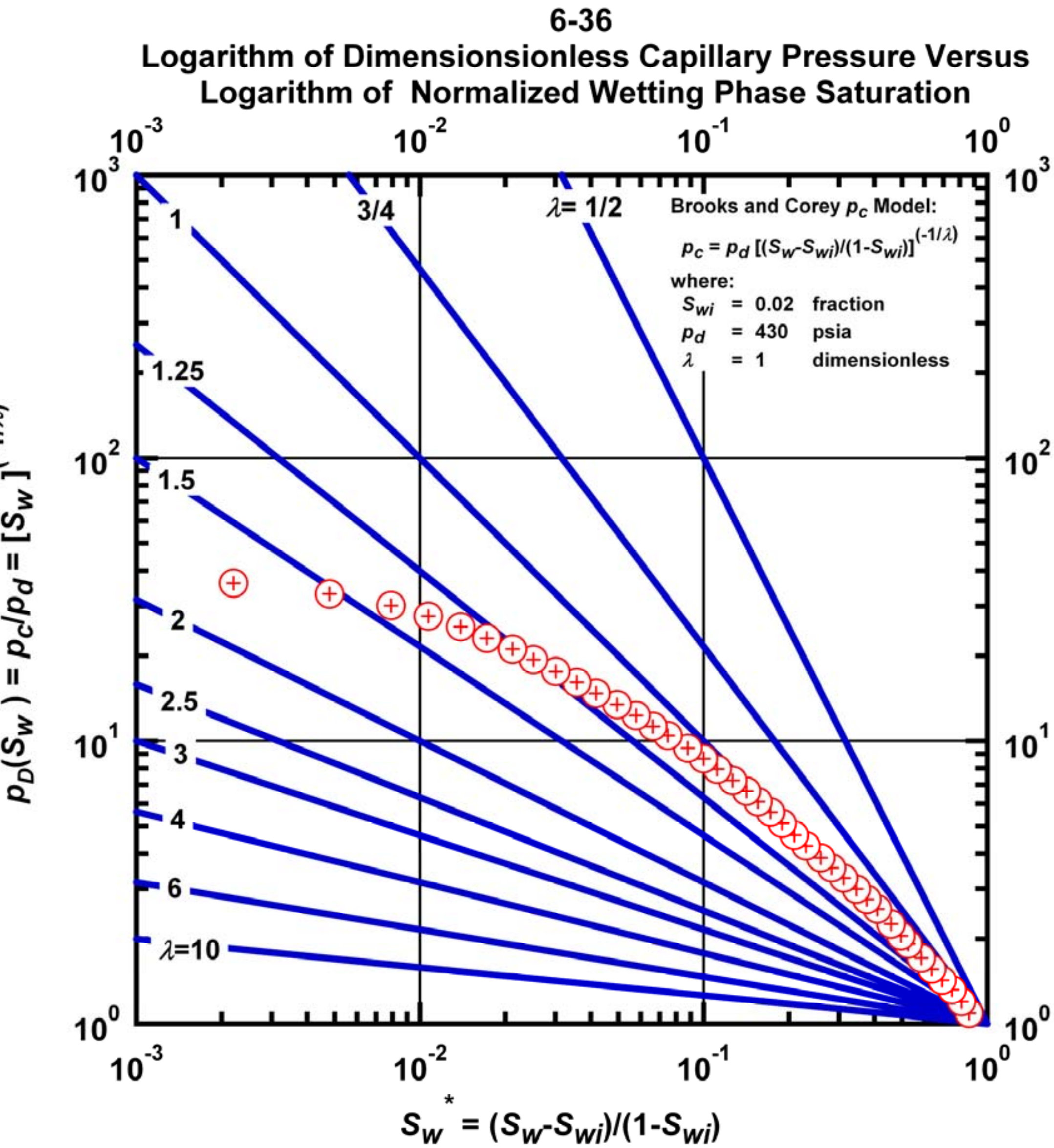

Figure L.17 – Plot of logarithm of dimensionless capillary pressure vs. logarithm of normalized wetting phase saturation — Case 6-36 HS1.

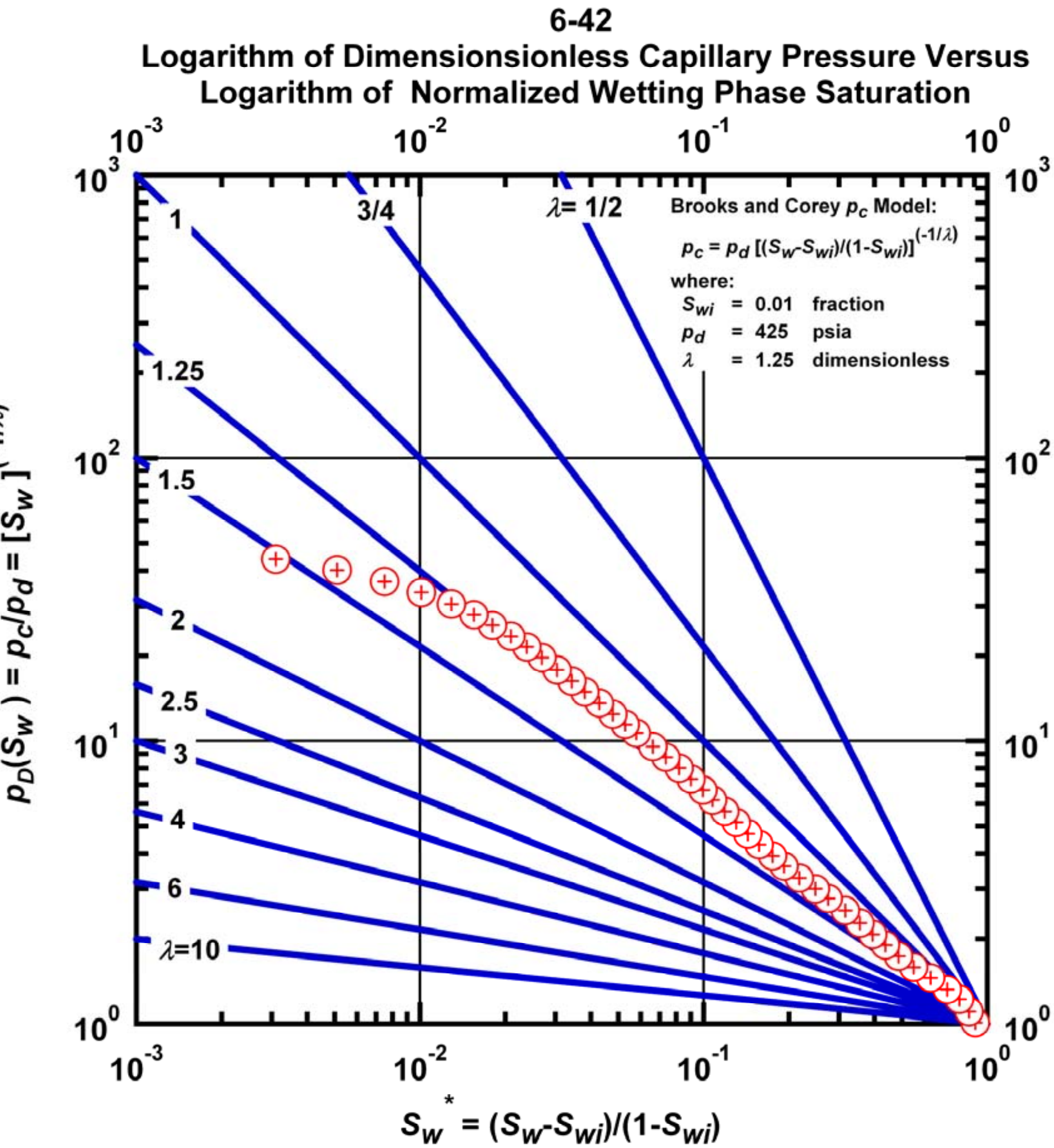

Figure L.18 – Plot of logarithm of dimensionless capillary pressure vs. logarithm of normalized wetting phase saturation — Case 6-42 HS1.

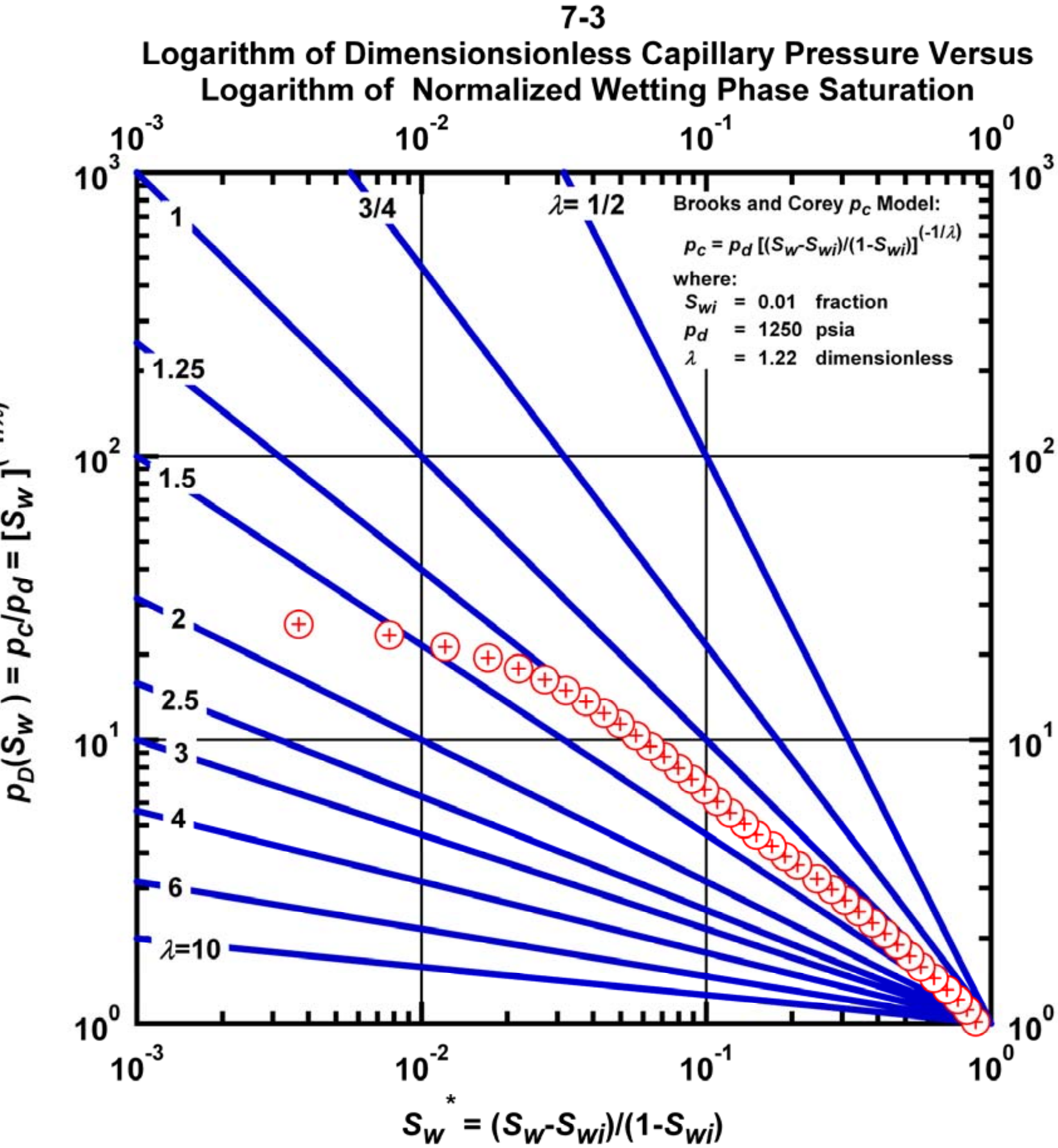

Figure L.19 – Plot of logarithm of dimensionless capillary pressure vs. logarithm of normalized wetting phase saturation — Case 7-3 HS1.

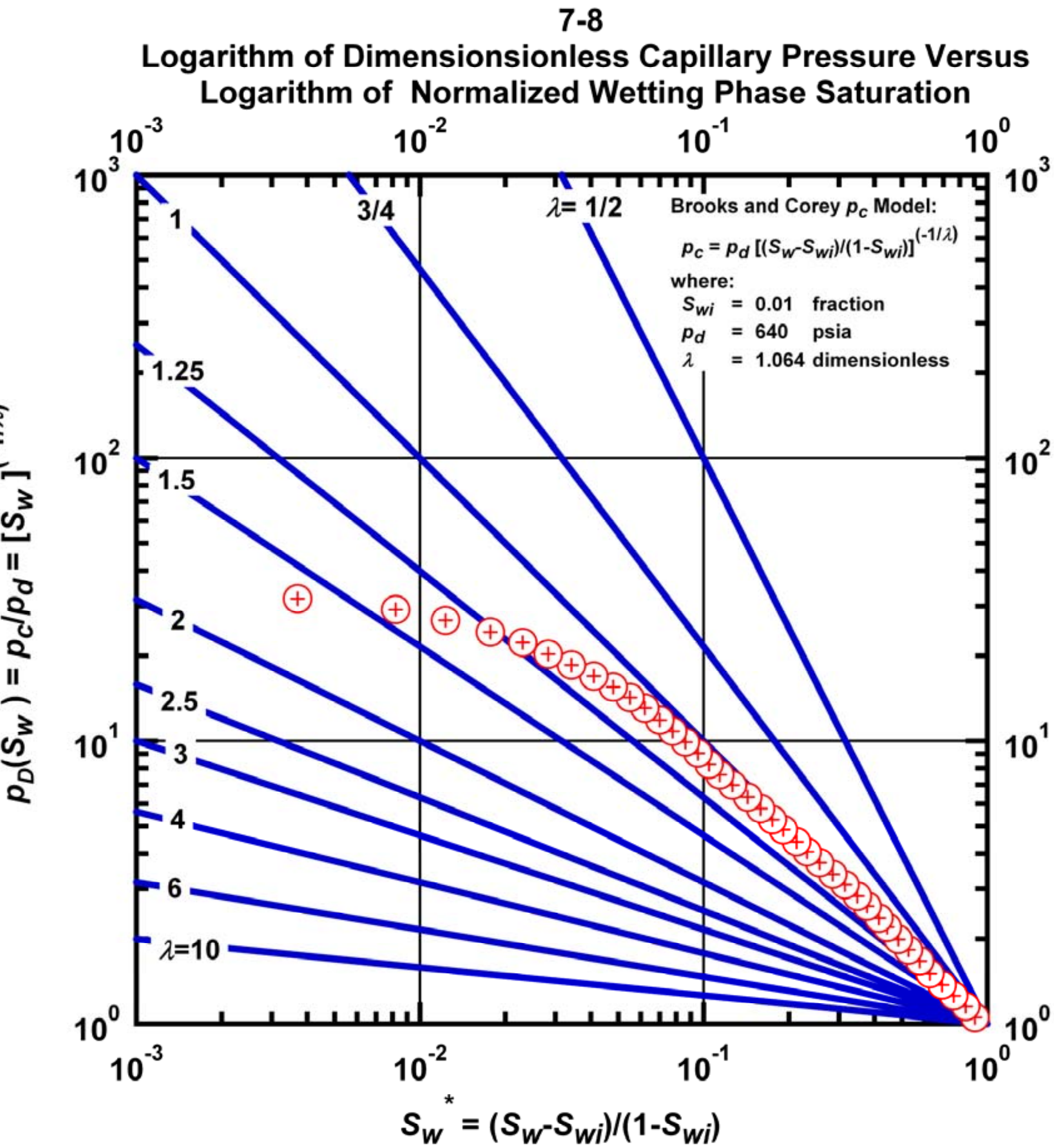

Figure L.20 – Plot of logarithm of dimensionless capillary pressure vs. logarithm of normalized wetting phase saturation — Case 7-8 HS1.

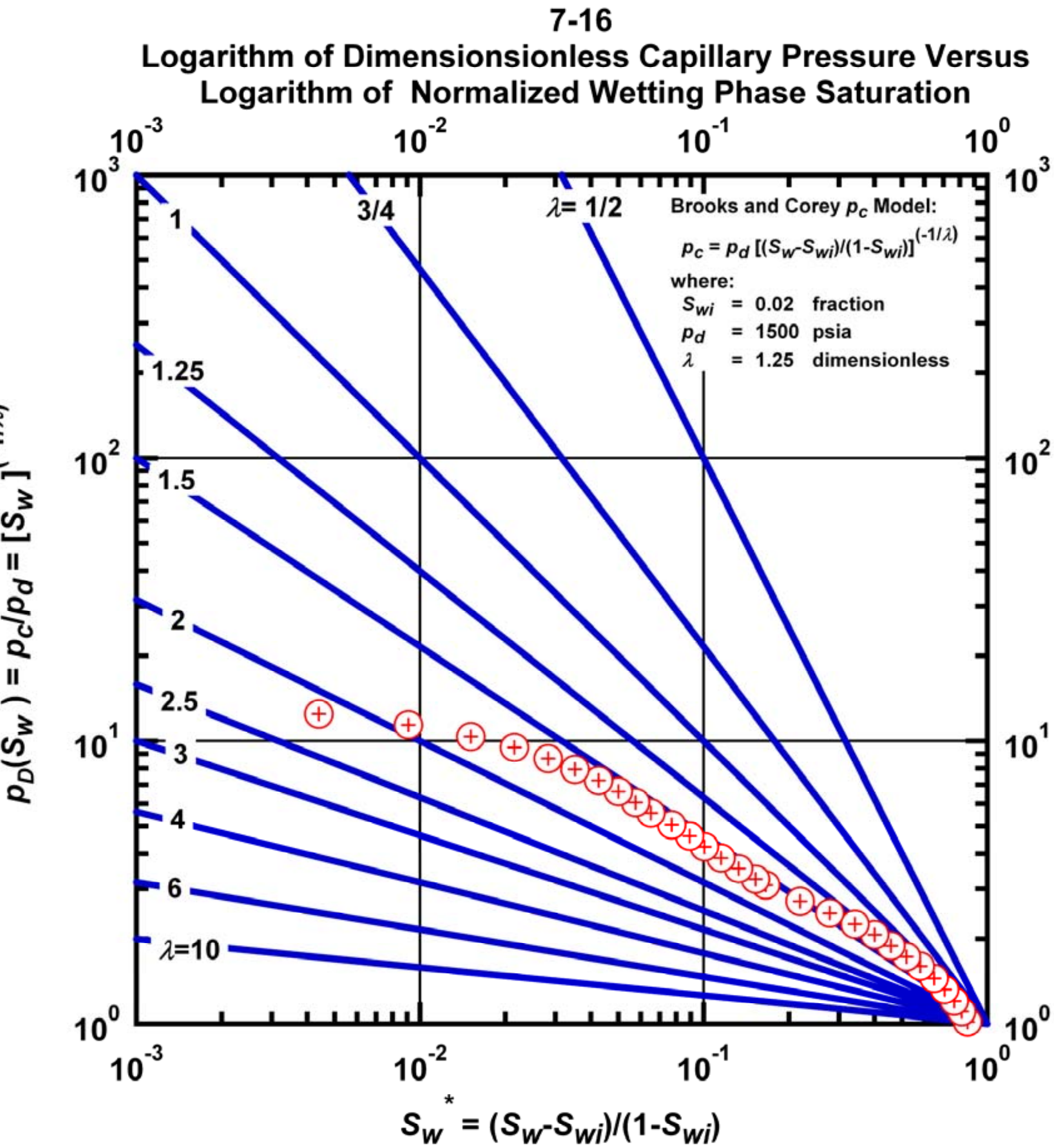

Figure L.21 – Plot of logarithm of dimensionless capillary pressure vs. logarithm of normalized wetting phase saturation — Case 7-16 HS1.

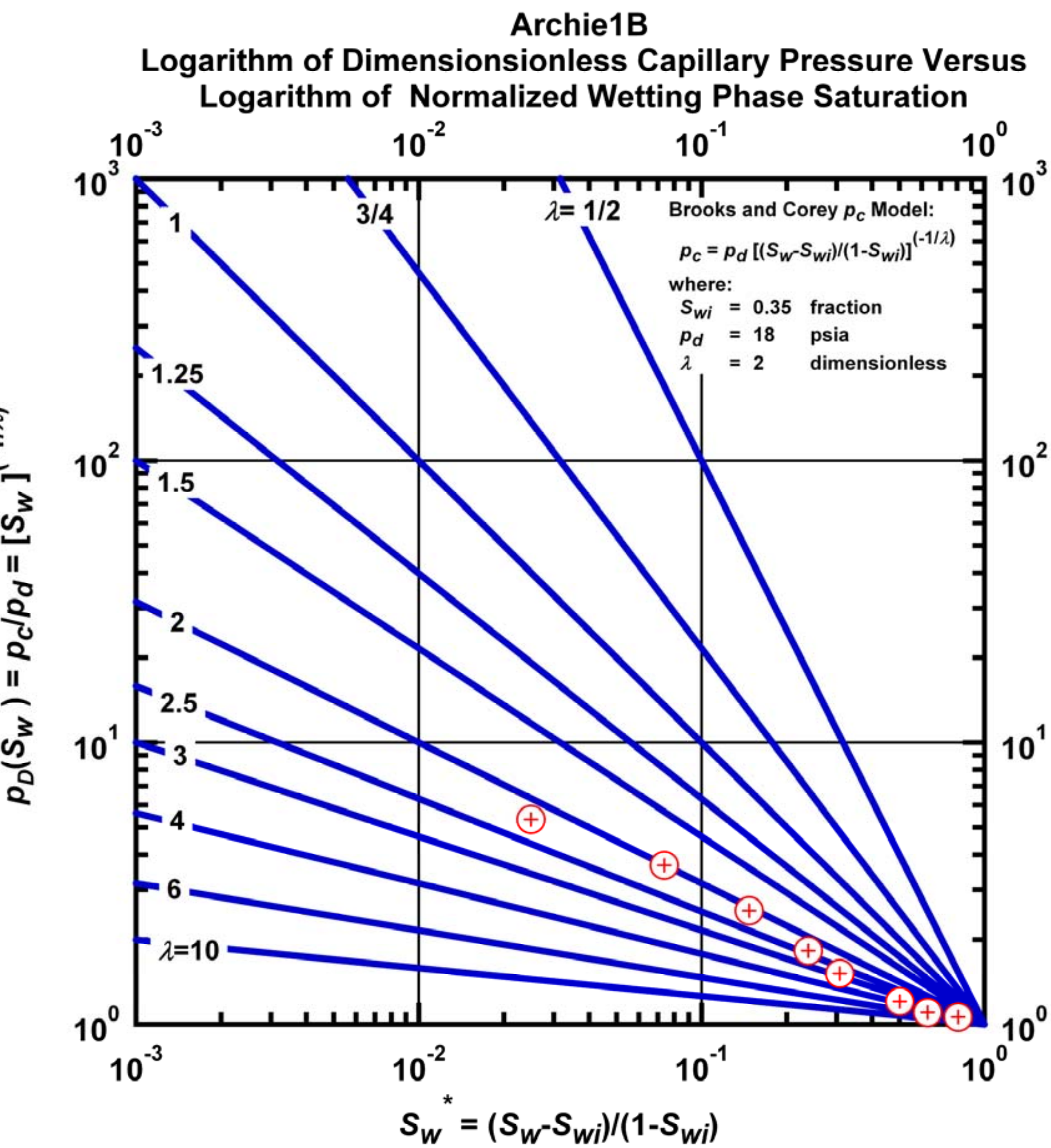

Figure L.22 – Plot of logarithm of dimensionless capillary pressure vs. logarithm of normalized wetting phase saturation — Case Archie1B.

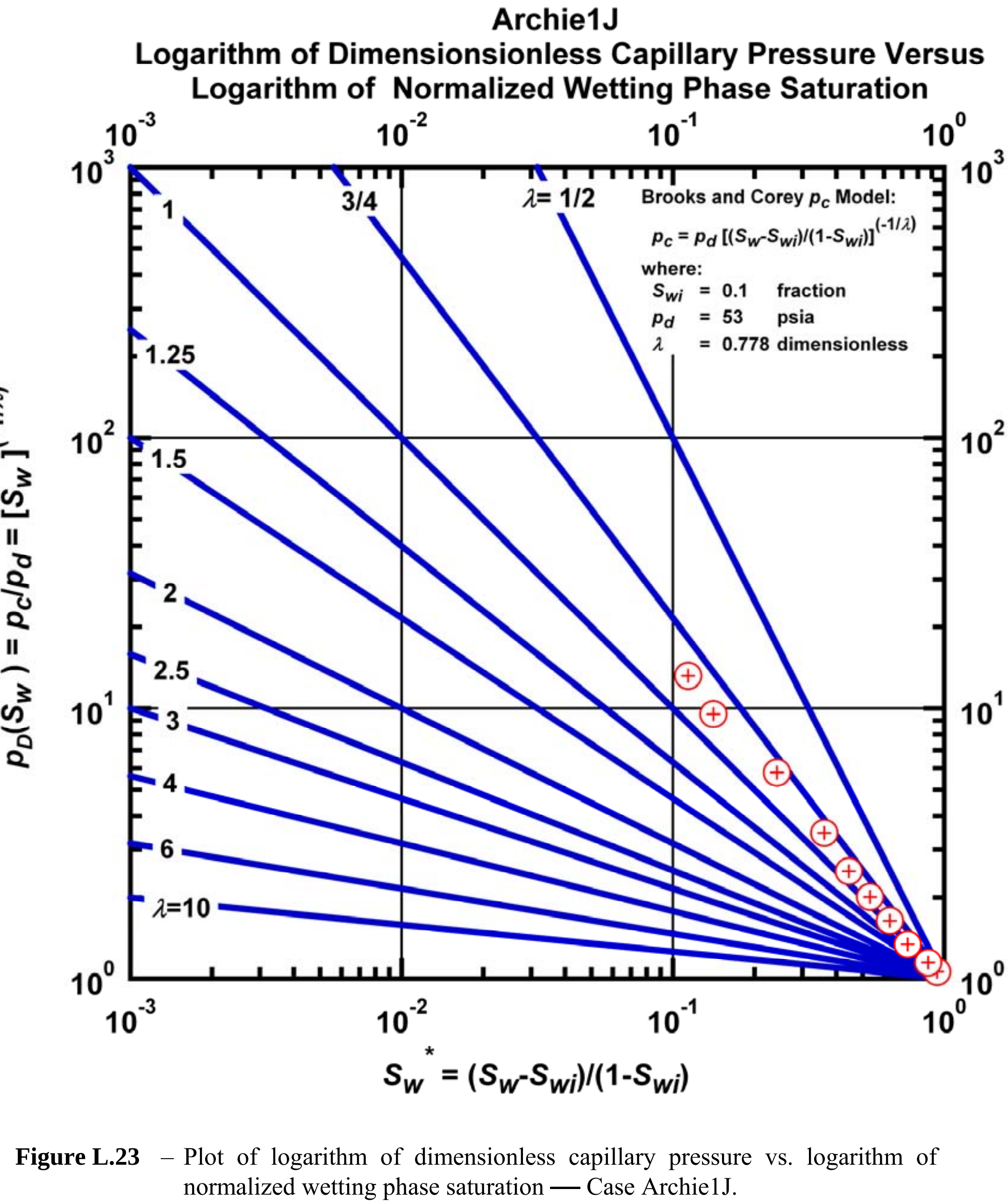

Figure L.23 – Plot of logarithm of dimensionless capillary pressure vs. logarithm of normalized wetting phase saturation — Case Archie1J.

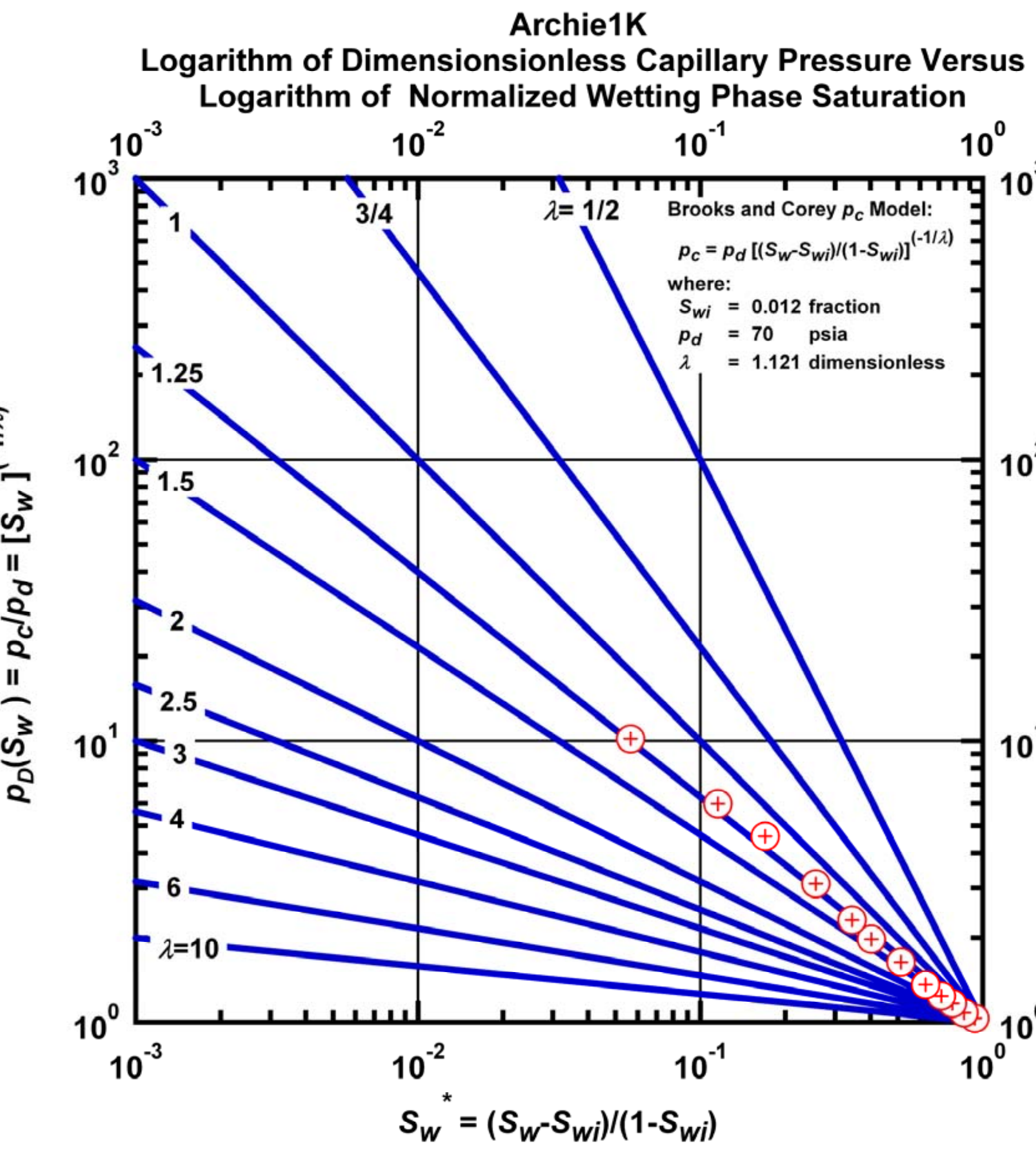

Figure L.24 – Plot of logarithm of dimensionless capillary pressure vs. logarithm of normalized wetting phase saturation — Case Archie1K.

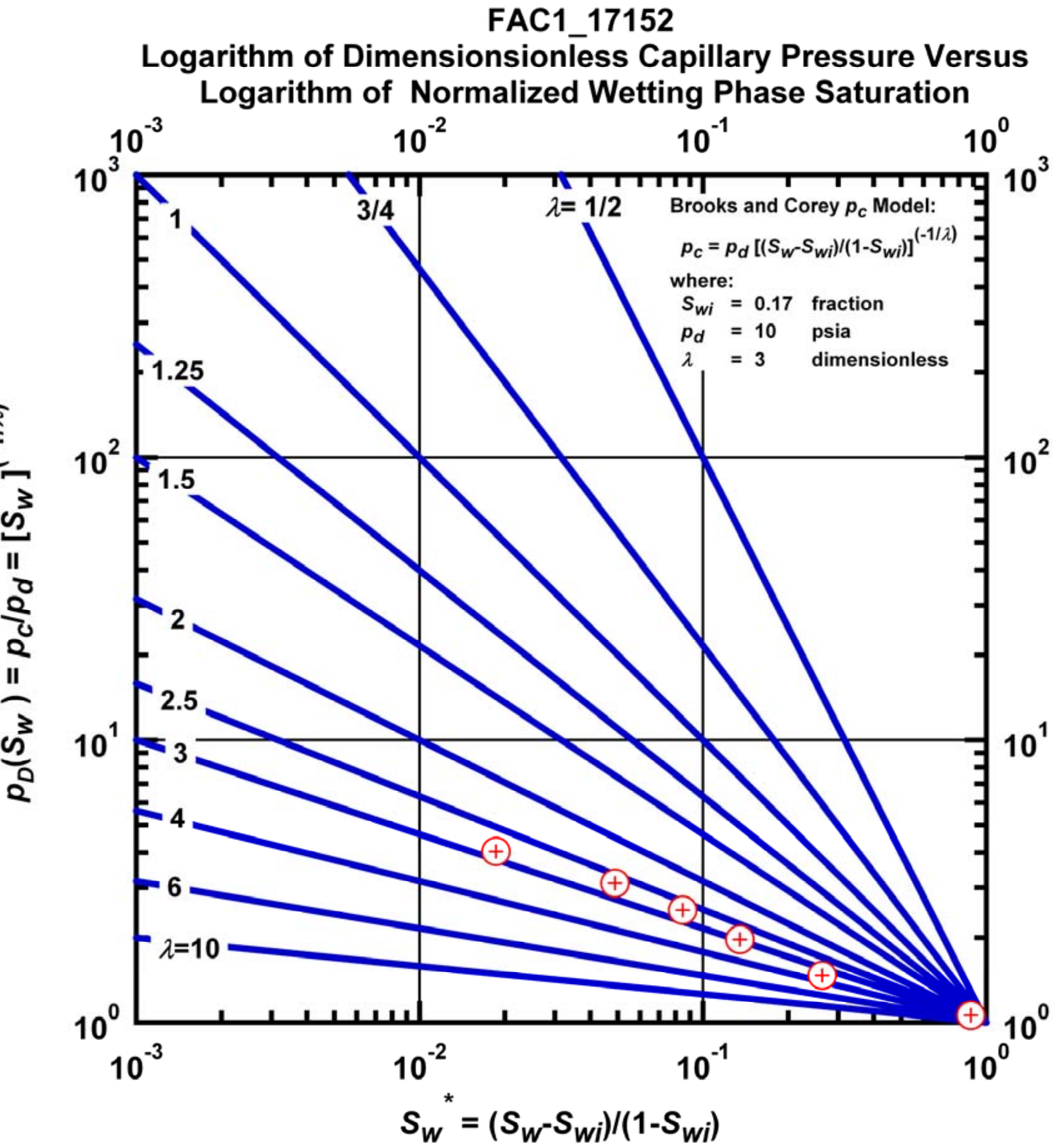

Figure L.25 – Plot of logarithm of dimensionless capillary pressure vs. logarithm of normalized wetting phase saturation — Case FAC1_17152.

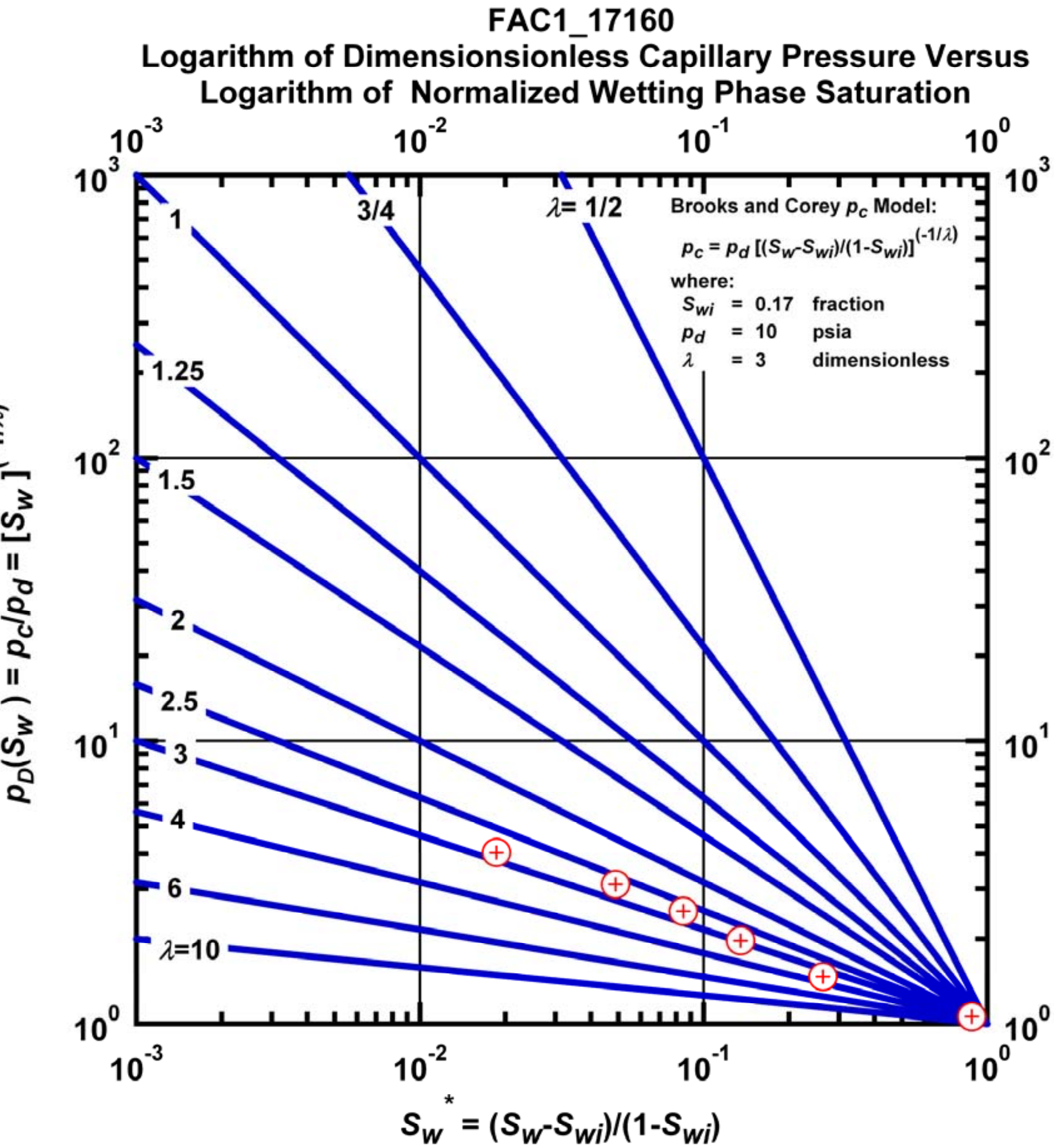

Figure L.26 – Plot of logarithm of dimensionless capillary pressure vs. logarithm of normalized wetting phase saturation — Case FAC1_17160.

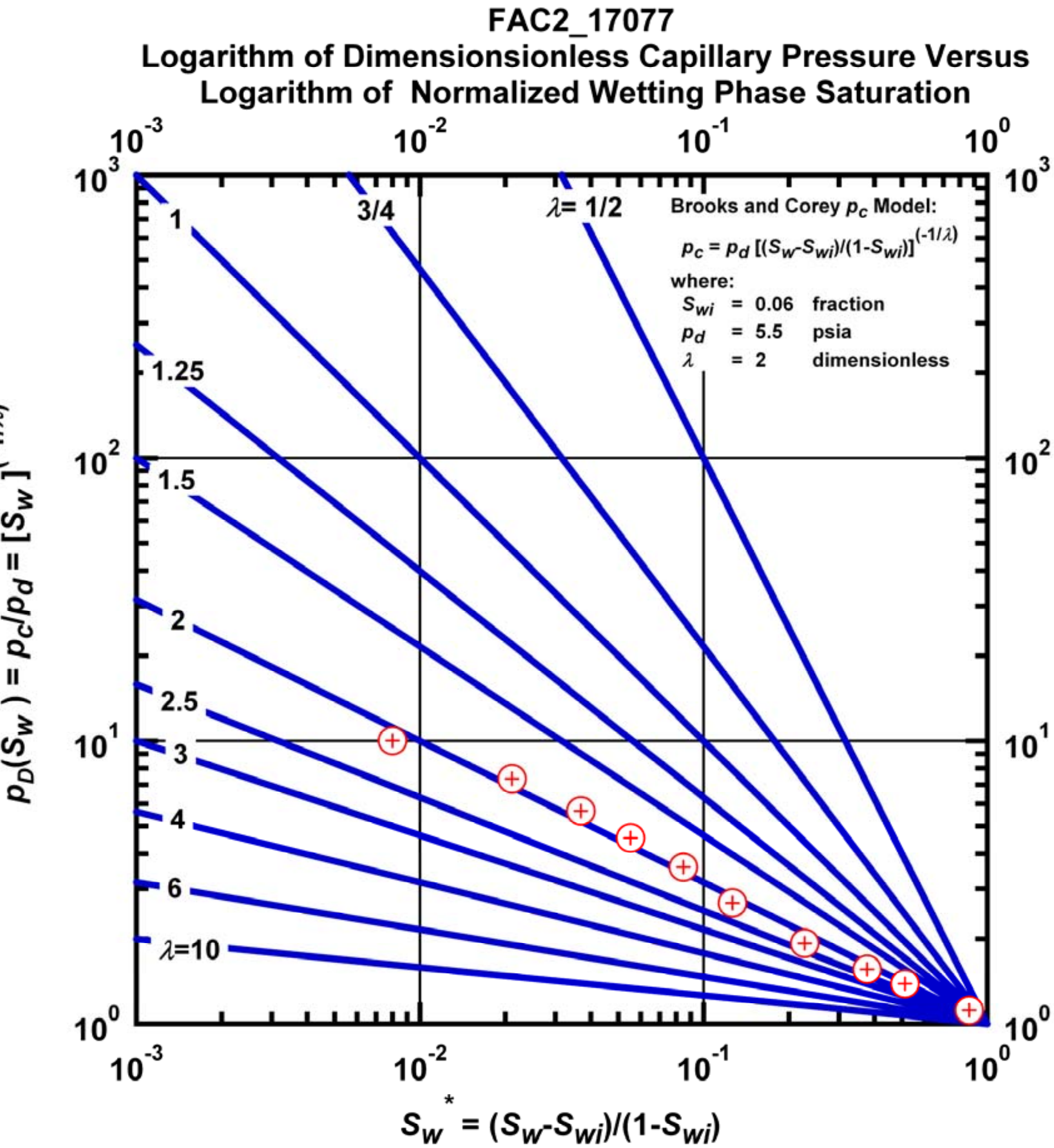

Figure L.27 – Plot of logarithm of dimensionless capillary pressure vs. logarithm of normalized wetting phase saturation — Case FAC2_17077.

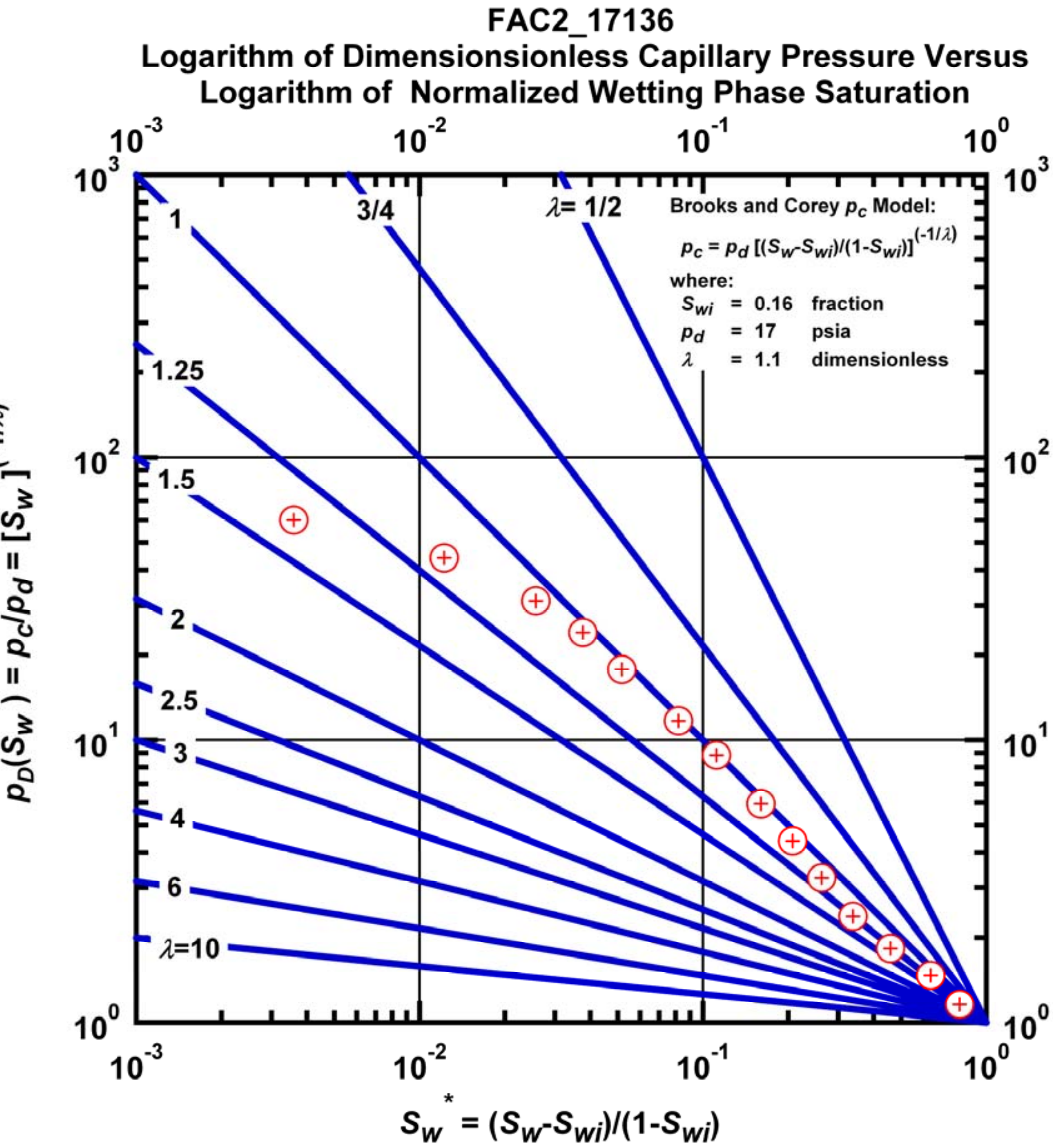

Figure L.28 – Plot of logarithm of dimensionless capillary pressure vs. logarithm of normalized wetting phase saturation ── Case FAC2_17136.

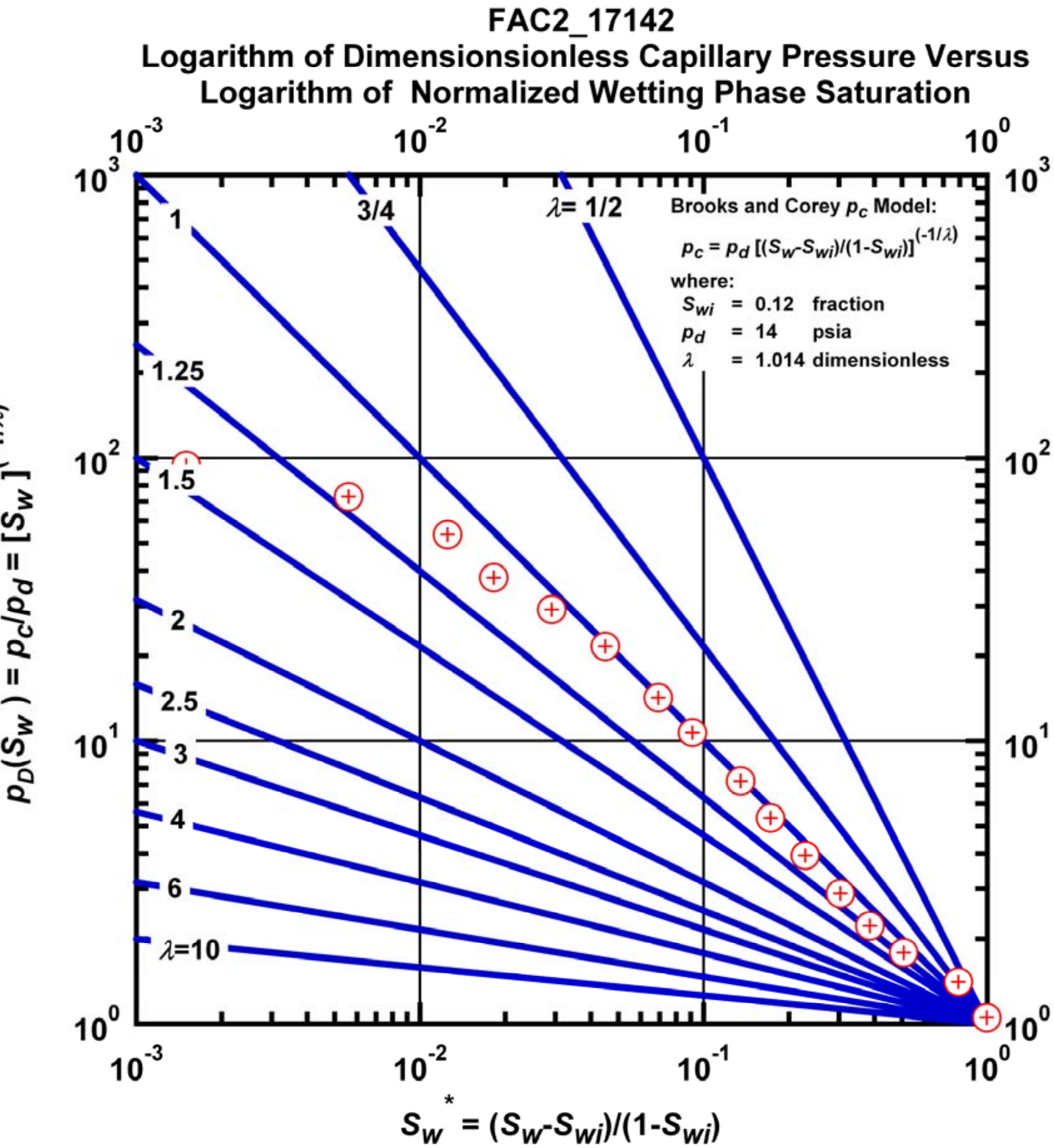

Figure L.29 – Plot of logarithm of dimensionless capillary pressure vs. logarithm of normalized wetting phase saturation — Case FAC2_17142.

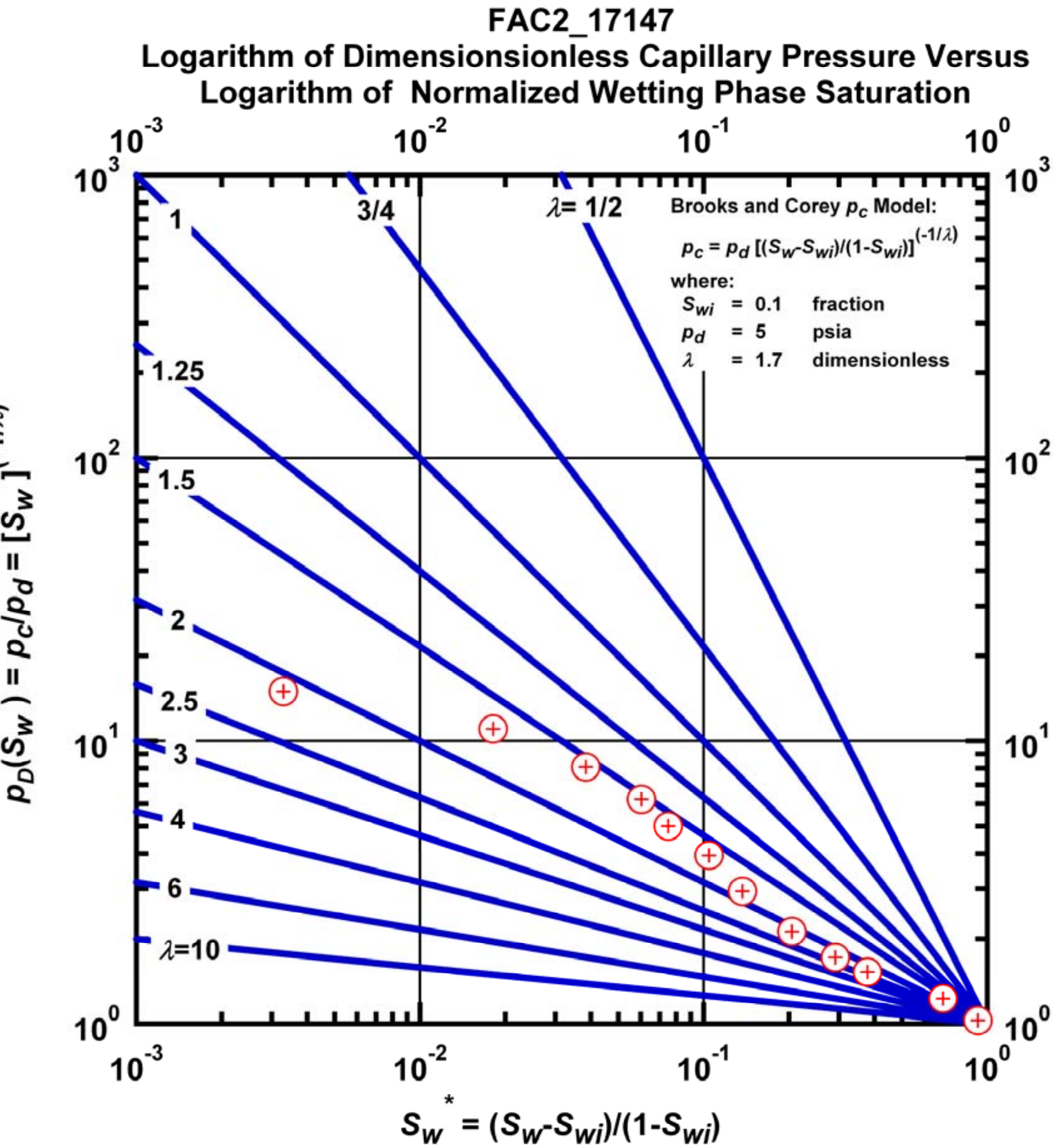

Figure L.30 – Plot of logarithm of dimensionless capillary pressure vs. logarithm of normalized wetting phase saturation — Case FAC2_17147.

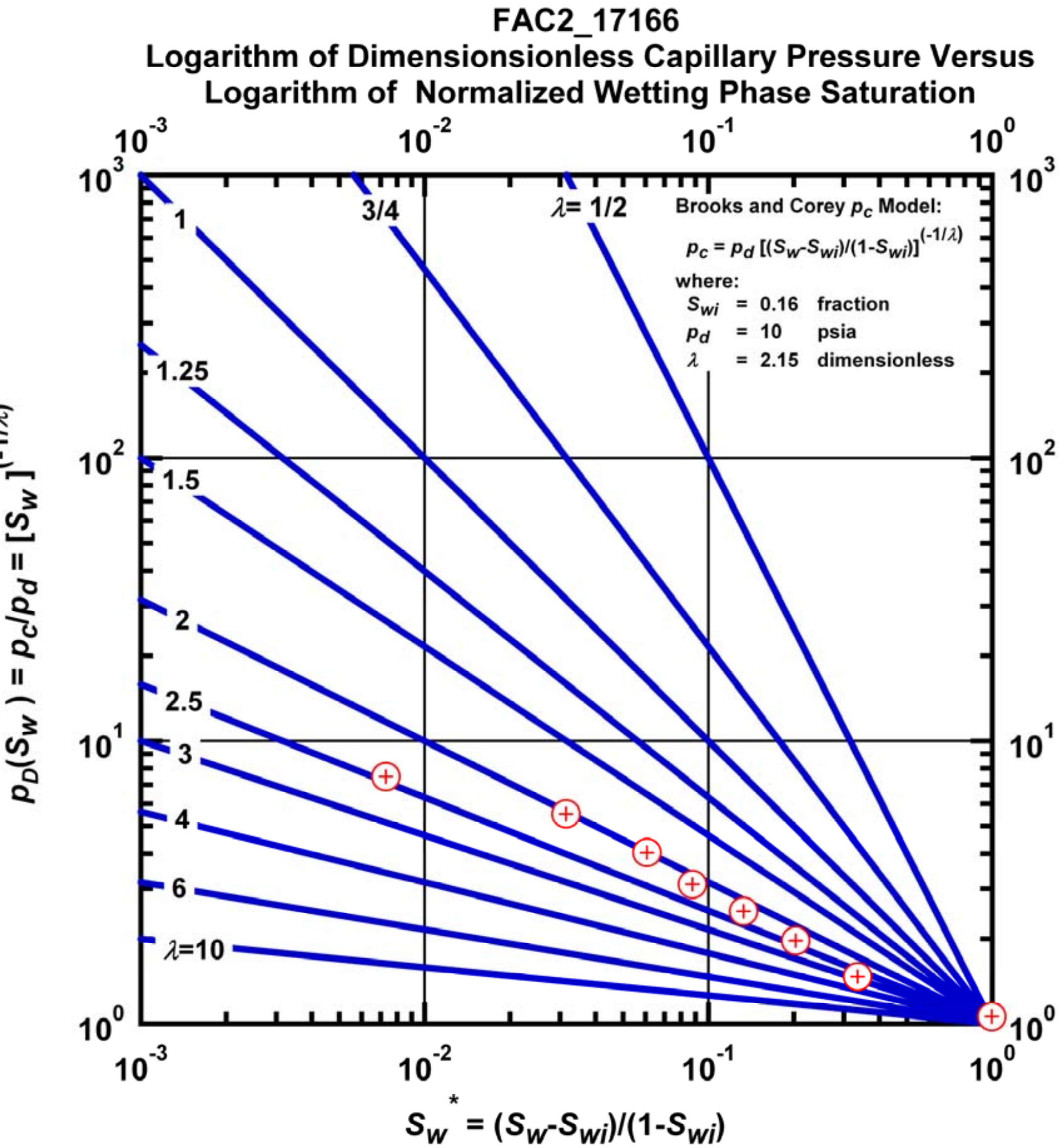

Figure L.31 – Plot of logarithm of dimensionless capillary pressure vs. logarithm of normalized wetting phase saturation — Case FAC2_17166.

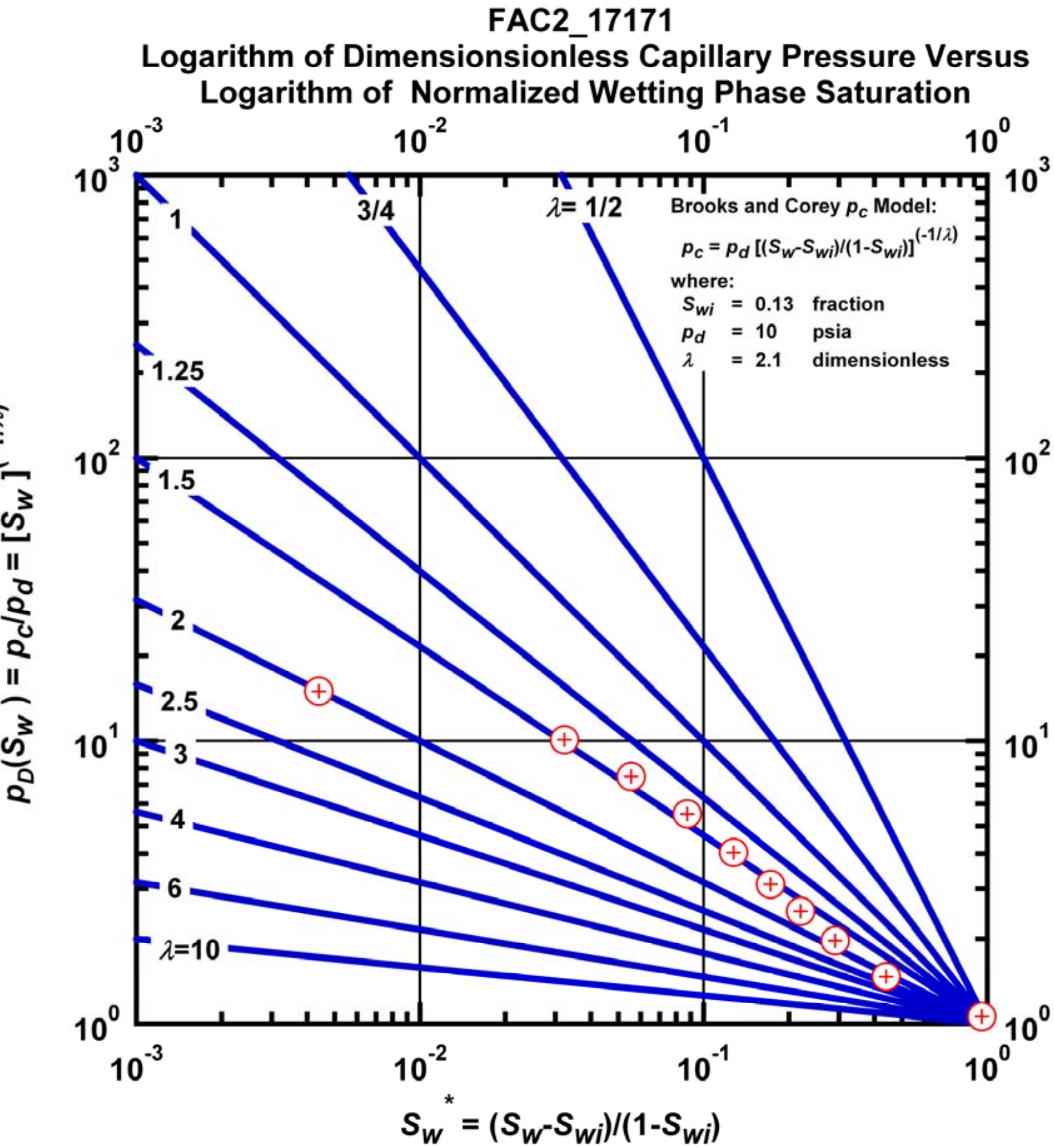

Figure L.32 – Plot of logarithm of dimensionless capillary pressure vs. logarithm of normalized wetting phase saturation — Case FAC2_17171.

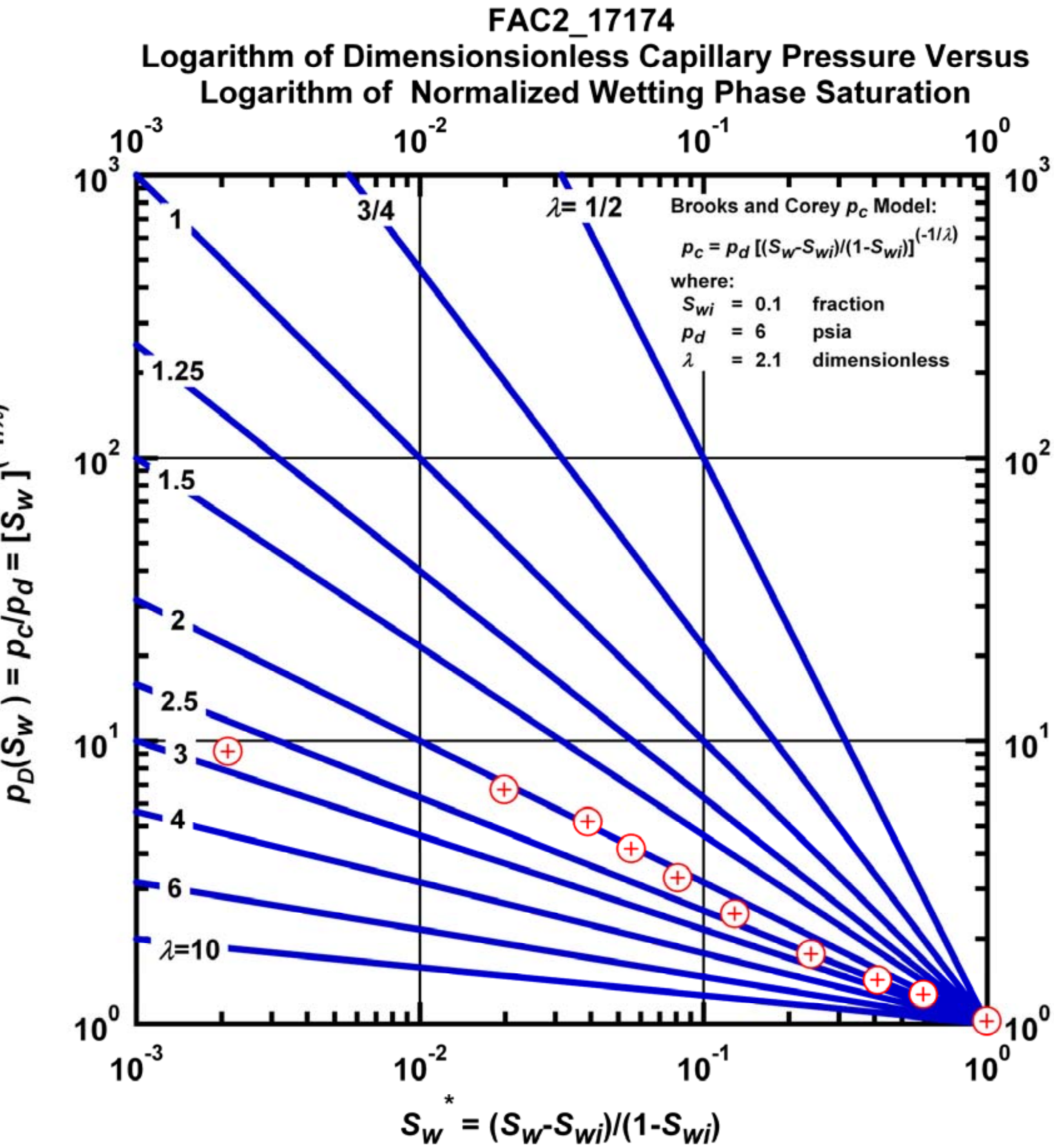

Figure L.33 – Plot of logarithm of dimensionless capillary pressure vs. logarithm of normalized wetting phase saturation — Case FAC2_17174.

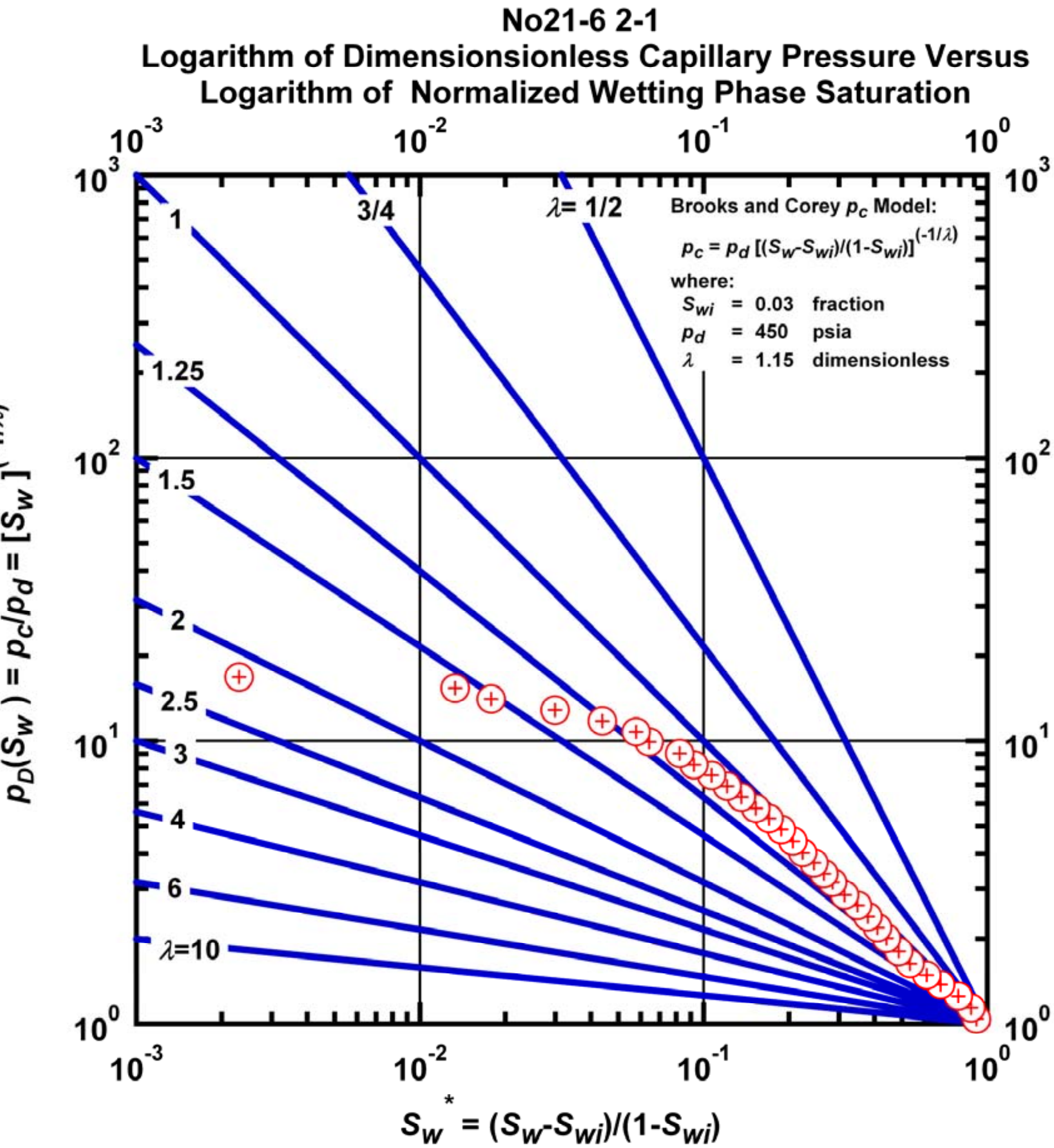

Figure L.34 – Plot of logarithm of dimensionless capillary pressure vs. logarithm of normalized wetting phase saturation ── Case No21-6 2-1.

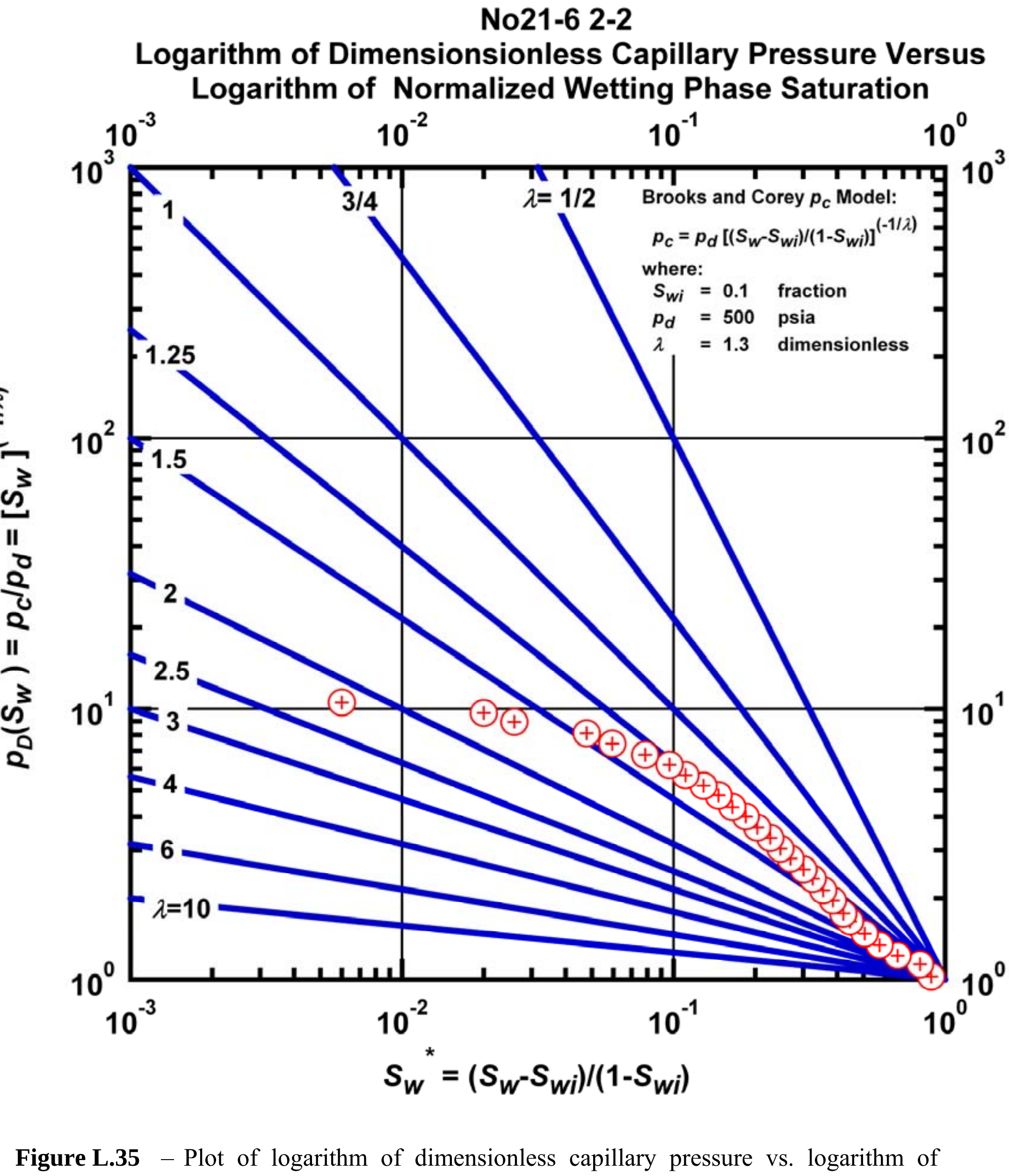

Figure L.35 – Plot of logarithm of dimensionless capillary pressure vs. logarithm of normalized wetting phase saturation — Case No21-6 2-2.

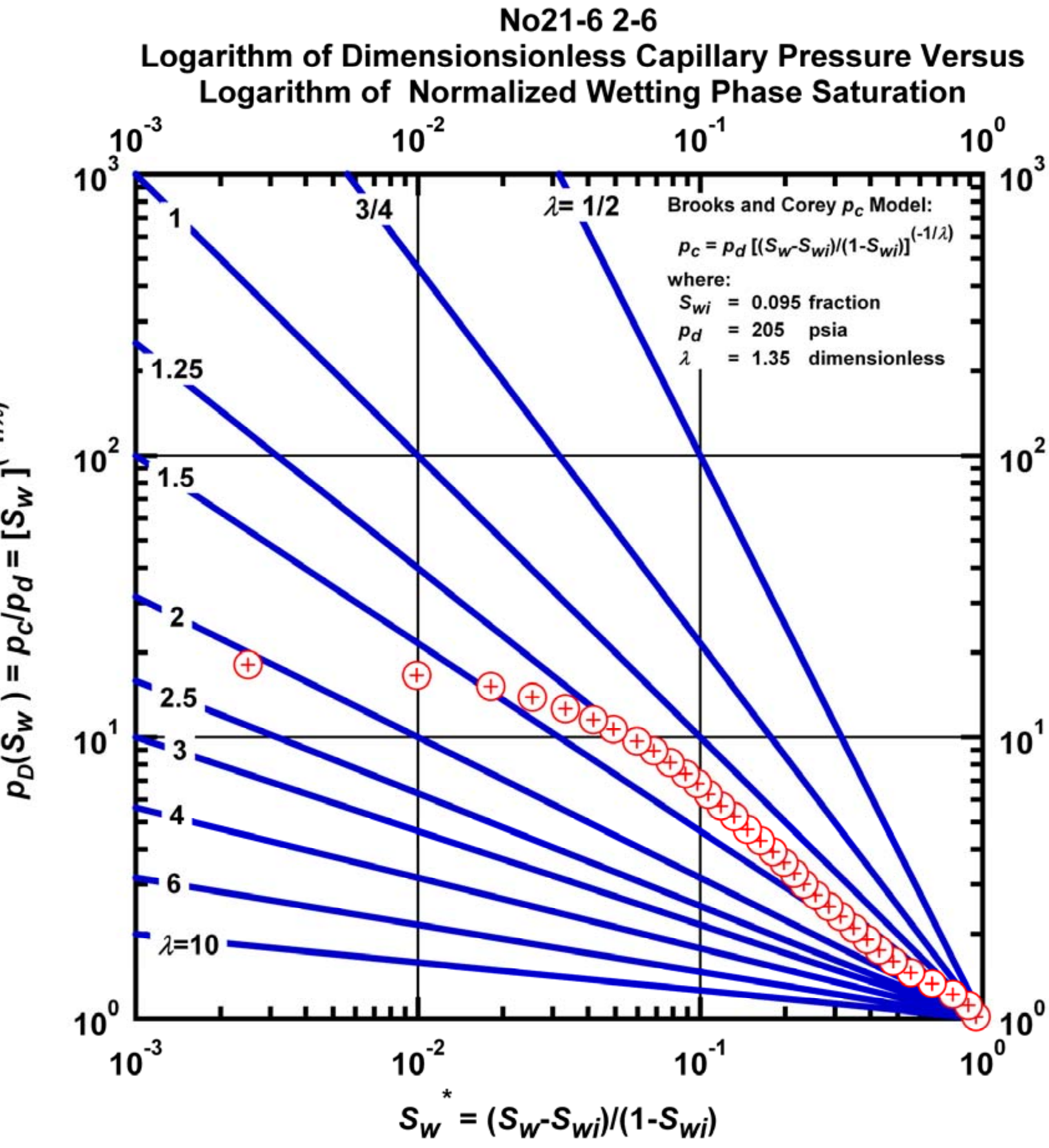

Figure L.36 – Plot of logarithm of dimensionless capillary pressure vs. logarithm of normalized wetting phase saturation — Case No21-6 2-6.

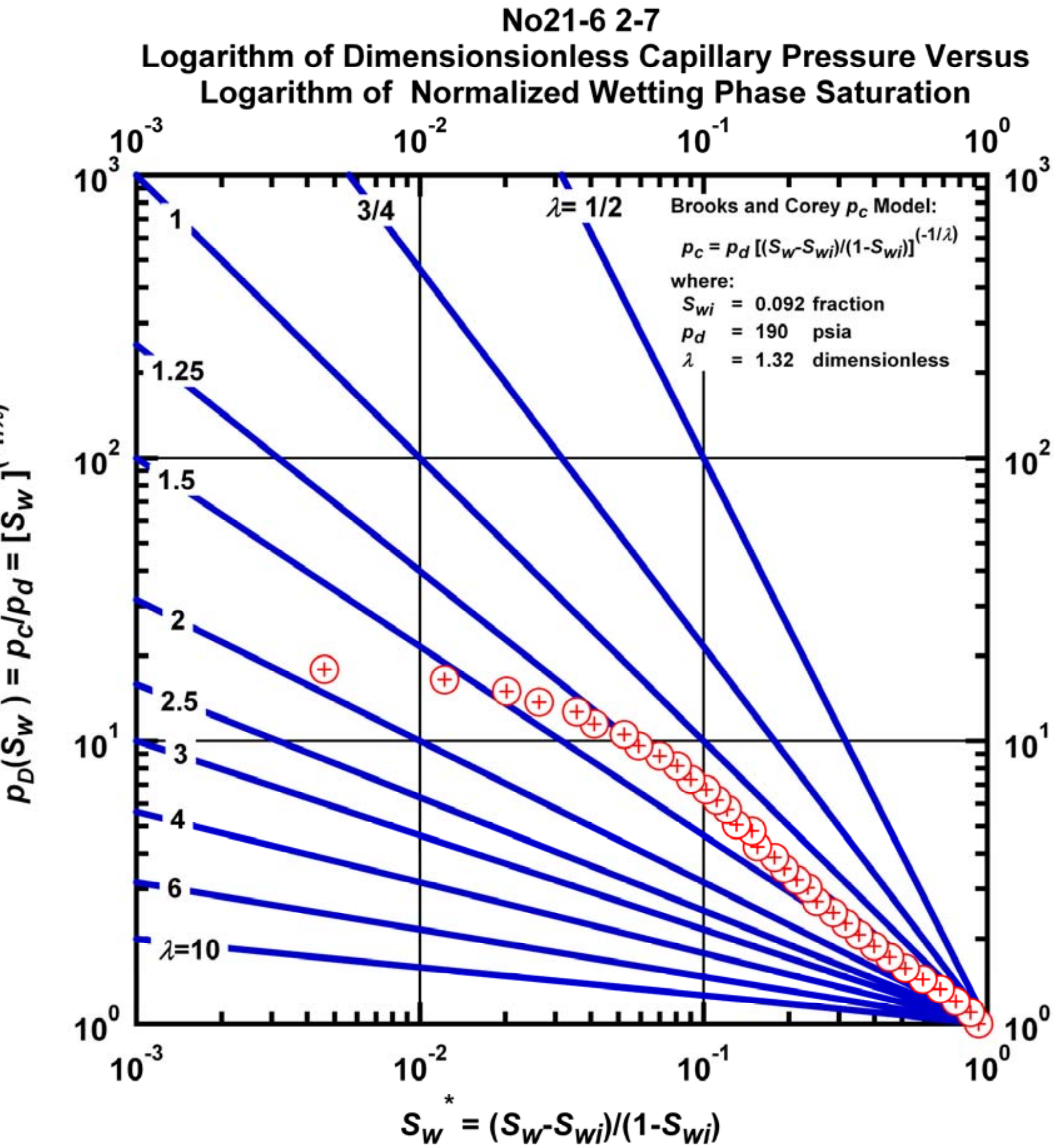

Figure L.37 – Plot of logarithm of dimensionless capillary pressure vs. logarithm of normalized wetting phase saturation — Case No21-6 2-7.

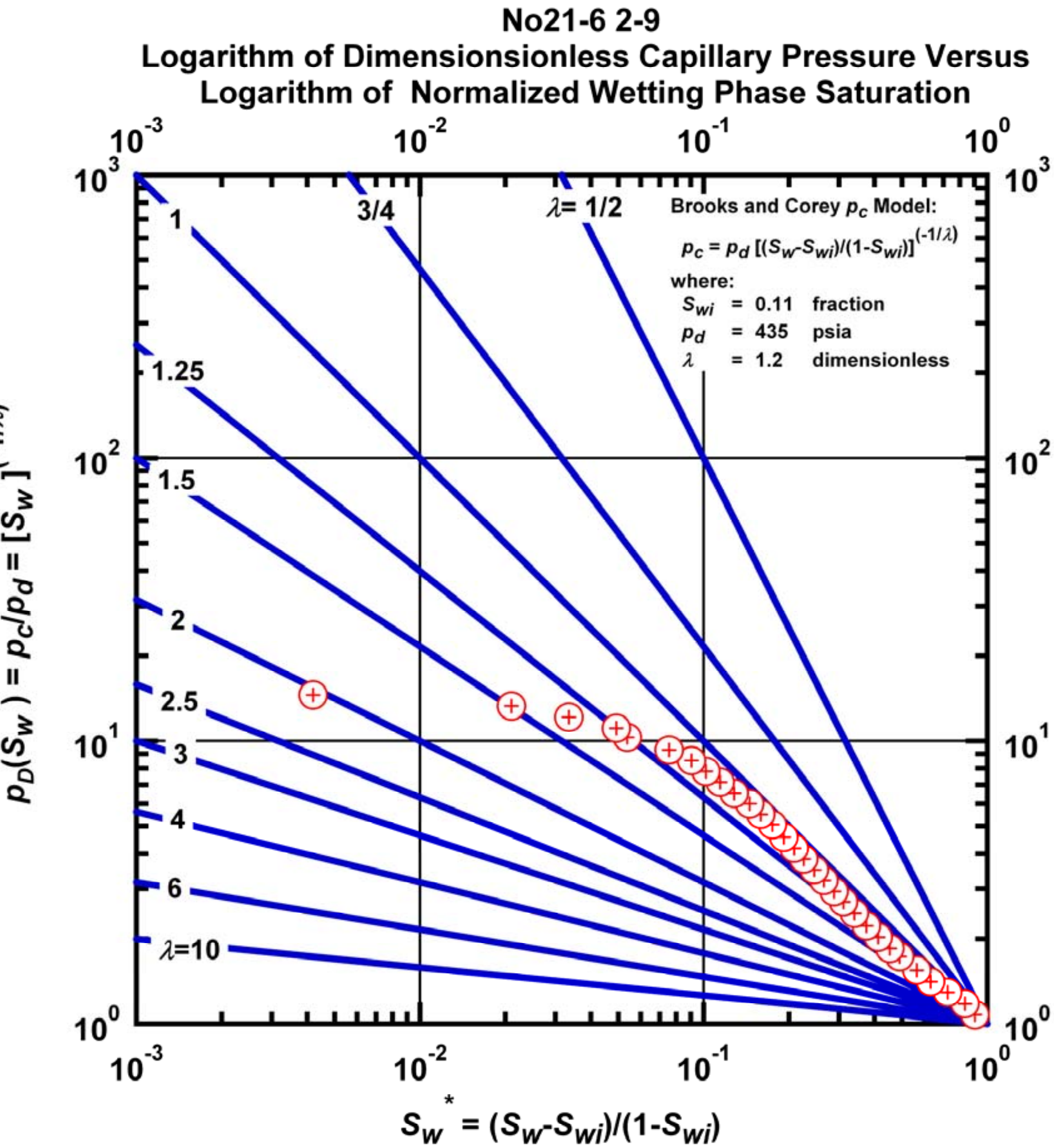

Figure L.38 – Plot of logarithm of dimensionless capillary pressure vs. logarithm of normalized wetting phase saturation — Case No21-6 2-9.

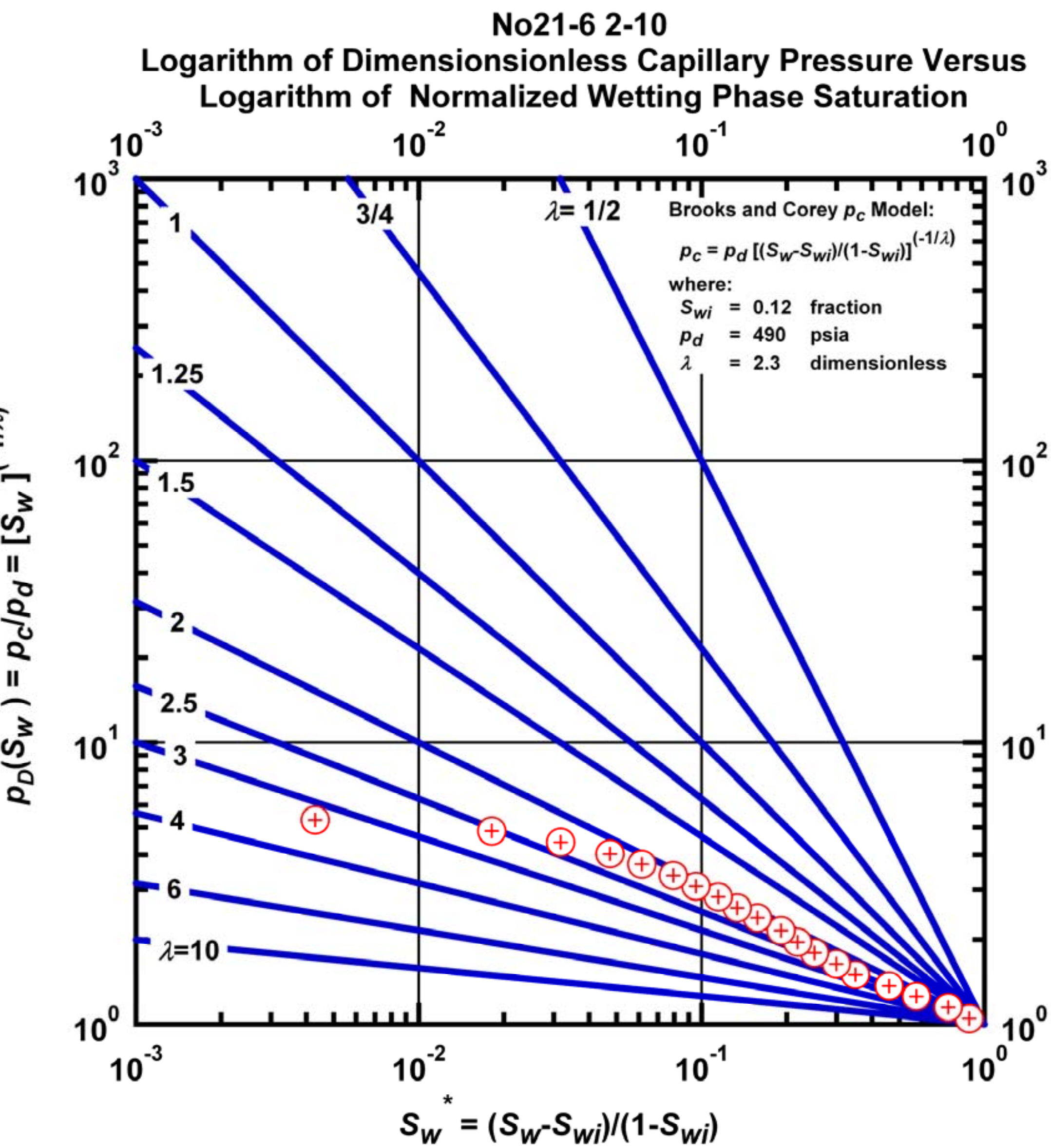

Figure L.39 – Plot of logarithm of dimensionless capillary pressure vs. logarithm of normalized wetting phase saturation — Case No21-6 2-10.

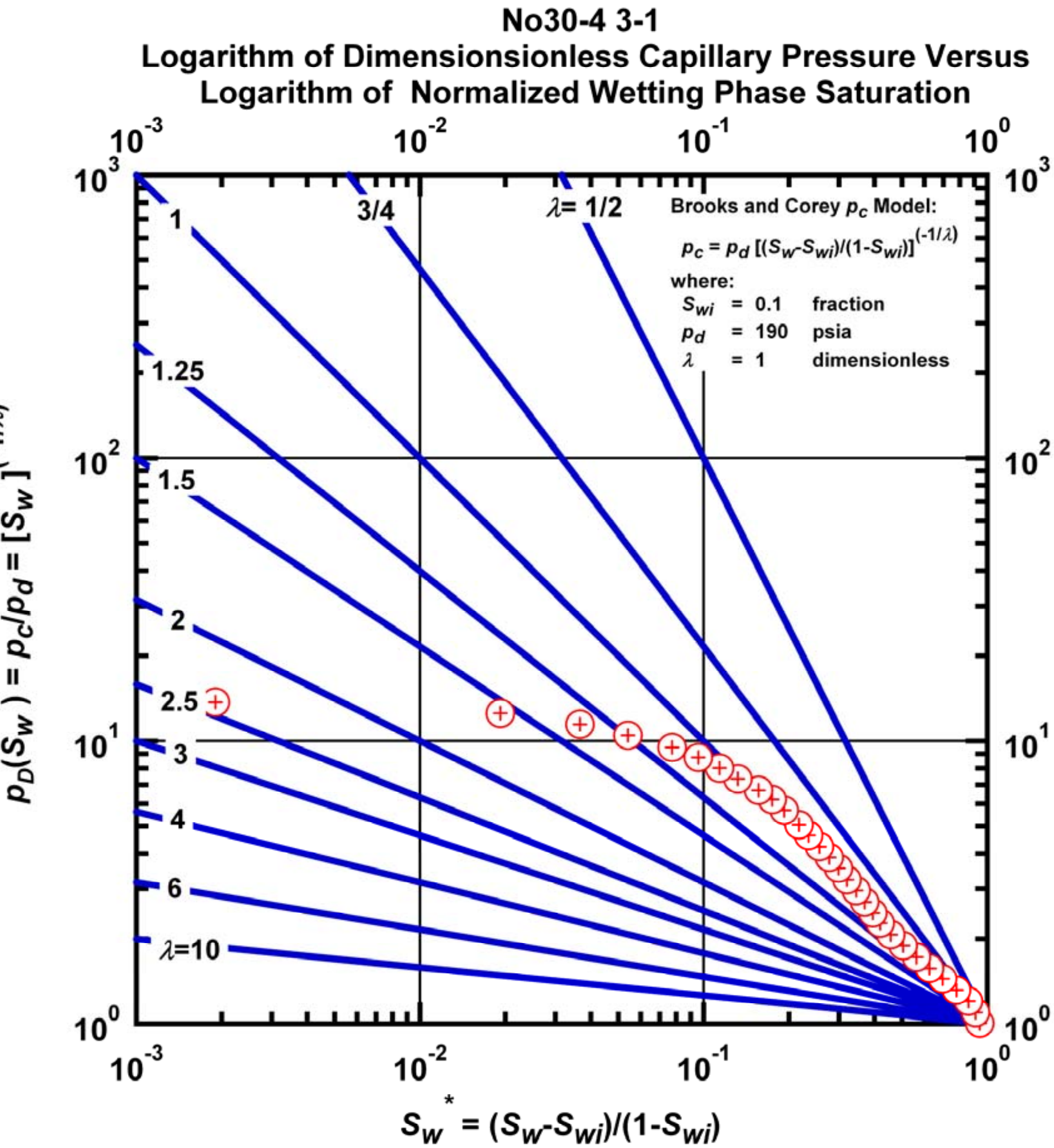

Figure L.40 – Plot of logarithm of dimensionless capillary pressure vs. logarithm of normalized wetting phase saturation — Case No30-4 3-1.

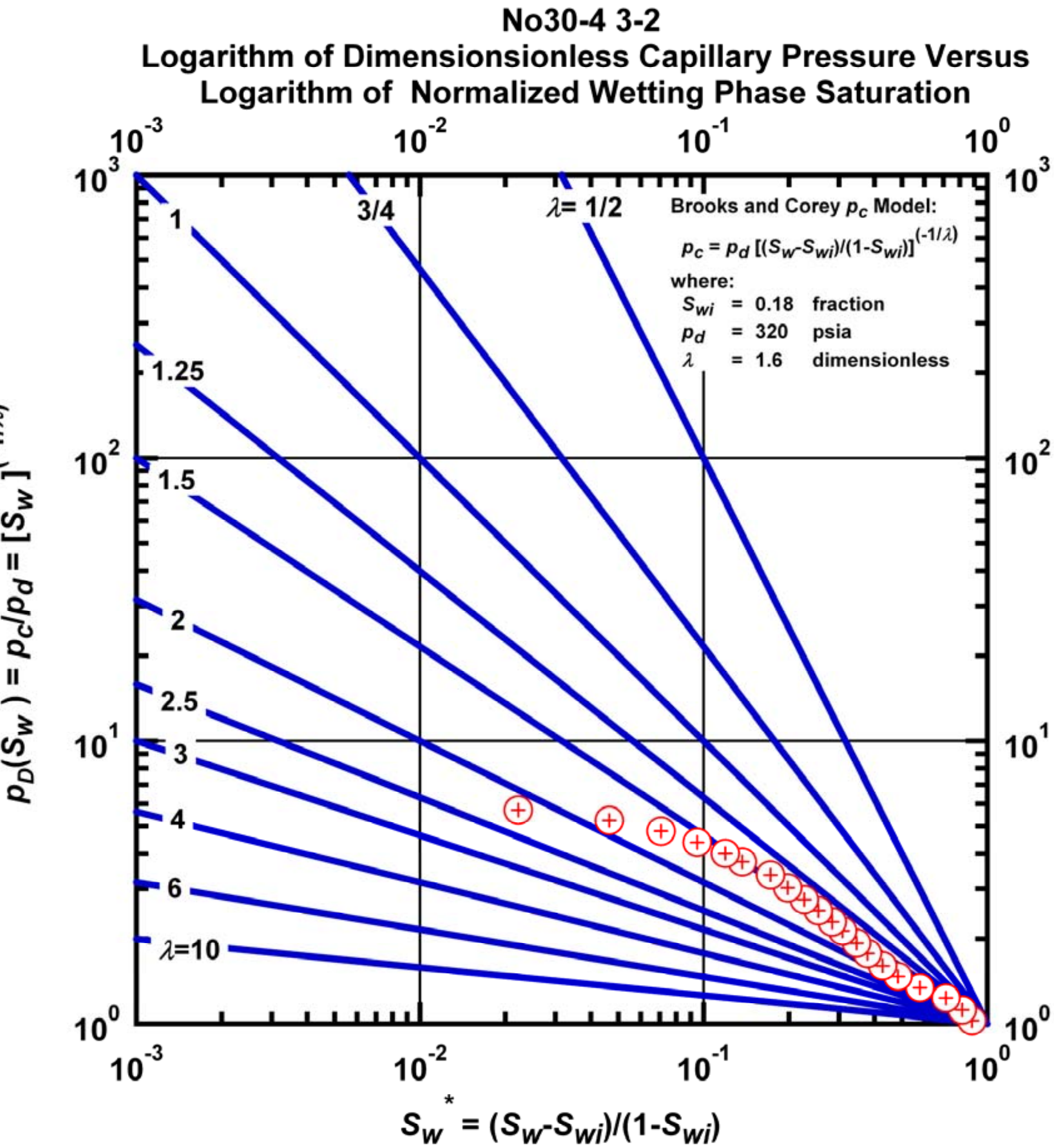

Figure L.41 – Plot of logarithm of dimensionless capillary pressure vs. logarithm of normalized wetting phase saturation — Case No30-4 3-2.

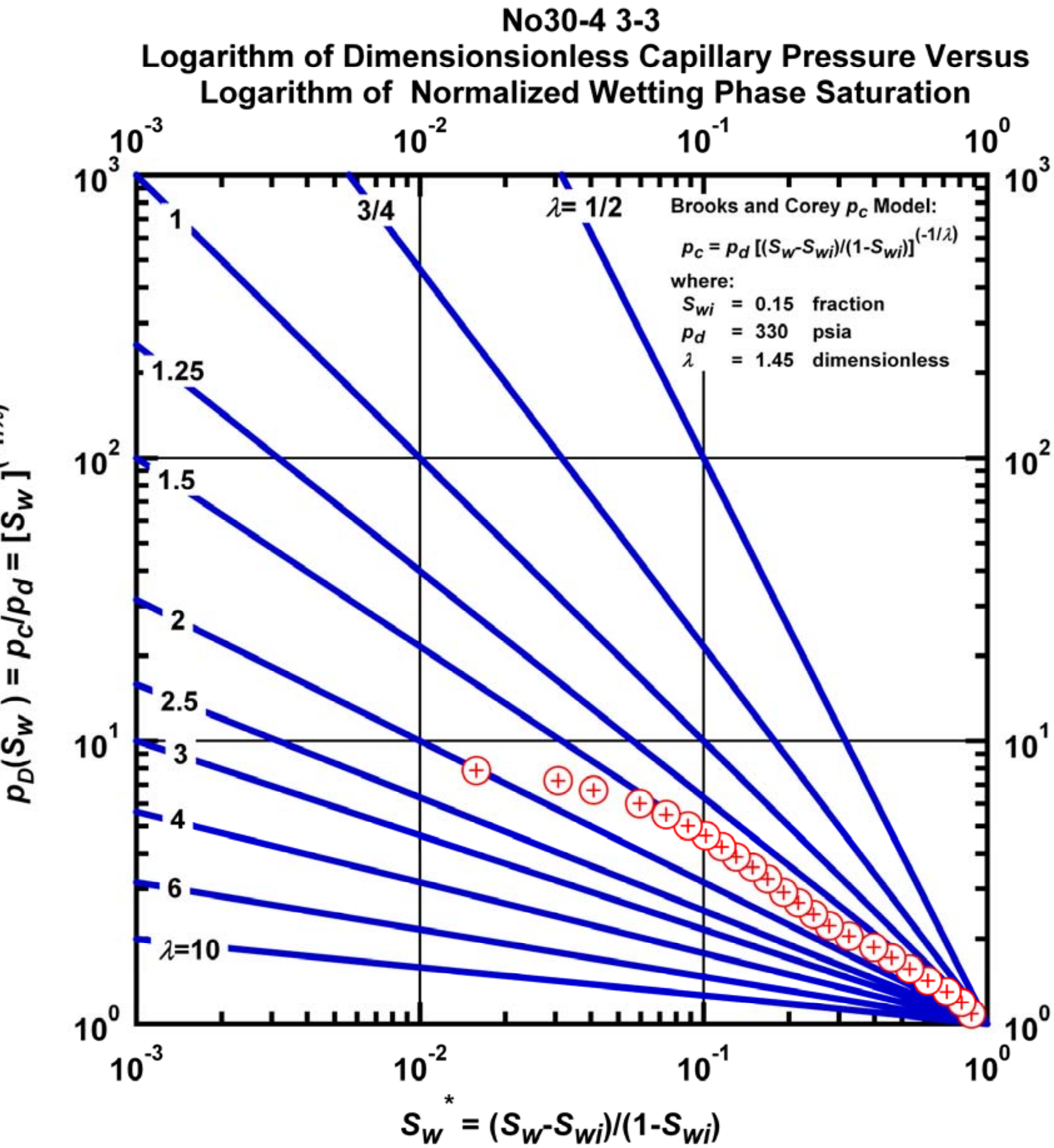

Figure L.42 – Plot of logarithm of dimensionless capillary pressure vs. logarithm of normalized wetting phase saturation — Case No30-4 3-3.

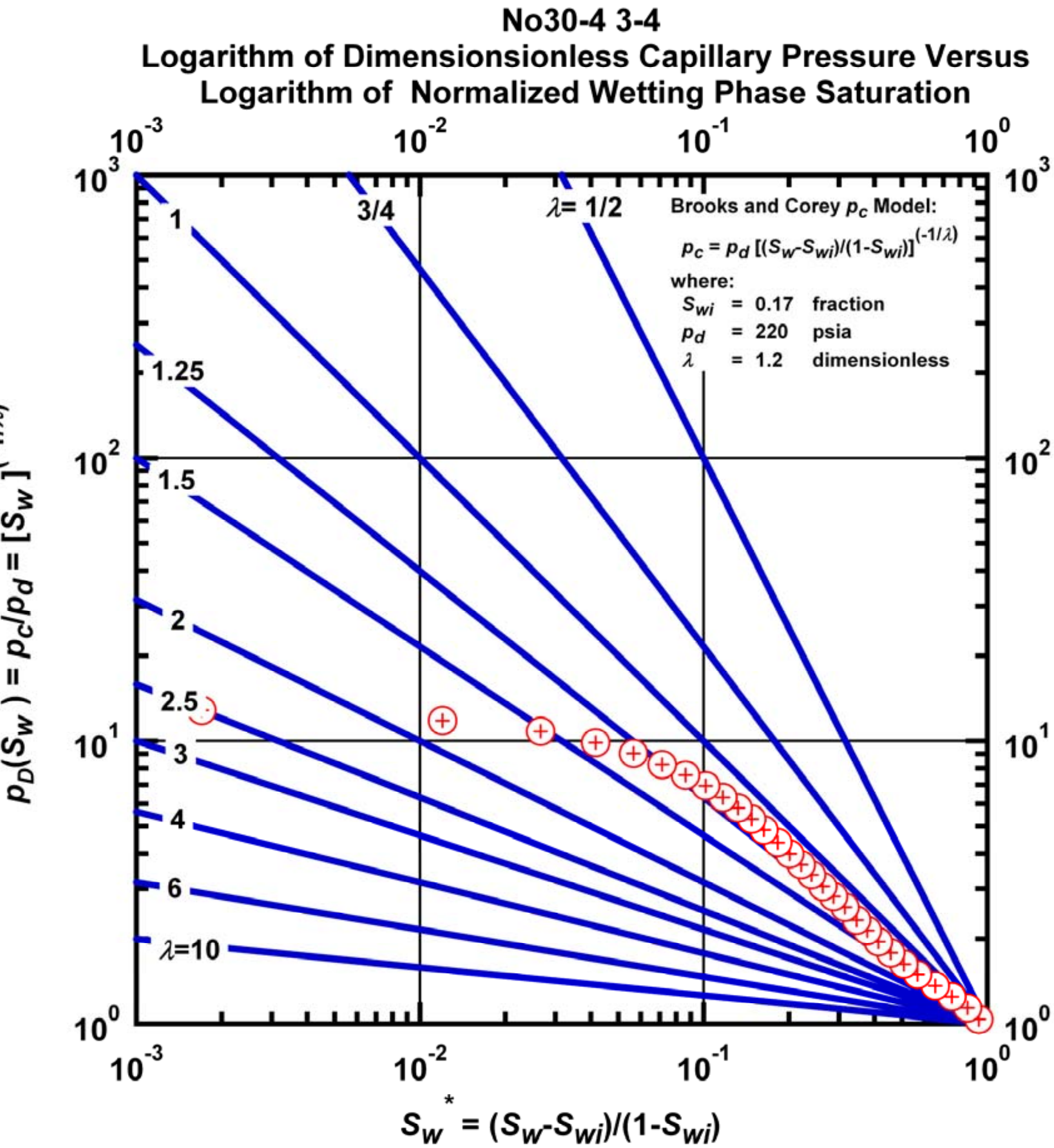

Figure L.43 – Plot of logarithm of dimensionless capillary pressure vs. logarithm of normalized wetting phase saturation — Case No30-4 3-4.

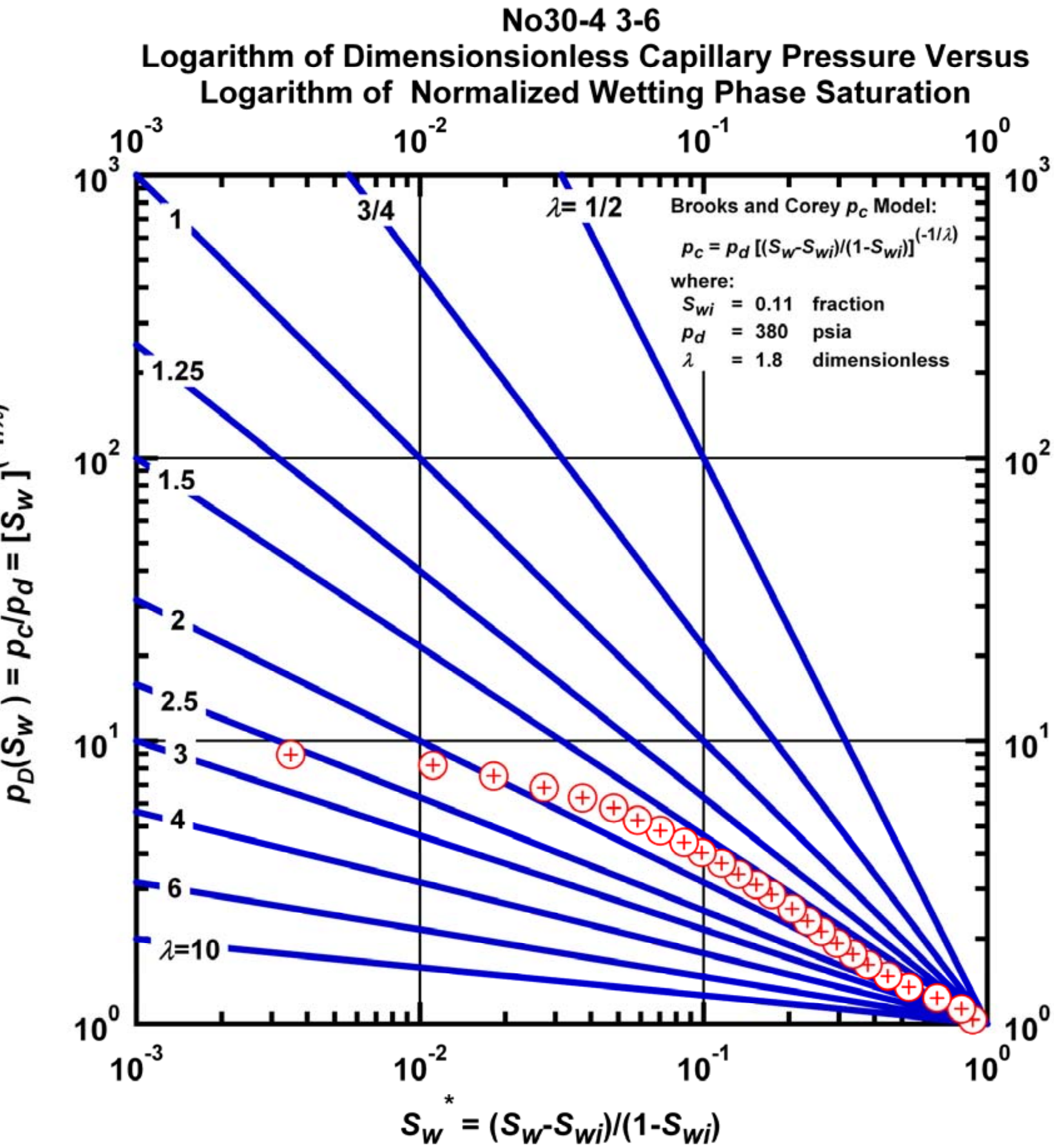

Figure L.44 – Plot of logarithm of dimensionless capillary pressure vs. logarithm of normalized wetting phase saturation — Case No30-4 3-6.

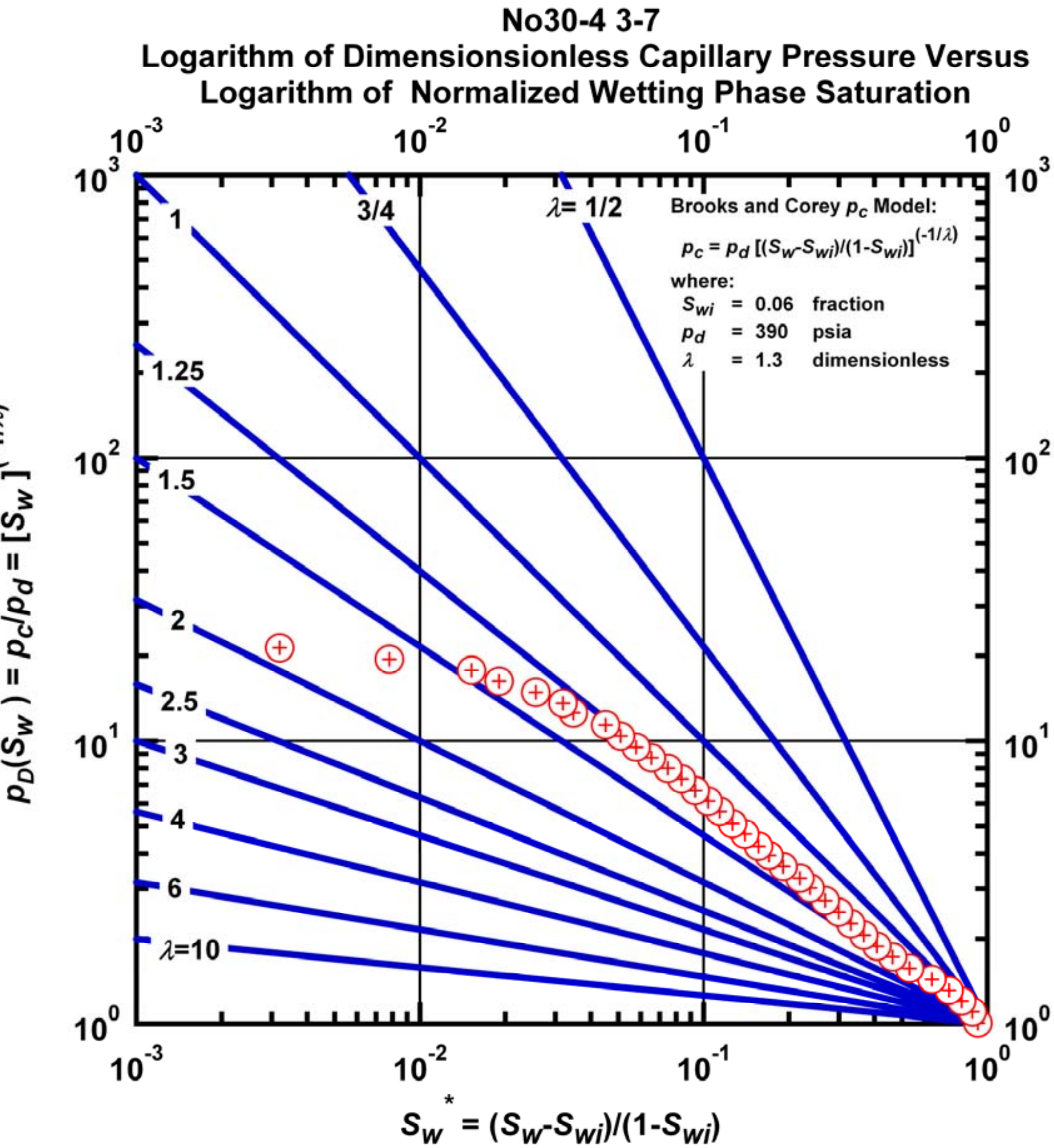

Figure L.45 – Plot of logarithm of dimensionless capillary pressure vs. logarithm of normalized wetting phase saturation — Case No30-4 3-7.

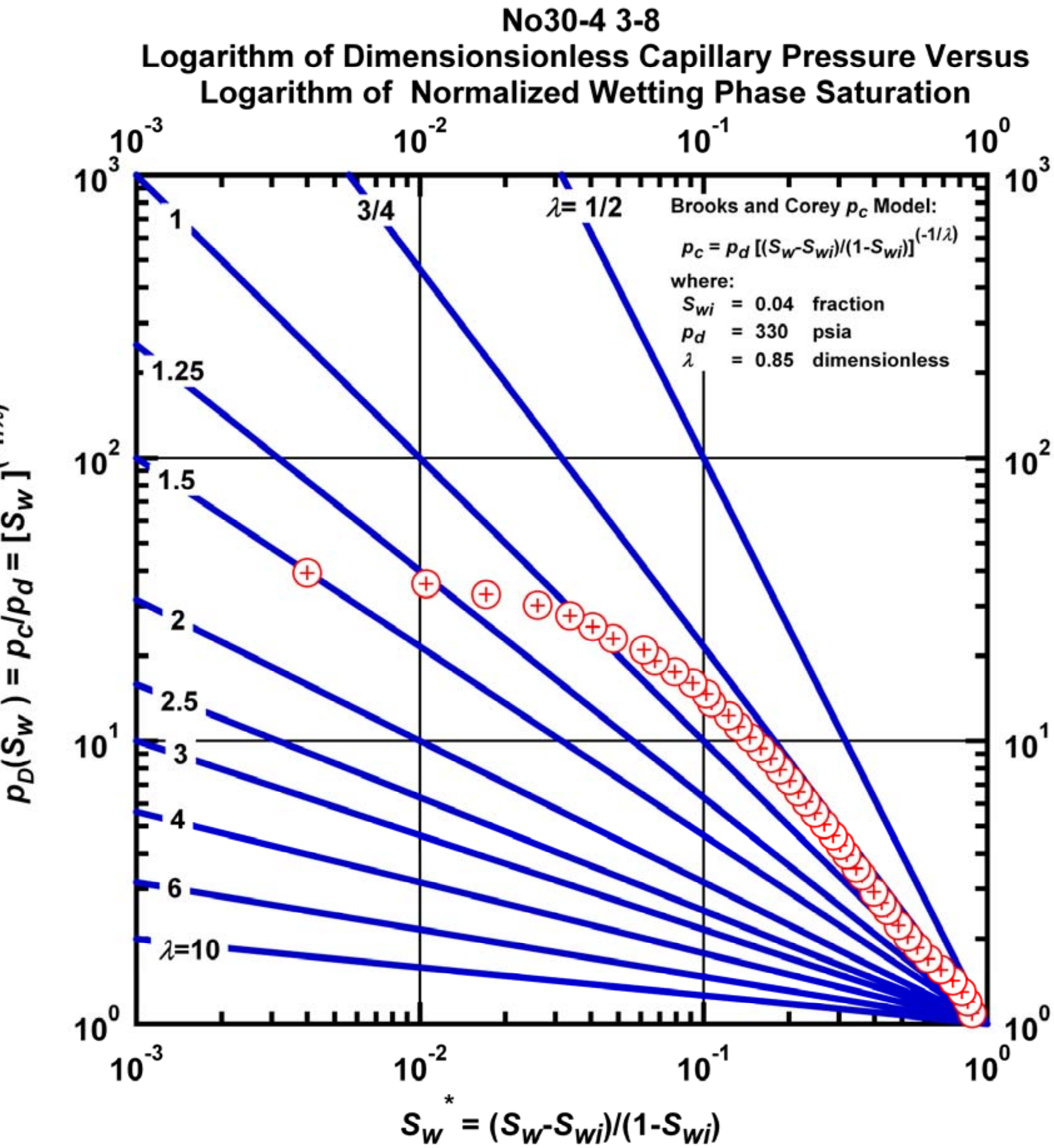

Figure L.46 – Plot of logarithm of dimensionless capillary pressure vs. logarithm of normalized wetting phase saturation — Case No30-4 3-8.

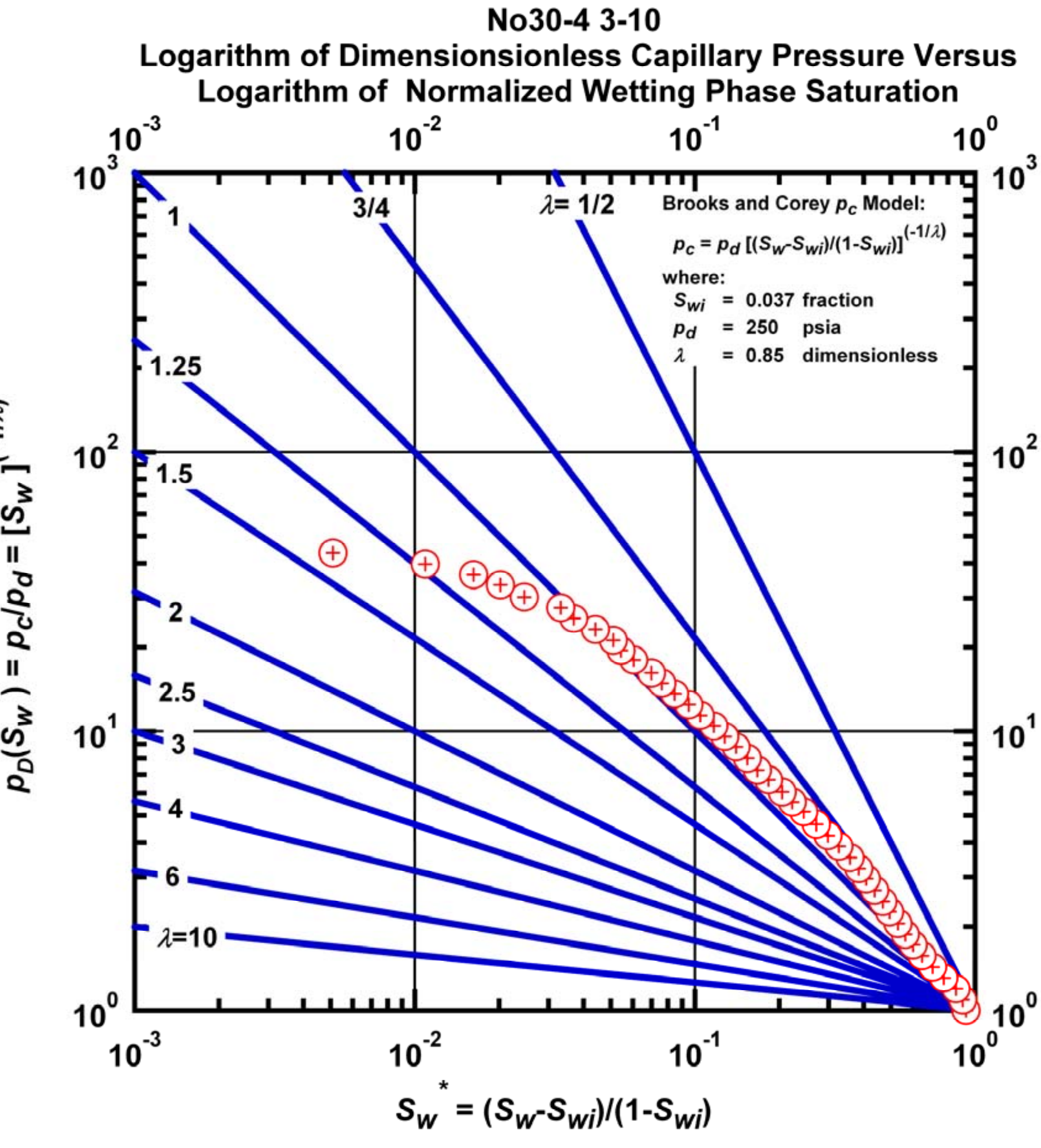

Figure L.47 – Plot of logarithm of dimensionless capillary pressure vs. logarithm of normalized wetting phase saturation — Case No30-4 3-10.

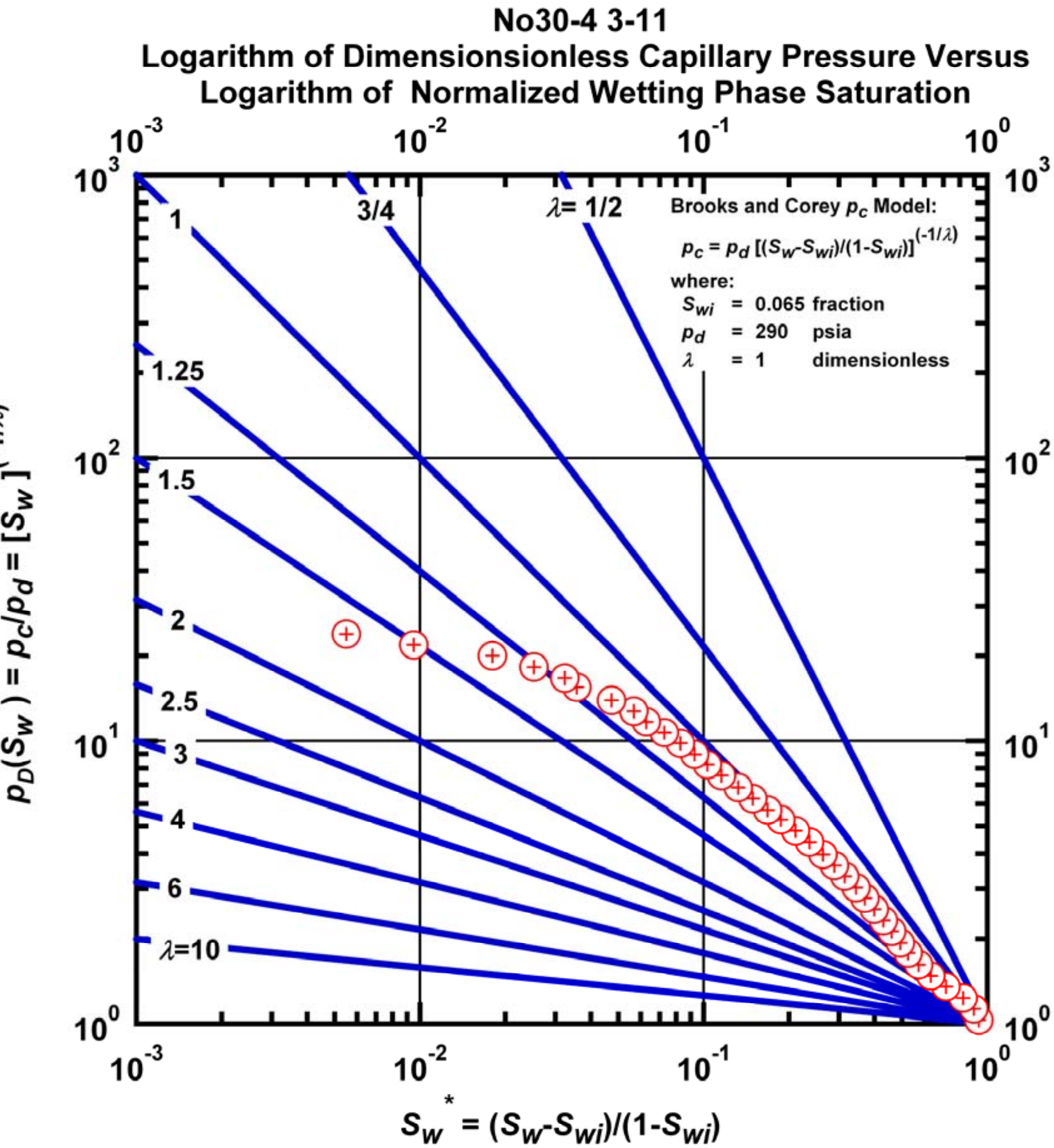

Figure L.48 – Plot of logarithm of dimensionless capillary pressure vs. logarithm of normalized wetting phase saturation — Case No30-4 3-11.

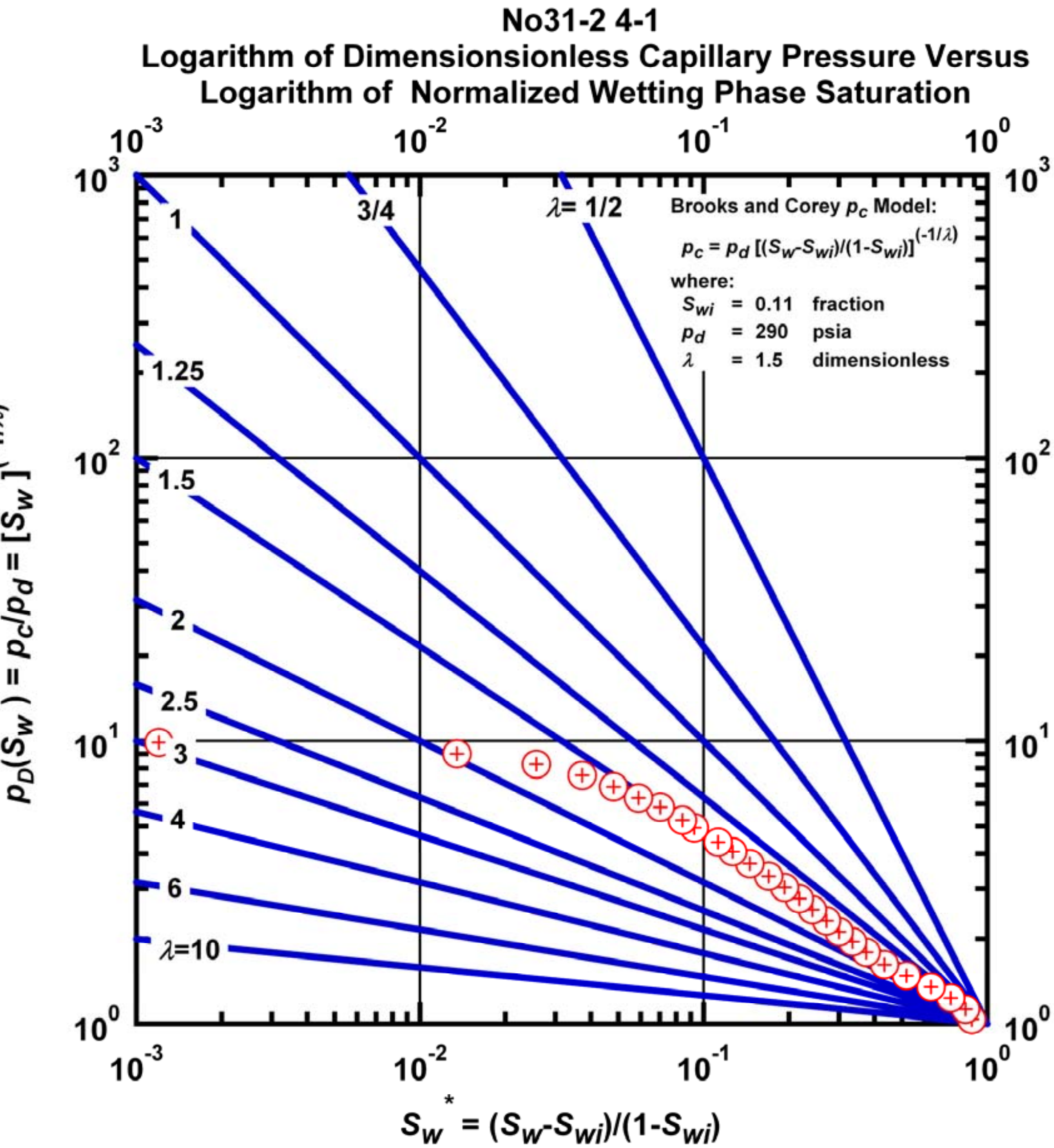

Figure L.49 – Plot of logarithm of dimensionless capillary pressure vs. logarithm of normalized wetting phase saturation —— Case No31-2 4-1.

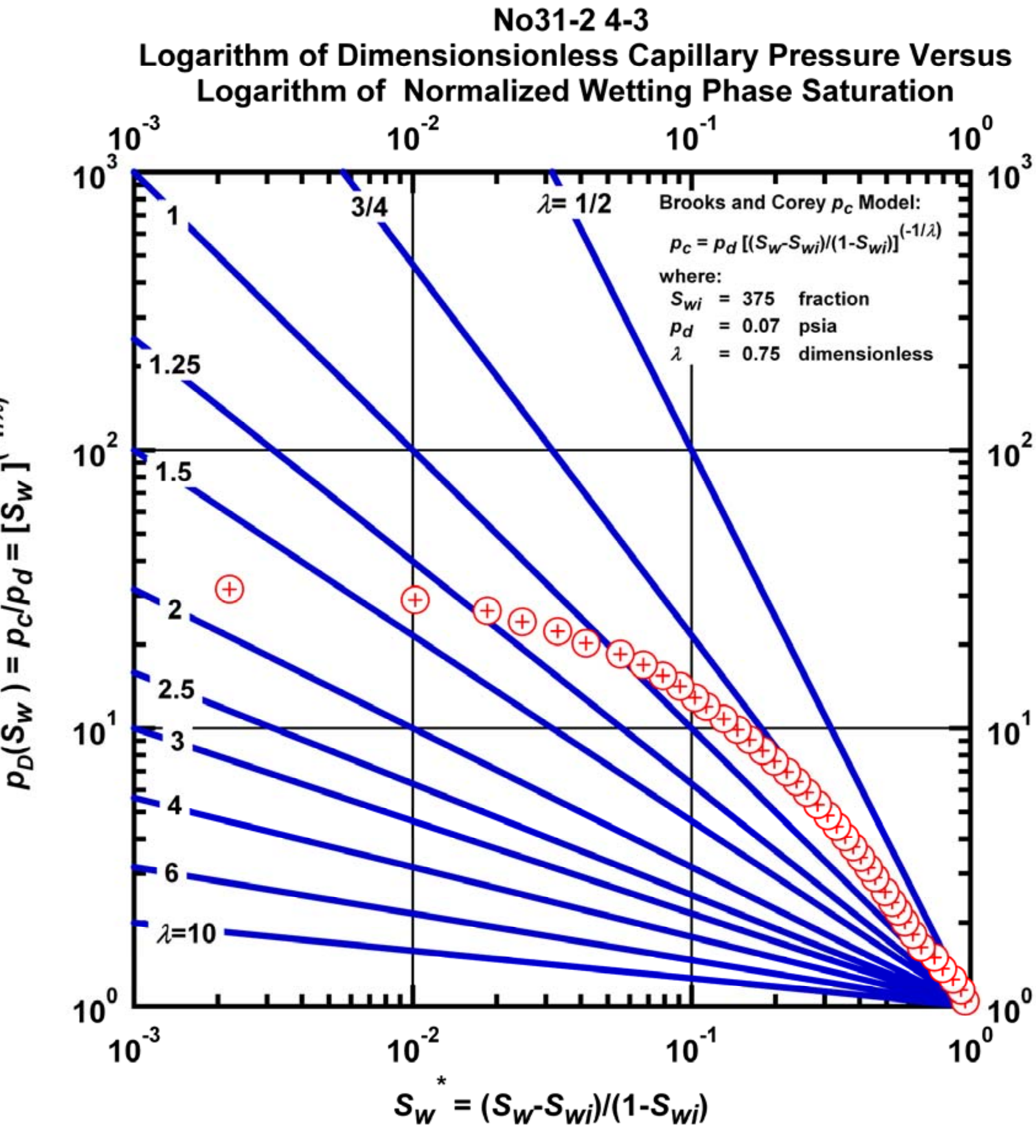

Figure L.50 – Plot of logarithm of dimensionless capillary pressure vs. logarithm of normalized wetting phase saturation ― Case No31-2 4-3.

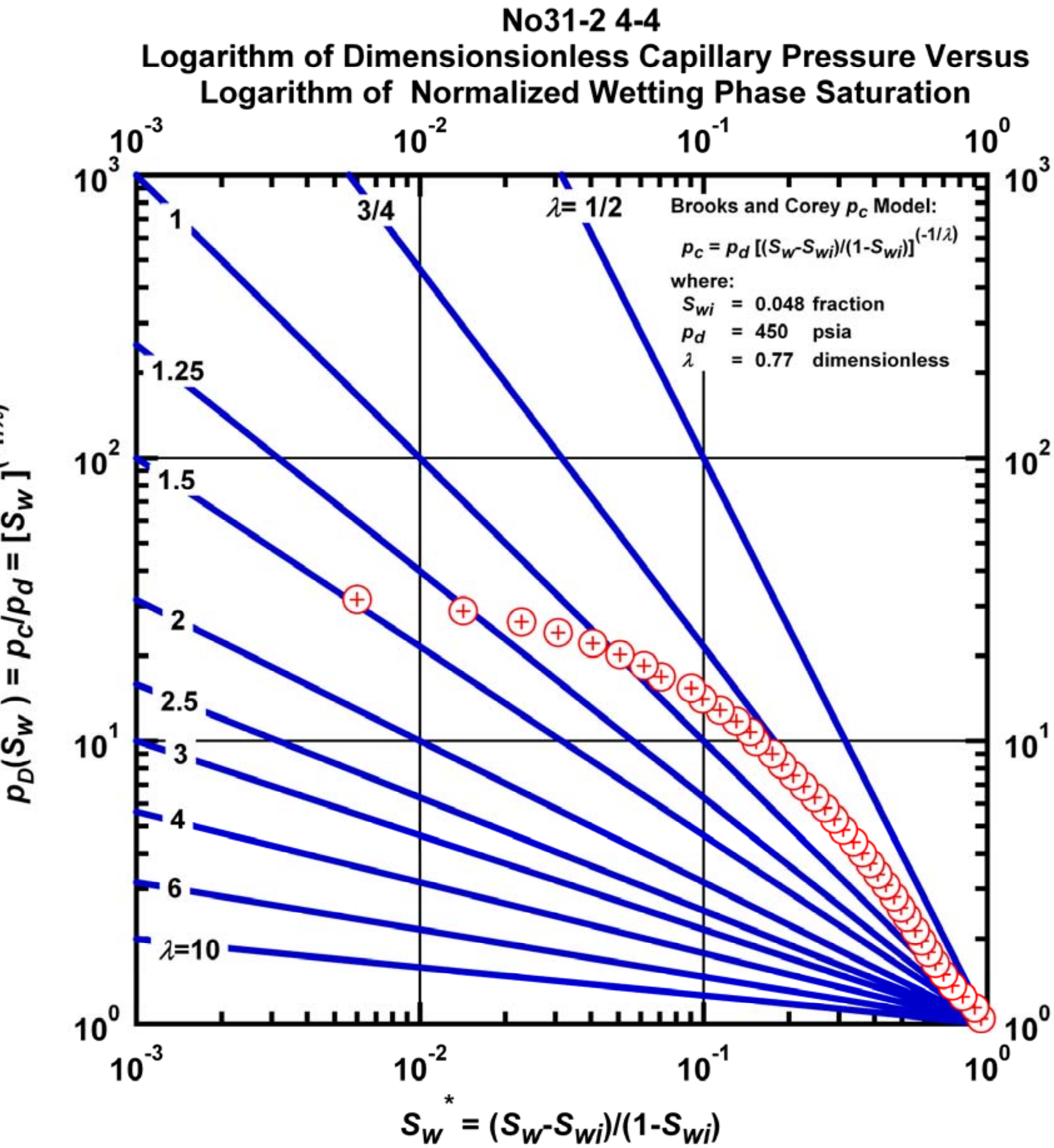

Figure L.51 – Plot of logarithm of dimensionless capillary pressure vs. logarithm of normalized wetting phase saturation — Case No31-2 4-4.

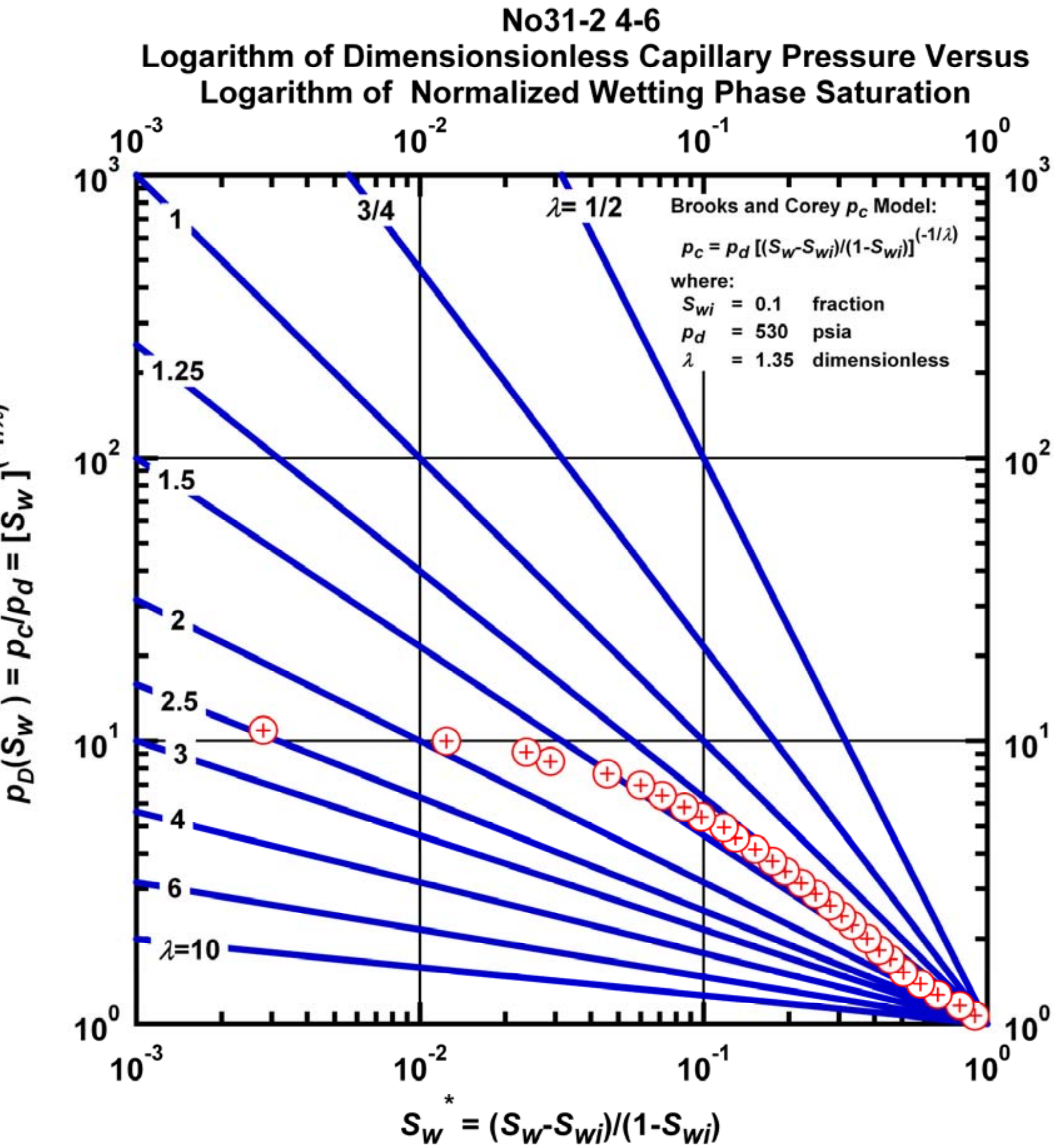

Figure L.52 – Plot of logarithm of dimensionless capillary pressure vs. logarithm of normalized wetting phase saturation — Case No31-2 4-6.

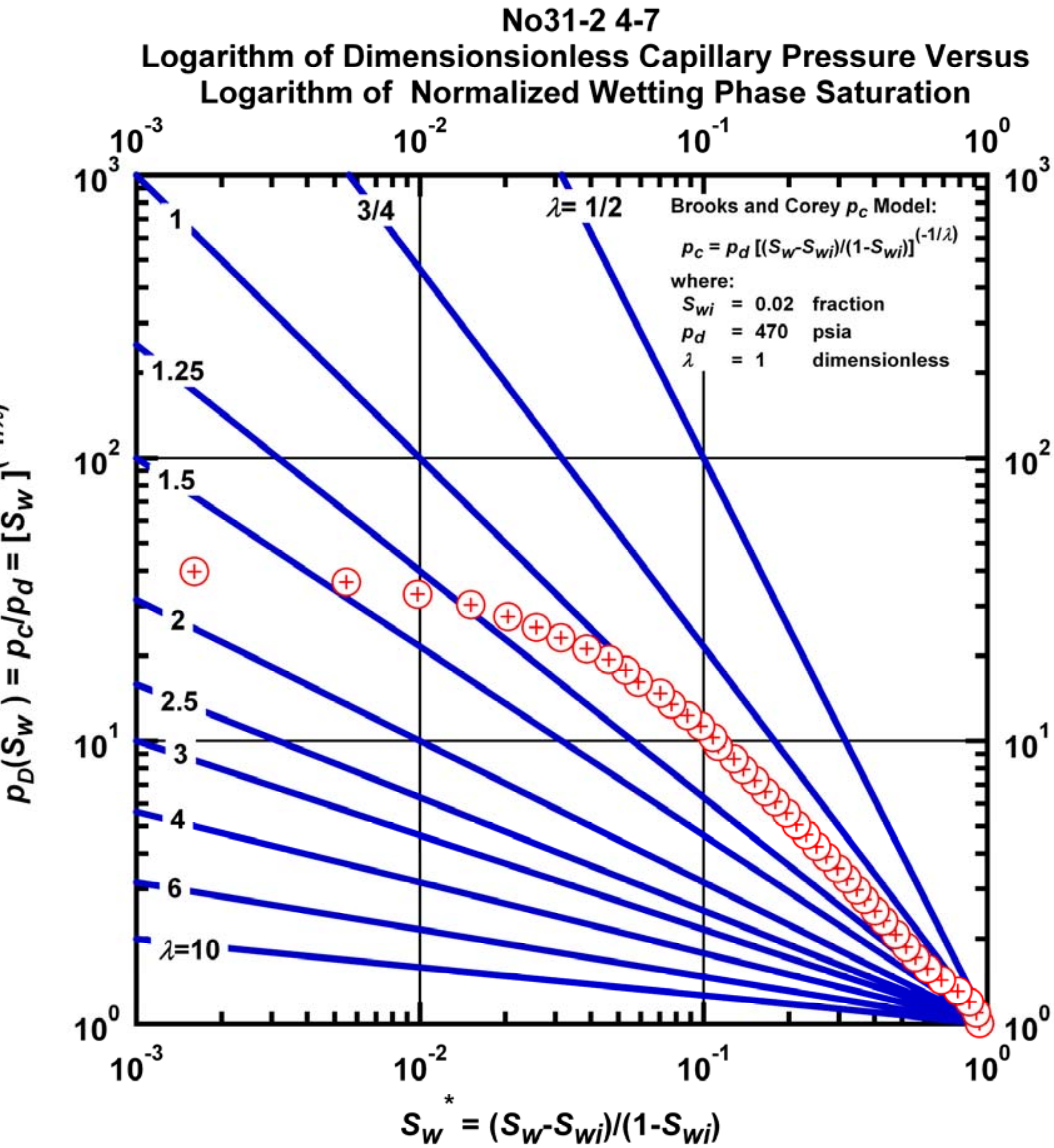

Figure L.53 – Plot of logarithm of dimensionless capillary pressure vs. logarithm of normalized wetting phase saturation — Case No31-2 4-7.

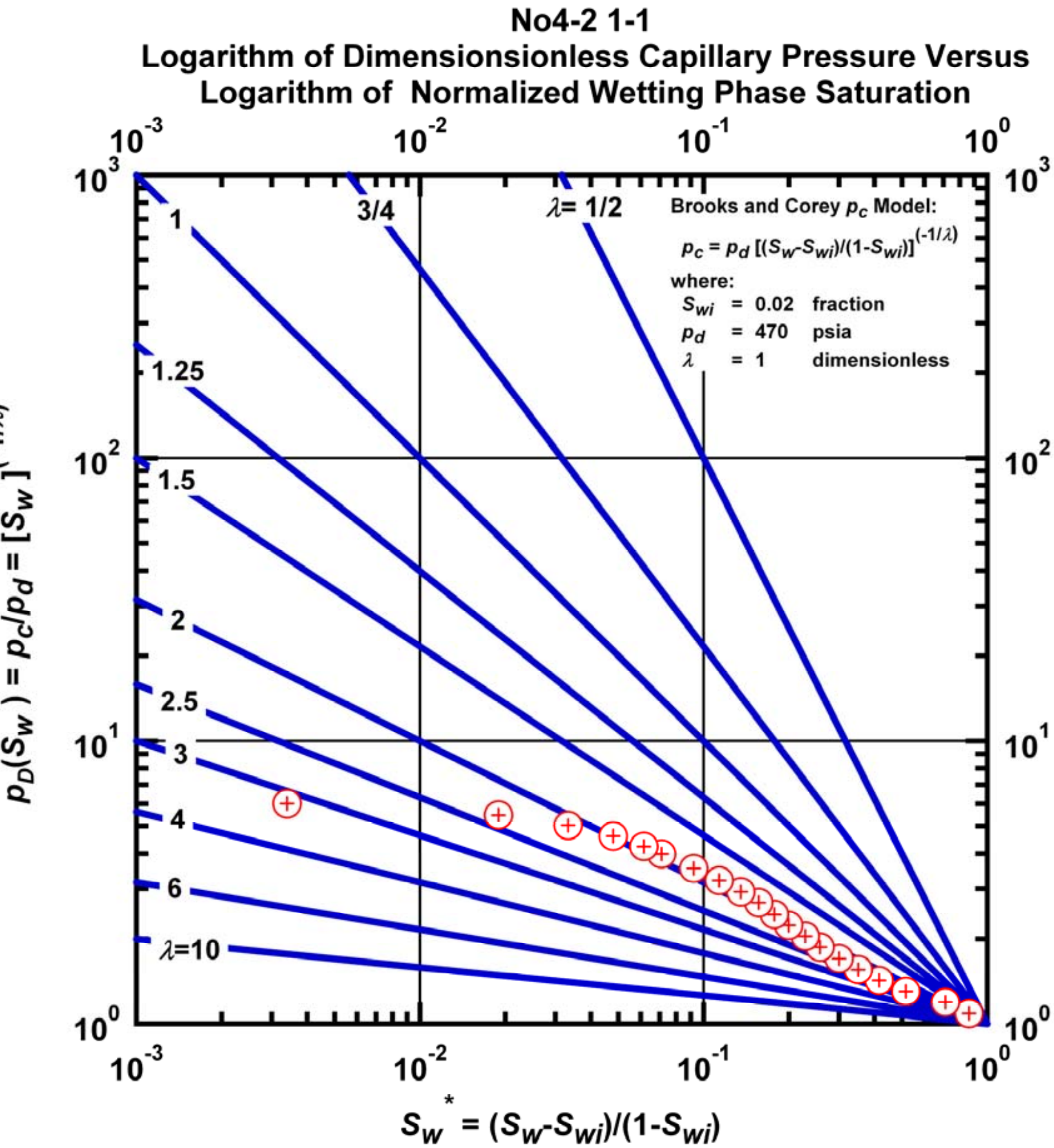

Figure L.54 – Plot of logarithm of dimensionless capillary pressure vs. logarithm of normalized wetting phase saturation — Case No4-2 1-1.

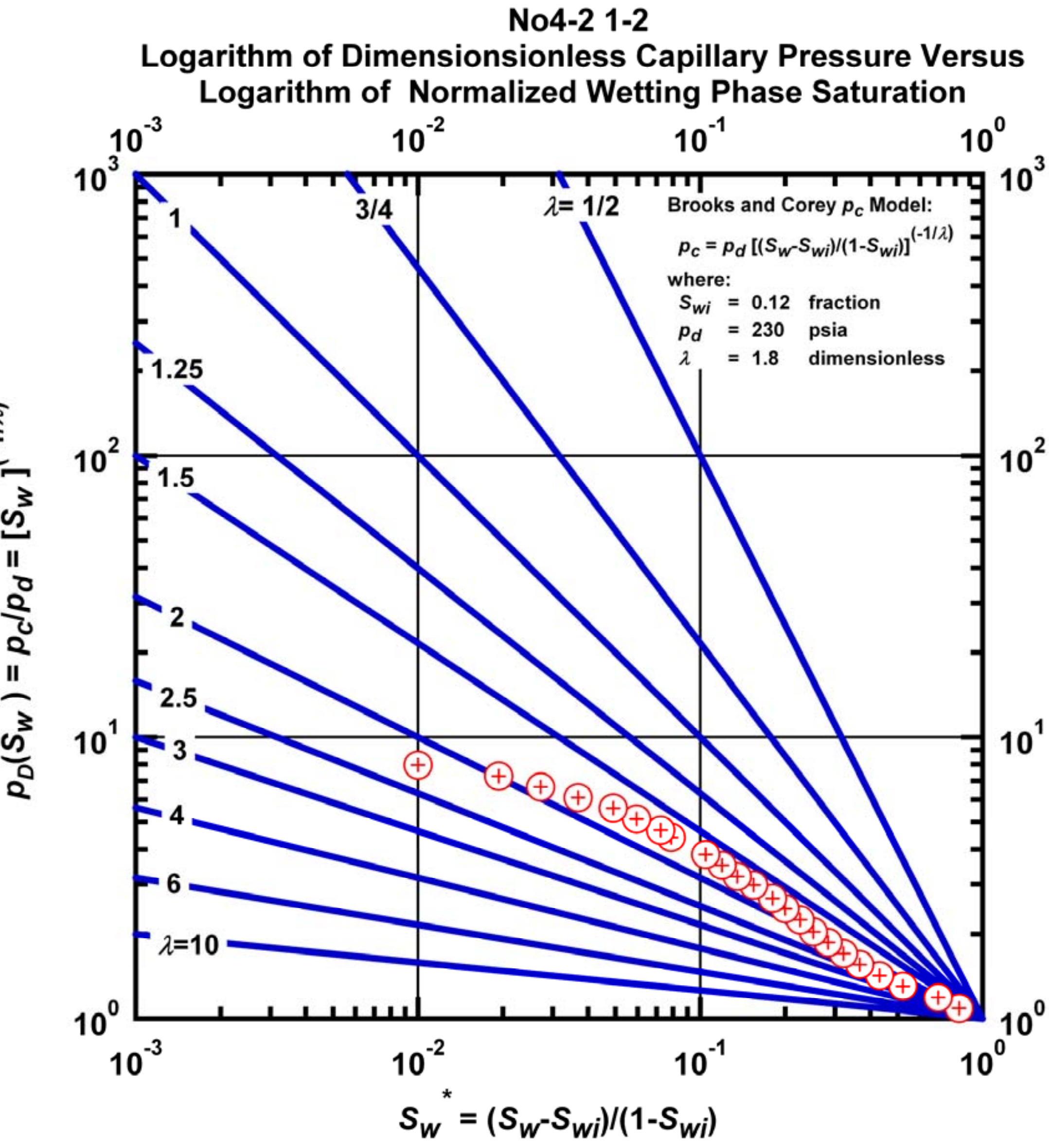

Figure L.55 – Plot of logarithm of dimensionless capillary pressure vs. logarithm of normalized wetting phase saturation — Case No4-2 1-2.

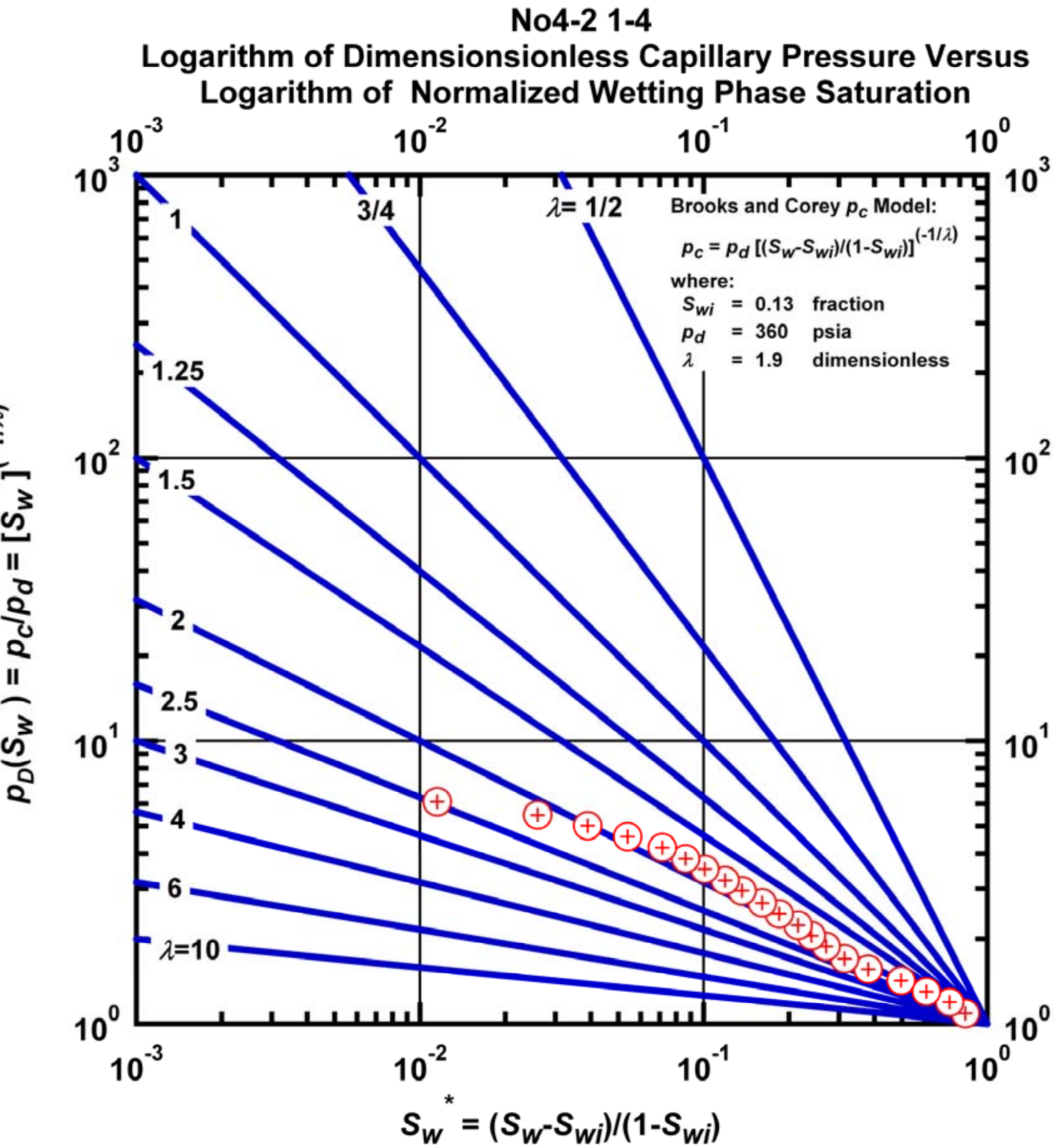

Figure L.56 – Plot of logarithm of dimensionless capillary pressure vs. logarithm of normalized wetting phase saturation — Case No4-2 1-4.

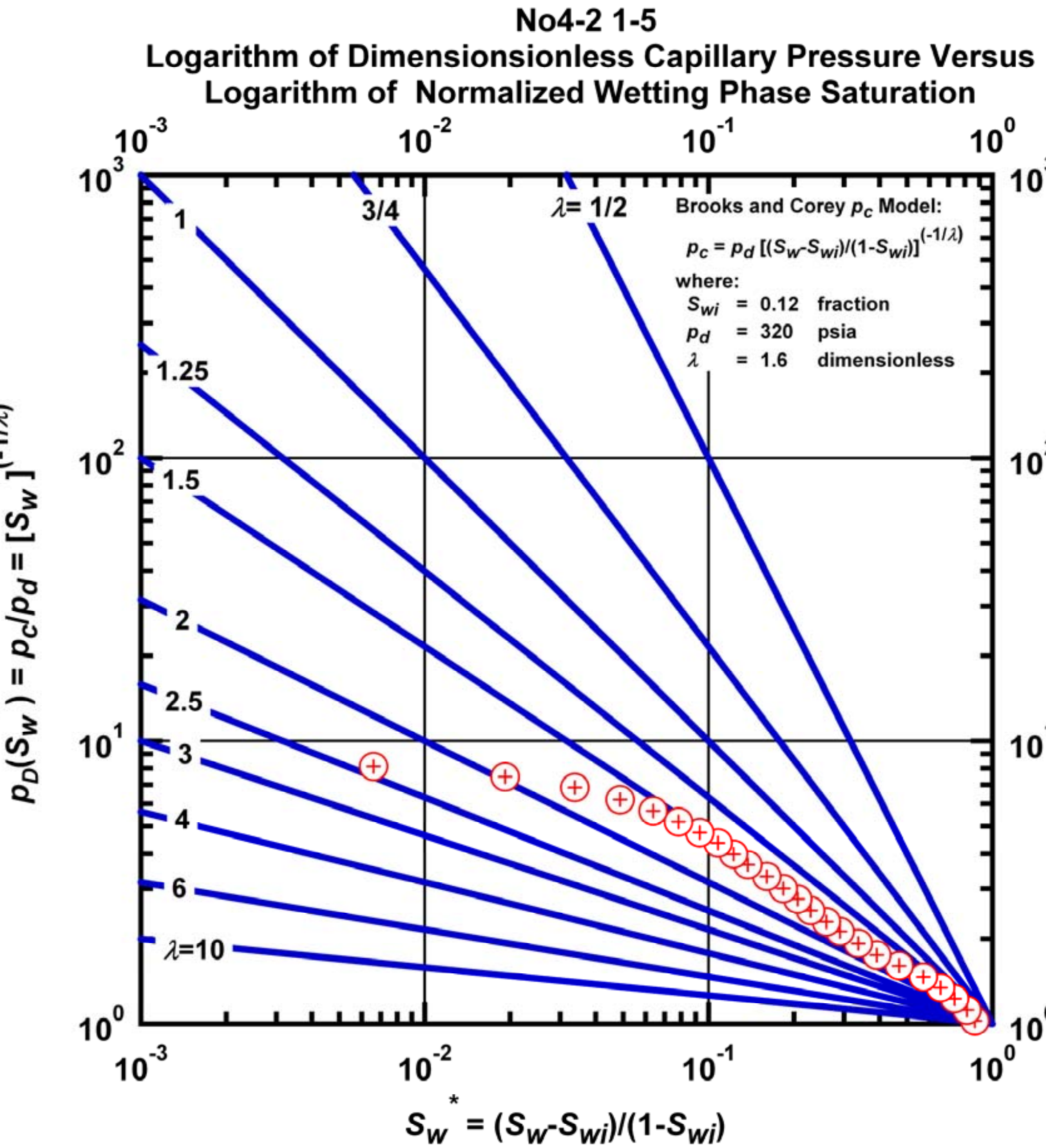

Figure L.57 – Plot of logarithm of dimensionless capillary pressure vs. logarithm of normalized wetting phase saturation — Case No4-2 1-5.

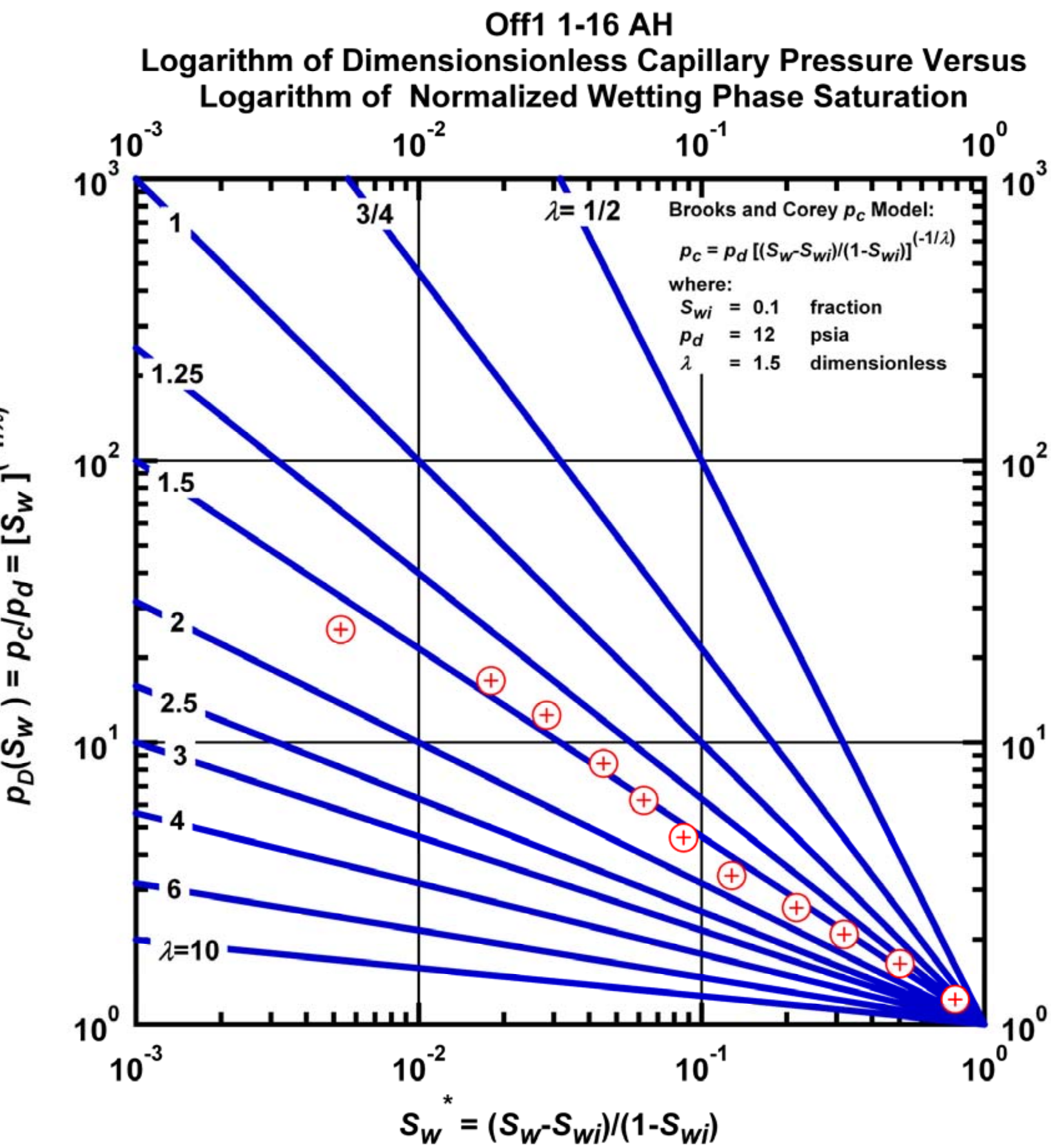

Figure L.58 – Plot of logarithm of dimensionless capillary pressure vs. logarithm of normalized wetting phase saturation — Case Off1 1-16AH.

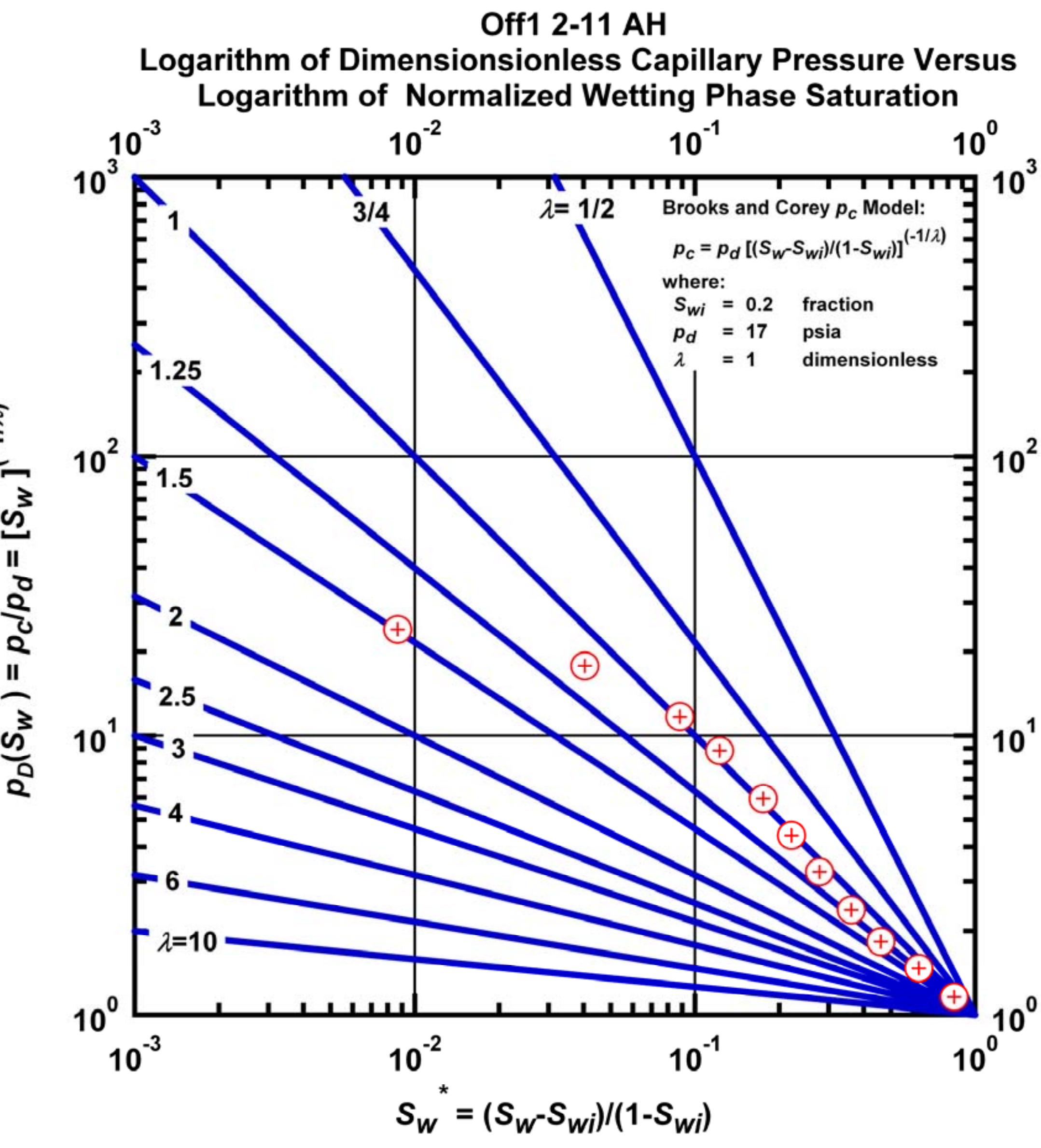

Figure L.59 – Plot of logarithm of dimensionless capillary pressure vs. logarithm of normalized wetting phase saturation — Case Off1 2-11 AH.

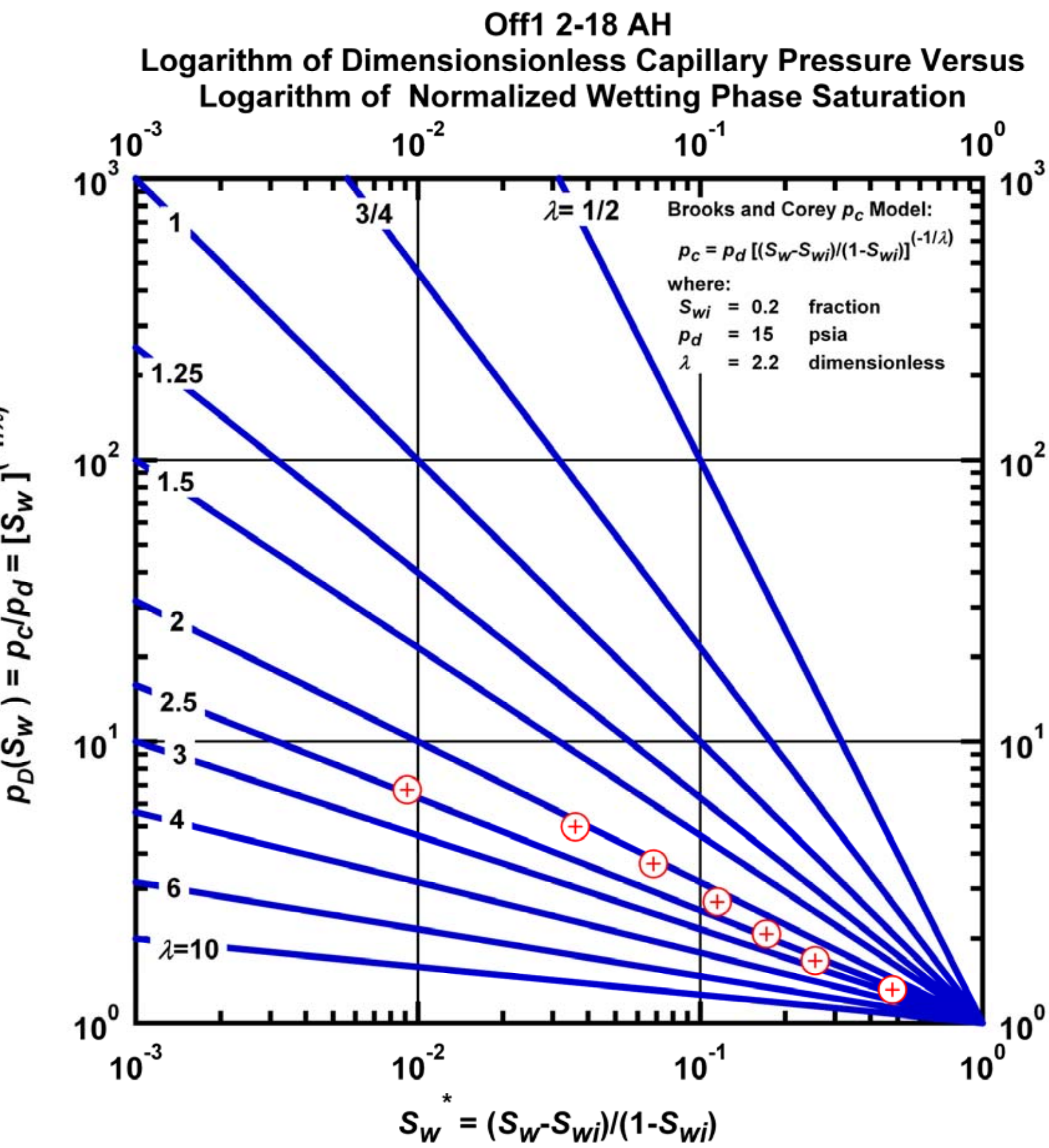

Figure L.60 – Plot of logarithm of dimensionless capillary pressure vs. logarithm of normalized wetting phase saturation — Case Off1 2-18 AH.

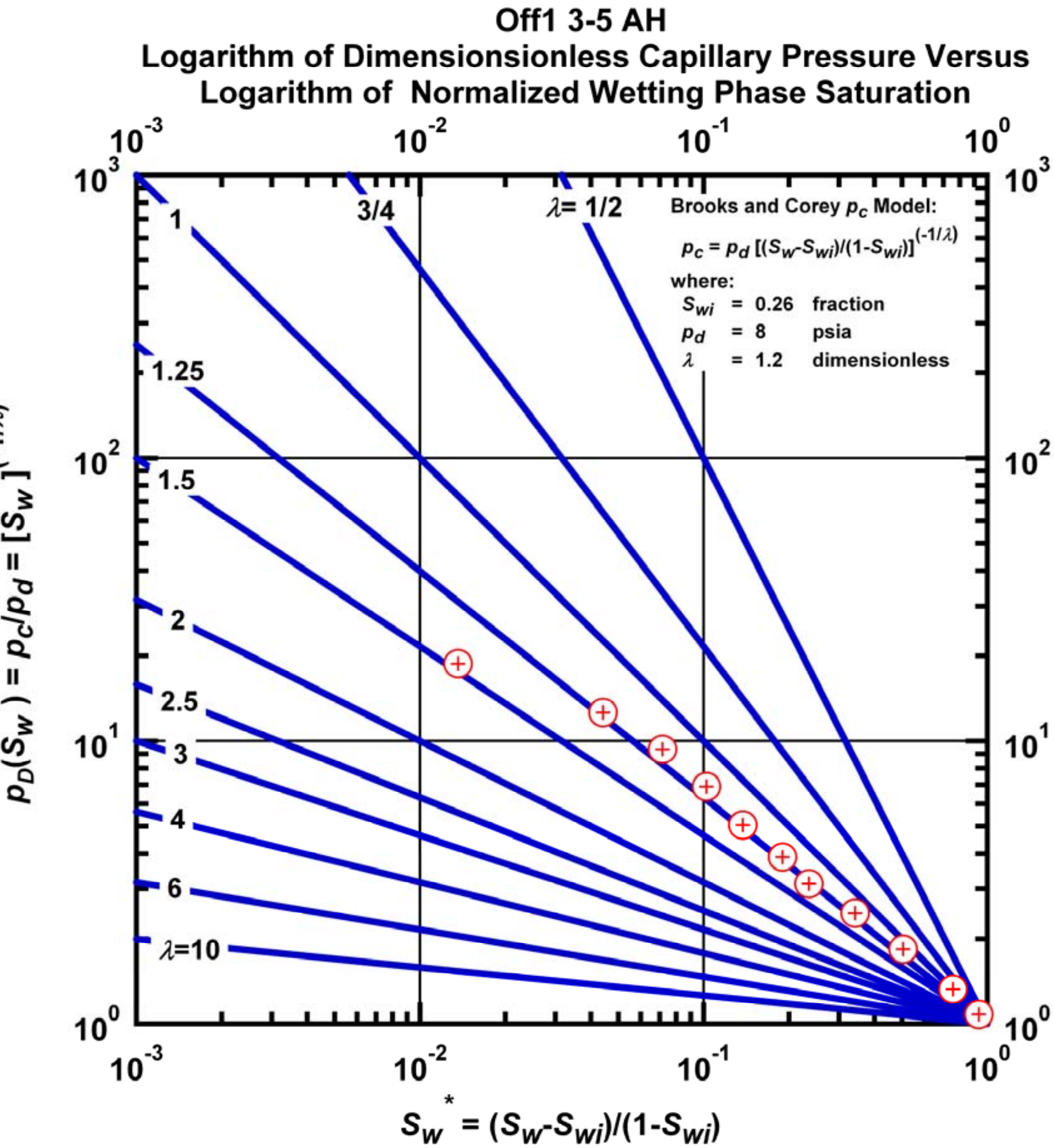

Figure L.61 – Plot of logarithm of dimensionless capillary pressure vs. logarithm of normalized wetting phase saturation — Case Off1 3-5 AH.

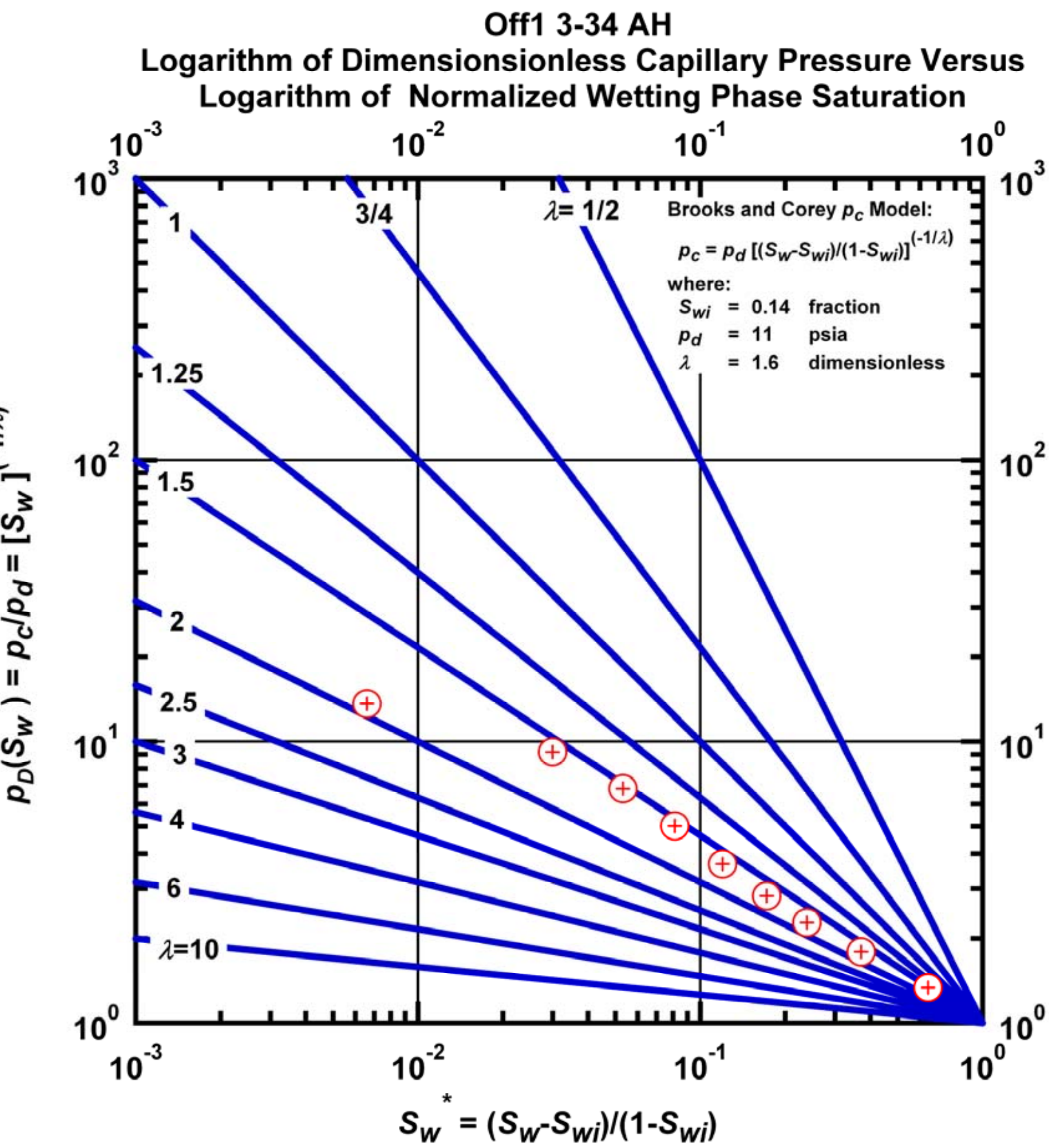

Figure L.62 – Plot of logarithm of dimensionless capillary pressure vs. logarithm of normalized wetting phase saturation — Case Off1 3-34 AH.

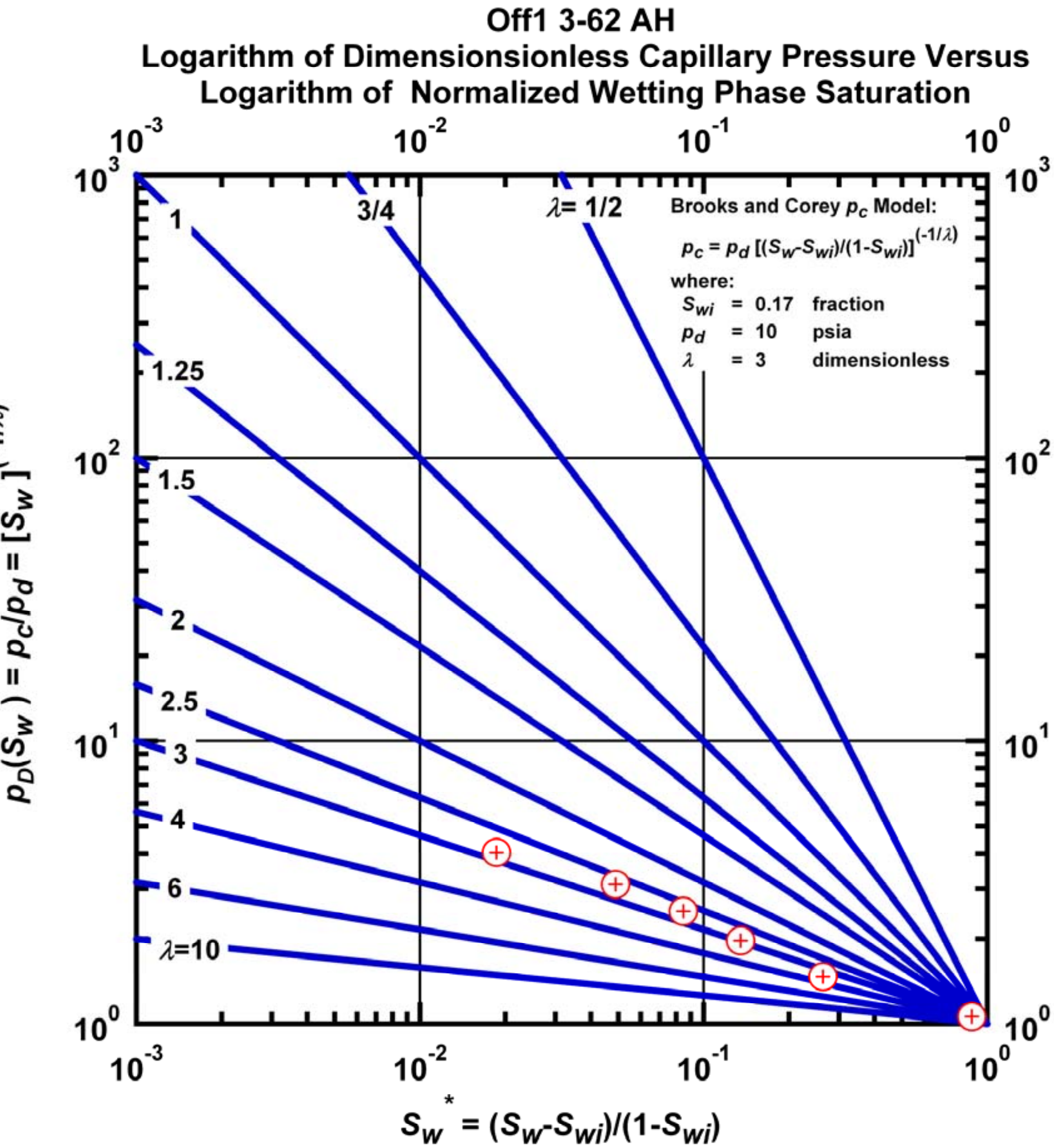

Figure L.63 – Plot of logarithm of dimensionless capillary pressure vs. logarithm of normalized wetting phase saturation ── Case Off1 3-62 AH.

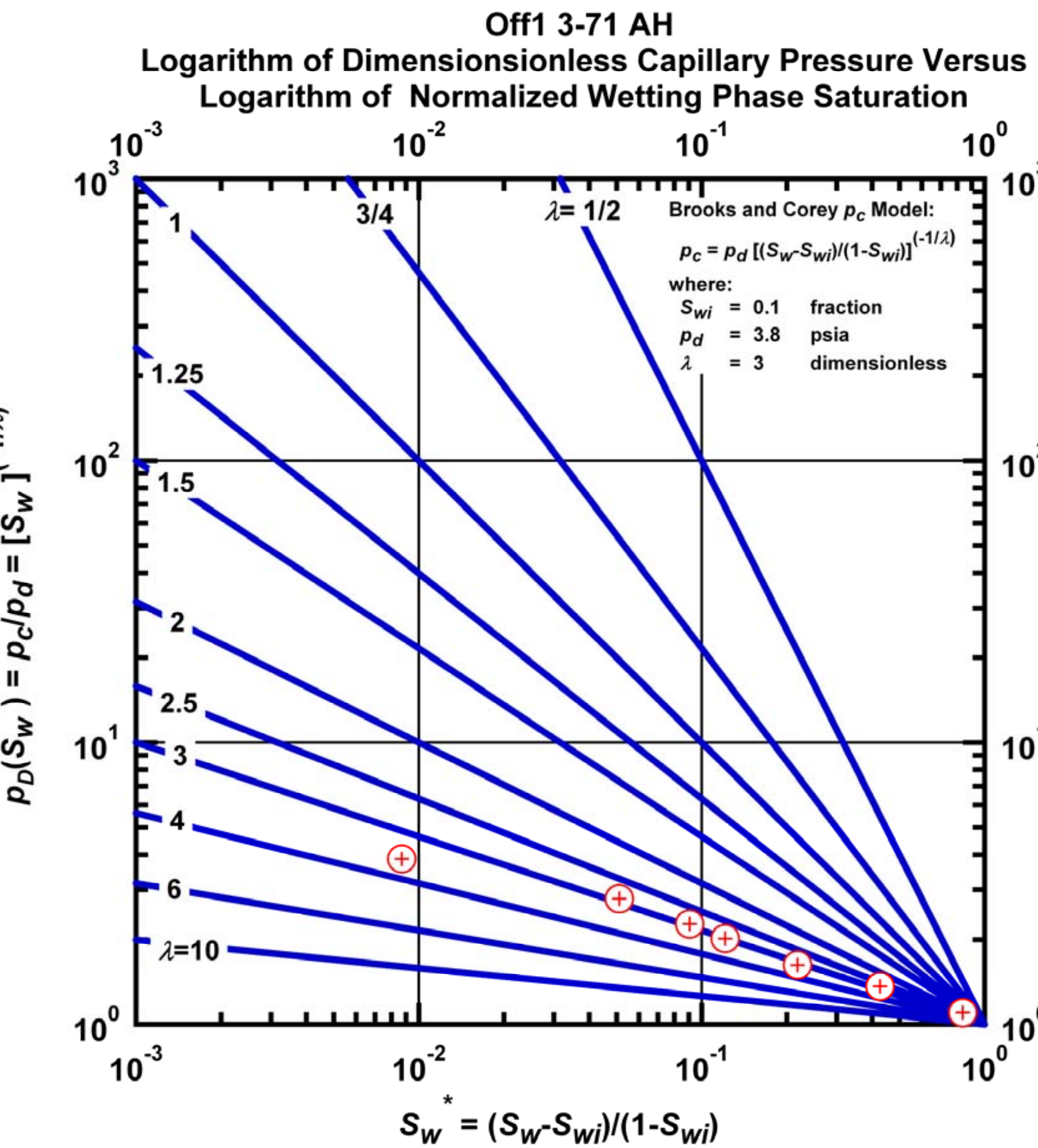

Figure L.64 – Plot of logarithm of dimensionless capillary pressure vs. logarithm of normalized wetting phase saturation — Case Off1 3-71 AH.

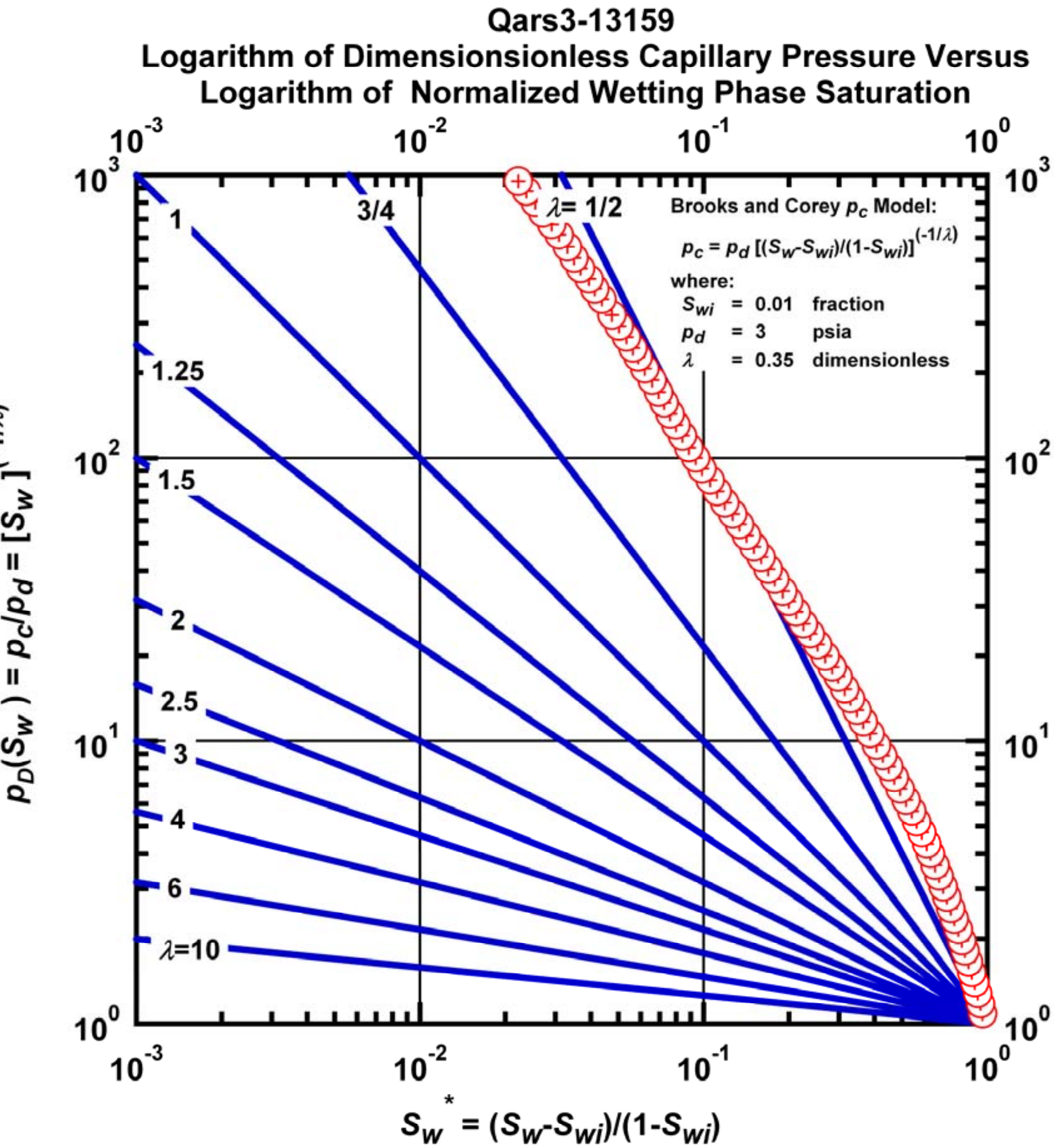

Figure L.65 – Plot of logarithm of dimensionless capillary pressure vs. logarithm of normalized wetting phase saturation — Case Qars3-13159.

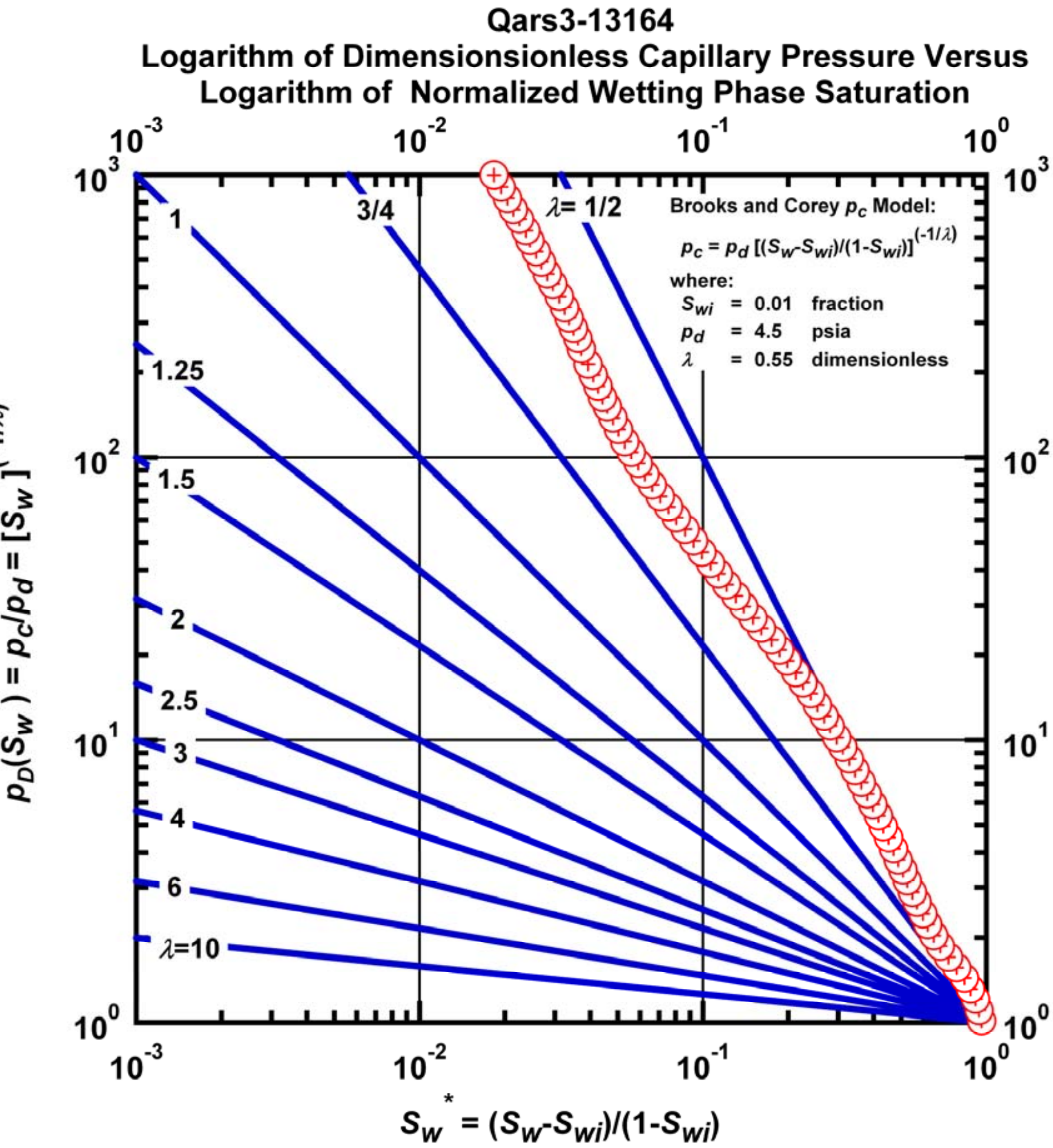

Figure L.66 – Plot of logarithm of dimensionless capillary pressure vs. logarithm of normalized wetting phase saturation — Case Qars3-13164.

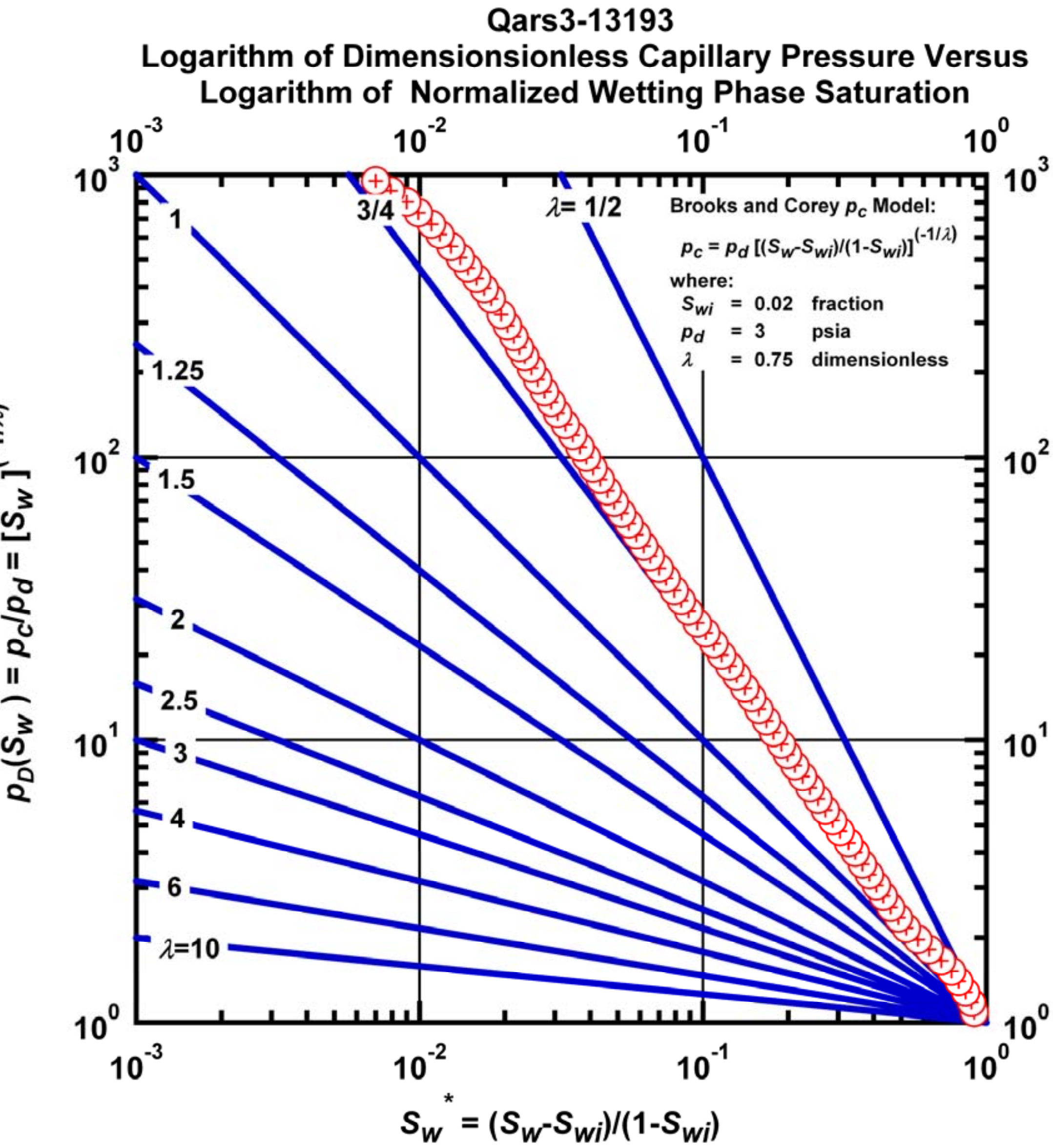

Figure L.67 – Plot of logarithm of dimensionless capillary pressure vs. logarithm of normalized wetting phase saturation — Case Qars3-13193.

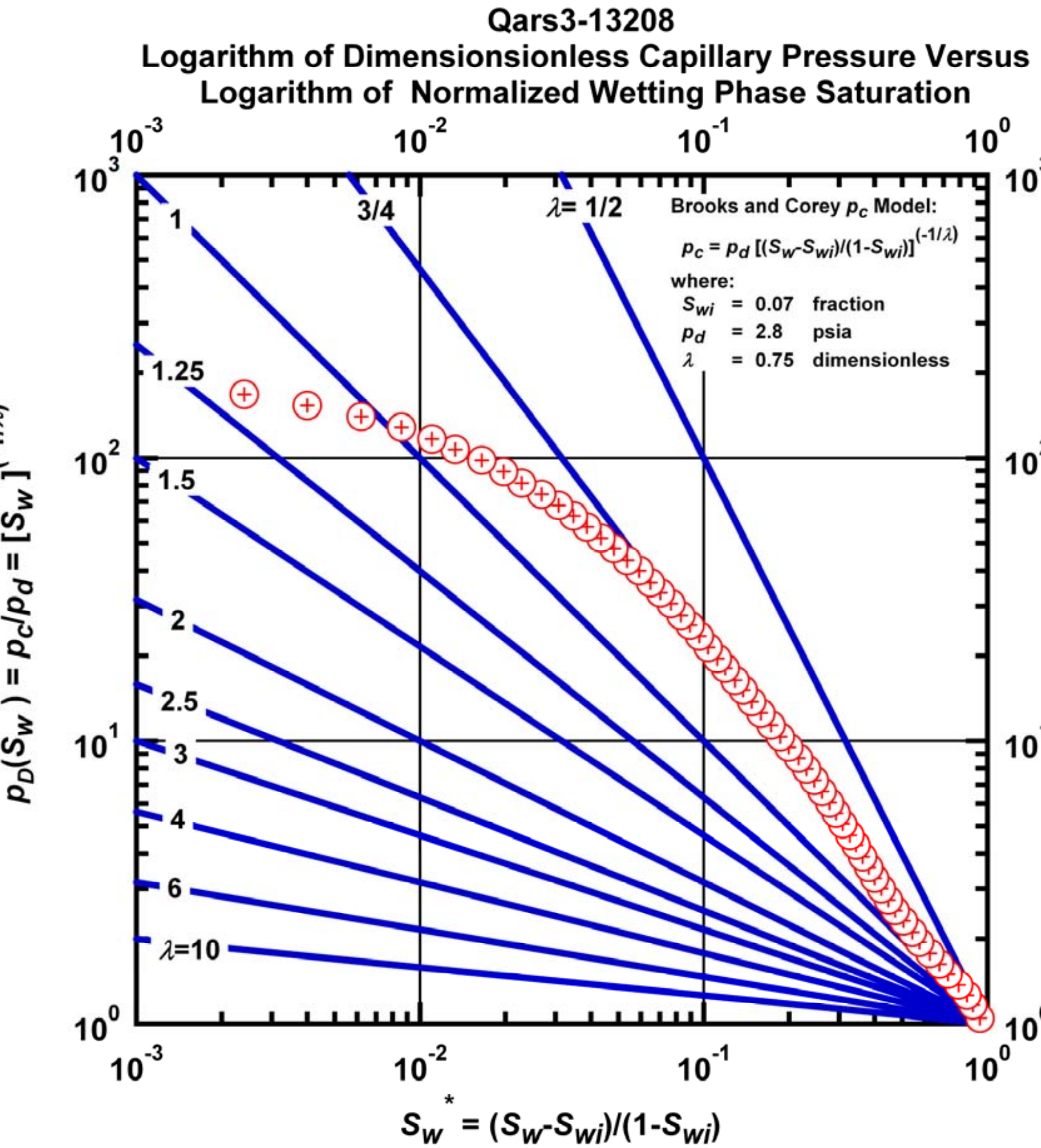

Figure L.68 – Plot of logarithm of dimensionless capillary pressure vs. logarithm of normalized wetting phase saturation — Case Qars3-13208.

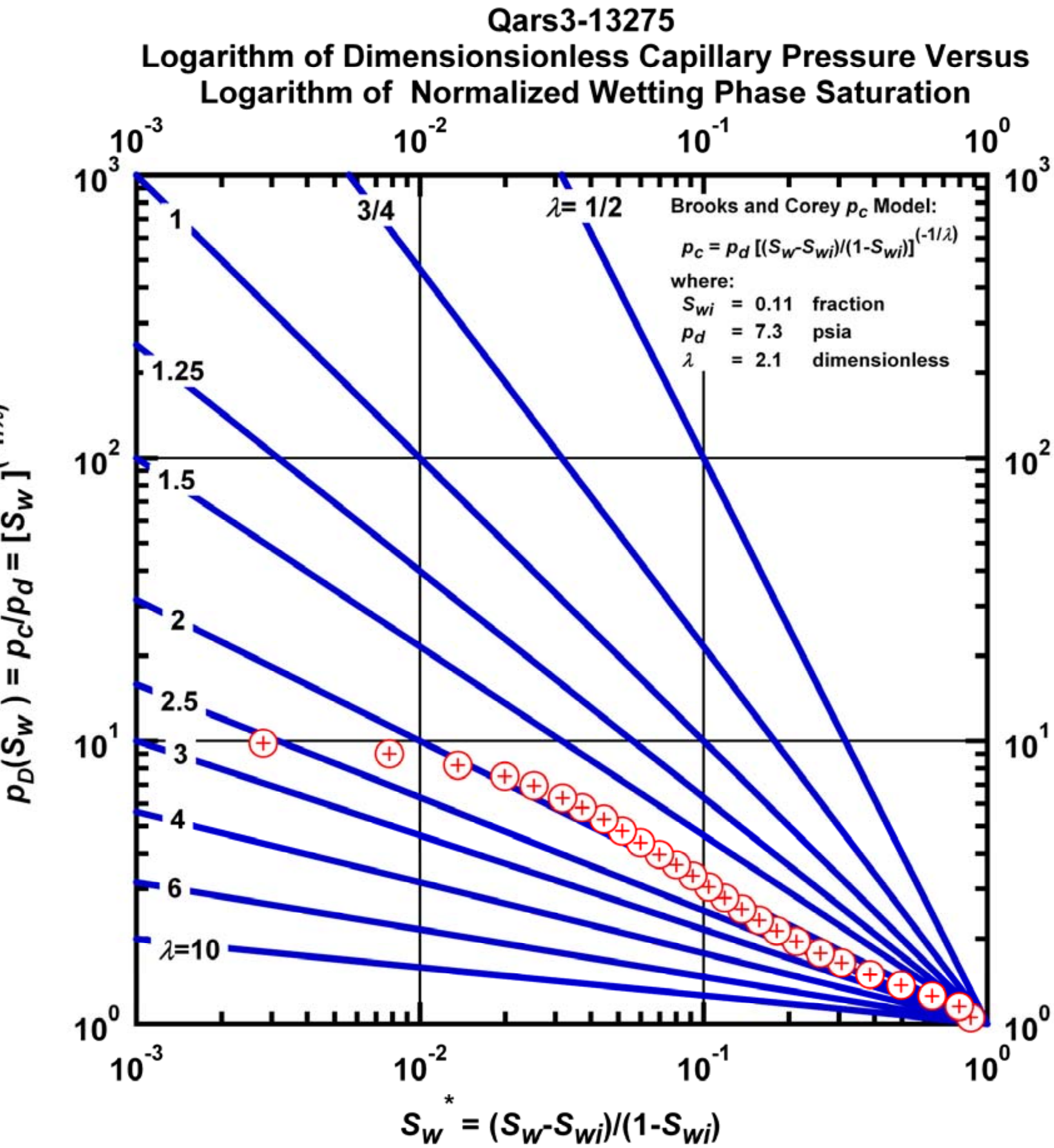

Figure L.69 – Plot of logarithm of dimensionless capillary pressure vs. logarithm of normalized wetting phase saturation — Case Qars3-13275.

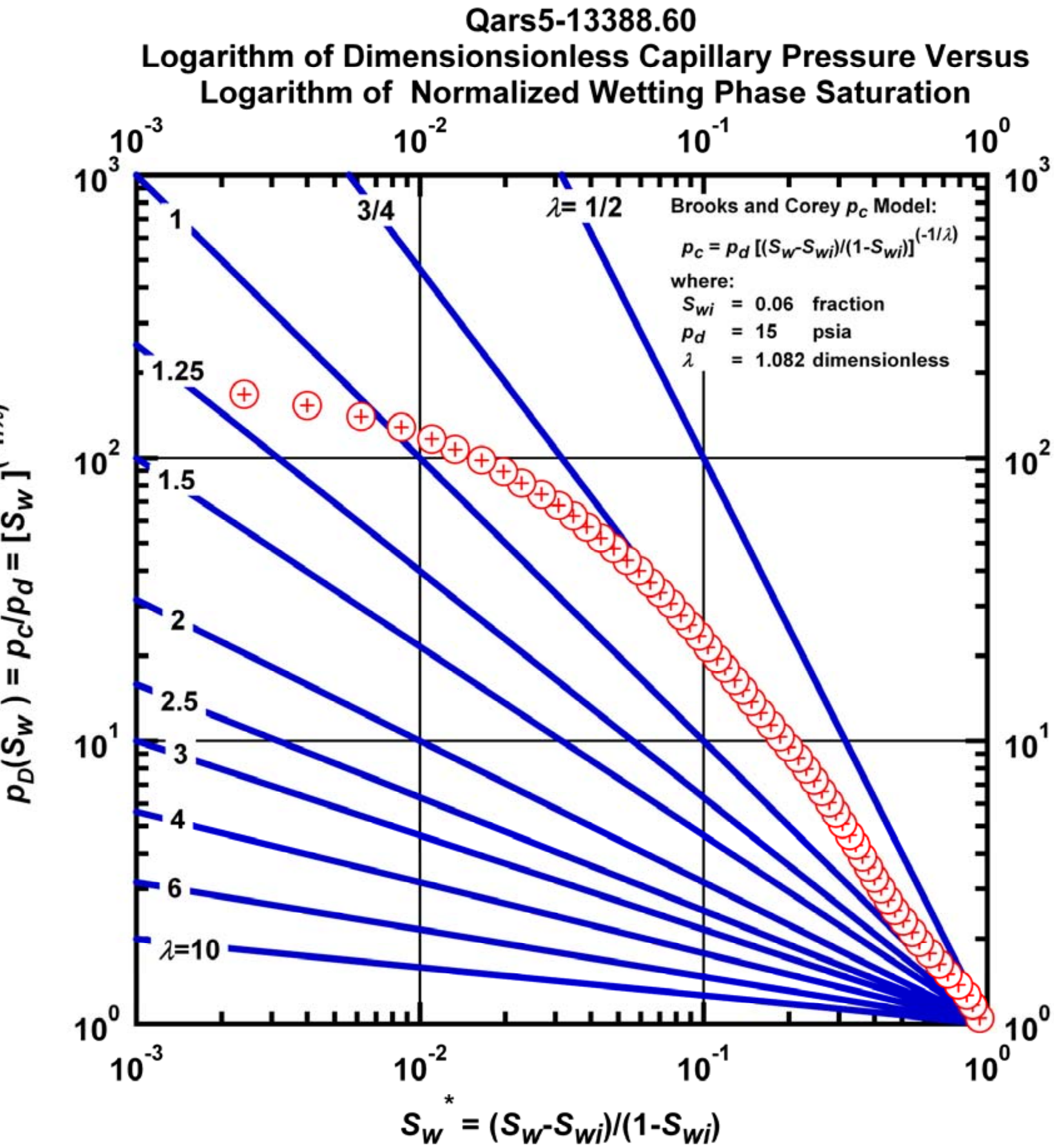

Figure L.70 – Plot of logarithm of dimensionless capillary pressure vs. logarithm of normalized wetting phase saturation ── Case Qars5-13388.6.

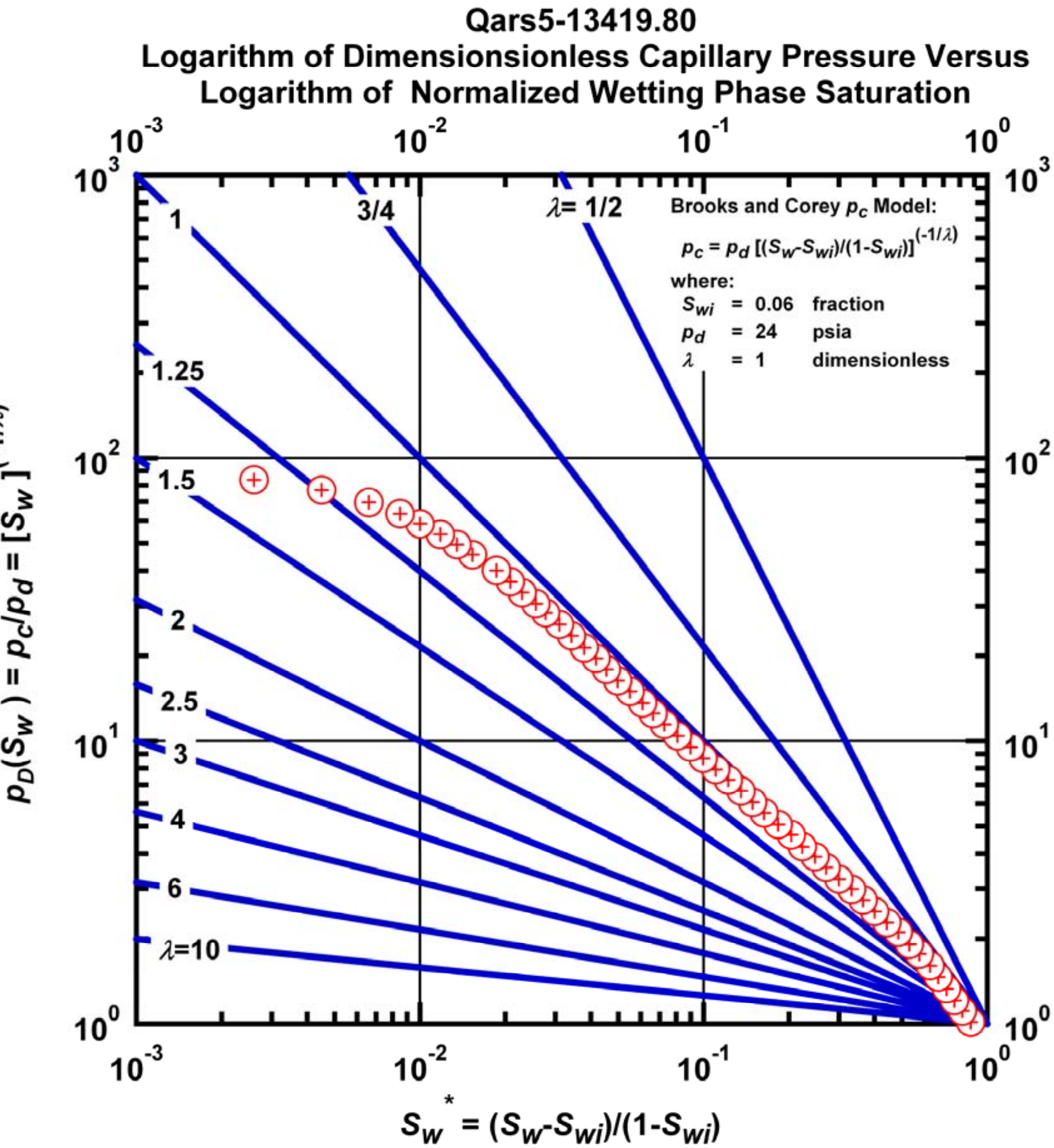

Figure L.71 – Plot of logarithm of dimensionless capillary pressure vs. logarithm of normalized wetting phase saturation — Case Qars5-13419.8.

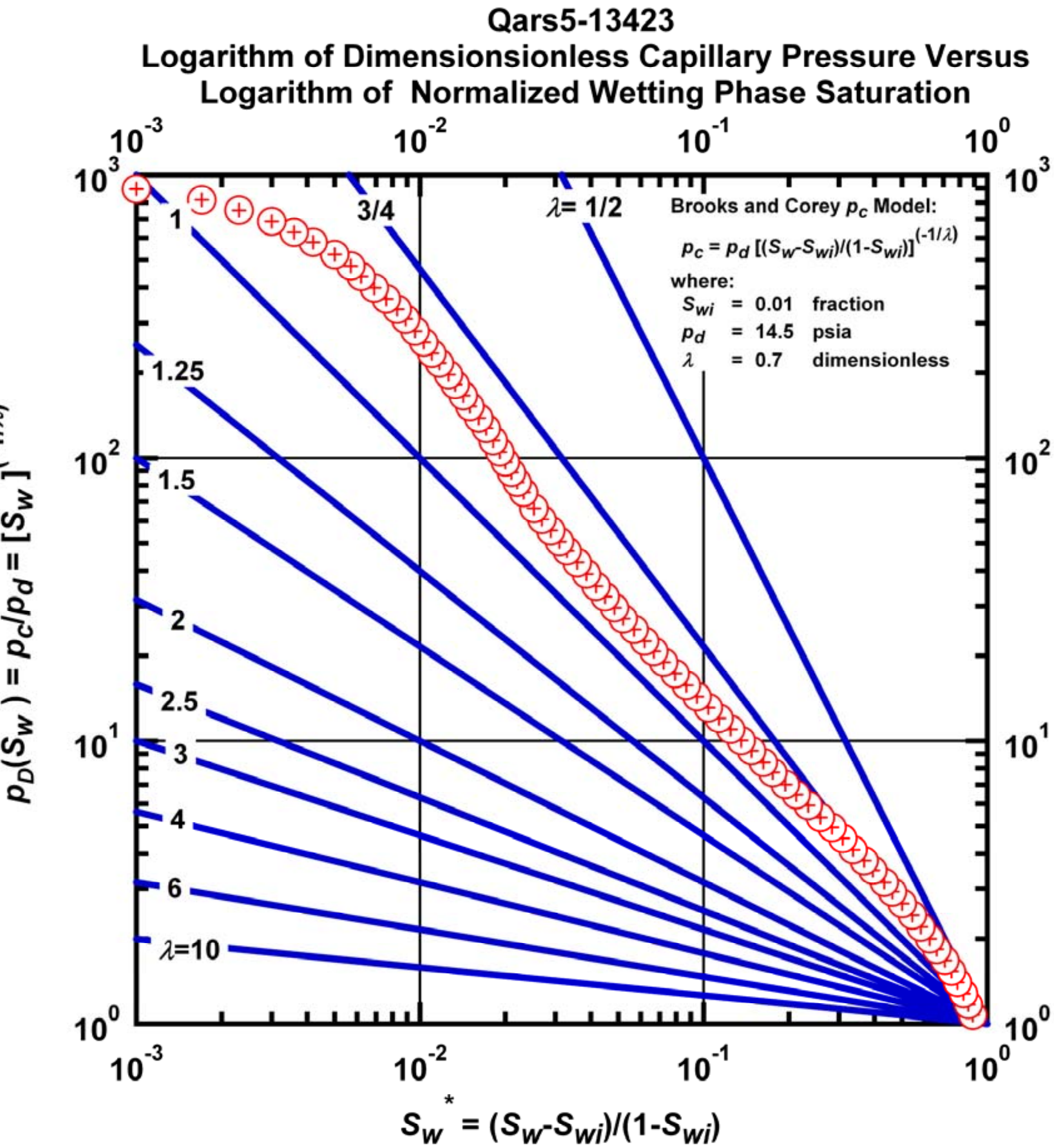

Figure L.72 – Plot of logarithm of dimensionless capillary pressure vs. logarithm of normalized wetting phase saturation — Case Qars5-13423.

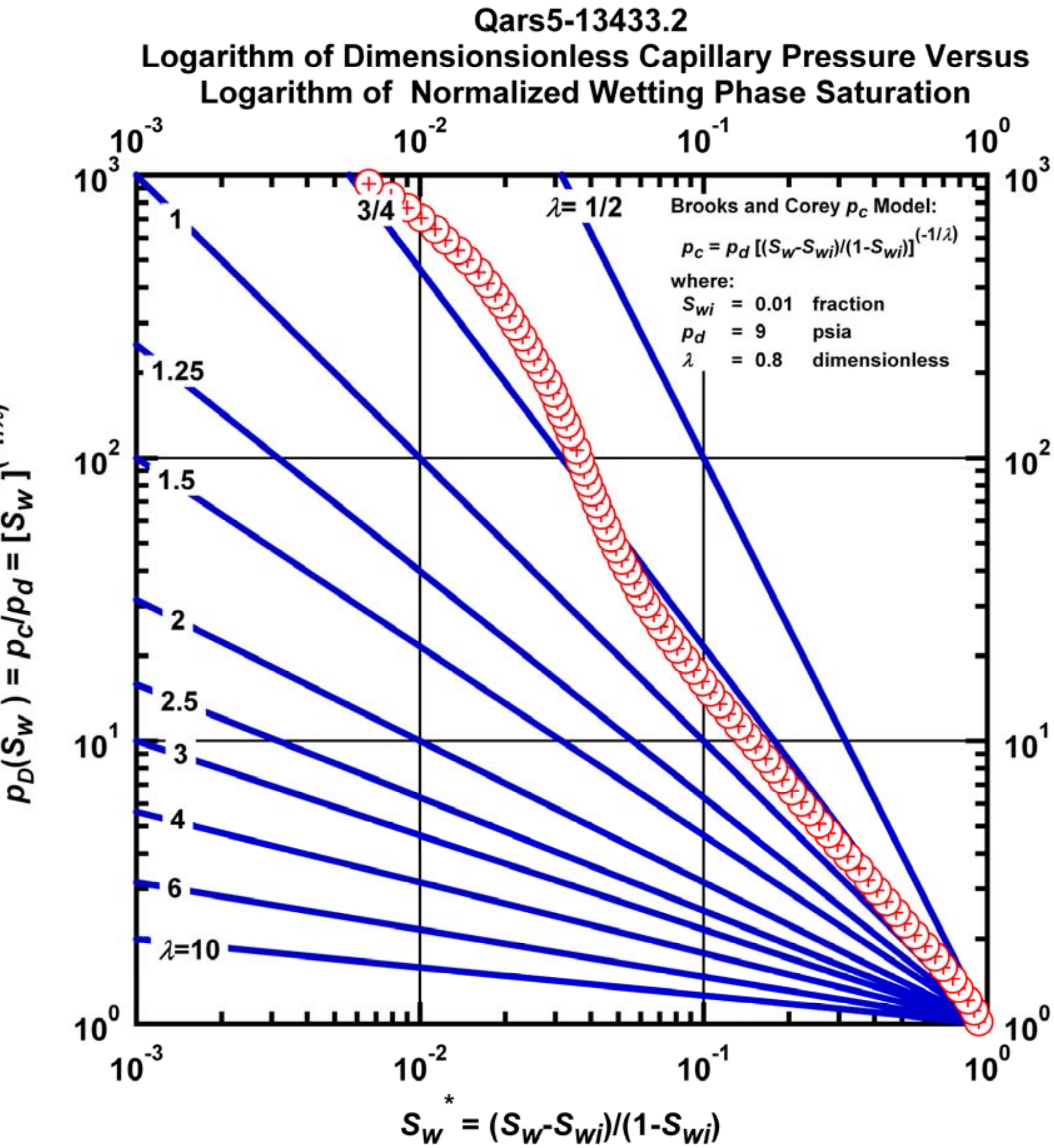

Figure L.73 – Plot of logarithm of dimensionless capillary pressure vs. logarithm of normalized wetting phase saturation — Case Qars5-13433.2.

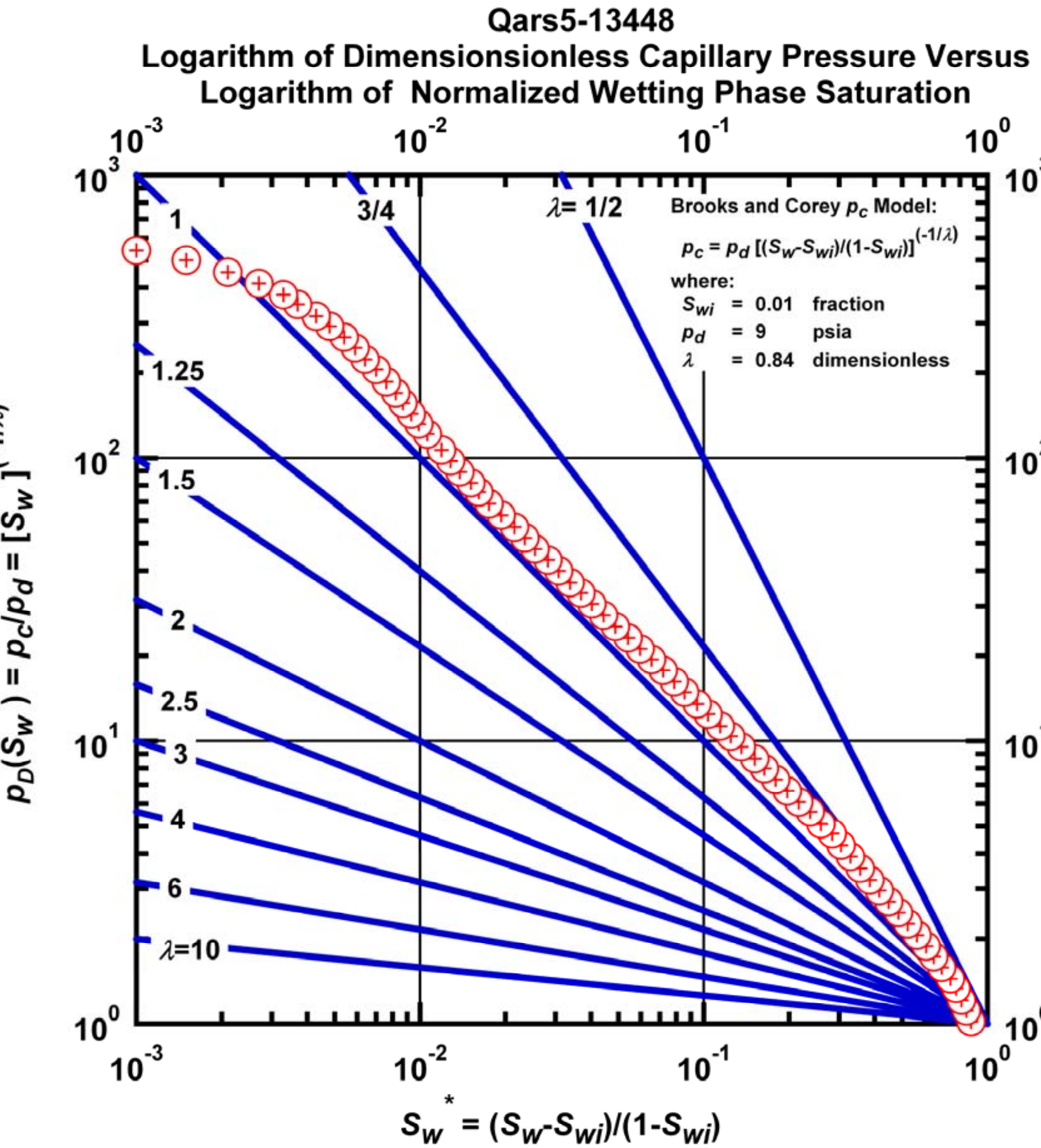

Figure L.74 – Plot of logarithm of dimensionless capillary pressure vs. logarithm of normalized wetting phase saturation — Case Qars5-13448.

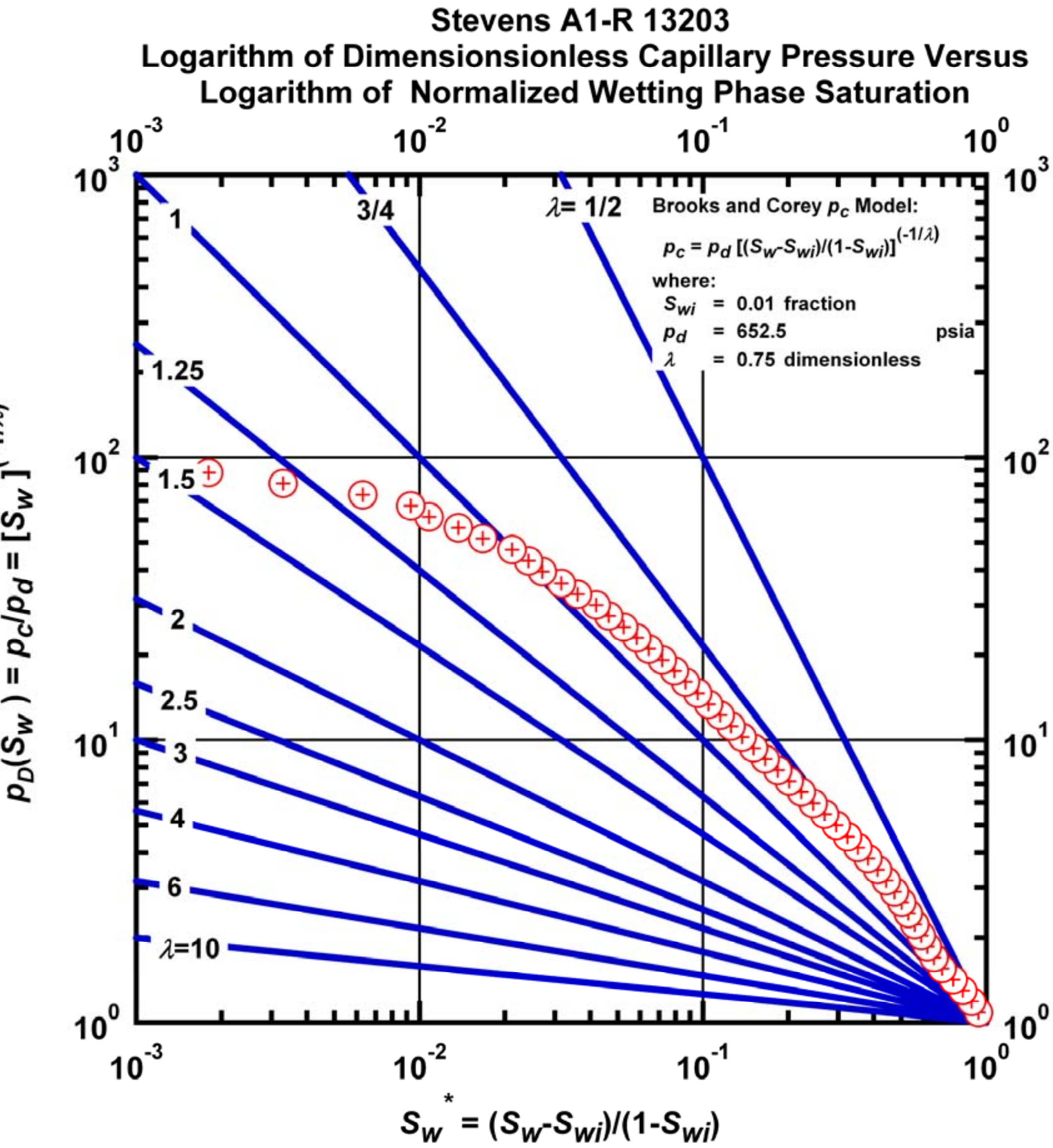

Figure L.75 – Plot of logarithm of dimensionless capillary pressure vs. logarithm of normalized wetting phase saturation — Case Stevens A1-R 13203.

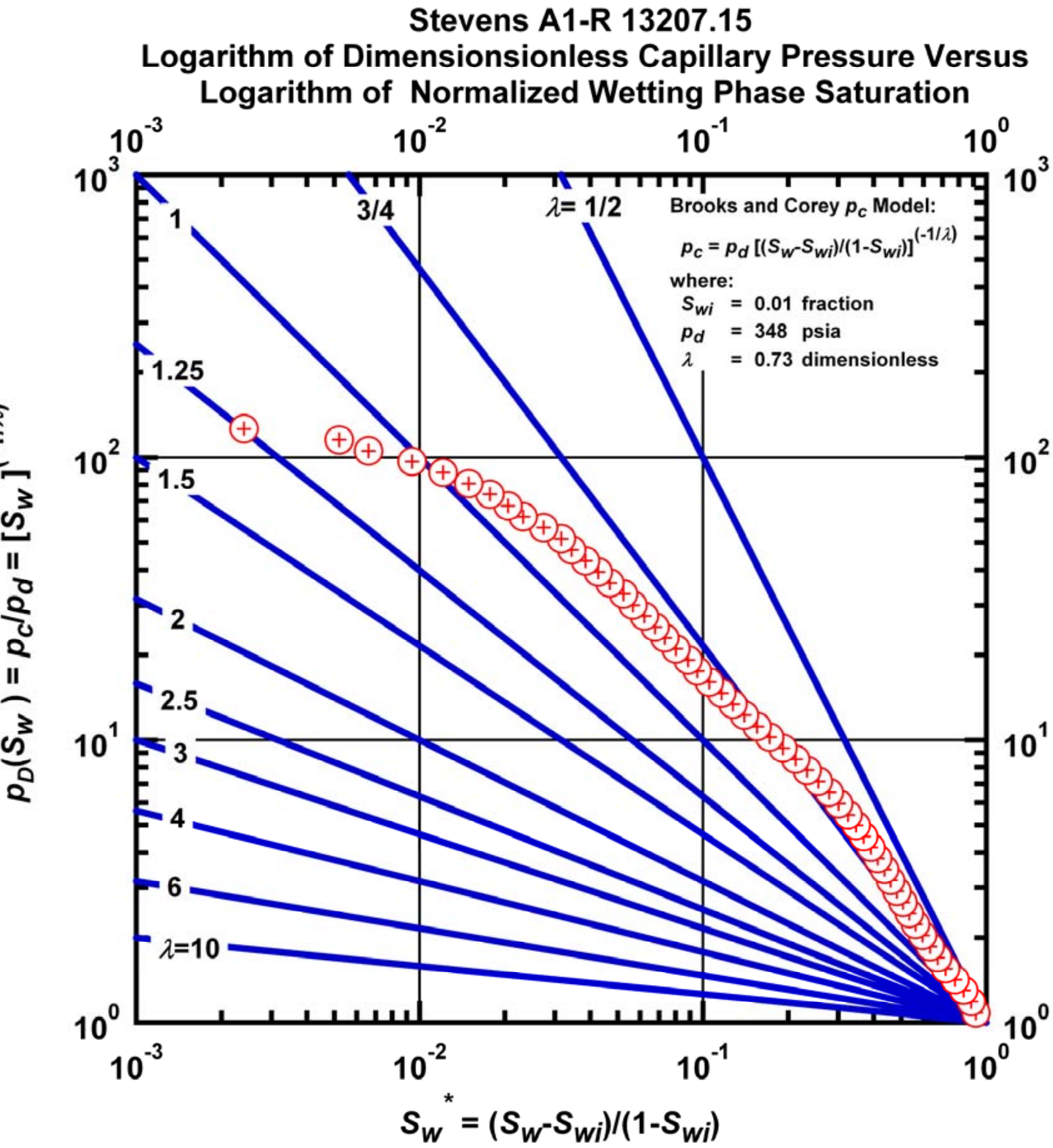

Figure L.76 – Plot of logarithm of dimensionless capillary pressure vs. logarithm of normalized wetting phase saturation ── Case Stevens A1-R 13207.15.

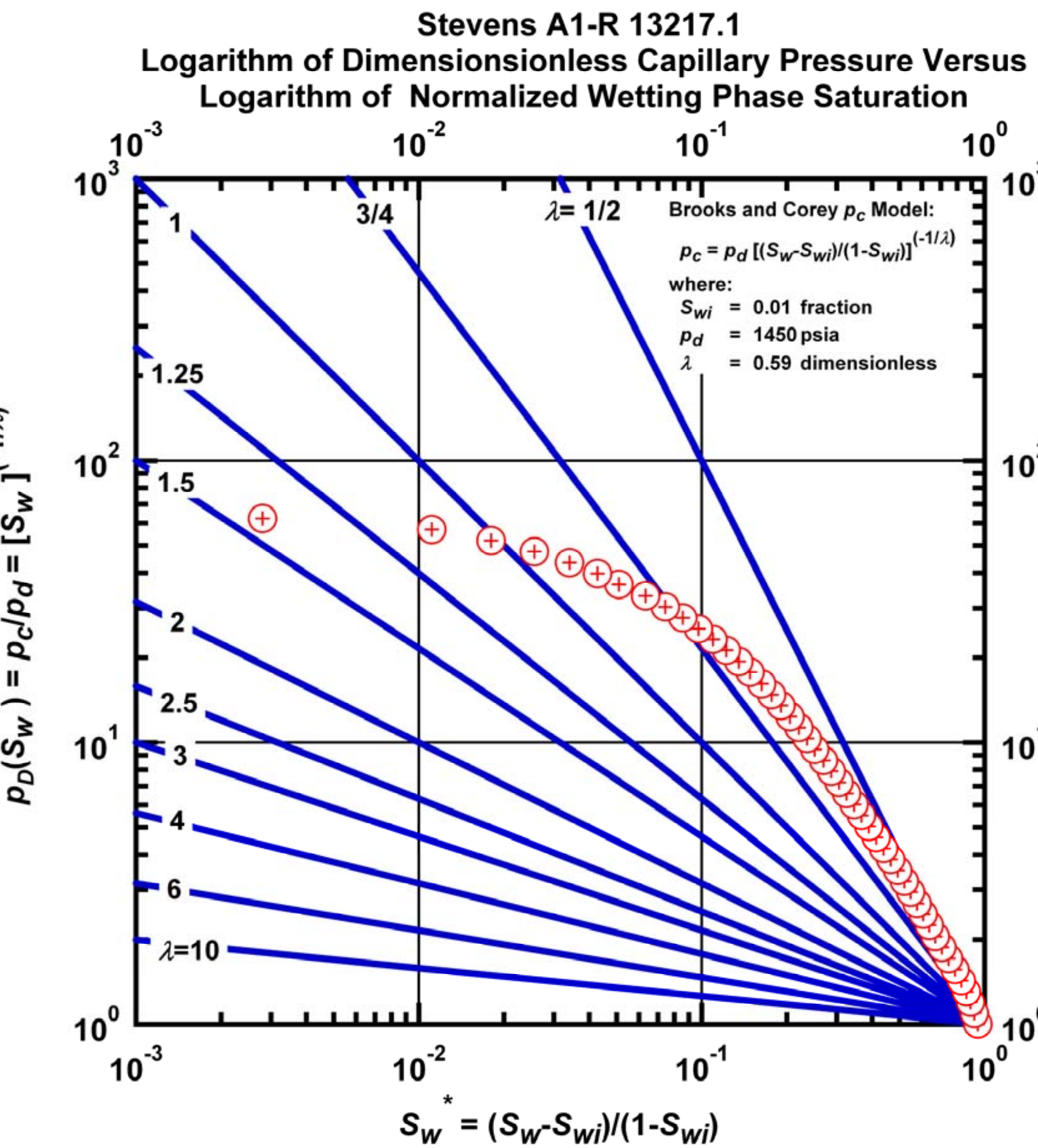

Figure L.77 – Plot of logarithm of dimensionless capillary pressure vs. logarithm of normalized wetting phase saturation ── Case Stevens A1-R 13217.1.

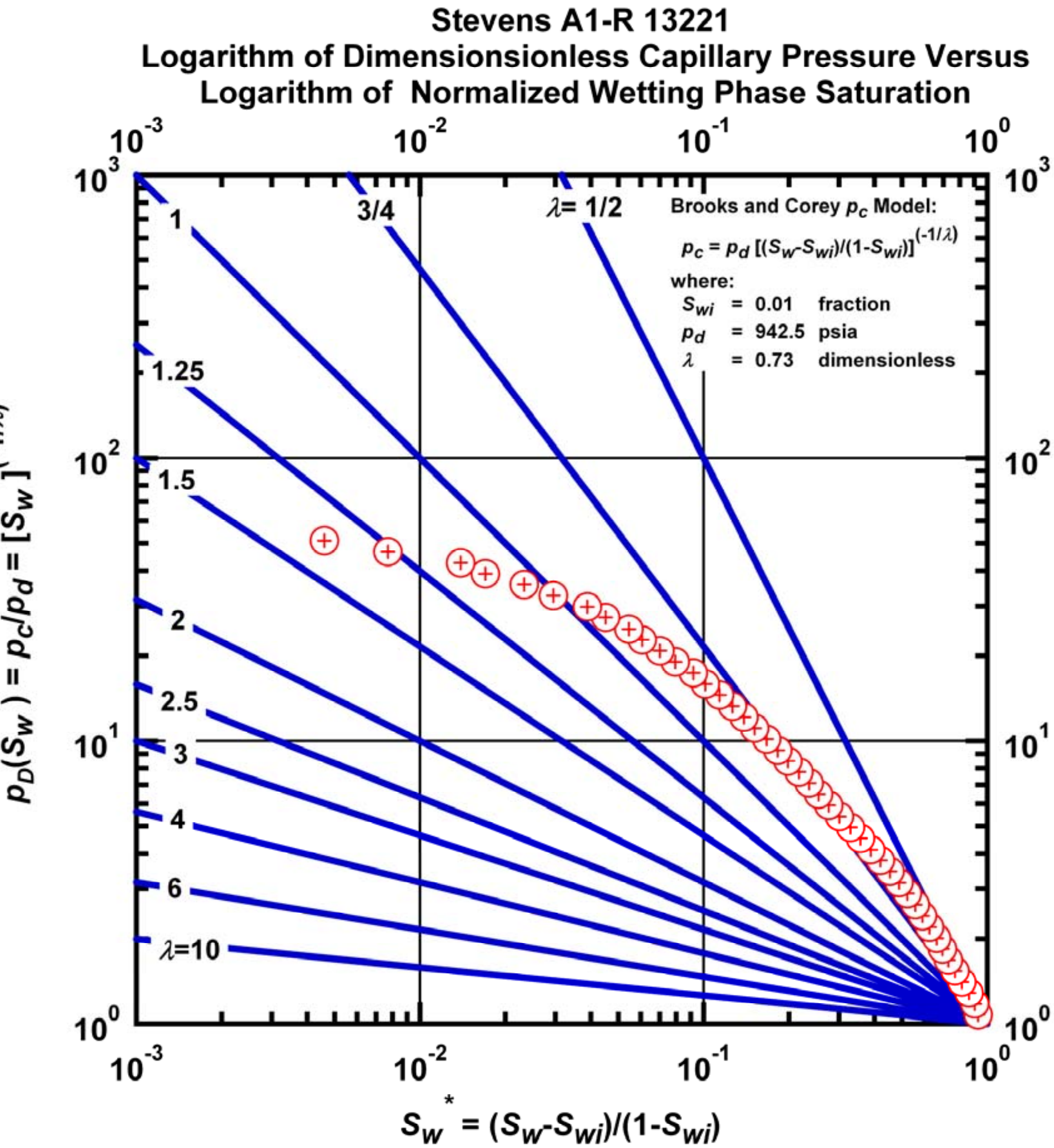

Figure L.78 – Plot of logarithm of dimensionless capillary pressure vs. logarithm of normalized wetting phase saturation ― Case Stevens A1-R 13221.

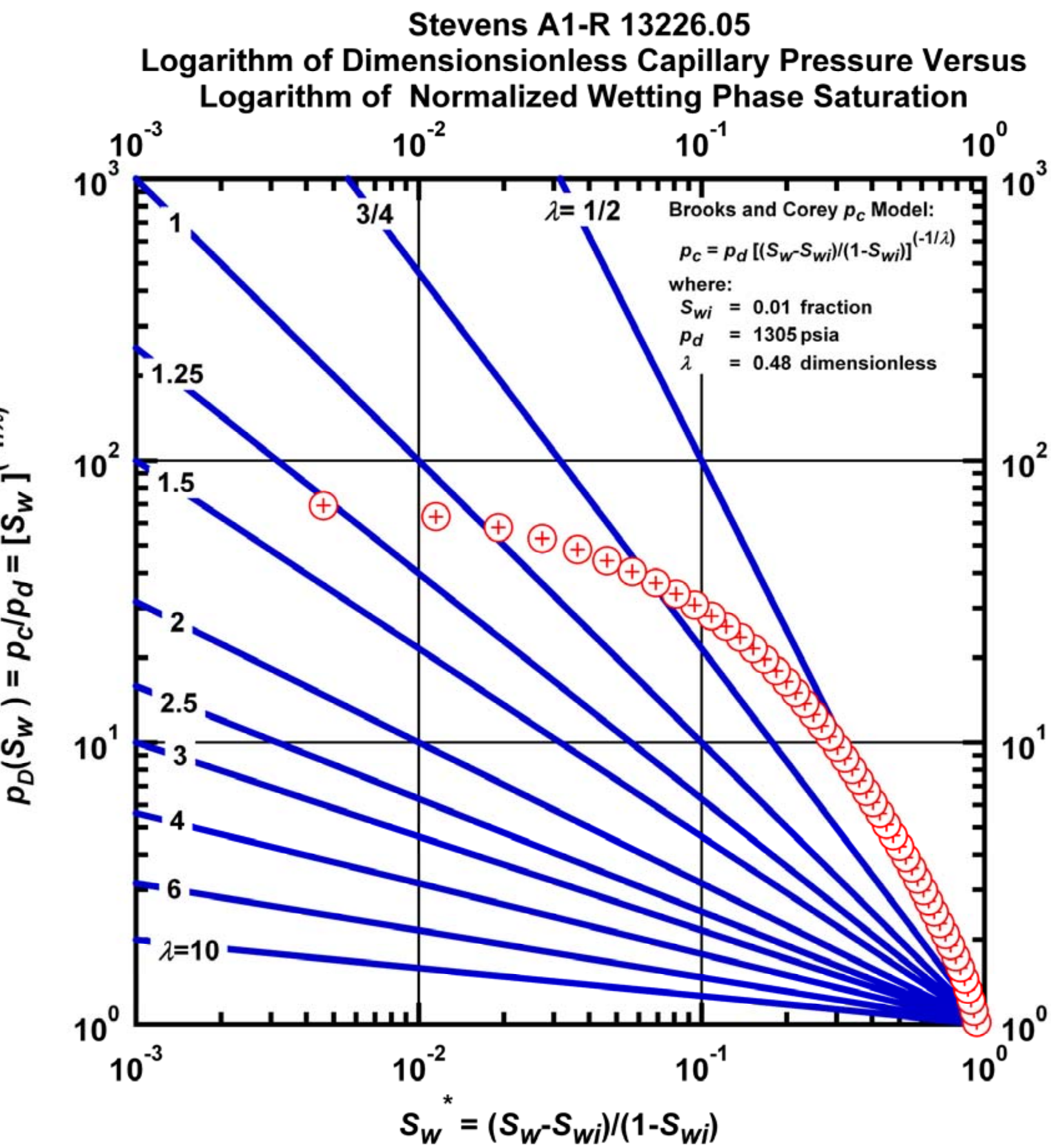

Figure L.79 – Plot of logarithm of dimensionless capillary pressure vs. logarithm of normalized wetting phase saturation — Case Stevens A1-R 13226.05.

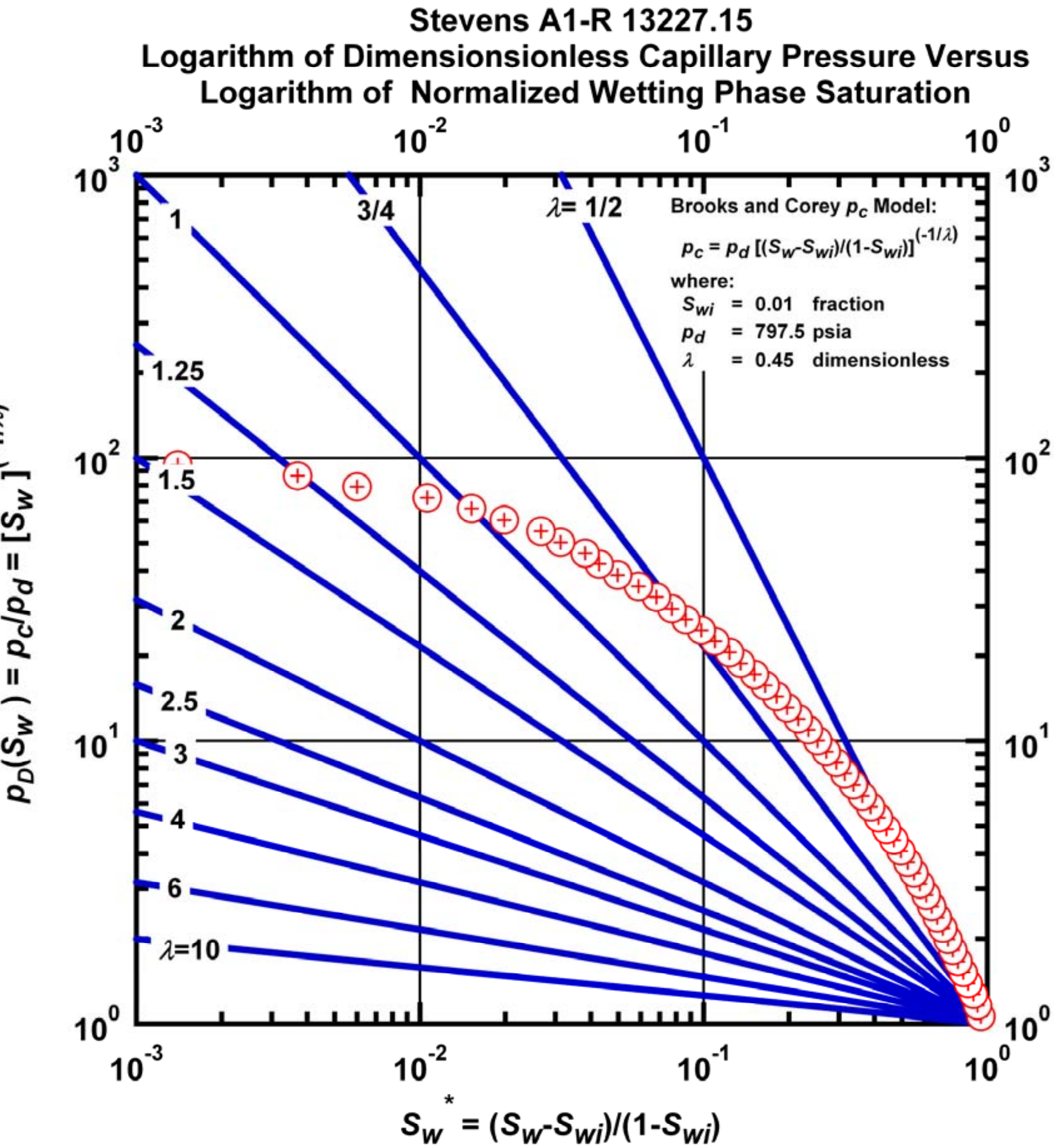

Figure L.80 – Plot of logarithm of dimensionless capillary pressure vs. logarithm of normalized wetting phase saturation — Case Stevens A1-R 13227.15.

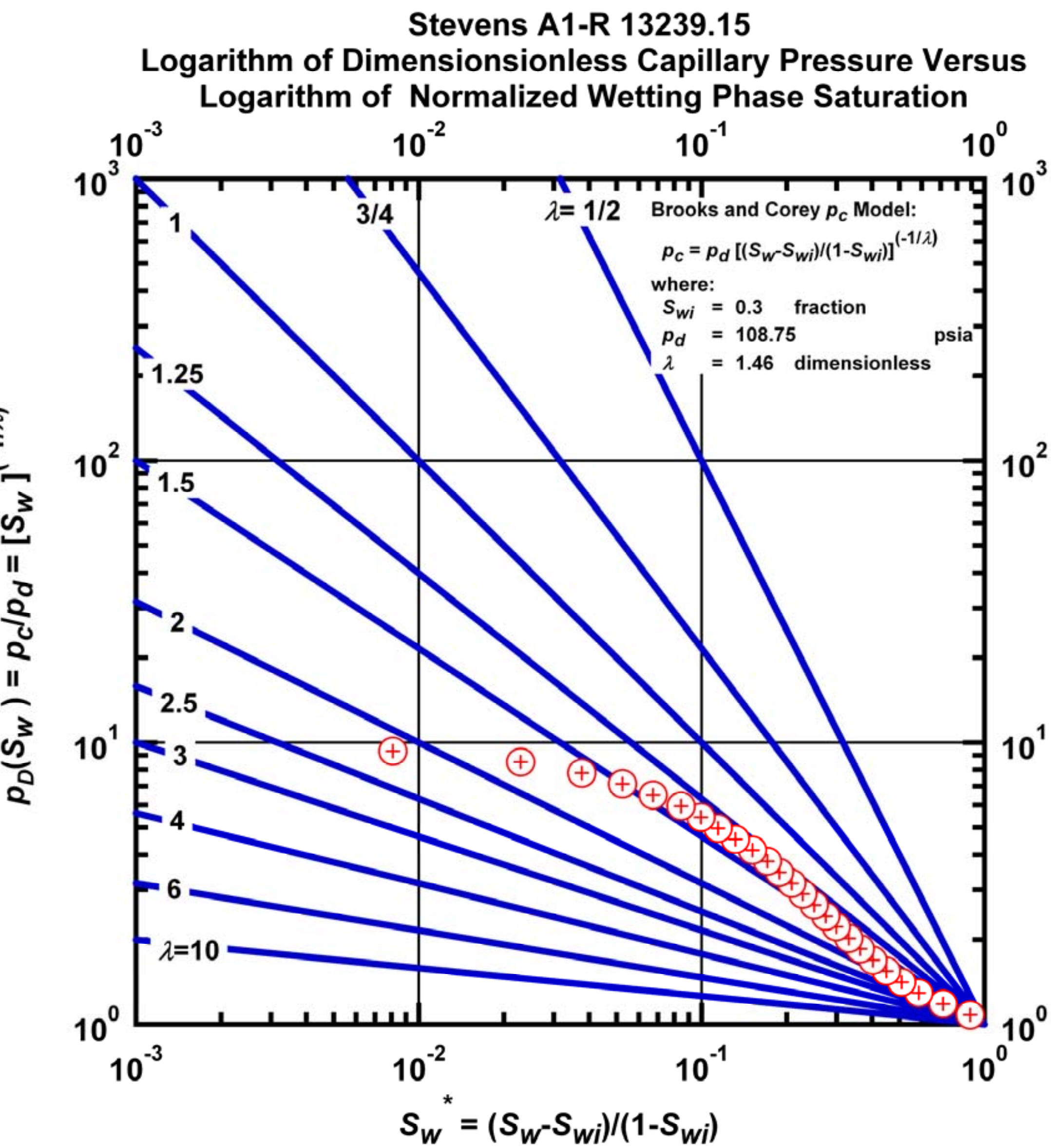

Figure L.81 – Plot of logarithm of dimensionless capillary pressure vs. logarithm of normalized wetting phase saturation — Case Stevens A1-R 13239.15.

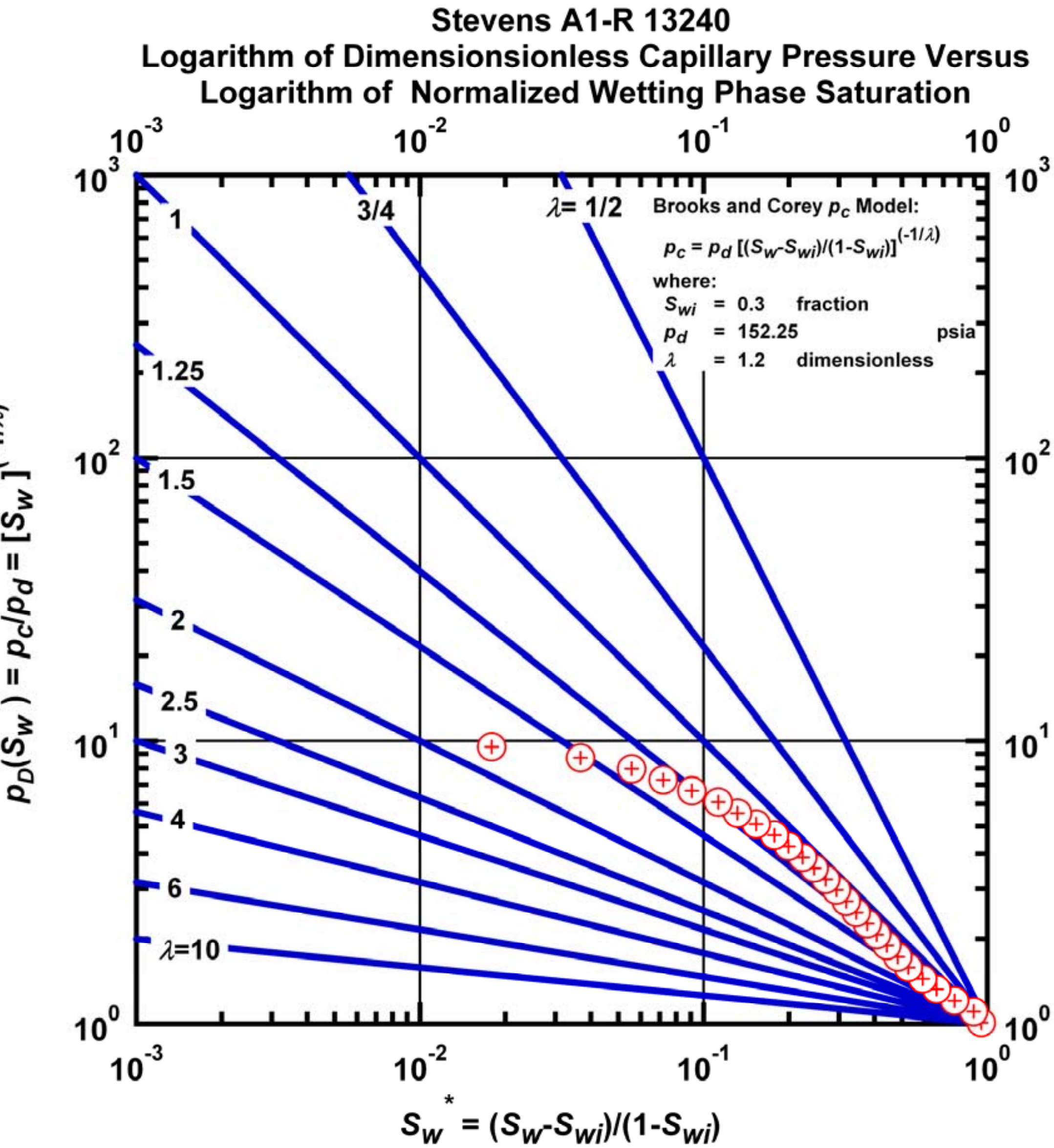

Figure L.82 – Plot of logarithm of dimensionless capillary pressure vs. logarithm of normalized wetting phase saturation — Case Stevens A1-R 13240.

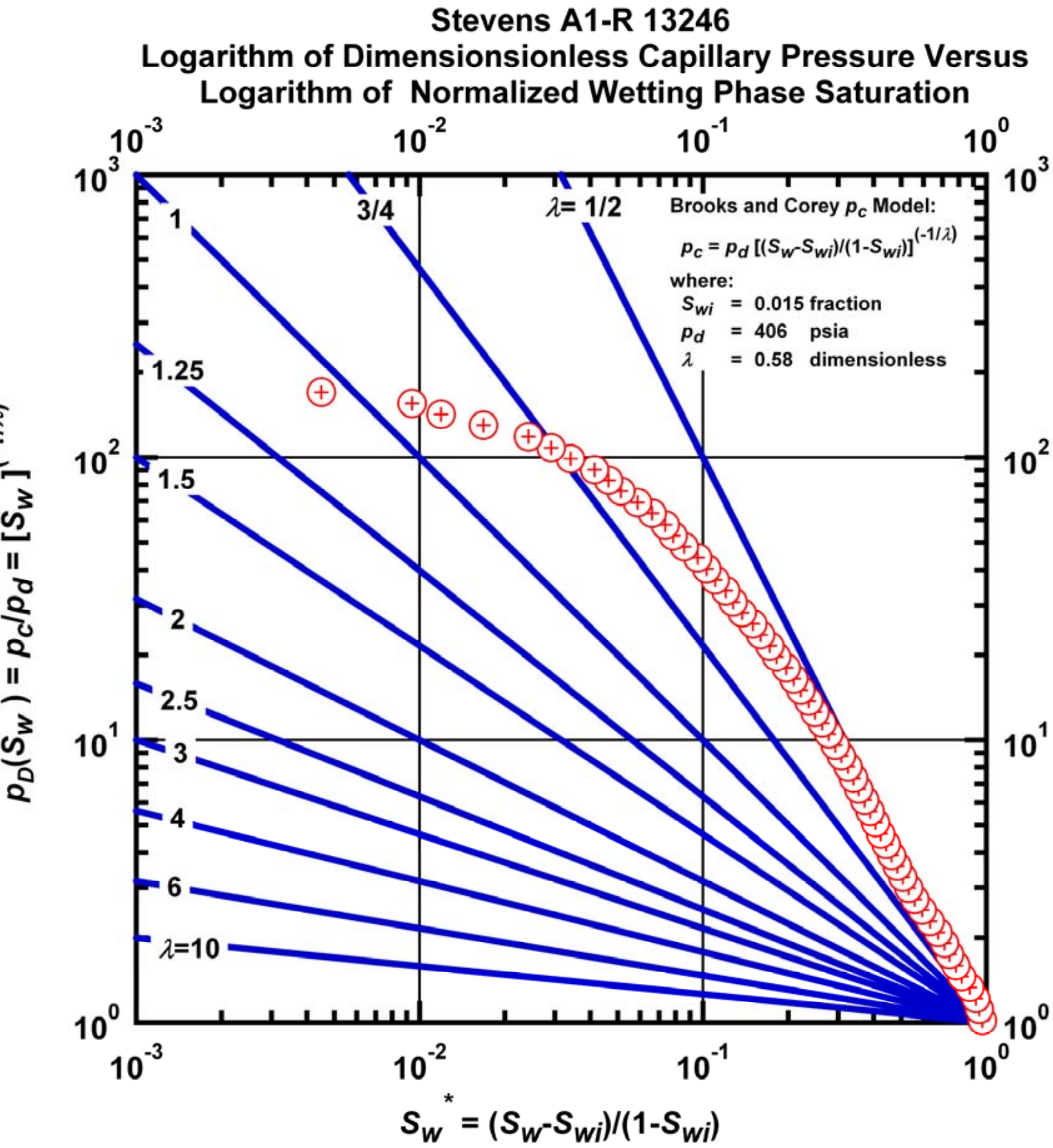

Figure L.83 – Plot of logarithm of dimensionless capillary pressure vs. logarithm of normalized wetting phase saturation — Case Stevens A1-R 13246.

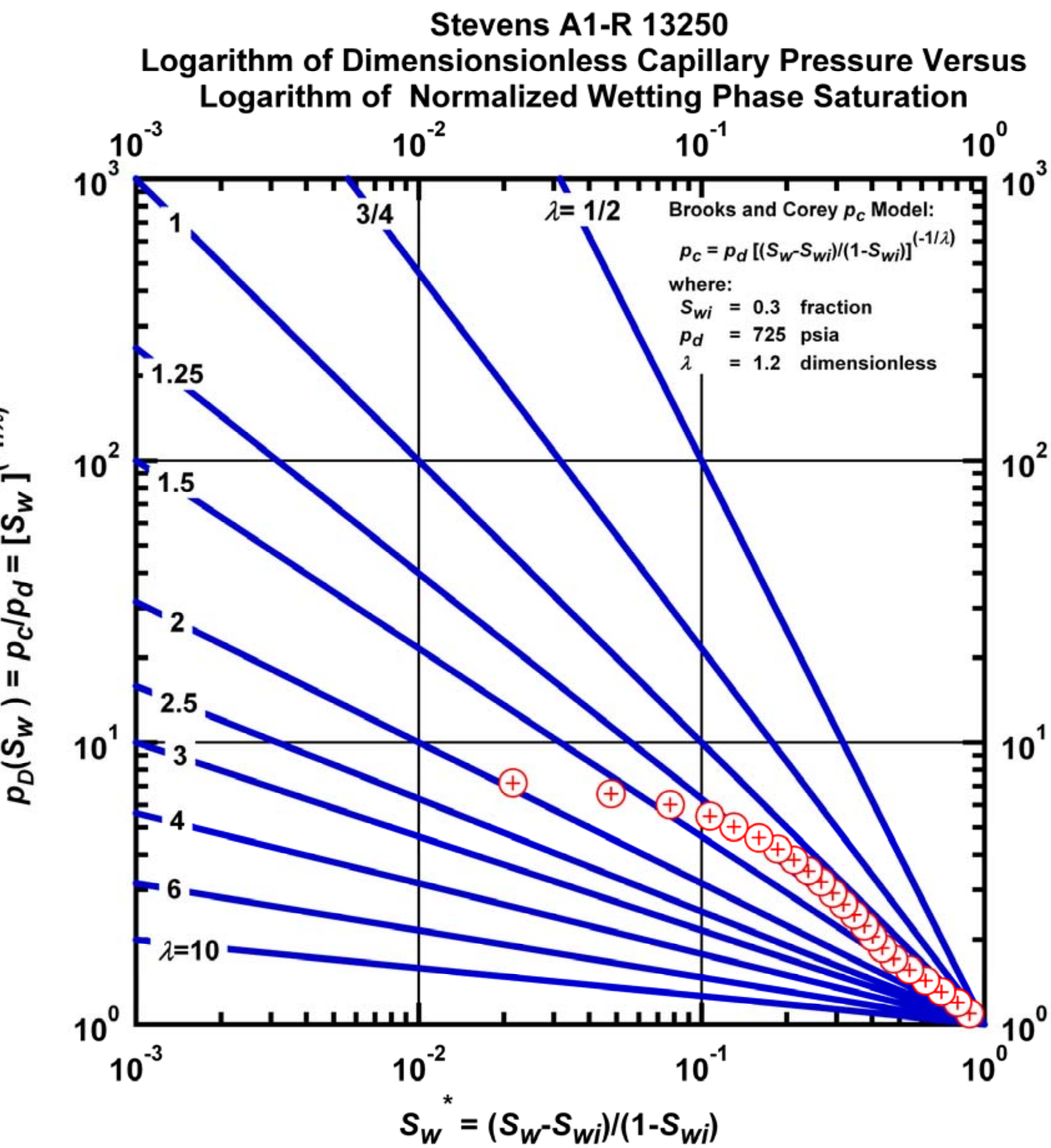

Figure L.84 – Plot of logarithm of dimensionless capillary pressure vs. logarithm of normalized wetting phase saturation — Case Stevens A1-R 13250.

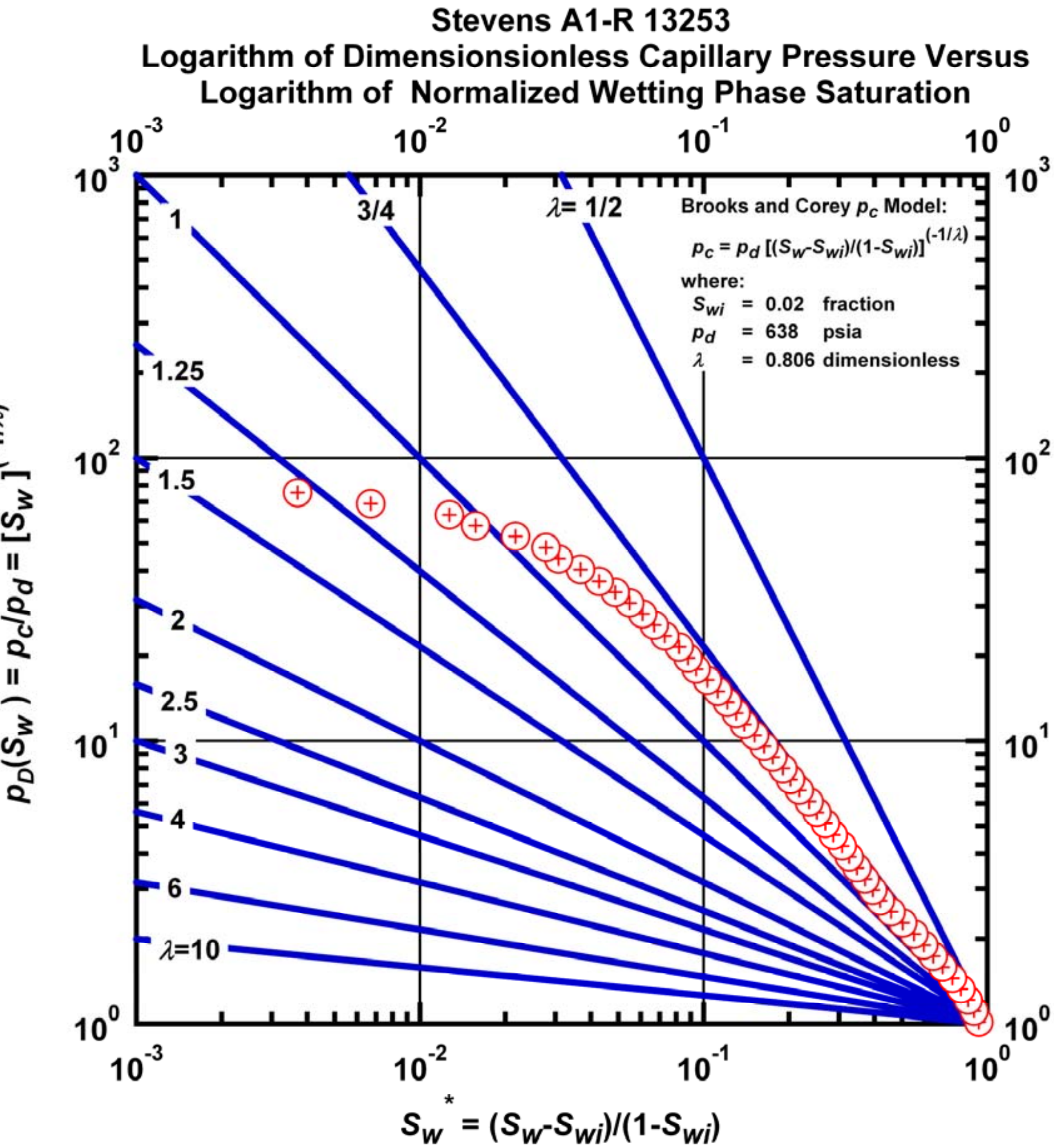

Figure L.85 – Plot of logarithm of dimensionless capillary pressure vs. logarithm of normalized wetting phase saturation — Case Stevens A1-R 13253.

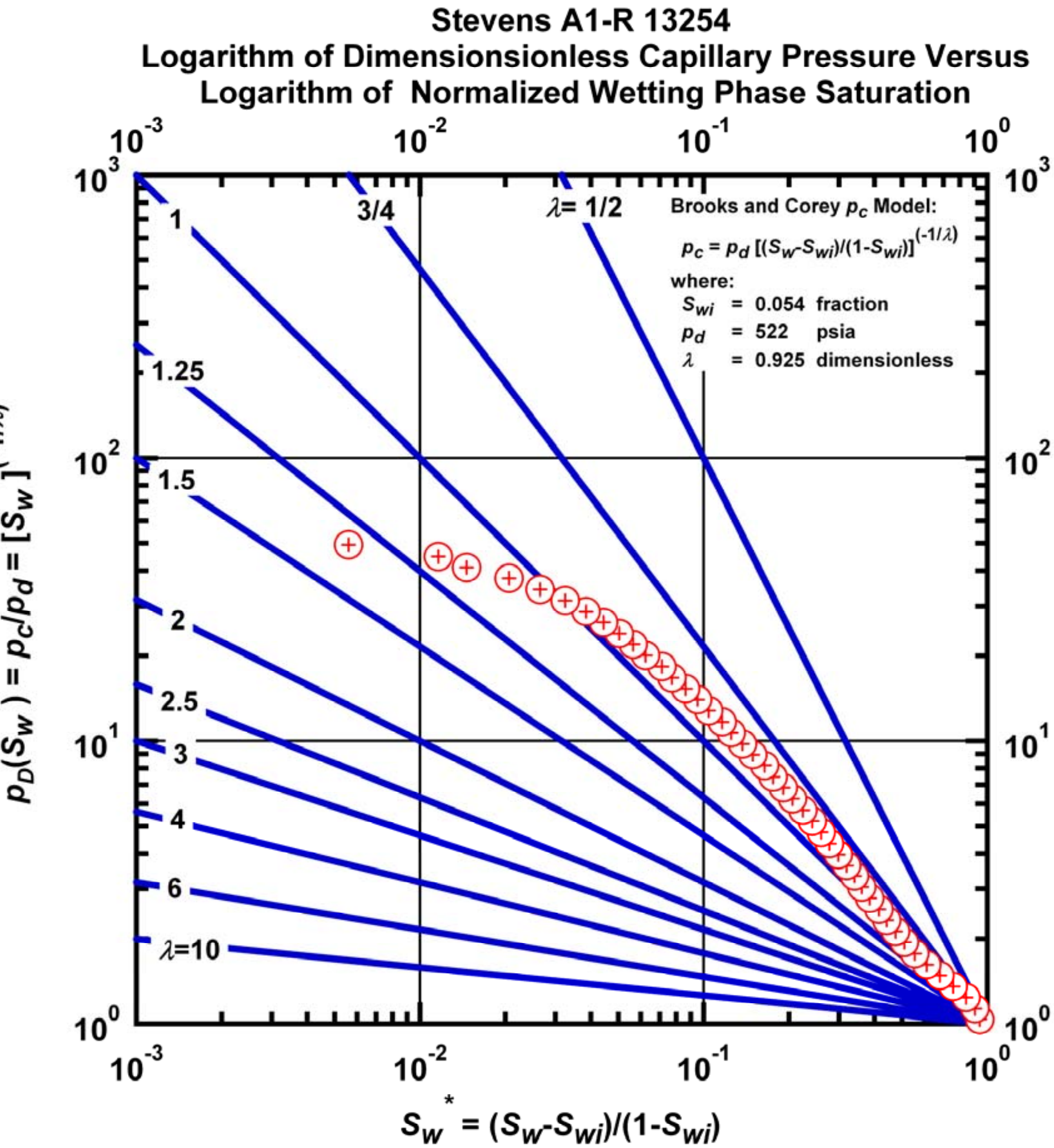

Figure L.86 – Plot of logarithm of dimensionless capillary pressure vs. logarithm of normalized wetting phase saturation — Case Stevens A1-R 13254.

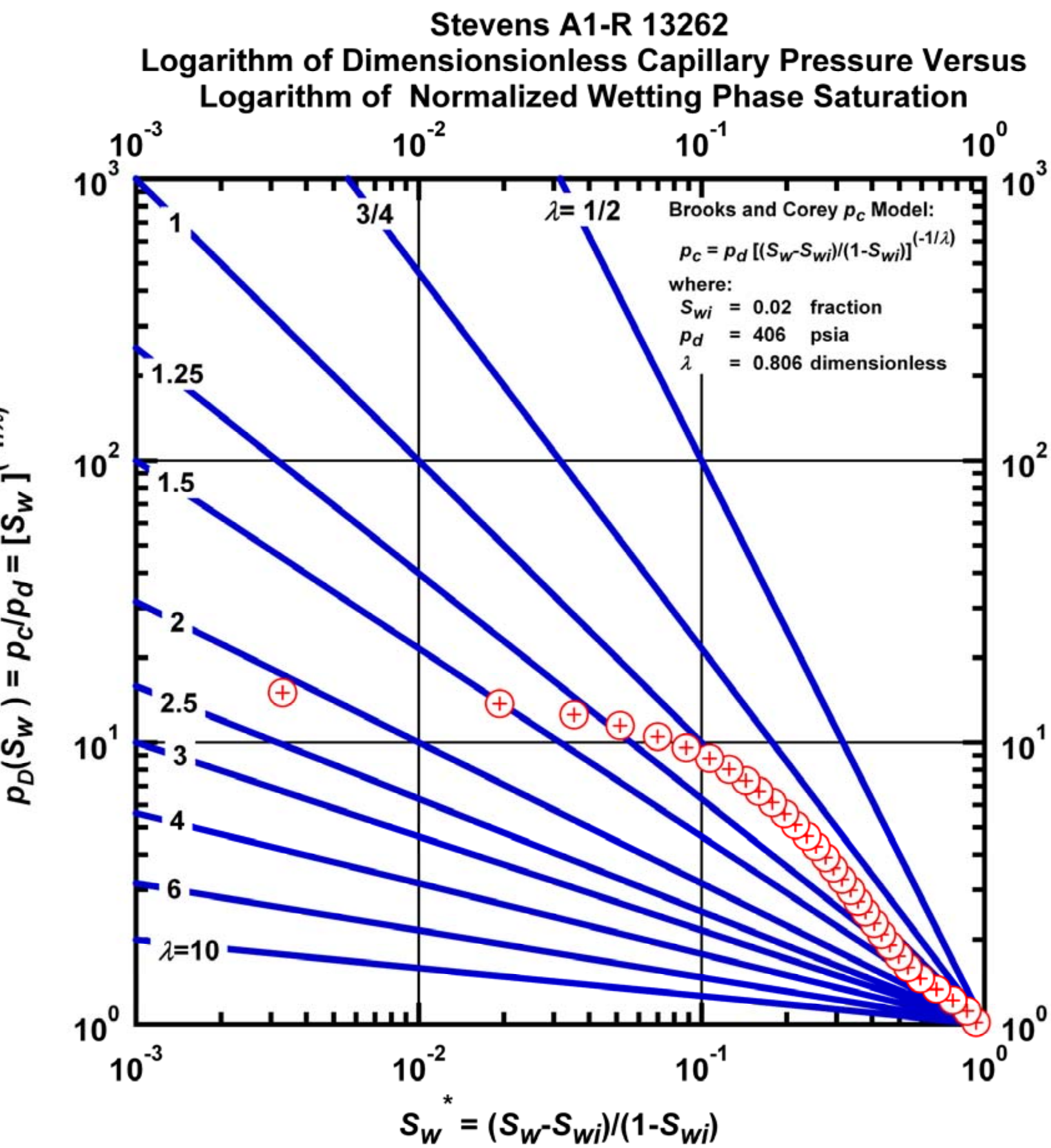

Figure L.87 – Plot of logarithm of dimensionless capillary pressure vs. logarithm of normalized wetting phase saturation — Case Stevens A1-R 13262.

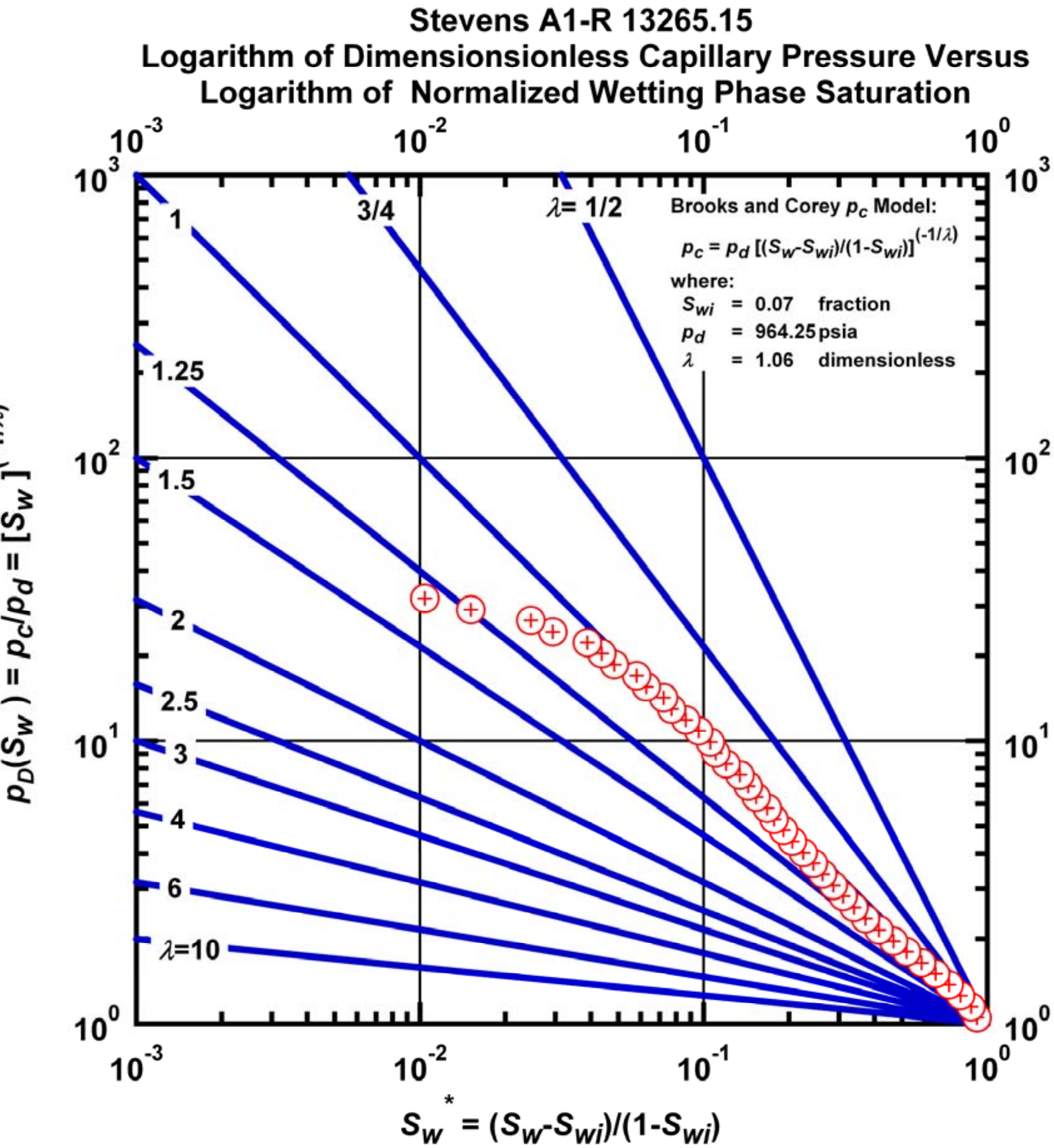

Figure L.88 – Plot of logarithm of dimensionless capillary pressure vs. logarithm of normalized wetting phase saturation — Case Stevens A1-R 13265.15.

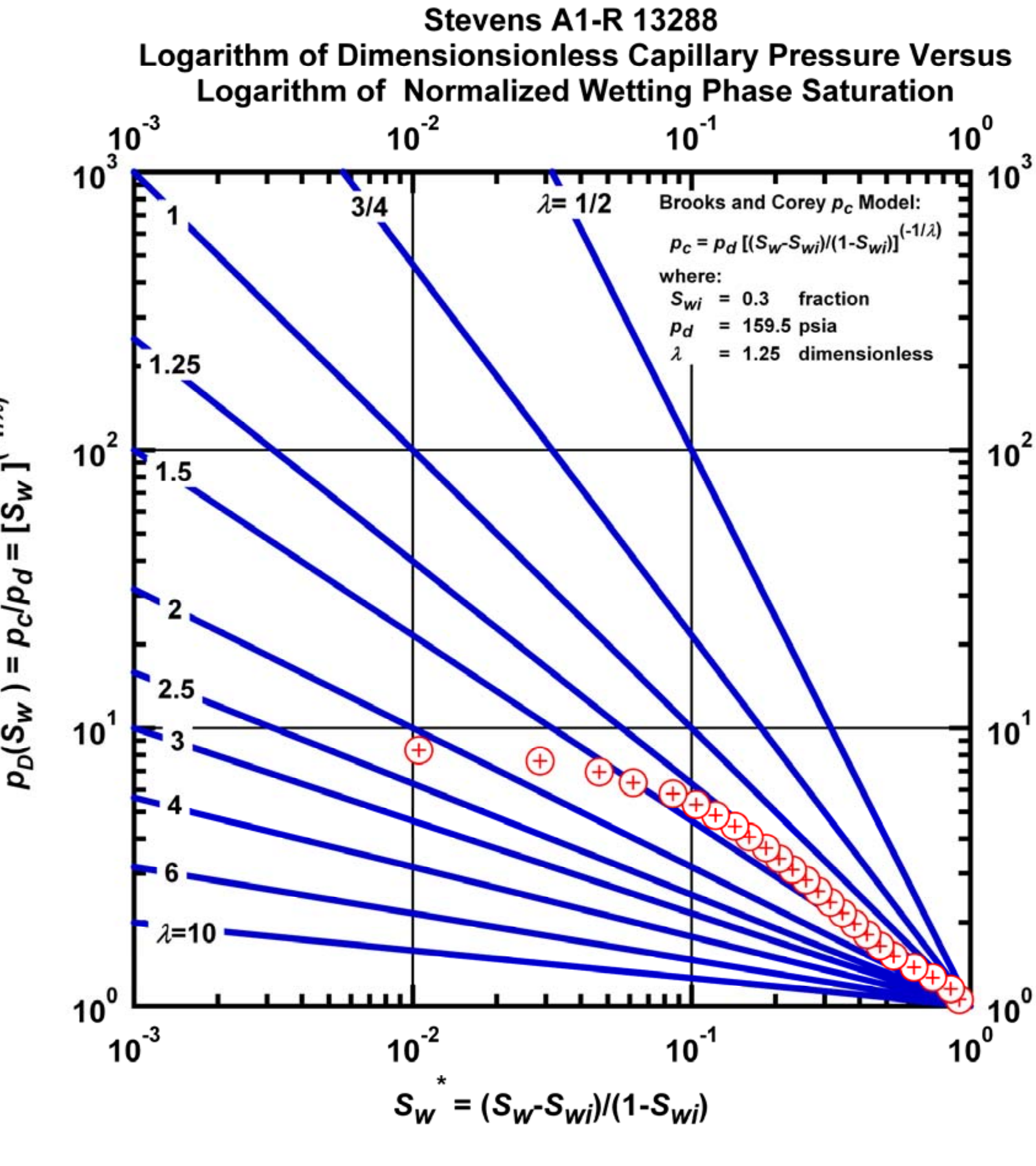

Figure L.89 – Plot of logarithm of dimensionless capillary pressure vs. logarithm of normalized wetting phase saturation — Case Stevens A1-R 13288.

APPENDIX M

LIBRARY OF DIMENSIONLESS CAPILLARY PRESSURE VERSUS DIMENSIONLESS WETTING PHASE SATURATION PLOTS — LOG-LOG FORMAT "TYPE CURVE" FOR CAPILLARY PRESSURE (BROOKS AND COREY CAPILLARY PRESSURE MODEL)

This Appendix presents the calibration of the capillary displacement pressure (p_d), irreducible wetting-phase saturation (S_{wi}), and the index of pore-size distribution (λ) on a sample-by-sample basis using the Brooks-Corey $p_c(S_w)$ model .

In this Appendix, we provide for each data a plot of dimensionless capillary pressure (p_c) vs. dimensionless wetting phase saturation (S_w) – log-log format "type curve" for capillary pressure.

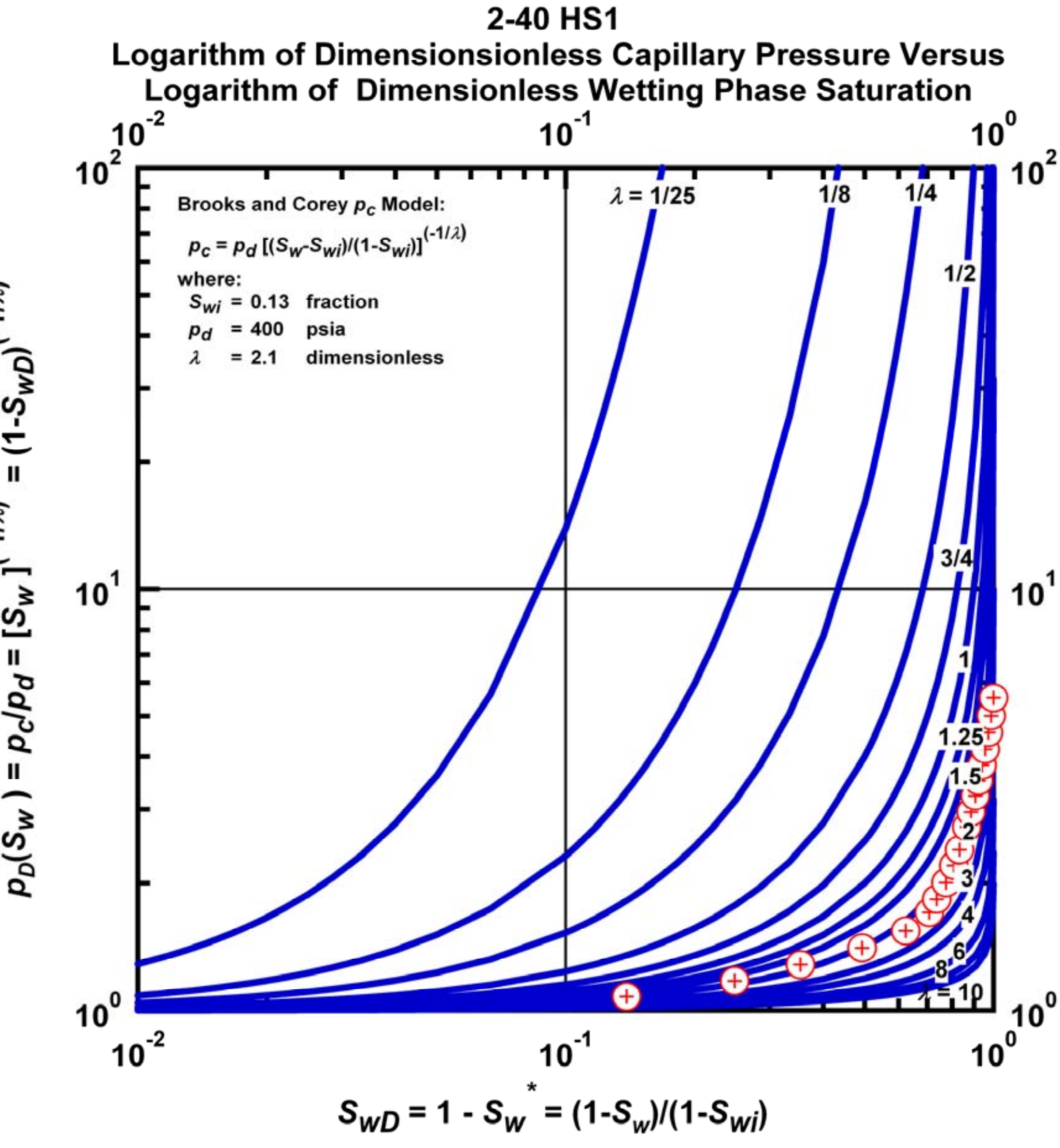

Figure M.1 – Plot of Logarithm of Dimensionless Capillary Pressure Versus Logarithm of Dimensionless Wetting Phase Saturation — Case 2-40 HS1.

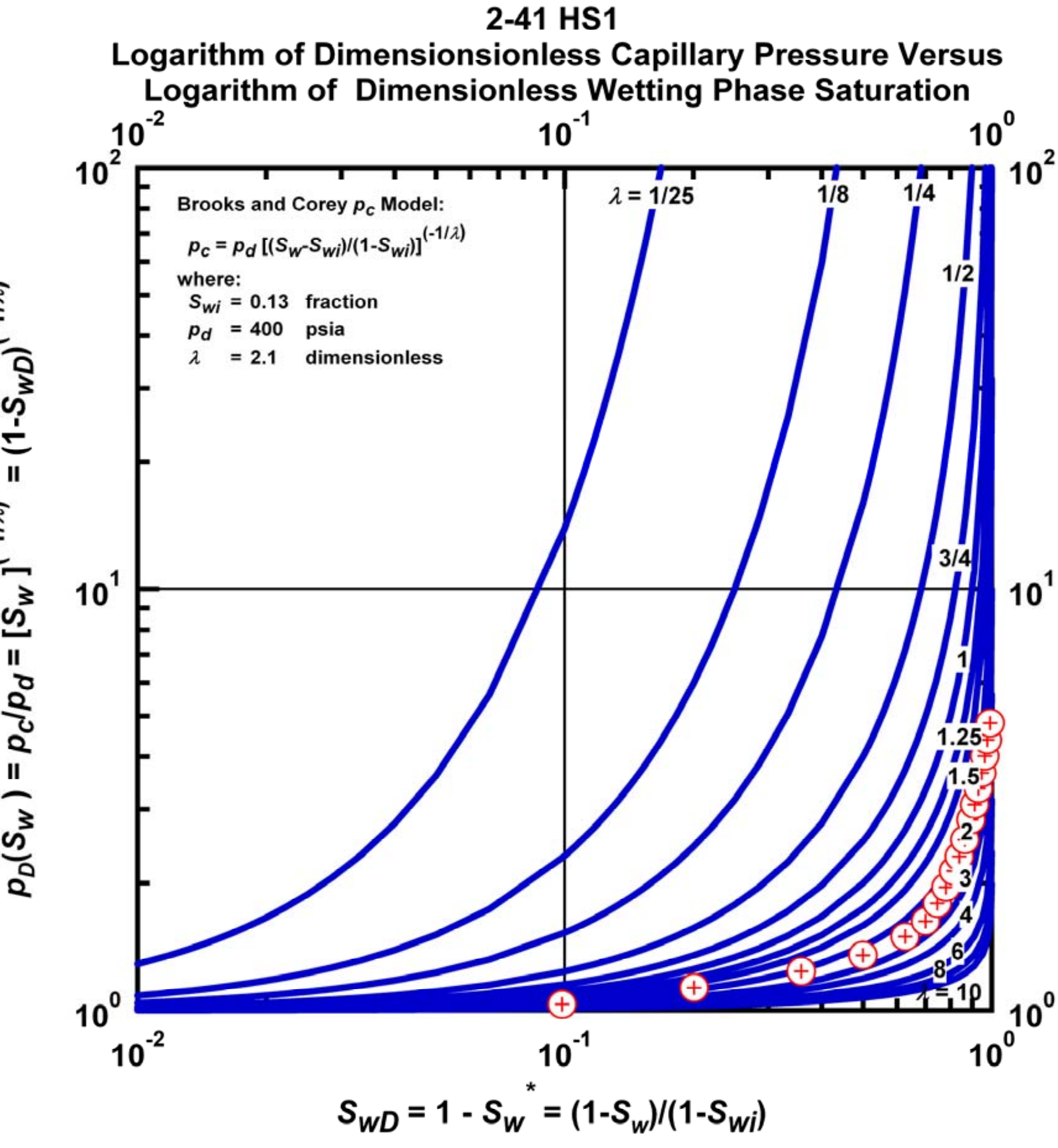

Figure M.2 – Plot of Logarithm of Dimensionless Capillary Pressure Versus Logarithm of Dimensionless Wetting Phase Saturation — Case 2-41 HS1.

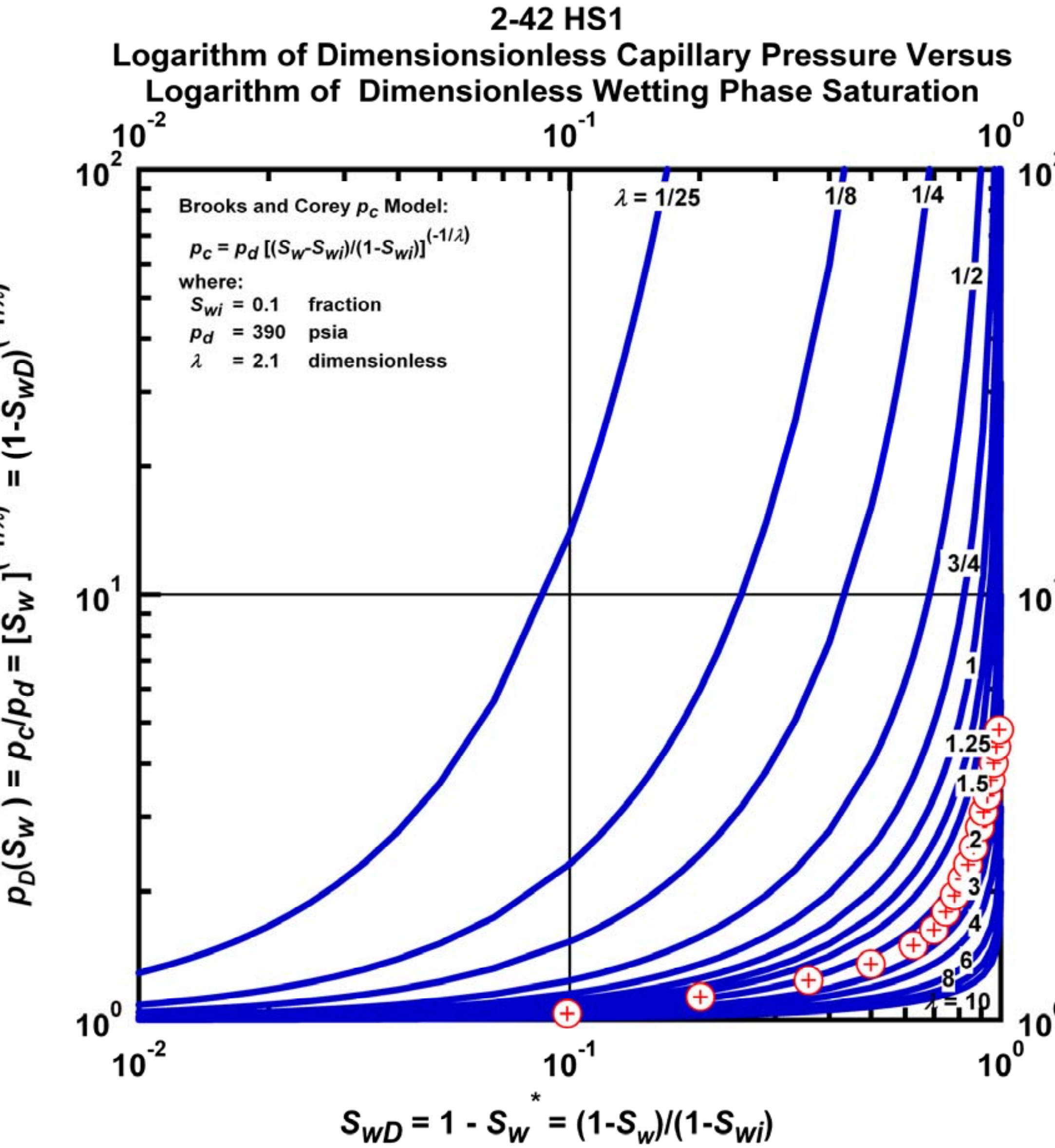

Figure M.3 – Plot of Logarithm of Dimensionless Capillary Pressure Versus Logarithm of Dimensionless Wetting Phase Saturation — Case 2-43 HS1.

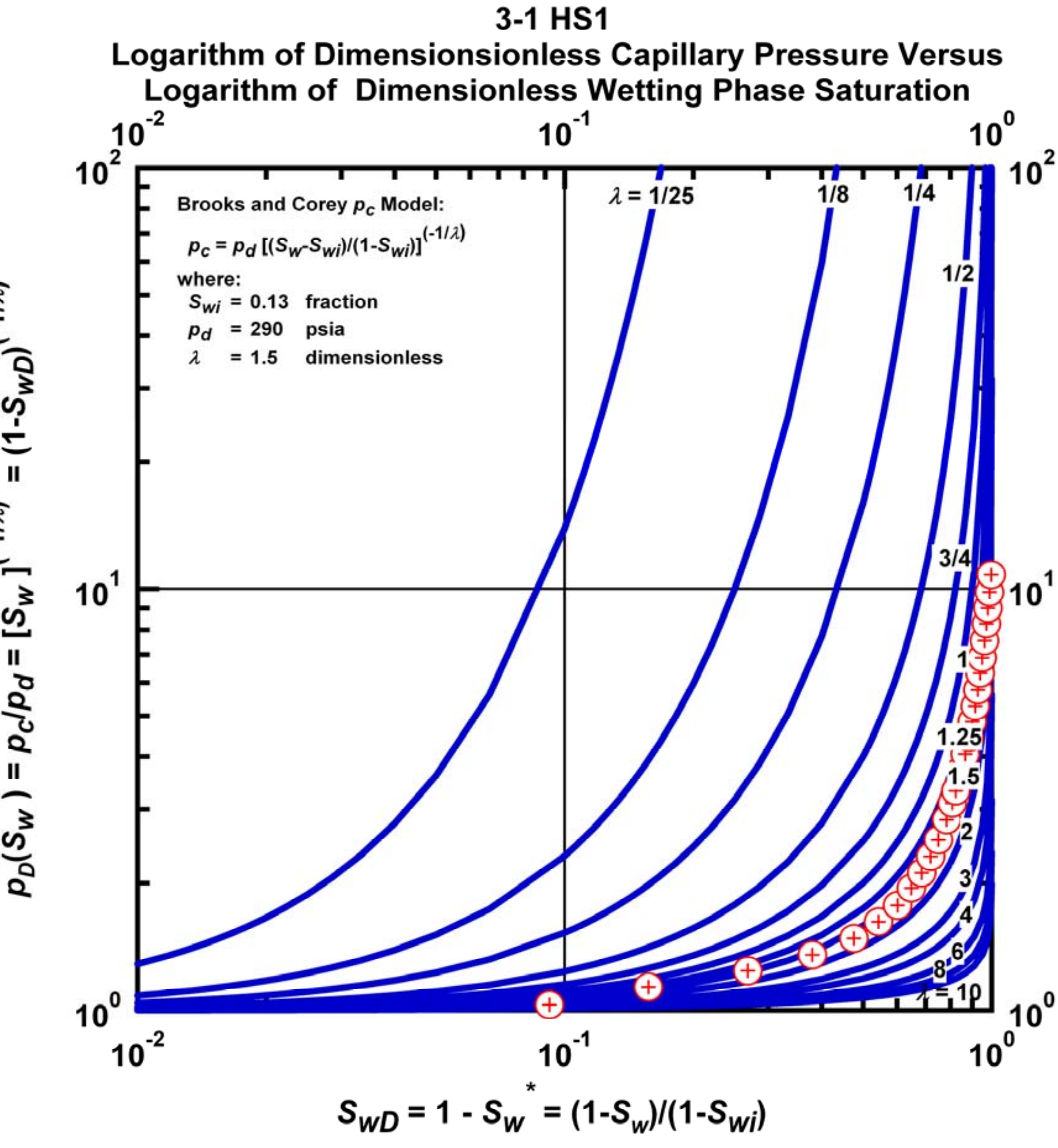

Figure M.4 – Plot of Logarithm of Dimensionless Capillary Pressure Versus Logarithm of Dimensionless Wetting Phase Saturation — Case 3-1 HS1.

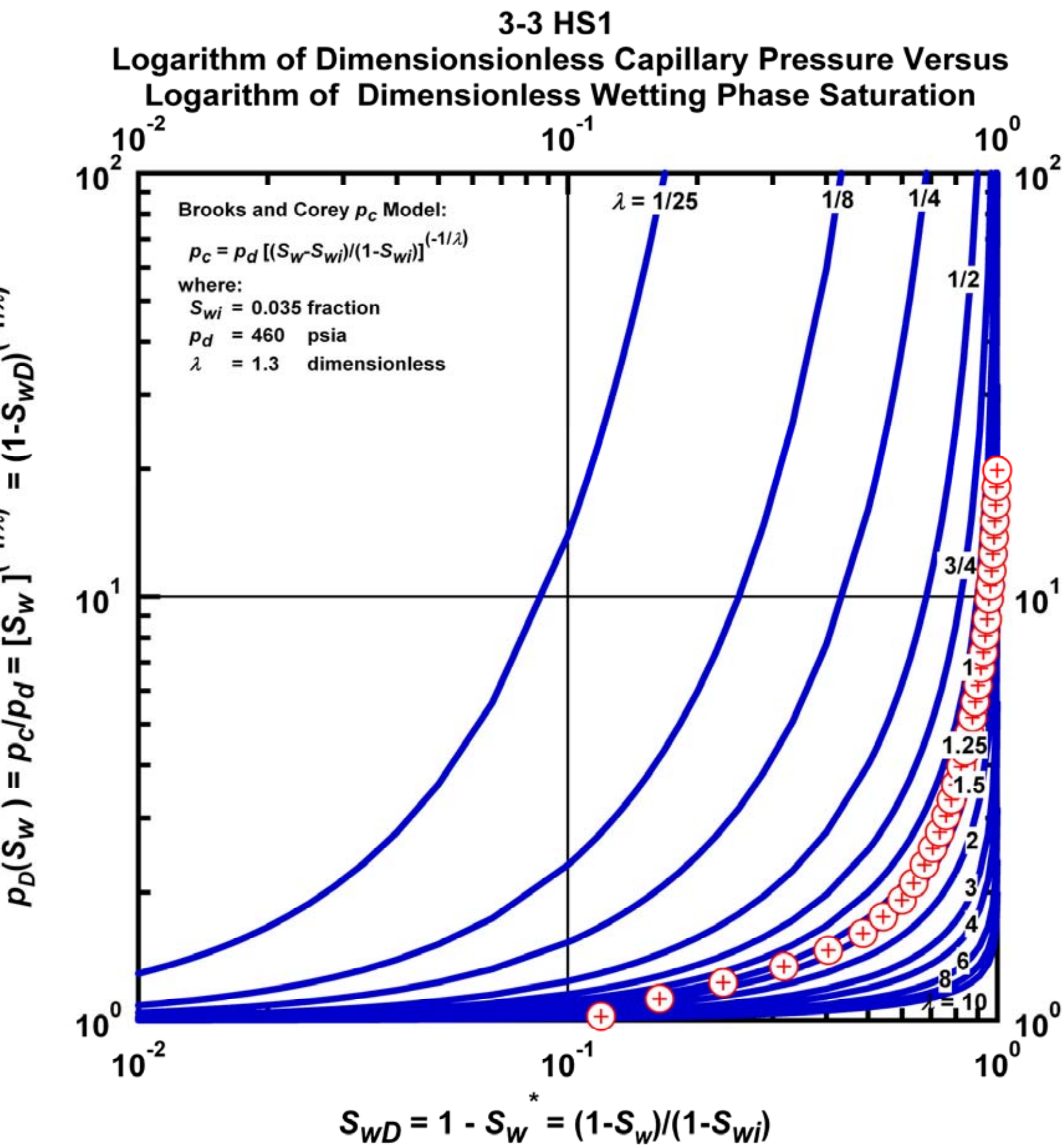

Figure M.5 – Plot of Logarithm of Dimensionless Capillary Pressure Versus Logarithm of Dimensionless Wetting Phase Saturation — Case 3-3 HS1.

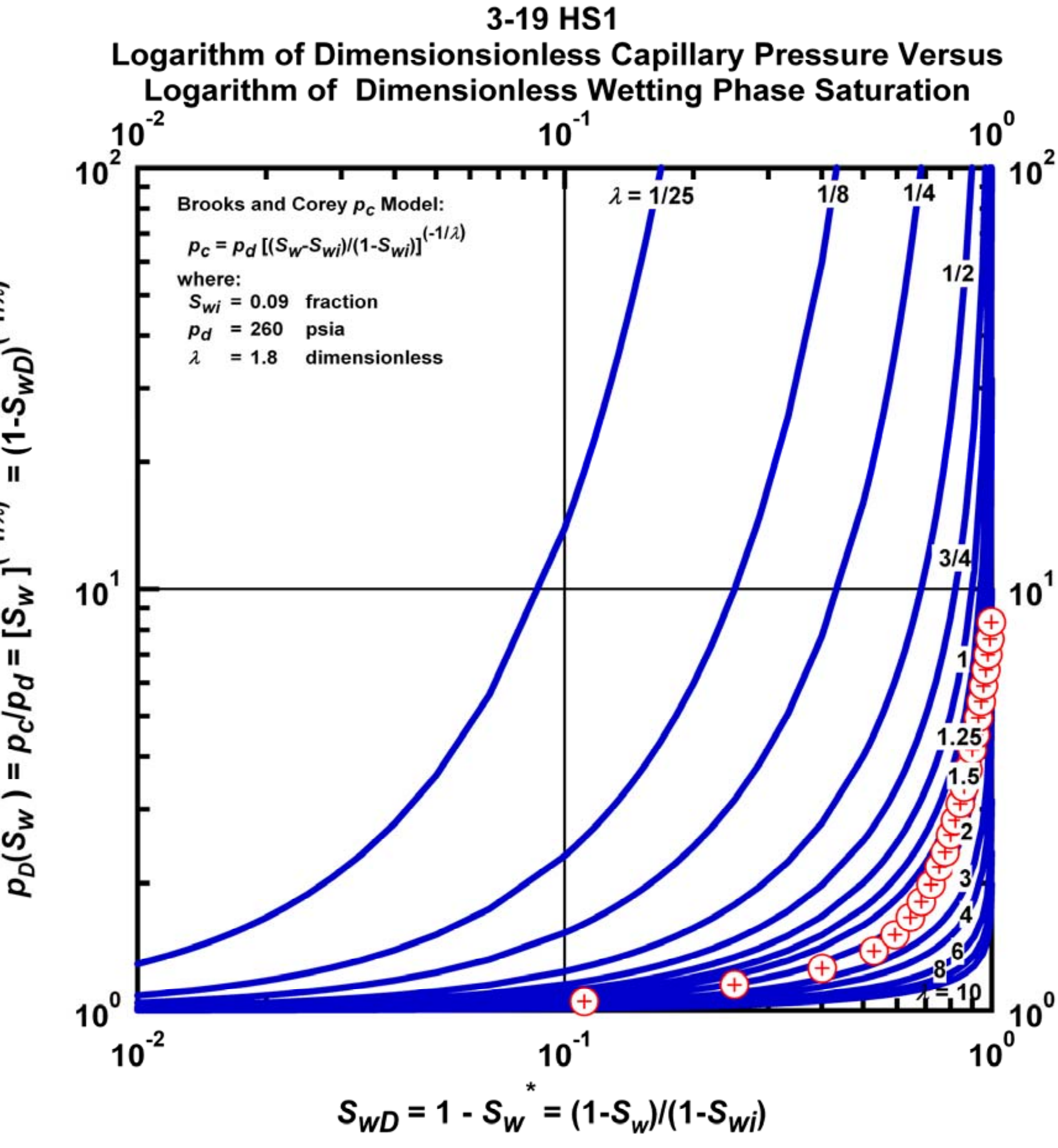

Figure M.6 – Plot of Logarithm of Dimensionless Capillary Pressure Versus Logarithm of Dimensionless Wetting Phase Saturation — Case 3-19 HS1.

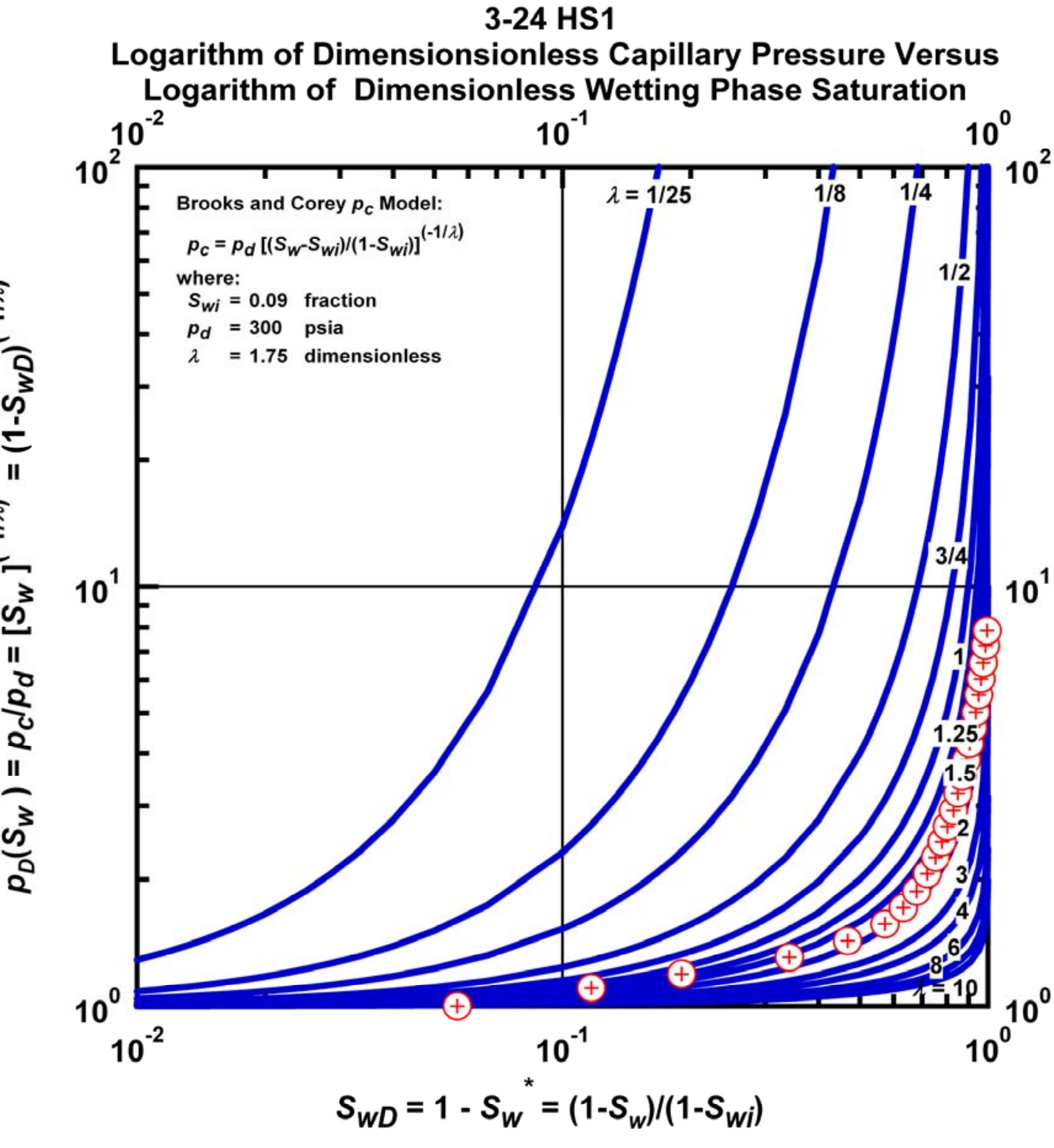

Figure M.7 – Plot of Logarithm of Dimensionless Capillary Pressure Versus Logarithm of Dimensionless Wetting Phase Saturation — Case 3-24 HS1.

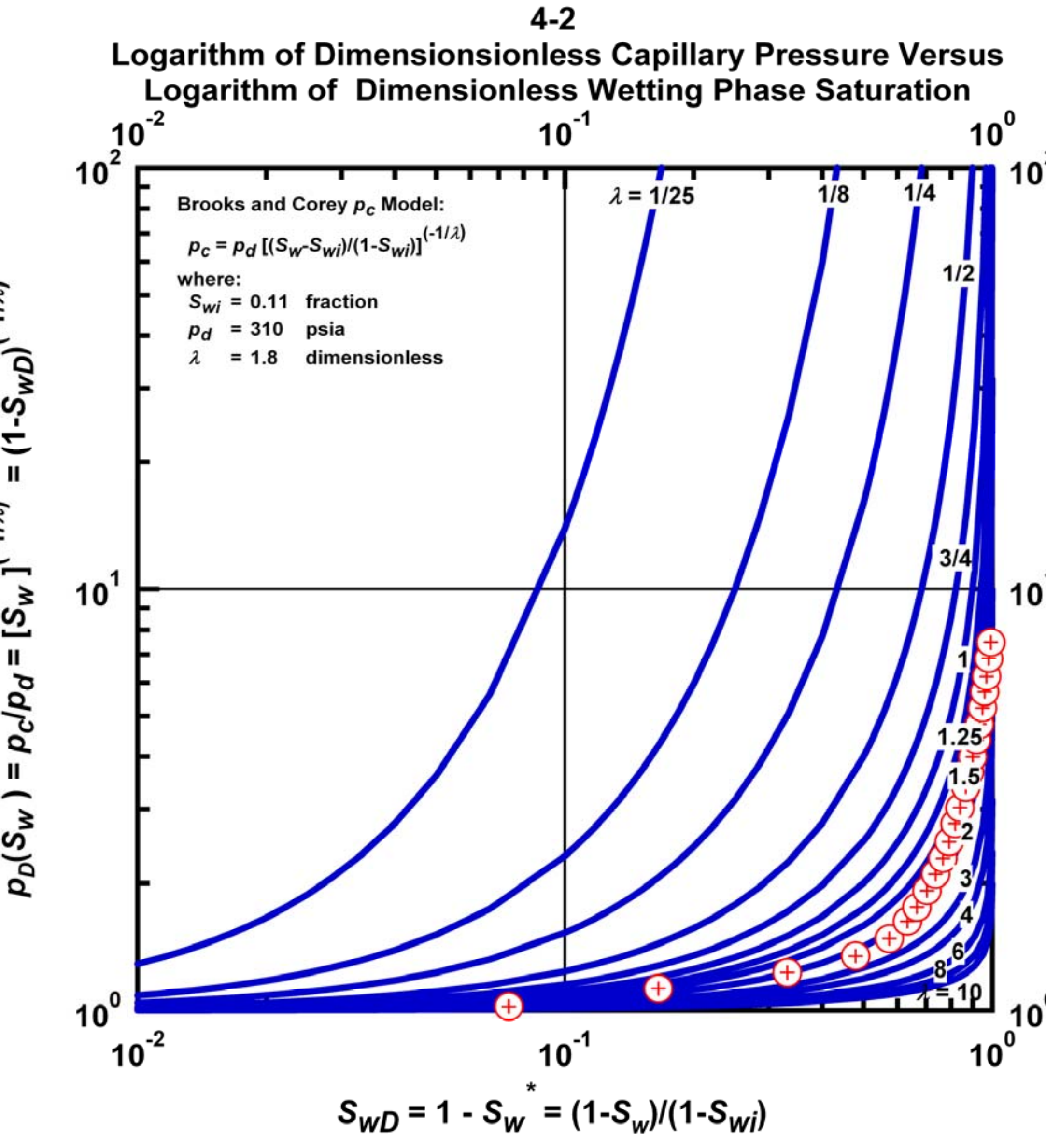

Figure M.8 – Plot of Logarithm of Dimensionless Capillary Pressure Versus Logarithm of Dimensionless Wetting Phase Saturation — Case 4-2 HS1.

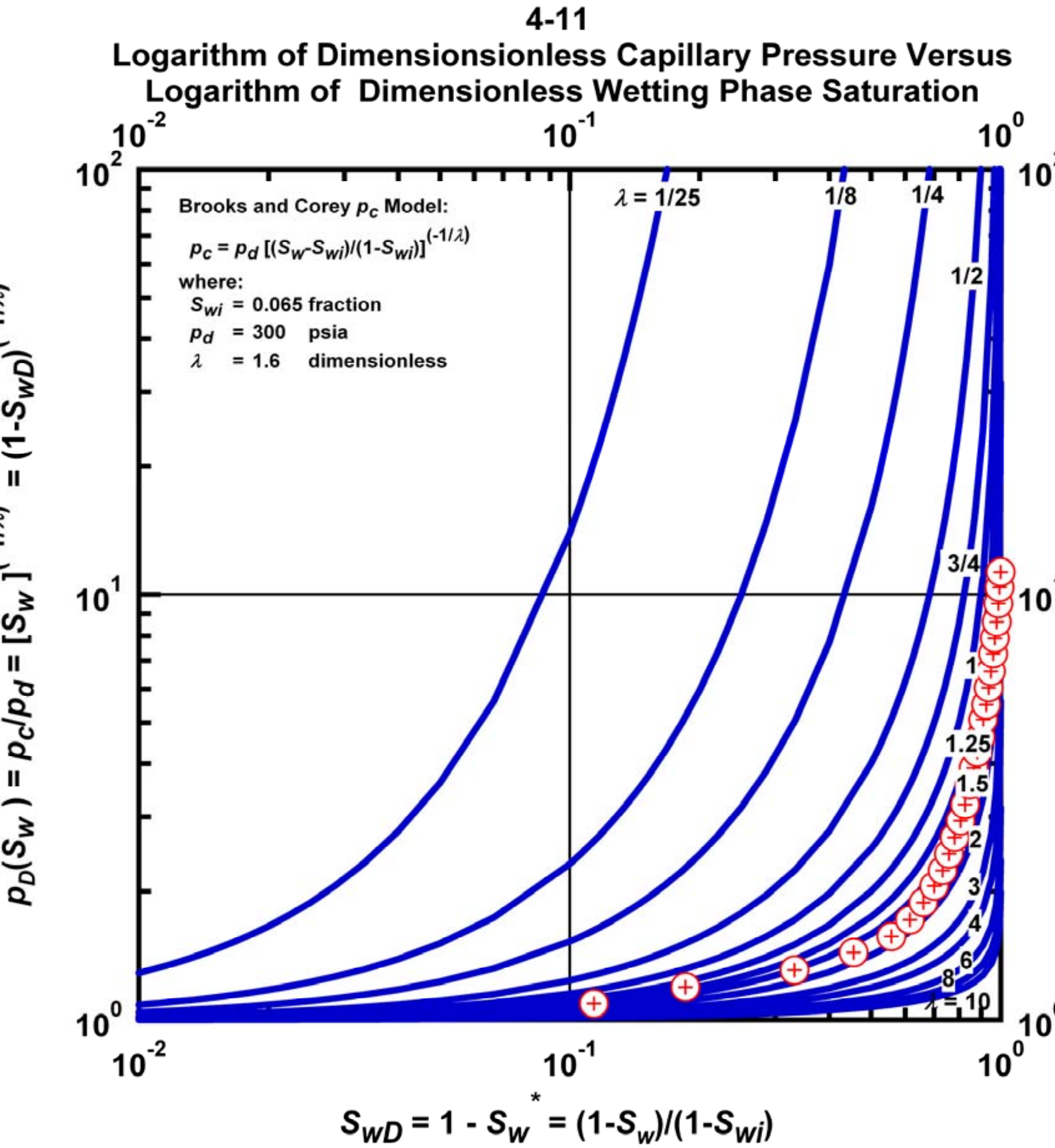

Figure M.9 – Plot of Logarithm of Dimensionless Capillary Pressure Versus Logarithm of Dimensionless Wetting Phase Saturation — Case 4-11 HS1.

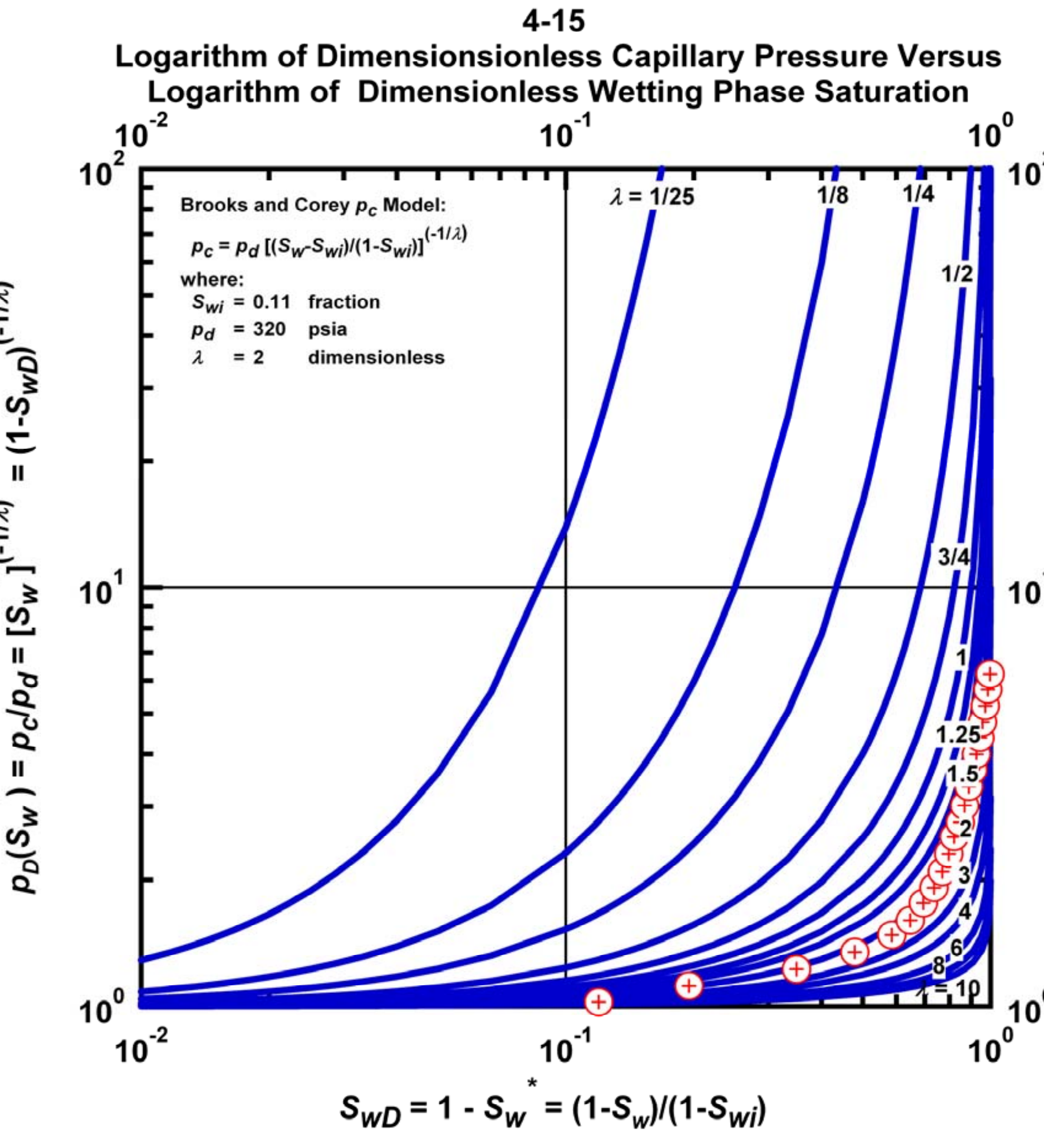

Figure M.10 – Plot of Logarithm of Dimensionless Capillary Pressure Versus Logarithm of Dimensionless Wetting Phase Saturation — Case 4-15 HS1.

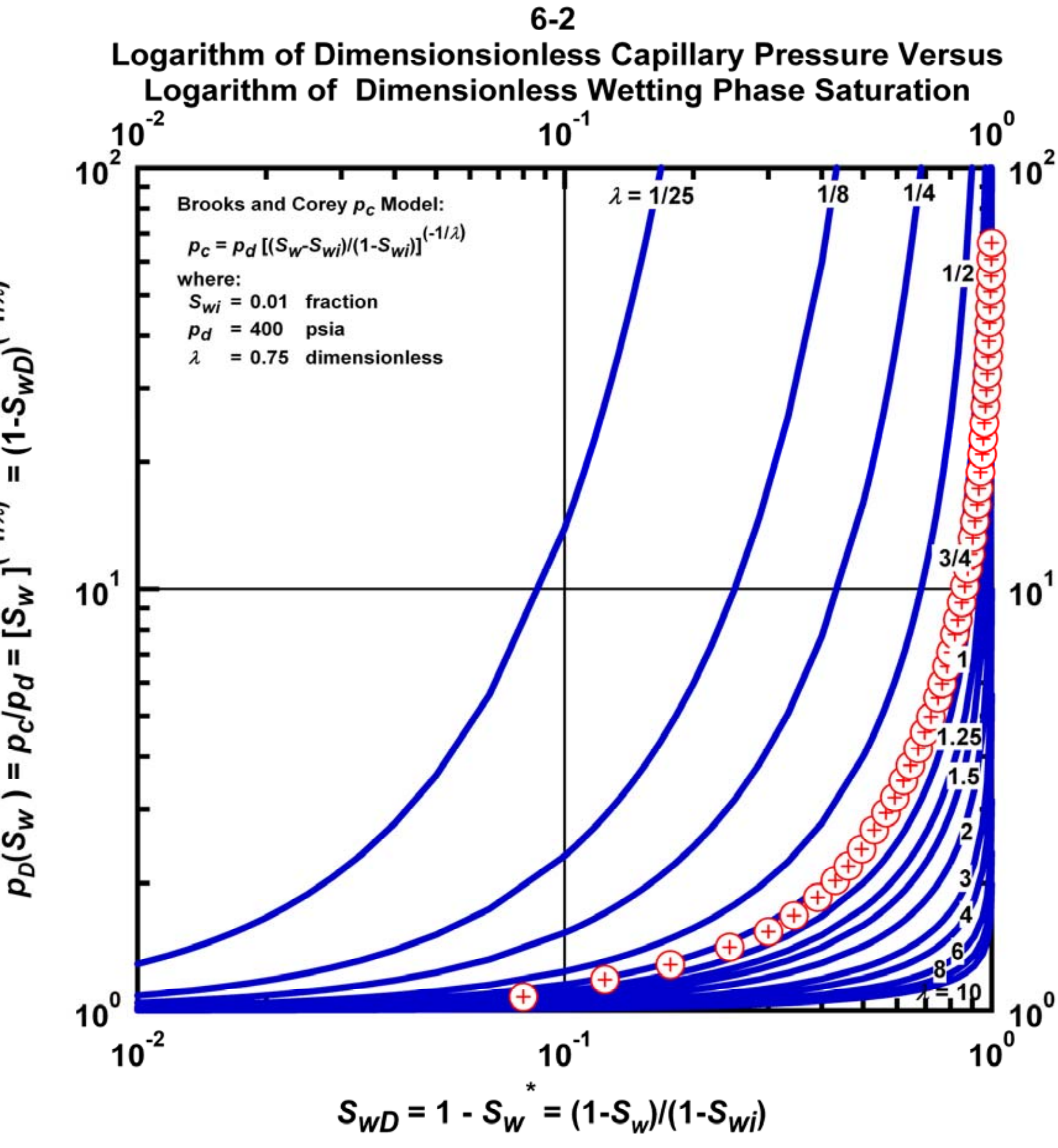

Figure M.11 – Plot of Logarithm of Dimensionless Capillary Pressure Versus Logarithm of Dimensionless Wetting Phase Saturation — Case 6-2 HS1.

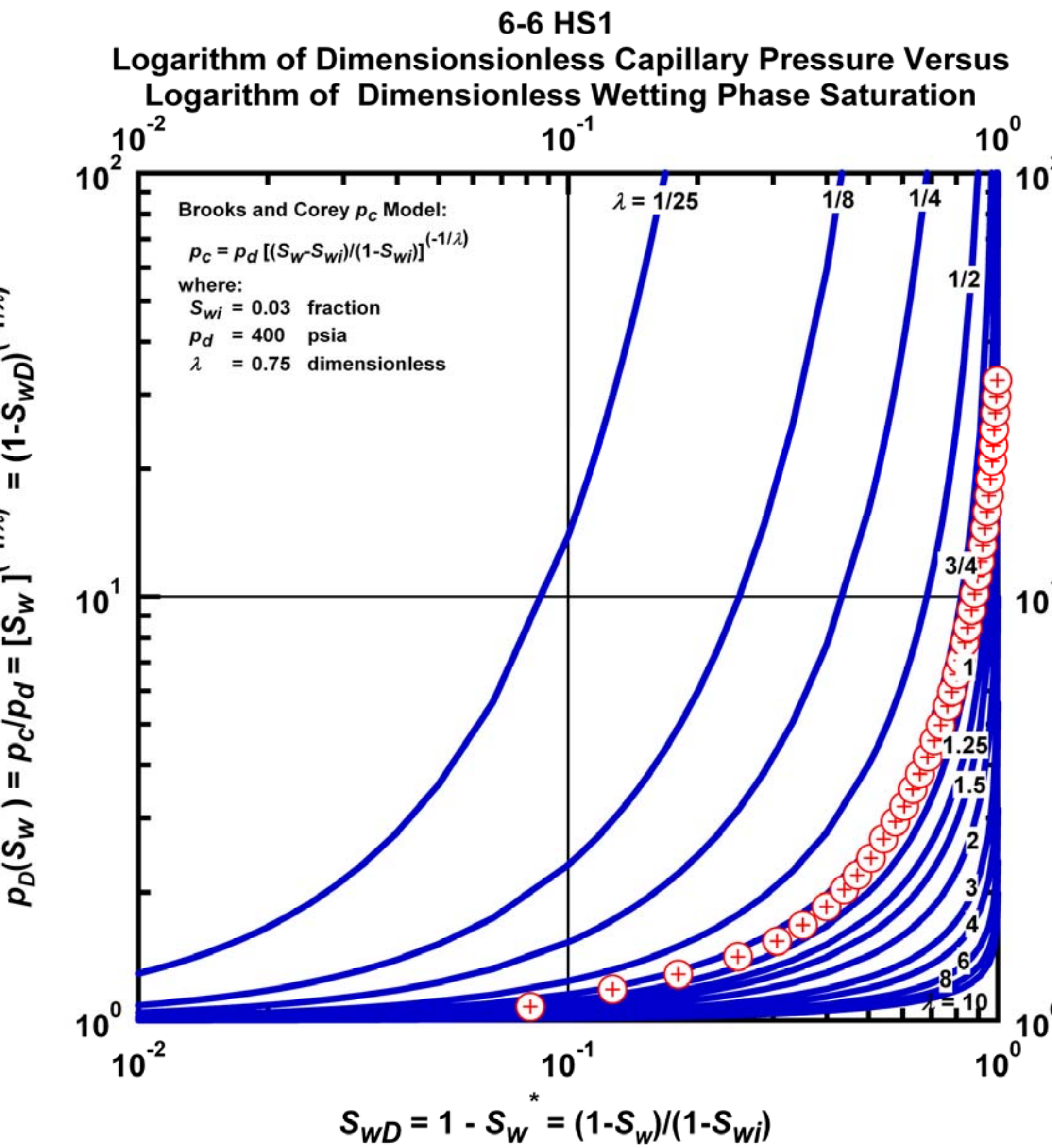

Figure M.12 – Plot of Logarithm of Dimensionless Capillary Pressure Versus Logarithm of Dimensionless Wetting Phase Saturation — Case 6-6 HS1.

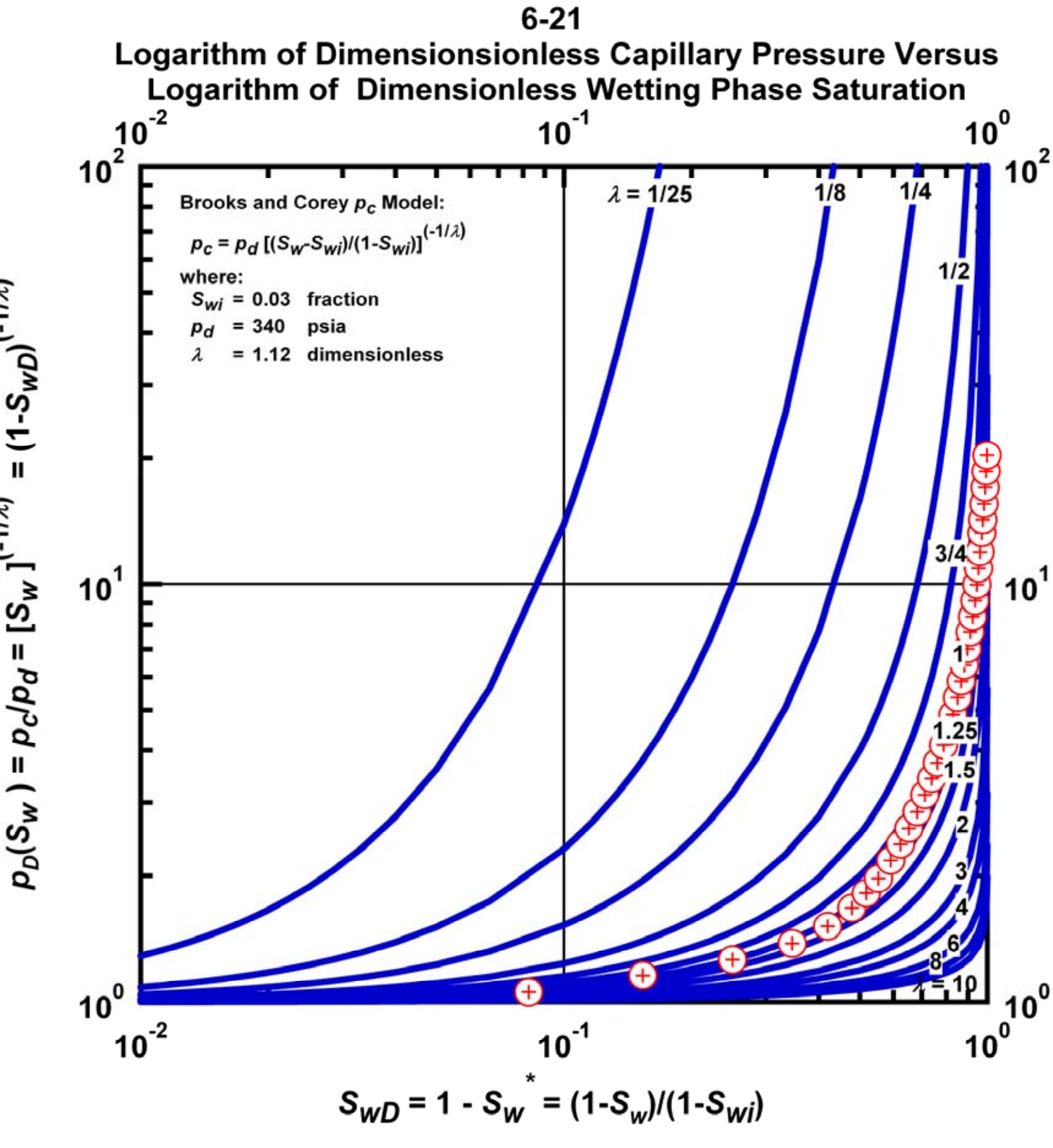

Figure M.13 – Plot of Logarithm of Dimensionless Capillary Pressure Versus Logarithm of Dimensionless Wetting Phase Saturation — Case 6-21 HS1.

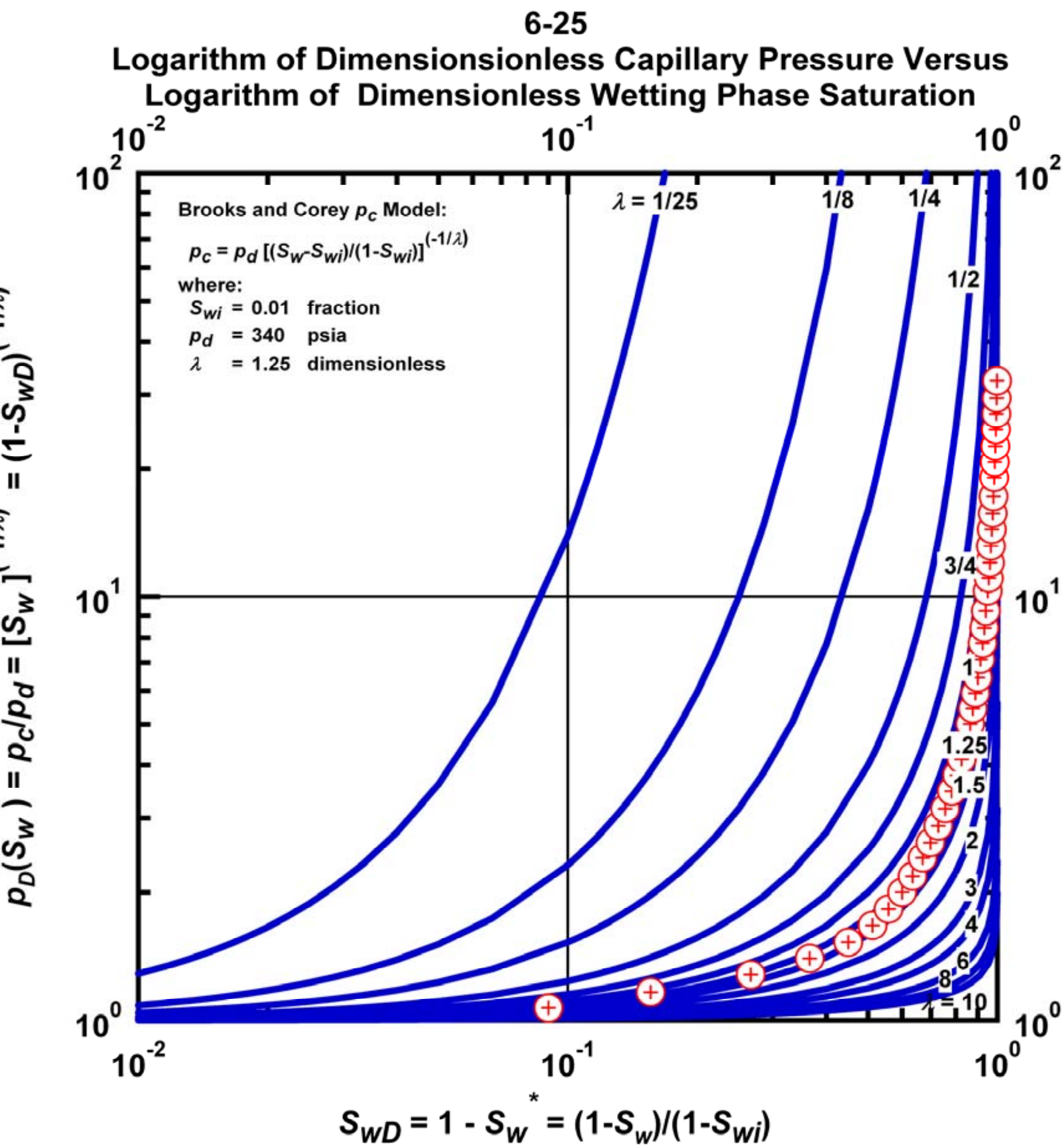

Figure M.14 – Plot of Logarithm of Dimensionless Capillary Pressure Versus Logarithm of Dimensionless Wetting Phase Saturation — Case 6-25 HS1.

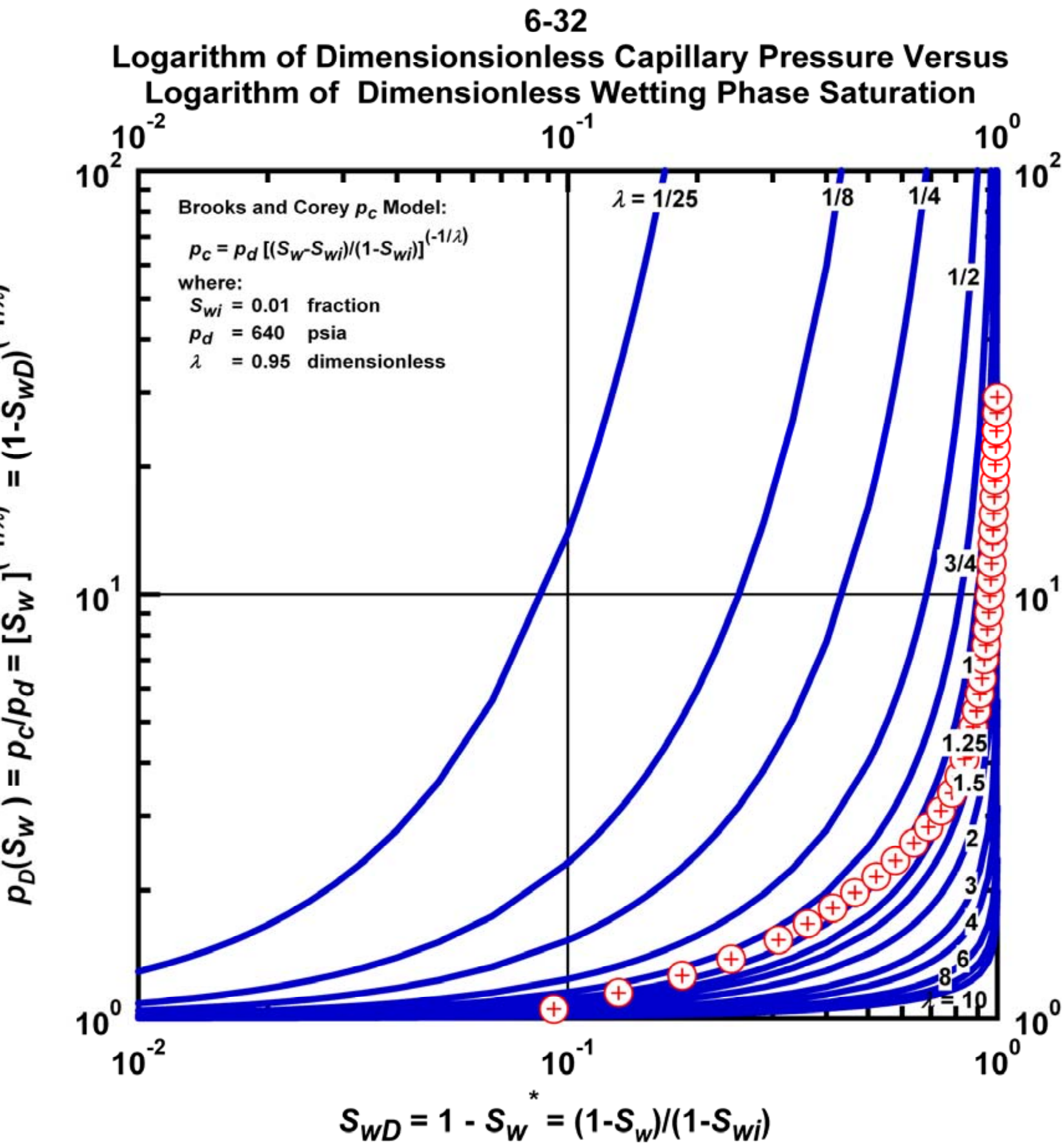

Figure M.15 – Plot of Logarithm of Dimensionless Capillary Pressure Versus Logarithm of Dimensionless Wetting Phase Saturation — Case 6-32 HS1.

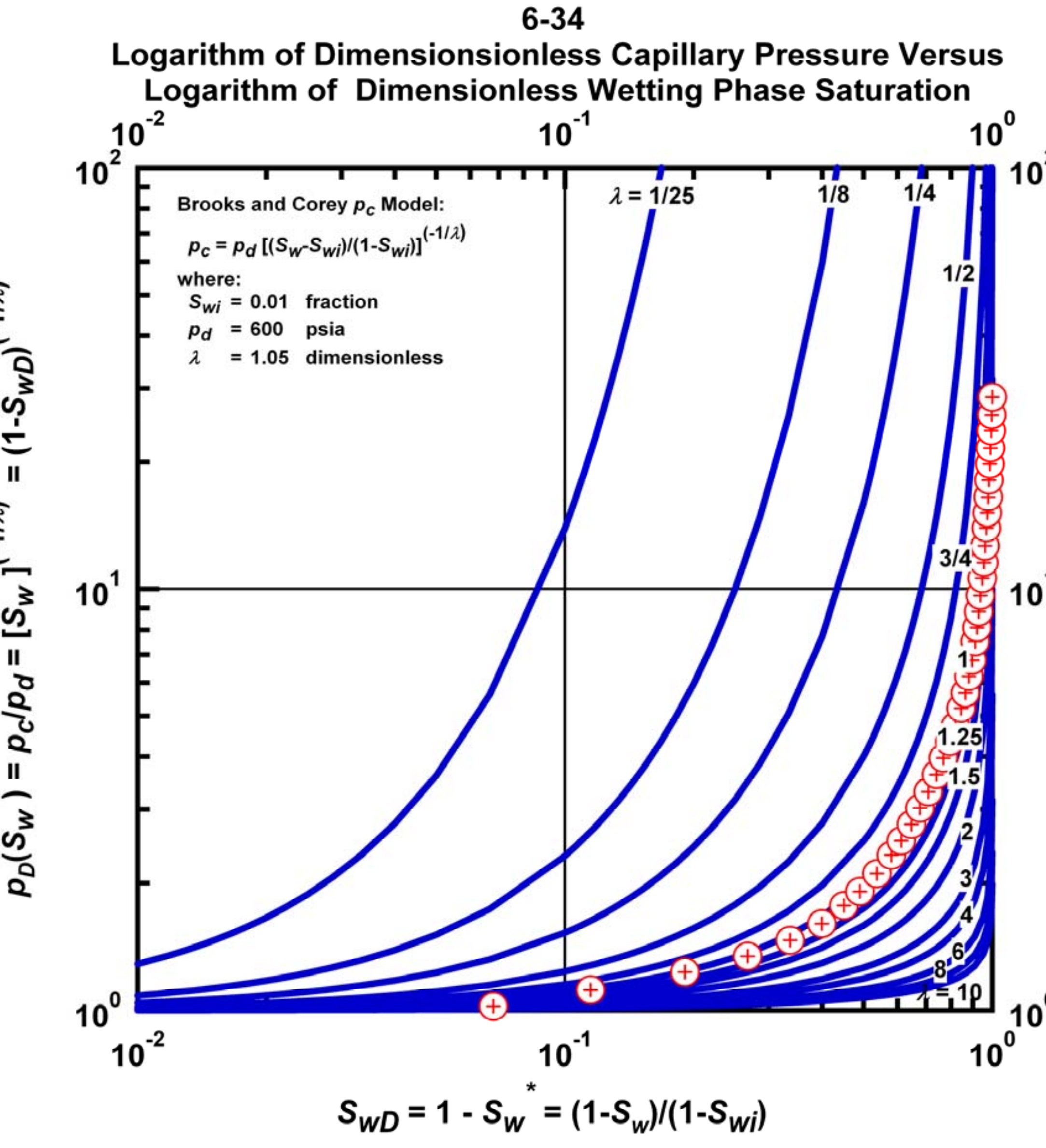

Figure M.16 – Plot of Logarithm of Dimensionless Capillary Pressure Versus Logarithm of Dimensionless Wetting Phase Saturation — Case 6-34 HS1.

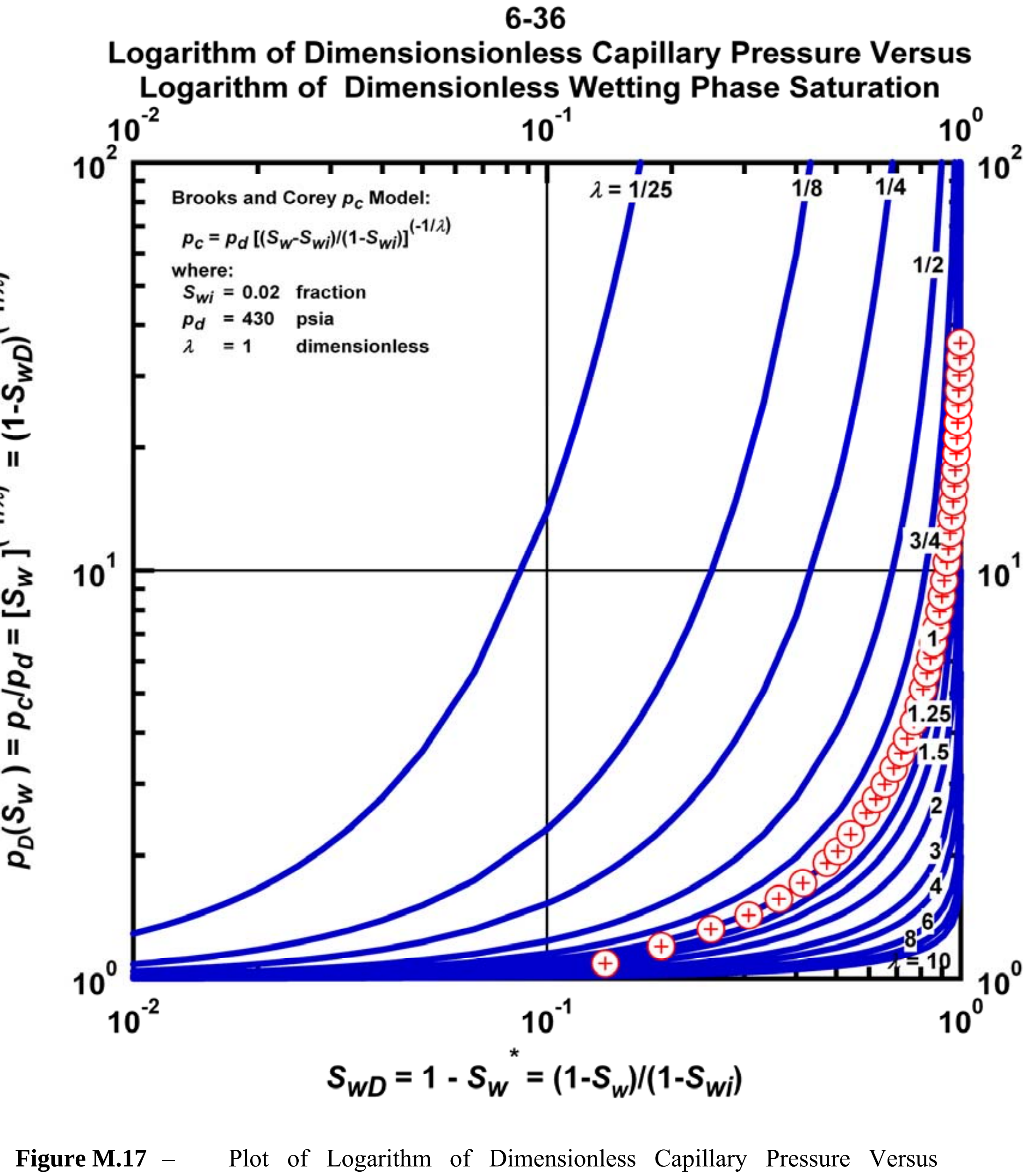

Figure M.17 – Plot of Logarithm of Dimensionless Capillary Pressure Versus Logarithm of Dimensionless Wetting Phase Saturation — Case 6-36 HS1.

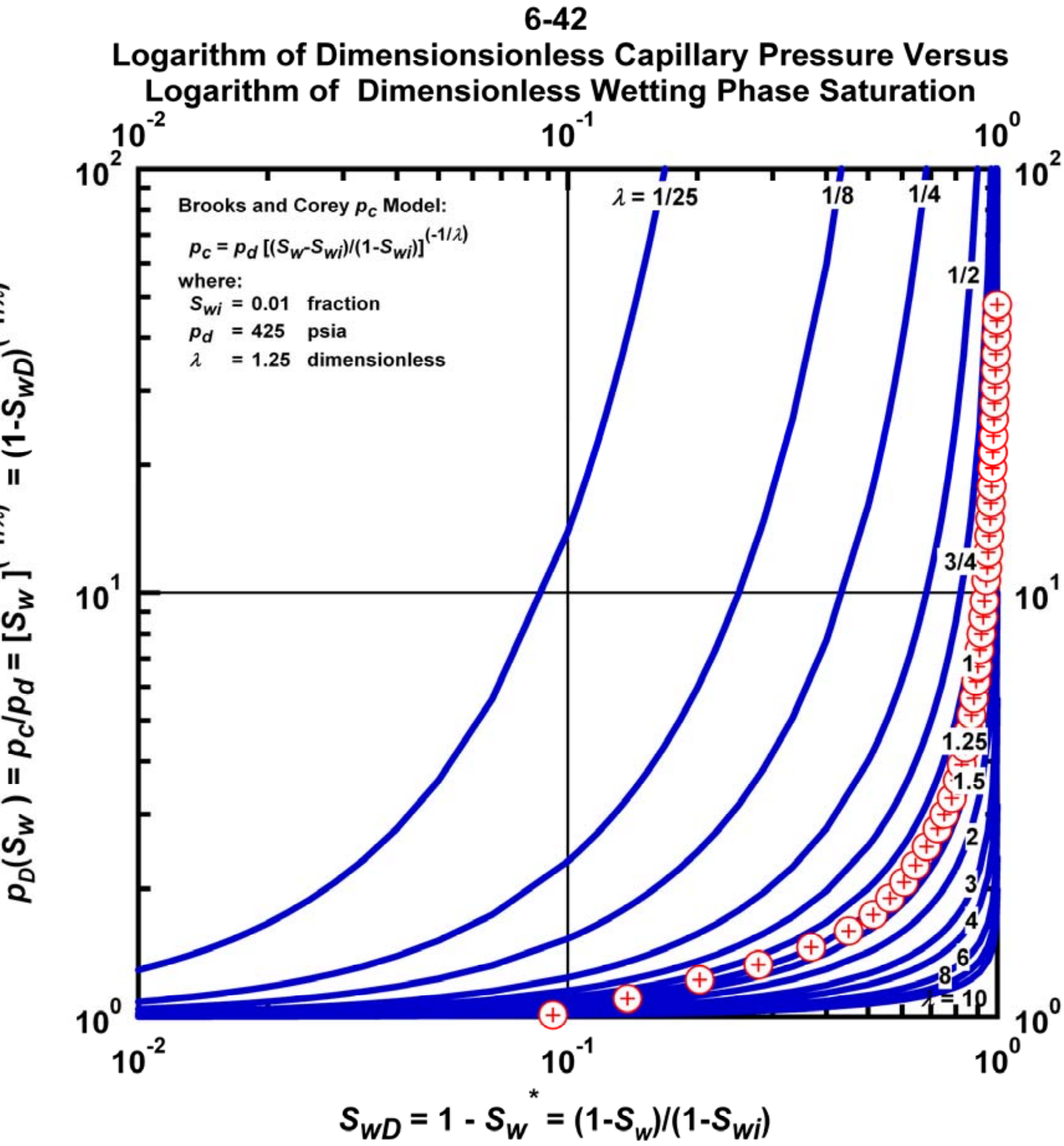

Figure M.18 – Plot of Logarithm of Dimensionless Capillary Pressure Versus Logarithm of Dimensionless Wetting Phase Saturation — Case 6-42 HS1.

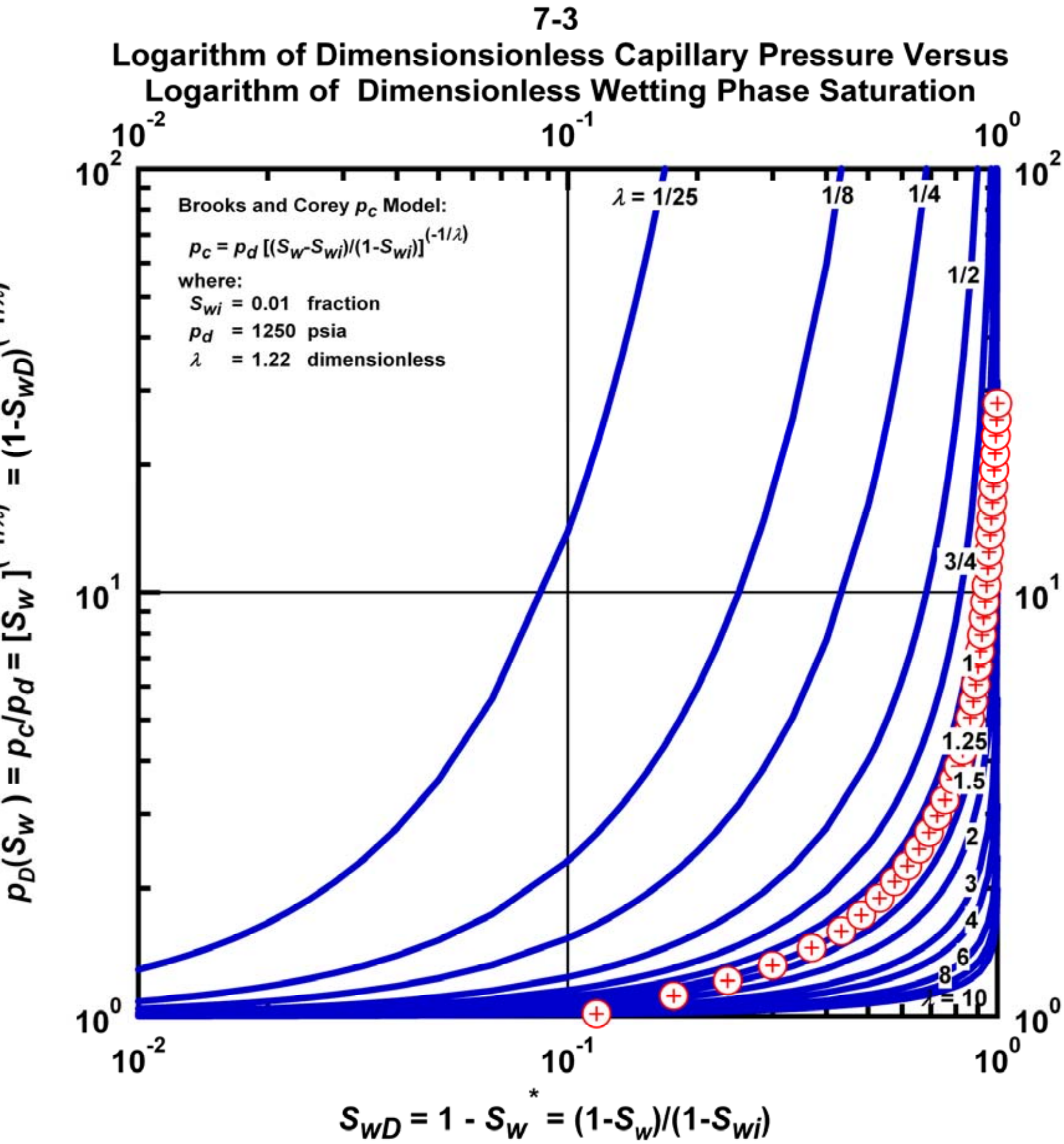

Figure M.19 – Plot of Logarithm of Dimensionless Capillary Pressure Versus Logarithm of Dimensionless Wetting Phase Saturation — Case 7-3 HS1.

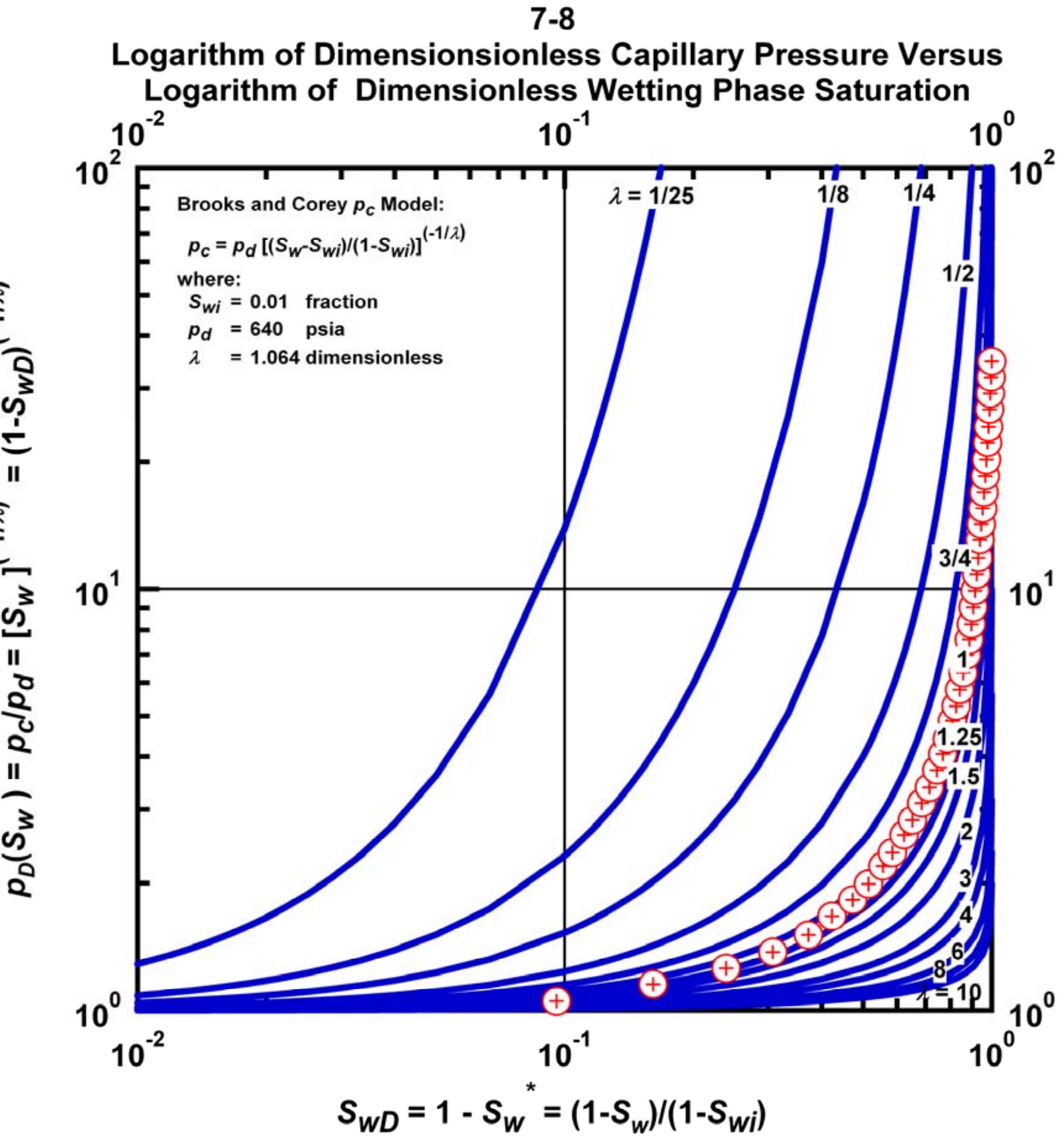

Figure M.20 – Plot of Logarithm of Dimensionless Capillary Pressure Versus Logarithm of Dimensionless Wetting Phase Saturation — Case 7-8 HS1.

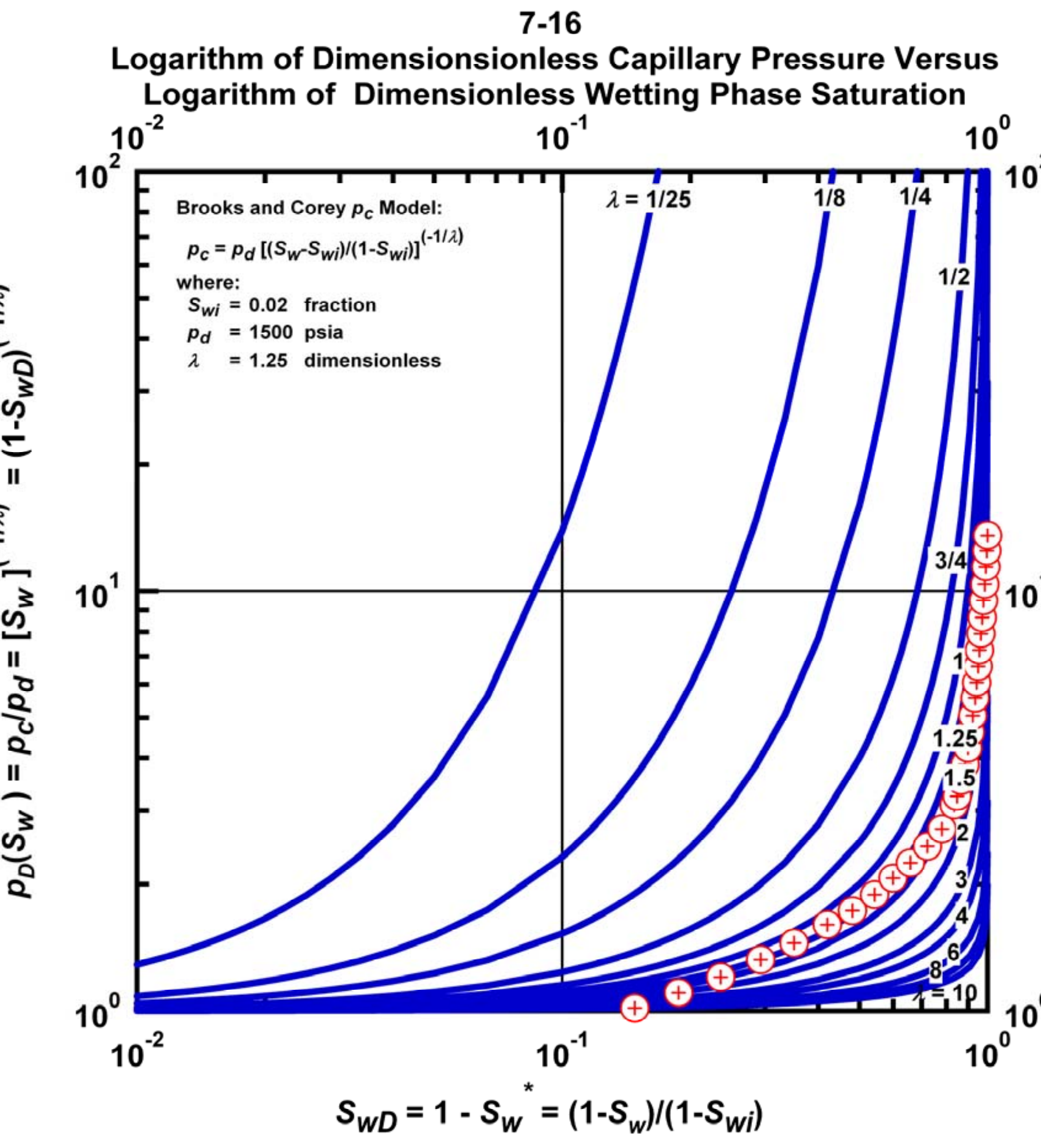

Figure M.21 – Plot of Logarithm of Dimensionless Capillary Pressure Versus Logarithm of Dimensionless Wetting Phase Saturation — Case 7-16 HS1.

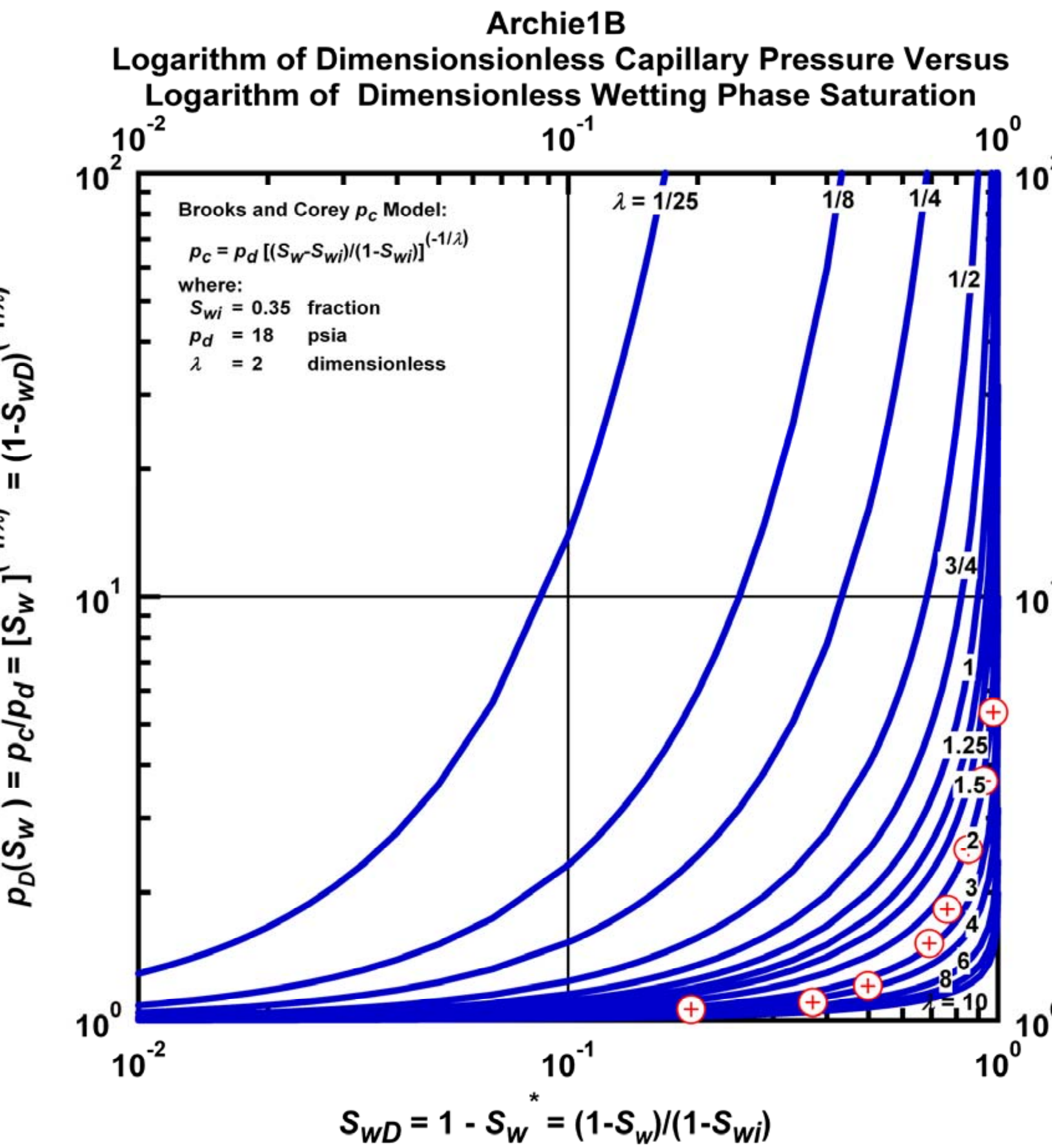

Figure M.22 – Plot of Logarithm of Dimensionless Capillary Pressure Versus Logarithm of Dimensionless Wetting Phase Saturation — Case Archie1B.

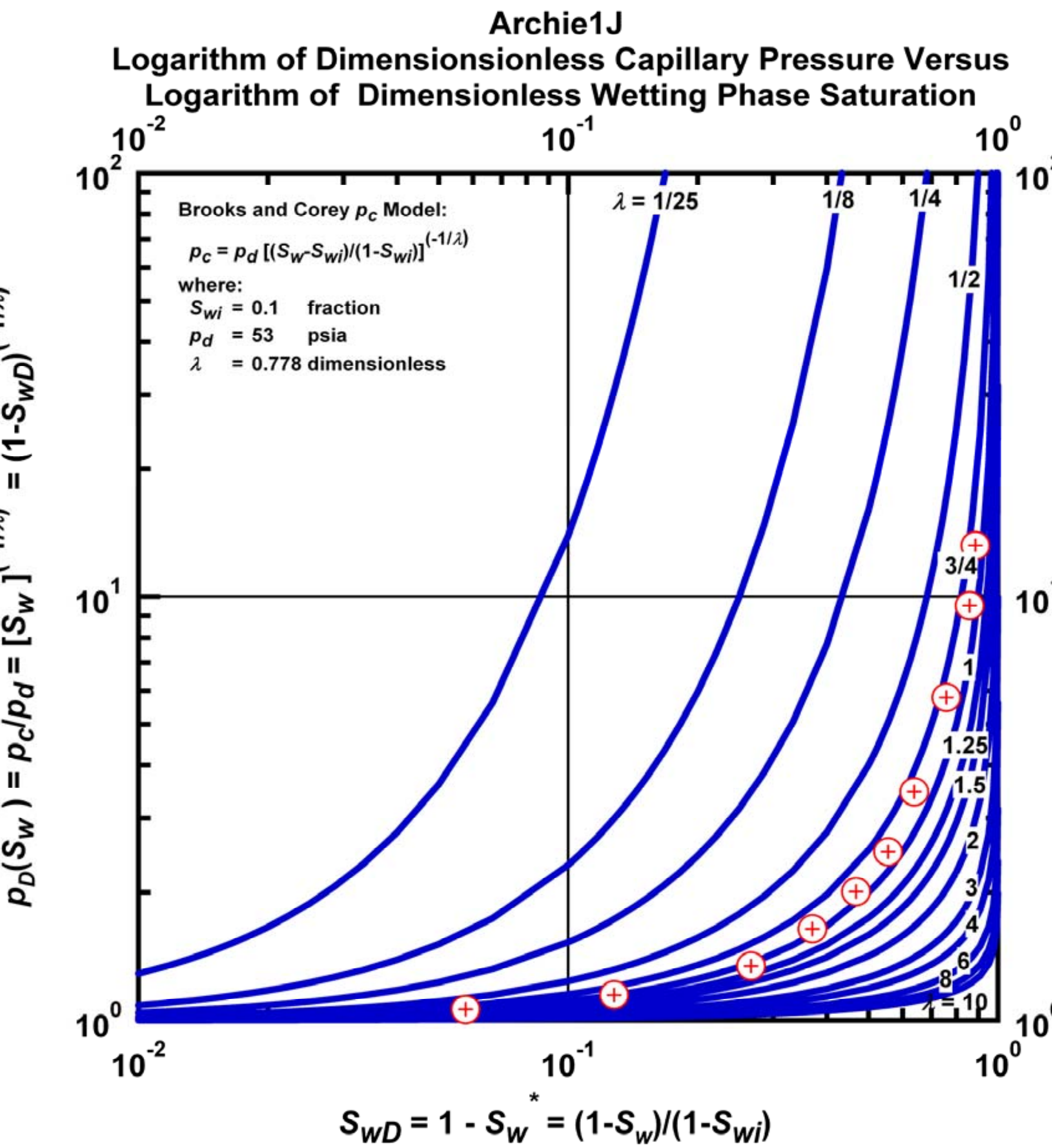

Figure M.23 – Plot of Logarithm of Dimensionless Capillary Pressure Versus Logarithm of Dimensionless Wetting Phase Saturation — Case Archie1J.

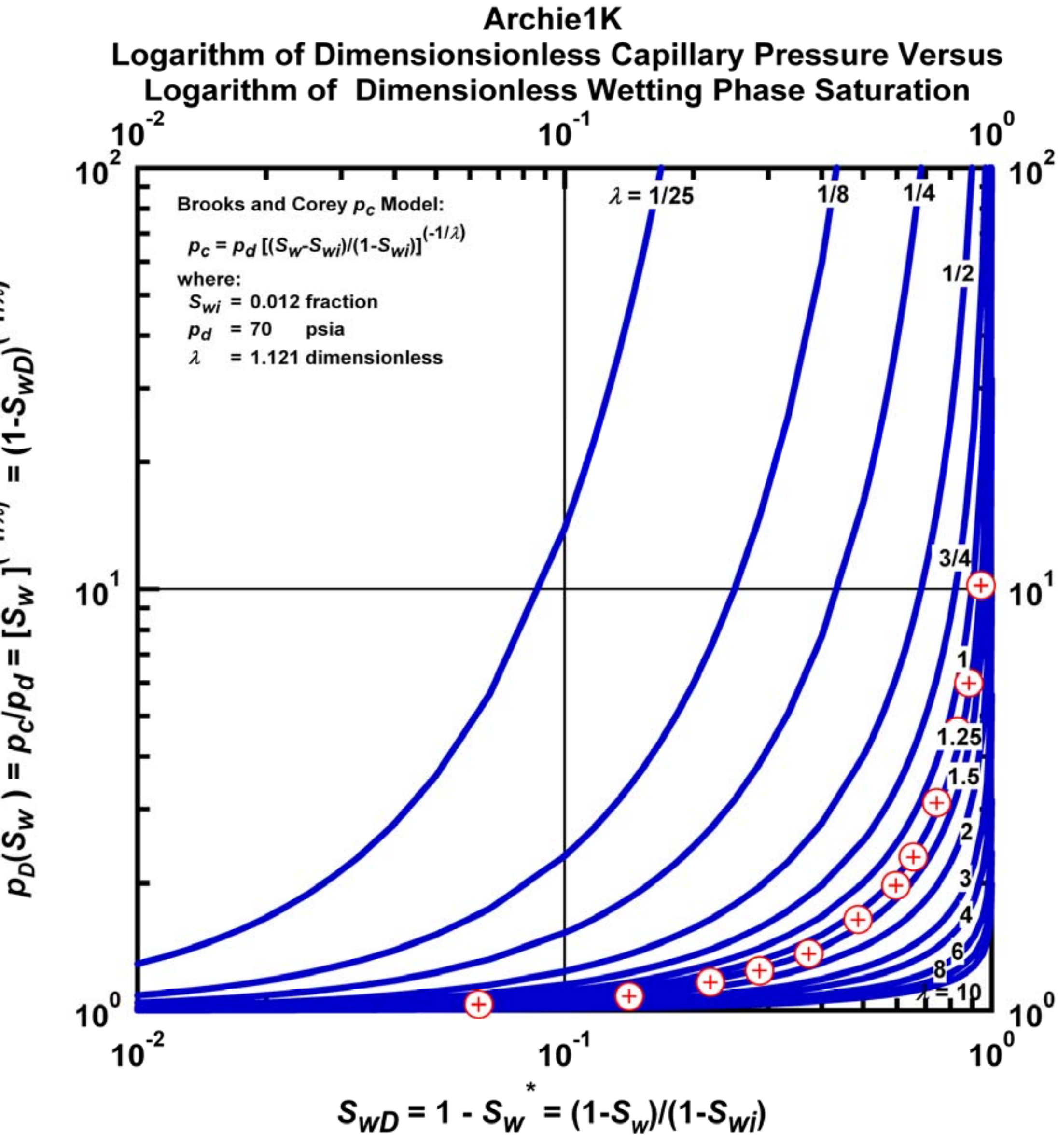

Figure M.24 – Plot of Logarithm of Dimensionless Capillary Pressure Versus Logarithm of Dimensionless Wetting Phase Saturation — Case Archie1K.

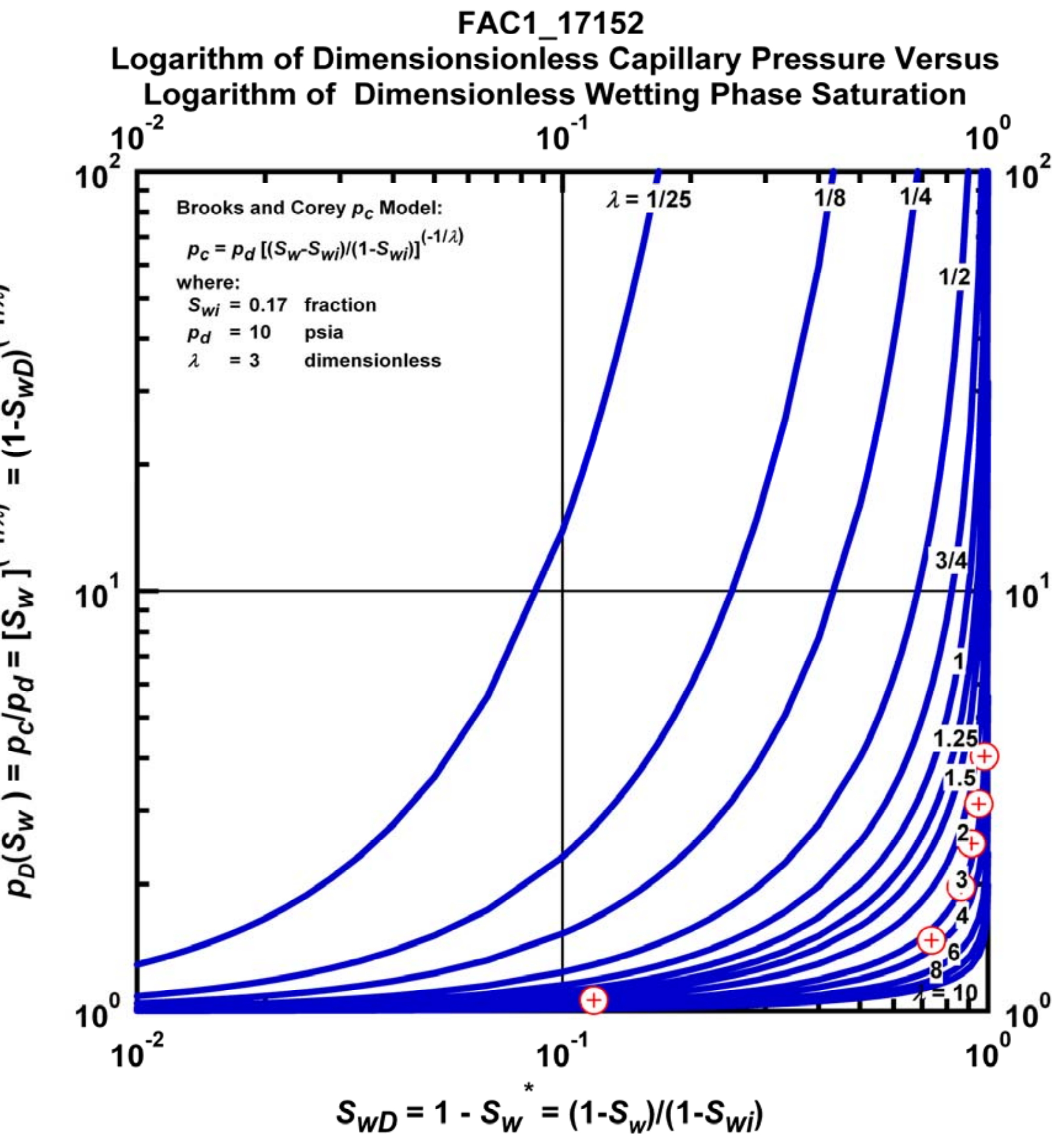

Figure M.25 – Plot of Logarithm of Dimensionless Capillary Pressure Versus Logarithm of Dimensionless Wetting Phase Saturation — Case FAC1_17152.

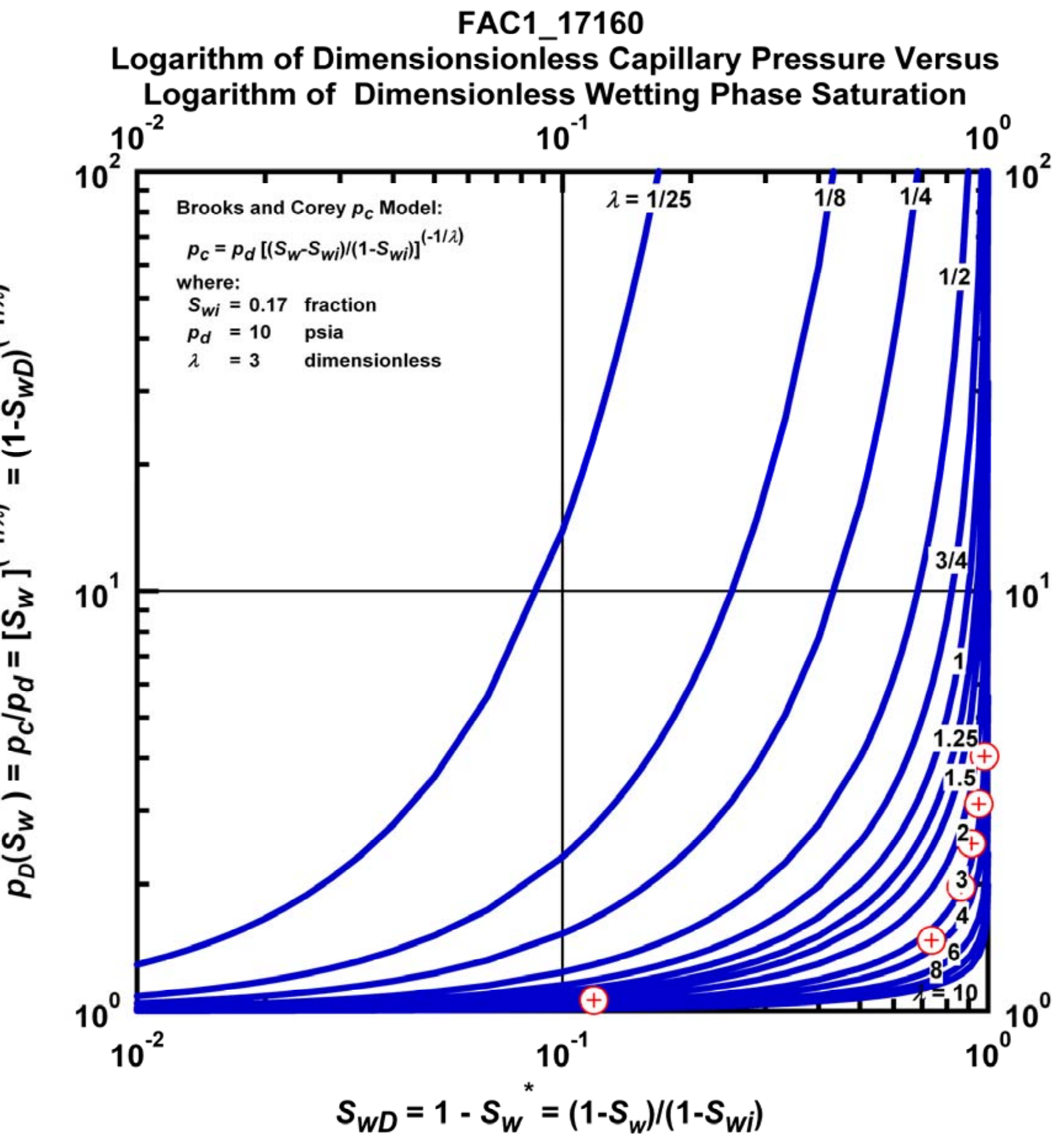

Figure M.26 – Plot of Logarithm of Dimensionless Capillary Pressure Versus Logarithm of Dimensionless Wetting Phase Saturation — Case FAC1_17160.

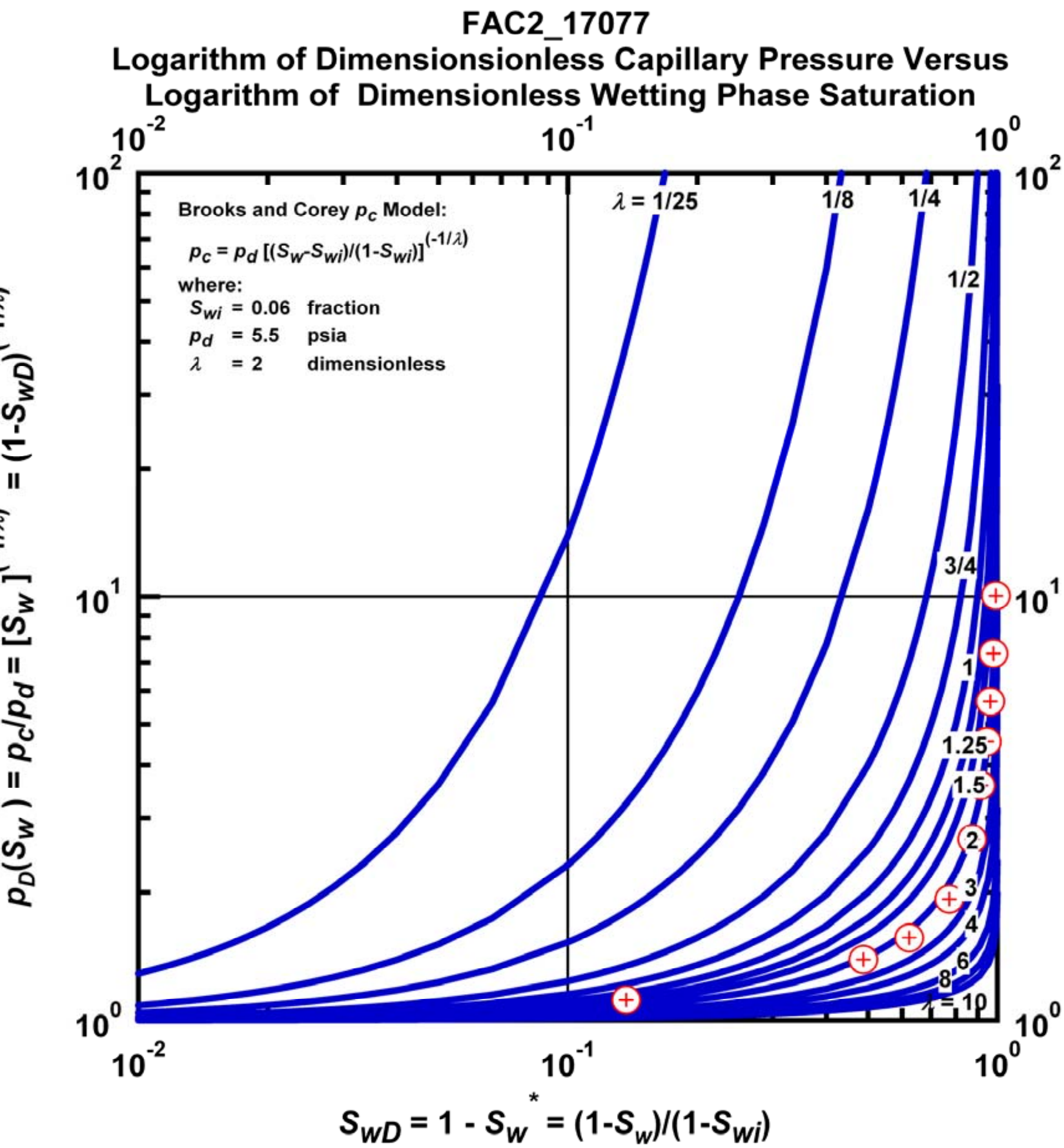

Figure M.27 – Plot of Logarithm of Dimensionless Capillary Pressure Versus Logarithm of Dimensionless Wetting Phase Saturation — Case FAC2_17077.

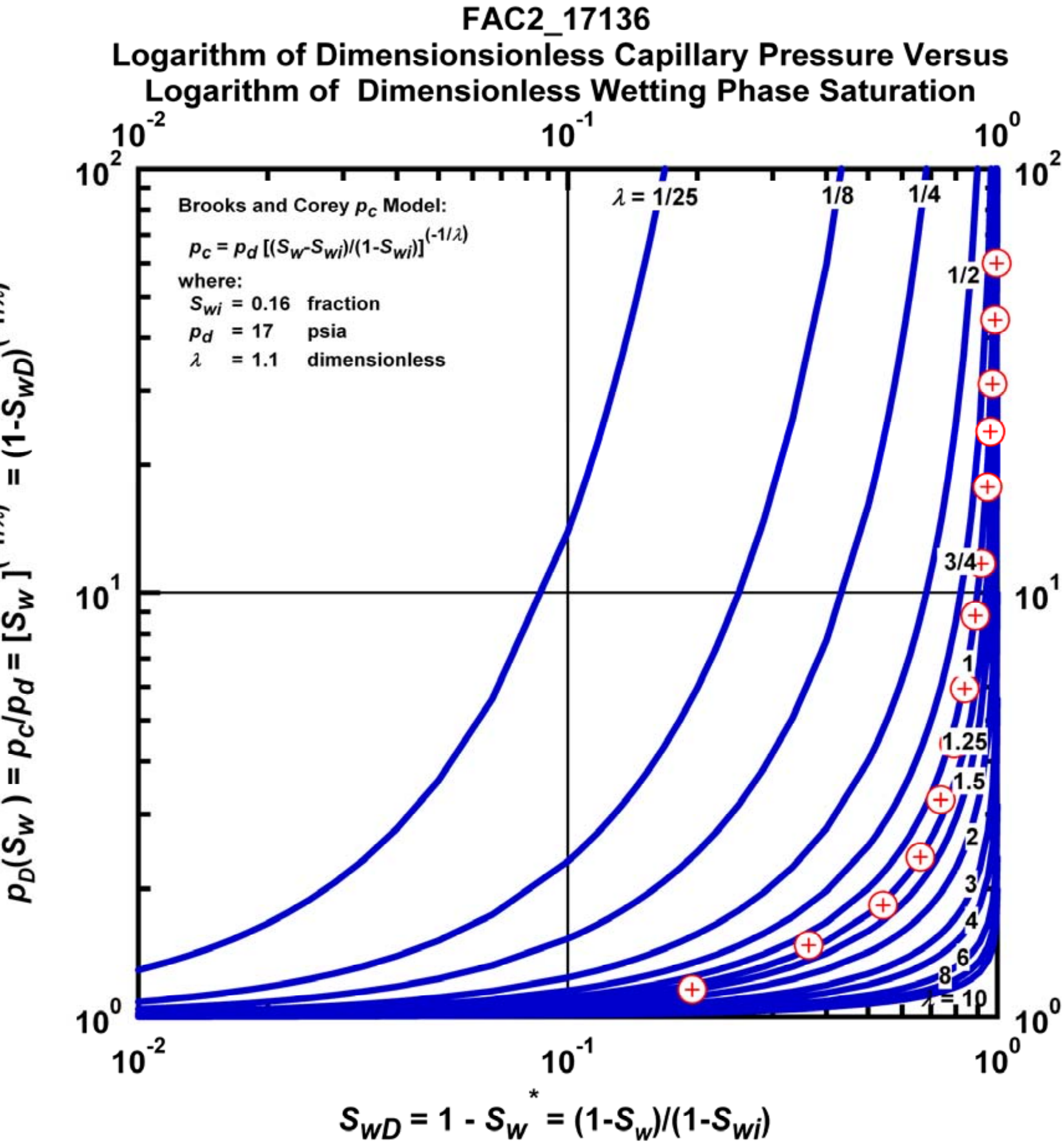

Figure M.28 – Plot of Logarithm of Dimensionless Capillary Pressure Versus Logarithm of Dimensionless Wetting Phase Saturation — Case FAC2_17136.

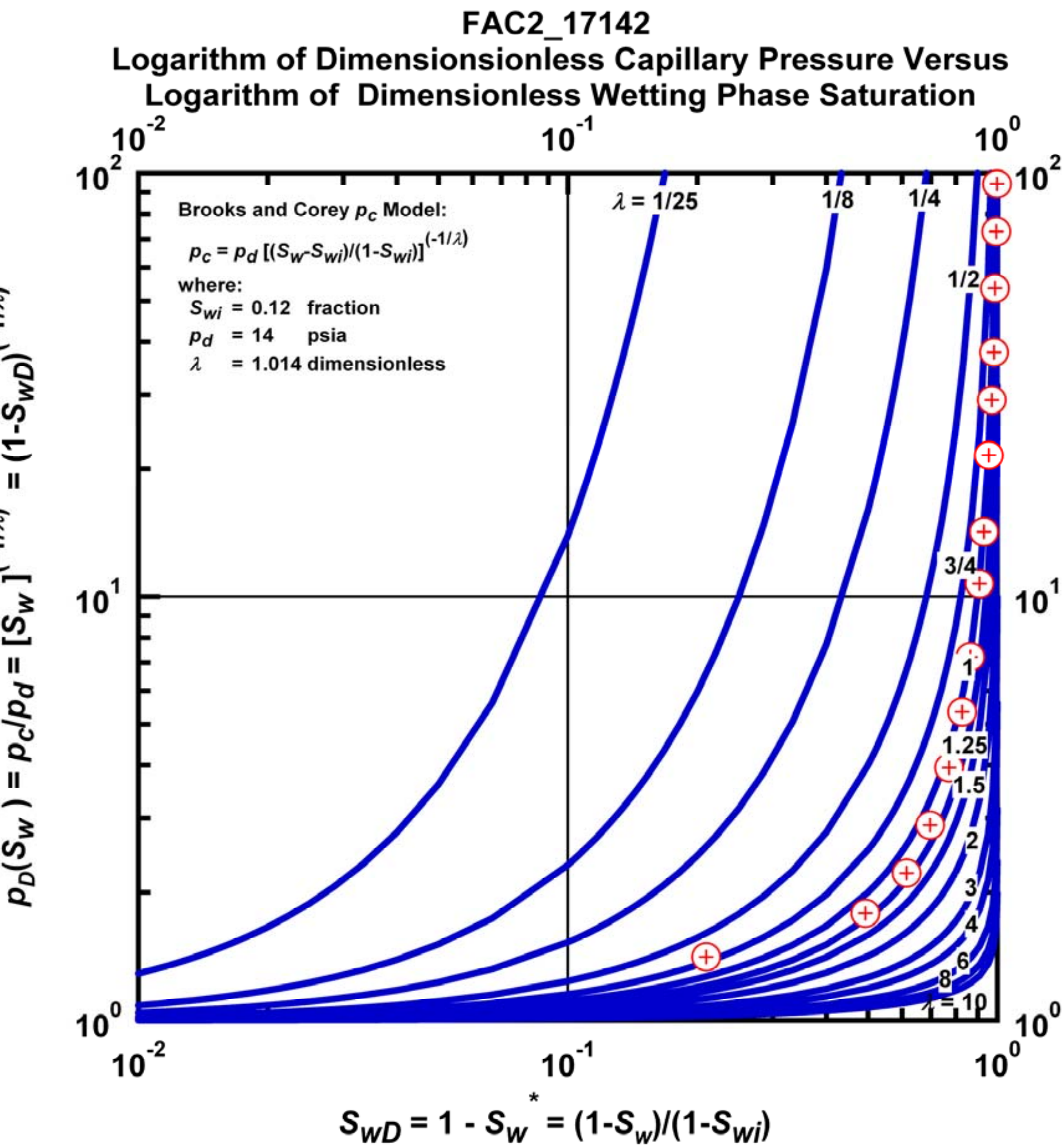

Figure M.29 – Plot of Logarithm of Dimensionless Capillary Pressure Versus Logarithm of Dimensionless Wetting Phase Saturation — Case FAC2_17142.

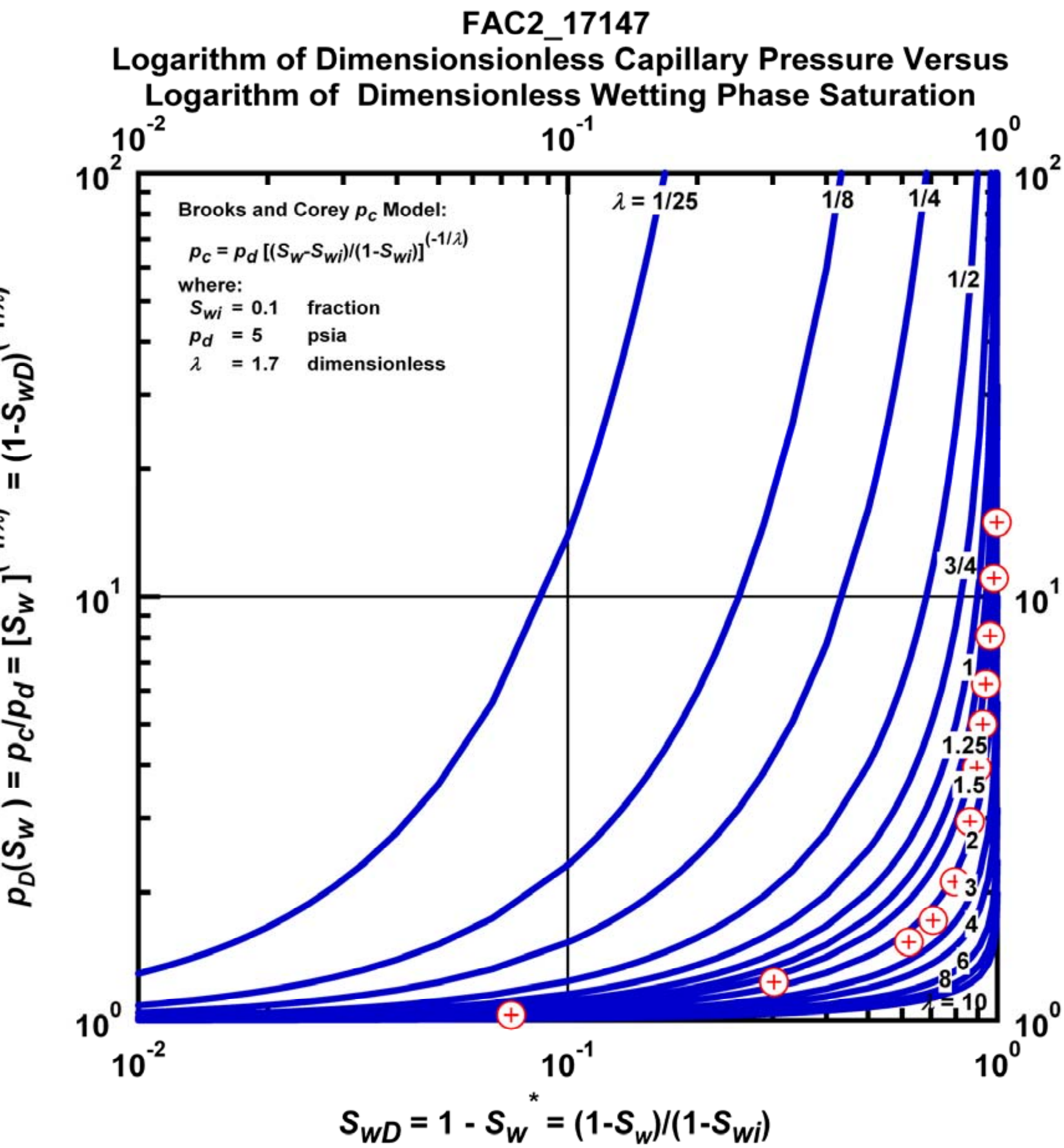

Figure M.30 – Plot of Logarithm of Dimensionless Capillary Pressure Versus Logarithm of Dimensionless Wetting Phase Saturation — Case FAC2_17147.

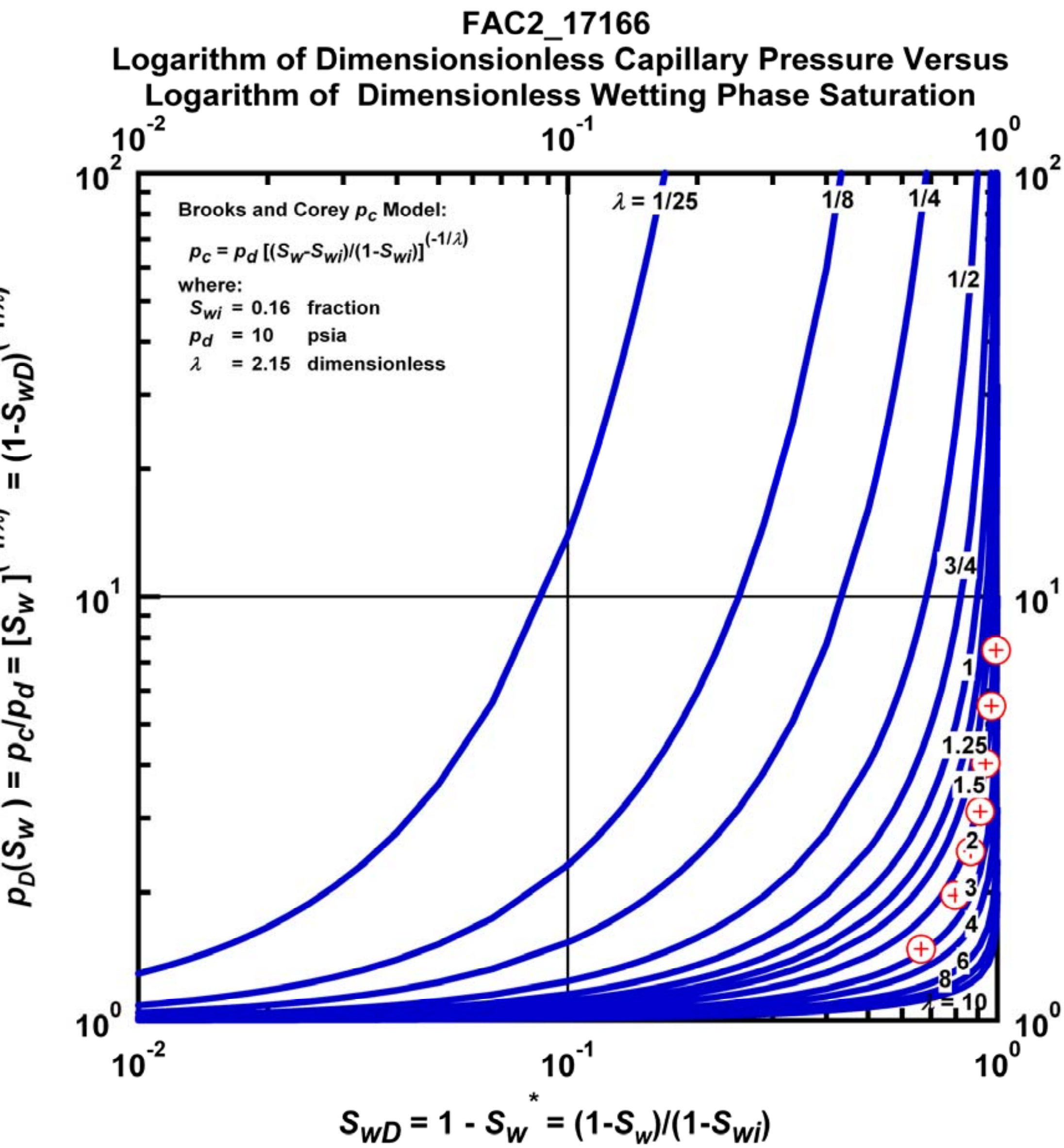

Figure M.31 – Plot of Logarithm of Dimensionless Capillary Pressure Versus Logarithm of Dimensionless Wetting Phase Saturation — Case FAC2_17166.

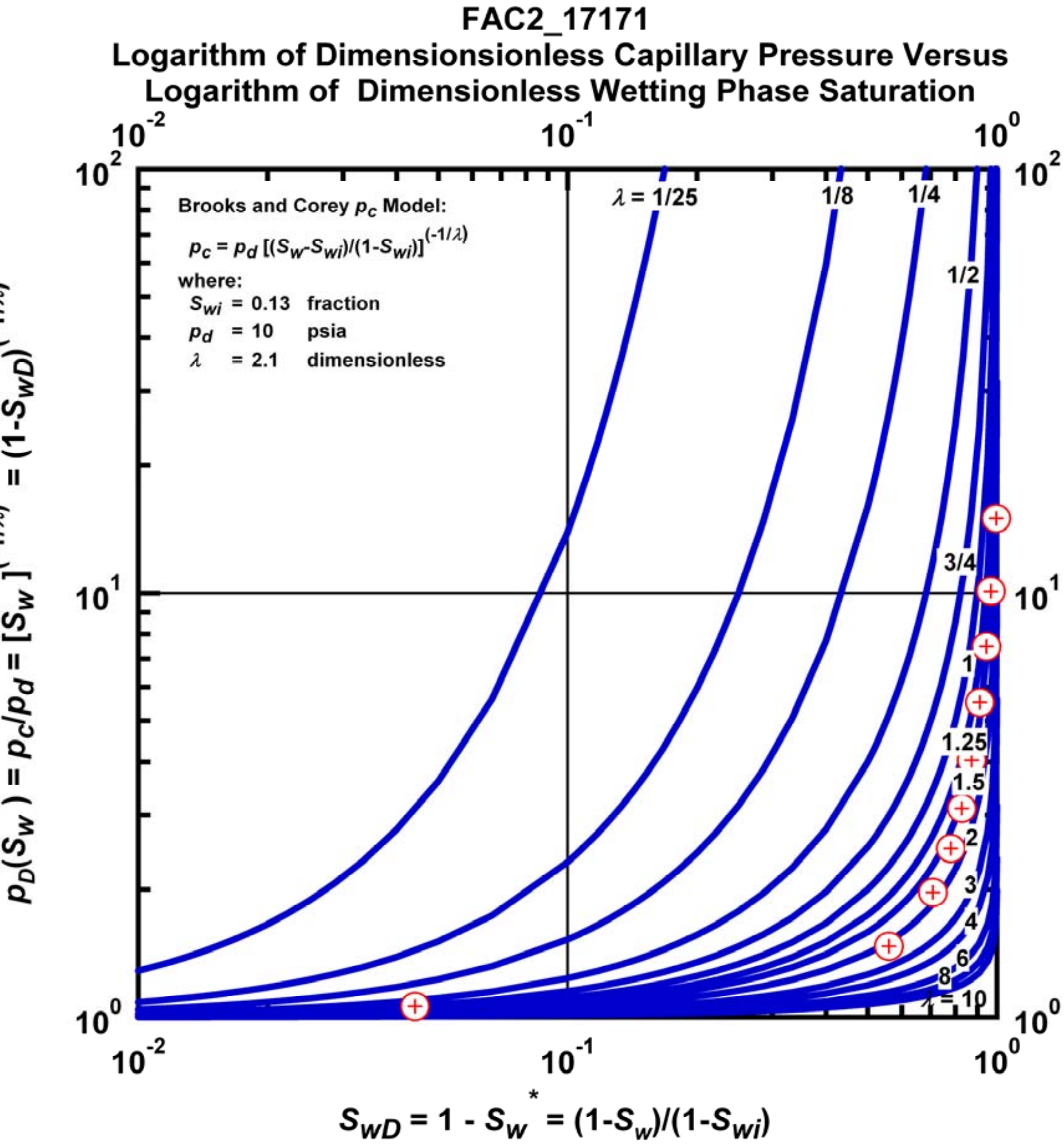

Figure M.32 – Plot of Logarithm of Dimensionless Capillary Pressure Versus Logarithm of Dimensionless Wetting Phase Saturation — Case FAC2_17171.

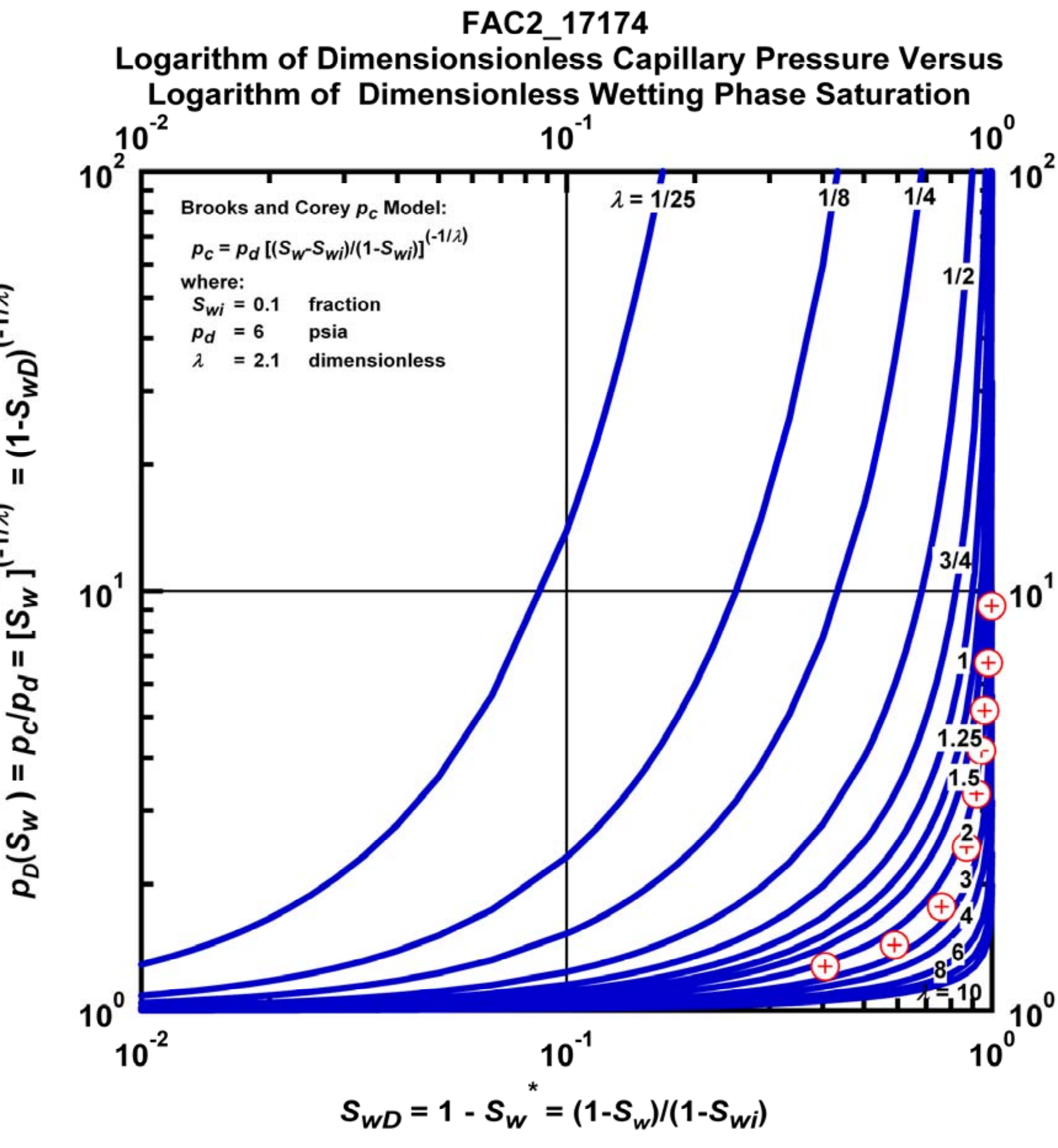

Figure M.33 – Plot of Logarithm of Dimensionless Capillary Pressure Versus Logarithm of Dimensionless Wetting Phase Saturation — Case FAC2_17174.

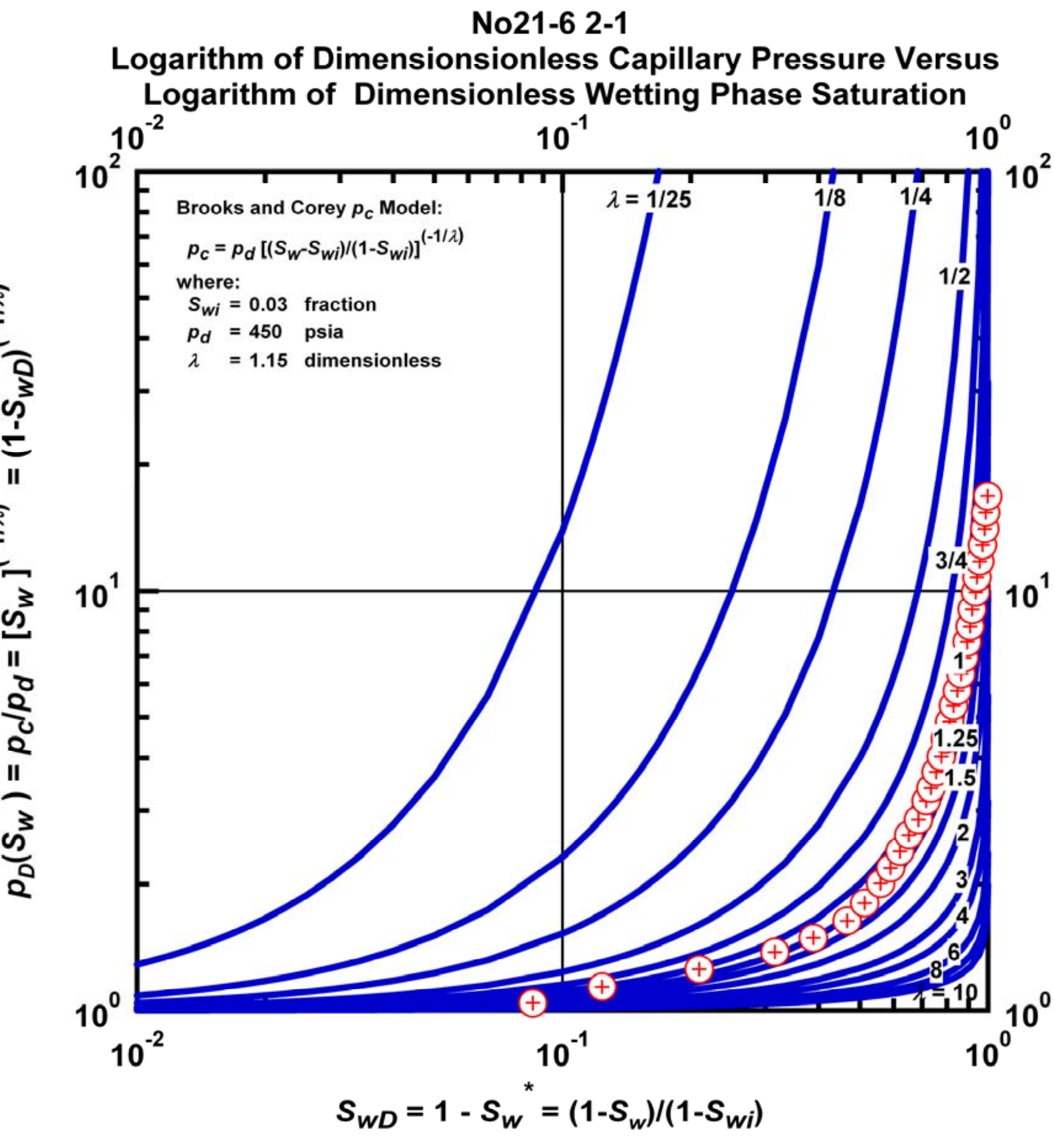

Figure M.34 – Plot of Logarithm of Dimensionless Capillary Pressure Versus Logarithm of Dimensionless Wetting Phase Saturation — Case No21-6 2-1.

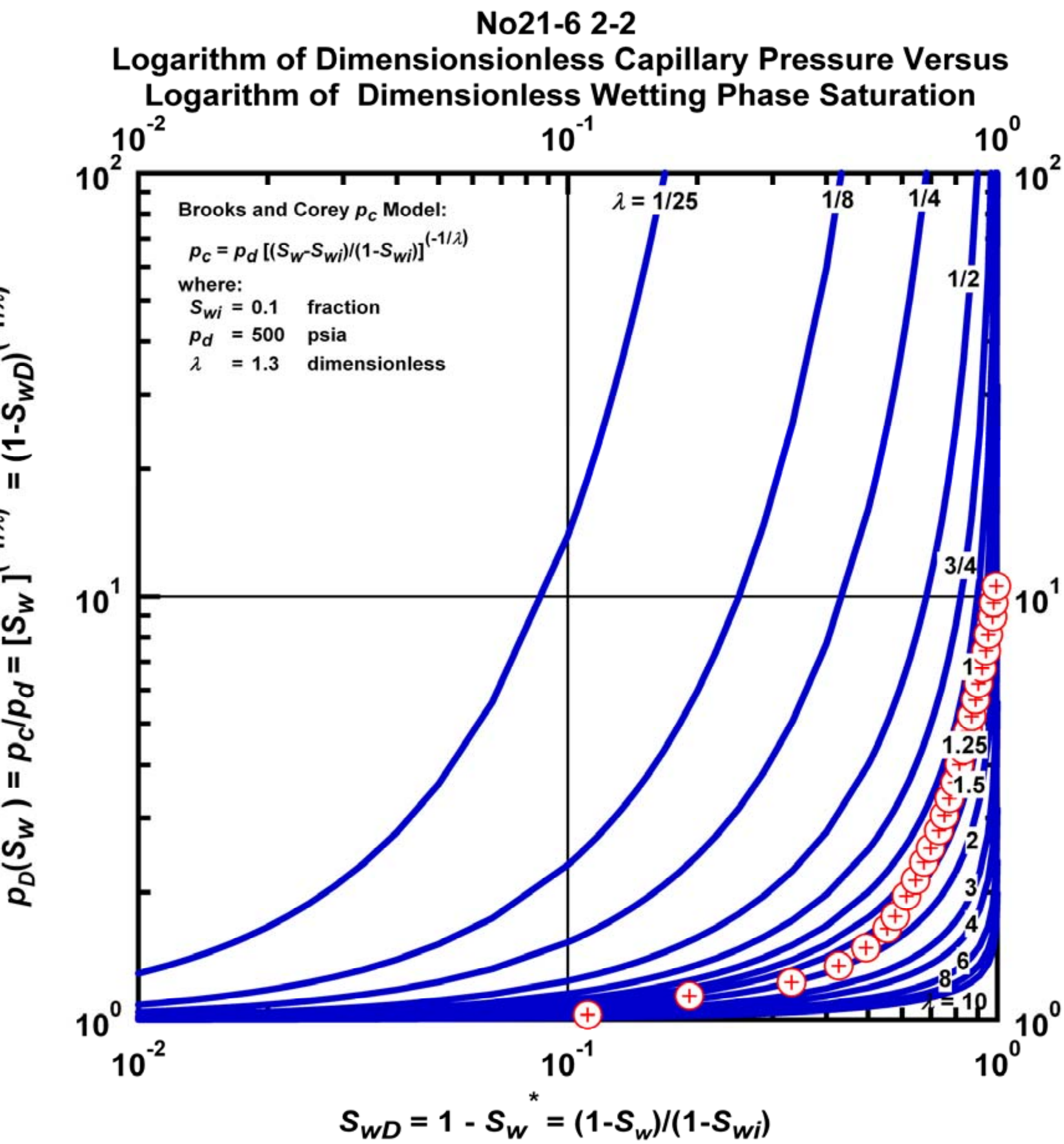

Figure M.35 – Plot of Logarithm of Dimensionless Capillary Pressure Versus Logarithm of Dimensionless Wetting Phase Saturation — Case No21-6 2-2.

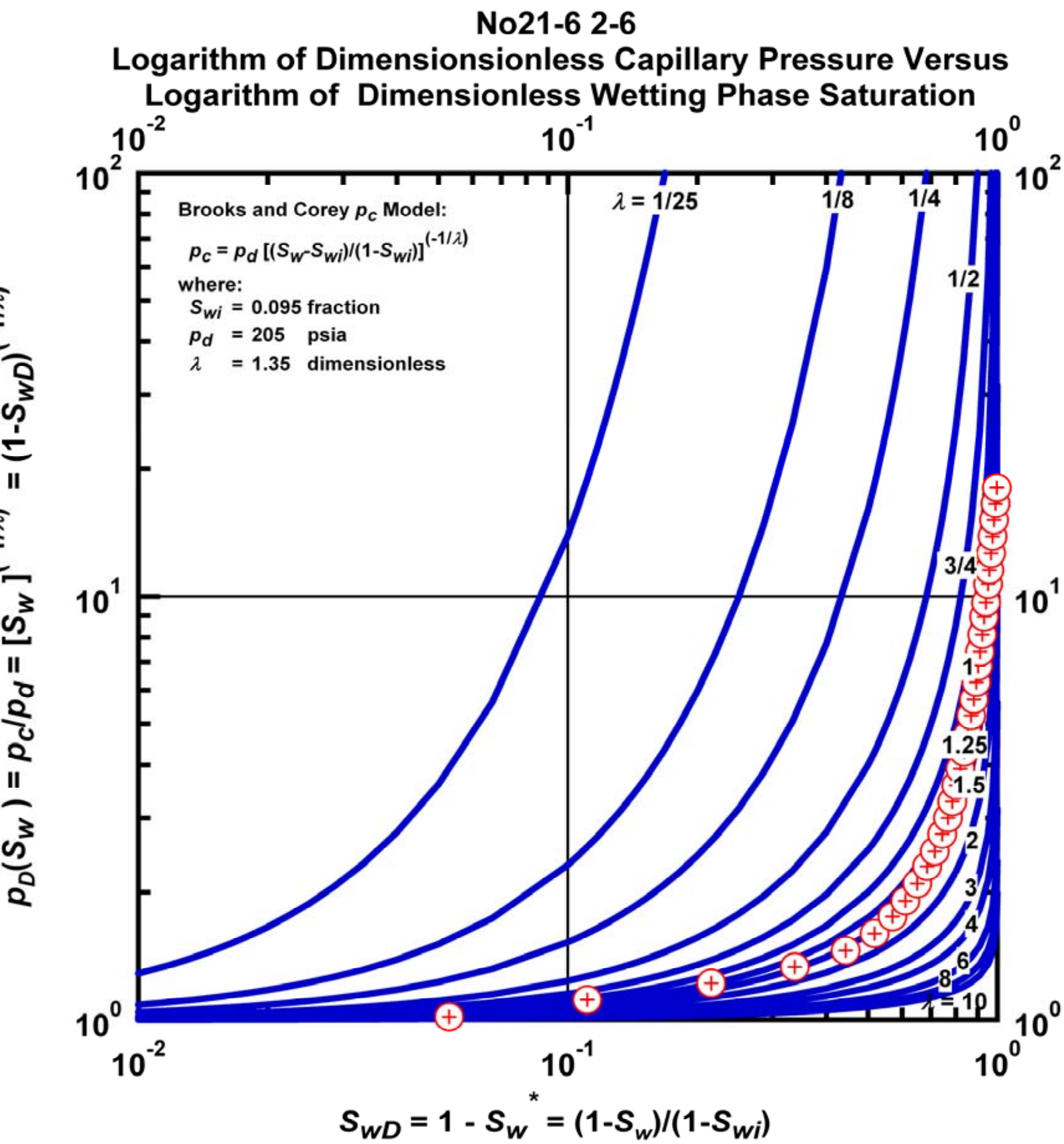

Figure M.36 – Plot of Logarithm of Dimensionless Capillary Pressure Versus Logarithm of Dimensionless Wetting Phase Saturation — Case No21-6 2-2.

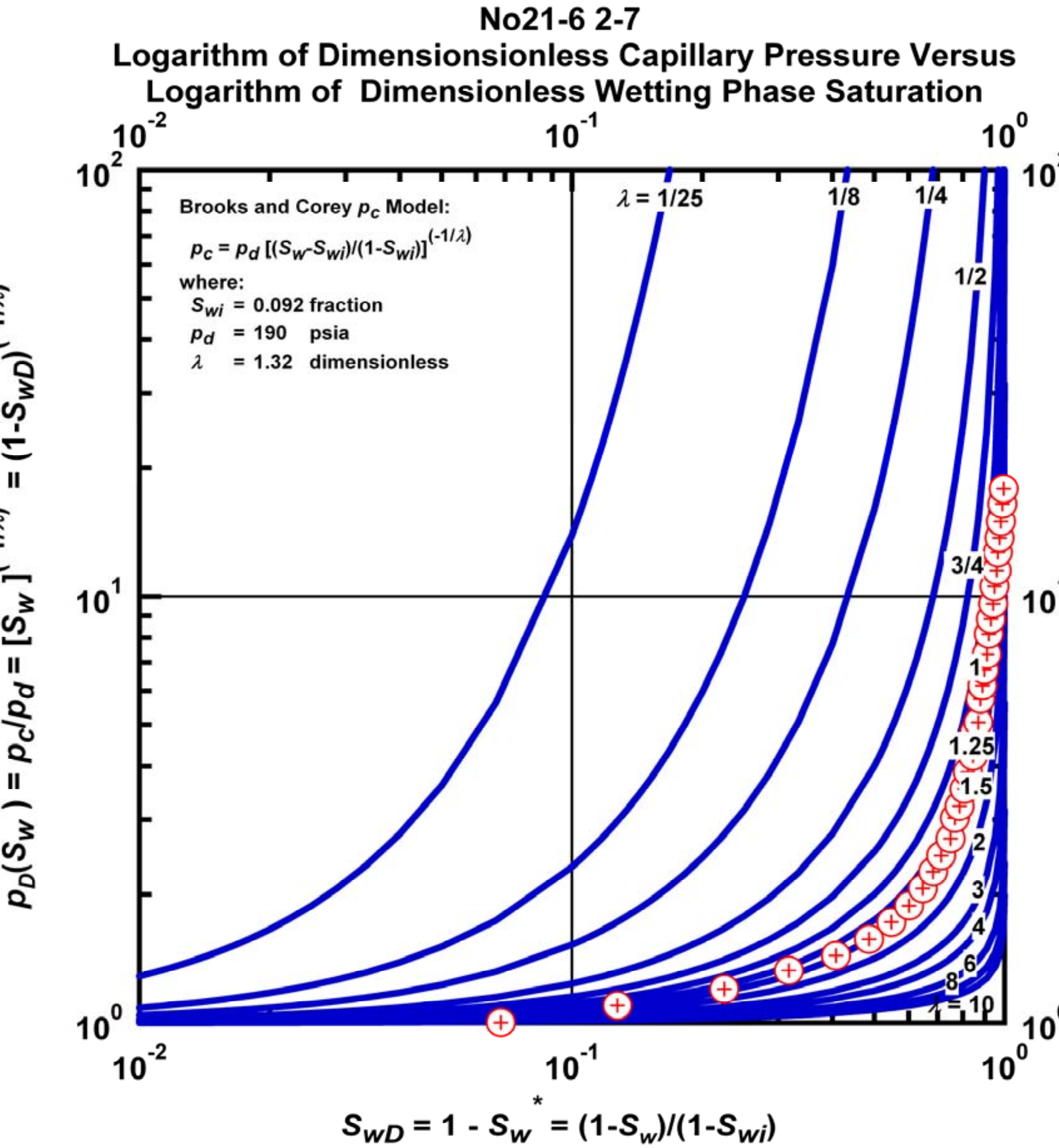

Figure M.37 – Plot of Logarithm of Dimensionless Capillary Pressure Versus Logarithm of Dimensionless Wetting Phase Saturation — Case No21-6 2-7.

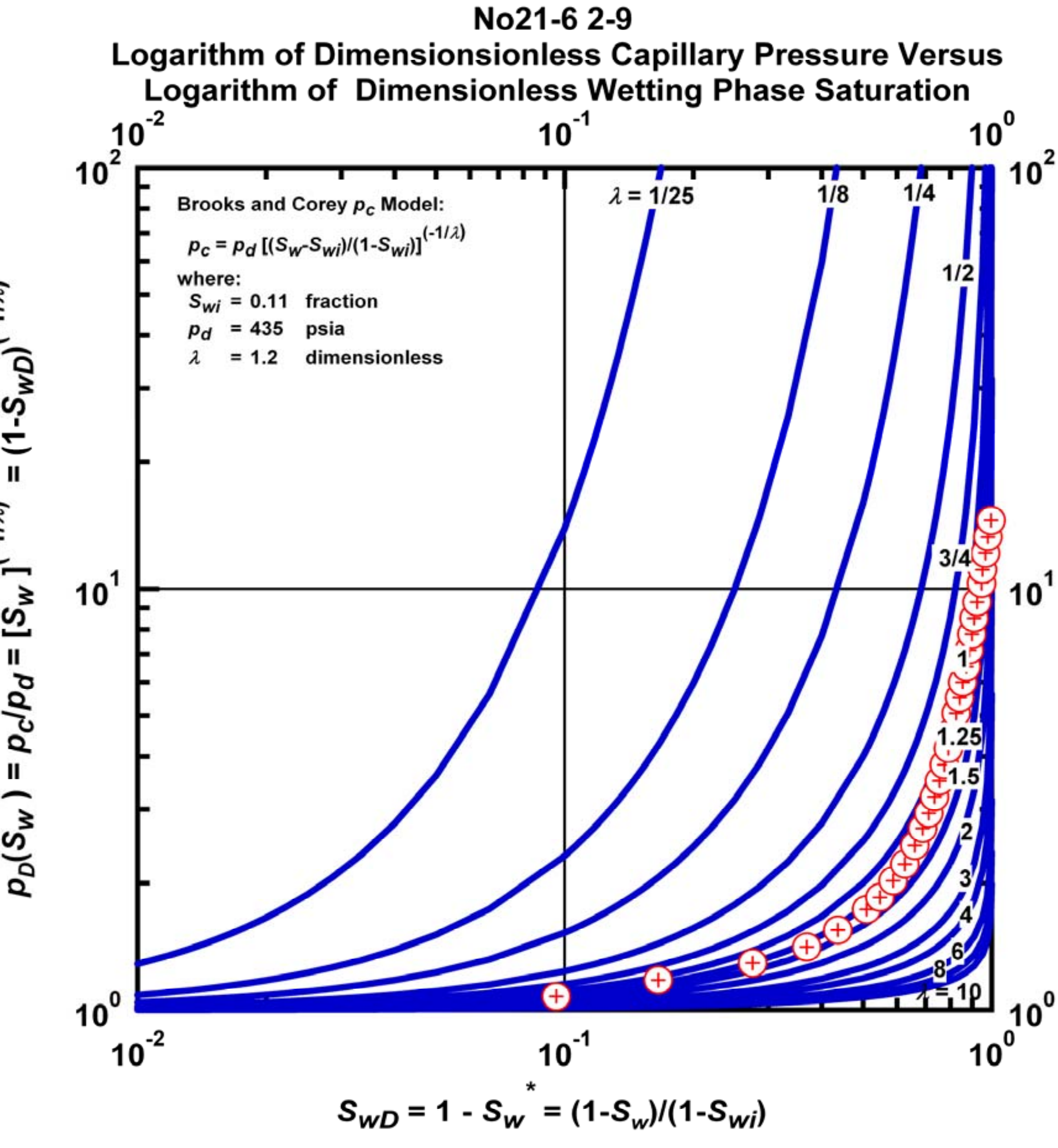

Figure M.38 – Plot of Logarithm of Dimensionless Capillary Pressure Versus Logarithm of Dimensionless Wetting Phase Saturation — Case No21-6 2-9.

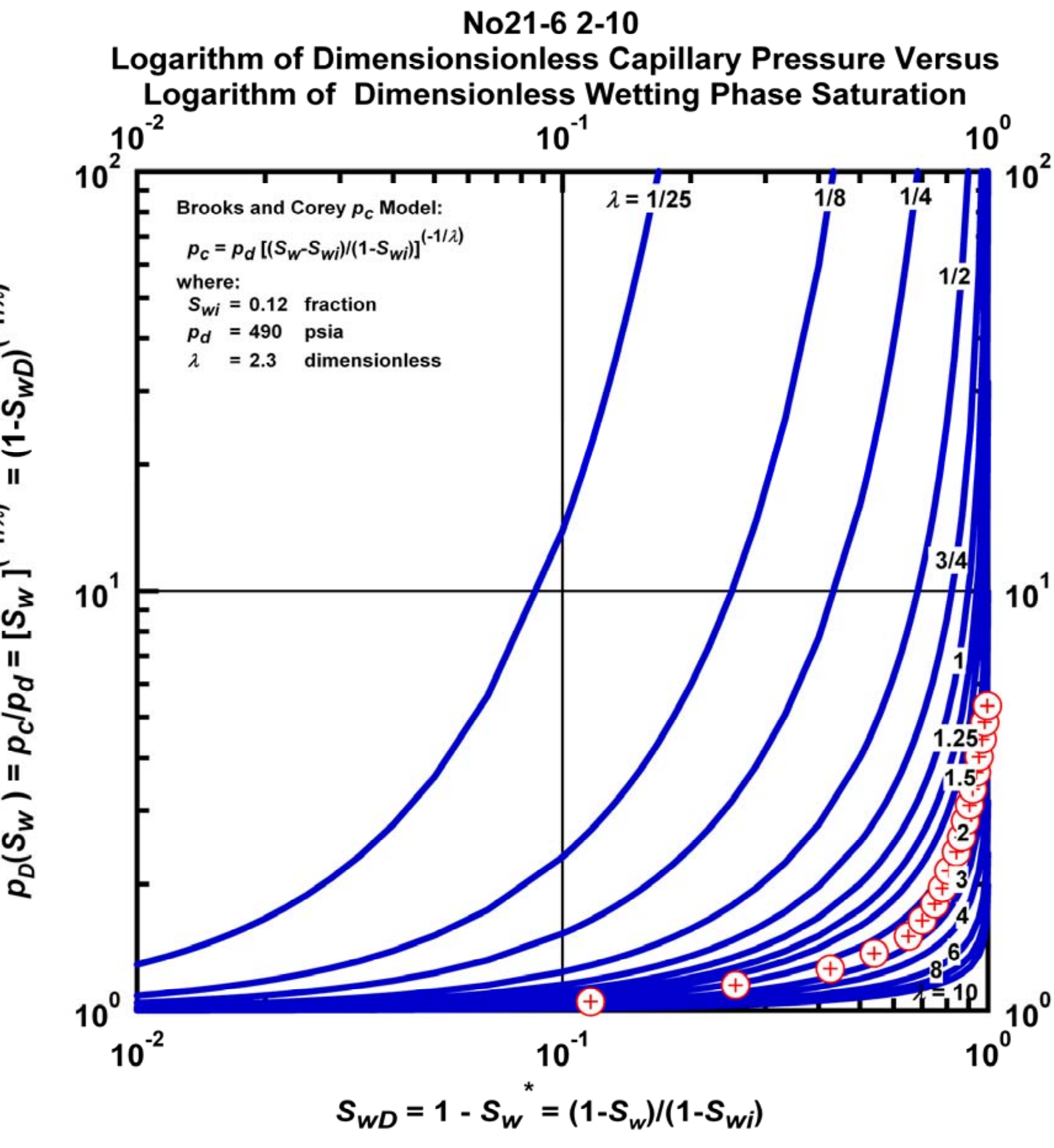

Figure M.39 – Plot of Logarithm of Dimensionless Capillary Pressure Versus Logarithm of Dimensionless Wetting Phase Saturation — Case No21-6 2-10.

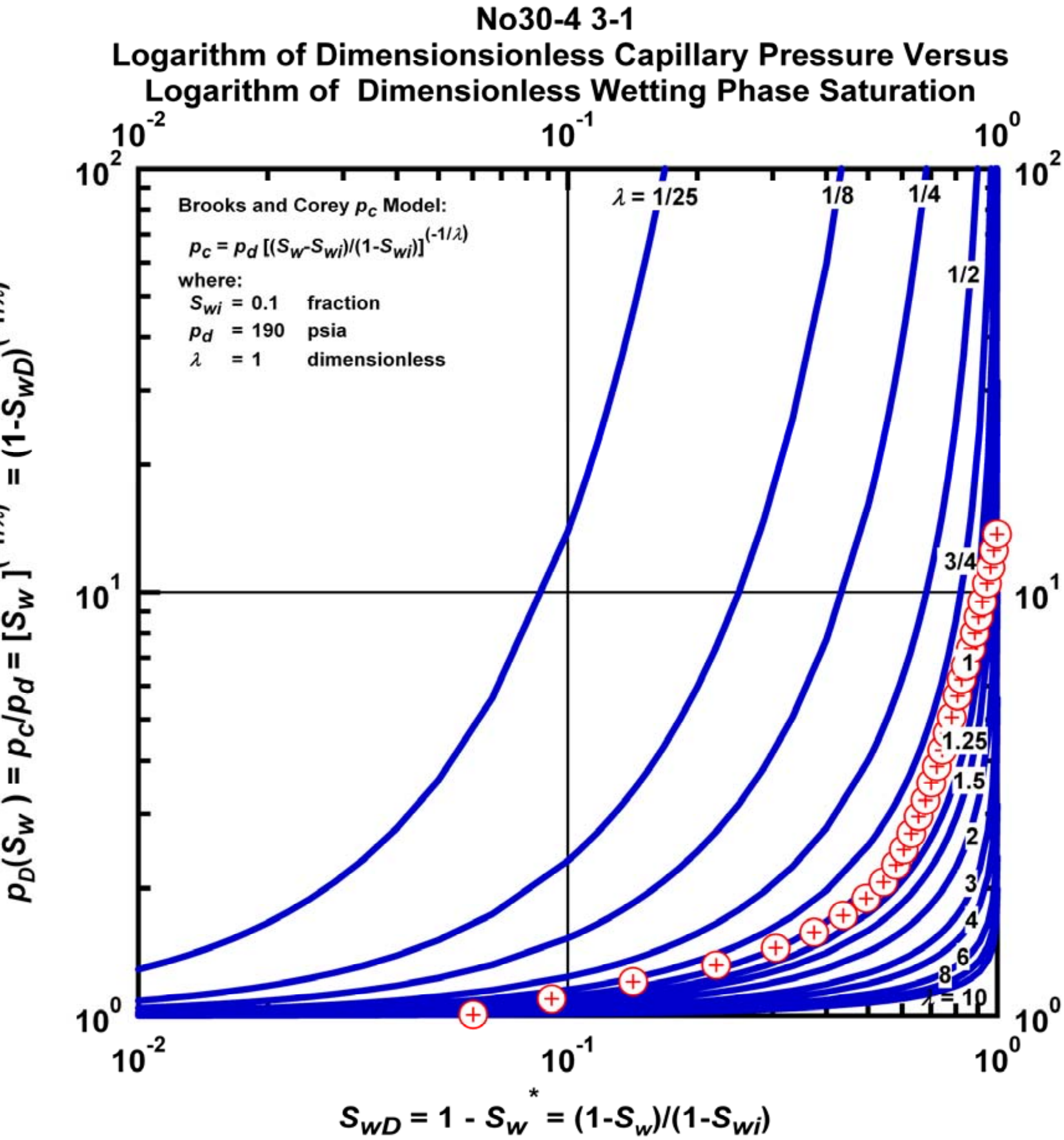

Figure M.40 – Plot of Logarithm of Dimensionless Capillary Pressure Versus Logarithm of Dimensionless Wetting Phase Saturation — Case No30-4 3-1.

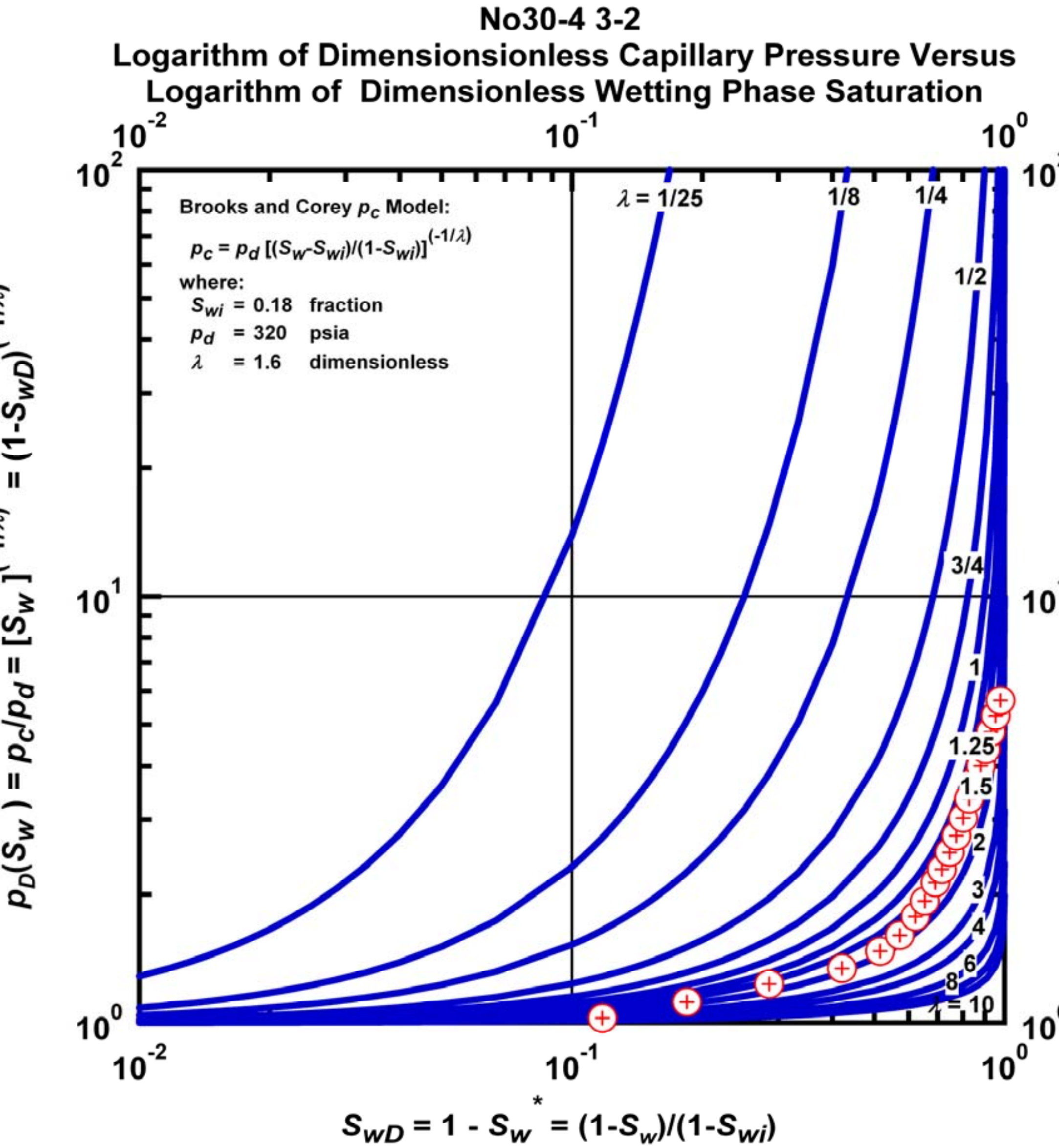

Figure M.41 – Plot of Logarithm of Dimensionless Capillary Pressure Versus Logarithm of Dimensionless Wetting Phase Saturation — Case No30-4 3-2.

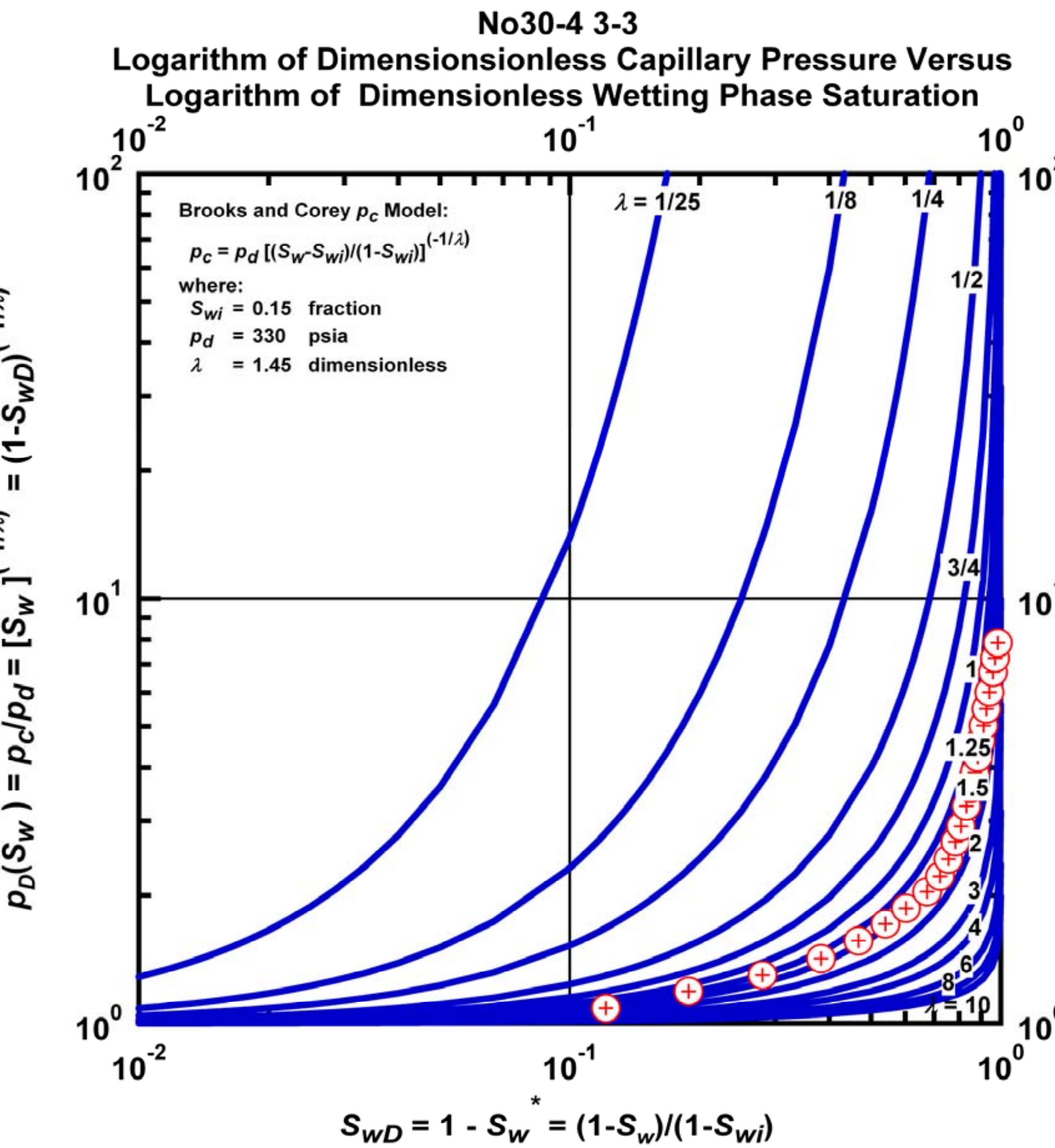

Figure M.42 – Plot of Logarithm of Dimensionless Capillary Pressure Versus Logarithm of Dimensionless Wetting Phase Saturation — Case No30-4 3-3.

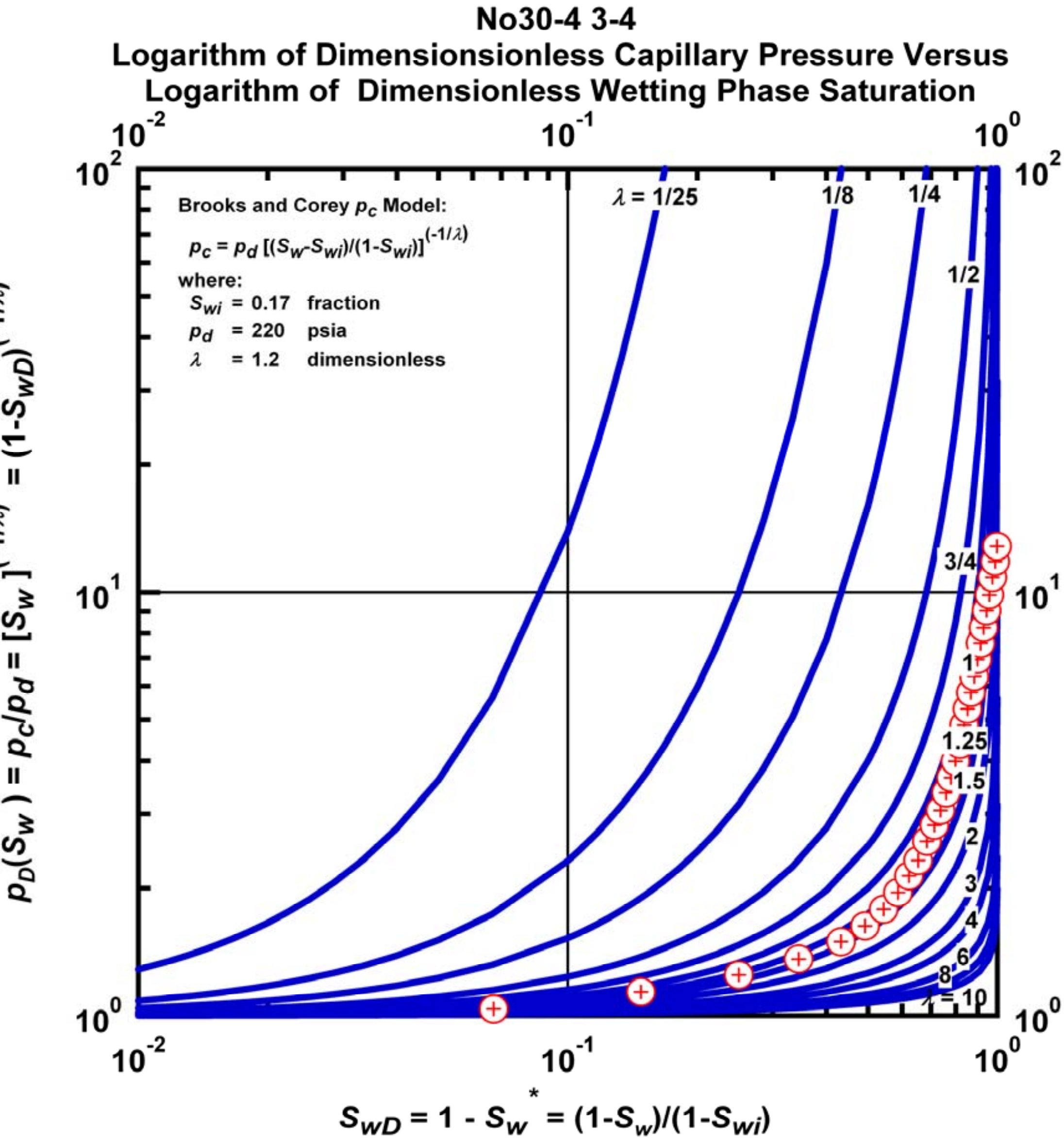

Figure M.43 – Plot of Logarithm of Dimensionless Capillary Pressure Versus Logarithm of Dimensionless Wetting Phase Saturation — Case No30-4 3-4.

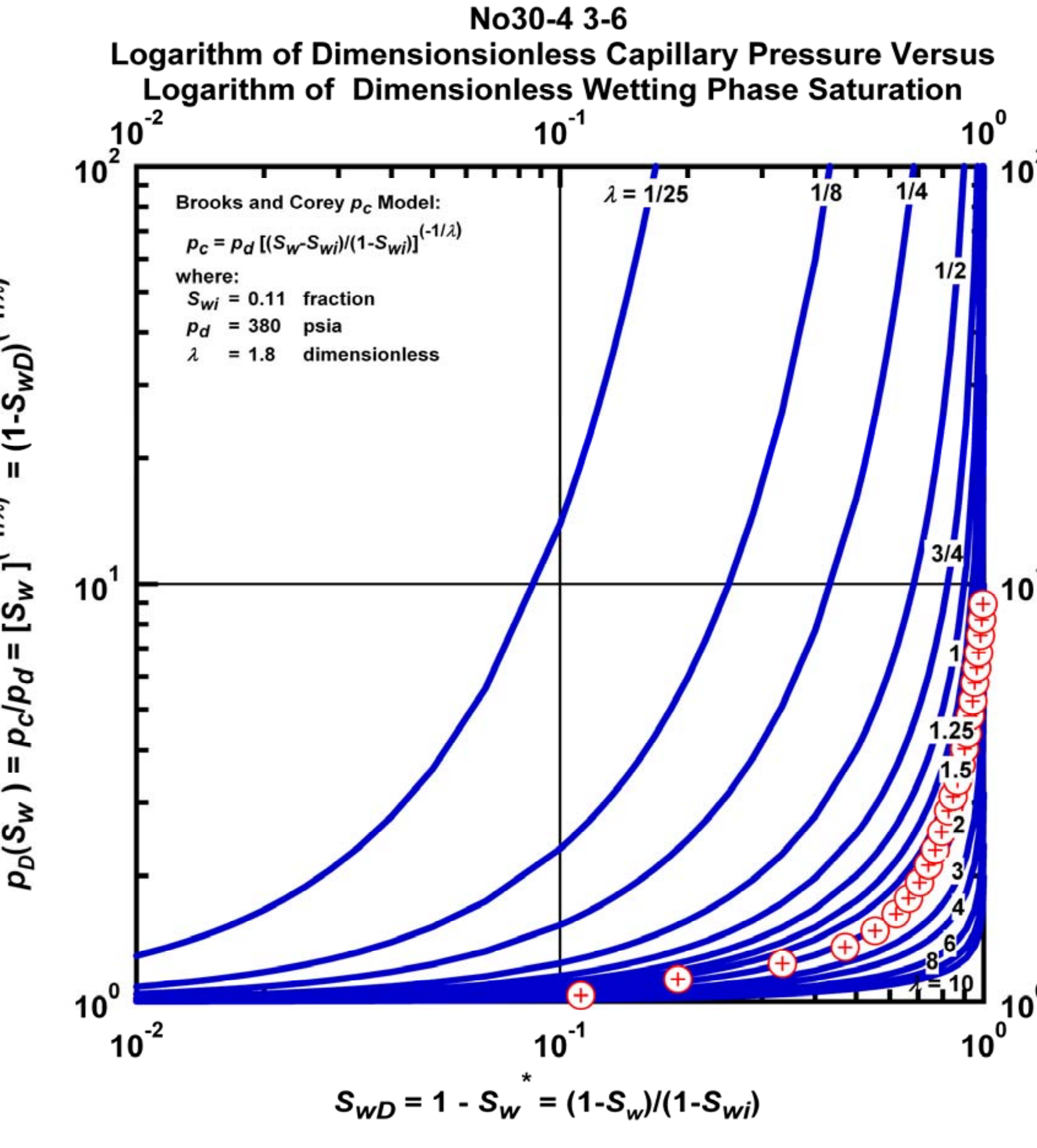

Figure M.44 – Plot of Logarithm of Dimensionless Capillary Pressure Versus Logarithm of Dimensionless Wetting Phase Saturation — Case No30-4 3-6.

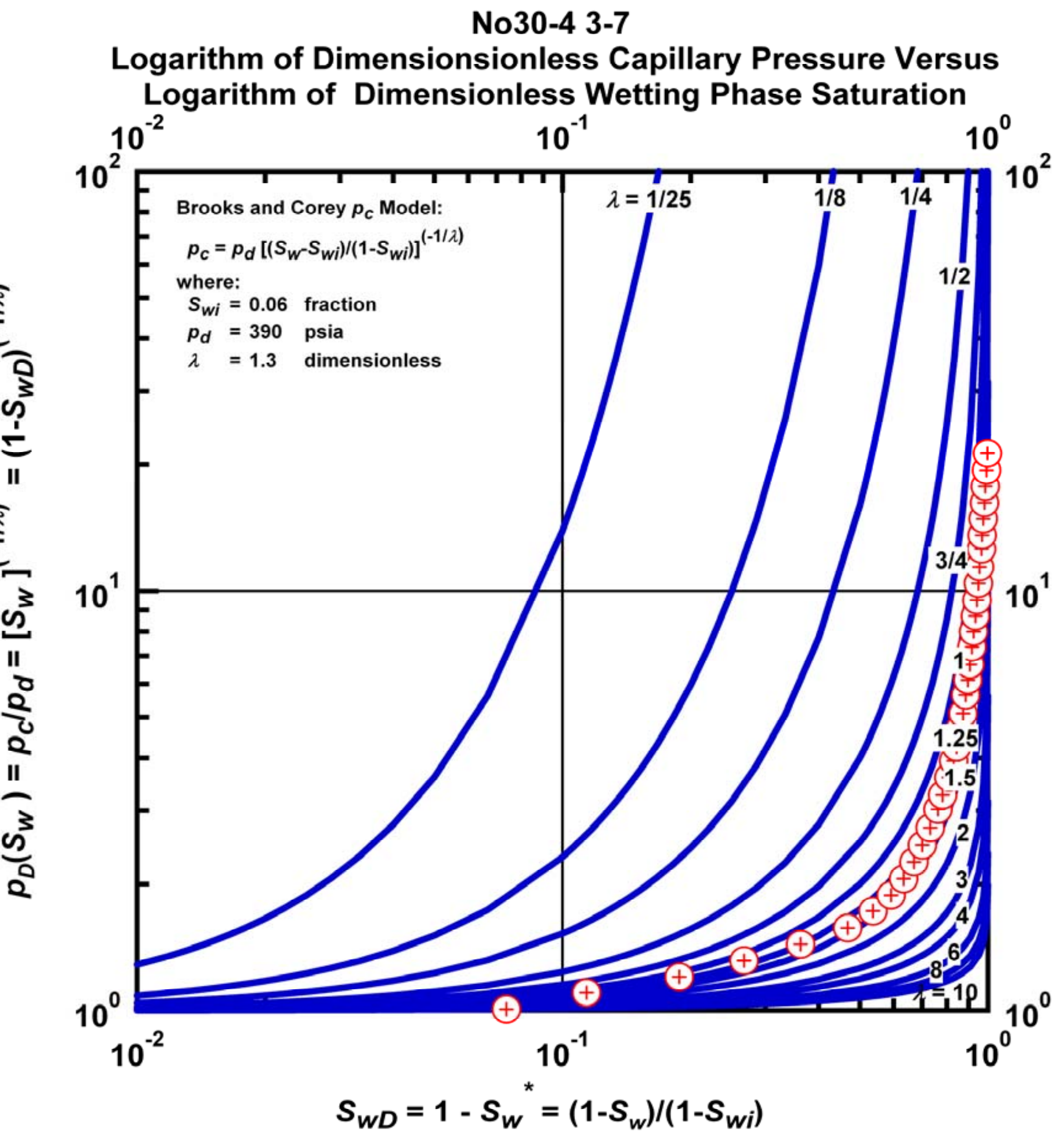

Figure M.45 – Plot of Logarithm of Dimensionless Capillary Pressure Versus Logarithm of Dimensionless Wetting Phase Saturation — Case No30-4 3-7.

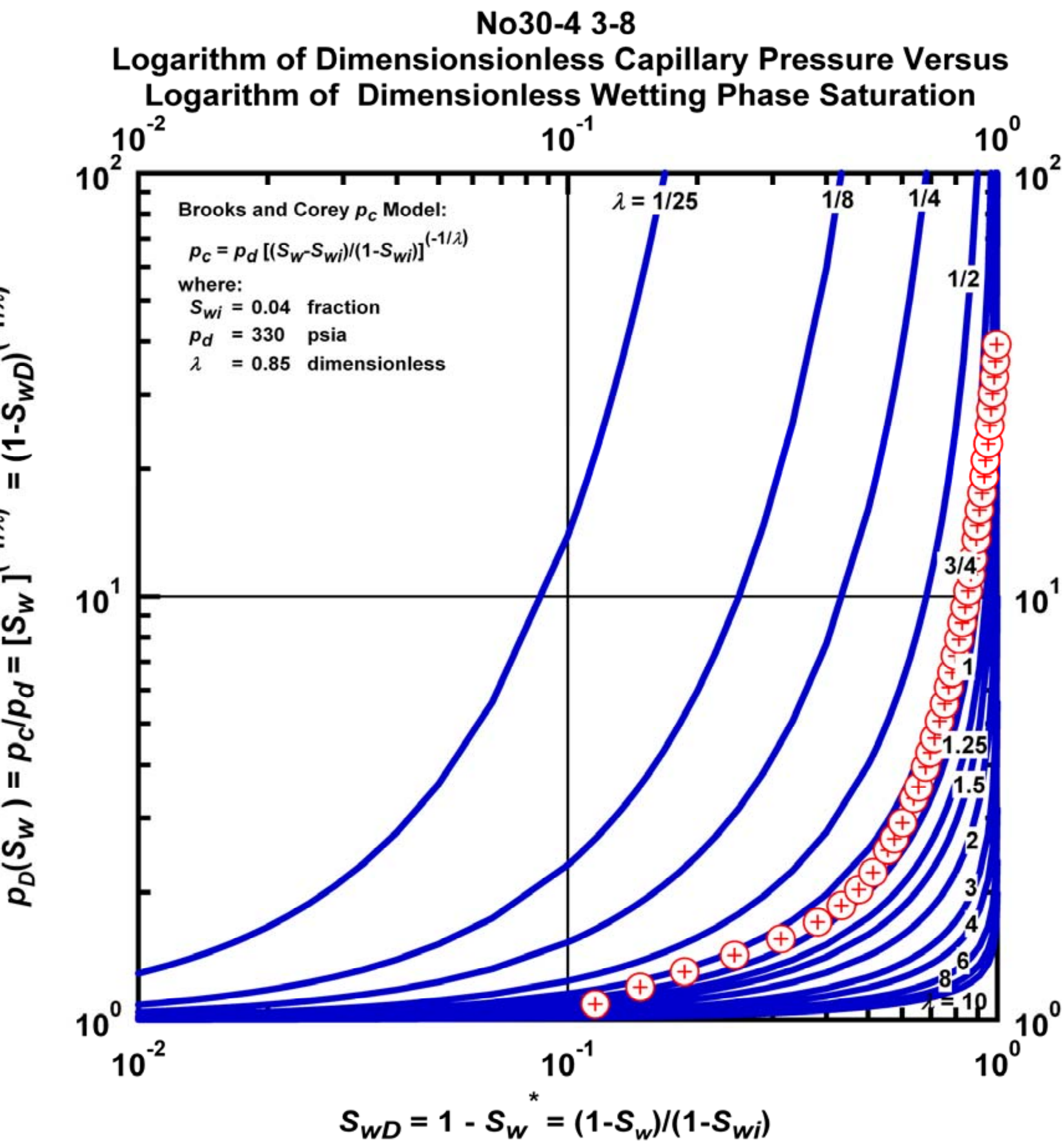

Figure M.46 – Plot of Logarithm of Dimensionless Capillary Pressure Versus Logarithm of Dimensionless Wetting Phase Saturation — Case No30-4 3-8.

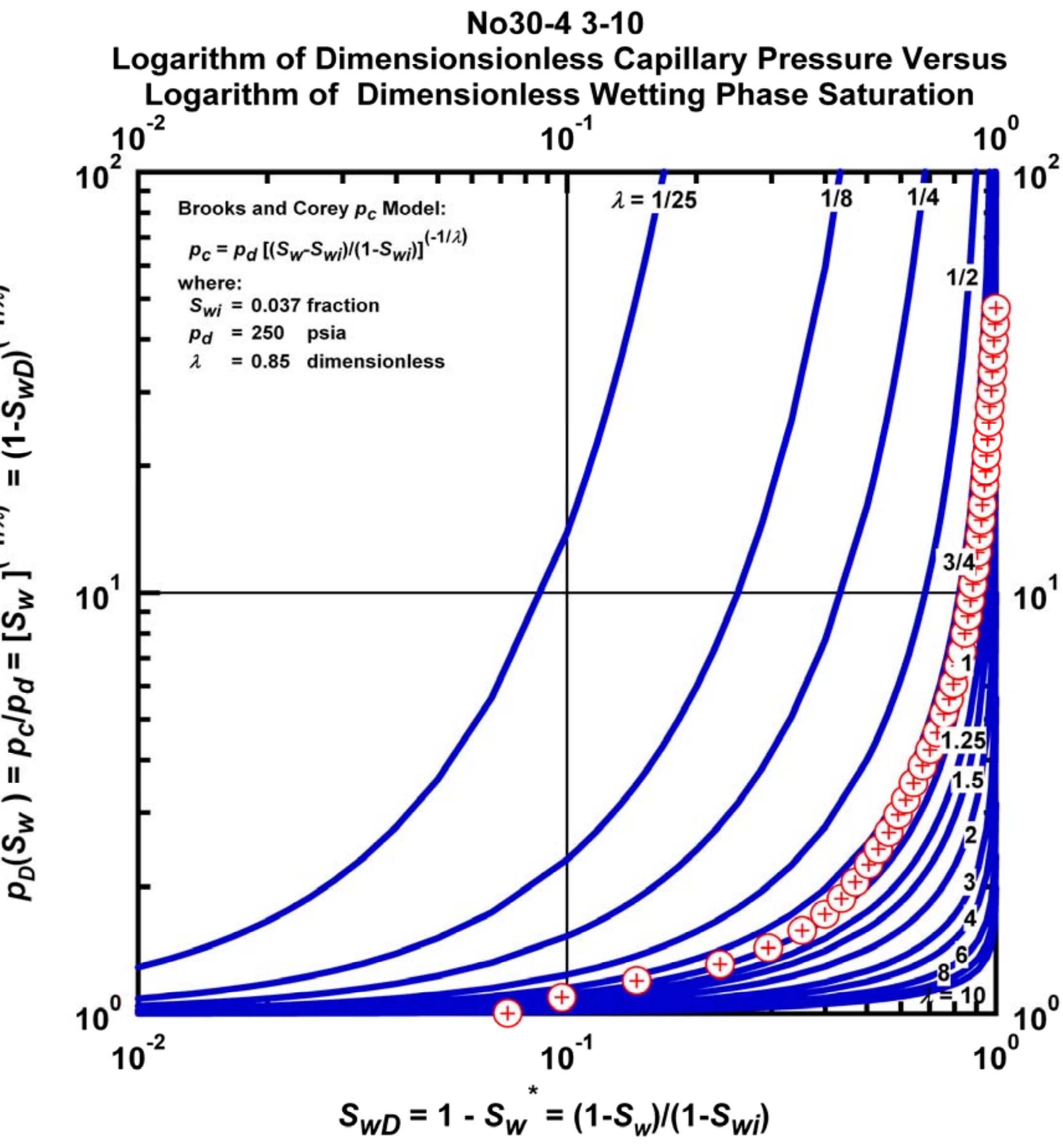

Figure M.47 – Plot of Logarithm of Dimensionless Capillary Pressure Versus Logarithm of Dimensionless Wetting Phase Saturation — Case No30-4 3-10.

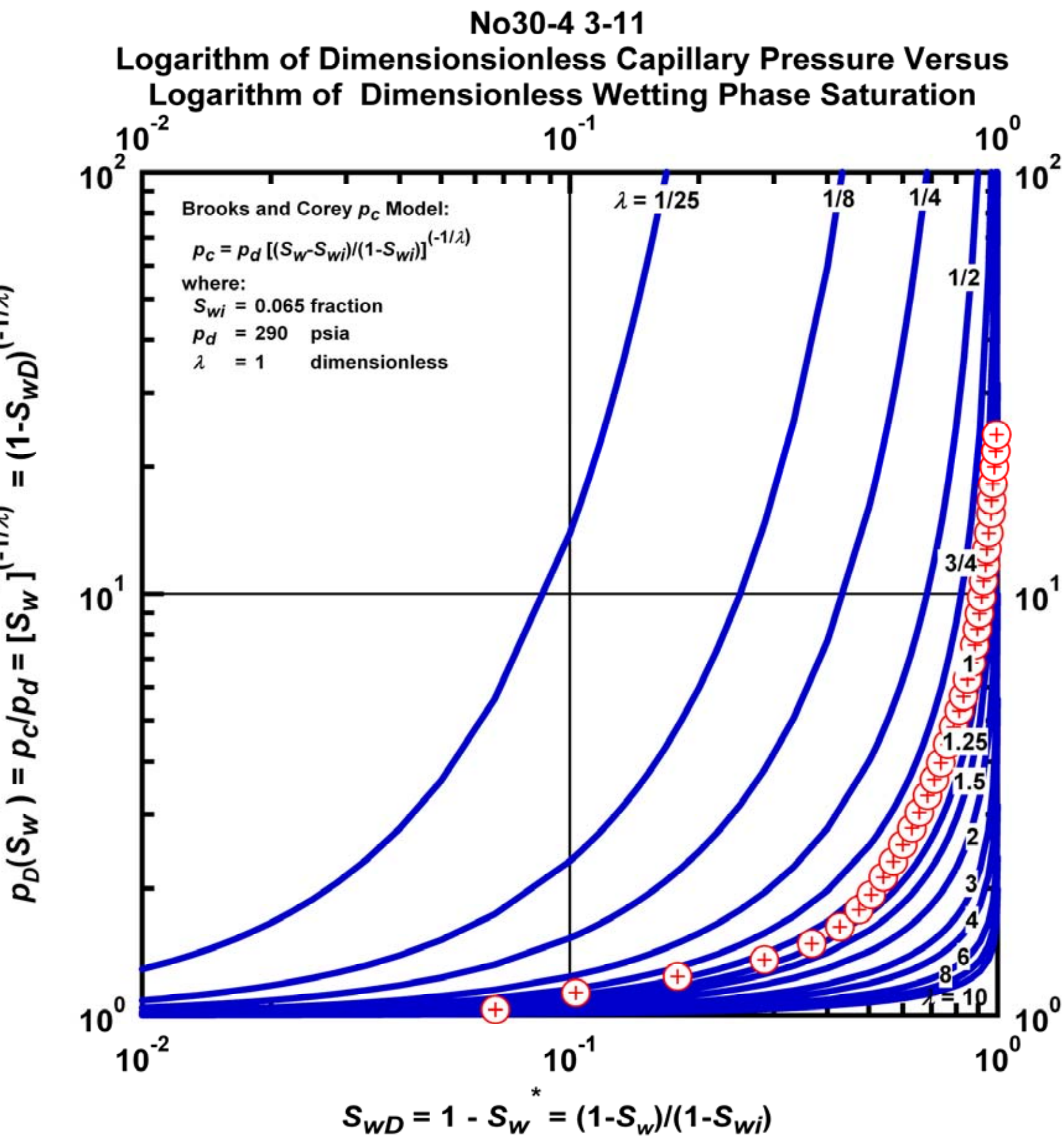

Figure M.48 – Plot of Logarithm of Dimensionless Capillary Pressure Versus Logarithm of Dimensionless Wetting Phase Saturation ── Case No30-4 3-11.

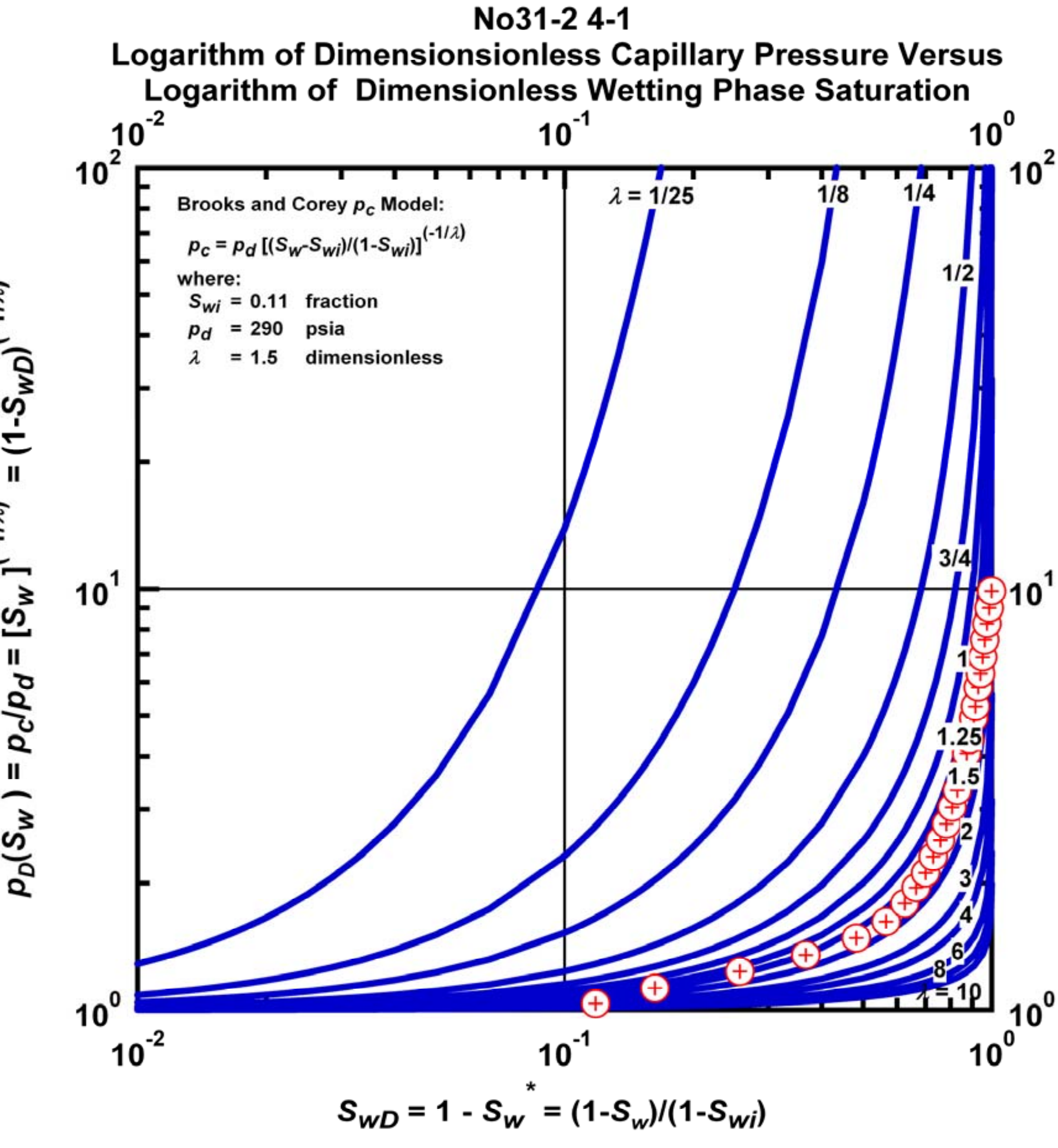

Figure M.49 – Plot of Logarithm of Dimensionless Capillary Pressure Versus Logarithm of Dimensionless Wetting Phase Saturation — Case No31-2 4-1.

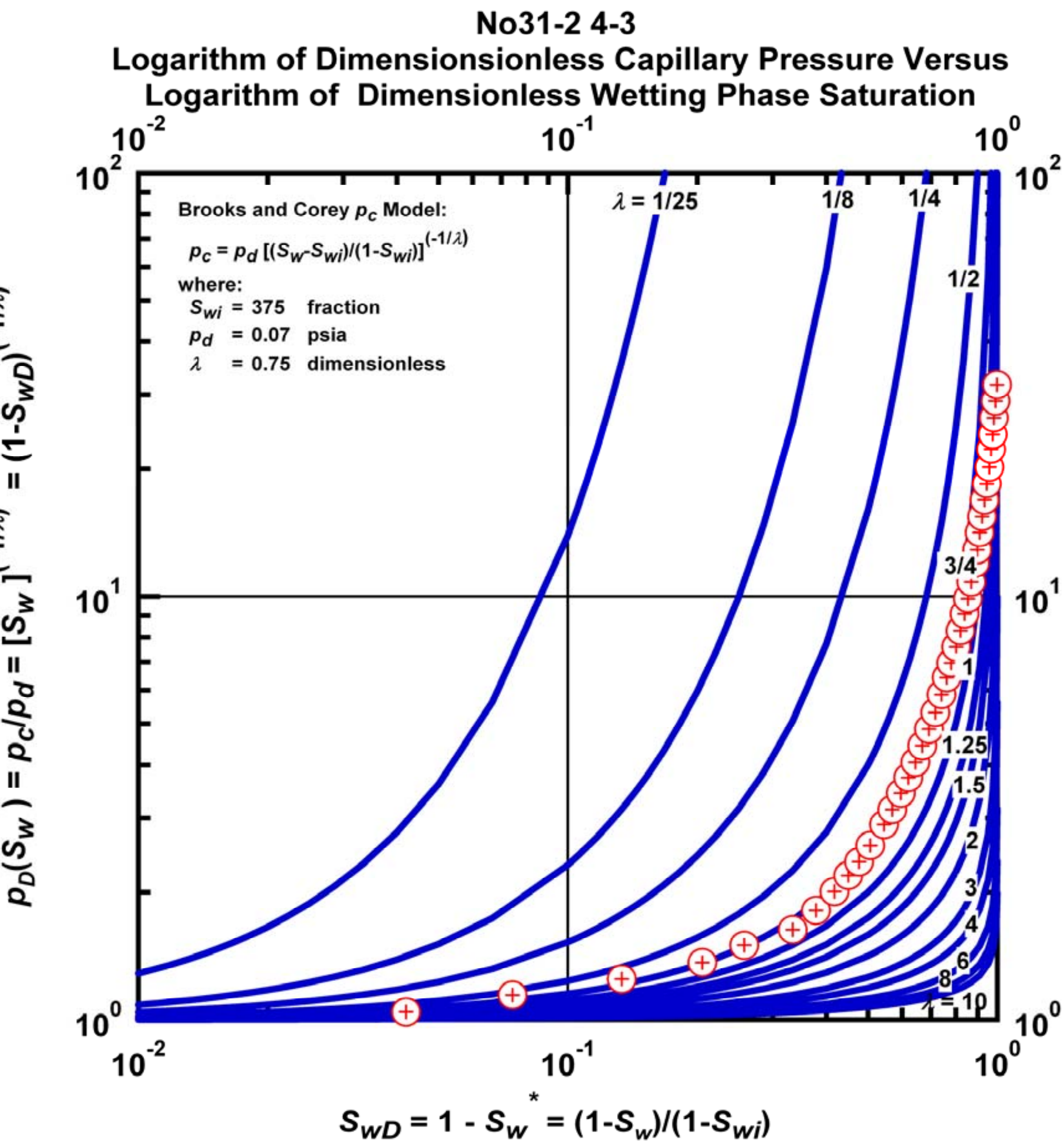

Figure M.50 – Plot of Logarithm of Dimensionless Capillary Pressure Versus Logarithm of Dimensionless Wetting Phase Saturation — Case No31-2 4-3.

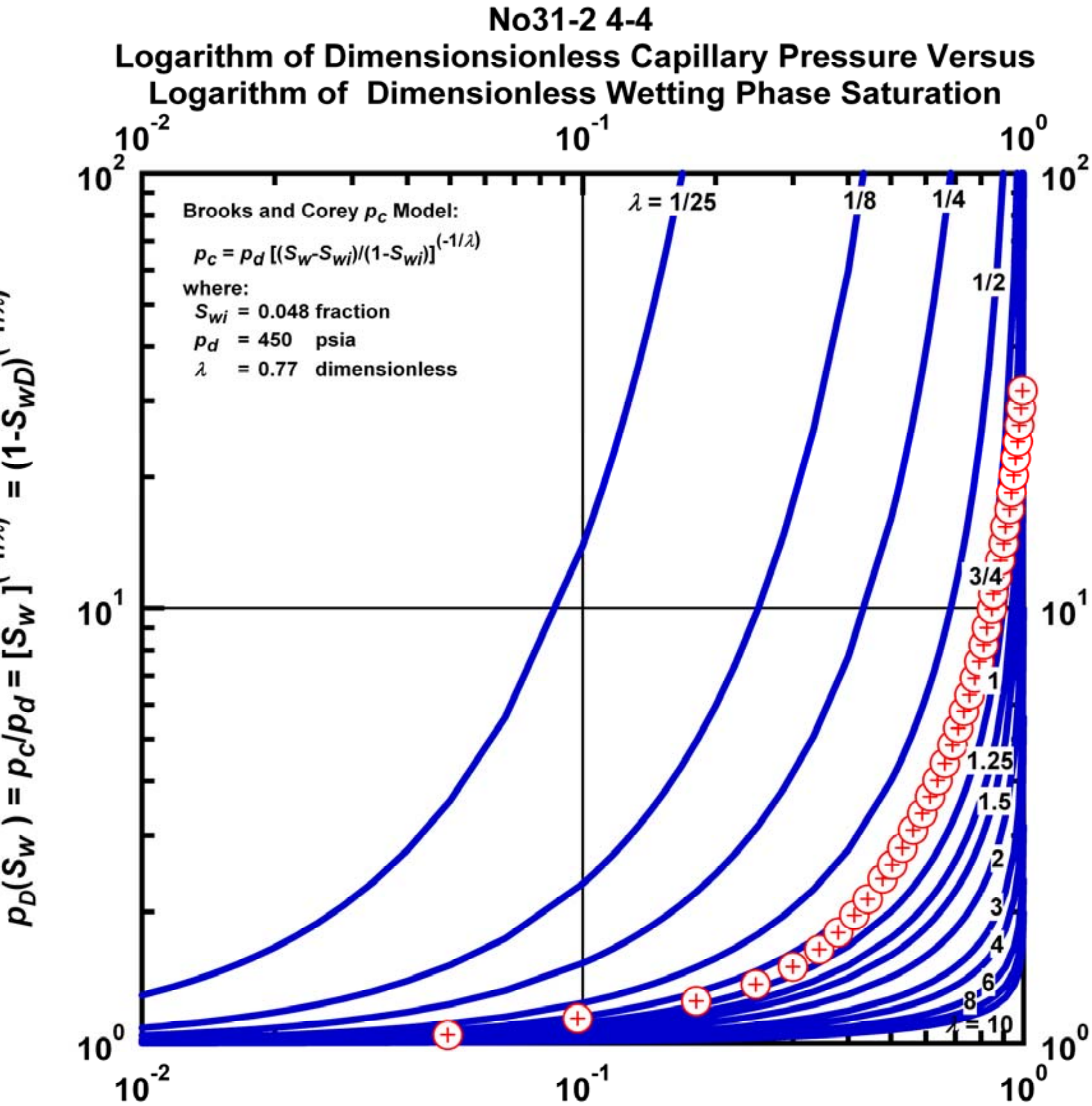

Figure M.51 – Plot of Logarithm of Dimensionless Capillary Pressure Versus Logarithm of Dimensionless Wetting Phase Saturation — Case No31-2 4-4.

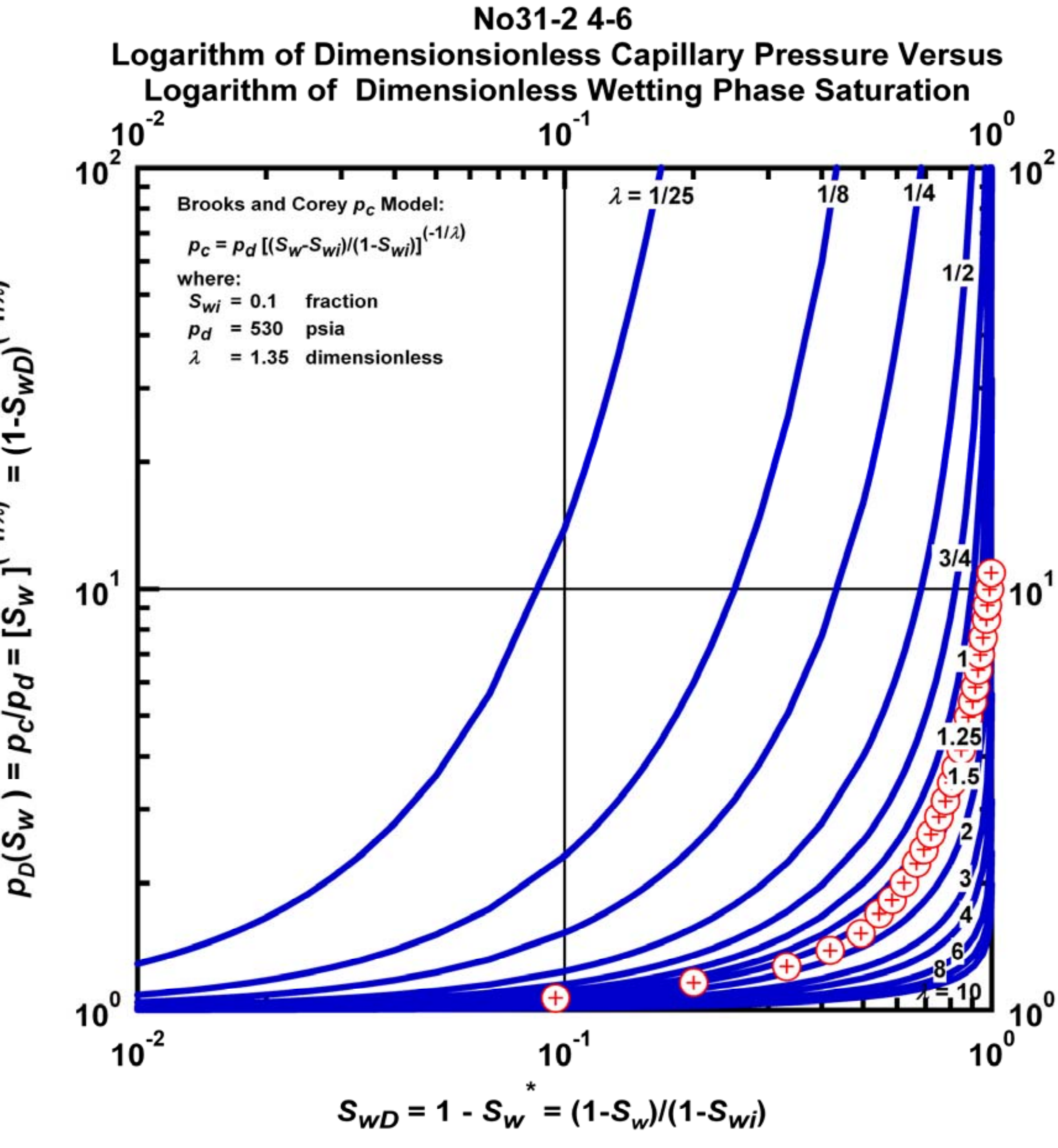

Figure M.52 – Plot of Logarithm of Dimensionless Capillary Pressure Versus Logarithm of Dimensionless Wetting Phase Saturation — Case No31-2 4-6.

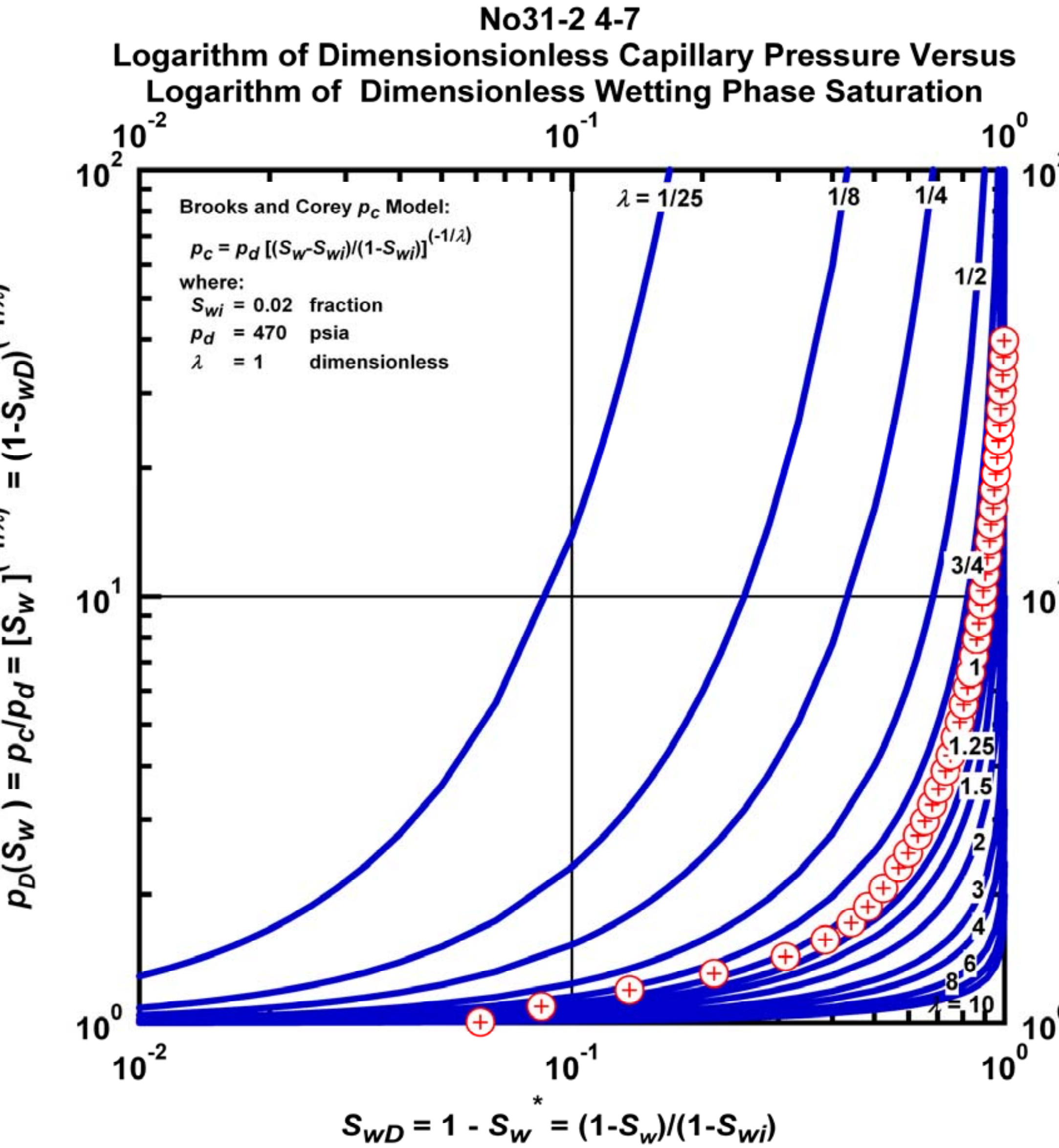

Figure M.53 – Plot of Logarithm of Dimensionless Capillary Pressure Versus Logarithm of Dimensionless Wetting Phase Saturation — Case No31-2 4-7.

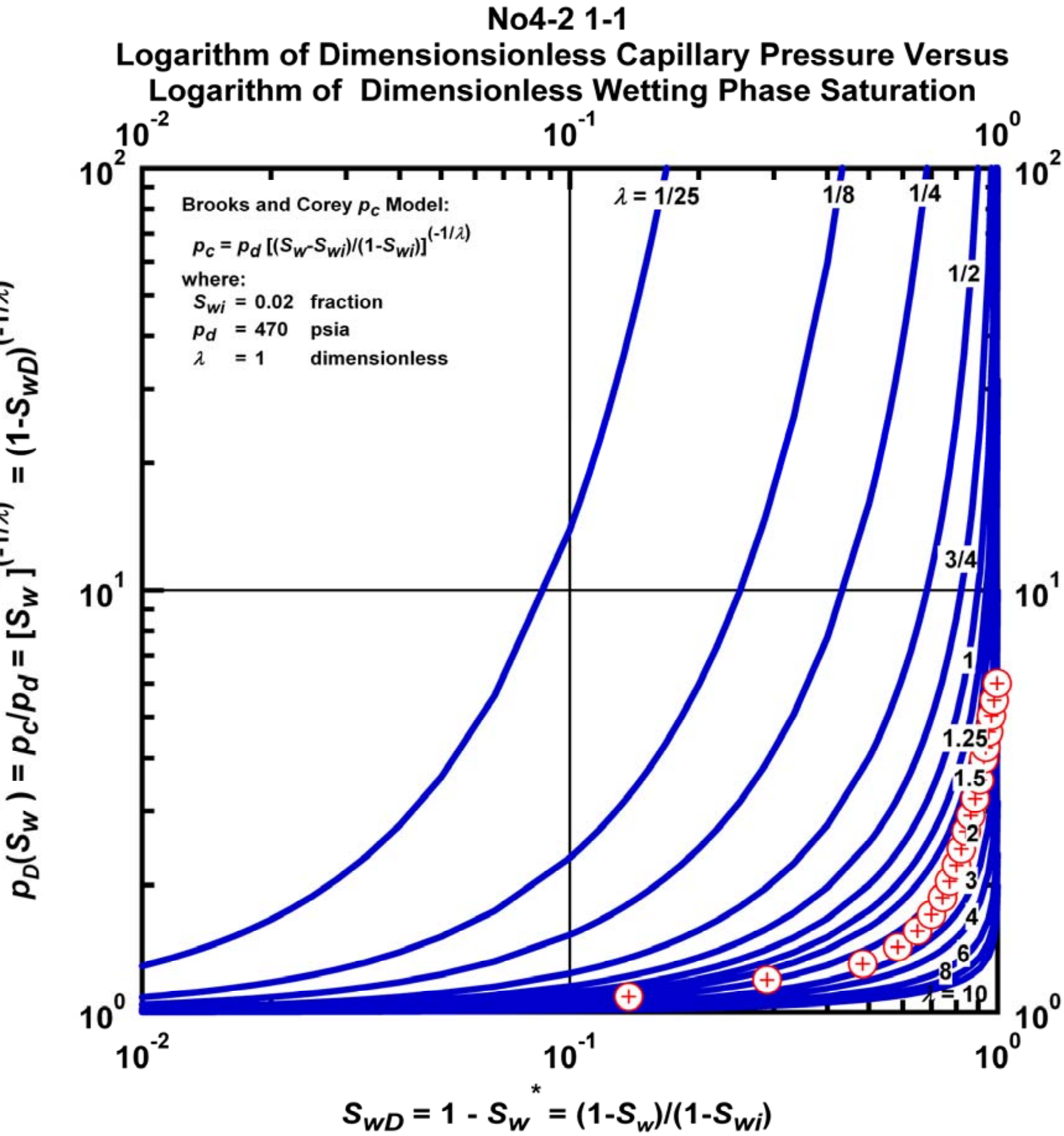

Figure M.54 – Plot of Logarithm of Dimensionless Capillary Pressure Versus Logarithm of Dimensionless Wetting Phase Saturation — Case No31-2 4-1.

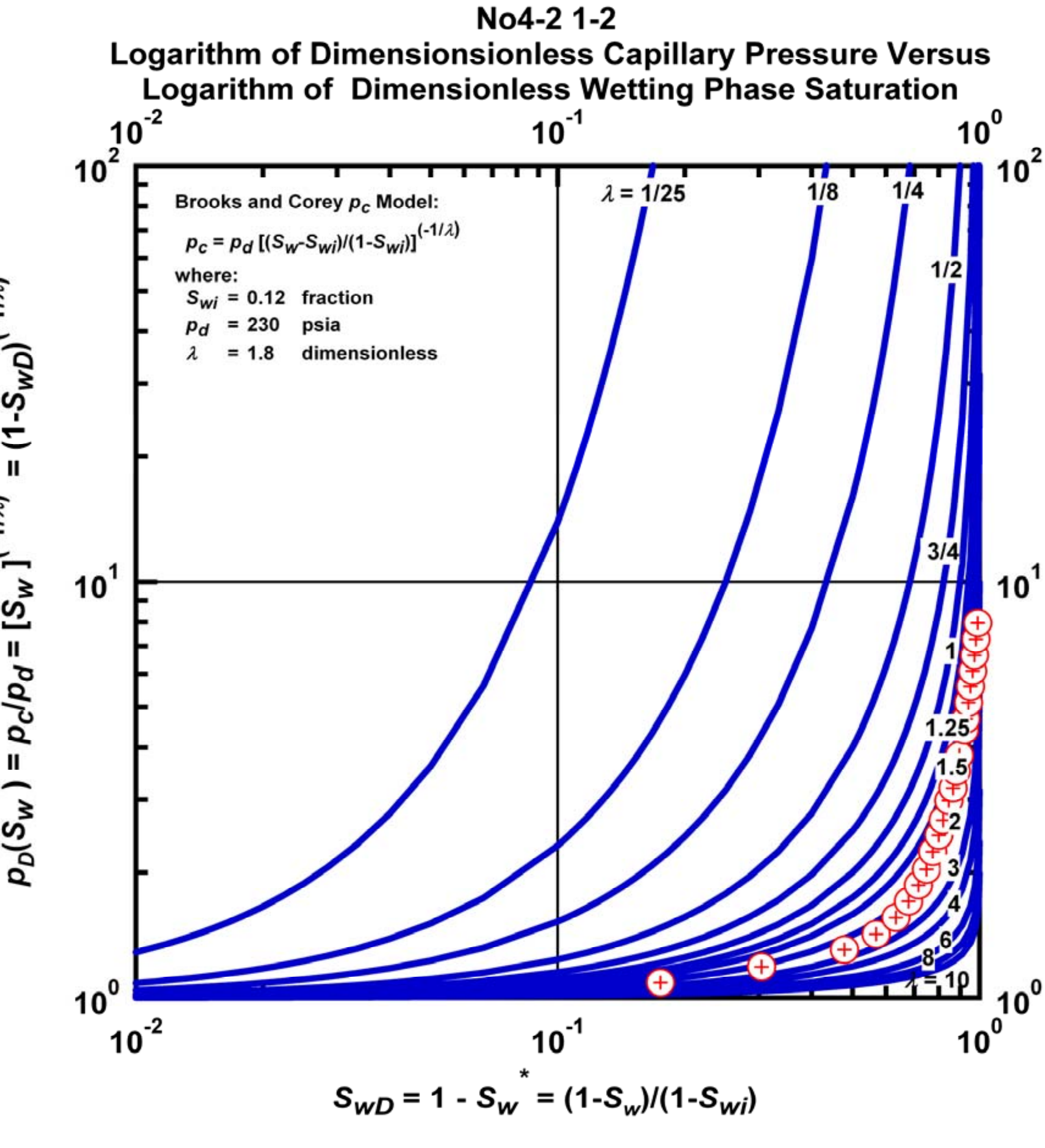

Figure M.55 – Plot of Logarithm of Dimensionless Capillary Pressure Versus Logarithm of Dimensionless Wetting Phase Saturation — Case No31-2 4-2.

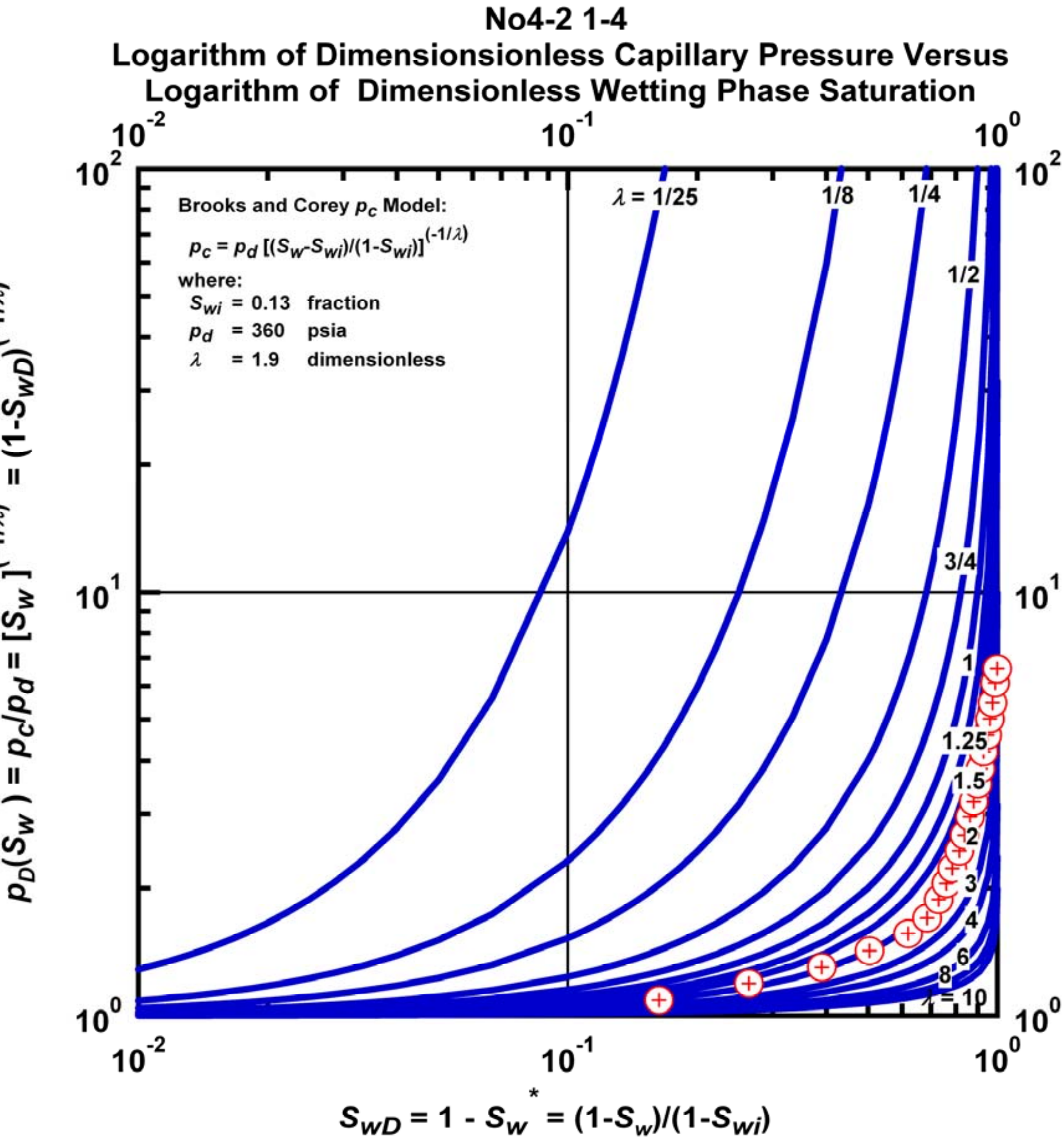

Figure M.56 – Plot of Logarithm of Dimensionless Capillary Pressure Versus Logarithm of Dimensionless Wetting Phase Saturation — Case No31-2 4-4.

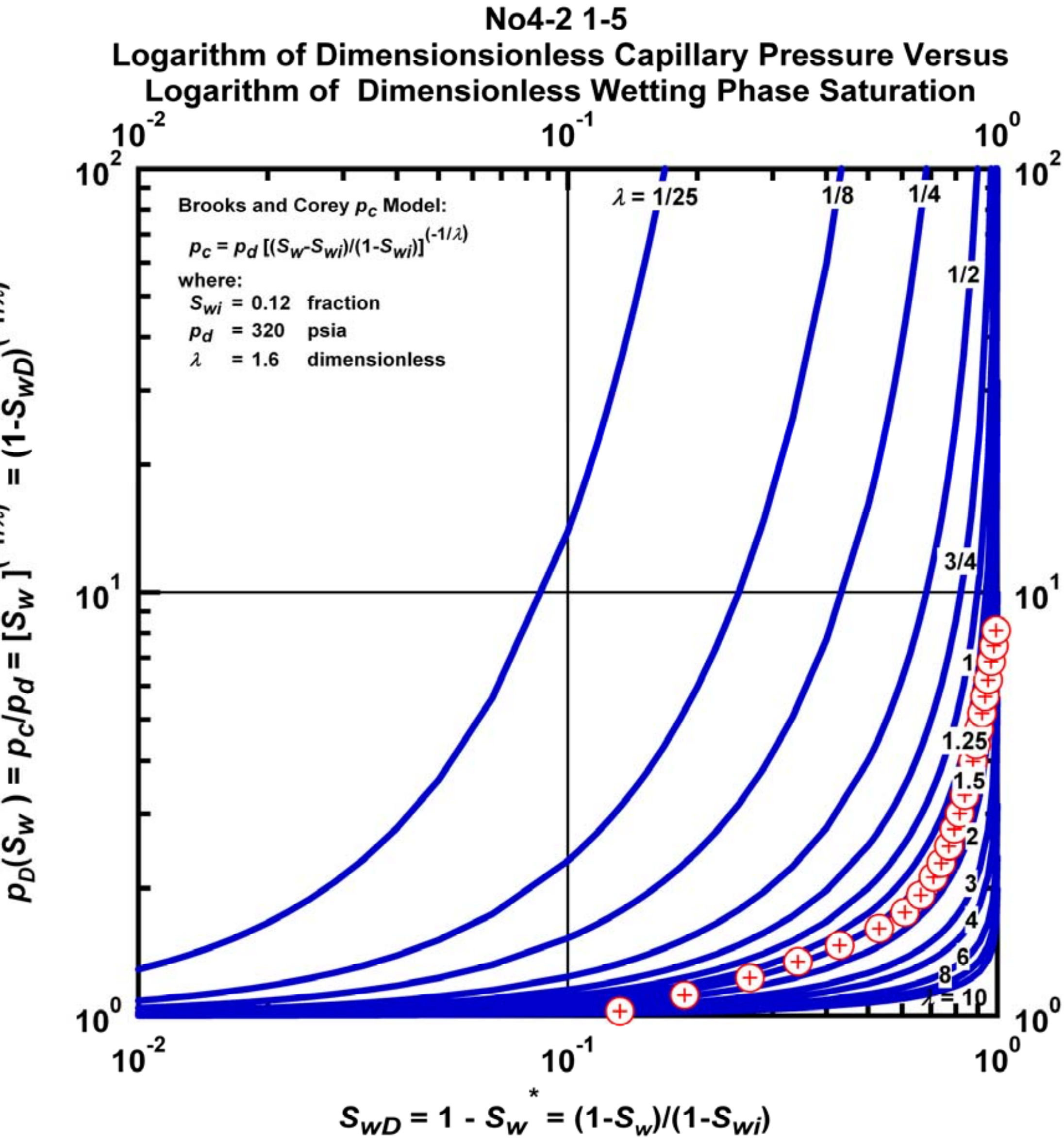

Figure M.57 – Plot of Logarithm of Dimensionless Capillary Pressure Versus Logarithm of Dimensionless Wetting Phase Saturation — Case No31-2 4-5.

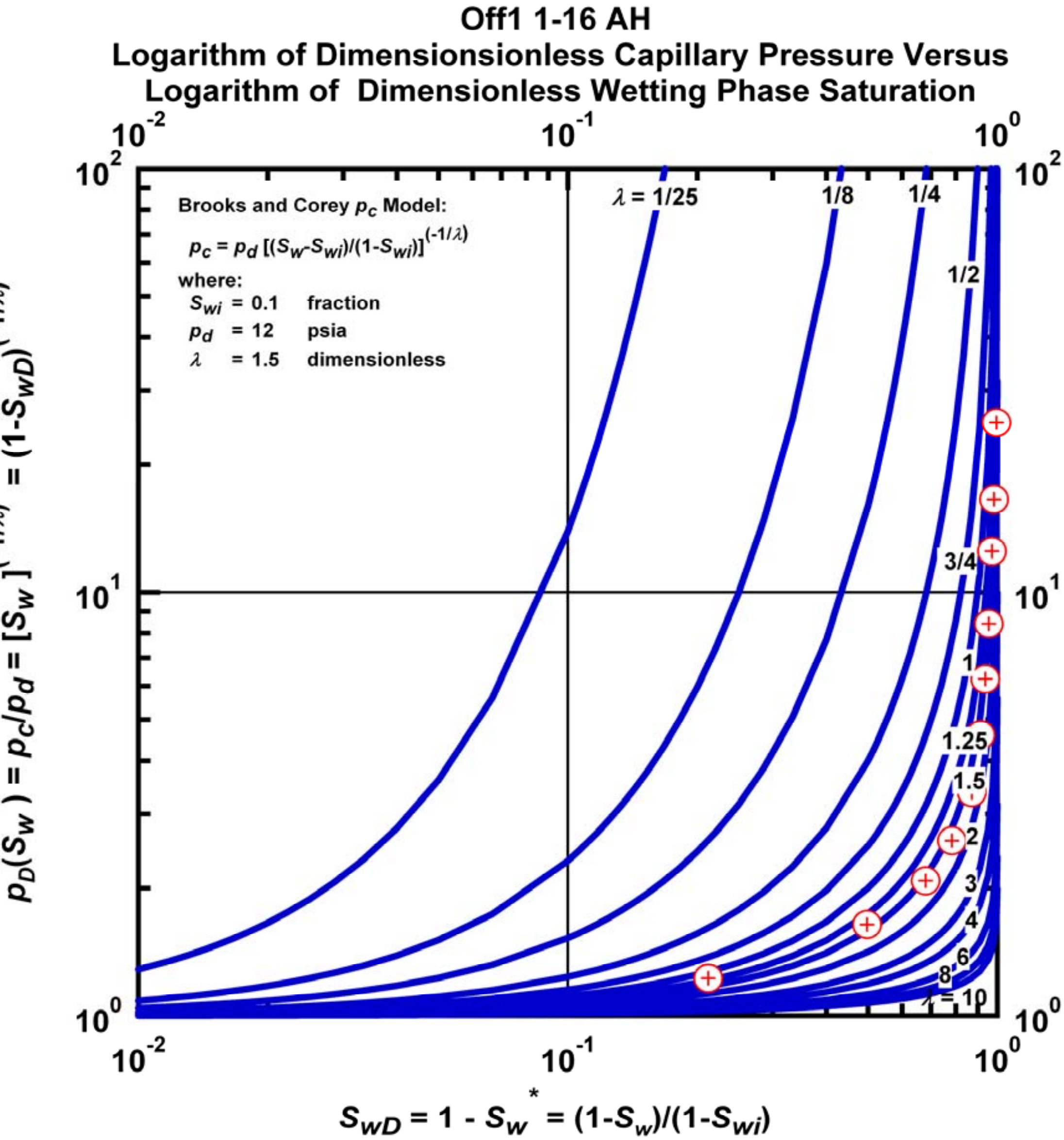

Figure M.58 – Plot of Logarithm of Dimensionless Capillary Pressure Versus Logarithm of Dimensionless Wetting Phase Saturation — Case Off1 1-16 AH.

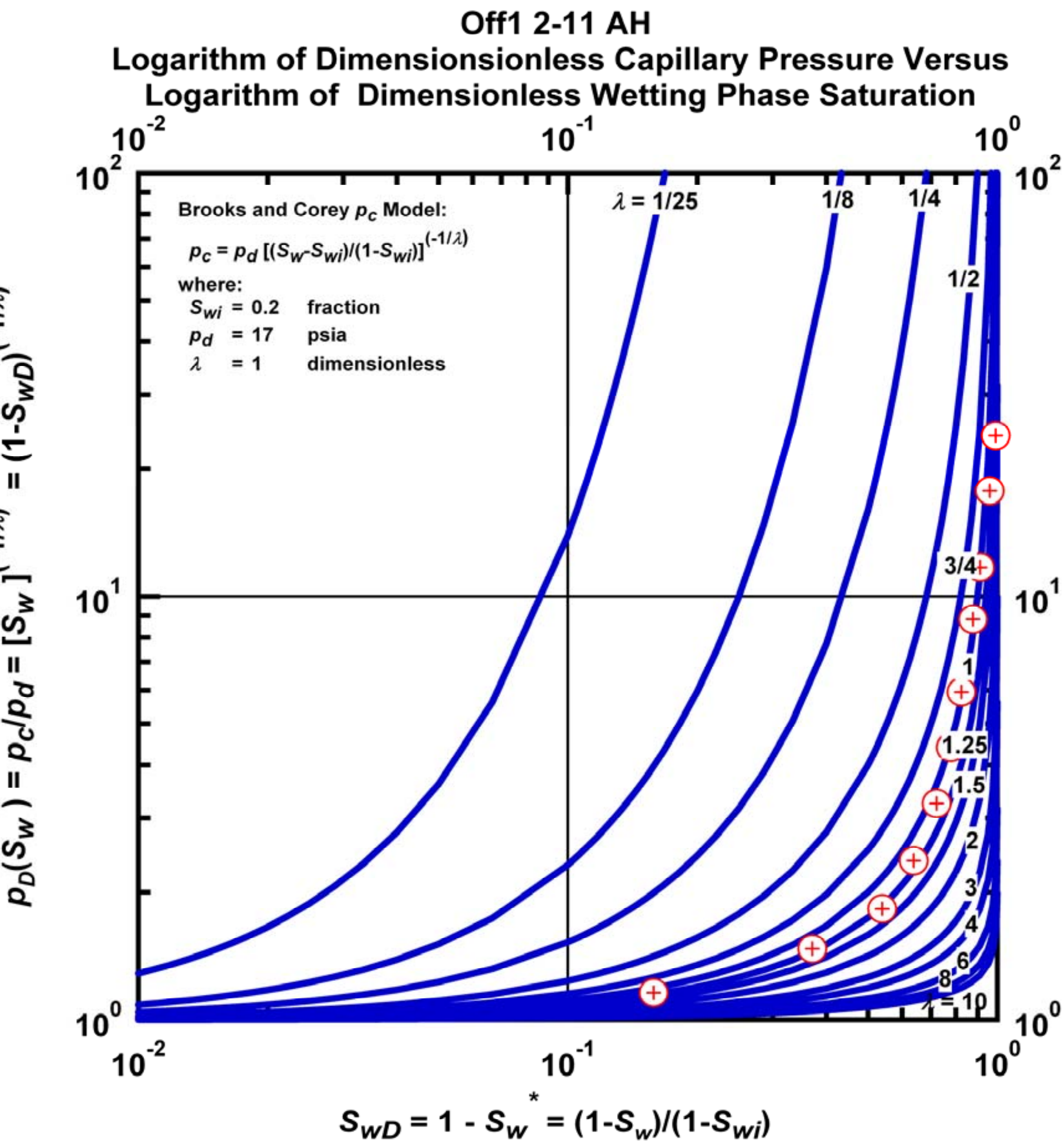

Figure M.59 – Plot of Logarithm of Dimensionless Capillary Pressure Versus Logarithm of Dimensionless Wetting Phase Saturation — Case Off1 2-11 AH.

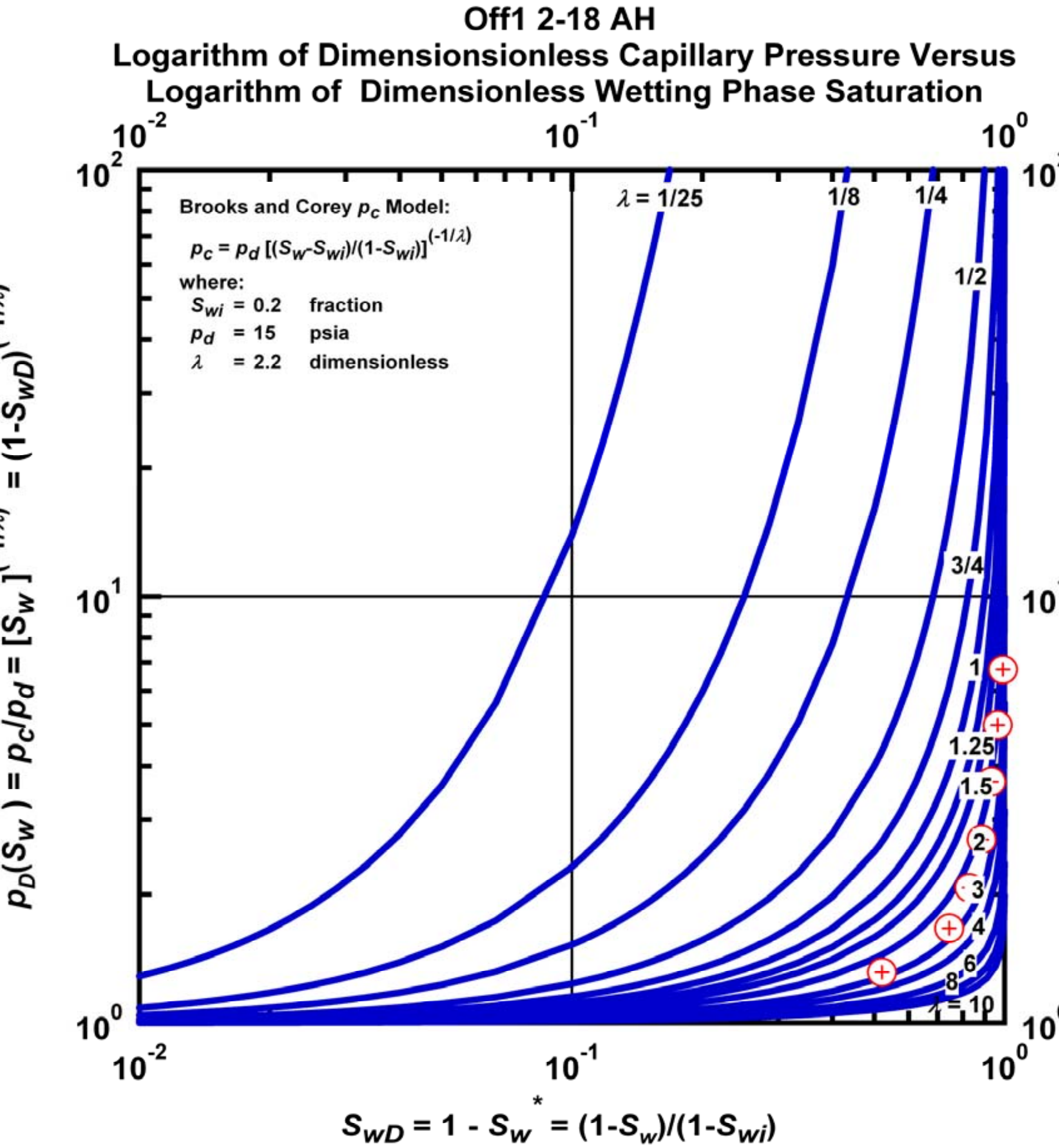

Figure M.60 – Plot of Logarithm of Dimensionless Capillary Pressure Versus Logarithm of Dimensionless Wetting Phase Saturation — Case Off1 2-18 AH.

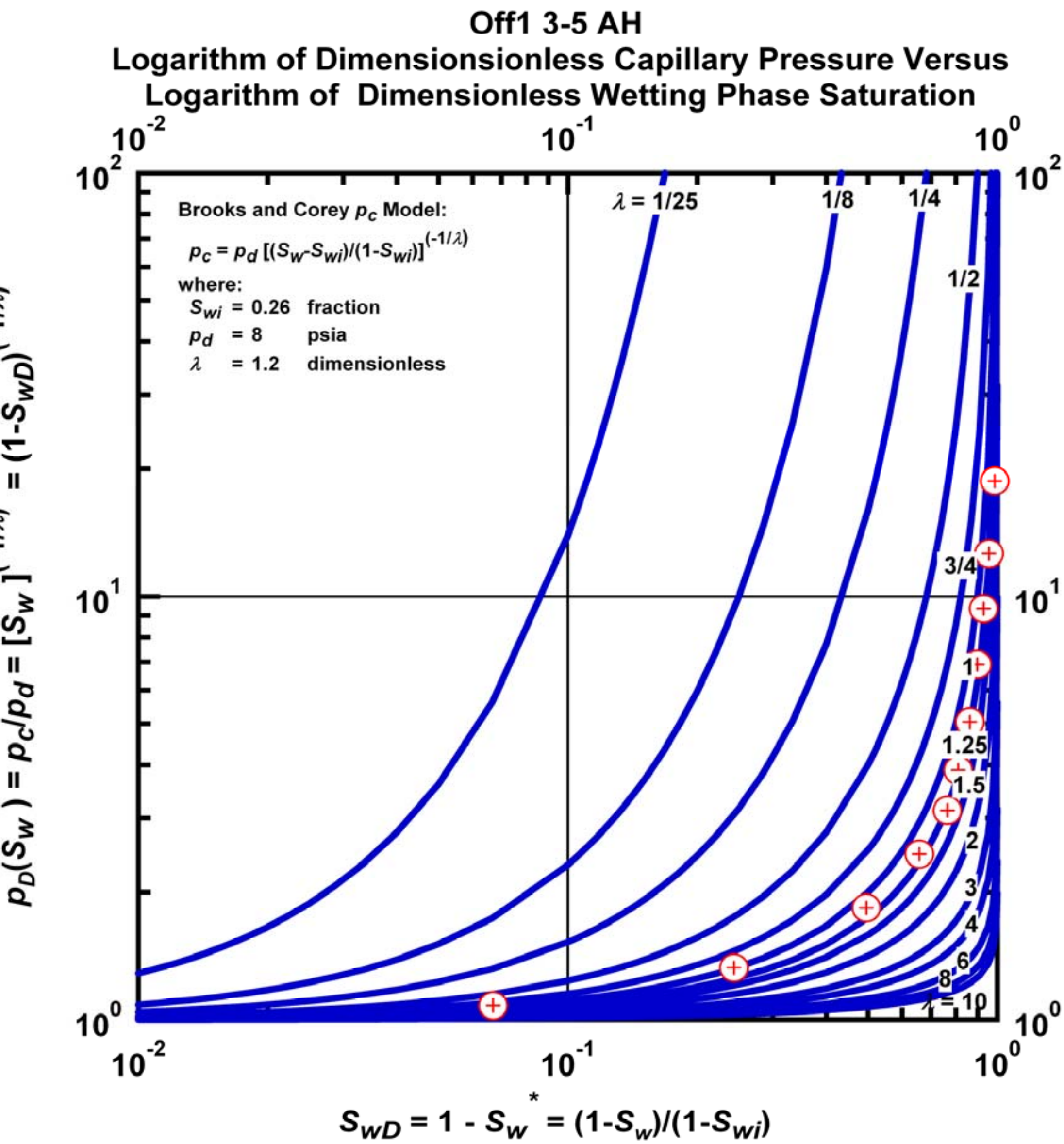

Figure M.61 – Plot of Logarithm of Dimensionless Capillary Pressure Versus Logarithm of Dimensionless Wetting Phase Saturation — Case Off1 3-5 AH.

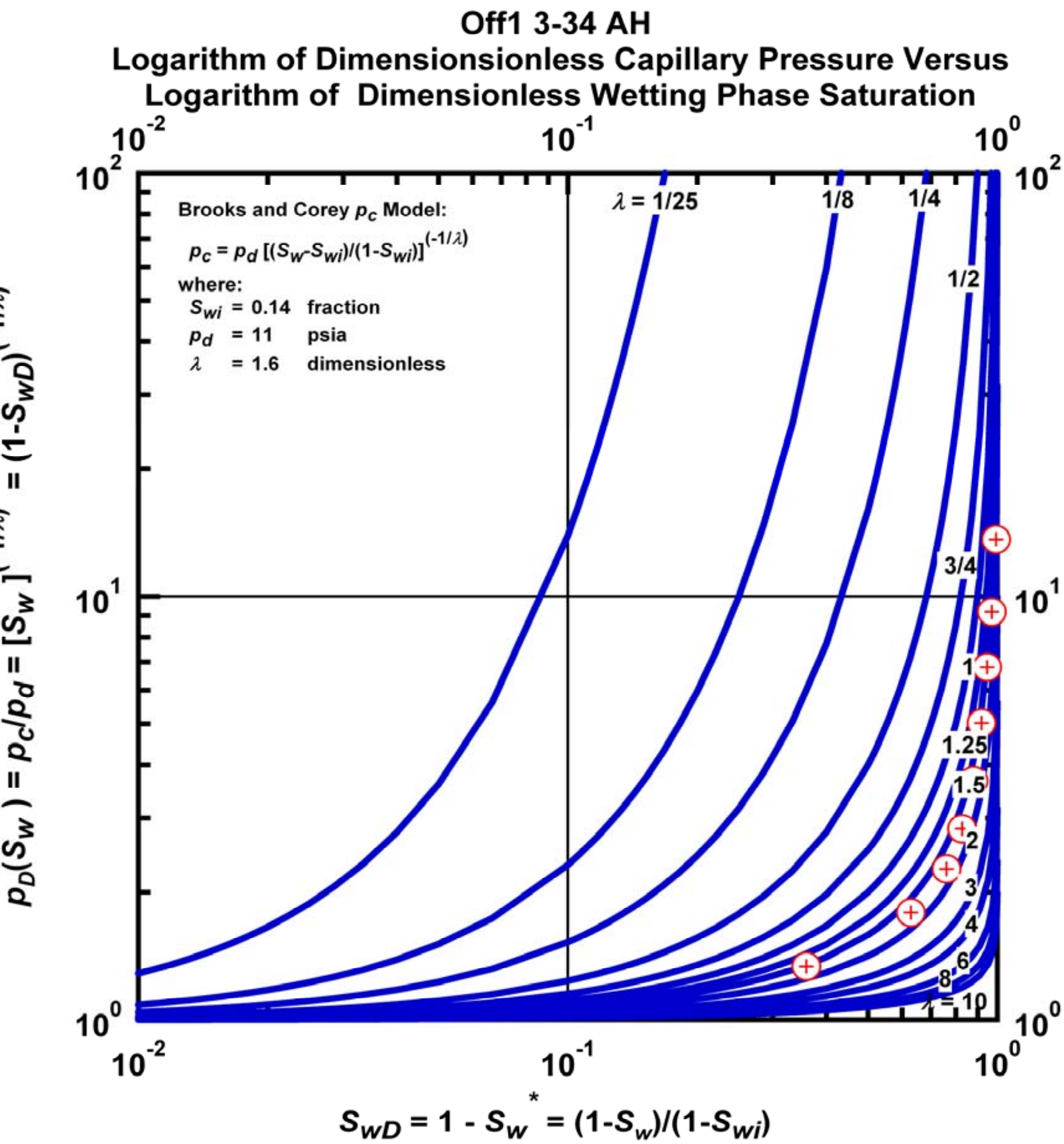

Figure M.62 – Plot of Logarithm of Dimensionless Capillary Pressure Versus Logarithm of Dimensionless Wetting Phase Saturation — Case Off1 3-34 AH.

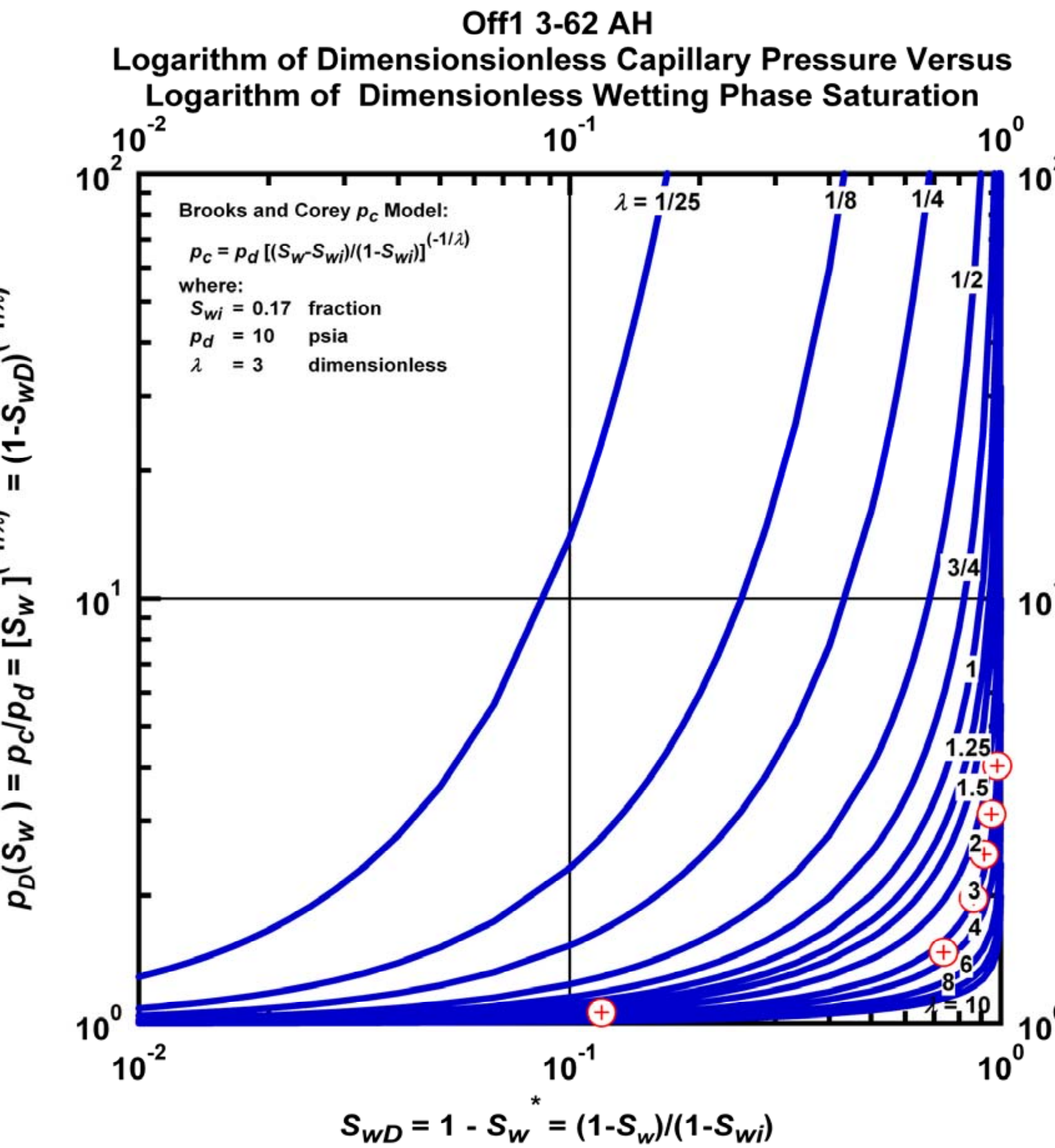

Figure M.63 – Plot of Logarithm of Dimensionless Capillary Pressure Versus Logarithm of Dimensionless Wetting Phase Saturation — Case Off1 3-62 AH.

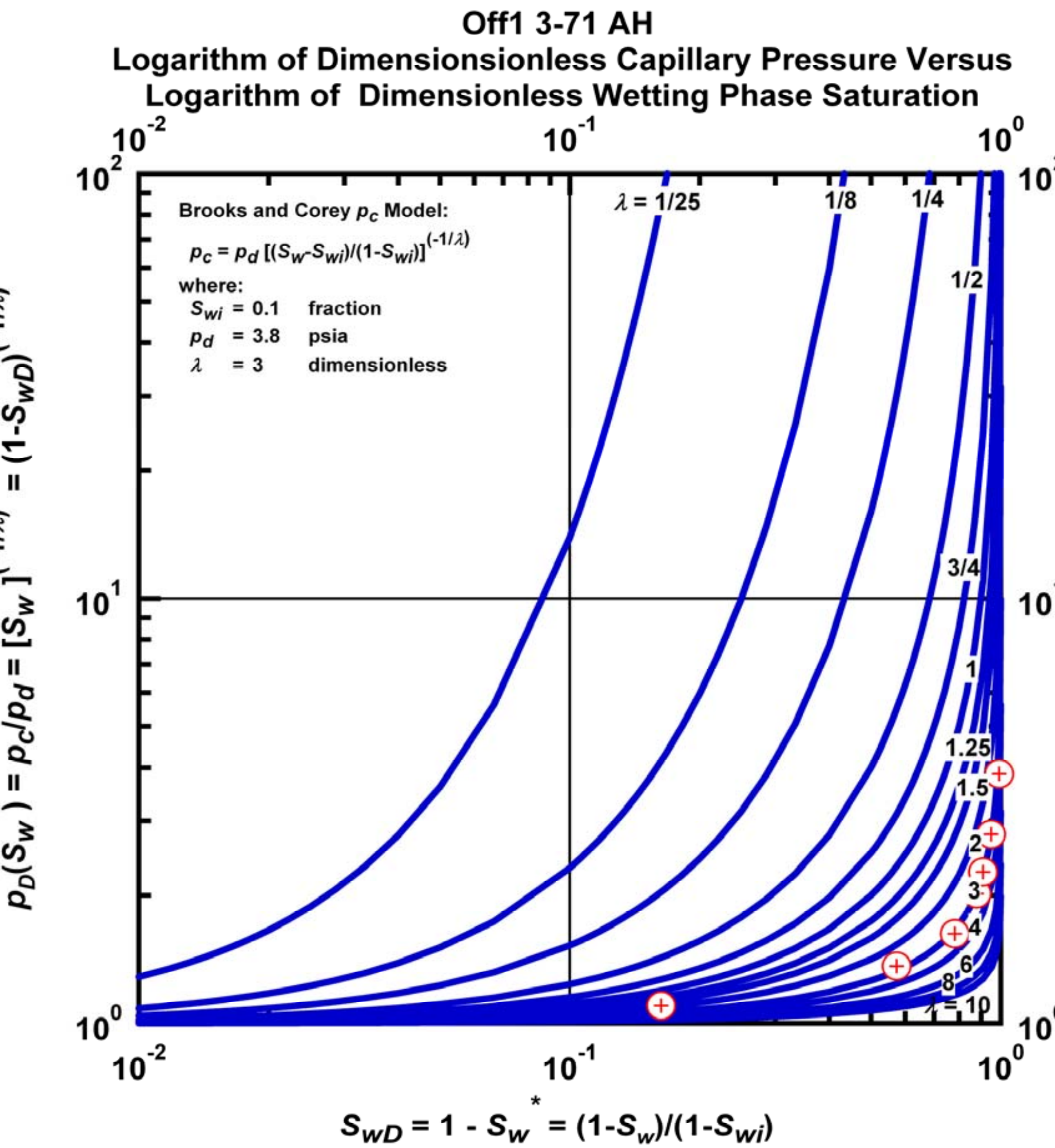

Figure M.64 – Plot of Logarithm of Dimensionless Capillary Pressure Versus Logarithm of Dimensionless Wetting Phase Saturation — Case Off1 3-71 AH.

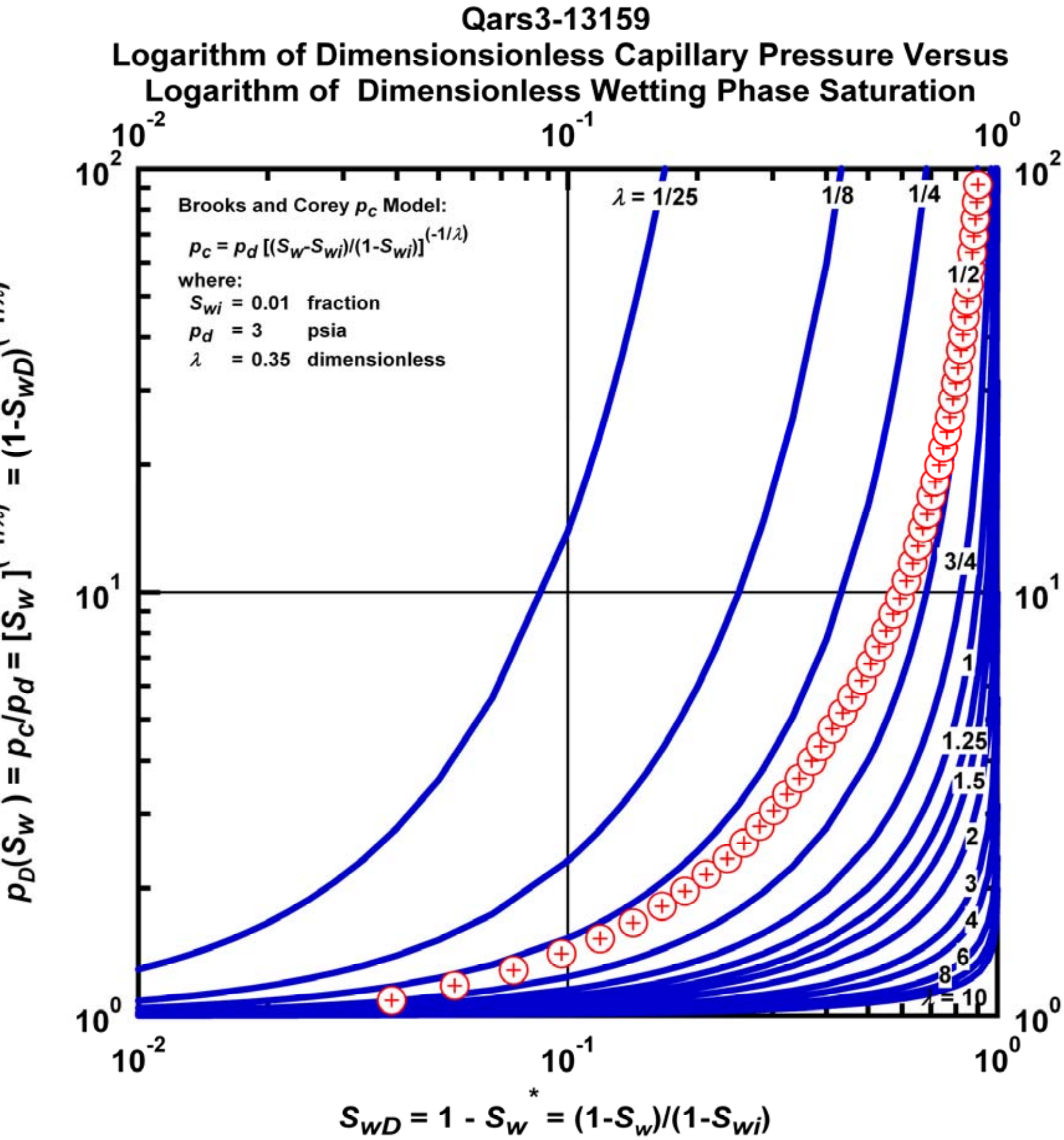

Figure M.65 – Plot of Logarithm of Dimensionless Capillary Pressure Versus Logarithm of Dimensionless Wetting Phase Saturation — Case Qars3-13159.

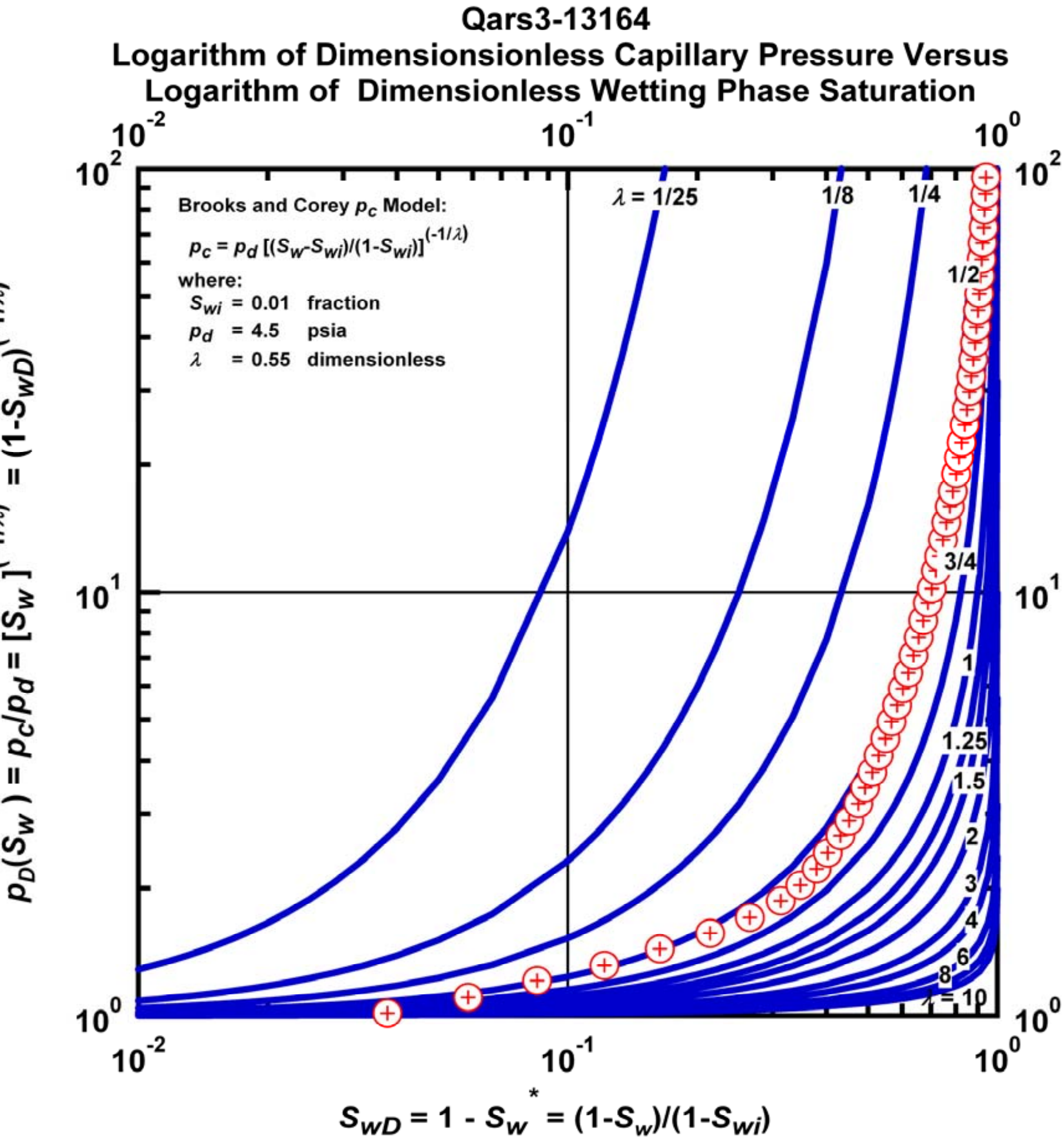

Figure M.66 – Plot of Logarithm of Dimensionless Capillary Pressure Versus Logarithm of Dimensionless Wetting Phase Saturation — Case Qars3-13164.

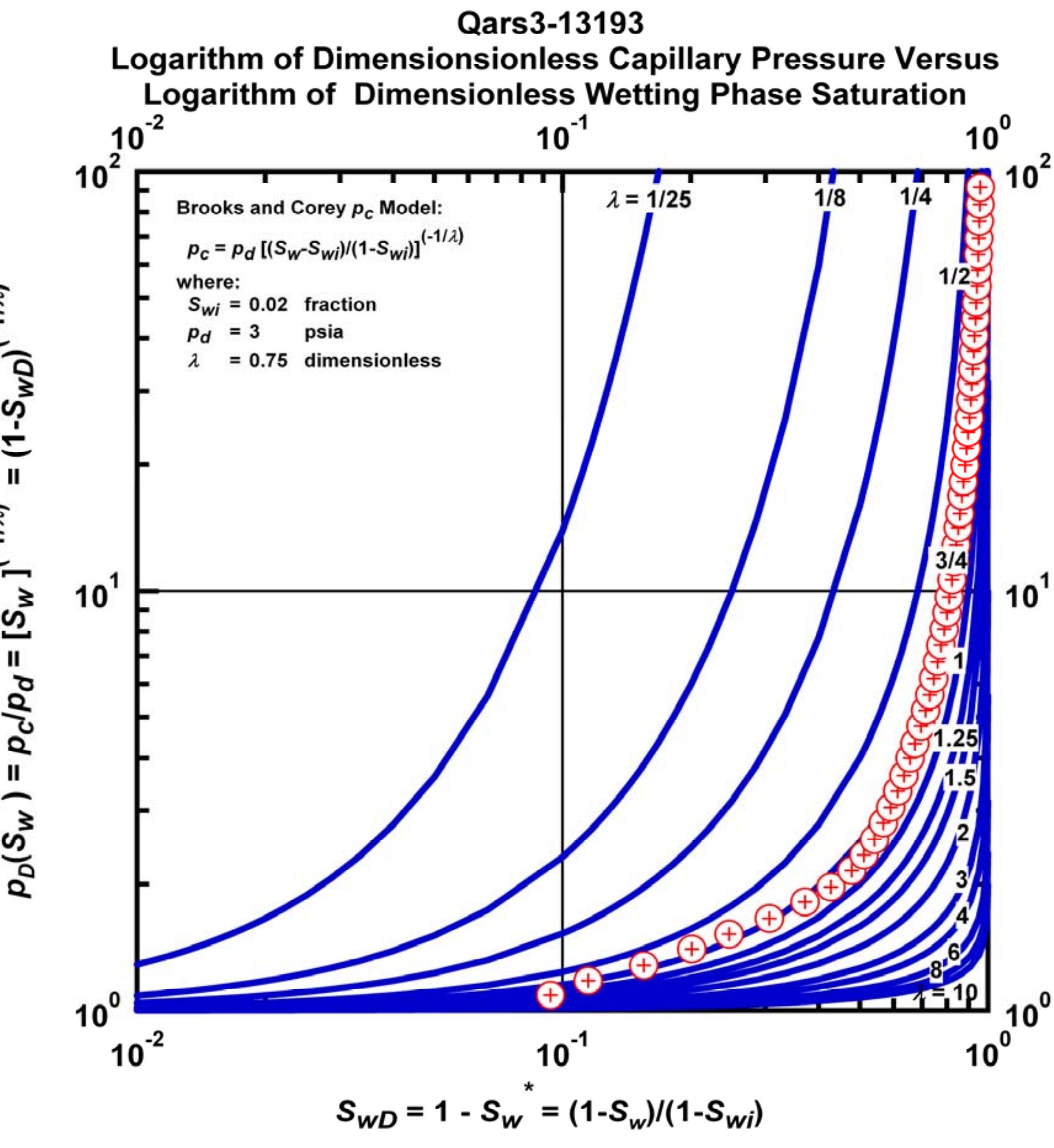

Figure M.67 – Plot of Logarithm of Dimensionless Capillary Pressure Versus Logarithm of Dimensionless Wetting Phase Saturation — Case Qars3-13193.

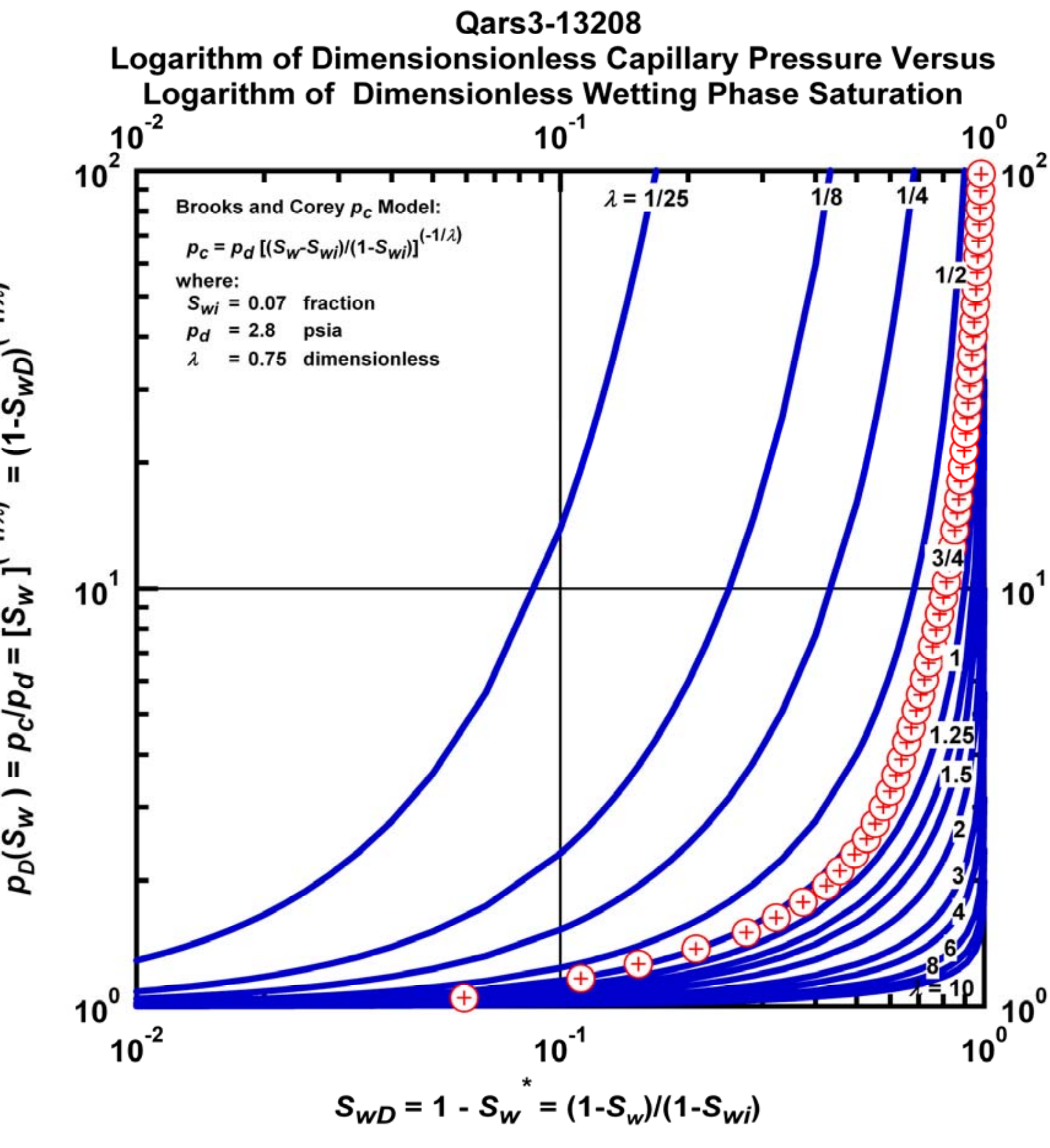

Figure M.68 – Plot of Logarithm of Dimensionless Capillary Pressure Versus Logarithm of Dimensionless Wetting Phase Saturation — Case Qars3-13208.

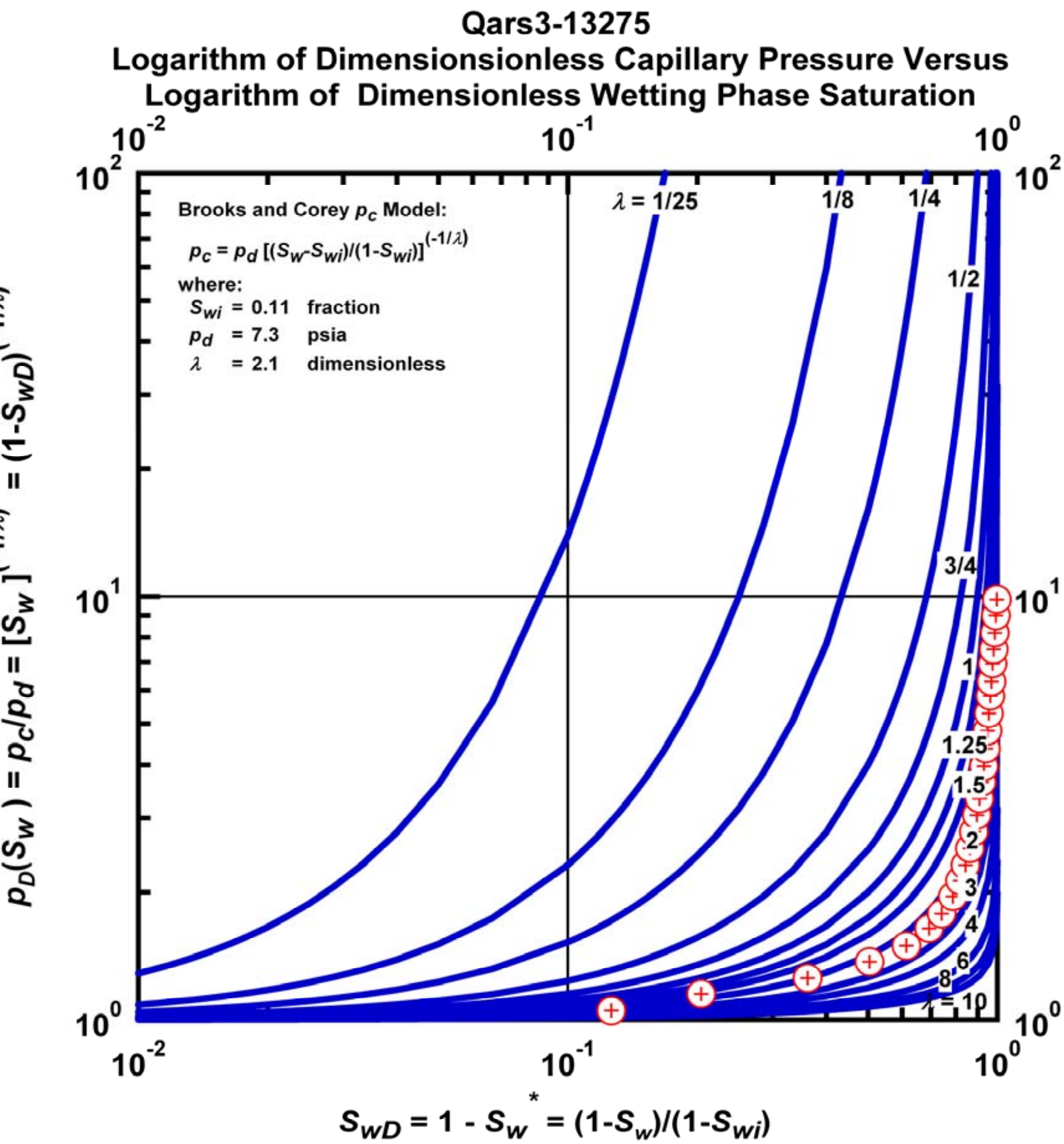

Figure M.69 – Plot of Logarithm of Dimensionless Capillary Pressure Versus Logarithm of Dimensionless Wetting Phase Saturation — Case Qars3-13275.

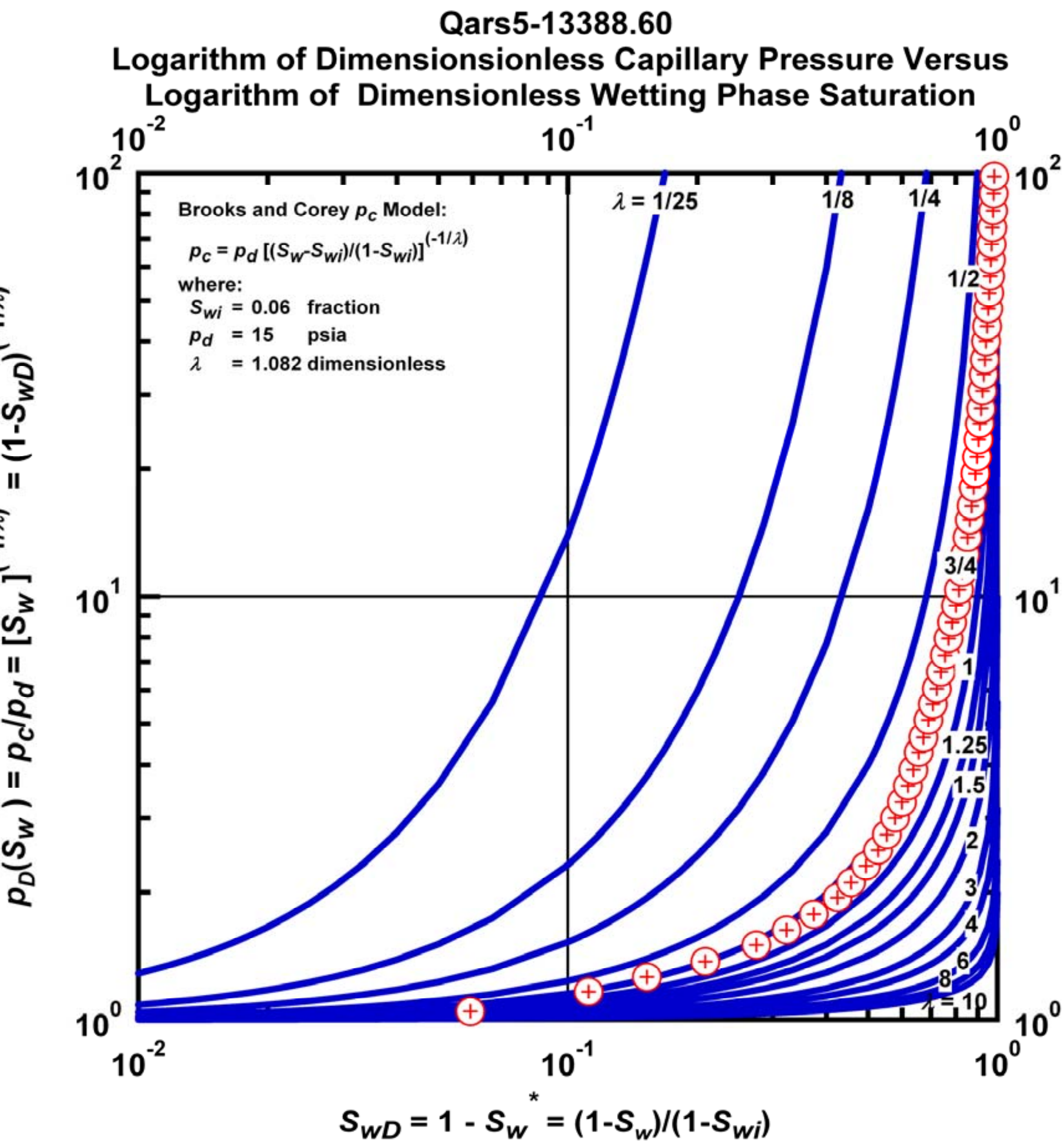

Figure M.70 – Plot of Logarithm of Dimensionless Capillary Pressure Versus Logarithm of Dimensionless Wetting Phase Saturation — Case Qars5-13388.6.

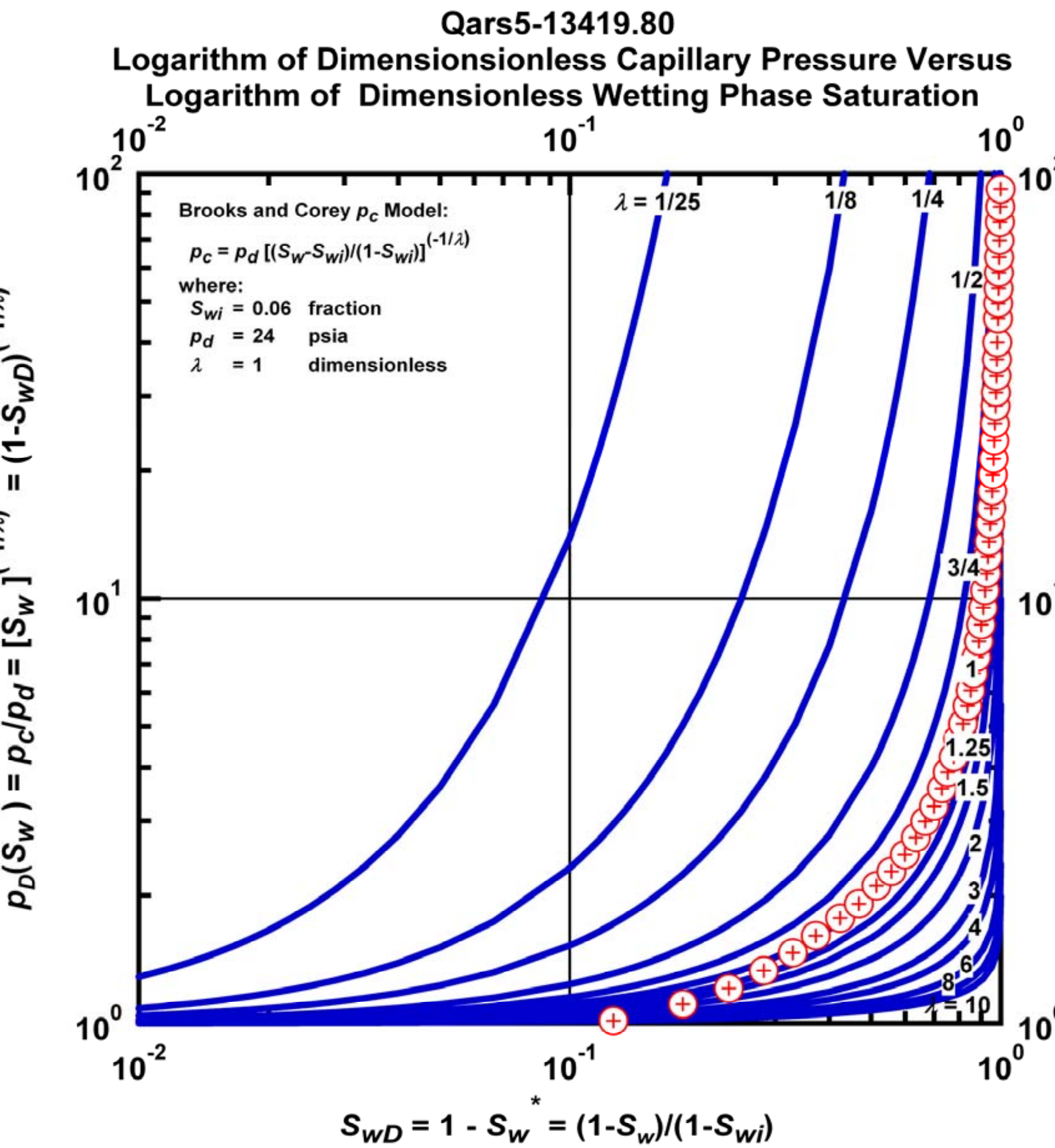

Figure M.71 – Plot of Logarithm of Dimensionless Capillary Pressure Versus Logarithm of Dimensionless Wetting Phase Saturation — Case Qars5-13419.8.

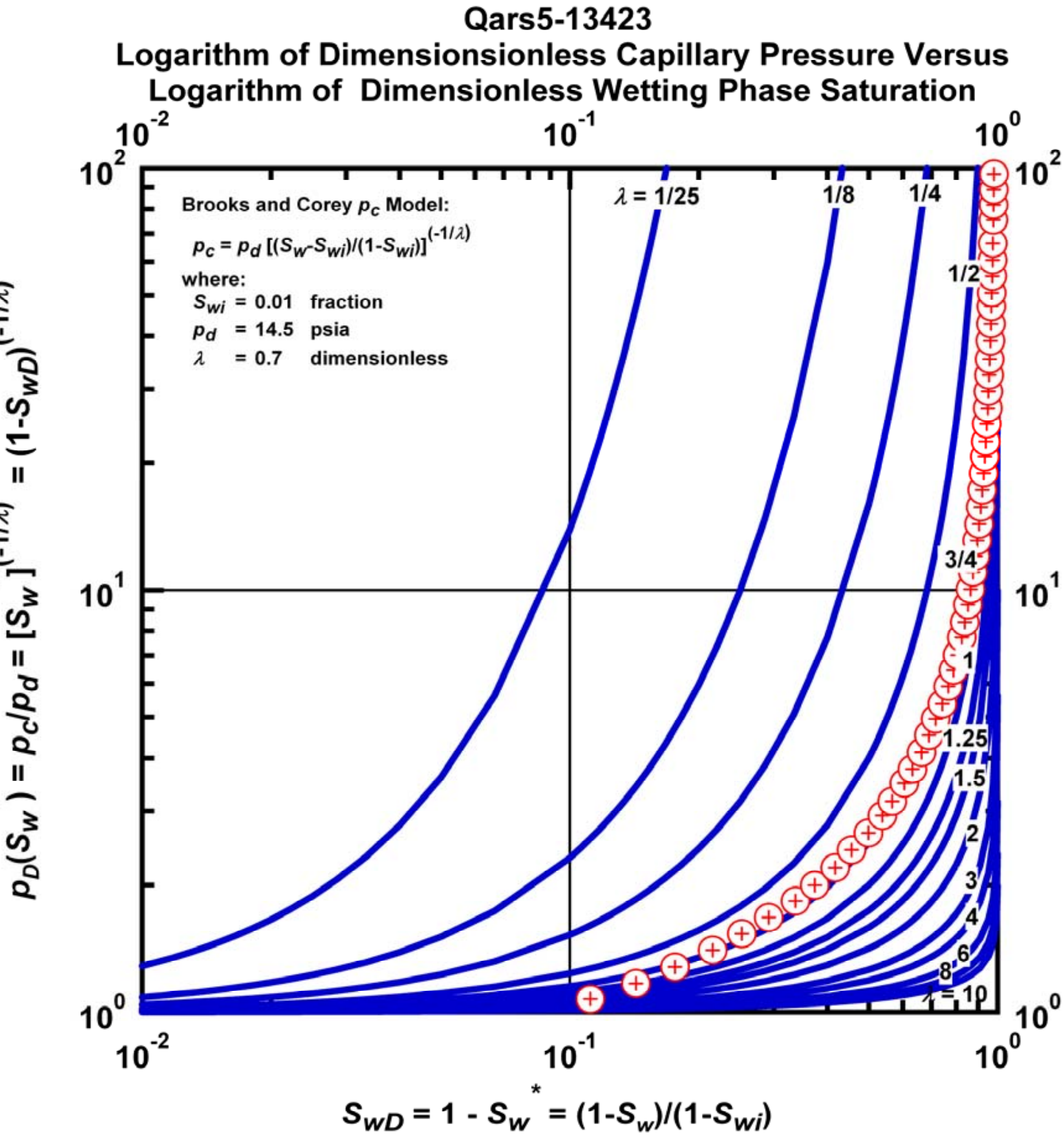

Figure M.72 – Plot of Logarithm of Dimensionless Capillary Pressure Versus Logarithm of Dimensionless Wetting Phase Saturation — Case Qars5-13423.

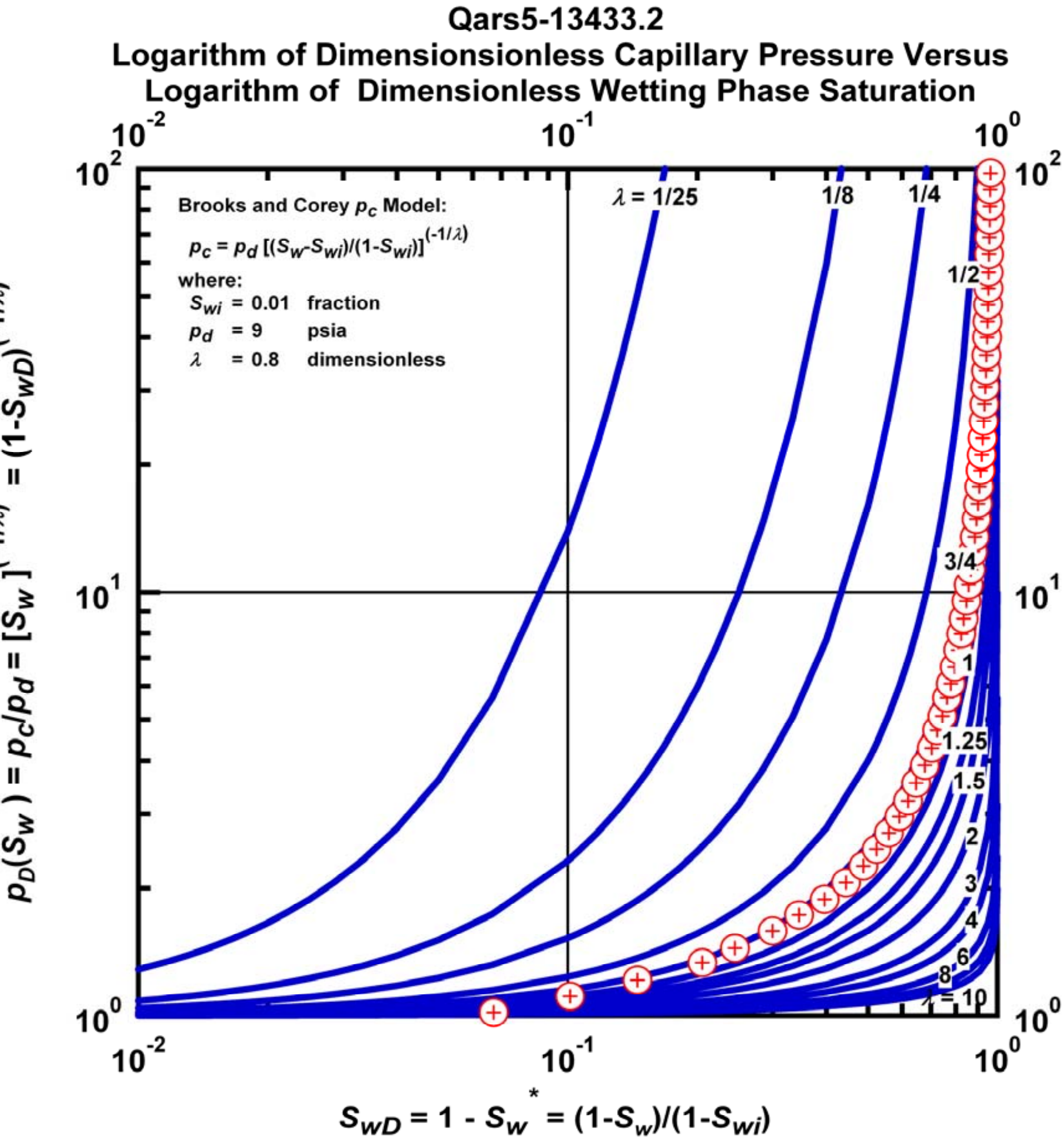

Figure M.73 – Plot of Logarithm of Dimensionless Capillary Pressure Versus Logarithm of Dimensionless Wetting Phase Saturation — Case Qars5-13433.2.

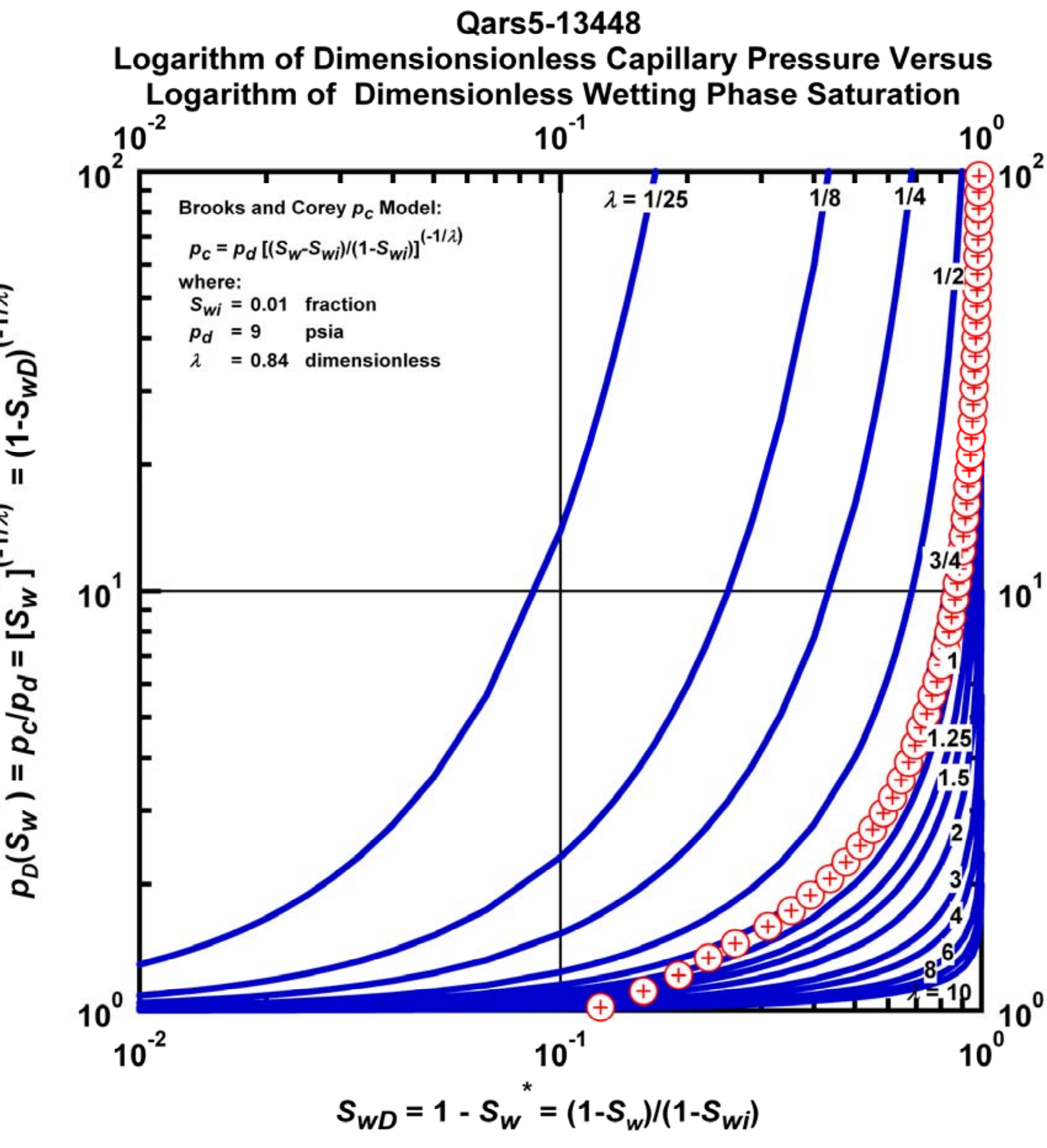

Figure M.74 – Plot of Logarithm of Dimensionless Capillary Pressure Versus Logarithm of Dimensionless Wetting Phase Saturation — Case Qars5-13448

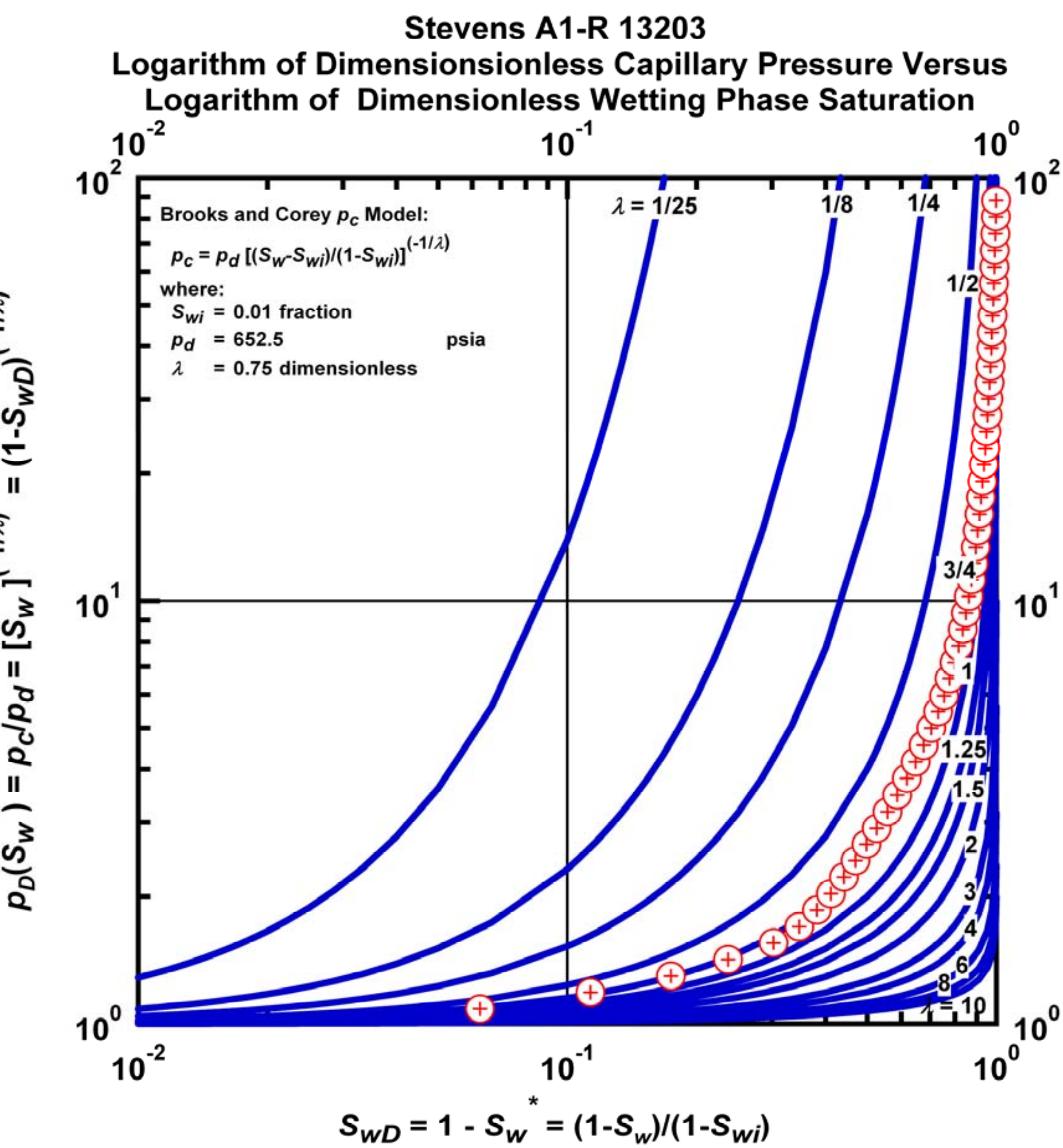

Figure M.75 – Plot of Logarithm of Dimensionless Capillary Pressure Versus Logarithm of Dimensionless Wetting Phase Saturation — Case Stevens A1-R 13203.

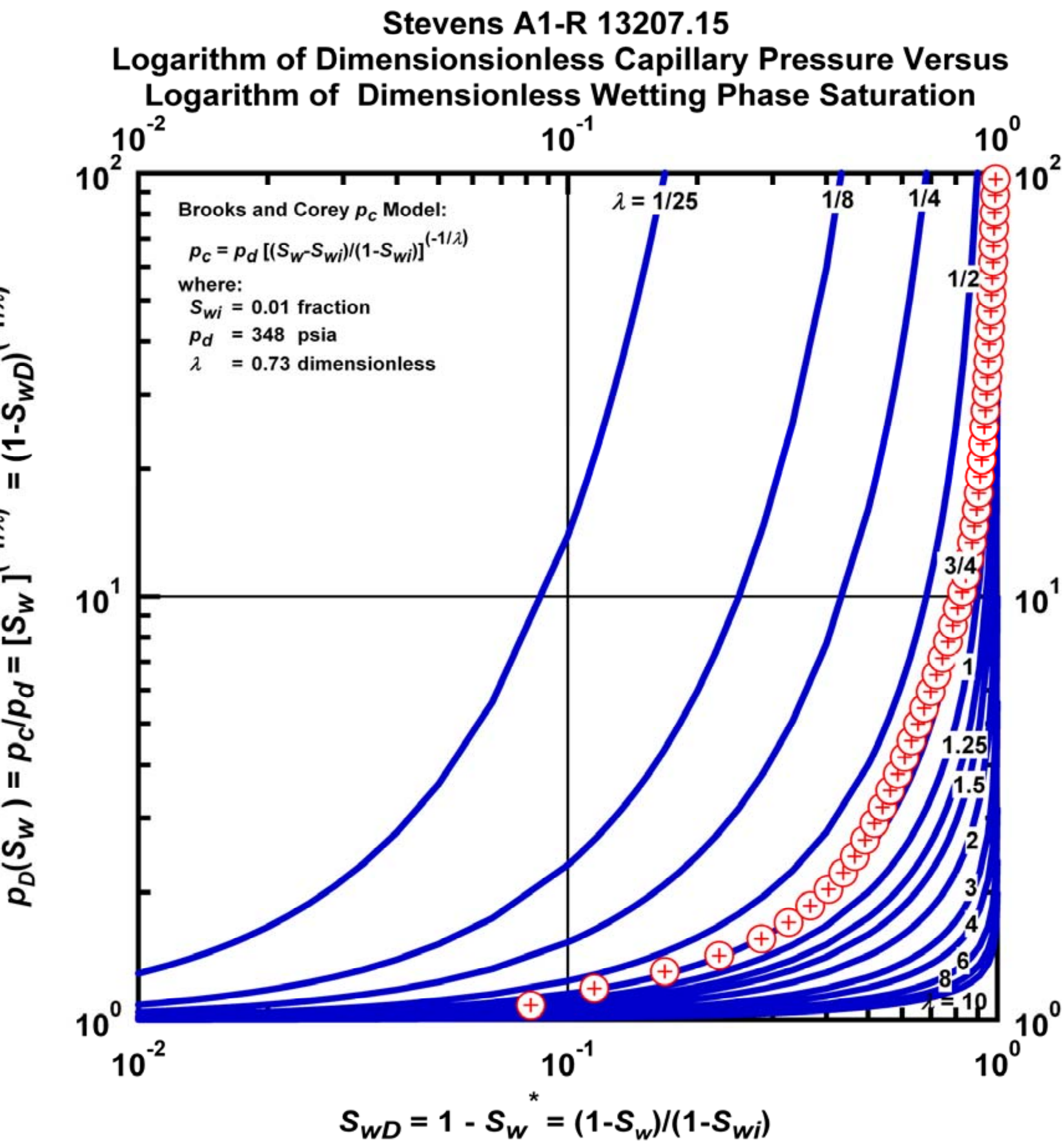

Figure M.76 – Plot of Logarithm of Dimensionless Capillary Pressure Versus Logarithm of Dimensionless Wetting Phase Saturation — Case Stevens A1-R 13207.15.

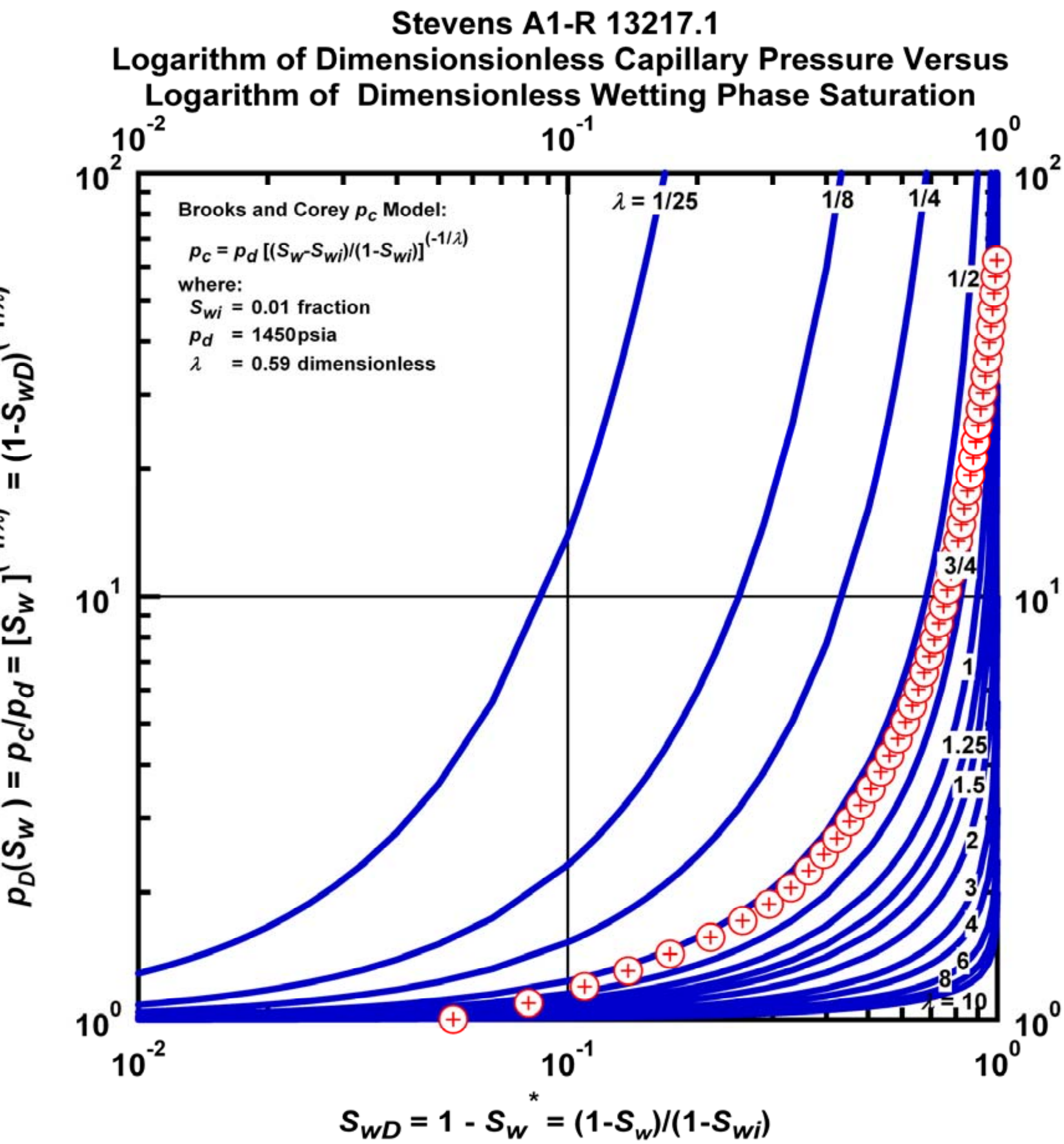

Figure M.77 – Plot of Logarithm of Dimensionless Capillary Pressure Versus Logarithm of Dimensionless Wetting Phase Saturation — Case Stevens A1-R 13217.1.

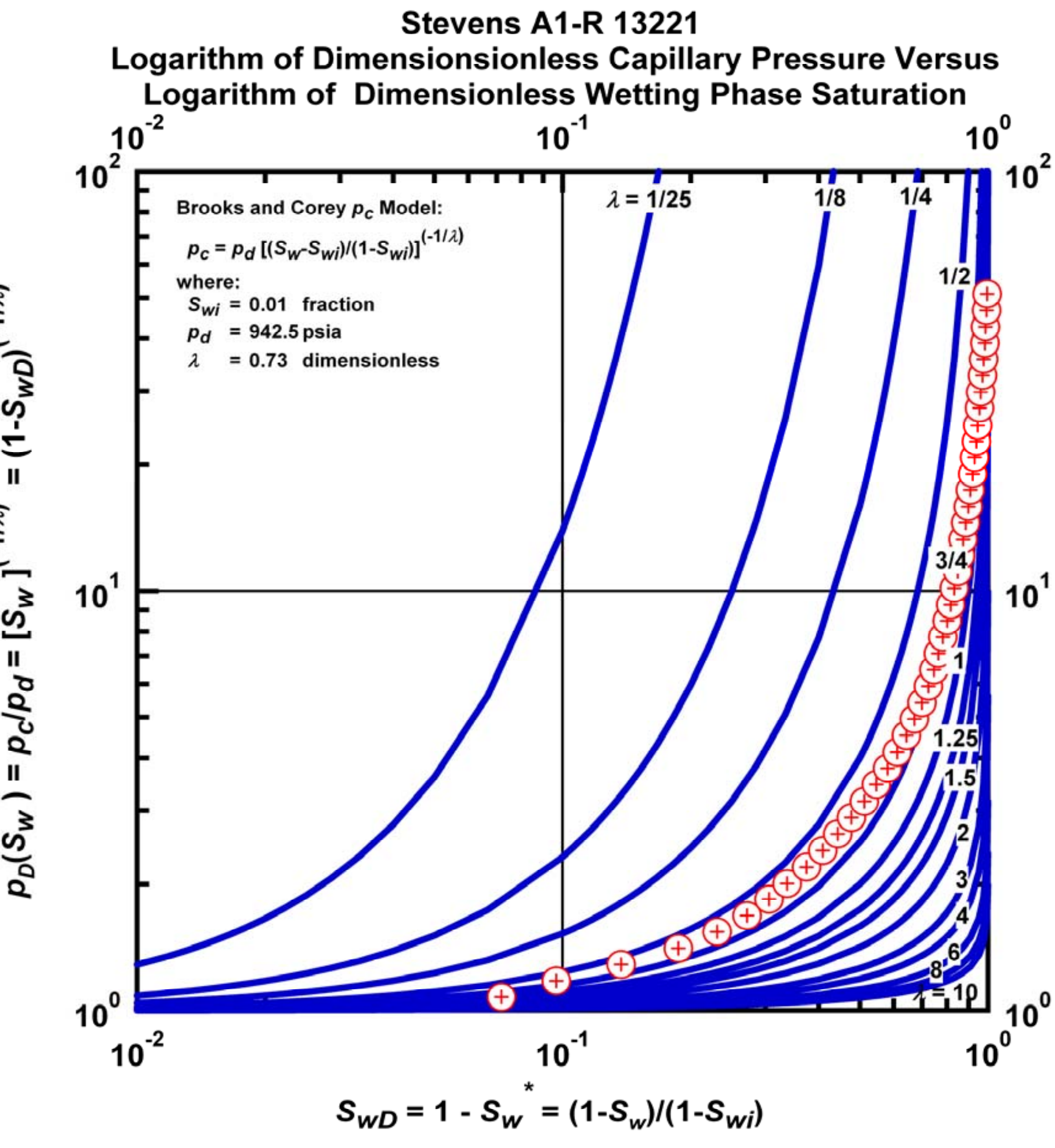

Figure M.78 – Plot of Logarithm of Dimensionless Capillary Pressure Versus Logarithm of Dimensionless Wetting Phase Saturation ── Case Stevens A1-R 13221.

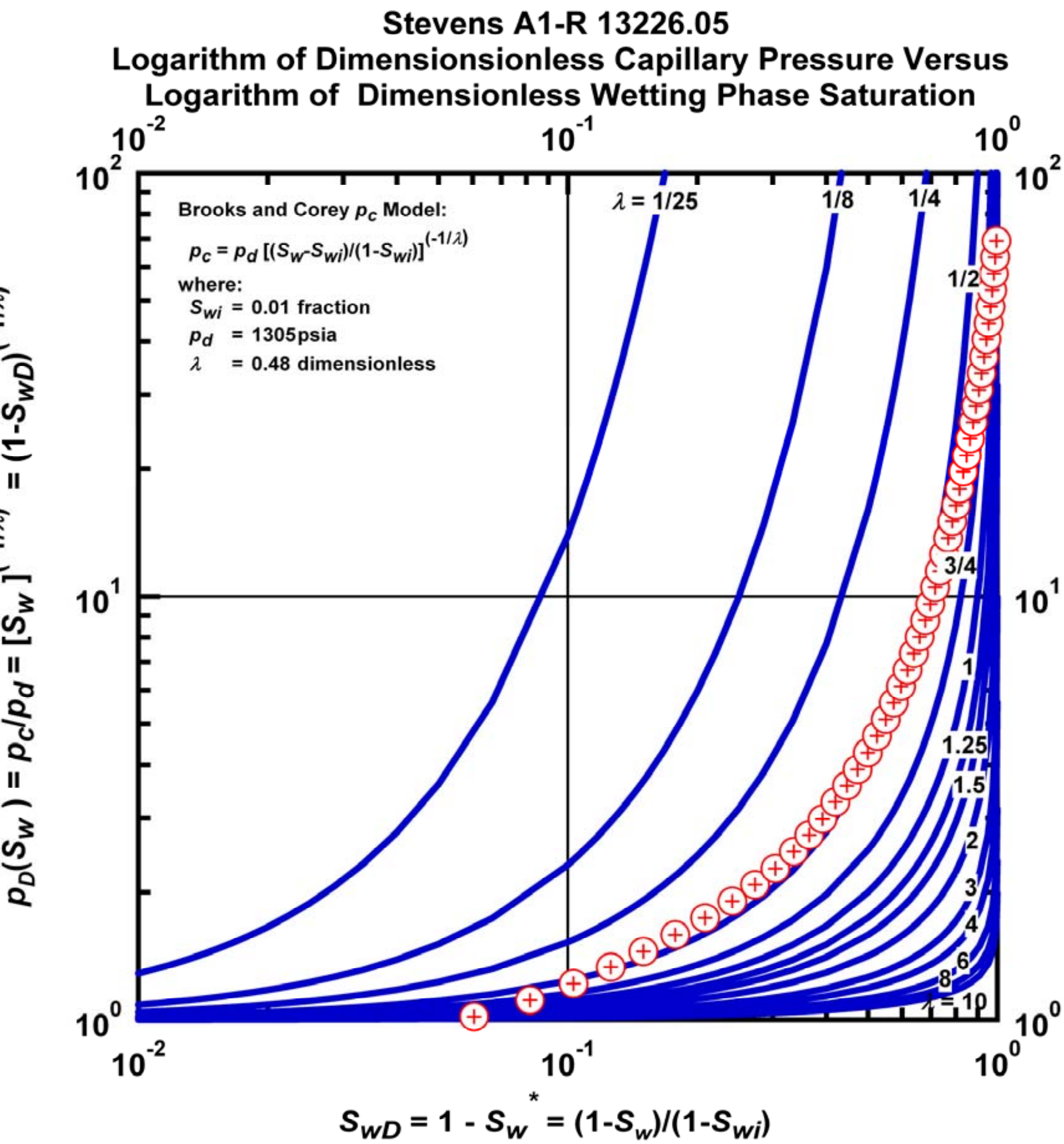

Figure M.79 – Plot of Logarithm of Dimensionless Capillary Pressure Versus Logarithm of Dimensionless Wetting Phase Saturation — Case Stevens A1-R 13226.05.

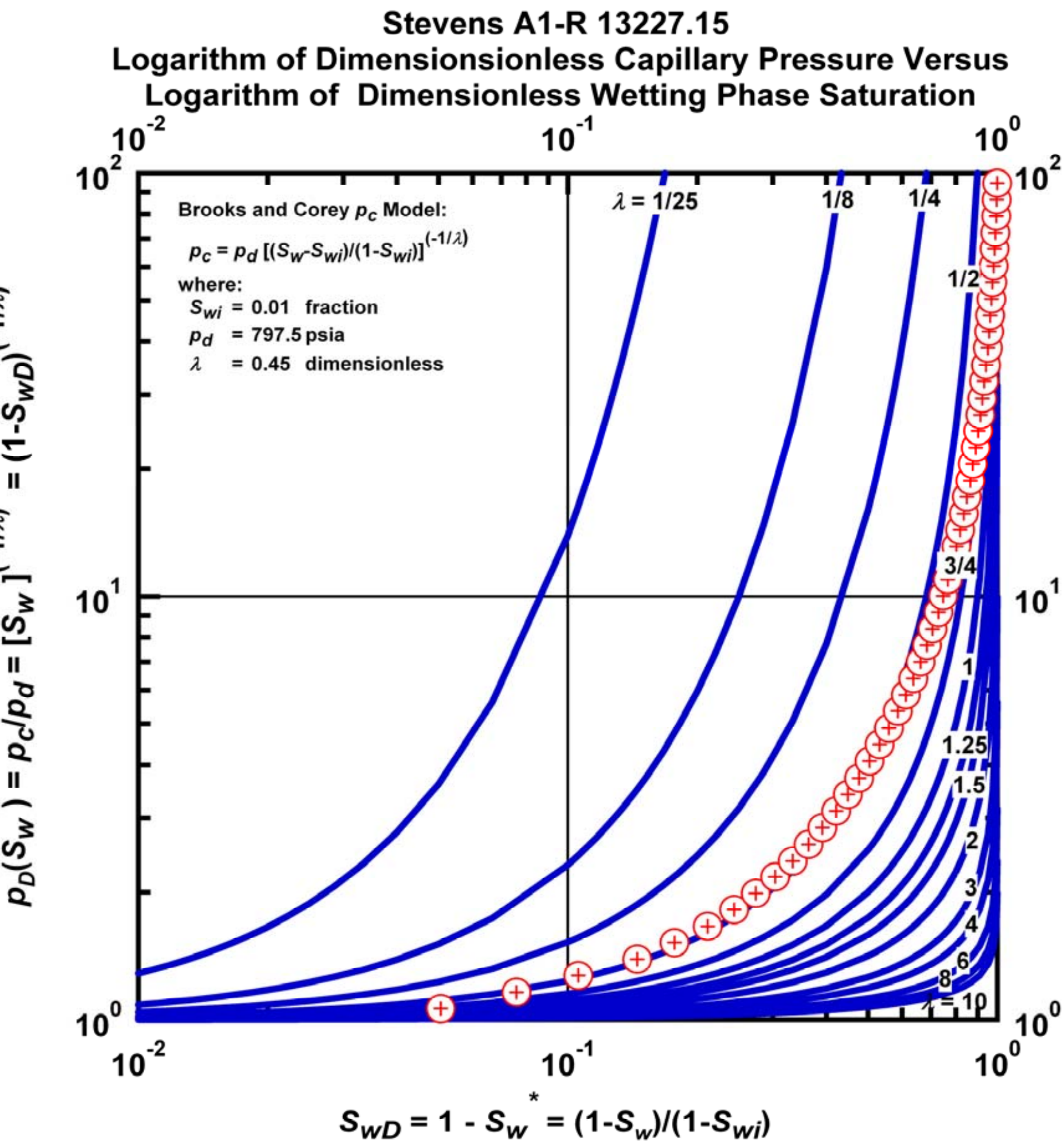

Figure M.80 – Plot of Logarithm of Dimensionless Capillary Pressure Versus Logarithm of Dimensionless Wetting Phase Saturation — Case Stevens A1-R 13227.15.

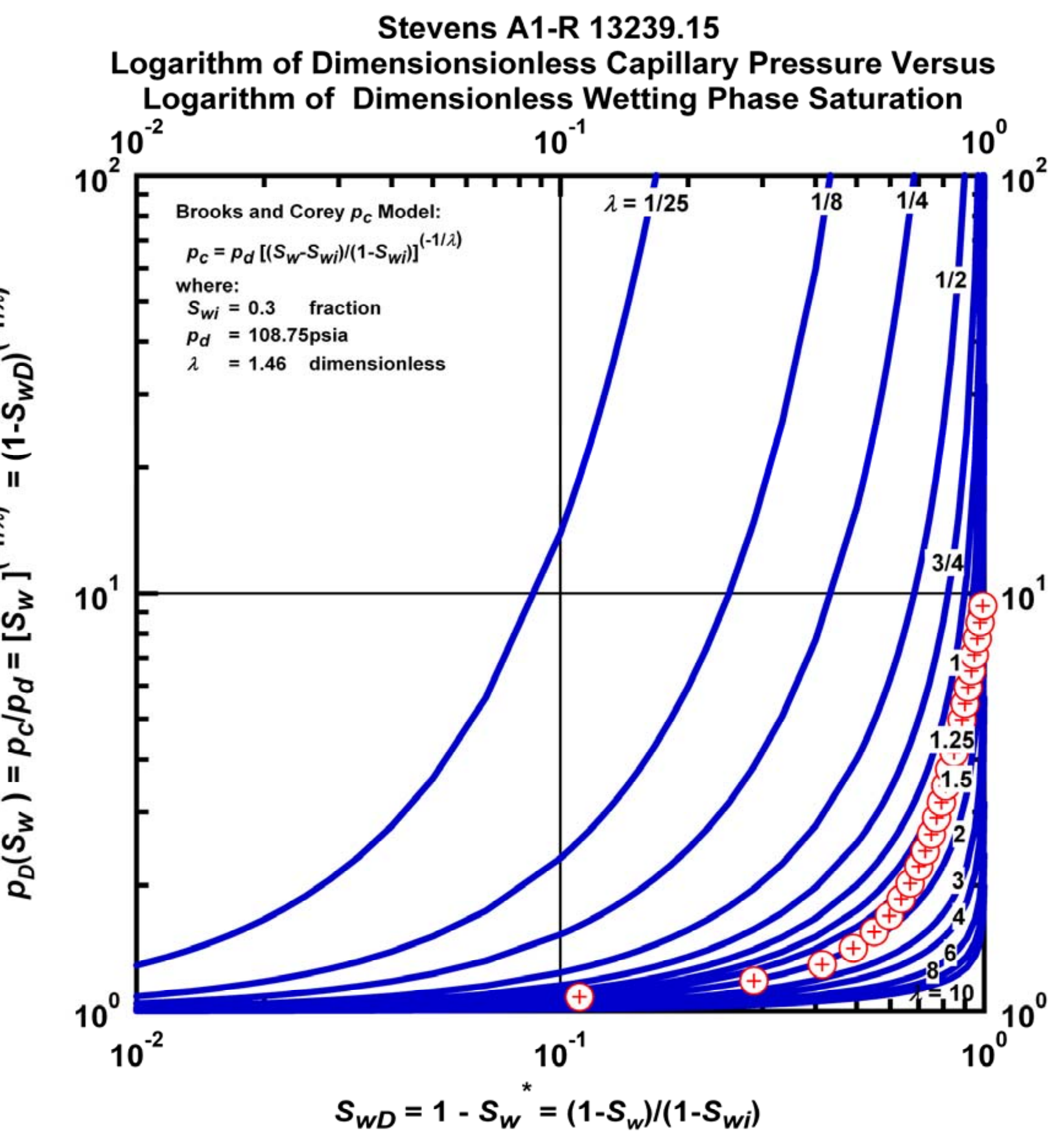

Figure M.81 – Plot of Logarithm of Dimensionless Capillary Pressure Versus Logarithm of Dimensionless Wetting Phase Saturation — Case Stevens A1-R 13239.15.

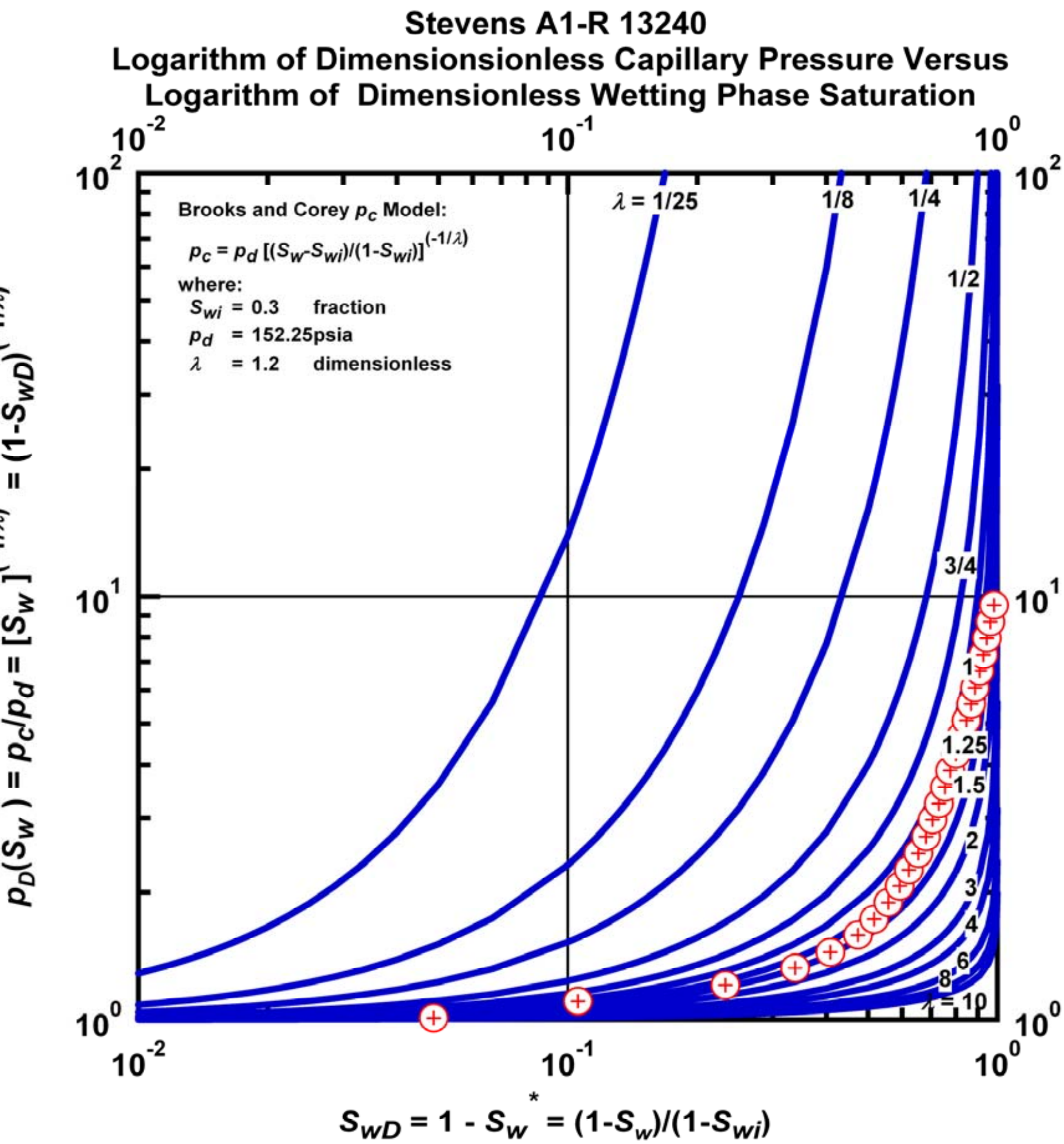

Figure M.82 – Plot of Logarithm of Dimensionless Capillary Pressure Versus Logarithm of Dimensionless Wetting Phase Saturation — Case Stevens A1-R 13240.

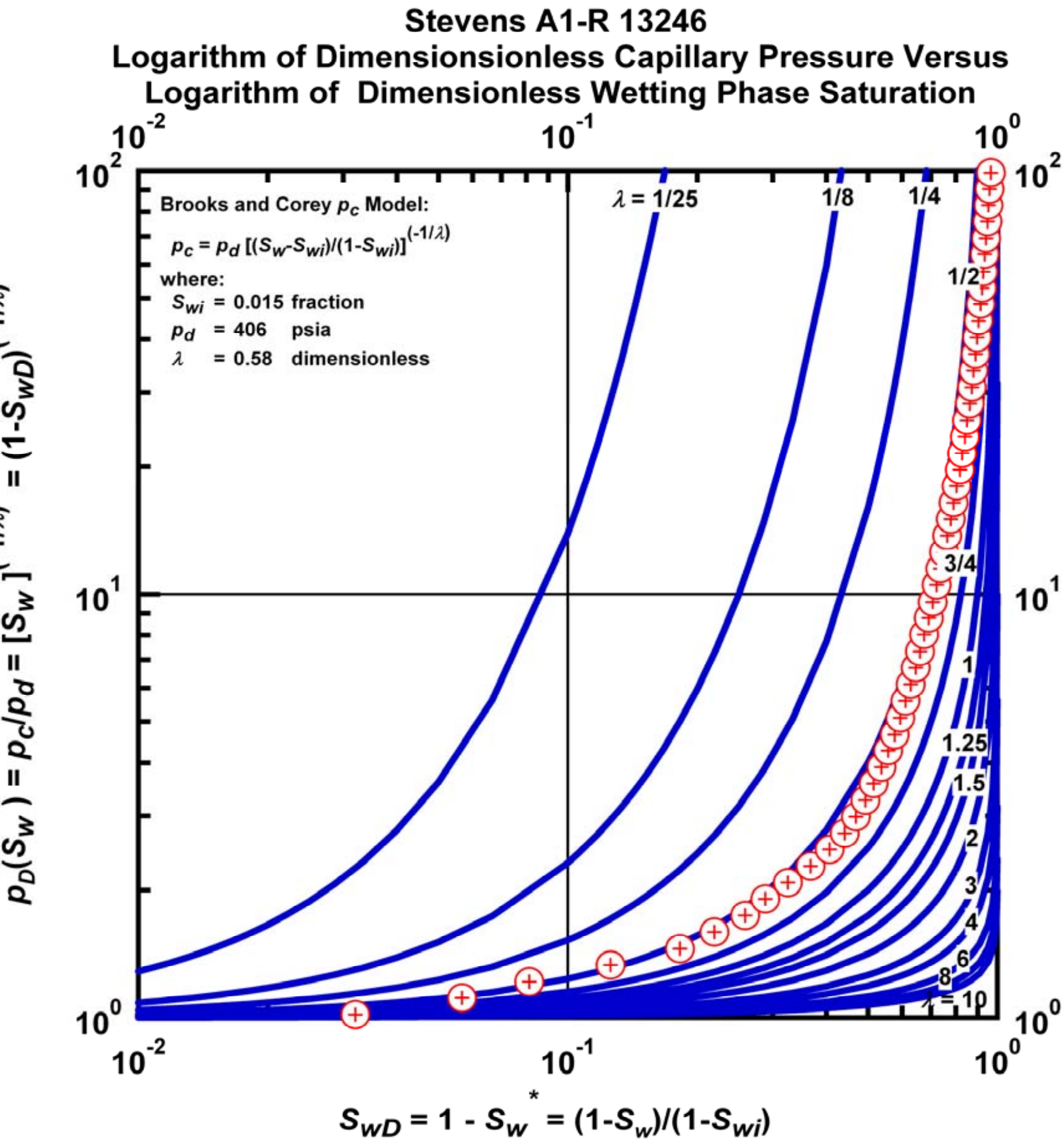

Figure M.83 – Plot of Logarithm of Dimensionless Capillary Pressure Versus Logarithm of Dimensionless Wetting Phase Saturation — Case Stevens A1-R 13246.

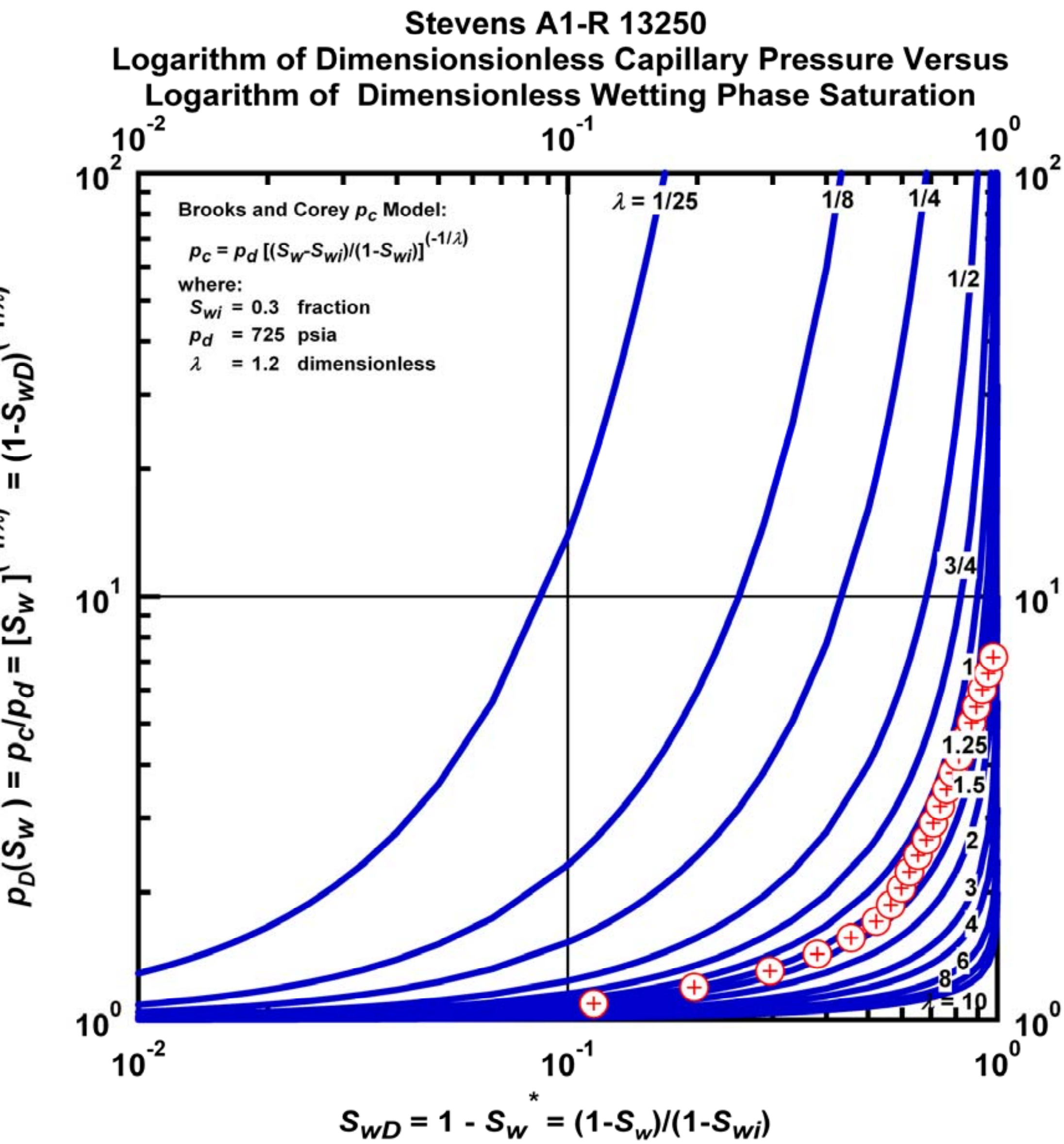

Figure M.84 – Plot of Logarithm of Dimensionless Capillary Pressure Versus Logarithm of Dimensionless Wetting Phase Saturation —— Case Stevens A1-R 13250.

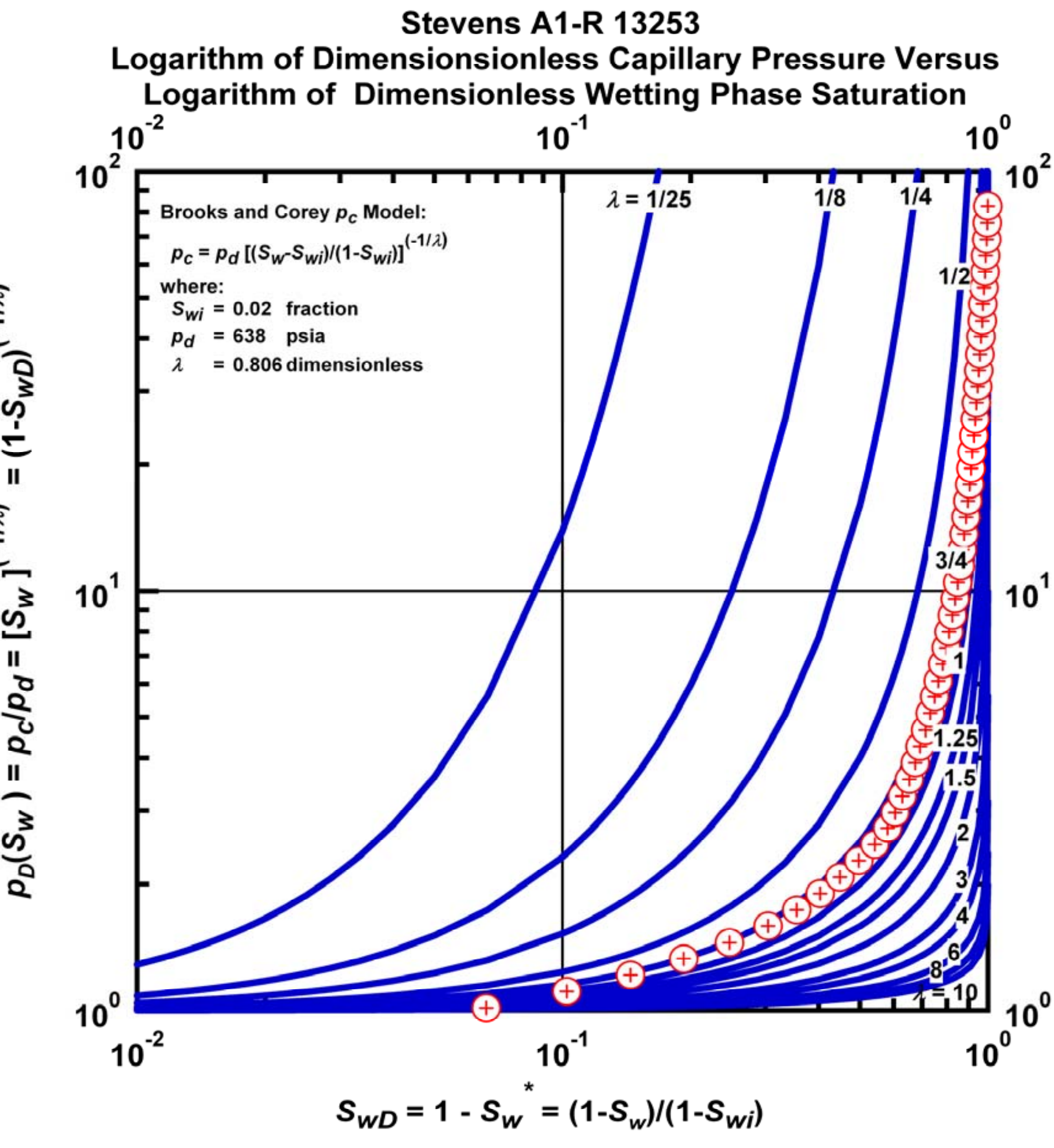

Figure M.85 – Plot of Logarithm of Dimensionless Capillary Pressure Versus Logarithm of Dimensionless Wetting Phase Saturation — Case Stevens A1-R 13253.

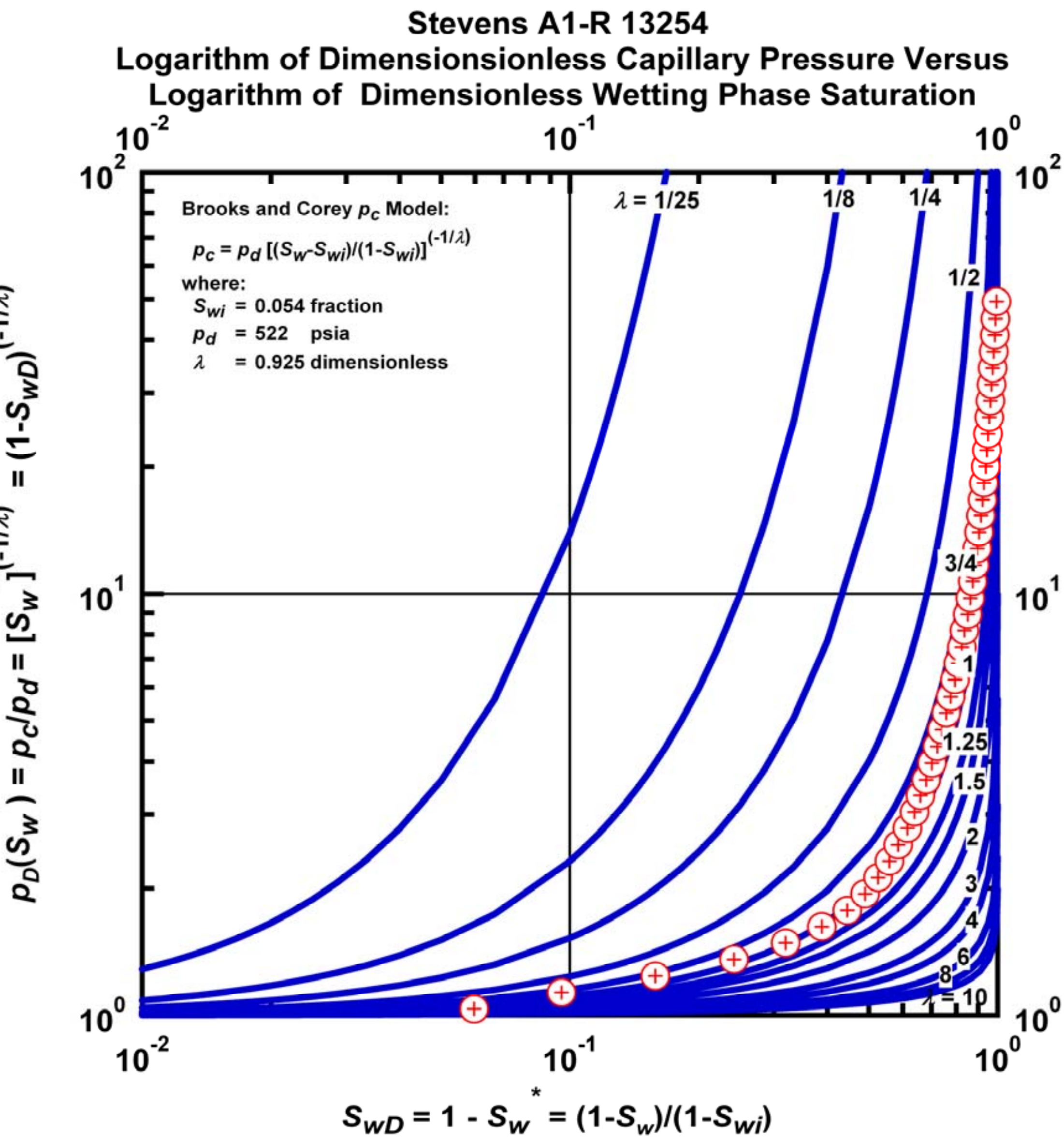

Figure M.86 – Plot of Logarithm of Dimensionless Capillary Pressure Versus Logarithm of Dimensionless Wetting Phase Saturation — Case Stevens A1-R 13254.

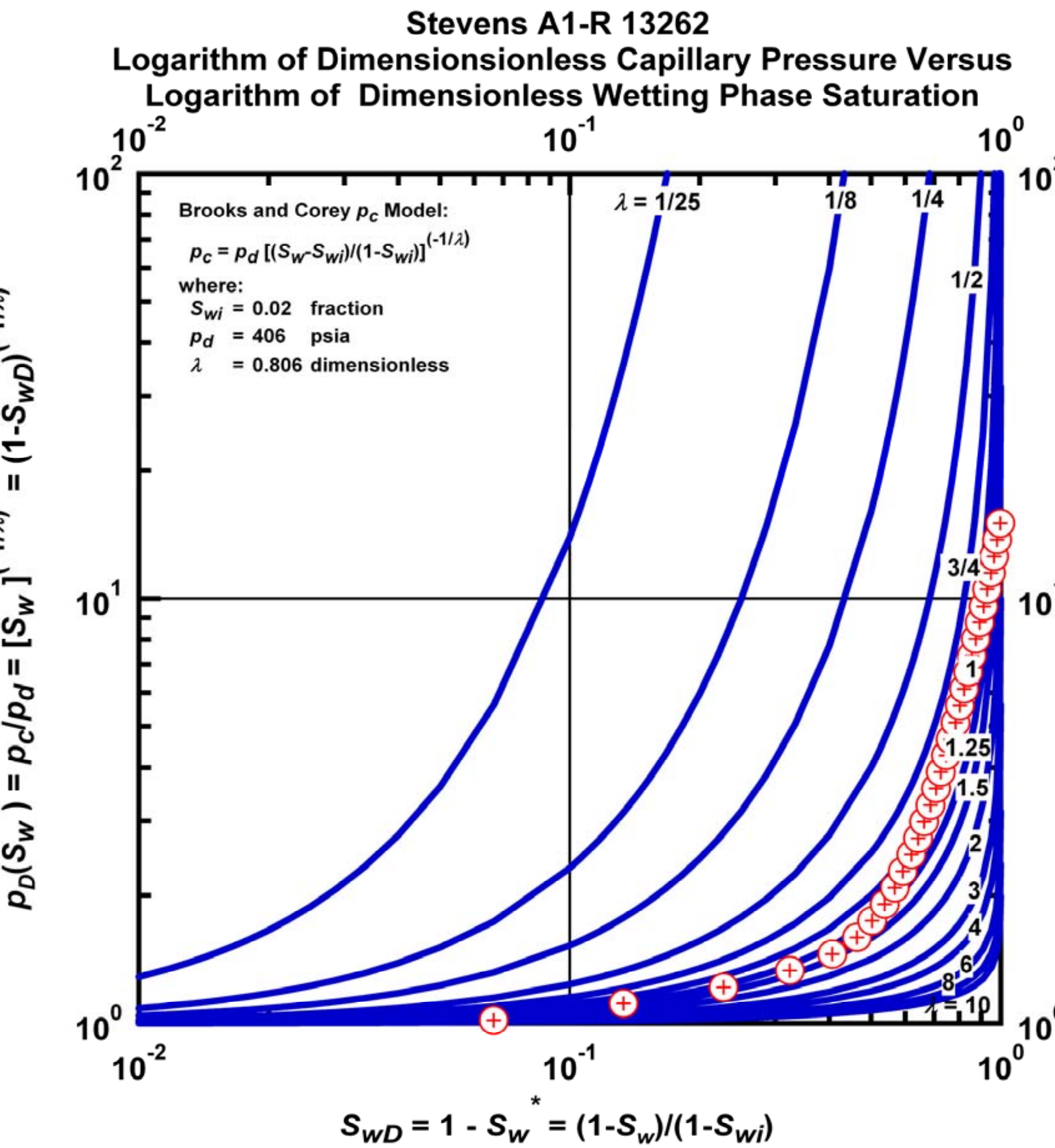

Figure M.87 – Plot of Logarithm of Dimensionless Capillary Pressure Versus Logarithm of Dimensionless Wetting Phase Saturation ── Case Stevens A1-R 13262.

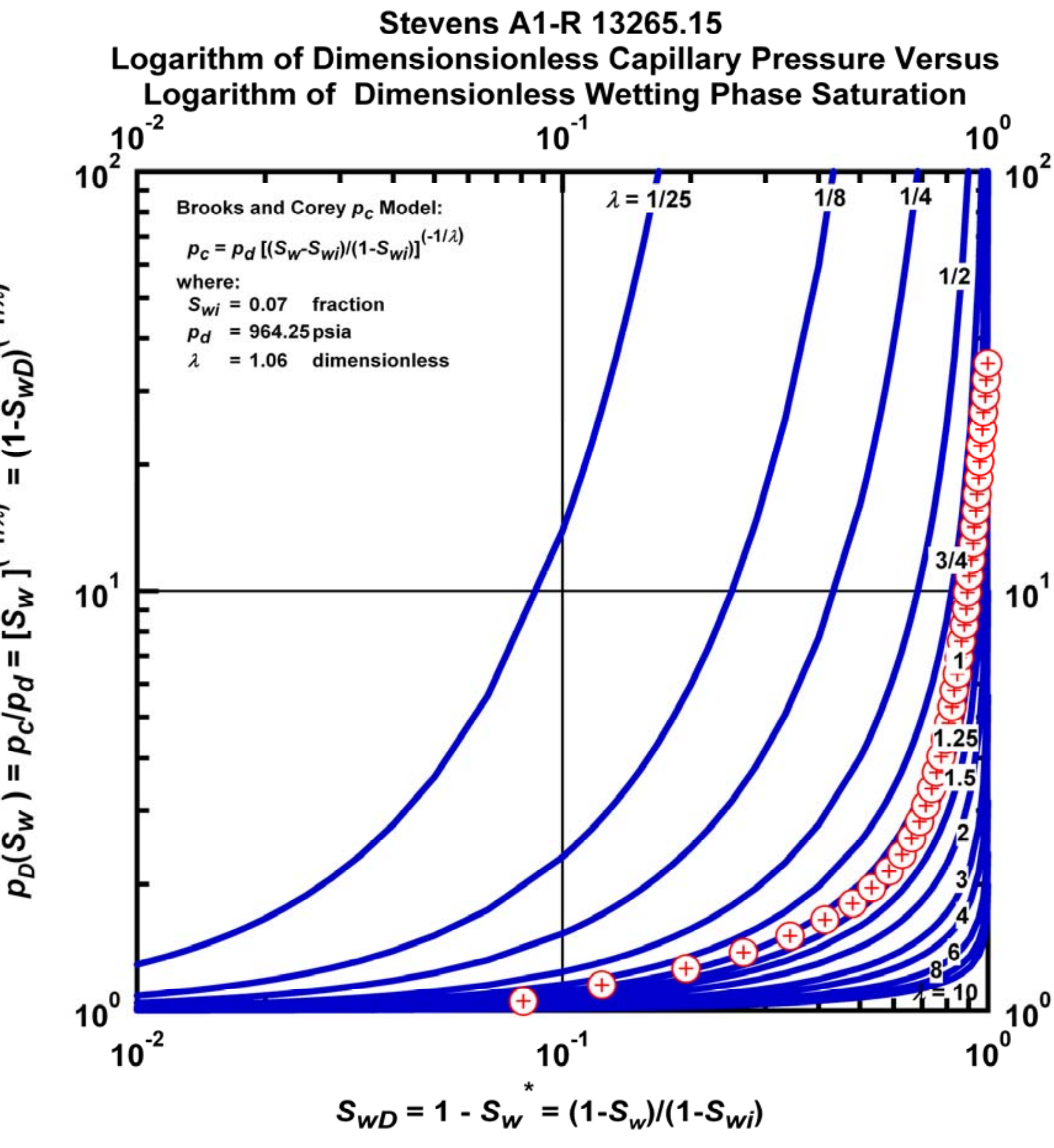

Figure M.88 – Plot of Logarithm of Dimensionless Capillary Pressure Versus Logarithm of Dimensionless Wetting Phase Saturation — Case Stevens A1-R 13265.15.

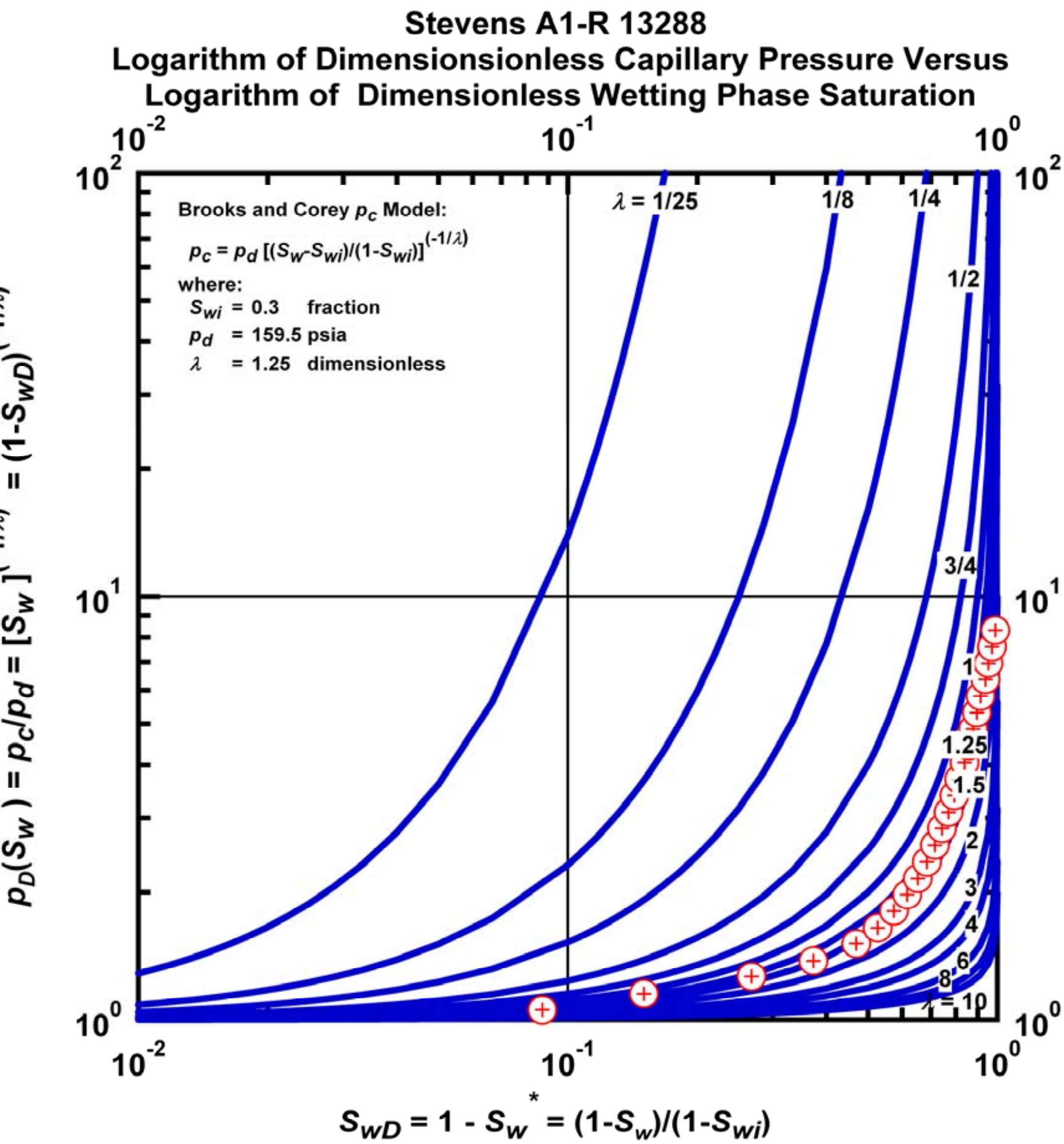

Figure M.89 – Plot of Logarithm of Dimensionless Capillary Pressure Versus Logarithm of Dimensionless Wetting Phase Saturation — Case Stevens A1-R 13288.

APPENDIX N
SUPPLEMENTAL REFERENCES

Capillary Pressure Measurement:

Forbes, P.L. Chen, Z.A. and Ruth D.W.: "Quantitative Analysis of Radial Effects on Centrifuge Capillary Pressure Curve," paper SPE 28182, UNSOLICITED, (January 19 1994).

Greder, H.N., Gallato, V., Cordelier, P., Laran, D., Munoz, V. and d'Abrigeon, O.: "Forty Comparisons of Mercury Injection Data with Oil/Water Capillary Pressure Measurements by the Porous Plate Technique," Society of Core Analysis, SCA 9710 (1997).

Honarpour, M., Djabbarah N.F. and Kralik J.G.: "Expert-Based Methodology for Primary Drainage Capillary Pressure Measurements and Modeling," Paper SPE 99709 presented at the 11th Abu Dhabi International Petroleum Exhibition and Conference held in Abu Dhabi, U.A.F., 10 – 13 October 2004.

Li, K. and Horne, R.N.: "Steam-Water Capillary Pressure," SPE 63224, presented at the 2000 SPE Annual Technical Conference and Exhibition, Dallas, TX, USA, October 1-4, 2000.

Melrose J.C., Dixon J.R. and Mallinson J.F.: "Comparison of Difference Techniques for Obtaining Capillary Pressure Date in the Low-Saturation Region," SPE 22690, presented at the 66th Annual Technical Conference and Exhibition of the Society of Petroleum Engineers held in Dallas, TX, 6 – 9 October 1991.

Melrose J.C. and Mallinson, J.F.: "Evaluation of the High-Speed Centrifuge Technique for Determining Capillary Pressure at Low Wetting-Phase Saturation," SPE 20597, SPE Advanced Technology Series, Vol. 1, No. 1 (1993)

Mitchell, P., Sincock, K. and Williams, J.: "On the Effect of Reservoir Confining Stress on Mercury Intrusion-Derived Pore Frequency Distribution," Society of Core Analysis, SCA 2003-23 (2003).

Neasham K.F., Rushing J.A., Lasswell P.M., Cox J.C. and Blasingame TA.: "A Comparative Study of Laboratory Techniques for Measuring Capillary Pressures in Tight Gas Sands," Paper SPE 89866 presented at the SPE Annual Technical Conference and Exhibition held in Houston, Texas, USA, 26 – 29 September 2004.

O'Meara, D.J., Hirasaki, G.J. and Rohan, J.A.: "Centrifuge Measurements of Capillary Pressure: Part 1 – Outflow Boundary Condition," Paper 18296, SPE Reservoir Engineering (1992).

Shafer, J. and Neasham, J.: "Mercury Porosimetry Protocol for Rapid Determination of Petrophysical and Reservoir Quality Properties," Society of Core Analysis, SCA 2000-21, (2001).

Smith, J.D, Chatzis, I. and Ioannidis M.A.: "A New Technique for Measuring the Breakthrough Capillary Pressure," Society of Core Analysis, SCA 2002-40 (2002)

Spindler, F.A. and Baldwin B.A.: "Capillary Pressure Scanning Curves by Direct Measurement of Saturation" Society of Core Analysis, SCA 9705 (1997).

Tiab D. and Donaldson, C.: "Petrophysics Second Edition – Theor vy and Practice of Measuring Reservoir Rock and Fluid Transport Properties," Golf Professional Publishing (2004) Chap 5, 313 – 360.

Capillary Pressure Data:

Archie, G.F.: "The Electrical Resistivity Log as an Aid in Determining Some Reservoir characteristics," *JPT* (1942), 5:1-8

Calhoun, J.C., Lewis, M.L. and Newman, .C.; "Experiments on the Capillary Properties of Porous Solids," *Trans. AIME*, (1949), 189

Gates, J. I. and Leitz, W. J.: "Relative Permeabilities of California Cores by the Capillary Pressure Method", paper presented at the API meeting, Los Angeles, California, May 11, 1950, 286.

Hidajat,I, Mohanty, K.K., Flaum, M. and Hirasaki, G.: "Study of Vuggy Carbonates using X-Ray CT Scanner and NMR" SPE 77396 presented at the SPE Annual Technical Conference and Exhibition held in San Antonio, Texas, 29 September – 2 October 2002.

Neasham, John W.: "The Morphology of Dispersed Clay in Sandstones Reservoirs and its effect on Sandstones Shaliness, Pore Space and Fluid Flow Properties," Society of Petroleum Engineers, paper SPE 6858, Annual Technical Conference and Exhibition held in Denver, CO, October 9 – 12, 1977.

Purcell, W.R.: "Capillary Pressures-Their Measurement Using Mercury and the Calculation of Permeability", *Trans. AIME*, (1949), 186, 39.

Thomas, L. K., Katz, D. L. and Tek, M. R.: "Threshold Pressure Phenomena in Porous Media", *SPEJ* (June 1968)

Capillary Pressure Models:

Amyx, J.W., Bass, D.M. and Whiting, R.L.: *Petroleum Reservoir Engineering*, 3rd edition, McGraw-Hill Book Company, New York, (1960)

Brooks, R.H., and Corey A.T.: "Hydraulic Properties of Porous Media," Hydrol. Paper 3, Colo. State Univ., Fort Collins, CO, 1964.

Brooks, R. H., and Corey, A. T.: "Properties of porous media affecting fluid flow." *Journal Irrigation and Drainage Division ASCF.* (1966) 92: 61-88.

El-Khatib, N.: "Development of a Modified Capillary Pressure J-Function," Paper SPE 29890, presented at the SPE Middle East Oil Show held in Bahtain, 11 – 14 March 1995.

Kosugi, K.: "Three-Parameter Lognormal Distribution Model for Soil Water Retention," *Water Resour. Res*., (1994) 30:891-901.

Leal, L., Barbato, R., Quaglia, A., Porras, J.C. and Lazarde, H.: "Bimodal Behavior of Mercury-Injection Capillary Pressure Curve and a Laminated and Heterogeneous Reservoir," SPE 69457, Presented at the SPE Latin American and Caribbean Petroleum Engineering Conference held in Buenos Aires, Argentina, 25 – 28 March 2001.

Leverett, M.C.: "Capillary Behavior in Porous Solids," *Trans. AIME* 142, 152. (1941).

Moulu, J.-C., Vizika, O., Kalaydjian, F., and Duquerroix, J.-P.:"A New Model for Three-Phase Relative Permeabilities Based on a Fractal Representation of the Porous Medium," SPE 38891 proceedings of the Annual Technical Conference and Exhibition of the Society of Petroleum Engineers, San Antonio, TX, October 5 – 8, 1997

Negahban, S. *et al*.: "An Improved Empirical Approach for Prediction of Formation Water Saturation and Free Water Level for Uni-modal Pore Systems," Paper SPE 63282, presented at the 2000 SPE Annual Technical Conference and Exhibition held in Dallas, Texas, 1 – 4 October 2000.

Sarwaruddin, M., Skauge A. and Torsaeter, O.: "Modeling of Capillary Pressure for Heterogeneous Reservoiurs by a Modified J-Function," Society of Core Analysis, SCA 2001-35 (2001).

van Genuchten, M .Th.: "A Closed-Form Equation For Predicting the Hydraulic Conductivity of Unsaturated Soils," *Soil Sci. Soc. Am. J.* (1980), 44:892–898.

van Genuchten, M .Th. and Nielson, D.R.: "On Describing and Predicting the Hydraulic Properties of Unsaturated Soils," *Annales Geophysicae*, Vol. 3, 5 (1985), 615-628.

Permeability Correlations:

Aguilera, R.: "Integration of Geology, Petrophysics, and Reservoir Engineering for Characterization of Carbonate Reservoirs through Pickett Plots," *AAPG Bulletin*, V. 88, No. 4 (April 2004), 433-446.

Amaefule J.O. *et al*.: "Reservoir Description: a Practical Synergistic Engineering and Geological Approach Based on Analysis of Core Data," Paper SPE 18267, presented at the 63rd Annual Technical Conference and Exhibition of the Society of Petroleum Engineers held in Houston, TX, October 2 – 5, 1988.

Amaefule J.O. *et al.:* "Enhanced Reservoir Description: Using Core and Log Data to Identify Hydraulic (Flow) Units and Predict Permeability in Uncored Intervals/Wells," Paper SPE 26436, presented at the 68th Annual Technical Conference and Exhibition of the Society of Petroleum Engineers held in Houston, Texas, 3 – 6 October 1993.

Amar, Z.H.B.T., Egbogah, F.O. and Nurdin, A.R.B.: "Core-log Data Integration for Improved Formation Evaluation in the Dulang Field, Offshore Peninsular Malaysia," Paper SPE 29262, presented at the SPE Asia Pacific Oil & Gas Conference held in Kuala Lumpur, Malaysia, 20 – 22 March 1995.

Amthor, J.F., Mountjoy, F.W. and Machel, H.G.: "Regional-Scale Porosity and Permeability Variations in Upper Devonian Leduc Buildups: Implications for Reservoir Development and Prediction in Carbonates," *AAPG Bulletin*, V. 78, No. 10 (Oct. 1994), 1541–1559.

Banik, A.K. and Schechter, D.S.: "Characterization of the Naturally Fractured Spraberry Trend Shaly Sands Based on Core and Log Data," Paper SPE 35224, presented at the SPE Permian Basin Oil and Gas Recovery Conference held in Midland, Texas, 27 – 29 March 1996.

Berg, R.R.: "Method for Determining Permeability from Reservoir Rock Properties," Gulf Coast Association of Geological Societies Transactions, Vol. 20 (1970), Pages 303-335

Bonnie, J.H.M. and Fens, T.W.: "Porosity and Permeability from SEM Based Image Analysis of Core Material," Paper SPE 23619, presented at the Second Latin American Petroleum Engineering Conference, II LAPEC, of the Society of Petroleum Engineers held in Caracas, Venezuela, March 8 – 11, 1992.

Bryant, S., Mellor, D., and Cade, C.: "Permeability Prediction from Geological Models," *AAPG Bulletin*, Vol. 77, No 8 (Aug. 1993), 1338-1350.

Bryant, S., Mellor, D., and Cade, C.: "Physically representative network models of transport in porous media," *AIChE Journal*, 39, 3 (1993), 387-396.

Coates, G.R. *et al*.: "The Magnetic Resonance Imaging Log Characterized by Comparison With Petrophysical Properties and Laboratory Core Data," Paper SPE 22723, presented at the 66th Annual Technical Conference and Exhibition of the Society of Petroleum Engineers held in Dallas, TX, October 6 – 9, 1991.

Civan,F.: "Fractal Formulation of the Porosity and Permeability Relationship Resulting in A Power-Law Flow Units Equation - A Leaky-Tube Model," Paper SPE 73785, presented at the SPE International Symposium and Exhibition on Formation Damage Control held in Lafayette, Louisiana, 20 – 21 February 2002.

Collins R.F. and Jordan, J.K.: "Porosity and Permeability Distribution of Sedimentary Rocks," Paper SPE 212, Unsolicited (1961).

Crawford, B.R., Myers, R.D., Woronow, A. and Faulkner, D.R.: "Porosity-Permeability Relationships in Clay-Bearing Fault Gouge," Paper SPE/ISRM 78214, presented at the SPE/ISRM Rock Mechanics Conference held in Irving, Texas, 20 – 23 October 2002.

Dutton, S.P. and Willis, B.J.: "Comparison of Outcrop and Subsurface Sandstone Permeability Distribution, Lower Cretaceous Fall River Formation, South Dakota and Wyoming," *Journal of Sedimentary Research*, Section A: Sedimentary Petrology and Processes, Vol. 68 (1998), No. 5. Pages 890-900

Evans, J., Crade, C. and Bryant, S.: "A Geological Approach to Permeability Prediction in Clastic Reservoirs," in *AAPG Memoir 69: Reservoir Quality Prediction in Sandstones and Carbonates* Edited by J. A. Kupecz, J. Gluyas, and S. Bloch (1997), 91-101

Everett, R.V., Culbertson, J.S. and Quircin, M.C.: "A Method for Porosity, Permeability, and Water-Saturation Estimates from Logs in Tight Gas Sands with Rugose Holes," Paper SPE 22737, presented at the 66th Annual Technical Conference and Exhibition of the Society of Petroleum Engineers held in Dallas, TX, October 6 – 9, 1991.

Finney, J.L.: "Random Packing and the Structure of Simple Liquids. I. The Geometry of Random Close Packing," *Proceedings of the Royal Society of London. Series A, Mathematical and Physical Sciences*, Vol. 319, No. 1539 (Nov. 10, 1970), 479-493.

Finney, J.L.: "Random Packing and the Structure of Simple Liquids. II. The Molecular Geometry of Simple Liquids," *Proceedings of the Royal Society of London. Series A, Mathematical and Physical Sciences*, Vol. 319, No. 1539 (Nov. 10, 1970), 495-507.

Gangi, A.F.: "Permeability of Unconsolidated Sands and Porous Rocks," *Journal of Geophysical Research*, Vol. 90, No B4 (March 1985), 3099 – 3104.

Gunter, G.W. *et al*.: "Early Determination of Reservoir Flow Units Using an Integrated Petrophysical Method," Paper SPE 38679, presented at the SPE Annual Technical Conference and Exhibition held in San Antonio, Texas, U.S.A., 5 – 8 October 1997.

Honarpour, M.M. *et al*.: "Effect of Rock Heterogeneity on Relative Permeability: Implications for Scale-up," Paper SPE 29311, presented at the SPE Asia Pacific Oil & Gas Conference held in Kuala Lumpur, Malaysia, 20 – 22 March 1995.

Iverson, W.P., Martinsen, R.S. and Surdam, R.C.: "Pressure Seal Permeability and Two-Phase Flow," Chapter 20 from: M 61: Basin Compartments and Seals Edited by Peter J. Ortoleva (1994)

Javalagi, M.I. and Iverson, W.P.: "Permeability Estimation from Sonic-Transit-Time Versus Porosity Gradients," Paper SPE 36658, presented at the 1996 SPE Annual Technical Conference and Exhibition held in Denver, Colorado, U.S.A., 6 – 9 October 1996.

Jennings, J. and Lucia, F.J.: "Predicting Permeability from Well Logs in Carbonates with a Link to Geology for Interwell Permeability Mapping," Paper 71336, presented at the 2001 SPE Annual Technical Conference and Exhibition held in New Orleans, Louisiana, 30 September – 3 October 2001.

Kane, T.V. and Henderson, R.P.: "Sequence Stratigraphic Model and Geology/Reservoir "Flow Unit" Study Improve Profitability and Recover Additional Reserves at the Sharon Ridge Canyon Unit," Paper SPE 35181, presented at the Permian Basin Oil & Gas Recovery Conference held in Midland, Texas, 27 – 29 March 1996.

Keelan, D.K.: "Core Analysis for Aid in Reservoir Description," Paper SPE 10011, *JPT* (1982).

Lim, J.S. and Kim, J.: "Reservoir Porosity and Permeability Estimation from Well Logs using Fuzzy Logic and Neural Networks," Paper 88476, presented at the SPE Asia Pacific Oil and Gas Conference and Exhibition held in Perth, Australia, 18 – 20 October 2004.

Lucia, F. J. and Conti, R. D.: "Rock fabric, permeability, and log relationships in an upward-shoaling, vuggy carbonate sequence," The University of Texas at Austin, Bureau of Economic Geology Geological Circular 87-5 (1987).

Lucia, F. J.: "Estimating Permeability from Porosity in Alabama Ferry Field: the Rock-Fabric Approach," Gulf Coast Association of Geological Societies Transactions, Vol. 52 (2002), 673-680

Luffel, D.L., Howard, W.F. and Hunt, F.R.: "Travis Peak Core Permeability and Porosity Relationships at Reservoir Stress," Paper SPE 19008, *SPEFE* (1991).

Magara, K.: "Porosity-Permeability Relationship of Shale," Paper SPE 2430, UNSOLICITED (1968).

Malik, M.A. and Lake, L.W.: "A Practical Approach to Scaling-Up Permeability and Relative Permeabilities in Heterogeneous Permeable Media," Paper SPE 38310, presented at the SPE Western Regional Meeting held in Long Beach, California, U.S.A., 25-27 June 1997.

Martin, A.J., Solomon, S.T. and Hartmann, D.J.: "Characterization of Petrophysical Flow Units in Carbonate Reservoirs," *AAPG Bulletin*, V. 81 (1997), No. 5, P. 734- 759

Nelson P.H.: "Permeability–porosity relationships in sedimentary rocks," *Log Analyst* 3, (1984), 38–62.

Nurmi, R.D. and Frisinger, M.R.: "Synergy of Core Petrophysical Measurements, Log Data, and Rock Examination in Carbonate Reservoir Studies," Paper SPE 11969, presented at the 58th Annual Technical Conference and Exhibition of the Society of Petroleum Engineers of AIME, held in San Francisco, California, Oct. 5 – 8, 1983.

Ohen, H.A. and Curby F.M.: "A Hydraulic (Flow) Unit Based Model for the Determination of Petrophysical Properties from NMR Relaxation Measurements," Paper SPE 30626, presented at the SPE Annual Technical Conference & Exhibition held in Dallas, TX, U.S.A., 22 – 25 October, 1995.

Ostermeier, R.M.: "Compaction Effects on Porosity and Permeability: Deepwater Gulf of Mexico Turbidites," Paper SPE 66479, *JPT* (2001).

Owolabi, O.O., LongJohn, T.F. and Ajienka, J.A.: "An Empirical Expression for Permeability in Unconsolidated Sands of the Eastern Niger Delta," *Journal of Petroleum Geology*, Vol.17, No.1, (1994) 111- 116.

Panda, M.N. and Lake, L.W.: "Estimation of Single-Phase Permeability from Parameters of Particle-Size Distribution," *AAPG Bulletin*, V. 78, No. 7 (July 1994), 1028–1039.

Panda, M.N. and Lake, L.W.: "A Physical Model of Cementation and Its Effects on Single-Phase Permeability," *AAPG Bulletin*, V. 79, No. 3 (March 1995), P. 431–443.

Rincones, J.G. et al.: "Effective Petrophysical Fracture Characterization Using the Flow Unit Concept-San Juan Reservoir, Orocual Field, Venezuela," Paper SPE 63072, presented at the 2000 SPE Annual Technical Conference and Exhibition held in Dallas, Texas, 1 – 4 October 2000.

Ringrose P.S., Jensen, J.L. and Sorbie, K.S.: "The Use of Geology in the Interpretation of Core-Scale Relative Permeability Data," Paper SPE 28448, presented at the SPE 69th Annual Technical Conference and Exhibition held in New Orleans, LA, U.S.A., 25 – 28 September 1994.

Rodriguez, A.: "Facies Modeling and the Flow Unit Concept as a Sedimentological Tool in Reservoir Description: A Case Study," Paper SPE 18154, presented at the 63rd Annual Technical Conference and Exhibition of the Society of Petroleum Engineers held in Houston, TX, October 2 – 5, 1988

Rogers, S.J. *et al*.: "Predicting Permeability from Porosity Using Artificial Neural Networks," Bulletin, V. 79 (1995), No. 12 1786-1796.

Saller, A.H. and Henderson, N.: "Distribution of Porosity and Permeability in Platform Dolomites: Insight from the Permian of West Texas," *AAPG Bulletin*, V. 82 (1998), No. 8 (August 1998), 1528 – 1550.

Schutjens P.M.T.M *et al*.: "Compaction-Induced Porosity/Permeability Reduction in Sandstone Reservoirs: Data and Model for Elasticity-Dominated Deformation," Paper 88441, *SPEREE* (June 2004).

Shang, B.Z., Hamman, J.G., Chen, H.L. and Caldwell, D.H.: "A Model to Correlate Permeability with Efficient Porosity and Irreducible Water Saturation," Paper SPE 84303, presented at the SPE Annual Technical Conference and Exhibition held in Denver, Colorado, U.S.A., 5 – 8 October 2003.

Soeder, D.J.: "Porosity and Permeability of Eastern Devonian Gas Shale," Paper SPE 15213, presented at the Unconventional Gas Technology Symposium of the Society of Petroleum Engineers held in Louisville, KY, May 18 – 21, 1986.

Soeder, D.J. and Randolph, P.L.: "Porosity, Permeability, and Pore Structure of the Tight Mesaverde Sandstone, Piceance Basin, Colorado," Paper SPE 13134, *SPEFE* (1987).

Sprunt, F.S., Gilliland R.F. and Barret, M.L.: "Predicting the Permeability of Unconsolidated Sediments from Grain Size Measurements," Gulf Coast Association of Geological Societies Transactions, Vol. 43 (1993), 373 – 380

Tsay, F.S. and Fang, J.H.: "A Core-Log Study of the Hartselle Sandstone in North Alabama with Emphasis in Log Interpretation Problems in Tight Gas Sands," Paper SPE 15211, presented at the Unconventional Gas Technology Symposium of the Society of Petroleum Engineers held in Louisville, KY, May 18 – 21, 1986.

Tyler, N., Barton, M.D. and Finley, R.J.: "Outcrop Characterization of Flow Unit and Seal Properties and Geometries, Ferron Sandstone, Utah," Paper SPE 22670, presented at the 66th Annual Technical Conference and Exhibition of the Society of Petroleum Engineers held in Dallas, TX, October 6 – 9, 1991.

Waite, M., Johansen, S. Betancourt, D. and Acharya, U.: "Modeling of Scale-Dependent Permeability Using Single-Well Micro-Models: Application to Hamaca Field, Venezuela," Paper SPE 86976, presented at the SPE International Thermal Operations and Heavy Oil Symposium and Western Regional Meeting, held in Bakersfield, California, U.S.A., 16 – 18 March 2004.

Zheng, S.Y., Corbett, P.W.M., Ryseth, A. and Stewart, G.: "Uncertainty in well test and core permeability analysis: a case study in fluvial channel reservoirs, northern North Sea, Norway," AAPG Bulletin, V. 84, No. 12 (December 2000), 1929-1954.

Permeability Models from Capillary Pressure:

Burdine, N. T.: "Relative Permeability Calculations from Pore Size Distribution Data", *Trans. AIME*, (1953), **198**, 71.

Gates, J. I. and Leitz, W. J.: "Relative Permeabilities of California Cores by the Capillary Pressure Method", paper presented at the API meeting, Los Angeles, California, May 11, 1950, 286.

Johnson, A.: "Permeability Averaged Capillary Data: A Supplement to Log Analysis in Field Studies," Proceedings of the SPWLA 28th Annual Logging Symposium (1987).

Kamath, J.: "Evaluation of Accuracy of Estimating Air Permeability from Mercury-Injection Data," SPE18181, *SPERE* (1992)

Katz, A. J., and Thompson A.H.: "Quantitative prediction of permeability in porous rock," *Physical Review B*,(1986) v. 34, p. 8179 – 8181.

Kolodzie, S., Jr.: "Analysis of Pore Throat Size and Use of the Waxman-Smits Equation to Determine OOIP in Spindle Field," Paper SPE-9382, SPE, 55th Annual Fall Technical Conference (1980), 10 p.

Pittman, F.D.: "Relationship of Porosity and Permeability to Various Parameters Derived from Mercury Injection-Capillary Pressure Curves for Sandstone," The American Association of Petroleum Geologists Bulletin V. 76, No. 2 (1992) 191 – 198.

Purcell, W.R.: "Capillary Pressures-Their Measurement Using Mercury and the Calculation of Permeability", *Trans. AIME*, (1949), **186**, 39.

Ma, S., Jiang, M.X., Morrow, N.R.: "Correlation of Capillary Pressure Relationships and Calculations of Permeability," SPE 22685, presented at the 66th Annual Technical Conference and Exhibition of the Society of Petroleum Engineers held in Dallas, TX, October 6-9, 1991.

Nakornthap, K. and Evans, R.D.: "Temperature-Dependent Relative Permeability and Its Effect on Oil Permeability and Its Effect on Oil Displacement by Thermal Methods," SPE 11217 *SPERE* (1986)

Rose W. and Bruce W.A.: "Evaluation of capillary character in petroleum reservoir rock," Petroleum *Trans. AIME* 186 (1949), 127 – 142.

Thomeer, J. H.: "Introduction of a Pore Geometrical Factor Defined by the Capillary Pressure Curve," *JPT* (1960), p. 73-77.

Thomeer, J. H.: "Air Permeability as a Function of Three Pore-Network Parameters," SPE 10922, *JPT* (1983).

Thompson, A. H., A. J. Katz, and Raschke R. A.: "Estimation of Absolute Permeability from Capillary Pressure Measurements," Paper SPE-16794, SPE, 62nd Annual Technical Conference 1987, p. 475-481.

Swanson, B. F.: "A Simple Correlation between Permeabilities and Mercury Capillary Pressures," Paper SPE 8234, *JPT*, (Dec. 1981), p. 2488-2504.

Ward, J.S. and Morrow N.R.: "Capillary Pressures and Gas Relative Permeabilities of Low-Permeability Sandstones," Paper SPE 13882, SPE Formation Evaluation (September 1987).

Wells, J.D. and Amaefule, J.O.: "Capillary Pressure and Permeability Relationships in Tight Gas Sands," Paper SPE 13879 presented at the 1985 Low Permeability Gas Reservoir held in Denver, Colorado, May 19-22.

Wyllie, M: "Some Theoretical Considerations Related to the Quantitative Evaluation of the Physical Characterizations of Reservoir Rock from Electrical Log Data," *JPT*, (1950).

Wyllie, M.R.J., and Gardner, G.H.F.: "The Generalized Kozeny–Carman Equation: Part II," *World Oil*, (1958), 146(5): 210–228.

Wyllie M.R. and Spangler M. B.: "The Application of Electrical Resistivity Measurements to the Problem of Fluid Flow in Porous Media," *Research Rroject 4-G-1 Geology division Report N°. 15* (March 1951) Gulf Research and Development Company.

Yuan H.H. and Swanson B.F.: "Resolving Pore-Space Characteristics by Rate-Controlled Porosimetry," SPE 14892, *SPEFE* (1986).

Relative Permeability:

Honarpour M., Koederitz L. and Herbert Harvey A.: "Relative permeability of petroleum reservoirs," Boca Raton, Fla. C.R.C. Press (1986) 1 – 43.

Al-Fattah S.M.: "Empirical Equation for Water/Oil Relative Permeability in Saudi Sandston Reservoirs," SPE 85652, presented at the 2003 SPE Annual International Conference and Exhibition held in Nigeria, Abuja, 4 – 6 August 2003.

Al-Omait, O. and Christiansen, R.L.: "Benefits of Saturation Profiles for Estimating Gas and Liquid Relative Permeabilities from Centrifuge Tests," Society of Core Analysis, SCA 2002-14 (2002).

Asar, H. and Handy, L.L.: "Influence of Interfacial Tension on Gas-Oil Relative Permeability in a Gas-Condensate System," paper SPE 11740, presented at the 1983 SPE Annual Technical Conference and Exhibition.

Cable, A. et al.: "Experimental Techniques For The Measurement Of Relative Permeability and In-Situ Saturation in Gas Condensate Near Well Bore and Drainage Studies," paper 9928, to be presented at the International Symposium of the Society of Core Analysts, Golden, Colorado, August 1999.

Cable A. et al.: "X-ray In-situ Saturation in Gas Condensate Relative Permeability Studies," SCA 2000-39, Presented at the SCA, Abu Dhabi, UAE, 18-22 Oct 2000.

Blom, S.M.P. and Hagoort, J.: "Relative Permeability at Near-Critical Conditions," paper SPE 38935 (accepted for publication in *SPEJ*).

Blom, S.P.M. and Hagoort J.: "The Combined Effect of Near-Critical Relative Permeability and Non-Darcy Flow on Well Impairment by Condensate Drop-Out," SPE 51367, presented ate the 1998 SPE Gas Technology Symposium held in Calgary, Alberta, Canada, 15 – 18 March 1998.

Blom, S.M.P. and Hagoort, J.: "How to Include the Capillary Number in Gas Condensate Relative Permeability Functions?" paper SPE 49268, presented at the SPE Annual Technical Conference and Exhibition, Dallas, 27-30 September 1998.

Chen, H.L. et al.: "Determination of Relative Permeability and Recovery for North Sea Gas Condensate Reservoirs," paper SPE 30769, presented at the SPE Annual Technical Conference and Exhibition, Dallas, October 1995.

Delshad, M., Lenhard, R.J., Oostrom, M. and Pope, G.A.: "A Mixed-Wet Hysteretic Relative Permeability and Capillary Pressure Model for Reservoir Simulations," Paper SPE 86916, revised for publication from paper SPE 51891, first presented at the 1999 SPE Reservoir Simulation Symposium, Houston, 14-17 February 1999.

Ebeltoft, F. et al.: "A novel experimental Apparatus for determination of three phase relative permeabilities at reservoir conditions," *JPSE* (1998) 119.

Fevang, Ø. and Whitson, C.H.: "Modeling Gas-Condensate Well Deliverability," *SPERE* (Nov. 1996).

Flett, M. Gurton, R. and Taggart I.: "The Function of Gas-Water Relative Permeability Hysteresis in the Sequestration of Carbon Dioxide in Saline Formations," Paper SPE 88485, prepared for presentation at the SPE Asia Pacific Oil and Gas Conference and Exhibition held in Perth, Australia, 18 – 20 October 2004.

Goda, H.M. and Behrenbruch, P.: "Using a Modified Brooks-Corey Model to Study Oil-Water Relative Permeability for Diverse Pore Structure," SPE 88538, presented at the SPE Asia Pacific Oil and Gas Conference and Exhibition held in Perth, Australia, 18 – 20 October 2004.

Haniff, M.S. and Ali, J.K.: "Relative Permeability and Low Tension Fluid Flow in Gas Condensate Systems,"Paper SPE 20917 presented at the 1990 EUROPEC meeting (Oct. 22-24).

Henderson, G.D., Danesh A., Teherani, D.H., Al-Shaidi, S. and Peden, J.M.: "Measurement and Correlation of Gas Condensate Relative Permeability by the Steady-State Method," *SPEJ*, 1(2), 191-201 (1995).

Honarpour, M.M., Cullick, A.S. and Saad, N.: "Influence of Small-Scale Rock Laminations on Core Plug Oil/Water Relative Permeability and Capillary Pressure," Paper SPE 27968, presented at the University of Tulsa Centennial Petroleum Engineering Symposium held in Tulsa, Oklahoma, U.S.A., 29-31 August 1994.

Huang D.D., Honarpour M.M., and Al-Hussainy, R.: "An Improved Model for Relative Permeability and Capillary Pressure Incorporating Wettability," Society of Core Analysis, SCA 9718 (1997)

Jamiolahmady, M., Danesh, A., Henderson, G. and Tehrani, G.D.: "Variations of Gas-Condensate Relative Permeability with Production Rate at Near Wellbore Conditions: A General Correlation," Paper SPE 83960, presented at Offshore Europe 2003 held in Aberdeen, UK, 2-5 September 2003.

Jan, B.M., Siagian, U.W. and Lee, R.L.: "Effect of Permeability Distribution and Interfacial Tension on Gas Condensate Relative Permeability: An Experimental Study," Paper SPE 80551, presented at the SPE Asia Pacific Oil and Gas Conference and Exhibition held in Jakarta, Indonesia, 9-11 September 2003.

Kjosavik, A., Ringen, J.K. and Skjaeveland,S.M.: "Relative Permeability Correlation for Mixed-Wet Reservoirs," Paper SPE 77328, *SPEJ*, (March 2002).

Li, K. and Horne, R.N.: "Experimental Verification of Methods to Calculate Relative Permeability Using Capillary Pressure Data," Paper SPE 76757 presented at the SPE Western Regional/ AAGP Pacific Section Joint Meeting held in Anchorage, Alaska, USA, 20 – 22 May 2002.

Li, K. and Horne, R.N.: "An Experimental Method of Measuring Steam-Water and Air-Water Capillary Pressures," paper 2001-84, presented at the Petroleum Society's Canadian International Petroleum Conference 2001, Calgary, Alberta, Canada, June 12–14, 2001.

McDougall, S.R., Cruickshank, J. and Sorbie, K.S.: "Anchoring Methodology or Pore-Scale Network Models: Application to Relative Permeability and Capillary Pressure Prediction," Society of Core Analysis, SCA 2001-15 (2001).

Mott, R.: "Calculating Well Deliverability in Gas Condensate Reservoirs," presented at the 10th European Symposium on Improved Oil Recovery, Brighton, UK, 18-20 August, 1999.

Mott, R., Cable, A. and Spearing, M.: "Measurement and Simulation of Inertial and High Capillary Number Flow Phenomena in Gas-Condensate Relative Permeability," Paper SPE 62932, presented at the 2000 SPE Annual Technical Conference and Exhibition held in Dallas, TX, 1-4 October 2000.

Mulyadi, H., Mason, T. and Steer D.: "Applying MAK Gas-Water Relative Permeability Correlations to Predict a Gas-Condensate Relative Permeability and Production Performance (Case Study)," Paper SPE 77935, presented at the SPE Asia Pacific Oil and Gas Conference and Exhibition held in Melbourne, Australia, 8-10 October 2002.

Narayanaswamy G., Pope, G.A. and Sharma, M.M.: "Predicting Gas Condensate Well Productivity Using Capillary Number and Non-Darcy Effects," SPE 51910 presented at the 1999 SPE Reservoir Simulation Symposium held in Houston, Texas, 14-17 February 1999.

Papatzacos, P. and Skjaeveland S.M.: "Relative Permeability from Capillary Pressure," SPE 77540, presented at the SPE Annual Technical Conference and Exhibition held in San Antonio, Texas, 29 September – 2 October 2002.

Papatzacos, P. and Skjaeveland S.M.: "Relative Permeability From Thermodynamics," Paper SPE 87674, *SPEJ*, March 2004.

Pope, G.A. et al: "Modeling Relative Permeability Effects in Gas Condensate Reservoirs," paper SPE 49266, presented at the SPE Annual Technical Conference and Exhibition, Dallas, 27-30 September 1998.

Rushing, J.A., Newsham, K.F. and Van Fraassen, K.C.: "Measurement of the Two-Phase Gas Slippage Phenomenon and Its Effect on Gas Relative Permeability in Tight Gas Sands," Paper SPE 84297, presented at the SPE Annual Technical Conference and Exhibition held in Denver, Colorado, USA, 5-8 October 2003.

Saevareid, O *et al*.: "An Engineering approach to Measuring gas condensate relative permeability," paper 9930, to be presented at the International Symposium of the Society of Core Analysts, Golden, Colorado, August 1999.

Wang, X. and Mohanty, K.K.: "Multiphase Non-Darcy Flow in Gas-Condensate Reservoirs," Paper SPE 56486, presented at the 1999 SPE Annual Technical Conference and Exhibition held in Houston, Texas, 3-6 October 1999.

Ward, J.S. and Morrow N.R.: "Capillary Pressures and Gas Relative Permeabilities of Low-Permeability Sandstones," Paper SPE 13882, *SPE Formation Evaluation* (September 1987).

Whitson C.H., Fevang O. and Saevareid, A.: "Gas Condensate Relative Permeability for Well Calculations," Paper SPE 56476, presented at the 1999 SPE Annual Technical Conference and Exhibition held in Houston, Texas, 3-6 October 1999.

Zapata J. F.: "Impact of Relative Permeability Models on Fluid Flow Behavior for Gas Condensate Reservoirs," Thesis, Texas A&M university, Texas, 2002